

申 报	系列：教学科研型
	专业：畜牧学
	职称：教授

业绩成果材料

（申报人的业绩成果材料包括论文、科研项目、获奖以及其他成果等）

单 位（二级单位） 动物科学学院

姓 名 孙加节

材料核对人：

单位盖章：

核对时间：

华南农业大学制

目 录

一、教学研究业绩

1. 教学研究项目

- 1.12 广东省 2022 年本科高校教学质量与教学改革工程建设项目落实：“育德”教育与实践，打造《饲料 生物技术》思政“金课”（主持）..... 1-5
- 1.2 广东省高等学校教育管理学会 2021 年度课程思政建设项目：饲料生物技术（主持）..... 6-7
- 1.3 华南农业大学 2022 年教学质量与教学改革工程建设项目（主持）..... 8-9
- 1.4 华南农业大学 2019 年教学质量与教学改革工程建设项目：在生物化学课程中构建低年级大学生研究性学习引导机制研究（主持）10-11

2. 第一作者发表教改论文

- 2.1 饲料生物技术课程改革与效果评价 12-15
- 2.2 动物生物化学线上线下混合式“金课”建设探索 16-18
- 2.3 饲料生物技术课程思政教育教学模式研究 19-23
- 2.4 《饲料生物技术》课程思政点挖掘与应用 24-29

3. 教学成果奖证书

- 3.1 国家教学成果二等奖，农科高校双创人才培养模式创新与实践（排十一）..... 30
- 3.2 广东省教学成果二等奖，契合新农科建设需求的动物生产类专业课“金课”建设的创新与实践（排三）..... 31
- 3.3 华南农业大学教学成果一等奖，契合新农科建设需求的动物生产类专业课“金课”建设的创新与实践（排三）..... 32
- 3.4 广东省课程思政改革示范项目，饲料生物技术-单细胞蛋白饲料的生产与应用（主持）..... 33
- 3.5 国家一流本科线下课程，《饲料生物技术》（排二）..... 34

3.6 广东省一流本科线下课程,《饲料生物技术》(排二)	35
3.7 广东省一流本科线上课程,《动物生物化学》(排四)	36
3.8 华南农业大学 2022 年度课程思政示范项目,《饲料生物技术》(主持)	37-39

4. 教学比赛证书

4.1 华南农业大学首届课程思政教学大赛三等奖	40
4.2 首届全国动物生理生化青年教师教学大赛获“突出教师”奖 ..	41

5. 编写教材

5.1 《生物信息基础》(第一主编)	42-47
--------------------------	-------

二、科研项目

1. 主持项目任务书

1.1 国家自然科学基金面上项目: 环状 RNA 介导 CNS1S1 基因影响热应激奶牛乳腺 α s1-casein 合成及机制研究	48-50
1.2 科技创新 2030-重大项目子课题: 基于产业链数据的猪适应性性状基因组选择方法研究与应用	51-78
1.3“十四五”国家重点研发子课题: 牛羊木本源饲料应用及高效转化关键技术研究	79-85
1.4 广东省基础与应用基础研究基金项目: CircLIMCH1 相关 ceRNA 网络调控猪骨骼肌纤维发育的机制研究	86-95
1.5 广东省重点领域研发计划子课题	96-105
1.6 广州市科技计划项目: LncRNA 竞争性结合 miR-21 调控 MSTN 在猪肌纤维类型转化中的分子机制	106-123
1.7 广州市科技计划项目: 关岭牛高效养殖与雪花肉生产技术 ..	124
1.8 猪禽种业全国重点实验室 2023 年度开放课题	125-132

三、论文、著作等

1. 检索证明	133-143
2. 以第一作者发表本专业论文情况	

2.1 Integrated meta-omics reveals the regulatory landscape involved in lipid metabolism between pig breeds.....	144-167
2.2 The effect of dietary ginseng polysaccharide supplementation on porcine milk - derived esRNAs involved in the host immune responses.....	168-174
2.3 Effect of Moringa oleifera supplementation on productive performance, colostrum composition and serum biochemical indexes of sow.....	175-183
2.4 Emerging Roles of Heat-Induced circRNAs Related to Lactogenesis in Lactating Sows.....	184-193
3. 以通讯作者发表本专业论文情况	
3.1 A novel protein encoded by circKANSL1L regulates skeletal myogenesis via the Akt-FoxO3 signaling axis	194-216
3.2 A novel protein encoded by porcine circANKRD17 activates the PPAR pathway to regulate intramuscular fat metabolism	217-232
3.3 Plant-derived miR166a-3p packaged into exosomes to cross-kingdom inhibit mammary cell proliferation and promote apoptosis by targeting APLNR gene.....	233-244
3.4 Milk exosome-derived miRNAs from water buffalo are implicated in immune response and metabolism process	245-249
3.5 Effects of Fermented Herbal Tea Residues on the Intestinal Microbiota Characteristics of Holstein Heifers Under Heat Stress.....	250-263
3.6 Fermentation quality of herbal tea residue and its application in fattening cattle under heat stress...	264-276
3.7 CircEZH2 Regulates Milk Fat Metabolism through miR-378b	

Sponge Activity.....	277-293
3.8 Effects of Herbal Tea Residue on Growth Performance, Meat Quality, Muscle Metabolome, and Rumen Microbiota Characteristics in Finishing Steers.....	294-305
3.9 Identification of circRNA-associated ceRNA networks using longissimus thoracis of pigs of different breeds and growth stages.....	306-320
3.10 The Characteristic Function of Blood-Derived Exosomes and Exosomal circRNAs Isolated from Dairy Cattle during the Dry Period and Mid-Lactation.....	221-339
3.11 The difference of intestinal microbiota composition between Lantang and Landrace newborn piglets.....	340-348
3.12 凉茶渣对育肥猪生长性能、胴体性状和肉品质的影响	349-357
3.13 Dietary supplementation with <i>Moringa oleifera</i> and mulberry leaf affects pork quality from finishing pigs	358-365
3.14 Effects of fermented feeds and ginseng polysaccharides on the intestinal morphology and microbiota composition of Xuefeng black-bone chicken.....	366-381
3.15 Identification of circRNA-Associated-ceRNA Networks Involved in Milk Fat Metabolism Under Heat Stress...	382-395
3.16 蓝塘猪与长白猪背最长肌全基因组 DNA 甲基化分析...	396-406
3.17 凉茶渣替代象草对育肥牛空肠组织形态、屏障功能以及菌群结构的影响.....	407-418
3.18 Effect of miR - 493 - 5p on proliferation and differentiation of myoblast by targeting ANKRD17....	419-432
3.19 非编码 RNA 对猪骨骼肌发育的影响.....	433-441
3.20 非编码 RNA 调控猪肌间脂肪沉积的研究进展.....	442-449

3.21 茶及其副产品在畜禽养殖中的应用.....	450-454
3.22 夏季热应激对肉牛养殖的影响及防控措施.....	455-459
3.23 茶渣资源再利用研究概况.....	460-464
3.24 调控乳蛋白合成信号通路的研究进展.....	465-470
3.25 Advances in the Evaluation and Application of Nutritionally Valuable Woody Feeding Plants.....	471-481
3.26 环境应激对圈养野生动物繁殖性能的影响.....	482-488
3.27 Exploration of long noncoding RNA in bovine milk exosomes and their stability during digestion in vitro.....	489-500
3.28 Plant MIR156 regulates intestinal growth in mammals by targeting the Wnt/ β -catenin pathway.....	501-515
3.29 Genomewide analysis of circular RNA in pituitaries of normal and heat-stressed sows.....	516-528
3.30 Biological Characteristics and Roles of Noncoding RNAs in Milk-Derived Extracellular Vesicles.....	529-539
3.31 Porcine milk exosome miRNAs protect intestinal epithelial cells against deoxynivalenol-induced damage.....	540-553
3.32 Rno_circ_0001004 Acts as a miR-709 Molecular Sponge to Regulate the Growth Hormone Synthesis and Cell Proliferation	554-564
3.33 Skeletal Muscle-Derived Exosomal miR-146a-5p Inhibits Adipogenesis by Mediating Muscle-Fat Axis and Targeting GDF5-PPAR γ Signaling.....	565-584
3.34 Plant MIR167e-5p Inhibits Enterocyte Proliferation by Targeting β -Catenin.....	585-598
3.35 Exploration of Long Non-coding RNAs and Circular RNAs in Porcine Milk Exosomes.....	599-610

四、学术专著

- 4.1 《环境生物学》(参编) 611-620
4.2 《中国黄牛遗传学》(参编) 621-641

五、知识产权

- 5.1 专利授权证书: 与猪胴体肉品质相关的 circRNA 标志物及其应用
..... 642
5.2 专利授权证书: 一种区分水牛和奶牛奶的 miRNA 标记物及其应用
..... 643
5.3 专利授权证书: 与猪胴体瘦肉率相关的 miRNA 标志物及其应用
..... 644
5.4 专利授权证书: 一种与猪肌纤维类型相关的 lncRNA 标志物及其
应用..... 645
5.5 专利授权证书: 与猪肌间脂肪相关的分子标记及其应用 646
5.6 专利授权证书: 与猪肌纤维类型发育相关的 circKANSL1L 及其
应用..... 647

六、其他个人荣誉

- 6.1 华南农业大学动科科学学院 2019 年度“青年教师成长奖”. 648
6.2 华南农业大学动科科学学院 2020 年度“服务管理工作先进个人”
..... 649
6.3 华南农业大学动科科学学院 2020 年度“青年教师优秀奖”. 650
6.4 华南农业大学动科科学学院 2021 年度“服务育人先进个人” 651
6.5 广东省高等教育学会第二届高等教育研究优秀成果奖..... 652

七. 社会服务

- 7.1 贵州关岭布依族苗族自治县国家级科技特派团产业组组长
7.2 贵州务川仡佬族苗族自治县国家科技特派团产业组组长
7.3 广州市农村科技特派员

广东省教育厅

粤教高函〔2023〕4号

广东省教育厅关于公布 2022 年广东省本科 高校教学质量与教学改革工程建设项目 立项名单的通知

各本科高校：

按照《广东省教育厅关于开展 2022 年度广东省本科高校教学质量与教学改革工程项目申报推荐工作的通知》等文件安排，经学校遴选推荐、省教育厅审核、评审、公示及异议复审等环节，现将 2022 年省本科高校质量工程建设项目立项名单予以公布，并就有关事项通知如下：

一、立项情况

确定立项建设省级实验教学示范中心 27 个、校企联合实验室 23 个、科产教融合实践教学基地 58 个、大学生社会实践教学基地 44 个、教师教学发展中心 2 个、课程教研室 112 个、现代产业学院 23 个、未来技术学院 1 个、专项人才培养计划 58 个、高等教育教学改革项目 781 个、高等教育教学改革项目（委托类）

5 个。具体立项名单见附件。

二、项目管理

（一）本次公布项目均为省质量工程建设项目，建设项目经学校组织建设、校内结题并通过省教育厅统一组织项目验收后，正式认定为省级项目。

（二）项目正式实施前，请确保已对项目建设目标、建设举措、预期成果、建设进度安排等进行科学论证，论证专家应不少于 5 人，且至少有三分之一来自外校。论证后的目标、任务等将作为项目结题验收时的重要依据。

（三）项目日常管理由学校主管部门负责，学校应统筹做好项目中期检查、校内结题验收等工作。校内结题时，邀请校外评审专家人数不得少于专家总人数的三分之二。满足以下条件的项目，经学校正式申请，可以参与省教育厅统一组织的项目验收：

1.项目已完成立项时设定的主要建设任务和目标；

2.项目已取得标志性建设成果，且该成果已在教学实践中得到检验和有效应用；

3.已按照要求完成项目校内结题；

4.符合当年度省统一验收规定的其他条件。

各校质量工程建设项目管理情况，将作为学校下一年度项目立项限额的参考依据。

（四）项目实施过程中，其名称、建设内容（任务）、建设目标、建设周期、主要负责人、预期成果等发生重大变更的，需

由时任项目负责人在发生变更后及时提出，经学校项目主管部门审核后由学校正式来函说明原因；擅自变更上述内容的，验收评定时列为不通过。

三、其他事项

（一）2022 年度各校向省教育厅推荐并获得立项的项目，学校须将项目校内评审、推荐及论证相关材料妥善保存，留底备查。

（二）各校要统筹本校“冲补强”提升计划资金及自有资金对立项项目予以资助，项目获得学校资助情况将作为项目结题验收时重要考察因素之一。如项目建设中取得具有推广价值的优秀成果，请及时形成书面材料报省教育厅高教处。

联系人：李成军、傅兴淙，联系电话：020-37626882、37627703。

附件：2022 年广东省本科高校教学质量与教学改革工程建设项目立项项目名单



公开方式：依申请公开

校对人：傅兴淙

430	高等教育教学改革项目	华南农业大学	融合“树医生”理念的《园林植物栽植与养护》课程思政与实践教学改革研究	刘天丽
431	高等教育教学改革项目	华南农业大学	教学高质量发展视域下本科生评教指标体系的优化	贾莉
432	高等教育教学改革项目	华南农业大学	融合课程思政的农林院校数学类公共基础课程评价体系的建立和实践	丁仕虹
433	高等教育教学改革项目	华南农业大学	问题驱动下农业院校的数学分析课程线上线下教学改革的研究与实践	王石宏
434	高等教育教学改革项目	华南农业大学	中外合作办学“学术英语”模块课程融合课程思政的探索	冯立新
435	高等教育教学改革项目	华南农业大学	助力乡村振兴的高阶性新型农商复合人才培养实践教学模式研究	齐文娥
436	高等教育教学改革项目	华南农业大学	“大思政课”视野下《中国近现代史纲要》教学改革与实践	崔芸
437	高等教育教学改革项目	华南农业大学	大数据背景下统计学专业产教融合人才培养机制的探索与实践	肖前
438	高等教育教学改革项目	华南农业大学	基于知识地图的高校实验室安全教育微课体系构建研究	刘小波
439	高等教育教学改革项目	华南农业大学	乡村美育实施背景下农林院校音乐专业人才培养改革研究	朱虹
440	高等教育教学改革项目	华南农业大学	教学核心素与“三农”情怀融合的《大学数学I》课程思政探索与实践	曹静
441	高等教育教学改革项目	华南农业大学	“双一流”背景下农林高校公共基础课的教学改革与实践 ——以大学数学课程群为例	李朗
442	高等教育教学改革项目	华南农业大学	基于“馆校协同+合作学习”的历史实践教学模式改革与探索	龚金红
443	高等教育教学改革项目	华南农业大学	思政教育融合双创教育在专业实验课程中的研究与探索	罗霞
444	高等教育教学改革项目	华南农业大学	基于课程思政建设的高校体育课程研究	周华锋
445	高等教育教学改革项目	华南农业大学	“双一流”建设农业院校本科人才培养目标与定位研究 ——以大数据管理与应用专业为例	熊俊涛
446	高等教育教学改革项目	华南农业大学	后疫情时代全英《植物学》国际化教学探索	龚维
447	高等教育教学改革项目	华南农业大学	基于“知农爱农”的农业高校课程思政模式建设研究	张运红
448	高等教育教学改革项目	华南农业大学	落实“育德”教育与实践，打造《饲料生物技术》思政“金课”	孙加节
449	高等教育教学改革项目	华南农业大学	基于“五维优化，三层互助”的专业课程改革、思政建设与实践 ——以《家具与室内材料学》为例	孙理超
450	高等教育教学改革项目	华南农业大学	新工科背景下风景园林历史与理论课程教学改革研究	夏宇
451	高等教育教学改革项目	华南农业大学	基于“SPDC+PBL”的《形势与政策》混合式教学模式改革与实践	项赠
452	高等教育教学改革项目	华南农业大学	强综合、重实践、补短板——面向专业认证的科产教融合式建筑设计课教学改革	陈乃华
453	高等教育教学改革项目	华南农业大学	新工科课程思政一体化教学改革与实践——以《测量学》课程为例	姚朝龙
454	高等教育教学改革项目	华南农业大学	基于PDCA与CDIO的实践教学模式研究与实践——以《汽车构造实验》为例	周锡恩
455	高等教育教学改革项目	华南农业大学	习近平生态文明思想融入思政课程机制研究	李俊宏
456	高等教育教学改革项目	华南农业大学	《用户体验设计》课程深度学习模式与效应研究	周秀
457	高等教育教学改革项目	南方医科大学	基于中医思维高阶培养的中医基础理论“IAC”教学法研究	安海燕
458	高等教育教学改革项目	南方医科大学	Python生物医学计算基础在线教学平台建设与应用	曹蕾
459	高等教育教学改革项目	南方医科大学	融合课程思政的《药物化学》课程教学综合改革实践	陈金香
460	高等教育教学改革项目	南方医科大学	基于计算机可视化的腹腔镜外科基础混合式教学改革实践	陈韬
461	高等教育教学改革项目	南方医科大学	基于OBE理念的医学生理学课程混合式教学改革实践	何江
462	高等教育教学改革项目	南方医科大学	新文科、大外语背景下英语读写主题教学的探索与实践	蒋文凭
463	高等教育教学改革项目	南方医科大学	大学附属医院课程思政教学改革探索与实践	金玥
464	高等教育教学改革项目	南方医科大学	医科院校专业课“纵横结合、德智交融”混合式教学模式的实践研究 ——以临床诊断学《症状学》为例	林春燕
465	高等教育教学改革项目	南方医科大学	基于标准化情景演练背景下的沉浸式教学在创伤急救课堂中的探索与实践	李旭
466	高等教育教学改革项目	南方医科大学	基于问题为导向的口腔组织病理学慕课课程构建及实践研究	麻丹丹
467	高等教育教学改革项目	南方医科大学	模拟高坠命案现场勘验的教学实验设计	缪启峰
468	高等教育教学改革项目	南方医科大学	基于成就需要激励理论的书院导师队伍建设研究	钱怡
469	高等教育教学改革项目	南方医科大学	基于知识图谱建设的《急危重症护理学》改革探索与实践	史雷
470	高等教育教学改革项目	南方医科大学	新时代医学生体育课程改革探索与实践	宋军
471	高等教育教学改革项目	南方医科大学	基于OBE理念的内科学课程体系改革实践	孙嘉
472	高等教育教学改革项目	南方医科大学	口腔医学专业临床实践线上线下混合式教学模式探索与实践	田智慧
473	高等教育教学改革项目	南方医科大学	《卫生事业管理学》课程思政的教学设计与实践	王冬
474	高等教育教学改革项目	南方医科大学	基于OSCE模式的《妇女健康与物理治疗》课程建设	王康玲
475	高等教育教学改革项目	南方医科大学	虚拟仿真实验结合CBCL教学模式在医学影像教学中研究与应用	文戈
476	高等教育教学改革项目	南方医科大学	融合课程思政的《小儿外科学》线上线下混合式教学改革探索与实践	吴凯
477	高等教育教学改革项目	南方医科大学	基础医学专业拔尖人才“四化优培”创新培养体系构建与实践	吴砂
478	高等教育教学改革项目	南方医科大学	《卫生经济学》课程思政设计与融入路径研究	向国春
479	高等教育教学改革项目	南方医科大学	基于“三黄方”不同剂型的中药学专业综合设计性实验教学改革实践	张璐
480	高等教育教学改革项目	南方医科大学	基于卓越护理人才培养的外科护理学课程改革与实践	张萍
481	高等教育教学改革项目	南方医科大学	高阶能力导向的《分子生物学》课程设计与实践	周洋宇
482	高等教育教学改革项目	南方医科大学	以创新能力培养为目标的《数理统计》项目驱动式教学改革与实践	庄严
483	高等教育教学改革项目	广州中医药大学	5 E教学模式下融入化学史教育的有机化学课程改革与实践	陈传兵
484	高等教育教学改革项目	广州中医药大学	中医骨伤科学影像判读与实践诊疗的教育研究	陈镇秋
485	高等教育教学改革项目	广州中医药大学	学习投入度视角下中医四诊技能混合式教学的设计与评价	陈卓群
486	高等教育教学改革项目	广州中医药大学	新医科背景下课程思政赋能本科订单定向应用型人才培养的探索与实践 ——以《中西医结合康复医学》为例	邓剑峰
487	高等教育教学改革项目	广州中医药大学	“三全育人”视域下《康复评定学》课程思政评价体系研究	郝曼
488	高等教育教学改革项目	广州中医药大学	大类招生下复合型创新药学人才培养为导向的化学基础课程 教学体系一体化构建与实践	何建峰
489	高等教育教学改革项目	广州中医药大学	基于人工智能优化学习者认知负荷的教学实践研究 ——以《Python程序设计》课程为例	洪佳明
490	高等教育教学改革项目	广州中医药大学	“五抓四促三融合”：新医科视域下整合课程的改革和探索 ——以风湿免疫整合课程建设为例	黄雅丽
491	高等教育教学改革项目	广州中医药大学	中国共产党精神谱系融入高校思政课程教学的实践路径研究	林志彬
492	高等教育教学改革项目	广州中医药大学	以OBE理念为基础，对分课堂为载体，开启生理学混合式教学新篇章	刘海梅
493	高等教育教学改革项目	广州中医药大学	基于多元化中医思维范式下夯实中医基础专业教育与人才培养的实践研究	刘凌云
494	高等教育教学改革项目	广州中医药大学	基于TBL真实岗位能力导向的眼视光专业教学改革	刘求红
495	高等教育教学改革项目	广州中医药大学	“思维引导”“多维融合”的课程思政教学实践模式 融入《中西医结合症学》的探索与实践	李志尚
496	高等教育教学改革项目	广州中医药大学	粤港澳大湾区中医药健康养老服务管理产教融合项目化课程体系构建	庆艳华
497	高等教育教学改革项目	广州中医药大学	基于案例的情景模拟在急危重症抢救护理临床教学中的应用	邱定荣
498	高等教育教学改革项目	广州中医药大学	数据驱动学习在高阶《医学英语》教学中的探索与实践	丘晓媛
499	高等教育教学改革项目	广州中医药大学	基于系统评价法的“三维三课”有效教学翻转模式研究	任溪海
500	高等教育教学改革项目	广州中医药大学	新医科建设背景下基于护教协同模式的护理学临床课程案例库建设研究 ——以《内科护理学》为例	吴燕
501	高等教育教学改革项目	广州中医药大学	“三师同堂”教学模式在中医康复规范化培训中的探索	谢韶东
502	高等教育教学改革项目	广州中医药大学	教师模拟标准化病人在中医骨伤科学正骨理伤手法临实践教学中的探索应用研究	杨文斌
503	高等教育教学改革项目	华南师范大学	定向师范生跨学科体育教学能力培养模式构建	陈荣杨
504	高等教育教学改革项目	华南师范大学	师生共享 研学共进 心智共育——《普通心理学》课程改革研究与实践	陈荆茜
505	高等教育教学改革项目	华南师范大学	基于产出导向的近代物理设计性实验教学改革与实践	丁格媛
506	高等教育教学改革项目	华南师范大学	基于大学生综合人文素质训练与提升的文学理论系列课程教学改革研究	段吉方
507	高等教育教学改革项目	华南师范大学	“五位一体”创新创业人才培养体系的构建与实践	侯永雄
508	高等教育教学改革项目	华南师范大学	基于线上线下混合式课程“学术前沿与文献导读”的英语师范生科研能力培养实践	金檀

广东省高等学校教学管理学会

广东省高等学校教学管理学会关于公布 2021 年度课程思政建设项目立项名单的通知

各会员单位：

根据《广东省高等学校教学管理学会关于开展 2021 年度课程思政建设项目申报的通知》，学会组织开展了 2021 年度课程思政建设项目的推荐与遴选工作。经专家评审，学会常务理事会审议，共遴选出《生命科学研究课》等 296 个项目立项为 2021 年度课程思政建设项目。现将名单（见附件）予以公布，并就有关事项通知如下：

一、立项建设项目由项目的牵头高校和共建高校共同开展建设与研究。

二、牵头高校要做好项目的监督与管理工作，保障项目的建设进度与成效。

三、项目负责人要积极整合团队力量，按照要求开展项目建设，确保项目目标任务如期完成。

四、项目建设期为 2 年，结题时需提供以下材料：

1. 一门或多门课程融入课程思政完整的教案（包含每章节的课程思政目标、课程思政元素、课程思政融入策略、课程思政考核要素）；

2. 一门或多门课程的思政案例集（每门课程至少 10 个）。

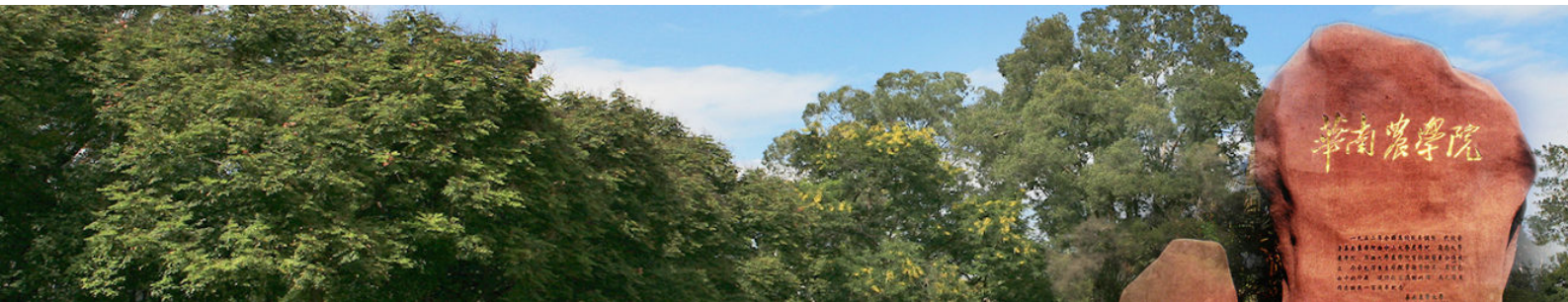
五、学会将按学科门类选出有示范、推广借鉴价值的优秀案例编制成册，并资助出版。

附件 1

广东省高等学校教学管理学会 2021 年度课程思政建设项目

立项名单（本科）

序号	项目编号	牵头单位	支持类别	课程名称	课程负责人	建设经费/元
1	X-KCSZ2021001	中山大学	重点	生命科学研究课	张雁	10000
2	X-KCSZ2021002	华南理工大学	重点	电工与电子技术	邓红雷	10000
3	X-KCSZ2021003	暨南大学	重点	生理学	王跃春	10000
4	X-KCSZ2021004	华南农业大学	重点	消费者行为学	贾莉	10000
5	X-KCSZ2021005	华南农业大学	重点	概率论	肖莉	10000
6	X-KCSZ2021006	华南农业大学	重点	饲料生物技术	孙加节	10000
7	X-KCSZ2021007	南方医科大学	重点	护士人文修养	翟惠敏	10000
8	X-KCSZ2021008	南方医科大学	重点	医学寄生虫学	彭鸿娟	10000
9	X-KCSZ2021009	华南师范大学	重点	微观经济学	瞿华	10000
10	X-KCSZ2021010	华南师范大学	重点	学习理论与学习心理研究	莫雷	10000
11	X-KCSZ2021011	广东外语外贸大学	重点	中级财务会计	王艳	10000
12	X-KCSZ2021012	广东外语外贸大学	重点	国际经济与贸易专业课程群	张建武	10000
13	X-KCSZ2021013	广州大学	重点	电路/电路实验	邹涛	10000
14	X-KCSZ2021014	广州大学	重点	环境监测实验	宋刚	10000
15	X-KCSZ2021015	广州大学	重点	结构力学	汪大洋	10000
16	X-KCSZ2021016	广州大学	重点	环境学概论	吴卓	10000
17	X-KCSZ2021017	广州大学	重点	民族乐舞欣赏与美学分析	何艳珊	10000
18	X-KCSZ2021018	广东石油化工学院	重点	审计学	张芹秀	10000
19	X-KCSZ2021019	广东石油化工学院	重点	高级财务会计	姚翠红	10000
20	X-KCSZ2021020	惠州学院	重点	新媒体概论	周海英	10000
21	X-KCSZ2021021	嘉应学院	重点	高级英语	张宏武	10000
22	X-KCSZ2021022	广东科技学院	重点	网络营销	王金良	10000
23	X-KCSZ2021023	广东东软学院	重点	综合商务英语 I-II	陈若静	10000
24	X-KCSZ2021024	北京理工大学珠海学院	重点	工业机器人	曹少泳	10000
25	X-KCSZ2021025	华南理工大学	一般	调查统计与分析	付佳	2000
26	X-KCSZ2021026	华南农业大学	一般	数字图像处理	薛月菊	2000

[学校概况](#)
[对外交流](#)[机构设置](#)
[思政在线](#)[师资队伍](#)
[服务社会](#)[人才培养](#)
[招生就业](#)[科学研究](#)
[信息公开](#)[校园文化](#)
[来访预约](#)

关于公示2022年省级教学质量与教学改革工程拟推荐项目和校级教学质量工程与教学改革工程拟立项项目的通知

审核发布：本科生院（招生办公室） 来源单位及审核人： 发布时间：2022-11-01 浏览次数：2313

各学院（部）、各相关单位：

根据学校《关于开展2022年度教学质量与教学改革工程建设项目申报推荐工作的通知》要求，学校组织开展了本年度教学质量工程与教学改革工程项目遴选工作。经项目负责人申请、所在单位遴选推荐和学校组织专家评审等环节，本年度拟计划立项校级质量工程项目44项，并在本年度校级立项的基础上，拟推荐“华南农业大学农学院广东省良种引进服务公司实践教学基地”等18个项目为省级质量工程项目，具体名单见附件1；拟计划立项校级教学改革项目136项，其中在本年度校级立项的基础上，拟推荐“新工科课程思政一体化教学改革与实践——以《测量学》课程为例”等31项为省级教学改革项目（其中2个项目不占用学校推荐指标），具体名单见附件2。现予以公示。

公示期自2022年11月1日至2022年11月5日。公示期间，如有异议请以书面方式提交（附必要的证据材料），并署真实姓名，否则不予受理。

联系人：王欢

地址：行政楼329

联系电话：85280052

邮箱：gjyj@scau.edu.cn

附件1：2022年省级质量工程拟推荐项目和校级质量工程拟立项项目名单.pdf

附件2：2022年省级教学改革拟推荐项目和校级教学改革拟立项项目名单.pdf

华南农业大学本科生院

2022年11月1日

[校长信箱](#)[国家科研平台](#)[招标采购](#)[阳光体育](#)[质量工程](#)[校园地图](#)[开放教育资源](#)[精品课程资源](#)

SCAU Copyright © 2018

华南农业大学 All rights reserved

地址：广州市天河区五山华南农业大学

备案编号：粤ICP备05008874号 4401060500010

[管理登录](#)

附件2：2022年省级教学改革拟推荐项目和校级教学改革拟立项项目名单

序号	类别	项目名称	所属单位	项目负责人	备注
1	重点项目	新工科课程思政一体化教学改革与实践——以《测量学》课程为例	资源环境学院	姚朝龙	拟校级立项，同时拟推荐省级
2	重点项目	“双一流”背景下农林高校公共基础课的教学改革与实践——以大学数学课程群为例	数学与信息学院、软件学院	李朗	拟校级立项，同时拟推荐省级
3	重点项目	基于知识地图的高校实验室安全教育微课体系构建研究	基础实验与实践训练中心	刘小波	拟校级立项，同时拟推荐省级
4	重点项目	新工科背景下风景园林历史与理论课程教学改革研究	林学与风景园林学院	夏宇	拟校级立项，同时拟推荐省级
5	重点项目	融合“树医生”理念的《园林植物栽植与养护》课程思政与实践教学改革研究	林学与风景园林学院	刘天颐	拟校级立项，同时拟推荐省级
6	重点项目	落实“育德”教育与实践，打造《饲料生物技术》思政“金课”	动物科学学院	孙加节	拟校级立项，同时拟推荐省级
7	重点项目	“大思政课”视野下《中国近现代史纲要》教学改革与实践	马克思主义学院	崔芸	拟校级立项，同时拟推荐省级
8	重点项目	基于“SPOC+PBL”的《形势与政策》混合式教学模式改革与实践	党委宣传部（党委统战部）	项赠	拟校级立项，同时拟推荐省级
9	重点项目	习近平生态文明思想融入思政课教学机制研究	马克思主义学院	李俊宏	拟校级立项，同时拟推荐省级
10	重点项目	思政教育融合双创教育在专业实验课程中的研究与探索	电子工程学院（人工智能学院）	罗霞	拟校级立项，同时拟推荐省级
11	重点项目	基于“知农爱农”的农业高校课程思政模式建设研究	公共管理学院	张运红	拟校级立项，同时拟推荐省级
12	重点项目	“双一流”建设农业院校本科人才的培养目标与定位研究——以大数据管理与应用专业为例	数学与信息学院、软件学院	熊俊涛	拟校级立项，同时拟推荐省级
13	重点项目	基于科教、产教双融合理念的《小动物临床病理学实验》教学改革与实践	兽医学院	李英	拟校级立项，同时拟推荐省级
14	重点项目	强综合、重实践、补短板——面向专业认证的科产教融合式建筑设计课教学改革	水利与土木工程学院	陈乃华	拟校级立项，同时拟推荐省级
15	重点项目	基于课程思政建设的高校体育课程研究	体育教学研究部	周华锋	拟校级立项，同时拟推荐省级
16	重点项目	中外合作办学“学术英语”模块课程融合课程思政的探索	国际教育学院（广州都柏林国际生命科学与技术学	冯立新	拟校级立项，同时拟推荐省级



关于公示2019年度华南农业大学教改立项项目及拟推荐申报省级教改项目的通知

来源：[文章出处] 2019-09-16 点击量：1509

学院、部处、各单位：

根据《广东省教育厅关于开展2019年度省高等教育教学改革项目推荐工作的通知》和华南农业大学《关于申报2019年度校级教育教学改革与研究项目的通知》，经组织申报、资格审查、专家评审等环节，拟确定“基于能力培养的多层级探究式教学改革研究及实践--以《土木工程材料》为例”等46个项目入选校级教改重点项目；“基于SPOC的混合式《形势与政策》教学模式构建研究”等69个项目入选校级教改一般项目；“以打造‘金课’为导向促进教师教学能力提升的探索和实践”等41个项目入选校级教改自筹项目。

结合省厅文件要求及组织专家评审，拟推荐“基于能力培养的多层级探究式教学改革研究及实践--以《土木工程材料》为例”等28个项目申报省级教改项目。现予以公示（见附件）。公示时间为2019年9月16日至9月20日，如有异议请于9月20日前以书面形式提交至教务处教学研究与评估中心，并署真实姓名附联系方式，匿名及其他形式的异议恕不受理。

联系人：曹广祥、伍鹏
地址：行政楼329
联系电话：85280052
邮箱：jgxm@scau.edu.cn

华南农业大学教务处
2019年9月16日

附件：

序号	学院名称	申报人	资助方式	项目类别	备注
1	基于能力培养的多层级探究式教学改革研究及实践--以《土木工程材料》为例	李庚英	重点资助		拟推荐申报省级
2	新工科背景下多维度提升工科高数课程教学质量的研究与实践	李娇娇	重点资助		拟推荐申报省级
3	以科研成果促进遗传学实验教学创新改革的研究与实践	刘自强	重点资助		拟推荐申报省级
4	基于蚕病学课程的全英教学和管理模式研究	孙京臣	重点资助		拟推荐申报省级
5	基于一流人才培养的“金课”标准与评价研究	欧阳娟	重点资助	金课改革类	拟推荐申报省级
6	知识传授、文化传承、价值引领三位一体的	徐初东	重点资助	课程思政类	拟推荐申报省级

请输入关键字

综合科

教务科

学籍科

考务科

教学质量监控科

实践学科

教学研究与评估中心

教师教学发展中心

语言文字工作委员会办公室

	教学模式创新与研究				
89	动物医学专业核心课程双语教学新模式的探索—以国家级双语示范课程《兽医寄生虫学》为例	李娜	一般资助		
90	基于雨课堂的《城市林业》课程智慧课堂建设与实践	邱权	一般资助	青年专项类	
91	思维导图在《微观经济学》教学中的应用研究	申津羽	一般资助	青年专项类	
92	基于OBE理论的全英教学模式创新研究—以农林产品国际贸易课程为例	张奕婧	一般资助	青年专项类	
93	基于库伯经验学习圈的宏观经济学翻转课堂模式设计与应用	段伟	一般资助	青年专项类/金课改革类	
94	乡村振兴背景下风景园林设计课程体系与教学改革研究	陈崇贤	一般资助	青年专项类	
95	国际认证背景下新工科专业的品牌化建设与实践——以家具专业为例	易欣	一般资助	青年专项类	
96	“线上”+“线下”混合式教学模式研究与实践—以《R语言及应用》课程为例	周磊	一般资助	青年专项类/金课改革类	
97	新工科视域下以农业机械设计为导向的人机工程学教学研究	付函	一般资助	青年专项类	
98	基于案例的情景模拟教学在公共事业管理类课程中的应用	张小娟	一般资助	青年专项类	
99	新农科背景下植物生理学实验教学模式的探索与实践	李淮源	一般资助	青年专项类	
100	文学影视作品融入《城市广场景观设计》课程的教学研究与实践	戚芳妮	一般资助	青年专项类	
101	“互联网+”背景下创新创业教育与农业生态学专业教学、实训教育的融合研究	向慧敏	一般资助	青年专项类	
102	珍贵植物真菌病害标本的整合与开放	孔广辉	一般资助	青年专项类	
103	《信息系统安全与保密》课程的翻转课堂教学模式研究与实践	宋歌	一般资助	青年专项类/金课改革类	
104	“线上-线下-实践”三位一体的《生态工程》课程建设研究	田纪辉	一般资助	青年专项类	
105	基于视频微课的《遗传学》教学改革与实践	金晶	一般资助	青年专项类	
106	新型开放性实验在植物学实验课程教学中的探索与实践	何韩军	一般资助	青年专项类	
107	工程教育认证下食品科学与工程专业多维实践教学体系及模式的探索与实践	黎攀	一般资助	青年专项类	
108	案例教学在环境化学课程中的应用	郑晓波	一般资助	青年专项类	
109	“新国标”背景下基于CBI教学理念的高级日语教学模式改革研究	张秀娟	一般资助	青年专项类	
110	协同教学在服装专业课程中的研究与应用——以服装结构设计课程为例	马宏林	一般资助	青年专项类	
111	基于人工智能背景下的教学教务管理信息化探索与研究	王宣琳	一般资助	青年专项类	
112	《人工智能》	陈琰	一般资助	继续教育类	
113	《城市绿地规划》	邱巧玲	一般资助	继续教育类	
114	以打造“金课”为导向促进教师教学能力提升的探索和实践	钟建英	自筹经费	金课改革类	
115	在生物化学课程中构建低年级大学生研究性学习引导机制研究	孙加节	自筹经费		
116	面向人工智能背景的会计学专业核心课程教学改革	董丽	自筹经费		

饲料生物技术课程改革与效果评价

孙加节, 罗君谊, 陈婷, 习欠云, 张永亮* (华南农业大学动物科学学院, 广东广州 510642)

摘要 饲料生物技术是现代生物技术与动物饲料科学交叉融合形成的一门理论与生产实践紧密联系的基础专业课程。为响应教育部打造“金课”的号召,从教学资源、教学内容、教学方法和手段及评价体系等方面对该课程进行教学改革与教学模式创新,旨在提高课程教学质量,为同类课程的建设提供参考。

关键词 饲料生物技术; 课程改革; 翻转课堂; 金课

中图分类号 S-01 文献标识码 A

文章编号 0517-6611(2021)14-0276-04

doi: 10.3969/j.issn.0517-6611.2021.14.074



开放科学(资源服务)标识码(OSID):

Curriculum Reform and Effect Evaluation of Feed Biotechnology Course

SUN Jia-jie, LUO Jun-yi, CHEN Ting et al (College of Animal Science, South China Agricultural University, Guangzhou, Guangdong 510642)

Abstract Feed biotechnology is a basic professional course formed by the integration of modern biotechnology and animal feed science. In response to the call of the Ministry of Education to create “golden course”, the curriculum actively carried out the reform and teaching mode innovation from the teaching resources, teaching content, teaching methods and means and evaluation system, so as to improve the teaching quality of the course and provide references for the construction of similar courses.

Key words Feed biotechnology; Curriculum reform; Flipped classroom; Golden class

随着生物技术和饲料产业的不断发展,生物技术在饲料工业上的应用研究日益深入^[1],饲料生物技术作为现代生物技术与动物饲料科学交叉融合形成的一门崭新学科分支应运而生。一般而言,饲料生物技术是以饲料原料和饲料添加剂为研究对象,运用生物技术或生物工程等先进技术研究 and 开发新型饲料资源和功能性饲料添加剂^[2]。饲料生物技术课程是华南农业大学动物生物技术专业必修课,为配合学分制改革,强化动物科学专业培养方案,2012年被列入动物科学专业选修课。该课程涵盖基因工程、微生物工程及酶工程等学科理论与技术在饲料工业中的研究成果和应用实践,包括饲料技术的基本理论、新工艺、新方法、新成果以及国内外相关研究的最新进展与发展趋势。该课程涉及面广,理论结合应用性强,内容更新快,若在教学过程中继续采用传统“填鸭式”教学方式,使课程内容与产业脱节、专业教育与创新创业脱节,将影响教学质量和学生的学习积极性与主动性。近年来,为贯彻落实教育部《关于一流本科课程建设的实施意见》,推动教师全员参与课程理念创新、内容创新和模式创新,形成打造“金课”、淘汰“水课”的教学改革氛围^[3-4]。饲料生物技术课程必须改变传统教学方法与教学模式,在教学内容上增加案例,在教学手段上采用“翻转课堂”与小组讨论等环节,培养学生发现问题、解决问题能力、创新意识和实践能力。

1 课程教学改革途径

1.1 更新教学内容、规划课程体系,融入思政元素,实现课程教学模块化 根据饲料行业现状,对接市场发展需求,及时调整课程教学内容、形成案例,更新补充新知识^[5]。目前,课

程教学内容主要分为6个模块,包括绪论、酶制剂及其在饲料中的应用、粗饲料资源开发、发酵技术与产品(单细胞蛋白)在饲料中的应用、植物提取物在动物养殖中的应用、抗生素替代与饲料资源开发进展,其中绪论2个学时,其他每个模块包括教学导学2学时、小组讨论2学时、课堂讨论与答疑2学时三部分,每个模块共计6个学时,加上课程绪论2个学时,课程共计32学时。在深化课程体系改革中,该课程从理论教学、实践活动和创新训练3个方面,在“基础、前沿、综合设计、研究创新”4个层面上规划教学体系,实现课程模块化和多元化。同时,在每个教学模块,根据教学内容,融入切题的思政元素,课程模块及思政点见表1。

1.2 网络教学平台建设 搭建课程网站和构建课程网络框架,丰富与课程相关的课件库、习题库、试题库、资料库等课程资源,紧跟饲料行业发展步伐,每年更新网络教学平台内容,确保网站资源每年更新30%以上,完善课程专门网站与教学资源库。各类教学文件、教学资料、教学动态、教学课件以及教学录像等在网上开放,创建课程教学互动交流平台等,实现了优质教学资源的校内与校间共享,使精品课程充分发挥了辐射功能与带动作用。

1.3 突出课堂讨论、学生互动参与,实现启发式的翻转教学模式 运用“翻转课堂”混合教学方式,教师讲授基础理论知识、课后布置讨论性或拓展学习课题,学生课后查阅文献、课堂讨论并自己讲解,教师点评并进行重点难点解析,以互动式、设问式、讨论式、翻转式的教学方法,引导学生的好奇心和参与意识,培养学生的创新思维和主动解决问题的能力,真正做到“以学生为中心、以教师为主导”的教学新模式^[6]。

1.4 强化现场教学、跟踪教学和连续教学方式,实现“教学练合一”的教学活动 在课程教学过程中或教学活动结束后,采取学生自由选题申请、教师联系安排对接企业的方式,把学生派驻下去进行实践教学,教师现场对各生产环节和工

基金项目 华南农业大学教育教学改革与研究项目(JG19131)。
作者简介 孙加节(1984—),男,江苏盐城人,副教授,博士,从事动物生化与营养研究。* 通信作者,教授,博士,从事动物生化与营养研究。
收稿日期 2020-10-28

艺流程进行系统讲解,通过这种“教-学-练”相融合的连续教学活动,让学生了解实际生产中的技术开发、技术流程、企业运作、管理模式以及工作环境,做到理论教学与实践教学同步,做到课程教学与专业实习或毕业设计同步。

表 1 饲料生物技术课程模块化设置及主要思政点
Table 1 Modularization setting of feed biotechnology course and its main ideological and political points

模块 Module	课程内容 Course contents	课程思政点 Ideological and political points of the course	学时 Class hour
模块一 Module 1	绪论	以我国畜牧业发展的历史、现状和问题为切入点,通过我国畜牧业改革开放以来取得的巨大成绩,强化学生“四个自信”;通过分析现状和问题,培养学生的责任感和专业情怀	2
模块二 Module 2	酶制剂及其在饲料中的应用	以植酸酶为例,宣扬姚斌院士在植酸酶国产化 and 产业化研发过程中的刻苦钻研精神,激励同学们勇于创新探索	6
模块三 Module 3	粗饲料资源开发	阐述我国粗饲料产业现状,以我国高蛋白苜蓿干草进口依赖和中美贸易战为切入点,强化学生的爱国主义精神和奋斗精神,增强对本专业的认同感和责任感	6
模块四 Module 4	发酵技术与产品(单细胞蛋白)在饲料中的应用	以现代生物技术的优势为切入点,体现以现代生物技术改造传统畜牧业的新农科建设,培养学生用新进展、新技术、新知识来提升我国畜牧业生产水平的意识	6
模块五 Module 5	植物提取物在动物养殖中的应用	以我国优秀传统文化中医中药为切入点,以屠呦呦获得诺贝尔奖为例,展示我国优秀的传统文化,增强文化自信	6
模块六 Module 6	抗生素替代与饲料资源开发进展	以抗生素使用的历史及存在问题为例,以生态与安全为切入点,培养学生食品安全、绿水青山就是金山银山的现代生态观	6

1.5 智慧教学工具与课程教学深度融合 采用雨课堂作为教学辅助管理工具^[7],课前发布预习讲义、课程 PPT 和课前思考题等,设置预习时间节点,掌握学生知识储备和预习效果;课堂通过 PPT 共享、弹屏与签到功能,实现线下实体课堂的师生互动;课后通过 PPT 回放、在线互动,强化学生的学习效果^[8]。

1.6 采用教学过程考核,实行多样化的课程考核体系 将培养学生素质贯穿整个考核评价过程,制定适合课程要求的考核评价体系,采用过程考察与课程期终理论考试相结合的方式^[9]。考核评价体系由 4 个部分组成:平时考勤 10%、文献综述与总结 20%、专题讨论(PPT) 20%、理论考试 50%。让学生积极归纳总结,以 PPT 和多媒体讲解的形式进行课堂讨论,拓宽对问题的了解和看法。学生针对课堂讨论,进行相互评价,在评价中反思自己,同时在互动中也能让教师及时了解教学动态,提高教学质量。

2 课程教学过程及效果评价

该课程以“教师理论讲授-学生分组讨论-小组课堂讲解-课外实践”为主线,使理论与实践相结合、行业和课堂相结合、传承与创新相结合,教室、实验室和基地三地联合。以 2016 级温氏班小班教学为例,构建翻转课堂,将课程模块化,并由教师导学、小组讨论、课堂讨论 3 个环节组成,实现了对分课堂。一般而言,各模块教学过程主要分为四大板块,以发酵技术与产品在饲料中的应用为例:①教师导学。主要讲授单细胞蛋白饲料的概念、原料来源、发酵微生物种类、生产工艺及其在动物饲料中的应用等方面的研究进展以及单细胞蛋白研究中存在的安全性问题及今后的研究方向。②学生小组讨论。导学后通过雨课堂布置讨论性和拓展性课题,学生与教师或同学之间可通过网络交流平台,如微信、QQ 等专业推送平台,将各自精心准备的学习资料或者课程相关微视频等学习资源通过约定的网络平台发布,同学可以根据自己的知识基础、学习能力、性格特点等自由组成 3~5 人的学

习协作小组,对发布的教学内容合理安排时间提前准备。各小组成员在学习过程中及时向教师和组员反馈学习效果以及遇到的问题,学生带着问题入课堂进行进一步小组讨论,教师在课堂上依据反馈问题有目的、有针对性地进行重点讲解,并补充遗漏点,最终进行选题和成果展示准备。③课堂讨论。各小组通过教师的引导和个体间的协作,从选题背景、国内外研究进展与现状、试验设计、预期效果等方面进行小组讨论成果展示、交流和评价打分,每组 15 min,10 min PPT 讲解,5 min 答疑。在课堂讨论教学活动中,教师应以答疑、解惑、引导、鼓励为主,使学生体会到合作学习的乐趣,激发学生的学习热情,挖掘学生学习的原动力,进而深化学习效果,实现课程理论知识的内化。④课外实践。结合教师研究团队科研项目,学生通过室内实验,测定和分析酱油渣、酒糟、凉茶渣等的基本营养成分,探究和认识生物饲料的发酵原理以及重点和难点,重点对比不同发酵菌种、不同发酵时间、不同发酵佐剂添加等对发酵效果的影响,进一步预估生产成本以及饲喂效果等。

此次整个温氏教学班共计 26 人选修,分为 6 个讨论小组,针对模块四,各小组分别以“在饲料中应用的酵母菌种类和营养特点”“酱香型茅台酒糟饲料化应用初步方案设计”“贵州茅台酒糟肉牛饲料化应用方案”“酱油渣开发育肥猪饲料设计方案”“酱油渣开发方案”“酵母菌在饲料中应用进展”为题进行小组讨论和课堂展示。总体来看,采用教师导学、小组讨论和课堂讨论相结合的翻转课堂教学模式,让学生更好地掌握理论知识,专业技能进步显著;获得了较好的口碑,学生参与感强,学生的学习兴趣高涨,综合评价良好,真正让学生“活起来”。调查显示,对饲料生物技术采用翻转课堂教学模式表示满意的学生有 23 人,占全部学生数的 88.46%,其中特别满意的学生占 26.92%(图 1);认为组织与口头表达能力提升的学生占 96.15%,认为获取知识的能力提升的学生占 76.92%(图 2)。

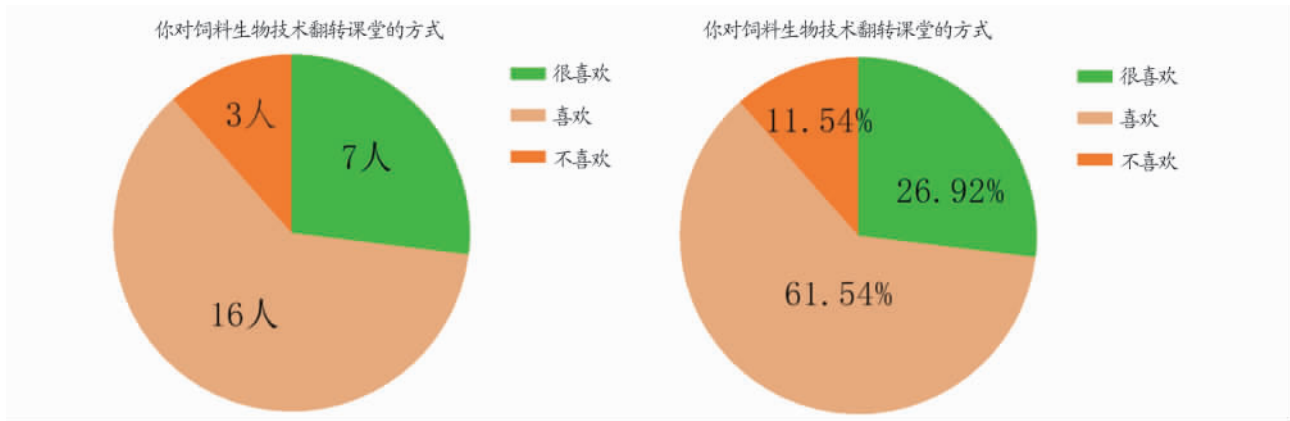


图1 学生对饲料生物技术翻转课堂的满意度调查

Fig.1 Satisfaction degree survey on flipped classroom of feed biotechnology course

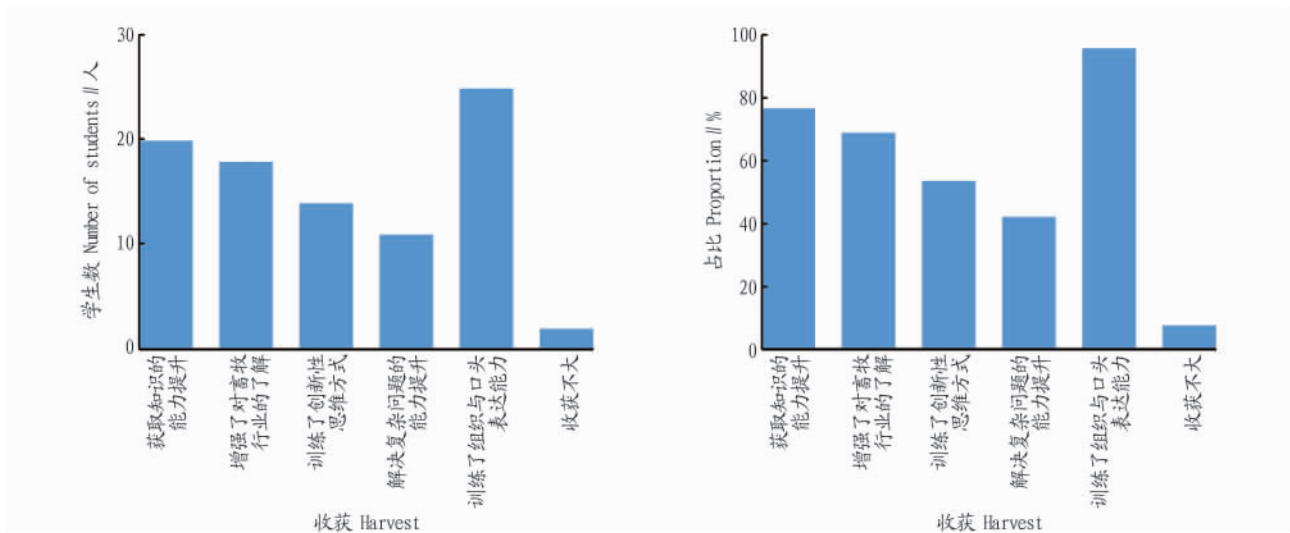


图2 学生学习饲料生物技术课程后的收获调查

Fig.2 Investigation on the students' harvest after studying feed biotechnology course

同时,课程与科研及生产实践相结合,把最新的科研成果融入课堂教学中,不仅丰富了课堂教学内容,而且使学生了解和掌握最新饲料生物技术,拓展学生的知识面,并提高学生解决科学难题的能力和创新思维能力。比如,在模块四教学过程中,让学生参与教师科研项目“酱油渣发酵饲料的工艺设计”“凉茶渣生物饲料应用方案研究”等,让学生了解实际生产中的技术开发、技术流程以及工作环境等,做到理论教学与科研及实践教学同步。同时,融入思政元素,以现代生物技术的优势为切入点,体现以现代生物技术改造传统畜牧业的新农科建设,培养学生用新进展、新技术和新知识来提升我国畜牧业生产水平的意识,实践过程中培养同学们不怕苦、不怕累、不怕脏的动科精神和专业情怀,端正学生的价值导向,激发学生的奋斗精神和专研精神。

由于教学内容不断更新,学习难度不断升级,考核标准不断提高,对学生提出了更高的要求。长期教学实践表明,学生的潜力是无限的。如果采用科学的教学方法,并从严格要求学生,通过系统的学习后学生的资料检索能力、动手能力、总结归纳能力、创新能力、材料撰写能力等各项素质均有所提升,基本符合新时代大学生的培养需求。调研结果显示,饲料生物

技术课程改革后,认为学习任务加重1倍以上的学生占69.2%,加重1倍以下的学生占26.9%(图3),真正让学生“忙起来”。2016级华南农业大学动物科学专业考研率达53.1%,位居全校第一,其中温氏教学班考研率为86%,效果显著。

3 小结

在新动科建设的大背景下,如何建设一门畜牧业特色金课是一个重要话题。对照金课标准,课程体现了以“两性一度”理念加强课程顶层设计,在高阶性、创新性和挑战度方面进行专门设计。高阶性方面,教师深入剖析饲料行业热点问题,广泛拓展理论知识,采用多元化考核方式对学生进行测评,尤其重视过程考核。创新性方面,建立开放式教学内容和课程体系。以产业发展为导向,课程内容与科研融合、与产业融合、与思政相融合。挑战度方面,教师备课充分,在知识传授、能力培养、情感认知3个方面精心设计,在各个教学环节,严格要求,不断提升难度,以期学生能系统掌握理论知识,熟悉行业背景,参与社会实践,提升专业能力,培养创新精神,提高综合素质。

经过长期的实践探索和不断完善,突破教学时数和教学空间的束缚,注重理论与实践的结合,取得了较好的教学效

果。但是,该课程教学还存在一些不足之处:①尚未建立线上、线下联合的混合式教学模式,今后将重点建设线上教学方式;②考核测评方法复杂,难度升级,学生短期可能不适应;③教学团队对信息化时代新技术的运用存在不足,目前

仅限于雨课堂和教育在线等少数平台,缺乏微课、慕课等新兴技术手段的应用实践。课程团队将继续投入建设,吸取学习者的建议,为课程学习者提供高质量的服务,也为其他同类课程的教学改革提供借鉴^[10]。

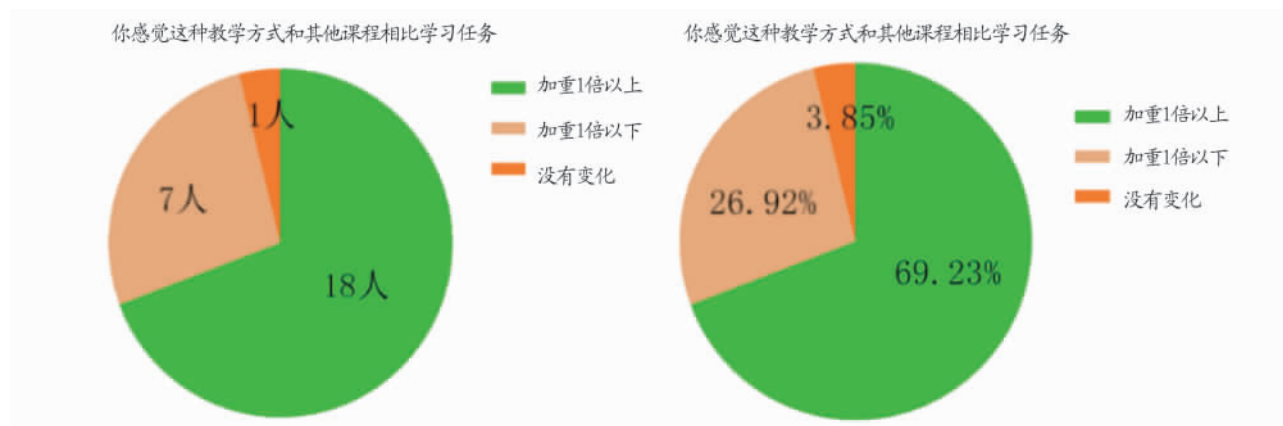


图3 饲料生物技术课程学习任务加重情况调查

Fig.3 Investigation on aggravating the learning tasks of feed biotechnology course

参考文献

- [1] 冷静,杨舒黎,鲁琼芬,等.饲料生物工程课程教学手段改革与创新模式[J].教育教学论坛,2018(48):98-100.
- [2] 张日俊.现代饲料生物技术与应用[M].北京:化学工业出版社,2009.
- [3] 任杰,司政.新工科背景下《水工建筑物》“金课”建设探究[J].中国电力教育,2020(4):70-71.
- [4] 谢一峰.羌族传统体育项目融入公体课的教学改革[J].当代体育科技,2020,10(22):75-77.
- [5] 杨光富,张宏菊.案例教学:从哈佛走向世界——案例教学发展历史研究[J].外国中小学教育,2008(6):1-5.

- [6] 齐惠云.运用启发式教学提升自主学习能力[J].中国校外教育,2008(S1):398,404.
- [7] 王秀珍,王粉梅,裴斌.基于雨课堂的智慧教学模式构建[J].计算机教育,2018(4):139-142.
- [8] 黄业伟,向泽敏.“雨课堂”教学模式在食品化学课程教学改革中的应用[J].安徽农业科学,2019,47(7):261-262,265.
- [9] 杨瀚涛.关于高校课程考核改革方式的研究和探索[J].科技视界,2015(24):89,78.
- [10] 张亚妮,左其生,吴信生,等.《动物遗传学》在线开放课程教学设计与评价体系[J].家畜生态学报,2019,40(12):94-96.

(上接第275页)

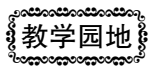
立完善的实践教学基地,引进具有工作经验的教师,增加对青年教师的实践教学培训等。加强实习考核内容等。例如园林植物实习I,在实习前期教师进行植物形态特征园林应用等方面的内容讲解,让学生学会认知植物并会应用植物,实习后半阶段采用半讲解半考核的方式,强化学生的认知水平;此外,实习结束会布置相应的作业,并进行考试(考试包括图片认知+实习相关内容+作业部分)。

4.4 优化师资队伍结构 对师资队伍进行重点建设,采取团队化教学模式,推荐有丰富教学经验的老教师与青年教师间的传、帮、带,实行“导师一助教”模式,促进教学研讨和交流,尽早让青年教师过教学质量关。鼓励并创造机会让青年教师积极参加培训,提高教师的实践教学水平,设立人才培育专项基金,帮助部分读博教师尽早完成学位,资助青年教师在国内外积极进修,弥补青年教师实践经验不足的问题。鼓励青年教师参加社会实践,积极参与到企业和社会服务中,提升基层工作及实践能力。邀请行业优秀企业家等进校做讲座,将行业新发展、新动态介绍给教师和学生。帮助中、老教师熟练应用线上资源,用与时俱进的方式参与到教学中。进行成长性评价,形成参与式教师评价,增强职能部门与授

课教师的良性互动,促进教师之间的相互学习改进。师资队伍结构的合理性和能力的提高,有助于 KAQP 人才培养质量的提高。

参考文献

- [1] 陈黎,潘健,马涛,等.地方应用型本科卓越农林人才培养模式探索与实践:以黄山学院园林专业为例[J].凯里学院学报,2020,38(3):104-107.
- [2] 杨贤均,危兆安.地方性本科院校风景园林专业应用型人才培养模式研究[J].中国园艺文摘,2015,31(4):191-195.
- [3] 姜新强,刘庆超,王奎玲,等.园林专业花卉采后生理与技术课程教学改革的探讨[J].安徽农业科学,2017,45(8):253-255.
- [4] 吴飞,王代钢.园林本科专业人才培养模式现状分析[J].安徽农业科学,2007,35(22):7020-7022.
- [5] 王桂清,吕福堂,张秀省.“3341”园林专业复合应用型卓越人才培养模式探索与实践[J].高等农业教育,2018(5):58-62.
- [6] 罗涛,刘相菊,杨帆,等.“合格+”卓越园林专业实用技能型人才培养模式改革研究[J].西南师范大学学报(自然科学版),2018,43(9):185-192.
- [7] 田忠平,李成忠,栾玲.“一带一路”背景下高职园林专业基于地产行业需求的人才培养模式探究[J].职业技术,2019,18(5):5-8.
- [8] 荣立革,高玉福,刘继生,等.边疆民族地区园林专业人才培养模式分析[J].江苏农业科学,2019,47(21):344-346.
- [9] 邹男男,曹锦丹.医学信息学专业研究生 KAQ 培养实践探讨[J].中国高等医学教育,2013(11):116-117.
- [10] 李瑞冬.论基于 KAQP 人才培养模式的风景园林本科教育专业教学目标体系的建构[J].中国园林,2009,25(11):55-58.



动物生物化学线上线下混合式“金课”建设探索

孙加节, 罗君谊, 陈 婷, 习欠云, 张永亮*

(华南农业大学动物科学学院, 广东 广州 510642)

摘 要:动物生物化学是畜牧兽医专业领域的一门重要专业基础课。随着现代信息技术的飞速发展,当前线上线下混合式教学模式在各个高校课程建设中得到了广泛的探索和实践。笔者在华南农业大学动物科学学院进行了动物生物化学课程的教学改革,将线上线下混合式教学模式应用于该课程中,旨在提高课程教学质量,响应教育部打造“金课”的号召。

关键词:动物生物化学;课程改革;混合式教学;金课

中图分类号: S823

文献标识码: A

文章编号: 1001-9111(2021)06-0081-03

动物生物化学是高等农业院校动物科学与动物医学等学科的专业基础课,是畜牧兽医专业动物育种学、动物营养学、动物病理学、动物药理学等主干课程的“语言”、“工具”和桥梁。课程主要涉及生物大分子如蛋白质、糖、脂类及核酸的组成、结构与功能,物质代谢与联系,基因表达及其调控,动物机体组成与器官功能等,课程既强调普通生物化学的原理与技术手段,又密切联系动物生产和动物医学实际,使学生获得的知识体系既有广泛的适应性,又与畜牧兽医专业后续课程保持着内在联系^[1]。课程理论性强、知识抽象,知识点多而杂,学习难度大。传统教学又以教师课堂讲授为主,填鸭式教学模式使学生的积极性和主动性没有得到充分发挥,自主学习与独立思考能力没有得到锻炼,课前预习流于形式,师生之间、学生之间互动交流少,教师对学生在学习过程中出现的问题无法真正了解,教学效果不理想。近年来,为贯彻落实教育部关于一流本科课程建设的实施意见,推动课程理念创新、内容创新和模式创新,形成打造“金课”、淘汰“水课”的教学改革氛围。华南农业大学畜牧专业《动物生物化学》在课程体系、课程内容、教学方法、教学手段等方面进行了积极探索和完善,尤其在新冠肺炎疫情全球蔓延,探索后疫情时代动物生物化学课程教学模式改革势在必行。

随着科技发展,“互联网+”和“智慧+”已经广泛用于现代教育探索,尤其是疫情期间线上网络教

学模式应运而生^[2]。线上教学是指以互联网为技术背景,以各种学习平台为技术支持,在师生之间展开的教学活动,能够打破地域限制,丰富学生学习和教师教学方式,但也存在师生互动少,学习氛围不足等缺点^[3]。因此如何利用现阶段新兴的线上教学模式与资源,探索与线下传统授课方式相结合,提高教学质量改善教学效果,我们进行了大胆尝试和积极探索。

1 教学改革的准备工作

1.1 转变思想,重塑教学理念

2018年6月,新时代全国高等学校本科教育工作会议上第一次提出“金课”概念^[4]，“打造金课”、“淘汰水课”已成为当前推进高等教育改革,改善本科教育质量的新途径,是广大高等教育工作者努力追求的新目标。对照金课标准,课程要符合“两性一度”的要求,即高阶性、创新性、挑战度^[5],教师要在思想认识上准确把握课程本质,转变教学理念。总体上来说,传统课堂教育教学形式单一,以教师为主体,以理论知识的讲解为主,采取满堂灌的教学方式,照本宣科严重。课程教学中没有学生能力的训练,也没有学生素质的养成,学生“填鸭式”学习,对老师讲课内容不感兴趣,看其他书籍、私下玩手机的比比皆是,甚至有部分学生课堂打游戏、睡大觉,“醉生梦死”混日子。师生关系是“授受关系”,教师掌管学生学习的主动权,教师在教学过程中是权威

收稿日期:2021-08-07 修回日期:2021-08-15

基金项目:华南农业大学教育教学改革与研究项目(JG19131)

作者简介:孙加节(1984—),男,江苏盐城人,博士,副教授,研究方向为动物生化与营养。

* 通讯作者:张永亮(1966—),男,河北黄骅人,博士,教授,研究方向为动物生化与营养。

和中心,这种把教学当作传递,把学生当作听众,把学习当作听讲的单向、灌输式课堂显然偏离了教学的本质。正如陈宝生部长所说,教学要体现“以学生发展为中心”的理念,这个也是世界高等教育共同的理念,课程是解决这个理念落地的“最后一公里”,要把课程作为人才培养的核心要素,学生从大学里受益的最直接、最核心、最显效的是课程,要给课程教学挤“水”添“金”,必须准确把握教学本质。教师要及时更新教学理念,应由知识的讲授者、灌输者、支配者变成学生学习的引导者、支持者、帮助者,引导学生独立思考、学会质疑,发现问题、解决问题进而学会创新创造。

1.2 更新教学内容、规划课程体系

教材是系统反映课程内容的教学用书,是教师教学和学生自主学习的首要参考资料,重要性不言而喻。目前国内农业院校畜牧专业所使用的生物化学教材各不相同,主要有朱圣庚、徐长法主编的《生物化学》(第4版,2016年)和邹思湘主编的《动物生物化学》(第5版,2013年),其中邹思湘主编的教材有两个显著特点:一是参编人员主要为国内主要农业院校专门从事动物生物化学教学科研的资深教师,课程内容专业针对性强,如包括乳和蛋的化学组成及形成等;二是该教材配套有国家精品资源共享课。因此该教材被选为华南农业大学动物科学专业课程教材。课程体系安排42学时,共包括14次课堂教学,每次3学时。结合学科培养方案与动物生物化学发展现状,我们对课程教学内容及体系进行了优化。课程教学内容除绪论外,主要分为6个模块:①生物大分子糖、脂、蛋白质的化学组成、结构和功能;②生物催化剂酶及生物氧化;③糖(葡萄糖)、脂类(甘油和脂肪酸)、蛋白质(氨基酸)在动物体内的代谢过程以及能量的产生、转移和利用;④物质代谢的相互联系与细胞调节;⑤核酸的结构和功能、中心法则、基因表达调节;⑥血液化学、乳蛋的化学组成及形成。在教学过程中安排了36个学时进行模块学习,另外预留两次讨论课,用于学生自行选择与生物化学相关的生产实践问题,进行专题汇报,教师参与课堂讨论。

1.3 基于智慧树在线教育平台建设课程 MOOC

智慧树是全球大型的学分课程运营服务平台,帮助高等院校完成优质课程的建设和服务配套落地,帮助教师完成教学发展培训,协助教师建设新课程,实现教育教学改革。华南农业大学动物科学学院前期利用该平台建设了动物生物化学在线课程(<https://coursehome.zhihuishu.com/courseHome/1000008753#>),主要由华南农业大学牵头,联合吉林大学、中国农业大学、南京农业大学、华中农业大学、

沈阳农业大学、黑龙江八一农垦大学等7所高校,共计11位教师,共享教学经验成果,建设动物生物化学 MOOC 平台。该在线开放课程包括“教学团队”、“课程设计”、“在线教程”、“见面课”、“课程公告”、“互动问答”、“作业测试”和“考核标准”等8个板块。根据动物生物化学课程教学要求,围绕课程体系基本知识点拍摄5-20分钟的教学视频,目前共上线93个单位,基本达到教材重要知识点全覆盖,而且每讲都配有课后作业,用于检测学生的学习效果,在学期中和学期末发布测试题,总体考核学生对生物化学基础知识的掌握情况。该课程既可以在PC端使用,也能在平板、手机上使用,操作简单,不受时间和地点的限制。学生进行实名认证后,任课老师还可以对教学班的学生学习情况进行统计。

2 混合式教学模式的具体实施

2.1 课前学习资料准备

根据教学进度的安排,利用智慧教学工具雨课堂等为教学辅助管理工具,提前一周发布预习讲义、课程PPT和课前思考题等,同时邀请学生登录智慧树在线教育平台进行自主预习,设置时间节点,掌握学生知识储备和预习情况。遇到问题可以在讨论区版块发帖,由教师或者其他学习者解答,也可以通过网络交流平台,如微信、QQ等专业推送软件直接与教师或同学进行即时沟通交流。教师也可根据智慧树在线教育平台后台数据和交流沟通情况,判定学生的学习效果,并且不定时在讨论区或借助教学辅助管理工具提问,进一步引导学生学习。

2.2 课堂教学活动设计

课堂教学时首先对学生自主预习过程中遇到的共性问题进行归纳总结,对于在线 MOOC 中尚未涵盖的内容或课程的重难点,采用多种教学方法进行教学或巩固学习。例如在讲述“蛋白质的化学组成、结构和功能”时,采用研究性学习的手段,将该部分内容分解为“氨基酸种类及性质”、“蛋白质化学结构”、“蛋白质高级结构”、“蛋白质理化性质及分离鉴定”、“蛋白质在生命活动中的重要作用”等5个单元,将班级学生分为小组,每组4-5人,分组查阅资料,进行讨论,并制作PPT,每个单元在课堂上进行讲解约15分钟。争取通过任务驱动让学生自主探究,以促进学生自主研究学习,提高学习能力,在整个学习过程中会极大地锻炼学生的逻辑思维能力,还会激发学生的创新思维能力。在讲授“乳蛋的化学组成及形成”时,采用案例现场实践教学法,教师联系并安排对接蛋鸡与奶牛等养殖企业,安排学生现场观摩,教师现场对蛋奶功能、形成等理论知识进行即时讲解,并联系企业生产中各个环节、技术

流程、企业运作、管理模式以及工作环境等,融入切题的思政元素,增强同学们不怕苦、不怕累、不怕脏的动科精神和专业情怀,端正学生价值导向,激发奋斗和专研精神。

2.3 课后拓展

借助雨课堂等智慧教学工具中 PPT 回放、在线互动答疑等功能板块,和动物生物化学在线 MOOC,学生可不受时空限制,随时随地回看,自主强化学习效果。教师可以布置线上作业、模块小测试及单元测试,通过线上测试,学生不仅可以检测自己的学习效果,教师也可以即时获得反馈,把握学生对所教内容的理解和掌握程度,反思和改善教学。同时利用网络资源优势,为学生提供更丰富的拓展素材与学习载体,如南京农业大学的国家精品在线课程、河南农业大学和西北农林科技大学在线 MOOC 等,加强学生所学知识的应用与迁移,丰富专业知识结构,开阔专业知识视野。

2.4 增加专题,拓展学生知识面

由于课程改革,提高了教学效率,节省了大量的课堂教学时间。课程设计了6个机动学时,学生可以选择与课程内容相关且感兴趣的专题,以“教师导学—学生分组讨论—小组课堂讲解”为主线,以互动式、设问式、讨论式、翻转式的教学方法,引导学生的好奇心与参与意识,培养学生创新性思维和主动解决问题的能力,真正做到“以学生为中心、以教师为主导”的教学模式创新。例如教师以“物质代谢的相互联系”为切入点进行导学,提出“畜禽体内能量如何生成、储存、转化及利用”、“畜禽添加能量饲料育肥机制”、“奶牛产后酮病发生”、“牛瘤胃酸中毒”等与动物生物化学理论知识密切相关的生产实践问题;班级学生可以根据各自的知识储备、学习能力、性格特点等自由组成3~5人的学习协作小组,各小组根据教师的引导,从选题背景、国内外研究进展与现状等方面进行小组讨论和成果展示;在课堂讨论教学活动中教师应以答疑、解惑、引导、鼓励为主,使学生体会到合作学习的乐趣,激发学生的

学习热情,挖掘学生学习的源动力,进而深化学习效果,实现课程理论知识的内化。

2.5 构建新教学考核体系

将培养学生素质贯穿整个考核评价过程,制定适合课程要求的评价体系,采用学生成绩由线上和线下两部分组成,各占50%。线上成绩包括章节作业、单元测试、在线课程期末考试成绩,以及学习进度、参与在线见面课讨论情况,线下成绩包括雨课堂考勤,专题讨论互动、期末理论考试。新的考核体系大幅增加了过程考核的比重,有效防止小部分同学在平时不认真学习,仅仅在考试前突击复习几天应付考试,能够真实地反映学生学习的整体情况。

3 结语

在新农科建设的大背景下,如何建设一门动物科学专业特色金课是一个有意义的话题。动物生物化学课程教育教学改革实践表明,线上线下混合式教学模式能有效提高学生的自主学习能力,显著提升课程的教学效果。但是课程还存在一些不足之处,如学生需要花费更多课后时间进行在线 MOOC 学习,学习任务加重,有时难以按预定完成,同时课程资源的覆盖面不全,即时交流也不方便。在未来的动物生物化学教学中,华南农业大学动物科学专业将不断进行改进和完善,力争将课程打造成“线上线下混合式金课”。

参考文献:

- [1] 张源淑,邹思湘,刘仪. 动物生物化学教学改革的探讨[J]. 甘肃农业大学学报, 2003, 38(2), 254-258.
- [2] 曲丹,刘敏,徐红娟,等. 浅谈线上线下混合式“金课”教学模式与课程建设的探析与思考[J]. 科教文汇(中旬刊), 2020, 497(6), 60-61.
- [3] 张双双,杨洪涛,张义龙. 疫情期间高校线上网络教学模式探讨[J]. 中国现代教育装备, 2020, 339(11), 14-16.
- [4] 陈宝生. 在新时代全国高等学校本科教育工作会议上的讲话[J]. 中国高等教育, 2018(15): 4-10.
- [5] 吴岩. 建设中国“金课”[J]. 中国大学教育, 2018(12): 4-9.

Exploration on Construction of Online – offline "Golden course" in Animal Biochemistry

SUN Jia-jie, LUO Jun-yi, CHEN Ting, XI Qian-yun, ZHANG Yong-liang*

(College of Animal Science in South China Agricultural University, Guangzhou, Guangdong 510642, China)

Abstract: Animal biochemistry is an important professional basic course in the field of animal husbandry and veterinary medicine. With the rapid development of modern information technology, online – offline blended teaching mode has been widely explored and practiced in the curriculum construction of many colleges and universities. The purpose of this paper is to improve the teaching quality of this course in South China University and respond to the ‘golden course’ appeal of the Ministry Of Education.

Key words: animal biochemistry; curriculum reform; blended teaching; golden course

新教育时代

2023年 6月 第26期

主管单位：天津出版传媒集团有限公司

主办单位：天津电子出版社有限公司

编辑出版：天津电子出版社有限公司

社 长：刘锦泉

执行主编：范洪武

特约策划：吴法源

责任编辑：张晓丹

采 编：张杏华 刘翔宇 杨晓莹 张 雪 张艳平

李 伟 孙 凡 陈晓明 王 芳 饶 蓉

李 萍 张 帅 良 辰 李 娜 李 扬

高 颖 王 楠 姜 萌 李会颖 郭 洋

李 静 王 薇 孔祥娟 王 欢 冯宇佳

陈 艳 贾会肖 高云哲 焦立涛 王 凯

李 霞 李 佳 刘秋新 林晓梅 刘丹丹

王丽娟 王 妍 王 静 修 睿 王海玲

张建楠

组稿电话：022-23678800

投稿邮箱：xjysdbjb@163.com

xjysdbjb@126.com

国际标准连续出版物号：ISSN 2095-4751

国内统一连续出版物号：CN 12-9205/G4

出版日期：2023年6月26日（逢周一出版）

光盘定价：20.00元

特别声明

1. 本刊所有文字、图片版权独家所有，未经授权，一律不得转载。
2. 除社评外，本刊所有文章内容均代表作者本人的观点，与本刊立场无关。
3. 所有稿件均要求作者是首次行使发表权的稿件，本刊对发表的稿件的版权和权利瑕疵情况不承担核实责任。
4. 本刊文章数据已入万方数据。来稿凡经本刊使用，如无特殊声明，本刊即视作同意上传传播。

CONTENTS

目 录

学生课堂

- 高中物理课堂多元教学策略研究.....龙 泽/1
- 浅论智慧课堂下阅读学习活动设计研究.....朱爱娟/4
- 高等数学课程思政元素分类与实施路径.....徐桂芳/7
- 中职思政课沉浸式教学的实践路径研究.....陈 艳/10
- 新课标下小学中低年级作文教学的策略与实践
-于秋菊/13
- 情景创设,开启小学数学“寓教于乐”之旅.....罗淑琴/16
- 审美支架在高中语文教学中的搭建策略.....刘修林/19
- 分层教学在特殊教育小学数学中的应用.....钱贝丽/22
- 学科大概念统摄下高中历史单元教学的设计路径研究
- 以《中外历史纲要上》第三单元为例.....周锐武/25
- 探讨空间想象能力对高中化学物质结构知识学习的影响
-韩 雪/28

幼儿教育

- 如何在幼儿学前教育中融入德育教学.....范 洁/31
- 幼儿学前教育当中存在的问题及对策.....付东旭/34

小学教育

- 利用课本提高学生写话能力教学初探.....王 霞/37
- 浅析小学英语高年段后进生教育观.....邱少渝/40
- 小学班主任如何做好班级管理工作.....卓 嘎/43
- 关于小学校园篮球开展现状的研究综述.....张 毅/46
- 新课程标准下小学英语写作教学策略研究.....汪兴东/49
- “五育”并举背景下的劳动教育研究.....李 玥/52
- 新时期小学学科教学中针对性辅导相关研究.....唐 昆/55
- “双减”政策下小学生语文素养提升路径与策略
-李 艳/58
- 小学语文教学中学生阅读能力的培养策略
-杨滨华 张誉馨/61
- 小学数学教学中提问技巧分析.....徐 进/64
- 思维导图在小学语文中高年级教学中运用的研究
-赵佳琦/67
- 论述如何在小学语文教学中激活学生思维
-高文超 刘艳玲/70

“双减”政策下小学语文学业监测和成效评价实施办法	
.....刘亚晶 张忠雾/73	

中学教育

巧设问题链,引领批判性思维发展.....吕 萍/76	
高中心理健康教育与班主任工作的问题与思考...宫庆宝/79	
引入趣味教学方法,提高初中英语教学效益.....周 莹/82	
“立德树人”指向下的高中德育创新研究	
.....韩兆梅 周真真/85	
高中语文群文阅读教学的实践模式探讨.....李 洁/88	
课程视域下的初中数学作业设计研究.....杨苏新/91	
谈初中音乐趣味教学策略研究.....李羚毓/94	
探讨初中历史教学对学生核心素养培养的研究	
.....张雪峰/97	
在初中体育教学中如何提升学生运动能力.....刘晓岩/100	
基于“双减”政策背景下初中语文作业优化与管理分析	
.....公美爻/103	
课堂提问技巧在初中英语教学中的作用与策略	
.....徐宏辉/106	
基于“三新”背景下的高中教学质量监测研究	
.....韦 美/109	
初中英语教学中如何构建高效课堂.....颜新祥/112	
“问题解决”模式下的初中数学教学研究.....邢 慧/115	
浅谈在高中美术教学中如何提高学生的鉴赏能力	
.....乔永磊/118	

高等教育

高校音乐表演专业应用型人才培养的创新思考	
.....段雯雯/121	
“三全育人”理念下的大学英语跨文化教学创新研究	
.....宋 佳/124	
高校思政课实践教学的内涵、价值及其实现.....陈 博/127	
饲料生物技术课程思政教育教学模式研究	
.....孙加节 罗君谊 陈 婷等/130	
大数据时代背景下英语阅读类软件的发展	
.....翟梓彤 肖 雨 金明浩/133	
工科专业大学生学情现状分析与对策	
.....张 超 张海红 魏 庆等/136	
社会语言学视角下《金星秀》中语码转换功能探究	
.....张 萍/139	
精确农业概论课程教研一体化探索与实践	
.....柯 健 徐 鹏 武立权/142	

教改理论

立足“三教”改革助力高职院校课程思政落地	
.....孙 伟/145	

图书馆管理

微阅读时代高校图书馆服务机制创新研究	
.....温盛勇 罗焕佑/148	

专题论坛

我国青少年身体素质下降的成因分析与对策研究	
.....刘北光/151	
新课标背景下落实体育学科核心素养的探究.....梁琳琳/154	
高职中药学专业教师“守正创新”实践能力培养路径探索	
.....王慧芳 周 扬/157	
高职护理专业实习生针刺伤发生情况及应对措施	
.....薛凯凯/160	
核心素养培育视域下中职学校心理健康教育路径研究	
.....吴海涛/163	
中外比较视角下中国高校教研室建设与管理探析	
.....王馨逸/166	
思政教育视域下高校电信网络诈骗防范对策研究	
.....彭建森 谢秉宸 潘斗超等/169	
教育督导保障机制的构建与实施研究	
.....康 杰 丁永钢/172	

职业教育

中等职业院校德育工作中工匠精神的作用及策略分析	
.....宋志鹏 张 琳/175	
新时代职业院校劳动教育评价的实施困境及优化策略探究实践	
.....孙方俊/178	
助力中职学生“学有所获”的教育管理实践尝试	
.....芦旭萍/181	
校企教育教学共同体视域下建设产业学院思维探析	
.....曹庆泽 仲 锐/184	
产教融合背景下的技工院校就业质量提升策略	
.....覃晓虹/187	
新专业目录下高职经管类专业群课程体系的构建	
.....延红兰/190	
四方协同、四轴驱动:中职学校	
瑶族非遗文化技艺人才培养的创新与实践	
.....曾瑞玲 黄 凯 陶 莉等/193	
地方红色文化融入中职思政教育的路径探析.....黄 凯/196	

饲料生物技术课程思政教育教学模式研究*

孙加节 罗君谊 陈 婷 习欠云 张永亮^{通讯作者}

(华南农业大学动物科学学院 广东广州 510642)

摘 要: 饲料生物技术是动物饲料科学与现代生物技术融合贯穿形成的一门新的学科分支, 具有理论与实践相结合的特点。如今高校对专业知识十分重视, 忽略了思想教育, 且思想认知存在偏差。该课程在传授专业知识的同时, 将思想政治和价值观融入课程中, 将课程思政与思政课程同向进行, 以充分发挥课程的思想教育功能, 培养一批“有理想、有道德、有文化、有纪律”的社会主义建设者和接班人。本文从教学目标和教学过程等角度阐述开展课程思政的具体方法和教学改革举措, 解决课程教学内容与思政脱节的问题, 并提高学生的情感认知。

关键词: 饲料生物技术 课程思政 教学改革

中图分类号: G816.9 **文献标志码:** A

DOI: 10.12219/j.issn.2095-4751.2023.26.130

随着国家对高校学科分工的不断完善, 科目间关联性逐步减弱, 思想政治教育似乎只是思想政治理论课的事情, 而造成高校其他课程对思想政治教育重视不够的现象。为此, 在全国高校思想政治工作中, 高校的根本任务应全面落实, 坚持尊重学生、服务学生, 做好课程、实践、文化、心理等方面的育人工作, 不断完善思政工作体系结构, 落实社会主义核心价值观; 在整个国民教育一体化的过程中, 与时俱进、因势利导是我们高校教师应该坚持的基本理念, 更加积极地探索新时期的教育教学方法, 通过德、智、体、美全面发展, 努力把学生培养成为社会主义建设者和接班人。

近年来, 国家不断发展饲料产业和生物技术, 并越来越重视生物技术 in 饲料工业中的应用。因此, 饲料科学和现代生物技术融合出现了一个新的研究领域, 称为饲料生物技术。饲料生物技术是利用生物技术或生物工程等先进技术分析饲料成分、研究功能性饲料添加剂和开发新的饲料资源。饲料生物技术课程是动物科学专业必修课, 此课程包含了微生物工程、基因工程等学科理论, 并介绍了这些技术和研究成果在饲料行业的应用, 既包括饲料技术的基本理论、工艺和方法, 也包括国内外的最新进展和发展。本文以饲料生物技术课程思政建设为例, 对该专业课思政教学模式进行探索。

一、课程现状分析

1. 重专业知识轻思想教育

课程思政是新时代高等教育的新要求, 传统的重专业知识传授的状况急需改变, 大思政的格局尚没形成。十八大以来, 党中央高度重视高校思想政治教育工作, 全面构建高校

思政工作体系, 紧紧抓住高校立德树人的根本任务。但过去很长一段时间, 思政教学在许多高校处于“边缘化”的地位, 其工作内容与学科专业之间也呈现“疏离化”的状态, 专业课程中涉及思政方面的内容更是少之又少, 在一定程度上影响了学生专业综合素质的培养与提升^[1]。因此, 专业课程应补充和加强思政内容建设, 将立德树人贯穿于整个课程。

2. 思想认知存在偏差

高校各种学科要和思想政治课程形成协同效应, 而各种学科不仅仅代表人文学科, 还包含了工程技术、自然科学等学科。哲、法、政、文、史等人文学关注人类发展和价值追求, 因此具有丰富的思政资源, 这在高校中乃至全社会已达成共识^[2]。而自然科学学科等本身以科研为主, 此类学科在教学课程中存在开设思政教育的空间和可能性并不大。《中共中央国务院关于进一步加强和改进大学生思想政治教育的意见》提出, “高等学校各门课程都具有育人功能, 所有教师都负有育人职责”。各个高校开展的所有课程都应该与思政教育共同进行, 形成协同育人、全员育人、全方位育人的效应。

3. 课程内容与产业脱节

目前, 以教材为中心的传统教学模式导致课程内容落后于产业发展, 需实现课程与产业发展的同频共振。在国家产业转型升级的关键时期, 饲料行业日益强调安全、优质、高效、资源节约和环境友好, 伴随着基因工程、酶工程及发酵工程为代表的现代生物技术发展, 现代畜牧业发展迅速, 国家广泛开发新型饲料资源以及饲料添加剂, 饲料转化率的逐

*基金项目: 广东省高等学校教学管理学会课程思政重点建设项目 (X-KCSZ2021006); 华南农业大学教育教学改革与研究项目与广东省本科高校教学质量与教学改革工程建设项目 (落实“育德”教育与实践, 打造《饲料生物技术》思政“金课”)。

渐提高,动物的生产性能的提高以及养殖业造成环境污染的降低已成为饲料行业发展的主要目标。目前,新产品、新技术不涌现,世界各国,尤其是发达国家普遍采用饲料生物技术作为饲料与饲料添加剂重大革新的重要手段。但课程内容局限于“教学大纲”“教材”,两者更新落后产业发展,影响学生整体专业素质的提升,同时知识体系落后,学生关注度也不够。

4. 传统教学模式滞后

当前,高等院校本科课堂教学普遍仍以教师为中心,多采用灌输和填鸭式的教学方法,教师自顾自讲课,全程多通过PPT授课,偶尔附带少量教学视频,少量板书或无板书,教学模式过于单一,极度缺乏与学生的互动、沟通和交流。这种一元单向式的传统陈旧教学形式容易引发学生无聊、厌烦等不良学习情绪,导致学生在课堂上玩手机、睡觉、私下聊天及思想漫游等,对课堂教学的氛围及学生学习效率有严重影响。

5. 专业教育与创新创业脱节。

专业教育与创新创业教育相融合,是高等教育的基本要求,但多数专业课程还没有实现。目前饲料生物技术课程教学仍以传统的课堂教学模式为主,创新创业等实践机会基本为零,教师侧重理论知识的讲授,不能与实践充分结合,未能让学生在实践过程中将课堂所学的理论知识运用起来,学生缺乏在实践中锻炼自己解决问题的机会和能力。

6. 考核制度缺乏创新,评价方式单调。

以闭卷考试为主,学生的学习成绩和掌握程度大多以考试得分来衡量,导致学生死记硬背,缺少学习活力。“上课记笔记、考前背笔记、考后忘笔记”,这种单一的考核制度及评价方式不利于培养学生创新思维、知识综合运用和实践能力。

二、课程思政教学目标

从古至今,中国一直非常重视人文教育的思想,从程朱理学到王阳明的精神哲学,这些思想一直指导和激励着中国人民。这些理论思想是当今青年最重要的思想营养,也是课程规范的主体^[3]。为了实现道德教育的目标,有必要将具体的思想和政治含义纳入课堂教学和教育改革。中国人心中,公民教育的根本目标是道德修养,“育人”是教育的落脚点。总的来说,应将职业知识教学与思想政治教育有机结合起来,完善当前的思想政治教育,将思想政治教育的内涵融入学科知识教学中,实现思想政治教育的目标^[4]。

饲料生物技术是一门应用核心课程,将理论与工程实践

相结合,让学生对当今的饲料相关技术有进一步认知。目前的课程应当加强思想政治教育,来进一步活跃课堂中的氛围,加强理解课程知识点,引导学生更认真地思考实际问题。生物技术知识体系应坚持历史唯物主义的观点,运用变化、发展和矛盾的基本原理,用“思想政治内涵”的典型事例补充课程。增强大学生的工匠精神、文化自信、社会责任感和爱国情怀^[5]。动物专业培养出的技术人才是社会所必需的,具有遵纪守法、社会责任感、良好的职业道德和职业精神。因此在饲料生物技术课程中,教师应根据课程教学特点,努力把握当代青年的脉搏,注重在教学中融入思想政治教育,使他们形成正确的人生观、历史观和世界观,为中国的产业转型和实现制造强国的目标作出贡献。

三、课程改革模式探索

更新课程中的思政要素,规划课程框架中的思政内容,实施模块化教学。根据饲料行业的现状和市场需求,将及时调整课程内容,更新相关案例,增加新知识。课程教学内容主要包括绪论、酶制剂及其在饲料中的应用、粗饲料资源开发、发酵技术与产品(单细胞蛋白)在饲料中的应用、植物提取物在动物养殖中的应用、抗生素替代与饲料资源开发进展6个模块,其中绪论2个学时,除绪论外,每个模块共计6个学时。其他每个模块以三部分构成,包括教学导学2个学时、小组讨论2个学时和课堂讨论与答疑2个学时,课程共计32个学时。为了实现课程的模块化、多元化,课程将从理论教学、实践活动和创新教学三个方面对课程进行规划,并将教育体系分为四个阶段:基础、前沿、综合设计、研究创新,从而达到深化课程体系的改革。同时,根据课程安排,课程在每个模块中纳入了相关的思想和政治内容。

四、课程思政实施过程

1. 在教学目标中融入思政元素

课程的主要目的是培养合格的技术性人才,能够在改革开放的背景下获得动物营养和饲料方面的专业知识,以满足社会主义市场的需要,并培养优秀的实践能力。不仅要学习相关理论,而且要在实践中培养专业和技术技能。该课程旨在使学生了解饲料生物技术的本质,了解国内外发展动态,将创新和创业教育结合起来,将课程思政元素联系起来,以培养学生的自学能力、解决复杂问题的能力、创新思维和能力、职业意识和责任感、领域知识框架和人际交往能力。

2. 在教学过程中融入思政内容

在教师理论导学过程中,通过案例、提问互动等方式融入思政元素。如,在单细胞饲用蛋白概念,我国饲用蛋白质

资源现状及主要替代方案等介绍时,通过讲述我国饲料产业现状,鉴于中国对饲料粮的进口依赖和中美贸易战,学生将增强爱国主义精神和自强不息的愿望,以及对专业的认同感和责任感;在介绍单细胞饲用蛋白工艺,菌种的选择及配伍,发酵等条件优化等时,发挥现代生物技术的优势,培养学生利用新发展、新技术和新知识来提高中国的畜牧业。认识到利用新进展、新技术、新知识来提高中国畜牧业的生产水平,为中国新农业科学的建设服务。

3. 线上线下、课内课外,进行价值观组合

利用媒体、互联网+等信息化平台,采取线上线下混合式教学模式,实现讲授、讨论等多元化教学手段,跨越时空限制,在课内和课外进行价值观的结合。与教师科研实践相结合,让学生参与团队科研项目。例如,开发将酱油残渣发酵成发酵饲料的工艺,研究茶叶残渣的有机饲料使用方案。让学生了解技术发展、技术流程和实际生产中的工作环境等。做到理论与实践教学同步,课内向课外延生。加深同学们对专业的了解,培养动科学子“一懂两爱”(懂农业、爱农村、爱农民)与三农情怀。

五、课程思政达到的效果

1. 解决课程教学内容与思政脱节的问题

将思想政治理论教育全面融入课程教学,同时结合网络、不同教材、专业文献等饲料生物技术课程相关的资料和素材,及时更新完善课程内容,完善知识体系建设,促进学生综合专业能力与思政素质全面均衡发展。

2. 提高学生的情感认知

通过教师导学,介绍我国畜牧与饲料产业取得的成绩,增强学生的“四个自信”,激发耕读精神;通过课堂展示讲解、教师点评,让学生体会畜禽生产科研工作的艰辛,培养大国“三农”情怀;通过参加课程实践,做到理论教学与实践教学同步,让学生了解服务乡村振兴的意义,增强学生建

设美丽乡村的责任感和使命感。

结语

通过目前教学改革使学生的眼界和思维得到提升,加强学生的文化自信。了解和掌握新时代课程思政的含义、特点和难点,积极寻求解决办法,充分挖掘不同课程的思想教育功能。培养一批“有理想、有道德、有文化、有纪律”的社会主义建设者和接班人,满足人民对美好生活的需要,对实现中华民族伟大复兴的中国梦具有十分重要的意义。

参考文献

- [1]田鸿芬,付洪.课程思政:高校专业课教学融入思想政治教育的实践路径[J].未来与发展,2018,42(04):99-103.
- [2]王学俭,石岩.新时代课程思政的内涵、特点、难点及应对策略[J].新疆师范大学学报(哲学社会科学版),2020,41(2):50-58.
- [3]高德毅,宗爱东.从思政课程到课程思政:从战略高度构建高校思想政治教育课程体系[J].中国高等教育,2017(1):43-46.
- [4]毛碧飞,张炳聪.创新创业背景下《食品生物技术》“课程思政”教学改革与实践[J].食品与发酵工业,2021,47(10):304-308.
- [5]王景云.论“思政课程”与“课程思政”的逻辑互构[J].马克思主义与现实,2019(6):186-191.

作者简介

孙加节,男,副教授,硕士生导师。研究方向:动物生物化学。

通讯作者:张永亮,男,教授,博士生导师。研究方向:动物生物化学。

主管单位：科技部西南信息中心

主办单位：重庆维普资讯有限公司

出版单位：重庆维普资讯有限公司

总 编：车东林

电 话：17316705750

网 址：<http://www.cqvip.com>

地 址：重庆市渝北区洪湖西路
18 号上丁企业公园

邮 编：401121

国际标准连续出版物号：ISSN 1671-5551

国内统一连续出版物号：CN 50-9207/G

法律顾问：闫 军

本刊声明

本刊版权归重庆维普资讯有限公司所有。作者稿件一经录用,均视为作者同意刊载以及同意在本刊合作的数据库及互联网站传播。如作者不同意文章被收录,请在来稿时向本刊声明。

目 次

CONTENTS

成人与职业教育

探究中职计算机教育中的实践教学策略和方法

..... 杨 兰 1

浅谈中职学校机械专业钳工实训改革 单崇巍 5

创新教育在中职计算机教学中的有效实施分析

..... 李 平 9

中职数控专业“一体化”教学的优化研究

..... 李红军 13

中职英语教学中的德育渗透策略分析 许冰滢 17

高等教育

新媒体时代高校辅导员网络思政教育工作路径研究

..... 赵 金 20

探究教育新业态背景下的高职学生创新创业能力培养

..... 熊 瑶 24

高校人工智能课程教学与实践研究 吴庆洪 28

立德树人视角下高校舞蹈课程思政建设的实施途径探讨

..... 魏 瑶 31

产业升级背景下高职测绘类专业实践教学改革创新探究

..... 杨单单 34

立德树人视域下的医学院校导师队伍建设探索与实践

..... 王志龙 张 珍 朱雁飞 郑慧哲 李鲁新 39

高职院校 AI+X 复合型人才培育新模式研究

..... 李桂春 42

中华优秀传统文化融入高校思政教育路径研究——以财会类专业为例

..... 李俊倩 45

高等代数学习中的思维转换 马毓正 48

初等教育

游戏精神视野中的幼儿艺术教育目标 张 琪 52

小学英语词汇教学改进策略研究 勒书兰 55

基于新时期背景下的幼儿学前教育策略分析

..... 毛燕琴 58

试分析提升小学体育教学的有效性策略

..... 杨 剑 61

数学文化融入小学数学教学研究 王 勇 64

小学低学段识字写字教学策略研究

..... 王艺嘉 刘佳怡 67

“双减”背景下初中语文名著阅读教学策略探微

..... 王雪仙 70

数形结合思想在小学数学教学中的渗透与应用探究

..... 魏 钦 73

基于微课的小学数学课堂教学模式探讨	叶 娟 76
小学语文阅读策略探讨	周 莉 79
体育游戏在初中体育教学中的应用及影响分析	张 强 82
“双减”下初中英语作业设计多样化策略探究	谭卫贤 85
小学劳动教育现状与有效实施对策	乔春玲 89
小学科学实验教学创新策略探究	夏希梅 93

教育论坛

《饲料生物技术》课程思政点挖掘与应用	孙加节 罗君谊 陈 婷 习欠云 张永亮 97
高中英语阅读教学在核心素养视域下的策略研究	于 淇 101
试论高中政治教学中学生思维能力的培养	尹佩文 105
1+X 制度下中职“机械零件数控铣加工”课程研究	姜 聪 109
中职学业水平考试背景下《汽车构造》课程教学的改革策略分析	罗鹏飞 113
高职院校基层教学组织内涵建设与实践研究	陈士龙 117
信息化背景下中职钳工实训教学的实践分析	袁 江 120
新课程下高中政治作业的研究与思考	赵顺健 124
现代信息技术背景下高等数学教学模式创新研究	盛茂林 128

跨国高等教育教学质量评价研究——以深圳市中外合作办学项目为例	彭 卓 王 瑛 132
高校房地产基本制度与政策课程思政元素挖掘研究	顾海玲 137
音乐审美教育在高中教学的实施探析	覃诗婷 141
大单元教学在高中化学教学中的应用研究	余小芳 145
高职院校 ERP 沙盘模拟课程教学问题研究	王 浩 148
基于 2022 版课程标准的小学体育与健康课程实施方案设计的研究	潘庆庆 孙继龙 152
基于 OBE 理念的中职《化工机械及设备》课程项目式学习研究	信熙卿 王化明 包 展 郭 雯 王海娇 156
中职学校机电专业实训课程教学的思考	安中锴 160
智慧教学种子教师培养的思考	田珍琳 164
“三全育人”视角下大学生心理健康教育路径探析	海庆玲 168
新媒体时代高职院校大学生网络意见表达与正向引导研究	杨 静 172
基于内驱力养成培养大学生创业能力的研究	李 军 卫舒春 张 海 176
分层教学法在高中足球教学中的应用策略探索	刘 磊 180

《饲料生物技术》课程思政点挖掘与应用

孙加节 罗君谊 陈婷 习欠云 张永亮

华南农业大学动物科学学院, 广东 广州 510642

摘要:课程思政就是课程作为载体,把思想政治教育作为一种内在价值纳入各类教学课程之中,从而实现课程学习和思想政治理论教育的有机结合,并最终取得协同效果的过程。《饲料生物技术》作为一门崭新的学科,它是由动物营养学,饲料科学以及现代生物技术等多门科学交叉融汇而形成的,它选用饲料原料和饲料添加剂作为研究对象,利用生物技术、发酵工程等新兴生物技术来开发新的饲料原料资源和饲料添加剂,对其生物学功能及作用机理进行了研究。挖掘《饲料生物技术》课程中的思政元素并将其应用到实际教学中,可以在传授专业知识的同时,提升学生的思想道德水平。

关键词:饲料生物技术;课程思政;教学改革

中图分类号:G64

生物饲料在过去十年中得到了越来越多的重视和快速发展,现已成为我国饲料工业中最热门的课题之一。2013年岁末,“在第一届生物饲料科技大会上”在国家生物饲料研究中心举行,有关专家及研究人员围绕产业发展中的重大问题及研发方向展开深入讨论,为实现饲料产品标准化、规范产业发展提供技术与理论支撑,这也标志着我国饲料生物加工技术研发进入到一个新的历史时期。“饲料生物技术”本质上是活性生物因子(具有生物活性的有益微生物、生物酶)与饲料物质在一定条件下发生生化反应的技术,也就是利用生物效应对饲料进行加工和利用,从而提高饲料的营养品质和利用效率^[1]。

近年来,在大学专业分工逐步细化的情况下,各大学课程间融通性减弱,对大学生进行思想政治教育似乎仅仅是思想政治理论课与课程教师双方的事,与其他课程和任课教师没有任何关系,导致学校思想政治教育在其他课程中存在重视程度不够,自觉性不高的现象。为此,习近平总书记在全国高校思想政治工作上明确提出了“其他各课程必须守住一条渠段,种下责任田,让各课程和思想政治理论课同舟共济,产生协同效应”,要把“将思想政治工作渗透到整个教育教学过程中去,做到全程育人和全方位育人,不断开创中国高等教育事业的新局面”。因此,我们的高等教育教师应当不断适应时代的发展和形势的变化,积极探索和研究新时代的教育教学方法,致力于培养学生成为全面发展的社会主义建设者和接班人;在此基础

上,要进一步加强课程改革,不断提高教学水平,以更好地适应人才培养需求。高校应当全面贯彻立德树人的根本任务,以学生为中心,积极开展课程、实践、文化、心理等多方面的育人工作,不断完善思政工作体系建设,将社会主义核心价值观有机融入国民教育全过程,以培养出最优秀的人才为目标。当前我国正处于改革攻坚期和深水区,在这个关键时期加强高校意识形态领域斗争,开展好高校课程思政是十分必要的。因此,深刻领会新时代课程思政的内核、特色和难点,积极探索应对之策,充分发挥各类课程的思想思想政治教育功能,推动课程思政与思政课程同步发展,培养一批具备理想、道德、文化和纪律的社会主义接班人和建设者,以满足人民对美好生活的需求,对于实现中华民族伟大复兴具有至关重要的意义。

1 《饲料生物技术》课程思政点挖掘的重要性

一般来说,《饲料生物技术》这门新兴学科的主要研究重点,是针对饲料原料及饲料添加剂,利用一些先进的技术,比如生物技术或发酵工程等,来开发新的饲料原料资源以及研发功能性饲料添加剂等系列产品,从而达到在最佳性价比的条件下使动物有最高的生产性能并尽可能地降低养殖业产生的环境污染的目的。随着生物技术及饲料产业的持续发展,人们对生物技术在饲料工业中应用的研究也越来越多,《饲料生物技术》是一门全新的专业学科,它是由现代生物技术与动物饲料科学交叉融汇而形成的,覆盖了两门学科的基础和共性,也具备其独有的理论和新概念。其

作为一门动物科学专业的选修课,内容涵盖了微生物工程、基因工程、和酶工程等学科的理论基础与科研成果以及它们在饲料产业中的应用实践,具体包括饲料技术的基本理论、新方法、新工艺、新成果以及国内外相关研究的最新进展与未来走向等。该课程涉及面广、理论结合应用性强、内容更新快,若在教学过程中继续沿用传统的注入式教学法,只一味地将知识灌输给学生而不能将理论解释清楚也不引导学生独立思考,使得课程内容脱离行业,脱离专业教育,脱离创新创业,就会影响教学质量以及学生学习的积极性和主动性。近年来,为贯彻落实教育部一流本科课程建设的实施意见,打破多数课程形式陈旧、内容枯燥的局面,鼓动所有教师共同参与课程理念、课程内容、课程模式的创新,形成创设高阶性、创新性和挑战性的“金课”、舍弃低阶性、陈旧性的“水课”的教学改革氛围。《饲料生物技术》一改传统教学方法与教学模式,在教学内容上增加对典型案例的呈现和分析,在教学手段上加入了新的环节,比如采用“翻转课堂”与小组讨论的教学模式相结合,给予学生更多的决定权和自由性,引导学生进行自主学习及探究式学习,它在培养学生发现问题、解决问题的能力时,也对他们的创新意识和实践能力进行了有效的锻炼,这对于强化饲料行业高素质专业人才的培养,促进畜禽业的优质快速发展有着重要的意义。基于上述背景及实践探索,围绕“育人”(立德树人)这一核心,创新《饲料生物技术》课程知识体系,创新课程建设模式,改革教学方法,发掘课程思政点,切实做到教学相长,对于培养品德高尚,热爱畜牧业的创新型和实践型复合人才至关重要。

2 《饲料生物技术》课程思政点挖掘的要点

课程作为思政建设的重要载体,是教师传播思想政治理念的主要通道。高校教师,不论是任何专业的任何科任教师,都要对课程教学内容进行全面而深刻的分析,并依据不同专业课的特点,思维方法和核心价值理念等,深挖专业课的思政元素并有机融入课堂教学之中,以达到潜移默化的育人效果。首先,要注重厚植学生的“大国三农”情怀,高等农业教育作为培养农业人才的主要阵地,需要积极引导同学们具备将强农兴农当作自己义不容辞的责任的觉悟、做到“懂农业,爱农村,爱农民”,提高将论文写进祖国大地的

个人自觉和精神信念,强化同学们为农业农村现代化服务的担当意识、心怀使命感、责任感为乡村整体振兴服务,培育知农爱农的创新型人才。二是课程教学中要强化生态文明教育,指导学生确立并实践绿水青山就是金山银山。再者在课程教学中要把马克思主义立场观点方法教育同科学精神培育高度融合,增强学生对问题的正确认识,理智地分析问题以及灵活地解决问题。最后,对学生的科学思维方法训练与科学伦理教育更是不容忽视的一部分,弘扬科学精神,培养学生的科学探究精神,激励学生有探求真理的主动性和积极性,鼓励学生攀登科学高峰,肩负科研的责任感与使命感。

3 《饲料生物技术》课程思政元素的挖掘途径

3.1 从课程发展历史中挖掘课程思政元素

我国饲料生物技术研究始于上世纪80年代,90年代开始商业化生产推广。从生物技术饲料的发展历程来看,我国的产品研发和产业化水平发展大致经历了三个阶段:第一阶段是以青贮饲料、糖化饲料等为代表的传统饲料产品,是我国饲料业早期发展的生物饲料,具有一定的技术含量和应用价值;第二阶段是以微生物饲料、单细胞蛋白(酵母粉)等为代表的生物发酵系列产品;第三阶段是以生物发酵系列产品为代表的生物发酵产业,在这一阶段中,我国的生物发酵产业发展迅猛。产品包括了饲料用酶制剂、有机微量元素细胞水解物、微生物饲料添加剂、益生菌及益生菌制剂、发酵饲料、细胞培养物、细胞产物或提取物、生物饲料新产品、生物药物饲料添加剂、酶解饲料、新型饲料蛋白等。目前全国有上千家生物饲料生产企业,年产量约500万吨,产品逐渐被市场认可^[2]。

总体上,我国饲料生物的发展较快,在整体的产品研发、规模化生产、市场化销售以及产业化应用等方面均有体现。对于生物饲料资源利用和饲料生物技术研究等方面,我国已经获得了很多具有国际领先水平的重要成果,比如,利用秸秆、木屑、发酵工业残余物等资源,将农副产品进行饲料化,在对这些资源高值化利用的同时,也为养殖业的饲料来源提供了新的方向和储备。已经开发的生物饲料添加剂产品,具体包括以下类别:酶制剂、益生菌、饲用氨基酸和生物药物饲料添加剂等等。经历多年的探究和沉淀,生物饲料产品的产业化技术已相对成熟,例如,中国农

业科学院建立了科学快速且行之有效的特殊酶生产菌的筛选系统,用来筛选能大量生产性能优良的饲料工业用酶,其中高表达的饲用植酸酶不仅占据了国内80%以上的市场,在国际市场上所占份额更是日趋上升,取得了显著的经济和社会效益^[3]。因此,以我国饲料生物技术的历史、现状和问题为切入点,通过我国在饲料生物技术上取得的巨大成绩,通过分析现状和问题,强化学生“四个自信”,培养学生的责任感和专业情怀。

3.2 从科学家成长中挖掘课程思政元素

在教学中,如果教师能够尝试去挖掘并引入一些与专业知识相关的科学史实和科学家的轶闻趣事等,能够让学生领悟科学的崇高和神圣,领会科学对于历史的巨大推动作用,感悟科学家们身上独特的科研精神和珍贵品质,极大地促进对学生科学精神的培养^[4]。饲料生物的科学研究者们的科研事迹蕴含着他们谨慎细致、锲而不舍的科研精神,通过介绍他们的故事,可以培养学生潜心钻研、持之以恒的工作作风和不忘初心、牢记使命的理想信念,始终本着脚踏实地、实事求是的工作态度投身于科学研究中。

以姚斌院士为例,姚斌院士很早就意识到了饲料用酶的重要性。1994年,姚斌博士从中国农业科学院研究生院毕业,来到中国农科院饲料研究所工作,潜心研究基因工程、蛋白质工程、发酵工程等酶制剂技术前沿,建立了国内饲料研究第一个分子生物学实验室。熟悉姚斌院士的人都知道,周末或节假日在实验室必能看到他的身影,这样持之以恒、不懈努力的作风大大影响着他的团队。“宝剑锋从磨砺出,梅花香自苦寒来”,不懈努力终于结出丰硕的果实,如今姚斌院士带领他的研究团队,已开发出多种达国际领先水平的饲料用酶新品种,其中植酸酶、 β -葡聚糖酶等10余种产品实现产业化生产且技术水平在国际上处于领先地位,植酸酶产品占据了95%以上的国内市场 and 较大份额的国际市场,打破了国际大公司的垄断,使我国饲料用酶发展成为具有国际竞争力的新兴产业。可以看出,正是通过不懈努力,姚斌带领他的团队,一步步实现了饲料用酶从基础研究到产业化生产的完整技术链条构建。因此,以植酸酶为例,宣扬姚斌院士在植酸酶国产化和产业化研发过程中的刻苦专研精神,能够激励同学们勇于创新探索。

3.3 从科学研究中挖掘思政元素

上世纪四十年代后期,抗生素被首次报道可能有饲用促畜禽生长特性。在畜禽养殖中,长期饲喂低于治疗剂量的抗生素的做法很容易被采用,并很快成为工业化畜牧业生产系统中的一个组成部分。在动物生产中,为了提高动物的生产发育,以亚治疗浓度(低剂量)添加到饲料中的抗生素被称为“饲用抗生素”,也就是饲用促生长抗生素。饲用抗生素在为养殖业的发展做出了巨大贡献的同时,也因为长期低剂量添加使用,造成耐药菌、环境污染、动物源性食品抗菌药残留、公共健康安全隐患等问题且愈演愈烈。1981年世界卫生组织抗生素慎用联盟成立,呼吁各国政府采取立法手段禁止滥用抗生素;1986年瑞典为缓解消费者对肉品药物残留和耐药性产生的恐惧心理,宣布全面禁止抗生素用作饲料添加剂,成为全球首个禁用饲用抗生素的国家;2002年欧洲理事会宣布决定逐步淘汰所有促生长用抗生素,2006年欧盟全面禁止抗生素在饲料中作为促生长剂使用的法规生效;我国自1989年以来,也对动物饲料中抗生素的使用进行了规范,并于2020年全面禁止使用促生长抗生素类饲用添加剂产品^[6]。至此,“饲用替抗”产品研发在全球养殖行业中成为研究热门。基于保障饲料与养殖行业绿色、高质量、健康发展的需要,目前植物提取物、精油、酸化剂、微生态制剂等类型饲料添加剂替抗产品开发研究如火如荼,这些“替抗产品”将遵循绿色健康、安全有效、提高生产效益和改善品质等原则进行。因此,以抗生素使用的历史及存在问题为例,以替抗产品研究为切入点,培养学生食品安全、绿水青山就是金山银山的现代生态观。

4 结束语

在新世纪,饲料生物技术无论是在理论研究还是实践应用上都有很大的发展前景^[7]。将《饲料生物技术》课程与思想政治教学的巧妙结合,是新时代对教育工作者提出的新要求,对未来行业接班人树立正确的世界观、价值观和人生观具有重要意义。将思政教育真正落到实处,对引导学生思想有启迪作用,灵魂有引领作用,人格有感召作用。

参考文献

[1] 李绍章,生物饲料技术内涵辨析[J].饲料工

业, 2014, 35(12): 1-5.

[2] 季益华, 生物饲料在畜牧业发展中的应用——评《生物兽药与生物饲料在畜牧业生产中的科学应用》

[J]. 中国饲料, 2022(01): 151.

[3] 王格, 生物饲料在生态畜牧业中的现状及发展趋势

[J]. 现代畜牧兽医, 2019(04): 53-58.

[4] 周莉君等, “植物学名”课程思政育人元素的挖掘与应用 [J]. 高校生物学教学研究 (电子版), 2022, 12(04): 60-64.

[5] 王永颖, 唐佩娟, 窦新艳, 窦广跃, 王鸿英, 饲用抗生素替代技术应用前景分析 [J]. 天津农林科技, 2022(05): 39-42.

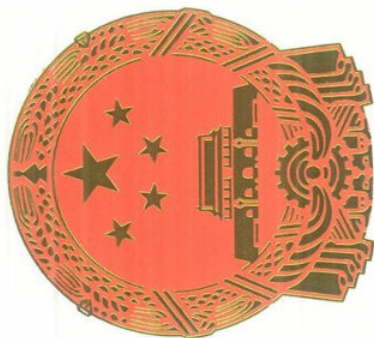
[6] 何文, 动物源食品中残留抗生素的危害和检测技术

[J]. 食品安全导刊, 2022(17): 157-159.

[7] 杨丽英, 周小燕, 生物饲料的现状与发展前景 [J]. 畜牧与饲料科学, 2010, 31(01): 34-36.

作者简介: 孙加节(1984—), 男, 江苏盐城人, 博士, 副教授, 研究方向为动物生物化学; 通讯作者: 张永亮(1966—), 男, 河北黄骅人, 博士, 教授, 研究方向为动物生物化学。

基金项目: 2022 年华南农业大学教育教学改革与研究项目与 2022 年广东省本科高校教学质量与教学改革工程建设项目 (落实“育德”教育与实践, 打造《饲料生物技术》思政“金课”); 2021 年广东省高等学校教学管理学会课程思政重点建设项目 (X-KCSZ2021006)。



国家级教学成果奖 证书

证书编号: G-2-2018354

为表彰国家级教学成果奖获得者,
特颁发此证书。

获奖成果: 农科高校双创人才培养的创新
与实践

获奖者: 张永亮 陈少雄 叶晖有 曾璇
曹广祥 陈永晴 李晨光 孙宝丽
陈婷 习欠云 孙加节

获奖等级: 二等奖



二〇一八年十二月



第十届广东省高等教育 教学成果奖

获奖证书

获奖成果：
契合新农科建设需求的动物生产实践
专业课“金课”建设的创新与实践

获奖者：张永亮、陈婷、孙加节、罗君谊、
习欠云、邓铭

获奖等级：二等奖

证书号：GJ2021E030



获奖成果：契合新农科建设需求的
动物生产类专业课“金
课”建设的创新与实践

获奖者：张永亮、陈 婷、
孙加节、罗君谊、
习欠云、邓 铭

获奖等级：一等奖

证书编号：JXCG21012



广东省课程思政改革示范项目

项目名称:饲料生物技术——单细胞蛋白
饲料的生产与应用第一章

项目类别:示范课堂

项目负责人:孙加节

主要建设单位:华南农业大学



证书编号:202123033

证书



国家级一流本科课程

课程类别：线下一流课程

课程名称：饲料生物技术

课程负责人：张永亮

课程团队其他主要成员：孙加节、习欠云、陈婷

主要建设单位：华南农业大学



2020年11月

证书编号：2020131168

证书



广东省一流本科课程

证书



课程名称: 动物生物化学

课程类别: 线上一流课程

课程负责人: 习欠云

课程团队其他主要成员: 张永亮、陈婷、孙加节、
罗君谊

主要建设单位: 华南农业大学



证书编号: 202011109

广东省一流本科课程

证书



课程名称：饲料生物技术

课程类别：线下一流课程

课程负责人：张永亮

课程团队其他主要成员：孙加节、习欠云、陈婷、
罗君谊

主要建设单位：华南农业大学



证书编号：202013067

华南农业大学文件

华南农教〔2023〕1号

关于公布华南农业大学 2022 年度 课程思政示范项目认定名单的通知

各学院、部处、各单位：

根据《华南农业大学课程思政实施方案》（华农党发〔2022〕26号）精神和《关于开展 2022 年度校级课程思政示范项目遴选认定工作的通知》要求，学校组织开展了 2022 年度课程思政示范项目遴选认定工作。

经项目负责人申请、所在单位遴选推荐、学校组织专家评审、校内公示等程序，现认定华南农业大学 2022 年度课程思政示范项目共 177 个，其中包括资源环境学院等课程思政试点学院 3 个、“动物生物化学与饲料生物技术教学团队”等课程思政示范团队 19 个、《动物组织学与胚胎学》等课程思政示范课程 43 门、“微观经济学-第八章第三节”等课程思政示范课堂 54 个、《概

- 1 -

率论与数理统计》等课程思政典型案例 58 个，现予以公布（名单详见附件）。

本次认定的试点学院建设期至 2024 年 9 月，其他示范项目

的有效期至 2026 年 12 月 31 日；有效期内，示范项目原则上不允许更换负责人或变更项目团队成员。获评为课程思政示范课程的，将同时认定为 2022 年度校级一流本科课程（课程思政）。试点学院要按照项目建设任务及要求，及时开展各项工作，加快推进课程思政改革，确保高质量完成建设目标。

请各学院充分认识课程思政改革的重要意义，认真贯彻《华南农业大学课程思政实施方案》，加强对教师的相关培训、指导、引领和支持，带动教师全员积极参与课程思政教学改革，持续深入抓典型、树标杆、推经验，全面提升本科人才培养质量。

附件：华南农业大学 2022 年度课程思政示范项目认定名单

华南农业大学

2023 年 1 月 8 日

公开方式：主动公开

华南农业大学党政办公室

2023 年 1 月 12 日印发

11	林学与风景园林学院	森林培育学课程思政示范团队	陈红跃
12	兽医学院	动物重大疫病防控团队	亓文宝
13	植物保护学院	植物保护课程思政示范团队	钟国华
14	食品学院	《食品化学》课程思政示范团队	周爱梅
15	数学与信息学院、软件学院	统计学专业课程思政示范教学团队	夏 强
16	公共管理学院	公共管理心理学	贾海薇
17	兽医学院	兽医药理学教学团队	蒋红霞
18	外国语学院	英语专业课程群课程思政教学团队	邓 飞
19	经济管理学院	金融学	柳 松

三、示范课程

序号	建设单位	示范课程名称	负责人
1	兽医学院	动物组织学与胚胎学	梁晓欢
2	农学院	遗传学	刘自强
3	材料与能源学院	家具与室内材料学	孙理超
4	动物科学学院	养猪学	洪林君
5	经济管理学院	宏观经济学	段 伟
6	经济管理学院	发展经济学	张沁岚
7	资源环境学院	土壤学	李 博
8	动物科学学院	饲料生物技术	孙加节
9	工程学院	汽车理论	王 昱
10	经济管理学院	广告管理	张 蓓
11	兽医学院	兽医产科学	杨世华
12	资源环境学院	农业生态学	章家恩

荣誉证书

孙加节 老师:

在华南农业大学首届课程思政教学大赛中
荣获“三等奖”。

特发此证，以资鼓励！



荣誉证书

HONORARY CREDENTIAL

孙加祥同志：

在首届全国动物生理生化青年教师教学大赛中，荣获“突出教师”。

特发此证，以资鼓励。

中国畜牧兽医学会动物生理生化分会

二零二三年七月

责任编辑 孟盟
封面设计 王振华

生物信息基础

生物信息基础

孙加节 李耀坤 主编

孙加节 李耀坤 主编

吉林科学技术出版社




定价：42.00元

吉林科学技术出版社

生物信息基础

主编 孙加节 李耀坤

 吉林科学技术出版社

图书在版编目 (CIP) 数据

生物信息基础 / 孙加节, 李耀坤主编. -- 长春 :
吉林科学技术出版社, 2021.12

ISBN 978-7-5578-9165-7

I. ①生… II. ①孙… ②李… III. ①生物信息论
IV. ①Q811.4

中国版本图书馆 CIP 数据核字 (2021) 第 274075 号

生物信息基础

SHENGWU XINXI JICHU

主 编 孙加节 李耀坤
出 版 人 宛 霞
责任编辑 孟 盟
封面设计 王振华
制 版 北京壹滴水文化传播有限公司
幅面尺寸 185mm×260mm 1/16
字 数 240 千字
印 张 13.5
印 数 1-1 000 册
版 次 2021 年 12 月第 1 版
印 次 2021 年 12 月第 1 次印刷

出 版 吉林科学技术出版社
发 行 吉林科学技术出版社
地 址 长春市净月区福祉大路 5788 号
邮 编 130118
编辑部电话 0431-81629514
印 刷 长春市华远印务有限公司

书 号 ISBN 978-7-5578-9165-7
定 价 42.00 元

版权所有 翻印必究 举报电话:0431-81629508

前 言

生物信息基础是分子生物学与信息技术的结合体,是随着生命科学和计算机科学的迅猛发展,相结合所形成的一门新学科,通过综合利用生物学,计算机科学和信息技术去揭示大量而复杂的生物数据所赋予的生物学奥秘。生物信息基础主要包括生物信息的采集、处理、存储、传播、分析和解释等各方面的理论知识及基础技术,作为一门新的学科技术领域,它是把基因组 DNA 序列信息作为源头,在转录和翻译等水平上,重点研究基因组学和蛋白质组学两方面,具体说就是从核酸和蛋白质序列出发,分析序列中表达的结构功能的生物信息。

本书分为 9 章,其内容包括:第一章 Linux 系统基本操作、第二章生物学数据库及其检索、第三章序列比对原理、第四章蛋白质结构预测与分析、第五章真核生物基因组的注释、第六章转录组学、第七章非编码 RNA、第八章蛋白质组学、第九章新一代测序技术及其应用。

本书在编写过程中,参阅了相关的文献资料,在此谨向作者表示衷心的感谢。由于水平有限,书中内容难免存在不妥、疏漏之处,敬请广大读者批评指正,以便进一步修订和完善。

目 录

第一章 Linux 系统基本操作.....	1
第一节 Linux 简介.....	1
第二节 Linux 常用命令行操作.....	2
第三节 在 Linux 下使用 SAMtools	6
第二章 生物学数据库及其检索	9
第一节 生物学数据库简介	9
第二节 生物学数据库的数据存储格式.....	14
第三节 生物学数据库的检索.....	27
第三章 序列比对原理.....	40
第一节 序列比对相关概念.....	40
第二节 序列比对打分方法.....	45
第三节 序列比对算法.....	52
第四节 序列比对工具.....	56
第五节 多序列比对.....	60
第四章 蛋白质结构预测与分析.....	65
第一节 蛋白质结构组织层次.....	65
第二节 蛋白质结构的测定和理论预测.....	72
第三节 蛋白质对接.....	89
第四节 蛋白质折叠与疾病.....	91
第五章 真核生物基因组的注释.....	97
第一节 蛋白质编码基因的注释.....	98
第二节 RNA 基因的注释	104

第三节 重复序列的注释	106
第四节 假基因的注释	108
第六章 转录组学	110
第一节 转录组学概述	110
第二节 试验设计和测序流程	114
第三节 转录组数据核心分析	117
第四节 功能分析	123
第七章 非编码 RNA	135
第一节 非编码 RNA 概述	135
第二节 非编码 RNA 的分类	139
第三节 MicroRNA	142
第四节 CircRNA	150
第五节 其他小分子 RNA	154
第八章 蛋白质组学	161
第一节 蛋白质组学概述	161
第二节 蛋白质的大规模分离鉴定技术	165
第三节 蛋白质的翻译后修饰	173
第四节 蛋白质分选	174
第五节 蛋白质相互作用	177
第九章 新一代测序技术及其应用	186
第一节 测序技术概述	186
第二节 第二代测序原理	188
第三节 第二代测序技术的应用	194
第四节 生物信息学在第二代测序中的应用	198
第五节 生物信息学新技术与发展趋势	204
参考文献	210



项目批准号	32072714
申请代码	C170303
归口管理部门	
依托单位代码	51064208A0499-0932



国家自然科学基金委员会 资助项目计划书

资助类别：面上项目

亚类说明：

附注说明：

项目名称：环状RNA介导CNS1S1基因影响热应激奶牛乳腺 α s1-casein合成及机制研究

直接费用：58万元 执行年限：2021.01-2024.12

负责人：孙加节

通讯地址：广东省广州市天河区五山路483号

邮政编码：510642 电 话：13925158841

电子邮件：jiajiesun@scau.edu.cn

依托单位：华南农业大学

联系人：倪慧群 电 话：020-85280070

填表日期：2020年09月19日

国家自然科学基金委员会制



简表

项目负责人信息	姓 名	孙加节	性 别	男	出生年月	1984年09月	民 族	汉族
	学 位	博士			职称	副教授		
	是否在站博士后	否			电子邮件	jiajiesun@scau.edu.cn		
	电 话	13925158841			个人网页			
	工 作 单 位	华南农业大学						
	所 在 院 系 所	动物科学学院						
依托单位信息	名 称	华南农业大学					代码	51064208A0499
	联 系 人	倪慧群			电子邮件	kycjkh@scau.edu.cn		
	电 话	020-85280070			网站地址	http://kjc.scau.edu.cn/		
合作单位信息	单 位 名 称							
项目基本信息	项 目 名 称	环状RNA介导CNS1S1基因影响热应激奶牛乳腺 α s1-casein合成及机制研究						
	资 助 类 别	面上项目				亚 类 说 明		
	附 注 说 明							
	申 请 代 码	C170303:反刍动物遗传育种				C170102:畜禽遗传、营养与环境互作		
	基 地 类 别							
	执 行 年 限	2021.01-2024.12						
	直 接 费 用	58万元						



项目摘要

中文摘要:

热应激与乳蛋白合成密切相关, 应激发生时奶牛乳腺 α s1-酪蛋白编码基因CSN1S1表达显著下调, 但具体机制尚不清楚。前期比较热应激与限饲配对适温奶牛乳腺全转录组数据, 发现4个circRNAs竞争性结合miRNA参与CSN1S1上游调控。因此, 项目拟通过RNA酶耐受、FISH及核质分离qPCR分析候选circRNA分子特征、亚细胞定位与出核规律; 利用荧光素酶报告系统、circRNA pull-down与RIP明确候选circRNA调控网络构成; 以乳腺原代细胞为材料, 干扰或过表达候选circRNA并设计桥梁miRNA恢复与CSN1S1回补性实验, 揭示候选circRNA影响乳腺 α s1-酪蛋白合成的分子机制; 最后构建候选circRNA腺相关病毒载体, 在活体水平上模拟热应激并验证相关ceRNA网络调控乳蛋白合成的作用机理, 这对阐明乳蛋白合成机制具有重要意义, 可为热应激条件下改善乳品质提供理论依据。

Abstract:

Heat stress is closely related to lactoprotein synthesis in mammary glands of dairy cows, and high ambient temperature can retard the expression of CSN1S1 gene. However, little is known about how heat stress mediates biosynthesis of milk protein in cows. Recently, we performed transcriptome analysis of mammary glands of Holstein cows between heat stress and moderate temperature individuals, and the results showed that 4 circRNA candidates can be as competitive endogenous RNAs to mediate CSN1S1 expression in α s1-casein synthesis. Based on the our previous researches, we will validate the reality, intracellular location and expression of circRNA candidates using RNase R treated analysis, RT-qPCR and Fluorescence in situ hybridization (FISH). In addition, the composition of circRNA-associated network will be further validated by luciferase reporter gene assays, circRNA pull-down and RNA Binding Protein Immunoprecipitation (RIP), respectively. Next, the functionary mechanism of α s1-casein biosynthesis regulated by circRNA candidates will be determined by transfection of over-expression or siRNA recombinant vector, as well as miRNA recovery and CSN1S1 complementation experiments. Finally, with the adeno-associated viral vector of circRNA candidates, we will double-check the circRNA-involved α s1-casein biosynthesis in vitro with heat stress model. In summary, our study will clarify the regulatory mechanisms of milk protein synthesis, and also lead to a new theoretical basis for milk quality improvement under heat stress.

关键词(用分号分开): 功能基因组; 非编码RNA; 奶牛; 泌乳性状; 遗传与环境互作

Keywords(用分号分开): Functional genomics; Non-coding RNA; Dairy cow; Milk production traits; Genetic and environmental interaction

子课题编号: 2023ZD0404405-02

密 级: 公开

科技创新 2030—重大项目 子课题任务书

子课题名称	基于产业链数据的猪适应性性状基因组选择方法研究与应用
所属课题名称:	猪适应性分子设计育种技术研发与应用
所属重大项目:	农业生物育种重大项目
重大项目实施管理机构:	农业农村部科技发展中心
子课题承担单位:	华南农业大学 (公章)
子课题负责人:	孙加节
执行期限:	2023 年 9 月至 2025 年 12 月

中华人民共和国科学技术部制

2023 年 9 月

填 写 说 明

一、任务书甲方即课题主持单位，乙方即子课题承担单位。

二、任务书中的单位名称，请按规范全称填写，并与单位公章一致。

三、任务书中文字须用宋体小四号字填写。

四、凡不填写内容的栏目，请用“无”表示。

五、乙方完成任务书的填写，提交甲方审核确认后，用 A4 纸打印、签章后邮寄给甲方。

六、任务书一式八份报课题主持单位签章，其中子课题承担单位四份，课题主持单位四份。

七、《项目申报书》、《项目任务书》和《课题任务书》是本任务书填报的重要依据，任务书填报不得降低考核指标，不得自行对主要研究内容作大的调整。《项目申报书》、《项目任务书》、《课题任务书》和本任务书将共同作为课题过程管理、综合绩效评价（验收）和监督评估的重要依据。

子课题基本信息表

子课题名称		基于产业链数据的猪适应性性状基因组选择方法研究与应用			
子课题编号		2023ZD0404405-01			
所属课题名称		猪适应性分子设计育种技术研发与应用			
课题编号		2023ZD0404405			
所属重大项目		农业生物育种重大项目			
密级		<input checked="" type="checkbox"/> 公开 <input type="checkbox"/> 秘密 <input type="checkbox"/> 机密		单位总数	1
课题成果技术就绪度		<input type="checkbox"/> 1. 发现基本原理 <input type="checkbox"/> 2. 形成技术方案 <input type="checkbox"/> 3. 方案通过验证 <input type="checkbox"/> 4. 形成单元并验证 <input type="checkbox"/> 5. 形成分系统并验证 <input type="checkbox"/> 6. 形成原型并验证 <input type="checkbox"/> 7. 现实环境的应用验证 <input type="checkbox"/> 8. 用户验证认可 <input checked="" type="checkbox"/> 9. 得到推广应用			
课题成果应用的主要国民经济行业		畜牧学			
课题的社会经济目标		一级目标： 研发猪强适应性分子设计育种技术 二级目标： 服务国家畜禽种业振兴			
经费预算		子课题总经费根据概算批复结果核定，子课题年度经费按照项目任务书约定下达。配套经费不得低于项目任务书约定要求。			
课题周期节点		起始时间	2023 年 9 月	结束时间	2025 年 12 月
		实施周期	共 28 个月	预计中期时间点	2024 年 12 月
子课题承担单位	单位名称	华南农业大学		单位法定代表人姓名	薛红卫
	单位性质	大专院校		组织机构代码	124400004554165634
	单位主管部门	广东省教育厅		隶属关系	<input type="checkbox"/> 中央/ <input checked="" type="checkbox"/> 地方
	单位所属地区	广东省广州市		地市（市、自治州、盟）	广州市
	通信地址	广东省广州市天河区五山路483 号		邮政编码	510642
	单位开户名称	华南农业大学			
	开户银行（全称）	中国工商银行股份有限公司广州五山支行		汇入地点	广东省广州市
	银行账号	3602002609000310520		银行机构代码	102581000546

子课题负责人	姓 名	孙加节	性 别	<input checked="" type="checkbox"/> 男 <input type="checkbox"/> 女	出生日期	1984.09.06
	证件类型	身份证	证件号码	320923198409064814		
	所在单位	华南农业大学				
	最高学位	<input checked="" type="checkbox"/> 博士 <input type="checkbox"/> 硕士 <input type="checkbox"/> 学士 <input type="checkbox"/> 其他				
	职 称	<input type="checkbox"/> 正高级 <input checked="" type="checkbox"/> 副高级 <input type="checkbox"/> 中级 <input type="checkbox"/> 初级 <input type="checkbox"/> 其他			职务	无
	电子邮箱	jiajiesun@scau.edu.cn		移动电话	13925158841	
子课题联系人	姓 名	孙加节	电子邮箱	jiajiesun@scau.edu.cn		
	固定电话	020-85280547	移动电话	13925158841		
	证件类型	身份证	证件号码	320923198409064814		
课题财务负责人	姓 名	何颖婷	电子邮箱	he_yingting@163.com		
	固定电话	020-85280547	移动电话	15521059247		
	证件类型	身份证	证件号码	620104199410110841		
子课题参加人数	<u>2</u> 人。其中：		高级职称 <u>1</u> 人，中级职称 <u>0</u> 人，初级职称 <u>0</u> 人，其他 <u>1</u> 人；			
			博士学位 <u>2</u> 人，硕士学位 <u>0</u> 人，学士学位 <u>0</u> 人，其他 <u>0</u> 人。			
子课题简介 (限 500 字以内)	<p>当前国内外针对猪的环境适应性和一般抗病力性状的遗传改良缺乏可度量、可选育的表型性状，对于有时间维度的纵向表型数据缺乏高效的遗传评估模型，同时二元猪、三元猪等杂交后代的一般抗病力表型数据难以在纯种的遗传改良中应用。课题研究目标是研发出环境适应性和一般抗病力遗传评定技术，构建强适应性新品系分子设计育种体系，并开发基于多维数据预测的基因组选择方法、多群体多性状基因组联合评估方法以及强适应性基因组精准选配与遗传传递技术体系。通过适应性和一般抗病力性状功能位点的评价和应用、分子设计育种体系的模拟和构建等策略，利用基因组选择、基因编辑、基因免疫等技术手段对分子设计育种方案进行应用，加速实现强适应性猪的育种进程。</p>					

填表说明：1. 组织机构代码指企事业单位国家标准代码，单位若已三证合一请填写单位统一社会信用代码，无组织机构代码的单位填写“000000000”；
2. 单位公章名称必须与单位名称一致；
3. 单位开户名称应与单位名称一致，如有开户名称不一致等特殊情况，必须提供证明文件。

一、子课题目标及考核指标、评测方式/方法

（一）课题目标

课题总体目标是研发出猪强环境适应性和一般抗病力遗传评定技术，构建强适应性新品系分子设计育种体系，并开发基于多维数据预测的基因组选择新方法、多群体多性状基因组联合评估方法以及强适应性基因组精准选配与遗传传递技术体系。

（二）考核指标

1、课题目标及考核指标（2023–2025 年）

本子课题总体目标是研发猪强环境适应性和一般抗病力遗传评定技术 1 套；筛选出能够科学准确评价个体环境适应性和一般抗病力的新靶标 2-3 个，研发出猪强适应性育种技术 1-2 个；申请或获得发明专利 2-3 件，软件著作权 1-2 件；发表相关学术论文 3-5 篇。

2、课题中期目标及考核指标（截至 2024 年底）

初步筛选出能够科学准确评价个体环境适应性和一般抗病力的新靶标 2-3 个，申请或获得发明专利 1-2 件，软件著作权 1-2 件；发表相关学术论文 2-3 篇。

（三）预期标志性成果

研发出基于全产业链的猪强适应性育种技术 1-2 个，实现强适应性猪新品系的高效快速选育。

子课题目标、成果与考核指标表

子课题目标 ¹	成果名称	成果简述	成果类型	考核指标 ²					考核方式（方法）及评价手段 ⁴
				指标名称	立项时已有指标值/状态	立项时重点国别指标值/状态	中期指标值/状态 ³	完成时指标值/状态	
研发猪强环境适应性和一般抗病力遗传评定技术1套；筛选出能够科学准确评价个体环境适应性和一般抗病力的新靶标2-3个，构建强适应性新品系分子设计育种体系1套；申请或获得发明专利2-3件，软件著作权1-2件；发表相关学术论文3-5篇。	1: 猪强适应性新品系分子设计育种体系1套。	新分子设计育种技术体系专门用于强适应性基因组选育，可利用全产业链多维数据，实现对群体精准选育，加快猪强环境适应性和一般抗病力性状的选育。	<input checked="" type="checkbox"/> 新理论 <input type="checkbox"/> 新原理 <input type="checkbox"/> 新产品 <input checked="" type="checkbox"/> 新技术 <input type="checkbox"/> 新方法 <input type="checkbox"/> 关键部件 <input type="checkbox"/> 数据库 <input checked="" type="checkbox"/> 软件 <input type="checkbox"/> 平台 <input type="checkbox"/> 应用解决方案 <input type="checkbox"/> 实验装置/系统 <input type="checkbox"/> 临床指南/规范 <input type="checkbox"/> 加工工艺 <input type="checkbox"/> 标准 <input checked="" type="checkbox"/> 论文 <input checked="" type="checkbox"/> 发明专利 <input type="checkbox"/> 其他	指标 1.1 新分子标记	无	无	1	2	学术论文
				指标 1.2 基因组选配技术	无	无	1	1	专利受理通知书、专利证书或学术论文
				指标 1.3 软件著作权	无	无	1	1~2	软件著作权登记证书
				指标 1.5 国家发明专利	无	无	1	2	专利受理通知书或专利证书

备注：

1. “课题目标”，应从以下方面明确描述：（1）研发主要针对什么问题和需求；（2）将要解决哪些科学问题、突破哪些核心/共性/关键技术；（3）预期成果；（4）成果将以何种方式应用在哪些领域/行业/重大工程等，并拟在科技、经济、社会、环境或国防安全等方面发挥何种的作用和影响。（5）所列主要成果原则上不超过5项，如有其他重要成果放在“其他”成果中表述。
2. “考核指标”，指相应成果的数量指标、技术指标、质量指标、应用指标和产业化指标等，其中，数量指标可以为论文、专利、产品等的数量，论文代表作应注重质量，不以数量作为评价标准；技术指标可以为关键技术、产品的性能参数等；质量指标可以为产品的耐震动、高低温、无故障运行时间等；应用指标可以为成果应用的对象、范围和效果等；产业化指标可以为成果产业化的数量、经济效益等。同时，对各项考核指标需填写立项时已有的指标值/状态、课题完成时要到达的指标值/状态，以及立项时重点国别指标值/状态。同时，考核指标也应包括支撑和服务其他重大科研、经济、社会发展、生态环境

境、科学普及需求等方面的直接和间接效益。如对国家重大工程、社会民生发展等提供了关键技术支撑，成果转让并带动了环境改善、实现了销售收入等。若某项成果属于开创性的成果，立项时已有指标值/状态可填写“无”，若某项成果在立项时已有指标值/状态难以界定，则可填写“/”。

3. **“中期指标”**，各重大项目根据管理特点，确定是否填写，阶段目标明确的项目课题应填写中期指标。

4. **“考核方式方法”**，应提出符合相关研究成果与指标的具体考核技术方法、测算方法等。

5. **“科技报告类型”**，包括课题综合绩效评价（验收）前撰写的全面描述研究过程和技术内容的最终科技报告、课题年度或中期检查时撰写的描述本年度研究过程和进展的年度技术进展报告以及在课题实施过程中撰写的包含科研活动细节及基础数据的专题科技报告（如实验报告、试验报告、调研报告、技术考察报告、设计报告、测试报告等）。其中，每个课题在综合绩效评价（验收）前应撰写一份最终科技报告；研究期限超过2年（含2年）的项目，应根据管理要求，每年撰写一份年度技术进展报告；每个课题可根据研究内容、期限和经费强度，撰写数量不等的专题科技报告。科技报告应按国家标准规定的格式撰写。

6. **“公开类别及时限”**，公开课题科技报告分为公开或延期公开，内容需要发表论文、申请专利、出版专著或涉及技术诀窍的，可标注为“延期公开”。需要发表论文的，延期公开时限原则上在2年（含2年）以内；需要申请专利、出版专著的，延期公开时限原则上在3年（含3年）以内；涉及技术诀窍的，延期公开时限原则上在5年（含5年）以内。涉密课题科技报告按照有关规定管理。

二、课题研究内容、研究方法及技术路线

（一）课题的主要研究内容

拟解决的关键科学问题、关键技术问题，针对这些问题拟开展的主要研究内容，限1000字以内。

1. 拟解决的重大科学问题或关键技术问题

当前国内外针对猪的强环境适应性和一般抗病力性状的遗传改良缺乏可度量、可选育的表型性状，对于多维度的纵向表型数据缺乏高效的遗传评估模型，同时二元猪、三元猪等杂交后代的适应性表型数据难以在纯种的遗传改良中应用。

2. 主要研究内容

通过强环境适应性和一般抗病力性状功能位点的评价和应用、分子设计育种体系的模拟和构建等策略，利用基因组选择、基因编辑等技术对分子设计育种方案进行完善和应用，以加速实现强适应性猪的育种进程。主要研究内容如下：

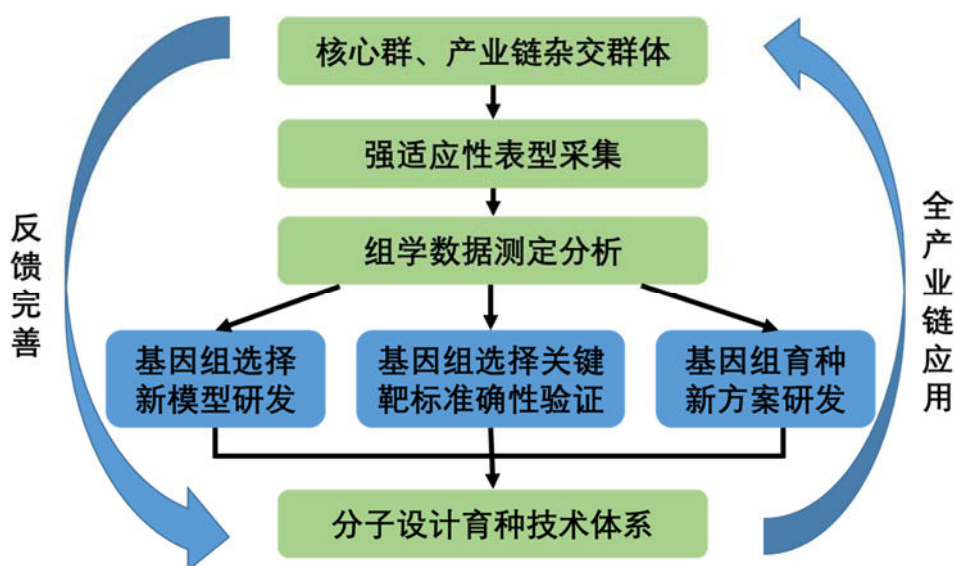


图1 子课题技术路线图

（1）通过测定特定性能纯种地方猪群与商品化杂交群体耐高温高湿、低氧、抗病等多种环境适应性表型，血常规参数（白细胞相关性状、红细胞相关性状以及血小板相关性状）、免疫细胞亚群、免疫与抗氧化等细胞因子、抗体水平等血清性状，个体物质与能量代谢指标，初步获得育种群体多种环境适应性和一般抗病力表型组学数据，结合群体基因组学数据，通过相关性整合分析等方法筛选出能够科学精准评价个体环境适应性的新指标，系统研发基于多维数据的基因组选择模型，实现对纵向数据的高效率利用。

(2) 基于不同育种群体及个体表型组学数据，以显著差异群体或个体特定组织与细胞类型为研究对象，结合微生物组学，代谢组学，转录组学、单细胞组学、修饰组学及现代分子生物学技术，从环境-基因-代谢-免疫轴出发，深入解析关键功能基因及调控网络对猪免疫等特定细胞类型发生与形成的影响及内在决定机制，通过进一步构建基因编辑动物或基因免疫的方法，检测基因缺失/激活对于目标组织或细胞及性状的调控，多层次分析目的基因的育种价值。

(二) 课题采取的研究方法

针对课题研究拟解决的问题，拟采用的方法、原理、机理、算法、模型等，限 1000 字以内。

(1) 结合表型组、基因组重测序、单细胞测序和高通量染色体构象捕获技术等，利用卷积神经网络、随机森林等深度学习方法进行多组学大数据的整合分析，准确鉴定影响猪适应性的 SNP、InDels 和 SV 等各类基因组变异。

(2) 采用多基因编辑和基因免疫技术实现猪适应性性状的多基因快速高效聚合，在群体水平，检测基因的遗传变异，并分析其对于目标性状的遗传效应；在细胞水平，基于功能获得和功能失活等常用的基因功能研究策略，利用基因过表达、基因干扰以及基因敲除技术，并结合下游的转录谱和表型分析完成候选基因功能验证；在个体水平，通过构建基因编辑动物，检测基因缺失/激活对于目标性状的调控；综合群体、细胞及个体水平的分析，对基因的育种价值进行评价。

三、主要创新点

围绕基础前沿、共性关键技术或应用示范等层面，简述课题的主要创新点。具体内容应包括该项创新的基本形态及其前沿性、时效性等，并说明是否具备方法、理论和知识产权特征。每项创新点的描述限 500 字以内。

创新性提出了应用以深度学习方法为代表的新一代人工智能技术构建针对猪适应性性状的全基因组选择新模型。新模型实现了首次将猪的适应性性状表型和多组学大数据应用到基因组选择遗传评估模型的计算中，多维度大数据的整合利用，有助于高效、精准的从全基因组位点中遴选潜在的功能基因和关键调控互作通路，实现了信息导向的数据精准降维，有效避免了常规基因组评估模型存在的有效信息丢失；新模型通过人工智能方法中的深度网络结构建立了“表型—基因型”的因果解析机制，通过互作网络中的

关键因子有效解释了表型、基因型和环境等多源信息间的复杂交互关系，与常规线性模型相比显著提高了模型的可解释性。新模型有望大幅提高适应性性状的遗传评估准确性，并加快适应性性状的遗传改良效率。

四、预期经济社会效益

课题的科学、技术、产业预期指标及科学价值、社会、经济、生态效益。限 500 字以内。

本课题以破解我国种业“卡脖子”技术、缺乏节粮耐粗饲猪重大新品系为导向，研究应用节粮耐粗饲表型精准测定技术、基因组选择技术、大数据智能 AI 育种技术等前沿生物育种技术，筛选科学精准的节粮耐粗饲育种新性状，构建针对性的表型数据库，遴选节粮耐粗饲性状的科学评价指标，科学评价相关的功能位点和分子遗传调控机制，深入研究精准的节粮性状的选种、选配和遗传传递体系，培育符合我国产业需求的节粮耐粗饲猪新品系，有效提高我国生猪的环境适应性和饲料利用效率，提升我国生猪产业的生产效率。

本课题强一般抗病力猪新品系的培育，能够满足我国当前生猪产业对猪抗病力新品系或配套系的产业重大需求，加快强一般抗病力新品系培育的速度和效率，为我国未来生猪产业的健康发展童工品种资源保障，加快实现我国的核心种源自主可控；另一方面课题能够加快我国猪的抗病力和生长、繁殖等重要经济性性状选育提升，加快繁殖性能、生长速度和肉质等重要经济性性状的改良，尤其是实现抗病力、适应性的大幅度提升，进而大幅提升我国生猪产业的生产效率和国际竞争力，降低生猪业的饲料能源消耗，加快满足老百姓对优质、健康和廉价猪肉产品的需求。同时，生猪生产性能的提升，能够大幅度缩短出栏日龄，减少饲料、疫苗和人工成本消耗，显著减少猪只的粪污及二氧化碳排放量，长远来看具有突出的社会生态效益。

五、课题年度计划

按每 6 个月制定形成课题的计划进度，应将课题的考核指标分解落实到年度计划中。

1、年度：2023 年 9 月—2023 年 12 月

任务：开展强环境适应性和一般抗病力评价新表型挖掘的研究。

考核指标：初步挖掘科学精准表型 1 个或以上。

成果形式：试验技术报告。

2、年度：2024 年 1 月—2024 年 6 月

任务：进一步研究强适应性评价表型指标，研究针对适应性性状的基因组选择靶标。

考核指标：基因组选择靶标 2-3 个。

成果形式：专利申请书或发表的学术论文。

3、年度：2024 年 7 月—2024 年 12 月

任务：基因组选择新模型的研发和基因组选配技术的研发。

考核指标：基因组选择或选配新模型 1 个。

成果形式：专利申请书或发表的学术论文。

4、年度：2025 年 1 月—2025 年 6 月

任务：强环境适应性和一般抗病力性状的基因组选择靶标功能验证。

考核指标：基因组选择理论机制 1 套或以上。

成果形式：专利申请书或发表的学术论文。

5、年度：2025 年 7 月—2025 年 12 月

任务：持续进行基因组选择新模型的研究，进行遗传评估和技术推广。

考核指标：开发遗传评估软件 1 个。

成果形式：软件著作权或发表的学术论文。

六、课题组织实施机制及保障措施

1、课题的内部组织管理方式、协调机制等，限 500 字以内。

课题负责人主要职责和工作机制如下：1、负责课题整体技术方案的制定及调整，做好实施进度和完成质量的全程管控，明确节点任务目标和考核指标，确保课题进度与计划匹配；2、负责对课题与单位承担任务完成进度的把控与指导；3、负责组建课题执行小组，根据课题实施情况，有权对课题参与单位、经费预算等提出调整建议以及对参与人员或团队提出奖惩建议；4、有权查阅课题技术、财务等文档资料，查验配套经费落实情况、配套研发试验条件 and 生产条件支撑能力和质量；5、课题负责人所在单位应支持其开展相关工作；6、课题负责人和项目负责人共同负责组织课题的年度、中期考核和结题考核，负责协调项目与课题、课题与课题之间的协调管理，负责建立课题内部的共性技术与资源共享机制、共性技术难题联合攻关机制、相关成果知识产权共享共用机制、人才人员互动协作机制等多项保障机制，统筹协调各个子课题研究任务的推进。

2、课题实施的相关政策，已有的组织、技术基础，支撑保障条件，限 500 字以内。

2021 年 12 月，习近平总书记在中央经济工作会议上强调，越是有粮食吃，越要想到没粮食的时候。中国人的饭碗任何时候都要牢牢端在自己手中，决不能在吃饭这一基本生存问题上让别人卡住我们的脖子。粮食安全首先是种业安全。习近平总书记指出，农业现代化，种子是基础，多次强调下决心把民族种业搞上去，抓紧培育具有自主知识产权的优良品种，从源头上保障国家粮食安全。2020 年中央经济工作会议和 2021 年中央一号文件都明确要“打好种业翻身仗”：对育种基础性研究以及重点育种项目给予长期稳定支持；深入实施农作物和畜禽良种联合攻关；实施新一轮畜禽遗传改良计划和现代种业提升工程。同时，国家高度重视种业领域的科技发展，2021 年出台了《种业振兴行动方案》。本课题研究内容符合政策相关要求，具有较好的政策支撑条件。

本课题将严格按照国家相关管理规定进行科学的项目管理，建立健全组织协调机制，注重完善协同创新管理体系和相应规章制度，将建立课题技术小组，专门负责课题的管理协调组织。本课题主要参加单位包括国内优势种猪育种企业 1 家和高校 3 所，其中的高校和科研院所在技术、人才等方面各有显著优势，形成了从基础研究、技术开发、产业应用、技术推广构成的多层次、多领域的人才团队和雄厚的技术力量，可为课题实施提供良好的组织保障和实施平台。

3、对实现项目总目标的支撑作用，及与项目内其他课题的协同机制，限 500 字以内。

由于我国地域广阔，长期以来引进猪种适应性差、抗病力低，导致种猪生产潜能不能充分发挥，生产效率低、成本高，严重制约了我国生猪产业发展。强一般抗病力猪新品系培育课题，是有针对性的培育适应我国产业需求的抗病力猪新品系特色猪新品系，通过建立多性状多群体的纵向时间维度基因组选择评估进行多世代高强度选育，并利用基因组选择等多项前沿技术培育出强一般抗病力猪群体。该课题的实施着眼生猪育种未来的产业方向，提前布局我国生猪产业未来发展需求，不但可以大幅提高我国种猪在国际市场上的核心竞争力，而且同时可以形成国际领先的育种技术，打造高效繁育技术体系，对实现重大项目的总体目标具有重要的支撑作用。

七、知识产权对策、成果管理及合作权益分配

限 500 字以内。

本课题依据中华人民共和国《科技进步法》、《促进科技成果转化法》、《专利法》、

《著作权法》等法律及《国务院关于深化中央财政科技计划（专项、基金等）管理改革的方案》、《教育部 科技部关于加强高等学校科技成果转移转化工作的若干意见》等国家科技计划相关管理规范政策，明确知识产权保护、成果管理和合作权益分配。本课题参加单位在本课题实施之前所获得的知识产权及相应权益均归各自所有。课题执行过程中，各参加单位取得的研究成果和相关的知识产权归各单位所有，但课题承担单位有权因非商业目的和课题研究需求（如：以政府性会议、报告、技术文件、统计资料、原始数据等）使用参加单位项目相关信息和数据资料，在课题执行期间进行知识产权共享；参加单位合作产生的研究成果和相关知识产权归双方或多方共有，依各方在成果中的实际分工和贡献大小署名和分配权益。

实行重要成果报告制度，实施过程中取得重要成果时，承担单位应及时填写重要成果报告表，并逐级向课题组、项目管理办公室以及相关管理机构报告。实行重要成果管理制度。重要成果产生后，需要对外宣传发布的，承担单位应及时填写国家科技计划重大成果发布申请表，并按计划管理渠道经计划管理机构汇总审核后向成果管理机构申请；未能安排发布的科研成果，经成果管理机构同意后，课题承担单位可自行发布；未向计划管理机构申报，并未经成果管理机构同意，课题承担单位不得自行发布。

八、需要约定的其他内容

限 500 字以内。

无。

九、课题参加人员基本情况表


填表说明： 1、专业技术职称：A、正高级 B、副高级 C、中级 D、初级 E、其他； 2、投入本课题的全时工作时间（人月）是指在课题实施期间该人总共为课题工作的满月度工作量；累计是指课题组所有人员投入人月之和； 3、课题固定研究人员需填写人员明细； 4、是否有工资性收入：Y、是 N、否； 5、人员分类代码： B、课题负责人 C、项目/课题骨干 D、其他研究人员； 6、工作单位：填写单位全称，其中高校要具体填写到所在院系。														
序号	姓名	性别	出生日期	证件类型	证件号码	专业技术职称	职务	最高学位	专业	投入本课题的全时工作时间（人月）	人员分类代码	在课题中分担的任务	是否有工资性收入	工作单位
1	孙加节	男	1984.09.06	身份证	320923198409064814	B	无	博士	动物遗传学	9	C	子课题负责人	Y	华南农业大学动物科学学院
2	何颖婷	女	1994.10.11	身份证	620104199410110841	E	无	博士	动物遗传育种与繁殖	18	D	参与人	Y	华南农业大学动物科学学院
固定研究人员合计										27	/	/	/	/
流动人员或临时聘用人员合计										0	/	/	/	/
累计										27	/	/	/	/

任务书签署

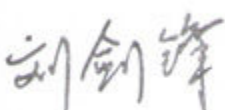
甲乙双方根据《国务院印发关于深化中央财政科技计划（专项、基金）管理改革方案的通知》（国发〔2014〕64号）、《国务院关于优化科研管理提升科研绩效若干措施的通知》（国发〔2018〕25号）、《国务院办公厅关于改革完善中央财政科研经费管理的若干意见》（国办发〔2021〕32号）、《科学技术活动违规行为处理暂行规定》（科学技术部令第19号）、《科技部 财政部关于印发〈中央财政科技计划（专项、基金等）监督工作暂行规定〉的通知》（国科发政〔2015〕471号）、《科技部 自然科学基金委关于进一步压实国家科技计划（专项、基金等）任务承担单位科研作风学风和科研诚信主体责任的通知》（国科发监〔2020〕203号）、《科技部、财政部、自然科学基金委关于进一步加强统筹国家科技计划项目立项管理工作的通知》（国科办资〔2022〕107号）等有关文件规定，以及有关法律、政策和管理要求，依据项目立项通知，签署本任务书。

同时，本单位和课题负责人郑重承诺：对本课题所有成果产出（包括但不限于新产品、新技术、标准、论文、专利等）的真实性、与项目（课题）的关联性等负责，将按要求落实科研作风学风和科研诚信主体责任；课题经费全部用于与本课题研究工作相关的支出，不截留、挪用、侵占，不用于与科学研究无关的支出；接受并积极配合相关部门的监督检查。如有违反，本单位和课题负责人以及相关成果产出者愿接受项目管理专业机构和相关部门做出的各项处理决定，包括但不限于终止课题执行、追回课题经费，取消一定期限国家科技计划项目（课题）申报资格，记入科研诚信严重失信行为数据库以及主要负责人接受相应党纪政纪处理等。

课题牵头承担单位（甲方）：中国农业大学

法定代表人签字（签章）：

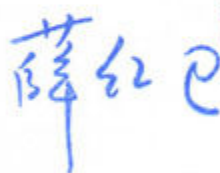


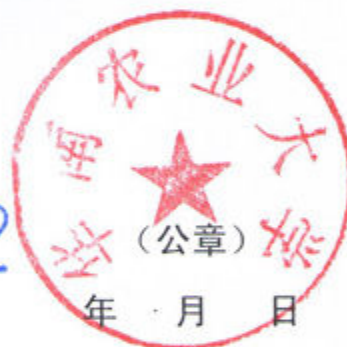
课题负责人签字（签章）：

23年12月22日

子课题承担单位（乙方）：华南农业大学

法定代表人签字（签章）：





子课题负责人签字（签章）：



23年12月20日

子课题编号: 2023ZD0404405-02

密级: 公开

科技创新 2030—重大项目 子课题年度预算书

子课题名称:	基于产业链数据的猪适应性性状基因组选择方法研究与应用
所属课题名称:	猪适应性分子设计育种技术研发与应用
所属重大项目:	农业生物育种重大项目
重大项目实施管理机构:	农业农村部科技发展中心
子课题承担单位:	华南农业大学 (公章)
子课题负责人:	孙加节
课题预算期间:	2023 年 9 月至 2024 年 6 月

中华人民共和国科学技术部制

2023 年 9 月

课题承担单位基本情况表

表 A1

填表说明：1. 组织机构代码指企事业单位国家标准代码，单位若已三证合一请填写单位统一社会信用代码，无组织机构代码的单位填写“000000000”； 2. 单位公章名称必须与单位名称一致； 3. 单位开户名称应与单位名称一致，如有开户名称不一致等特殊情况，必须提供证明文件。					
课题牵头单位	单位名称	华南农业大学			
	单位性质	大专院校			
	单位主管部门	广东省教育厅	隶属关系	■地方	
	单位组织机构代码	124400004554165634			
	单位法定代表人姓名	薛红卫			
	单位开户名称	华南农业大学			
	开户银行（全称）	中国工商银行股份有限公司广州五山支行	汇入地点	广东省广州市	
	银行账号	3602002609000310520	银行机构代码	102581000546	
	单位所属地区	广东省	地市 (市、自治州、盟)	广州市	
	电子邮箱	dongkekeyan@scau.edu.cn			
	通信地址	广东省广州市天河区五山路 483 号			
邮政编码	510642				
相关责任人	子课题负责人	姓名	孙加节		
		身份证号码	320923198409064814		
		工作单位	华南农业大学		
		电话号码	020-85280547	手机号码	13925158841
		电子邮箱	jiajiesun@scau.edu.cn	邮政编码	510642
		通信地址	广东省广州市天河区五山路 483 号		
	子课题联系人	姓名	孙加节		
		电话号码	020-85280547	手机号码	13925158841
		传真号码	020-85280547		
		电子邮箱	jiajiesun@scau.edu.cn		
	子课题财务负责人	姓名	何颖婷		
		身份证号码	620104199410110841		
		电话号码	020-85280547	手机号码	15521059247
		电子邮箱	he_yingting@163.com		

子课题预算表（2023-2024 年）

表 B1 子课题编号：02 子课题名称：基于产业链数据的猪适应性性状基因组选择方法研究与应用
金额单位：万元

序号	预算科目名称	金额
	(1)	(2)
1	一、中央财政专项资金	78.00
2	（一）直接费用	68.00
3	1. 设备费	0
4	其中：购置设备费	0
5	2. 业务费	52.40
6	3. 劳务费	15.60
7	（二）间接费用	10.00
8	二、其他来源资金	0
9	三、合计	78.00

注：1、间接费用无需编制预算说明；2、绩效支出在间接费用中无比例限制。承担单位在统筹安排间接费用时，要处理好合理分摊间接成本和对科研人员激励的关系，绩效支出安排与科研人员在课题工作中的实际贡献挂钩。

设备费——购置/试制设备预算明细表（2023-2024 年）

表 B2 子课题编号：02 子课题名称：基于产业链数据的猪适应性性状基因组选择方法研究与应用 金额单位：万元

填表说明：1. 设备分类：购置、试制； 2. 购置设备类型：通用、专用； 3. 试制设备不需填列本表（9）列、（10）列、（11）列、（12）列； 4. 设备单价的单位为万元/台套，设备数量的单位为台套； 5. 单价 50 万元以下的设备不用填写。 6. 本表只填写中央财政资金购置（试制）的设备												
序号	设备名称	设备分类	功能和技术指标	单价	数量	金额	购置或试制单位	安置单位	购置设备类型	主要生产厂 家及国别	规格型号	拟开放共享 范围
	(1)	(2)	(3)	(4)	(5)	(6)	(7)	(8)	(9)	(10)	(11)	(12)
单价 50 万元以上购置设备合计							/	/	/	/	/	/
单价 50 万元以上试制设备合计							/	/	/	/	/	/
累计							/	/	/	/	/	/

课题单位经费预算明细表（2023-2024 年）

表 B3 子课题编号：02 子课题名称：基于产业链数据的猪适应性性状基因组选择方法研究与应用 金额单位：万元

填表说明：1. 单位类型分课题承担单位、课题参与单位； 2. 组织机构代码指企事业单位国家标准代码，单位若已三证合一请填写单位统一社会信用代码，无组织机构代码的单位填写“000000000”。										
序号	单位名称	组织机构代码-统一社会信用代码		单位类型	任务分工	研究任务负责人	合计	中央财政资金		其他来源资金
		小计	其中：间接费用							
	(1)	(2)	(3)	(4)	(5)	(6)	(7)	(8)	(9)	(10)
1	华南农业大学	124400004554165634		课题参与单位	基于产业链数据的猪适应性性状基因组选择方法研究与应用	孙加节	78.00	78.00	10.00	0.00
累计							78.00	78.00	10.00	0.00

预算说明

一、中央财政资金

预算的编制要坚持任务相关性、政策相符性和经济合理性，实事求是编制提出课题预算。填报时，直接费用应按设备费、业务费、劳务费三个类别填报，每个类别结合科研任务按支出用途进行说明。除 50 万元以上的设备外，其他费用只提供基本测算说明，不需要提供明细。

1. **设备费**（是指项目实施过程中购置或试制专用仪器设备，对现有仪器设备进行升级改造，以及租赁外单位仪器设备而发生的费用等。计算类仪器设备和软件工具可在设备费科目编列。填报时，50 万元以上的设备详细说明，50 万元以下的设备费用分类说明）

无。

2. **业务费**（是指在项目实施过程中消耗的各种材料、低值易耗品等、发生的测试化验加工、燃料动力、出版文献、信息传播、知识产权事务、会议、差旅、国际合作与交流以及其他与项目实施直接相关的各项费用。编报时，对单笔大额支出、对外委托支出重点说明）

本年度课题业务费用共计 **52.40 万元**，其中材料费 16.00 万元，测试化验加工费 28.00 万元，燃料动力费 1.50 万元，出版费和知识产权事务费 1.90 万元，差旅与国际交流合作费 5.00 万元。具体预算如下：

2.1 材料费：16.00 万元

在项目执行过程中需要对特定群体全程跟踪测定，以收集完整的纵向数据，并将该数据用于构建新的基因组选择新模型。同时对于重要的功能位点在使用多组学数据进行挖掘后需要进行相应的实验验证。经过验证的位点将用于芯片。实施过程中需要消耗各种基因组、转录组等提取实验耗材以及相关涉及基因表达研究等的实验耗材。

（1）实验动物样本采集及提取检测试剂费：8.679 万元

本课题需要对群体进行组织或者血样采集，采集后的样本进行后续基因组、转录组等多组学测序。以上工作均涉及组织和血液等样本 DNA 和 RNA 提取、纯化及检测相关试剂，包括动物基因组提取试剂盒、基因组纯化试剂盒、琼脂糖凝胶纯化回收试剂盒、DNA Ladder、RNA 提取试剂盒和 Trizol 等，共计 8.679 万元。见表 3-1。

表 3-1 实验动物样本采集及提取检测试剂费用明细

名称	规格	单价 (元)	数量	金额 (万元)
动物组织基因组提取试剂盒	盒	980.00	20	1.96
血液 DNA 提取试剂盒	盒	1200.00	10	1.20
琼脂糖凝胶纯化回收试剂盒	盒	2900.00	10	2.90
组织 RNA 提取试剂盒	盒	1800.00	3	0.54
血液 RNA 提取试剂盒	盒	1600.00	3	0.48
Trizol (Invitrogen, 200 mL)	瓶	2500.00	3	0.75
250 bp DNA Ladder	50T	90.00	3	0.027
100 bp DNA ladder	250 mg/支	1500.00	3	0.45
1 kb DNA Ladder	250 mg/支	800.00	3	0.24
Agarose 琼脂糖	100 g	440.00	3	0.132
合计				8.679

(2) 基因表达分析及功能验证所需试剂：4.72 万元

主要用于将筛选得到的重要功能基因开展表型检测及分子机制研究，主要包括反转录试剂盒、RNAase 抑制剂、Supper II 反转录酶、SMART RACE cDNA Amplification 试剂盒、SYBR Green PCR Master Mix 和 Western Blotting 试剂盒及相关抗体等，共计 4.72 万元。见表 3-2。

表3-2 基因表达分析及功能验证相关试剂费用明细

名称	规格	单价 (元)	数量	金额 (万元)
100 次反转录试剂盒	盒	1000.00	2	0.20
RNAase 抑制剂 (1 mL)	支	800.00	2	0.16
Supper II 反转录酶 (Invitrogen, 50 次)	支	1800.00	2	0.36
M-MLV 逆转录酶 (Invitrogen)	支	2300.00	1	0.23
Smart race cDNA Amplification 试剂盒	盒	2500.00	1	0.25
cDNA 第一链合成试剂盒 (50 次)	盒	4000.00	2	0.80
SYBR Green qPCR Mix	盒	4000.00	1	0.40
SYBR Premix Ex Tap (Perfect Real Time)	盒	1800.00	1	0.18
Western 制胶试剂盒	盒	400.00	5	0.20
Western 及 IP 裂解液	支	200.00	5	0.10
蛋白 Marker	支	500.00	3	0.15

Western 封闭液	瓶	200.00	1	0.02
一抗	支	3000.00	2	0.60
二抗	支	500.00	1	0.05
Western 转膜液	瓶	200.00	5	0.1
Western 显色液	瓶	200.00	1	0.02
超敏 ECL 化学发光盒	支	1000.00	1	0.1
ELISA 试剂盒	盒	2500.00	2	0.5
细胞凋亡试剂盒	盒	3000.00	1	0.3
合计				4.72

(3) 分子生物学操作常用化学试剂及耗材：2.601 万元

分子生物学实验中常用化学试剂，主要包括无水乙醇、苯酚等，实验耗材，主要包括细胞培养板、细胞培养瓶、离心管、枪头、乳胶手套等，共计 2.601 万元。见表 3-3。

表 3-3 分子生物学操作常用化学试剂

名称	规格	单价（元）	数量	金额（万元）
无水乙醇	瓶	15	10	0.015
苯酚	瓶	50	10	0.05
异丙醇	瓶	40	5	0.02
氯仿	瓶	40	10	0.04
细胞培养板	箱	1000	5	0.5
细胞培养瓶	箱	1000	5	0.5
Eppendorf 1.5 ml、2 ml 离心管	箱	800	5	0.4
Eppendorf 10ul、20ul、100ul、1000ul 枪头	箱	800	5	0.4
乳胶手套	箱	600	5	0.3
液氮	45L/罐	/	/	0.376
合计				2.601

2.2 测试化验加工费：28 万元

需要进行环境适应性和一般抗病力性状功能位点的挖掘和鉴定，并采用分子设计育种的方法将重要的功能位点导入到选育群体中，从而形成新的强一般抗病力的新品系。此外，本课题还需要对于选育群体的一般抗病力表型情况进行数据采集与处理，构建用于持续性选育的参考群，以辅助本课题对新品系进行快速选

育。涉及到表型测定、基因组测序、免疫指标的测定以及 SNP 芯片检测和评估计算等工作，为保证质检与测试的精准性和高效性，需委托专业技术检测公司或利用学校仪器设备共享平台开展，具体预算如下：

（1）全基因组测序费用：4.50 万元

本课题需要对适应性和一般抗病力性状功能位点进行挖掘，预计对 60 头个体的基因组与血液生化指标、免疫指标等进行整合分析，挖掘重要功能位点。每个个体测序数据量为 50GB，每 GB 数据费用 15.00 元/GB，合计为 $50\text{GB}/\text{头} \times 15\text{元}/\text{GB} \times 60\text{头} = 4.50\text{万元}$ 。

（2）转录组测序费用：3.60 万元

本课题对 60 头个体的血液进行转录组测序，平均每个样品 600 元，合计为 $600\text{元}/\text{头} \times 60\text{头} = 3.60\text{万元}$ 。

（3）单细胞测序费用：6.00 万元

需要对 6 个显著差异个体血液等组织细胞类型进行鉴定，平均每个样品 10000 元，合计为 $10000\text{元}/\text{头} \times 6\text{头} = 6.00\text{万元}$ 。

（4）血液性状、免疫及抗氧化细胞因子、抗体水平等重要指标的测定：9.00 万元

血液性状、免疫与抗氧化细胞因子、抗体水平可以反应群体所处的健康状况和所具有的抗病能力，需要测定 60 个个体的细胞因子、免疫因子等免疫指标，单个个体测定费用预计为 1500 元/个，合计为 $1500\text{元}/\text{个} \times 60\text{个} = 9.00\text{万元}$ 。

（5）高性能计算费：1.40 万元

在课题执行过程中，需要对多组学数据进行分析，共需 14 万核时，费用为 0.10 元/核时，共计 $14\text{万核时} \times 0.10\text{元}/\text{核时} = 1.40\text{万元}$ 。

（6）纵向数据基因组选择模型的开发与计算：2.00 万元

本课题将设计行程一个新的基于全套纵向数据的基因组选择新模型，该模型的开发费用预计为 0.5 万元，测试所需核时预计为 15 万核时，费用为 0.10 元/核时，合计为 2.0 万元。

（7）高性能数据存储费：1.50 万元

课题实施过程中会产生大量数据，需租赁高性能服务器进行遗传数据存储。本年度存放数据需求为 10TB，每 TB 存储每年费用 1500.00 元，共计为 $1500.00\text{元}/\text{TB}/\text{年} \times 10\text{TB} = 1.50\text{万元}$ 。

2.3 燃料动力费：1.50 万元

用于项目执行过程中所耗用的燃料、电力、水等费用，合计 1.50 万元。

2.4 出版费及知识产权事务费：1.90 万元

专利申请代理费 0.50 万元，论文版面费 1.0 万元，合计 1.90 万元。

2.5 差旅及与国际交流合作费：5.00 万元

主要用于采集样品、往返实验室和猪场，共计 50 人次，当天返还，平均每人每次 300 元，共计 1.50 万元；项目实施过程中技术交流和学术研讨等差旅费，本年度出差 5 人次，平均往返路费 3000 元/人次，按照《中央和国家机关工作人员赴地方差旅住宿费标准明细表》（财行[2016]71 号），平均住宿费、注册费、伙食补助等，每人每次 2000 元，共计 2.50 万元；其他专家接送等市内交通费，共计 1.00 万元。

3. 劳务费（是指在项目实施过程中支付给参与项目的研究生、博士后、访问学者以及项目聘用的研究人员、科研辅助人员、科研（财务）助理等的劳务性费用；支付给临时聘请的咨询专家的费用等。项目聘用人员由单位缴纳的社会保险补助、住房公积金等可纳入劳务费列支。）

劳务费用：15.60 万元。主要用于支付参与该项目的博士后、研究生、聘用科研（财务）助理及临时工作人员等劳务费用。具体预算如下：

3.1 本项目在本年度执行期间，共需 2 名博士生和 2 名硕士生，每人投入 5 月。博士研究生 1000.00 元/月×2 人×10 月/人=2.00 万元；硕士研究生 500.00 元/月×2 人×10 月/人=1.00 万元。合计 3.00 万元。

3.2 项目聘用科研（财务）助理 1 名，本年度每人投入 6 月，按每月 5000.00 元/月标准支付，合计为 5000 元/月×1 人×6 月/人=3.00 万元。

3.3 本项目在本年度执行期间，需要 1 名博士后人员，本年度每人投入 10 月，按每月 8000.00 元/月标准支付，合计为 8000 元/月×1 人×10 月/人=8.00 万元。

3.4 项目执行期间涉及大量项目相关种猪屠宰、种猪饲养、性能测定、妊娠观察、仔猪护理、血样和组织样本采集及初生重、日增重、繁殖数据采集等工作，共需聘请临时工协助完成，预计需要 1.60 万元。

4. 间接费用

本课题间接经费 10.00 万元。主要用于在项目组织实施过程中发生的无法由直接费用中列支的相关费用。主要包括承担单位为项目研究提供的现有仪器设备

及房屋占有费、日常水电气暖消耗费、有关管理费用及科研人员绩效支出等。

二、其他来源资金（包括地方财政资金、单位自筹资金、社会资本等渠道资金）


对其他来源资金主要用途、支出预算做简要说明。

无。

子课题年度经费预算签章页

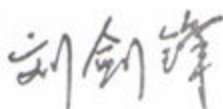
课题承担单位（甲方）：中国农业大学

法定代表人签字（签章）：





课题负责人签字：



23年12月20日

子课题承担单位（乙方）：华南农业大学

法定代表人签字（签章）：





子课题负责人签字（签章）：



23年12月20日

课题编号：2022YFD1300905

密 级：公开

国家重点研发计划 课题任务书

课题名称：牛羊木本源饲料应用及高效转化关键技术研究

所属项目：木本源新型蛋白饲料加工与高效转化技术

所属专项：畜禽新品种培育与现代牧场科技创新

项目牵头承担单位：贵州大学

课题承担单位：中国科学院亚热带农业生态研究所

课题负责人：李铁军

执行期限：2022 年 12 月 至 2026 年 06 月

中华人民共和国科学技术部制

2022 年 11 月 28 日

0003YF 2022YFD1300905 2022-11-28 17:44:36



九、课题参加人员基本情况表

填表说明： 1. 专业技术职称：A、正高级 B、副高级 C、中级 D、初级 E、其他；
2. 投入本课题的全时工作时间（人月）是指在课题实施期间该人总共为课题工作的满月度工作量；累计是指课题组所有人员投入人月之和；
3. 课题固定研究人员需填写人员明细；
4. 是否有工资性收入：Y、是 N、否；
5. 人员分类代码：B、课题负责人 C、项目/课题骨干 D、其他研究人员；
6. 工作单位：填写单位全称，其中高校要具体填写到所在院系。

序号	姓名	性别	出生日期	证件类型	证件号码	专业技术职称	职务	最高学位	专业	投入本课题的全时工作时间（人月）	人员分类代码	在课题中分担的任务	是否有工资性收入	工作单位
1	李铁军	男	1967-11-22	身份证	430111196711220416	正高级	无	博士	动物生产与兽医类	24	课题负责人	课题设计，精准饲喂	是	中国科学院亚热带农业生态研究所
2	刘勇	男	1986-08-03	身份证	511623198608035397	副高级	无	博士	农业资源与自然科学	24	课题骨干	肉品质的干预	是	中国科学院亚热带农业生态研究所
3	汤少勋	男	1972-09-10	身份证	430802197209104918	副高级	无	博士	动物生态营养	24	课题骨干	蛋白质消化代谢	是	中国科学院亚热带农业生态研究所
4	孙加节	男	1984-09-06	身份证	320923198409064814	副高级	无	博士	动物遗传学	24	课题骨干	负责任务 2，营养消化代谢	是	华南农业大学动物科学学院
5	左建军	男	1976-08-01	身份证	433127197608011016	正高级	副系主任	博士	动物营养与饲料科学	24	课题骨干	营养品质评定	是	华南农业大学动物科学学院
6	孙宝丽	女	1981-09-24	身份证	411024198109241823	副高级	无	博士	动物营养与饲料科学	24	课题骨干	牛乳品质干预	是	华南农业大学动物科学学院



课题预算表

表B1 课题编号： 2022YFD1300905 课题名称： 牛羊木本源饲料应用及高效转化关键技术研究 金额单位： 万元

序号	预算科目名称	金额
	(1)	(2)
1	一、中央财政专项资金	450.00
2	（一）直接费用	347.00
3	1. 设备费	
4	其中：购置设备费	
5	2. 业务费	289.70
6	3. 劳务费	57.30
7	（二）间接费用	103.00
8	二、其他来源资金	
9	三、合计	450.00

注：1. 间接费用无需编制预算说明；2. 绩效支出在间接费用中无比例限制。承担单位在统筹安排间接费用时，要处理好合理分摊间接成本和对科研人员激励的关系，绩效支出安排与科研人员在课题工作中的实际贡献挂钩。



课题单位经费预算明细表

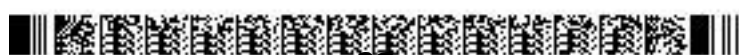
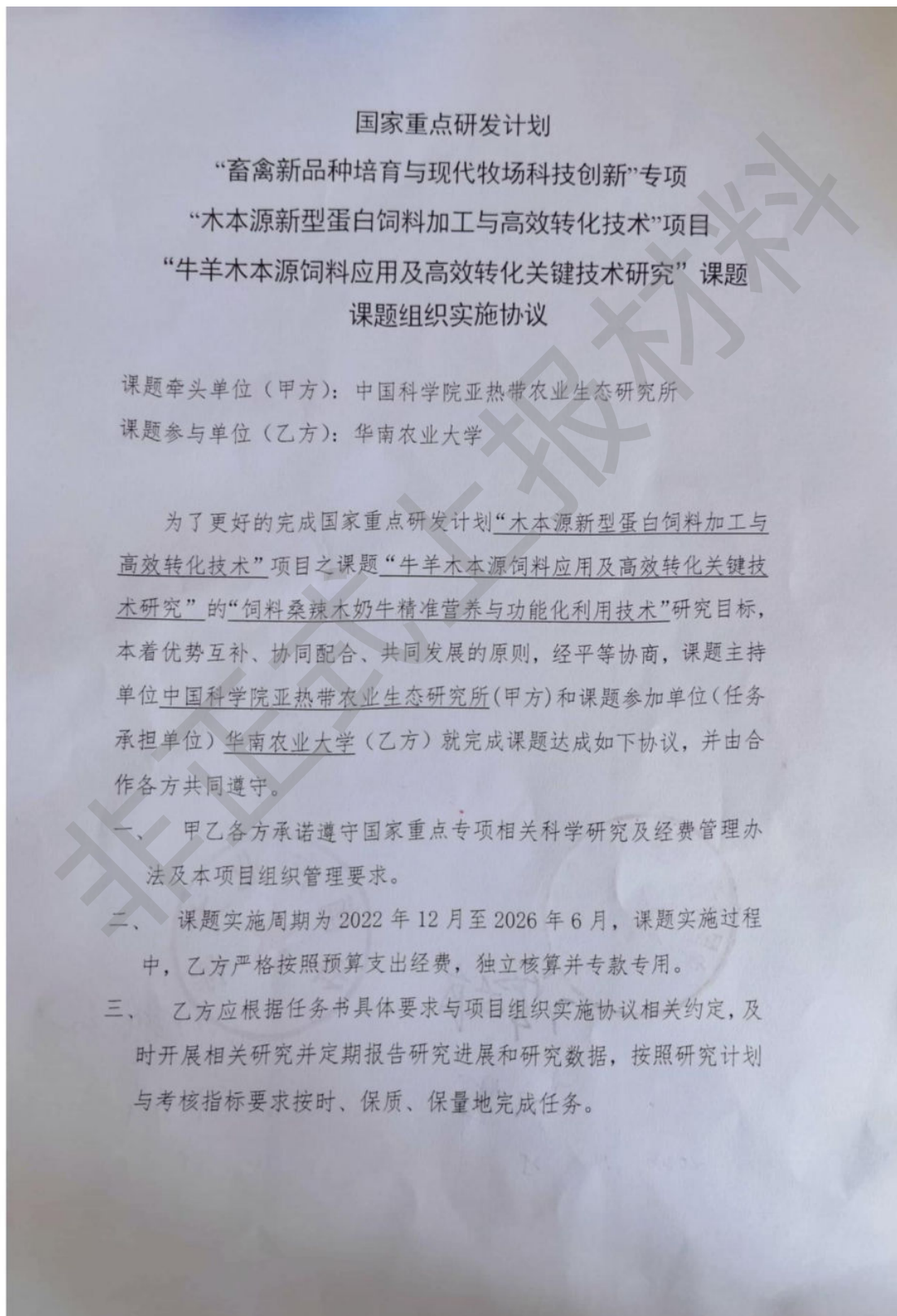
表B3 课题编号： 2022YFD1300905 课题名称： 牛羊木本源饲料应用及高效转化关键技术研究 金额单位：万元

填表说明：1.单位类型分课题承担单位、课题参与单位； 2.组织机构代码指企事业单位国家标准代码，单位若已三证合一请填写单位统一社会信用代码，无组织机构代码的单位填写“000000000”。										
序号	单位名称	组织机构代码-统一社会信用代码		单位类型	任务分工	研究任务负责人	合计	中央财政专项资金		其他来源资金
		(2)	(3)					小计	其中：间接费用	
	(1)	(2)	(3)	(4)	(5)	(6)	(7)	(8)	(9)	(10)
1	中国科学院亚热带农业生态研究所	统一社会信用代码	12100000717807303X	课题承担单位	饲料桑辣木肉牛肉羊精准营养与功能化利用技术	李铁军	200.00	200.00	45.00	
2	华南农业大学	统一社会信用代码	124400004554165634	课题参与单位	饲料桑辣木奶牛精准营养与功能化利用技术	孙加节	100.00	100.00	23.00	
3	宁夏大学	统一社会信用代码	1264000045400005H	课题参与单位	柠条肉牛肉羊精准营养与功能化利用技术	张桂杰	150.00	150.00	35.00	
累计							450.00	450.00	103.00	



十一、相关附件

1. 乙方与参加单位有关协议（须加盖乙方与参加单位公章、法人签字签章；协议文件须扫描上传。如无参加单位，则不填）；



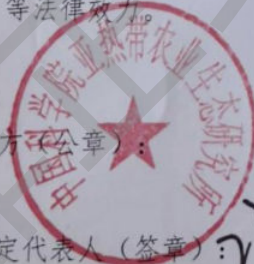
四、 如乙方在执行过程中出现研究进展严重滞后、研究方案的重大改动、经费不合理开支等方面的情形，应及时上报给项目及课题组织单位，以便及时采取应对措施。

五、 课题获批国拨专项经费 450 万元，其中乙方 100 万元。乙方的任务分工、考核指标如下表：

研究任务名称	负责人	国拨经费(万元)	主要任务	考核指标
饲料桑辣木奶牛精准营养与功能化利用技术	孙加节	100	构建奶牛饲料桑辣木蛋白质、氨基酸、纤维素等营养数据库。比较研究奶牛对辣木与豆粕蛋白利用差异，揭示其消化代谢特征；重点开展奶牛对辣木“全混合型”与“精粗料配比型”日粮蛋白转化研究，建立豆粕减量替代节粮型饲料配方及饲养技术，并示范推广。通过风味物质筛选，建立优质风味牛乳的敏感参数，探讨辣木对牛乳关键风味物质干预规律，开发基于辣木的优质牛乳木本源资源调控技术。	构建节粮型饲料配制与高效饲喂技术体系2套以上；制定标准或规程1项；授权发明专利1件；发表/接受论文2-3篇；培养研究生2-3名；技术就绪度达到9级。

六、 本协议自各方盖章（签字）之日起生效，有效期至项目结题验收结束。协议一式6份，甲方保留3份，乙方保留3份，具有同等法律效力。

甲方（公章）：



乙方（公章）：



法定代表人（签章）：

李铁军

法定代表人（签章）：

刘雅红

课题负责人（签章）：

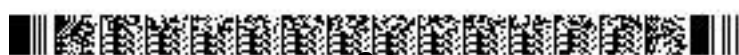
李铁军

任务负责人（签章）：

刘雅红

2022年11月25日

2022年11月25日



项目牵头承担单位（甲方）：

法定代表人签字（签章）：

李宝安



项目负责人签字（签章）：

杨富裕

2022年12月20日

课题承担单位（乙方）：

法定代表人签字（签章）：

谭文良



课题负责人签字（签章）：

李铁军

2022年12月20日



受理编号: c20140500000725

项目编号: 2020A1515010062

文件编号: 粤基金字(2020)4号

广东省基础与应用基础研究基金项目

合同书

项目名称: CircLIMCH1 相关ceRNA网络调控猪骨骼肌纤维发育的机制研究

项目类别: 广东省自然科学基金-面上项目

项目起止时间: 2019-10-01 至 2022-09-30

管理单位(甲方): 广东省基础与应用基础研究基金委员会

依托单位(乙方): 华南农业大学

通讯地址: 广东省广州市天河区五山路483号

邮政编码: 510642

单位电话: 020-85283435

项目负责人: 孙加节

联系电话: 02085280547



(广东科技微信公众号)

广东省基础与应用基础研究
基金委员会
二〇一九年制



(受理纸质材料二维码)

一、主要研究内容和要达到的目标

1、主要研究内容

(1) circLIMCH1克隆及出核规律研究

前期研究发现存在circLIMCH1→miR-423-5p→HDAC4调控网络影响猪肌纤维发育过程。由于circRNAome-Seq分析结果存在假阳性，同时circRNA功能发挥也依赖于其细胞定位，位于胞液中的circRNA主要发挥竞争性内源RNA的作用。因此，首先针对circLIMCH1拼接位点，设计特异性Divergent引物，结合T载体测序确定circLIMCH1是否真实成环并克隆全长序列；进一步根据全长序列设计荧光原位杂交探针，在猪骨骼肌卫星细胞增殖分化不同时间点对候选circLIMCH1进行定位，结合核质分离RT-qPCR技术明确目标circLIMCH1出核规律。

(2) circLIMCH1与miR-423-5p靶向验证及互作研究

前期研究证实miR-423-5p可以通过与HDAC4的3' UTR序列结合调控HDAC4基因表达。因此，在circLIMCH1→miR-423-5p→HDAC4调控网络中，circLIMCH1是否作为竞争性内源RNA发挥对miR-423-5p的吸附调控作用，关键在于候选circRNA与miR-423-5p之间是否存在直接靶向关系。因此，首先利用RT-PCR技术扩增候选circLIMCH1序列中与miR-423-5p互补部分，构建候选circRNA野生型和突变型双荧光素酶重组载体，并与miR-423-5p共转染，通过检测荧光活性初步确定候选circLIMCH1与miR-423-5p是否存在靶向关系。进一步利用RNA纯化染色质分离技术(ChIP)鉴定候选circRNA是否与miR-423-5p结合，将biotin标记的miR-423-5p转染猪骨骼肌卫星细胞，利用链霉亲和素磁珠分离与miR-423-5p结合的mRNA，RT-qPCR检测分离物中是否存在目标circRNA。此外，由于AGO2蛋白是miRNA调控靶基因表达的必需中间组分，因此可利用RNA免疫共沉淀技术(RIP)，将与AGO2蛋白互作的RNA沉淀下来，再对其进行定量分析，即可确定与miR-423-5p互作的目标circRNA，从侧面证明miR-423-5p是否受候选circLIMCH1调控。

(3) circLIMCH1作为ceRNA调控猪肌纤维发育机制研究

构建目标circLIMCH1过表达及干扰腺病毒载体，包装病毒，感染猪骨骼肌卫星细胞，并进行细胞增殖培养与诱导分化。EdU法检测细胞增殖情况；流式细胞术检测细胞周期；qRT-PCR、Northern blot及Western blot用于mRNA和蛋白水平检测，检测基因包括细胞周期相关基因Cyclin D和Cyclin E，肌分化标志基因Pax7、MEF2C、MyoG、MyoD和MSTN，肌纤维类型相关基因NFAT、PGC-1 α 、MyHC1、MyHC2a、MyHC2x和MyHC2b。同时设计功能拯救实验，过表达目标circLIMCH1同时添加miR-423-5p的mimics，干扰目标circRNA同时添加miR-423-5p的inhibitor，观察肌细胞增殖分化情况，最终明确候选circLIMCH1作为ceRNA参与miR-423-5p调控猪肌纤维发育的分子机制。

2、研究目标

本课题以miRNA上游调控机制为出发点，探究候选circLIMCH1作为竞争性内源RNA对miR-423-5p的上游吸附调控方式，明确miR-423-5p相关ceRNA调控网络的构成及影响猪肌纤维发育的分子机制，从环状RNA层面填补猪骨骼肌发育研究领域的一些科学数据，为猪遗传改良和优质高效生产提供新思路。

二、研究成果及形式

论文及专著情况	国家统计源刊物以上刊物 发表论文（篇）		2		科技报告（篇）		1	
	专著（册）		0					
专利情况(项)	发明专利		实用新型专利		外观设计专利		国外专利	
	申请	授权	申请	授权	申请	授权	申请	授权
	2	0	0	0	0	0	0	0

三、项目进度和阶段目标

1. 项目起止时间： 2019-10-01 至 2022-09-30		
2. 项目实施进度及阶段主要目标：		
开始日期	结束日期	主要工作内容
2019-10-01	2020-09-30	(1) circLIMCH1验证及全长克隆； (2) circLIMCH1肌细胞FISH定位及出核规律研究。
2020-10-01	2021-09-30	(1) 利用荧光素酶报告基因、ChiRP及RIP技术验证miR-423-5p与circLIMCH1的靶向关系； (2) 构建circLIMCH1过表达和干扰腺病毒载体及病毒包装； (3) 发表SCI学术论文1篇。
2021-10-01	2022-09-30	(1) 候选circLIMCH1对猪骨骼肌卫星细胞增殖、分化及肌纤维类型转化的影响； (2) 设计miR-423-5p功能拯救实验，解析circLIMCH1作为ceRNA参与miR-423-5p调控猪肌纤维发育机制； (3) 参加全国性学术会议1人次；撰写结题报告，发表SCI论文1篇。

五、人员信息

项目负责人

姓名	证件号码	年龄	性别	职称	学历	在项目中承担的任务	所在单位	签名
孙加节	320923198409064814	36	男	副教授	博士研究生	项目负责人	华南农业大学	孙加节

项目组主要成员

姓名	证件号码	年龄	性别	职称	学历	在项目中承担的任务	所在单位	签名
王翀	420111196802135020	52	男	教授	博士研究生	实验指导	华南农业大学	王翀
陈婷	430426198312192147	37	女	讲师	博士研究生	CircRNA克隆、细胞定位及出核规律研究	华南农业大学	陈婷
罗君谊	440103199302262426	27	女	实验员	博士研究生	实验准备与样品保存	华南农业大学	罗君谊
曾斌	43110319911130571X	29	男	未取得	硕士研究生	双荧光素酶靶基因验证、ChiRP及RIP分析	华南农业大学	曾斌
谢月琴	522224199410110824	26	女	未取得	硕士研究生	RT-qPCR、Northern blot及Western blot分析	华南农业大学	谢月琴
汪东阳	342623199605025373	24	男	未取得	硕士研究生	细胞培养与转染	华南农业大学	汪东阳

六、依托单位与合作单位的合作协议

承担/参与单位名称 (盖章)	工作分工	总经费分摊 (万元)	省基金委经费分配 (万元)
华南农业大学		10.00	10.00
	合计	10.00	10.00

七、合同条款

第一条 甲方与乙方根据《中华人民共和国合同法》及国家有关法规和规定，为顺利完成（2020）年 CircLIMCH1 相关ceRNA网络调控猪骨骼肌纤维发育的机制研究 专项项目（文件编号： 粤基金字〔2020〕4号）经协商一致，特订立本合同，作为甲乙双方在项目实施管理过程中共同遵守的依据。

第二条 甲方的权利义务：

1. 按合同书规定进行经费核拨的有关工作协调。
2. 根据甲方需要，在不影响乙方工作的前提下，定期或不定期对乙方项目的实施情况和经费使用情况进行检查或抽查。
3. 根据《广东省科技计划项目信用管理办法(试行)》对乙方进行科技计划信用管理。

第三条 乙方的权利义务：

1. 确保落实自筹经费及有关保障条件。
2. 乙方是项目资金管理的责任主体，应当建立健全科研项目资金管理制度，严格按照省科技经费使用范围和有关规定管好用好财政资金；应当按合同书规定，对甲方核拨的经费实行专款专用，单独列账，并随时配合甲方进行监督检查。
3. 实施“包干制”的面上项目及青年基金项目，依托单位应参照国家杰出青年科学基金试点项目经费使用“包干制”要求，制定经费使用“包干制”内部管理规定。项目经费支出应实际用于研发活动相关支出，使用范围限于设备费、材料费、测试化验加工费、燃料动力费、差旅/会议/国际合作与交流费、出版/文献/信息传播/知识产权事务费、劳务费、专家咨询费、依托单位管理费用、绩效支出以及其他合理支出。依托单位管理费用由依托单位根据实际管理支出情况与项目负责人协商确定。绩效支出由项目负责人根据实际科研需要和相关薪酬标准自主确定，依托单位按照现行工资制度进行管理。其余用途经费无额度限制，由项目负责人根据实际需要自主决定使用。项目验收时应提交经费决算表。
4. 项目负责人是项目资金使用的直接责任人，对资金使用的合规性、合理性、真实性和相关性承担法律责任。
5. 使用财政资金采购设备、原材料等，按照《广东省实施〈中华人民共和国招标投标法〉办法》有关规定，符合招标条件的须进行招标。
6. 项目合同任务完成后，或合同书规定的任务、指标及经费投入等提前完成的，乙方可按照《广东省省级科技计划项目结题管理实施细则（试行）》提出验收结题申请，并按甲方要求做好项目验收结题工作。
7. 若项目发生需要终止结题的情况，乙方须按照《广东省省级科技计划项目结题管理的实施细则（试行）》提出终止结题申请，并按甲方要求做好项目终止结题工作。
8. 在每年规定时间内向甲方如实提交上年度工作情况报告，报告内容包含上年度项目进展情况、经费决算和取得的成果等。
9. 按照国家和省有关规定，提交科技报告及其他材料。
10. 利用甲方的经费获得的研究成果，项目负责人和参与者应当注明获得“广东省基础与应用基础研究基金（英文：Guangdong Basic and Applied Basic Research Foundation）（项目编号）”资助或作有关说明。

11. 乙方要恪守科学道德准则，遵守科研活动规范，践行科研诚信要求，不得抄袭、剽窃他人科研成果或者伪造、篡改研究数据、研究结论；不得购买、代写、代投论文，虚构同行评议专家及评议意见；不得违反论文署名规范，擅自标注或虚假标注获得科技计划（专项、基金等）等资助；不得弄虚作假，骗取科技计划（专项、基金等）项目、科研经费以及奖励、荣誉等；不得有其他违背科研诚信要求的行为。

12. 确保本项目开展的研究工作符合我国科研伦理管理相关规定。

第四条 在履行本合同的过程中，如出现广东省相关政策法规重大改变等不可抗力情况，甲方有权对所核拨经费的数量和时间进行相应调整。

第五条 在履行本合同的过程中，当事人一方发现可能导致项目整体或部分失败的情形时，应及时通知另一方，并采取适当措施减少损失，没有及时通知并采取适当措施，致使损失扩大的，应当就扩大的损失承担责任。

第六条 本项目技术成果的归属、转让和实施技术成果所产生的经济利益的分享，除双方另有约定外，按国家和广东省有关法规执行。

第七条 根据项目具体情况，经双方另行协商订立的附加条款，作为本合同正式内容的一部分，与本合同具有同等效力。

第八条 本合同一式三份，各份具有同等效力。甲、乙方及项目负责人各执一份，三方签字、盖章后即生效，有效期至项目结题后一年内。各方均应负合同的法律责任，不应受机构、人事变动的影响。

第九条 乙方必须接受甲方聘请的本项目合同监理单位的监督和管理。监理单位按照甲方赋予的权利对本项目合同的履行进行审核、进度调查，对项目合同变更、经费使用情况进行监督管理及组织项目验收。

说明：1. 本合同书中，凡是当事人约定无需填写的内容，应在空白处划（/）。

2. 委托代理人签订本合同书的，应出具合法、有效的委托书。

八、本合同签约各方

管理单位（甲方）：广东省基础与应用基础研究基金委员会（盖章）

法定代表人（或法人代理）：（签章）

年 月 日

依托单位（乙方）：华南农业大学（盖章）

法定代表人（或法人代理）：刘雅红（签章）

联系人（项目主管）姓名：郑鹏（签章）

Email: kjcgxk@scau.edu.cn

电话：020-85283435 / 13560344902

开户单位名称：华南农业大学

开户银行名称：广东广州工行五山支行

开户银行帐号：3602002609000310520

2019年3月29日

联系人（项目负责人）姓名：孙加节

（签名）

Email: jiajiesun@scau.edu.cn

电话：02085280547

2019年3月19日

项目编号：2018B020203002

广东省重点领域研发计划项目 子课题任务书

课题名称：新一代瘦肉型种猪育种技术研究

项目名称：新一代瘦肉型种猪育种技术与品种（品系）创建

项目来源：广东省重点领域研发计划项目

课题承担单位：华南农业大学

课题负责人：刘德武

子课题名称：猪肌纤维类型转化关键 circRNA 鉴定及功能研究

子课题承担单位：华南农业大学

子课题负责人：孙加节

项目执行期限：2019.01.01--2021.12.31

二零一九年一月

填写说明

- 1、任务书为课题验收的依据，其各项内容应尽可能详细填写。
- 2、课题任务的目标要强调形成主导品种（产品、装备）、主推技术、重要标准（规程规范）、决策支持方案、知识产权等；考核指标应具体、量化、可考核。
- 3、经费的使用应严格按有关经费管理办法执行。
- 4、本协议书要求用 A4 纸、正文小四号宋体、双面打印并装订。
- 5、任务书填报不得降低考核指标，不得自行对主要研究内容作大的调整。
- 6、任务书正式文本一式 2 份。项目牵头承担单位和子课题承担单位各 1 份。

一、研究任务目的和意义简述

1、研究目的：

以 miRNA 上游调控机制为出发点，探究候选 circRNA 作为竞争性内源 RNA 对 miRNA 的上游吸附调控方式，明确 miRNA 相关 ceRNA 调控网络的构成及影响猪肌纤维发育的分子机制，从环状 RNA 层面填补猪骨骼肌发育研究领域的一些科学数据，为猪遗传改良和优质高效生产提供新思路。

2、研究意义

生猪产业是我国畜牧业的支柱产业，猪肉产品是城乡居民肉类消费的主要来源。目前，国内商品猪主要是从国外引进的瘦肉型猪种及其杂交后代，引进品种具有生长速度快，胴体瘦肉率及饲料转化率高等优点；但与我国地方猪种相比，猪应激能力与肉品质却显著降低。近年来，随着消费者对猪肉品质要求越来越高，亟需改善肉质，培育优质肉猪。因此，开展猪优良品种选育，培育出具有中国特色的优良猪种，符合当前国情。

猪肉品质与肌纤维类型密切相关，瘦肉型长白猪与脂肪型蓝塘猪肌纤维类型存在明显差异。前期结合长白猪和蓝塘猪背最长肌 mRNAome、circRNAome 及 miRNAome 测序数据，通过整合基因组学的方法初步构建猪肌发育调控网络，发现存在候选 circRNAs 可能作为竞争性内源 RNA 参与肌肉发育过程。因此课题拟首先通过克隆测序、FISH、核质分离 RT-qPCR 技术明确候选 circRNA 是否真实成环、亚细胞定位及出核规律；利用荧光素酶报告基因、ChiRP 及 RIP 技术验证 miRNA 与候选 circRNA 的靶向关系；以猪骨骼肌卫星细胞为材料，过表达或干扰候选 circRNA 并设计 miRNA 拯救实验，确定候选 circRNA 作为 ceRNA 所调控的网络构成及影响猪肌纤维发育的分子机制，这不仅对阐明肌肉发育这一生命现象具有重要意义，还可以为优质肉猪选育提供理论依据。

二、任务研究主要内容（详细说明研究任务的主要内容，并明确要重点解决的主要技术难点和问题）

1、研究内容：

(1) 候选 circRNA 克隆及亚细胞定位研究。首先针对 circRNA 拼接位点，设计特异性 Divergent 引物，结合 T 载体测序确定候选 circRNA 是否真实成环并克隆目标 circRNA 全长序列；进一步根据全长序列设计荧光原位杂交 (Fluorescence in Situ Hybridization, FISH) 探针，在猪骨骼肌卫星细胞增殖分化不同时间点对候选 circRNA 进行定位，结合核质分离 RT-qPCR 技术明确目标 circRNA 是否存在出核现象并研究其表达规律。

(2) 候选 circRNA 作为 ceRNA 调控猪肌纤维发育机制研究。构建目标 circRNA 过表达及干扰腺病毒载体，包装病毒，感染猪骨骼肌卫星细胞，并进行细胞增殖培养与诱导分化。EdU 法检测细胞增殖情况；流式细胞术检测细胞周期；qRT-PCR、Northern blot 及 Western blot 用于 mRNA 和蛋白水平检测，检测基因包括细胞周期相关基因 Cyclin D 和 Cyclin E，肌分化标志基因 Pax7、MEF2C、MyoG、MyoD 和 MSTN，肌纤维类型相关基因 NFAT、PGC-1 α 、MyHC1、MyHC2a、MyHC2x 和 MyHC2b。同时设计功能拯救实验，过表达目标 circRNA 同时添加 miRNA 的 mimics，干扰目标 circRNA 同时添加 miRNA 的 inhibitor，观察肌细胞增殖分化情况，最终明确候选 circRNA 作为 ceRNA 参与 miR-423-5p 调控猪肌纤维发育的分子机制。

2、主要技术难点和问题：

近年来随着人们对 miRNA 功能研究的深入，相关 miRNA 在肌增殖、分化及凋亡等生命过程中的作用被不断揭示，但 miRNAs 自身又是通过什么方式被调控的，尤其在猪骨骼肌发育过程中相关 miRNA 上游是否存在调节分子？到目前为止还鲜有报道，近期相关报道已表明，miRNA 上游存在竞争性内源 RNA，可通过竞争性抑制 miRNAs 与靶基因 mRNA 3' UTR 的结合，发挥对 miRNAs 和靶基因的调控作用。本项目主要解决以下两个关键问题。候选 circRNA 作为 miRNA 上游竞争性内源 RNA 的验证及特征分析；CircRNA 网络调控猪肌纤维发育的作用机制。

三、研究任务总体目标及年度考核指标		
总体目标	阐明 miRNA 调控猪肌纤维发育的 ceRNA 网络及分子机制； 在本领域权威期刊发表论文 2 篇以上； 申报国家发明专利 2 项；	
年度	年度目标	考核指标
2019 年 1 月-12 月	(1) 候选 circRNA 验证及全长克隆； (2) 候选 circRNA 肌细胞 FISH 定位及出核规律研究；	候选 circRNA 克隆及亚细胞定位。
2020 年 1 月-12 月	(1) 利用荧光素酶报告基因、ChiRP 及 RIP 技术验证 miRNA 与候选 circRNA 的靶向关系； (2) 构建目标 circRNA 过表达和干扰腺病毒载体及病毒包装；	候选 circRNA 与 miRNA 靶关系验证。申报专利 1 件, 发表论文 1 篇。
2021 年 1 月-12 月	(1) 候选 circRNA 对猪骨骼肌卫星细胞增殖、分化及肌纤维类型转化的影响； (2) 设计 miRNA 功能拯救实验, 解析候选 circRNA 作为 ceRNA 参与 miRNA 调控猪肌纤维发育机制；	揭示候选 circRNA 作为 ceRNA 调控猪肌纤维发育机制。申报专利 1 件, 发表论文 1 篇。

四、主要考核指标（具体、量化）（可根据实际要求增加项目）	
解决的关键问题或技术难点	miRNA 调控猪肌纤维发育的 ceRNA 网络及分子机制
主要技术指标	
主要新产品	
标准制定	
论文发表（注明 SCI 论文）	发表科技论文 2 篇（其中 SCI 1 篇）
专利申报	申报发明专利 2 件
中试生产线	
研发平台建设	
人才队伍建设	培养研究生 1 人
推广应用	
经济、社会、生态效益	
年度进展报告、中期检查报告、验收总结报告	
其 他	

五、参加人员名单								
	姓名	单位	身份证号	性别	专业	职称/职务	责任分工	电话
主持人	孙加节	华南农业大学	320923198409064814	男	动物生物化学	副教授	主持	13925158841
主要参加人员	谢月琴	华南农业大学	522224199410110824	女	动物生物化学	无	细胞培养	1834165424
	汪东阳	华南农业大学	342623199605025373	男	动物营养与饲料科学	无	候选 circRNA 功能验证	18819268297
通讯地址：广东省广州市天河区五山路 483 号								
邮编：510642								

六、经费预算表

预算科目名称	合计 (万元)	中央财政资金 (万元)	单位自有资金 (万元)
一、经费支出			
（一）直接费用	30	30	0
1、设备费	7.8	7.8	0
（1）购置设备费	7.8	7.8	0
（2）试制设备费	0	0	0
（3）设备改造与租赁费	0	0	0
2、材料费	12.0	12.0	0
3、测试化验加工费	0.3	0.3	0
4、燃料动力费	0	0	0
5、差旅费	3.0	3.0	0
6、会议费	0.6	0.6	0
7、国际合作与交流费	0	0	0
8、出版/文献/信息传播/知识产权事务费	0.9	0.9	0
9、劳务费	5.4	5.4	0
10、专家咨询费	0	0	0
11、其它支出			
（二）间接费用	0	0	0
其中：绩效支出	0	0	0
二、经费来源			
（一）申请从专项经费获得的资助	30.0	30.0	0
（二）自筹经费来源	0	0	0
1、地方财政拨款	0	0	0
2、单位自有货币资金	0	0	0
3、其他资金	0	0	0
合计	30.0	30.0	0

七、共同条款

签约各方共同遵守《关于改进加强中央财政科研项目和资金管理的若干意见》（以下简称《意见》）、《财政部 科技部关于调整国家科技计划和公益性行业科研专项经费管理办法若干规定的通知》（以下简称《通知一》）、《财政部 科技部关于中央财政科技计划管理改革过渡期资金管理有关问题的通知》（以下简称《通知二》）、《关于国家重点研发计划重点专项预算管理有关规定（试行）的通知》（以下简称《通知三》）等文件的有关规定。

1. 课题经费要专款专用，不得挪作它用。经费的使用要严格按照《意见》、《通知一》、《通知二》和《通知三》的有关规定执行。若经费超支，由乙方自筹解决，但不得因此影响项目的执行。

2. 甲方根据《意见》、《通知一》、《通知二》和《通知三》经费开支的规定，监督乙方经费的使用情况。

3. 课题执行过程中，乙方如需调整任务，应根据《意见》、《通知一》、《通知二》和《通知三》中有关规定，向甲方提出变更内容的申请报告，经甲方审核后逐级上报项目管理部门、项目组织部门审定后实施。

4. 乙方因某种原因（如：与可行性研究内容有出入、挪用经费、技术措施或某些条件不落实）致使计划无法执行，并要求中止任务，应视不同情况，部分或全部退还所拨经费；若乙方没有提出中止任务的要求，甲方根据调查情况有权提出中止任务的处理建议，经上报项目管理部门、项目组织部门批准后执行。

5. 乙方因不可抗力不能履行协议书规定的工作内容时，应及时通知甲方，并在合理期间内出具不能履行的证明。

6. 乙方应保证课题任务主持人及主要承担人员的稳定，不得随意调换；如确需调换，应征得甲方同意，否则，由于人员安排问题造成课题任务不能正常实施，其损失由乙方负责，本课题任务按撤销处理。

7. 合作各方根据在合作期间所获取的成果，包括论文、专著、专利以及鉴定、成果报道等均须注明 广东省重点领域研发计划 2018-2019 年度“精准农业”重点专项项目计划资助及项目编号。

8. 本协议书签订各方均负有相应责任。若有争议或纠纷时，按照《意见》、《通知一》、《通知二》和《通知三》有关条款处理。

八、任务合同书签约各方

课题承担单位（甲方）：华南农业大学



单位负责人签字（签章）：

刘雅红

2019年10月20日

课题负责人签字（签章）：

刘德武

2019年10月20日

子课题承担单位（公章）：华南农业大学



单位负责人签字（签章）：

刘雅红

2019年10月20日

子课题负责人签字（签章）：

刘德武

2019年10月20日

项目编号： 202002030037

广州市科技计划项目 合同书

项目名称： LncRNA竞争性结合miR-21调控MSTN在猪肌纤维类型转化中的分子机制

计划类别： 基础研究计划

专题名称： 基础与应用基础研究项目

起止时间： 2020年04月01日 至 2022年03月31日

承担单位： 华南农业大学

组织单位： 华南农业大学

责任处室： 基础研究处

填表日期： 2020年04月09日

广州市科学技术局制
(2019年版)

填写说明

一、本合同书的项目编号由市科学技术局（以下简称“市科技局”）统一确定。

二、本合同书由申报书在后台自动转换生成，如有错漏之处需修正，请联系市科技局项目责任处室退回承担单位修正。

三、项目经费管理试点实行“包干制”。经费分为直接费用和间接费用。

（一）直接费用是指在项目研究过程中发生的与之直接相关的费用。直接经费支出不设科目比例限制。

（二）间接费用是指项目承担单位在组织实施项目过程中发生的无法直接列支的相关费用，主要用于补偿项目承担单位为了项目研究提供的现有仪器设备及房屋，水、电、气、暖消耗，有关提高科研管理、服务能力等费用，以及绩效支出等。间接经费根据市级财政科研项目资金管理办法按不超过直接经费扣除设备费后的一定比例核定。

（三）项目经费不得列支基建费。

（四）实行项目负责人承诺制，承诺项目经费用于项目研究支出。

（五）项目结题验收时提交经费决算表。

（六）组织对试点单位和项目监督检查，对发现问题的及时督促整改，对违反相关规定的作出处理或移送有关机关处理。

四、本项目如涉及多家（包含两家）单位参加，乙方应在签订本合同书前与合作单位就任务分工、经费和知识产权分配等问题签订有关合同或协议（仅委托其他单位进行常规试验、提供社会化科技服务和少量辅助科研工作的情况除外），作为本合同书的附件。

五、项目承担单位是在广州市行政区域内设立、登记、注册的具有独立法人资格的企业、高校、科研院所等机构。高等院校、科研院所不具备独立法人资格的二级单位不得作为项目承担单位。

六、项目组织单位是指项目承担单位的上级主管部门。项目组织单位包括广州市各区科技行政主管部门，以及其他经市科学技术局同意作为项目组织单位的行政事业单位、企业集团、高等院校、科研院所等。除经市科学技术局同意或科技计划类别另有规定的外，项目组织单位为项目承担单位注册地所属的区科技行政主管部门。

七、项目基本信息表中单位特性指项目承担单位的资质或获得的称号，如高新技术企业、软件企业、技术先进型服务企业、创新型企业、科技小巨人企业等。单位类型按以下类型填写：高等院校、科研院所、国有企业、民营企业、股份制企业、中外合资企业、港/澳/台商投资企业、外商投资企业等。

八、本合同书适用于广州市事前资助类科技计划项目，有特殊要求另行制定的除外。

一、项目基本信息

项目名称	LncRNA竞争性结合miR-21调控MSTN在猪肌纤维类型转化中的分子机制			
研究类别/ 所属技术领域	农业与食品-畜牧业-禽畜的遗传育种			
承担单位	名 称	华南农业大学		
	通信地址	广东省广州市天河区五山路483号		
	邮政编码	510642	传 真	85281885
	单位特性		单位类型	高等院校
	统一社会信用代码 或组织机构代码	124400004554165634		
	法定代表人	刘雅红	电子邮箱	gale@scau.edu.cn
	联系人	侯建国	联系电话	02038632413

二、项目组人员信息

项目负责人	姓名	孙加节		证件类型		身份证		证件号码	320923198409064814		性别	男	
	出生年月	1984年09月06日		民族		汉族		国籍	中国		学历	博士研究生	
	学位	博士		学位授予国家（或地区）		中国		职务	无		职称	副教授	
	所学专业	动物遗传学		手机号码		13925158841		办公电话	13925158841		电子邮箱	jiajiesun@scau.edu.cn	
项目组成员（含项目负责人）													
序号	姓名	证件类型	证件号码	年龄	性别	职务	职称	学历	现从事专业	分工	所在单位	签名	
1	孙加节	身份证	320923198409064814	34	男	无	副教授	博士研究生	动物生物化学	项目负责人	华南农业大学		
2	张永亮	身份证	220106196604209617	53	男	教务处长	教授	博士研究生	动物生物化学	项目指导	华南农业大学		
3	习欠云	身份证	362223197209136832	46	男	无	教授	博士研究生	动物生物化学	生物信息学	华南农业大学		
4	罗君谊	身份证	440103199302262426	26	女	无	实验员	硕士研究生	动物生物化学	样品保存与实验准备	华南农业大学		
5	曾斌	身份证	43110319911130571X	27	男	无	未取得	博士研究生	动物生物化学	RACE克隆候选lncRNAs全长及细胞定位研究	华南农业大学		
6	谢月琴	身份证	522224199410110824	24	女	无	未取得	硕士研究生	动物生物化学	分子生物学实验	华南农业大学		

7	汪东阳	身份证	342623199605 025373	23	男	无	未取得	硕士研究生	动物生物化学	猪高纯度肌卫星细胞原代培养	华南农业大学	
---	-----	-----	------------------------	----	---	---	-----	-------	--------	---------------	--------	--

202002030037

三、项目实施内容

(一)项目概述

肌纤维类型与猪肉品质密切相关。申请人前期发现6个候选lncRNA可作为ceRNA参与miR-21调控猪纤维发育。因此，拟在前期研究的基础上对候选lncRNA进行验证和细胞内定位研究，并确定候选lncRNA作为ceRNA调控猪肌纤维发育的作用机制，对阐明肌肉发育这一生命现象和猪优质选育具有重要意义。

(二)项目研究内容

(1. 研究目标和内容。2. 拟解决的关键技术问题。3. 主要创新点。4. 采用的方法、技术路线以及工艺流程。5. 项目的协同创新机制模式。6. 其他。)

1、研究目标

- (1) 明确miR-21相关ceRNA调控网络的构成；
- (2) 揭示lncRNA作为ceRNA参与miR-21调控猪纤维发育，进而影响猪肉品质的分子机制。

2、研究内容

- (1) 候选lncRNA验证及细胞内定位
- (2) miR-21与候选lncRNA靶向验证及互作研究
- (3) miR-21靶向MSTN调控猪肌纤维发育
- (4) 候选lncRNA作为ceRNA参与miR-21调控猪肌纤维发育

3、拟解决的关键技术问题

- (1) miR-21相关ceRNA有哪些？

近年来随着miRNA功能研究的不断深入，竞争性内源RNA（ceRNA）学说被提出，即具有相同miRNA应答元件的mRNA、假基因转录物、lncRNA等可通过竞争性结合同种miRNA来调控各自的表达水平。申请人通过前期实验，已成功筛选得到6个lncRNA候选，能通过与MSTN基因竞争结合miR-21，减少miR-21对MSTN基因的表达抑制，来参与猪纤维发育的调控过程。其中，这6个lncRNA候选即为ceRNA，但需实验进一步验证。

- (2) LncRNA作为ceRNA调控猪纤维发育的分子基础是什么？

该问题是本项目拟解决的核心科学问题。对该问题的解决需要系统地分析相关lncRNA作为ceRNA候选在猪肌细胞增殖分化过程中，对肌细胞数量、形态和细胞周期的影响，及与肌发育调控网络的相关性，最终达到本项目研究的目的和意义。

4、主要创新点

- (1) 项目选题和研究内容有特色

目前有关猪肉品质的研究，主要从动物营养调控、肌肉脂肪含量等角度展开。而本研究以肌纤维类型与猪肉品质之间的关系为出发点，探究ceRNA调控猪肌纤维发育的作用机制，为猪优质选育提供理论依据，在选题和内容设计上新颖、有特色。

- (2) 研究策略具有明显创新性

与既往孤立地研究lncRNA或miRNA不同，本研究以竞争内源性RNA（ceRNA）理论作为桥梁，将转录组、lncRNAome及miRNAome表达数据整合起来分析，基于ceRNA→miRNA→mRNA网络，研究猪纤维发育的调控机制，研究策略具有明显创新性。

5、采用的方法

- (1) RT-qPCR及Northern blot验证候选lncRNA；
- (2) cDNA末端快速扩增法（RACE）克隆候选lncRNA全长序列；
- (3) 荧光原位杂交法（FISH）细胞内定位候选lncRNA；
- (4) 组织块分离方法培养猪肌卫星细胞原代细胞系；
- (5) 采用psiCHECK-2双荧光素酶重组载体系统、ChIRP及RIP检测miR-21与候选lncRNA互作；
- (6) EdU细胞增殖检测；
- (7) 流式细胞术检测细胞周期；
- (8) RT-qPCR检测肌增殖分化标志基因mRNA表达，Western blot检测蛋白表达。

(三)项目预期风险及规避措施

(1. 预期风险。2. 规避措施。)

1、预期风险

我国虽然是世界上猪种资源最丰富的国家，在繁殖、肉质和抗逆等方面均有优异种质特性。但影响优良性状发生的机制复杂多样，主效与微效基因作用如何区分显现，功能代偿效应及基因网络等还不清楚，项目实施挖掘调控猪肌纤维类型发育相关ceRNA网络是否准确，项目后期执行是否严谨、科学，预算是否合理等存在风险。

2、规避措施

(1) 聘请咨询专家：拟聘请1-2名国内知名领域专家，负责参与本项目的咨询工作，负责对项目实施过程中技术方案的审定，针对项目问题和实施中遇到的困难提出意见。

(2) 实行课题依托单位负责制：课题负责人负责制定本项目的总体目标、任务设计和任务分解，实行“定专题、定内容、定目标、定人员、定预期效果”的五定责任制，增强科技人员的责任感。

(3) 加强课题内部的交流和专项财务管理，建立实时课题交流平台，定期汇报。

四、项目主要验收指标

(一) 主要技术指标

- (1) 明确miR-21调控猪肌纤维发育的ceRNA 网络及分子机制;
- (2) 发表学术论文2-3篇 (至少2篇SCI 论文), 培养研究生3 名。

202002030037

(二) 主要技术成果			
序号	成果形式		成果数量
1	新产品（或新材料、新装备、新品种/系）	无	0
2	新工艺（或新方法、新模式、新技术、新服务）	无	0
3	发明专利（件）	申请	2
		授权	0
4	实用新型专利（件）	申请	0
		授权	0
5	外观设计专利（件）	申请	0
		授权	0
6	国外专利（件）	PCT受理	0
		授权	0
7	技术标准制定（个）	牵头	0
		参与	0
8	软件著作权（项）		0
9	论文论著（篇）	SCI/EI/ISTP	2
		其他	1
10	创新平台（载体）项目	技术服务数量（项）	0
		服务企业数量（家）	0
11	获得国家级奖项（项）		0
12	获得省级奖项（项）		0
13	科技人才奖励（人）		0
14	引进人才（人）		0
15	培养人才（人）	博士	0
		硕士	2
其他成果及形式说明（新药证书、动植物新品种、创新特色、成果宣传推介措施等）			
无			

(三) 主要经济指标及社会效益		
序号	指标名称	指标值
1	实施期内项目销售收入（万元）	0.00
2	实施期内项目利税（万元）	0.00
3	实施期内项目出口创汇（万美元）	0.00
4	实施期内项目新增就业人数（人）	0
其他经济指标及社会效益说明		

无

202002030037

五、项目经费预算

(单位：万元)

项目经费： 20.00				
资金来源	小计	市科技局经费	自筹资金	其他财政经费
2020年	20.00	20.00	0.00	0.00
2021年	0.00	0.00	0.00	0.00
2022年	0.00	0.00	0.00	0.00
合计	20.00	20.00	0.00	0.00

202002030037

六、工作进度安排

序号	起止时间	阶段目标主要内容及成果
1	2020-04-01至2020-09-30	(1) 候选lncRNAs Northern blot及RT-qPCR定性和定量验证; (2) SMARTer™ RACE 克隆候选lncRNAs 全长; (3) 创建猪高纯度肌卫星细胞原代培养技术体系。
2	2020-10-01至2021-03-31	(1) FISH 定位猪肌细胞中候选lncRNAs 成熟序列; (2) miR-21 与候选lncRNAs 互作研究; (3) 探索miR-21 调控猪肌纤维发育机制。
3	2021-04-01至2021-09-30	(1) 候选lncRNAs siRNA干扰和过表达载体构建; (2) 在猪肌细胞水平上, 候选lncRNAs→miR-21→MSTN调控网络验证。
4	2021-10-01至2022-03-31	(1) 解析候选lncRNAs作为ceRNA参与miR-21调控猪肌纤维发育机制; (2) 研究结果整理。

七、共同条款

第一条 甲、乙、丙三方根据《中华人民共和国合同法》及国家有关法规和规定，经协商一致，特订立本合同，作为甲、乙、丙三方在合同执行中共同遵守的依据。

第二条 甲、乙、丙三方应当严格履行《广州市科技计划项目管理办法》《市级财政科研项目资金绩效提升和管理监督方法》、中规定的职责，严格按照《市级财政科研项目资金绩效提升和管理监督方法》、《广州市科技创新发展专项资金管理办法》实施项目经费管理。

第三条 甲方应在项目执行期满（执行期以本《合同书》“六、工作进度安排”为准，下同）时按相关管理办法组织项目验收。

1. 对通过验收的项目，签发《验收证书》；

2. 对未通过验收的项目，要求其承担单位限期整改，整改后仍不能通过验收的，终止合同。

第四条 乙方应：

1. 为本单位提供的与本项目有关的全部材料真实、合法、有效性负责；

2. 按照《合同书》规定的内容组织实施项目，接受并配合甲方、丙方以及各级财政、审计部门，或上述部门委托的机构进行评估、稽查、审计、检查和绩效评价，并按要求提供项目任务与预算执行情况和有关财务资料；

3. 保证自筹资金按时到位和其它配套条件的落实；

4. 在项目研究开发过程中优先考虑使用“广东省科技资源共享服务平台”的仪器设备，项目购置的设备仪器若符合入网条件应及时办理入网手续对社会共用共享，提高设备仪器的使用率。按照《中华人民共和国采购法》要求，对符合政府采购范围的设备仪器，执行政府采购；

5. 项目合同执行期内确需进行变更的，须按照《广州市科技计划项目管理办法》、《市级财政科研项目资金绩效提升和管理监督方法》、《广州市科技创新发展专项资金管理办法》相关程序办理；

6. 项目合同执行期满3个月内向甲方提出验收申请，提前完成合同规定任务的可提前申请验收；

7. 项目未通过验收的，按相关管理办法限期整改并重新提出验收申请；

8. 办理《验收证书》和科技成果登记手续；

9. 按照科技经费管理相关要求对项目资金单独设帐，按照预算专款专用；

10. 项目验收时，须提交科技报告；

11. 配合甲方开展对财政资金绩效的跟踪，在项目实施期内及实施期结束后的3年内，按照甲方要求提供相关信息和数据；

12. 对合作单位承担监管责任，与合作单位签署合作协议，作为本合同的附件，因合作单位违反合作协议或其他导致本合同书项目建设未能按约定完成的行为，应向甲方承担违约责任。

第五条 乙方因某种原因（如技术或市场情况发生变化，项目所依托的技术、资金、设备仪器或人力条件不能落实，原定技术方案及路线不合理等）或不可抗力因素，致使项目计划无法执行，须终止合同的，应向甲方提出申请，经丙方同意，由甲方审核批准，尚未使用和使用不符合规定的财政经费予以收回；如乙方没有提出终止申请，甲方根据项目研究开发过程监督检查情况，有权终止项目，财政经费予以收回；乙方在执行期满无故不提交验收申请，经甲方催办仍不提交的，甲方有权终止项目，财政经费予以收回，因乙方不及时报告或申请所导致的各方损失，由乙方承担。乙方违反约定造成项目工作停滞、延误或失败，未能通过验收的，应承担违约责任。

第六条 丙方应：

1. 协助甲方对项目的实施过程进行跟踪、检查和提供相关信息，并对所提供信息的客观真实性负责；
2. 负责监管乙方严格遵守《合同书》规定的任务；
3. 督促乙方按时到位自筹资金并保证和落实其他配套条件。

第七条 在履行本合同的过程中，当事人一方发现可能导致项目失败或部分失败的情形时，应及时通知另一方，并采取适当措施减少损失，没有及时通知并采取适当措施，致使损失扩大的，应当就扩大的损失承担责任。

第八条 在履行本合同的过程中，如遇到市财政计划改变等不可抗力情况，甲方对所核拨经费的数量和时间可进行相应变更。

第九条 本项目技术成果及知识产权的归属、转让和实施技术成果所产生的经济利益的分享，除另有约定外，按国家和省、市有关规定执行；正式发表的论文、论著应标注“广州市科技计划项目资助”字样及项目编号；项目所取得的技术成果和知识产权应优先广州产业化或推广转让；需向外地转让或产业化的，须事先以书面形式征得甲方同意。

第十条 属技术保密的项目，经协商订立如下技术保密条款：

1. 本合同书保密内容范围为：本合同及其补充协议和附件、乙方因履行本合同所接触或知晓的甲方工作秘密（包括但不限于甲方的任何技术性资料、以及甲方为完成本合同提供的任何其他信息资料并且在提供时未说明是公开信息的）；

2. 本合同书保密期限为：\；

3. 乙方（包括但不限于乙方雇员、代理人、顾问等人员，下同）采取有效的保密措施以避免泄露给任何第三方；在本合同有效存续期间及合同终止后，未经甲方事先的书面同意，不得以任何方式公布、发表、公开、披露、散播、复制此种保密信息的任何部分，或对其加以任何形式的利用或使用；如甲方要求，乙方必须签署甲方提供的保密协议。乙方应与可能知悉保密内容的人员签订技术保密保护协议，保密义务不得低于本合同书的约定；

4. 双方应建立技术保密制度；

5. 属技术保密的项目必须经市负责技术保密部门审查后，方可确定可否发表或用于国际合作与交流。

第十一条 根据项目具体情况，经协商订立如下附加条款作为本合同正式内容的一部分：

1. 甲方同意给予乙方人民币（¥20.00万）的资助，立项后一次性拨付；

2. \

第十二条 违约责任

乙方无正当理由造成项目工作停滞、延误或失败，未能通过验收的，甲方有权终止项目，财政经费予以收回，由此造成的经济损失由乙方承担；经检查确认项目计划进度不符合合同书约定的，甲方有权警告并责令乙方整改，由此产生的损失由乙方负担；情节严重的，甲方有权终止项目，财政经费予以收回。

第十三条 廉洁责任

乙方应严格遵守国家、省、市关于科技专项经费使用的有关法律、法规，相关政策以及廉洁建设的各项规定，积极开展人员廉洁从业教育，防范科技项目组成员在科研活动中出现下列违法违规行为：

1. 向甲方、组织单位、评审机构及其工作人员赠送礼金、有价证券、任何形式的贵重物品和回扣、好处费、感谢费等；
2. 为甲方、组织单位、评审机构及其工作人员报销应由对方或个人支付的费用；
3. 为甲方、组织单位、评审机构工作人员个人装修住房、婚丧嫁娶、配偶子女的工作安排以及出国（境）、旅游等提供方便；
4. 为甲方、组织单位、评审机构及其工作人员组织有可能影响公正执行公务的宴请、健身、娱乐等活动；
5. 其他：\

乙方及其工作人员有上述行为之一的，一经查实，甲方有权按照相关规定采取终止项目合同、不拨付财政经费、限制项目申报等处理；涉嫌犯罪的，移交司法机关追究刑事责任。甲方、组织单位、评审机构及其工作人员有涉及上述行为之一的，乙方应及时向甲方或其上级机关或纪检监察、司法等有关机关检举举报。

第十四条 科研诚信和科研伦理要求

乙方应建立健全促进科研诚信和科研伦理的规章制度，落实以下职责：

1. 建立健全本单位学术论文发表诚信承诺制度、科研过程可追溯制度、科研成果检查和报告制度等成果管理制度。对本项目形成的科研成果的署名、研究数据真实性、实验可重复性等进行诚信审核和学术把关。防范科技项目组成员在项目申报、研发过程中提供虚假信息或材料，抄袭、剽窃他人科研成果，捏造、变造或篡改科研数据；
2. 加强对科技项目参加人员的科研诚信和科研伦理教育，督促科技项目组成员恪守科学道德准则，遵守科研活动规范。对在科研诚信和科研伦理方面存在问题情节较严重的，应及时调整出项目团队并及时以书面形式报告甲方；
3. 加强对项目合作单位的科研诚信管理，正确履行管理、指导、监督职责，全面落实科研诚信和科研伦理要求；
4. 乙方或项目合作单位及其相关人员被纳入科研严重失信行为记录或相关社会领域信用“黑名单”，乙方应及时以书面形式报告甲方；
5. 其他：\

在项目实施过程中，对乙方或项目合作单位及其相关人员有严重违背科研诚信和科研伦理要求的行为，甲方和相关部门可对乙方采取约谈主要负责人、停拨或核减经费、记入科研诚信严重失信行为数据库、将不良行为向社会公开、移送至有管理权限的纪检监察部门等处理处罚措施。

第十五条 争议解决

因本合同书所产生的争议，各方应友好协商解决；协商不成的，各方同意由本合同签订地人民法院管辖。

第十六条 通知与送达

甲方在本合同履行过程中向乙方或丙方发出或者提供的所有通知、文件、文书、资料等，均以本合同所列明的乙方或丙方地址送达。乙方或丙方如果迁址，应当书面通知甲方；未履行书面通知义务的，甲方按原地址邮寄相关材料即视为已履行送达义务。当面交付上述材料的，在交付之时视为送达。

本合同一式五份，各份具有同等效力。甲方、市财政局和丙方各存一份，乙方存二份。本合同签订各方均负有相应的法律责任，不受机构、人事变动而影响。

说明：本《合同书》中，凡是三方约定无需填写的条款，在该条款的空白处划（\）。

202002030037

八、合同书各方签章

签订地点：广州市越秀区

广州市科学技术局（甲方）：广州市科学技术局

项目经办人（签章）：

责任处室负责人（签章）：

李石磊

莫雪华

联系电话：83124052



项目承担单位（乙方）：华南农业大学

二级部门：华南农业大学动物科学学院

项目负责人（签章）：

2020年5月26日

动物科学学院

项目经费汇入帐号

帐户名：华南农业大学

帐号：3602002609000310520

开户银行：广东广州工行五山支行

财务负责人（签章）：

- 有 梁

财务负责人联系电话：02085287402

法定代表人（签章）：

刘雅红



组织单位（丙方）：华南农业大学

项目经办人（签章）：

侯建国



附件：项目承担单位（乙方）及项目负责人承诺书

承诺书

本单位/本人作为广州市科技计划项目承担单位/项目负责人，将严格遵守广州市科技计划管理相关规定，严格履行自身责任，加强对项目组人员及合作单位的管理，在此郑重承诺：

（一）确保与本项目有关的全部材料真实、合法、有效，未侵犯其他方的权利；

（二）严格遵守《广州市科技计划项目管理办法》相关规定，积极推动项目实施，按时完成项目并按规定提交验收材料；

（三）严格遵守《市级财政科研项目资金绩效提升和管理监督办法》、《广州市科技创新发展专项资金管理办法》及相关财经法规规定，实施项目经费管理，确保财政经费使用合法合规；

（四）严格遵守国家、省、市关于科研诚信和科研伦理的有关法律、法规，相关政策以及各项规定，加强项目实施过程中的科研诚信及科研伦理管理，恪守科研道德准则。

如有违反，本单位/本人愿意接受相关部门做出的各项处理决定，包括但不限于终止项目，停拨或核减经费，追回项目经费，取消一定期限广州市科技计划项目申报资格，记入科研诚信严重失信行为数据库，将不良行为向社会公开以及主要责任人接受相应党纪政纪处理等。

项目承担单位签章：

日期：2020.5.26

项目负责人签章：

日期：2020.5.26

任务书编号：2023E04J0056

广州市科技计划项目 任务书

项目名称：关岭牛高效养殖与雪花肉生产技术研究

承担单位：华南农业大学

项目负责人：孙加节

计划类别：创新环境计划

专题名称：2023年度农村科技特派员专题

方向名称：市外帮扶方向

组织单位：华南农业大学

起止时间：2023-04-01 至 2025-03-31

主管处室：农村和社会发展科技处

广州市科学技术局制

二〇二三年

关于公布 2023 年度猪禽种业全国重点实验室开放课题立项结果的通知

各有关单位：

根据《关于发布猪禽种业全国重点实验室 2023 年开放课题申请指南的通知》，经遴选，决定对“惠阳胡须鸡 RFI 形状形成的相关微生物挖掘”等 26 个项目予以立项资助（详见附件）。请各项目主持人根据合同书模板，于 2023 年 7 月 15 日前完成项目合同书的签订。合同书纸质签字盖章版一式 4 份报送猪禽种业全国重点实验室，同时将合同书电子版（Word 版）发送到 gdxms@163.com。请各项目承担单位严格按照合同要求和相关经费管理规定实施，认真做好项目组织管理工作，确保项目按期完成。

附件：1. 2023 年度猪禽种业全国重点实验室开放课题立项清单

2. 合同书模板

猪禽种业全国重点实验室
广东省农业科学院动物科学研究所
2023 年 6 月 30 日

附件 1:

2023 年度猪禽种业全国重点实验室开放课题立项清单

项目编号	项目名称	主持人	承担单位	经费(万元)
2023GZ01	惠阳胡须鸡 RFI 性状形成的相关微生物挖掘	梁启颖	华南农业大学	2
2023GZ02	利用长期 RFI 双向选择群体解析影响肉鸡饲料利用效率性状基因的遗传及调控网络	刘德武	华南农业大学	2
2023GZ03	IGF2BPs 基因多态性与粤西卷羽鸡生长及屠宰性能的关联分析	林树带	广东海洋大学	2
2023GZ04	栀子对仔猪肠道微生物组成和肠屏障功能的影响	刘世龙	华南农业大学	2
2023GZ05	不同组合红光照射时间和强度对公猪精液品质和母猪繁殖性能的影响	朱晓萍	佛山科学技术学院	2
2023GZ06	低蛋白下精氨酸比例对母猪生产性能及仔猪肠道健康的影响	李帅	广西大学	2
2023GZ07	不同杂粕替代豆粕对肥育猪生长性能、营养物质表观消化率、血清氨基酸含量及肠道微生物组成的影响	何振涛	佛山科学技术学院	1
2023GZ08	高温应激诱导家禽肠道先天免疫功能损伤的分子机制及调控	尚秀国	佛山科学技术学院	1
2023GZ09	中速型黄羽肉鸡净能需要量研究	白银山	佛山科学技术学院	1
2023GZ10	姜黄素对黄羽肉种鸡繁殖性能、免疫功能及其子代生长的影响	兰瑞霞	广东海洋大学	1.5
2023GZ11	基于 NLRP3/Caspase1/IL-1 β 信号解析黑水虻肠道微生物预防鼠伤寒沙门氏菌诱导的肝脏炎症效果研究	彭杰	仲恺农业工程学院	1
2023GZ12	25(OH)VD3 调控产蛋后期蛋鸭脂肪肝的机制研究	刘文超	广东海洋大学	1
2023GZ13	蛋鸭促卵泡激素对卵泡自噬的影响	洪亮	天津农学院	1.5

2023GZ14	钙信号参与蛋鸭卵泡成熟调控机制研究	靳二辉	安徽科技学院	1
2023GZ15	植物废弃物在动物养殖低碳减排中应用效果评价	吴文佳	中国科学院华南植物园	1.5
2023GZ16	猪不同生长阶段粪便在自然堆放过程中温室气体排放特征研究	李欢	仲恺农业工程学院	1.5
2023GZ17	体外法研究益生菌或益生元调控粪臭素生成的微生物学机制	张瑞阳	沈阳农业大学	1.5
2023GZ18	高产罗伊氏菌素基因工程菌的构建及其抗菌分子机制研究	杨桥	浙江海洋大学	2
2023GZ19	猪卵泡颗粒细胞 Caskin1 调控雌激素合成的机制研究	陶晨雨	河北农业大学	2
2023GZ20	环状 RNA 编码蛋白 KANSL1L-421aa 调控猪肌纤维发育机制研究	孙加节	华南农业大学	2
2023GZ21	稻渔鸭立体生态农业技术研究	王广军	中国水产科学研究院珠江水产研究所	1
2023GZ22	凉茶渣对白羽肉鸡肠道健康的调节研究	陈婷	华南农业大学	1
2023GZ23	一种新型耐盐异养硝化好氧反硝化细菌及应用	舒琥	广州大学	1
2023GZ24	α -月桂酸单甘油酯促进麻黄仔鸡肠道屏障发育机制的初步研究	王宏	暨南大学	1
2023GZ25	大花白猪耐粗饲的肠道微生物菌群研究	柴建民	佛山科学技术学院	1
2023GZ26	单细胞/核数据挖掘骨骼肌生长发育、再生和疾病的调控基因	黄波	华南农业大学	2
合计				38.5

附件 2:

猪禽种业全国重点实验室 开放课题合同书

课 题 名 称: 环状 RNA 编码蛋白 KANSL1L-421aa

调控猪肌纤维发育机制研究

项 目 编 号: 2023GZ20

起 止 年 限: 2023 年 6 月 15 日-2023 年 10 月 15 日

课题负 责 人: 孙加节

负责人所在单位: 华南农业大学动物科学学院

通讯地址及邮编: 广州市天河区五山路 483 号

联 系 电 话: 13925158841

签 订 时 间: 2023 年 7 月 14 日

猪禽种业全国重点实验室
广东省农业科学院动物科学研究所

一、项目内容与目标

(一) 主要研究内容

项目拟首先通过 RNase R 消化耐受与放线菌素 D 干扰转录实验研究候选 circKANS1L1 稳定性, FISH 和核质分离 RT-qPCR 技术确定候选 circKANS1L1 亚细胞定位与出核规律; 通过构建标签蛋白重组载体和 RNC-seq 手段, 分别利用 Western blot 及 RT-qPCR 技术间接验证候选环状 RNA 分子是否翻译, 利用蛋白质谱技术, 直接验证是否翻译; Cap-independent translation 双荧光素酶报告载体及 RIP 技术探究启动环状分子翻译的作用机理; 以猪骨骼肌卫星细胞为材料, 过表达或干扰 circKANS1L1 并设计起始密码子删除和突变实验作为对照, 阐明候选 circKANS1L1 通过编码蛋白影响猪肌纤维发育的分子机制。研究结果能拓展蛋白质翻译新机制, 对完善肌肉发育这一生命现象的理论基础具有重要意义, 还可以为优质肉猪选育提供数据支撑。

(二) 计划达到的目标

本研究以前期发现的猪肌纤维发育相关候选 circKANS1L1 为出发点, 明确环状分子序列全长、分子稳定性与亚细胞定位, 确定其出核现象及规律; 阐明候选 circKANS1L1 编码肽链的组成及启动翻译的作用机制, 揭示其通过编码蛋白调控猪肌纤维发育的分子机理, 从环状 RNA 编码蛋白层面填补猪骨骼肌发育研究领域的一些科学数据, 为猪遗传改良和优质高效生产提供新思路。

(三) 将提供的研究开发成果及形式

成果形式		成果数量	成果形式		成果数量
专利	申请	2	引进人才（人）		
	授权		培养人才（人）		
新产品（或信材料、新装备、新品种（系））			论文论著（篇）		2
新工艺（或新方法、新模式、新技术）			其中：被收录论文数	SCI	1
技术标准制定	牵头（个）			EI	
	参与（个）				

二、项目实施方案

(一) 技术路线或实施方案

(1) 候选 circKANS1L1 分子特征及亚细胞定位研究
环状 RNA 分子功能发挥依赖其分子稳定性与细胞定位等, 因此课题拟首先通过 RNase R

消化耐受和放线菌素 D 干扰转录实验, 研究候选 circKANS1L 的稳定性; 针对接头序列, 设计特异性 Divergent 引物, 结合 T 载体测序克隆候选 circKANS1L 全长序列; 根据全长序列设计荧光原位杂交 (Fluorescence in Situ Hybridization, FISH) 探针, 在猪骨骼肌卫星细胞增殖分化不同阶段对候选 circKANS1L 进行亚细胞定位, 结合核质分离 RT-qPCR 技术确定候选 circKANS1L 出核现象并阐述其规律。

(2) 候选 circKANS1L 翻译验证及机制研究

通过在候选 circKANS1L 原有 ORF 前端增加标签序列, 构建环状 RNA 过表达融合载体, 主要包括 3×Flag、V5 或 HA 等标签, 利用 Western blot 初步验证环状 RNA 在生理条件下是否可以实现翻译; 进一步利用核糖体-新生肽链复合物测序 (Ribosome nascent-chain complex sequencing, RNC-seq) 对与核糖体结合的正在翻译的全长 RNA 进行测序, 间接验证候选 circKANS1L 能否与核糖体结合形成复合物, 启动翻译过程; 根据 circKANS1L 可能翻译的蛋白质序列, 通过体外合成相应肽段, 作为质谱的标准图谱, 分析过表达 circKANS1L 的猪肌卫星细胞产物质谱数据中是否有符合标准图谱的蛋白, 直接证明 circKANS1L 是否翻译。

环状 RNA 是以非帽子依赖的方式启动翻译, 目前 IRES 序列和 m6A 修饰位点被认为是环状分子潜在的启动翻译方式。因此, 首先基于海肾荧光素酶 (Renilla Luciferase, R-Luc) 和萤火虫荧光素酶 (Firefly Luciferase, F-Luc) 的 cap-independent translation 报告载体, 验证 F-Luc 是否只有插入候选 circKANS1L 的 IRES 活性序列才能介导翻译起始, 同时设计 Luc2 空载体为阴性对照, 插入脑心肌炎病毒 (Encephalomyocarditis Virus, EMCV) IRES 序列的 Luc2 报告载体为阳性对照。此外, 由于 YTHDF3 可识别 circRNA 上发生的 m6A 修饰, 并招募翻译起始因子启动编码, 拟利用 RNA 免疫共沉淀技术 (RNA Binding Protein Immunoprecipitation, RIP), 以 anti-YTHDF3 为目的的抗体, 将与 YTHDF3 蛋白结合的 circRNA 沉淀下来, 再对其进行定性和定量分析, 确定候选 circKANS1L 能否由 m6A 修饰启动翻译过程。

(3) 候选 circKANS1L 编码蛋白调控猪肌纤维发育的分子机制研究

构建候选 circKANS1L 过表达及干扰腺病毒载体, 包装病毒, 感染猪骨骼肌卫星细胞, 并进行细胞增殖培养与诱导分化。CKK8 及 EdU 法检测细胞增殖情况; 流式细胞术检测细胞周期; qRT-PCR、Northern blot 及 Western blot 用于 mRNA 和蛋白水平检测, 检测基因包括细胞周期相关基因 Cyclin D 和 Cyclin E, 肌分化标志基因 Pax7、Myf5、MyoD、MyoG 和 MSTN, 肌纤维类型相关基因 NFAT、PGC-1 α 、MyHC I、MyHC IIa、MyHC IIx 和 MyHC IIb, 同时删除和突变 circKANS1L 的 ORF 起始密码子作为对照。

(二) 工作计划与进度安排

开始时间	结束时间	主要工作内容
2023 年 6 月	2023 年 10 月	circKANSL1L 编码蛋白载体构建及调控猪肌纤维发育的分子机制研究

三、人员信息

姓名	证件号码	学历	职称	工作分工	所在单位
胡斌	430922198207235813	博士	副研究员	试验指导	广东省农科院动物科学研究所
谢芳	360781199905161060	硕士研究生	硕士生	过表大载体构建	华南农业大学动科学院
何潇	42070420000408428X	硕士研究生	硕士生	细胞培养	华南农业大学动科学院
聂影	41022320010114802X	硕士研究生	硕士生	功能研究	华南农业大学动科学院

四、经费预算

甲方核定用于乙方开放课题研究的经费 2 万元，供乙方进行课题研究时使用。经费使用必须专款专用、专账核算。

经费可用于材料费、测试化验加工外协费、燃料动力费、差旅费、会议费、国际合作与交流费、出版/文献/信息传播/知识产权事物、劳务费、人员费、专家咨询费、小型设备费等。不能用于基建费。其中设备费比例不能超过 15%，其余科目不设比例限制。

五、合同条款

1. 甲方与乙方根据《中华人民共和国民法典》及国家有关法规和规定，为顺利完成 环状 RNA 编码蛋白 KANSL1L-421aa 调控猪肌纤维发育机制研究 项目，经协商一致，特订立本合同，作为甲乙双方在项目实施管理过程中共同遵守的依据。

2. 乙方应按计划与本重点实验室合作开展课题研究，甲方为该课题研究提供必要的支持。课题到期后乙方须向甲方提交结题报告，并办理相关的项目结题手续。

3. 在合同执行过程中，任何一方不得擅自修改合同内容，如确需修改，应由甲方乙方共同商定，重新签定合同方能生效。

4. 甲方乙方对相关技术资料负有保密责任。

5. 乙方在开放课题研究中形成的论文、专著、成果评议鉴定资料以及其他知识产权，必须标注“猪禽种业全国重点实验室”为第一完成单位。成果所有权归甲乙双方。

6. 本合同一式四份，双方各执两份，具有同等效力。签字、盖章后即生效，有效期至项目结题后一年内。各方均应负合同的法律责任，不应受机构、人事变动的影响。

7. 本合同未尽事宜双方协商解决。

六、签约各方

下达单位(甲方): 猪禽种业全国重点实验室
广东省农业科学院动物科学研究所

实验室主任(签字):

联系电话:

2023年8月1日

承担单位(乙方): 华南农业大学

承担单位联系人(签字): 孙加节

联系电话: 13925158841

开户单位名称: 华南农业大学

开户银行名称: 中国工商银行广州五山支行

开户银行帐号: 3602-0026-0900-0310-520

年 月 日

项目负责人(签字): 孙加节

联系电话: 13925158841

年 月 日

备注: 1. 涉及经费, 合同书必须盖学校/单位公章

2. 经费需要在 2023 年 11 月前支出完毕。

检索证明

根据委托人提供的论文材料, 委托人华南农业大学动物科学学院 孙加节 36 篇论文收录情况如下表。

序号	* 论文名称	发表刊物及发表的年月卷期/页码等	作者排名	论文等级	作者文中单位	收录情况	影响因子	中科院大类分区
1	The effect of dietary ginseng polysaccharide supplementation on porcine milk-derived esRNAs involved in the host immune responses	JOURNAL OF ANIMAL PHYSIOLOGY AND ANIMAL NUTRITION 出版年: 2019 卷期: 103 1 页码: 276-282 文献号: 文献类型: Article	第一作者	B 类	华南农业大学	SCI	IF2-year=1.597 IF5-year=1.74 (2019)	农林科学 3 区 Top 期刊: 否 (2019)
2	Effect of Moringa oleifera supplementation on productive performance, colostrum composition and serum biochemical indexes of SOW	JOURNAL OF ANIMAL PHYSIOLOGY AND ANIMAL NUTRITION 出版年: 2020 卷期: 104 1 页码: 291-299 文献号: 文献类型: Article, Early Access	第一作者	B 类	华南农业大学	SCI	IF2-year=2.13 IF5-year=2.322 (2020)	农林科学 3 区 Top 期刊: 否 (2020)
3	Emerging Roles of Heat-Induced circRNAs Related to Lactogenesis in	FRONTIERS IN GENETICS 出版年: 2020 卷期: 10 页码: - 文献号: 1347	第一作者	B 类	华南农业大学	SCI	IF2-year=4.599 IF5-year=4.888 (2020)	生物学 3 区 Top 期刊: 否 (2020)

	Lactating Sows	文献类型: Article						
4	Integrated meta-omics reveals the regulatory landscape involved in lipid metabolism between pig breeds	MICROBIOME 出版年: 2024 卷期: 12 1 页码: - 文献号: 33 文献类型: Article	第一作者	T2 类	华南农业大学	SCI	IF2-year=15.5 IF5-year=19.4 (2022)	生物学 1 区 Top 期刊: 是 (2023)
5	Milk exosome-derived miRNAs from water buffalo are implicated in immune response and metabolism process	BMC VETERINARY RESEARCH 出版年: 2020 卷期: 16 1 页码: - 文献号: 123 文献类型: Article	共同通讯作者 (倒数第一)	A 类	华南农业大学	SCI	IF2-year=2.741 IF5-year=2.955 (2020)	农林科学 2 区 Top 期刊: 否 (2020)
6	Effects of Fermented Herbal Tea Residues on the Intestinal Microbiota Characteristics of Holstein Heifers Under Heat Stress	FRONTIERS IN MICROBIOLOGY 出版年: 2020 卷期: 11 页码: - 文献号: 1014 文献类型: Article	共同通讯作者 (倒数第一)	A 类	华南农业大学	SCI	IF2-year=5.64 IF5-year=6.32 (2020)	生物学 2 区 Top 期刊: 是 (2020)
7	Fermentation quality of herbal tea residue and its application in fattening cattle under	BMC VETERINARY RESEARCH 出版年: 2021 卷期: 17 1 页码: -	共同通讯作者 (倒数第一)	A 类	华南农业大学	SCI	IF2-year=2.792 IF5-year=3.008 (2021)	农林科学 2 区 Top 期刊: 否 (2021)

	heat stress	文献号: 348 文献类型: Article						
8	CircEZH2 Regulates Milk Fat Metabolism through miR-378b Sponge Activity	ANIMALS 出版年: 2022 卷期: 12 6 页码: - 文献号: 718 文献类型: Article	共同通讯作者 (倒数第一)	A 类	华南农业大学	SCI	IF2-year=3.0 IF5-year=3.2 (2022)	农林科学 2 区 Top 期刊: 否 (2022)
9	Effects of Herbal Tea Residue on Growth Performance, Meat Quality, Muscle Metabolome, and Rumen Microbiota Characteristics in Finishing Steers	FRONTIERS IN MICROBIOLOGY 出版年: 2022 卷期: 12 页码: - 文献号: 821293 文献类型: Article	共同通讯作者 (倒数第一)	A 类	华南农业大学	SCI	IF2-year=5.2 IF5-year=6.2 (2022)	生物学 2 区 Top 期刊: 是 (2022)
10	Identification of circRNA-associated ceRNA networks using longissimus thoracis of pigs of different breeds and growth stages	BMC GENOMICS 出版年: 2022 卷期: 23 1 页码: - 文献号: 294 文献类型: Article	通讯作者	A 类	华南农业大学	SCI	IF2-year=4.4 IF5-year=4.7 (2022)	生物学 2 区 Top 期刊: 是 (2022)

11	The Characteristic Function of Blood-Derived Exosomes and Exosomal circRNAs Isolated from Dairy Cattle during the Dry Period and Mid-Lactation	INTERNATIONAL JOURNAL OF MOLECULAR SCIENCES 出版年: 2023 卷期: 24 15 页码: - 文献号: 12166 文献类型: Article	共同通讯作者 (倒数第一)	A 类	华南农业大学 信息科学部 华南农业大学 SCI	IF2-year=5.6 IF5-year=6.2 (2022)	生物学 2 区 Top 期刊: 否 (2023)
12	The difference of intestinal microbiota composition between Lantang and Landrace newborn piglets	BMC VETERINARY RESEARCH 出版年: 2023 卷期: 19 1 页码: - 文献号: 174 文献类型: Article	共同通讯作者 (倒数第一)	A 类	华南农业大学 SCI	IF2-year=2.6 IF5-year=2.9 (2022)	农林科学 2 区 Top 期刊: 否 (2023)
13	凉茶渣对育肥猪生长性能、胴体性状和肉品质的影响	动物营养学报 出版年: 2019 卷期: 2019, 31(10) 10 页码: 4776-4783 文献号: 文献类型: 期刊论文	共同通讯作者 (倒数第一)	B 类	华南农业大学 北大核心	无	无
14	Dietary supplementation with Moringa oleifera and mulberry leaf affects pork	JOURNAL OF ANIMAL PHYSIOLOGY AND ANIMAL NUTRITION 出版年: 2021 卷期: 105 1 页码: 72-79 文献号:	共同通讯作者 (倒数第一)	B 类	华南农业大学 SCI	IF2-year=2.718 IF5-year=2.747 (2021)	农林科学 3 区 Top 期刊: 否 (2021)

	quality from finishing pigs	文献类型: Article, Early Access						
15	Effects of fermented feeds and ginseng polysaccharides on the intestinal morphology and microbiota composition of Xuefeng black-bone chicken	PLOS ONE 出版年: 2020 卷期: 15 8 页码: - 文献号: e0237357 文献类型: Article	共同通讯作者 (倒数第一)	B 类	华南农业大学	SCI	IF2-year=3.24 IF5-year=3.788 (2020)	综合性期刊 3 区 Top 期刊: 否 (2020)
16	Identification of circRNA-Associated-ceRNA Networks Involved in Milk Fat Metabolism under Heat Stress	INTERNATIONAL JOURNAL OF MOLECULAR SCIENCES 出版年: 2020 卷期: 21 11 页码: - 文献号: 4162 文献类型: Article	共同通讯作者 (倒数第一)	B 类	华南农业大学	SCI	IF2-year=5.924 IF5-year=6.132 (2020)	生物学 3 区 Top 期刊: 否 (2020)
17	蓝塘猪与长白猪背最长肌全基因组 DNA 甲基化分析	西北农林科技大学学报(自然科学版) 出版年: 2022 卷期: 2023, 51 (06) 06 页码: 1-10+17 文献号: 文献类型: 期刊论文	共同通讯作者 (倒数第一)	B 类	华南农业大学	北大核心	无	无

18	凉茶渣替代象草对育肥牛空肠组织形态、屏障功能以及菌群结构的影响	动物营养学报 出版年: 2021 卷期: 2022, 34 (02) 02 页码: 1087-1097 文献号: 文献类型: 期刊论文	共同通讯作者 (倒数第一)	B 类	华南农业大学	北大核心	无	无
19	Effect of miR-493-5p on proliferation and differentiation of myoblast by targeting ANKRD17	CELL AND TISSUE RESEARCH 出版年: 2023 卷期: 393 1 页码: 119-132 文献号: 文献类型: Article, Early Access	共同通讯作者 (倒数第一)	B 类	华南农业大学	SCI	IF2-year=3.6 IF5-year=4.4 (2022)	生物学 3 区 Top 期刊: 否 (2023)
20	A novel protein encoded by circKANS1L1L regulates skeletal myogenesis via the Akt-FoxO3 signaling axis	INTERNATIONAL JOURNAL OF BIOLOGICAL MACROMOLECULES 出版年: 2024 卷期: 257 页码: - 文献号: 128609 文献类型: Article	通讯作者	T2 类	华南农业大学	SCI	IF2-year=8.2 IF5-year=7.8 (2022)	化学 1 区 Top 期刊: 是 (2023)
21	非编码 RNA 对猪骨骼肌发育的影响	中国畜牧兽医 出版年: 2021 卷期: 2021, 48 (10) 10 页码: 3595-3603 文献号: 文献类型: 期刊论文	通讯作者	B 类	华南农业大学	北大核心	无	无

22	非编码 RNA 调控猪肌间脂肪沉积的研究进展	中国畜牧兽医 出版年: 2023 卷期: 2023, 50(10) 10 页码: 4133-4140 文献号: 文献类型: 期刊论文	通讯作者	B 类	华南农业大学	北大核心	无	无
23	茶及其副产品在畜禽养殖中的应用	中国草食动物科学 出版年: 2019 卷期: 2019, 39(03) 03 页码: 51-54+65 文献号: 文献类型: 期刊论文	通讯作者	普刊类	华南农业大学	CNKI	无	无
24	茶渣资源再利用研究概况	中国农学通报 出版年: 2019 卷期: 2019, 35(33) 33 页码: 141-145 文献号: 文献类型: 期刊论文	通讯作者	普刊类	华南农业大学	CNKI	无	无
25	调控乳蛋白合成信号通路的研究进展	中国奶牛 出版年: 2020 卷期: 2020(05) 05 页码: 6-11 文献号: 文献类型: 期刊论文	通讯作者	普刊类	华南农业大学	CNKI	无	无

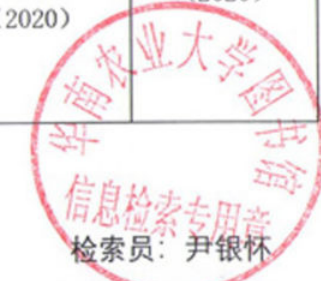
26	Advances in the Evaluation and Application of Nutritionally Valuable Woody Feeding Plants	Journal of Food and Nutrition 出版年: 2020 卷期: 页码: - 文献号: doi: 10.17303/jfn.2020.6.205 文献类型:	通讯作者		华南农业大学	已发表	无	无
27	环境应激对圈养野生动物繁殖性能的影响	特产研究 出版年: 2023 (排版定稿) 网络首发 时间: 2023-03-30 09:46:07 卷期: 页码: - 文献号: 10.16720/j.cnki.tcyj.2023.032 文献类型:	通讯作者	普刊类	华南农业大学	CNKI	无	无
28	Exploration of long noncoding RNA in bovine milk exosomes and their stability during digestion in vitro	JOURNAL OF DAIRY SCIENCE 出版年: 2019 卷期: 102 8 页码: 6726-6737 文献号: 文献类型: Article	共同通讯作者	T2 类	华南农业大学	SCI	IF2-year=3.333 IF5-year=3.432 (2019)	农林科学 1 区 Top 期刊: 是 (2019)
29	Plant MIR156 regulates intestinal growth in mammals by targeting the Wnt/ β -catenin pathway	AMERICAN JOURNAL OF PHYSIOLOGY-CELL PHYSIOLOGY 出版年: 2019 卷期: 317 3 页码: C434-C448 文献号:	10 共同通讯作者	A 类	华南农业大学	SCI	IF2-year=3.485 IF5-year=3.73 (2019)	生物学 2 区 Top 期刊: 否 (2019)

		文献类型: Article						
30	Genomewide analysis of circular RNA in pituitaries of normal and heat-stressed sows	BMC GENOMICS 出版年: 2019 卷期: 20 1 页码: - 文献号: 1013 文献类型: Article	共同通讯作者	A 类	华南农业大学	SCI	IF2-year=3.594 IF5-year=4.093 (2019)	生物学 2 区 Top 期刊: 是 (2019)
31	Porcine milk exosome miRNAs protect intestinal epithelial cells against deoxynivalenol-induced damage	BIOCHEMICAL PHARMACOLOGY 出版年: 2020 卷期: 175 页码: - 文献号: 113898 文献类型: Article	共同通讯作者	A 类	华南农业大学	SCI	IF2-year=5.858 IF5-year=5.675 (2020)	医学 2 区 Top 期刊: 是 (2020)
32	Biological Characteristics and Roles of Noncoding RNAs in Milk-Derived Extracellular Vesicles	ADVANCES IN NUTRITION 出版年: 2021 卷期: 12 3 页码: 1006-1019 文献号: 文献类型: Review	共同通讯作者	A 类	华南农业大学	SCI	IF2-year=11.567 IF5-year=13.607 (2021)	医学 2 区 Top 期刊: 否 (2021)
33	Rno_circ_0001004 Acts as a miR-709 Molecular Sponge to Regulate the Growth Hormone Synthesis and Cell	INTERNATIONAL JOURNAL OF MOLECULAR SCIENCES 出版年: 2022 卷期: 23 3 页码: -	共同通讯作者	A 类	华南农业大学	SCI	IF2-year=5.6 IF5-year=6.2 (2022)	生物学 2 区 Top 期刊: 是 (2022)

	Proliferation	文献号: 1413 文献类型: Article						
34	Skeletal Muscle-Derived Exosomal miR-146a-5p Inhibits Adipogenesis by Mediating Muscle-Fat Axis and Targeting GDF5-PPAR γ Signaling	INTERNATIONAL JOURNAL OF MOLECULAR SCIENCES 出版年: 2023 卷期: 24 5 页码: - 文献号: 4561 文献类型: Article	共同通讯作者	A 类	华南农业大学	SCI	IF2-year=5.6 IF5-year=6.2 (2022)	生物学 2 区 Top 期刊: 否 (2023)
35	Plant MIR167e-5p Inhibits Enterocyte Proliferation by Targeting β -Catenin	CELLS 出版年: 2019 卷期: 8 11 页码: - 文献号: 1385 文献类型: Article	共同通讯作者	B 类	华南农业大学	SCI	IF2-year=4.366 IF5-year=5.276 (2019)	生物学 3 区 Top 期刊: 否 (2019)
36	Exploration of Long Non-coding RNAs and Circular RNAs in Porcine Milk Exosomes	FRONTIERS IN GENETICS 出版年: 2020 卷期: 11 页码: - 文献号: 652 文献类型: Article	共同通讯作者	B 类	华南农业大学	SCI	IF2-year=4.599 IF5-year=4.888 (2020)	生物学 3 区 Top 期刊: 否 (2020)

说明: 论文等级和中科院大类分区按《华南农业大学学术论文评价方案(试行)》划分。

报告免责声明: 如未盖章, 报告无效



检索员: 尹银怀

检索证明

根据委托人提供的论文材料，委托人华南农业大学动物科学学院 孙加节 4 篇论文收录情况如下表。

序号	论文名称	发表刊物及发表的年月卷期/页码等	作者排名	论文等级	作者文中单位	收录情况	影响因子	中科院大类分区
1	Plant-derived miR166a-3p packaged into exosomes to cross-kingdom inhibit mammary cell proliferation and promote apoptosis by targeting APLNR gene	INTERNATIONAL JOURNAL OF BIOLOGICAL MACROMOLECULES 出版年：2025 出版日期：JAN 卷期：286 页码：- 文献号：138470 文献类型：Article	通讯作者	A 类	华南农业大学动物科学学院	SCI	IF2-year=8.5 IF5-year=8.7 (2024)	生物学 2 区 Top 期刊：是 (2025)
2	A novel protein encoded by porcine circANKRD17 activates the PPAR pathway to regulate intramuscular fat metabolism	JOURNAL OF ANIMAL SCIENCE AND BIOTECHNOLOGY 出版年：2025 出版日期：FEB 5 卷期：16 1 页码：- 文献号：19 文献类型：Article	通讯作者	T2 类	华南农业大学动物科学学院	SCI	IF2-year=6.5 IF5-year=7.2 (2024)	农林科学 1 区 Top 期刊：是 (2025)

RESEARCH

Open Access



Integrated meta-omics reveals the regulatory landscape involved in lipid metabolism between pig breeds

Jiajie Sun^{1†}, Fang Xie^{1†}, Jing Wang³, Junyi Luo¹, Ting Chen¹, Qingyan Jiang¹, Qianyun Xi^{1*}, George E. Liu^{2*} and Yongliang Zhang^{1*}

Abstract

Background Domesticated pigs serve as an ideal animal model for biomedical research and also provide the majority of meat for human consumption in China. Porcine intramuscular fat content associates with human health and diseases and is essential in pork quality. The molecular mechanisms controlling lipid metabolism and intramuscular fat accretion across tissues in pigs, and how these changes in response to pig breeds, remain largely unknown.

Results We surveyed the tissue-resident cell types of the porcine jejunum, colon, liver, and longissimus dorsi muscle between Lantang and Landrace breeds by single-cell RNA sequencing. Combining lipidomics and metagenomics approaches, we also characterized gene signatures and determined key discriminating markers of lipid digestibility, absorption, conversion, and deposition across tissues in two pig breeds. In Landrace, lean-meat swine mainly exhibited breed-specific advantages in lipid absorption and oxidation for energy supply in small and large intestinal epitheliums, nascent high-density lipoprotein synthesis for reverse cholesterol transport in enterocytes and hepatocytes, bile acid formation, and secretion for fat emulsification in hepatocytes, as well as intestinal-microbiota gene expression involved in lipid accumulation product. In Lantang, obese-meat swine showed a higher synthesis capacity of chylomicrons responsible for high serum triacylglycerol levels in small intestinal epitheliums, the predominant characteristics of lipid absorption in muscle tissue, and greater intramuscular adipocytogenesis potentials from muscular fibro-adipogenic progenitor subpopulation.

Conclusions The findings enhanced our understanding of the cellular biology of lipid metabolism and opened new avenues to improve animal production and human diseases.

Keywords Animal model, Intermuscular fat, Single-cell RNA sequencing, Lipidomics, Metagenome

[†]Jiajie Sun and Fang Xie contributed equally to this work.

*Correspondence:

Qianyun Xi
xiqianyun_scau@163.com
George E. Liu
george.liu@usda.gov
Yongliang Zhang
zhangyl_scau@163.com

¹ Guangdong Provincial Key Laboratory of Animal Nutrition Control, National Engineering Research Center for Breeding Swine Industry, College of Animal Science, South China Agricultural University, Guangzhou, Guangdong 510642, China

² Animal Genomics and Improvement Laboratory, USDA-ARS, BARC-East, Beltsville, MD 20705, USA

³ Institute of Animal Husbandry and Veterinary Medicine, Henan Academy of Agricultural Sciences, Zhengzhou 450002, China



© The Author(s) 2024. **Open Access** This article is licensed under a Creative Commons Attribution 4.0 International License, which permits use, sharing, adaptation, distribution and reproduction in any medium or format, as long as you give appropriate credit to the original author(s) and the source, provide a link to the Creative Commons licence, and indicate if changes were made. The images or other third party material in this article are included in the article's Creative Commons licence, unless indicated otherwise in a credit line to the material. If material is not included in the article's Creative Commons licence and your intended use is not permitted by statutory regulation or exceeds the permitted use, you will need to obtain permission directly from the copyright holder. To view a copy of this licence, visit <http://creativecommons.org/licenses/by/4.0/>. The Creative Commons Public Domain Dedication waiver (<http://creativecommons.org/publicdomain/zero/1.0/>) applies to the data made available in this article, unless otherwise stated in a credit line to the data.

Introduction

Pork is the most consumed meat in China [1], though only slightly less than poultry meat globally in recent years [2]. The consumer acceptance and perception of pork are affected by numerous quality traits of meat [3]. In farm animals, the quantity and distribution of intramuscular fat (IMF), referred to as marbling fat, is highly desirable for enhancing meat quality [4], including tenderness, flavor, juiciness, firmness, and palatability [5]. In humans, muscle tissues accumulate IMF through age, diet, gender, and genetics [6], and excess accumulation of IMF is also responsible for metabolic abnormalities and is associated with a variety of increasing prevalence of obesity, insulin resistance, muscular dystrophies, and sarcopenia [6, 7]. In general, domestic pigs share genetic, anatomical, and physiological similarities with humans [8, 9] and therefore are considered to be an excellent model for studying lipid metabolic disease [10].

The adipose tissue is a specialized loose connective tissue and highly active metabolic endocrine organ that is composed mostly of adipocytes [11, 12]. In general, adipose cells are derived from mesenchymal stem cells (MSCs), further developing into a pool of progenitor cells with dual potentials of adipogenic and fibrogenic differentiation, thus are termed fibro-adipogenic progenitors (FAPs) [13]. FAPs commit into adipocyte lineage and eventually give rise to preadipocytes and then undergo terminal differentiation into mature adipocytes [14]. In animals, adipogenesis is initiated around mid-gestation with the formation of preadipocytes, the majority of which differentiate into mature adipocytes in late gestation or early postpartum period [15]; new adipocytes generated in adulthood are mainly located in subcutaneous, visceral, and retroperitoneal connective tissues, with few located in the intramuscular fat depot [16]. Thus, maternal nutritional management during pregnancy and lactation, which enhances the number of mesenchymal cells committed to intramuscular adipogenesis, will provide more sites for fat accumulation during fattening and further marbling [17]. This physiological process involves a complex homeostatic orchestration of diverse metabolic tissues, such as digestion and absorption of nutrients by the intestinal tract [18], as well as gut microbiota [19], metabolism and biotransformation with the liver [20], and communication with muscle tissue [21]. During the past decades, substantial progress has been made in identifying the dynamic and integrative functions of these key tissues in adipogenesis. However, the underlying cell types and composition of these tissues, and especially the functions of these cell subpopulations, are not completely understood.

In particular, the application of high-dimensional approaches, such as single-cell RNA sequencing

(scRNA-seq), has revealed finer levels of heterogeneity across various tissues, providing in-depth snapshots of individual cell activity and function in several physiological and pathological processes [22]. A recent scRNA-seq study of chicken skeletal muscles elucidated the cell subtypes and captured the gene expression of individual cells, revealing novel insights into myogenesis and intramuscular adipogenesis [23]. Here, we performed scRNA-seq to construct the single-cell atlases of jejunum, colon, liver, and longissimus dorsi muscle between fat-type (Lantang, LT) and lean-type (Landrace, LW) piglets and revealed hitherto unappreciated cell-specific features across different tissues in lipid metabolism. Our study opens potential avenues to further improve pork quality for human consumption and broadens our understanding of the mechanisms that underpin lipid metabolic diseases.

Results and discussion

The domestic pig is an indispensable agricultural species for meat sources [1] and a powerful biomedical model for studying human developmental processes and diseases [24]. In general, intramuscular fat, described as marbling for meat quality, is defined as a unique adipose depot interspersed between and around myofiber groups, and in parallel, strongly associated with human health and disease [25]. Therefore, we systematically assessed cell type heterogeneity and transcriptional profiles of multiple tissues that are involved in lipid digestion, absorption, transport, conversion, and deposition between different breeds of pigs, which allowed us to propose a unified annotation of adipocytogenesis and lipogenesis processes at cellular levels in piglets. We profiled single-cell transcriptomes of the porcine jejunum, colon, liver, and longissimus dorsi muscle, with two for each tissue as biological replicates and one replicate for each breed, on a 10× genomics system. In total, we obtained more than 3405.28 million sequencing reads, and on average, more than 425.66 ± 17.17 million sequencing reads for each sample. After quality filtering, we retained a total of 60,514 high-quality single cells for downstream analysis, of which 10,227, 12,906, 18,152, and 19,229 belonged to the jejunum, colon, liver, and muscle, respectively. We then identified a total of 40 cell clusters using t-distributed stochastic neighbor embedding (t-SNE) analysis, with a resolution value=0.8 (Fig. 1A). These clusters were divided into 20 major cell populations (Fig. 1B) based on the expression levels of canonical cell-type-specific markers (Fig. 1C; Table S1A) and the annotated functions of differentially expressed genes (DEGs) in each cluster (Fig. 1D; Table S1B). Consistent with the characteristics and function of various tissues, immune-related cells, such as T cells, B cells, macrophages, eosinophils,

and neutrophils, clearly exhibited in liver tissue, as well as hepatocytes and dendritic cells; enterocytes, enteroendocrine cells, goblet cells, Paneth cells, and tuft cells, a series of intestinal epithelium cells, were significantly enriched in the jejunum and colon tissues, while multiple myogenesis-related subtypes and intramuscular adipocytes were mainly identified in the longissimus dorsi tissue (Fig. 1E). In recent, another study used a similar strategy to elucidate the chicken intermuscular fat cells in skeletal muscle [23], and in addition, our findings here fully corroborated this approach while extending it across additional tissues and breeds. To our knowledge, this study is one of the first to constitute a comprehensive resource describing the molecular signatures of porcine lipid metabolism across tissues, potentially benefiting the scientific community to better apprehend the lipogenesis and adipogenesis processes in humans.

Characterization and function of porcine intestinal cells

To characterize the cellular diversity of porcine intestines, a total of 23,133 intestinal cells were pooled together, and their transcriptome profiles were classified into 28 cell clusters with unsupervised graph-based clustering (Table S2A). We assigned cell identities based on a panel of previously established markers (Table S2B) and visualized the data using t-SNE. From this analysis, we identified 14 specific intestine-resident subtypes (Fig. 2A), including T cells, B cells, macrophages, eosinophils, stem cells, enterocytes, BEST4/OTOP2 epithelial cells, endothelium cells, enteroendocrine cells, goblet cells, Paneth cells, tuft cells, fibroblasts, and muscle cells. These major cell types were also identified in the jejunum and colon segments when analyzed separately (Fig. S1A–B). In total, we identified 16 and 14 specific jejunum- and colon-resident subtypes, including the major subpopulations identified in the mouse and human intestinal epithelium [26, 27]. Specifically, the previously described population of type 3 innate lymphoid cells (ILC3) was only identified in the small intestine with the expression of the *PTPRC*, *ETS1*, *TOX*, *IL7R*, *ID2*, and *RORC* genes (Fig. S1C), as well as pericytes stably expressing *KCNJ8*, *ABCC9*, and *RGS5* (Fig. S1D). In contrast, a small proportion of subpopulations were observed and termed as

distal mature enterocytes in the large intestinal enterocytes with high expression of *EPCAM*, *FABP1*, *FAM3D*, and *AQP8* (Fig. S1E). Our data captured 12,409 epithelial cells, accounting for nearly half of high-quality intestinal cells (Table S2C), which were demarcated by highly specific gene expressions such as *EPCAM* and *FABP1* (Fig. S1F) and were readily distinguished on their top 5 gene signatures (Fig. 2B). In addition, t-SNE analysis of the enterocyte cluster revealed the presence of two juxtaposed clusters (Fig. S1G), and we observed substantial locational divergence between proximal (jejunal) and distal (colonic) population demarcated by specific gene expression of *FABP2*, *APOC3*, *AQP8*, and *SLC26A2* (Fig. S1H–I), in agreement with the previous description [26].

In general, the intestinal epithelium is the major organ for a wide range of nutrients digestion, absorption, and processing, including lipids, glucose, amino acids, vitamins, and metallic trace elements. In this study, we captured a total of 1321 significantly upregulated genes in the enterocyte subtype cells (Table S2D), and these candidates were enriched in a number of distinct categories at the organismal systems level based on KEGG analysis (Table S2E), such as mineral absorption, protein digestion and absorption, fat digestion and absorption, and carbohydrate digestion and absorption (Fig. 2C). In detail, the genes participating in lipid transport (*SLC27A4*, *FABP1*, *FABP2*), triglyceride assembly (*DGAT1*) [28], lipid homeostasis (*PLIN2* and *PLIN3*) [29], β -oxidation (*ACOX1* and *ACADM*), and lipid assimilation (*APOA1*, *APOA2*, *APOA4*, *APOB*, *APOC2*, and *APOC3*) [30] were highly expressed in the jejunum (Fig. 2D). In contrast, the genes related to short-chain fatty acid (SCFA) transport were enriched in the colon segment and obviously enriched in LW breed (Fig. 2E), including *SLC16A1*, *SLC9A2*, *SLC12A2*, and *CLDN1* [31]. High expression of the genes related to the transport of lipids in the jejunum indicated that lipid absorption was mainly accomplished in the small intestine, which was consistent with an earlier report [30], while the expression of the genes involved in the transport of SCFA was obviously enriched in the colon segments, which were also in line with previous findings [32]. Both the jejunum and colon were involved in sugar absorption (Fig. 2F), but the small

(See figure on next page.)

Fig. 1 Construction of the single-cell landscape of porcine jejunum, colon, liver and muscle tissues. **A** tSNE plots showing the distribution of the main tissue-resident clusters in the tested tissues. **B** t-SNE analysis of 60,514 single cells from tested samples, with 20 major cell types labeled in different colors. IMF, intramuscular fat; SMMCs, smooth muscle cells; MuSCs, Muscle stem cells; DC, dendritic cells; FAP, fibroadipogenic precursors/myofibroblast. **C** Dot plots showing the expression of representative marker genes; dot color reflects average gene expression, and dot size represents percent of cells expressing the gene. **D** Heatmap representing the top 5 most variably expressed genes (row) between the given cell subpopulations (column); colors and numbers correspond to the cell types shown in B. **E** Proportions of the 20 major cell types in the tested tissues; JE, jejunum; RE, colon; LI, liver; MU, longissimus dorsi muscle

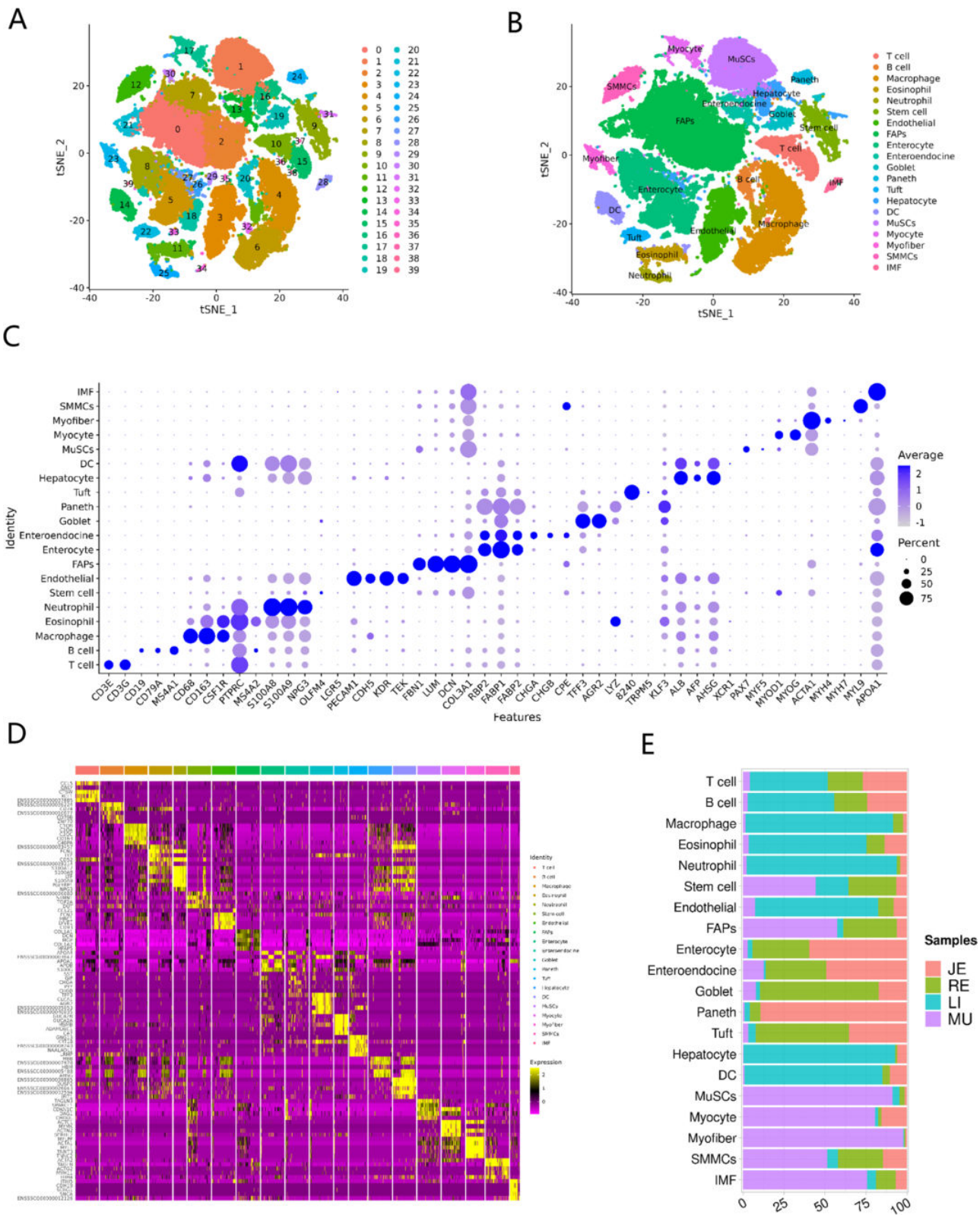
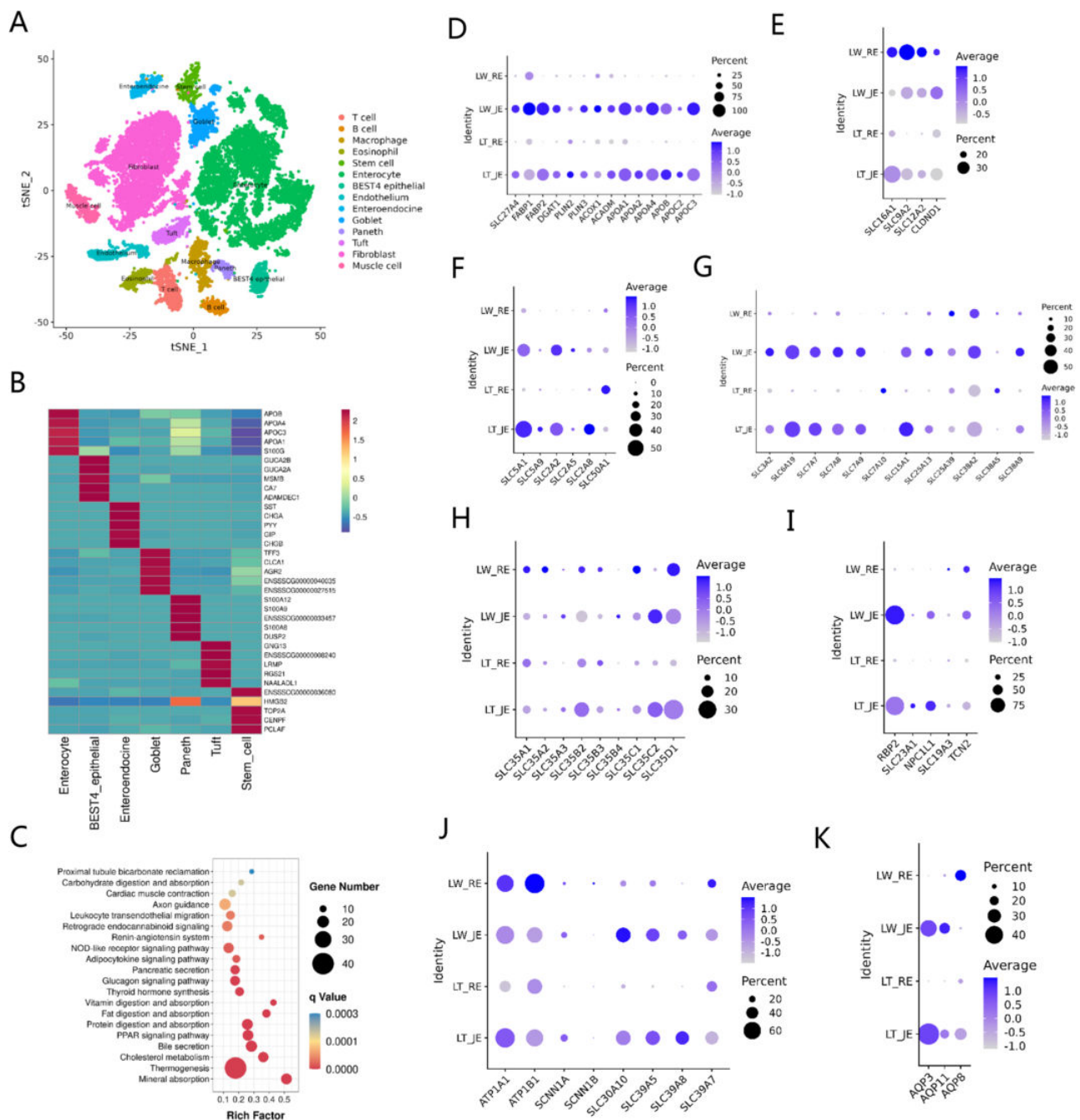


Fig. 1 (See legend on previous page.)



intestinal segments are mainly members of the *SLC3A*, *SLC6A*, *SLC7A*, *SLC15A*, *SLC25A*, and *SLC38A* families (Fig. 2G) [30–33]. The channels of *SLC3A2*, *SLC25A13*, and *SLC25A39* for essential amino acid transport were mainly expressed in both the jejunum and colon, especially in the jejunum [35], while *SLC6A19*, *SLC7A7*, *SLC7A8*, and *SLC7A9* were enriched in jejunum for neutral and cationic amino acid transport such as leucine or arginine [33]. In addition, *SLC38A9* is specifically expressed in the jejunum and exhibits low amino acid-sensing activity for arginine transport [36]. *SLC15A1* was substantially expressed in the jejunum tissue and responsible for the absorption of different di- and tripeptides [37, 38]. In the colon segment, *SLC7A10* and *SLC38A5* were highly expressed and mainly moved small neutral amino acids such as alanine, serine, cysteine, glycine, and threonine [39], while glutamine transporter *SLC38A2* displayed similar expression patterns in the jejunum and colon tissues [40]. Our data also suggested that the colon was the major site for nucleotide or nucleotide sugar absorption with the *SLC35* family (Fig. 2H) [41], in agreement with an earlier report [30]. For vitamin (Fig. 2I), the genes related to vitamin A, C, D, and E absorption were enriched in the jejunum, such as *RBP2* for the absorption of vitamin A [42], *SLC23A1* for vitamin C [43], and *NPC1L1* for vitamin D and E [44, 45], while the whole intestinal segments could transport vitamin B1, B6, and B12 through the expression of *SLC19A3* [46] and *TCN2* [47]. For metal ions (Fig. 2J), the Na and K channels of *ATP1A1*, *ATP1B1*, *SCNN1A*, and *SCNN1B* were mainly expressed in the jejunum and colon [48], while the transporters for bivalent metal ions like Fe, Zn, and Mn (*SLC30A10*, *SLC39A5*, *SLC39A8*) were highly expressed in the jejunum and *SLC39A7* in the jejunum and colon segments [49, 50]. The expression of *AQP3* and *AQP11* was mainly found in the jejunum and *AQP8* in the colon (Fig. 2K), supporting the results that most water was absorbed in the small intestine and further dehydration occurred in the large intestine [51].

As small intestines show breed-specific differences, they likely play emerging roles in lipid absorption and metabolism between the indigenous fat-type and lean-type piglets [52, 53]. We therefore compared the gene expression between LT and LW piglets in small intestinal epithelial cells (Table S3A) and captured a total of 1381 DEGs (Fig. 3A), including 761 upregulated and 620 downregulated candidates in the LT breed. Kyoto Encyclopedia of Genes and Genomes (KEGG) analysis revealed that these DEGs were significantly enriched in modulating intestinal energy and nutrient metabolism (Table S3B), such as oxidative phosphorylation, glycolysis/gluconeogenesis, and fatty acid degradation in the

metabolism category, as well as fat digestion and absorption at the organismal systems level. In fat digestion and absorption enrichment, the *APOB*, *NPC1L1*, and *PLA2G12B* genes were significantly up-expressed in the intestinal enterocytes of the LT breed, while the *APOA1*, *APOA4*, *ABCA1*, *ABCG5*, *ABCG8*, *DGAT1*, *FABP1*, *FABP2*, and *SLC27A4* genes were highly expressed in the LW enterocytes (Fig. 3B). The transporters of intestinal FABPs are intracellular lipid-binding proteins and display high affinity binding for long-chain fatty acids [54], and FABP1 preferentially directs fatty acid toward oxidative pathways while FABP2 directs fatty acids to triacylglycerol (TAG) synthesis [55]. In addition, small intestine-rich *SLC27A4* (fatty acid transport protein 4, FATP4) is a cell-surface fatty acid transport protein for the trafficking of long-chain fatty acids [56] and exhibits acyl-CoA synthetase activity for lipid beta-oxidation [57]. In general, high activity by intestinal *FABP1*, *FABP2*, and *SLC27A4* contributed to the transport of fatty acids across the cell membrane [58]. Once intestinal lipids are digested and absorbed by the intestinal epithelium, and they mainly undergo β -oxidation for energy supply or intracellular TAG re-synthesis and subsequent translocation around the body for later use [52]. The KEGG enrichment of fatty acid degradation was most significant at the lipid metabolism level (Table S3B), and the pathway genes of *ACAA1* [59], *ACOX1* [60], *ACADVL* [61], and *HADHA* [62] encoded rate-limiting enzymes for fatty acid beta-oxidation were significantly increased in LW breed (Table S3A), strongly implying the high-energy requirements of LW piglets. In addition, the *ABCA1*, *ABCG5*, and *ABCG8* mediated the secretion of cellular cholesterol and phospholipids to extracellular acceptors, APOA protein families, to form nascent high-density lipoprotein (HDL) [63, 64]. In this study, the relatively high expression of these genes was observed in the LW piglets when compared to LT piglets, and their functions suggested a panel of breed-specific advantages of the LW breed in lipid uptake, lipid cytoplasmic oxidation, and HDL biogenesis in the intestinal epithelium. In contrast, *NPC1L1* was enriched in the small intestine absorptive enterocytes and transported dietary sterols to target the encoding product of the *APOB* gene, resulting in the formation of chylomicron (CM) [65, 66]. In addition, the *PLA2G12B* expression governed intestinal and hepatic cytosolic lipoprotein production and secretion, such as CM and very low-density lipoprotein (VLDL) [67, 68], and is associated with serum triglycerides (TG) level in part [69]. We further utilized lipidomic technology and subsequently detected 398 negative and 701 positive lipid metabolites in porcine serum (Table S3C), while phosphatidylcholine (PC), phosphatidylethanolamine (PE) and TG were

obviously rich in the blood (Fig. 3C). The PCA analysis demonstrated that the metabolite composition between LT and LW was clearly distinguished (Fig. 3D), and a total of 405 metabolites were significantly regulated, including 344 increased and 61 decreased candidates in the LT breed (Fig. 3E). In detail, 4 fatty acids, 7 diacylglycerols, and 129 triacylglycerols were all significantly upregulated in the LT serum (Fig. 3F; Table S3D), in agreement with the high level of *APOB*, *NPC1L1*, and *PLA2G12B* expression for triglyceride-rich lipoprotein synthesis and secretion in the LT enterocytes.

The large intestine is the site of bacterial fermentation, mainly producing SCFA in monogastric animals [32], and these bacteria-derived SCFA generally contribute to maintaining intestinal homeostasis by acting not only as an energy source but also as multiple signaling modalities [70]. To reveal colonic metabolic characteristics between different breeds, we detected 1464 DEGs between LT and LW piglets in colonic enterocytes (Table S3E), and a total of 662 were upregulated and 802 were downregulated in the LT breed (Fig. 4A). The monocarboxylate transporters (MCTs) and sodium-coupled monocarboxylate transporters (SMCTs) are the dominant transmission routes for the entry of SCFA into intestinal epithelium, thereby providing energy to epithelial cells [71]. In our study, *SLC16A1* (MCT1) was a major route for SCFA absorption in porcine colonic enterocytes (Fig. 4B) and was highly expressed in the LW breed (Table S3E), whereas *SLC5A12* (SMCT2) showed an essential role for SCFA transfer in jejunal epithelial cells (Fig. 4C). In addition, the DEGs were significantly associated with several nutrient metabolisms (Table S3F), including butanoate metabolism and citrate cycle (Fig. 4D). In butanoate metabolism, the expressed levels of *SLC16A1*, *ACADS*, *HADH*, and *ACAT1* involved in β -oxidation were significantly increased in the LW breed (Fig. 4E), as well as the core gene of citrate synthase (CS) in the mitochondrial tricarboxylic acid (TCA) cycle (Fig. 4F). In LW piglets, an

overall increase in the expression of these essential genes related to β -oxidation and TCA cycle, in particular, such as *ACADS* and *CS*, the enzymes that catalyze the rate-limiting steps of short-chain fatty acid dehydrogenation in the large intestines [72]. Our findings suggested that large-intestinal SCFA that was taken up with epithelium in the LW breed was preferentially trafficked toward oxidative pathways releasing energy, in line with high energy requirements for the rapid growth of the LW breed. In addition, over the past decade, it has been identified that a widespread receptor system exists for SCFA [73]. The SCFA-activated G-coupled protein receptors, FFAR2 and HCAR2, were significantly enriched in porcine Paneth cells in the small and large intestinal segments (Fig. 4B, C). In general, Paneth cells are specialized intestinal epithelial cells associated with autophagy activity [74] and regulate host-bacterial interactions by producing antimicrobial peptides [75]. In the Paneth cells of the LT breed, we found a total of 408 upregulated genes (Fig. 4G; Table S3G), and these candidates were significantly enriched in multiple immune-related events (Table S3H), in agreement with increased immune-related cell numbers (Table S3I) and enhanced disease resistance in LT piglets [76]. In addition, lysozyme is an innate enzyme with potent antibacterial properties mainly found in Paneth cells [77]. However, we discovered that the lysozyme gene was highly expressed in the Paneth cells of the LW breed (Fig. 4H), and by contrast, the SCFA-related G-coupled protein receptor genes were obviously downregulated in the LW breed (Fig. 4I), probably implying the alternative synthesis and secretion system of lysozyme [78].

The catalog of metagenome-assembled genomes from porcine gut microbiota

The gut microbiota is a central regulator of host metabolism [79]. The composition and function of the gut microbiota are dynamic and affected by various genetic, nutritional, and environmental factors [80]. In this study,

(See figure on next page.)

Fig. 3 Breed-specific differences involved in lipid digestion and absorption in porcine small intestinal enterocytes. **A** Differentially expressed genes in small intestinal epithelial cells between LW and LT piglets. The outer ring represented 1 to 18 porcine autosomal and X and Y chromosomes. The middle ring indicated the differentially expressed genes involved in lipid metabolism; red symbols represented upregulated genes in LT pigs, and green represented downregulated genes. The scatter plot in the inner ring represented all genes presented in porcine enterocytes; the size of the solid circles represented for $\log(Q \text{ value}, 2)$. **B** Expression patterns of identified genes in fat digestion and absorption enrichment in small intestinal enterocytes between LW and LT piglets. **C** Lipid metabolites identified in porcine serum. PC, phosphatidylcholine; PE, phosphatidylethanolamine; PS, phosphatidylserine; PI, phosphatidylinositols; PG, phosphatidylglycerols; PA, phosphatidic acids; SM, sphingomyelins; Cer, ceramides; GlcCer, glucosyl ceramides; FA, free fatty acids; DAG, diacylglycerol; TAG, triacylglycerol; GM3, monosialodihexosyl ganglioside; GlcADG, glucuronosyl diacylglycerol; ACer, acylcarnitine; DGTS, diacylglycerol trimethylhomoserine. **D** PCA analysis of the identified metabolites in porcine serum between LT and LW piglets. **E** Volcano plot showing the differential lipid metabolites in porcine serum between LT and LW piglets. The red circles represented increased metabolites in LT pigs, and green represented decreased metabolites. **F** Violin plots showing FA, DAG, and TAG concentrations in porcine serum between LT and LW piglets

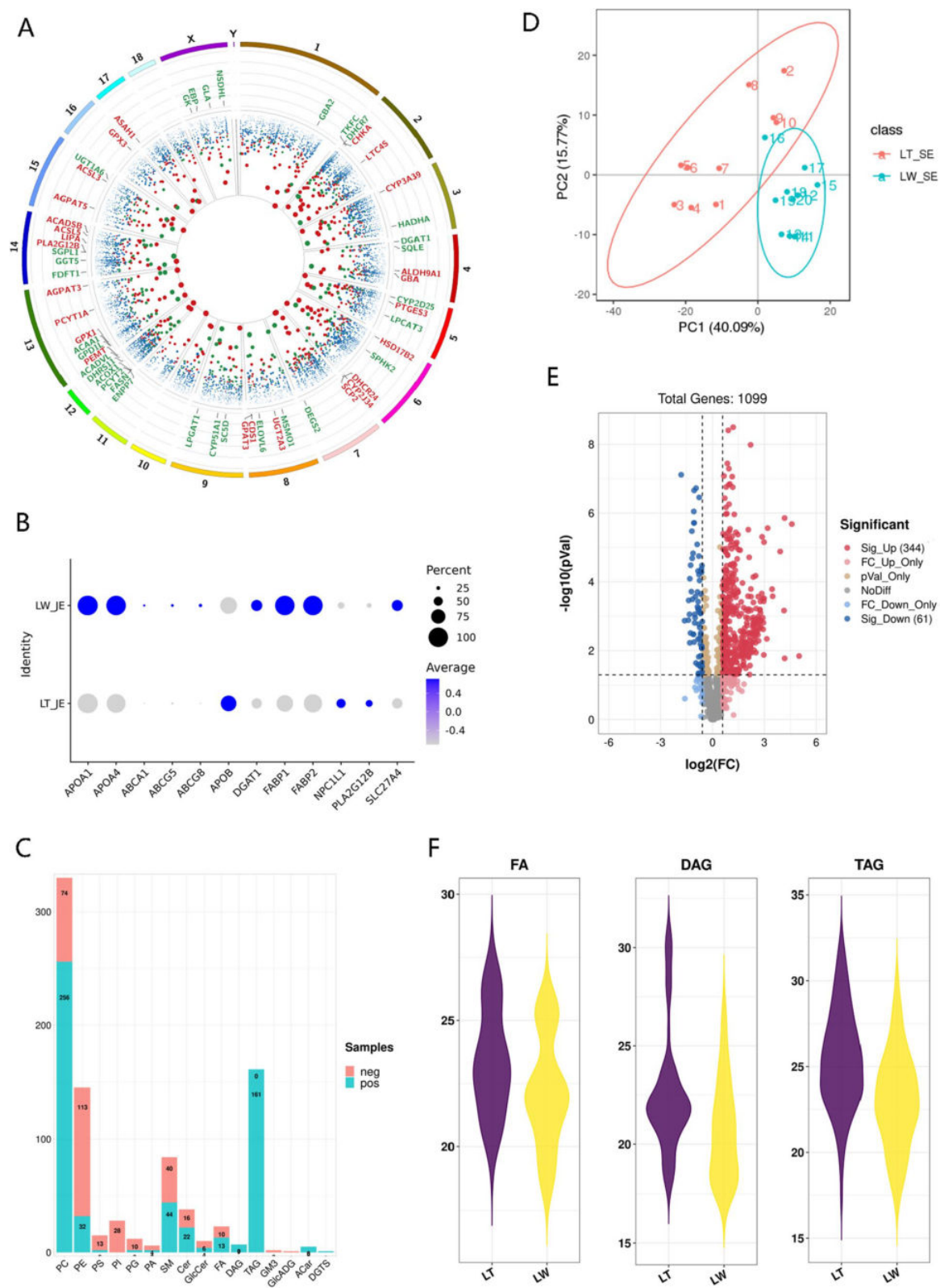


Fig. 3 (See legend on previous page.)

we examined the composition and function of the jejunal and colonic microbiota in 10 LT and 10 LW piglets. We obtained a total of 265.19 gigabases (GB) of paired-end reads and achieved an average sequencing depth of 6.63 ± 0.44 Gb (mean \pm s.d.) for each sample. Approximately $11.57\% \pm 4.42\%$ and $81.31\% \pm 15.67\%$ of original reads from jejunal and colonic segments were considered as non-host, quality-filtered microbial sequences for further analysis (Table S4A). The reads were then assembled into scaffolds for each sample using the assembly software MEGAHIT [81], and the diversity of metagenome-assembled scaffolds varied with pig breed and intestinal location (Table S4B). In detail, a total of $68,318.90 \pm 3029.54$, $74,771.88 \pm 13,214.48$, $45,487.00 \pm 10,648.78$, and $21,950.60 \pm 4925.64$ fragments with least 500-bp length were successfully assembled in the jejunal sites of LT and LW, and the colonic sites of LT and LW, respectively. We then performed MetaGeneMark to construct a gene catalog [82], and the program predicted 681,230 non-redundant open reading frames (ORFs) using a 100-bp cutoff, with an average length of 407-bp (Table S4C). The jejunal and colonic catalogs contained 308,508 and 478,568 unigenes, respectively, and a total of 302,864 (44.46%) were complete genes, while 378,366 (55.54%) were incomplete.

To determine the composition of the gut microbiota, we blasted the identified genes to 3302 non-redundant references extracted from the National Center for Biological Information (NCBI), including bacteria, fungi, archaea, and viruses, and only 264,438 genes could be taxonomically classified. More than 99.86% of the classified genes were assigned to bacteria, whereas the remaining 0.13% and 0.14% belonged to eukaryota and archaea, respectively. These classified genes were annotated to 53 phyla, 71 classes, 149 orders, 284 families, and 861 genera. At the phylum level, Proteobacteria dominated the intestinal microbial communities of all samples (Fig. 5A), representing $8.49\% \pm 2.86\%$ of the jejunum and $72.57\% \pm 10.88\%$ of the colon, respectively, followed by Firmicutes, Fusobacteria, and Bacteroidetes (Table S4D). This distribution was in agreement with a previous observation [83]. At the genus level, *Escherichia*, *Neisseria*, and *Campylobacter* were the dominant phylotypes in the jejunal group, while *Escherichia*,

Clostridium, and *Turicibacter* were the most abundant genera in the colonic group (Table S4E). The bacterial taxa detected in all tested samples were defined as the core bacteria of pig gut microbiome, and 27 (81.82% in all annotated phyla) phyla, 111 (29.68%) genera, and 143 (14.61%) species were identified as core bacteria in the jejunal samples, as well as 15 (28.30%) phyla, 60 (7.06%) genera, and 95 (2.91%) species in the colonic samples (Table S4D-F). The abundances of these 143 species in the jejunum and 95 in the colon occupied more than $97.02 \pm 2.90\%$ and $87.04\% \pm 12.59\%$ of the total abundance of the annotated bacterial species, implying their high prevalence and important roles in the gut microbiome of pigs. We readily separated the tested samples with pig breed and intestinal location based on genera profiles by principal component analysis (Fig. 5B), non-metric multi-dimensional scaling analysis (Fig. S2A), or hierarchical clustering analysis (Fig. S2B). We then removed two outliers of LTJC3 and LWJC9 and explored whether some microbial candidates were significantly different in the gut microbiota between LT and LW piglets. Based on LefSe analysis [84], a total of 60 microbial candidates were estimated to be discriminative features in the jejunum (Table S4G), and 41 were inferred to be putative genomic biomarkers in the colon (Table S4H). In detail, the genera *Bacteroides*, *Deinococcus*, *Lactobacillus*, *Lactococcus*, *Neisseria*, *Campylobacter*, and *Francisella* were significantly enriched in the small intestine segment of the LT breed, whereas *Enterobacter*, *Photobacterium*, and *Serratia* were enriched in the LW breed. In the large intestine segment, genera of *Lactobacillus*, *Niameybacter*, *Neisseria*, *Campylobacter*, and *Francisella* showed higher levels in the LT breed, as well as *Veillonella*, the species of *Enterococcus hirae* from *Enterococcus* genus, the species of *Fusobacterium russii* from *Fusobacterium* genus, and the species of *Actinobacillus succinogenes* from *Actinobacillus* genus in the LW breed.

To investigate microbial functions of porcine intestines, we annotated the metagenome-assembled genes in our catalog to the KEGG and eggNOG datasets. A total of 243,614 (35.76%) and 245,158 (35.99%) non-redundant genes were successfully annotated to 6645 KEGG orthologues (Table S5A) and 7014 eggNOG orthologues (Table

(See figure on next page.)

Fig. 4 Breed-specific differences involved in SCFA functions in porcine large intestinal enterocytes and Paneth cells. **A** Volcano plot showing differentially expressed genes between LT and LW piglets in large intestinal epithelial cells. **B, C** Expression patterns of SCFA transport-related and receptor genes in distinct cell types from the small intestine (**B**) and large intestine (**C**), respectively. **D** KEGG functional enrichment analysis of differently expressed genes in large intestinal epithelial cells between LT and LW piglets at metabolism classification. **E, F** Expression patterns of β -oxidation (**E**) and TCA cycle (**F**) genes in porcine colonic enterocytes between LT and LW piglets. **G** Scatter plot showing the differentially expressed genes between LT and LW piglets in large intestinal Paneth cells. **H** Ridge plot showing the expression of LYZ gene in large intestinal Paneth cells between LT and LW piglets. **I** Dot plot of the SCFA-related receptor gene FFAR2 and HCAR2 in large intestinal Paneth cells between LT and LW piglets

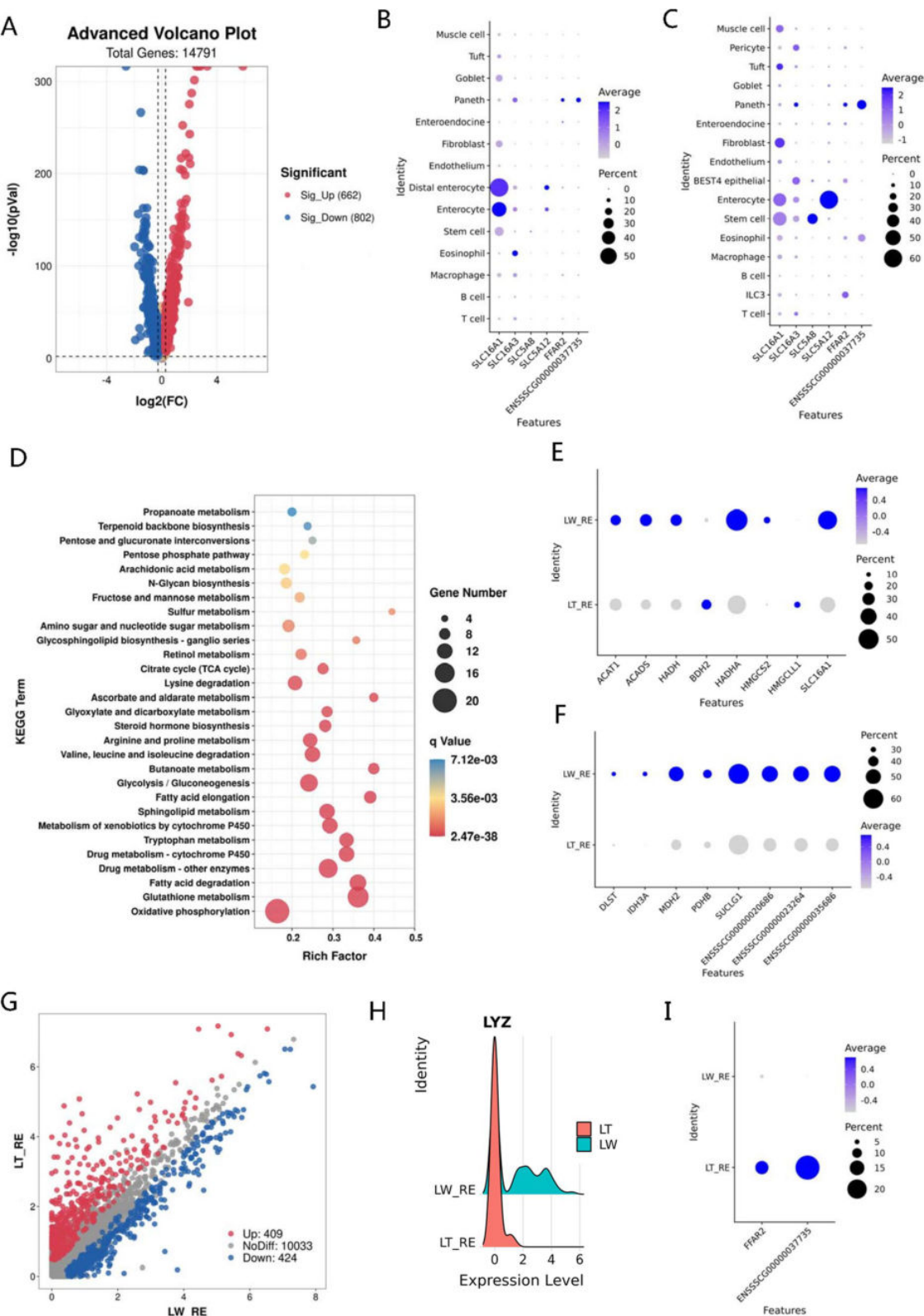


Fig. 4 (See legend on previous page.)

S5B), respectively. A large number of KEGG-annotated genes were enriched in various metabolic processes, including carbohydrate metabolism, amino-acid metabolism, metabolism of cofactors and vitamins, nucleotide metabolism, and energy metabolism (Fig. S2C), while the eggNOG-annotated genes were associated with carbohydrate transport and metabolism, amino-acid transport and metabolism, cell membrane biogenesis, inorganic transport and metabolism, and energy production and conversion (Fig. S2D). These results were in agreement with the physiological structure and biological function of intestinal tracts in nutrient transport and metabolism. In the jejunum segment, a total of 2494 KEGG ortholog groups (KOs) were differentially presented between LT and LW piglets, and only 70 KOs were significantly enriched in the LT breed (Table S5C). At the pathway level, we detected a total of 398 functional terms annotated with metagenome-assembled genes (Table S5D), and more than 56.76% (105) functional differences were enriched in the Metabolism level, including 11 functional categories associated with lipid metabolisms, such as alpha-linolenic acid metabolism, sphingolipid metabolism, glycerophospholipid metabolism, and arachidonic acid metabolism (Table S5E), in agreement with the high sphingolipid and glycerophospholipid contents in porcine jejunum of our study. We obtained a total of 2134 metabolites with lipidomic technology in porcine jejunum, and 1585 had identification information (Table S5F). In detail, 346 molecules in the lipidome belonged to sphingolipids, including 163 ceramide and 120 sphingomyelins (SM), while 909 metabolites were primarily from glycerophospholipids, consisting of 348 phosphatidylcholine (PC), 279 phosphatidylethanolamine (PE), and 90 phosphatidylserine (PS) molecules (Fig. 5C and Fig. S2E). In general, the gut microbiota is now considered as one of the key elements contributing to the regulation of intestinal lipid metabolism and composition through interaction with the diet [85]. In our study, a large number of phospholipid metabolites were identified in the jejunum of the tested sucking piglets, and glycerophospholipids and sphingolipids were obviously enriched in the intestinal contents, in agreement with the concentration and composition of the milk lipids [86]. Comparing the metabolomic data between LT and LW piglets, there were 731 significantly changed metabolites, and 9

of 12 free fatty acids (FFAs) were highly enriched in LW groups (Table S5G). In general, a number of long-chain free fatty acid (LCFA) releases were mainly from lipid digestion and bacterial fatty acid biosynthesis in the small intestine [87, 88]. For lipid digestion, pathway analysis of KEGG orthologs found that genes for glycerophospholipid digestion via phospholipase (*K01058*, *K01048*, *K06999*) were highly enriched in LW groups, whereas the gene expression of triacylglycerol lipase (*TGL2*, *K01046*) and lipoprotein lipase (*LPL*, *K01059*) involved in lipolysis appeared no differences in comparison to LT groups (Table S5C). The results implied more obvious advantages in lipid digestion by hydrolyzing phospholipids to FFAs in the lean-meat type piglets. In recent, several data have provided pieces of evidence in animal models that milk phospholipids affect infant gastrointestinal health and development [89], and the possible mechanism to benefit from milk phospholipid may occur via microbiota-lipid interaction [90]. These biological interactions allow gut microbiota to bind dietary lipids and express lipolytic and phospholipolytic enzymes to digest milk-fat [91], and these enzymes within the gut microbiome thus act like a second liver to break down and transform lipids [92]. Previous analysis indicated that the majority of phospholipase-positive strains mainly belong to the phylum Firmicutes [91], Bacteroidetes [93], Enterobacteria and Actinobacteria [94], and Proteobacteria [95]. In line with our study, Proteobacteria and Firmicutes were the predominant intestinal microbial phyla and characterized as phospholipase producers, including the genera of *Clostridium*, *Turicibacter*, *Escherichia*, and *Moraxella* (Table S5H). We observed that only the strains from *Escherichia*, dominated the intestinal microbial communities during the first week of life [96, 97], were significantly presented in LW piglets (Table S4I), and exhibited the accumulation of membrane phospholipase [98], strongly implying their biological functions in lipid accumulation of small intestinal tract in response to pig breed. For fatty acid biosynthesis, *FabA* (*K01716*), *FabB* (*K00647*), *FabD* (*K00645*), *FabH* (*K00648*), and *FabZ* (*K02372*), encoding to synthetases, responsible for bacterial LCFA synthesis and elongation [99], showed elevated relative abundances in the LW group (Fig. 5D). These genes that were indispensable for LCFA synthesis were mainly expressed in the genera *Staphylococcus*,

(See figure on next page.)

Fig. 5 The composition, abundance, and annotation of porcine intestinal microbiota and lipidome in LT and LW piglets. **A** Bar plot showing the relative abundance of intestinal microbiota at the phylum level. **B** Principal component analysis of the tested samples at the genus level. **C** Lipid metabolites identified at positive ion mode in porcine jejunal contents. **D** Heatmap showing the gene expression levels involved in bacterial fatty acids synthesis in porcine jejunum. **E** The distribution of *FabA*, *FabB*, *FabD*, *FabH* and *FabZ* genes on jejunal bacteria at phylum and genus levels. The colors of the lines represented different taxonomy levels

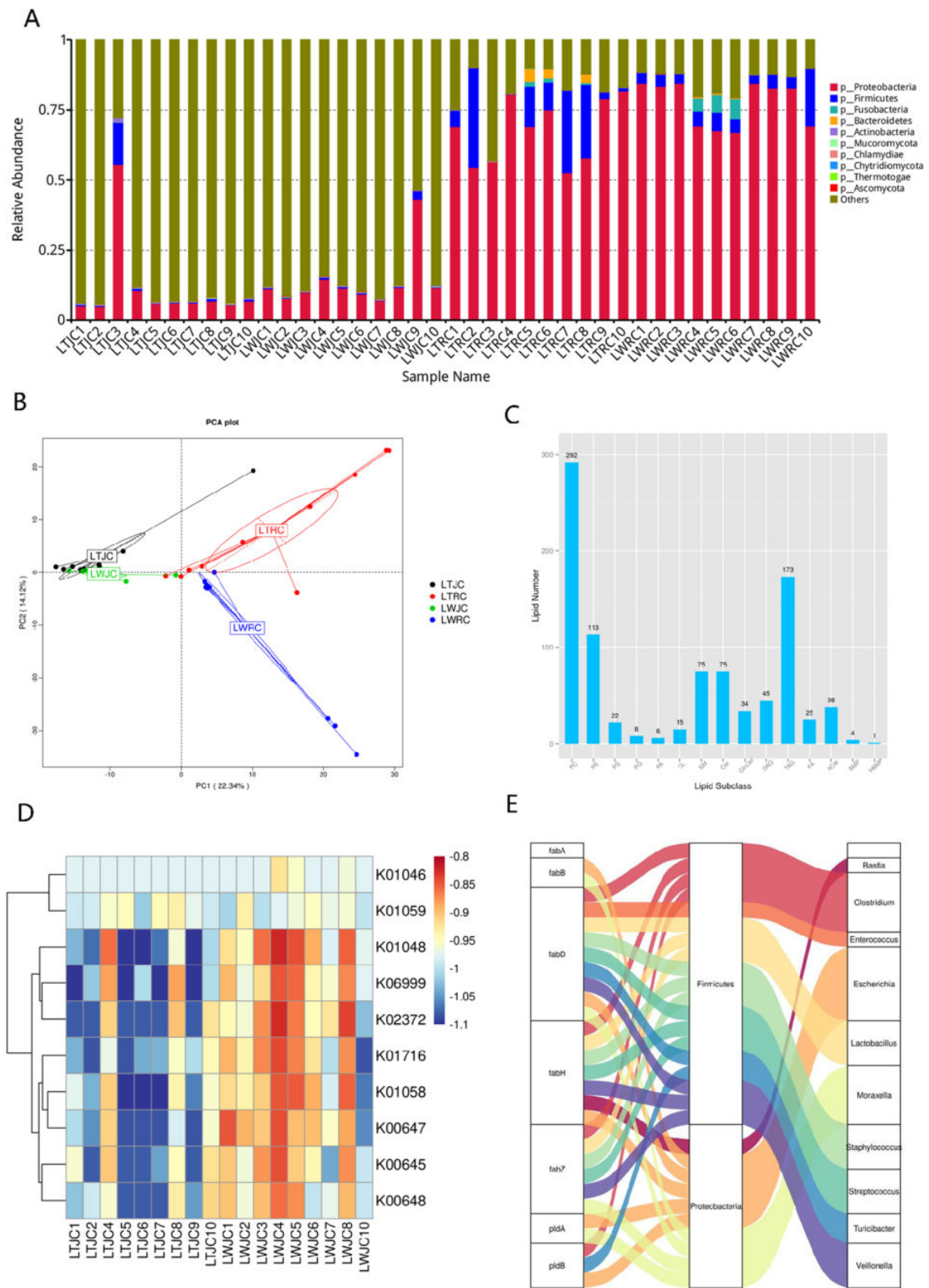


Fig. 5 (See legend on previous page.)

Enterococcus, *Lactobacillus*, *Streptococcus*, *Clostridium*, *Turicibacter*, *Veillonella*, *Escherichia*, *Basfia*, and *Moraxella* (Fig. 5E; Table S5H), suggesting that they participated LCFA accumulation. In general, the hindgut microbiota has been well recognized in maintaining intestinal homeostasis and symbiosis by fermenting indigestible dietary components and thereby producing SCFA, such as acetate, butyrate, and propionate [70, 71]. The potential for SCFA production is frequently a focus of many mammalian gut microbiome studies, as even in monogastric animals like pigs, up to 25% of daily energy requirements are met by SCFAs [100]. In the pre-weaning period of piglets, breast milk oligosaccharides are indigestible to the infant and, for this reason, reach the colon intact, thereby acting as metabolic substrate necessary for intestinal microbiota to generate SCFAs that are critical for gut health [101]. In the colon segment, we identified a total of 1455 differentially regulated KOs (Table S5I), as well as 103 KEGG pathways between LT and LW groups (Table S5J). Here, we found that the SCFA-producing enzymes, namely acetate kinase (*ackA*, K00925), phosphate acetyltransferase enzymes (*pta*, K00625, or K13788), propionate CoA-transferase (*pct*, K01026), butyryl-CoA to acetate CoA-transferase (*bua*, K01034, or K01035) and butyrate kinase (*buk*, K00634, or K00929) [102], were mainly encoded in the Actinobacteria, Bacteroidetes, Firmicutes, Fusobacteria, and Proteobacteria phyla and widely distributed in 23 genera (Fig. S2F), and notably, *Clostridioides* encoding butyrate kinases, were significantly enriched in LT groups (Table S4J). Butyrate production by *Clostridioides* has been demonstrated in a previous report [32] and can regulate apoptosis, enhance barrier function, and reduce inflammation in the host [103], associated with the strong disease-resistance characteristic of LT pigs. In addition, the total expression levels of the above genes were further compared between LT and LW breeds, but no significant differences were found (Table S5I), the results demonstrating that there were no differences in SCFA synthesis between pig breeds, at least in the pre-weaning period. Our findings suggested an additional mechanism involved in crosstalk between the early intestinal microbiota and lipids and expanded our

understanding of lipid metabolism for animal production and human health.

The landscape of porcine liver cell types

To identify resident liver cells, we used scRNA-seq to measure the entire transcriptome of more than 18,000 dissociated liver cells. Our analysis revealed 25 distinct populations, and our atlas comprised all of the main liver cell types consisting of T cells, $\gamma\delta$ T cells, B cells, Kupffer cells, monocyte-derived macrophages, neutrophils, eosinophils, dendritic cells, monocytes, hepatic stellate cells, hepatocytes, endothelial cells, and erythrocytes (Fig. 6A) based on a panel of landmark genes (Fig. 6B; Table S6A). In general, hepatocytes play a series of key roles in detoxification, lipolysis, and gluconeogenesis based on their zonation [104]. We therefore re-clustered 1671 hepatocytes (Table S6B) that generally showed enriched *ALB* expression (Fig. 6B) and found two diverse zonation patterns that showed dynamic differences in the gene expression profiles (Table S6C), known as periportal and central hepatocytes (Fig. 6C). KEGG enrichment analysis of the zonated genes demonstrated that periportal hepatocytes were enriched in genes responsible for biological oxidations, lipid, and cholesterol metabolism (Table S6D), including fatty acid degradation, glycolysis/gluconeogenesis, primary bile acid biosynthesis, and cholesterol metabolism (Fig. 6D), whereas central hepatocytes showed enrichment of drug metabolism genes along with numerous active immune pathways (Table S6E), based on the expression patterns of the periportal gene *ARG1*, *ASS1*, *CPS1*, *PCK1*, and *SCD* [104, 105] and the central gene *GLUL* [106] (Fig. 6E).

In general, bile acids are important physiological agents that are required for intestinal solubilization, digestion, and absorption of lipids [107], and the gut-to-liver axis plays a critical role in the regulation of bile acid synthesis, especially in the periportal hepatocytes [108]. To explore how pig breed affects hepatocytic function in lipid metabolism, we therefore compared the periportal hepatocyte transcriptomes of LT and LW piglets in our scRNA-seq datasets. We detected a total of 796 and 1143 genes that exhibited significant decreases or increases in LT groups, respectively (Table S6F). KEGG

(See figure on next page.)

Fig. 6 Distinct expression patterns of genes related to cholesterol metabolism and bile secretion in porcine liver tissues. **A** t-SNE analysis of 18,152 single cells from porcine liver tissues, with 13 major cell types labeled in different colors. **B** Dot plots showing the expression of representative marker genes in porcine livers. **C** Graph-based re-clustering of porcine hepatocytes revealed two subpopulations: periportal and central hepatocytes. **D** KEGG enrichment analysis of the periportal hepatocyte-specific genes. **E** Dot plots showing the expression of representative marker genes in porcine periportal and central hepatocytes. **F** Expression patterns of breed-specific genes involved in cholesterol metabolism and bile secretion at the digestive system categories in porcine periportal hepatocytes. **G** Heatmap showing the differential cholesteryl esters in porcine liver tissues between LT and LW piglets

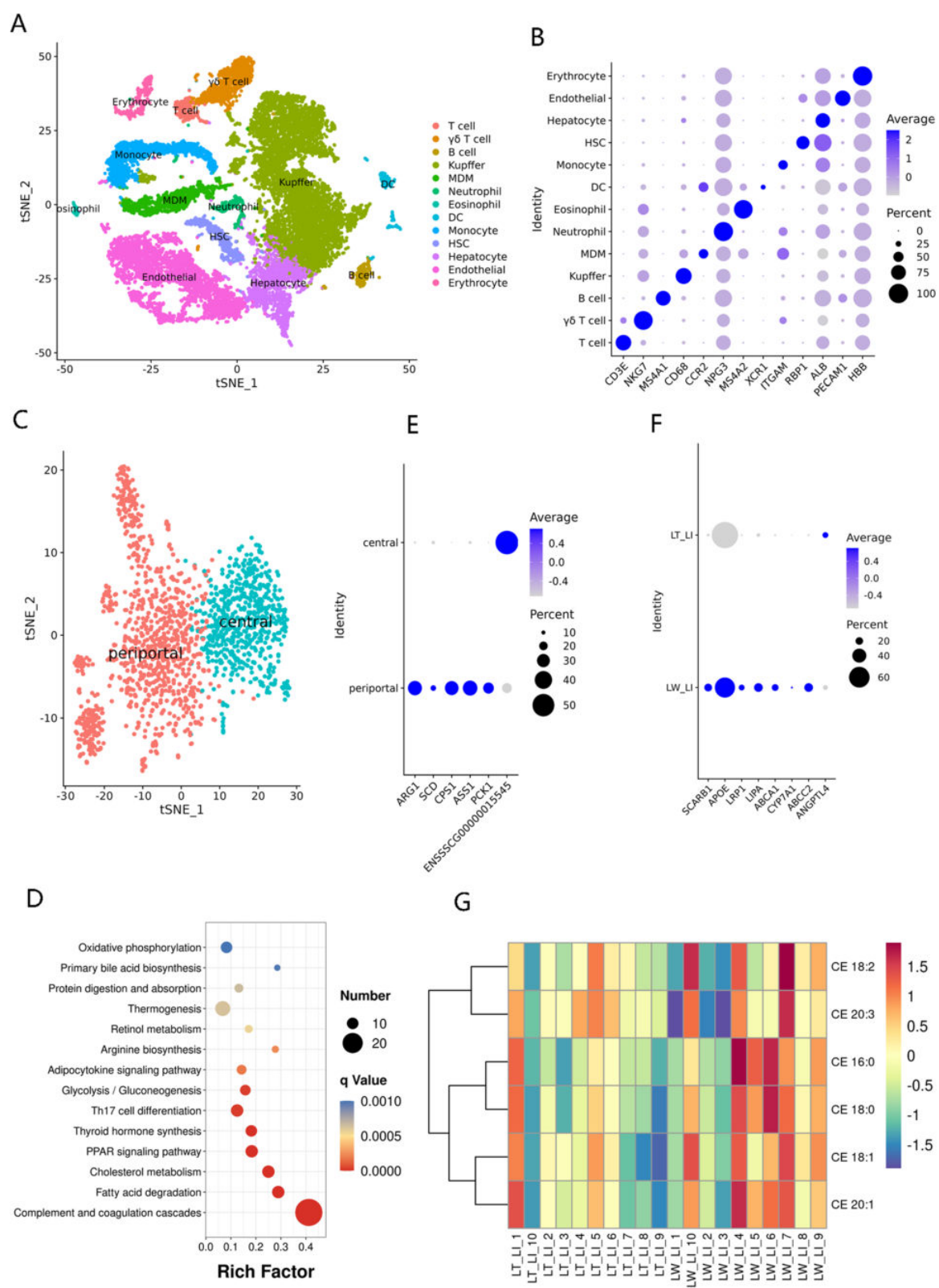


Fig. 6 (See legend on previous page.)

analysis on these DEGs revealed that the breed-related genes were highly enriched in the pathways responsible for energy and nutrient metabolism, and a range of significantly upregulated genes involved in cholesterol metabolism and bile secretion were observed in digestive system categories in the LW liver (Table S6G; Fig. 6F). Among them, the HDL receptor gene *SCARB1* involved in the selective uptake of HDL-associated esterified cholesterol [109], as well as the apolipoprotein E (APOE) receptor gene *LRP1* linked to hepatocytic absorption of CM remnant [110], was strongly increased in the periportal hepatocytes isolated from the LW liver, thereby improved the transfer of cholesteryl esters (CEs) from HDL or CM remnant to the hepatic cells for bile acid biosynthesis [111]. The lipid composition and metabolite profiling of porcine liver tissues were further investigated by lipidomic technology, and a total of 2202 metabolite molecules were found in our study (Table S6H), including 552 significantly regulated metabolites between LT and LW groups (Table S6I). The results showed that five CEs were all obviously upregulated in the LW liver, and CE 16:0 and CE 18:0 were significantly enriched in the LW groups (Fig. 6G), in agreement with the high level of *SCARB1* and *LRP1* expression for HDL-associated CEs and CM remnant uptake in the LW hepatocytes. Notably, blood HDL, mainly generated from the small intestine and liver tissues, is a main carrier of cholesterol in the circulation and transports excess peripheral cholesterol to the liver for bile acid synthesis [112]. The biogenesis of HDL requires APOA1 and the cholesterol transporter ABCA1 [113]. In mammals, ABCA1, a transmembrane protein that mediates the rate-controlling step in HDL particle formation, is highly expressed in the liver and intestine, and its major function is to mediate the transport of free cholesterol and phospholipids from peripheral cells to APOA1 protein for generating HDL particles [114]; deletion of intestinal ABCA1 gene in mice considerably reduces approximately 30% of the steady-state plasma HDL pool [115]. In LW hepatocytes, our survey showed that the expression levels of *ABCA1* and *APOA1* were significantly upregulated, as well as in the jejunal enterocytes of the LW breed, strongly implying the high efficiency of nascent HDL synthesis in the LW breed. For bile acid biosynthesis, lysosomal acid lipase (LIPA) has major roles in hydrolyzing CEs to cholesterol in the endocytic compartment [116], while cholesterol 7 α -hydroxylase (CYP7A1), a rate-limiting enzyme of bile acid biosynthesis, contributes to catalyze the hydroxylation of cholesterol [117]. The ABCG2 generally serves as a transporter for exporting bile acids from hepatocytes to bile [118]. The expression patterns of these LW-enriched genes illustrated high efficiency in bile acid biosynthesis and secretion in the LW breed. In contrast,

angiopoietin-like 4 (ANGPTL4), a secretory protein that inhibits lipoprotein lipase and modulates extracellular triacylglycerol homeostasis [119], was upregulated in the liver of LT piglets in keeping with high plasma triglyceride levels in LT piglets. A previous study has showed that bile acids influence ANGPTL4 secretion [120], in accordance with a decreased expression level of *ANGPTL4* in LW piglets and an increased level of plasmatic lipid in LT piglets. Our studies have been instrumental in elucidating the major advantages of HDL enterohepatic cycling and bile acid biosynthesis in LW piglets, and the molecular mechanisms regulating those advantages. In recent, the cholesterol contained within HDL has been extensively proven to be associated with cholesterol homeostasis and the risk of cardiovascular diseases, such as atherosclerosis in humans [121], and these key regulators and additional mechanisms delineated in our study also opened new possibilities for therapeutic interventions for the treatment of cholesterol-related diseases.

Single-cell RNA sequencing analysis of porcine longissimus dorsi tissues

To elucidate cell heterogeneity and dynamic breed-induced changes in porcine muscle tissues, we performed single-cell RNA sequencing on porcine longissimus dorsi tissues obtained from LT and LW piglets. We obtained a total of 19,229 single-cell transcriptomes, and further performed unsupervised shared nearest neighbor clustering, which partitioned cells into 23 groups based on their transcriptomic programs (Fig. S3A). To identify these populations, we examined the normalized expression level of canonical cell type genes (Table S7A), and revealed 12 known muscle-resident cell types (Fig. 7A), which correspond to FAPs, tenocyte-like cells, endothelial cells, T and B cells, muscle stem cells (MuSCs), myoblasts, myocytes, oxidative and glycolytic myofibers, smooth muscle cells (SMMCs), and a cluster representing IMF, based on marker gene expression (Fig. 7B). These findings are similar to those reported in other studies [122, 123].

We observed a population of myogenic progenitors, containing MuSCs and myoblasts, which expressed the myogenic transcription factors *PAX7*, *MYF5*, and *MYOD1* [124], and a population of mature myocytes, which expressed *MYOG*, involved in the regulation of myocyte fusion during myogenesis [125]. In general, the terminally differentiated muscle cells displayed distinct fiber type composition and exhibited oxidative and glycolytic metabolic phenotypes, revealing a high degree of heterogeneity within the myofiber compartment [126]. In our study, the identities of cell candidates supported by high expression of *MYH7*, encoding MyHC I, were related to oxidative fibers, while subtype with unique

expression of *MYH4*, encoding MyHC Iib, contributed to glycolytic fibers (Table S7B). The glycolytic fibers within our atlas exhibited notable dynamics, and more than 4.53% (426) identified cells belonged to LW piglets, as well as 2.26% (222) in LT piglets, with the number of oxidative fibers remaining constant between two breeds (Fig. 7C; Table S7C). In muscle tissues, IMF accumulates both in (intramyocellular) and out (extramyocellular) of the muscle fibres [127]. Between cell clusters, we found a total of 658 and 1010 significantly up-expressed genes in oxidative and glycolytic myofibers, respectively (Table S7B), and KEGG annotation confirmed that the two mature myofibers were transcriptionally similar (Table S7D and E). These KEGG pathways are mainly related to energy and nutrient metabolism, such as oxidative phosphorylation, citrate cycle, pyruvate metabolism, and fatty acid degradation, consistent with biological functions of intramyocellular lipids. The intramyocellular lipids, composed mainly of triglycerides, were known to be metabolically active, providing an important energy source for muscle cells [128]. In addition, 242 (2.47%) cells revealed gene expression patterns which could be assigned to intramuscular adipocytes in LT groups, as well as 115 (1.22%) in LW groups (Fig. 7C; Table S7C). Within this cluster, cells were observed to specially express variable levels of IMF marker *APOA1* [23], while a large number of genes also preferentially detected in the clusters corresponding to IMF cells, such as *SNCA*, *SCRG1*, *CDH19*, *CNP*, and *MBP* genes (Fig. 7D), strongly suggesting them as marker candidates for intramuscular adipocytes. In addition, we observed that the 1138 IMF-specific genes had strong associations with the biosynthesis of unsaturated fatty acids and fatty acid elongation (Table S7F; Fig. S3B), including *ELOVL2*, *ELOVL5*, *ELOVL6*, *FADS1*, *FADS2*, *HSD17B1*, *HSD17B12*, *PPT2*, and *SCD*, and the co-expression modular scores of above genes were also higher in IMF (Fig. S3C). Our findings suggested that the intramuscular adipocytes were mostly associated with adipogenesis and lipid accumulation. To explore the process of lipogenesis in intramuscular, we further analyzed the transcriptomic atlas to assess how the IMF subtypes were dynamically altered in incidence

and gene expression across the porcine breeds. In total, we only discerned 244 and 233 genes that exhibited significant increases or decreases in LT piglets (Table S7G), but KEGG annotation revealed no significant differences in lipid metabolism between breeds (Table S7H), including the genes of *DGAT1* and *DGAT2* (the final step in triglyceride synthesis) [129] and *acyl-CoA synthetase* family (the activation of intracellular FFA) [130]. These observations strongly supported that the IMF cells of the LT breed in muscle tissues were obviously linked to adipocytogenesis than lipogenesis processes in comparison with the LW breed.

The FAPs are the lineage precursors of specialized cells, including activated fibroblasts, adipocytes, and osteogenic cells [131]. We detected that FAP subpopulations comprised 39.76% and 49.09% of the LT and LW muscle tissues (Table S7C), consistent with human skeletal muscle, illustrating that FAPs were the most represented cell population in human skeletal muscle [132]. As expected, we found the FAP population highly expressed for *LUM* and *COL1A1*, as well as partly expressing *THY1* (*CD90*) (Fig. 7E). A previous report showed that the *THY1*-subset of FAPs was associated with adipogenesis, while *THY1*+ FAPs were involved in fibrogenesis [133]. We therefore took advantage of our scRNA-seq data and re-clustered the FAP population with high resolution, which resulted in 10 subpopulations (Fig. S3D; Table S7I). To further understand the differentiation process of FAP populations, we performed the slingshot pseudotime inference analysis to predict lineage patterns within the FAP cells (Fig. 7F), and the result indicated an origin in clusters 2, 3, and 4 (Fig. S3E), where a high proportion of *THY1*+ cells were observed (Fig. S3F). The lineage then progressed through branch point 2 to clusters 0 and 1 (Fig. S3E), consisting of a large number of *THY1*- cells and accounting for 50.65% of total identified FAPs in the LT breed (1977/3903) and 50.40% in the LW breed (2329/4621), respectively (Fig. S3F). These lines of evidences suggested that *THY1*- cells arose from *THY1*+ FAPs, and *THY1*+ cells could represent a progenitor subpopulation, in accordance with the previous study [133]. We then examined the pseudotime

(See figure on next page.)

Fig. 7 Clustering and pseudotemporal trajectories identified transcriptional dynamics of porcine muscle tissues. **A** t-SNE analysis of 19,229 single cells from porcine muscle tissues, with 12 major cell types labeled in different colors. **B** Expression of representative genes in distinct cell clusters. **C** The proportions of the 12 major cell types in porcine muscle tissues. **D** Expression of IMF-enriched genes, including *APOA1*, *SNCA*, *SCRG1*, *CDH19*, *CNP*, and *MBP* genes. **E** t-SNE plot showing the expression of *LUM*, *COL1A1* and *THY1* in porcine FAPs. **F** Pseudotime single-cell trajectory reconstructed by Monocle2 for FAP subpopulation. Pseudotime was shown in a gradient from dark to light blue. **G** Pseudotemporal heat map showing gene expression dynamics for significant marker genes. The genes (rows) were clustered into three modules, and the cells (columns) were ordered according to pseudotime. **H** The differentially expressed genes between LT and LW piglets increased along with pseudotime trajectory in porcine FAP subtypes. **I** The differentially expressed genes between LT and LW piglets decreased along with pseudotime trajectory in porcine FAP subtypes

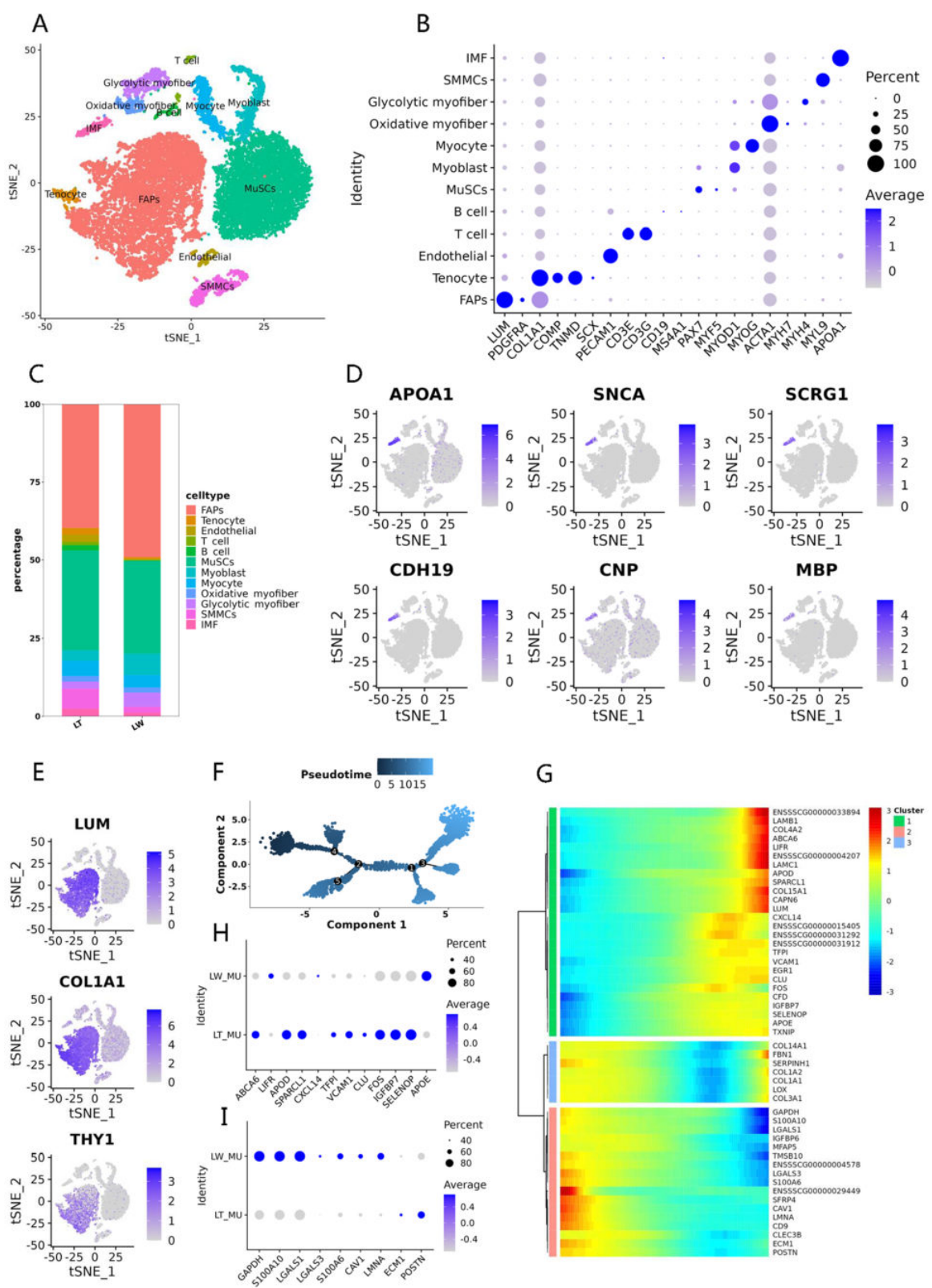


Fig. 7 (See legend on previous page.)

dynamics, which identified pseudotime-dependent genes and arranged them into clusters. This analysis revealed three gene modules, and top 50 DEGs were displayed in accordance with distinct pseudotime tracks (Fig. 7G). In detail, a series of genes, evidently increased along with the pseudotime trajectory, were significantly differential expression between LT and LW groups (Fig. 7H; Table S7J). In particular, some LT-enriched genes were predominantly involved in lipid trafficking (*ABCA6*, *APOD*) [134, 135], lipid synthesis (*FOS*) [136], lipid accumulation (*CLU*) [137], and preadipocyte differentiation (*SPARCL1*, *IGFBP7*) [138, 139], while several LW-enriched genes contributed to a significant decrease in the accumulation of triglycerides during adipogenesis (*LIFR*) [140] and lipid phagocytosis (*CXCL14*) [141]. In contrast, a number of genes seemed to lose expression along from *THY1*⁺ cells to *THY1*[−] cells, including the significantly upregulated genes in the LW group such as *GAPDH*, *S100A10*, *LGALS1*, *LGALS3*, *S100A6*, *CAVI*, and *LMNA*, as well as the *ECM1* and *POSTN* genes enriched in the LT group (Fig. 7I; Table S7J). Among them, some genes highly expressed at the beginning points of pseudotime trajectory were associated with adipocyte differentiation and adipogenesis (*LGALS1*, *POSTN*) [142, 143], lipoprotein transcytosis and lipid droplet formation (*CAVI*) [144, 145], and fat loss (*LMNA*) [144]. The results illustrated that pseudotime analysis established a basis for exploring gene candidates of FAP differentiation programs, and these breed-responsive genes that related to lipid metabolism maybe resulted in the functional differences in adipocytogenesis between LT and LW piglets.

The muscle tissues mainly rely on plasma TGs as an important source of fatty acids for subsequent oxidation or storage, and plasma TGs are generally packaged into the TG-rich CM and VLDL synthesized by the intestine and liver, respectively [146]. In our study, a significantly higher level of serum TGs was found accordingly in LT piglets, and in agreement with previous observations, similar results were identified in other Chinese native fatty breeds, such as Jinhua pigs [147], Erhualian pigs [148], and Meishan pigs [149]. The high TG concentration in local Chinese pigs illustrated that these breeds might have a lower ability to clear circulating chylomicron-TG. In the postprandial state, the clearance of circulating chylomicrons is largely dependent on hepatocyte, myocyte, and adipocyte LPL activities [150]. In general, LPL secreted by different cells is trafficked across capillary endothelial cells and anchored to the capillary wall by GPIHBP1, where it then hydrolyzes TG to release FFA [151]. The GPIHBP1 protein, an endothelial cell transporter for TG-rich lipoprotein lipase, is mainly located in capillary endothelial cells [152]. In our study, a total of

223 (2.27%) cells exhibited gene expression pattern of endothelial cells in LT groups, as well as only 29 (0.31%) in LW groups (Table S7C), and we found that the *GPIHBP1* gene was enriched in the endothelial cells (Table S7B) and significantly upregulated in the LT piglets compared to LW piglets (Table S7K), as well as the expression levels of *CD36* and *FABP5* genes in endothelial cells (Fig. S3G). The CD36 protein, located on various cell membranes, transports fatty acids in response to dietary fat [153], while *FABP5* expression is most prominent in the epidermis and considered a transporting and binding agent for lipid homeostasis [154]. These results demonstrated that the muscular differences in lipid metabolism, probably linked to pig breed, were associated primarily with the physiological functions of epithelium in TG-rich lipoprotein hydrolysis and FFA absorption.

In conclusion, we provided a comprehensive resource describing the cell dynamics and transcriptomic profiles involved in lipid metabolism in the porcine jejunum, colon, liver, and longissimus dorsi muscle, as well as the breed-specific differences in gut microbiota composition responsible for dietary fat metabolism. Our findings could open a new avenue to understanding several molecular characteristics of lipid digestibility, absorption, conversion, and deposition across tissues, which may be particularly useful for improving pork quality and developing therapies for human lipid metabolic diseases.

Material and methods

Animals and samples

This study included 10 Chinese fat-type piglets of LT and 10 typical lean-type piglets of LW. All piglets were collected from a large-scale pig breeding farm (Xinfeng County, Shaoguan City, Guangdong Province, China). One healthy and purebred LT or LW male piglet per litter was slaughtered on day 3 postnatal, and samples of the jejunum, colon, liver, and longissimus dorsi muscle tissues were freshly collected and immediately subjected to single-cell isolation. The jejunum digesta, colon content, serum, liver, and longissimus dorsi muscle in each piglet were harvested separately and snap-frozen in liquid nitrogen for further analysis.

Preparation for scRNA-seq

The jejunum, colon, liver, and longissimus dorsi isolated from 10 experimental individuals in each breed were pooled and stripped of non-purpose tissues, such as blood stains, muscle, and fatty layers. Next, the harvested tissues were cut into 1 mm³ pieces on ice and dissociated into single cells in a dissociation solution (0.35% collagenase I, 2 mg/mL papain, 120 units/mL Dnase I) in

a 37 °C water bath with shaking for 20 min at 100 rpm. Digestion was terminated with 1×PBS (Hyclone, Logan, UT) containing 10% fetal bovine serum (Life Technologies, Foster City, CA), followed by a filtration step through 70 µm and 30 µm strainer (Miltenyi Biotec, Bergisch Gladbach, Germany). Digested cells were centrifuged at 300×g for 5 min at 4 °C and then resuspended in 100µL 1×PBS (0.04% BSA) and added with 1 mL 1×red blood cell lysis buffer (MACS 130-094-183) and incubated on ice for 10 min. After incubation, the suspension was centrifuged at 300×g for 5 min at 4 °C and resuspended in 100 µL Dead Cell Removal MicroBeads (MACS 130-090-101) and removed dead cells using Miltenyi Dead Cell Removal Kit (MACS 130-090-101). The overall cell viability was confirmed by trypan blue exclusion (Thermo Fisher Scientific, Waltham, MA), which needed to be above 85%, while single-cell suspensions were counted using a Countess II Automated Cell Counter (Thermo Fisher Scientific) and further diluted to a concentration of 700–1200 cells/µL for 10×Genomics sequencing. Live cells were loaded to 10×chromium to capture approximately 5000 single cells by 10×Genomics Chromium Single-Cell v3 kit (10×Genomics, San Francisco, CA) following the manufacturer's protocol. The libraries were multiplexed and sequenced on NovaSeq 6000 sequencing system (paired-end multiplexing run, 150 bp) (Illumina, San Francisco, CA) at a minimum depth of 20,000 reads per cell.

scRNA-seq computational analysis

Sequencing results were demultiplexed and converted to FASTQ format using Illumina bcl2fastq software v2.20 (<https://support.illumina.com>). Sample demultiplexing, barcode processing, and single-cell 3' gene counting were carried out using the cell ranger pipeline (<https://www.10xgenomics.com/support>), and sequencing reads were aligned to *Sscrofa11.1* reference genome to obtain the raw digital gene expression matrix with the unique molecular identifier (UMI) counts per gene per cell. The cell ranger outputs were then loaded into Seurat v4.0.3 [155], and the cell candidates were removed if they expressed fewer than 500 unique genes, more than 50,000 UMI counts, or greater than 25% mitochondrial reads. To visualize the data, we further reduced the dimensionality of all high-quality cells using Seurat, and applied the t-SNE algorithm to project the cells into 2D space. In detail, the “normalization” function in the Seurat package was used to calculate the expression levels of genes; the “FindClusters” function with default parameters was performed to perform cell clustering; the “FindAllMarkers” function was used to determine the DEGs or marker genes with $|\text{Log}(\text{Fold Change})| > 0.25$ and P value < 0.05 .

GO and KEGG annotation of DEGs were performed by the “enrichGO” and “enrichKEGG” functions in the clusterProfiler package v4.0.5 [156].

Metagenomic library construction and quality control

The frozen contents of the jejunum and colon were thawed on ice, and total genomic DNAs were extracted by a Quick Gel Extraction Kit (Qiagen, Hilden, Germany) as described in the manufacturer's protocol. We then measured the DNA concentration and purity with a NanoDrop ND-1000 spectrophotometer (NanoDrop Technologies, Wilmington, DE). The total DNAs were subjected to library construction through DNA-fragmentation, end-repair, adapter-ligation, and unbiased PCR amplification using NEBNext Ultra II DNA Library Prep Kit (New England Biolabs, Ipswich, MA). Agilent 2100 Bioanalyzer (Agilent Technologies, Palo Alto, CA) was used for quality control of the DNA libraries, and the qualified libraries were sequenced with an Illumina platform.

Bioinformatics analysis of metagenome

Readfq v8 (<https://github.com/cjfields/readfq>) was used for preprocessing raw data, and then, clean reads were blasted with the *Sscrofa11.1* reference to filter out fragments that came from the host genome by Bowtie2 software v2.2.4 (<http://bowtie-bio.sourceforge.net/bowtie2/index.shtml>). MEGAHIT software v1.0.4 was further used for assembly analysis of the filtered clean data, and Scaffigs without N were obtained by breaking the resulting Scaffolds from the N junction [157]. With the default parameters, MetaGeneMark v3.05 (<http://topaz.gatech.edu/GeneMark/>) was applied to perform ORF prediction for Scaffigs (≥ 500 bp) in each library, and the candidates with a length less than 100nt in the prediction results were filtered out [158]. For the ORF prediction results, CD-HIT software v4.5.8 (<http://www.bioinformatics.org/cd-hit/>) was used to eliminate redundancy and obtain the non-redundant initial gene catalog. The clean reads in each library were then aligned to the initial gene catalog using Bowtie2 and calculated the abundance of identified genes, while genes with reads ≤ 2 in each sample were removed to finally determine the gene catalog (Unigenes) for subsequent analysis [159]. DIAMOND software v2.9.10 (<https://github.com/bbuchfink/diamond/>) was used for the alignment of Unigene sequences with those of bacteria, fungi, archaea, and viruses extracted from NCBI-nr database (<https://www.ncbi.nlm.nih.gov/>) with e value $< 1e-5$ [160]. Gene functional annotations were made by BLASTP search (e value $< 1e-5$) with KEGG (<http://www.kegg.jp/kegg/>), eggNOG (<http://eggno5.embl.de/#/app/home>), and CAZy (<http://www.cazy.org/>) databases.

Lipid extraction

About 0.75 mL of methanol was added to 100 μ L serum (100 mg tissue powder) in a glass tube with a Teflon-lined cap and vortexed the tubes well. Then, 2.5 mL of Methyl Tert-Butyl Ether (MTBE) was mixed and incubated for 1 h at room temperature in a shaker. Phase separation was induced by adding 0.625 mL of MS-grade water, and the tested samples were centrifuged at $1000\times g$ for 10 min. The upper (organic) phase was collected, while the lower phase was re-extracted with 1 mL of MTBE/methanol/water mixture (10:3:2.5; v/v/v) and centrifuged to collect the upper phase. Combined organic phases were dried and dissolved in 100 μ L of isopropanol for LC-MS/MS analysis.

UHPLC-MS/MS analysis

All analyses were performed on a Vanquish UHPLC system (Thermo Fisher) coupled with an Orbitrap Q Exactive HF mass spectrometer (Thermo Fisher). The raw data generated by UHPLC-MS/MS were processed using the Compound Discoverer (Thermo Fisher) to perform peak alignment, peak picking, and quantitation for each metabolite. After that, peak intensities were normalized to the total spectral intensity, and the normalized data was further used to predict the molecular formula based on additive ions, molecular ion peaks, and fragment ions. Then, peaks were matched with the Lipidmaps and Lipidblast database to obtain accurate qualitative and relative quantitative results. We applied univariate analysis (t test) to calculate the statistical significance (P value). The metabolites with $VIP > 1$ and P value < 0.05 and fold change ≥ 2 or ≤ 0.5 were considered to be differential metabolites between LT and LW.

Supplementary Information

The online version contains supplementary material available at <https://doi.org/10.1186/s40168-023-01743-3>.

Additional file 1: Fig. S1. Identification of distinct cell populations in porcine small and large intestines. A t-SNE analysis of 10,227 single-cell RNA-sequencing cells in the porcine jejunal segment, with 16 major cell types labeled in different colors. B t-SNE analysis of 12,906 single-cell RNA-sequencing cells in the porcine colonic segment, with 14 major cell types labeled in different colors. C, D Violin plots showing the representative genes of ILC3 cells (C) and pericytes (D) in porcine jejunum. E Violin plots showing the representative genes of distal mature enterocytes in the porcine colon. F dot plots showing the expression of representative markers for intestinal epithelial cells. G graph-based clustering and t-SNE plot of porcine epithelial cells revealed two subpopulations: proximal and distal enterocytes. H, I Expression of representative genes between proximal and distal enterocytes by t-SNE plot (H) and dot plot (I).

Additional file 2: Fig. S2. Taxonomic annotation of porcine intestinal microbiota and lipidomic analysis of porcine intestinal contents. A Non-metric multi-dimensional scaling analysis (NMDS) of the tested samples at the genus level. B Hierarchical clustering analysis of the tested samples at the genus level. On the left were the Bray-Curtis distances between different samples at the genus level, and on the right was

the relative abundance distribution map of each sample at the genus level. C The KEGG ortholog annotation of the metagenome-assembled genes in porcine intestinal tracts. D The eggNOG ortholog annotation of the metagenome-assembled genes in porcine intestinal tracts. E Lipid metabolites identified at negative ion mode in porcine jejunal contents. F The distribution of the metagenome-assembled genes involved in SCFA synthesis on colonic bacteria at phylum and genus levels. The colors of the lines represented different taxonomy levels.

Additional file 3: Fig. S3. The single-cell landscapes and functional annotation of porcine muscle-resident cell types. A tSNE plot showing the distribution of the muscle-resident clusters in LT and LW piglets. B KEGG pathway analysis of IMF-specific genes. C The gene set scores were calculated across various muscle-resident cell types based on the AddModuleScore method. D Graph-based re-clustering of porcine FAPs revealed 10 clusters that were labeled in different colors. E Pseudotime trajectory analysis corresponds to the differentiation of the FAP subpopulation from THY1-positive cells to THY1-negative cells. The cells were colored by cluster types. F Dot plots showing the expression of LUM, COL1A1 and THY1 genes in each cluster of the FAP subpopulation. G The expression levels of CD36 and FABP5 genes in porcine endothelial cells between LT and LW piglets.

Additional file 4: Table S1A. The list of canonical cell type-specific markers. **Table S1B** The cluster-specific genes identified for 40 major cell clusters.

Additional file 5: Table S2A. The proportions of the 28 major clusters in porcine intestinal tracts. **Table S2B** List of canonical cell type-specific markers in porcine intestinal tracts. **Table S2C** The proportions of the 14 major cell types in porcine intestinal tracts. **Table S2D** The enterocyte-enriched genes identified in porcine intestinal tracts. **Table S2E** KEGG analysis of the enterocyte-enriched genes identified in porcine intestinal tracts.

Additional file 6: Table S3A. Differentially expressed genes between LT and LW piglets in small intestinal epithelial cells. **Table S3B** KEGG analysis of differentially expressed genes between LT and LW piglets in small intestinal epithelial cells. **Table S3C** Lipid metabolites identified in porcine serum. **Table S3D** Differential lipid metabolites in porcine serum between LT and LW piglets. **Table S3E** Differentially expressed genes between LT and LW piglets in large intestinal epithelial cells. **Table S3F** KEGG analysis of differentially expressed genes between LT and LW piglets in large intestinal epithelial cells. **Table S3G** Differentially expressed genes between LT and LW piglets in large intestinal Paneth cells. **Table S3H** KEGG analysis of differentially expressed genes between LT and LW piglets in large intestinal Paneth cells. **Table S3I** The cell composition of porcine colon tissues.

Additional file 7: Table S4A. Quality control and preprocessing of metagenomic datasets. **Table S4B** Basic statistics of the metagenome-assembled scaffolds. **Table S4C** Basic statistics of the gene catalogues. **Table S4D** The relative abundance of intestinal microbiota at the phylum level. **Table S4E** The relative abundance of intestinal microbiota at the genus level. **Table S4F** The relative abundance of intestinal microbiota at the species level. **Table S4G** Comparison of the classification of jejunal microbiota between two breeds by linear discriminant analysis effect size (LefSe) method. **Table S4H** Comparison of the classification of colonic microbiota between two breeds by linear discriminant analysis effect size (LefSe) method. **Table S4I** List of genus differentially abundant in porcine jejunum between LT and LW samples. **Table S4J** List of genus differentially abundant in porcine colon between LT and LW samples.

Additional file 8: Table S5A. Functional profiles of the metagenome-assembled genes with KEGG ortholog annotation in porcine intestinal tracts. **Table S5B** Functional profiles of the metagenome-assembled genes with eggNOG ortholog annotation in porcine intestinal tracts. **Table S5C** List of KEGG orthologs differentially abundant in porcine jejunum segment between LT and LW samples. **Table S5D** Functional terms annotated with KEGG pathway in porcine jejunal segment. **Table S5E** List of KEGG pathways differentially abundant in porcine jejunal segment between LT and LW samples. **Table S5F** Lipid metabolites identified in porcine jejunal contents. **Table S5G** Differential lipid metabolites in porcine jejunal contents between LT and LW piglets. **Table S5H** The

distribution of the metagenome-assembled genes on bacteria at different taxonomy levels. **Table S5I** Functional terms annotated with KEGG pathway in porcine colonic segment. **Table S5J** List of KEGG pathways differentially abundant in porcine colonic segment between LT and LW samples.

Additional file 9: Table S6A. List of canonical cell type-specific markers in porcine liver tissues. **Table S6B** The proportions of the 13 major cell types in porcine liver tissues. **Table S6C** The zonation-specific genes in porcine periportal and central hepatocytes. **Table S6D** KEGG analysis of the periportal hepatocyte-specific genes. **Table S6E** KEGG analysis of the central hepatocyte-specific genes. **Table S6F** Differentially expressed genes between LT and LW piglets in porcine periportal hepatocytes. **Table S6G** KEGG analysis of differentially expressed genes in porcine periportal hepatocytes between LT and LW piglets. **Table S6H** Lipid metabolites identified in porcine liver tissues. **Table S6I** Differential lipid metabolites in porcine liver tissues between LT and LW piglets.

Additional file 10: Table S7A. List of canonical cell type-specific markers in porcine muscle tissues. **Table S7B** The cell type-specific genes identified in porcine muscle. **Table S7C** The proportions of the 12 major cell types in porcine muscle tissues. **Table S7D** KEGG analysis of the significantly up-expressed genes in oxidative myofibers. **Table S7E** KEGG analysis of the significantly up-expressed genes in glycolytic myofibers. **Table S7F** KEGG analysis of the significantly up-expressed genes in intermuscular fat cells. **Table S7G** Differentially expressed genes between LT and LW piglets in porcine IMF subtypes. **Table S7H** KEGG analysis of differentially expressed genes in porcine IMF subtypes between LT and LW piglets. **Table S7I** The expression levels of identified genes in each cluster of FAP subpopulation. **Table S7J** Differentially expressed genes in porcine FAP subtypes between LT and LW piglets. **Table S7K** Differentially expressed genes in porcine endothelial cells between LT and LW piglets.

Acknowledgements

We thank the high-performance computing center of South China Agricultural University for providing computational resources in this work.

Authors' contributions

Jiajie Sun: Conceptualization, Methodology, Data curation, Software, Writing-Original draft preparation. Fang Xie: Data curation, Investigation. Jing Wang: Conceptualization, Supervision. Junyi Luo: Investigation. Ting Chen: Investigation. Qingyan Jiang: Supervision. Qianyun Xi: Supervision. George E. Liu: Software, Reviewing and Editing, Methodology, Visualization, Investigation. Yongliang Zhang: Supervision. All authors have read and approved the final version of the manuscript.

Funding

This work was supported by the Sci-Tech Innovation 2030 Agenda [grant numbers 2023ZD04044], the Natural Science Foundation of China Program [grant numbers 32072714, 31802032], the Opening Foundation of State Key Laboratory of Swine and Poultry Breeding Industry [2023GZ20], the Natural Science Foundation of Guangdong Province [grant number 2020A151010062], and the Science and Technology Project of Guangzhou [grant number 202002030037].

Availability of data and materials

The raw sequences were deposited into Sequence Read Archive (SRA) database with the BioProject accession number PRJNA1019009 (<https://dataview.ncbi.nlm.nih.gov/object/PRJNA1019009?reviewer=vqi08r93cjqd1vmi3f994tik79>).

Declarations

Ethics approval and consent to participate

Our study was carried out in compliance with the ARRIVE guidelines, and any anesthesia or euthanizing agent was not used in our study. This study was approved by the Animal Care Committee of South China Agricultural University (animal care protocol number 2022F096), and all applicable institutional and national guidelines for the care and use of animals were followed.

Consent for publication

Not applicable.

Competing interests

The authors declare no competing interests.

Received: 17 September 2023 Accepted: 19 December 2023

Published online: 20 February 2024

References

- Whitnall T, Pitts N. Global trends in meat consumption. *Agric Commod Stat.* 2019;1:96–9.
- Parlasca MC, Qaim M. Meat consumption and sustainability. *Annu Rev Resour Econ.* 2022;14:17–41.
- Font-i-Furnols M, Skrlep M, Aluwe M. Attitudes and beliefs of consumers towards pig welfare and pork quality. *Earth Environ Sci.* 2019;333:012002.
- Kim JA, Cho ES, Jeong YD, Choi YH, Kim YS, Choi JW, et al. The effects of breed and gender on meat quality of Duroc, Pietrain, and their cross-bred. *J Anim Sci Technol.* 2020;62:409–19.
- Huang Y, Zhou L, Zhang J, Liu X, Zhang Y, Cai L, et al. A large-scale comparison of meat quality and intramuscular fatty acid composition among three Chinese indigenous pig breeds. *Meat Sci.* 2020;168:108182.
- Hausman GJ, Basu U, Du M, Fernyhough-Culver M, Dodson MV. Intermuscular and intramuscular adipose tissues: bad vs. good adipose tissues. *Adipocyte.* 2014;3(4):242–55.
- Consitt LA, Bell JA, Houmard JA. Intramuscular lipid metabolism, insulin action, and obesity. *IUBMB Life.* 2009;61:47–55.
- Yan S, Tu Z, Liu Z, Fan N, Yang H, Yang S, et al. A Huntingtin knockin pig model recapitulates features of selective neurodegeneration in Huntington's disease. *Cell.* 2018;173:989–1002.
- Lunney JK, Van Goor A, Walker KE, Hailstock T, Franklin J, Da C. Importance of the pig as a human biomedical model. *Sci Transl Med.* 2021;13:eabd5758.
- Gao X, Nowak-Imialek M, Chen X, Chen D, Herrmann D, Ruan D, et al. Establishment of porcine and human expanded potential stem cells. *Nat Cell Biol.* 2019;21:687–99.
- Kershaw EE, Flier JS. Adipose tissue as an endocrine organ. *J Clin Endocrinol Metab.* 2004;89:2548–56.
- Li X, Fu X, Yang G, Du M. Review: enhancing intramuscular fat development via targeting fibro-adipogenic progenitor cells in meat animals. *Animal.* 2020;14:312–21.
- Uezumi A, Fukada S, Yamamoto N, Ikemoto-Uezumi M, Nakatani M, Morita M, et al. Identification and characterization of PDGFR α + mesenchymal progenitors in human skeletal muscle. *Cell Death Dis.* 2014;5:e1186.
- Ambele MA, Dhanraj P, Giles R, Pepper MS. Adipogenesis: a complex interplay of multiple molecular determinants and pathways. *Int J Mol Sci.* 2020;21:4283.
- Fève B. Adipogenesis: cellular and molecular aspects. *Best Pract Res Clin Endocrinol Metab.* 2005;19:483–99.
- Valet P, Tavernier G, Castan-Laurell I, Saulnier-Blache JS, Langin D. Understanding adipose tissue development from transgenic animal models. *J Lipid Res.* 2002;43:835–60.
- Du M, Tong J, Zhao J, Underwood KR, Zhu M, Ford SP, et al. Fetal programming of skeletal muscle development in ruminant animals. *J Anim Sci.* 2010;88:E51–60.
- Luo H, Jiang M, Lian G, Liu Q, Shi M, Li TY, et al. AIDA selectively mediates downregulation of fat synthesis enzymes by ERAD to retard intestinal fat absorption and prevent obesity. *Cell Metab.* 2018;27:843–53.
- Ha C, Martin A, Sepich-Poore GD, Shi B, Wang Y, Gouin K, et al. Translocation of viable gut microbiota to mesenteric adipose drives formation of creeping fat in humans. *Cell.* 2020;183:666–83.
- Trefts E, Gannon M, Wasserman DH. The liver. *Curr Biol.* 2017;27:R1147–51.
- Rodríguez A, Becerril S, Hernández-Pardos AW, Frühbeck G. Adipose tissue depot differences in adipokines and effects on skeletal and cardiac muscle. *Curr Opin Pharmacol.* 2020;52:1–8.

22. Jovic D, Liang X, Zeng H, Lin L, Xu F, Luo Y. Single-cell RNA sequencing technologies and applications: a brief overview. *Clin Transl Med*. 2022;12:e694.
23. Li J, Xing S, Zhao G, Zheng M, Yang X, Sun J, et al. Identification of diverse cell populations in skeletal muscles and biomarkers for intramuscular fat of chicken by single-cell RNA sequencing. *BMC Genomics*. 2020;21:752.
24. Bergen WG. Pigs (*Sus Scrofa*) in biomedical research. *Adv Exp Med Biol*. 2022;1354:335–43.
25. Laurens C, Moro C. Intramyocellular fat storage in metabolic diseases. *Horm Mol Biol Clin Investig*. 2016;26(1):43–52.
26. Fawcner-Corbett D, Antanaviciute A, Parikh K, Jagielowicz M, Gerós AS, Gupta T, et al. Spatiotemporal analysis of human intestinal development at single-cell resolution. *Cell*. 2021;184:810–26.
27. Haber AL, Biton M, Rogel N, Herbst RH, Shekhar K, Smillie C, et al. A single-cell survey of the small intestinal epithelium. *Nature*. 2017;551:333–9.
28. Dávalos-Salas M, Mariadason JM, Watt MJ, Montgomery MK. Molecular regulators of lipid metabolism in the intestine—underestimated therapeutic targets for obesity? *Biochem Pharmacol*. 2020;178:114091.
29. Sztalryd C, Brasaemle DL. The perilipin family of lipid droplet proteins: gatekeepers of intracellular lipolysis. *Biochim Biophys Acta Mol Cell Biol Lipids*. 2017;1862:1221–32.
30. Wang Y, Song W, Wang J, Wang T, Xiong X, Qi Z, et al. Single-cell transcriptome analysis reveals differential nutrient absorption functions in human intestine. *J Exp Med*. 2020;217:e20191130.
31. Stumpff F. A look at the smelly side of physiology: transport of short chain fatty acids. *Pflugers Arch*. 2018;470:571–98.
32. Louis P, Flint HJ. Formation of propionate and butyrate by the human colonic microbiota. *Environ Microbiol*. 2017;19:29–41.
33. Chen C, Yin Y, Tu Q, Yang H. Glucose and amino acid in enterocyte: absorption, metabolism and maturation. *Front Biosci*. 2018;23:1721–39.
34. Wright EM. Glucose transport families SLC5 and SLC50. *Mol Aspects Med*. 2013;34:183–96.
35. Nicklin P, Bergman P, Zhang B, Triantafellow E, Wang H, Nyfeler B, et al. Bidirectional transport of amino acids regulates mTOR and autophagy. *Cell*. 2009;136:521–34.
36. Wolfson RL, Sabatini DM. The dawn of the age of amino acid sensors for the mTORC1 pathway. *Cell Metab*. 2017;26:301–9.
37. Hu Y, Xie Y, Wang Y, Chen X, Smith DE. Development and characterization of a novel mouse line humanized for the intestinal peptide transporter PEPT1. *Mol Pharm*. 2014;11:3737–46.
38. Spanier B. Transcriptional and functional regulation of the intestinal peptide transporter PEPT1. *J Physiol*. 2014;592:871–9.
39. Nakauchi J, Matsuo H, Kim DK, Goto A, Chairoungdua A, Cha SH, et al. Cloning and characterization of a human brain Na(+)-independent transporter for small neutral amino acids that transports D-serine with high affinity. *Neurosci Lett*. 2000;287:231–5.
40. Morotti M, Zois CE, El-Ansari R, Craze ML, Rakha EA, Fan SJ, et al. Increased expression of glutamine transporter SNAT2/SLC38A2 promotes glutamine dependence and oxidative stress resistance, and is associated with worse prognosis in triple-negative breast cancer. *Br J Cancer*. 2021;124:494–505.
41. Song Z. Roles of the nucleotide sugar transporters (SLC35 family) in health and disease. *Mol Aspects Med*. 2013;34:590–600.
42. de Oliveira MR. Vitamin A and retinoids as mitochondrial toxicants. *Oxid Med Cell Longev*. 2015;2015:140267.
43. Subramanian VS, Teafatiller T, Moradi H, Marchant JS. Histone deacetylase inhibitors regulate vitamin C transporter functional expression in intestinal epithelial cells. *J Nutr Biochem*. 2021;98:108838.
44. Reboul E. Intestinal absorption of vitamin D: from the meal to the enterocyte. *Food Funct*. 2015;6:356–62.
45. Reboul E. Vitamin E intestinal absorption: regulation of membrane transport across the enterocyte. *IUBMB Life*. 2019;71:416–23.
46. Miyake K, Yasujima T, Takahashi S, Yamashiro T, Yuasa H. Identification of the amino acid residues involved in the species-dependent differences in the pyridoxine transport function of SLC19A3. *J Biol Chem*. 2022;298:102161.
47. Benoit CR, Walsh DJ, Mekerishvili L, Houerbi N, Stanton AE, McGaughey DM, et al. Loss of the vitamin B-12 transport protein Tcn2 results in maternally inherited growth and developmental defects in zebrafish. *J Nutr*. 2021;151:2522–32.
48. Hummler E, Beermann F. Scnn1 sodium channel gene family in genetically engineered mice. *J Am Soc Nephrol*. 2000;11:S129–34.
49. Eide DJ. The SLC39 family of metal ion transporters. *Pflugers Arch*. 2004;447:796–800.
50. Zogzas CE, Mukhopadhyay S. Putative metal binding site in the transmembrane domain of the manganese transporter SLC30A10 is different from that of related zinc transporters. *Metallomics*. 2018;10:1053–64.
51. Verkman AS, Anderson MO, Papadopoulos MC. Aquaporins: important but elusive drug targets. *Nat Rev Drug Discov*. 2014;13:259–77.
52. Ko CW, Qu J, Black DD, Tso P. Regulation of intestinal lipid metabolism: current concepts and relevance to disease. *Nat Rev Gastroenterol Hepatol*. 2020;17:169–83.
53. Xie C, Zhu X, Xu B, Niu Y, Zhang X, Ma L, et al. Integrated analysis of multi-tissues lipidome and gut microbiome reveals microbiota-induced shifts on lipid metabolism in pigs. *Anim Nutr*. 2022;10:280–93.
54. Wu G, Tawfeeq HR, Lackey AI, Zhou Y, Sifnakis Z, Zacharisen SM, et al. Gut microbiota and phenotypic changes induced by ablation of liver- and intestinal-type fatty acid-binding proteins. *Nutrients*. 2022;14:1762.
55. Lagakos WS, Gajda AM, Agellon L, Binas B, Choi V, Mandap B, et al. Different functions of intestinal and liver-type fatty acid-binding proteins in intestine and in whole body energy homeostasis. *Am J Physiol Gastrointest Liver Physiol*. 2011;300:G803–14.
56. Anderson CM, Stahl A. SLC27 fatty acid transport proteins. *Mol Aspects Med*. 2013;34:516–28.
57. Lenz LS, Marx J, Chamulitrat W, Kaiser I, Gröne HJ, Liebisch G, et al. Adipocyte-specific inactivation of Acyl-CoA synthetase fatty acid transport protein 4 (Fatp4) in mice causes adipose hypertrophy and alterations in metabolism of complex lipids under high fat diet. *J Biol Chem*. 2011;286:35578–87.
58. Straub RH. The memory of the fatty acid system. *Prog Lipid Res*. 2020;79:101049.
59. Wang Y, Li X, Cao Y, Xiao C, Liu Y, Jin H, et al. Effect of the ACAA1 gene on preadipocyte differentiation in sheep. *Front Genet*. 2021;12:649140.
60. Zhang F, Xiong Q, Tao H, Liu Y, Zhang N, Li XF, et al. ACOX1, regulated by C/EBPα and miR-25-3p, promotes bovine preadipocyte adipogenesis. *J Mol Endocrinol*. 2021;66:195–205.
61. Chen T, Tong F, Wu XY, Zhu L, Yi QZ, Zheng J, et al. Novel ACADVL variants resulting in mitochondrial defects in long-chain acyl-CoA dehydrogenase deficiency. *J Zhejiang Univ Sci B*. 2020;21:885–96.
62. Pan A, Sun XM, Huang FQ, Liu JF, Cai YY, Wu X, et al. The mitochondrial β-oxidation enzyme HADHA restrains hepatic glucagon response by promoting β-hydroxybutyrate production. *Nat Commun*. 2022;13:386.
63. Wang S, Smith JD. ABCA1 and nascent HDL biogenesis. *BioFactors*. 2014;40:547–54.
64. Yu XH, Qian K, Jiang N, Zheng XL, Cayabyab FS, Tang CK. ABCG5/ABCG8 in cholesterol excretion and atherosclerosis. *Clin Chim Acta*. 2014;428:82–8.
65. Betters JL, Yu L. NPC1L1 and cholesterol transport. *Febs Lett*. 2010;584:2740–7.
66. Sirwi A, Hussain MM. Lipid transfer proteins in the assembly of apoB-containing lipoproteins. *J Lipid Res*. 2018;59:1094–102.
67. Chen L, Wu M, Zhang S, Tan W, Guan M, Feng L, et al. Estrogen-related receptor γ regulates hepatic triglyceride metabolism through phospholipase A2 G12B. *FASEB J*. 2019;33:7942–52.
68. Zhang M, Yang M, Wang N, Liu Q, Wang B, Huang T, et al. Andrographolide modulates HNF4α activity imparting on hepatic metabolism. *Mol Cell Endocrinol*. 2020;513:110867.
69. Liu Q, Yang M, Fu X, Liu R, Sun C, Pan H, et al. Activation of farnesoid X receptor promotes triglycerides lowering by suppressing phospholipase A2 G12B expression. *Mol Cell Endocrinol*. 2016;436:93–101.
70. Martin-Gallausiaux C, Marinelli L, Blottière HM, Larraufie P, Lapaque N. SCFA: mechanisms and functional importance in the gut. *Proc Nutr Soc*. 2021;80:37–49.
71. Sivaprakasam S, Bhutia YD, Yang S, Ganapathy V. Short-chain fatty acid transporters: role in colonic homeostasis. *Compr Physiol*. 2017;8:299–314.
72. Lin Y, Zhang W, Chen D, Lin C, Zheng Z, Fu Q, et al. Newborn screening and genetic characteristics of patients with short- and very long-chain acyl-CoA dehydrogenase deficiencies. *Clin Chim Acta*. 2020;510:285–90.

73. Morrison DJ, Preston T. Formation of short chain fatty acids by the gut microbiota and their impact on human metabolism. *Gut Microbes*. 2016;7:189–200.
74. Shankman LS, Fleury ST, Evans WB, Penberthy KK, Arandjelovic S, Blumberg RS, et al. Efferocytosis by Paneth cells within the intestine. *Curr Biol*. 2021;31:2469–76.
75. Adolph TE, Mayr L, Grabherr F, Tilg H. Paneth cells and their antimicrobials in intestinal immunity. *Curr Pharm Des*. 2018;24:1121–9.
76. Sun J, Xie M, Huang Z, Li H, Chen T, Sun R, et al. Integrated analysis of non-coding RNA and mRNA expression profiles of 2 pig breeds differing in muscle traits. *J Anim Sci*. 2017;95:1092–103.
77. Bel S, Pendse M, Wang Y, Li Y, Ruhn KA, Hassell B, et al. Paneth cells secrete lysozyme via secretory autophagy during bacterial infection of the intestine. *Science*. 2017;357:1047–52.
78. Bel S, Hooper LV. Secretory autophagy of lysozyme in Paneth cells. *Autophagy*. 2018;14:719–21.
79. Sonnenburg WK, Yu D, Lee EC, Xiong W, Gololobov G, Key B, et al. GPIHBP1 stabilizes lipoprotein lipase and prevents its inhibition by angiopoietin-like 4 and angiopoietin-like 4. *J Lipid Res*. 2009;50:2421–9.
80. Goma E. Human gut microbiota/microbiome in health and diseases: a review. *Antonie Van Leeuwenhoek*. 2020;113:2019–40.
81. Wang Z, Wang Y, Fuhrman JA, Sun F, Zhu S. Assessment of metagenomic assemblers based on hybrid reads of real and simulated metagenomic sequences. *Brief Bioinform*. 2020;21:777–90.
82. Qin N, Yang F, Li A, Pifti E, Chen Y, Shao L, et al. Alterations of the human gut microbiome in liver cirrhosis. *Nature*. 2014;513:59–64.
83. Chen C, Zhou Y, Fu H, Xiong X, Fang S, Jiang H, et al. Expanded catalog of microbial genes and metagenome-assembled genomes from the pig gut microbiome. *Nature Commun*. 2021;12:1106.
84. Segata N, Izard J, Waldron L, Gevers D, Miropolsky L, Garrett WS, et al. Metagenomic biomarker discovery and explanation. *Genome Biol*. 2011;12:R60.
85. Schoeler M, Caesar R. Dietary lipids, gut microbiota and lipid metabolism. *Rev Endocr Metab Disord*. 2019;20:461–72.
86. Ortega-Anaya J, Jiménez-Flores R. Symposium review: the relevance of bovine milk phospholipids in human nutrition-evidence of the effect on infant gut and brain development. *J Dairy Sci*. 2019;102:2738–48.
87. Lindquist S, Hernell O. Lipid digestion and absorption in early life: an update. *Curr Opin Clin Nutr Metab Care*. 2010;13:314–20.
88. Zhao L, Huang Y, Lu L, Yang W, Huang T, Lin Z, et al. Saturated long-chain fatty acid-producing bacteria contribute to enhanced colonic motility in rats. *Microbiome*. 2018;6:107.
89. Yadav M, Kapoor A, Verma A, Ambatipudi K. Functional significance of different milk constituents in modulating the gut microbiome and infant health. *J Agric Food Chem*. 2022;70:3929–47.
90. Santiago-Rodriguez TM, Cano R, Jiménez-Flores R. Potential applications of metagenomics to assess the biological effects of food structure and function. *Food Funct*. 2016;7:4160–9.
91. Hitt C, Masson JM, Streidl T, Fischöder T, Elling L, Clavel T. Diversity and function of microbial lipases within the mammalian gut. *bioRxiv*. 2020. <https://doi.org/10.1101/2020.09.08.287425>.
92. Brown EM, Clardy J, Xavier RJ. Gut microbiome lipid metabolism and its impact on host physiology. *Cell Host Microbe*. 2023;31:173–86.
93. Sitaraman R. Phospholipid catabolism by gut microbiota and the risk of cardiovascular disease. *J Med Microbiol*. 2013;62:948–50.
94. Vulevic J, McCartney AL, Gee JM, Johnson IT, Gibson GR. Microbial species involved in production of 1,2-sn-diacylglycerol and effects of phosphatidylcholine on human fecal microbiota. *Appl Environ Microbiol*. 2004;70:5659–66.
95. Flores-Díaz M, Monturiol-Gross L, Naylor C, Alape-Girón A, Flieger A. Bacterial sphingomyelinases and phospholipases as virulence factors. *Microbiol Mol Biol Rev*. 2016;80:597–628.
96. Olivares M, Neef A, Castillejo G, Palma GD, Varea V, Capilla A, et al. The HLA-DQ2 genotype selects for early intestinal microbiota composition in infants at high risk of developing coeliac disease. *Gut*. 2015;64:406–17.
97. Zhuang L, Chen H, Zhang S, Zhuang J, Li Q, Feng Z. Intestinal microbiota in early life and its implications on childhood health. *Genomics Proteomics Bioinformatics*. 2019;17:13–25.
98. May KL, Silhavy TJ. The *Escherichia coli* phospholipase PldA regulates outer membrane homeostasis via lipid signaling. *mBio*. 2018;9:e00379-18.
99. Cronan JE, Thomas J. Bacterial fatty acid synthesis and its relationships with polyketide synthetic pathways. *Methods Enzymol*. 2009;459:395–433.
100. Iyayi EA, Adeola O. Quantification of short-chain fatty acids and energy production from hindgut fermentation in cannulated pigs fed graded levels of wheat bran. *J Anim Sci*. 2015;93:4781–7.
101. Walsh C, Lane JA, van Sinderen D, Hickey RM. Human milk oligosaccharides: shaping the infant gut microbiota and supporting health. *J Funct Foods*. 2020;72:104074.
102. Holman DB, Kommadath A, Tingley JP, Abbott DW. Novel insights into the pig gut microbiome using metagenome-assembled genomes. *Microbiol Spectr*. 2022;10:e0238022.
103. Bach Knudsen KE, Lærke HN, Hedemann MS, Nielsen TS, Ingerslev AK, Gundelund Nielsen DS, et al. Impact of diet-modulated butyrate production on intestinal barrier function and inflammation. *Nutrients*. 2018;10:1499.
104. Halpern KB, Shenhav R, Matcovitch-Natan O, Toth B, Lemze D, Golan M, et al. Single-cell spatial reconstruction reveals global division of labour in the mammalian liver. *Nature*. 2017;542:352–6.
105. MacParland SA, Liu JC, Ma XZ, Innes BT, Bartczak AM, Gage BK, et al. Single cell RNA sequencing of human liver reveals distinct intrahepatic macrophage populations. *Nature Commun*. 2018;9:4383.
106. Aizarani N, Saviano A, Sagar-Mailly L, Durand S, Herman JS, Pessaux P, et al. A human liver cell atlas reveals heterogeneity and epithelial progenitors. *Nature*. 2019;572:199–204.
107. Chiang JYL, Ferrell JM. Bile acids as metabolic regulators and nutrient sensors. *Annu Rev Nutr*. 2019;39:175–200.
108. Chiang JYL, Ferrell JM. Discovery of farnesoid X receptor and its role in bile acid metabolism. *Mol Cell Endocrinol*. 2022;548:111618.
109. Yu H. HDL and scavenger receptor class B type I (SRBI). *Adv Exp Med Biol*. 2022;1377:79–93.
110. Laatsch A, Panteli M, Sornsakrini M, Hoffzimer B, Grewal T, Heeren J. Low density lipoprotein receptor-related protein 1 dependent endosomal trapping and recycling of apolipoprotein E. *PLoS One*. 2012;7:e29385.
111. Pal R, Ke Q, Pihan GA, Yesilaltay A, Penman ML, Wang L, et al. Carboxy-terminal deletion of the HDL receptor reduces receptor levels in liver and steroidogenic tissues, induces hypercholesterolemia, and causes fatal heart disease. *Am J Physiol Heart Circ Physiol*. 2016;311:H1392–408.
112. Rosenson RS, Brewer HB Jr, Davidson WS, Fayad ZA, Fuster V, Goldstein J, et al. Cholesterol efflux and atheroprotection: advancing the concept of reverse cholesterol transport. *Circulation*. 2012;125:1905–19.
113. Han YH, Onufer EJ, Huang LH, Sprung RW, Davidson WS, Czeplinski RS, et al. Enterically derived high-density lipoprotein restrains liver injury through the portal vein. *Science*. 2021;373:eabe6729.
114. Li G, Gu HM, Zhang DW. ATP-binding cassette transporters and cholesterol translocation. *IUBMB Life*. 2013;65:505–12.
115. Brunham LR, Kruit JK, Iqbal J, Fievet C, Timmins JM, Pape TD, et al. Intestinal ABCA1 directly contributes to HDL biogenesis in vivo. *J Clin Invest*. 2006;116:1052–62.
116. Viaud M, Ivanov S, Vujic N, Duta-Mare M, Aira LE, Barouillet T, et al. Lyso-somal cholesterol hydrolysis couples efferocytosis to anti-inflammatory oxysterol production. *Circ Res*. 2018;122:1369–84.
117. Rizzolo D, Kong B, Taylor RE, Brinker A, Goedken M, Buckley B, et al. Bile acid homeostasis in female mice deficient in Cyp7a1 and Cyp27a1. *Acta Pharm Sin B*. 2021;11:3847–56.
118. Lei Z, Rong H, Yang Y, Yu S, Zhang T, Chen L, et al. Loperamide induces excessive accumulation of bile acids in the liver of mice with different diets. *Toxicology*. 2022;477:153278.
119. Singh AK, Chaube B, Zhang X, Sun J, Citrin KM, Canfrán-Duque A, et al. Hepatocyte-specific suppression of ANGPTL4 improves obesity-associated diabetes and mitigates atherosclerosis in mice. *J Clin Invest*. 2021;131:e140989.
120. Janssen AWF, Dijk W, Boekhorst J, Kuipers F, Groen AK, Lukovac S, et al. ANGPTL4 promotes bile acid absorption during taurocholic acid supplementation via a mechanism dependent on the gut microbiota. *Biophys Acta Mol Cell Biol Lipids*. 2017;1862:1056–67.
121. Kjeldsen EW, Nordestgaard LT, Frikke-Schmidt R. HDL cholesterol and non-cardiovascular disease: a narrative review. *Int J Mol Sci*. 2021;22:4547.

122. Dell'Orso S, Juan AH, Ko KD, Naz F, Perovanovic J, Gutierrez-Cruz G, et al. Single cell analysis of adult mouse skeletal muscle stem cells in homeostatic and regenerative conditions. *Development*. 2019;146:dev174177.
123. Giordani L, He GJ, Negroni E, Sakai H, Law JYC, Siu MM, et al. High-dimensional single-cell cartography reveals novel skeletal muscle-resident cell populations. *Mol Cell*. 2019;74:609–21.
124. Wu J, Matthias N, Lo J, Ortiz-Vitali JL, Shieh AW, Wang SH, et al. A myogenic double-reporter human pluripotent stem cell line allows prospective isolation of skeletal muscle progenitors. *Cell Rep*. 2018;25:1966–81.
125. Ganassi M, Badodi S, Wanders K, Zammit PS, Hughes SM. Myogenin is an essential regulator of adult myofibre growth and muscle stem cell homeostasis. *eLife*. 2020;9:e60445.
126. Pette D, Staron RS. Transitions of muscle fiber phenotypic profiles. *Histochem Cell Biol*. 2001;115(5):359–72.
127. Rahemi H, Nigam N, Wakeling JM. The effect of intramuscular fat on skeletal muscle mechanics: implications for the elderly and obese. *J R Soc Interface*. 2015;12:20150365.
128. Umek N, Horvat S, Cvetko E. Skeletal muscle and fiber type-specific intramyocellular lipid accumulation in obese mice. *J Basic Med Sci*. 2021;21:730–8.
129. Coleman RA, Lee DP. Enzymes of triacylglycerol synthesis and their regulation. *Prog Lipid Res*. 2004;43:134–76.
130. Gargiulo CE, Stuhlsatz-Krouper SM, Schaffer JE. Localization of adipocyte long-chain fatty acyl-CoA synthetase at the plasma membrane. *J Lipid Res*. 1999;40:881–92.
131. Contreras O, Rossi FMV, Theret M. Origins, potency, and heterogeneity of skeletal muscle fibro-adipogenic progenitors-time for new definitions. *Skelet Muscle*. 2021;11:16.
132. Farup J, Just J, de Paoli F, Lin L, Jensen JB, Billeskov T, et al. Human skeletal muscle CD90+ fibro-adipogenic progenitors are associated with muscle degeneration in type 2 diabetic patients. *Cell Metab*. 2021;33:2201–14.
133. Chazaud B, Mounier R. Diabetes-induced skeletal muscle fibrosis: fibro-adipogenic precursors at work. *Cell Metab*. 2021;33:2095–6.
134. Perdomo G, Henry DH. Apolipoprotein D in lipid metabolism and its functional implication in atherosclerosis and aging. *Aging*. 2009;1:17–27.
135. Tachikawa M, Toki H, Watanabe M, Tomi M, Hosoya KI, Terasaki T. Gene expression of A6-like subgroup of ATP-binding cassette transporters in mouse brain parenchyma and microvessels. *Anat Sci Int*. 2018;93:456–63.
136. Caputto BL, Cardozo-Gizzi AM, Gil GA. c-Fos: an AP-1 transcription factor with an additional cytoplasmic, non-genomic lipid synthesis activation capacity. *Biochim Biophys Acta*. 2014;1841:1241–6.
137. Heo JY, Kim JE, Dan Y, Kim YW, Kim JY, Cho KH, et al. Clusterin deficiency induces lipid accumulation and tissue damage in kidney. *J Endocrinol*. 2018;237:175–91.
138. Hu Z, Wu J, Qin L, Jin H, Cao Y, Zhao Y. IGFBP7 downregulation or overexpression effect on bovine preadipocyte differentiation. *Anim Biotechnol*. 2021;32:21–30.
139. Xiao C, Jin HG, Zhang LC, Liu JQ, He M, Ma HH, et al. Effects of SPARC1 on the proliferation and differentiation of sheep preadipocytes. *Adipocyte*. 2021;10:658–69.
140. Hogan JC, Stephens JM. Effects of leukemia inhibitory factor on 3T3-L1 adipocytes. *J Endocrinol*. 2005;185:485–96.
141. Tong W, Duan Y, Yang R, Wang Y, Peng C, Huo Z, et al. Foam cell-derived CXCL14 multi-functionally promotes atherogenesis and is a potent therapeutic target in atherosclerosis. *J cardiovasc Transl Res*. 2020;13:215–24.
142. Baek JH, Kim DH, Lee J, Kim SJ, Chun KH. Galectin-1 accelerates high-fat diet-induced obesity by activation of peroxisome proliferator-activated receptor gamma (PPAR γ) in mice. *Cell Death Dis*. 2021;12:66.
143. Qi R, Han X, Wang J, Qiu X, Wang Q, Yang F. MicroRNA-489-3p promotes adipogenesis by targeting the Postn gene in 3T3-L1 preadipocytes. *Life Sci*. 2021;278:119620.
144. Garg A, Agarwal AK. Lipodystrophies: disorders of adipose tissue biology. *Biochim Biophys Acta*. 2009;1791:507–13.
145. Ramírez CM, Zhang X, Bandyopadhyay C, Rotllan N, Sugiyama MG, Aryal B, et al. Caveolin-1 regulates atherogenesis by attenuating low-density lipoprotein transcytosis and vascular inflammation independently of endothelial nitric oxide synthase activation. *Circulation*. 2019;140:225–39.
146. Feingold KR. Lipid and lipoprotein metabolism. *Endocrinol Metab Clin North Am*. 2022;51:437–58.
147. Yang H, Xiang Y, Robinson K, Wang J, Zhang G, Zhao J, et al. Gut microbiota is a major contributor to adiposity in pigs. *Front Microbiol*. 2018;9:3045.
148. Zheng Y, Pan S, Huang Y, Ci L, Zhao R, Yang X. Breed-specific lipid-related gene expression in the subcutaneous fat of Large White and Erhualian pigs at weaning. *Arch Anim Breed*. 2015;58:33–41.
149. Nakajima I, Kojima M, Oe M, Ojima K, Muroya S, Chikuni K. Comparing pig breeds with genetically low and high backfat thickness: differences in expression of adiponectin, its receptor, and blood metabolites. *Domest Anim Endocrinol*. 2019;68:54–63.
150. Pagliarunga S, Cianflone K. Regulation of postprandial lipemia: an update on current trends. *Appl Physiol Nutr Metab*. 2007;32:61–75.
151. Davies BS, Beigneux AP, Barnes RH, Tu Y, Gin P, Weinstein MM, et al. GPIHBP1 is responsible for the entry of lipoprotein lipase into capillaries. *Cell Metab*. 2010;12:42–52.
152. Young SG, Fong LG, Beigneux AP, Allan CM, He C, Jiang H, et al. GPIHBP1 and lipoprotein lipase, partners in plasma triglyceride metabolism. *Cell Metab*. 2019;30:51–65.
153. Li Y, Huang X, Yang G, Xu K, Yin Y, Breccia G, et al. CD36 favours fat sensing and transport to govern lipid metabolism. *Prog Lipid Res*. 2022;88:101193.
154. Nowowiejska J, Baran A, Flisiak I. Fatty acid-binding proteins in psoriasis—a review. *Metabolites*. 2022;12:833.
155. Stuart T, Butler A, Hoffman P, Hafemeister C, Papalexi E, Mauck WM, et al. Comprehensive integration of single-cell data. *Cell*. 2019;177:1888–902.
156. Yu G, Wang LG, Han Y, He QY. clusterProfiler: an R package for comparing biological themes among gene clusters. *OMICS*. 2012;16:284–7.
157. Nielsen HB, Almeida M, Juncker AS, Rasmussen S, Li J, Sunagawa S, et al. Identification and assembly of genomes and genetic elements in complex metagenomic samples without using reference genomes. *Nature Biotechnol*. 2014;32:822–8.
158. Karlsson FH, Tremaroli V, Nookaew I, Bergström G, Behre CJ, Fagerberg B, et al. Gut metagenome in European women with normal, impaired and diabetic glucose control. *Nature*. 2013;498:99–103.
159. Oh J, Byrd AL, Deming C, Conlan S, NISC Comparative Sequencing Program, Kong HH, et al. Biogeography and individuality shape function in the human skin metagenome. *Nature*. 2014;514:59–64.
160. Buchfink B, Reuter K, Drost HG. Sensitive protein alignments at tree-of-life scale using DIAMOND. *Nat Methods*. 2021;18:366–8.

Publisher's Note

Springer Nature remains neutral with regard to jurisdictional claims in published maps and institutional affiliations.

SHORT COMMUNICATION

The effect of dietary *ginseng polysaccharide* supplementation on porcine milk-derived esRNAs involved in the host immune responses

Jiajie Sun* | Jiali Xiong*  | Liyuan Yao | Ting Chen | Junyi Luo | Qianyun Xi | Yongliang Zhang

Guangdong Provincial Key Laboratory of Animal Nutrition Control, College of Animal Science, National Engineering Research Center for Breeding Swine Industry, South China Agricultural University, Guangzhou, Guangdong, China

Correspondence

Yongliang Zhang, College of Animal Science, South China Agricultural University, Guangzhou, Guangdong, China.
Email: zhangyl@scau.edu.cn

Funding information

Innovative projects of General Colleges and Universities of Guangdong Province, Grant/Award Number: 2017KTSCX023; Opening Foundation of the State Key Laboratory for Conservation and Utilization of Subtropical Agro-bioresources, Grant/Award Number: OSKL201502; National Key Research and Development Program of China, Grant/Award Number: 2016YFD0500503; Natural Science Foundation of China, Grant/Award Number: 31472163

Abstract

Ginseng polysaccharides (GPS) have been well known as an immune modulator. This study was conducted to investigate the effects of dietary supplemental GPS on the immune responses involved in sow's milk-derived exosomal shuttle RNAs (esRNAs) using RNA-Seq and miRNA-Seq. Of the 213 identified miRNA types, a total of 26 conserved miRNAs were differently expressed in response to GPS supplementation, including 10 up-regulated and 16 down-regulated miRNAs in GPS feeding group. In addition, exosomal transcriptome analysis identified 14,696 protein-coding genes in sow's milk exosomes, and 283 genes with 204 and 79 candidates showing up and down-regulation were significantly responded to GPS supplementation. Integrated analysis of each differently expressed miRNA with significantly expressed genes further revealed the presence of 51 highly conserved miRNA-gene interactions that were annotated to be related to immunoregulatory functions. This work provided an important advance in the functional identification of dietary GPS supplementation and more fundamental information about how GPS promoted the immune response and healthy growth of the infant from mothers at molecular levels.

KEYWORDS

esRNAs, exosome, ginseng polysaccharide, milk, sow

1 | INTRODUCTION

Ginseng (*Panax ginseng* C.A. Meyer), one of the most well-known oriental medicines for several thousand years, has been widely used with mysterious powers as a tonic, prophylactic and restorative agent, etc. (Sun, 2011) The polysaccharide extracted from the medicinal ginseng root (mostly), stems and leaves was demonstrated to have many functions, including inhibition of tumours (Li et al., 2014), suppression of bacterial (Fukuyama, Shibuya, & Orihara, 2012) and viral (Kim & Kim, 2011) activity, anti-peroxidatic reactions (Luo & Fang, 2008) and innate (Shin et al., 2002) or acquired (Sumiyoshi,

Sakanaka, & Kimura, 2010) immune modulation. In recent years, there has been growing interests in the use of polysaccharides as new, alternative immunological additives for agricultural animals. Chen et al. (Chen, Liu, & He, 2009) indicated an increase in cellular and humoral immunities by modulating the production of antibodies, complements and cytokines in the *Achyranthes bidentata* polysaccharide supplemented weaned piglets, conferring an important protective role in the non-specific defence against infections. In our previous study, dietary GPS significantly increased immune enzyme activity and modified expression of immune genes in shrimp (Liu et al., 2011). However, to date, the effects of dietary polysaccharide supplementation on lactating sows were deficient.

*These authors contributed equally to this work.

In general, breast milk supplied the chief nutrient source during the natural suckling period of the neonates, and milk liquid with immune-related composition also provided immunity to the infant and affected the maturation of the infant's immune system (Admyre et al., 2007). Previous research has reported that exosomes were identified to present in the breast milk (Zhou et al., 2012), which were small membrane vesicles of endocytic origin that were released from the producing cell into the extracellular environment (Théry, Zitvogel, & Amigorena, 2002). And exosomes have been proposed to signal by binding to the recipient cell surface receptors or by internalization with the cell membrane (Valadi et al., 2007), potentially donating substantial amounts of exosomal RNAs such as mRNAs, microRNAs (miRNAs) and other non-coding RNAs (ncRNAs) to other cells and subsequently affecting the protein production of a recipient cell (Sato-Kuwabara, Melo, Soares, & Calin, 2015). In addition, previous research has revealed the ability of human breast milk exosomes to potentially influence the immune system of the infant (Admyre et al., 2007).

Overall, we therefore hypothesized that dietary supplementation with GPS influenced the composition of sow milk, especially for immune-related esRNAs, and further enhanced the immune responses in suckling piglets. This hypothesis was performed by miRNA and RNA sequencing to analyse the porcine breast milk exosomes in response to GPS supplementation.

2 | MATERIALS AND METHODS

2.1 | Animals and feeding

The GPS were extracted from the roots of *P. ginseng* according to the protocols described in our previous research (Liu et al., 2011). A total of 20 large white sows at 90 days of gestation were acquired from WENS breeding pig farm (Qingyuan, Guangdong, China) and equally allocated to two dietary treatment groups on the basis of age, body weight and parities. Control group (Con) was fed the basal diet, and the diet of treatment group was added with 400 mg/kg GPS until 14th day after delivery. Porcine milk samples were collected at days 1, 3, 7 and 14 after parturition and kept at -80°C until use.

2.2 | Milk exosome collection and sequencing analysis

Preparation of exosomes from porcine milk was operated as our previous descriptions (Chen et al., 2014). Total RNAs were extracted from pelleted exosomes using TRIzol[®] Reagent (Life Technologies, Carlsbad, CA, USA) by the manufacturer's protocol, and the quantity and purity were analysed using Bioanalyzer 2100 and RNA 6000 Nano LabChip Kit (Agilent, CA, USA) with RNA Integrity Number (RIN) value ≥ 7.0 . Prior to constructing Illumina-indexed libraries, the total RNAs from four different time points were pooled equally in each treatment group. Subsequently, indexed miRNAome and transcriptome sequencing libraries were constructed with Illumina TruSeq Small RNA Library Preparation

Kits and TruSeq RNA Library Preparation Kits (Illumina, San Diego, CA, USA), respectively, which included size selection of the final library amplicons. Finally, the libraries were sequenced using Illumina HiSeq[™] 2000, and the raw reads were demultiplexed and the indexed adapter sequences were trimmed using the CASAVA v1.8.2 software.

2.3 | miRNA analysis

Firstly, the raw reads of control and GPS-supplemented group were processed with ACGT101-miR program (LC Sciences, Houston, TX, USA) to trim 3' adapter and discard reads with polyN and reads shorter than 17 bp. Then, using BLAST search, all clean reads were aligned to porcine miRNA mature and precursor sequences published in miRBase v21.0 (<https://www.mirbase.org/>) to identify conserved miRNAs. The read count of each identified miRNA was firstly normalized to reads per million, and the R v3.0.2 Bioconductor package EDGER v2.4.6 (Robinson, McCarthy, & Smyth, 2010) was applied to identify differentially expressed (DE) miRNAs with p value < 0.05 and fold change ≥ 2 between different groups.

2.4 | Align the RNA-Seq reads to genome and assemble-expressed transcripts

Raw reads of fastq format were firstly processed by removing the low-quality reads and the reads that contain adapter or polyN. Then, the clean reads from each library were aligned to the Sscrofa10.2 reference genome (<https://hgdownload.soe.ucsc.edu/goldenPath/susScr3/bigZips/susScr3.fa.gz>) downloaded from the University of California Santa Cruz (UCSC) website with TopHat v2.0.12 (Trapnell, Pachter, & Salzberg, 2009). The mapped reads of each group were assembled by Cufflinks 2.2.1 (Trapnell et al., 2012), and using Cuffmerge two assemblies were merged to create a single transcriptome annotation with porcine Ensembl's genes generated by UCSC table browser for subsequent protein-coding gene analysis. The gene expression level was analysed using RPKM method (reads per kilobase transcriptome per million mapped reads) (Mortazavi, Williams, McCue, Schaeffer, & Wold, 2008), and only genes with false discovery rate (FDR) value < 0.05 that calculated by Cuffdiff program and $|\log_2 \text{fold change}| \geq 1$ were considered as differently expressed candidates.

2.5 | miRNA target prediction and network construction

Putative targets of DE miRNAs were evaluated using miRanda (Betel, Koppal, Agius, Sande, & Leslie, 2010), and only alignments with energies ≤ -20.0 kcal/mol and no mismatch in the seed region (positions 2–8 in the 5' end) were used for further analysis. The construction of interaction networks included three steps: (a) DE mRNAs and DE protein-coding genes were first retained; (b) then mRNA–miRNA negative interactions were predicted by miRanda analysis; and (c)

Type	Con		GPS	
	Count	Percentage (%)	Count	Percentage (%)
Total reads	13,256,489	100	11,349,485	100
3' adapter NULL	193,785	1.46	39,610	0.35
Insert NULL	147,791	1.11	106,849	0.94
5' adapter contaminants	14,380	0.11	4,129	0.04
Removed inferior quality	95,210	0.72	61,994	0.55
Smaller than 17 nt	549,207	4.14	482,024	4.25
Poly-A/T/C/G/N	43	0.00	123	0.00
Clean reads	12,256,073	92.45	10,654,756	93.88

TABLE 1 Summary of small RNA sequencing data

potential interactions between targets and miRNA were established and visualized using Cytoscape V3.4 (<https://cytoscape.org/>).

3 | RESULTS AND DISCUSSION

3.1 | Sequence analysis of milk exosomal miRNAs

Solexa sequencing provided a total of 13,256,489 and 11,349,485 raw reads of 51 nt from the Con and GPS libraries respectively. After removing 3' adapter null or 5' adapter contaminants, low-quality reads and reads contained polyN or smaller than 17 nt, a total of 12,256,073 and 10,654,756 clean reads of 17–31 nt were obtained (Table 1). Subsequently, clean reads were mapped to porcine miRNA mature and precursor sequences published in miRBase 21.0 by BLAST search to identify known miRNAs, and length variation at both 3' and 5' ends and one mismatch inside of the sequences were allowed in the alignment. In total, we identified 213 unique miRNA types aligned to 181 independent pre-miRNA loci with read number more than 10, and 188 known miRNAs were expressed in both Con and GPS groups (Table S1A). The 10 most highly expressed miRNAs in each group accounted for $89.64\% \pm 3.07\%$ of the total counts of all unique miRNAs, and four of these miRNAs (ssc-miR-148a-3p, ssc-miR-30a-5p, ssc-miR-21 and ssc-miR-26a) were found in common across two tested groups, indicating that the majority of miRNAs were expressed from very few loci that maybe play very important roles in milk. Recently, similar miRNAs were identified by sequencing of porcine (Chen et al., 2014), bovine (Sun et al., 2015) and human (Chen et al., 2010) milk exosomes, and miR-148a-3p and miR-30a were also represented as the top 10 miRNAs. Of the identified miRNAs, the most abundant was miR-148a-3p, which represented $56.02\% \pm 5.88\%$ reads across two libraries. The predominance of miR-148a was consistent with its well-established function as a nutritional biomarker corresponding to the protein content of various bovine-derived milk products (Chen et al., 2010). Interestingly, feeding studies that have shown exogenous plant (Zhang et al., 2012) or milk (Baier, Nguyen, Xie, Wood, & Zemleni, 2014) miRNAs can be found in the sera and tissues and influence regulation of

target genes in recipient animals, suggesting that the enrichment of specific miRNAs derived from milk in our study may also influence the growth and development of neonates. Specifically, miR-148a influenced dendritic cell activation and maturation by down-regulating calcium/calmodulin-dependent protein kinase IIa (CaMKIIa) expression and finally associated with anti-inflammatory responses (Turner, Schnorfeil, & Brocker, 2011). MiR-30a attenuated immunosuppressive functions of IL-1 β -elicited mesenchymal stem cells via targeting transforming growth factor- β -activated kinase 1 binding protein 3 (TAB3) (Hu et al., 2015). Also widely studied for possible involvement in the pathogenesis of multiple autoimmune and chronic inflammatory disorders, miR-21 expression was specifically elevated in Th17 cells, and T-cell-intrinsic expression of miR-21 was important for effective Th17 differentiation (Murugaiyan, Garo, & Weiner, 2015). In addition, cellular miR-26a suppressed replication of porcine reproductive and respiratory syndrome virus by activating innate antiviral immunity (Jia et al., 2015). Even though there were compelling evidences that the most prevalent miRNAs in our study could potentially exert an influence on immune response, the specific functional roles of these miRNAs need further detailed investigations to obtain a thorough understanding of the specific targets and mechanistic effects on consumption of miRNA-loaded porcine milk exosomes by a recipient animal.

3.2 | Expression analysis on porcine milk exosomal transcriptome

The single-end RNA reads generated from sequencing of the exosomal libraries were trimmed to remove adapter sequences and then filtered. After filtering procedures, a total of 77,106,888 and 82,953,484 high-quality reads were considered for further analysis, which resulted in ~ 6.46 and ~ 6.95 gigabases (Gb) from Con and GPS libraries respectively. We aligned all these high-quality reads onto the porcine Sscrofa10.2 reference genome and found that over $63.59\% \pm 0.25\%$ of the reads were mapped to the genome, including $58.31\% \pm 0.23\%$ of the mapped reads that were aligned uniquely in each library (Table S2A). Transcripts assembled with mapped reads using Cufflinks revealed a total of 14,696 protein-coding genes across

the two libraries, and Con-specific units accounted for 95.30% of all identified genes, and 94.55% existed in the GPS library (Table S2B), consistent with previous study indicating that 19,320 mRNA transcripts were present in bovine milk exosomes (Izumi, Tsuda, Sato, & Kosaka, 2015). In addition, the top 100 highly expressed genes in sequencing libraries accounted for $72.91\% \pm 0.96\%$ of the total expression levels calculated by RPKM value, and a total of 98 genes were common to both groups. We then performed Gene Ontology (GO) enrichment analysis of these highly expressed genes using the DAVID bioinformatics resource, which employs a Fisher's exact test with Benjamini-Hochberg correction. A total of 82 enriched GO categories were derived using a cut-off of $p < 0.05$, including 56 biological process (BP), 19 cell component (CC) and seven molecular function (MF) categories (Table S2C) respectively. These categories were mainly focused on translational elongation, ribosome biogenesis, rRNA processing and rRNA metabolic process, clearly indicating that the exosomal RNAs were enriched in rRNA family species (Jenjaroenpun et al., 2013). Jenjaroenpun et al. found that cellular exosomes contained various classes of RNA molecules with the major class represented by fragmented ribosomal RNA (rRNA), in particular 28S and 18S subunits. The observation in our and previous studies suggested that the majority of exosomal rRNAs were fragmented, and these results may explain why the 28S and 18S rRNA cannot be detected in exosomal total RNAs (Gu et al., 2012).

3.3 | miRNA and their target expression in response to GPS supplementation

After normalization, miRNAs that changed more than 2-fold and p value < 0.05 were considered to be differently up- or down-regulated in response to GPS supplementation. In total, there were 10 miRNAs up-regulated in the milk exosomes of GPS group in relation to control, as well as 16 down-regulated miRNAs (Table S1B). To identify the potential function of these DE miRNAs, target prediction was performed using miRanda software. Prediction analyses yielded a total of 3,525 unique genes potentially regulated by DE miRNAs. This resulted in 4,902 miRNA-target interactions; 3,271 of these were targeted by up-regulated miRNAs, and 1,631 were targeted by down-regulated miRNAs (Table S1C). The KEGG pathway analysis of the predicted targets by DAVID Bioinformatics Resources revealed 22 unique KEGG terms with p value < 0.05 , which had been previously implicated in immune and disease. These pathways included the top five statistical enrichment, namely pancreatic cancer, MAPK signalling pathway, B cell receptor signalling pathway, T-cell receptor signalling pathway and Fc gamma R-mediated phagocytosis (Table S1D), suggesting the functions of GPS in immune enhancement and regulation.

Previous reports have documented the functional connection between RNA editing and miRNA-mediated post-transcriptional

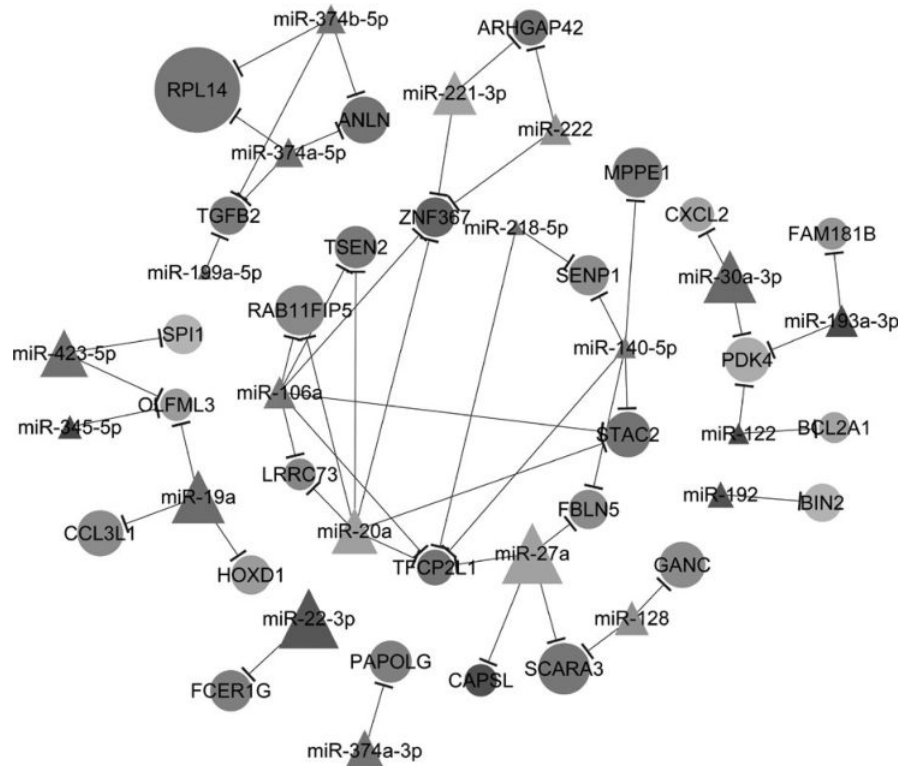


FIGURE 1 miRNA-mRNA correlation networks. Circular nodes represented targets and triangular nodes represented miRNAs. Red nodes represented an up-regulation, and green represented a down-regulation relative to match in GPS group. The size of each node represented average expressed level of each gene between two groups, and the significant levels between different groups were associated with the colour of node deepening

gene silencing (Bartel, 2009). To characterize the potential effects of RNA editing on miRNAs in porcine milk exosomes, we first profiled porcine milk exosomal transcriptome between Con and GPS groups. Of 14,696 identified protein-coding genes, a total of 283 exosomal genes were further considered to be differently expressed in response to GPS supplementation based on $|\log_2 \text{fold change}| \geq 1$, $\text{FDR} < 0.05$ and gene coverage $\geq 60\%$, including 204 up-regulated and 79 down-regulated genes in GPS groups (Table S2D). Next, we aimed at computing all possible interactions of each DE miRNA with significantly expressed genes. Generally, an up-regulation of a target gene indicates a decrease activity of the corresponding miRNA; therefore, a miRNA-mRNA interaction pair means antiregulation of a miRNA and a corresponding gene. In final, miRanda analysis revealed the presence of 51 highly conserved miRNA-mRNA interactions. Of these negative interactions, a total of nine down-regulated genes appeared to be targeted by eight up-regulated miRNAs in GPS group, and 17 up-regulated genes were targeted by 12 down-regulated miRNAs (Figure 1). By applying a cut-off criterion of FDR value < 0.05 , GO enrichment analysis of these target candidates revealed a few important terms those were significantly enriched in the functions of immunity, such as neutrophil chemotaxis (CCL3L1, FCER1G, TGF- β 2), phagocytosis (FCER1G, BIN2), cell chemotaxis (CXCL2, BIN2) and chemokine-mediated signalling pathway (CCL3L1, CXCL2) (Table S2E). In details, CCL3L1 dramatically influenced cell-mediated immunity (Dolan et al., 2007) and was targeted by ssc-miR-19a in our previous study. Phagocytosis-related molecule FCER1G played a role in the uptake of antigens bound to immunoglobulin E (Landi & Babiuk, 2011), and cytokine TGF- β 2 acted an integral role in regulating immune responses (Rautava, Lu, Nanthakumar, Dubert-Ferrandon, & Walker, 2012), these implying the biological functions of their anticorresponding miR-22-3p and miR-374b-5p in porcine milk exosomes. In addition, kidney-specific miR-192 (Liang, Ridzon, Wong, & Chen, 2007) significantly involved in immune-related gene expression (Wu et al., 2012), consistent with our results in negative regulation of BIN2, a membrane sculpting protein that influenced leucocyte podosomes, motility and phagocytosis (Sánchez-Barrena et al., 2013). And mast cell and macrophage chemokine CXCL2, a target gene of miR-30a-3p, controlled the early stage of neutrophil recruitment during tissue inflammation (De Filippo et al., 2013). Taken together, we found that the expression of several key miRNAs and genes in porcine milk-derived exosomes was induced or decreased under GPS supplementation in porcine basal diets, and these miRNA-mRNA interactions were reported to be significantly related to immunoregulatory functions. Meanwhile, previous research has showed that exosomal mRNAs or miRNAs, termed esRNAs, can be delivered to another cell and take effect on the new location (Valadi et al., 2007). Therefore, the findings suggested the functions of dietary GPS supplementation in enhancing the immune-related esRNA expression in milk-derived exosomes, and these candidates may be further transferred to suckling piglets for immune system development and healthy growth.

In conclusion, we detected 26 miRNAs and 283 genes in porcine milk-derived exosomes that showed differential expression in response to GPS supplementation in sow's basal diets. Integrated analysis and functional annotation revealed 51 highly conserved miRNA-mRNA interactions that were significantly related to immunoregulatory functions. This work provided an important advance in the functional identification of dietary GPS supplementation and more fundamental information about how GPS promoted the immune response and healthy growth of the infant at the molecular level.

ACKNOWLEDGEMENTS

This research was supported by grants from Innovative projects of General Colleges and Universities of Guangdong Province [2017KTSCX023], the Opening Foundation of the State Key Laboratory for Conservation and Utilization of Subtropical Agro-bioresources [OSKL201502], the National Key Research and Development Program of China [2016YFD0500503] and the Natural Science Foundation of China programme [31472163].

CONFLICT OF INTEREST

The authors declare that they have no conflict of interest.

ORCID

Jiali Xiong  <https://orcid.org/0000-0003-0274-2211>

REFERENCES

- Admyre, C., Johansson, S. M., Qazi, K. R., Filén, J. J., Lahesmaa, R., ... Gabrielsson, S. (2007). Exosomes with immune modulatory features are present in human breast milk. *The Journal of Immunology*, 179(3), 1969–1978. <https://doi.org/10.4049/jimmunol.179.3.1969>
- Baier, S. R., Nguyen, C., Xie, F., Wood, J. R., & Zemleni, J. (2014). MicroRNAs are absorbed in biologically meaningful amounts from nutritionally relevant doses of cow milk and affect gene expression in peripheral blood mononuclear cells, HEK-293 kidney cell cultures, and mouse livers. *The Journal of Nutrition*, 144(10), 1495–1500. <https://doi.org/10.3945/jn.114.196436>
- Bartel, D. P. (2009). MicroRNAs: Target recognition and regulatory functions. *Cell*, 136(2), 215–233. <https://doi.org/10.1016/j.cell.2009.01.002>
- Betel, D., Koppal, A., Agius, P., Sande, C., & Leslie, C. (2010). Comprehensive modeling of microRNA targets predicts functional non-conserved and non-canonical sites. *Genome Biology*, 11(8), R90. <https://doi.org/10.1186/gb-2010-11-8-r90>
- Chen, X., Gao, C., Li, H., Huang, L., Sun, Q., Dong, Y., ... Hu, X. (2010). Identification and characterization of microRNAs in raw milk during different periods of lactation, commercial fluid, and powdered milk products. *Cell Research*, 20(10), 1128. <https://doi.org/10.1038/cr.2010.80>
- Chen, Q., Liu, Z., & He, J. H. (2009). *Achyranthes bidentata* polysaccharide enhances immune response in weaned piglets. *Immunopharmacology and Immunotoxicology*, 31(2), 253–260.

- Chen, T., Xi, Q. Y., Ye, R. S., Cheng, X., Qi, Q. E., Wang, S. B., ... Zhang, Y. L. (2014). Exploration of microRNAs in porcine milk exosomes. *BMC Genomics*, 15(1), 100. <https://doi.org/10.1186/1471-2164-15-100>
- De Filippo, K., Dudeck, A., Hasenberg, M., Nye, E., van Rooijen, N., Hartmann, K., ... Hogg, N. (2013). Mast cell and macrophage chemokines CXCL1/CXCL2 control the early stage of neutrophil recruitment during tissue inflammation. *Blood*, 121(24), 4930–4937. <https://doi.org/10.1182/blood-2013-02-486217>
- Dolan, M. J., Kulkarni, H., Camargo, J. F., He, W., Smith, A., Anaya, J. M., ... Marconi, V. (2007). CCL3L1 and CCR9 influence cell-mediated immunity and affect HIV-AIDS pathogenesis via viral entry-independent mechanisms. *Nature Immunology*, 8(12), 1324. <https://doi.org/10.1038/ni1521>
- Fukuyama, N., Shibuya, M., & Orihara, Y. (2012). Antimicrobial polyacetylenes from *Panax ginseng* hairy root culture. *Chemical and Pharmaceutical Bulletin*, 60(3), 377–380.
- Gu, Y., Li, M., Wang, T., Liang, Y., Zhong, Z., Wang, X., ... Chen, X. (2012). Lactation-related microRNA expression profiles of porcine breast milk exosomes. *PloS One*, 7(8), e43691. <https://doi.org/10.1371/journal.pone.0043691>
- Hu, E., Ding, L., Miao, H., Liu, F., Liu, D., Dou, H., & Hou, Y. (2015). MiR-30a attenuates immunosuppressive functions of IL-1 β -elicited mesenchymal stem cells via targeting TAB3. *FEBS Letters*, 589(24), 3899–3907. <https://doi.org/10.1016/j.febslet.2015.11.001>
- Izumi, H., Tsuda, M., Sato, Y., & Kosaka, N. (2015). Bovine milk exosomes contain microRNA and mRNA and are taken up by human macrophages. *Journal of Dairy Science*, 98(5), 2920–2933. <https://doi.org/10.3168/jds.2014-9076>
- Jenjaroenpun, P., Kremenska, Y., Nair, V. M., Kremenskoy, M., Joseph, B., & Kurochkin, I. V. (2013). Characterization of RNA in exosomes secreted by human breast cancer cell lines using next-generation sequencing. *Peer Journal*, 1, e201. <https://doi.org/10.7717/peerj.201>
- Jia, X., Bi, Y., Li, J., Xie, Q., Yang, H., & Liu, W. (2015). Cellular microRNA miR-26a suppresses replication of porcine reproductive and respiratory syndrome virus by activating innate antiviral immunity. *Scientific Reports*, 5, 10651. <https://doi.org/10.1038/srep10651>
- Kim, J. Y., & Kim, H. J. (2011). Effect of Oral Administration of Korean Red Ginseng on Influenza A (H1N1) Virus Infection. *Journal of Ginseng Research*, 35(1), 104–110. <https://doi.org/10.5142/jgr.2011.35.1.104>
- Landi, A., & Babiuk, L. A. (2011). Dendritic cells matured by a prostaglandin E2-containing cocktail can produce high levels of IL-12p70 and are more mature and Th1-biased than dendritic cells treated with TNF- α or LPS. *Immunobiology*, 216(6), 649–662. <https://doi.org/10.1016/j.imbio.2010.11.004>
- Li, C., Tian, Z. N., Cai, J. P., Chen, K. X., Zhang, B., Feng, M. Y., ... Geng, J. S. (2014). *Panax ginseng* polysaccharide induces apoptosis by targeting Twist/AKR1C2/NF-1 pathway in human gastric cancer. *Carbohydrate Polymers*, 102, 103–109. <https://doi.org/10.1016/j.carbpol.2013.11.016>
- Liang, Y., Ridzon, D., Wong, L., & Chen, C. (2007). Characterization of microRNA expression profiles in normal human tissues. *BMC Genomics*, 8(1), 1. <https://doi.org/10.1186/1471-2164-8-166>
- Liu, X. L., Xi, Q. Y., Yang, L., Li, H. Y., Jiang, Q. Y., Shu, G., ... Zhang, Y. L. (2011). The effect of dietary *Panax ginseng* polysaccharide extract on the immune responses in white shrimp, *Litopenaeus vannamei*. *Fish & Shellfish Immunology*, 30(2), 495–500. <https://doi.org/10.1016/j.fsi.2010.11.018>
- Luo, D., & Fang, B. (2008). Structural identification of ginseng polysaccharides and testing of their antioxidant activities. *Carbohydrate Polymers*, 72(3), 376–381. <https://doi.org/10.1016/j.carbpol.2007.09.006>
- Mortazavi, A., Williams, B. A., McCue, K., Schaeffer, L., & Wold, B. (2008). Mapping and quantifying mammalian transcriptomes by RNA-Seq. *Nature Methods*, 5(7), 621–628. <https://doi.org/10.1038/nmeth.1226>
- Murugaiyan, G., Garo, L. P., & Weiner, H. L. (2015). MicroRNA-21, T helper lineage and autoimmunity. *Oncotarget*, 6(12), 9644. <https://doi.org/10.18632/oncotarget.3928>
- Rautava, S., Lu, L., Nanthakumar, N. N., Dubert-Ferrandon, A., & Walker, W. A. (2012). TGF- β 2 induces maturation of immature human intestinal epithelial cells and inhibits inflammatory cytokine responses induced via the NF- κ B pathway. *Journal of Pediatric Gastroenterology and Nutrition*, 54(5), 630. <https://doi.org/10.1097/MPG.0b013e31823e7c29>
- Robinson, M. D., McCarthy, D. J., & Smyth, G. K. (2010). edgeR: A Bioconductor package for differential expression analysis of digital gene expression data. *Bioinformatics*, 26(1), 139–140. <https://doi.org/10.1093/bioinformatics/btp616>
- Sánchez-Barrena, M. J., Vallis, Y., Clatworthy, M. R., Doherty, G. J., Veprintsev, D. B., Evans, P. R., & McMahon, H. T. (2013). Correction: Bin2 is a membrane sculpting N-BAR protein that influences leucocyte podosomes, motility and phagocytosis. *PloS One*, 8(8). <https://doi.org/10.1371/annotation/3bdc487b-5e25-4cd7-a354-b2952eec943d>
- Sato-Kuwabara, Y., Melo, S. A., Soares, F. A., & Calin, G. A. (2015). The fusion of two worlds: Non-coding RNAs and extracellular vesicles—diagnostic and therapeutic implications. *International Journal of Oncology*, 46(1), 17–27.
- Shin, J. Y., Song, J. Y., Yun, Y. S., Yang, H. O., Rhee, D. K., & Pyo, S. (2002). Immunostimulating effects of acidic polysaccharides extract of *Panax ginseng* on macrophage function. *Immunopharmacology and Immunotoxicology*, 24(3), 469–482.
- Sumiyoshi, M., Sakanaka, M., & Kimura, Y. (2010). Effects of Red Ginseng extract on allergic reactions to food in Balb/c mice. *Journal of Ethnopharmacology*, 132(1), 206–212. <https://doi.org/10.1016/j.jep.2010.08.012>
- Sun, Y. (2011). Structure and biological activities of the polysaccharides from the leaves, roots and fruits of *Panax ginseng* CA Meyer: An overview. *Carbohydrate Polymers*, 85(3), 490–499. <https://doi.org/10.1016/j.carbpol.2011.03.033>
- Sun, J., Aswath, K., Schroeder, S. G., Lippolis, J. D., Reinhardt, T. A., & Sonstegard, T. S. (2015). MicroRNA expression profiles of bovine milk exosomes in response to *Staphylococcus aureus* infection. *BMC Genomics*, 16(1), 806. <https://doi.org/10.1186/s12864-015-2044-9>
- Théry, C., Zitvogel, L., & Amigorena, S. (2002). Exosomes: Composition, biogenesis and function. *Nature Reviews Immunology*, 2(8), 569–579. <https://doi.org/10.1038/nri855>
- Trapnell, C., Pachter, L., & Salzberg, S. L. (2009). TopHat: Discovering splice junctions with RNA-Seq. *Bioinformatics*, 25(9), 1105–1111. <https://doi.org/10.1093/bioinformatics/btp120>
- Trapnell, C., Roberts, A., Goff, L., Pertea, G., Kim, D., Kelley, D. R., ... Pachter, L. (2012). Differential gene and transcript expression analysis of RNA-seq experiments with TopHat and Cufflinks. *Nature Protocols*, 7(3), 562. <https://doi.org/10.1038/nprot.2012.016>
- Turner, M. L., Schnorfeil, F. M., & Bocker, T. (2011). MicroRNAs regulate dendritic cell differentiation and function. *The Journal of Immunology*, 187(8), 3911–3917. <https://doi.org/10.4049/jimmunol.1101137>
- Valadi, H., Ekström, K., Bossios, A., Sjöstrand, M., Lee, J. J., & Lötvall, J. O. (2007). Exosome-mediated transfer of mRNAs and microRNAs is a novel mechanism of genetic exchange between cells. *Nature Cell Biology*, 9(6), 654. <https://doi.org/10.1038/ncb1596>
- Wu, T. H., Pan, C. Y., Lin, M. C., Hsieh, J. C., Hui, C. F., & Chen, J. Y. (2012). In vivo screening of zebrafish microRNA responses to bacterial infection and their possible roles in regulating immune response genes after lipopolysaccharide stimulation. *Fish Physiology and Biochemistry*, 38(5), 1299–1310. <https://doi.org/10.1007/s10095-012-9617-1>

- Zhang, L., Hou, D., Chen, X., Li, D., Zhu, L., Zhang, Y., ... Yin, Y. (2012). Exogenous plant MIR168a specifically targets mammalian LDLRAP1: Evidence of cross-kingdom regulation by microRNA. *Cell Research*, 22(1), 107. <https://doi.org/10.1038/cr.2011.158>
- Zhou, Q., Li, M., Wang, X., Li, Q., Wang, T., Zhu, Q., ... Li, X. (2012). Immune-related microRNAs are abundant in breast milk exosomes. *International Journal of Biological Sciences*, 8(1), 118. <https://doi.org/10.7150/ijbs.8.118>

How to cite this article: Sun J, Xiong J, Yao L, et al. The effect of dietary *ginseng polysaccharide* supplementation on porcine milk-derived esRNAs involved in the host immune responses. *J Anim Physiol Anim Nutr*. 2019;103:276–282. <https://doi.org/10.1111/jpn.12993>

SUPPORTING INFORMATION

Additional supporting information may be found online in the Supporting Information section at the end of the article.

ORIGINAL ARTICLE

Effect of *Moringa oleifera* supplementation on productive performance, colostrum composition and serum biochemical indexes of sow

Jia-Jie Sun | Peng Wang | Guo-Ping Chen | Jun-Yi Luo | Qian-Yun Xi | Geng-Yuan Cai |
Jia-Han Wu | Bin Zeng | Yue-Qin Xie | Qing-Yan Jiang | Ting Chen | Yong-Liang Zhang

Guangdong Provincial Key Laboratory of Animal Nutrition Control, National Engineering Research Center For Breeding Swine Industry, Guangdong Engineering & Research Center for Woody Fodder Plants, College of Animal Science, South China Agricultural University, Guangzhou, China

Correspondence

Yong-Liang Zhang, Ting Chen, Guangdong Provincial Key Laboratory of Animal Nutrition Control, National Engineering Research Center For Breeding Swine Industry, College of Animal Science, South China Agricultural University, Guangzhou 510642, China.
Emails: zhangyl@scau.edu.cn (YL Z); 36391538@qq.com (T C)

Funding information

National Key Research and Development Program of China, Grant/Award Number: 2016YFD0500503 and 2018YFD0501706; Technical System of Modern Agricultural Industry in Guangdong Province, Grant/Award Number: 2018LM1121 and 2018LM2158

Abstract

Moringa oleifera has been considered as a potential functional feed or food, since it contains multiple components beneficial to animal and human. However, little is known about the effects of *Moringa oleifera* supplementation on productive performances in sows. In the current study, the results showed that dietary *Moringa oleifera* significantly decreased the farrowing length and the number of stillborn ($p < .05$), while had an increasing trend in the number of live-born ($0.05 < p < .10$). Furthermore, 8% *Moringa oleifera* supplementation significantly elevated protein levels in the colostrum ($p < .05$); 4% *Moringa oleifera* lowered serum urea nitrogen of sows after 90 days of gestation ($p < .05$) and significantly decreased serum glucose on 10 days of lactation ($p < .05$). Both groups showed significant elevation in serum T-AOC activity ($p < .05$). The serum malondialdehyde (MDA) of sows declined significantly in 4% *Moringa oleifera* addition group ($p < .05$). 8% *Moringa oleifera* meal significantly elevated serum CAT activity after 60 days of gestation ($p < .05$), while decreased the serum MDA level and increased the serum GSH-Px activity of sows at 10 days of lactation ($p < .05$). Of piglets, both two dosages of *Moringa oleifera* supplementation essentially reduced the serum urea nitrogen ($p < .05$), and 4% *Moringa oleifera* meal increased serum total protein ($p < .05$). In addition, piglets that received 8% *Moringa oleifera* had the highest serum CAT and SOD activities among all groups ($p < .05$). The present study indicated that *Moringa oleifera* supplementation could enhance the reproduction performances, elevate protein levels in the colostrum and improve the serum antioxidant indices in both sows and piglets.

KEYWORDS

antioxidant, farrowing length, *Moringa oleifera* leave meal, sows

1 | INTRODUCTION

Reproductive performance is a key factor in controlling the efficiency of swine production and is considered economically important to

the swine industry. Low levels of reproductive performance may not only result in low profit per sow, but also limit the attempts to improve the herd genetically (Rekwot, Jegede, Ehoche, & Tsb, 2001). Various factors can induce oxidative stress in pig industry, including intensive production mode for sows, housing environmental deterioration, disease, stress, dietary fat, antibiotics drugs, chemical feed

Sun and Wang are contributed equally to this work.

additive and hypermetabolism in the reproductive cycle. Previous studies showed that birth and weaning processes also impair antioxidant balance (Yin et al., 2013, 2014). It is well known free radicals cause oxidative stress as a result of an imbalance between the antioxidant defence system and reactive oxygen species. Almost all biological macromolecules, including DNA, lipid and carbohydrates, could be attacked, causing a decline in the reproductive performance of sows by damaging histocytes (Yazdanparast & Ardestani, 2007).

Antioxidants play an important role in inhibiting and scavenging free radicals, thus providing protection to animals against infections and degenerative diseases. The current research is directed towards natural antioxidants originated from plants due to safe therapeutics (Sreelatha & Padma, 2009). *Moringa oleifera* is commonly known as drumstick, horseradish or benzoil tree, a perennial tropical deciduous tree native to the north-western India and north-eastern Africa, and is considered as the "Nature nutrition of the tropics" (Naidoo & Cooposamy, 2011). *Moringa* leaves, the most utilized part of the plant, is rich in protein, amino acids, vitamins and minerals that meet animal nutritional requirements (Moyo, Masika, Hugo, & Muchenje, 2011; Teixeira, Carvalho, Neves, Silva, & Arantes-Pereira, 2014). Generally, the dried leaves of *Moringa* had crude protein levels of 30.3% and contained 19 amino acids (Moyo et al., 2011). Moreover, *Moringa* leaves contain an abundance of bioactive compounds, principally rich in antioxidant substances including phenols, flavonoids, proanthocyanidins, flavonols, vitamin C, vitamin E, β -carotene, zinc and selenium, which have been documented to possess strong antioxidant potential and is important in the inhibition and scavenge of free radicals (Ahmad, 2006; Iqbal & Bhanger, 2006; Lako et al., 2007). Although numerous extensive studies have indicated that antioxidants can improve reproductive performance of sows, *Moringa oleifera* has not been tried in sows so far. The present study was designed to evaluate the effects of oral supplement of *Moringa oleifera* on sows, as well as on their piglets.

2 | MATERIALS AND METHODS

2.1 | Plant Material

The *Moringa oleifera* leaves fodder was purchased from the Xiamen Qiuting *Moringa Oleifera* Raw Materials Co., Ltd. The *Moringa oleifera* is grown commercially in Dali Yunnan, and fresh leaves are processed by hot air drying in baking room, after which they are grounded into *Moringa oleifera* leave meal (MOLM) through a 400-mesh sieve.

2.2 | Animal and experimental diets

The experiment was carried out in WENS Shuitai Breeding Pig Farm. Forty-five Landrace backup sows at 7.5 months old and initially weighing 140 kg on average were randomly divided into the control and two treatment groups, each group with 15 sows ($n = 15$). The pigs were allocated to one of three balance dietary treatments formulated to contain 0%, 4% and 8% of MOLM. The ingredient composition and proximate composition of the dietary treatments are shown in Tables 1 and 2.

TABLE 1 Composition of gestation diets

Items	<i>Moringa oleifera</i> inclusion level (%)		
	0	4	8
Feed ingredients (g/kg)			
Moringa meal ^a	0	40	80
Corn	378.6	401.63	445.41
Hulled barley	283.71	234.41	160.16
Wheat bran	152	154	162
Soya bean meal	136	119	101
Limestone powder	16.2	14.4	12.6
Dicalcium phosphate	16	16.8	17.5
NaCl	3.6	3.6	3.7
Lysine sulphate	2.61	3.61	4.61
Sodium sulphate	2	3	3
Choline chloride	1.3	1.3	1.3
Threonine	1.16	1.5	1.61
Methionine	0.82	0.65	0.88
Tryptophan	0	0.1	0.23
Premix ^b	6	6	6
Total	1,000	1,000	1,000
Calculated nutrient levels			
Crude protein (%)	14.5	14.5	14.5
Crude fibre (%)	3.9	3.9	3.9
Calcium (%)	1.05	1.05	1.05
Total phosphorus (%)	0.69	0.71	0.73
Electrolyte balance (mEq/kg)	171	159	147
Digestible energy (kcal/kg)	3,031	3,031	3,031
DLys-S (%)	0.7	0.7	0.7
DMet/DLy-S	0.392	0.35	0.365
DMC/DLy-S	0.701	0.636	0.63
DThr/DLy-S	0.75	0.75	0.72
DTrp/DLy-S	0.204	0.2	0.201
DVal/DLy-S	0.804	0.738	0.671

^a*Moringa oleifera* leaves digestible energy 13.93 MJ/kg, digestible crude fibre 7.20%, digestible fat 4.81%, digestible crude protein 23.21%, which measured by digestive experiments.

^bThe premix provided the following per kilogram of complete diet: vitamin A 11,000 IU, vitamin D 3,000 IU, vitamin E 65 IU, vitamin K 4.4 mg, vitamin B₁ 3 mg, vitamin B₂ 10 mg, vitamin B₆ 4 mg, vitamin B₁₂ 40 μ g, nicotinic acid 50 mg, pantothenic acid 30 mg, folic acid 4 mg, biotin 0.45 mg, choline chloride 750 mg, 16.5 mg Cu as copper sulphate, 100 mg Fe as iron sulphate, 0.25 mg I as potassium iodate, 100 mg Zn as zinc oxide, 40 mg Mn as manganous oxide, 0.25 mg Se as sodium selenite.

The sows were allowed seven days to adjust to the experimental diets before the trial. The experiment started from two weeks before mating to the end of weaning. Sows had ad libitum access to feed and unrestricted access to water throughout the lactation, which continued until piglets were weaned at 21 days old.

TABLE 2 Composition of pre-breeding and lactation diets

Items	Different levels of <i>Moringa Oleifera</i> (%)		
	0	4	8
Feed ingredients (g/kg)			
Moringa meal ^a	0	40	80
Corn	605.39	611.7	619.16
Soya bean meal	192	177	161
Wheat bran	63	36	10
Expanded soya bean	39	40	39
Soya oil	36	30.1	24.5
Fish meal	20	20	20
Dicalcium phosphate	11.4	12.2	13
Limestone powder	11.2	9.3	7.5
NaCl	4	4.1	4.2
KCl	1	1	1
Lysine sulphate	3.97	4.87	5.83
Choline chloride	1.3	1.3	1.3
Threonine	1.07	1.37	1.92
Methionine	0.45	0.72	0.59
Tryptophan	0.22	0.34	1
Premixture ^b	10	10	10
Total	1,000	1,000	1,000
Calculated nutrient levels			
Crude protein (%)	17.5	17.5	17.5
Crude fibre (%)	2.5	2.5	2.5
Calcium (%)	0.9	0.9	0.9
Total phosphorus (%)	0.62	0.62	0.63
Electrolyte balance (mEq/kg)	186	171	155
Digestible energy (kcal/kg)	3,442	3,442	3,442
DLys-S (%)	1	1	1
DMet/DLy-S	0.293	0.307	0.282
DMC/DLy-S	0.54	0.54	0.5
DThr/DLy-S	0.65	0.65	0.672
DTrp/DLy-S	0.19	0.19	0.241
DVal/DLy-S	0.63	0.591	0.55

^a*Moringa oleifera* leaves digestible energy 13.93 MJ/kg, digestible crude fibre 7.20%, digestible fat 4.81%, digestible crude protein 23.21%, which measured by digestive experiments.

^bThe premix provided the following per kilogram of complete diet: vitamin A 9,500 IU, vitamin D 1,400 IU, vitamin E 60 IU, vitamin K 3.5 mg, vitamin B₁ 3 mg, vitamin B₂ 10 mg, vitamin B₆ 4 mg, vitamin B₁₂ 40 µg, nicotinic acid 50 mg, pantothenic acid 30 mg, folic acid 4 mg, biotin 0.45 mg, choline chloride 750 mg, 30 mg Cu as copper sulphate, 100 mg Fe as iron sulphate, 0.25 mg I as potassium iodate, 80 mg Zn as zinc oxide, 50 mg Mn as manganous oxide, 0.25 mg Se as sodium selenite.

Before mating, females were fed 2.5 kg/d of pre-breeding diets. The sows were given 1.8, 2.0, 2.3 and 2.5 kg/d of gestation diets during the pregnancy period of days 1–50, 50–80, 80–95 and

95 farrowing, respectively, and thin sows were provided an extra amount of feed (0.45 kg/d). On the day of farrowing, sows did not receive any feed and the amount of feed was increased by about 1.1 kg per day for the first 5 days post-farrowing, followed by ad libitum feeding.

Thirty days after insemination, the sows were scanned by ultrasound for pregnancy. Gilts who failed to conceive were removed from the experiment. Pregnant gilts were transferred to pens, each equipped with a concrete feeding trough and a nipple drinker. At day 111 of gestation, the animals were moved to the farrowing house. The farrowing room was equipped with pens on a metal slatted floor and infrared lights to keep the temperature for the newborn piglets at a constant 35°C.

2.3 | Data recording, Sample collection and examination

The following parameters were recorded including the number of total born, live-born and stillborn, piglet birth weight per litter, weaned piglets alive per litter, weaned piglet weight and survival rate of lactation. Farrowing length was calculated as time from birth of first piglet to birth of last piglet and as time from birth of first piglet to birth of last live-born piglet. Approximately 30 ml of colostrum was collected within 6 hr after farrowing and stored at –20°C until further analysis for milk composition with milk composition analyzer (SSF-m120420).

On days 60, 90 of pregnancy and 10 of lactation, 5 ml blood samples were collected via ear venipuncture from each sow into separate 10-ml vacuum blood collection tubes. On the day of weaning, 5 ml blood samples from 30 piglets per group were collected with a one-off sterile syringe from the pre-caval vein into centrifuge tubes. The samples were allowed to coagulate at room temperature for 60 min and then centrifuged at 4°C, 2,000 g for 10 min. The serum was transferred to another tube and stored at –80°C for further analysis.

Antioxidant capacities, including total antioxidant capacity (T-AOC), superoxide dismutase (SOD), catalase (CAT), malondialdehyde (MDA) and glutathione peroxidase (GSH-Px), and serum biochemical parameters, including urea nitrogen, glucose, triglyceride, total cholesterol and total protein, were tested using a commercial kit (Nanjing Jiancheng Bioengineering Institute). All operations are in accordance with the instructions.

2.4 | Statistical analysis

Data for reproduction performances, colostrum composition, serum biochemical and antioxidant indices of sows, and serum biochemical and antioxidant indices of piglets were analysed using a one-way analysis of variance (ANOVA) and a protected least significant difference test (LSD) between groups by SPSS 22.0 statistical software package. The analytical data were presented in the following tables as “means ± SE,” and $p < .05$ was considered statistically significant.

3 | RESULTS

3.1 | Productive performance

Significance of main effects and interactions among treatments on productive performance are shown in Table 3. Our results indicated that *Moringa oleifera* had certain effects in decreasing farrowing length and the number of stillborn, and increasing the number live-born piglets ($p < .05$). However, dietary inclusion of *Moringa oleifera* did not significantly affect the piglet birth weight, weaned piglet weight, number of weaned per litter and survival rate of lactation.

3.2 | Colostrum composition

As shown in Table 4, only 8% *Moringa oleifera* supplementation significantly elevated protein levels in the colostrum ($p < .05$), while having no effects on fat, solid non-fat extract (SNF), lactose, density and freezing point in colostrum.

3.3 | Serum parameters of sows

As shown in Table 5, dietary *Moringa oleifera* reduced the serum urea nitrogen and glucose. Relative to the control group, sows that received 4% *Moringa oleifera* showed significantly lower serum urea nitrogen on day

90 of gestation ($p < .05$), and significantly decreased glucose on day 10 of lactation ($p < .05$). Also, the serum triglyceride reduced slowly in three different trial periods, while total protein only increased after receiving *Moringa oleifera* on day 90 of gestation and day 10 of lactation. No significant effect on total cholesterol was found between three periods.

As shown in Table 6, at 60 days of gestation, additions of both 4% and 8% *Moringa oleifera* significantly increased serum T-AOC activity of the sows relative to control ($p < .01$), 8% *Moringa oleifera* significantly elevated serum CAT activity relative to control group ($p < .05$) but not afterwards. At 90 days of gestation, *Moringa oleifera* meal significantly increased the serum T-AOC of sows ($p < .05$), and the serum MDA of sows declined significantly in 4% *Moringa oleifera* addition group ($p < .05$). At 10 days of lactation, additions of both 4% and 8% *Moringa oleifera* significantly increased serum T-AOC activity of the sows ($p < .05$), 8% *Moringa oleifera* meal significantly decreased the serum MDA level ($p < .05$) and increased the serum GSH-Px activity of sows ($p < .05$), relative to control. The serum SOD had not seen significant alterations.

3.4 | Serum parameters of piglets

As shown in Table 7, both levels of *Moringa oleifera* supplementation in sow feed significantly reduced the serum urea nitrogen of piglets ($p < .05$), relative to the control group. 4% *Moringa oleifera*

TABLE 3 Reproduction performances

Items	Different levels of <i>Moringa Oleifera</i> (%)			SEM	p-Value
	0%	4%	8%		
Total born (n)	12.08 ± 0.82	11.77 ± 0.48	13.50 ± 0.68	0.40	.25
Live-born (n)	10.00 ± 0.58	11.25 ± 0.39	11.57 ± 0.69	0.69	.09
Stillborn (n)	1.10 ± 0.23 ^a	0.31 ± 0.13 ^b	0.36 ± 0.15 ^b	0.11	.01
Farrowing length (h)	3.30 ± 0.22 ^a	2.61 ± 0.28 ^b	2.52 ± 0.21 ^b	0.15	.04
Piglet birth weight (kg)	1.41 ± 0.05	1.35 ± 0.05	1.38 ± 0.03	0.03	.65
Weaned piglets alive per litter (n)	8.71 ± 1.01	10.15 ± 0.36	9.16 ± 1.14	0.51	.38
Weaned piglet weight (kg)	5.60 ± 0.24	5.45 ± 0.12	5.98 ± 0.14	0.11	.14
Survival rate of lactation (%)	95.13 ± 2.33	98.00 ± 1.06	98.60 ± 0.95	0.98	.30

^{a,b}Values that differ significantly at $P < .05$.

TABLE 4 Colostrum composition

Items	Different leaves of <i>Moringa Oleifera</i>			SEM	p-Value
	0%	4%	8%		
Fat/%	6.75 ± 0.47	7.04 ± 0.32	6.54 ± 0.59	0.27	.71
SNF/%	19.29 ± 0.92	18.97 ± 0.64	19.54 ± 0.56	0.40	.85
Protein/%	7.05 ± 0.40 ^b	7.08 ± 0.26 ^b	8.00 ± 0.17 ^a	0.18	.04
Lactose/%	11.34 ± 0.88	10.20 ± 0.38	10.88 ± 0.40	0.36	.43
Density/g/ml	1.07 ± 0.00	1.06 ± 0.00	1.06 ± 0.00	0.00	.34
Freezing Point/°C	-0.84 ± 0.05	-0.79 ± 0.02	-0.80 ± 0.03	0.02	.50

^{a,b}Values that differ significantly at $P < .05$.

TABLE 5 Serum biochemical indices of sows

	Different levels of <i>Moringa Oleifera</i>				
Items	0%	4%	8%	SEM	p-Value
Gestation 60 day					
Urea nitrogen (mmol/L)	3.56 ± 0.06	3.55 ± 0.03	3.44 ± 0.04	0.03	.16
Glucose (mmol/L)	4.13 ± 0.13	3.81 ± 0.11	3.98 ± 0.20	0.09	.37
Triglyceride (mmol/L)	0.44 ± 0.05	0.34 ± 0.06	0.38 ± 0.03	0.03	.35
Total cholesterol (mmol/L)	1.61 ± 0.03	1.65 ± 0.06	1.58 ± 0.06	0.03	.68
Total protein (g/L)	68.06 ± 1.51	67.86 ± 1.95	67.54 ± 1.28	0.86	.97
Gestation 90 day					
Urea nitrogen (mmol/L)	4.11 ± 0.23 ^a	3.58 ± 0.09 ^b	3.67 ± 0.27 ^{ab}	0.13	.02
Glucose (mmol/L)	5.16 ± 0.40	4.45 ± 0.20	4.58 ± 0.22	0.17	.22
Triglyceride (mmol/L)	0.64 ± 0.04	0.49 ± 0.05	0.55 ± 0.04	0.03	.09
Total cholesterol (mmol/L)	1.70 ± 0.07	1.74 ± 0.04	1.77 ± 0.08	0.04	.72
Total protein (g/L)	63.54 ± 1.29	64.48 ± 2.21	69.42 ± 3.15	1.13	.11
Lactation 10 day					
Urea nitrogen (mmol/L)	5.45 ± 0.53	5.40 ± 0.21	4.80 ± 0.48	0.24	.49
Glucose (mmol/L)	5.54 ± 0.17 ^a	4.54 ± 0.31 ^b	4.99 ± 0.26 ^{ab}	0.18	.04
Triglyceride (mmol/L)	0.30 ± 0.06	0.26 ± 0.01	0.30 ± 0.04	0.02	.67
Total cholesterol (mmol/L)	2.17 ± 0.19	2.02 ± 1.68	1.94 ± 0.10	0.08	.52
Total protein (g/L)	62.88 ± 2.70	67.14 ± 1.94	66.62 ± 1.14	1.13	.30

^{a,b}Values that differ significantly at $P < .05$.

significantly increased the serum total protein and serum glucose in piglets relative to control group ($p < .05$). The serum total cholesterol was significantly higher in 8% *Moringa oleifera* diet group than control group ($p < .05$).

As shown in Table 8, dietary *Moringa oleifera* enhanced serum CAT and SOD activities of piglets, and 8% supplementation had the best improvement on serum CAT and SOD activities among groups ($p < .05$). Dietary addition of *Moringa oleifera* did not lead to a significant alteration of T-AOC, GSH-Px and MDA.

4 | DISCUSSION

This study was performed to investigate the effects of dietary supplement of 4% or 8% *Moringa oleifera* on reproductive traits of sows. We determined the total number of born and live-born piglets as well as piglet and litter weights at birth and on day 21 of lactation. The results indicate that both supplementation levels of 4% and 8% *Moringa oleifera* diet were able to shorten the farrowing length and decreased the number of stillborn. This finding agrees with previous studies that the length of farrowing and the number of stillborn are directly connected (Van Dijk, van Rens, van der Lende, & Taverne, 2014; Zaleski & Hacker, 1993), and stillbirth risk is higher in sows with prolonged farrowing (Oliviero, Heinonen, Valros, & Peltoniemi, 2010; Thodberg, Jensen, & Herskin, 2002). The average of farrowing length is 2.5 hr; hence, parturitions that last more than 3 or 4 hr are considered potentially problematic (Borges, Bernardi, Bortolozzo,

& Wentz, 2005; Lucia et al., 2002). Longer farrowing lengths have previously been proved to be related to stillbirth, which is likely due to increased risk of asphyxia during delivery (Oliviero et al., 2010). As the farrowing progresses, it increases the proportion of stillborn. After 80% of the piglets have been born, the number of stillbirths increases, with most of them occurring in the last three piglets (Borges et al., 2005).

The consumption of *Moringa oleifera* leaves by both human and animals have been shown to possess high nutritive value and antioxidant compounds (Khalafalla et al., 2010; Mendieta-Araica, Spöndly, Reyes-Sánchez, & Spöndly, 2011; Siddhuraju & Becker, 2003). Previous research reported that *Moringa oleifera* leaves have a high amount of phenols and potent antioxidant properties, and it could prevent morphological changes and oxidative damages in animals effectively by increasing the activities of antioxidant enzymes (Osman, Shayoub, & Babiker, 2012; Sreelatha & Padma, 2009; Verma, Vijayakumar, Mathela, & Rao, 2009). These antioxidants are molecules that prevent uncontrolled formation of free radical and activated species by quenching or chelating their catalytic metal ions. In our study, the decreased MDA and increased T-AOC, CAT and GSH-Px activities indicated an enhanced antioxidative status in the sows fed with *Moringa oleifera*. The findings obtained in this study agreed with Moyo et al. (Moyo et al., 2011) who found a significant elevation of the antioxidative status and reduction of MDA in goats supplemented with *Moringa oleifera* leaves as compared with the control group. MDA is produced during the process of lipid peroxidation, and the content of MDA in body blood reflects the

TABLE 6 Serum antioxidant indices of sows

	Different levels of <i>Moringa Oleifera</i>				
Items	0%	4%	8%	SEM	p-Value
Gestation 60 day					
T-AOC (U/ml)	0.66 ± 0.07 ^b	1.26 ± 0.13 ^a	1.66 ± 0.16 ^a	0.13	<.01
CAT (U/ml)	7.67 ± 0.32 ^b	8.40 ± 0.46 ^{ab}	9.42 ± 0.49 ^a	0.29	.04
MDA (mmol/ml)	3.56 ± 0.27	3.21 ± 0.25	3.45 ± 0.16	0.13	.56
SOD (U/ml)	31.68 ± 3.86	29.67 ± 2.40	27.48 ± 1.04	1.51	.56
GSH-PX (U/ml)	2,572.20 ± 29.66	2,683.39 ± 45.11	2,627.80 ± 47.24	25.25	.21
Gestation 90 day					
T-AOC (U/ml)	0.86 ± 0.13 ^b	1.43 ± 0.16 ^a	1.63 ± 0.06 ^a	0.11	<.01
CAT (U/ml)	9.11 ± 0.35	8.56 ± 0.21	8.90 ± 0.63	0.24	.67
MDA (mmol/ml)	4.14 ± 0.26 ^a	3.33 ± 0.12 ^b	3.83 ± 0.223 ^{ab}	0.15	.06
SOD (U/ml)	25.22 ± 2.57	24.65 ± 2.02	23.43 ± 1.64	1.14	.83
GSH-PX (U/ml)	2,618.64 ± 57.75	2,794.58 ± 74.41	2,735.59 ± 78.71	42.62	.24
Lactation 10 day					
T-AOC (U/ml)	0.79 ± 0.19 ^b	1.43 ± 0.10 ^a	1.45 ± 0.18 ^a	0.12	.02
CAT (U/ml)	11.64 ± 1.36	11.08 ± 0.64	11.36 ± 1.21	0.60	.94
MDA (mmol/ml)	5.60 ± 0.34 ^a	5.06 ± 0.18 ^{ab}	4.82 ± 0.25 ^b	0.17	.15
SOD (U/ml)	23.73 ± 1.61	23.69 ± 2.34	29.30 ± 2.64	1.33	.28
GSH-PX (U/ml)	2,197.63 ± 62.60 ^b	2,317.29 ± 75.19 ^{ab}	2,478.64 ± 66.21 ^a	47.71	.04

^{a,b}Values that differ significantly at $P < .05$.**TABLE 7** Serum biochemical indices of piglets

Items	Different levels of <i>Moringa Oleifera</i>			SEM	p-Value
	0%	4%	8%		
Urea nitrogen (mmol/L)	3.62 ± 0.23 ^a	2.35 ± 0.33 ^b	2.31 ± 0.45 ^b	0.25	.03
Glucose (mmol/L)	6.68 ± 0.49 ^b	7.88 ± 0.20 ^a	7.42 ± 0.31 ^{ab}	0.22	.04
Triglyceride (mmol/L)	0.69 ± 0.06	1.02 ± 0.07	0.77 ± 0.17	0.07	.14
Total cholesterol (mmol/L)	3.52 ± 0.48 ^b	4.40 ± 0.23 ^{ab}	4.92 ± 0.46 ^a	0.27	.04
Total protein (g/L)	40.10 ± 2.06 ^b	45.88 ± 0.89 ^a	43.52 ± 2.19 ^{ab}	1.16	.12

^{a,b}Values that differ significantly at $P < .05$.**TABLE 8** Serum antioxidant indices of piglets

Items	Different levels of <i>Moringa Oleifera</i>			SEM	p-Value
	0%	4%	8%		
T-AOC (U/ml)	1.97 ± 0.30	2.00 ± 0.26	1.58 ± 0.20	0.15	.46
CAT (U/ml)	9.90 ± 1.10 ^b	14.41 ± 0.82 ^{ab}	17.36 ± 2.26 ^a	1.16	.02
MDA (mmol/ml)	5.55 ± 0.19	5.31 ± 0.37	5.31 ± 0.41	0.18	.85
SOD (U/ml)	50.42 ± 2.48	52.72 ± 2.20	55.20 ± 2.01	1.30	.35
GSH-PX (U/ml)	1678.62 ± 51.51	1728.2759 ± 48.93	1744.83 ± 44.13	26.88	.61

^{a,b}Values that differ significantly at $P < .05$.

level of lipid peroxidation in animals (Xi et al., 2016). Also, Sun et al. (2017) reported that the 20% *Moringa oleifera* leaves substitution group had highest serum CAT activity. It was found that dietary

supplementation of *Moringa oleifera* was of great benefits to improve ability of oxidation resistance of sows in the present research. While previous studies show that prolonged farrowing induces many free

radicals in sows and piglets, leading to oxidative stress (Szczeniowski, Dąbrowski, Bochniarz, & Komar, 2013). Therefore, in this research, shortening farrowing length may relate to antioxidant properties of *Moringa oleifera*.

In addition, dietary crude fibre can reduce sow constipation and shorten farrowing length of sows (Oliviero, Kokkonen, Heinonen, Sankari, & Peltoniemi, 2009). Reducing constipation may be a potential mechanism for shorten farrowing length. Thus, the crude fibre in *Moringa oleifera* reduced constipation may be the second mechanism to shorten farrowing length. In this study, all two dosages of *Moringa oleifera* supplementation have a tendency to increase the number of born alive piglets. The reason responsible for this phenomenon may relate to the fact that dietary *Moringa oleifera* was shown to shorten the farrowing length.

Colostrum is produced during the last month of gestation but mainly during the last week before farrowing (Devillers, Dividich, & Prunier, 2006), which supplies energy, maternal immunity and growth factors to piglets (Herpin, Louveau, Damon, & Dividich, 2005; Rooke & Bland, 2002; Xu, Wang, & Zhang, 2000). Our results indicate that dietary supplement of *Moringa oleifera* leaves elevated protein levels in the colostrum. Previous studies have suggested that the coefficients of variation in total protein concentration reach their highest during early stages of lactation (5% to 26%) (Klobasa, Werhahn, & Butler, 1987), and immunoglobulins account for most of the total protein in the colostrum (Declercq, Dewulf, Piepers, Decaluwé, & Maes, 2015). Beyond the neonatal period, the supply of maternal immunity by colostrum is relatively more important to survival than the supply of energy (Herpin et al., 2005; Le Dividich, Rooke, & Herpin, 2005). In the current context of demanding antibiotic reduction, sows are preferred to be vaccinated to protect their offspring against diseases through maternal immunity. However, a good maternal immunity can only be achieved by an adequate colostrum intake by the piglets (Farmer & Quesnel, 2009; Quesnel, Farmer, & Devillers, 2012). Thus, we tentatively put forward that dietary substitution of *Moringa oleifera* leaves may be conducive to growth and health of piglets at later stage, by elevating protein levels in the colostrum. Since three diets in the present study have very similar crude protein level, the elevation of colostrum protein is possibly due to the addition of *Moringa oleifera* leaves and their special active components. Further investigation is needed to explore its exact mechanisms.

Blood analysis is a defined method to evaluate health and clinical status of an animal (Church, Judd, Young, Kelsay, & Kim, 1984). Hassan et al., 2016 have shown the supplement of *Moringa oleifera* leaves meal improves haematological and biochemical parameters. In contrast, Ahemen, Abu, and Iorgilim (2013) reported no significant influence on serum biochemical parameters in rabbits which were fed diets containing 0, 5%, 10% and 15% *Moringa oleifera* leaves. Our results showed that supplement of *Moringa oleifera* leave meal decreased the serum urea nitrogen of sows, suggesting an improved protein utilization in sows that received *Moringa oleifera* addition. Urea nitrogen concentration reflects the balance between amino acid metabolism and protein synthesis in vivo. A reduced level of

urea nitrogen corresponds to a higher rate of protein synthesis (Malmolf, 1988). A previous study have demonstrated that balance of N in animals is positively influenced by introducing *Moringa* foliage meal in the diet of *Mong Cai* pigs (Ly, Samkol, Phiny, & Bustamante, 2016). N balance in pigs fed with other non-leguminous species has also been positive, according to data obtained for that purpose (Caro, Ly, Delgado, & Samkol, 2013). Supplementation of *Moringa oleifera*, as are other arboreal or bushy foliage non-leguminous species, leads to a benign N balance, according to what was observed in this study. Moreover, the addition of *Moringa oleifera* leave meal decreased serum glucose. Gupta et al., 2012 demonstrated that the progression of diabetes significantly reduced after receiving *Moringa oleifera* which induced a significant reduction in serum glucose and nitric oxide with concomitant increase in serum insulin and protein levels. So, it was found that dietary supplementation of *Moringa oleifera* was conducive to improves serum biochemical index of sows, which could elevate nitrogen utilization and help to maintain optimum health of sows.

More interestingly, *Moringa oleifera* supplementation essentially reduced the serum urea nitrogen and increased total protein not only in sows but also in the offspring, suggesting that maternal supplement of *Moringa oleifera* leaves improve nitrogen utilization in their piglets. Leonard et al. (2010) suggested that the supplementation of laminarin and fucoidan positively influenced colostrum IgG levels and was accompanied by enhanced serum IgG concentrations in suckled piglets. It is consistent with our view that the rise of serum total protein in piglets probably accounts for dietary *Moringa oleifera* to increase the protein in the colostrum. Confusingly, maternal supplement of *Moringa oleifera* leaves increased the serum glucose and total cholesterol of piglets. These results are fully in conflict with that *Moringa oleifera* is able to decrease both serum glucose and cholesterol in animals. Abd El Latif, El Bialy, Mahboub, & Abd Eldaim, 2014 reported that *Moringa oleifera* leave extract counteracted the alloxan-induced diabetic effects in rats as it normalized the elevated serum levels of glucose, triglycerides, cholesterol and malondialdehyde. The hydroalcoholic extract of *Moringa oleifera* leaves contains 90 mg/g of β -sitosterol which is a plant sterol with close chemical resemblance to cholesterol which enables it to block the absorption of cholesterol by competitive inhibition (Rajanandh & Kavitha, 2010). These counteracting bioactive compounds probably have not secreted into the colostrum but the mechanisms accounting for these increases in piglets remain further investigation. Furthermore, serum SOD and CAT activities were also improved in piglets whose mothers received *Moringa oleifera* leave meal. Maternal effects occur when the phenotype of the mother or the environment she experiences influences the phenotype of her offspring over and above the direct effect of transmitted genes (Marshall & Uller, 2007). A previous study suggested that mammalian maternal nutrition could modulate the islet function of mice by regulating gene expression (Aalinkeel, Srinivasan, Song, & Patel, 2001). Waterland and Garza (2002) also found that maternal nutrition may affect the offspring by influencing the epigenetic regulation of genomically imprinted genes. Therefore, maternally received *Moringa oleifera* improved

serum antioxidant indices in offspring, which probably count to the maternal effects.

5 | CONCLUSION

Overall, the present results provide a comprehensive overview on *Moringa oleifera* supplementation improved the reproduction performance and also had positive effects on the serum antioxidant and biochemical indices in both sows and piglets. Particularly, *Moringa oleifera* addition could significantly increase the protein levels in the colostrum. It can be concluded that *Moringa oleifera* can be used as a kind of feedstuff for sows, which has a positive effect on the reproductive performance and the health status of sows and piglets.

ACKNOWLEDGEMENTS

This work was supported by grants from The National Key Research and Development Program of China [2016YFD0500503, 2018YFD0501706] and Technical System of Modern Agricultural Industry in Guangdong Province [2018LM1121, 2018LM2158].

CONFLICT OF INTEREST

None of the authors declare any conflicts of interests.

ANIMAL WELFARE STATEMENT

This experiment was conducted in accordance with the guidelines of the Department of College of Animal Science, South China Agricultural University, China. The study was approved by the Ethics Committee of Local Experimental Animals Care Committee and conducted in accordance with the guidelines of South China Agricultural University, China (No.201004152). All efforts were made to minimize animal suffering.

REFERENCES

- Aalinkeel, R., Srinivasan, M., Song, F., & Patel, M. S. (2001). Programming into adulthood of islet adaptations induced by early nutritional intervention in the rat. *American Journal of Physiology. Endocrinology and Metabolism*, 281(3), E640–E648. <https://doi.org/10.1152/ajpen.2001.281.3.E640>
- Abd El Latif, A., El Bialy, B. E. S., Mahboub, H. D., & Abd Eldaim, M. A. (2014). *Moringa oleifera* leaf extract ameliorates alloxan-induced diabetes in rats by regeneration of β cells and reduction of pyruvate carboxylase expression. *Biochemistry and Cell Biology*, 92(5), 413–419.
- Ahemen, T., Abu, A. H., & Iorgilim, L. K. (2013). Physiological responses of rabbits fed graded levels of *Moringa oleifera* leaf meal (MOLM): some aspects of haematology and serum biochemistry. *Archives of Applied Science Research*, 5(2), 172–176.
- Ahmad, I. (2006). Antioxidant and free radical scavenging properties of twelve traditionally used Indian medicinal plants. *Turkish Journal of Biology*, 30(3), 177–183.
- Borges, V. F., Bernardi, M. L., Bortolozzo, F. P., & Wentz, I. (2005). Risk factors for stillbirth and foetal mummification in four Brazilian swine herds. *Preventive Veterinary Medicine*, 70(3–4), 165–176. <https://doi.org/10.1016/j.prevetmed.2005.03.003>
- Caro, Y., Ly, J., Delgado, E. J., & Samkol, P. (2013). Digestibilidad in vitro ileal y total de *Morus alba* L. y *Trichanthera gigantea* (H & B), como alimento para cerdos. *Zootecnia Tropical*, 31, 331–336.
- Church, J. P., Judd, J. T., Young, C. W., Kelsay, J. L., & Kim, W. W. (1984). Relationships among dietary constituents and specific serum clinical components of subjects eating self-selected diets. *American Journal of Clinical Nutrition*, 40(6), 1338–1344. <https://doi.org/10.1093/ajcn/40.6.1338>
- Declerck, I., Dewulf, J., Piepers, S., Decaluwé, R., & Maes, D. (2015). Sow and litter factors influencing colostrum yield and nutritional composition. *Journal of Animal Science*, 93(3), 1309–1317. <https://doi.org/10.2527/jas.2014-8282>
- Devillers, N., Dividich, J. L., & Prunier, A. (2006). Physiologie de la production de colostrum chez la truie. *Productions Animales -Paris-Institut National De La Recherche Agronomique-*, 19(1), 29–38.
- Farmer, C., & Quesnel, H. (2009). Nutritional, hormonal, and environmental effects on colostrum in sows. *Journal of Animal Science*, 87(13), 56–65.
- Gupta, R., Mathur, M., Bajaj, V. K., Katariya, P., Yadav, S., Kamal, R., & Gupta, R. S. (2012). Evaluation of antidiabetic and antioxidant activity of *Moringa oleifera* in experimental diabetes. *Journal of Diabetes*, 4(2), 164–171. <https://doi.org/10.1111/j.1753-0407.2011.00173.x>
- Hassan, H. M. A., El-Moniary, M. M., Hamouda, Y., El-Daly, E. F., Youssef, A. W., & El-Aze, N. A. A. (2016). Effect of different levels of *Moringa oleifera* leaves meal on productive performance, carcass characteristics and some blood parameters of broiler chicks reared under heat stress conditions. *Asian Journal of Animal & Veterinary Advances*, 11(1), 60–66. <https://doi.org/10.3923/ajava.2016.60.66>
- Herpin, P., Louveau, I., Damon, M., & Dividich, J. L. (2005). Chapter 14 Environmental and hormonal regulation of energy metabolism in early development of the pig. *Biology of Growing Animals*, 3, 351–374.
- Iqbal, S., & Bhanger, M. I. (2006). Effect of season and production location on antioxidant activity of *Moringa oleifera* leaves grown in Pakistan. *Journal of Food Composition and Analysis*, 19(6–7), 544–551. <https://doi.org/10.1016/j.jfca.2005.05.001>
- Khalafalla, M. M., Abdellatef, E., Dafalla, H. M., Nassrallah, A. A., Aboul-Enein, K. M., Lightfoot, D. A., ...El-Shemy, H. A. (2010). Active principle from *Moringa oleifera* Lam leaves effective against two leukemias and a hepatocarcinoma. *African Journal of Biotechnology*, 9(49), 8467–8471.
- Klobasa, F., Werhahn, E., & Butler, J. E. (1987). Composition of sow milk during lactation. *Journal of Animal Science*, 64(5), 1458. <https://doi.org/10.2527/jas1987.6451458x>
- Lako, J., Trenerry, V. C., Wahlqvist, M., Wattanapenpaiboon, N., Sotheeswaran, S., & Premier, R. (2007). Phytochemical flavonols, carotenoids and the antioxidant properties of a wide selection of Fijian fruit, vegetables and other readily available foods. *Food Chemistry*, 101(4), 1727–1741. <https://doi.org/10.1016/j.foodchem.2006.01.031>
- Le Dividich, J., Rooke, J. A., & Herpin, P. (2005). Nutritional and immunological importance of colostrum for the new-born pig. *Journal of Agricultural Science*, 143(6), 469–485. <https://doi.org/10.1017/S0021859605005642>
- Leonard, S. G., Sweeney, T., Bahar, B., Pierce, K. M., Lynch, B. P., & O'Doherty, J. V. (2010). The effects of maternal dietary supplementation with seaweed extract and fish oil on the humoral immune response and performance of suckling piglets. *Livestock Science*, 134(1–3), 211–214. <https://doi.org/10.1016/j.livsci.2010.06.144>
- Lucia, T., Corrêa, M. N., Deschamps, J. C., Bianchi, I., Donin, M. A., Machado, A. C., ...Matheus, J. E. M. (2002). Risk factors for stillbirths in

- two swine farms in the south of Brazil. *Preventive Veterinary Medicine*, 53(4), 285–292. [https://doi.org/10.1016/S0167-5877\(01\)00288-4](https://doi.org/10.1016/S0167-5877(01)00288-4)
- Ly, J., Samkol, P., Phiny, C., & Bustamante, D. (2016). Balance of nitrogen (n) in pigs fed with *Moringa Oleifera* foliage meal. *Revista Bio Ciencias*, 3(4), 349–358.
- Malmolf, K. (1988). Amino acid in farm animal nutrition metabolism, partition and consequences of imbalance. *Swedish Journal of Agricultural Research*, 18(4), 191–193.
- Marshall, D. J., & Uller, T. (2007). When is a maternal effect adaptive? *Oikos*, 116(12), 1957–1963. <https://doi.org/10.1111/j.2007.0030-1299.16203.x>
- Mendieta-Araica, B., Spörndly, R., Reyes-Sánchez, N., & Spörndly, E. (2011). *Moringa (Moringa oleifera)* leaf meal as a source of protein in locally produced concentrates for dairy cows fed low protein diets in tropical areas. *Livestock Science*, 137(1–3), 10–17. <https://doi.org/10.1016/j.livsci.2010.09.021>
- Moyo, B., Masika, P. J., Hugo, A., & Muchenje, V. (2011). Nutritional characterization of *Moringa (Moringa oleifera)* leaves. *African Journal of Biotechnology*, 10(60), 12925–12933. <https://doi.org/10.5897/AJB10.1599>
- Naidoo, K. K., & Cooposamy, R. M. (2011). Review on herbal remedies used by the 1860 South African Indian settlers. *African Journal of Biotechnology*, 10(43), 8533–8538.
- Oliviero, C., Heinonen, M., Valros, A., & Peltoniemi, O. (2010). Environmental and sow-related factors affecting the duration of farrowing. *Animal Reproduction Science*, 119(1–2), 85–91. <https://doi.org/10.1016/j.anireprosci.2009.12.009>
- Oliviero, C., Kokkonen, T., Heinonen, M., Sankari, S., & Peltoniemi, O. (2009). Feeding sows with high fibre diet around farrowing and early lactation: Impact on intestinal activity, energy balance related parameters and litter performance. *Research in Veterinary Science*, 86(2), 314–319. <https://doi.org/10.1016/j.rvsc.2008.07.007>
- Osman, H. M., Shayoub, M. E., & Babiker, E. M. (2012). The effect of *Moringa oleifera* leaves on blood parameters and body weights of albino rats and rabbits. *Jordan Journal of Biological Sciences*, 5(3), 147–150.
- Quesnel, H., Farmer, C., & Devillers, N. (2012). Colostrum intake: Influence on piglet performance and factors of variation. *Livestock Science*, 146(2–3), 105–114. <https://doi.org/10.1016/j.livsci.2012.03.010>
- Rajanandh, M. G., & Kavitha, J. (2010). Quantitative estimation of β -sitosterol, total phenolic and flavonoid compounds in the leaves of *Moringa oleifera*. *International Journal of Pharmtech Research*, 2(2), 1409–1414.
- Rekwot, P. I., Jegede, J. O., Ehoche, O. W., & Tsb, T. (2001). Reproductive performance in smallholder piggeries in northern Nigeria. *Tropical Agriculture*, 78(2), 130–133.
- Rooke, J. A., & Bland, I. M. (2002). The acquisition of passive immunity in the new-born piglet. *Livestock Production Science*, 78(1), 13–23. [https://doi.org/10.1016/S0301-6226\(02\)00182-3](https://doi.org/10.1016/S0301-6226(02)00182-3)
- Siddhuraju, P., & Becker, K. (2003). Antioxidant properties of various solvent extracts of total phenolic constituents from three different agroclimatic origins of drumstick tree (*Moringa oleifera* Lam.) leaves. *Journal of Agricultural and Food Chemistry*, 51(8), 2144–2155.
- Sreelatha, S., & Padma, P. R. (2009). Antioxidant activity and total phenolic content of *Moringa oleifera* leaves in two stages of maturity. *Plant Foods for Human Nutrition*, 64(4), 303–311. <https://doi.org/10.1007/s11130-009-0141-0>
- Sun, B., Zhang, Y., Ding, M., Xi, Q., Liu, G., Li, Y., ... Chen, X. (2017). Effects of *Moringa oleifera* leaves as a substitute for alfalfa meal on nutrient digestibility, growth performance, carcass trait, meat quality, antioxidant capacity and biochemical parameters of rabbits. *Journal of Animal Physiology & Animal Nutrition*, 102(1), 194–203.
- Szczubiał, M., Dąbrowski, R., Bochniarz, M., & Komar, M. (2013). The influence of the duration of the expulsive stage of parturition on the occurrence of postpartum oxidative stress in sows with uncomplicated, spontaneous farrowings. *Theriogenology*, 80(7), 706–711. <https://doi.org/10.1016/j.theriogenology.2013.05.015>
- Teixeira, E. M. B., Carvalho, M. R. B., Neves, V. A., Silva, M. A., & Arantes-Pereira, L. (2014). Chemical characteristics and fractionation of proteins from *Moringa oleifera* Lam. leaves. *Food Chemistry*, 147, 51–54. <https://doi.org/10.1016/j.foodchem.2013.09.135>
- Thodberg, K., Jensen, K. H., & Herskin, M. S. (2002). Nest building and farrowing in sows: Relation to the reaction pattern during stress farrowing environment and experience. *Applied Animal Behaviour Science*, 77(1), 21–42. [https://doi.org/10.1016/S0168-1591\(02\)00026-6](https://doi.org/10.1016/S0168-1591(02)00026-6)
- van Dijk, A. J., van Rens, B., van der Lende, T., & Taverne, M. (2014). Factors affecting duration of the expulsive stage of parturition and piglet birth intervals in sows with uncomplicated, spontaneous farrowings. *Theriogenology*, 64(7), 1573–1590. <https://doi.org/10.1016/j.theriogenology.2005.03.017>
- Verma, A. R., Vijayakumar, M., Mathela, C. S., & Rao, C. V. (2009). In vitro and in vivo antioxidant properties of different fractions of *Moringa oleifera* leaves. *Food and Chemical Toxicology*, 47(9), 2196–2201. <https://doi.org/10.1016/j.fct.2009.06.005>
- Waterland, R. A., & Garza, C. (2002). Early postnatal nutrition determines adult pancreatic glucose-responsive insulin secretion and islet gene expression in rats. *Journal of Nutrition*, 132(3), 357–364. <https://doi.org/10.1093/jn/132.3.357>
- Xi, Q. Y., Jiang, Y., Zhao, S., Zeng, B., Wang, F., Wang, L. N., ... Zhang, Y. L. (2016). Effect of ginseng polysaccharides on the immunity and growth of piglets by dietary supplementation during late pregnancy and lactating sows. *Animal Science Journal*, 88(6), 863–872. <https://doi.org/10.1111/asj.12678>
- Xu, R. J., Wang, F., & Zhang, S. H. (2000). Postnatal adaptation of the gastrointestinal tract in neonatal pigs: A possible role of milk-borne growth factors. *Livestock Production Science*, 66(2), 95–107. [https://doi.org/10.1016/S0301-6226\(00\)00217-7](https://doi.org/10.1016/S0301-6226(00)00217-7)
- Yazdanparast, R., & Ardestani, A. (2007). In vitro antioxidant and free radical scavenging activity of *Cyperus rotundus*. *Journal of Medicinal Food*, 10(4), 667–674.
- Yin, J., Ren, W., Liu, G., Duan, J., Yang, G., Wu, L., ... Yin, Y. (2013). Birth oxidative stress and the development of an antioxidant system in newborn piglets. *Free Radical Research*, 47(12), 1027–1035. <https://doi.org/10.3109/10715762.2013.848277>
- Yin, J., Wu, M. M., Xiao, H., Ren, W. K., Duan, J. L., Yang, G., ... Yin, Y. L. (2014). Development of an antioxidant system after early weaning in piglets. *Journal of Animal Science*, 92(2), 612–619.
- Zaleski, H. M., & Hacker, R. R. (1993). Variables related to the progress of parturition and probability of stillbirth in swine. *The Canadian Veterinary Journal*, 34(2), 109–113.

How to cite this article: Sun J-J, Wang P, Chen G-P, et al. Effect of *Moringa oleifera* supplementation on productive performance, colostrum composition and serum biochemical indexes of sow. *J Anim Physiol Anim Nutr*. 2019;00:1–9. <https://doi.org/10.1111/jpn.13224>



Emerging Roles of Heat-Induced circRNAs Related to Lactogenesis in Lactating Sows

Jiajie Sun^{1†}, Haojie Zhang^{1†}, Baoyu Hu¹, Yueqin Xie¹, Dongyang Wang¹, Jinzhi Zhang², Ting Chen¹, Junyi Luo¹, Songbo Wang¹, Qinyan Jiang¹, Qianyun Xi¹, Zujing Chen^{1*} and Yongliang Zhang^{1*}

¹ College of Animal Science, Guangdong Provincial Key Laboratory of Animal Nutrition Control, Guangdong Engineering & Research Center for Woody Fodder Plants, National Engineering Research Center for Breeding Swine Industry, South China Agricultural University, Guangzhou, China, ² College of Animal Science, Zhejiang University, Hangzhou, China

OPEN ACCESS

Edited by:

David E. MacHugh,
University College Dublin, Ireland

Reviewed by:

Gary Rohrer,
United States Department of
Agriculture, United States
Nicolas Nalpas,
University of Tübingen, Germany

*Correspondence:

Zujing Chen
zujingchen@scau.edu.cn
Yongliang Zhang
zhangyl@scau.edu.cn

[†]These authors have contributed
equally to this work

Specialty section:

This article was submitted to
Livestock Genomics,
a section of the journal
Frontiers in Genetics

Received: 29 May 2019

Accepted: 10 December 2019

Published: 11 February 2020

Citation:

Sun J, Zhang H, Hu B, Xie Y, Wang D,
Zhang J, Chen T, Luo J, Wang S,
Jiang Q, Xi Q, Chen Z and Zhang Y
(2020) Emerging Roles of Heat-
Induced circRNAs Related to
Lactogenesis in Lactating Sows.
Front. Genet. 10:1347.
doi: 10.3389/fgene.2019.01347

Heat stress negatively influences milk production and disrupts normal physiological activity of lactating sows, but the precious mechanisms by which hyperthermia adversely affects milk synthesis in sows still remain for further study. Circular RNAs are a novel class of non-coding RNAs with regulatory functions in various physiological and pathological processes. The expression profiles and functions of circRNAs of sows in lactogenesis remain largely unknown. In the present study, long-term heat stress (HS) resulted in a greater concentration of serum HSP70, LDH, and IgG, as well as decreased levels of COR, SOD, and PRL. HS reduced the total solids, fat, and lactose of sow milk, and HS significantly depressed CSN α s1, CSN α s2, and CSN κ biosynthesis. Transcriptome sequencing of lactating porcine mammary glands identified 42 upregulated and 25 downregulated transcripts in HS vs. control. Functional annotation of these differentially-expressed transcripts revealed four heat-induced genes involved in lactation. Moreover, 29 upregulated and 21 downregulated circRNA candidates were found in response to HS. Forty-two positively correlated circRNA-mRNA expression patterns were constructed between the four lactogenic genes and differentially expressed circRNAs. Five circRNA-miRNA-mRNA post-transcriptional networks were identified involving genes in the HS response of lactating sows. In this study we establish a valuable resource for circRNA biology in sow lactation. Analysis of a circRNA-miRNA-mRNA network further uncovered a novel layer of post-transcriptional regulation that could be used to improve sow milk production.

Keywords: heat stress, lactating sow, circRNA, ceRNA, casein

INTRODUCTION

In seasonal climates, high ambient temperature is the primary environmental stress impacting domestic animal performance, including growth, reproduction, and lactation (Das et al., 2016). In general, high-yielding animals are especially susceptible to thermal stress since they generate considerably more metabolic heat (Kadzere et al., 2002). In response to heat stress (HS), dairy

animals experience a sustained reduction in appetite and nutrient uptake (Bohmanova et al., 2007) and a subsequent reallocation of energy for heat acclimation (Renaudeau et al., 2012), thereby resulting in decreased milk yield and milk quality, which negatively affects the efficiency and profitability of animal farms worldwide (Hill and Wall, 2015).

In modern swine husbandry, lactating sows have been heavily selected for increased productivity (fertility, disease resistance, feed conversion efficiency, and so on) during the last two decades, and are especially at risk of HS (Renaudeau, 2005), as they have a thermal neutral zone between 16 and 22°C (Messias de Bragança et al., 1998). It is noteworthy that high temperatures above 25° are sustained for half a year in the south of China; thus, local sows are often exposed to hot conditions. Under thermal stress, individuals normally increase respiration rates and reduce feed intake (Quiniou and Noblet, 1999), in an effort to generate a negative energy balance to promote metabolic heat loss to counter HS (Renaudeau et al., 2001; Renaudeau et al., 2012). In addition, HS also influences milk production in lactating sows, perhaps through an indirect effect associated with reduction in feed intake (Ribeiro et al., 2018); however, previous reports of Messias de Bragança et al. (1998) and Silanikove et al. (2009) suggested that there may be a direct effect of ambient temperature on mammary gland metabolism in connection with low milk yield. Thus, identifying key differences in the mammary gland of lactating sows in response to high ambient temperatures has the potential to improve the productivity of sows in adverse environments (Collier et al., 2006). The ability to use powerful genomic tools to evaluate genetic differences associated with thermal tolerance can provide important information on the underlying mechanisms of HS on lactation, and will permit the selection of sows for resistance to HS.

Circular RNAs (circRNAs) are a recently identified genetic element that are abundantly expressed, highly conserved between different animal species (Hanan et al., 2017), and are involved in the foundation of mammary gland growth and development (Zhang et al., 2015; Zhu et al., 2016), milk synthesis (Zhang C. et al., 2016), and secretion and transportation (Wang et al., 2019). HS greatly impacts circRNA biogenesis, and heat-induced circRNAs perform substantial regulatory functions through circRNA-mediated competing endogenous RNA (ceRNA) networks (Pan et al., 2018). Although patterns of circRNA expression and function have been revealed among various developmental stages and physiological conditions (Lai et al., 2018; Patop and Kadener, 2018), little is known about how HS affects circRNAs in lactation. In this study, we focused on circRNAs involved in the HS response of lactating sows, and we explored potential mechanisms underlying circRNA regulation in mammary tissue.

MATERIALS AND METHODS

Study Design and Sample Collection

A total of 60 healthy purebred Landrace sows (2–3 parity and without genetic relationships) were separated into two balanced

cohorts of 30 animals each, and HS tests were conducted at a local thoroughbred farm during December 2016 and during August 2017 (WENS Shuitai Breeding Pig Farm, Guangdong, China). All sows were fed the same commercial formula diet and raised under the same management conditions. In the experimental stage, the ambient temperatures and relative humidity were measured at 14:00pm in everyday. In details, one cohort of 30 sows was selected in the winter months with a moderate average temperature, designated as the non-heat stress (NS) population; other cohort of 30 animals was selected in the summer months with a higher average temperature, designated as the HS population. Within each cohort, the number of piglets born alive was recorded, and litter birth weights of piglets were obtained within 24 hours after farrowing. Piglets were not offered creep feed, and sow milk was the only feed available to the piglets during lactation. On day 21, weaning survival and the weights of living piglets per litter were recorded and used to calculate average daily weight gain. Blood samples (10 ml) were collected at 10:00am from fasted sows using jugular venipuncture at weaning, and ELISA kits (Nanjing Jiancheng Bioengineering Institute, Nanjing, China) were used to determine serum LDH, IgG, SOD, HSP70, COR, and PRL concentrations. Sow milk samples (approximate 20 ml) were obtained on d 3, 15, and 20 of lactation from the last two pairs of sow nipples at 10:30–11:30am in each animal, and oxytocin was used to stimulate let-down. Three milk samples from each animal was pooled equally to evaluate the effect of environmental temperature on milk composition. In each environmental group, six animals that balanced for weaned backfat thickness and weight were chosen and humanely slaughtered at 21 day postpartum, and suckled mammary glands were split down the mid-line and tissues were excised from the center portion of four glands from the fourth and fifth pairs of nipples. Connective tissue and fat were removed. Mammary tissues were cut into small pieces and snap-frozen in liquid nitrogen prior to subsequent processing. In general, the collected mammary tissues contain primarily secretory epithelial cells, with a small amount of myoepithelial cells, endothelial cells, adipocytes, fibroblasts, and immune cells (Kensinger et al., 1986). All procedures were conducted under protocols approved by the Institutional Animal Care and Use Committee of South China Agricultural University, China.

RNA Preparation and Sequencing

Total RNA was extracted from mammary tissue and purified using Trizol reagent (Invitrogen, Carlsbad, CA), according to the manufacturer's instructions. Each RNA sample was treated with DNase I (Takara, Dalian, China) for 15 minutes at 37°C to remove residual genomic DNA. RNA quantity and purity were analyzed using a Bioanalyzer 2100 (Agilent, Palo Alto, CA), and RNA samples with Integrity Number (RIN) value ≥ 7.5 were used for further analysis. In each experimental condition, we randomly selected two RNA samples and pooled 5 μ g of RNA from each sample. In total, six RNA pools were depleted of ribosomal RNA using an Ribo-Zero™ rRNA Removal Kit (Illumina, San Diego, USA), and the left poly-A^{+/+} RNA fractions were

then reverse-transcribed to create the final cDNA using a mRNA-Seq sample preparation kit (Illumina, San Diego, CA). Finally, we performed paired-end sequencing on an Illumina Hiseq 4000 (LC Bio, Hangzhou, China) to yield 2×150 nucleotide reads, following the manufacturer's recommended protocol.

Bioinformatics Analysis

Raw sequences quality was verified using FastQC (<http://www.bioinformatics.babraham.ac.uk/projects/fastqc/>), and the reads that contained adaptor contamination, low quality, and undetermined bases were removed by Cutadapt (Martin, 2011). Filtered data from each library was aligned to the *Sscrofa11.1* reference genome downloaded from Ensembl genome website (ftp://ftp.ensembl.org/pub/release-94/fasta/sus_scrofa/dna/) with TopHat v2.1.1 (Kim et al., 2013), and transcript assembly and abundance estimation were performed using Cufflinks v2.2.1 (Trapnell et al., 2012). Each assembly was then merged using Cuffmerge to create a single transcriptome annotation with known porcine genes in gtf format (ftp://ftp.ensembl.org/pub/release-94/gtf/sus_scrofa) for subsequent protein-coding gene analysis. To predict circRNA candidates, five different algorithms including CIRCexplorer2 (Zhang X. et al., 2016), circRNA_Finder (Fu and Liu, 2014), CIRI (Gao et al., 2015), find_circ (Memczak et al., 2013), and MapSplice (Wang et al., 2010) were performed on each RNAseq library. Only circRNA candidates identified by all five approaches were considered for further evaluation. Following the above primary analysis, expression levels of all coding genes in each library were estimated from the TopHat alignments as fragments per kilobase of exon per million mapped reads (FPKM), and Cuffdiff, included in the Cufflinks package, was used to compare expression levels between NS and HS with a false discovery rate (FDR) value < 0.05 . The abundance of circRNA candidates was calculated with back-spliced junction read count (Zhang et al., 2014). Then, the edgeR software package (Robinson et al., 2010) was used to examine the differential expression (DE) of circRNA candidates with P value < 0.05 and fold change ≥ 2 . Finally, Biological Processes GO terms and KEGG pathway analysis of the DE genes were performed using DAVID gene functional classification (<https://david.ncifcrf.gov/>).

CeRNA Network Construction

Putative interactions between the DE circRNAs and lactation-related coding genes that responded to HS in our paper were evaluated by competing to bind with shared miRNAs. Porcine mature miRNAs published in miRBase (<http://www.mirbase.org/>) were prepared for further analysis. In details, the construction of ceRNA networks included three steps: (1) the correlations between DE circRNAs and lactation-related genes were calculated by the Pearson test, and only nodes in positive circRNA-gene interactions were retained; (2) the circRNA-miRNA and mRNA-miRNA interactions were predicted by miRanda algorithm (Betel et al., 2010) with with energies of ≤ -20.0 kcal/mol and no mismatch in the seed region (positions 2–8 in the 5' end); (3) potential circRNA-miRNA-gene interactions were established and visualized using Cytoscape V3.4 (<http://cytoscape.org/>).

Validation of Sequencing Data by Reverse transcription quantitative real-time polymerase chain reaction (RT-qPCR)

Total RNA from the NS and HS samples were isolated with Trizol reagent (Invitrogen, Carlsbad, CA), and cDNA synthesis was conducted using PrimeScript RT reagent Kit (Takara, Dalian, China) with random hexamers. Quantitative PCR was used to analyze the expression changes of the chosen transcripts with SYBR Premix Ex Taq II (Takara). All primers are listed in **Table S1**, and final expression data were calculated using the $2^{-\Delta\Delta C_t}$ method using porcine GAPDH as a reference gene.

Sequencing Data Submission

All sequencing raw datasets have been deposited into the National Center for Biotechnology Information (NCBI) Sequence Read Archive (SRA) database (<https://www.ncbi.nlm.nih.gov/sra/>) with the BioProject accession number PRJNA578241.

Statistical Analysis

The statistical analysis was performed using by SPSS 17.0 Statistics Software (Chicago, IL, USA). The results of ELISA and RT-qPCR analysis between two groups were compared with independent t-test; the correlation analyses of DE circRNAs with lactation-related coding genes were tested by function cor (x, y, use = "p"), and illustrated with function labeledHeatmap (Matrix, xLabels, yLabels) in R package WGCNA (<http://127.0.0.1:11153/library/stats/html/cor.html>).

RESULTS

Sow and Litter Performance

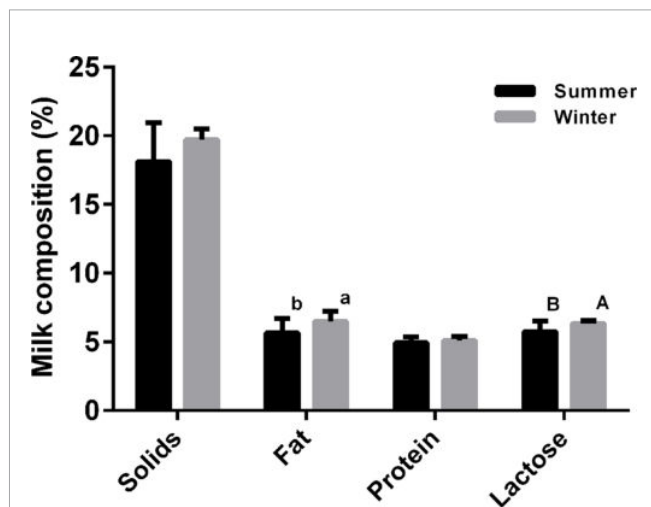
This study was performed during December 2016 and during August 2017. During the winter experimental stage, ambient temperatures and relative humidity averaged $14.3 \pm 0.81^\circ\text{C}$ and $65.0\% \pm 0.69\%$, while the corresponding values for the hot season were $32.7 \pm 1.40^\circ\text{C}$ and $76.1\% \pm 0.38\%$, respectively. The effects of ambient temperature on the serum stress-associated variables of lactating sows are presented in **Figure S1**. Blood heat shock protein 70 (HSP70), lactate dehydrogenase (LDH), and immunoglobulin G (IgG) levels were significantly higher in the HS cohort compared with the NS group ($P < 0.05$). In contrast, serum superoxide dismutase (SOD) and prolactin (PRL) concentrations were lower in the HS population ($P < 0.05$). The high temperature group had significantly lower serum cortisol (COR) concentration than the NS group ($P < 0.05$). In addition, there was no effect of thermal stress on the number of piglets born alive, litter birth weights, or piglets alive per litter at weaning ($P > 0.05$, **Table 1**). In contrast, litter weights at weaning were significantly higher in the NS cohort than the HS cohort ($P < 0.05$). And a reduced average daily weight gain of piglets (193.9 ± 2.19 vs. 218.0 ± 1.89 g, respectively, for the HS and NS cohorts) was associated with the environment with a high temperature. Thermal stress also altered the milk composition of lactating sows. In particular, sow milk had less butterfat, and lactose when sows lactated in the hot environment ($P < 0.05$), and milk in the

TABLE 1 | Production traits of tested sows and piglets between summer and winter.

Variables	Summer (N = 30)	Winter (N = 30)
Number born alive	10.8 ± 0.13	10.9 ± 0.09
Weaning survival	10.4 ± 0.13	10.5 ± 0.11
Litter birth weight, kg	14.9 ± 0.18	15.2 ± 0.17
Weight of weaning litter, kg	61.3 ± 0.73 ^B	67.2 ± 1.59 ^A
Average daily gain, g	193.9 ± 2.19 ^B	218.0 ± 1.89 ^A

A and B denote values that differ significantly at $P < 0.01$.

HS group had a downward trend for total milk solids and milk protein levels (**Figure 1**). HS individuals tended to have much lower casein alpha s1 (CSN α s1) and s2 (CSN α s2) distributions ($P < 0.01$), while casein beta (CSN β) and casein kappa (CSN κ) concentrations decreased from 343.59 ± 6.42 μ g/ml and 7.47 ± 0.16 μ g/ml in the HS group to 259.14 ± 7.96 μ g/ml and 6.35 ± 0.12 μ g/ml in the NS group ($P < 0.01$), respectively. Under HS, we found no overall differences in whey acidic protein (WAP) concentrations between the NS and HS groups ($P = 0.067$), although there was a slightly decreasing trend in the HS group (**Table 2**).

**FIGURE 1 |** Effect of thermal stress on milk composition of lactating sows. a and b denote values that differ significantly at $P < 0.05$, and A and B denote values that differ significantly at $P < 0.01$ (N = 30).**TABLE 2 |** Effect of thermal stress on lactoprotein distribution of lactating sows.

Variables	Summer (N = 30)	Winter (N = 30)
CSN α s1, μ g/ml	592.03 ± 23.31 ^B	693.63 ± 16.35 ^A
CSN α s2, μ g/ml	282.31 ± 15.00 ^B	409.85 ± 9.27 ^A
CSN β , μ g/ml	259.14 ± 7.96 ^B	343.59 ± 6.42 ^A
CSN κ , μ g/ml	6.35 ± 0.12 ^B	7.47 ± 0.16 ^A
WAP, ng/ml	447.87 ± 14.67	484.14 ± 13.65

CSN α s1, casein alpha s1; CSN α s2, casein alpha s2; CSN2, casein beta; CSN3, casein kappa; WAP, whey acidic protein. a and b denote values that differ significantly at $P < 0.05$, and A and B denote values that differ significantly at $P < 0.01$.

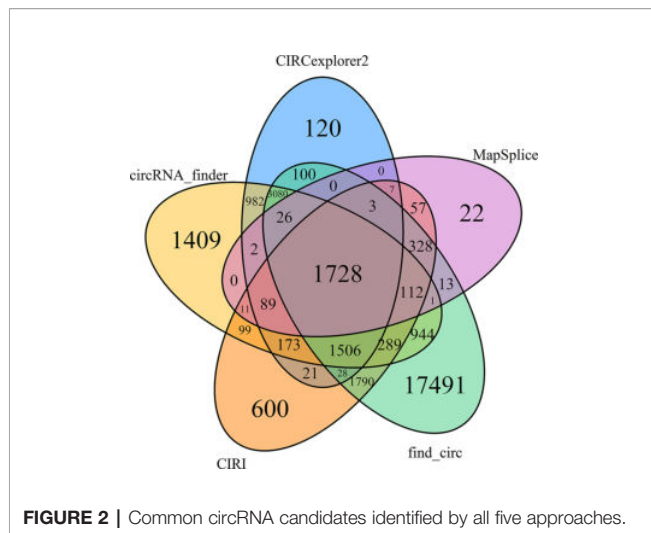
RNA Sequencing and Transcript Analysis

Six cDNA libraries were constructed from porcine mammary tissues exposed to thermal stress or to suitable temperatures. Each RNA-seq library generated approximately 94.52 ± 2.83 million raw reads of 110 nt in length, representing about 3.70 ± 0.11 fold coverage of the porcine genome. After quality control trimming, a total of 88.08 ± 2.65 million valid reads were obtained, accounting for $93.19\% \pm 0.23\%$ of the raw reads in each library. We aligned all valid reads onto the porcine *Sscrofa11.1* reference genome and found that over $80.55\% \pm 1.63\%$ of the reads could be mapped successfully to the genome, including $76.13\% \pm 1.63\%$ of the mapped reads with proper pair alignment in the six libraries (**Table S2A**). In addition, most valid reads were mapped to exons ($77.51\% \pm 2.64\%$), $17.27\% \pm 2.02\%$ were mapped to introns, and the rest to intergenic regions ($5.22\% \pm 0.62\%$), indicating confidence in the quality of library construction and sequencing analysis.

Transcript assemblies from porcine mammary tissue with Cufflinks revealed a total of 133,145 isoforms across six samples, including approximately 37.33% identified candidates that completely matched Ensembl transcript regions (**Table S2B**). A comparison of known Ensembl transcripts revealed that 36,271 isoforms were expressed across all tissues; NS-specific units accounted for 82.08% of known Ensembl isoforms, while 81.37% of the known isoforms existed in the HS libraries (**Table S2C**). Raw Ensembl gene expression levels were quantified by the FPKM algorithm, and the 10 most prevalent functional isoforms accounted for $7.97\% \pm 0.62\%$ of the total raw reads. In addition, seven gene candidates of *PAEP*, *CSN1S1*, *CSN3*, *CSN2*, *JCHAIN*, *COX1*, and *NUPR1* were shared in the top 10 expressed genes in each sequencing library. These highly expressed isoforms are well-known as having key functions in the lactation process, consistent with the physiological roles of genes expected to be found in mammary gland tissues.

Identification of circRNA

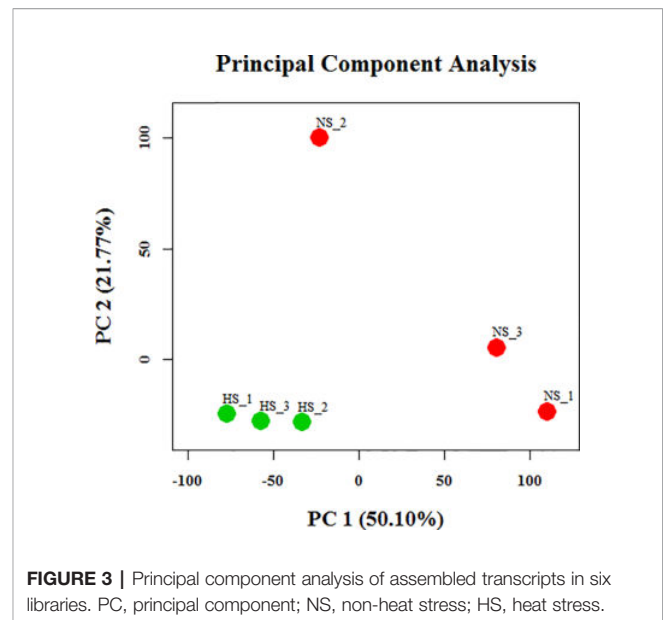
Several tools have been developed for identification of circRNAs based on back-spliced reads produced from high-throughput RNA sequencing datasets (Hansen et al., 2015). Due to the rearranged exon ordering, these back-spliced events usually cannot be mapped onto the reference genomes (Zhang et al., 2014). In the present study, we identified 17.07 ± 0.25 ($19.75\% \pm 0.80\%$ of the valid reads) and 17.07 ± 3.19 ($19.16\% \pm 3.55\%$) million unmapped reads in the NS and HS libraries, respectively. Among them, we found a total of 948.00 ± 23.98 thousand back-spliced junction events ($1.09\% \pm 0.04\%$ of the valid reads) in the rRNA-depleted libraries of NS animals, as well as 892.49 ± 80.27 thousand candidates in the HS libraries. We then compared five different circRNA predicting algorithms and found a total of 31,031 unique circRNAs identified across six libraries. Of these, 19,642 were found by a single algorithm, accounting for 63.29% of all the circRNAs identified (**Figure 2**), indicating that the circRNA landscape differs quite dramatically depending on the algorithm used. In particular, find_circ and MapSplice exhibited the highest and lowest level of sensitivity; this is in part reflected in the total number of circRNAs predicted, where find_circ and



MapSplice output the highest and lowest number of circRNA species (27,439 and 2,399, respectively) compared to CIRCEXPLORER2, circRNA_finder, and CIRI methods (7,865, 10,451, and 6,841 species, respectively; **Table S3**). To limit the level of false positive circRNAs, only circRNA candidates identified by all five approaches were considered for further evaluation. Of the 31,031 predicted circRNAs, only a modest overlap of 1,728 circRNAs (5.57%) was observed among the five prediction pipelines. These 1,728 circularization events were found to be produced from 1,157 hosting isoform loci, including 571 transcripts that generated more than one circRNA. For instance, we found that the porcine genes *SEC24A* and *SLC5A10* had nine and eight predicted circRNAs, respectively, and there were seven circularization events predicted from the *BAZ2B*, *PIAS1*, and *CCAR1* genes (**Table S4A**).

Differential Expression and Functional Analysis

To identify dissimilarities between the tested individuals, principal component analysis (PCA) of the globally expressed transcript with the FPKM levels was performed (**Figure 3**). This analysis indicated that the differences in expression between the NS and HS groups were greater than the differences between pools from each particular group. Therefore, we employed the Cuffdiff algorithm to analyze differences in mammary gland gene expression between the NS and HS groups to identify candidate transcripts that are responsive to thermal stress. In our dataset there were over 40,000 unique Ensembl transcripts sequenced, most of which had a very small FPKM value in total across all libraries. In order to filter out false-positive results, we only kept confident transcripts that were expressed in at least three libraries, and finally 9,789 tags were identified in our study (**Table S5A**). Among these, we detected a total of 67 differentially expressed (DE) transcript events by a limited cut-off of $FDR < 0.05$, representing 63 protein-coding genes, with 42 transcripts increased and 25 transcripts decreased in the HS groups compared to the NS group (**Table S5A**). Analysis of gene



ontology (GO) enrichment for DE genes, using identified porcine genes as background in the current experiment, revealed that these genes were significantly enriched in lactation-related functions or stress-inducible biological processes, including “lactation”, “defense response”, “inflammatory response”, “response to stimulus”, and “regulation of immune system process” (**Table S5B**). These 67 DE genes are significantly involved in only one KEGG signaling pathways, termed as toll-like receptor signaling pathway. Although the role of these genes needs to be validated experimentally, the GO and KEGG pathway analyses collectively illustrate some possible avenues to improve HS resistance of lactating sows. In addition, we also clustered differential porcine circRNA expression counts between NS and HS libraries, as determined by the CIRCEXPLORER2 algorithm, and normalized with trimmed mean of M-values (TMM) (Robinson et al., 2010). In total, only 50 out of 1,728 identified circRNAs were DE, including 29 up-regulated candidates and 21 down-regulated candidates in the NS samples compared with the HS samples (**Table S4B**).

Functional Interactions Between circRNA and mRNA

To identify possible correlations between circRNA and mRNA expression, we first used the Pearson test and found a total of 1,423 significant interactions between DE circRNAs and DE genes in our study (**Table S6**). In **Table S6** we identified 464 sponge modulators participating in 100 miRNA-mediated regulatory interactions, including 45 circRNAs and 36 unique mRNAs. In addition, the Pearson analysis also revealed 84 significant interactions between DE circRNAs and four lactation-related coding genes (*CSN1S1*, *CSN1S2*, *CSN3*, *WAP*) that were annotated by GO analyses, and these interactions included 42 positive significant interactions and 42 negative interactions (**Table S6**). We observed that the highest expressed circRNA, *circCSN1S1_2*, was significantly and

positively associated with the expression of the *CSN1S1*, *CSN1S2*, *CSN3*, and *WAP* genes; interestingly, these gene products represent the main components of lactoprotein. Recent reports also showed that diverse RNA species can communicate with and co-regulate each other by competing to bind with shared miRNAs, acting as competing endogenous RNAs (ceRNAs) (Tay et al., 2014). We constructed circRNA-miRNA-mRNA networks by pairing the shared miRNA recognition sequences. In total, we generated a network that contained eight nodes and five connections formed between four circRNAs, three miRNAs, and *CSN1S1* gene, including five circRNA-miRNA interactions and three mRNA-miRNA interactions (Table S7). Of these, the circCSN1S1_2-miR-204 (miR-670)-*CSN1S1* ceRNA axis was established, corresponding well with the ceRNA hypothesis.

RT-qPCR Analysis

Based on ceRNA networks involved in mammapoiesis and lactogenesis under HS that we constructed, we identified a total of 10 interaction core genes (Figure S2). We validated expression of these core genes by RT-qPCR, including eight lactation-related coding genes, one heat-response gene, and circCSN1S1_2, which had the highest expression levels in our study. Divergent and convergent primers were designed for circRNA candidates according to the method described in previous study (Sun et al., 2017). All tested candidate genes showed consistent expression patterns between RT-qPCR and sequencing analysis, suggesting that our estimation of abundance was accurate. Briefly, the expression of coding genes for lactoprotein were significantly lower in HS sows ($P < 0.05$), except for *CSN3*, which decreased in HS sows, but the change was not significant. Usually, HSP family member proteins have important roles as molecular chaperones that help prevent apoptosis under various stress conditions, including HS (Sakatani et al., 2012). In agreement with the sequencing analysis, HSP90AA1 showed a strong induction in response to HS, and it had high expression levels in the HS group. In addition, expression of circCSN1S1_2 was significantly lower in HS sows, demonstrating the validity of our post-transcriptional ceRNA regulatory model.

DISCUSSION

In general, HS is caused by a combination of environmental temperature, relative humidity, solar radiation, air movement and precipitation, and the majority of studies on HS in livestock have focused mainly on temperature and relative humidity (Bohmanova et al., 2007). In our experiment, the average temperatures and humidity levels during the HS challenge were $32.7 \pm 0.40^\circ\text{C}$ and $76.1 \pm 0.38\%$, respectively; thus, the lactating sows in our test might be under HS (Bergsma and Hermes, 2012). We observed greater concentrations of LDH and HSP70, and a decrease of COR levels in sows under HS conditions, compared with those in an NS climate; these values are generally considered as indicators of stress in pigs (Yu et al., 2010; Belhadj Slimen et al., 2016). Enhanced levels of serum LDH is a biomarker of liver damage in hyperthermic animals (Ozaki

et al., 1995). Cao et al. (2011) reported that chronic HS induces significant increases LDH levels in rat plasma; this report was similar to what we observed in lactating sows. HSPs are molecular chaperones that differ in regards to their biological functions and molecular weights (Feder and Hofmann, 1999). Among the various HSP classes, HSP70 levels are associated with the acquisition of thermotolerance (Bedulina et al., 2013). In farm animals, HS significantly increases serum HSP70 concentrations in beef cattle (Gaughan et al., 2013), dairy cow (Min et al., 2015), buffalo (Manjari et al., 2015), sheep (Romero et al., 2013), goat (Dangi et al., 2015), and broiler chicken (Gu et al., 2012); these reports are in excellent agreement with the experimental results in our study. In addition, Wang et al. (2015) reported that acute heat exposure significantly elevated levels of COR in rats, and porcine serum COR levels rapidly increased when individuals were subjected to 40°C for 5 hours (Yu et al., 2010). In contrast, summer temperature-induced HS dramatically repressed COR concentrations in the present study. This finding may be due to the different effects between short-term acute HS and chronic HS. Generally, short-term heat exposure increases plasma COR levels, while long-term exposure decreases them (Du Preez, 2000). Christison and Johnson (1972), and Wiersma and Stott (1974) noted a similar trend in dairy cattle exposed to hot summer conditions. HS has been suggested to be responsible for inducing oxidative stress and immune responses in livestock animals during the summer (Das et al., 2016). In the present study, serum SOD and IgG levels were higher in the HS group than in the NS group, suggesting that the antioxidative and immune function of sows increases to adapt to the adverse environment. Recently, elevated concentrations of SOD and IgG were also reported to be sensitive to ambient temperature in broiler chickens (Azad et al., 2010), lactating buffaloes, and cows (Lallawmkimi et al., 2013; Yatoo et al., 2014). PRL is vital for lactogenesis (Akers et al., 1981), and concentrations of plasma PRL decrease in dairy cows during thermal stress (Tao et al., 2011). In agreement with previous studies, our data demonstrated a significant reduction in porcine PRL levels due to elevated ambient temperature.

In our study, no significant effects of HS were observed on the number of live piglets born per litter, nor on litter birth weight; similar findings were reported by Lucy and Safranski (2017), who demonstrated no clear influences of gestational HS on the number of piglets born live per litter. The seasonal influences of our study and that have been reported previously on piglet traits at birth are mainly caused by a delayed response to ambient temperature, i.e. sows were mated and conceived during the cool season and subsequently farrowed in the hot season; it is established that the primary effects of temperature on litter traits in piglets primarily occur during the first 4 weeks of gestation (Tummaruk et al., 2004). The HS sows weaned piglets that were approximately 0.5 kg lighter in our study than the NS sows. This represented an about 8.47% decrease in weaning weight, and is in accordance with the results of Williams et al. (2013). In addition, piglets were more susceptible to heat-induced reductions in piglet weight gain during early lactation, in concordance with a study by Spencer

et al. (2003), who reported a 17% decrease in piglet weaning weight when lactation period lasted 14 days. We observed a downward trend of high temperature on total milk solids, which were reduced by approximately 8.77%, including specific losses in milk fat and lactose content by about 14.69% and 10.45%, respectively. Generally, milk composition varies considerably throughout the seasons, as showed in multiple farm animals included Holstein cows (Shwartz et al., 2009; Bernabucci et al., 2015), dairy goats (Chornobai et al., 1999), and mares (Markiewicz-Kęszycka et al., 2015). In dairy cows, lower milk fat (Bernabucci et al., 2015) and lactose (Shwartz et al., 2009) values are recorded during the summer months, in correspondence with an increase in Temperature Humidity Index. A similar trend of variation in milk composition was also reported for goat milk, and high air temperature in the summer was significantly negatively correlated with goat milk physico-chemical characteristics (Chornobai et al., 1999). In particular, the milk characteristics most highly affected by air temperature were fat and lactose contents, with correlation coefficients of -0.90 and -0.77 , respectively. In contrast, mare milk collected in summer had a significantly higher fat content than in autumn, but the average concentration of lactose was similar for milk collected in summer and in autumn, and showed no specific significant seasonal variations (Markiewicz-Kęszycka et al., 2015). These large discrepancies observed in lactating mares may be due to differences in experimental animals (sows and cows vs. mares) or differences in climate conditions ($32.7 \pm 0.40^\circ\text{C}$ vs. $23.15 \pm 1.61^\circ\text{C}$ in the summer). In agreement with a study comparing lactating sows exposed to high ambient temperature (Renaudeau and Noblet, 2001), our results showed no significant effects of elevated ambient temperature on milk protein, but HS during summer significantly decreased CSN α s1, CSN α s2, and CSN κ concentrations in milk. These results confirmed those obtained by Bernabucci et al. (2015) carried out in dairy cows, in which it was reported that the concentration of CSN α during summer months was 22.6% lower than in the winter, and was 16% lower than in the spring. CSN κ levels were also 9.7% lower during summer than in the winter. Our study agrees with previous studies, and indicates that there is a significant seasonal effect on CSN fractions in domestic livestock milk.

Generally, heat-stressed lactating sows reduce their feed intake, leading to loss of milk production, which can negatively affect piglet growth and development during lactation (Ribeiro et al., 2018). However, Rhoads et al. (2009) and Wheelock et al. (2010) have recently demonstrated that reduced nutrient intake only accounts for about 35%–50% of the HS-induced decrease in milk synthesis. A large portion of the thermal effects on animal lactation may be a consequence of energy intake-independent changes (Wheelock et al., 2010), resulting from genetic regulation of nutrient partitioning during HS (Collier et al., 2008). In the current study, we therefore used RNA-Seq to find the underlying molecular mechanisms of milk synthesis under HS in lactating sows. Sequencing revealed a total of 19,032 unique Ensembl genes in lactating porcine mammary tissues, while genes encoding caseins, whey proteins, and enzymes

involved in lactogenesis pathways showed higher expression than other genes with RPKM values. Similar results were obtained in cows (Wickramasinghe et al., 2012), goats (Shi et al., 2015; Crisà et al., 2016), and humans (Lemay et al., 2013). A total of 16,892 genes were expressed in bovine milk somatic cells during early lactation, as well as 19,094 in peak lactation and 18,070 in late lactation, and *LGB* (β -lactoglobulin), *CSN2* (β -casein), *CSN1S1* (α -S1-casein), *LALBA* (α -lactalbumin), *CSN3* (κ -casein), and *CSN1S2* (casein- α -S2) were identified as having the highest expression in milk, based on RPKM values (Wickramasinghe et al., 2012). Approximately 16,024 ovine NCBI unigenes were found to be expressed in mammary glands (Shi et al., 2015), and *CSN2*, *CSN3*, *CSN1S1*, *CSN1S2*, *LALBA*, and *LGB* were the most abundant in the mammary gland transcriptome (Shi et al., 2015; Crisà et al., 2016). In human mammary cells, Lemay et al. (2013) reported 14,629, 14,529, and 13,745 unique genes expressed in colostrum, transitional, and mature stages of lactation, and β -casein and α -lactalbumin transcripts made up 45% of the total mRNA expression during lactation. Of the top genes identified in our study, *CSN1S2* had the highest expression among the CSN family, followed by *CSN2*, *CSN1S1*, and *CSN3*, which were in discordance with the composition of caseins identified by ELISA analysis. We found that porcine casein- α -S1 constituted up to 51.94% of the caseins in our study. One possibility for this discrepancy was that the abundant caseins are broken into bio-active peptides, and therefore their concentrations are not accurately reflected in the analysis of major milk component proteins. The expression of bio-active peptides formed by cleavage of caseins are higher toward the beginning of lactation (Silva and Malcata, 2005). Another possible explanation is that even though there was high expression of the genes encoding caseins, the protein synthesis may not be efficient in sows that were in negative energy balance, or that were limited in dietary intake of essential amino acids (Wickramasinghe et al., 2012).

In order to further reveal the mechanism of response of lactating sows to HS, we focused on identification of differently expressed genes in response to high ambient temperature. Functional annotation analysis identified that four of these DE genes have principal roles in lactogenesis, including four down-regulated genes (*CSN1S1*, *CSN1S2*, *CSN3*, and *WAP*) in the heat stressed individuals. The *CSN1S1*, *CSN1S2*, *CSN3*, and *WAP* proteins are the main components of lactoprotein that is usually reduced in response to HS in dairy animals (Bernabucci et al., 2015), and the gene expression analysis was in accordance with the results of the ELISA assay.

Recently, a class of non-coding RNAs, called circRNAs, has been identified across the animal kingdoms (Memczak et al., 2013). These circRNAs usually act as ceRNAs to regulate other coding genes by sharing specific miRNA binding sites (Salmena et al., 2011). Multiple types of circRNA-mediated ceRNA interactions have been linked to various physiological or pathological states, including members of the miRNA-2284 family that are sponged by circCSN1S1 to regulate bovine casein translation (Zhang et al., 2015). Therefore, in the

present study we carried out a circRNAome analysis of porcine mammary tissues between NS and HS groups. We identified 50 candidate circRNAs out of 1,728 identified circRNAs that were DE between the NS and HS groups. Based on the ceRNA hypothesis, 42 positively correlated circRNA-mRNA interactions were constructed between the four lactogenic genes and the DE circRNAs using the Pearson algorithm. Of these interaction pairs, analysis by the miRanda application (Enright et al., 2003) revealed four circRNA-mRNA interactions that were predicted to share the same miRNA regulatory elements. In particular, the circCSN1S1_2 binds competitively with miR-204 to increase expression of its hosting gene, *CSN1S1*. A similar ceRNA network was strongly suggested between circFoxo3 and *Foxo3* mRNA in tumor growth and angiogenesis (Yang et al., 2016). Yang et al. reported that circFoxo3 shared identical sequences with the *Foxo3* gene to bind miR-22, miR-136, miR-138, miR-149, miR-433, miR-762, miR-3614-5p, and miR-3622b-5p. These observations indicated that the expression of circRNAs might be related to the expression of their parental genes. Taken together, several circRNA-miRNA-mRNA axes were shown to be likely involved in porcine lactogenesis under HS, and these findings provide novel perspectives on circRNA-associated ceRNA networks for future research in sow lactation.

CONCLUSION

We found that constant elevated ambient temperature and HS has negative consequences on piglet growth and performances due to decreased milk production and characteristics of lactating sows. Thermal stress altered genome-wide profiles of circRNAs dramatically in lactating porcine mammary tissue, and these heat-induced circRNAs might participate in mammapoiesis and lactogenesis by post-transcriptional regulation of ceRNA networks. Our results provide novel rationale to investigate circRNA functions in the lactating sow response to HS, and additional research is necessary to quantify and understand these effects.

REFERENCES

- Akers, M. R., Bauman, D. E., Capuco, A. V., Goodman, G. T., and Tucker, A. H. (1981). Prolactin regulation of milk secretion and biochemical differentiation of mammary epithelial cells in periparturient cows. *Endocrinology* 109 (1), 23–30. doi: 10.1210/endo-109-1-23
- Azad, M. A. K., Kikusato, M., Maekawa, T., Shirakawa, H., and Toyomizu, M. (2010). Metabolic characteristics and oxidative damage to skeletal muscle in broiler chickens exposed to chronic heat stress. *Comp. Biochem. Physiol. Part A: Mol. Integr. Physiol.* 155 (3), 401–406. doi: 10.1016/j.cbpa.2009.12.011
- Bedulina, D. S., Evgen'ev, M. B., Timofeyev, M. A., Protopopova, M. V., Garbuz, D. G., Pavlichenko, V. V., et al. (2013). Expression patterns and organization of the hsp70 genes correlate with thermotolerance in two congener endemic amphipod species (*Eulimnogammarus cyaneus* and *E. verrucosus*) from Lake Baikal. *Mol. Ecol.* 22 (5), 1416–1430. doi: 10.1111/mec.12136
- Belhadj Slimen, I., Najjar, T., Ghram, A., and Abdrrabba, M. (2016). Heat stress effects on livestock: molecular, cellular and metabolic aspects, a review. *J. Anim. Physiol. Anim. Nutr.* 100 (3), 401–412. doi: 10.1111/jpn.12379

DATA AVAILABILITY STATEMENT

All sequencing raw datasets have been deposited into the National Center for Biotechnology Information (NCBI) Sequence Read Archive (SRA) database (<https://www.ncbi.nlm.nih.gov/sra/>) with the BioProject accession number PRJNA578241.

ETHICS STATEMENT

The animal study was reviewed and approved by the Institutional Animal Care and Use Committee of South China Agricultural University, China.

AUTHOR CONTRIBUTIONS

All authors were involved in project conception and design. JS led the lab assays, analyses of data, and writing of the manuscript. JS and YZ contributed reagents, materials, and analysis tools. All authors gave final approval for publication.

FUNDING

This research was financially supported by the National Key Research and Development Program of China (2016YFD0500503), the Natural Science Foundation of China Program (31802032), the major scientific projects in general colleges and Universities of Guangdong Province (2017KTSCX023), and the Natural Science Foundation of Guangdong Province (2018B030311015).

SUPPLEMENTARY MATERIAL

The Supplementary Material for this article can be found online at: <https://www.frontiersin.org/articles/10.3389/fgene.2019.01347/full#supplementary-material>

- Bergsma, R., and Hermes, S. (2012). Exploring breeding opportunities for reduced thermal sensitivity of feed intake in the lactating sow. *J. Anim. Sci.* 90 (1), 85–98. doi: 10.2527/jas.2011-4021
- Bernabucci, U., Basiricò, L., Morera, P., Dipasquale, D., Vitali, A., Cappelli, F. P., et al. (2015). Effect of summer season on milk protein fractions in Holstein cows. *J. Dairy Sci.* 98 (3), 1815–1827. doi: 10.3168/jds.2014-8788
- Betel, D., Koppal, A., Agius, P., Sander, C., and Leslie, C. (2010). Comprehensive modeling of microRNA targets predicts functional non-conserved and non-canonical sites. *Genome Biol.* 11 (8), R90. doi: 10.1186/gb-2010-11-8-r90
- Bohmanova, J., Myszal, I., and Cole, J. B. (2007). Temperature-humidity indices as indicators of milk production losses due to heat stress. *J. Dairy Sci.* 90 (4), 1947–1956. doi: 10.3168/jds.2006-513
- Cao, D., Li, H., Yi, J., Zhang, J., Che, H., Cao, J., et al. (2011). Antioxidant properties of the mung bean flavonoids on alleviating heat stress. *PLoS One* 6 (6), e21071. doi: 10.1371/journal.pone.0021071
- Chornobai, C. A., Damasceno, J. C., Visentainer, J. V., and Matsushita, M. (1999). Physical-chemical composition of in natura goat milk from cross Saanen throughout lactation period. *Archiv. Latinoamericanas Nutricion* 49 (3), 283–286.

- Christison, G. I., and Johnson, H. D. (1972). Cortisol turnover in heat-stressed cows. *J. Anim. Sci.* 35 (5), 1005–1010. doi: 10.2527/jas1972.3551005x
- Collier, R. J., Dahl, G. E., and VanBaale, M. J. (2006). Major advances associated with environmental effects on dairy cattle. *J. Dairy Sci.* 89 (4), 1244–1253. doi: 10.3168/jds.S0022-0302(06)72193-2
- Collier, R. J., Collier, J. L., Rhoads, R. P., and Baumgard, L. H. (2008). Invited review: genes involved in the bovine heat stress response. *J. Dairy Sci.* 91 (2), 445–454. doi: 10.3168/jds.2007-0540
- Crisà, A., Ferrè, F., Chillemi, G., and Moiola, B. (2016). RNA-Sequencing for profiling goat milk transcriptome in colostrum and mature milk. *BMC Veterinary Res.* 12 (1), 264. doi: 10.1186/s12917-016-0881-7
- Dangi, S. S., Gupta, M., Dangi, S. K., Chouhan, V. S., Maurya, V. P., Kumar, P., et al. (2015). Expression of HSPs: an adaptive mechanism during long-term heat stress in goats (*Capra hircus*). *Int. J. Biometeorol.* 59 (8), 1095–1106. doi: 10.1007/s00484-014-0922-5
- Das, R., Sailo, L., Verma, N., Bharti, P., and Saikia, J. (2016). Impact of heat stress on health and performance of dairy animals: a review. *Veterinary World* 9 (3), 260. doi: 10.14202/vetworld.2016.260-268
- Du Preez, J. H. (2000). Parameters for the determination and evaluation of heat stress in dairy cattle in South Africa. *Onderstepoort J. Vet Res.* 67 (4), 263–271.
- Enright, A. J., John, B., Gaul, U., Tuschl, T., Sander, C., and Marks, D. S. (2003). MicroRNA targets in *Drosophila*. *Genome Biol.* 5 (1), R1. doi: 10.1186/gb-2003-5-1-r1
- Feder, M. E., and Hofmann, G. E. (1999). Heat-shock proteins, molecular chaperones, and the stress response: evolutionary and ecological physiology. *Annu. Rev. Physiol.* 61 (1), 243–282. doi: 10.1146/annurev.physiol.61.1.243
- Fu, X., and Liu, R. (2014). “CircRNAFinder: a tool for identifying circular RNAs using RNA-Seq data” in *Proceedings of the 6th International Conference on Bioinformatics and Computational Biology*. (Las Vegas, Nevada, USA: BICOB).
- Gao, Y., Wang, J., and Zhao, F. (2015). CIRI: an efficient and unbiased algorithm for *de novo* circular RNA identification. *Genome Biol.* 16 (1), 4. doi: 10.1186/s13059-014-0571-3
- Gaughan, J. B., Bonner, S. L., Loxton, I., and Mader, T. L. (2013). Effects of chronic heat stress on plasma concentration of secreted heat shock protein 70 in growing feedlot cattle. *J. Anim. Sci.* 91 (1), 120–129. doi: 10.2527/jas.2012-5294
- Gu, X. H., Hao, Y., and Wang, X. L. (2012). Overexpression of heat shock protein 70 and its relationship to intestine under acute heat stress in broilers: 2. Intestinal oxidative stress. *Poultry Sci.* 91 (4), 790–799. doi: 10.3382/ps.2011-01628
- Hanan, M., Soreq, H., and Kadener, S. (2017). CircRNAs in the brain. *RNA Biol.* 14 (8), 1028–1034. doi: 10.1080/15476286.2016.1255398
- Hansen, T. B., Venø, M. T., Damgaard, C. K., and Kjems, J. (2015). Comparison of circular RNA prediction tools. *Nucleic Acids Res.* 44 (6), e58–e58. doi: 10.1093/nar/gkv1458
- Hill, D. L., and Wall, E. (2015). Dairy cattle in a temperate climate: the effects of weather on milk yield and composition depend on management. *Animal* 9 (1), 138–149. doi: 10.1017/S1751731114002456
- Kadzere, C. T., Murphy, M. R., Silanikove, N., and Maltz, E. (2002). Heat stress in lactating dairy cows: a review. *Livestock Prod. Sci.* 77 (1), 59–91. doi: 10.1016/S0301-6226(01)00330-X
- Kensinger, R. S., Collier, R. J., and Bazer, F. W. (1986). Ultrastructural changes in porcine mammary tissue during lactogenesis. *J. Anat.* 145, 49.
- Kim, D., Perte, G., Trapnell, C., Pimentel, H., Kelley, R., and Salzberg, S. L. (2013). TopHat2: accurate alignment of transcriptomes in the presence of insertions, deletions and gene fusions. *Genome Biol.* 14 (4), R36. doi: 10.1186/gb-2013-14-4-r36
- Lai, X., Bazin, J., Webb, S., Crespi, M., Zubieta, C., and Conn, S. J. (2018). “CircRNAs in plants,” in *Circular RNAs* (Singapore: Springer), 329–343.
- Lallawmkimi, M. C., Singh, S. V., Upadhyay, R. C., and De, S. (2013). Impact of vitamin E supplementation on heat shock protein 72 and antioxidant enzymes in different stages of Murrah buffaloes during seasonal stress. *Indian J. Anim. Sci.* 83 (9), 909–915.
- Lemay, D. G., Ballard, O. A., Hughes, M. A., Morrow, A. L., Horseman, N. D., and Nommsen-Rivers, L. A. (2013). RNA sequencing of the human milk fat layer transcriptome reveals distinct gene expression profiles at three stages of lactation. *PLoS One* 8 (7), e67531. doi: 10.1371/journal.pone.0067531
- Lucy, M. C., and Safranski, T. J. (2017). Heat stress in pregnant sows: thermal responses and subsequent performance of sows and their offspring. *Mol. Reprod. Dev.* 84 (9), 946–956. doi: 10.1002/mrd.22844
- Manjari, R., Yadav, M., Ramesh, K., Uniyal, S., Rastogi, S. K., Sejian, V., et al. (2015). HSP70 as a marker of heat and humidity stress in Tarai buffalo. *Trop. Anim. Health Prod.* 47 (1), 111–116. doi: 10.1007/s11250-014-0692-4
- Markiewicz-Kęszycka, M., Czyżak-Runowska, G., Wójtowski, J., Jóźwik, A., Pankiewicz, R., Łęska, B., et al. (2015). Influence of stage of lactation and year season on composition of mares' colostrum and milk and method and time of storage on vitamin C content in mares' milk. *J. Sci. Food Agric.* 95 (11), 2279–2286. doi: 10.1002/jsfa.6947
- Martin, M. (2011). Cutadapt removes adapter sequences from high-throughput sequencing reads. *EMBnet. J.* 17 (1), 10–12. doi: 10.14806/ej.17.1.200
- Memczak, S., Jens, M., Elefsinioti, A., Torti, F., Krueger, J., Rybak, A., et al. (2013). Circular RNAs are a large class of animal RNAs with regulatory potency. *Nature* 495 (7441), 333. doi: 10.1038/nature11928
- Messias de Bragança, M., Mounier, A. M., and Prunier, A. (1998). Does feed restriction mimic the effects of increased ambient temperature in lactating sows. *J. Anim. Sci.* 76 (8), 2017–2024. doi: 10.2527/1998.7682017x
- Min, L., Cheng, J. B., Shi, B. L., Yang, H. J., Zheng, N., and Wang, J. Q. (2015). Effects of heat stress on serum insulin, adipokines, AMP-activated protein kinase, and heat shock signal molecules in dairy cows. *J. Zhejiang University-Sci. B* 16 (6), 541–548. doi: 10.1631/jzus.B1400341
- Ozaki, M., Fuchinoue, S., Teraoka, S., and Ota, K. (1995). The *in vivo* cytoprotection of ascorbic acid against ischemia/reoxygenation injury of rat liver. *Arch. Biochem. Biophys.* 318 (2), 439–445. doi: 10.1006/abbi.1995.1252
- Pan, T., Sun, X., Liu, Y., Li, H., Deng, G., Lin, H., et al. (2018). Heat stress alters genome-wide profiles of circular RNAs in Arabidopsis. *Plant Mol. Biol.* 96 (3), 217–229. doi: 10.1007/s11103-017-0684-7
- Patop, I. L., and Kadener, S. (2018). circRNAs in cancer. *Curr. Opin. In Genet. Dev.* 48, 121–127. doi: 10.1016/j.canlet.2018.03.035
- Quiniou, N., and Noblet, J. (1999). Influence of high ambient temperatures on performance of multiparous lactating sows. *J. Anim. Sci.* 77 (8), 2124–2134. doi: 10.2527/1999.7782124x
- Renaudeau, D., and Noblet, J. (2001). Effects of exposure to high ambient temperature and dietary protein level on sow milk production and performance of piglets. *J. Anim. Sci.* 79 (6), 1540–1548. doi: 10.2527/2001.7961540x
- Renaudeau, D., Quiniou, N., and Noblet, J. (2001). Effects of exposure to high ambient temperature and dietary protein level on performance of multiparous lactating sows. *J. Anim. Sci.* 79 (5), 1240–1249. doi: 10.2527/2001.7951240x
- Renaudeau, D., Collin, A., Yahav, S., De Basilio, V., Gourdi, J. L., and Collier, R. J. (2012). Adaptation to hot climate and strategies to alleviate heat stress in livestock production. *Animal* 6 (5), 707–728. doi: 10.1017/S1751731111002448
- Renaudeau, D. (2005). Effects of short-term exposure to high ambient temperature and relative humidity on thermoregulatory responses of European (Large White) and Caribbean (Creole) restrictively-fed growing pigs. *Anim. Res.* 54 (2), 81–93. doi: 10.1051/animres:2005005
- Rhoads, M. L., Rhoads, R. P., VanBaale, M. J., Collier, R. J., Sanders, S. R., Weber, W. J., et al. (2009). Effects of heat stress and plane of nutrition on lactating Holstein cows: I. Production, metabolism, and aspects of circulating somatotropin. *J. Dairy Sci.* 92 (5), 1986–1997. doi: 10.3168/jds.2008-1641
- Ribeiro, B. P. V. B., Lanferdini, E., Palencia, J. Y. P., Lemes, M. A. G., de Abreu, M. L. T., de Souza Cantarelli, V., et al. (2018). Heat negatively affects lactating swine: a meta-analysis. *J. Thermal Biol.* 74, 325–330. doi: 10.1016/j.jtherbio.2018.04.015
- Robinson, M. D., McCarthy, D. J., and Smyth, G. K. (2010). edgeR: a Bioconductor package for differential expression analysis of digital gene expression data. *Bioinformatics* 26 (1), 139–140. doi: 10.1093/bioinformatics/btp616
- Romero, R. D., Pardo, A. M., Montaldo, H. H., Rodríguez, A. D., and Cerón, J. H. (2013). Differences in body temperature, cell viability, and HSP-70 concentrations between Pelibuey and Suffolk sheep under heat stress. *Trop. Anim. Health Prod.* 45 (8), 1691–1696. doi: 10.1007/s11250-013-0416-1
- Sakatani, M., Alvarez, N. V., Takahashi, M., and Hansen, P. J. (2012). Consequences of physiological heat shock beginning at the zygote stage on embryonic development and expression of stress response genes in cattle. *J. Dairy Sci.* 95 (6), 3080–3091. doi: 10.3168/jds.2011-4986
- Salmena, L., Poliseno, L., Tay, Y., Kats, L., and Pandolfi, P. P. (2011). A ceRNA hypothesis: the Rosetta Stone of a hidden RNA language? *Cell* 146 (3), 353–358. doi: 10.1016/j.cell.2011.07.014
- Shi, H., Zhu, J., Luo, J., Cao, W., Shi, H., Yao, D., et al. (2015). Genes regulating lipid and protein metabolism are highly expressed in mammary gland of lactating dairy goats. *Funct. Integr. Genomics* 15 (3), 309–321. doi: 10.1007/s10142-014-0420-1

- Shwartz, G., Rhoads, M. L., VanBaale, M. J., Rhoads, R. P., and Baumgard, L. H. (2009). Effects of a supplemental yeast culture on heat-stressed lactating Holstein cows. *J. Dairy Sci.* 92 (3), 935–942. doi: 10.3168/jds.2008-1496
- Silva, S. V., and Malcata, F. X. (2005). Caseins as source of bioactive peptides. *Int. Dairy J.* 15 (1), 1–15. doi: 10.1016/j.idairyj.2004.04.009
- Silanikove, N., Shapiro, F., and Shinder, D. (2009). Acute heat stress brings down milk secretion in dairy cows by up-regulating the activity of the milk-borne negative feedback regulatory system. *BMC Physiol.* 9 (1), 13. doi: 10.1186/1472-6793-9-13
- Spencer, J. D., Boyd, R. D., Cabrera, R., and Allee, G. L. (2003). Early weaning to reduce tissue mobilization in lactating sows and milk supplementation to enhance pig weaning weight during extreme heat stress. *J. Anim. Sci.* 81 (8), 2041–2052. doi: 10.2527/2003.8182041x
- Sun, Y., Yang, Z., Zheng, B., Zhang, X. H., Zhang, M. L., Zhao, X. S., et al. (2017). A novel regulatory mechanism of smooth muscle α -actin expression by NRG-1/circACTA2/miR-548f-5p axis. *Circ. Res.* 121 (6), 628–635. doi: 10.1161/CIRCRESAHA.117.311441
- Tao, S., Bubolz, J. W., Do Amaral, B. C., Thompson, I. M., Hayen, M. J., Johnson, S. E., et al. (2011). Effect of heat stress during the dry period on mammary gland development. *J. Dairy Sci.* 94 (12), 5976–5986. doi: 10.3168/jds.2011-4329
- Tay, Y., Rinn, J., and Pandolfi, P. P. (2014). The multilayered complexity of ceRNA crosstalk and competition. *Nature* 505 (7483), 344. doi: 10.1038/nature12986
- Trapnell, C., Roberts, A., Goff, L., Pertea, G., Kim, D., Kelley, D. R., et al. (2012). Differential gene and transcript expression analysis of RNA-seq experiments with TopHat and Cufflinks. *Nat. Protoc.* 7 (3), 562. doi: 10.1038/nprot.2012.016
- Tummaruk, P., Tantasuparuk, W., Techakumphu, M., and Kunavongkrit, A. (2004). Effect of season and outdoor climate on litter size at birth in purebred Landrace and Yorkshire sows in Thailand. *J. Veterinary Med. Sci.* 66 (5), 477–482. doi: 10.1292/jvms.66.477
- Wang, K., Singh, D., Zeng, Z., Coleman, S. J., Huang, Y., Savich, G. L., et al. (2010). MapSplice: accurate mapping of RNA-seq reads for splice junction discovery. *Nucleic Acids Res.* 38 (18), e178–e178. doi: 10.1093/nar/gkq622
- Wang, L. I., Liu, F., Luo, Y., Zhu, L., and Li, G. (2015). Effect of acute heat stress on adrenocorticotrophic hormone, cortisol, interleukin-2, interleukin-12 and apoptosis gene expression in rats. *Biomed. Rep.* 3 (3), 425–429. doi: 10.3892/br.2015.445
- Wang, Y., Li, D., Wang, Y., Li, M., Fang, X., Chen, H., et al. (2019). The landscape of circular RNAs and mRNAs in bovine milk exosomes. *J. Food Composition Anal.* 76, 33–38. doi: 10.1016/j.jfca.2018.12.004
- Wheelock, J. B., Rhoads, R. P., VanBaale, M. J., Sanders, S. R., and Baumgard, L. H. (2010). Effects of heat stress on energetic metabolism in lactating Holstein cows. *J. Dairy Sci.* 93 (2), 644–655. doi: 10.3168/jds.2009-2295
- Wickramasinghe, S., Rincon, G., Islas-Trejo, A., and Medrano, J. F. (2012). Transcriptional profiling of bovine milk using RNA sequencing. *BMC Genomics* 13 (1), 45. doi: 10.1186/1471-2164-13-45
- Wiersma, F., and Stott, F. M. (1974). “Response of dairy cattle to an evaporative cooled environment”, in *Proceedings of the livestock environment*. (St. Joseph: American Society of Agricultural Engineers), 88–95.
- Williams, A. M., Safranski, T. J., Spiers, D. E., Eichen, P. A., Coate, E. A., and Lucy, M. C. (2013). Effects of a controlled heat stress during late gestation, lactation, and after weaning on thermoregulation, metabolism, and reproduction of primiparous sows. *J. Anim. Sci.* 91 (6), 2700–2714. doi: 10.2527/jas.2012-6055
- Yang, W., Du, W. W., Li, X., Yee, A. J., and Yang, B. B. (2016). Foxo3 activity promoted by non-coding effects of circular RNA and Foxo3 pseudogene in the inhibition of tumor growth and angiogenesis. *Oncogene* 35 (30), 3919. doi: 10.1038/onc.2015.460
- Yatoo, M. I., Dimri, M., and Sharma, M. C. (2014). Seasonal changes in certain blood antioxidants in cattle and buffaloes. *Indian J. Anim. Sci.* 84 (2), 173–176.
- Yu, J., Yin, P., Liu, F., Cheng, G., Guo, K., Lu, A., et al. (2010). Effect of heat stress on the porcine small intestine: a morphological and gene expression study. *Comp. Biochem. Physiol. Part A: Mol. Integr. Physiol.* 156 (1), 119–128. doi: 10.1016/j.cbpa.2010.01.008
- Zhang, X. O., Wang, H. B., Zhang, Y., Lu, X., Chen, L. L., and Yang, L. (2014). Complementary sequence-mediated exon circularization. *Cell* 159 (1), 134–147. doi: 10.1016/j.cell.2014.09.001
- Zhang, C., Wu, H., Wang, Y., Zhao, Y., Fang, X., Chen, C., et al. (2015). Expression patterns of circular RNAs from primary kinase transcripts in the mammary glands of lactating rats. *J. Breast Cancer* 18 (3), 235–241. doi: 10.4048/jbc.2015.18.3.235
- Zhang, C., Wu, H., Wang, Y., Zhu, S., Liu, J., Fang, X., et al. (2016). Circular RNA of cattle casein genes are highly expressed in bovine mammary gland. *J. Dairy Sci.* 99 (6), 4750–4760. doi: 10.3168/jds.2015-10381
- Zhang, X. O., Dong, R., Zhang, Y., Zhang, J. L., Luo, Z., Zhang, J., et al. (2016). Diverse alternative back-splicing and alternative splicing landscape of circular RNAs. *Genome Res.* 26, 1277–1287. doi: 10.1101/gr.202895.115
- Zhu, S. Q., Wang, Y., Zhao, Y. L., Chen, J., Chen, C., Jiang, Y. M., et al. (2016). Identification and partial characterization of a novel circular transcript of the Tc2n gene from rat mammary gland. *Arch. Biol. Sci.* 68 (2), 257–262. doi: 10.2298/ABS151015013Z

Conflict of Interest: The authors declare that the research was conducted in the absence of any commercial or financial relationships that could be construed as a potential conflict of interest.

Copyright © 2020 Sun, Zhang, Hu, Xie, Wang, Zhang, Chen, Luo, Wang, Jiang, Xi, Chen and Zhang. This is an open-access article distributed under the terms of the Creative Commons Attribution License (CC BY). The use, distribution or reproduction in other forums is permitted, provided the original author(s) and the copyright owner(s) are credited and that the original publication in this journal is cited, in accordance with accepted academic practice. No use, distribution or reproduction is permitted which does not comply with these terms.



A novel protein encoded by circKANSL1L regulates skeletal myogenesis via the Akt-FoxO3 signaling axis

Zekun Lin^{a,1}, Fang Xie^{a,1}, Xiao He^a, Jing Wang^b, Junyi Luo^a, Ting Chen^a, Qingyan Jiang^a, Qianyun Xi^a, Yongliang Zhang^a, Jiajie Sun^{a,*}

^a Guangdong Provincial Key Laboratory of Animal Nutrition Control, National Engineering Research Center for Breeding Swine Industry, State Key Laboratory of Swine and Poultry Breeding Industry, College of Animal Science, South China Agricultural University, Guangzhou, Guangdong 510642, China

^b Institute of Animal Husbandry and Veterinary Medicine, Henan Academy of Agricultural Sciences, Zhengzhou 450002, China

ARTICLE INFO

Keywords:

Meat quality
Myofiber types
Single-cell sequencing
Metabolome
Ribosome profiling

ABSTRACT

Skeletal muscle is one the largest organs of the body and is involved in animal production and human health. Circular RNAs (circRNAs) have been implicated in skeletal myogenesis through largely unknown mechanisms. Herein, we report the phenotypic and metabolomic analysis of porcine longissimus dorsi muscles in Lantang and Landrace piglets, revealing a high-content of slow-oxidative fibers responsible for high-quality meat product in Lantang piglets. Using single-cell transcriptomics, we identified four myogenesis-related cell types, and the Akt-FoxO3 signaling axis was the most significantly enriched pathway in each subpopulation in the different pig breeds, as well as in fast-twitch glycolytic fibers. Using the multi-dimensional bioinformatic tools of circRNAome-seq and Ribo-seq, we identified a novel circRNA, circKANSL1L, with a protein-coding ability in porcine muscles, whose expression level correlated with myoblast proliferation and differentiation *in vitro*, as well as the transformation between distinct mature myofibers *in vivo*. The protein product of circKANSL1L could interact with Akt to decrease the phosphorylation level of FoxO3, which subsequently promoted FoxO3 transcriptional activity to regulate skeletal myogenesis. Our results established the existence of a protein encoded by circKANSL1L and demonstrated its potential functions in myogenesis.

1. Introduction

Skeletal muscle is an important tissue in humans and farm animals, accounting for about 40 % of the body weight and 50–75 % of all body proteins [1]. It plays a vital role in multiple physiological and pathological functions, such as mechanical exercise [2], basal energy metabolism [3], and meat quality of livestock [4]. In general, prenatal muscle growth is determined by the proliferation of myogenic cells, whereas postnatal muscle growth is primarily derived from an increase in myofiber size and regeneration with muscle satellite stem cells (MuSCs) [5]. Recently, non-coding RNAs (ncRNAs), such as microRNAs (miRNAs), long non-coding RNAs (lncRNAs) and circular RNAs (circRNAs), have been proven to be widely involved in the regulation of skeletal muscle proliferation and differentiation, as well as a series of subsequent myogenesis processes [6].

In general, circRNAs are generated by back-splicing of pre-mRNA, forming a covalently closed circular structure without a 5' end cap and

3' poly(A) tail [7]. Most circRNAs are expressed from protein coding genes and consist of multiple exons [8]. In addition, circRNAs are considered to have low abundance and occur *via* splicing errors, and exhibit cell and tissue specific patterns in eukaryotes [9]. The functions of most circRNAs remain largely unexplored; however, their known functions include sequestration of miRNAs [10] and proteins [11], modulation of transcription and interference with splicing [12], and even translation to produce proteins or functional polypeptides [13], adding yet a dimension to circRNA function. In detail, translated circRNAs tend to share a start codon with the host gene and contain an open reading frame (ORF), internal ribosome entry site (IRES) or N6-methyladenosine (m⁶A) for the cap-independent translation initiation mechanism [14].

Domestic pigs are genetically, anatomically, and physiologically close to humans [15], and are an excellent model for various human biological processes, such as skeletal myogenesis and muscle diseases [16]. Lantang (LT), a Chinese indigenous lard type breed, and Landrace

* Corresponding author.

E-mail address: jiajiesun@scau.edu.cn (J. Sun).

¹ Zekun Lin and Fang Xie contributed equally to this article.

(LW), a typical lean breed, show obvious differences in muscle fiber characteristics particularly in terms of meat quality [17]. In this study, we profiled the porcine circRNAome landscape of the longissimus dorsi muscle between LT and LW piglets and revealed the translational functions of circRNA candidates involved in the emergence and progression of myogenesis, as well as the functional mechanism of proteins and peptides encoded by circRNA candidates. The discovery of these circRNAs and their encoded products could help us to determine the causes of muscle growth and development, and promote the development of muscle biology.

2. Results

2.1. Myofiber type distribution between pig breeds and muscle metabolome

We performed hematoxylin and eosin (H&E) staining to compare the myofiber characteristics between LT and LW piglets, and obvious differences in myofiber phenotype were observed (Fig. 1A). The cross-sectional areas (CSAs) of single muscle fibers in LT ($99.23 \pm 3.24 \mu\text{m}^2$) were significantly smaller than those of LW ($132.69 \pm 6.34 \mu\text{m}^2$) (Fig. 1B). By detecting the mRNA expression levels of different isoforms of the myosin heavy chain (MyHC) (Fig. 1C), the expression level of *MYH1* (encoding oxidative muscle fiber MyHC type I (MyHC I)) in LT was observed to be significantly higher than that in LW, while a higher amount of *MYH4* (encoding glycolytic muscle fiber MyHC IIb) was observed in LW. In addition, western blotting was performed to assess the relative levels of muscle-specific proteins MYOD, MYOG, MyHC, MyHC I and MyHC IIb (Fig. 1D and E). The results showed that the levels of MYOD and MyHC I were markedly increased in LT compared with that in LW, while the levels of MYOG, MyHC, and MyHC IIb were significantly decreased in LT compared with those in LW.

To explore global metabolic variations, an untargeted metabolomic approach was performed, which identified 19,386 annotated metabolites from 36,048 ion features within LT and LW muscle tissues. In detail, 16,951 and 19,097 compounds were identified in the positive and negative ion modes, respectively, of which 10,000 positive and 9386 negative metabolites were annotated and categorized from different databases (Table S1A). According to their annotations, a number of metabolites were assigned to at least one primary or secondary metabolic category. In total, 6901 positive and 6375 negative metabolites were associated with Kyoto Encyclopedia of Genes and Genomes (KEGG) identifiers (Table S1B); 8689 positive and 7718 negative metabolites were associated with Human Metabolome Database (HMDB) identifiers (Table S1C); and 939 positive and 734 negative metabolites were associated with an in-house fragment spectrum library (Table S1D). To examine the quality of the acquired mass spectrogram (MS) datasets, total ion chromatograms (TICs) were generated with the overall MS signal intensity, which revealed a high degree of overlap between different samples (Fig. S1A), while the *m/z* and retention-time width analyses suggested that individual *m/z* peaks tended to cluster together rather than retention-time values (Fig. 2A). These metabolites belonged to 52 different KEGG-based metabolic pathways, with the top pathways being amino acid metabolism, lipid metabolism, carbohydrate metabolism, and metabolism of cofactors and vitamins (Fig. S1B). The metabolites were further assigned to the HMDB dataset, of which >67.65 % and 61.08% were matched and classified into lipids and lipid-like molecules in positive and negative models (Fig. 2B). A total of 1673 metabolites annotated from in-house fragment spectrum library were classified into 6 main categories and 66 second-grade terms; the top priority was metabolic pathways, followed by ABC transporters, central carbon metabolism in cancer, biosynthesis of amino acids, and protein digestion and absorption (Fig. S1C). To ensure reliability, a principal component analysis (PCA) score plot was generated (Fig. 2C), and the quality control (QC) samples (blue) clustered together tightly, reflecting the stability of the instrument and showing that the quality of all the MS

data for this study were satisfactory [18]. Using partial least squares-discriminant analysis (PLS-DA) analysis, the R² and Q² points were lower on the left than on the right, and the regression line of the Q² point and the vertical axis intersected below the origin (Fig. S1D), this implied that the model was not over-fitted and was reliable [19]. Besides, the PCA and PLS-DA score plots showed that the samples in the LT group were distinctly separated from those of the LW group (Fig. 2C; Fig. S1E), indicating that the breed of piglets altered the muscle metabolome significantly. In addition to our assessment of the qualitative differences between groups, we evaluated the metabolite abundance data for their quantitative variations. To this end, we evaluated the coefficient of variation (CV), a measure of variance of quantified metabolites [20], and a total of 32,492 high-quality metabolites with CV values ≤ 30 % were used to screen the differentially accumulated metabolites (DAMs) (Table S1E). The statistical analysis identified 1588 significant DAMs (Fig. 2D), including 774 predominantly accumulated metabolites in LT piglets and 814 predominantly accumulated metabolites in LW piglets (Table S1F). All of the DAMs were then assigned to various major metabolic categories, while 111 putative metabolites matching with the in-house fragment spectrum library were confirmed and summarized (Fig. S1F). Among them, a number of metabolites were predominantly enriched in biosynthesis of amino acids, glycerophospholipid metabolism, purine metabolism, and the citrate cycle (TCA cycle) (Fig. 2E). More interestingly, citric acid was highly accumulated in LT piglets, while D-Fructose 1,6-bisphosphate was significantly accumulated in LW piglets; these two compounds were significantly associated with oxidative and glycolytic metabolism, respectively.

2.2. Discovery of putative circRNA candidates

We performed deep RNA sequencing (RNA-seq) of rRNA-deleted libraries and RNase R-digested libraries to characterize the circRNA landscape and expression in porcine longissimus dorsi tissues between the LT and LW piglets. For the rRNA-depletion, we identified 35,893 unique circRNAs across six libraries using five distinct prediction algorithms, as showed in Fig. 3A, highlighting the sensitivity of different algorithms in circRNA detection. In detail, a total of 17,994, 20,606, 7773, 25,274, and 3445 circRNA candidates were detected using CIR-Cexplorer2, circRNA_Finder, CIRI, find_circ, and MapSplice, respectively (Table S2A-E); however, only 1123 circRNAs were commonly found by all algorithms for further analyses (Table S2F). For RNase R-digestion, Illumina sequencing provided 6.06 ± 0.89 and 8.14 ± 0.86 million reads from the LT and LW libraries, respectively, and approximately 5.63 ± 0.88 and 7.57 ± 0.79 million valid reads, respectively, were obtained after removing low-quality sequences, sequencing adapters, and primers, accounting for 92.52 ± 0.94 % and 92.95 ± 0.31 % of the raw reads in the LT and LW libraries (Table S3A). We then aligned all valid reads against the porcine reference genome, and identified over 43.21 ± 4.21 % and 44.33 ± 2.59 % of the unmapped reads in the LT and LW piglets, respectively. Among them, over 3.26 ± 0.19 % back-spliced junction reads in the LT libraries were obtained for circRNA prediction, as well as 3.28 ± 0.25 % in the LW libraries (Table S3B). In addition, find_circ predicted the most circRNA types ($n = 34,425$), and MapSplice predicted the fewest candidates ($n = 6887$); CIR-Cexplorer2, circRNA_finder, and CIRI identified 31,817, 34,309, and 14,853 circRNAs, respectively (Table S3C-G). In total, 59,626 unique circRNA candidates were found across six libraries, and only 4453 candidates were detected by all five algorithms (Fig. 3B; Table S3H). For a single sample, an average of 654.67 ± 98.86 and 2914.67 ± 203.73 circRNAs, respectively, were found in each rRNA-deleted or RNase R-digested library (Fig. 3C), indicating that rRNA-depletion and RNase R-digestion exhibited obvious difference in sensitivity for circRNA detection. With the normalized back-splice junction reads, we performed PCA of globally expressed circRNAs (Fig. S2A), and the results showed that the differences between groups caused by breed were much greater than those between tested individuals. Of the 1123 identified circRNAs in

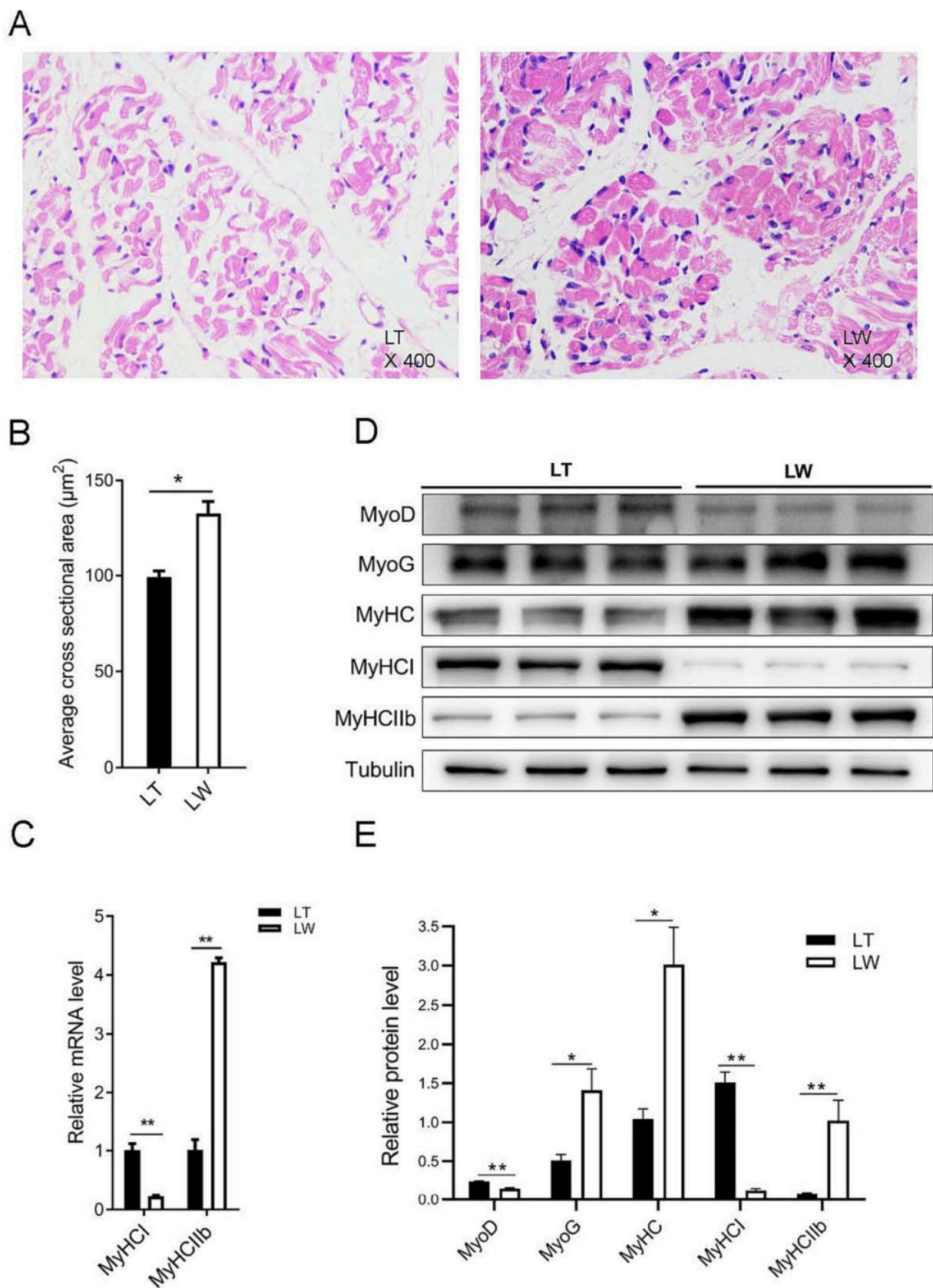


Fig. 1. Comparison of porcine myofiber features between the LT and LW piglets. (A) The structural traits of the longissimus thoracis muscle analyzed by H&E staining and scanned at 400 \times magnification. (B) Average cross-sectional areas of myofibers in LT and LW. (C) Relative RNA expression level of *MTH1* and *MYH4* in LT and LW by qRT-PCR analysis. (D-E) Protein levels of MYOD1, MYOG, MyHC, MyHC I, and MyHC IIb in LT and LW (D), and the band intensities quantified by Image J and normalized against internal reference Tubulin (E). Student's *t*-test was used to compare expression levels or values between different groups, and * and ** indicate significant differences at $P < 0.05$ and $P < 0.01$, respectively.

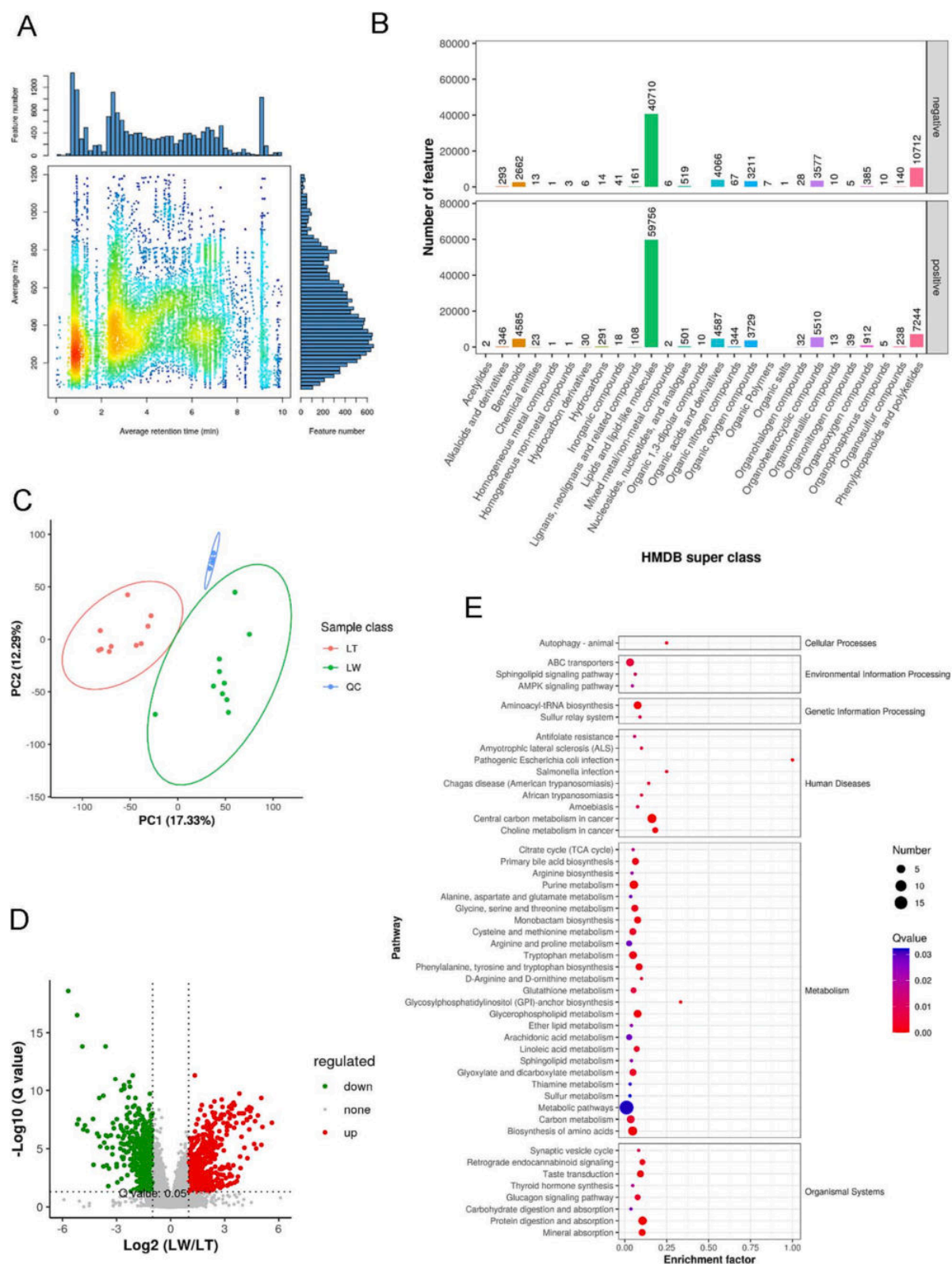


Fig. 2. Analysis of porcine muscle metabolome between the LT and LW breeds.

(A) The m/z and retention-time distribution of the identified metabolites. The X-axis and Y-axis represent the retention time and m/z values, respectively; each point represents a metabolite, and the colour represents the density of the metabolites in that area. (B) The metabolite annotation statistics in the HMDB database in the positive ion mode (lower panel) and the negative ion mode (upper panel). The X-axis represents the KEGG term, and the Y-axis represented the number of metabolites. (C) PCA scatter plot of each tested sample in porcine muscles. Each point represents a sample, and the differences between all samples are reflected in the separation and aggregation trends in the graph. (D) Volcano map of differentially accumulated metabolites in porcine muscles. Each point in the volcano map represents a metabolite; the significantly upregulated metabolites are represented by red dots, whereas the significantly downregulated metabolites are represented by green dots. (E) The differentially accumulated metabolite annotation statistics in the HMDB database. (For interpretation of the references to colour in this figure legend, the reader is referred to the web version of this article.)

rRNA-deleted libraries, only 5 candidates were differentially expressed between LT and LW (Fig. 3D); circARHGAP10 was upregulated, while circAGL, circLIFR, circSLC25A3, and circSTXBP3 were downregulated in the LT samples compared with those in the LW samples (Fig. 3E). In the RNase R-digested libraries, a total of 30 differentially expressed circRNAs were identified, among which 15 were upregulated and 15 were downregulated in the LT libraries (Fig. 3F). Between the rRNA-deleted and RNase R-digested libraries, the differentially expressed circAGL and circSLC25A3 were shared; therefore, 33 unique candidates were significantly regulated between LT and LW. We verified the junction sites of these differentially expressed circRNAs using PCR amplification and Sanger sequencing, and 16 differentially expressed candidates were confirmed to have head-to-tail splicing (Fig. S2B).

2.3. Identification of coding circRNA candidates

A total of 4759 porcine circRNA candidates were detected in our rRNA-deleted and RNase R-digested datasets (Fig. 4A), and we identified those with Open reading frames (ORFs) across the backspliced junction using the ORF_finder pipeline. The ORF length was set to ≥ 300 bp, and the longest ORF was selected when multiple ORFs overlapped in the same circRNA. We obtained a group of 3864 candidates with high-confidence circRNA ORFs (cORFs) (Table S4A). Among them, 3800 cORFs spanned the head-to-tail junction sites of the identified circRNAs, termed as HEAD-TO-TAIL cORFs; 453 cORFs contained start codon coincident with that of the host gene, named as KNOWN_START cORF; and 1581 cORFs had no stop codon and thus theoretically never terminated, abbreviated as MOEBIUS_ORF cORF (Fig. 4A). We then searched for evidence of their translation using four different algorithms, including CPC2 (Table S4B), CPAT (Table S4C), CNCI (Table S4D), and Pfam (Table S4E), and 2050 unique cORFs were detected in common (Fig. 4C). In addition, we utilized ribosome footprinting (RFP) data and searched for sequencing reads across the circRNA-specific junction sites, and found only nine circRNA events with at least one specific RFP read (Fig. 4D), referred hereafter as ribo-circRNAs. Among them, only circKANSL1L was supported with multiple translating features and was significantly differently expressed between the LT and LW piglets. In detail, circKANSL1L originated from the circularization of the exons 2–5 of its hosting gene (*KANSL1L*, encoding KAT8 regulatory NSL complex subunit 1 like), and a 1653-nt open reading frame was present and matched with human has_circ_26165 from the circRNADb database (<http://reprod.njmu.edu.cn/cgi-bin/circrnadb/circRNADb.php>), spanning from the putative ATG of the host gene to a STOP codon created 103-nt after the splice junction site. The head-to-tail splicing of circKANSL1L in mouse was successfully confirmed based on reverse transcription PCR (RT-PCR) and Sanger sequencing (Fig. 5A). We used cDNA and genomic DNA (gDNA) isolated from porcine muscle tissues as PCR templates, and divergent primers produced amplicons only from cDNA samples and not from the gDNA (Fig. 5B). In general, linear RNA molecules are susceptible to exonuclease R digestion, while circRNA candidates are resistant. In our study, circKANSL1L was resistant to RNase R digestion compared with its linear parental gene based on quantitative real-time reverse transcription PCR (qRT-PCR) analysis, as well as the *GAPDH* (encoding glyceraldehyde-3-phosphate dehydrogenase) expression pattern detected using agarose gel electrophoresis (Fig. 5C). In addition, circKANSL1L was successfully reversed transcribed using the random primer but was resistant to amplification using the oligo Dt primer (Fig. 5D). The above findings indicated the circular structure of circKANSL1L. Further nuclear and cytoplasmic fractionation (Fig. 5E) and fluorescence *in situ* hybridization (FISH) (Fig. 5F) examinations further revealed that circKANSL1L was mainly localized in the cytoplasm but was also presented in the nucleus.

2.4. Single-cell atlas of porcine longissimus dorsi tissues

To characterize the cellular diversity of porcine muscle tissues, we performed single-cell RNA-seq on muscular cell suspensions obtained from LT and LW piglets after birth. A total of 11,908 cells in LT and 12,646 cells in LW were obtained. In the LT piglets, 17,718 genes were detected, with a median of 4194 unique molecular identifiers (UMIs) and 1628 genes per cell; in the LW piglets, 17,967 genes were identified, with a median of 5636 UMIs and 1896 genes per cell (Table S5A). We retained 9936 cells in the LT group and 9370 cells in the LW group after QC, and the two samples were tested for similarity and therefore merged for downstream analysis (Fig. S3A). In a global view, the porcine longissimus dorsi tissues were grouped into 21 major clusters, termed C0 to C20 (Fig. S3B). In C5, C14, C15, C16, C17, and C19, over 80 % of all single cells belonged to LT, while >80 % in C3 and C4 belonged to LW (Table S5B; Fig. S3C), revealing a huge difference in muscle-resident cell types between the LT and LW piglets. We assigned cell identities based on the expression of previously established markers [21–23] and visualized the data using t-distributed stochastic neighborhood embedding (t-SNE) (Fig. 6A; Table S5C). From this analysis, we identified 12 major subpopulations composed of 11 known muscle-resident cell types, including fibroadipogenic precursors (FAPs), tenocyte-like cells, endothelial cells, B cells, T cells, smooth muscle cells (SMCs), muscle stem cells (MuSCs), myoblasts, myocytes, myofibers, and intermuscular fat (IMF), and one previously understudied population. We used differential gene expression analysis to determine cell type-specific marker genes between clusters (Table S5D), and the results showed that the unknown population significantly expressed *ACTA1*, *MYLPF*, and *MYL1*, which are generally presented in mature skeletal muscle [24], but not *MYH7* and *CKM*, thus distinguishing the cells from myofibers (Table S5D). We further visualized the top five most variably expressed markers between cell types, and the results documented distinct transcriptional programs of the 11 subpopulations (Fig. 6B). In detail, we compared our identified markers for each cell type with previously published marker genes for known cell types. We found 8416 cells (43.59 %) that were FAPs (*PDGFRA*), 229 (1.19 %) tenocyte-like cells (*TNMD*), 277 (1.44 %) endothelial cells (*PECAM1*), 186 (0.96 %) B cells (*FOLR1*), 132 (0.68 %) T cells (*CD3E*), 797 (4.13 %) SMCs (*FHL5*), 5903 (30.58 %) MuSCs (*PAX7*), 1013 (5.25 %) myoblasts (*PCLAF*), 750 (3.89 %) myocytes (*MYOG*), 1098 (5.69 %) myofibers (*CKM*), and 354 (1.83 %) IMFs (*SNCA*) (Fig. 6C and D). Within these cells, we compared the cluster identities of our dataset with the recently published muscle-resident atlas, and found a few differences in cluster identities and annotation (Fig. S3D). To explain, B cells were observed to express variable levels of *FOLR1*, which was more advantageous than *CD22* and *PTPRC* derived from a previous report [22]. In addition to being positive for myosin (*MYL9*, *MYL6*) [25], the clusters corresponding to SMCs specifically expressed *FHL5* in our datasets. A cluster of myoblasts was characterized by *PCLAF* expression and were negative for *MYF5* in our study, which disagreed with a previous report in mouse in which they were labeled by the *Myod1* gene [21]. The *CKM* gene was preferentially detected in the clusters corresponding to myofibers, with higher expression than *MYH* genes [26]. In addition to the *APOA1* and *COL1A1* genes identified in chicken intramuscular fat, the subpopulation of the IMF cluster was also enriched with *SNCA* expression in our data [27].

To explore the process of myogenesis, we firstly performed pseudo-time trajectory analysis of MuSCs (cluster 0, 3, and 20), myoblasts (cluster 9 and 12), and myocytes (cluster 6) (Fig. 6E; Fig. S3E). The results showed that cluster 0, 3 and 20 were located in the early stage of the development trajectory and were MuSCs, while cluster 9 branched off in two distinct trajectories. In detail, one trajectory progressed through a branch point to cluster 6 and identified cells progressing towards differentiation, as indicated by activation of *MYOG* and myoblast fusion factor *MYMK* in cluster 6. In addition, the gene encoding *CCND1* was downregulated and cell cycle inhibitor *CDKN1C* was upregulated significantly in cells located within cluster 6. Another trajectory

stemming out of the differentiation process identified cells that retained *PCNA* and *CCND2* expression with a low level of *MYOG* expression in cluster 12 (Table S5E and S5F). This branch corresponded to proliferating myoblasts that had not entered the differentiation program and might contain a self-renewal subpopulation, termed as 'reserve cells' [28]. The genes associated with Myosin formation, such as *MYH3*, *MYH4*, *MYH7*, *MYH8*, and *MYL1*, were enriched in the myofiber population (cluster 7 and 10) (Fig. S3F). The distribution of myofiber cells simulated the development process from cluster 10 to cluster 7 (Fig. S3G), while homeostatic cluster 10 was located at one end along a linear trajectory and cluster 7 branched off in two distinct trajectories (Fig. S3H). To automatically annotate the myofiber subpopulations, we next applied high-resolution to classification to divide cluster 7 into three specific subtypes including $CKM^+/MYH4^-/MYH7^-$, $CKM^+/MYH4^+/MYH7^-$, and $CKM^+/MYH4^-/MYH7^+$ cells (Fig. S3I), revealing a high degree of heterogeneity within the myofiber compartments. The identities of cell candidates supported by high expression of *MYH4*, encoding MyHC IIb, were related to glycolytic fibers; whereas, the subtype with unique expression of *MYH7*, encoding MyHC I, contributed to oxidative fibers (Fig. S3J). We found a total of 881 and 141 significantly upregulated genes (marker genes) in glycolytic and oxidative fibers, respectively (Table S5G and S5H). These marker genes were strongly enriched in several biological processes associated with myogenesis (Table S5I and S5J), such as the PI3K-Akt and FoxO signaling pathways in glycolytic fibers, and Apelin and mTOR signaling pathways in oxidative fibers (Fig. S3K).

Next, we analyzed the transcriptomic atlas to assess how these populations with gene expression were dynamically altered between the LT and LW piglets in myogenesis. In MuSCs, we discerned 253 significantly regulated genes, including 141 downregulated and 92 upregulated candidates in the LT samples (Table S6A). A total of 194 genes were significantly expressed in the myoblast subpopulation; 117 candidates were significantly upregulated and 77 were downregulated in the LT libraries (Table S6B). In the myocyte subtypes, we detected 206 differentially expressed genes; 140 candidates were significantly increased in LT piglets, while 96 were markedly decreased (Table S6C). There were 362 differentially expressed genes in the myofiber subgroup, including 176 upregulated and 186 downregulated genes identified in the LT breed (Table S6D). In addition, we used lists of differentially expressed genes for KEGG analysis, and the obtained terms were significantly enriched in several biological processes that are significantly associated with myogenesis, including the PI3K-Akt signaling pathway and the FoxO signaling pathway identified in each subpopulation (Fig. S3L). In four myocyte types, we observed a strong increase in *FoxO3*, the core gene of FoxO signaling pathway, in LW piglets, which is an important transcription factor involved in muscle biology [29].

2.5. *circKANS1L* inhibits C2C12 cell proliferation

We constructed an overexpression vector for the full-length fragment of *circKANS1L* (pCD2.1-ciR-*circKANS1L*) and synthesized two small interfering RNA (siRNA) fragments targeting the splice junction (*circKANS1L*-si-1 and *circKANS1L*-si-2). qRT-PCR showed that transfection of pCD2.1-ciR-*circKANS1L* and *circKANS1L*-si-1 significantly increased and decreased the expression levels of *circKANS1L* in C2C12 cells, respectively, with no significant effects on the host gene (Fig. S4A and S4B). Western blotting was performed to detect the proliferation-related proteins PCNA, Cyclin D, and Cyclin E, as well as the core proteins in the Akt-FoxO3 signaling axis, such as FoxO3, phosphorylated (p)-FoxO3, Akt and AMPK. Overexpression of *circKANS1L* significantly decreased the levels of PCNA and Cyclin E, and that of Cyclin D showed the same trend but not significantly (Fig. 7A and B). The FoxO3 level was significantly increased, while p-FoxO3 (S253) and Akt levels were significantly decreased (Fig. 7C and D). According to the 5-ethynyl-2'-deoxyuridine (EdU) assay results, overexpression of *circKANS1L* significantly reduced the number of EdU positive cells

(Fig. 7E). After *circKANS1L* overexpression, flow cytometry showed that the cells were arrested in the G0/G1 phase, and the number of cells entering the S phase was significantly reduced compared with those in the control groups (Fig. 7F). In contrast, knockdown of *circKANS1L* significantly increased the protein levels of PCNA, Cyclin D, and Cyclin E compared with those in the control group (Fig. 8A and B). The levels of FoxO3 were significantly decreased, while the levels of p-FoxO3 and Akt were significantly increased (Fig. 8C and D). The EdU results showed that knockdown *circKANS1L* significantly increased the number of EdU positive cells (Fig. 8E), and cell cycle analysis showed that knockdown of *circKANS1L* promoted the progression of cells from G0/G1 phase to S phase (Fig. 8F).

2.6. *circKANS1L* promotes C2C12 cell differentiation

We transfected pCD2.1-ciR-*circKANS1L* and *circKANS1L*-si-1 into C2C12 cells and induced differentiation with 2 % horse serum for 48 h and 96 h. In the 48 h differentiation group, overexpression of *circKANS1L* significantly increased the protein levels of MYOD, MYOG, MYH6, and MyHC (Fig. 9A and B), as well as the levels of FoxO3, and significantly decreased the levels of p-FoxO3 and Akt (Fig. 9C and D). Similar results were observed in the 96-h differentiation group (Fig. 9E-H). In addition, a cell immunofluorescence assay was performed at 96 h after transfection, which showed that overexpression of *circKANS1L* significantly promoted the expression level of MyHC and formation of myotubes (Fig. 9I). In comparison with the control group, knockdown of *circKANS1L* significantly reduced the protein levels of MYOD, MYOG, MYH6, and MyHC in the 48 h differentiation group (Fig. 10A and B). Meanwhile, knockdown of *circKANS1L* significantly decreased the levels of FoxO3, and significantly increased the levels of p-FoxO3 and Akt (Fig. 10C and D). These trends were also observed in the 96 h group (Fig. 10E-H). An immunofluorescence assay showed that knockdown of *circKANS1L* significantly inhibited the expression of MyHC and myotube formation (Fig. 10I).

2.7. *circKANS1L* regulates skeletal myogenesis in vivo

We constructed a lentiviral vector encoding a short hairpin RNA (*circKANS1L*-si-1), termed as LV-sh-*circKANS1L* (Fig. S4B-G). LV-sh-*circKANS1L* and the empty vector, termed as LV-sh-NC, were injected into the gastrocnemius of six 6-week-old C57BL/6 mice, respectively. The first injection was denoted as day 0 and thereafter was injected once a week, with a total of four injections followed by collection of gastrocnemius samples (Fig. 11A). The qRT-PCR results showed that LV-sh-*circKANS1L* significantly reduced the expression level of *circKANS1L* in the gastrocnemius of the tested mice, with no significant effects on mouse *Kans1l* expression (Fig. 11B). After four weeks, treadmill exercise experiments showed that the running distance and time of the tested mice were significantly enhanced after knockdown of *circKANS1L* (Fig. 11C). H&E staining showed that the average cross-sectional area and diameter of the muscle in the LV-sh-*circKANS1L* groups were significantly smaller than those in the control groups (Fig. 11D and E). The levels of proliferation-related proteins, such as PCNA and Cyclin E, were significantly increased compared with those in the control group, while the level of Cyclin D showed an upregulated trend but not significantly (Fig. 11F and G). Among differentiation-related proteins, the levels of MYOG and MyHC decreased significantly in the LV-sh-*circKANS1L* group, while the oxidative myofiber marker MyHC I and glycolytic myofiber marker MyHC IIb levels were significantly increased and decreased after knockdown of *circKANS1L*, respectively (Fig. 11H and I). In the Akt-FoxO3 signaling axis, we found that the FoxO3 level was significantly decreased compared with that in the control group, and the p-FoxO3 and Akt levels were significantly increased in the LV-sh-*circKANS1L* group (Fig. 11J and K). These results indicated that knockdown of *circKANS1L* *in vivo* affected the proliferation and differentiation of

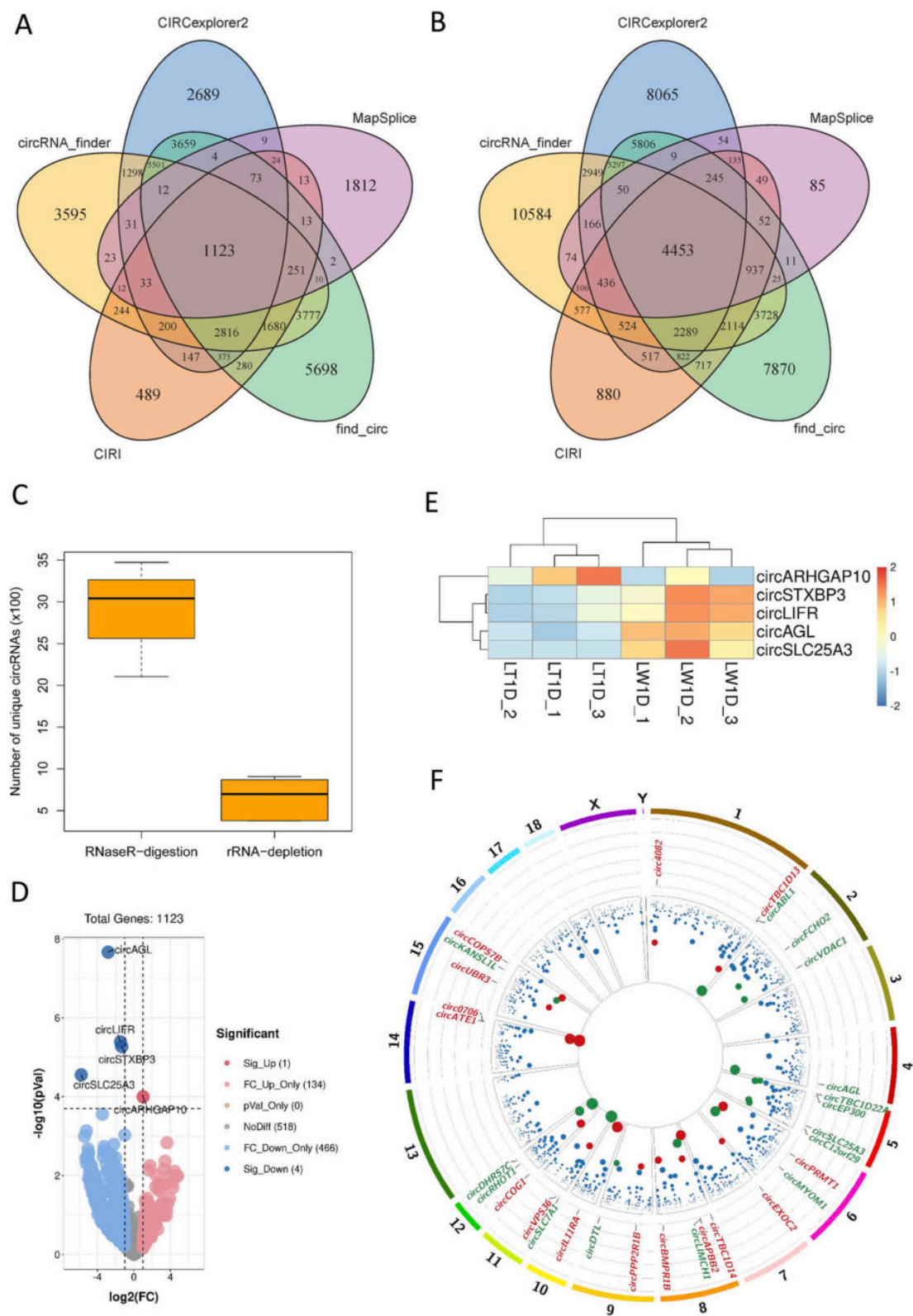
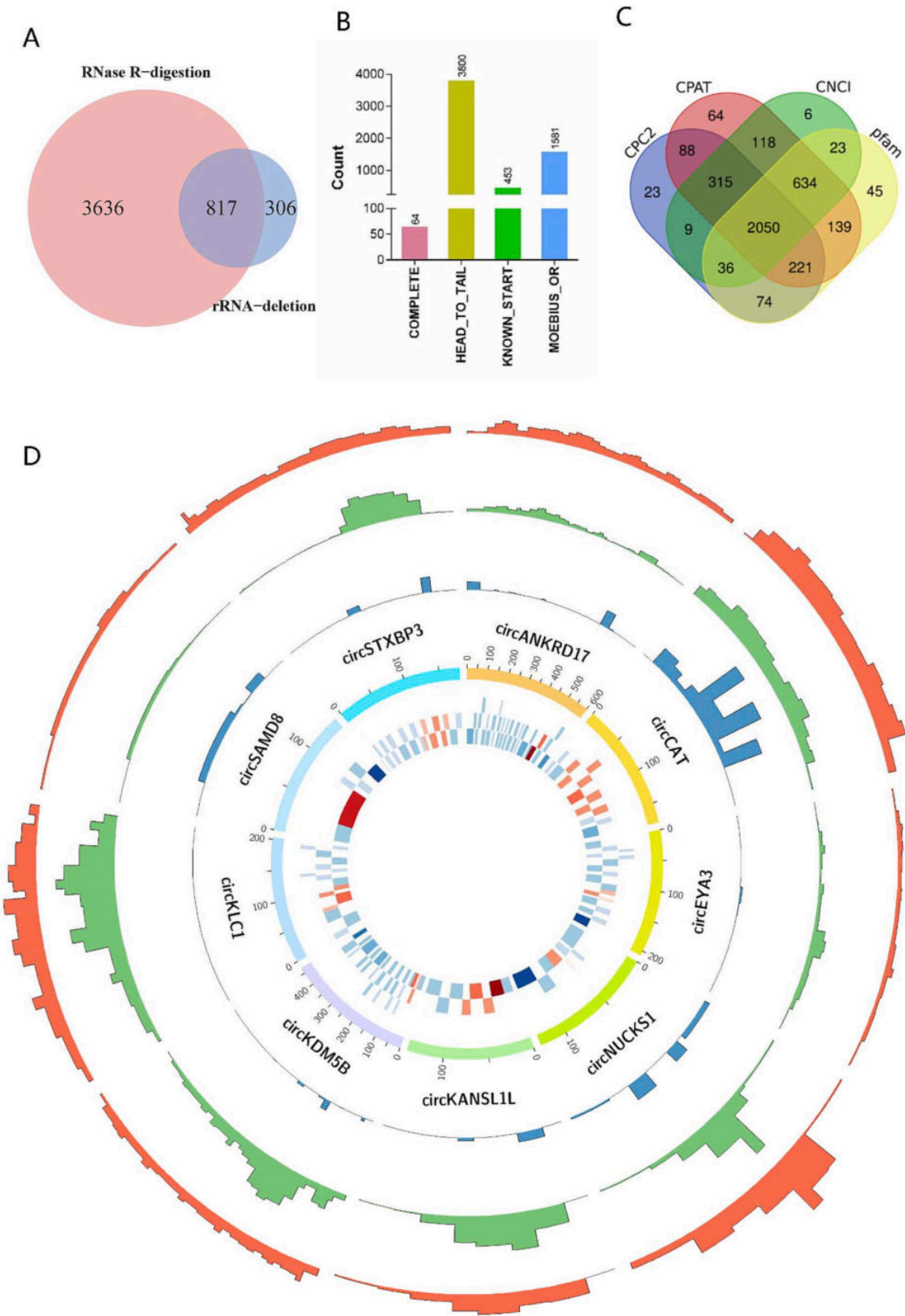


Fig. 3. Identification of the circRNA landscape and expression between the LT and LW breeds. (A-B) The shared circRNA candidates identified using five predictive algorithms in rRNA-deleted (A) and RNase R-digested libraries (B), respectively. (C) Effect of number of unique circRNAs verified in the sequencing libraries that were constructed using different approaches. (D-E) Volcano plot (D) and heatmap (E) showing differentially expressed circRNAs in the rRNA-deleted libraries. (F) Circos plot displaying the differentially expressed circRNAs in the RNase R-digested libraries. The outer ring represents the porcine autosomal and X, Y sex-chromosomes. The middle ring indicates the differentially expressed circRNA symbols, and the text marked with red and green represent up and downregulated circRNAs, respectively, in LT piglets. In the inner ring, the size of the solid circle represents $-\log(P \text{ value}, 2)$, while the red circles represent upregulated candidates and green represent downregulated candidates in LT piglets. (For interpretation of the references to colour in this figure legend, the reader is referred to the web version of this article.)



(caption on next page)

Fig. 4. Characteristics of the coding circRNA candidates in porcine muscles.

(A) Venn diagram showing the circRNA candidates identified in our rRNA-deleted and RNase R-digested datasets. (B) The characteristics of the circRNA ORFs identified in porcine muscles. COMPLETE, the coding region covered the entire circRNA candidate; HEAD_TO_TAIL, the coding region spanned the splice junction site (it is possible to form unique peptides at the end of the encoded product); KNOWN_START, the start codon of the circRNA candidates was same as their host mRNAs; MOEBIUS_ORF, no stop codon that was identified in the ORF of the circRNA candidates, which led to infinite translation. (C) Venn diagram showing the protein-coding potential of circRNA candidates calculated using four different algorithms. (D) The protein-encoding potential of circRNA candidates analyzed using Ribo-seq. In the inner circle, the tiles represent the exons of host genes. The exons marked with red represented the circRNA exons, while those in blue represent non-circRNA exons. The darker the colour, the larger the exon. In the second inner circle, the histogram shows the abundance of reads in each exon of the host genes in the Ribo-seq library. In the third inner circle, the histogram shows the abundance of reads in each exon of the host genes in the RNase R-digested libraries. In the outer circle, the histogram shows the abundance of reads in each exon of the host genes in the rRNA-deleted libraries. (For interpretation of the references to colour in this figure legend, the reader is referred to the web version of this article.)

myoblasts, and especially promoting a glycolytic-to-oxidative muscle fiber switch.

2.8. circKANSLL1L encodes a novel protein that regulate myogenesis by binding to Akt

We found that circKANSLL1L has an initiation codon and terminator near the splicing site, which could form an 1653-nt ORF with the ability to encode a 551 amino acid protein (Fig. 12A). The linear sequence of the ORF in circKANSLL1L was cloned into pcDNA3.1 vector, and 3 × Flag tag was placed before the stop codon, which was designated as Flag-KANSLL1L-551aa. The above vector was transfected into C2C12 cells, and the western blotting results showed that the protein expression of Flag-KANSLL1L-551aa could be detected using anti-Flag antibodies (Fig. 12B). After incubation for 48 h in growth medium, Flag-KANSLL1L-551aa transfection significantly decreased the levels of the cell proliferation-related proteins PCNA, Cyclin D, and Cyclin E (Fig. 12C and D), whereas the level of FoxO3 was significantly increased and p-FoxO3 and Akt levels were significantly decreased after Flag-KANSLL1L-551aa overexpression (Fig. 12E and F). After 96 h of incubation in differentiation medium, the levels of MYOG, MYH6 and MyHC were significantly increased in the Flag-KANSLL1L-551aa group (Fig. 12G and H), while the core protein expression of the Akt-FoxO3 signaling axis showed a consistent change in C2C12 cells incubated with growth medium in the Flag-KANSLL1L-551aa group (Fig. 12I and J). A co-immunoprecipitation experiment (CO-IP) using the anti-Flag antibody confirmed that Akt interacts with the novel protein encoded by circKANSLL1L (Fig. 12K).

3. Discussion

A previous study suggested that the variations in myofiber characteristics of porcine muscle tissues could explain the differences in meat quality [30]. There are four fiber types in mammalian muscles, one slow (type I) and three fast types (type IIA, IIX, and IIB), each characterized by the expression of one specific isoform of MyHC [31]. The slow and fast muscle fibers largely differ in their phenotype, contraction mechanism, and metabolism [32]. In general, the slow-twitch myofibers are characterized by smaller cross-sectional areas and diameters, and make the meat ruddy, fresh, and juicy, thereby improving the flavor of meat [33]. In our study, significantly smaller cross-sectional areas were observed in the muscle of the LT breed, and much higher mRNA and protein levels of MyHC I were detected in LT piglets, indicating that LT pigs had more slow muscle fibers for high-quality meat production. The myofiber types, however, also differ in their metabolic profiles, ranging between slow and fast myofibers [34]. The metabolomic profiles of the porcine longissimus dorsi muscles were therefore demonstrated between the LT and LW breeds, and a large number of DAMs were significantly enriched in several annotated pathways responsible for substance and energy metabolism, such as amino acid metabolism, glycerophospholipid metabolism, and the TCA cycle. The similar results were found between Luchuan pig (a type of fatty pig) and Duroc pig (a lean-type pig) [35]. The TCA cycle plays an important role in energy homeostasis and cell metabolism of skeletal muscle [36], and is

significantly associated with oxidative metabolism, which is responsible for meat tenderness [37]. Recently, several studies have indicated that skeletal muscles with greater oxidative metabolism are more tender than muscles that are more prone to glycolytic metabolism [38,39]. As an important TCA-cycle intermediate, citric acid accumulation was considerably increased in the muscle tissues of the LT piglets, consistent with the composition and metabolic characteristics of muscle fibers in the LT breed. By contrast, D-Fructose 1,6-bisphosphate, an intermediate metabolite of glycolysis [40], was significantly accumulated in the LW piglets. Our findings confirmed substantial intergroup differences between the LT and LW piglets, indicating that the two pig breeds not only have distinctive myofiber composition, but also have exclusive metabolic profiles in their muscle tissues.

In the past decade, bulk RNA-seq technologies have been widely used to study gene expression patterns at the population level [41], while single-cell RNA sequencing technology is revolutionizing the identification of cell types and transcriptome heterogeneity in various species, especially in diverse animal tissues [42]. Exploring the function of muscle tissue has benefitted enormously from the emergence of single-cell technology, because the complex composition of muscle-resident cell types makes it difficult to decipher genome-wide transcriptome data using bulk RNA-seq data. To date, a handful of muscle-focused single-cell RNA-seq projects have been reported in humans [43], mice [21,22,25], beef cattle [44], cows [45], pigs [46], and chickens [27]. In this work, a comprehensive single-cell compendium of the porcine longissimus dorsi muscle was identified in the LT and LW piglets, with a special emphasis on the subpopulations involved in myogenesis. The major cell types in porcine muscle tissues were similar to those in other species. In general, skeletal myogenesis is a complex-multistep process that originates from the earliest myogenic progenitor stage to the formation of mature myofibers [47]. The myogenic program is controlled by a core network of transcription factors, including PAX7 and a set of muscle regulatory factors consisting of MYF5, MYOD, MYOG, and MYHs [26]. In the present study, two subpopulations of myogenic progenitors were found, including MuSCs and myoblasts, which expressed the myogenic transcription factors PAX7, MYF5, and MYOD [48], and a population of mature myocytes, which expressed MYOG, which are involved in the formation of multinucleated myofibers from the fusion of mononucleated myocytes during myogenesis [49]. Several phases of proliferation and differentiation lead to the formation of terminally differentiated myofibers; however, how these differ among pig breeds remains largely unknown. We therefore discussed the key cellular and molecular events that regulate the progression through these developmental steps. In our work, the differentially expressed genes between the LT and LW breeds were most significantly enriched in the PI3K-Akt and FoxO signaling pathways in MuSCs, myoblasts, myocytes, and myofibers, respectively. The FoxO transcription factors are regulated by several modifications, among which the most critical is phosphorylation and nuclear exclusion by Akt [50]. The phosphorylation of FoxOs promote their translocation from the nucleus to the cytosol, subsequently reducing FoxO transcriptional activity [51], which is highly poised to regulate skeletal myogenesis [52]. In addition, the terminally differentiated myofibers usually exhibit oxidative and glycolytic metabolic phenotypes, revealing a high degree of heterogeneity within the

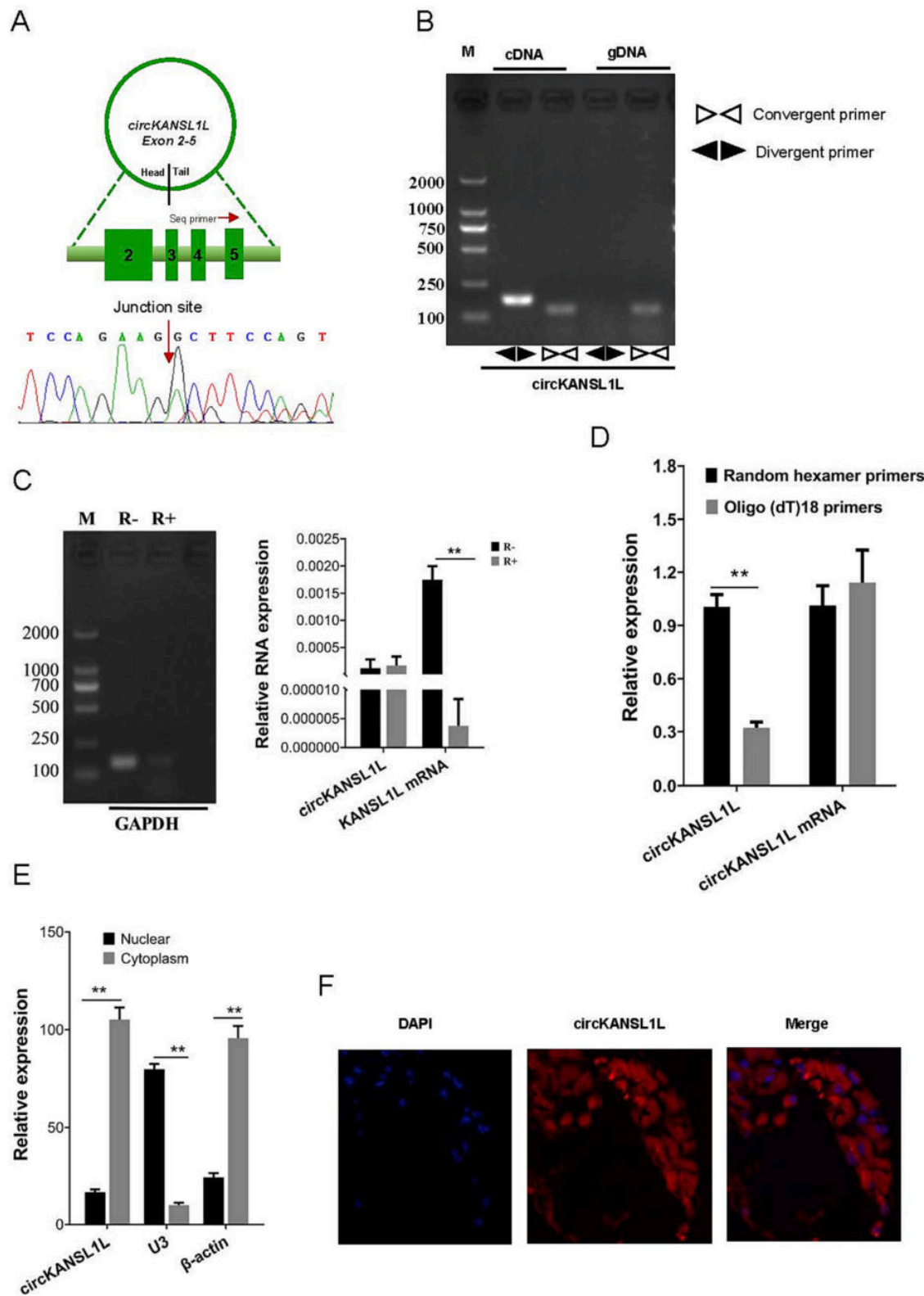


Fig. 5. Characterization of circKANSL1L in porcine muscles. (A) The genomic locus of circKANSL1L (upper panel), and Sanger sequencing confirmed the head-to-tail splicing of murine circKANSL1L (lower panel). (B) Divergent primers amplified circKANSL1L in cDNA but not genomic DNA. (C) qRT-PCR analysis of the expression of circKANSL1L and *KANSL1L* mRNA after treatment with RNase R in porcine muscles. (D) qRT-PCR using oligo dT primers and random primers confirmed the circular characteristics of circKANSL1L. (E) circKANSL1L was mainly situated in the cytoplasm, as validated by cytoplasmic and nuclear fractionation assays. (F) The location of circKANSL1L as observed by fluorescence *in situ* hybridization. The Cy3-labeled circRNA appeared red, whereas DAPI-stained nuclei appeared blue. Scale bar =10 μm. (For interpretation of the references to colour in this figure legend, the reader is referred to the web version of this article.)

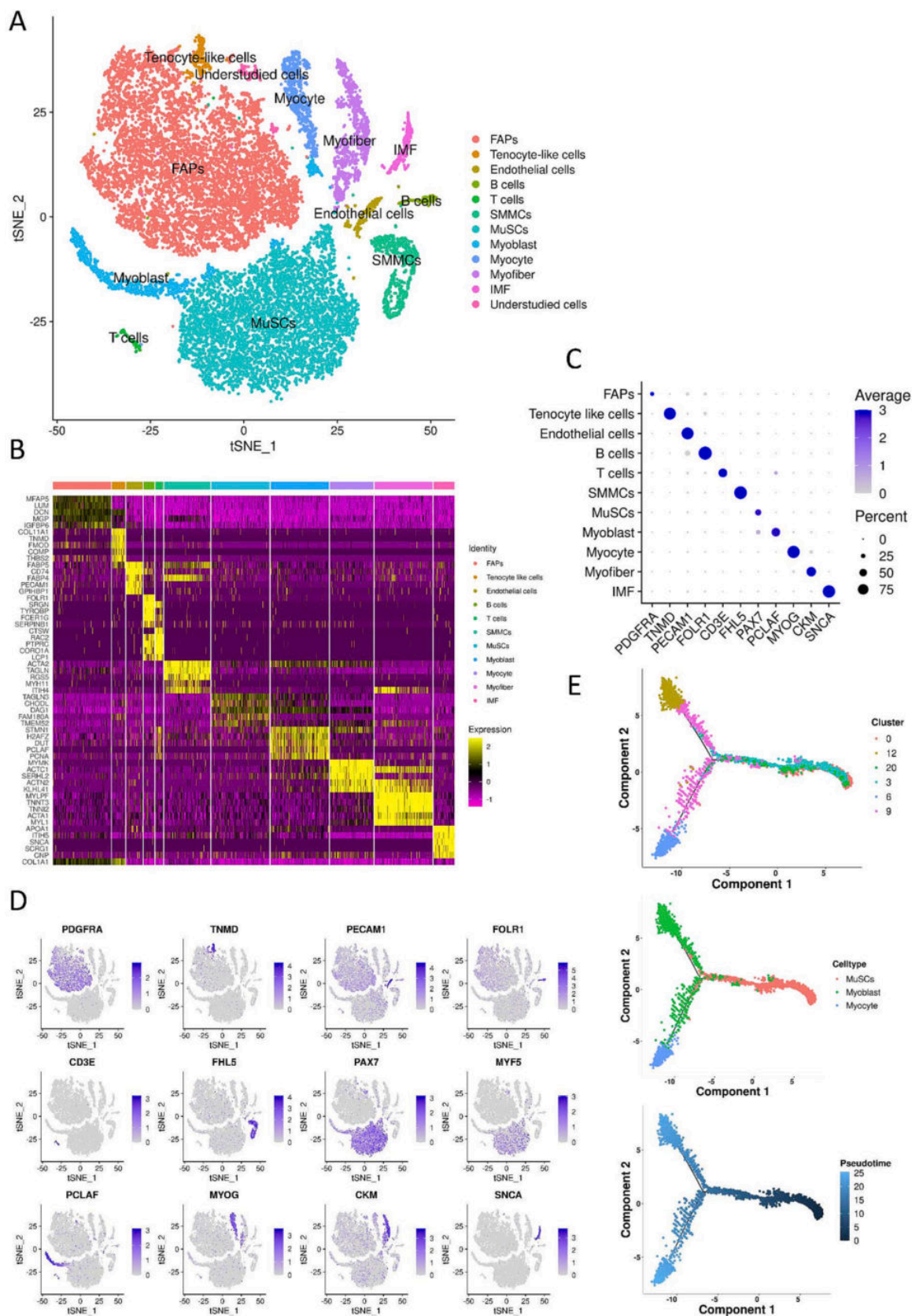


Fig. 6. Identification of distinct cell populations in porcine muscles. (A) The t-Stochastic neighbor embedding (tSNE) plot showing the distribution of the main muscle-resident cell populations. (B) Heatmap representing the top five most variably expressed genes between the different clusters identified. (C) Dot plot for the expression of marker genes in distinct cell populations. (D) Individual gene t-SNE plots showing the expression level and distribution of representative marker genes. (E) Pseudotime single cell trajectory reconstructed by Monocle2 for MuSCs, myoblasts, and myocytes. The cells are colored by pseudotime and cell types.

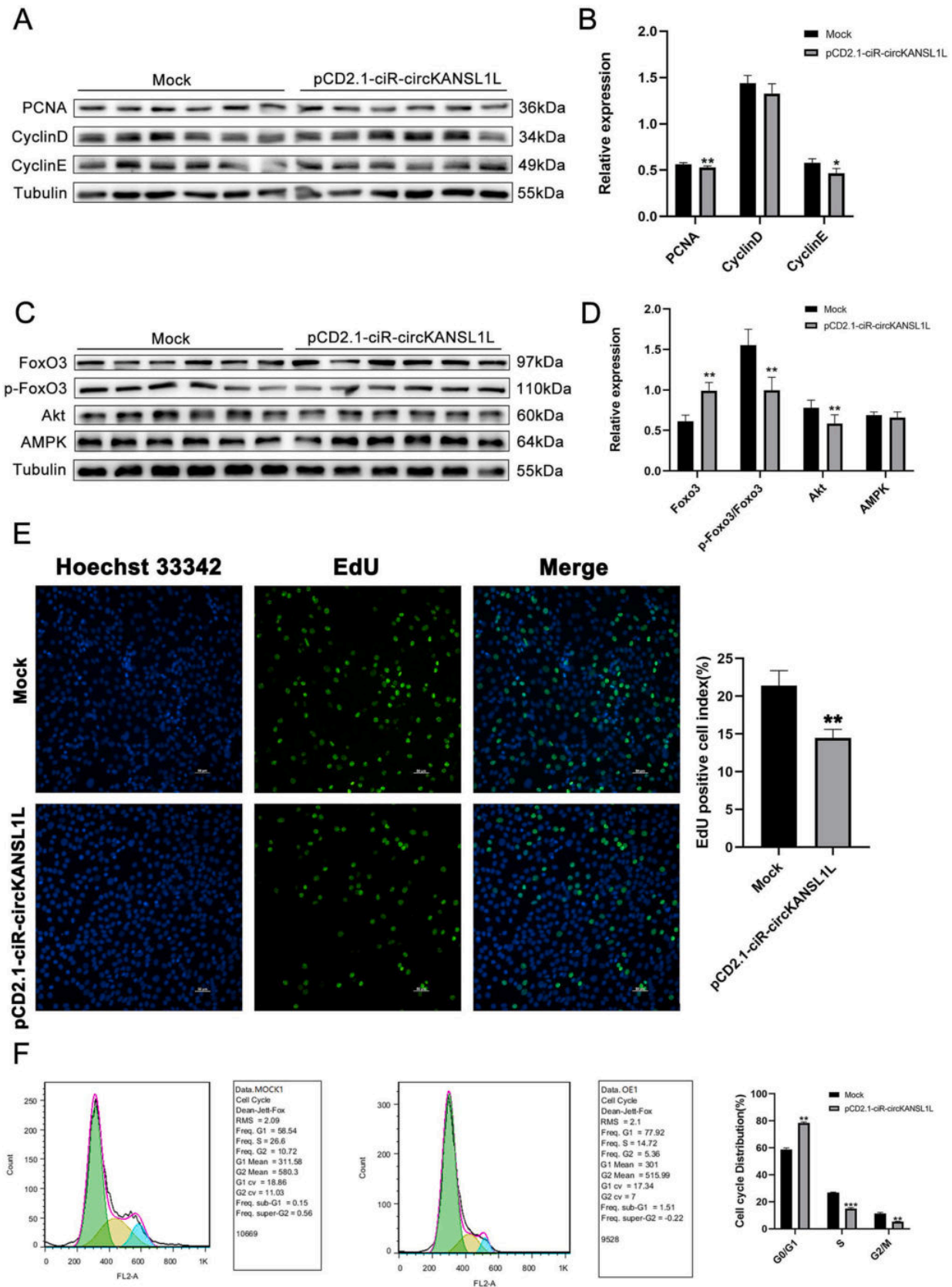


Fig. 7. Overexpression of circKANSL1L inhibited C2C12 cell proliferation. (A-D) After treatment with pCD2.1-ciR-circKANSL1L and incubation for 48 h in growth medium, western blotting analysis of the levels of proliferation marker proteins (A and B) and the core proteins in the Akt-FoxO3 signaling axis (C and D) was carried out. (E) The proliferation ability of C2C12 cells as detected using an EdU assay (bar = 100 μ m). (F) The changes to the cell cycle in C2C12 cells as assessed using flow cytometry.

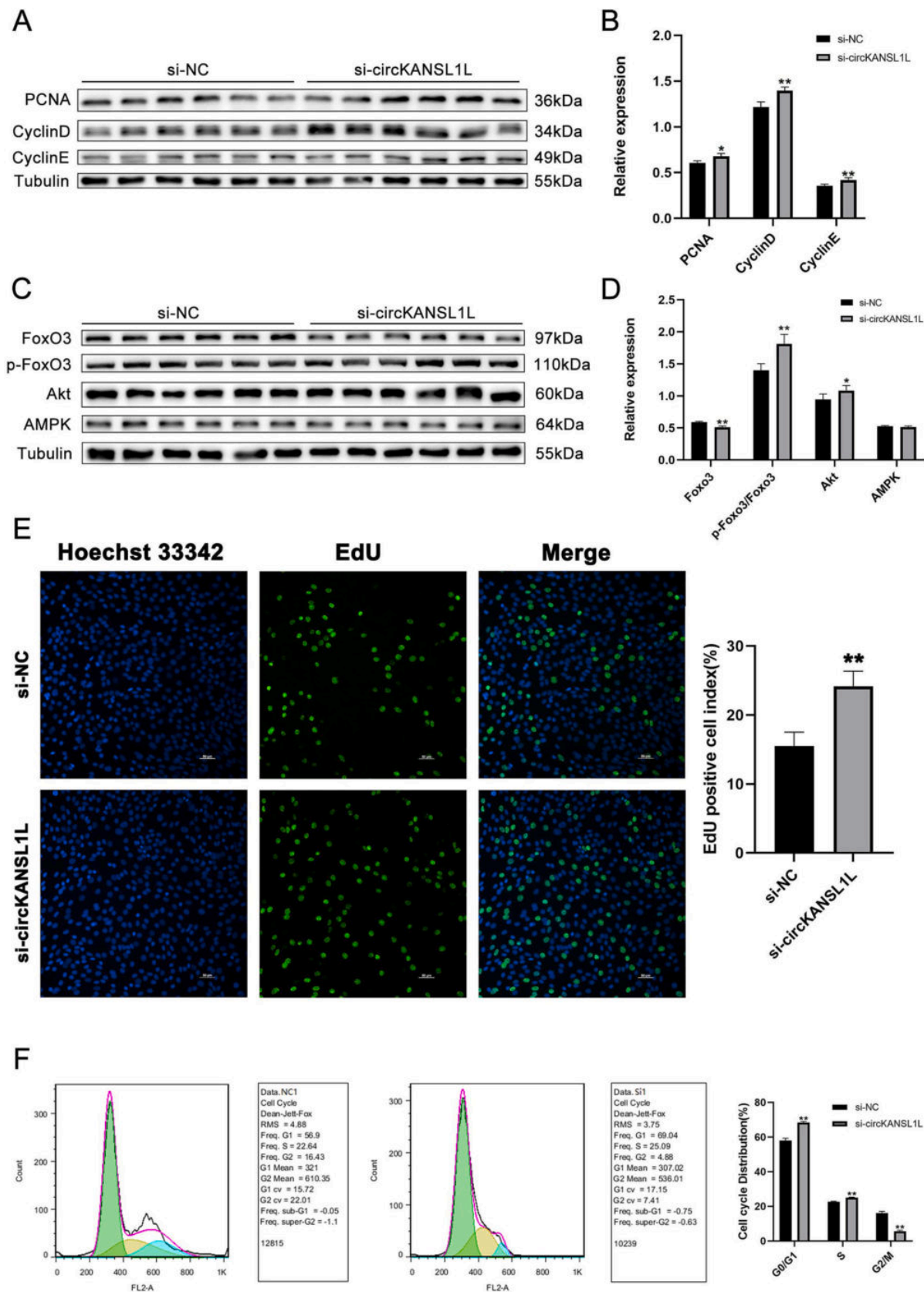


Fig. 8. Knockdown of circKANSL1L promoted C2C12 cell proliferation. (A-D) After treatment with circKANSL1L-si-1 and incubation for 48 h in growth medium, western blotting analysis of the levels of proliferation marker proteins (A and B) and the core proteins in the Akt-FoxO3 signaling axis (C and D) was carried out. (E) The proliferation ability of C2C12 cells was detected using an EdU assay (bar = 100 μ m). (F) The changes to the cell cycle in C2C12 cells as assessed using flow cytometry.

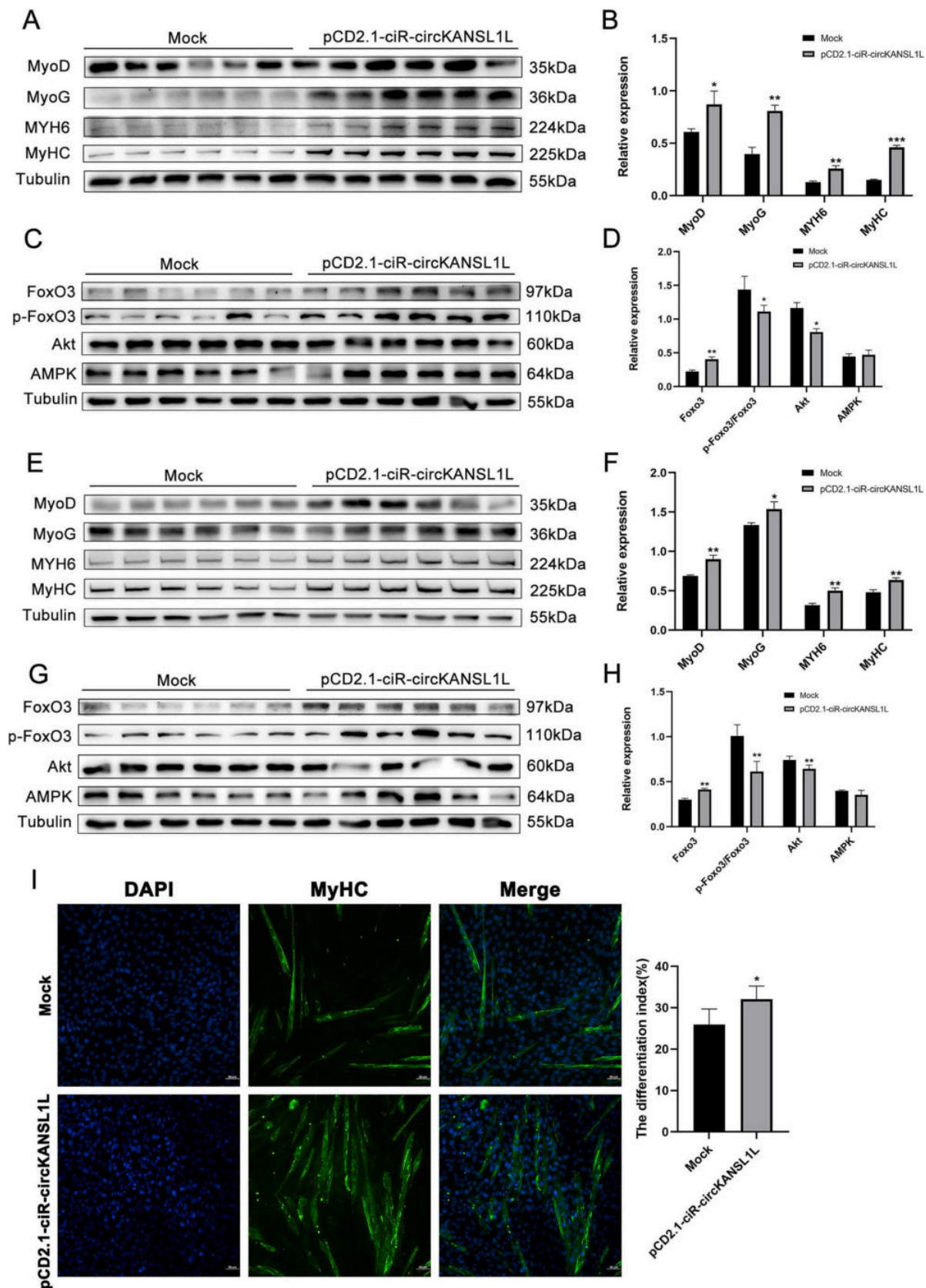


Fig. 9. Overexpression of circKANSL1L promoted C2C12 cell differentiation. (A-D) After treatment with circKANSL1L-si-1 and incubation for 48 h in growth medium, western blotting analysis of the levels of proliferation marker proteins (A and B) and the core proteins in the Akt-FoxO3 signaling axis (C and D) was carried out. (E-H) After 96 h of incubation with differentiation medium, western blotting analysis was carried out to determine the levels of differentiation marker proteins (E and F) and Akt-FoxO3 pathway proteins (G and H). (I) Immunofluorescence analysis of the MyHC colocalization in pCD2.1-ciR-circKANSL1L-transfected C2C12 cells after 96 h of incubation.

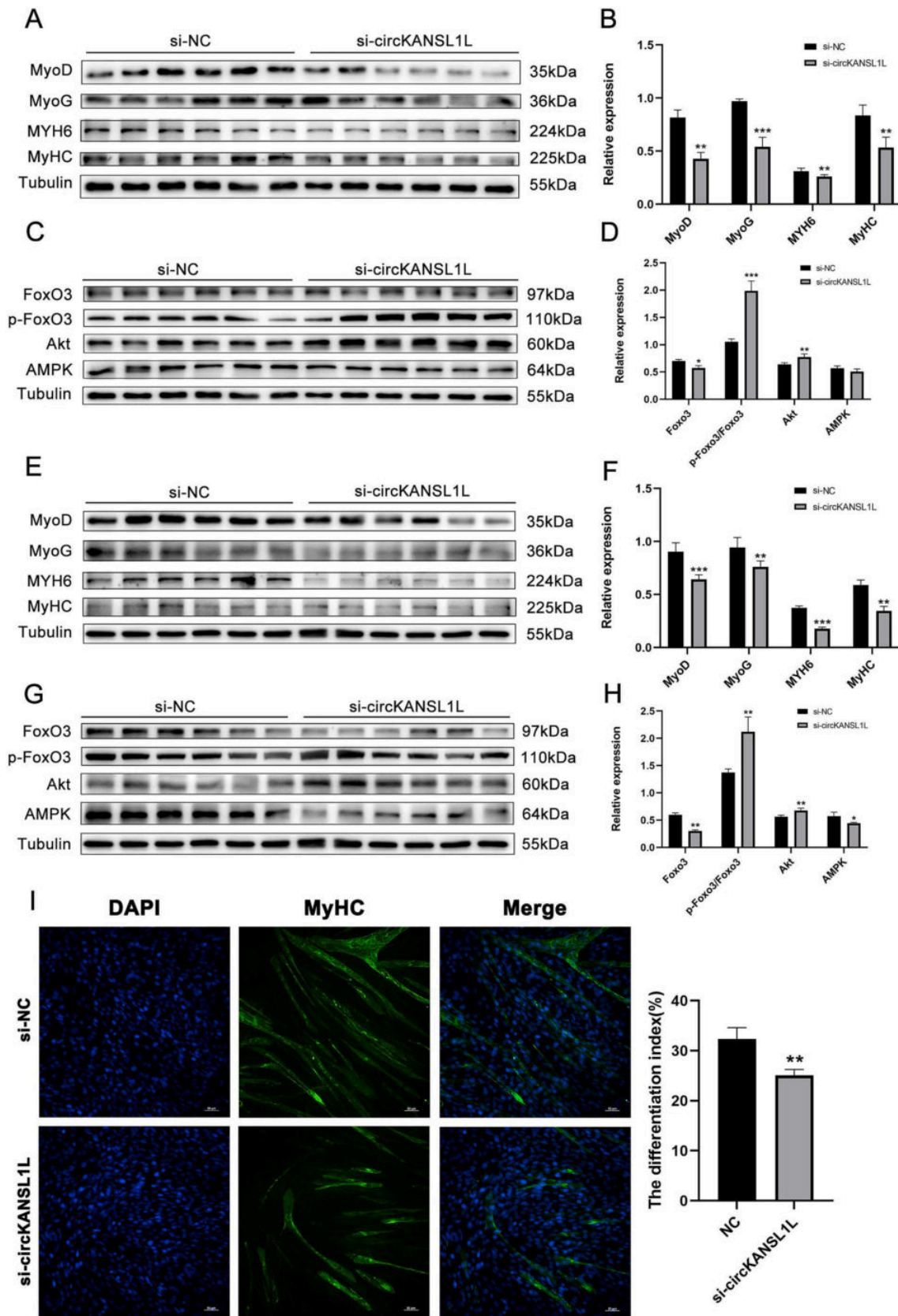


Fig. 10. Knockdown of circKANS1L inhibited C2C12 cell differentiation. (A-D) After treatment with circKANS1L-si-1 and incubation for 48 h with differentiation medium, western blotting analysis was carried out to determine the levels of differentiation marker proteins (A and B) and Akt-FoxO3 pathway proteins (C and D). (E-H) After 96 h of incubation with differentiation medium, western blotting analysis was carried out to determine the levels of differentiation marker proteins (E and F) and Akt-FoxO3 pathway proteins (G and H). (I) Immunofluorescence was performed to determine MyHC colocalization in circKANS1L-si-1-transfected C2C12 cells after 96 h of incubation.

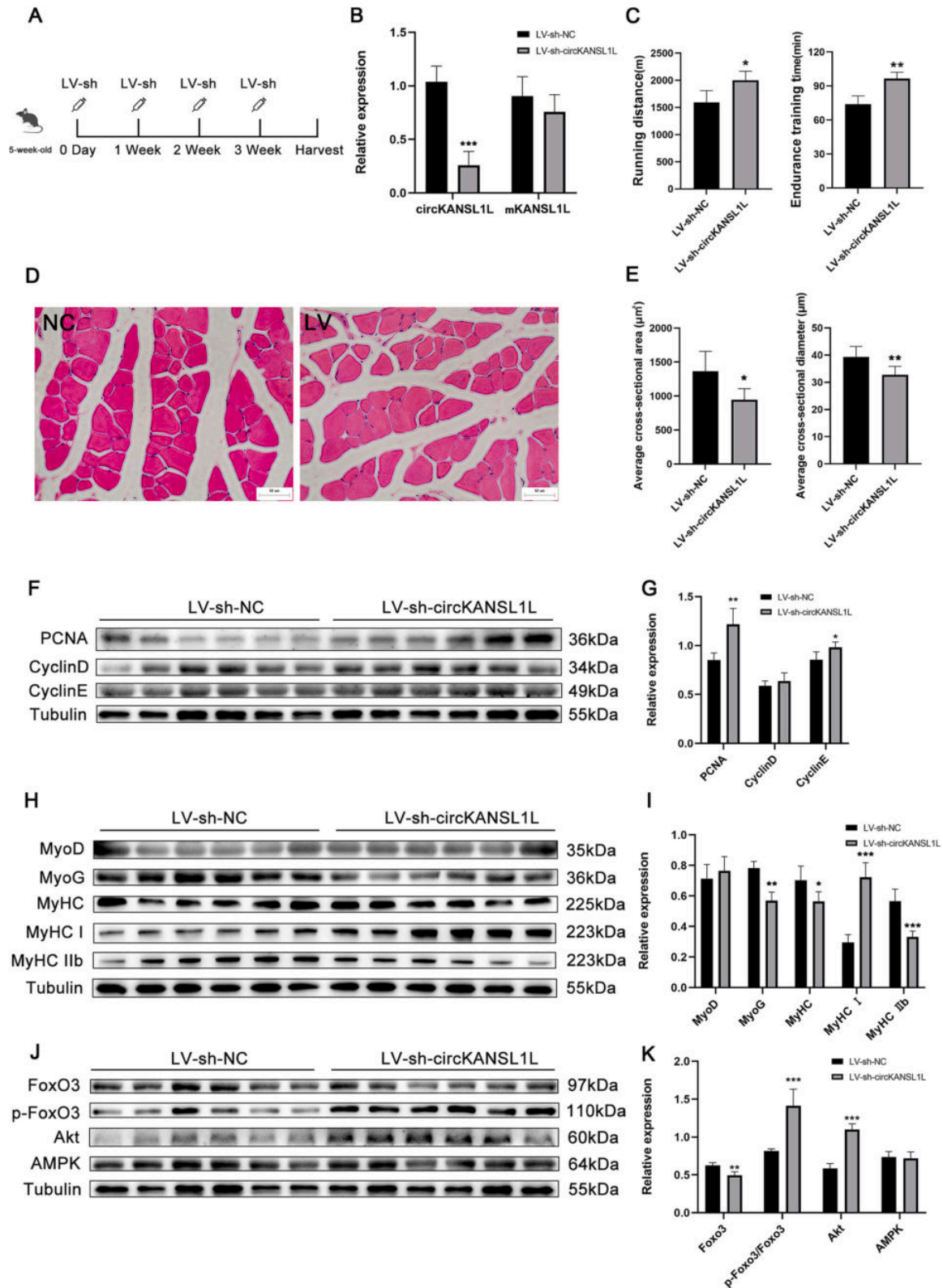


Fig. 11. Knockdown of circKANSL1L regulated skeletal myogenesis *in vivo*. (A) Flowchart illustrating the *in vivo* experimental study. (B) The relative expression of circKANSL1L and *Kansl1* mRNA in mouse gastrocnemius muscles infected with LV-sh-circKANSL1L lentivirus or control (GFP). (C) Treadmill exercise experiments revealed the running distance and time of the tested mice. (D) H&E staining of mouse gastrocnemius muscles from tested individuals infected with LV-sh-circKANSL1L lentivirus or control (GFP), scale bar = 50 μ m. (E) Average cross-sectional areas of myofibers in the tested individuals. (F-K) Western blotting analysis of the levels of proliferation marker proteins (F and G), differentiation marker proteins (H and I), and Akt-FoxO3 pathway proteins (J and K).

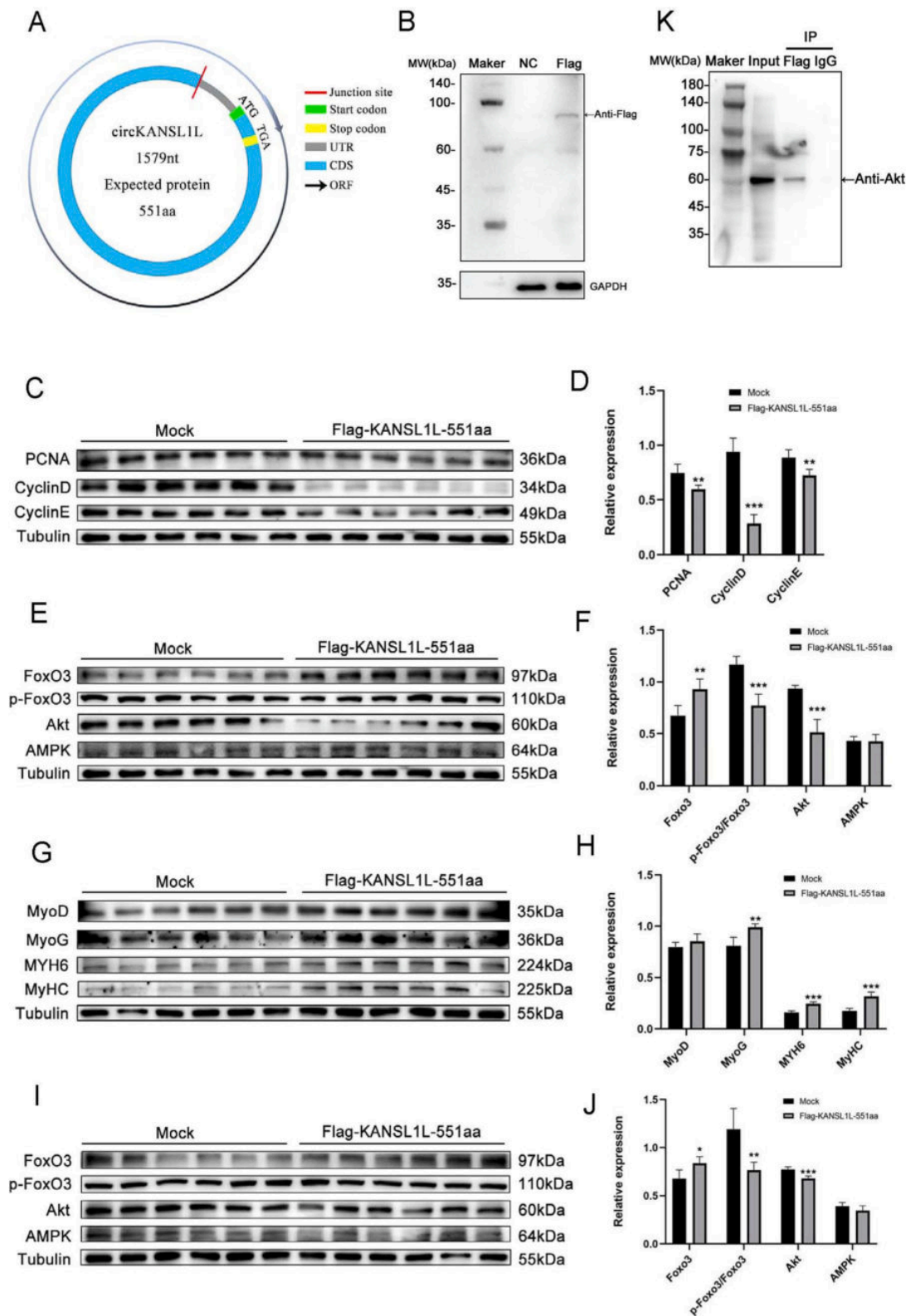


Fig. 12. circKANS1L1L encodes a novel protein in C2C12 cells. (A) Schematic diagram of circKANS1L1L's translation potential. (B) After transfection of Flag-KANS1L1L-551aa or control plasmids into C2C12 cells, total proteins from the transfected cells were extracted and western blotting was performed using an anti-Flag antibodies. (C–F) After 48 h of incubation with growth medium, western blotting analysis of the expression of proliferation marker proteins (C and D) and the core proteins in the Akt-FoxO3 signaling axis (E and F). (G–J) After 96-h incubation with differentiation medium, western blot analysis of the expression of differentiation marker proteins (G and H) and Akt-FoxO3 pathway proteins (I and J). (K) After transfection with Flag-KANS1L1L-551aa for 24 h, C2C12 cells were lysed for Immunoprecipitation and western blot with anti-Akt antibody.

myofiber compartment [53]. We therefore re-clustered myofibers and found three diverse cell types that showed dynamic differences in their gene expression profiles. In glycolytic fibers, the subtype-specific marker genes were also the most significantly enriched in the Akt-FoxO signaling axis. These observations implied that Akt-mediated phosphorylation of FoxO and the relatively high expression of FoxO3 in the LW pigs were strongly associated with muscle cell proliferation and differentiation, and muscle fiber type conversion.

Recently, a growing body of evidence suggests that circRNAs are a widespread RNA species in eukaryotes, playing important roles in skeletal myogenesis [54]. Using high-throughput sequencing technologies, a large number of circRNA events have been identified in muscle tissues of humans [55] and various animals, such as monkeys [56], mice [57], cattle [58], buffaloes [59], yaks [60], goats [61], sheep [62], rabbits [63], pigs [17], chickens [64], ducks [65], and geese [66]. In this work, the rRNA-depletion and RNase R-digestion approaches were applied for circRNAome-seq library construction, and approximately 4-fold more circRNA candidates were discovered using the RNase R-digestion approach. The results suggested that the potential use of RNase R-digested RNA sources for circRNA prediction could greatly reduce the background noise and improve the reliability and efficiency of circRNA identification [67]. In this study, a novel circRNA was found, termed as circKANSL1L, consisting of exons 2–5 of its host gene, which is conserved between pig and mouse, and was differentially expressed between the two pig breeds. In our previous study, we also identified a circRNA candidate, consisting of exons 2–3 of KANSL1L gene, and it was found to inhibit the proliferation of myocytes but promote differentiation [68]. Through circRNA overexpression and siRNA-mediated silencing, the circKANSL1L is proved to be significantly associated with myoblast proliferation and differentiation *in vitro*. Furthermore, *in vivo* experiments showed that the differentiation of muscle cells was significantly inhibited after circKANSL1L knockdown, while the proliferation of muscle cells was obviously promoted, as well as the transformation from fast-glycolytic to slow-oxidative fibers. In addition to acting as regulators by adsorbing miRNAs and proteins, recent evidence has confirmed the existence of functional peptides or proteins translated from certain circRNAs [13], suggesting that the coding potential of these non-coding RNAs has been largely underestimated. In general, most translatable circRNAs share similar ORFs to their related linear mRNAs, and a spanning junction ORF is the distinctive feature of these circRNA candidates [69]. Herein, using a combination of bioinformatic tools, we confirmed that the circKANSL1L ORF spanned from the putative initiator codon of the host gene to a stop codon after the splice junction. In addition, the coding ability and functions of this circRNA were further proven using Ribo-seq analysis and the use of artificial constructs expressing the circular ORF with Flag tags. Our data demonstrated that eukaryotic endogenous circKANSL1L is involved in skeletal myogenesis.

A previous study and our single-cell RNA sequencing analysis of porcine muscle tissues revealed that the Akt-FoxO axis is an important and conserved evolutionary signaling pathway involved in skeletal myogenesis [52]. In our work, further experiments showed that circKANSL1L correlated negatively with the expression of Akt and phosphorylated FoxO3 *in vitro* and *in vivo*, indicating that the Akt-FoxO pathway was activated. Recently, other studies indicated that a subset of circRNAs, such as circPINTexon2 [12], circGprc5a [70], and circUBE4B [71], have been reported to be translated, and the encoding products could interact with target proteins in various physiological and pathological processes. In our study, a co-IP assay was performed, and the result showed that the protein encoded by circKANSL1L interacted with Akt directly. Taken together, the circKANSL1L protein could interact with Akt and promote the phosphorylation of FoxO3 to eventually activate the Akt-FoxO signaling pathway.

In conclusion, the histological features and transcriptome information of porcine longissimus dorsi muscles were compared between the LT and LW breeds, and we found that circKANSL1L, encoding a novel protein, was significantly associated with skeletal myogenesis. The

encoded protein of circKANSL1L interacted with Akt and changed the phosphorylation level of FoxO3, and subsequently affecting FoxO3 transcriptional activity and maybe regulating myoblast proliferation and differentiation, and muscle fiber composition.

4. Material and methods

4.1. Sample collection

A total of 10 Chinese fat-type Lantang (LT) piglets, and 10 typical lean-type Landrace (LW) piglets were collected from a large-scale pig breeding farm (Xinfeng County, Shaoguan City, Guangdong Province, China). One healthy and purebred LT or LW male piglet per litter was slaughtered after birth, and the longissimus dorsi muscle tissues were collected, and immediately subjected to single-cell isolation. Meanwhile, a part of the muscle tissue was cut into approximately $0.5 \times 0.5 \times 0.5$ cm pieces and then immediately fixed in 4 % paraformaldehyde for H&E staining analysis. For the metabolomics ($n = 10$) and bulk RNA-seq ($n = 3$) analyses, porcine muscle tissues were harvested separately and snap-frozen in liquid nitrogen for further analysis. This study was approved by the Animal Care Committee of South China Agricultural University, and all applicable institutional and national guidelines for the care and use of animals were followed.

4.2. Myofiber characteristics

All muscles were fixed with paraformaldehyde, dehydrated in graded alcohols, cleared in xylene, and paraffin embedded for sectioning. Cross-sections of 5 μ m thickness were cut longitudinally using a manual rotary microtome (Olympus, Tokyo, Japan). The sections were stained using H&E and scanned using Olympus VS120 microscope at 400 \times magnification. Using Image J software (Media Cybernetics, Rockville, MD, USA), total cross-sectional areas were measured, and cell nuclei were then counted. The relative expression level of the mRNAs encoding MyHC I and MyHC IIb isoforms were assessed using RT-PCR, while equal amounts of protein in LT and LW muscles were extracted and separated using 10 % sodium dodecyl sulfate-polyacrylamide gel electrophoresis (SDS-PAGE) for western blotting, using antibodies recognizing MyoD, MyoG, MyHC, MyHC I and MyHC IIb.

4.3. Sample preparation and metabolomic analysis

The muscle homogenates were prepared by grinding tissue in liquid nitrogen, and approximately 100 mg of muscle powder was mixed immediately with 120 mL of precooled 50 % methanol, vortexed for 3 min, and incubated at room temperature for 10 min. The mixture was then stored overnight at -20°C . After centrifugation at 4000 \times g for 20 min, the supernatants were transferred into 96-well plates for LC-MS analysis.

All chromatographic separations were performed using a Thermo Fisher Scientific UltiMate 3000 HPLC (Thermo Fisher Scientific, Waltham, MA, USA), with an Acquity UPLC BEH C18 column (100 mm \times 2.1 mm, 1.8 μ m) (Waters, Wilmslow, Manchester, UK). The column oven was maintained at 35 $^{\circ}\text{C}$, and the flow rate was 0.4 mL/min. The mobile phase consisted of solvent A (water, 0.1 % formic acid) and solvent B (Acetonitrile, 0.1 % formic acid). Gradient elution conditions were set as follows: 0–0.5 min, 5 % B; 0.5–7 min, 5 % to 100 % B; 7–8 min, 100 % B; 8–8.1 min, and 100 % to 5 % B; 8.1–10 min, 5 % B. The injection volume for each sample was 4 μ L. The HPLC system was coupled to a high-resolution tandem TripleTOF 5600 mass spectrometer (Sciex, Framingham, MA, USA), while detection was performed in positive and negative ion mode using electrospray ionization with a Turbo V source. The following settings were applied: gas 1 (nebulizer) and gas 2 (heater) were set at 60 psi; curtain gas (nitrogen) was set at 30 psi; the interface heater temperature was 650 $^{\circ}\text{C}$; and the positive and negative Ion Spray Voltage Floating were set at 5000 V and -4500 V, respectively.

LC-MS raw data files were converted into the mzXML format and further processed by XCMS [72], CAMERA [73], and metaX toolbox [74]. The combined retention time (RT) and m/z value were used to identify each ion. The online KEGG (<https://www.kegg.jp/>), HMDB (<http://www.hmdb.ca/>), and in-house fragment spectrum library (<http://spldatabase.saskatoonlibrary.ca/>) were used to annotate the metabolites by matching the exact molecular mass of the m/z value. Student's t -tests were conducted to detect differences in metabolite concentrations between the LT and LW piglets, and the P value was adjusted for multiple tests using a false discovery rate (FDR) (Benjamini-Hochberg) algorithm.

Supervised PLS-DA was conducted through metaX to discriminate the different variables between groups, and a variable importance in projection (VIP) cut-off value of 1.0 was used to select important features.

4.4. Bulk circRNA-sequencing and circRNA prediction

A total of three muscle samples in each breed were randomly selected for circRNA-seq analysis. Total RNA was extracted using the Trizol reagent (Invitrogen, Carlsbad, CA, USA) following the manufacturer's procedure, while the quantity and purity were assessed using a Bioanalyzer 2100 and RNA 6000 Nano LabChip Kit (Agilent, Santa Clara, CA, USA) with an RNA integrity number (RIN) number > 7 . We then used an Epicentre Ribo-Zero Gold Kit (Illumina, San Diego, CA, USA) to deplete ribosomal RNA, and applied RNase R (Geneseed, Guangzhou, Guangdong, China) digestion to remove linear RNA molecules. Following purification, the RNase R-digested RNA fractions were fragmented and reverse-transcribed to create the final cDNA library using the mRNA-Seq sample preparation kit (Illumina). Next, we performed paired-end sequencing on an Illumina HiSeq 4000 platform (LC Sciences, Hangzhou, Zhejiang, China) to obtain raw sequencing reads. As in our previous publication [68], the raw data generated from rRNA-deleted libraries were collected under accession number PRJNA778795. Then, the preliminary quality of the raw sequences in the Fastq format was evaluated using FastQC v0.11.9, and further processed by removing low-quality reads and reads that contained sequencing adapters or primers. We combined TopHat [75] and TopHat-Fusion [76] to obtain back-spliced junction reads for circRNA prediction. In general, five different algorithms were used to obtain circRNA candidates, including CIR-Cexplorer2 [77], circRNA_Finder [78], CIRI [79], find_circ [80], and MapSplice [81], and only circRNA candidates identified by all five approaches were considered for further analysis. We calculated circRNA expression levels with back-spliced junction reads, while the edgeR algorithm was used to examine the differentially expressed (DE) circRNA candidates according to an FDR < 0.05 . We designed a pair of unique primers that crossed the cyclization site for each DE circRNA candidate. Total RNA was reverse-transcribed into cDNA, which was used as the template for PCR amplification using PrimeScript RT Reagent Kit (Takara, Dalian, China) and PrimeSTAR GXL DNA Polymerase (Takara) according to the manufacturer's protocol. The authenticity of circRNA head and tail splicing was preliminarily verified by 1 % agarose gel electrophoresis and Sanger sequencing of the PCR products; the primers are shown in Table S7.

4.5. Prediction of potential coding circRNA candidates and ribosome profiling

To predict the open reading frames of circRNAs (cORFs), we utilized circRNA candidates obtained from our previous rRNA-deleted and RNase R-digested libraries. Each circRNA sequence, excluding intronic sequences, was multiplied three times, and the longest ORF spanning the junction site was selected (minimum cORF length threshold was 100 aa) using the ORF_finder pipeline (<https://www.ncbi.nlm.nih.gov/orffinder/>). We then combined four types of evidence, CPC2 [82], CPAT [83], CNCI [84], and Pfam [85], to evaluate the coding potential

of the cORF sequences.

For ribosome profiling sequencing (Ribo-seq), six frozen muscle tissues used for circRNA-sequencing were pooled equally and pulverized manually under liquid nitrogen, and the powdered tissue was then lysed for 10 min on ice in 1 mL of lysis buffer consisting of $1 \times$ TruSeq Ribo Profile mammalian polysome buffer (Illumina), 1 % Triton X-100, 0.1 % NP-40, 1 Mm dithiothreitol, 10 U DNase I, 0.1 mg cycloheximide (Sigma, St. Louis, MO, USA) and nuclease-free H_2O to a final volume. The tissue was homogenized further by repeatedly passing the lysate through a 21 gauge syringe needle. For complete lysis, the sample was kept on ice for 15 min and subsequently centrifuged at $20,000 \times g$ for 10 min at $4^\circ C$ to precipitate cell and tissue debris. Next, 400–800 mL of the lysate was processed using the TruSeq Ribo Profile mammalian Library Preparation Kit (Illumina) exactly according to the supplier's protocol. The library size distributions were checked on the Bioanalyzer 2100 using a high sensitivity DNA assay (Agilent), while the Ribo-seq library was sequenced using the Illumina HiSeq 4000 platform (LC Sciences).

Raw data was demultiplexed using the CASAVA v1.8 pipeline and the 3' end adapter was removed using fastx_clipper (http://hannonlab.cshl.edu/fastx_toolkit/). Before mapping, the ribosome-profiling reads were filtered for mitochondrial, ribosomal RNA, and tRNA sequences, and subsequently aligned with the porcine reference genome using bowtie2 [86]. The reads that mapped to the genome that were derived from linear RNA were discarded, while the remaining unmapped reads potentially harboring junction reads of circRNAs were collected to identify ribosome-associated circRNA candidates according to a previous description [87]. In detail, we first extracted the exonic sequences surrounding the backsplice junction (50 bp on either side), and aligned all unmapped ribosome profiling reads (*i.e.*, Ribo-seq reads that could not be aligned to the linear transcriptome or genome) to the circRNA backsplice junctions using the BLASTn algorithm (<https://blast.ncbi.nlm.nih.gov/Blast.cgi>). We did not allow any mismatches and required a minimum read-junction overlap of 9 bp on either side of the junction.

4.6. Single-cell RNA sequencing preparation and computational analysis

The longissimus dorsi tissues isolated from three experimental individuals were immediately transferred to cold Dulbecco's phosphate-buffered saline (PBS; Thermo Fisher) and minced into pieces (~ 0.5 mm) on ice using scissors. The tissue pieces were pooled equally for each piglet breed and transferred to a 15 mL centrifuge tube, rinsed twice with cold PBS, and suspended in 5 mL of solution containing dissociation enzymes (0.35 % collagenase I, 2 mg/mL papain, 120 U/mL DNase I). During dissociation, the tissue pieces were pipetted up and down gently several times until no tissue fragments were visible. Enzyme activity was then inhibited by adding 5 mL of PBS supplemented with 10 % fetal calf serum (Life Technologies, Foster City, CA, USA). After passage through 70 μm and 30 μm strainers (Miltenyi Biotec, Bergisch Gladbach, Germany), the cells were washed twice, centrifuged at $300 \times g$ for 5 min at $4^\circ C$, and then treated with red blood cell lysis buffer (Thermo Fisher) and a Miltenyi Dead Cell Removal Kit (Miltenyi Biotec) following the manufacturer's procedure. The overall cell viability was confirmed using trypan blue exclusion (Thermo Fisher), while single cell suspensions were counted using a Countess II Automated Cell Counter (Thermo Fisher) and further diluted to a concentration of 700–1200 cells/mL for $10 \times$ Genomics sequencing using a Single-Cell v3 kit ($10 \times$ Genomics, San Francisco, CA, USA). The libraries were sequenced on a NovaSeq 6000 instrument (Illumina).

Sequencing datasets were demultiplexed and converted to the Fastq format using Illumina bcl2fastq software v2.20 (<https://support.illumina.com>). Sample demultiplexing, barcode processing, and single-cell 3' gene counting were carried out using Cell Ranger v3.1.0 (<https://www.10xgenomics.com/support>), and sequencing reads were then aligned against the *Sscrofa11.1* reference genome using STAR [88] to obtain the raw digital gene expression data matrices (DGE). Seurat [89] was used to perform clustering analysis of single-cell data with the DGE

data as inputs. In detail, we firstly filtered out cells with fewer than 500 detected transcripts, while cells with a mitochondrial transcript ratio of >25 % were also excluded using the PercentageFeatureSet function. Filtered data were applied to normalize the expression levels of identified genes using the NormalizeData function. Using the FindVariableGenes and ScaleData functions, about 2000 genes with an average expression of >0.01 and a dispersion >0.5 were used as inputs for initial principal component analysis (PCA). The number of principal components (PCs) generated from the RunPCA function were applied for nonlinear dimensional reduction analysis (t-SNE) using the JackStraw-Plot function. For clustering, we set different resolution parameters between 0.6 and 4 in the FindAllCluster function and narrowed down to certain cluster numbers by distinguishing differential genes among the clusters. The default Wilcoxon rank-sum test was used by running the FindAllMarkers function to detect differentially expressed markers in each cluster or between different breeds. Finally, we annotated each cell type by extensive literature reading and searching for their specific gene expression patterns. In addition, we performed trajectory analysis using Monocle2 [90] for various myocytes according to the general pipeline.

4.7. RNase R treatment

About 2 µg of total RNA extracted from porcine muscle tissues was incubated with 3 U/µg of RNase R (Epicentre Technologies, Madison, WI, USA) for 15 min at 37 °C. After treatment with RNase R, the treated RNA was further subjected to qRT-PCR detection, comprising reverse transcription to cDNA followed by detection of the expression levels of circRNAs and their host mRNAs using the quantitative real-time PCR (qPCR) step of the qRT-PCR protocol.

4.8. Oligo Dt (18T) primers and random hexamer primers amplification

The total RNAs of porcine muscle tissues were reverse transcribed using random hexamer primers and Oligo dT (18T) primers with a PrimeScript™ RT Reagent Kit with gDNA Eraser (Takara), respectively. The expression levels of circRNAs and their hosting mRNAs were then detected using qPCR.

4.9. Nuclear and cytoplasmic extraction

The cytoplasmic and nuclear fractions of porcine muscles were isolated using reagents supplied in the mirVana™ PARIS™ Kit (Invitrogen). In detail, the samples were treated with lysis buffer on ice for 10 min. After centrifugation at 500 ×g for 3 min at 4 °C, the supernatant was collected as the cytoplasmic fraction. The pellet was washed and the nuclei were collected. Total RNA in each fraction was extracted and subjected to qRT-PCR analysis to detect the level of nuclear control transcript (U6), cytoplasmic control transcript (ACTB, encoding β-actin), and circKANS1L1L.

4.10. Fluorescence in situ hybridization (FISH)

The 5'-Cy3-labeled probe sequence for circKANS1L1L was synthesized by Sangon Biotech (Shanghai, China). The experiment was performed using a Fluorescence *In situ* Hybridization Kit (RiboBio, Guangzhou, China) according to the manufacturer's instructions. The oligonucleotide-modified probes targeting the reverse splice site of circKANS1L1L were used to determine its subcellular localization. Images were acquired using a Zeiss LSM 710 laser scanning confocal microscope system (Zeiss, Oberkochen, Germany).

4.11. Vector construction and RNA oligonucleotides

The linear sequence of circKANS1L1L was cloned into vector pCD2.1-ciR (Genesee Biotech, Guangzhou, China), named as pCD2.1-ciR-circKANS1L1L, and the empty pCD2.1-ciR vector was used as the

negative control. The circKANS1L1L-si-1 and circKANS1L1L-si-2 targeting circKANS1L1L junction sites and the negative control siRNA were designed and synthesized by GenePharma Co., Ltd. (Shanghai, China). The linear sequence of the ORF present in circKANS1L1L was cloned into vector pCDNA3.1 (Invitrogen), with a sequence encoding 3 × Flag tags placed before the stop codon, named as Flag-KANS1L1L-551aa; the pCDNA3.1 empty vector was used as the corresponding negative control.

4.12. Cell culture and treatment

C2C12 cells (mouse myoblasts) were purchased from the China National Collection of Authenticated Cell Cultures (Beijing, China). When the cells reached approximately 60 % confluence, they were transfected with the overexpression vector, knockdown vector, and their negative controls using Lipofectamine 2000 (Invitrogen). The transfected cells were harvested for protein and RNA analysis after 48 h to study cell proliferation, and switched to differentiation medium and cultured for 48 and 96 h to study cell differentiation.

4.13. 5-ethynyl-2'-deoxyuridine (EdU) staining and flow cytometry assay

C2C12 cells were inoculated into 48-well plates and transfected with pCD2.1-ciR-circKANS1L1L or circKANS1L1L-si. After 48 h, a Beyoclick™ Edu-488 Kit (Biyuntian Biotechnology, Shanghai, China) was used to detect cell proliferation. The results were observed and photographed under a fluorescence microscope (Nikon, Tokyo, Japan), and further analyzed using Image J software (Media Cybernetic). For the flow cytometry assay, the cells were collected, fixed with 75 % ethanol, and stored overnight at −20 °C. Next day, the cells were resuspended in 500 µL of propidium iodide (PI)/RNase staining buffer solution (BD Biosciences, Franklin Lakes, NJ, USA) and incubated at 37 °C for 30 min. A BD Accuri C6 flow cytometer and FACSDiVa software (BD Biosciences) were used to perform the flow cytometry analysis.

4.14. Western blotting

The muscle tissues and C2C12 cells were lysed in Radio-immunoprecipitation assay (RIPA) lysis buffer (Solarbio, Beijing, China) to collect cell total proteins. Identical quantities of proteins were separated using SDS-PAGE and then transferred onto polyvinylidene fluoride (PVDF) membranes (Millipore, Bedford, MA). After incubation with the corresponding primary antibodies, the membranes were incubated with goat anti-rabbit IgG-horseradish peroxidase (HRP) or goat anti-mouse IgG-HRP (Biorworld, Minneapolis, MN, USA). Enhanced chemiluminescence solution (Solarbio Life Sciences) was used to visualize the immunoreactive protein bands.

4.15. Cellular immunofluorescence

The C2C12 cells were inoculated into 12-well plates, transfected with pCD2.1-ciR-circKANS1L1L or circKANS1L1L-si, and then cultured for 96 h of differentiation. The cells were washed in ice-cold PBS before being fixed in 4 % paraformaldehyde. Then, the samples were permeabilized and blocked with blocking solution (PBS, 5 % goat serum, and 0.2 % Triton X-100) for 1 h at room temperature before being incubated overnight at 4 °C with anti-MyHC primary antibodies (R&D Systems, Minneapolis, MN, USA). Samples were washed with PBS and incubated for 2 h at room temperature with secondary fluorescent conjugated anti-mouse antibodies and nuclei were counterstained using Hoechst 33342. The wells were washed with PBS and then covered with PBS containing 10 % glycerol before imaging. A fluorescence inverted microscope (Nikon) equipped with an RGB digital camera was used for microscopic examination, while the images were taken under a 20× objective. Image J software (Media Cybernetics) was used to analyze the images.

4.16. Lentivirus production and transduction

The short hairpin (sh) RNA sequence against circKANS1L1-si-1 was cloned into pshRNA-copGFP lentivector for LV-sh-circKANS1L1 construction. Then, LV-sh-circKANS1L1, psPAX2, and pMD2.G were co-transfected into 293T cells using Lipofectamine 2000 (Invitrogen). At 48 and 72 h after transfection, the virus supernatant was collected and concentrated for titer determination. The C57BL/6 mice (6-week-old) were infected with lentiviruses (10^7 U/ μ L, 100 μ L per mouse) by direct injection into the tibialis anterior (TA) muscles.

4.17. Statistical analysis

The differences in the experimental data between two groups were assessed using analysis of variance followed by Student's *t*-test. A value of $P < 0.05$ was considered statistically significant, and was denoted with 1, 2, or 3 asterisks when lower than 0.05, 0.01, or 0.001, respectively. Statistical analysis was performed using GraphPad Prism 9.5 software (GraphPad Software Inc., San Diego, CA, USA).

Supplementary data to this article can be found online at <https://doi.org/10.1016/j.ijbiomac.2023.128609>.

CRediT authorship contribution statement

ZL, FX and XH gathered samples, and conducted the experiments; JW, JL, TC, QJ, QX, and YZ conceived the study and improved the manuscript; JS conceived the study, performed data analysis, and drafted the manuscript. All authors have read and approved the final version of the manuscript.

Funding

This work was supported by the Open Project Program of State Key Laboratory of Swine and Poultry Breeding Industry [2023GZ20]; the Natural Science Foundation of China Program [grant numbers 32072714, 31802032]; the Natural Science Foundation of Guangdong Province [grant number 2020A1515010062]; and the Science and Technology Project of Guangzhou [grant number 202002030037].

Declaration of competing interest

The authors declare that they have no known competing financial interests or personal relationships that could have appeared to influence the work reported in this paper.

Data availability

Data will be made available on request.

Acknowledgements

We thank the High Performance Computing Center of South China Agricultural University for providing computational resources in this work.

References

- [1] O. Hernández-Hernández, R.D. Ávila-Avilés, J.M. Hernández-Hernández, Chromatin landscape during skeletal muscle differentiation, *Front. Genet.* 11 (2020), 578712, <https://doi.org/10.3389/fgene.2020.578712>.
- [2] M. Widmann, A.M. Nieß, B. Munz, Physical Exercise and Epigenetic Modifications in Skeletal Muscle. *Sports Medicine* (Auckland, N.Z.) vol. 49, 2019, pp. 509–523, <https://doi.org/10.1007/s40279-019-01070-4>.
- [3] M. Hargreaves, L.L. Spriet, Skeletal muscle energy metabolism during exercise, *Nat. Metab.* 2 (2020) 817–828, <https://doi.org/10.1038/s42255-020-0251-4>.
- [4] S.K. Matarneh, S.L. Silva, D.E. Gerrard, New insights in muscle biology that alter meat quality, *Ann. Rev. Anim. Biosci.* 9 (2021) 355–377, <https://doi.org/10.1146/annurev-animal-021419-083902>.
- [5] B. Yue, H. Yang, J. Wu, J. Wang, W. Ru, J. Cheng, et al., circSVIL regulates bovine myoblast development by inhibiting STAT1 phosphorylation, *Sci. China Life Sci.* 65 (2022) 376–386, <https://doi.org/10.1007/s11427-020-1908-2>.
- [6] A. Das, A. Das, D. Das, K. Abdelmohsen, A.C. Panda, Circular RNAs in myogenesis. *Biochimica et biophysica acta, Gene Regulat. Mech.* 1863 (2020), 194372, <https://doi.org/10.1016/j.bbaggm.2019.02.011>.
- [7] L.S. Kristensen, M.S. Andersen, L. Stagsted, K.K. Ebbesen, T.B. Hansen, J. Kjems, The biogenesis, biology and characterization of circular RNAs, *Nat. Rev. Genet.* 20 (2019) 675–691, <https://doi.org/10.1038/s41576-019-0158-7>.
- [8] J.U. Guo, V. Agarwal, H. Guo, D.P. Bartel, Expanded identification and characterization of mammalian circular RNAs, *Genome Biol.* 15 (2014) 409, <https://doi.org/10.1186/s13059-014-0409-z>.
- [9] B. Li, D. Yin, P. Li, Z. Zhang, X. Zhang, H. Li, et al., Profiling and functional analysis of circular RNAs in porcine fast and slow muscles, *Front. Cell Dev. Biol.* 8 (2020) 322, <https://doi.org/10.3389/fcell.2020.00322>.
- [10] D.W. Thomson, M.E. Dinger, Endogenous microRNA sponges: evidence and controversy, *Nat. Rev. Genet.* 17 (2016) 272–283, <https://doi.org/10.1038/nrg.2016.20>.
- [11] C.J. Ulshöfer, C. Pfaffenrot, A. Bindereif, T. Schneider, Methods to study circRNA-protein interactions, *Methods (San Diego, Calif.)* 196 (2021) 36–46, <https://doi.org/10.1016/j.ymeth.2021.04.014>.
- [12] X.O. Zhang, H.B. Wang, Y. Zhang, X. Lu, L.L. Chen, L. Yang, Complementary sequence-mediated exon circularization, *Cell* 159 (2014) 134–147, <https://doi.org/10.1016/j.cell.2014.09.001>.
- [13] Y. Shi, X. Jia, J. Xu, The new function of circRNA: translation, *Clin. Transl. Oncol.* 22 (2020) 2162–2169, <https://doi.org/10.1007/s12094-020-02371-1>.
- [14] T. Sinha, C. Panigrahi, D. Das, Panda A. Chandra, Circular RNA translation, a path to hidden proteome, *Wiley Interdiscip. Rev. RNA* 13 (2022), e1685, <https://doi.org/10.1002/wrna.1685>.
- [15] S. Yan, Z. Tu, Z. Liu, N. Fan, H. Yang, S. Yang, et al., A Huntingtin Knockin Pig Model recapitulates features of selective neurodegeneration in Huntington's disease, *Cell* 173 (2018) 989–1002.e13, <https://doi.org/10.1016/j.cell.2018.03.005>.
- [16] X. Gao, M. Nowak-Imialek, X. Chen, D. Chen, D. Herrmann, D. Ruan, et al., Establishment of porcine and human expanded potential stem cells, *Nat. Cell Biol.* 21 (2019) 687–699, <https://doi.org/10.1038/s41556-019-0333-2>.
- [17] J. Sun, M. Xie, Z. Huang, H. Li, T. Chen, R. Sun, et al., Integrated analysis of non-coding RNA and mRNA expression profiles of 2 pig breeds differing in muscle traits, *J. Anim. Sci.* 95 (2017) 1092–1103, <https://doi.org/10.2527/jas.2016.0867>.
- [18] J. Li, L. Luu, X. Wang, X. Cui, X. Huang, J. Fu, et al., Metabolomic analysis reveals potential biomarkers and the underlying pathogenesis involved in Mycoplasma pneumoniae pneumonia, *Emerg. Microb. Infect.* 11 (2022) 593–605, <https://doi.org/10.1080/22221751.2022.2036582>.
- [19] Z. Yang, M. Jiang, Z. Yue, P. Wang, H. Wang, G. Zhang, et al., Metabonomics analysis of semen euphorbiae and semen Euphorbiae Pulveratum using UPLC-Q-TOF/MS, *Biomed. Chromatogr.* 36 (2022), e5279, <https://doi.org/10.1002/bmc.5279>.
- [20] B.B. Misra, E. Bassey, A.C. Bishop, D.T. Kusel, L.A. Cox, M. Olivier, High-resolution gas chromatography/mass spectrometry metabolomics of non-human primate serum, *Rapid Commun. Mass Spectr.* RCM 32 (2018) 1497–1506, <https://doi.org/10.1002/rcm.8197>.
- [21] S. Dell'Orso, A.H. Juan, K.D. Ko, F. Naz, J. Perovanovic, G. Gutierrez-Cruz, et al., Single cell analysis of adult mouse skeletal muscle stem cells in homeostatic and regenerative conditions, *Development (Cambridge, England)* 146 (2019), dev174177, <https://doi.org/10.1242/dev.174177>.
- [22] L. Giordani, G.J. He, E. Negroni, H. Sakai, J.Y.C. Law, M.M. Siu, et al., High-dimensional single-cell cartography reveals novel skeletal muscle-resident cell populations, *Mol. Cell* 74 (2019) 609–621, <https://doi.org/10.1016/j.molcel.2019.02.026>.
- [23] J. Saber, A. Lin, M.A. Rudnicki, Single-cell analyses uncover granularity of muscle stem cells, *F1000Research* 9:F1000 Faculty Rev-31 (2020), <https://doi.org/10.12688/f1000research.20856.1>.
- [24] A.F. Rosa, C.T. Moncau, M.D. Poletti, L.D. Fonseca, J. Balieiro, S. Silva, et al., Proteome changes of beef in Nellore cattle with different genotypes for tenderness, *Meat Sci.* 138 (2018) 1–9, <https://doi.org/10.1016/j.meatsci.2017.12.006>.
- [25] A.J. De Micheli, E.J. Laurillard, C.L. Heinke, H. Ravichandran, P. Fraczek, S. Soueïd-Baumgarten, et al., Single-cell analysis of the muscle stem cell hierarchy identifies heterotypic communication signals involved in skeletal muscle regeneration, *Cell Rep.* 30 (2020) 3583–3595, <https://doi.org/10.1016/j.celrep.2020.02.067>.
- [26] J. Chal, O. Pourquie, Making muscle: skeletal myogenesis in vivo and in vitro, *Development* 144 (2017) 2104–2122, <https://doi.org/10.1242/dev.151035>.
- [27] J. Li, S. Xing, G. Zhao, M. Zheng, X. Yang, J. Sun, et al., Identification of diverse cell populations in skeletal muscles and biomarkers for intramuscular fat of chicken by single-cell RNA sequencing, *BMC Genomics* 21 (2020) 752, <https://doi.org/10.1186/s12864-020-07136-2>.
- [28] D. Cacchiarelli, X. Qiu, S. Srivatsan, A. Manfredi, M. Ziller, E. Overbey, et al., Aligning single-cell developmental and reprogramming trajectories identifies molecular determinants of myogenic reprogramming outcome, *Cell Syst.* 7 (2018) 258–268, <https://doi.org/10.1016/j.cels.2018.07.006>.
- [29] S. Choi, H.J. Jeong, H. Kim, D. Choi, S.C. Cho, J.K. Seong, et al., Skeletal muscle-specific Prmt1 deletion causes muscle atrophy via deregulation of the PRMT6-FOXO3 axis, *Autophagy* 15 (2019) 1069–1081, <https://doi.org/10.1080/15548627.2019.1569931>.
- [30] G.D. Kim, Y.C. Ryu, J.Y. Jeong, H.S. Yang, S.T. Joo, Relationship between pork quality and characteristics of muscle fibers classified by the distribution of myosin

- heavy chain isoforms, *J. Anim. Sci.* 91 (2013) 5525–5534, <https://doi.org/10.2527/jas.2013-6614>.
- [31] K.C. Chang, N. da Costa, R. Blackley, O. Southwood, G. Evans, G. Plastow, et al., Relationships of myosin heavy chain fibre types to meat quality traits in traditional and modern pigs, *Meat Sci.* 64 (2003) 93–103, [https://doi.org/10.1016/s0309-1740\(02\)00208-5](https://doi.org/10.1016/s0309-1740(02)00208-5).
- [32] D. Rakus, A. Gizak, A. Deshmukh, J.R. Wiśniewski, Absolute quantitative profiling of the key metabolic pathways in slow and fast skeletal muscle, *J. Proteome Res.* 14 (2015) 1400–1411, <https://doi.org/10.1021/pr5010357>.
- [33] S.T. Joo, G.D. Kim, Y.H. Hwang, Y.C. Ryu, Control of fresh meat quality through manipulation of muscle fiber characteristics, *Meat Sci.* 95 (2013) 828–836, <https://doi.org/10.1016/j.meatsci.2013.04.044>.
- [34] M.P. Fabrice, S. Ghidini, M. Conter, M.O. Varrà, A. Ianieri, E. Zanardi, Filling gaps in animal welfare assessment through metabolomics, *Front. Vet. Sci.* 10 (2023) 1129741, <https://doi.org/10.3389/fvets.2023.1129741>.
- [35] L. Deng, W. Li, W. Liu, Y. Liu, B. Xie, M.A.M. Groenen, et al., Integrative metabolomic and transcriptomic analysis reveals difference in glucose and lipid metabolism in the longissimus muscle of Luchuan and Duroc pigs, *Front. Genet.* 14 (2023) 1128033, <https://doi.org/10.3389/fgene.2023.1128033>.
- [36] T. Wang, Y.Q. Xu, Y.X. Yuan, P.W. Xu, C. Zhang, F. Li, et al., Succinate induces skeletal muscle fiber remodeling via SUCNR1 signaling, *EMBO Rep.* 22 (2021), e53027, <https://doi.org/10.15252/embr.202153027>.
- [37] D. Antonelo, J.F. Gómez, N.R. Consolo, M. Beline, L.A. Colnago, W. Schilling, et al., Metabolites and metabolic pathways correlated with beef tenderness, *Meat Muscle Biol.* (2020) 4, <https://doi.org/10.22175/mmb.10854>.
- [38] Y.H. Hwang, G.D. Kim, J.Y. Jeong, S.J. Hur, S.T. Joo, The relationship between muscle fiber characteristics and meat quality traits of highly marbled Hanwoo (Korean native cattle) steers, *Meat Sci.* 86 (2010) 456–461, <https://doi.org/10.1016/j.meatsci.2010.05.034>.
- [39] G.D. Kim, M.F. Overholt, J.E. Lowell, B.N. Harsh, B.J. Klehm, A.C. Dilger, et al., Evaluation of muscle fiber characteristics based on muscle fiber volume in porcine longissimus muscle in relation to pork quality, *Meat Muscle Biol.* (2018) 2, <https://doi.org/10.22175/mmb2018.07.0018>.
- [40] M. Kim, Y. Zhang, C. Birchmeier, Fructose 1, 6-bisphosphate sensing by pyruvate kinase isozymes M2 (PKM2) controls MyoD stability and myogenic differentiation, *bioRxiv* (2020) 12, <https://doi.org/10.1101/2020.12.22.424062>.
- [41] X. Li, C.Y. Wang, From bulk, single-cell to spatial RNA sequencing, *Int. J. Oral Sci.* 13 (2021) 36, <https://doi.org/10.1038/s41368-021-00146-0>.
- [42] G. Chen, B. Ning, T. Shi, Single-cell RNA-Seq technologies and related computational data analysis, *Front. Genet.* 10 (2019) 317, <https://doi.org/10.3389/fgene.2019.00317>.
- [43] A.B. Rubenstein, G.R. Smith, U. Raue, G. Begue, K. Minchev, F. Ruf-Zamojski, et al., Single-cell transcriptional profiles in human skeletal muscle, *Sci. Rep.* 10 (2020) 229, <https://doi.org/10.1038/s41598-019-57110-6>.
- [44] C. Cai, P. Wan, H. Wang, X. Cai, J. Wang, Z. Chai, et al., Transcriptional and open chromatin analysis of bovine skeletal muscle development by single-cell sequencing, *Cell Prolif.* 1 (2023), e13430. Advance online publication. <https://doi.org/10.1111/cpr.13430>.
- [45] J.J. Wu, S. Zhu, F. Gu, T.G. Valencak, J.X. Liu, H.Z. Sun, Cross-tissue single-cell transcriptomic landscape reveals the key cell subtypes and their potential roles in the nutrient absorption and metabolism in dairy cattle, *J. Adv. Res.* 37 (2021) 1–18, <https://doi.org/10.1016/j.jare.2021.11.009>.
- [46] S. Cai, B. Hu, X. Wang, T. Liu, Z. Lin, X. Tong, et al., Integrative single-cell RNA-seq and ATAC-seq analysis of myogenic differentiation in pig, *BMC Biol.* 21 (2023) 19, <https://doi.org/10.1186/s12915-023-01519-z>.
- [47] L. Lehka, M.J. Redowicz, Mechanisms regulating myoblast fusion: a multilevel interplay, *Semin. Cell Dev. Biol.* 104 (2020) 81–92, <https://doi.org/10.1016/j.semcdb.2020.02.004>.
- [48] J. Wu, N. Matthias, J. Lo, J.L. Ortiz-Vitali, A.W. Shieh, S.H. Wang, et al., A myogenic double-reporter human pluripotent stem cell line allows prospective isolation of skeletal muscle progenitors, *Cell Rep.* 25 (2018) 1966–1981, <https://doi.org/10.1016/j.celrep.2018.10.067>.
- [49] M. Ganassi, S. Badodi, K. Wanders, P.S. Zammit, S.M. Hughes, Myogenin is an essential regulator of adult myofibre growth and muscle stem cell homeostasis, *eLife* 9 (2020), e60445, <https://doi.org/10.7554/eLife.60445>.
- [50] D.N. Gross, M. Wan, M.J. Birnbaum, The role of FOXO in the regulation of metabolism, *Curr. Diab. Rep.* 9 (2009) 208–214, <https://doi.org/10.1007/s11892-009-0034-5>.
- [51] X. Zhang, N. Tang, T.J. Hadden, A.K. Rishi, Akt, FoxO and regulation of apoptosis, *Biochim. Biophys. Acta* 1813 (2011) 1978–1986, <https://doi.org/10.1016/j.bbamcr.2011.03.010>.
- [52] A.M. Sanchez, R.B. Candau, H. Bernardi, FoxO transcription factors: their roles in the maintenance of skeletal muscle homeostasis, *Cell. Mol. Life Sci.* 71 (2014) 1657–1671, <https://doi.org/10.1007/s00018-013-1513-z>.
- [53] D. Pette, R.S. Staron, Transitions of muscle fiber phenotypic profiles, *Histochem. Cell Biol.* 115 (2001) 359–372, <https://doi.org/10.1007/s004180100268>.
- [54] P. Zhang, Z. Chao, R. Zhang, R. Ding, Y. Wang, W. Wu, et al., Circular RNA regulation of myogenesis, *Cells* 8 (2019) 885, <https://doi.org/10.3390/cells8080885>.
- [55] D. Tsitsipatis, K. Mazan-Mamczarz, Y. Si, A.B. Herman, J.H. Yang, A. Guha, et al., Transcriptomic analysis of human ALS skeletal muscle reveals a disease-specific pattern of dysregulated circRNAs, *Aging* 14 (2022) 9832–9859, <https://doi.org/10.18632/aging.204450>.
- [56] K. Abdelmohsen, A.C. Panda, S. De, I. Grammatikakis, J. Kim, J. Ding, et al., Circular RNAs in monkey muscle: age-dependent changes, *Aging* 7 (2015) 903–910, <https://doi.org/10.18632/aging.100834>.
- [57] M. Guo, J. Qiu, F. Shen, S. Wang, J. Yu, H. Zuo, et al., Comprehensive analysis of circular RNA profiles in skeletal muscles of aging mice and after aerobic exercise intervention, *Aging* 12 (2020) 5071–5090, <https://doi.org/10.18632/aging.102932>.
- [58] R. Liu, X. Liu, X. Bai, C. Xiao, Y. Dong, Identification and characterization of circRNA in longissimus dorsi of different breeds of cattle, *Front. Genet.* 11 (2020), 565085.
- [59] K. Huang, M. Chen, D. Zhong, X. Luo, T. Feng, M. Song, et al., Circular RNA profiling reveals an abundant circEch1 that promotes myogenesis and differentiation of bovine skeletal muscle, *J. Agric. Food Chem.* 69 (2021) 592–601, <https://doi.org/10.1021/acs.jafc.0c06400>.
- [60] C. Huang, F. Ge, X. Ma, R. Dai, R. Dingkao, Z. Zhaxi, et al., Comprehensive analysis of mRNA, lncRNA, circRNA, and miRNA expression profiles and their ceRNA networks in the Longissimus dorsi muscle of cattle-yak and yak, *Front. Genet.* 12 (2021), 772557, <https://doi.org/10.3389/fgene.2021.772557>.
- [61] J. Shen, H. Zhen, L. Li, Y. Zhang, J. Wang, J. Hu, et al., Identification and characterization of circular RNAs in Longissimus dorsi muscle tissue from two goat breeds using RNA-Seq, *Molec. Gen. Genom.* 297 (2022) 817–831, <https://doi.org/10.1007/s00438-022-01887-1>.
- [62] A. Robic, C. Cerutti, C. Kühn, T. Faraut, Comparative analysis of the circular transcriptome in muscle, liver, and testis in three livestock species, *Front. Genet.* 12 (2021), 665153, <https://doi.org/10.3389/fgene.2021.665153>.
- [63] K. Du, X. Zhao, Y. Li, Z. Wu, W. Sun, J. Wang, et al., Genome-wide identification and characterization of circular RNAs during skeletal muscle development in meat rabbits, *Animals* 12 (2022) 2208, <https://doi.org/10.3390/ani12172208>.
- [64] P. Wu, K. Zhou, J. Zhang, X. Ling, X. Zhang, L. Zhang, et al., Identification of crucial circRNAs in skeletal muscle during chicken embryonic development, *BMC Genomics* 23 (2022) 330, <https://doi.org/10.1186/s12864-022-08588-4>.
- [65] J. Liu, S. Liu, W. Zhang, X. Hu, H. Mao, S. Liu, et al., Transcriptome RNA sequencing reveals that circular RNAs are abundantly expressed in embryonic breast muscle of duck, *Vet. Sci.* 10 (2023) 75, <https://doi.org/10.3390/vetsci10020075>.
- [66] J. Chen, S. Zhang, G. Chen, X. Deng, D. Zhang, H. Wen, et al., Transcriptome sequencing reveals pathways related to proliferation and differentiation of Shitou goose myoblasts, *Animals* 12 (2022) 2956, <https://doi.org/10.3390/ani12212956>.
- [67] C. Wang, S. Tan, W.R. Liu, Q. Lei, W. Qiao, Y. Wu, et al., RNA-Seq profiling of circular RNA in human lung adenocarcinoma and squamous cell carcinoma, *Mol. Cancer* 18 (2019) 134, <https://doi.org/10.1186/s12943-019-1061-8>.
- [68] X. Zhuang, Z. Lin, F. Xie, J. Luo, T. Chen, Q. Xi, et al., Identification of circRNA-associated ceRNA networks using longissimus thoracis of pigs of different breeds and growth stages, *BMC Genomics* 23 (2022) 294, <https://doi.org/10.1186/s12864-022-08515-7>.
- [69] M. Zhang, K. Zhao, X. Xu, Y. Yang, S. Yan, P. Wei, et al., A peptide encoded by circular form of LINC-PINT suppresses oncogenic transcriptional elongation in glioblastoma, *Nat. Commun.* 9 (2018) 4475, <https://doi.org/10.1038/s41467-018-06862-2>.
- [70] C. Gu, N. Zhou, Z. Wang, G. Li, Y. Kou, S. Yu, et al., circGprc5a promoted bladder oncogenesis and metastasis through Gprc5a-targeting peptide, *Molec. Ther. Nucleic Acids* 13 (2018) 633–641, <https://doi.org/10.1016/j.omtn.2018.10.008>.
- [71] Y. Lyu, B. Tan, L. Li, R. Liang, K. Lei, K. Wang, et al., A novel protein encoded by circUBE4B promotes progression of esophageal squamous cell carcinoma by augmenting MAPK/ERK signaling, *Cell Death Dis.* 14 (2023) 346, <https://doi.org/10.1038/s41419-023-05865-2>.
- [72] C.A. Smith, E.J. Want, G. O'Maille, R. Abagyan, G. Siuzdak, XCMS: processing mass spectrometry data for metabolite profiling using nonlinear peak alignment, matching, and identification, *Anal. Chem.* 78 (2006) 779–787, <https://doi.org/10.1021/ac051437y>.
- [73] C. Kuhl, R. Tautenhahn, C. Böttcher, T.R. Larson, S. Neumann, CAMERA: an integrated strategy for compound spectra extraction and annotation of liquid chromatography/mass spectrometry data sets, *Anal. Chem.* 84 (2012) 283–289, <https://doi.org/10.1021/ac202450g>.
- [74] B. Wen, Z. Mei, C. Zeng, S. Liu, metaX: a flexible and comprehensive software for processing metabolomics data, *BMC Bioinforma.* 18 (2017) 183, <https://doi.org/10.1186/s12859-017-1579-y>.
- [75] C. Trapnell, A. Roberts, L. Goff, G. Pertea, D. Kim, D.R. Kelley, et al., Differential gene and transcript expression analysis of RNA-seq experiments with TopHat and Cufflinks, *Nat. Protoc.* 7 (2012) 562–578, <https://doi.org/10.1038/nprot.2012.016>.
- [76] D. Kim, S.L. Salzberg, TopHat-fusion: an algorithm for discovery of novel fusion transcripts, *Genome Biol.* 12 (2011) R72, <https://doi.org/10.1186/gb-2011-12-8-r72>.
- [77] X.O. Zhang, R. Dong, Y. Zhang, J.L. Zhang, Z. Luo, J. Zhang, et al., Diverse alternative back-splicing and alternative splicing landscape of circular RNAs, *Genome Res.* 26 (2016) 1277–1287, <https://doi.org/10.1101/gr.202895.115>.
- [78] F. Xing, R. Liu, Circrnafinder: A tool for identifying circular RNAs using RNA-Seq data, in: *The 6th International Conference on Bioinformatics and Computational Biology (BICOB-2014)*, 2014.
- [79] Y. Gao, J. Wang, F. Zhao, CIRI: an efficient and unbiased algorithm for de novo circular RNA identification, *Genome Biol.* 16 (2015) 4, <https://doi.org/10.1186/s13059-014-0571-3>.
- [80] S. Memczak, M. Jens, A. Elefsinioti, F. Torti, J. Krueger, A. Rybak, et al., Circular RNAs are a large class of animal RNAs with regulatory potency, *Nature* 495 (2013) 333–338, <https://doi.org/10.1038/nature11928>.
- [81] K. Wang, D. Singh, Z. Zeng, S.J. Coleman, Y. Huang, G.L. Savich, et al., MapSplice: accurate mapping of RNA-seq reads for splice junction discovery, *Nucleic Acids Res.* 38 (2010), e178, <https://doi.org/10.1093/nar/gkq622>.


- [82] Y.J. Kang, D.C. Yang, L. Kong, M. Hou, Y.Q. Meng, L. Wei, et al., CPC2: a fast and accurate coding potential calculator based on sequence intrinsic features, *Nucleic Acids Res.* 45 (2017) W12–W16, <https://doi.org/10.1093/nar/gkx428>.
- [83] L. Wang, H.J. Park, S. Dasari, S. Wang, J.P. Kocher, W. Li, CPAT: coding-potential assessment tool using an alignment-free logistic regression model, *Nucleic Acids Res.* 41 (2013), e74, <https://doi.org/10.1093/nar/gkt006>.
- [84] L. Sun, H. Luo, D. Bu, G. Zhao, K. Yu, C. Zhang, et al., Utilizing sequence intrinsic composition to classify protein-coding and long non-coding transcripts, *Nucleic Acids Res.* 41 (2013), e166, <https://doi.org/10.1093/nar/gkt646>.
- [85] J. Mistry, S. Chuguransky, L. Williams, M. Qureshi, G.A. Salazar, E. Sonnhammer, et al., Pfam: the protein families database in 2021, *Nucleic Acids Res.* 49 (2021) D412–D419, <https://doi.org/10.1093/nar/gkaa913>.
- [86] B. Langmead, S.L. Salzberg, Fast gapped-read alignment with Bowtie 2, *Nat. Methods* 9 (2012) 357–359, <https://doi.org/10.1038/nmeth.1923>.
- [87] S. van Heesch, F. Witte, V. Schneider-Lunitz, J.F. Schulz, Faber A.B. AdamiE, et al., The translational landscape of the human heart, *Cell* 178 (2019) 242–260, <https://doi.org/10.1016/j.cell.2019.05.010>.
- [88] A. Dobin, C.A. Davis, F. Schlesinger, J. Drenkow, C. Zaleski, S. Jha, et al., STAR: ultrafast universal RNA-seq aligner, *Bioinformatics* (Oxford, England) 29 (2013) 15–21, <https://doi.org/10.1093/bioinformatics/bts635>.
- [89] A. Butler, P. Hoffman, P. Smibert, E. Papalexi, R. Satija, Integrating single-cell transcriptomic data across different conditions, technologies, and species, *Nat. Biotechnol.* 36 (2018) 411–420, <https://doi.org/10.1038/nbt.4096>.
- [90] X. Qiu, Q. Mao, Y. Tang, L. Wang, R. Chawla, H.A. Pliner, et al., Reversed graph embedding resolves complex single-cell trajectories, *Nat. Methods* 14 (2017) 979–982, <https://doi.org/10.1038/nmeth.4402>.

RESEARCH

Open Access



A novel protein encoded by porcine circANKRD17 activates the PPAR pathway to regulate intramuscular fat metabolism

Xiao He^{1†}, Fang Xie^{1†}, Ying Nie¹, Xuefeng Wang¹, Junyi Luo¹, Ting Chen¹, Qianyun Xi¹, Yongliang Zhang¹ and Jiajie Sun^{1*} 

Abstract

Background Intramuscular fat is an important factor in evaluating pork quality and varies widely among different pig breeds. However, the regulatory mechanism of circular RNAs (circRNAs) in lipid metabolism remains largely unexplored.

Results We combined circRNA-seq and Ribo-seq data to screen a total of 18 circRNA candidates with coding potential, and circANKRD17 was found to be significantly elevated in the longissimus dorsi muscle of Lantang piglets, with a length of 1,844 nucleotides. Using single-cell sequencing, we identified 477 differentially expressed genes in IMF cells between Lantang and Landrace piglets, with enrichment in the PPAR signaling pathway. These genes included *FABP4*, *FABP5*, *CPT1A*, and *UBC*, consistent with the high levels of acylcarnitines observed in the longissimus dorsi muscles of the Lantang breed, as determined by lipidomic analysis. Further in vitro and in vivo experiments indicated that circANKRD17 can regulate lipid metabolism through various mechanisms involving the PPAR pathway, including promoting adipocyte differentiation, fatty acid transport and metabolism, triglyceride synthesis, and lipid droplet formation and maturation. In addition, we discovered that circANKRD17 has an open reading frame and can be translated into a novel 571-amino-acid protein that promotes lipid metabolism.

Conclusions Our research provides new insights into the role of protein-coding circANKRD17, especially concerning the metabolic characteristics of pig breeds with higher intramuscular fat content.

Keywords CircRNAs, Intramuscular fat, Meat quality, PPAR pathway

[†]Xiao He and Fang Xie contributed equally to this work.

*Correspondence:

Jiajie Sun

jiajiesun@scau.edu.cn

¹ Guangdong Provincial Key Laboratory of Animal Nutrition Control, National Engineering Research Center for Breeding Swine Industry, State Key Laboratory of Swine and Poultry Breeding Industry, College of Animal Science, South China Agricultural University, Guangzhou, Guangdong 510642, China



© The Author(s) 2025. **Open Access** This article is licensed under a Creative Commons Attribution 4.0 International License, which permits use, sharing, adaptation, distribution and reproduction in any medium or format, as long as you give appropriate credit to the original author(s) and the source, provide a link to the Creative Commons licence, and indicate if changes were made. The images or other third party material in this article are included in the article's Creative Commons licence, unless indicated otherwise in a credit line to the material. If material is not included in the article's Creative Commons licence and your intended use is not permitted by statutory regulation or exceeds the permitted use, you will need to obtain permission directly from the copyright holder. To view a copy of this licence, visit <http://creativecommons.org/licenses/by/4.0/>. The Creative Commons Public Domain Dedication waiver (<http://creativecommons.org/publicdomain/zero/1.0/>) applies to the data made available in this article, unless otherwise stated in a credit line to the data.

Introduction

Intramuscular fat (IMF) is a key indicator for evaluating pork quality [1] as it is closely linked to sensory qualities, such as color, flavor, tenderness [2], and marbling [3]. In general, the IMF content varies among different pig breeds [4]. Compared to western commercial pigs, Chinese local pigs have higher IMF content and better meat quality [5]. Specifically, Lantang (LT, a typical fatty pig breed) has fine marbling and high IMF, resulting in significantly superior meat quality compared to the Landrace (LW, a typical lean meat breed) [6]. In addition, the physiology and structure of pigs are similar to those of humans, making them excellent models for studying fat metabolism [7], thereby enabling more in-depth research into related diseases such as human obesity and insulin resistance [8].

In recent, several studies indicate that non-coding RNAs (ncRNAs), including microRNAs (miRNAs), long non-coding RNAs (lncRNAs), and circRNAs, are potential regulators of IMF, participating in the regulation of animal fat deposition processes [9]. In general, circRNAs are covalently closed RNA molecules generated through a process known as back-splicing. They are widely present in eukaryotic cells without a 5' cap structure or 3' polyA tail [10] and are composed of one or multiple exons [11]; circRNAs have long been considered functional RNAs that directly participate in various biological processes [12]. Previously, circRNAs were primarily studied for their non-coding functions, such as acting as miRNA sponges [13], participating in parental gene transcription [14], and interacting with proteins [15]. However, recent studies have found that circRNAs can directly code for proteins, as many of them contain translatable open reading frames (ORFs) [16]. Most endogenous circRNAs rely on Internal Ribosome Entry Sites (IRES) and N⁶-methyladenosine (m⁶A) modifications to initiate cap-independent translation mechanisms [17]. Despite this, the role of circRNA-encoded proteins in lipid metabolism remains largely unexplored.

In our study, we combined our previous circRNA-seq data [18] with Ribo-seq data [19] to evaluate the coding potential of circRNAs. We also investigated the functions and mechanisms of the circANKRD17 candidate in fat metabolism. These findings could lead to advancements in animal breeding strategies to improve meat quality and may also have implications in studying obesity-related conditions in humans.

Materials and methods

Ethics statement and animal tissue samples

A total of 20 healthy, purebred LT and LW pigs, 10 of each breed, were obtained post-birth from Banling Breeding Farm (Xinfeng County, Shaoguan City,

Guangdong Province, China). The longissimus dorsi muscle tissues were collected and immediately snap-frozen in liquid nitrogen for lipid metabolomics and RT-qPCR analysis.

Prediction of potential coding circRNA candidates with ribosome profiling

We utilized circRNA candidates obtained from our previous rRNA-depleted and RNase R-digested libraries [18] and predicted using CIRCexplorer2 [20]. For ribosome profiling data [19], the sequencing reads were filtered to remove mitochondrial, ribosomal RNA, and tRNA sequences and were subsequently aligned to the porcine reference genome. The unmapped reads, potentially containing junction reads of circRNAs, were collected to identify ribosome-associated circRNA candidates. We first extracted the exonic sequences surrounding the backsplice junction (50 bp on either side) and aligned all unmapped ribosome profiling reads (Ribo-seq reads that could not be aligned to the linear transcriptome or genome) to the circRNA backsplice junctions (100 bp sequences) using the BLASTn algorithm (<https://blast.ncbi.nlm.nih.gov/Blast.cgi>). We did not allow any mismatches and required a minimum read-junction overlap of 9 bp on either side of the junction. Furthermore, we developed a set of specific primers targeting the cyclization junction of these circRNA candidates. After reverse-transcribing total RNA into cDNA, this cDNA served as the template for subsequent PCR amplification. The head-to-tail splicing of circRNA was initially confirmed through 1% agarose gel electrophoresis and Sanger sequencing of the PCR products. The details of the primers used can be found in Table S1A.

Characterization of IMF cells between LT and LW breeds

Based on our previous single-cell sequencing data, a total of 242 and 115 cells exhibited gene expression patterns that could be attributed to IMF cells in the LT and LW groups, respectively [21]. Using Seurat v4.0.3 [22], the “Normalization” function was employed to calculate gene expression levels, while the “FindAllMarkers” function was utilized to identify DEGs between LT and LW pigs with $|\log(\text{Fold Change})| > 0.25$ and a $P\text{-value} < 0.05$. The KEGG annotation of DEGs was performed using the “enrichKEGG” function in the clusterProfiler package v4.0.5 [23].

Lipid metabolome determination and analysis in muscle tissue

The frozen longissimus dorsi muscle tissues were ground into a fine powder under liquid nitrogen using a pre-chilled mortar and pestle. For lipid extraction,

ice-cold methanol and chloroform were added to the tissue samples at a ratio of 2:1 (v/v). The mixture was thoroughly vortexed and incubated on ice for 30 min to ensure efficient lipid solubilization. Following the

incubation, chloroform and water were added to the samples to achieve a final solvent ratio of 1:1:0.9 (chloroform/methanol/water, v/v/v). The samples were then centrifuged at 4 °C for 10 min at 12,000 × *g* to facilitate

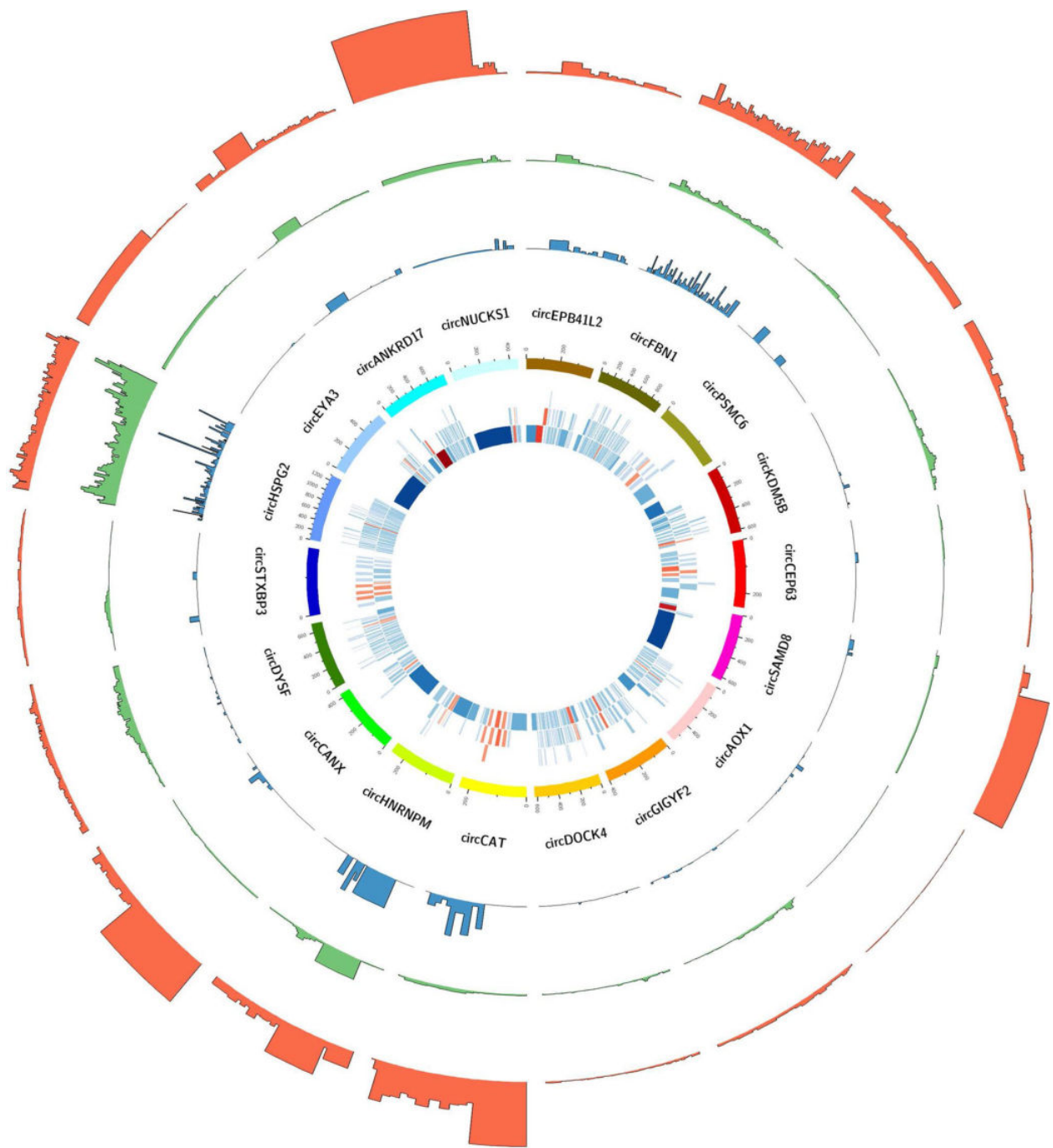


Fig. 1 Identification of coding-Potential circRNAs in porcine muscle tissues. In the inner circle, the tiles represent the exons of host genes. Exons marked in red indicate circRNA exons, while those in blue represent non-circRNA exons. The darker the color, the larger the exon. In the second inner circle, the histogram displays the abundance of reads for each exon of the host genes in the Ribo-seq library. In the third inner circle, the histogram shows the abundance of reads for each exon of the host genes in the RNase R-digested libraries. In the outer circle, the histogram presents the abundance of reads for each exon of the host genes in the rRNA-depleted libraries

phase separation. The lower organic phase, containing the lipids, was carefully collected using a glass pipette and transferred to a new tube for UHPLC-MS/MS analysis (LC-Bio Technology, Hangzhou, China). The raw mass spectrometry data were processed using proprietary software for peak detection, alignment, and integration. The peak intensities were then normalized to the total spectral intensity, and the normalized data were further used to predict the molecular formula based on additive ions, molecular ion peaks, and fragment ions. Next, the peaks were matched with the LipidMaps and LipidBlast databases to obtain accurate qualitative and relative quantitative results. Finally, the univariate analysis (*t*-test) was applied to calculate statistical significance (*P*-value). Metabolites with a $VIP > 1$, $P\text{-value} < 0.05$, and a fold change ≥ 2 or ≤ 0.5 were considered differential metabolites between LT and LW.

Actinomycin D and RNase R treatment

The 3T3-L1 cells were seeded into 6-well plates. After reaching approximately 60% confluency at 24 h, the cells were treated with either 5 $\mu\text{g/mL}$ Actinomycin D or DMSO (Sigma, St. Louis, MO, USA) and harvested at 6, 12, 18, and 24 h for further analysis. For RNase R treatment, around 2 μg of total RNA extracted from porcine muscle tissues was incubated with 3 U/ μg of RNase R (Epicentre Technologies, Madison, WI, USA) for 15 min at 37 °C. Following RNase R treatment, the RNA was subjected to RT-qPCR analysis, including reverse transcription to cDNA, followed by the measurement of circRNAs and their host mRNAs expression levels using the RT-qPCR protocol.

Nuclear and cytoplasmic extraction

The nuclear and cytoplasmic fractions of porcine muscle were separated using the PARIS™ Kit (Thermo Fisher Scientific, Waltham, USA). Samples were lysed on ice for 10 min, followed by centrifugation at $500\times g$ for 3 min at 4 °C. The supernatant was collected as the cytoplasmic fraction, while the pellet, containing nuclei, was washed and collected separately. Total RNA was then extracted from both fractions and analyzed

by RT-qPCR to measure the levels of nuclear marker U6, cytoplasmic marker ACTB (encoding β -actin), and circANKRD17.

Fluorescence in situ hybridization (FISH)

A 5'-Cy3-labeled probe specific to circANKRD17 was synthesized (Sangon Biotech, Shanghai, China). The experiment was carried out using a Fluorescence In Situ Hybridization Kit (RiboBio, Guangzhou, China). Probes targeting the reverse splice site of circANKRD17 were used to determine its subcellular localization. Images were captured with a Zeiss LSM 710 confocal microscope (Zeiss, Oberkochen, Germany).

Vector construction and RNA oligonucleotides

The linear sequence of circANKRD17 was cloned into the pCD2.1-ciR vector (Genesee Biotech, Guangzhou, China) and designated as OE-circANKRD17, with the empty pCD2.1-ciR vector serving as the negative control. Two small interfering RNAs (siRNAs), si-circANKRD17-1 and si-circANKRD17-2, targeting the junction sites of circANKRD17, along with a negative control siRNA, were designed and synthesized (GenePharma, Shanghai, China). Additionally, the 1716-nt ORF sequence within murine circANKRD17 was cloned into the pcDNA3.1 vector (Invitrogen, Carlsbad, CA, USA) with a 3 \times Flag tag sequence inserted before the stop codon, referred to as pcDNA3.1-circANKRD17-Flag; the empty pcDNA3.1 vector was used as the corresponding negative control.

Cell culture and treatment

Mouse immortalized 3T3-L1 preadipocytes were obtained from the China National Collection of Authenticated Cell Cultures (Beijing, China) and cultured at 37 °C in 5% CO₂. Differentiation was induced 2 d after the cells reached confluence by supplementing the growth media with 3 nmol/L insulin, 0.25 $\mu\text{mol/L}$ dexamethasone, and 0.5 mmol/L 1-methyl-3-isobutyl-xanthine (Beyotime Biotechnology, Shanghai, China). Then, the cells were transfected with the overexpression vector, knockdown vector, and their respective negative controls using Lipofectamine 2000

(See figure on next page.)

Fig. 2 Characteristics of IMF cells and lipid metabolism differences between pig breeds. **A** KEGG pathway enrichment analysis of differentially expressed genes. **B** Expression levels of genes related to the PPAR pathway. **C** Fat metabolites identified in porcine serum. Abbreviations: PC, phosphatidylcholine; PE, phosphatidylethanolamine; PS, phosphatidylserine; PI, phosphatidylinositol; PG, phosphatidylglycerols; PA, phosphatidic acids; CL, cardiolipin; SM, sphingomyelins; Cer, ceramides; GlcCer, glucosyl ceramides; ShexCer, sulfated hexosyl ceramides; DAG, diacylglycerol; MGDG, monogalactosyldiacylglycerol; TAG, triacylglycerol; FA, free fatty acids; ACarn, acylcarnitine; BMP, bis (monoacylglycerol) phosphate; FAHFs, branched fatty acid esters of hydroxy fatty acids; GM3, monosialodihexosyl ganglioside; PetOH, phosphatidylethanol. **D** PCA scatter plot of lipid profiles for each test sample. Each point represents a sample, with differences between samples reflected in the separation and clustering trends in the plot. **E** Heatmap of differentially expressed acylcarnitines between LT and LW breeds

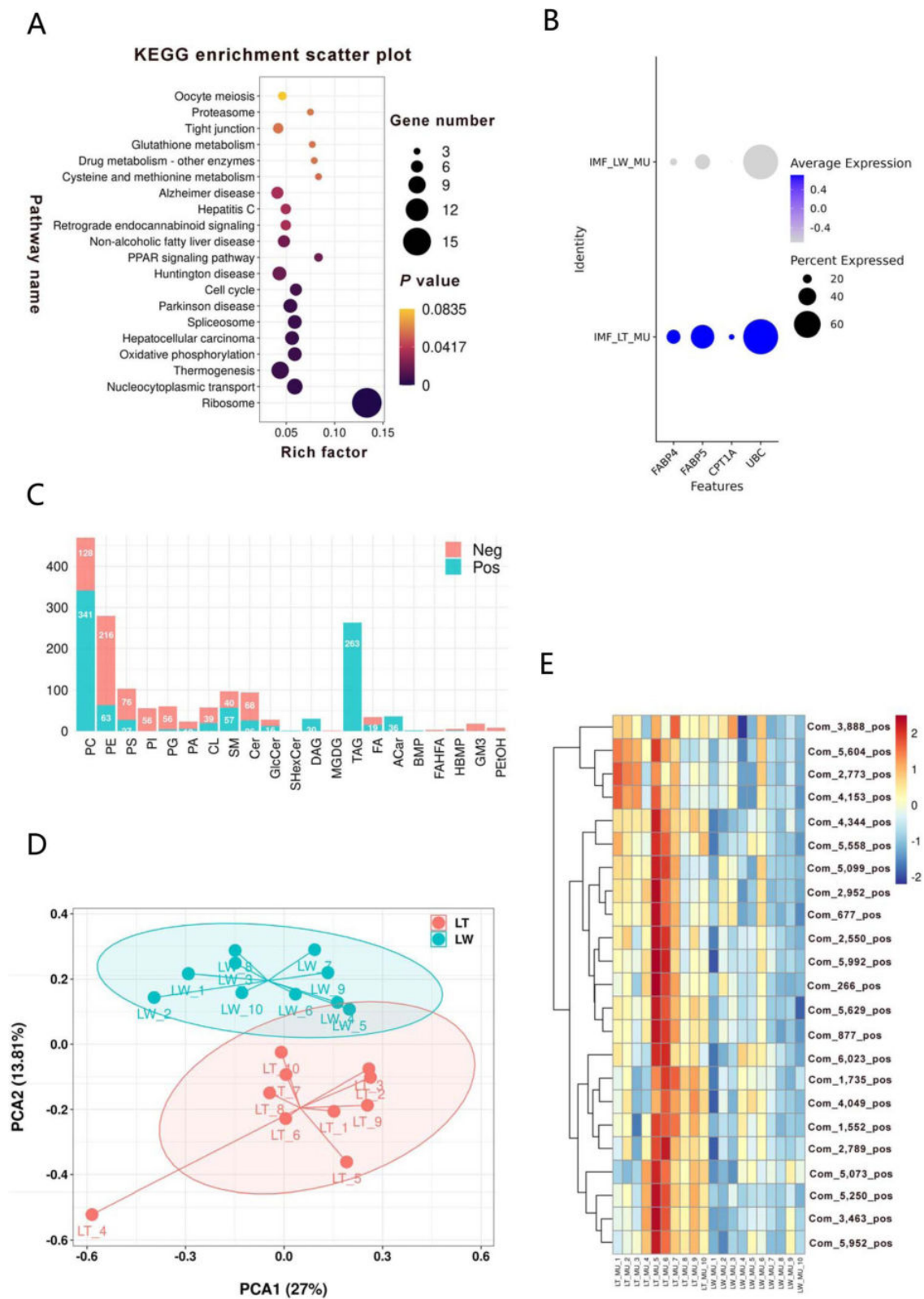


Fig. 2 (See legend on previous page.)

(Invitrogen). The transfected cells were harvested for protein and RNA analysis 48 h later.

Oil red O, Nile red staining and triglyceride content assay

The medium of 3T3-L1 cells was removed, and the cells were fixed with 4% paraformaldehyde (Solarbio, Beijing, China) for 30 min. Oil red O staining solution (Sigma) was added for 1 h, or Nile red working solution (Sigma) was applied for 10 min. After rinsing with PBS, the staining results were observed and photographed under a microscope (Olympus, Tokyo, Japan). The triglyceride content was determined using a triglyceride test kit (Jiancheng Bioengineering Institute, Nanjing, China). The liver tissues of the tested mice were fixed with paraformaldehyde, dehydrated in graded alcohol, washed in xylene, and then paraffin-embedded for sectioning. Sections of 5 μ m thickness were cut longitudinally using a manual rotary slicer (Olympus, Tokyo, Japan). The sections were then stained with Oil red O and scanned.

Protein isolation and western blot

Total proteins were extracted from 3T3-L1 cells or gastrocnemius muscle using RIPA lysis buffer (Solarbio, Beijing, China). A total of 15 μ g of protein was subjected to SDS-PAGE and subsequently transferred onto polyvinylidene fluoride (PVDF) membranes (Millipore, Bedford, MA, USA). The membranes were then probed with specific primary antibodies, followed by incubation with goat anti-rabbit IgG-HRP or goat anti-mouse IgG-HRP secondary antibodies (Bioworld, Minneapolis, MN, USA). Immunoreactive protein bands were visualized using an enhanced chemiluminescence solution (Solarbio). The antibodies used targeted proteins including PPAR γ , CEBP α , CD36, FABP4, FABP5, FASN, LPL, and CPT1A.

Statistical analysis

Differences between the two groups were analyzed using ANOVA followed by a Student's *t*-test. Statistical significance was set at $P < 0.05$, with significance levels indicated by one asterisk for $P < 0.05$ and two for

$P < 0.01$. Each experiment included at least three biological replicates.

Results

Identification of coding-potential circRNAs in porcine muscle tissues

A total of 25,295 circRNA candidates were predicted by CIRCexplorer2 in the longissimus dorsi tissues of LT and LW piglets. Among these, 18 circRNAs with coding potential were identified by combining the ribosome profiling sequencing in porcine longissimus dorsi tissues (Table S1B). We then designed divergent primers based on the junction sequences of the circRNAs and successfully confirmed the circular characteristic of 8 circRNA candidates based on reverse transcription PCR (RT-PCR) and Sanger sequencing (Fig. S1A). Among them, circANKRD17, which consists of exon 28 and exon 29 of its parental gene, has a fragment size of 1,844-nt, while the sequencing reads was obviously concentrated in the exon 28–29 region in the rRNA removal, RNase R digestion, and Ribo-seq libraries (Fig. 1). In our study, only the expression level of circANKRD17 was significantly elevated in the longissimus dorsi muscle of LT pigs (Fig. S1B, $P < 0.01$), suggesting that circANKRD17 may be related to porcine intramuscular fat metabolism.

Analysis of IMF cell characteristics and lipid metabolism differences between pig breeds

Based on our single-cell RNA data [21], a total of 477 differentially expressed genes were identified in IMF cells between LT and LW piglets. These candidates were enriched in the PPAR signaling pathway according to KEGG enrichment analysis (Fig. 2A). The pathway genes *FABP4*, *FABP5*, *CPT1A*, and *UBC* showed significantly higher expression levels in LT piglets (Fig. 2B). In general, FABPs are typically described as intracellular proteins that mediate lipid uptake and intracellular transport [24], while CPT1A, a key enzyme in mitochondrial fatty acid oxidation, influences the balance between lipolysis and liposynthesis [25]. Our findings may provide novel insights into the regulatory factor for higher intramuscular fat content observed in local pig breeds. We further utilized

(See figure on next page.)

Fig. 3 Characterization of circANKRD17 in adipocytes. **A** Circular structure diagram and Sanger sequencing results for circANKRD17. **B** Polymerase chain reaction (PCR) and agarose gel electrophoresis analysis of complementary DNA (cDNA) and genomic DNA (gDNA) using a double-primer method. **C** and **D** Analysis of circANKRD17 using RNase R digestion and actinomycin D treatment. circANKRD17 indicates a fragment with a junction sequence amplified by divergent primers, while linear ANKRD17 refers to a linear fragment amplified by convergent primers. **E** Distribution of circANKRD17 gene transcripts in 3T3-L1 cells, with U6 serving as a nuclear control gene and ACTB as a cytoplasmic control gene. **F** Localization of circANKRD17 observed via fluorescence in situ hybridization (FISH). Cy3-labeled circRNA appears red, while DAPI-stained nuclei appear blue. Scale bar = 10 μ m

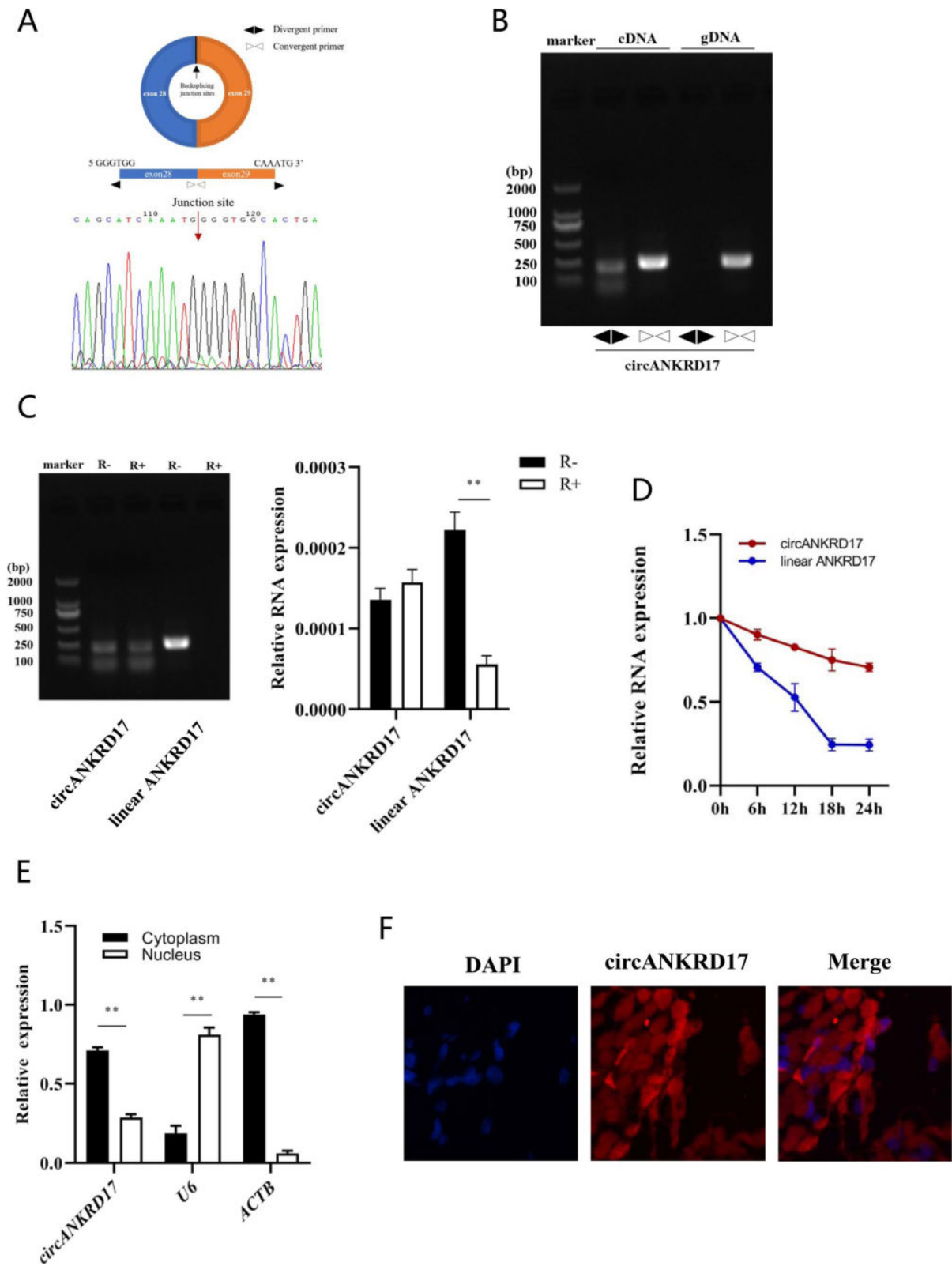


Fig. 3 (See legend on previous page.)

lipidomic technology and detected 944 negative and 1,113 positive lipid metabolites in porcine longissimus dorsi muscles (Table S1C), with significant enrichment in phosphatidylcholine (PC), phosphatidylethanolamine (PE), and triacylglycerol (TAG) (Fig. 2C). The PCA analysis demonstrated a clear distinction in metabolite composition between LT and LW breeds (Fig. 2D). A total of 229 metabolites were significantly regulated ($P < 0.05$), with 142 candidates increased and 87 decreased in the LT breed (Table S1D). In detail, a total of 23 acylcarnitines (ACar) were significantly upregulated in the LT breed (Fig. 2E), consistent with the high level of CPT1A expression, which catalyzes the conversion of fatty acids into acyl-carnitine in LT IMF cells.

Characterization of circANKRD17 in adipocytes

The head-to-tail splicing of circANKRD17 in mouse was successfully confirmed by RT-PCR and Sanger sequencing (Fig. 3A). The murine circANKRD17 contained a 1,653-nt open reading frame (Fig. S1C) and matched with the human hsa_circ_13463 from the circRNADb database (<http://reprod.njmu.edu.cn/circrnadb>) (Fig. S1D). This sequence spans from the putative ATG start codon to a STOP codon located 170-nt and 36-nt after the splice junction site, respectively. We used cDNA and genomic DNA (gDNA) isolated from 3T3-L1 cells as PCR templates, and divergent primers produced amplicons only from cDNA samples and not from the gDNA (Fig. 3B). Typically, linear RNA molecules are vulnerable to digestion by exonuclease R, whereas circRNA candidates exhibit resistance to this digestion. In our study, circANKRD17 was resistant to RNase R digestion compared with its linear parental gene based on agarose gel electrophoresis and RT-qPCR analysis (Fig. 3C). After treatment with Actinomycin D, a transcription inhibitor, RT-qPCR analysis revealed that the half-life of circANKRD17 exceeded 24 h, while the associated linear transcript had a half-life of approximately 4 h (Fig. 3D), indicating that circANKRD17 is more stable in 3T3-L1 cells. Further nuclear and cytoplasmic fractionation (Fig. 3E) and FISH (Fig. 3F) analyses revealed that circANKRD17 was primarily localized in the cytoplasm,

as well as being present in the nucleus. These results collectively reveal that circANKRD17 is conserved across species and is expressed abundantly and stably in adipocytes.

Overexpression and knockdown of circANKRD17 in lipid metabolism in vitro

We amplified the 1,844-nt full-length fragment of murine circANKRD17 (Fig. S1E) and constructed a recombinant plasmid (OE-circANKRD17) using the circRNA overexpression vector pCD2.1-ciR (Fig. S1F and Fig. S1G). In addition, we synthesized two siRNA fragments targeting the splice junction (si-circANKRD17-1 and si-circANKRD17-2). RT-qPCR showed that transfection of OE-circANKRD17 and si-circANKRD17-1 significantly increased and decreased the expression levels of circANKRD17 in 3T3-L1 cells ($P < 0.01$), respectively, with no significant effects on the host gene (Fig. S1H and Fig. S1I). After transfection with OE-circANKRD17, Oil red O staining revealed a obviously increase in the number of lipid droplets (Fig. 4A), while Nile red staining showed a substantial rise in triglyceride levels and content (Fig. S1J). The RT-qPCR results demonstrated that overexpression of OE-circANKRD17 significantly increased the mRNA expression levels of *CEBPα* involved in adipocyte differentiation (Fig. 4B, $P < 0.05$), *FAT1*, *FABP4*, and *FABP5* involved in fatty acid transport (Fig. 4C, $P < 0.01$ or $P < 0.05$), *FASN*, *LPL*, and *CPT1A* involved in fatty acid synthesis, hydrolysis, and oxidation (Fig. 4D, $P < 0.01$ or $P < 0.05$), *DGAT2* involved in intracellular triglyceride synthesis (Fig. 4E, $P < 0.05$), and *PLIN3* involved in lipid droplet formation and maturation (Fig. 4F, $P < 0.01$). In similar, OE-circANKRD17 significantly increased the protein expression levels of PPARγ, CEBPα, CD36 (FAT), FABP4, FABP5, FASN, LPL, and CPT1A (Fig. 4G, $P < 0.01$ or $P < 0.05$). We selected si-circANKRD17-1 for the follow-up knockdown experiments. In contrast, circANKRD17 knockdown effectively reduced lipid droplet production (Fig. 5A). Nile red staining and triglyceride content assays indicated a decrease in triglyceride levels (Fig. S1K). RT-qPCR analysis showed that si-circANKRD17-1 knockdown significantly suppressed

(See figure on next page.)

Fig. 4 Overexpression of circANKRD17 promotes lipid metabolism in vitro. **A** 3T3-L1 cells stained with Oil red O after transfection with either NC (negative control) or OE-circANKRD17 (overexpression of circANKRD17). **B** The mRNA levels of adipocyte differentiation genes. **C** The mRNA levels of fatty acid transport genes. **D** The mRNA levels of fatty acid synthesis, hydrolysis, and oxidation genes. **E** The mRNA levels of triglyceride synthesis genes. **F** The mRNA levels of lipid droplet maturation genes. **G** Protein levels related to lipid metabolism after treatment with either the negative control or OE-circANKRD17

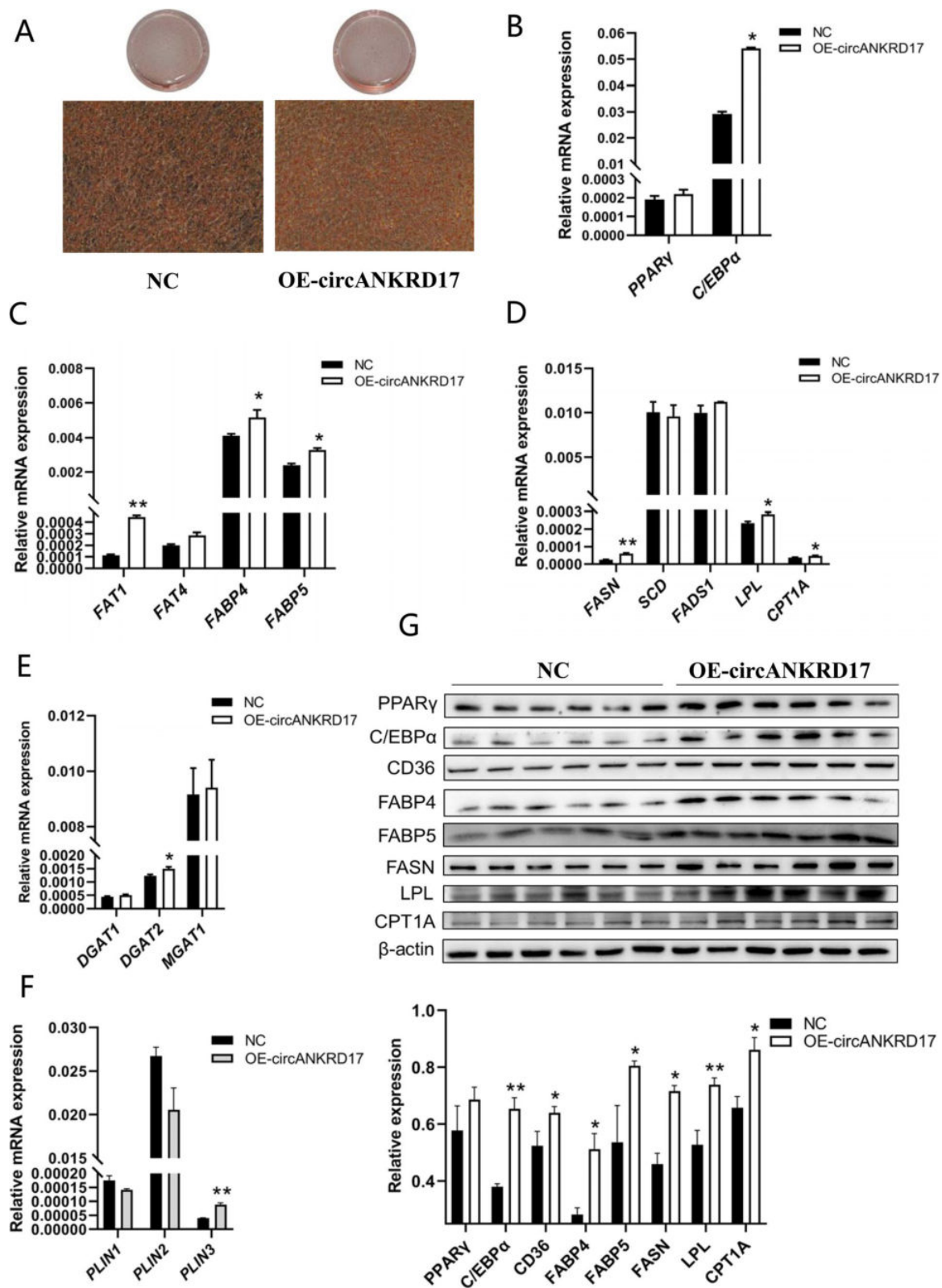


Fig. 4 (See legend on previous page.)

the mRNA expression of *PPAR γ* and *CEBP α* (Fig. 5B, $P < 0.01$ or $P < 0.05$), as well as *FAT1*, *FABP4*, *FABP5* (Fig. 5C, $P < 0.05$). The mRNA levels of *FASN*, *SCD*, *LPL*, and *CPT1A* were also significantly reduced (Fig. 5D, $P < 0.01$ or $P < 0.05$). In similar, *MGAT1* (Fig. 5E, $P < 0.01$) and *PLIN2*, *PLIN3* (Fig. 5F, $P < 0.05$) mRNA levels were significantly down-regulated. Western blot results confirmed that circANKRD17 knockdown significantly reduced the protein expression levels of *PPAR γ* , *CEBP α* , *CD36* (FAT), *FABP4*, *FABP5*, *FASN*, *LPL*, and *CPT1A* (Fig. 5G, $P < 0.01$ or $P < 0.05$). Our results suggest that circANKRD17 plays an important role in various aspects of lipid metabolism in vitro.

Analysis of circANKRD17 in lipid metabolism in vivo

We constructed a lentiviral vector encoding a short hairpin RNA (circANKRD17-si-1), referred to as LV-sh-circANKRD17 (Fig. S1L–M). Both LV-sh-circANKRD17 and an empty vector (NC) were injected into six 6-week-old C57BL/6 mice via tail vein injection. The first injection was administered on day 0, followed by weekly injections for a total of four doses. During the injection period, the mice were fed either a standard diet or a high-fat diet. Liver and gastrocnemius muscle samples were subsequently collected. In the standard diet groups, Oil red O staining demonstrated that no significant changes in lipid metabolism were observed in the livers between the LV-sh-circANKRD17 and NC groups (Fig. S1O). In the high-fat diet groups, RT-qPCR analysis revealed that LV-sh-circANKRD17 significantly reduced the expression of circANKRD17 in the gastrocnemius muscle of the test mice ($P < 0.01$), while it had no significant effect on the mRNA expression of linear *ANKRD17* (Fig. S1P). Oil red O staining demonstrated that the lipid droplet content in the liver of the LV-sh-circANKRD17 group was obviously lower than that of the control group (Fig. 6A). Compared to NC, LV-sh-circANKRD17 significantly inhibited adipocyte differentiation (*PPAR γ* and *CEBP α*) (Fig. 6B, $P < 0.01$ or $P < 0.05$), fatty acid transport (*FAT1*, *FABP4*, and *FABP5*) (Fig. 6C, $P < 0.01$), fatty acid synthesis (*FASN*, *SCD*, *FADS1*), lipid oxidation (*CPT1A*) (Fig. 6D, $P < 0.01$), triglyceride synthesis (*DGAT2* and *MGAT1*) (Fig. 6E, $P < 0.01$), and lipid droplet maturation (*PLIN1*, *PLIN2*, and *PLIN3*) (Fig. 6F, $P < 0.01$). The levels of lipid

metabolism-related proteins (*PPAR γ* , *CEBP α* , *CD36*, *FABP4*, *FABP5*, *FASN*, *LPL*, *CPT1A*) were also significantly decreased (Fig. 6G, $P < 0.01$ or $P < 0.05$). These results suggest that LV-sh-circANKRD17 can significantly reduce lipid metabolism in vivo.

A novel protein encoded by circANKRD17 regulates lipid metabolism

We discovered that circANKRD17 contains an initiation codon and a terminator near the splice site, allowing it to encode a protein of 571 amino acids (Fig. S1C). To verify whether the predicted ORF of circANKRD17 has the ability to encode a protein, we cloned the linear sequence of the circANKRD17 ORF into the pcDNA3.1 vector, adding a 3×Flag tag before the stop codon to construct the pCD3.1-circANKRD17-3×Flag overexpression vector, and performed double enzyme digestion for verification (Fig. S1Q). The recombinant vector was then transfected into 3T3-L1 cells, and western blotting results showed that the protein expression of pCD3.1-circANKRD17-Flag could be detected using anti-Flag antibodies (Fig. 7A). Overexpression of pCD3.1-circANKRD17-Flag increased the number of intracellular lipid droplets, as evidenced by Oil red O staining (Fig. 7B) and Nile red staining (Fig. 7C). RT-qPCR analysis revealed that overexpression of pCD3.1-circANKRD17-Flag increased the expression of genes related to adipocyte differentiation (Fig. 7D), fatty acid transport (Fig. 7E), fatty acid synthesis and oxidation (Fig. 7F), triglyceride synthesis, and lipid droplet maturation (Fig. 7G). Western blotting was also used to verify the expression of the relevant proteins, showing that overexpression of pCD3.1-circANKRD17-Flag significantly increased the protein expression of *PPAR γ* , *CEBP α* , *CD36*, *FABP4*, *FABP5*, *FASN*, *LPL*, and *CPT1A* (Fig. S1R, $P < 0.01$ or $P < 0.05$). Our results indicate that circANKRD17 can influence lipid metabolism through its encoded protein.

Discussion

In recent years, the functions of non-coding RNAs have been extensively studied in the field of circRNA research. With continued in-depth investigation, recent studies have uncovered the coding ability of circRNAs to produce functional peptides in vivo

(See figure on next page.)

Fig. 5 Knockdown of circANKRD17 inhibits lipid metabolism in vitro. **A** 3T3-L1 cells transfected with si-NC (negative control) or si-circANKRD17 (small interfering RNA targeting circANKRD17) and stained with Oil red O. **B** The mRNA levels of adipocyte differentiation genes. **C** The mRNA levels of fatty acid transport genes. **D** The mRNA levels of genes involved in fatty acid synthesis, hydrolysis, and oxidation. **E** The mRNA levels of triglyceride synthesis genes. **F** the mRNA levels of lipid droplet maturation genes. **G** Protein levels related to lipid metabolism after treatment with either si-NC or si-circANKRD17

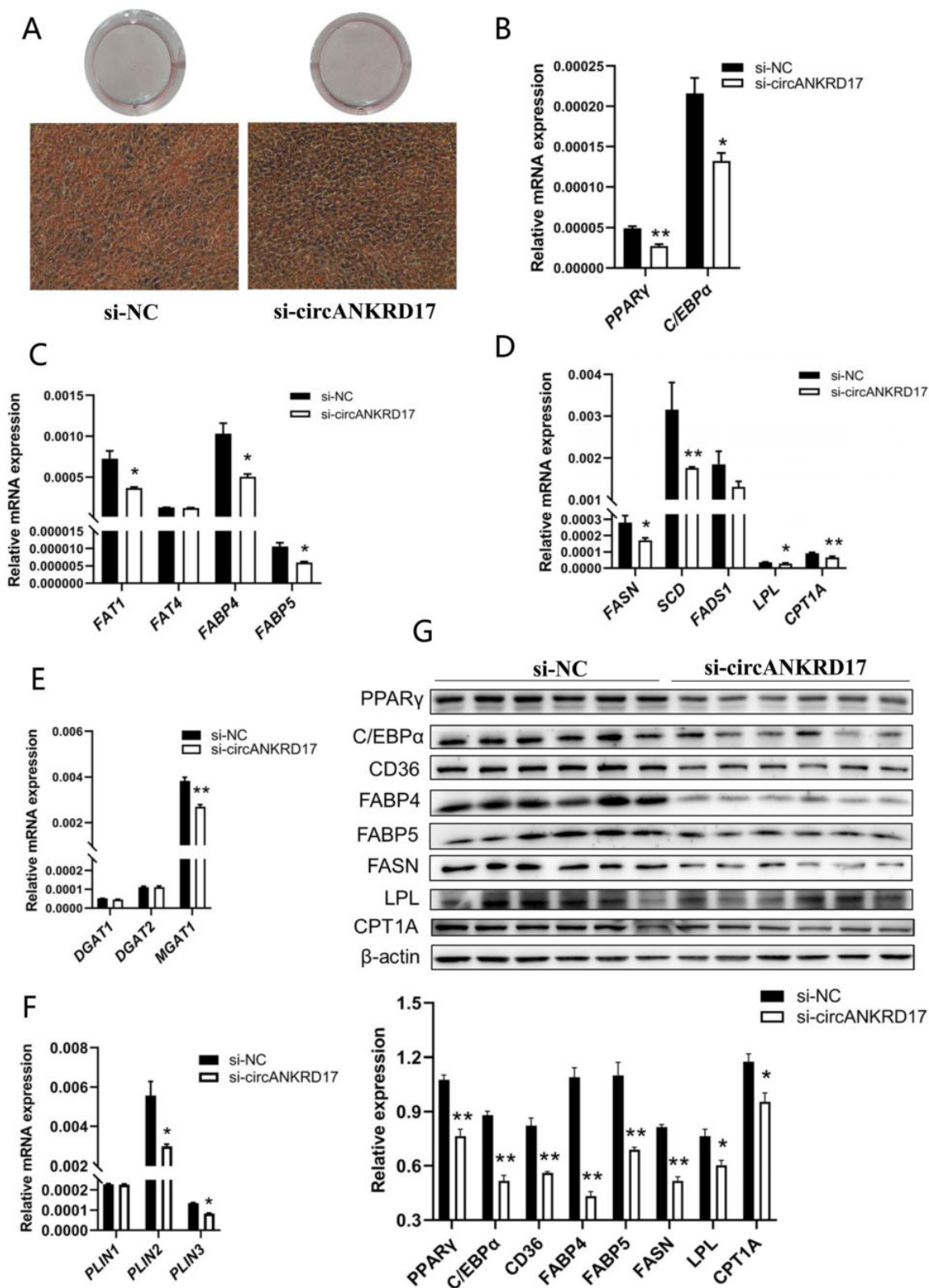


Fig. 5 (See legend on previous page.)

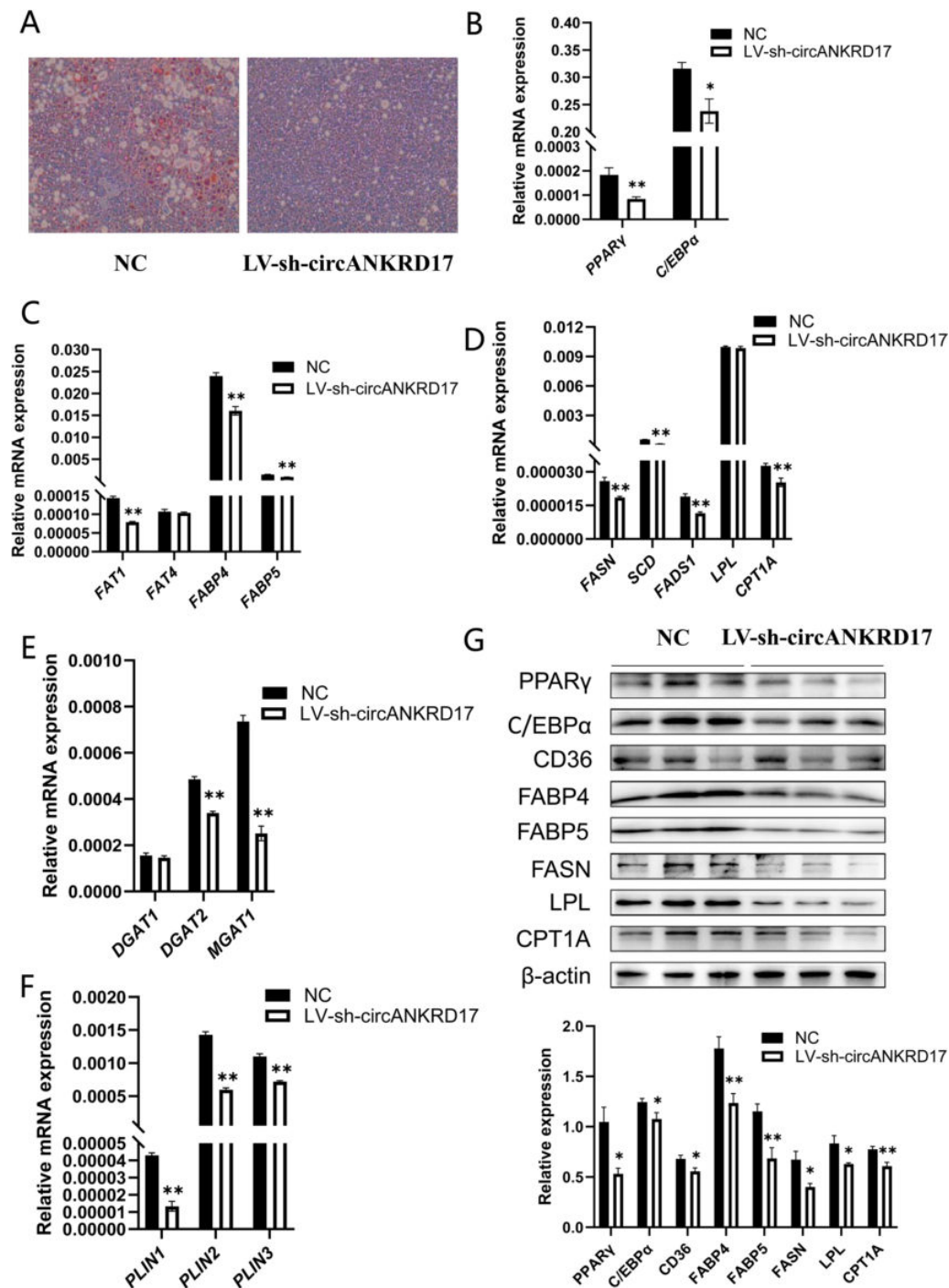


Fig. 6 Knockdown of circANKRD17 inhibits lipid metabolism in vivo. **A** Oil red O staining of mouse livers infected with either LV-sh-circANKRD17 lentivirus or control, with high-fat diet treatments, scanned at 20× magnification. **B** The mRNA levels of adipocyte differentiation genes. **C** The mRNA levels of fatty acid transport genes. **D** The mRNA levels of genes involved in fatty acid synthesis, hydrolysis, and oxidation. **E** The mRNA levels of triglyceride synthesis genes. **F** The mRNA levels of lipid droplet maturation genes. **G** Protein levels related to lipid metabolism after treatment with either the negative control (NC) or LV-sh-circANKRD17

[26]. For instance, a novel protein encoded by circ-ZNF609 was first discovered in adult myoblasts [27]. In our previous study, we demonstrated that a new protein encoded by circKANS1L could regulate skeletal myogenesis [19]. Therefore, we combined previous circRNAome-seq data [18] and Ribo-seq data [19] to screen circRNA candidates with coding potential. We verified that circANKRD17 has a cyclic structure and is differentially expressed in LT and LW breeds. Based on our single-cell sequencing data [21], we found that in IMF cells, *FABP4*, *FABP5*, *CPT1A*, and *UBC* showed significantly higher expression levels in LT piglets and were enriched in the PPAR signaling pathway. The PPAR signalling pathway plays a key role in lipid metabolism, including controlling fatty acid transport (PPAR α), lipid storage (PPAR γ) and glucose metabolism (PPAR δ) [28]. In detail, FABP can coordinate lipid transport [24], while CPT1A can transport fatty acid from the cytosol into mitochondria [29]. In agree with our study, FABP4 was found to be highly expressed in Laiwu pigs (a local pig breed) compared to Duroc \times Landrace \times Yorkshire pigs [30]. Consequently, we concluded that circANKRD17 may have coding potential and could play a role in lipid metabolism through the PPAR pathway.

In comparison to lean pigs, fat-type pigs exhibit a greater capacity for adipocyte proliferation and differentiation, giving them a significant advantage in IMF deposition [31]. To further investigate the function of circANKRD17, we utilized 3T3-L1 cells as a model in vitro and C57BL/6 mice as a model in vivo, selecting a series of adipose-related genes to examine the effects on lipid metabolism through the PPAR pathway. Among these, PPAR γ and CEBP α are known as key regulators of early adipogenesis [32]; *FAT1*, *FAT4*, *FABP4*, and *FABP5* are involved in fatty acid transport [33]; *FASN* converts carbohydrates into fatty acids for storage as triglycerides [32]; *SCD* is a key rate-limiting enzyme that convert saturated fatty acids to monounsaturated fatty acids [34]; and *FADS1* is primarily responsible for the synthesis of polyunsaturated fatty acids [35]. Additionally, *LPL* serves as the rate-limiting enzyme for triglyceride degradation [36], while *CPT1A* facilitates the transfer of fatty acids to mitochondria for subsequent oxidative metabolic processes [25]. *DGAT1* and *DGAT2* are two forms of acylglycerol acyltransferases

involved in triglyceride storage within adipocytes [37], with *MGAT1* playing a critical role as an initiator of triglyceride synthesis and fat uptake in the body [38]. Furthermore, *PLIN1*, *PLIN2*, and *PLIN3* are key genes involved in the formation of neutral lipids [39]. Our study revealed that overexpression of circANKRD17 significantly upregulated the expression of these genes and proteins, whereas interference resulted in the opposite trend. Additionally, the expression of genes related to lipolysis, such as *LPL*, also showed an upregulation trend. Generally, *LPL* can interact with lipoproteins, anchoring them to the vessel wall to facilitate the uptake of lipoprotein particles and the exchange of lipids between lipoproteins [40]. Typically, fatty acid synthesis, cholesterol uptake, and β -oxidation are tightly balanced [41]. *CPT1A*, a crucial enzyme in β -oxidation [29], may experience increased expression in response to elevated lipid metabolism demands, potentially to avoid lipid over-accumulation. However, the underlying mechanisms require further investigation. These findings demonstrate that circANKRD17 can regulate fat deposition through multiple pathways, highlighting its significant role in various aspects of lipid metabolism.

At present, the main methods for verifying the coding ability of circRNAs include adding tagged proteins to the ORF coding region of circRNAs to detect the expression of fusion proteins, or inserting the ORF coding region of circRNAs into a dual-luciferase coding sequence to determine whether the ORF coding region is readable [42]. In this study, to verify the coding ability of circANKRD17, we constructed the vector pcDNA3.1-circANKRD17-Flag, which allowed for the fusion expression of the ORF of circANKRD17 with a Flag-tagged protein. We performed western blot analysis using a Flag-tagged antibody and detected a protein of the expected size for the circANKRD17-Flag fusion, thereby confirming the coding ability of circANKRD17. Cap-independent translation of circRNAs driven by internal ribosome entry site (IRES) or N⁶-methyladenosine (m⁶A)-containing short sequence [17]. However, the translation mechanism of circANKRD17 remains unclear, and it constitutes a key research objective for our subsequent experiments. One might argue that the protein encoded by circANKRD17 specifically interacts with the PPAR pathway to influence intramuscular fat metabolism and that the

(See figure on next page.)

Fig. 7 circANKRD17 encodes a novel protein to regulate lipid metabolism. **A** Levels of Flag-tagged protein in 3T3-L1 cells transfected with pcDNA3.1-circANKRD17-Flag. **B** Oil red O staining of 3T3-L1 cells transfected with either pcDNA3.1 or pcDNA3.1-circANKRD17-Flag. **C** Nile red staining of 3T3-L1 cells transfected with either pcDNA3.1 or pcDNA3.1-circANKRD17-Flag. **D** The mRNA levels of adipocyte differentiation genes. **E** The mRNA levels of fatty acid transport genes. **F** The mRNA levels of genes involved in fatty acid synthesis, hydrolysis, and oxidation. **G** The mRNA levels of triglyceride synthesis genes and lipid droplet maturation genes

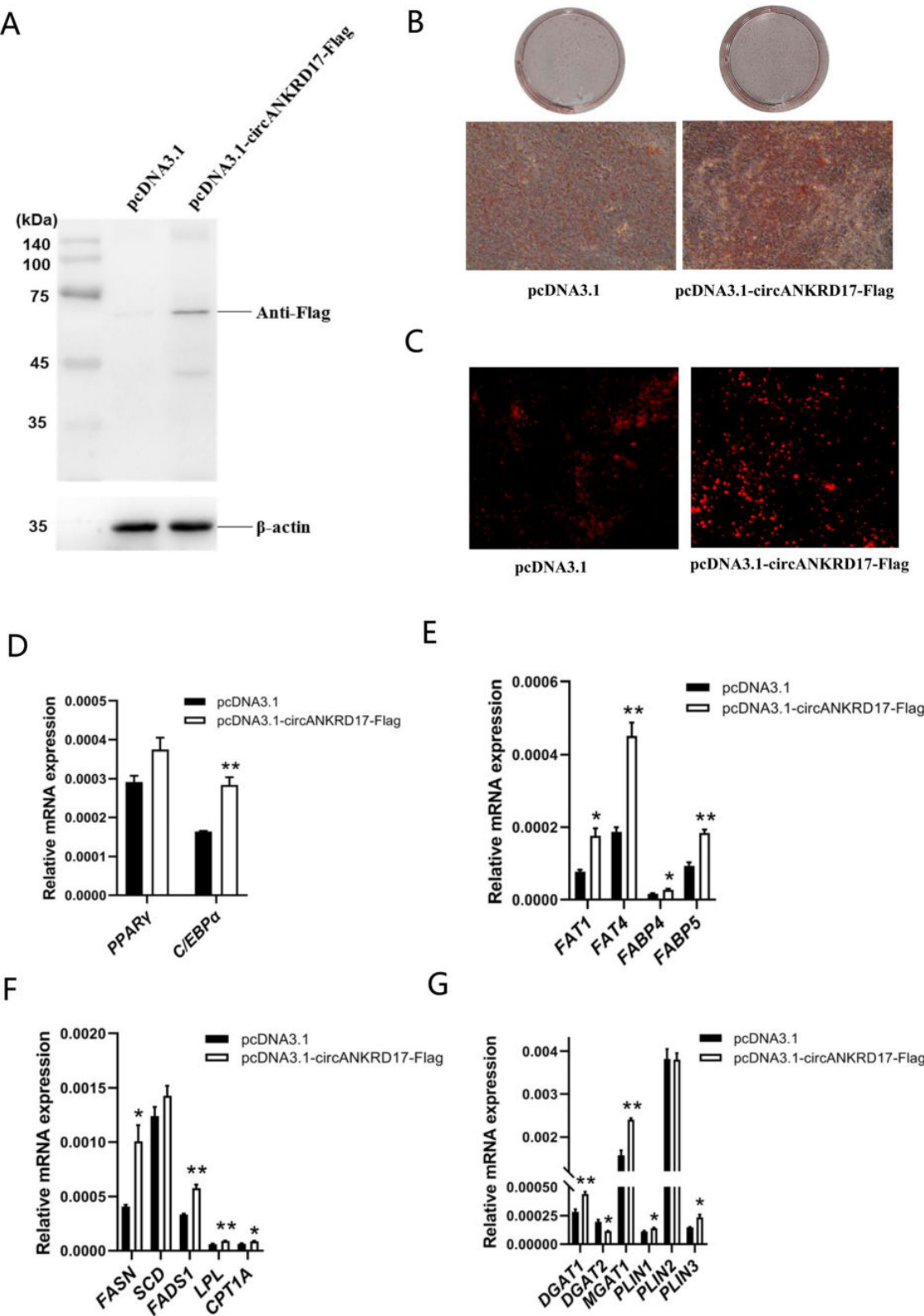


Fig. 7 (See legend on previous page.)

proposed molecular mechanisms underlying this interaction are based on the findings of this investigation.

Conclusion

In summary, our study identifies circANKRD17 as a key regulator of lipid metabolism, with its encoded protein significantly contributing to adipogenesis and lipid metabolism. These findings provide new insights into the metabolic characteristics of pig breeds with higher intramuscular fat content.

Abbreviations

ACar	Acylcarnitines
circRNA	Circular RNA
FISH	Fluorescence in situ hybridization
gDNA	Genomic DNA
IMF	Intramuscular fat
IRES	Internal ribosome entry site
lncRNA	Long non-coding RNA
miRNA	MicroRNA
ncRNA	Non-coding RNA
ORF	Open reading frame
PC	Phosphatidylcholine
PE	Phosphatidylethanolamine
TAG	Triacylglycerol

Supplementary Information

The online version contains supplementary material available at <https://doi.org/10.1186/s40104-025-01153-5>.

Additional file 1: Table S1A. The primer sequences used in our study. Table S1B. The protein-coding circRNA candidates identified with the ribosome profiling sequencing. Table S1C. Lipid metabolites identified in porcine longissimus dorsi muscles. Table S1D. Differential lipid metabolites in porcine longissimus dorsi muscles between LT and LW piglets.

Additional file 2: Fig. S1A. RT-PCR and Sanger sequencing to validate the junction sites of candidate circRNAs. Fig. S1B. Relative expression levels of candidate circRNAs between LT and LW. Fig. S1C. Schematic diagram illustrating the translation potential of circANKRD17. Fig. S1D. Schematic representation of the open reading frame of human circANKRD17. Fig. S1E. RT-PCR amplification of the full-length sequence of murine-derived circANKRD17. Fig. S1F. Diagram of the pCD2.1-ciR overexpression vector. Fig. S1G. Identification of the OE-circANKRD17 overexpression plasmid by double digestion. Fig. S1H. Expression levels of circANKRD17 and ANKRD17 mRNA in 3T3-L1 cells transfected with circANKRD17 overexpression vectors. Fig. S1I. Knockdown efficiency of two siRNA sequences targeting circANKRD17 in 3T3-L1 cells. Different lowercase letters indicate $P < 0.05$. Fig. S1J. Nile red staining fluorescence and triglyceride content assay of 3T3-L1 cells transfected with circANKRD17 overexpression vectors. Fig. S1K. Nile red fluorescence and triglyceride content assay of 3T3-L1 cells transfected with circANKRD17 knockdown vectors. Fig. S1L. Diagram of the pshRNA-copGFP Lentivector. Fig. S1M. Colony PCR and Sanger sequencing results of the recombinant plasmid sh-circANKRD17. The horizontal segment represents the inserted interfering sequence. Fig. S1N. Diluted lentivirus supernatant was transfected into 293T cells, and the titer of the lentivirus was determined by observing green fluorescent protein under a fluorescence microscope. Fig. S1O. Oil red O staining of mouse livers infected with either LV-sh-circANKRD17 lentivirus or control in the standard diet groups. Fig. S1P. Expression of circANKRD17 and mANKRD17 mRNA in LV-sh-circANKRD17-transfected 293T cells. Fig. S1Q. Diagram of the pCDNA3.1 vector and identification of the pCDNA3.1-circANKRD17-3xFlag overexpression plasmid by double digestion. Fig. S1R. Protein levels related to lipid metabolism after treatment with either the negative control or pCDNA3.1-circANKRD17-Flag.

Acknowledgements

We thank the High Performance Computing Center of South China Agricultural University for providing computational resources in this work.

Authors' contributions

XH, FX, YN and XW gathered samples, and conducted the experiments; JL, TC, QX, and YZ conceived the study and improved the manuscript; JS conceived the study, performed data analysis, and drafted the manuscript. All authors have read and approved the final version of the manuscript.

Funding

This work was supported by the Biological Breeding-Major Projects in National Science and Technology [grant numbers 2023ZD04044], and the Natural Science Foundation of China Program [grant numbers 32072714].

Data availability

Not applicable.

Declarations

Ethics approval and consent to participate

This study was approved by the Animal Care Committee of South China Agricultural University, and all applicable institutional and national guidelines for the care and use of animals were followed (2023F148).

Consent for publication

Not applicable.

Competing interests

The authors declare that they have no financial interests.

Received: 7 October 2024 Accepted: 2 January 2025

Published online: 05 February 2025

References

1. Yu T, Tian X, Li D, He Y, Yang P, Cheng Y, et al. Transcriptome, proteome, and metabolome analysis provide insights on fat deposition and meat quality in pig. *Food Res Int*. 2023;166:112550. <https://doi.org/10.1016/j.foodres.2023.112550>.
2. Miller R. Drivers of consumer liking for beef, pork, and lamb: A review. *Foods*. 2020;9(4):428. <https://doi.org/10.3390/foods9040428>.
3. Gao Y, Zhang YH, Jiang H, Xiao SQ, Wang S, Ma Q, et al. Detection of differentially expressed genes in the longissimus dorsi of northeastern indigenous and large white pigs. *Genet Mol Res*. 2011;10(2):779–91. <https://doi.org/10.4238/vol10-2gmr1170>.
4. Hocquette JF, Gondret F, Baéza E, Médale F, Jurie C, Pethick DW. Intramuscular fat content in meat-producing animals: Development, genetic and nutritional control, and identification of putative markers. *Animal*. 2010;4(2):303–19. <https://doi.org/10.1017/S1751731109991091>.
5. Hou X, Zhang R, Yang M, Niu N, Wu J, Shu Z, et al. Metabolomics and lipidomics profiles related to intramuscular fat content and flavor precursors between Laiwu and Yorkshire pigs. *Food Chem*. 2023;404:134699. <https://doi.org/10.1016/j.foodchem.2022.134699>.
6. Sun J, Xie M, Huang Z, Li H, Chen T, Sun R, et al. Integrated analysis of non-coding RNA and mRNA expression profiles of 2 pig breeds differing in muscle traits. *J Anim Sci*. 2017;95(3):1092–103. <https://doi.org/10.2527/jas.2016.0867>.
7. Yan S, Tu Z, Liu Z, Fan N, Yang H, Yang S, et al. A huntingtin knockin pig model recapitulates features of selective neurodegeneration in Huntington's disease. *Cell*. 2018;173(4):989–1002.e13. <https://doi.org/10.1016/j.cell.2018.03.005>.
8. Consitt LA, Bell JA, Houmard JA. Intramuscular lipid metabolism, insulin action, and obesity. *IUBMB Life*. 2009;61:47–55. <https://doi.org/10.1002/iub.142>.

9. Zou C, Li J, Luo W, Li L, Hu A, Fu Y, et al. Transcriptome analysis reveals long intergenic non-coding RNAs involved in skeletal muscle growth and development in pig. *Sci Rep*. 2017;7:8704. <https://doi.org/10.1038/s41598-017-07998-9>.
10. Kristensen LS, Andersen MS, Stagsted LVW, Ebbesen KK, Hansen TB, Kjems J. The biogenesis, biology and characterization of circular RNAs. *Nat Rev Genet*. 2019;20(11):675–91. <https://doi.org/10.1038/s41576-019-0158-7>.
11. Qu S, Yang X, Li X, Wang J, Gao Y, Shang R, et al. Circular RNA: a new star of noncoding RNAs. *Cancer Lett*. 2015;365:141–8. <https://doi.org/10.1016/j.canlet.2015.06.003>.
12. Zhou WY, Cai ZR, Liu J, Wang DS, Ju HQ, Xu RH. Circular RNA: Metabolism, functions, and interactions with proteins. *Mol Cancer*. 2020;19(1):172. <https://doi.org/10.1186/s12943-020-01286-3>.
13. Tay Y, Rinn J, Pandolfi PP. The multilayered complexity of ceRNA crosstalk and competition. *Nature*. 2014;505(7483):344–52. <https://doi.org/10.1038/nature12986>.
14. Ashwal-Fluss R, Meyer M, Pamudurti NR, Ivanov A, Bartok O, Hanan M, et al. circRNA biogenesis competes with pre-mRNA splicing. *Mol Cell*. 2014;56:55–66. <https://doi.org/10.1016/j.molcel.2014.08.019>.
15. Huang A, Zheng H, Wu Z, Chen M, Huang Y. Circular RNA-protein interactions: Functions, mechanisms, and identification. *Theranostics*. 2020;10(8):3503–17. <https://doi.org/10.7150/thno.42174>.
16. Shi Y, Jia X, Xu J. The new function of circRNA: Translation. *Clin Transl Oncol*. 2020;22(12):2162–9. <https://doi.org/10.1007/s12094-020-02371-1>.
17. Wen SY, Qadir J, Yang BB. Circular RNA translation: Novel protein isoforms and clinical significance. *Trends Mol Med*. 2022;28(5):405–20. <https://doi.org/10.1016/j.molmed.2022.03.003>.
18. Zhuang X, Lin Z, Xie F, Luo J, Chen T, Xi Q, et al. Identification of circRNA-associated ceRNA networks using longissimus thoracis of pigs of different breeds and growth stages. *BMC Genomics*. 2022;23:294. <https://doi.org/10.1186/s12864-022-08515-7>.
19. Lin Z, Xie F, He X, Wang J, Luo J, Chen T, et al. A novel protein encoded by circKANS1L1 regulates skeletal myogenesis via the Akt-FoxO3 signaling axis. *Int J Biol Macromol*. 2024;257:128609. <https://doi.org/10.1016/j.ijbio.2023.128609>.
20. Zhang XO, Dong R, Zhang Y, Zhang JL, Luo Z, Zhang J, et al. Diverse alternative back-splicing and alternative splicing landscape of circular RNAs. *Genome Res*. 2016;26(9):1277–87. <https://doi.org/10.1101/gr.202895.115>.
21. Sun J, Xie F, Wang J, Luo J, Chen T, Jiang Q, et al. Integrated meta-omics reveals the regulatory landscape involved in lipid metabolism between pig breeds. *Microbiome*. 2024;12:33. <https://doi.org/10.1186/s40168-023-01743-3>.
22. Stuart T, Butler A, Hoffman P, Hafemeister C, Papalexi E, Mauck WM, et al. Comprehensive integration of single-cell data. *Cell*. 2019;177(7):1888–1902.e21. <https://doi.org/10.1016/j.cell.2019.05.031>.
23. Yu G, Wang LG, Han Y, He QY. clusterProfiler: An R package for comparing biological themes among gene clusters. *OMICS*. 2012;16(5):284–7. <https://doi.org/10.1089/omi.2011.0118>.
24. Hotamisligil GS, Bernlohr DA. Metabolic functions of FABPs: Mechanisms and therapeutic implications. *Nat Rev Endocrinol*. 2015;11(10):592–605. <https://doi.org/10.1038/nrendo.2015.122>.
25. Schlaepfer IR, Joshi M. CPT1A-mediated fat oxidation: mechanisms and therapeutic potential. *Endocrinology*. 2020;161(2):bqz046. <https://doi.org/10.1210/endo/bqz046>.
26. Nelson BR, Makarewich CA, Anderson DM, Winders BR, Troupes CD, Wu F, et al. A peptide encoded by a transcript annotated as long noncoding RNA enhances SERCA activity in muscle. *Science*. 2016;351(6270):271–5. <https://doi.org/10.1126/science.aad4076>.
27. Legnini I, Di Timoteo G, Rossi F, Morlando M, Briganti F, Sthandier O, et al. Circ-ZNF609 is a circular RNA that can be translated and functions in myogenesis. *Mol Cell*. 2017;66(1):22–37.e9. <https://doi.org/10.1016/j.molcel.2017.02.017>.
28. Montaigne D, Butruille L, Staels B. PPAR control of metabolism and cardiovascular functions. *Nat Rev Cardiol*. 2021;18(9):809–23. <https://doi.org/10.1038/s41569-021-00569-6>.
29. Lee K, Kerner J, Hoppel CL. Mitochondrial carnitine palmitoyltransferase 1a (CPT1a) is part of an outer membrane fatty acid transfer complex. *J Biol Chem*. 2011;286(29):25655–62. <https://doi.org/10.1074/jbc.M111.228692>.
30. Wang H, Wang J, Yang DD, Liu ZL, Zeng YQ, Chen W. Expression of lipid metabolism genes provides new insights into intramuscular fat deposition in Laiwu pigs. *Asian-Australas J Anim Sci*. 2020;33(3):390–7. <https://doi.org/10.5713/ajas.18.0225>.
31. Huang W, Zhang X, Li A, Xie L, Miao X. Genome-wide analysis of mRNAs and lncRNAs of intramuscular fat related to lipid metabolism in two pig breeds. *Cell Physiol Biochem*. 2018;50(6):2406–22. <https://doi.org/10.1159/000495101>.
32. Moseti D, Regassa A, Kim WK. Molecular regulation of adipogenesis and potential anti-adipogenic bioactive molecules. *Int J Mol Sci*. 2016;17(1):124. <https://doi.org/10.3390/ijms17010124>.
33. Solly EL, Dimasi CG, Bursill CA, Psaltis PJ, Tan JTM. MicroRNAs as therapeutic targets and clinical biomarkers in atherosclerosis. *J Clin Med*. 2019;8(12):2199. <https://doi.org/10.3390/jcm8122199>.
34. Kikuchi K, Tsukamoto H. Stearoyl-CoA desaturase and tumorigenesis. *Chem Biol Interact*. 2020;316:108917. <https://doi.org/10.1016/j.cbi.2019.108917>.
35. O'Neill CM, Minihane AM. The impact of fatty acid desaturase genotype on fatty acid status and cardiovascular health in adults. *Proc Nutr Soc*. 2017;76:64–75. <https://doi.org/10.1017/S0029665116000732>.
36. Jiang S, Ren Z, Yang Y, Liu Q, Zhou S, Xiao Y. The GPIIb/IIIa-LPL complex and its role in plasma triglyceride metabolism: Insights into chylomicronemia. *Biomed Pharmacother*. 2023;169:115874. <https://doi.org/10.1016/j.biopha.2023.115874>.
37. Hung YH, Carreiro AL, Buhman KK. Dgat1 and Dgat2 regulate enterocyte triacylglycerol distribution and alter proteins associated with cytoplasmic lipid droplets in response to dietary fat. *Biochim Biophys Acta Mol Cell Biol Lipids*. 2017;1862(6):600–14. <https://doi.org/10.1016/j.bbalip.2017.02.014>.
38. Liss KHH, Lutkewitte AJ, Pietka T, Finck BN, Franczyk M, Yoshino J, et al. Metabolic importance of adipose tissue monoacylglycerol acyltransferase 1 in mice and humans. *J Lipid Res*. 2018;59(9):1630–9. <https://doi.org/10.1194/jlr.M084947>.
39. Ramos SV, Turnbull PC, MacPherson RE, LeBlanc PJ, Ward WE, Peters SJ. Changes in mitochondrial perilipin 3 and perilipin 5 protein content in rat skeletal muscle following endurance training and acute stimulated contraction. *Exp Physiol*. 2015;100(4):450–62. <https://doi.org/10.1113/expphysiol.2014.084434>.
40. Lookene A, Beckstead JA, Nilsson S, Olivecrona G, Ryan RO. Apolipoprotein A-V-heparin interactions: Implications for plasma lipoprotein metabolism. *J Biol Chem*. 2005;280(29):25383–7. <https://doi.org/10.1074/jbc.M501589200>.
41. Yang H, Zhao H, Ren Z, Yi X, Zhang Q, Yang Z, et al. Overexpression of CPT1A reduces lipid accumulation via PPARα/CD36 axis to suppress the cell proliferation in ccRCC. *Acta Biochim Biophys Sin*. 2022;54(2):220–31. <https://doi.org/10.3724/abbs.2021023>.
42. Li Q, Wang Y, Wu S, Zhou Z, Ding X, Shi R, et al. CircACC1 regulates assembly and activation of AMPK complex under metabolic stress. *Cell Metab*. 2019;30:157–173.e7. <https://doi.org/10.1016/j.cmet.2019.05.009>.



Plant-derived miR166a-3p packaged into exosomes to cross-kingdom inhibit mammary cell proliferation and promote apoptosis by targeting *APLNR* gene

Yiru Shi¹, Junjie Wei¹, Ying Nie, Junyi Luo, Ting Chen, Qianyun Xi, Yongliang Zhang, Jiajie Sun*

Guangdong Provincial Key Laboratory of Animal Nutrition Control, College of Animal Science, South China Agricultural University, Guangzhou, Guangdong 510642, China

ARTICLE INFO

Keywords:
miRNA
Cross-kingdom
Mammary gland

ABSTRACT

Plant-derived microRNAs (miRNAs) have attracted significant attention for their potential in cross-kingdom gene regulation, but the mechanisms of their entry, stability, and function in animal bodies need further investigation. We provided an in-depth analysis of tissue-specific miRNA expression in dairy cows, identifying 347 miRNAs, including 16 novel candidates, across 21 normal tissues. Our findings revealed that specific miRNAs, such as miR-192, miR-143, miR-148a, miR-486, and miR-21-5p, showed distinct tissue enrichment. In addition, a total of 167 maize-derived miRNAs were identified in dairy cow tissues, particularly in the rumen, mammary glands, serum, and exosomes. These exogenous miRNAs, which are abundant and conserved among plants, may be absorbed by the SLC46A2 transporter in the rumen epithelium during feeding and distributed to other tissues via exosomal encapsulation. The maize-derived miR166a-3p was highly abundant. Transfection experiments confirmed that miR166a-3p reduces the expression of proliferation markers (PCNA, Cyclin D, and Cyclin E) and the anti-apoptotic gene Bcl2, while upregulating the pro-apoptotic gene Bax. Moreover, exosomes derived from bovine serum were found to mediate these effects, as miR166a-3p-enriched exosomes inhibited cell proliferation and promoted apoptosis, further supporting the cross-kingdom role of plant-derived miRNAs in regulating biological processes. This study enhances the understanding of miRNA regulatory mechanisms, particularly the absorption and systemic transport of plant-derived miRNAs in dairy cows. The findings underscore the potential for using exogenous miRNAs, like miR166a-3p, in agricultural and medical contexts, warranting further investigation into their functions and cross-species interactions.

1. Introduction

MicroRNAs (miRNAs) are a class of small non-coding RNAs that act as pivotal regulators of gene expression by mediating post-transcriptional gene expression and degrading target mRNA, thus playing many important roles in living organisms [1]. In various organisms, miRNA candidates are differentially expressed at distinct developmental stages, cell types, and tissues [2]. Numerous reports have demonstrated that the unique expression patterns of tissue-specific miRNAs reflect various physiological and pathological conditions [3–5]. In recent years, an increasing number of studies have shown that miRNAs can be transferred between species and regulate gene

expression in recipient cells [6,7]. Stable miRNA molecules derived from food plants may enter the circulatory systems of mammals and inhibit the production of specific mammalian proteins [8]. For example, the plant miRNA-168a, originating from a food source specifically *Oryza sativa* (rice), is present and stable in human serum. Further studies showed that miRNA-168a can reduce LDLRAP1 protein levels in the blood and liver of mice fed rice [9]. Another plant miRNA enriched in honeysuckle decoction, named miRNA-2911, has been shown to directly target various influenza A subtypes [10]. In addition, plant miRNAs in bee bread delay development and decrease body and ovary size in honeybees, thereby preventing larval differentiation into queens and inducing development into worker bees [11]. These studies suggest that

* Corresponding author at: South China Agricultural University, 483# Wushan Road, Guangzhou, Guangdong 510642, China.

E-mail address: jiajiesun@scau.edu.cn (J. Sun).

¹ Yiru Shi and Junjie Wei contributed equally to this work.

<https://doi.org/10.1016/j.ijbiomac.2024.138470>

Received 26 October 2024; Received in revised form 2 December 2024; Accepted 4 December 2024

Available online 5 December 2024

0141-8130/© 2024 Elsevier B.V. All rights are reserved, including those for text and data mining, AI training, and similar technologies.

plant food-derived miRNAs may transfer to animals and regulate gene expression within their cells [12,13].

Exosomes are nanoscale cell-derived vesicles that encapsulate functional molecules, including proteins, lipids, DNA, and various RNA species [14,15]. To date, many miRNAs have been identified in serum and other body fluids, serving as biomarkers for disease [16–18]. These secreted miRNAs, particularly those found in exosomes, may facilitate paracrine and endocrine communication between different tissues, thereby modulating gene expression and the function of distant cells [19]. Furthermore, more than half of the plant-derived miRNAs detected in human and animal blood are found in exosomes [9]. In detail, exosome-derived miRNAs from ginger have been extensively studied and shown to provide versatile therapeutic benefits against inflammatory diseases [20]. A substantial proportion of the miRNAs in milk is encapsulated within exosomes, enabling the delivery of the entire miRNA cargo to cells that uptake dietary miRNAs [21]. In porcine breast milk exosomes, plant-derived miRNAs have been identified in particularly large quantities [22]. These studies suggest that miRNAs may be protected and transported via exosomes or microvesicles, allowing them to maintain stability and activity during cross-species transfer [23–25].

In the present study, we analyzed the miRNA expression profiles of various tissues and cell types in dairy cows using public miRNA sequencing datasets, and evaluated tissue-specific miRNAs through bioinformatics analysis. We were surprised to detect a substantial number of exogenous plant miRNAs in dairy cows, particularly in various types of exosomes. Analysis of maize miRNA sequencing data indicates that the maize-derived miRNA species found in dairy cows correspond to the miRNA species that are highly enriched in forage maize tissues. Moreover, further in vitro analysis demonstrated that the food-derived exogenous miR166a-3p can cross kingdoms to regulate APLNR protein expression, as well as the proliferation and apoptosis of mammary cells.

2. Material and methods

2.1. miRNA analysis

A total of 558 miRNA sequencing datasets from dairy cows were downloaded from NCBI (<https://www.ncbi.nlm.nih.gov/sra/>) with SRA-Toolkit v3.1.1 (<https://github.com/ncbi/sra-tools/wiki/01.-Downloading-SRA-Toolkit>), representing 21 different tissue or cell types. These include the rumen, liver, duodenum, jejunum, ileum, cecum, colon, and mammary gland, as well as plasma, serum, blood cells, whole blood, plasma exosomes, serum exosomes, blood exosomes, whole milk, milk exosomes, preadipocytes, adipocytes, alveolar macrophages, and follicular fluid extracellular vesicles (Table S1A). The preliminary quality control of raw reads was carried out using FastQC software v0.12.0 (<https://www.bioinformatics.babraham.ac.uk/projects/fastqc/>). The adaptor sequences were trimmed, and reads with poly-A tails and those shorter than 18-nt were removed using Fastx-Toolkit v0.0.14 (https://github.com/agordon/fastx_toolkit). Then, the clean reads from each library were aligned to the *Bos taurus* reference genome (https://ftp.ensembl.org/pub/release-110/fasta/bos_taurus/dna/) using Bowtie v1.3.1 [26]. The mappable sequences were used for bovine miRNA prediction with the miRDeep2 program [27], while the unmapped reads were further screened against the *Zea mays* genome (https://ftp.ebi.ac.uk/ensemblgenomes/pub/release-59/plants/fasta/zea_mays/dna/) for the analysis of plant-derived exogenous miRNAs in dairy cows. In addition, we obtained 31 miRNA libraries of *Zea mays* from NCBI for the prediction of maize-enriched miRNAs, including anthers, embryos, leaves, ovaries, pollen, roots, stems, seeds, shoots, seedlings, and tassels (Table S1B).

2.2. Transcriptome analysis

We acquired 18 rRNA-depleted RNA-seq libraries, focusing on six

different bovine gastrointestinal tissues, including the rumen, duodenum, jejunum, ileum, colon, and rectum (Table S1C). After quality control, the clean reads from the RNA-seq libraries were mapped to the bovine reference genome using HISAT2 v2.1.0, and StringTie v2.0.6 was used to assemble and quantify the transcripts in each library [28]. The transcript expression levels were measured and normalized as fragments per kilobase of exon per million mapped reads (FPKM), and Ballgown v2.20.0 [28] was used to identify and compare differentially expressed transcripts, as well as to produce tables and plots. For bovine MAC-T cells, total RNA was isolated using Trizol Reagent (Invitrogen, Life Technologies, Carlsbad, CA), and the RNA-seq library was constructed using the NEBNext Ultra RNA Library Prep Kit (NEB#7530, New England Biolabs, Ipswich, MA). The libraries were then sequenced on an Illumina NovaSeq 6000 sequencer. Low-quality reads were filtered and discarded using fastp v0.18.0 [29]. The paired-end clean reads were mapped to the reference genome using HISAT2 v2.1.0, and the mapped reads of each library were assembled using StringTie v2.0.6 with a reference-based approach. The differentially expressed genes (DEGs) between the two groups were identified with FPKM values by DESeq2 v1.1.25 [30]. The DEGs were screened with a $|\log_2 \text{fold change}|$ of ≥ 1 and an FDR of < 0.05 .

2.3. Cell culture

MAC-T and MDA-MB-231 cells were cultured in Dulbecco's Modified Eagle Medium (DMEM) supplemented with 10 % FBS. The cells were maintained in a humidified incubator at 37 °C with 5 % CO₂.

2.4. miRNA transfection

The cells were seeded into 12, 24, 48, or 96-well plates at 70 % confluence and kept in the incubator overnight. The miR166a-3p mimic, negative control mimic, inhibitor negative control, or mir166a-3p inhibitor were transfected using Lipofectamine 2000 (Invitrogen, Life Technologies, Carlsbad, CA). The transfected cells were then incubated for 48 h. The total RNA and protein were harvested separately and stored at −80 °C for further analysis.

2.5. Total RNA isolation and RT-qPCR

Total RNA was isolated from MAC-T and MDA-MB-231 cells using Trizol Reagent (Invitrogen), and cDNA was synthesized using the PrimeScript™ RT Reagent Kit with gDNA Eraser (Takara, Tokyo, Japan). The Quantitative PCR (qPCR) was performed with SYBR Premix Ex TaqII (Takara) using a Bio-Rad CFX96 Real-Time PCR system (Bio-Rad Laboratories, Hercules, CA). Gene expression levels were calculated by the 2^{−ΔCt} method using porcine *GAPDH* as a reference gene, and the reactions were always performed in quadruplicates. For mir166a-3p, the mature molecules were polyadenylated and reverse transcribed using a mir-X miRNA First-Strand Synthesis Kit (Clontech, Palo Alto, CA). A miR-X miRNA RT-qPCR SYBR Kit (Clontech) was then used to quantify their expression relative to the level of U6 snRNA (U6 primers were included in the kits).

2.6. Protein isolation and western blot

The proteins were extracted from MAC-T and MDA-MB-231 cells using RIPA lysis buffer (Solarbio, Beijing, China). Equal amounts of proteins were subjected to SDS-PAGE and subsequently transferred onto polyvinylidene fluoride (PVDF) membranes (Millipore, Bedford, MA). The membranes were then probed with specific primary antibodies, followed by incubation with goat anti-rabbit IgG-HRP or goat anti-mouse IgG-HRP secondary antibodies (Bioworld, Minneapolis, MN). Immunoreactive protein bands were visualized using an enhanced chemiluminescence solution (Solarbio). The antibodies targeted proteins including PCNA, Cyclin D, Cyclin E, Bcl2, Bax, and Tubulin.

2.7. Immunofluorescence assay

The MAC-T and MDA-MB-231 cells for immunofluorescence staining were cultured and treated in 48-well plates, fixed in 4 % formaldehyde, permeabilized with 0.2 % Triton X-100, and finally blocked with bovine serum albumin (BSA). Primary antibodies against APLNR (Proteintech, Wuhan, China) were diluted to 1:100 in PBS containing 1 % BSA and incubated for 12 h at 4 °C. The corresponding fluorescently labeled secondary antibody was incubated at room temperature for 1 h, while DAPI was incubated at room temperature for 5 min. Images were captured with the Nikon TS2 microscope (Nikon, Tokyo, Japan).

2.8. Cell Counting Kit-8 (CCK-8)

We used the CCK-8 assay kit (EZBioscience, Roseville, MN) to evaluate the viability of the treated cells. Approximately 100 μ L of cell suspension was dispensed into a 96-well plate, and the cells received different treatments according to the experimental design. Then, 10 μ L of CCK-8 solution was added to each well, and the cells were incubated for an additional 4 h. The cell viability was measured with a microplate reader (Thermo Fisher Scientific, Waltham, MA) by assessing the absorbance at a wavelength of 450 nm.

2.9. EdU proliferation assay

The cells were inoculated into 48-well plates and transfected with miR166a-3p mimics, inhibitors, or controls. After 48 h, the Beyoclick™ Edu-488 Kit (Biyuntian Biotechnology, Shanghai, China) was used for cell proliferation detection. A fluorescence inverted microscope (Nikon, Tokyo, Japan) was used to capture images, which were then analyzed using Image J software (Media Cybernetics, Bethesda, MD).

2.10. Flow cytometric analysis

The cells harvested during logarithmic growth were resuspended in PI/RNase staining buffer (BD Biosciences, Franklin Lakes, NJ) and cultured in the dark at 37 °C for 30 min. Finally, the cell cycles were analyzed using a BD Accuri C6 flow cytometer (BD Biosciences) and FACSDiVa software (BD Biosciences).

2.11. Dual luciferase assay

The potential target genes of maize-derived miR166a-3p were successfully predicted using miRanda software [31]. The mutant (APLNR-mut) fragments were generated by deleting the reverse complementary binding sites of the miRNA seed region. Both the wild type (APLNR-wild) and mutant fragments were then cloned into the pmirGLO vector (Promega, Madison, WI). HEK293 cells were inoculated in 96-well plates, and the recombinant plasmids were co-transfected with miR166a-3p mimics or bovine sera exosomes. After 48 h of culture, luciferase activity was detected using the Dual-Glo® Reagent and Dual-Glo® Stop & Glo Reagent (Promega, Madison, WI).

2.12. Statistical analysis

Differences between the two groups were analyzed using ANOVA followed by a Student's *t*-test. Statistical significance was defined as $P < 0.05$, with significance levels indicated by one asterisk for $P < 0.05$ and two asterisks for $P < 0.01$.

3. Results

3.1. Tissue-specific analysis of miRNA expression in dairy cows

To analyze the miRNA profiles of dairy cows, we first obtained miRNA expression profiles from 558 samples across 21 normal tissues

(Table S1A). We then used these profiles to assess the tissue specificity of miRNAs in dairy cows. Based on PCA analysis of the miRNA expression levels, 23 outlier samples were removed (Figs. 1A; S1A). In detail, a total of 347 miRNAs were identified through bioinformatics analysis, including 16 novel miRNAs (Table S1D). Interestingly, we found that specific miRNAs were linked to distinct tissue types (Fig. S1B). For example, miR-192 was significantly enriched in the liver, miR-143 in digestive and absorptive tissues such as the gastrointestinal tract, miR-148a in tissues like mammary glands and breast exosomes, miR-486 in blood-related samples, and miR-21-5p in adipose tissue.

3.2. Maize-derived miRNAs are present in the circulatory system and organs of dairy cows

A total of 167 maize-derived miRNAs were detected across various dairy cow tissues (Table S1E), showing major enrichment in the rumen, mammary glands, as well as in other circulatory tissues or cell types, such as serum, whole milk, and a variety of exosomes, while there was little enrichment in intestinal tissues. The results suggest that the absorption of plant-derived miRNAs may primarily occur through rumen tissue. In detail, zma-miR166, zma-miR159, zma-miR156, and zma-miR167 are enriched in these tissues (Fig. S1C), with zma-miR166 showing the highest level of enrichment in dairy cow (Fig. 1B). To investigate miRNA expression in different maize tissues, we obtained miRNA expression profiles from 31 samples across 11 tissues (Table S1B). A total of 319 miRNAs were detected in maize samples (Table S1F), among which miR166a-3p is specifically expressed and highly abundant in some tissues commonly used as feed materials, such as maize leaf, shoot apex, and seeds (Figs. 1C, S1D). In addition, sequence comparison of maize miR166a-3p with miR166a-3p from other edible plant sources indicated that miR166a-3p is highly conserved across species (Table S1G). Our results indicated that zma-miR166 is highly conserved across species and may be absorbed by animals through non-intestinal tissues via a saturation adsorption mechanism.

3.3. Transcriptomic analysis of gastrointestinal tissues in dairy cows

Consistent with our results, a previous study showed that the stomach is the main organ for exogenous miRNA uptake, while the intestine does not contribute to this process [9]. These findings suggest that the uptake might be attributed to the presence of specific transport protein carriers associated with miRNA in the rumen tissue. Therefore, we obtained transcriptome datasets of 18 samples across gastrointestinal tissues in dairy cows to explore the differentially expressed genes between rumen and intestinal tissues (Table S1C). Principal component analysis (PCA) and clustering analyses clearly demonstrated that the rumen samples were distinct from other intestinal samples (Fig. 1D). In total, 2083 differentially expressed transcripts were identified between the rumen and intestinal tissues, with 771 transcripts significantly upregulated and 1312 transcripts significantly downregulated in the rumen tissue (Fig. 1E, Table S1H). A total of 38 solute carrier genes related to transport were differentially expressed, among which 12 were highly expressed in the rumen (Fig. 1F), representing potential transmembrane carrier genes for the absorption and transport of plant-derived miRNAs.

3.4. miR166a-3p inhibits MAC-T cell proliferation and promotes apoptosis

To further investigate the role of miR166a-3p in the proliferation and apoptosis of MAC-T cells, we conducted transfection with miR166a-3p mimics, along with CCK-8, EdU, and flow cytometric analyses. The transfection efficiency of the mimics was validated by RT-qPCR, showing that miR166a-3p was highly upregulated following mimic transfection. In contrast, the inhibitor group showed no significant difference compared to the control group (Fig. 2A), indicating that

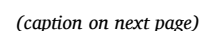


Fig. 1. Bioinformatics analysis of miRNA expression in dairy cows.

(A) PCA analysis of 535 miRNA sequencing samples from dairy cows. AD, adipocytes; AM, alveolar macrophage; BC, blood cell; BE, blood exosomes; CE, cecum; CO, colon; DU, duodenum; FV, follicular fluid extracellular vesicles; IL, ileum; JE, jejunum; LI, liver; MG, mammary gland; ME, milk exosome; PL, plasma; PE, plasma exosomes; PA, preadipocytes; RU, rumen; SE, serum; SV, serum extracellular vesicle; WB, whole blood; WM, whole milk.

(B) Relative enrichment levels of miR166a-3p in various dairy cow tissues.

(C) Relative enrichment levels of miR166a-3p in maize tissues. AN, anther; EM, embryo; LE, leaf; OV, ovary; PO, pollen; RO, root; SD, seed; SL, seedling; SA, shoot apex; SH, shoot; TP, tassel primordia.

(D) PCA analysis of 18 RNA sequencing samples from the gastrointestinal tract of dairy cows.

(E) Differentially expressed genes between the rumen and other intestinal tissues in dairy cows.

(F) Differentially expressed transporter genes between the rumen and other intestinal tissues in dairy cows.

miR166a-3p was not originally present in MAC-T cells. The CCK-8 assay was performed to examine the growth of MAC-T cells, and the results showed that miR166a-3p mimic transfection inhibited cell proliferation (Fig. 2B). The results of the EdU assay were consistent with those of the CCK-8 proliferation assay (Fig. 2C). We analyzed the effect of miR166a-3p on apoptosis in MAC-T cells using flow cytometry. The results showed that the apoptosis rate in the miR166a-3p mimics group was significantly higher than in the control group (Fig. 2D). We found that the expression levels of proliferation marker genes, *PCNA*, *Cyclin D*, and *Cyclin E*, were significantly decreased in mimic-transfected cells compared to the control group. Furthermore, the expression level of *Bcl2*, a gene associated with the inhibition of apoptosis, was decreased, while the expression level of the apoptosis marker gene *Bax* was significantly increased in mimic-transfected cells compared to the control group (Fig. 2E). In addition, the mimics-transfected group significantly downregulated the protein expression levels of *PCNA*, *Cyclin D*, *Cyclin E*, and *Bcl2*, and significantly upregulated the expression level of *Bax* compared to the control group. These results suggest that the plant-derived miR166a-3p inhibits the proliferation of mammary epithelial cells and promotes apoptosis.

3.5. The predicted target genes of miR166a-3p

We conducted an in-depth analysis of global gene expression using Illumina HiSeq to compare miR166a-3p mimics with control groups. Three cDNA libraries were constructed for each group, with an average of 52.26 ± 4.02 million clean reads per library. The average unique mapping rate was 94.58 ± 0.11 %, and the overall mapping rate was 96.76 ± 0.09 % (Table S2A). These findings validated the successful construction of the libraries and confirmed their suitability for subsequent analyses. A total of 16,203 known transcripts were identified across all six libraries, and transcript abundance was quantified using FPKM values (Table S2B). PCA analysis using these FPKM values revealed that the tested individuals were distinctly separated into two groups, reflecting the differences in gene expression in response to miR166a-3p transfection (Fig. 3A). Compared to the control group, we identified 172 significantly DEGs, consisting of 94 up-regulated and 78 down-regulated genes in miR166a-3p transfected cells (Fig. 3B). To determine miRNA-DEGs interactions, target prediction of miR166a-3p was performed using miRanda software, with the 78 down-regulated genes as the target reference genes (Table S2C). The results suggested that *APLNR* was targeted by miR-166a-3p, which was consistent with the expression level of *APLNR* in miR-166a-3p transfected cells (Fig. 3C), as well as the protein expression assessed by Western blot analysis (Fig. 3D) and immunofluorescence assay (Fig. 3E). We co-transfected *APLNR*-wild and *APLNR*-mut with miR166a-3p mimics (or bovine sera exosomes) into HEK293 cells, and measured changes in the ratio of Firefly/Renilla luciferase activity (Fig. 3F). In the *APLNR*-wild group, the luciferase activity ratio decreased significantly compared to the *APLNR*-mut group, as well as with bovine serum exosomes supplementation.

3.6. Serum-derived exosomes inhibit MAC-T cell proliferation and promote apoptosis

Our results showed that plant-derived miR166a-3p is enriched in bovine serum exosomes. Further investigation is necessary to determine whether miR166a-3p influences the development of mammary gland cells via serum exosome transport. The MAC-T cells were cultured and treated with PBS or exosomes extracted from the sera of dairy cows. In the other two groups, the cells were treated with exosomes following transfection with either a miR166a-3p inhibitor or control. We found that the expression levels of *PCNA*, *Cyclin D*, *Cyclin E*, and *Bcl2* were significantly downregulated after exosome treatment compared with the control group, while the expression level of *Bax* was upregulated (Fig. 4A). These changes were reversed in the MAC-T cells following exosome treatment with miR166a-3p inhibitor transfection (Fig. 4B). Western blotting also showed that the protein expression levels of *PCNA*, *Cyclin D*, *Cyclin E*, and *Bcl2* were significantly downregulated after exosome treatment compared with the control group, while the protein expression level of *Bax* was upregulated (Fig. 4C). These changes were also reversed in the exosome treatment with miR166a-3p inhibitor transfection group (Fig. 4D). In addition, after exosome treatment, the expression level of *APLNR* was significantly downregulated (Fig. 4E), but this change was reversed in the exosome treatment with miR166a-3p inhibitor transfection group (Fig. 4F). We further validated this using Western blot, which yielded consistent results (Fig. 4G–H). The results suggest that miR166a-3p can target *APLNR* and exert biological effects via exosomes.

3.7. miR166a-3p inhibits the proliferation and promotes the apoptosis of MDA-MB-231 cells

To further confirm the role of miR166a-3p in regulating the proliferation and apoptosis of breast cancer cells, MDA-MB-231 cells were transfected with miR166a-3p mimics. The CCK-8 analysis indicated that transfection with miR166a-3p mimics inhibited cell proliferation (Fig. 5A). The Edu assay results were consistent with the findings of the CCK-8 proliferation assay (Fig. 5B). Flow cytometry was used to assess the impact of miR166a-3p on apoptosis in MDA-MB-231 cells, revealing that the apoptosis rate in the miR166a-3p mimic group was significantly higher than that in the control group (Fig. 5C). We observed that the expression levels of *PCNA*, *Cyclin D*, *Cyclin E*, and *Bcl2* were markedly decreased in cells transfected with the mimics, while the expression level of *Bax* was significantly increased (Fig. 5D). These findings were supported by Western blotting analysis in protein levels (Fig. 5E). In addition, the expression of *APLNR* was reduced following transfection with miR166a-3p mimics compared to the control group (Fig. 5F), as corroborated by RT-qPCR (Fig. 5G) and western blot analysis (Fig. 5H). The results suggest that miR166a-3p targets *APLNR* to inhibit the proliferation and promote the apoptosis of breast cancer cells.

4. Discussion

A large number of miRNAs exhibit tissue-specific expression patterns. For instance, miR-192 serves as a liver-specific biomarker across multiple species [32,33]. It has been confirmed that miR-143 is

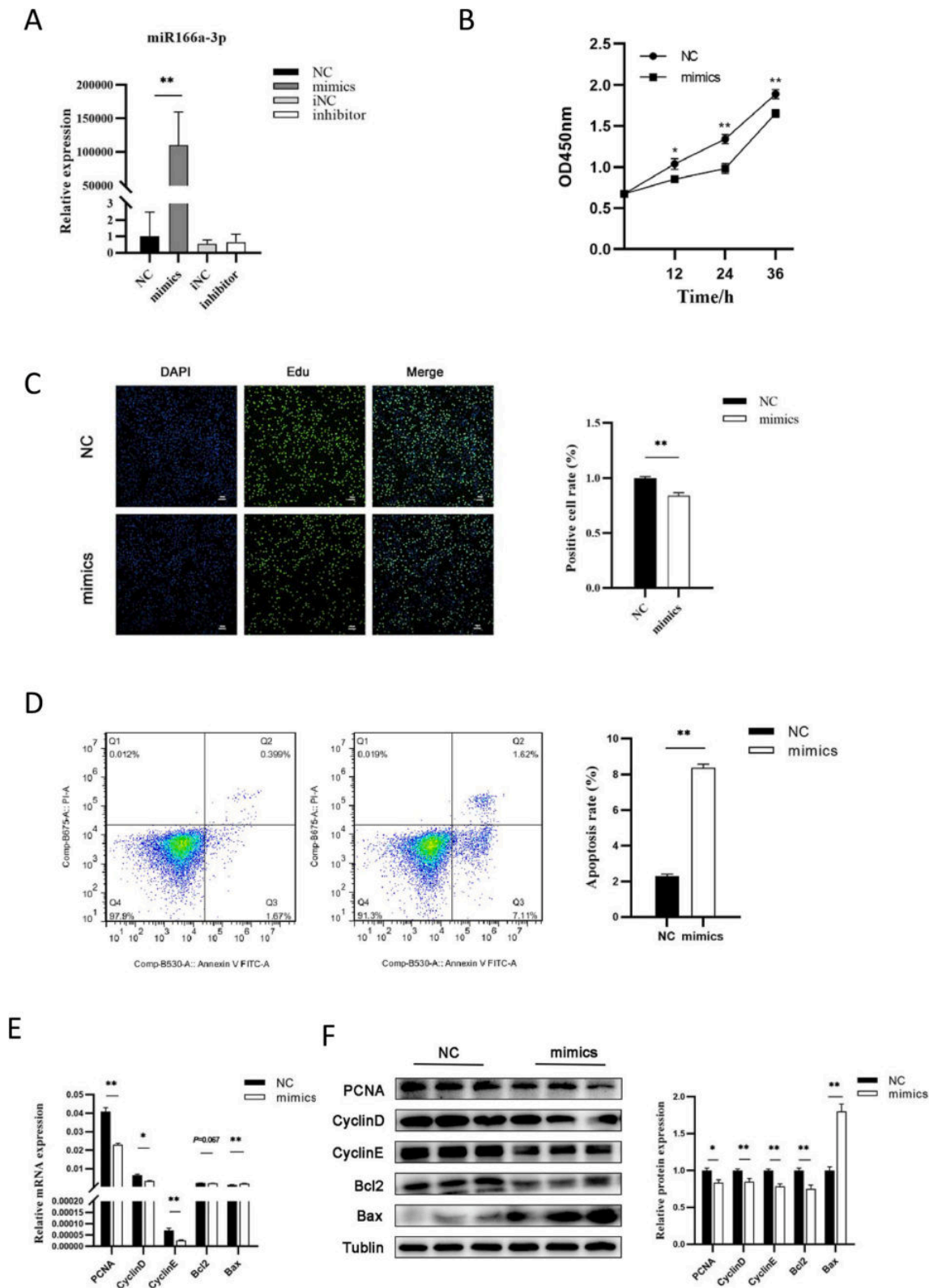


Fig. 2. miR166a-3p inhibits proliferation and promotes apoptosis in MAC-T cells. (A) Validation of miR166a-3p transfection efficiency. (B) CCK-8 assay showing proliferation in MAC-T cells. (C) Edu assay showing proliferation in MAC-T cells. (D) Flow cytometric analysis of apoptosis in MAC-T cells. (E) RT-qPCR analysis showing expression levels of genes related to cell proliferation and apoptosis. (F) Western blot analysis showing expression levels of proteins related to cell proliferation and apoptosis.

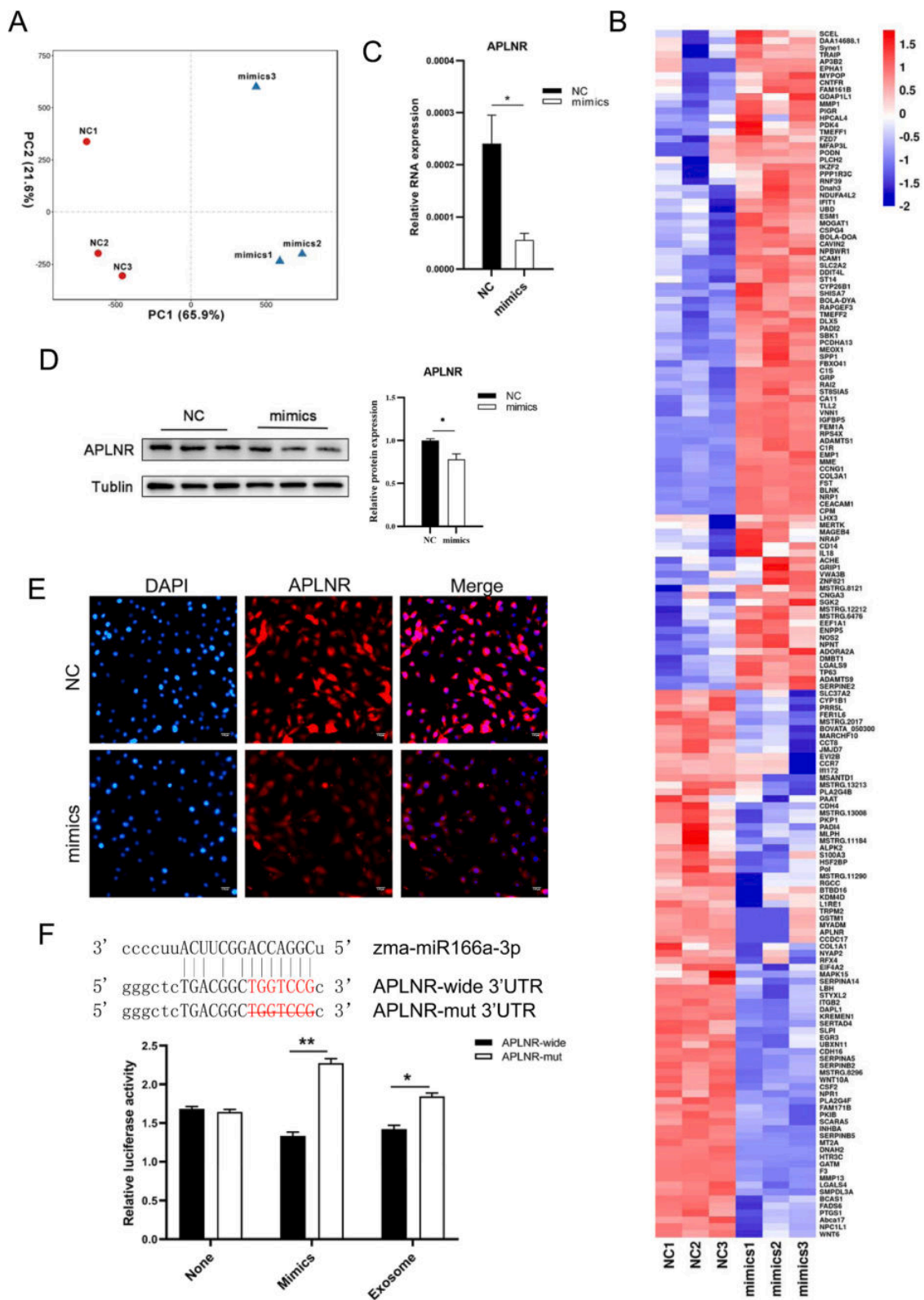


Fig. 3. The analysis of target genes for plant-derived miR166a-3p. (A) PCA analysis based on the transcriptome of MAC-T cell samples transfected with miR166a-3p. (B) Heatmap showing differentially expressed genes between the miR166a-3p mimic and control groups. (C) RT-qPCR assay of *APLNR* gene expression in MAC-T cells after transfection with miR166a-3p. (D) Western blot assay of *APLNR* protein expression in MAC-T cells after transfection with miR166a-3p. (E) Immunofluorescence assay of *APLNR* protein expression in MAC-T cells after transfection with miR166a-3p. (F) Targeting sites and dual-luciferase assay results for miR166a-3p and *APLNR*.

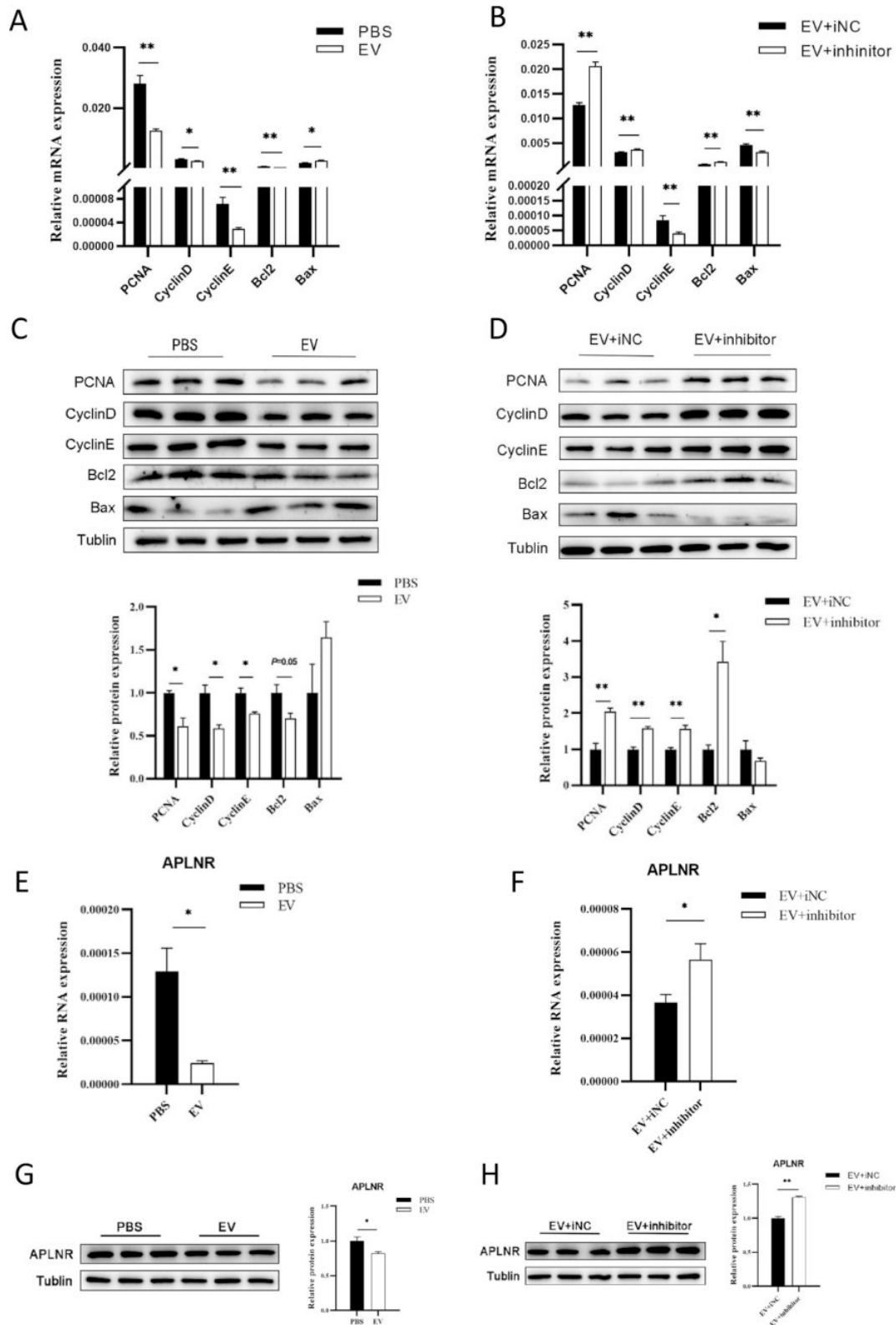


Fig. 4. Sera-derived exosomes inhibit MAC-T cell proliferation and promote apoptosis.

(A) Expression levels of cell proliferation-related and apoptosis-related genes in MAC-T cells treated with exosomes.

(B) Expression levels of cell proliferation-related and apoptosis-related genes in exosome-treated MAC-T cells transfected with a miR166a-3p inhibitor.

(C) Expression levels of cell proliferation-related and apoptosis-related proteins in MAC-T cells treated with exosomes.

(D) Expression levels of cell proliferation-related and apoptosis-related proteins in exosome-treated MAC-T cells transfected with a miR166a-3p inhibitor.

(E) Expression levels of APLNR in MAC-T cells treated with exosomes.

(F) Expression levels of APLNR in exosome-treated MAC-T cells transfected with a miR166a-3p inhibitor.

(G) Western blot assay of APLNR protein expression in MAC-T cells after treated with exosomes.

(H) Western blot assay of APLNR protein expression in exosome-treated MAC-T cells after transfection with a miR166a-3p inhibitor.

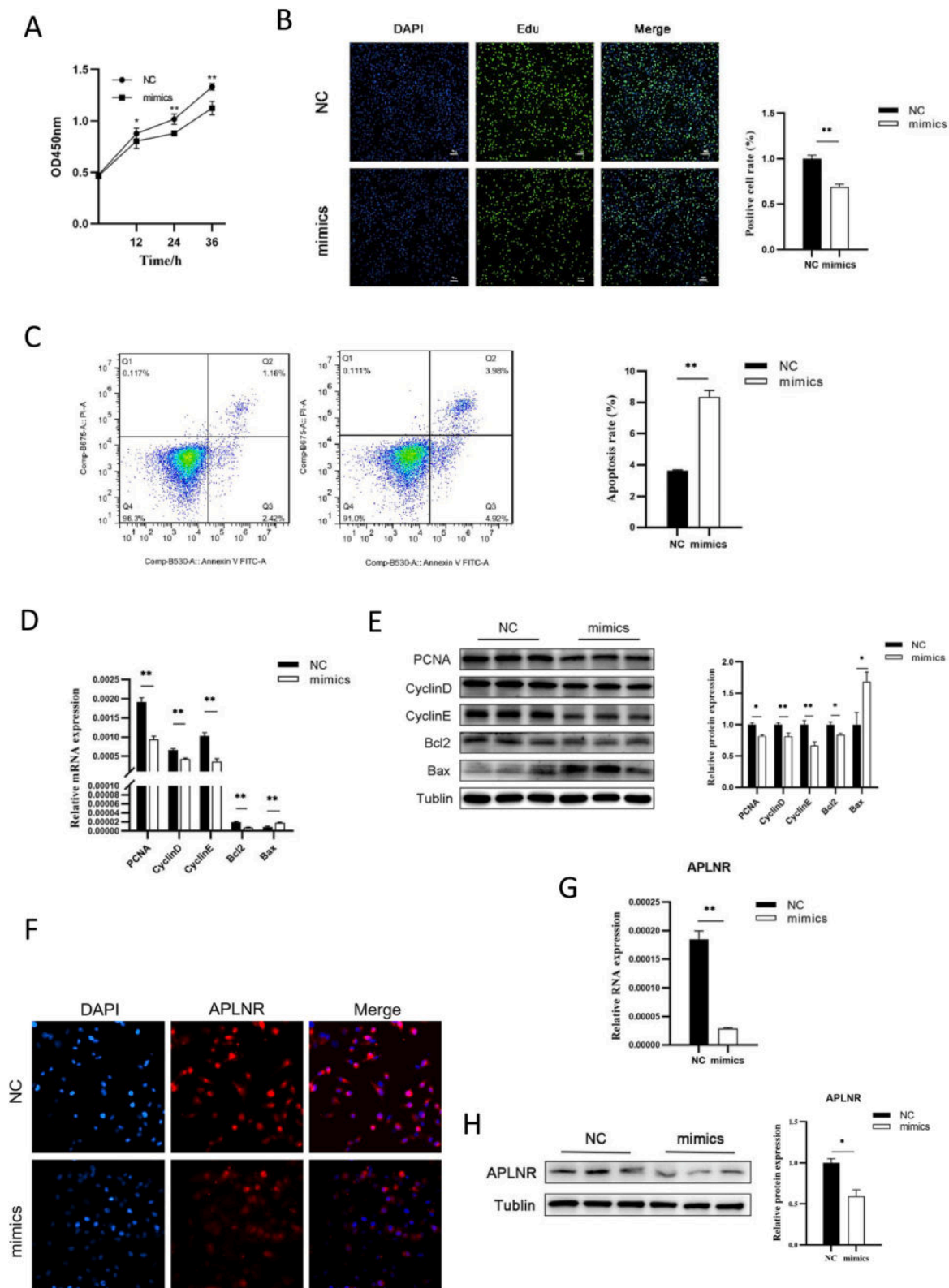


Fig. 5. miR166a-3p inhibits MDA-MB-231 cell proliferation and promotes apoptosis.

(A) CCK-8 assay of proliferation in MDA-MB-231 cells.

(B) EdU assay of proliferation in MDA-MB-231 cells.

(C) Flow cytometric analysis of apoptosis in MDA-MB-231 cells.

(D) RT-qPCR showing the expression levels of cell proliferation-related and apoptosis-related genes in MDA-MB-231 cells treated with miR166a-3p.

(E) Western blot analysis showing the expression levels of cell proliferation-related and apoptosis-related proteins in MDA-MB-231 cells treated with miR166a-3p.

(F) Immunofluorescence assay of APLNR protein expression in MDA-MB-231 cells after transfection with miR166a-3p.

(G) RT-qPCR assay of APLNR gene expression in MDA-MB-231 cells after transfection with miR166a-3p.

(H) Western blot assay of APLNR protein expression in MDA-MB-231 cells after transfection with miR166a-3p.

predominantly expressed in the gastrointestinal tract, where its high abundance likely plays an important role in regulating the rapid development and growth of the gastrointestinal tract during early life [34,35]. Meanwhile, miR-148a belongs to a highly conserved family and is abundantly expressed in mammary gland tissue [36,37]. Researchers have also linked miR-148a to mammary gland development, lactation, and disease [38–41]. In addition, miR-486, the most dominant micro-RNA in peripheral blood [42,43], has been identified as a promising diagnostic marker for the early detection and recurrence prediction of certain diseases [44–46]. Moreover, miR-21-5p is associated with adipose tissue deposition and the development of obesity [47,48]. Based on the analysis of the miRNA expression profiles of dairy cows, we have identified a series of tissue-specific miRNAs that align with previous findings. The expression patterns of these tissue-specific miRNAs may reflect the growth and developmental status of the organism, and their aberrant expression could serve as a marker of biological progression.

Since Zhang et al. introduced the concept of cross-kingdom gene expression regulation by miRNAs [9], there has been increasing interest in exploring how miRNAs derived from food and plants can potentially regulate gene expression across different kingdoms, providing insights into their functions and applications. To date, a growing number of studies have detected several miRNA candidates originating from various exogenous species, including dietary plants, in humans and animals [22,49,50]. These stable exogenous miRNAs have demonstrated regulatory functions and therapeutic potential [25,51]. For instance, mtr-miR-5754 and gma-miR4995 have been shown to reduce cancer cell production by targeting tumor-associated genes [52]. Plant-derived miR156a inhibits the proliferation of mammalian intestinal epithelial cells by targeting Wnt10b in the Wnt/ β -catenin pathway [13], while miR167e-5p was found to inhibit the proliferation of mammalian intestinal epithelial cells by down-regulating the gene and protein levels of β -catenin [12]. In our study, we identified maize-derived miRNAs in dairy cows, including in the rumen, serum, mammary gland, milk, and various exosomes. Among them, miR166a-3p was enriched at the highest level and was also the most abundant miRNA in tissues commonly used as maize feed ingredients. We found that miR166a-3p is highly conserved across species, suggesting that miR166a-3p from other plant sources may also be transported and stabilized in the animal organism through foraging. There are studies on which dietary miRNAs are absorbed by animals and how they regulate host gene expression, but few focus on the mechanisms underlying their absorption. A previous study indicated that SIDT1/2, RNA transporters expressed in gastric pit epithelial cells, mediates the absorption of dietary miRNAs in the mammalian stomach [53]. Consistent with our results, we detected plant-derived miRNAs that were mainly enriched in the rumen samples of dairy cows, while they were scarcely found in other intestinal tissues. Therefore, we conducted a transcriptome expression analysis comparing the rumen and other intestinal tissues of dairy cows, and no significant differences were found for SIDT1/2 between the rumen and other intestinal tissues. In addition, our results showed that numerous transporter genes were highly expressed in the rumen, including SLC46A2, a novel nucleic acid transporter [54], which was significantly enriched in the rumen compared to other intestinal tissues. Our findings indicate that exogenous miRNAs are primarily absorbed in the rumen of dairy cows through SLC46A2, though additional studies are required to verify this conclusion.

Several studies have demonstrated that exogenous miRNAs play cross-kingdom roles in regulating gene expression in animal organisms [10,55,56]. In our study, miR166a-3p was found to inhibit the proliferation of breast epithelial cells and promote apoptosis by targeting the APLNR gene. One mechanism by which exogenous miRNAs facilitate cross-kingdom regulation is their stable existence within exosome-like vesicles in animals [57–59]. We therefore treated mammary epithelial cells with blood-derived exosomes from dairy cows and found that these exosomes had the same effect as miR166a-3p, suggesting that it is the miR166a-3p within the exosomes that is responsible for this action. In

addition, APLNR has been identified as a prognostic marker in several types of cancers and a promising target for cancer treatment [60,61]. Therefore, we speculated that miR166a-3p might have a therapeutic effect on breast cancer. We transfected MDA-MB-231 cells with miR166a-3p mimics, which were found to inhibit the proliferation of these cells and promote apoptosis. Although the inhibition of mammary cell proliferation and promotion of apoptosis are negative outcomes for dairy production, miR166a-3p shows potential for inhibiting breast cancer cell growth. However, further research is needed to explore its specific practical applications and regulatory mechanisms. Currently, a great number of studies have provided evidence for the presence of plant-derived miRNAs in mammals and have demonstrated the ability of plant-derived miRNAs to mediate cross-kingdom gene regulation [9,62,63]. Additionally, research has found and summarized the application prospects of exogenous plant-derived miRNAs as therapeutics for some human diseases, suggesting that plant-derived miRNAs have the potential to enhance human health [64–66]. These findings have raised our hopes to explore the therapeutic potential and dietary supplement applications of plant miRNAs.

In summary, we identified several tissue-specific miRNAs and confirmed the presence of plant-derived miRNAs in dairy cows. These exogenous miRNAs, which are abundant and conserved in plants, may be absorbed by the SLC46A2 transporter in the rumen epithelium during feeding and distributed to other tissues via exosomal encapsulation. We found that plant-derived miR166a-3p inhibits cell proliferation and promotes apoptosis by targeting the APLNR gene. These findings enhance our understanding of miRNA regulatory mechanisms and provide data supporting the cross-kingdom application of plant-derived miRNAs.

Supplementary data to this article can be found online at <https://doi.org/10.1016/j.ijbiomac.2024.138470>.

CRedit authorship contribution statement

Yiru Shi: Writing – original draft, Validation, Investigation. **Junjie Wei:** Validation, Investigation. **Ying Nie:** Validation, Investigation. **Junyi Luo:** Project administration. **Ting Chen:** Conceptualization. **Qianyun Xi:** Conceptualization. **Yongliang Zhang:** Conceptualization. **Jiajie Sun:** Writing – review & editing, Validation, Supervision, Software, Project administration, Funding acquisition, Formal analysis, Conceptualization.

Funding

This work was supported by the Natural Science Foundation of China Program [grant numbers 32072714].

Declaration of competing interest

The authors declare that they have no known competing financial interests or personal relationships that could have appeared to influence the work reported in this paper.

Acknowledgements

We thank the High Performance Computing Center of South China Agricultural University for providing computational resources in this work.

Data availability

Not applicable.

References

- [1] W. Filipowicz, N. Sonenberg, S.N. Bhattacharyya, Mechanisms of post-transcriptional regulation by micrnas: are the answers in sight? *Nat. Rev. Genet.* 9 (2) (2008) 102–114, <https://doi.org/10.1038/nrg2290>.
- [2] B. John, A.J. Enright, A. Aravin, T. Tuschl, C. Sander, D.S. Marks, Human microrna targets, *PLoS Biol.* 2 (11) (2004) e363, <https://doi.org/10.1371/journal.pbio.0020363>.
- [3] G. Divisato, S. Piscitelli, M. Elia, E. Cascone, S. Parisi, Micrnas and stem-like properties: the complex regulation underlying stemness maintenance and cancer development, *Biomolecules* (Basel, Switzerland) 11 (8) (2021) 1074, <https://doi.org/10.3390/biom11081074>.
- [4] Q. Ji, Y. Ji, J. Peng, X. Zhou, X. Chen, H. Zhao, T. Xu, L. Chen, Y. Xu, Increased brain-specific mir-9 and mir-124 in the serum exosomes of acute ischemic stroke patients, *PLoS One* 11 (9) (2016) e163645, <https://doi.org/10.1371/journal.pone.0163645>.
- [5] A. Ninawe, S.A. Guru, P. Yadav, M. Masroor, A. Samadhiya, N. Bhutani, N. Gupta, R. Gupta, A. Saxena, Mir-486-5p: a prognostic biomarker for chronic myeloid leukemia, *ACS Omega* 6 (11) (2021) 7711–7718, <https://doi.org/10.1021/acsomega.1c00035>.
- [6] S.R. Baier, C. Nguyen, F. Xie, J.R. Wood, J. Zemleni, Micrnas are absorbed in biologically meaningful amounts from nutritionally relevant doses of cow milk and affect gene expression in peripheral blood mononuclear cells, hek-293 kidney cell cultures, and mouse livers, *J. Nutr.* 144 (10) (2014) 1495–1500, <https://doi.org/10.3945/jn.114.196436>.
- [7] Y. Gu, M. Li, T. Wang, Y. Liang, Z. Zhong, X. Wang, Q. Zhou, L. Chen, Q. Lang, Z. He, X. Chen, J. Gong, X. Gao, X. Li, X. Lv, Lactation-related microrna expression profiles of porcine breast milk exosomes, *PLoS One* 7 (8) (2012) e43691, <https://doi.org/10.1371/journal.pone.0043691>.
- [8] Y. Li, Z. Teng, D. Zhao, Plant-derived cross-kingdom gene regulation benefits human health, *Trends Plant Sci.* 28 (6) (2023) 626–629, <https://doi.org/10.1016/j.tplants.2023.03.004>.
- [9] L. Zhang, D. Hou, X. Chen, D. Li, L. Zhu, Y. Zhang, J. Li, Z. Bian, X. Liang, X. Cai, Y. Yin, C. Wang, T. Zhang, D. Zhu, D. Zhang, J. Xu, Q. Chen, Y. Ba, J. Liu, Q. Wang, J. Chen, J. Wang, M. Wang, Q. Zhang, J. Zhang, K. Zen, C.Y. Zhang, Exogenous plant mir168a specifically targets mammalian ldlr1: evidence of cross-kingdom regulation by microrna, *Cell Res.* 22 (1) (2012) 107–126, <https://doi.org/10.1038/cr.2011.158>.
- [10] Z. Zhou, X. Li, J. Liu, L. Dong, Q. Chen, J. Liu, H. Kong, Q. Zhang, X. Qi, D. Hou, L. Zhang, G. Zhang, Y. Liu, Y. Zhang, J. Li, J. Wang, X. Chen, H. Wang, J. Zhang, H. Chen, K. Zen, C.Y. Zhang, Honeyuckle-encoded atypical microrna2911 directly targets influenza a viruses, *Cell Res.* 25 (1) (2015) 39–49, <https://doi.org/10.1038/cr.2014.130>.
- [11] K. Zhu, M. Liu, Z. Fu, Z. Zhou, Y. Kong, H. Liang, Z. Lin, J. Luo, H. Zheng, P. Wan, J. Zhang, K. Zen, J. Chen, F. Hu, C.Y. Zhang, J. Ren, X. Chen, Plant micrnas in larval food regulate honeybee caste development, *PLoS Genet.* 13 (8) (2017) e1006946, <https://doi.org/10.1371/journal.pgen.1006946>.
- [12] M. Li, T. Chen, J.J. He, J.H. Wu, J.Y. Luo, R.S. Ye, M.Y. Xie, H.J. Zhang, B. Zeng, J. Liu, Q.Y. Xi, Q.Y. Jiang, J.J. Sun, Y.L. Zhang, Plant mir167e-5p inhibits enterocyte proliferation by targeting β -catenin, *Cells* 8 (11) (2019), <https://doi.org/10.3390/cells8111385>.
- [13] M. Li, T. Chen, R. Wang, J.Y. Luo, J.J. He, R.S. Ye, M.Y. Xie, Q.Y. Xi, Q.Y. Jiang, J. J. Sun, Y.L. Zhang, Plant mir156 regulates intestinal growth in mammals by targeting the wnt/ β -catenin pathway, *Am. J. Phys. Cell Phys.* 317 (3) (2019) C434–C448, <https://doi.org/10.1152/ajpcell.00030.2019>.
- [14] V. Sokolova, A.K. Ludwig, S. Hornung, O. Rotan, P.A. Horn, M. Eppele, B. Giebel, Characterisation of exosomes derived from human cells by nanoparticle tracking analysis and scanning electron microscopy, *Colloid Surf. B-Biointerf.* 87 (1) (2011) 146–150, <https://doi.org/10.1016/j.colsurfb.2011.05.013>.
- [15] Y. Zhang, Y. Liu, H. Liu, W.H. Tang, Exosomes: biogenesis, biologic function and clinical potential, *Cell Biosci.* 9 (2019) 19, <https://doi.org/10.1186/s13578-019-0282-2>.
- [16] M. Shew, H. Wichova, P.M. St. A. Warnecke, H. Staeker, Distinct microrna profiles in the perilymph and serum of patients with menière's disease, *Front. Neurol.* 12 (2021) 646928, <https://doi.org/10.3389/fneur.2021.646928>.
- [17] Z. Ramshani, C. Zhang, K. Richards, L. Chen, G. Xu, B.L. Stiles, R. Hill, S. Senapati, D.B. Go, H.C. Chang, Extracellular vesicle microrna quantification from plasma using an integrated microfluidic device, *Commun. Biol.* 2 (2019) 189, <https://doi.org/10.1038/s42003-019-0435-1>.
- [18] Y. Yang, L. Ma, X. Qiao, X. Zhang, S.F. Dong, M.T. Wu, K. Zhai, H.Z. Shi, Salivary micrnas show potential as biomarkers for early diagnosis of malignant pleural effusion, *Transl. Lung Cancer Res.* 9 (4) (2020) 1247–1257, <https://doi.org/10.21037/tlcr-19-530>.
- [19] M.A. Mori, R.G. Ludwig, R. Garcia-Martin, B.B. Brandão, C.R. Kahn, Extracellular micrnas: from biomarkers to mediators of physiology and disease, *Cell Metab.* 30 (4) (2019) 656–673, <https://doi.org/10.1016/j.cmet.2019.07.011>.
- [20] S.P. Kalarikkal, G.M. Sundaram, Edible plant-derived exosomal micrnas: exploiting a cross-kingdom regulatory mechanism for targeting SARS-cov-2, *Toxicol. Appl. Pharmacol.* 414 (2021) 115425, <https://doi.org/10.1016/j.taap.2021.115425>.
- [21] J. Zemleni, S.R. Baier, K.M. Howard, J. Cui, Gene regulation by dietary micrnas, *Can. J. Physiol. Pharmacol.* 93 (12) (2015) 1097–1102, <https://doi.org/10.1139/cjpp-2014-0392>.
- [22] A. Lukasik, P. Zielenkiewicz, V. Scaria, In silico identification of plant mirnas in mammalian breast milk exosomes—a small step forward? *PLoS One* 9 (6) (2014) e99963 <https://doi.org/10.1371/journal.pone.0099963>.
- [23] N. Kosaka, H. Izumi, K. Sekine, T. Ochiya, Microrna as a new immune-regulatory agent in breast milk, *Silence* 1 (1) (2010) 7, <https://doi.org/10.1186/1758-907X-1-7>.
- [24] Q. Zhou, M. Li, X. Wang, Q. Li, T. Wang, Q. Zhu, X. Zhou, X. Wang, X. Gao, X. Li, Immune-related micrnas are abundant in breast milk exosomes, *Int. J. Biol. Sci.* 8 (1) (2012) 118–123, <https://doi.org/10.7150/ijbs.8.118>.
- [25] A.R. Chin, M.Y. Fong, G. Somlo, J. Wu, P. Swiderski, X. Wu, S.E. Wang, Cross-kingdom inhibition of breast cancer growth by plant mir159, *Cell Res.* 26 (2) (2016) 217–228, <https://doi.org/10.1038/cr.2016.13>.
- [26] B. Langmead, C. Trapnell, M. Pop, S.L. Salzberg, Ultrafast and memory-efficient alignment of short dna sequences to the human genome, *Genome Biol.* 10 (3) (2009) R25, <https://doi.org/10.1186/gb-2009-10-3-r25>.
- [27] M.R. Friedländer, S.D. Mackowiak, N. Li, W. Chen, N. Rajewsky, Mirdeep2 accurately identifies known and hundreds of novel microrna genes in seven animal clades, *Nucleic Acids Res.* 40 (1) (2012) 37–52, <https://doi.org/10.1093/nar/gkr688>.
- [28] M. Pertea, D. Kim, G.M. Pertea, J.T. Leek, S.L. Salzberg, Transcript-level expression analysis of rna-seq experiments with hisat, stringtie and ballgown, *Nat. Protoc.* 11 (9) (2016) 1650–1667, <https://doi.org/10.1038/nprot.2016.095>.
- [29] S. Chen, Y. Zhou, Y. Chen, J. Gu, Fastp: an ultra-fast all-in-one fastq preprocessor, *Bioinformatics* 34 (17) (2018) i884–i890, <https://doi.org/10.1093/bioinformatics/bty560>.
- [30] M.I. Love, W. Huber, S. Anders, Moderated estimation of fold change and dispersion for rna-seq data with DESeq2, *Genome Biol.* 15 (12) (2014) 550, <https://doi.org/10.1186/s13059-014-0550-8>.
- [31] D. Betel, A. Koppal, P. Agius, C. Sander, C. Leslie, Comprehensive modeling of microrna targets predicts functional non-conserved and non-canonical sites, *Genome Biol.* 11 (8) (2010) R90, <https://doi.org/10.1186/gb-2010-11-8-r90>.
- [32] O.F. Laterza, L. Lim, P.W. Garrett-Engle, K. Vlasakova, N. Muniappa, W. K. Tanaka, J.M. Johnson, J.F. Sina, T.L. Fare, F.D. Sistare, W.E. Glaab, Plasma micrnas as sensitive and specific biomarkers of tissue injury, *Clinical Chemistry* (Baltimore, Md.) 55 (11) (2009) 1977–1983, <https://doi.org/10.1373/clinchem.2009.131797>.
- [33] P.J. Starkey Lewis, J. Dear, V. Platt, K.J. Simpson, D.G.N. Craig, D.J. Antoine, N. S. French, N. Dhaun, D.J. Webb, E.M. Costello, J.P. Neoptolemos, J. Moggs, C. E. Goldring, B.K. Park, Circulating micrnas as potential markers of human drug-induced liver injury, *Hepatology* (Baltimore, Md.) 54 (5) (2011) 1767–1776, <https://doi.org/10.1002/hep.24538>.
- [34] C. Archambaud, O. Sismeiro, J. Toedling, G. Soubigou, C. Becavin, P. Lechat, A. Lebreton, C. Ciaudo, P. Cossart, The intestinal microbiota interferes with the microrna response upon oral listeria infection, *Mbio* 4 (6) (2013) e707–e713, <https://doi.org/10.1128/mBio.00707-13>.
- [35] G. Liang, N. Malmuthuge, T.B. Mcfadden, H. Bao, P.J. Griebel, P. Stothard, L. L. Guan, Potential regulatory role of micrnas in the development of bovine gastrointestinal tract during early life, *PLoS One* 9 (3) (2014) e92592, <https://doi.org/10.1371/journal.pone.0092592>.
- [36] R. Li, F. Beaudoin, A.A. Ammah, N. Bissonnette, C. Benchaar, X. Zhao, C. Lei, E. M. Ibeagha-Awemu, Deep sequencing shows microrna involvement in bovine mammary gland adaptation to diets supplemented with linseed oil or safflower oil, *BMC Genomics* 16 (881) (2015) 884, <https://doi.org/10.1186/s12864-015-1965-7>.
- [37] I. Manaster, D. Goldman-Wohl, C. Greenfield, D. Nachmani, P. Tsukerman, Y. Hamani, S. Yagel, O. Mandelboim, P. Bobé, Mirna-mediated control of hla-g expression and function, *PLoS One* 7 (3) (2012) e33395, <https://doi.org/10.1371/journal.pone.0033395>.
- [38] A. Iqbal, H. Yu, P. Jiang, Z. Zhao, Deciphering the key regulatory roles of klf6 and bta-mir-148a on milk fat metabolism in bovine mammary epithelial cells, *Genes* 13 (10) (2022) 1828, <https://doi.org/10.3390/genes13101828>.
- [39] A. Dwivedi, C. Padala, A. Kumari, S.S. Khumukcham, V. Penugurti, S. Ghosh, A. Mazumder, V. Goffin, B. Manavathi, Hematopoietic pbx-interacting protein is a novel regulator of mammary epithelial cell differentiation, *FEBS J.* 289 (6) (2022) 1575–1590, <https://doi.org/10.1111/febs.16242>.
- [40] B.C. Melnik, G. Schmitz, Exosomes of pasteurized milk: potential pathogens of western diseases, *J. Transl. Med.* 17 (1) (2019) 3–33, <https://doi.org/10.1186/s12967-018-1760-8>.
- [41] H.J. Wu, M. Hao, S.K. Yeo, J.L. Guan, Fak signaling in cancer-associated fibroblasts promotes breast cancer cell migration and metastasis by exosomal mirnas-mediated intercellular communication, *Oncogene* 39 (12) (2020) 2539–2549, <https://doi.org/10.1038/s41388-020-1162-2>.
- [42] S. Juzenas, C.M. Lindqvist, G. Ito, Y. Dolshanskaya, J. Halfvarson, A. Franke, G. Hemmrich-Stanisak, Depletion of erythropoietic mir-486-5p and mir-451a improves detectability of rare micrnas in peripheral blood-derived small rna sequencing libraries, *Nar Genom. Bioinform.* 2 (1) (2020) lqaa8, <https://doi.org/10.1093/nargab/lqaa008>.
- [43] M. El-Mogy, B. Lam, T.A. Haj-Ahmad, S. MCGowan, D. Yu, L. Nosal, N. Rghei, P. Roberts, Y. Haj-Ahmad, Diversity and signature of small rna in different bodily fluids using next generation sequencing, *BMC Genomics* 19 (1) (2018) 408, <https://doi.org/10.1186/s12864-018-4785-8>.
- [44] W. Li, Y. Wang, Q. Zhang, L. Tang, X. Liu, Y. Dai, L. Xiao, S. Huang, L. Chen, Z. Guo, J. Lu, K. Yuan, Microrna-486 as a biomarker for early diagnosis and recurrence of non-small cell lung cancer, *PLoS One* 10 (8) (2015) e134220, <https://doi.org/10.1371/journal.pone.0134220>.
- [45] D.G. Weber, A. Brik, S. Casjens, K. Burek, M. Lehnert, B. Pesch, D. Taeger, T. Bruning, G. Johnen, Are circulating micrnas suitable for the early detection of malignant mesothelioma? Results from a nested case-control study, *BMC. Res. Notes* 12 (1) (2019) 77, <https://doi.org/10.1186/s13104-019-4113-7>.


- [46] J. Shen, Q. Hu, M. Schrauder, L. Yan, D. Wang, L. Medico, Y. Guo, S. Yao, Q. Zhu, B. Liu, M. Qin, M.W. Beckmann, P.A. Fasching, R. Strick, C.S. Johnson, C. B. Ambrosone, H. Zhao, S. Liu, Circulating mir-148b and mir-133a as biomarkers for breast cancer detection, *Oncotarget* 5 (14) (2014) 5284–5294, <https://doi.org/10.18632/oncotarget.2014>.
- [47] V. Toro, N. Jutras-Beaudoin, O. Boucherat, S. Bonnet, S. Provencher, F. Potus, Right ventricle and epigenetics: a systematic review, *Cells* (Basel, Switzerland) 12 (23) (2023) 2693, <https://doi.org/10.3390/cells12232693>.
- [48] O. Ramos-Lopez, Epigenetic biomarkers of metabolic responses to lifestyle interventions, *Nutrients* 15 (19) (2023) 4251, <https://doi.org/10.3390/nu15194251>.
- [49] K. Wang, H. Li, Y. Yuan, A. Etheridge, Y. Zhou, D. Huang, P. Wilmes, D. Galas, L. J. de Windt, The complex exogenous rna spectra in human plasma: an interface with human gut biota? *PLoS One* 7 (12) (2012) e51009 <https://doi.org/10.1371/journal.pone.0051009>.
- [50] H. Liang, S. Zhang, Z. Fu, Y. Wang, N. Wang, Y. Liu, C. Zhao, J. Wu, Y. Hu, J. Zhang, X. Chen, K. Zen, C.Y. Zhang, Effective detection and quantification of dietetically absorbed plant micrornas in human plasma, *J. Nutr. Biochem.* 26 (5) (2015) 505–512, <https://doi.org/10.1016/j.jnutbio.2014.12.002>.
- [51] S. Mlotshwa, G.J. Pruss, J.L. Macarthur, M.W. Endres, C. Davis, L.J. Hofseth, M. M. Peña, V. Vance, A novel chemopreventive strategy based on therapeutic micrornas produced in plants, *Cell Res.* 25 (4) (2015) 521–524, <https://doi.org/10.1038/cr.2015.25>.
- [52] F. Marzano, M.F. Caratozzolo, A. Consiglio, F. Licciulli, S. Liuni, E. Sbisà, D. D'Elia, A. Tullo, D. Catalano, Plant mirnas reduce cancer cell proliferation by targeting malat1 and neat1: a beneficial cross-kingdom interaction, *Front. Genet.* 11 (2020) 552490, <https://doi.org/10.3389/fgene.2020.552490>.
- [53] Q. Chen, F. Zhang, L. Dong, H. Wu, J. Xu, H. Li, J. Wang, Z. Zhou, C. Liu, Y. Wang, Y. Liu, L. Lu, C. Wang, M. Liu, X. Chen, C. Wang, C. Zhang, D. Li, K. Zen, F. Wang, Q. Zhang, C. Zhang, Sidt1-dependent absorption in the stomach mediates host uptake of dietary and orally administered micrornas, *Cell Res.* 31 (3) (2021) 247–258, <https://doi.org/10.1038/s41422-020-0389-3>.
- [54] A.F. Cordova, C. Ritchie, V. Böhnert, L. Li, Human slc46a2 is the dominant cgamp importer in extracellular cgamp-sensing macrophages and monocytes, *ACS Cent. Sci.* 7 (6) (2021) 1073–1088, <https://doi.org/10.1021/acscentsci.1c00440>.
- [55] Y. Qin, B. Zheng, G. Yang, H. Yang, J. Zhou, Z. Yang, X. Zhang, H. Zhao, J. Shi, J. Wen, Salvia miltiorrhiza-derived sal-mir-58 induces autophagy and attenuates inflammation in vascular smooth muscle cells, *Molecular Therapy. Nucleic Acids* 21 (2020) 492–511, <https://doi.org/10.1016/j.omtn.2020.06.015>.
- [56] T.S. Trivedi, N. Mangukia, M. Bhavsar, A.U. Mankad, R.M. Rawal, S.K. Patel, A novel insight of picrorrhiza kurroa mirnas in human cystic fibrosis: a transcriptome-wide cross-kingdom study, *Hum. Gene Ther.* (2023), <https://doi.org/10.1016/j.humgen.2023.201153>.
- [57] C. Zhao, X. Sun, L. Li, Biogenesis and function of extracellular mirnas, *Exrna* 1 (1) (2019) 38, <https://doi.org/10.1186/s41544-019-0039-4>.
- [58] A. Lukasik, I. Brzozowska, U. Zielenkiewicz, P. Zielenkiewicz, Detection of plant mirnas abundance in human breast milk, *Int. J. Mol. Sci.* 19 (1) (2017), <https://doi.org/10.3390/ijms19010037>.
- [59] S. Ju, J. Mu, T. Dokland, X. Zhuang, Q. Wang, H. Jiang, X. Xiang, Z.B. Deng, B. Wang, L. Zhang, M. Roth, R. Welti, J. Mobley, Y. Jun, D. Miller, H.G. Zhang, Grape exosome-like nanoparticles induce intestinal stem cells and protect mice from dss-induced colitis, *Mol. Ther.* 21 (7) (2013) 1345–1357, <https://doi.org/10.1038/mt.2013.64>.
- [60] S. Lv, Y. An, H. Dong, L. Xie, H. Zheng, X. Cheng, L. Zhang, T. Teng, Q. Wang, Z. Yan, X. Guo, Z. Junli, J. Zhao, High apln expression predicts poor prognosis for glioma patients, *Oxidative Med. Cell. Longev.* 2022 (2022) 1–16, <https://doi.org/10.1155/2022/8393336>.
- [61] A. Pathak, A.K. Pal, S. Roy, M. Nandave, K. Jain, Role of angiogenesis and its biomarkers in development of targeted tumor therapies, *Stem Cells Int.* 2024 (2024) 9077926, <https://doi.org/10.1155/2024/9077926>.
- [62] G. Liang, Y. Zhu, B. Sun, Y. Shao, A. Jing, J. Wang, Z. Xiao, Assessing the survival of exogenous plant microrna in mice, *Food Sci. Nutr.* 2 (4) (2014) 380–388, <https://doi.org/10.1002/fsn3.113>.
- [63] X. Chen, G.H. Dai, Z.M. Ren, Y.L. Tong, F. Yang, Y.Q. Zhu, Identification of dietetically absorbed rapeseed (*Brassica campestris* L.) bee pollen micrornas in serum of mice, *Biomed. Res. Int.* 2016 (2016) 5413849, <https://doi.org/10.1155/2016/5413849>.
- [64] M. Saquib, P. Agnihotri, S. Biswas Monu, Exogenous mirna: a perspective role as therapeutic in rheumatoid arthritis, *Curr. Rheumatol. Rep.* 23 (6) (2021) 43, <https://doi.org/10.1007/s11926-021-01009-7>.
- [65] B. Alshehri, Plant-derived xenomirs and cancer: cross-kingdom gene regulation, *Saudi J. Biol. Sci.* 28 (4) (2021) 2408–2422, <https://doi.org/10.1016/j.sjbs.2021.01.039>.
- [66] Sanchita, R. Trivedi, M.H. Asif, P.K. Trivedi, Dietary plant miRNAs as an augmented therapy: cross-kingdom gene regulation, *RNA Biol.* 15 (12) (2018) 1433–1439, <https://doi.org/10.1080/15476286.2018.1551693>.

RESEARCH ARTICLE

Open Access



Milk exosome-derived miRNAs from water buffalo are implicated in immune response and metabolism process

Zujing Chen^{1,2†}, Yueqin Xie^{3†}, Junyi Luo³, Ting Chen^{1,3}, Qianyun Xi^{1,3}, Yongliang Zhang^{1,3*} and Jiajie Sun^{1,3*} 

Abstract

Background: Buffalo milk is rich in various nutritional components and bioactive substances that provide more essential health benefits to human body. Recently, exosome identified in the breast milk has been reported as a neotype nutrient and can mediate intercellular communication with exosomal miRNAs. In the present study, we therefore hypothesized that exosome-derived miRNAs from buffalo milk would play the potential physiological importance of consumption of buffalo milk.

Results: We isolated exosomes from buffalo and cow milk samples that were obtained at mid-lactation period, and the exosomal miRNA profiles were then generated using miRNA-seq. In addition, miRNAomes of pig, human and panda milk exosomes were downloaded from GEO database. Finally, a total of 27 milk exosomal miRNA profiles that included 4 buffalo, 4 cow, 8 pig, 4 human and 7 panda were analyzed using the miRDeep2 program. A total of 558 unique miRNA candidates existed across all species, and the top 10 highly expressed miRNA were evolutionarily conserved across multiple species. Functional analysis revealed that these milk enriched miRNAs targeted 400 putative sites to modulate disease resistance, immune responsiveness and basic metabolism events. In addition, a total of 32 miRNAs in buffalo milk were significantly up-regulated compared with non-buffalo milks, while 16 were significantly down-regulated. Of interest, functional analysis showed that up-regulated miRNAs were mainly related to host metabolism processes, while the predicted functions of down-regulated miRNAs were enriched in immune response.

Conclusion: In this study, we explored the exosomal miRNAome differences between milks of different animals, expanding the theoretical basis for potential applications of the miRNA-containing vesicles.

Keywords: Buffalo milk, Exosomal miRNA, Cell-cell communication, Immune and metabolism

Background

Water buffaloes are predominant dairy animals, contributing the most important source of 13% to the milk production worldwide [1]. In recent years, buffalo milk has received increasing research interest and investment in various countries, owing mainly to its attractive nutrient

content. Compared with cow milk, buffalo milk is characterized by a rich composition with fat [2], proteins [3], amino acids [4], vitamins and minerals [5, 6], as well as a healthier (i.e. lower) concentration of cholesterol and higher magnitude of unsaturated fatty acids [7]. In addition to nutritional ingredients, increasing evidences have reported that a type of membrane-bound carriers termed as exosomes were identified in the breast milk of human [8, 9], cow [10, 11] and pig [12], which have recently been considered as major players in cell-cell communication [13]. Exosomes are 40–100 nm diameter

* Correspondence: jiajiesun@scau.edu.cn; jiajiesun@scau.edu.cn

[†]Zujing Chen and Yueqin Xie contributed equally to this work.

¹Guangdong Engineering & Research Center for Woody Fodder Plants, South China Agricultural University, Guangzhou 510642, China

Full list of author information is available at the end of the article



© The Author(s). 2020 **Open Access** This article is licensed under a Creative Commons Attribution 4.0 International License, which permits use, sharing, adaptation, distribution and reproduction in any medium or format, as long as you give appropriate credit to the original author(s) and the source, provide a link to the Creative Commons licence, and indicate if changes were made. The images or other third party material in this article are included in the article's Creative Commons licence, unless indicated otherwise in a credit line to the material. If material is not included in the article's Creative Commons licence and your intended use is not permitted by statutory regulation or exceeds the permitted use, you will need to obtain permission directly from the copyright holder. To view a copy of this licence, visit <http://creativecommons.org/licenses/by/4.0/>. The Creative Commons Public Domain Dedication waiver (<http://creativecommons.org/publicdomain/zero/1.0/>) applies to the data made available in this article, unless otherwise stated in a credit line to the data.

vesicles that are widely present in almost all biological fluids [14]. Exosomes have been proposed to signal by binding to the recipient cell surface receptors or by internalisation with the cell membrane [15], potentially donating substantial amounts of exosomal miRNAs to the recipient tissue/cells and subsequently playing pivotal roles in the post-transcriptional regulation of gene expression [14]. Previous report showed that human breast milk exosomes with immune modulatory features were important for the development of the infant's immune system [8]. Further, the roles of bovine milk exosomes have been proved as transporters of miRNAs for eliciting regulatory functions in the recipient cells [10]. Overall, we therefore hypothesized that buffalo milk exosomes also provided novel information on miRNA composition differing from other types of non-buffalo milks, and highlighted the unrealized physiological importance of exosomes on drinking behaviour.

Results

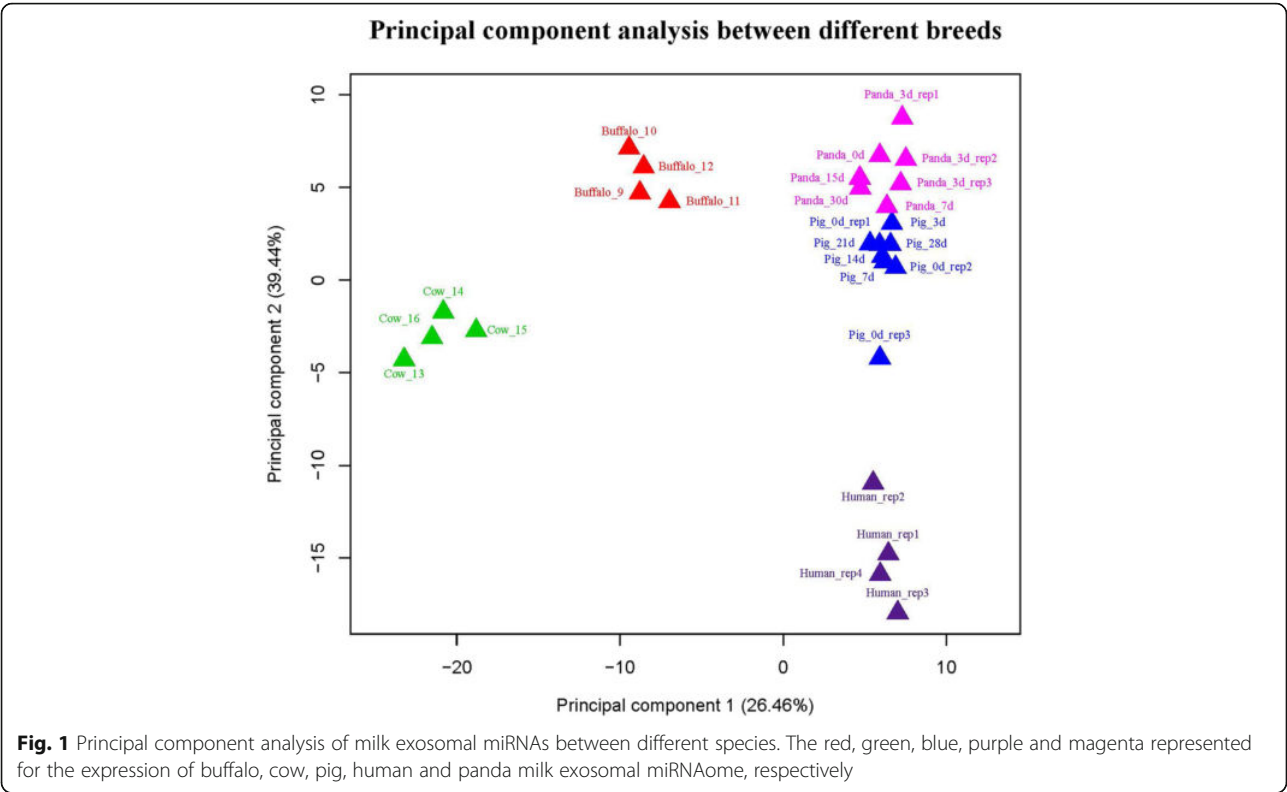
In 27 sequencing libraries, there were 558 unique miRNA candidates sequenced across all species, and only 395 miRNAs which were identified at least in four libraries were considered further (Additional file 1). Of these, the top 10 highly expressed miRNA in four buffalo libraries, which accounted for $75.45 \pm 1.18\%$ of all aligned reads, were evolutionarily conserved across multiple species. These miRNAs represented four different miRNA families; miR-let-7 (bta-let-7a-5p, bta-let-7b, bta-let-7c, bta-let-7e and bta-let-7f), miR-30 (bta-miR-30a-5p, bta-miR-30d and bta-miR-30e-5p), miR-148 (bta-miR-148a), and miR-26 (bta-miR-26a). In addition, four of these miRNAs (miR-148a, miR-30a-5p, bta-miR-30d, bta-let-7c) shared common ranking as top 10 expressed miRNAs when parsing the sequence data based on different species (buffalo, cow, pig, human and panda milks). To further identify the potential function of the top expressed miRNAs, target prediction was performed using miRanda software. A total of 400 putative target sites for the top 10 expressed miRNAs were identified (Additional file 2), and then all of these target candidates were submitted for homology and functional annotation using an online version of the DAVID program. These target genes belonged to 5 KEGG annotated categories that significantly related to a wide variety of disease resistance, immune responsiveness and basic metabolism events, including microRNAs in cancer, lysosome, glycerophospholipid metabolism, proteoglycans in cancer, galactose metabolism and neurotrophin signaling pathway (Additional file 3).

For validation and identification of species-specific miRNAs in buffalo milk, we compared the sequencing libraries between buffalo and non-buffalo milks and found that 27 indexed libraries were obviously divided into five groups

based on breed differences (Fig. 1). To comparison with miRNA expression in non-buffalo milks, a total of 32 miRNAs in buffalo milk were significantly up-regulated (Fig. 2a), while 16 were significantly down-regulated (Fig. 2b) using the R Bioconductor package EdgeR analysis with TMM-normalized algorithm. In addition, target prediction revealed a total of 4372 miRNA-target interactions between significantly expressed miRNAs and NCBI RefSeq genes. This resulted in 1759 unique genes targeted by up-regulated miRNAs (Additional file 4), 1761 genes targeted by down-regulated miRNAs (Additional file 5), and 477 genes targeted by both up and down-regulated miRNAs. Especially, pathway analysis revealed that 39 predicted targets of up-regulated miRNAs were significantly enriched in categories annotated as a role in endocytosis (Additional file 6). On the contrary, the targets of down-regulated miRNAs were annotated with a total of 31 significantly KEGG pathways (Additional file 7).

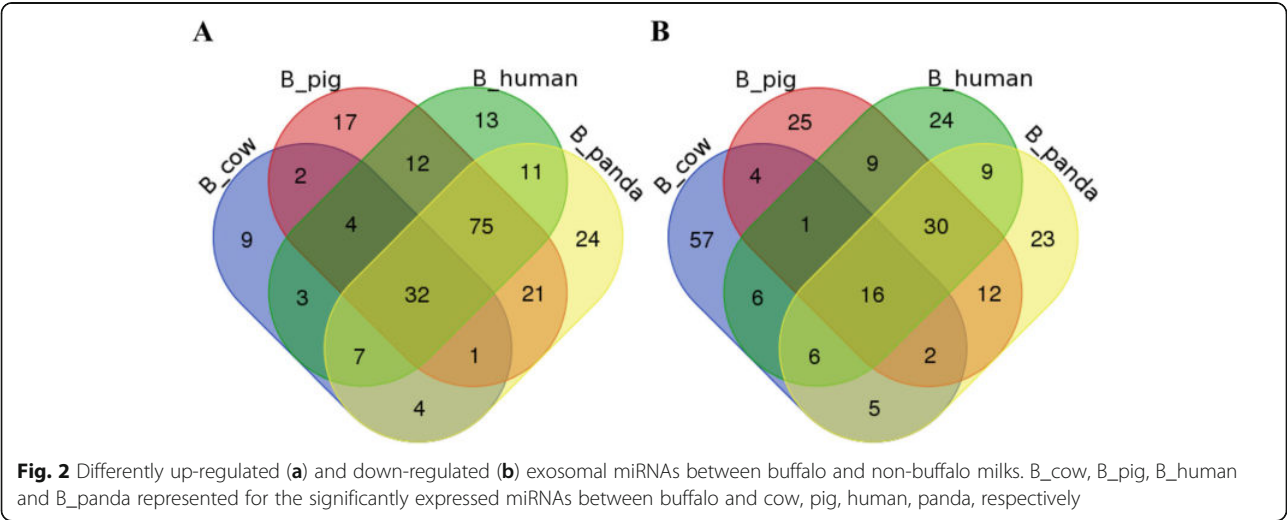
Discussion

In our sequencing libraries, miR-148a, miR-30a-5p, bta-miR-30d, bta-let-7c shared common ranking as top 10 expressed miRNAs when parsing the sequence data based on different species (buffalo, cow, pig, human and panda milks), suggesting these miRNAs could be important nutritional components of milk [16]. In details, the most abundant was bta-miR-148a accounting for $38.88 \pm 3.12\%$ in each buffalo library, which was consistent with previous reports in cow [17], pig [12] and human [9] milks. Recent characterizations of the human salivary exosome have also highlighted the miR-148a expression at high levels that expected to modulate oral cavity defence [18]. To date, although the underlying regulatory mechanism of the most predominant miRNA (miR-148a) packaged into milk exosomes was still unclear, it was intriguing to suggest that miR-148a was a potential biomarker for the quality control of mammalian milk [19]. The miR-30a was highly enriched in exosomes from the serum of acute myocardial infarction patients in vivo, and inhibition of miR-30a or exosome release contributed to maintaining of autophagy after hypoxia [20]. In addition to miR-30a, exosome-enriched miR-30d in endometrial fluid was proposed to be taken up by the pre-implantation embryo, thereby resulting in the observed modifications to the transcriptome and embryo adhesion [21]. The enrichment of let-7 miRNA family in the extracellular fractions, particularly, in the exosomes from gastric cancer cells reflected their oncogenic characteristics including tumorigenesis and metastasis [22]. These data implied the roles of highly expressed miRNAs with a specified function in the milk exosomes. Compared with non-buffalo milks, 32 miRNAs were significantly up-regulated, and 16 were down-regulated. Pathway analysis revealed that the targets of up-regulated miRNAs were significantly enriched in



categories annotated as a role in endocytosis. The endocytosis pathway, for instance, has been highlighted as an important step in the delivery of bovine exosomes and their cargo to human vascular endothelial cells and peripheral tissues by endocytosis [23]. Additionally, we also revealed many of the other pathways which have been previously implicated in series basic metabolism processes in animals. These pathways included metabolic pathways enriched with 127 targets, glycerophospholipid metabolism enriched with 18 targets, protein processing

in endoplasmic reticulum enriched with 26 targets, glycosaminoglycan biosynthesis enriched with 6 targets, biosynthesis of amino acids enriched with 13 targets, etc. Taken together, these analyses strongly suggested that up-regulated miRNAs that were differentially expressed between buffalo and non-buffalo milks were key regulators of the host metabolism processes shuttling within exosomes by endocytosis. In addition to metabolic pathways shared with the target annotation of up-regulated miRNAs, computational analysis of the down-regulated



miRNA targets has identified the statistical over-representation of several terms previously implicated in response to immunity events, such as T cell receptor signaling pathway, NF-kappa B signaling pathway, AMPK signaling pathway, HTLV-I infection, lysosome, inflammatory mediator regulation of TRP channels, etc. The evidences indicated that the down-expressed miRNAs identified in this study were likely central regulators of the immune response and thus represented potential targets or novel biomarkers of infection and inflammation.

Conclusions

Milk exosomal miRNA profiles that included 4 buffalo, 4 cow, 8 pig, 4 human and 7 panda were analyzed, and milk enriched miRNA candidates across all species were annotated to modulate disease resistance, immune responsiveness and basic metabolism events. This study provided an important mechanistic framework for future studies of dietary extracellular vesicles and the roles of milk miRNAs in human health and disease.

Methods

Milk exosomes collection and sequencing analysis

Buffalo (*Murrah* breed) and cow (*Friesian* breed) milk samples were obtained respectively from 4 healthy mid-lactating animals in a local farm (Panyu town, Guangzhou city, Guangdong province, China), and crude exosomes were purified following our previous method [24]. In brief, approximate 40 mL raw milk samples were subjected to 2 successive centrifugations at 2000 and 12,000×g at 4°C for 30 min to remove somatic cells and debris. The supernatant was mixed with an equal volume of 0.25 M EDTA (pH 7.0) and incubated on ice for 15 min to precipitate casein and exosomes coated with casein. The suspension was ultracentrifuged at 80,000 g at 4°C for 60 min (Sorvall WX Ultra 80, F37L-8 × 100 rotor; Thermo Scientific) to remove precipitated protein, milk fat globules, and microvesicles larger than exosomes. Exosomes were collected by centrifugation at 120,000 g at 4°C for 90 min, resuspended in sterile phosphate-buffered saline, and filtered through a 0.22-μm membrane filter to obtain exosome solutions. Then, exosomal RNAs from each milk sample were used for library construction and subjected to single-end sequencing in the length of 40 nt with an Illumina Genome Analyzer (Biomarker Technologies, Beijing city, China). All procedures were conducted under protocols approved by the Institutional Animal Care and Use Committee of South China Agricultural University, China.

MiRNA analysis

In addition to the indexed sequencing data of buffalos and cows, we downloaded the exosomal small RNA data of pig [12], human [8] and panda [25] in the GEO

database (<https://www.ncbi.nlm.nih.gov/gds/>), respectively. Using the miRDeep2 program [17], a total of 27 sequencing libraries that included 4 buffalo, 4 cow, 8 pig, 4 human and 7 panda were further analyzed by blasting against bovine miRBase miRNA annotation (<http://www.mirbase.org/>) to identify conserved candidates between different species. The read count of each identified miRNA was firstly normalized with TMM-normalized algorithm, and the R Bioconductor package EdgeR analysis (<http://bioconductor.org/packages/edgeR/>) was applied to identify differentially expressed (DE) miRNAs with *P* value < 0.05 and fold change ≥ 2 between different groups.

Target predictions and annotation

The 3'UTR sequences of the bovine RefSeq genes were downloaded from the University of California Santa Cruz (UCSC) table browser (<http://genome.ucsc.edu/cgi-bin/hgTables>). The targets of highly and differentially expressed miRNAs were successfully predicted using miRanda software (<http://34.236.212.39/microrna/home.do>), and the biological KEGG pathway analysis of the predicted targets were further performed by an online version of the DAVID program (<https://david.ncifcrf.gov/>).

Supplementary information

Supplementary information accompanies this paper at <https://doi.org/10.1186/s12917-020-02339-x>.

Additional file 1. Exosomal miRNA expression between buffalo and non-buffalo milks. Buffalo_9, buffalo_10, buffalo_11 and buffalo_12 represented for 4 buffalo milk samples; cow_13, cow_14, cow_15 and cow_16 represented for 4 cow milk samples; pig_0_rep1, pig_0_rep2, pig_0_rep3, pig_3d, pig_7d, pig_14d, pig_21d and pig_28d represented for 8 pig milk samples; human_rep1, human_rep2, human_rep3 and human_rep4 represented for 4 human milk samples; panda_0d, panda_3d_rep1, panda_3d_rep2, panda_3d_rep3, panda_7d, panda_15d and panda_30d represented for 7 panda milk samples; logFC, log fold change; logCPM, log counts per million; FDR, false discovery rate.

Additional file 2. Predicted targets of top 10 expressed miRNAs in buffalo milk exosome. Query represented for miRNA candidates; Ref represented for reference genes.

Additional file 3. The KEGG analysis of top 10 expressed miRNAs' targets

Additional file 4. Predicted targets of significantly up-regulated miRNAs in buffalo milk exosome

Additional file 5. Predicted targets of significantly down-regulated miRNAs in buffalo milk exosome

Additional file 6. The KEGG analysis of the up-regulated miRNAs' targets

Additional file 7. The KEGG analysis of the down-regulated miRNAs' targets

Abbreviations

GEO: NCBI Gene Expression Omnibus; DAVID: The Database for Annotation, Visualization and Integrated Discovery; KEGG: Kyoto Encyclopedia of Genes and Genomes; TMM: the trimmed mean of M-values; AMPK: Adenosine 5'-monophosphate-activated protein kinase

Acknowledgements

We thank the High Performance Computing center of South China Agricultural University for providing computational resources in this work. We also thank Gu et al., Admyre et al., and Ma et al. for sharing their miRNA-seq data in NCBI platform.

Authors' contributions

YQX and JJS collected data, perform analysis and also drafted the manuscript. ZJC contributed to data analysis. JYL, TC, QYX and YLZ conceived this study and revised the manuscript. All authors read and proved the final manuscript.

Funding

This research was supported by the projects of Guangdong Provincial Promotion Project on Preservation and Utilization of Local Breed of Livestock and Poultry, the major scientific projects in general colleges and Universities of Guangdong Province [2017KTSCX023], the Opening Foundation of The State Key Laboratory for Conservation and Utilization of Subtropical Agro-bioresources [OSKL201502], and the Natural Science Foundation of China Program [31802032].

Availability of data and materials

The miRNA-seq raw datasets of buffalo and cow milk exosome have been deposited into NCBI SRA database with the BioProject accession number PRJNA606117. The exosomal small RNA datas of pig, human and panda were free downloaded from the publicly accessible NCBI GEO database with the Accession Nnumber GSE36590, GSE32253 and GSE89755, and this is an open science data sharing platform and allowed to shared the datas for scientific research.

Ethics approval and consent to participate

Verbal consent for collecting milk samples was obtained from the owner of a private farm as part of routine milking. This method is widely used in China and all procedures were conducted under protocols of SCAU-AEC-2010-0416 approved by the ethics committee of South China Agricultural University, China.

Consent for publication

Not applicable.

Competing interests

The authors declare that they have no competing interests.

Author details

¹Guangdong Engineering & Research Center for Woody Fodder Plants, South China Agricultural University, Guangzhou 510642, China. ²College of Forestry and Landscape Architecture, South China Agricultural University, Guangzhou 510642, Guangdong, China. ³College of Animal Science, Guangdong Provincial Key Laboratory of Animal Nutrition Control, National Engineering Research Center for Breeding Swine Industry, South China Agricultural University, Guangzhou 510642, China.

Received: 7 November 2019 Accepted: 22 April 2020

Published online: 29 April 2020

References

- Murtaza MA, Pandya AJ, Khan MMH. Buffalo milk: 4.1 buffalo milk production. In: Handbook of Milk of Non-Bovine Mammals; 2017. p. 261–83.
- Abbas HM, Hassan FA, El-Gawad MA, Enab AK. Physicochemical characteristics of goat's milk. *Life Sci J*. 2014;11:307–17.
- Mahmood A, Usman S. A comparative study on the physicochemical parameters of milk samples collected from buffalo, cow, goat and sheep of Gujrat, Pakistan. *Pak J Nutr*. 2010;9:1192–7.
- El-Salam MHA, El-Shibiny S. A comprehensive review on the composition and properties of buffalo milk. *Dairy sci Technol*. 2011;91:663.
- Ahmad S, Gaucher I, Rousseau F, Beaucher E, Piot M, Grongnet JF, Gaucheron F. Effects of acidification on physico-chemical characteristics of buffalo milk: a comparison with cow's milk. *Food Chem*. 2008;106:11–7.
- Ahmad S, Anjum FM, Huma N, Sameen A, Zahoor T. Composition and physico-chemical characteristics of buffalo milk with particular emphasis on lipids, proteins, minerals, enzymes and vitamins. *J Anim Plant Sci*. 2013;23: 62–74.
- Bhanger MI, Memon NN, Talpur FN. Comparison of fatty acid and cholesterol content of Pakistani water buffalo breeds. *Pak J Anal Environ Chem*. 2007;8:15–20.
- Admyre C, Johansson SM, Qazi KR, Filén JJ, Lahesmaa R, Norman M, Gabrielsson S. Exosomes with immune modulatory features are present in human breast milk. *J Immunol*. 2007;179:1969–78.
- Zhou Q, Li M, Wang X, Li Q, Wang T, Zhu Q, Li X. Immune-related microRNAs are abundant in breast milk exosomes. *Int J Biol Sci*. 2012;8:118.
- Hata T, Murakami K, Nakatani H, Yamamoto Y, Matsuda T, Aoki N. Isolation of bovine milk-derived microvesicles carrying mRNAs and microRNAs. *Biochem Biophys Res Commun*. 2010;396:528–33.
- Yamada T, Inoshima Y, Matsuda T, Ishiguro N. Comparison of methods for isolating exosomes from bovine milk. *J Vet Med Sci*. 2012;74:1523–5.
- Gu Y, Li M, Wang T, Liang Y, Zhong Z, Wang X, Chen X. Lactation-related microRNA expression profiles of porcine breast milk exosomes. *PLoS One*. 2012;7:e43691.
- Mathivanan S, Ji H, Simpson RJ. Exosomes: extracellular organelles important in intercellular communication. *J Proteome*. 2010;73:1907–20.
- Zhang J, Li S, Li L, Li M, Guo C, Yao J, Mi S. Exosome and exosomal microRNA: trafficking, sorting, and function. *Genomics Proteomics Bioinformatics*. 2015;13:17–24.
- Valadi H, Ekström K, Bossios A, Sjöstrand M, Lee JJ, Lötvall JO. Exosome-mediated transfer of mRNAs and microRNAs is a novel mechanism of genetic exchange between cells. *Nat Cell Biol*. 2015;9:654.
- Melnik BC, Kakulas F, Geddes DT, Hartmann PE, John SM, Carrerabastos P, Cordain L, Schmitz G. Milk mirnas: simple nutrients or systemic functional regulators? *Nutr Metab*. 2016;13:1–5.
- Friedländer MR, Mackowiak SD, Li N, Chen W, Rajewsky N. Mirdeep2 accurately identifies known and hundreds of novel microRNA genes in seven animal clades. *Nucleic Acids Res*. 2012;40:37–52.
- Ogawa Y, Taketomi Y, Murakami M, Tsujimoto M, Yanoshita R. Small RNA transcriptomes of two types of exosomes in human whole saliva determined by next generation sequencing. *Biol Pharm Bull*. 2013;36:66–75.
- Chen X, Gao C, Li H, Huang L, Sun Q, Dong Y, Hu X. Identification and characterization of microRNAs in raw milk during different periods of lactation, commercial fluid, and powdered milk products. *Cell Res*. 2010;20:1128.
- Yang Y, Li Y, Chen X, Cheng X, Liao Y, Yu X. Exosomal transfer of miR-30a between cardiomyocytes regulates autophagy after hypoxia. *J Mol Med*. 2016;94:711–24.
- Vilella F, Moreno-Moya JM, Balaguer N, Grasso A, Herrero M, Martínez S, Simón C. 2015 Hsa-miR-30d, secreted by the human endometrium, is taken up by the pre-implantation embryo and might modify its transcriptome. *Development*. 2015;142:3210–21.
- Ohshima K, Inoue K, Fujiwara A, Hatakeyama K, Kanto K, Watanabe Y, Mochizuki T. Let-7 microRNA family is selectively secreted into the extracellular environment via exosomes in a metastatic gastric cancer cell line. *PLoS One*. 2010;5:e13247.
- Kusuma RJ, Manca S, Friemel T, Sukreet S, Nguyen C, Zemleni J. Human vascular endothelial cells transport foreign exosomes from cow's milk by endocytosis. *Am J Physiol Cell Physiol*. 2016;310:C800.
- Sun J, Aswath K, Schroeder SG, Lippolis JD, Reinhardt TA, Sonstegard TS. MicroRNA expression profiles of bovine milk exosomes in response to *Staphylococcus aureus* infection. *BMC Genomics*. 2015;16:806.
- Ma J, Wang C, Long K, Zhang H, Zhang J, Jin L, Tang Q, Jiang A, Wang X, Tian S, Chen L, He D, Li D, Huang S, Jiang Z, Li M. Exosomal microRNAs in giant panda (*Ailuropoda melanoleuca*) breast milk: potential maternal regulators for the development of newborn cubs. *Sci Rep*. 2017;7:1–11.

Publisher's Note

Springer Nature remains neutral with regard to jurisdictional claims in published maps and institutional affiliations.



Effects of Fermented Herbal Tea Residues on the Intestinal Microbiota Characteristics of Holstein Heifers Under Heat Stress

Yueqin Xie^{1,2†}, Zujing Chen^{1†}, Dongyang Wang², Guoping Chen², Xiaohong Sun², Qian He¹, Junyi Luo², Ting Chen^{1,2}, Qianyun Xi^{1,2}, Yongliang Zhang^{1,2*} and Jiajie Sun^{1,2*}

¹ Guangdong Engineering & Research Center for Woody Fodder Plants, South China Agricultural University, Guangzhou, China, ² Guangdong Provincial Key Laboratory of Animal Nutrition Control, National Engineering Research Center for Breeding Swine Industry, College of Animal Science, South China Agricultural University, Guangzhou, China

OPEN ACCESS

Edited by:

George Tsiamis,
University of Patras, Greece

Reviewed by:

Marcello Chieppa,
European Biomedical Research
Institute of Salerno (EBRIS), Italy
Junjun Wang,
China Agricultural University, China

*Correspondence:

Yongliang Zhang
zhangyl@scau.edu.cn
Jiajie Sun
jiajiesun@scau.edu.cn

[†] These authors have contributed
equally to this work

Specialty section:

This article was submitted to
Systems Microbiology,
a section of the journal
Frontiers in Microbiology

Received: 10 October 2019

Accepted: 24 April 2020

Published: 26 May 2020

Citation:

Xie Y, Chen Z, Wang D, Chen G,
Sun X, He Q, Luo J, Chen T, Xi Q,
Zhang Y and Sun J (2020) Effects
of Fermented Herbal Tea Residues on
the Intestinal Microbiota
Characteristics of Holstein Heifers
Under Heat Stress.
Front. Microbiol. 11:1014.
doi: 10.3389/fmicb.2020.01014

Herbal tea residue (HTR) is a reusable resource with high nutritional value and bioactive substances content, which can be used as a feed additive. In the present study, HTRs were fermented by lactic acid bacteria, and then fed to a total of 90 Holstein heifers, termed as CN, LC, and HC groups. The supplementation improved physiological indices of respiratory frequency and rectal temperature, increased the concentrations of immunoglobulins and antioxidant capacity-related parameters, and reduced the concentrations of heat stress-related parameters and serum hormones. The heifers' body height increased considerably, while their energy metabolism rates were stimulated in response to fermented HTRs. We also studied the fecal microbial community composition of 8 Holstein heifers in each group, and employed correlation analysis with tested parameters. We found that the bacteria were closely related to characteristics including the energy utilization rate, growth performance, serum biochemical indexes, and fecal SCFA levels of the heifers. Based on our findings, the 5% fermented HTRs replaced corn silage might be advantageous for the heifers' characteristics under heat stress.

Keywords: bacterial microbiome, heat stress, HTR, Holstein heifers, feed additive

INTRODUCTION

Herbal teas made from fresh or dried leaves, flowers, fruit, seeds, roots, and barks of various plant species have long been used as heat-clearing and detoxifying health care drinks in China (Li et al., 2017). In general, these herbal mixtures contain various biologically active compounds such as polysaccharides, flavones, organic acids, alkaloids, and volatile oils (Liu et al., 2011), which are involved in essential functions in humans and animals, including anti-oxidant, anti-inflammatory, anti-proliferative, anti-mutagenic, anti-bacterial, and anti-viral properties (Pardau et al., 2017). Thus, herbal teas are favored by people in the subtropical region of China because of these properties. Consumers believe that herbal teas have therapeutic effectiveness, are inexpensive, and have minimal or no toxic side effects compared with synthetic drugs (Abd et al., 2014). Thus, the demand for herbal teas has gradually increased and herbal teas are now produced on a large scale, which has led to increased production of herbal tea residues (HTRs). According to our

survey, most producers treat HTRs by directly dumping or burning them, which not only poses a threat to the environment, but also wastes resources. In fact, HTRs can be recycled and reused. For example, HTRs can be used as a viable material for water purification, because they contain functional groups, such as carboxylate, aromatic carboxylate, phenolic hydroxyl, and oxyl, which have unusually high adsorption capabilities for toxic and harmful heavy metals (Yang and Cui, 2013). Many researchers have reported that tea residues could be used as adsorbent for Cesium [Cs (I)] (Gurung et al., 2013), Mercury (Hg) (Shen et al., 2017), and Chromium [Cr (VI)] (Ahsan et al., 2018). HTRs can also be used as composting materials to enhance soil fertility because of their high content of organic matter and nitrogen (Iqbal Khan et al., 2007). Moreover, some studies have shown that tea residues, because of their high content of polysaccharides and alkaloids, could be used as feed additives to improve the meat quality of goats (Zhong et al., 2009), change the gut environment of weaned piglets (Su et al., 2018), and improve the immune function in dairy cows under heat stress conditions (Shan et al., 2018). However, HTRs may be difficult to store, digest, and absorb because of their high content of moisture and fiber. This is a key issue when using them as feed additives. Therefore, the problem of how to store, digest, and absorb HTRs efficiently is attracting increased research attention. Microbial fermentation might improve the nutritive value, palatability, and digestibility of HTRs (Niba et al., 2009). A recent study confirmed that microbial fermentation also improved biological activities and exerted a greater immune effect on animals (Kim et al., 2017; Kumar et al., 2017). To date, however, no studies have focused on how to efficiently store and utilize HTRs. Therefore, in the present study, we aimed to develop a method to preserve HTRs and evaluated the possibility of using them as functional feed additives for Holstein heifers under heat stress.

MATERIALS AND METHODS

Preparation of HTRs and Fermentation

HTR was obtained from Wong Lo Kat Limited (Guangzhou, China). It was cut into 2–3 cm pieces and mixed with oat hay (640:360 on a wet weight basis). The minor material, including 10% of corn flour, 2% of molasses, and 1% of lactic acid bacteria (*Lactobacillus plantarum* GIM1.191) (5×10^9 colony forming units/g) were added and mixed thoroughly using a feed-stuff mixer. Finally, the HTR mixture was pressed into polyethylene bags (50 kg each) and fermented by anaerobic fermentation for 20 days.

Nutritive Value Analysis

The samples of HTR and fermented HTR (days 0 and 20) were analyzed for dry matter (DM), crude protein (CP), ether extract (EE), and ash according to the AOAC International guidelines (Horwitz, 2010). The crude fiber (CF), neutral detergent fiber (NDF), and acid detergent fiber (ADF) contents were determined using the method reported by Van Soest et al. (1991). In detail, the contents of fermented HTR were determined from a water extract. Wet fermented HTR (20 g) was transferred to a glass

bottle filled with 180 mL of deionized water, sealed, mixed, and stored at 4°C overnight (Fang et al., 2016). Then, the water extract was passed through filter paper and the filtrate pH was measured using a glass-electrode pH meter (Horiba D-21; Horiba, Tokyo, Japan). The lactic acid content of the filtrate was determined using the method of Barker and Summerson (1941).

Animals, Experimental Design, and Treatments

The study was conducted in a scaled cow farm in Guangzhou, China. Ninety Holstein heifers (8 months of age and balanced for body weight) were used in a completely randomized design for a 7 days adaptation period and a 31 days experimental period. The heifers were randomly divided into three groups (30 heifers per group) in the same cowshed: CN group (no fermented HTRs or control, fed a basal diet); LC group (5% fermented HTRs replaced corn silage); HC group (10% fermented HTRs replaced corn silage). All heifers were fed a total mixed ration (TMR) twice daily. To meet their nutritional requirements, the TMR was based on corn silage as the main forage component and corn grain as the major concentrate component, according to Chinese feeding standards (China Standard NY/T34, 2004). The ingredients and nutrient composition of the HTRs, pre- and post- fermenting HTRs, and the three treatment diets are shown in **Supplementary Table S1**. All heifers were housed in an open sand-bedded cowshed, and water was available *ad libitum* throughout the experimental period. All animal procedures were approved by the Animal Care Committee at South China Agricultural University according to the university's guidelines for animal research.

Measurements and Sampling

The ambient temperature (AT) and relative humidity (RH) were recorded using a KTH-350-I temperature and humidity data-logger (Kimo Industry Co., Biarritz, France) at 08.00, 15.00, and 22.00 h. The temperature-humidity index (THI) was calculated as:

$$THI = (1.8 \times AT + 32) - [(0.55 - 0.0055 \times RH) \times (1.8 \times AT - 26.8)]$$

(Naderi et al., 2016). Respiration rates were determined by counting the number of flank movements in a 60-s period and were measured at 08.00, 15.00, and 22.00 h on Monday of each week (Srikandakumar and Johnson, 2004). Rectal temperature (RT) was measured immediately after respiratory rate (RR) observation using a 10 s digital thermometer (Digi-Vet SC 12, Kruuse, Langeskov, Denmark) that was inserted 8 cm into the rectum and determined at 08.00, 15.00, and 22.00 h (Kovács et al., 2018). The average daily feed intake (ADFI) was recorded on a daily basis. Body dimensions, including body length (BL), body oblique length (BOL), body height (BH), rump length (RL), and hip width (HW) were measured using a measuring stick and tape according to the method of Ozkaya and Bozkurt (2008).

On days 28–30, the diet offered to the heifers was sampled and used for nutrient analysis, chemical analysis, and gross energy (GE) measurement. The methods of nutrient determination, including CP, NDF, and ADFI, were consistent with the method described in Nutrition Value Analysis section. Chemical analysis of the calcium (Ca) and phosphorus (P) contents was performed

using inductively coupled plasma spectroscopy (Chemists and Horwitz, 1990). The GE of the diet was determined using an automatic bomb calorimeter according to the method of Zou et al. (2016).

On the last experimental day, blood samples were collected from eight heifers in each group via the jugular vein before the morning feeding. Blood was placed on ice for more than 2 h and then centrifuged at $3,000 \times g$ for 20 min at 4°C. The serum was stored at -80°C for further analysis of serum biochemistry parameters. Blood serum samples were analyzed for heat shock protein 70 (HSP 70), cortisol (Cor), lactate dehydrogenase (LDH), immunoglobulin A (IgA), immunoglobulin (IgG), alanine transaminase (ALT), creatine kinase (CK), total-antioxidant capacity (T-AOC), malondialdehyde (MDA), superoxide dismutase (SOD), and glutathione-peroxidase (GSH-PX) using the relevant commercial enzyme linked immunosorbent assay kits (Jiancheng Bioengineering Institute, Nanjing, China).

At the end of the experiment, we sampled feces from eight heifer rectums from each group and 400 g of feces per individual were collected at 08:00 h. One aliquot (100 g) was immediately mixed with 3 mL of 10% formaldehyde and stored at -20°C to determine fecal energy. The second aliquot (100 g) was used to determine nutrient apparent digestibility of DM, CP, NDF, and ADF using acid-insoluble ash (AIA) as a marker (Van Keulen and Young, 1977). The third aliquot (100 g) was used to determine fecal volatile fatty acids, including acetic acid (Aa), propionic acid (Pa), isobutyric acid (Ia), butyric acid (Ba), isovaleric acid (Iva), and valeric acid (Va) using high performance liquid chromatography analysis (Actlabs, Ancaster, ON, Canada). The fourth aliquot (100 g) was used to extract total genomic DNA. Total genomic DNA from feces was extracted using the cetyltrimethylammonium bromide/sodium dodecyl sulfate method. The DNA samples were tested for integrity using 1% agarose gel electrophoresis and their concentration was determined using a Qubit fluorometer (Invitrogen, Carlsbad, CA, United States). According to the concentration, DNA was diluted to 1 ng/μL using sterile water. The V3-V4 regions of the 16S ribosomal DNA (rDNA) genes were amplified by polymerase chain reaction based on the method of Sun et al. (2017). In details, the amplification was performed with the universal primers (forward primer, 341F: CCTAYGGGRBGCASCAG; reverse primer, 806R: GGACTACNNGGTATCTAAT). Sequencing libraries were generated using an ThermoFisher Ion Plus Fragment Library Kit (Thermo Scientific, Waltham, MA, United States) on an ThermoFisher Ion S5TMXL sequencer.

16S rRNA Gene Sequencing and Annotation Analysis

Single-end reads were assigned to samples based on their unique barcode in the adaptor sequence. Quality filtering of the raw reads was performed to obtain high-quality clean reads according to the Cutadapt quality controlled process (Martin, 2011). The reads were compared with the reference database (Quast et al., 2012) using the UCHIME algorithm (Edgar et al., 2011) to detect chimeric sequences (Haas et al., 2011), and clean

reads were finally obtained using the Uparse software (Uparse v7.0.1001) (Edgar, 2013). Sequences with $\geq 97\%$ similarity were assigned to the same operational taxonomic units (OTUs). For each representative OTU, the Silva Database was used to annotate taxonomic information based on the Mothur algorithm (Quast et al., 2012). To study the phylogenetic relationships between different OTUs, multiple sequence alignment was conducted using the MUSCLE software (Version 3.8.31) (Edgar, 2004). Alpha diversity was applied to analyze the complexity of species diversity within groups, including the Observed-species, Chao1, ACE, and Shannon indices. Beta diversity analysis was used to evaluate differences between groups using non-metric multi-dimensional scaling (NMDS). Two different complementary analyses including analysis of similarity (ANOSIM) and multiresponse permutation procedure (MRPP), were used to determine the significant differences of the fecal microbiota in response to fermented HTRs. All these indices were calculated using the quantitative insights into microbial ecology (QIIME) pipeline (Version 1.7.0) and displayed using the R software (Version 2.15.3). The raw sequences were deposited into Sequence Read Archive (SRA) database¹ with the BioProject accession number PRJNA624971.

Statistical Analysis

All data, including physiological parameters, serum biochemical indices, growth traits, energy metabolism rates, and the fecal concentrations of short-chain fatty acids (SCFAs) were analyzed using one-way analysis of variance (ANOVA) and Duncan's test (SPSS 17.0, IBM Corp., Armonk, NY, United States). The R software was used to perform Metastat analysis to determine the differences in the relative abundance of fecal microbiomes (White et al., 2009). The correlation analyses of fecal microbiota with the tested traits were tested by function cor (x, y, use = "p")², and illustrated with function labeledHeatmap (Matrix, xLabels, yLabels) in R package WGCNA².

RESULTS

Chemical Compositions and Fermentation Quality of HTRs

The HTR had low DM, CP, EE, and ash contents of 205.88, 97.75, 35.17, and 66.85 g/kg, respectively. Additionally, it had high CF, NDF, and ADF contents of 288.28, 612.18, and 452.88 g/kg, respectively. After twenty days of anaerobic fermentation, the pH value dropped from 5.60 to 3.72; and the DM, NDF, and ADF contents decreased from 441.0 to 436.2 g/kg, 567.8 to 510.0 g/kg, and 332.0 to 301.2 g/kg, respectively. Simultaneously, the acetic acid, CP, and ash contents increased from 0 to 21.09 g/kg, 79.2 to 82.3 g/kg, and 50.0 to 55.0 g/kg, respectively (Supplementary Table S1). Additionally, compared with that of the CN group, the LC and HC groups were formulated to contain similar content of Ca (5.8, 5.6, and 5.6 g/kg, respectively) and P (4.0, 3.9, and

¹<https://www.ncbi.nlm.nih.gov/sra/>

²<http://horvath.genetics.ucla.edu/html/CoexpressionNetwork/Rpackages/WGCNA/>

3.9 g/kg, respectively), a lower content of CP (130.1, 128.2, and 127.9 g/kg, respectively), but a higher content of DM (554.8, 560.2, and 563.8 g/kg, respectively), NDF (467.2, 473.1, and 479.8 g/kg, respectively), and ADF (220.9, 235.8, and 241.9 g/kg, respectively) (Supplementary Table S1).

Physiological Index, Energy Utilization Rate, Nutrient Apparent Digestibility, and Growth Performance

The mean THI values in the morning (08:00), afternoon (15:00), and evening (22:00) in the barn during the study were 77.9 (range 75.4–80.7), 82.1 (range 79.6–83.9), and 77.6 (range 75.8–78.6), respectively (Supplementary Figure S1). The overall mean THI was 79.2. The results for the physiological index and ADFI are shown in Table 1. The RR and RT were affected by fermented HTR ($P < 0.05$). In detail, compared with that in the CN group, the RR in LC and HC groups decreased ($P < 0.05$) at 15.00 h, to 51.75, 47.02, and 48.29 breaths/min, respectively. The RT in LC group was similar at 8.00, 15.00, and 22.00 h (39.02, 39.10, and 39.08°C, respectively), which was significantly lower than that in the CN group (39.13, 39.27, and 39.19°C, respectively) ($P < 0.05$). Additionally, no differences in the RT were observed between the LC and HC groups ($P > 0.05$). The ADFI in the CN, LC, and HC groups were 14.24, 16.34, and 15.05 kg/day, respectively. The ADFI was the highest ($P < 0.01$) in the LC group and decreased significantly ($P < 0.01$) in the presence of an elevated dietary fermented HTR content.

The energy utilization rate is shown in Table 2. The DE/GE and ME/GE ratios in the CN, LC, and HC groups were 67.51 and 54.81%, 69.85 and 57.63%, and 69.22 and 57.77%, respectively. The values of DE/GE and ME/GE in the LC group were significantly higher than those in the CN group ($P < 0.05$). However, no differences in energy utilization rates were observed between the LC and HC groups. In addition, the apparent digestibility of DM, CP, NDF, and ADF was not different between the CN, LC, and HC groups ($P > 0.05$, Supplementary Table S1).

TABLE 1 | Food intake, respiratory rate, and rectal temperature of Holstein heifers fed HTR.

Item	Time	Groups		
		CN	LC	HC
Dry matter intake (kg/day)		14.24 ± 0.12 ^C	16.34 ± 0.21 ^A	15.05 ± 0.18 ^B
Respiratory rate (breaths/min)	8:00	46.54 ± 2.81	45.75 ± 2.13	45.66 ± 2.11
	15:00	51.75 ± 1.79 ^a	47.02 ± 2.26 ^c	48.29 ± 2.73 ^b
	22:00	46.44 ± 2.15	46.04 ± 1.68	46.17 ± 1.64
Rectal temperature (°C)	8:00	39.13 ± 0.31 ^a	39.02 ± 0.18 ^b	39.07 ± 0.25 ^{ab}
	15:00	39.27 ± 0.21 ^a	39.10 ± 0.25 ^b	39.11 ± 0.27 ^b
	22:00	39.19 ± 0.23 ^a	39.08 ± 0.23 ^b	39.14 ± 0.21 ^{ab}

The values were calculated as the means ± standard error of the mean ($N = 30$); a and b denote values that differ significantly at $P < 0.05$, while A and B denote values that differ significantly at $P < 0.01$. HTR, herbal tea residue; CN, control no HTR; LC, 5% fermented HTRs replaced corn silage; HC, 10% fermented HTRs replaced corn silage.

TABLE 2 | Energy metabolism rate and quantitative analysis of short-chain fatty acids (SCFAs) in the feces of Holstein heifers among the three groups.

Item	Groups		
	CN	LC	HC
DE/GE (%)	67.506 ± 0.792 ^b	69.851 ± 0.602 ^a	69.219 ± 0.719 ^{ab}
ME/GE (%)	54.812 ± 0.914 ^b	57.634 ± 0.692 ^a	57.774 ± 0.763 ^{ab}
Acetic acid (mmol/L)	11.637 ± 0.153 ^C	15.547 ± 0.154 ^A	13.297 ± 0.329 ^B
Propionic acid (mmol/L)	2.298 ± 0.034 ^c	3.162 ± 0.029 ^a	2.920 ± 0.123 ^b
Isobutyric acid (mmol/L)	0.190 ± 0.013 ^b	0.251 ± 0.007 ^a	0.243 ± 0.005 ^a
Butyric acid (mmol/L)	1.100 ± 0.044 ^c	1.750 ± 0.037 ^a	1.280 ± 0.073 ^b
Isovaleric acid (mmol/L)	0.161 ± 0.005 ^b	0.192 ± 0.005 ^a	0.184 ± 0.006 ^a
Valeric acid (mmol/L)	0.118 ± 0.004 ^b	0.206 ± 0.007 ^a	0.193 ± 0.003 ^a

DE, Digestive energy; ME, Metabolizable Energy; GE, Gross Energy; CN, control no HTR; LC, 5% fermented HTRs replaced corn silage; HC, 10% fermented HTRs replaced corn silage. The values were calculated as the means ± standard error of the mean ($N = 30$); a and b denote values that differ significantly at $P < 0.05$, while A and B denote values that differ significantly at $P < 0.01$.

TABLE 3 | Analysis of serum biochemical indices in Holstein heifers between three groups.

Item	Groups		
	CN	LC	HC
HSP70 (pg/mL)	294.91 ± 5.20 ^A	198.93 ± 7.24 ^C	238.34 ± 3.64 ^B
Cor (mg/mL)	116.30 ± 3.30 ^A	76.52 ± 2.37 ^C	104.64 ± 2.58 ^B
LDH (U/L)	430.56 ± 8.51 ^A	292.65 ± 8.09 ^C	342.02 ± 8.28 ^B
IgA (μg/mL)	215.11 ± 6.03 ^C	317.14 ± 8.46 ^A	280.15 ± 3.28 ^B
IgG (μg/mL)	367.82 ± 7.32 ^C	522.55 ± 6.04 ^A	451.99 ± 12.89 ^B
ALT (U/L)	4.54 ± 0.31 ^A	2.92 ± 0.39 ^B	3.06 ± 0.43 ^B
CK (U/mL)	0.443 ± 0.062 ^A	0.23 ± 0.021 ^B	0.38 ± 0.041 ^A
T-AOC (mmol/L)	0.167 ± 0.014	0.17 ± 0.018	0.17 ± 0.007
MDA (nmol/mL)	4.12 ± 0.47	3.76 ± 0.27	3.90 ± 0.19
SOD (U/mL)	78.30 ± 3.38 ^b	94.80 ± 5.74 ^a	82.43 ± 3.75 ^{ab}
GSH-PX (U/mL)	100.23 ± 6.85 ^b	121.61 ± 4.85 ^a	120.05 ± 5.90 ^a

HSP70, Heat shock protein 70; COR, Cortisol; LDH, Lactate dehydrogenase; IgA, Immunoglobulin G; IgG, Immunoglobulin G; ALT, Alanine aminotransferase; CK, Creatine kinase; T-AOC, Total antioxidant capacity; MDA, Malondialdehyde; SOD, Superoxide Dismutase; GSH-PX, Glutathione peroxidase; CN, control no HTR; LC, 5% fermented HTRs replaced corn silage; HC, 10% fermented HTRs replaced corn silage. a and b denote values that differ significantly at $P < 0.05$, while A and B denote values that differ significantly at $P < 0.01$. The values were calculated as the means ± standard error of the mean ($N = 8$); a and b denote values that differ significantly at $P < 0.05$, while A and B denote values that differ significantly at $P < 0.01$.

Results of growth traits measurements are shown in Table 3. The BH value was higher ($P < 0.05$) for the LC and HC group compared with that in the CN group. There was no significant difference between the LC and HC groups ($P > 0.05$). Other growth parameters including BL, BOL, RL, and HW were not affected by fermented HTR ($P > 0.05$).

TABLE 4 | Growth traits of Holstein heifers between three groups.

Item	Groups		
	CN	LC	HC
Body length (cm)	109.25 ± 0.55	113.13 ± 1.48	109.38 ± 2.17
Body oblique length (cm)	120.25 ± 1.16	126.25 ± 1.75	123.88 ± 3.02
Body height (cm)	113.13 ± 0.76 ^b	117.00 ± 1.60 ^a	117.25 ± 0.95 ^a
Rump length (cm)	36.38 ± 0.86	38.75 ± 0.83	38.13 ± 1.61
Hip width (cm)	39.00 ± 0.26	41.38 ± 1.20	40.00 ± 1.95

The values were calculated as the means ± standard error of the mean ($N = 30$), while *a* and *b* denote values that differ significantly at $P < 0.05$. CN, control no HTR; LC, 5% fermented HTRs replaced corn silage; HC, 10% fermented HTRs replaced corn silage.

Serum Biochemical Indexes

Serum concentrations of heat stress-related parameters (HSP70, Cor, and LDH), immunoglobulins (IgA and IgG), serum hormones (ALT and CK), and antioxidant capacity-related parameters (SOD, GSH-PX, T-AOC, and MDA) are listed in **Table 4**. For the heat stress-related parameters, the concentrations of HSP70 in the CN, LC, and HC groups were 294.91, 198.93, and 238.34 pg/ml, respectively, indicating a significant decrease ($P < 0.01$) when Holstein heifers were offered 5 or 10% fermented HTRs. The concentrations of Cor and LDH in the CN, LC, and HC groups were 116.30 mg/mL and 430.56 U/L, 76.52 mg/mL and 292.65 U/L, and 104.64 mg/mL and 342.02 U/L, respectively. The concentrations in the LC and HC groups were significantly lower than those in the CN group ($P < 0.01$). The concentrations of IgA and IgG were greater ($P < 0.01$) in the LC and HC groups than in the CN group. The concentrations of IgA and IgG in CN, LC, and HC groups were 215.11 and 367.82 μg/mL, 317.14 and 522.55 μg/mL, and 280.15 and 451.99 μg/mL, respectively. For the serum hormones, the concentrations of ALT in the CN, LC, and HC groups were 14.54, 2.92, and 3.06 U/L, respectively and the concentrations of CK in were 0.443, 0.23, and 0.38 U/mL, respectively. The ALT level was significantly lower ($P < 0.01$) in the LC and HC groups compared with that in the CN group. Whereas the CK level in the LC group was lower ($P < 0.01$) than that in the CN and HC groups. For the antioxidant capacity-related parameters, the concentrations of SOD and GSH-PX in the CN, LC, and HC groups were 78.30 and 100.23 U/mL, 94.80 and 121.61 U/mL, and 82.43 and 120.05 U/mL, respectively. There levels in the LC group were significantly higher than those in CN group ($P < 0.05$). However, the concentrations of T-AOC and MDA were not affected ($P > 0.05$) by the fermented HTRs.

Fecal SCFA Concentrations

The fecal SCFA concentrations are listed in **Table 2**. The concentrations of Aa in the CN, LC, and HC groups were 11.64, 15.55, and 13.30 mmol/L, respectively, with the LC and HC groups showing significantly higher levels than the CN group ($P < 0.01$). The concentrations of other fecal SCFAs, including Pa, Ia, Ba, Iva, and Va in the LC or HC groups were also significantly higher than those in the CN group ($P < 0.05$). However, no

differences were found between LC and HC groups except for the concentrations of Pa and Ba.

16S rRNA Gene Sequencing and Annotation Analysis

After DNA extraction, the hypervariable V3–V4 regions of the 16S rDNA were enriched, and a random rarefaction of sample reads was carried out to avoid errors caused by sequencing depth differences. The subsequent high-throughput analysis generated a total of 2,002,175 raw reads. On average, each sample produced approximately 83,423 joined tags (min = 70,458, max = 88,696). Over $94.33\% \pm 2.55\%$ of the total joined tags from each sample passed quality control and were processed for further analysis (**Supplementary Table S2A**). Venn diagrams analysis of the high-quality tags yielded 2,573 unique OTU candidates at 97% sequence similarity, and 1,898 candidates that were shared across all samples were defined as core OTUs. The core OTUs comprised approximately 73.77% of the total candidates, while only 89, 136, and 119 OTUs were identified uniquely in the CN, LC, and HC groups, respectively (**Figure 1A** and **Supplementary Table S2B**). We annotated all these OTU tags to the Greengenes database, and found that $98.98 \pm 0.25\%$ of the sequences could be aligned at the phyla taxonomic level, while $98.12 \pm 0.37\%$, $90.36 \pm 2.11\%$, $82.95 \pm 1.97\%$, $28.29 \pm 4.02\%$, and $4.73 \pm 1.64\%$ of the annotated OTUs were assigned at the class, order, family, genus, and species levels, respectively (**Supplementary Table S2C**). Additionally, the microbial diversity in the feces of dairy cows was assessed using the QIIME pipeline based on the OTU annotation, which identified the top 10 phyla (**Figures 1B,C**). In detail, the most abundant phylum in the feces of Holstein heifers was *Firmicutes*, which accounted for approximately $65.79 \pm 3.90\%$ of all sequences, followed by *Bacteroidetes* ($18.93 \pm 4.57\%$), and *Tenericutes* ($7.42 \pm 1.94\%$) (**Supplementary Tables S3A,B**). At the class level, a total of 38 classes were detected, five classes had a relative abundance greater than 1.0%, including *Clostridia*, *Bacteroidia*, *Mollicutes*, *Erysipelotrichia*, and *unidentified_Bacteria*. The most abundant class in the feces of Holstein heifers was *Clostridia* ($60.92 \pm 3.84\%$) (**Supplementary Tables S3C,D**). At the order level, we detected four orders with a relative abundance greater than 1.0% (**Supplementary Tables S3E,F**). Specifically, the most abundant order in the feces of Holstein heifers was *Clostridiales*, which accounted for approximately $60.87 \pm 3.83\%$ of all sequences, followed by *Bacteroidales* ($18.77 \pm 4.39\%$), *Erysipelotrichales* ($4.23 \pm 1.18\%$), and *unidentified_Bacteria* ($2.37 \pm 0.65\%$). At family level, among the 137 families detected, eleven families had a relative abundance greater than 1.0%, including *Ruminococcaceae*, *Rikenellaceae*, *Christensenellaceae*, *unidentified_Clostridiales*, *Bacteroidaceae*, *Lachnospiraceae*, *unidentified_Bacteria*, *Peptostreptococcaceae*, *Erysipelotrichaceae*, *Muribaculaceae*, and *Prevotellaceae*, and the most abundant family in the feces of Holstein heifers was *Ruminococcaceae* ($35.88 \pm 3.73\%$) (**Supplementary Tables S3G,H**). Among the 257 genera detected, eight genera had a relative abundance greater than 1.0%, such as *Bacteroides*,

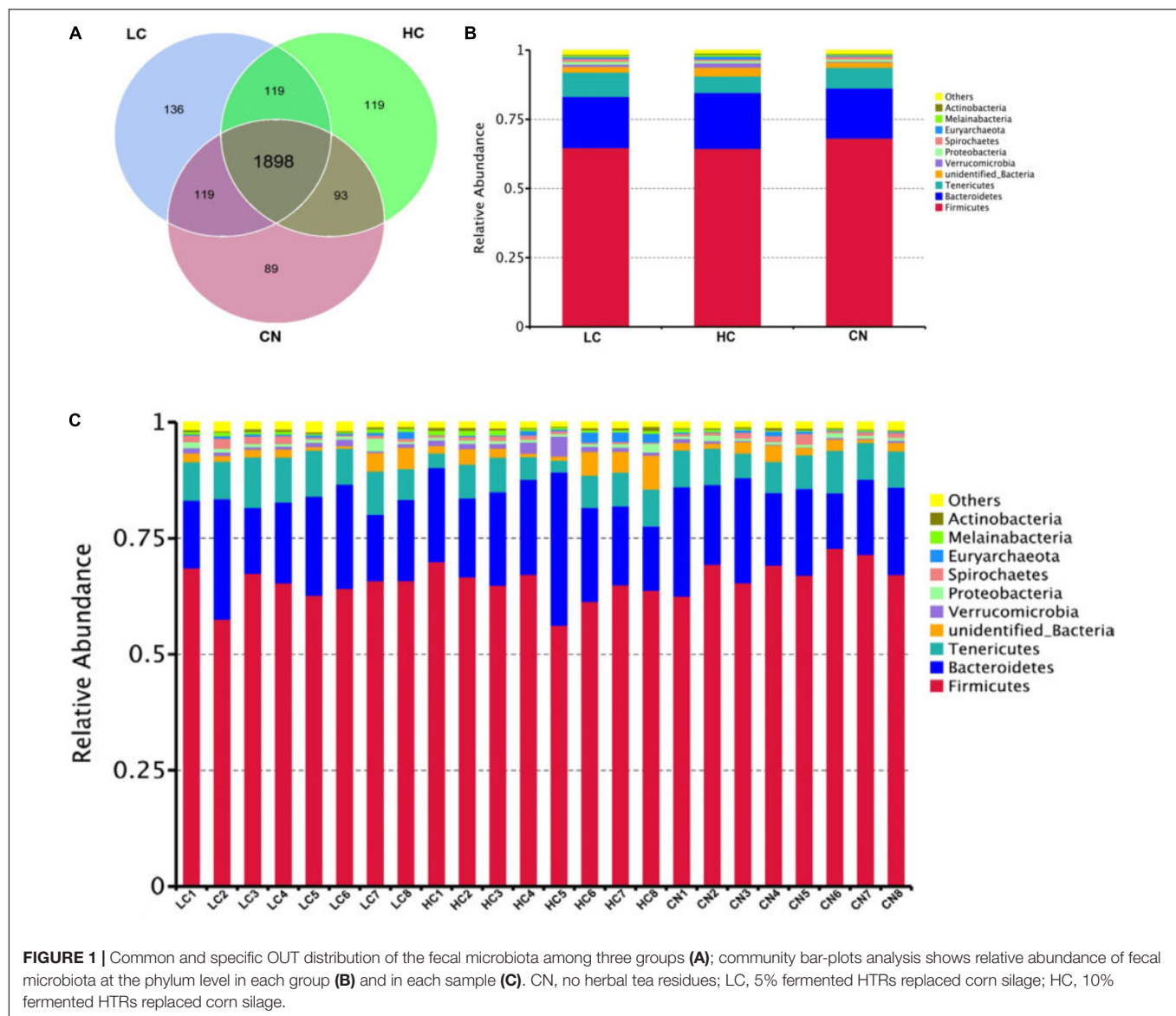


FIGURE 1 | Common and specific OUT distribution of the fecal microbiota among three groups (A); community bar-plots analysis shows relative abundance of fecal microbiota at the phylum level in each group (B) and in each sample (C). CN, no herbal tea residues; LC, 5% fermented HTRs replaced corn silage; HC, 10% fermented HTRs replaced corn silage.

Clostridiales, *Ruminococcaceae*, *Candidatus_Saccharimonas*, *Turicibacter*, *Alistipes*, *Romboutsia*, and *Paeniclostridium* (Supplementary Tables S3I,J). At the species level, among the 168 species detected, nine species had a relative abundance greater than 0.10%, including *Clostridium disporicum*, *Clostridium papyrosolvens*, *Methanobrevibacter ruminantium*, *Spirochaetes bacterium* GWE2 31 10, *Treponema porcinum*, *Ruminococcus bromii*, *rumen bacterium* NK4A214, *Pseudomona fragi*, and *bacterium* LD2013. The most abundant species in the feces of Holstein heifers was *Clostridium disporicum* ($1.61 \pm 0.22\%$) (Supplementary Tables S3K,L).

Microbial Diversity in the Feces of Holstein Heifers

We compared the alpha-diversity (within-sample diversity or estimate of species richness and evenness) of each sample

with differing sequence counts or sampling efforts. Rarefaction curve analysis indicated that the number of sequences and the sequencing depth was sufficient for this study (Supplementary Figure S2). We further used Observed species, Chao1, ACE, and Shannon indices among the different groups to evaluate the fecal diversity of Holstein heifers affected by fermented HTRs treatments (Figure 2). Although there was a trend toward decreased alpha diversity in the LC and HC groups compared with those of the control, these differences did not significantly affect the species-level microbial diversity as assessed using Observed species ($P = 0.175$), Chao 1 ($P = 0.190$), and ACE ($P = 0.212$). However, the Shannon diversity index showed a significant decrease in the diversity of the LC and HC groups compared with that of the CN group ($P = 0.031$). For the Beta diversity, NMDS showed distinct diversity differences between the groups (Stress = 0.161) (Figure 3). In addition, pairwise ANOSIM analyses suggested that there were extremely significant

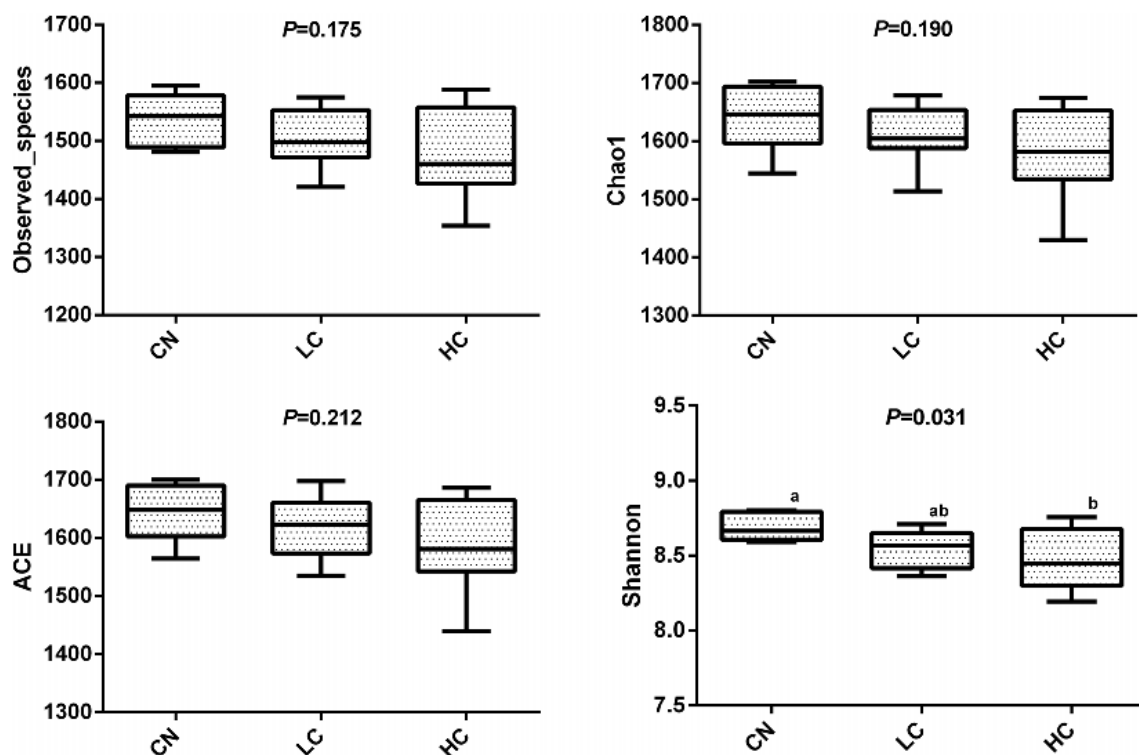


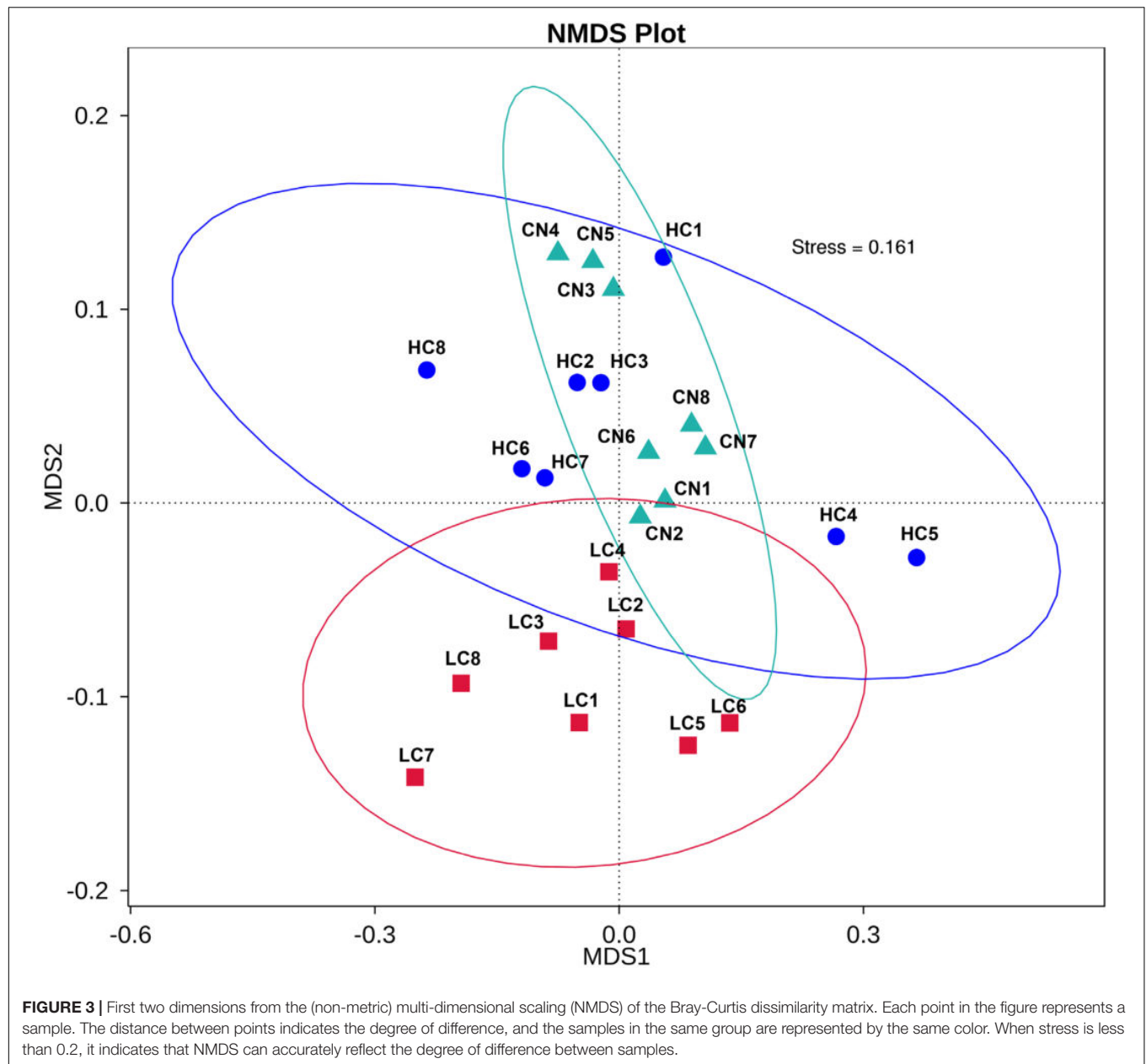
FIGURE 2 | Microbial diversity indices in the fecal microbiome. Four measures of α -diversity include observed species, Chao 1 index, ACE and Shannon.

differences between the CN and LC groups (global $R = 0.4905$, $P = 0.001$), between the CN and HC groups (global $R = 0.3245$, $P = 0.001$), and between the LC and HC groups (global $R = 0.2366$, $P = 0.008$) (Table 5). We also performed an MRPP analysis in within- and between-group populations. The differences for between-group homogeneity were higher than those for within-group with an A -value > 0 , and the change degree reached a significant level between the CN and LC groups ($P = 0.001$), between the CN and HC groups ($P = 0.003$), and between the LC and HC groups ($P = 0.003$) (Table 5).

Alternative Diets Containing Fermented HTR Changed the Composition of the Fecal Microbiota

The changes in the fecal microbiota at the genus and species levels were determined using a ternary plot method and are shown in Supplementary Figure S3. Compared with the CN and HC groups, the LC group showed a remarkably increased abundance of *Oxyphotobacteria* at the Genus level, while the abundances of *Bifidobacterium*, *Aerosphaera*, *Erysipelothrix*, *Enterobacteriaceae*, *Jeotgalibaca*, and *Acinetobacter* were remarkably enhanced in the HC group. At the species level, the LC group showed significant increases in *Lolium perenne*, *Spirochaetes bacterium*, and *Clostridium* sp. MC 40, and the HC group showed significant increases in *Escherichia coli*, *Treponema porcinum* and *Ruminococcus* sp. YE281 were significantly enhanced in the CN group. The differences in the microbial composition

(relative abundance) of the fecal microbiome between the CN and LC groups and the CN and HC groups were compared using the Metastat method with Fisher's exact test (White et al., 2009). A total of 17 genera displayed a significant difference between the CN and LC groups. Among them, *Negativibacillus*, *Eisenbergiella*, *Anaerovibrio*, *Mollicutes*, *Anaerovorax*, *Mailhella*, *Bacteroidales*, *Flavonifractor*, *Pseudoramibacter*, *Oscillibacter*, *Ruminococcaceae*, and *Butyrivibrio* were decreased, and *Bacillus*, *Akkermansia*, *Parvibacter*, *Turicibacter*, and *Lysinibacillus* were increased in the LC group (Supplementary Table S4A). Compared with the CN group, six genera (*Enterobacteriaceae*, *Brochothrix*, *Akkermansia*, *Rummeliibacillus*, *Campylobacter*, and *Methanocorpusculum*) displayed a significant increase and 11 genera (*Pygmaibacter*, *Roseburia*, *Rhodospirillales*, *Anaerocolumna*, *Erysipelotrichaceae*, *Eisenbergiella*, *Succinivibrio*, *Butyrivibrio*, *Sanguibacteroides*, *Oxyp*, and *Prevotellaceae*) displayed a significant decrease in the HC group (Supplementary Table S4B). At the species level, a total of eight species displayed a significant difference between the CN and LC groups (Supplementary Table S5A). Among them, *Bacillus oleronius*, *Ruminococcus* sp., *Marseille*, *Bacillus thermoamylovorans*, *Clostridium* sp. MC 40, and *Lysinibacillus massiliensis* were upregulated, and *Lactobacillus reuteri*, *Acholeplasmatales bacterium*, and *rumen bacterium* YS3 were downregulated (Figure 4A). A total of nine species displayed a significant difference between CN and HC groups (Supplementary Table S5B). Among them, *Alphaproteobacteria bacterium*, *bacterium* YGD2005, *Ruminococcus* sp. YE281, *Bacteroides*



ovatus, *bacterium* YE57, and *Spirochaetes bacterium* were downregulated, and *Escherichia coli*, *Brochothrix thermosphacta*, and *Rummeliibacillus pycnus* were upregulated (Figure 4B).

Correlations of Fecal Microbiota With the Energy Utilization Rate and SCFAs

To further identify genera that significantly correlated with the energy utilization rate and the SCFAs concentrations of heifers, we used the Pearson correlation test and found that the bacterial abundance of *Turicibacter* was slightly and positively related to the ratio of DE/GE and ME/GE, but did not reach significance ($P = 0.09$ and $P = 0.08$, respectively) (Supplementary Figure S4). At the genus level,

the concentration of Aa, Pa, Ba, and Va displayed strong positive correlations with relative abundance of *Turicibacter* ($P = 0.009$, $P = 0.04$, $P = 0.01$, and $P = 0.008$, respectively). The concentration of Aa, Pa, Ia, Iva, and Va showed significant negative correlations with relative abundance of *Butyrivibrio* ($P = 0.05$, $P = 0.004$, $P = 0.01$, $P = 0.005$, and $P = 0.004$, respectively) (Supplementary Figure S4). At the species level, the relative abundance of *Ruminococcus* sp. *marseille* correlated positively with the concentrations of Aa, Ia, Ba, and Va ($P = 0.01$, $P = 0.04$, $P = 0.04$, and $P = 0.02$, respectively). The relative abundance of *Lysinibacillus massiliensis* correlated positively with the concentrations of Aa, Pa, and Ia ($P = 0.03$, $P = 0.02$, and $P = 0.02$, respectively). In addition, the concentration of Aa and Ba displayed a strong positive correlation with

TABLE 5 | Significant differences in community structure in the fecal microbiota of Holstein heifers among the three groups.

Group	Anosim		MRPP			
	R-value	P-value	A-value	Observed delta	Expected delta	P-value
CN-LC	0.4905	0.001	0.09894	0.2821	0.3131	0.001
CN-HC	0.3245	0.001	0.0739	0.306	0.3304	0.003
LC-HC	0.2366	0.008	0.0746	0.3252	0.3515	0.003

Anosim, analysis of similarity; MRPP, multiresponse permutation procedure. The R-value ranged from -1 to 1, and an R-value > 0 showed a significant difference in the between-group population compared with those in the within-group population, as well as the A-value (analyzed by MRPP, multiresponse permutation procedure). The P-values indicated the significant differences at the levels of $P < 0.05$ or $P < 0.01$. CN, control no HTR; LC, 5% fermented HTRs replaced corn silage; HC, 10% fermented HTRs replaced corn silage.

relative abundance of *Clostridium* sp. MC 40 ($P = 0.008$ and $P = 0.002$, respectively) and a negative correlation with relative abundance of *Acholeplasmatales bacterium* ($P = 0.008$, $P = 0.004$, respectively) (Figure 5).

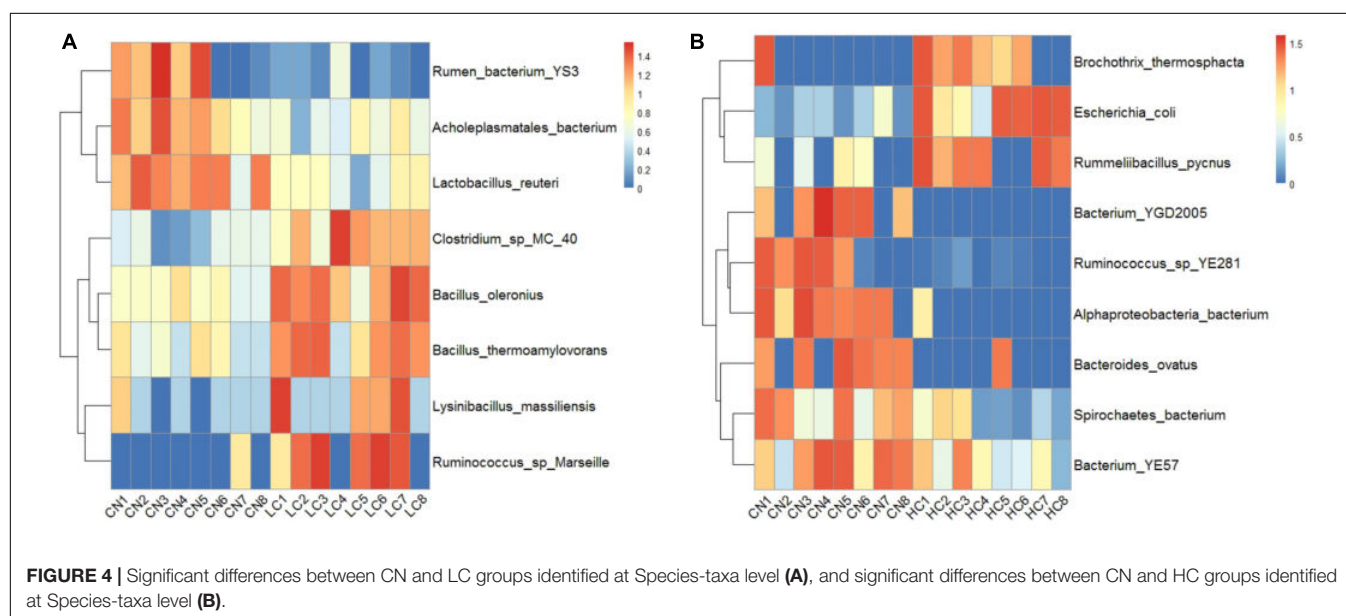
Correlations of Fecal Microbiota With Serum Biochemical Indexes

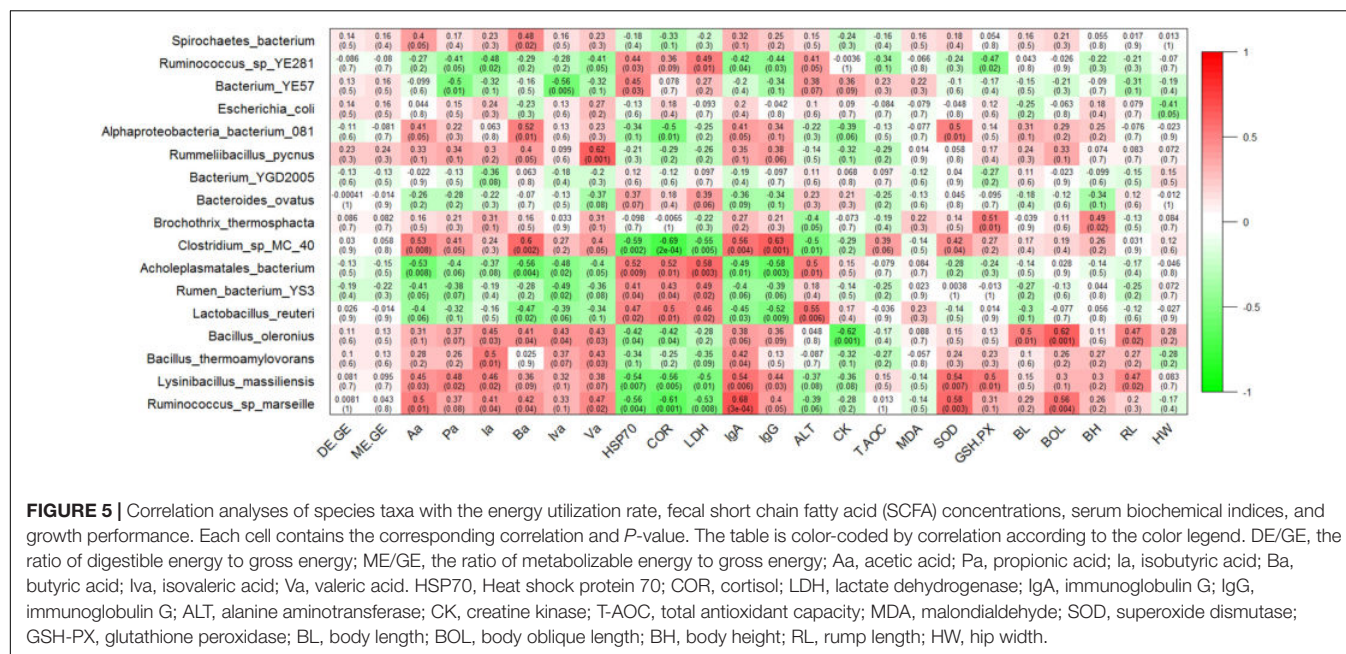
At the genus level, the concentration of HSP70, Cor, and LDH correlated positively with the relative abundance of *Mollicutes* ($P = 0.01$, $P = 0.01$ and $P = 0.003$, respectively) and *Eisenbergiella* ($P = 0.003$, $P = 0.007$ and $P = 0.002$, respectively), while the correlated significantly negatively with the relative abundance of *Lysinibacillus* ($P = 0.007$, $P = 0.005$, and $P = 0.01$, respectively). The concentration of IgA and IgG showed significant positive correlations with relative abundance of *Lysinibacillus* ($P = 0.006$ and $P = 0.03$, respectively) and *Turicibacter* ($P = 0.03$ and $P = 0.03$, respectively), and negative correlations with relative abundance of *Eisenbergiella* ($P = 0.002$

and $P = 0.002$, respectively) and *Negativibacillus* ($P = 0.001$ and $P = 0.008$, respectively). The bacterial abundance of *Butyrivibrio* correlated positively with the concentration of ALT ($P = 0.002$) and CK ($P = 0.003$). Additionally, the bacterial abundance of *Lysinibacillus* correlated positively with the concentration of SOD ($P = 0.007$) and GSH.PX ($P = 0.01$) (Supplementary Figure S4). At the species level, the relative abundance of *Acholeplasmatales bacterium* correlated positively with the concentrations of HSP70, Cor, LDH, and ALT, and correlated significantly negatively with the concentration of IgA and IgG. In contrast, the relative abundance of *Clostridium* sp. MC 40, *Lysinibacillus massiliensis*, and *Ruminococcus* sp. marseille correlated negatively with the concentrations of HSP70, Cor, and LDH, and correlated positively with the concentrations of IgA and IgG. In addition, the relative abundance of *Lysinibacillus massiliensis* correlated positively with the concentrations of SOD and GSH.PX (Figure 5).

Correlations of Fecal Microbiota With Growth Performance

At the genus level, the relative abundances of *Bacillus* and *Anaerovibrio* displayed strong positive (Pearson's $r = 0.59$, $P = 0.002$) and negative correlations (Pearson's $r = -0.5$, $P = 0.01$) with the BOL value. The RL value correlated positively with the relative abundance of *Lysinibacillus* (Pearson's $r = 0.47$, $P = 0.02$) and *Bacillus* (Pearson's $r = 0.42$, $P = 0.04$), and correlated negatively with the relative abundance of *Anaerovibrio* (Pearson's $r = -0.49$, $P = 0.01$) and *Mailhella* (Pearson's $r = -0.48$, $P = 0.02$) (Supplementary Figure S4). At the species level, the relative abundances of *Bacillus oleronius* displayed a strong positive correlation with the values of BL, BOL, and RL ($P = 0.01$, $P = 0.001$, and $P = 0.02$, respectively). The relative abundance of *Ruminococcus* sp. marseille also showed a strong positive correlation with the BOL value ($P = 0.004$) and the relative





abundance of *Lysinibacillus massiliensis* correlated positively with the value of RL ($P = 0.02$) (Figure 5).

DISCUSSION

Herbal teas have heat-clearing and detoxifying effects and are favored by the population of southern China, leading to gradually increasing demand for herbal teas and the production of massive amounts HTRs. The main herbal tea production enterprises in Guangdong Province can produce about 680 tons of HTRs per day currently, which wastes resources and pollutes the environment. Some studies have shown that tea residues could be used as feed additives (Zhong et al., 2009). However, HTRs are difficult to store because of their high moisture content. Therefore, this study used oat hay to control the moisture content, because it contains high concentrations of non-structural carbohydrates and provides abundant carbohydrates for silage fermentation (Chatterton et al., 2006). In this study, the CP, NDF, and ADF contents (82.3 g/kg of DM, 510.0 g/kg of DM, and 301.2 g/kg of DM, respectively) of the HTRs fermented for 20 days were higher than that of maize straw silage (78.6 g/kg of DM, 462.1 g/kg of DM, and 265.2 g/kg of DM, respectively) (Zeng et al., 2018). Simultaneously, the fermented HTR was well preserved with a low pH and high lactic acid content. Hence, the fermented HTR could be used as good-quality roughage for ruminants. Additionally, HTR fermented with oat hay was used as a partial substitute for corn silage in the feed of Holstein heifers, representing a new use for HTRs as forage for livestock.

An early study suggested that Holstein cows are sensitive to heat stress (HS) conditions when the THI is over 72 (Rhoads et al., 2009). In this study, the average THI was 79.2, which this indicated that the experimental Holstein heifers in South China were substantially affected by HS during summer months.

Additionally, the RT and RR are also excellent indicators of an animal's susceptibility to heat load (Yan et al., 2016). In the presents study, the results showed that both the RT and RR were affected by the fermented HTR, and the optimal dietary supplement was 5% fermented HTRs replaced corn silage, at which the RT and RR of the heifers were the lowest. This finding is consistent with a study conducted by Song et al. (2014), who demonstrated that traditional Chinese medicine reduced the body temperature or maintained the normal temperature of cows in a high temperature environment. The current study demonstrated that the ADFI and BH were greater for the LC and HC groups ($P < 0.05$) compared with those of the CN group. This is in agreement with the results of Wang et al. (2011), who showed that Chinese herbal mixture feed additives had growth-promoting effects in beef cattle. This could be caused by Chinese herbs, which contain abundant protein, carbohydrate, vitamin, fat, and minerals, which can play an important role in the nutritive equilibrium, thus enhancing growth performance (Liu et al., 2011). Currently, there is no information on the effects of fermented HTRs on the energy utilization of ruminants. However, the energy utilization data showed that the fermented HTR had improved the energy utilization efficiency of ruminants. We suspected that this might be caused by a certain effect on microbial fermentation. Studies have shown that microbial fermented feed may provide more rich nutrition, better palatability, increased digestibility, and improved energy efficiency (Niba et al., 2009).

In the present study, the decreased level of HSP70, Cor, and LDH in the serum of the experimental group indicated that consuming fermented HTR might improve the heat stress resistance of heifers. This result corroborates the report of Wang et al. (2011), who observed that a microbially fermented Chinese herbal combination might improve the heat stress resistance of Jersey cattle. In addition, the levels of IgA and

IgG in the heifers' serum were significantly increased in the LC and HC groups. Previous studies reported that fermented Chinese herbal medicines improve the immune function in dairy cows under HS conditions (Shan et al., 2018). Interestingly, we also found that the concentrations of ALT and CK in the heifers' serum decreased significantly. These results indicated that feeding heifers with fermented HTR has important health effects. However, the specific molecular mechanism is unclear. In terms of antioxidant capacity, the levels of SOD and GSH-PX in the heifers' serum increased significantly. This result illustrates that fermented HTR might exert an antioxidative effect via its antioxidative constituents. Studies have shown that herbal feed with anti-oxidant properties, which can cope with an excess of free radicals produced upon oxidative stress, could be used to alleviate the negative effects of high ambient temperature (Tuzcu et al., 2008; Wang et al., 2008). Based on the above results, we believe that this might be related to HTR's rich and diverse active substances, however, the specific mechanism needs further research.

There is little information on the effects of the fermented HTRs on fecal SCFA concentrations in heifers. In this study, the fermented HTR had a positive effect on the fecal SCFA concentrations of Aa, Pa, Ia, Ba, Iva, and Va. Therefore, we hypothesized that the fermented HTR might improve SCFA metabolism of ruminants under HS conditions via an as-yet-unidentified mechanism. We also investigated the association between fecal microbial composition and the heifers' characteristics, including energy utilization rate, fecal SCFA concentrations, serum biochemical indexes, and growth performances under HS conditions. We believe that this is the first study to evaluate the difference in the fecal microbiota between heifers with different performances and to explore the correlation of fecal microbiota with the characteristics of Holstein heifers under HS conditions. The Chao1 index indicated that this sequencing depth was sufficient for further analysis. Clustering analysis revealed that the *Firmicutes* and *Bacteroidetes* were the most dominant phyla among the total sequences, which was consistent with studies conducted by Wang et al. (2018). Additionally, in this study, the composition and structure of the fecal microbial community was affected by fermented HTRs. At the genus level, the abundance of *Turicibacter* and *Butyrivibrio* increased and decreased, respectively, in the feces of Holstein heifers fed fermented HTRs. Interestingly, we found that the bacterial abundance of *Turicibacter* was slightly and positively related to the DE/GE and ME/GE ratios. In addition, the relative abundance of *Turicibacter* correlated positively with the fecal concentrations of Aa, Pa, Ba, and Va and the serum concentrations of IgA, IgG, and GSH-PX; and correlated negatively with the serum concentrations of Cor and CK. In contrast, the relative abundance of *Butyrivibrio* correlated negatively with the fecal concentrations of Aa, Pa, Ia, Iva, and Va and the serum concentrations of IgA and IgG; and correlated positively with the concentration of HSP70, LDH, ALT, and CK. A previous study reported that *Turicibacter* deficiency alters the colonic microbiota and results in damage to the normal function of the colonic epithelium (Zenewicz et al., 2013). Moreover, it also associated positively with immunoregulation (Presley et al., 2010). However, *Butyrivibrio* is more involved in epithelial

proliferation and diseases (Mao et al., 2015). At the species level, we discovered that *Ruminococcus* sp. *Marseille*, *Clostridium* sp. *MC 40*, and *Lysinibacillus massiliensis* in the LC group were upregulated, and *Acholeplasmatales bacterium* in the LC or HC groups was downregulated compared with those in the CN group. The abundance of *Ruminococcus* sp. *Marseille* correlated positively with the fecal concentration of Aa, Ia, Ba, and Va; the serum concentrations of IgA and IgG; SOD; and the BOL value, and correlated negatively with the serum concentrations of HSP70, Cor, LDH, and ALT. Park et al. (2017) reported that members of the genus *Ruminococcus* protected neurons from oxidative damage by increasing SOD and GSH levels. The abundance of *Lysinibacillus massiliensis* and *Clostridium* sp. *MC 40* correlated positively with the fecal concentrations of Aa, Pa, Ba, and Va; the serum concentrations of IgA, IgG, and SOD; and the BOL value; and correlated negatively with the serum concentrations of HSP70, Cor, LDH, and ALT. The bacterial abundance of *Acholeplasmatales bacterium* correlated negatively with the fecal concentrations of Aa, Ba, Iva and Va; and the serum concentrations of IgA and IgG; and correlated positively with the serum concentrations of HSP70, Cor, LDH, and ALT. Recent studies have revealed that members of the species *Lysinibacillus* have potential antimicrobial properties against foodborne bacterial and fungal pathogens (Ahmad et al., 2014; Seelam et al., 2018). Zeng et al. (2011) reported that a decrease in *Clostridium* resulted in enterotoxemic diseases and other colonic epithelium diseases. However, *Acholeplasmatales bacterium* was established as pathogenic by Nicolet (1996). In addition, a study reported that the relative abundance of *Acholeplasmatales* also correlated with intestinal inflammation (Dicksveld et al., 2015). Therefore, a hypothesis was proposed that fermented HTRs might improve growth traits and energy utilization efficiency, increased antioxidant capacity, enhance immunity, and relieve HS by altering the microbial communities. However, more in-depth and detailed research is needed to confirm this hypothesis.

CONCLUSION

The results of the present study indicated that fermented HTRs promoted physiological traits, increased growth performance, improved energy utilization efficiency, enhanced immunity, strengthened antioxidant function, and mitigated heat stress in Holstein heifers. Additionally, we also detailed the fecal microbial community composition of Holstein heifers in response to HTRs. The bacteria are closely related to characteristics including the energy utilization rate, growth performance, serum biochemical indexes, and fecal SCFA levels of the heifers. Based on our findings, the 5% fermented HTRs replaced corn silage might be advantageous for the heifers' characteristics. This might be related to the inclusion of a variety of biologically active substances; however, the specific mechanism requires further research.

DATA AVAILABILITY STATEMENT

All datasets generated for this study are included in the article/**Supplementary Material**.

ETHICS STATEMENT

The animal study was reviewed and approved by South China Agricultural University.

AUTHOR CONTRIBUTIONS

YX and JS led the lab assays, analyses of data, and writing of the manuscript. JS and YZ contributed reagents, materials, and analysis tools. All authors gave final approval for publication and were involved in project conception and design.

FUNDING

This work was supported by grants from the National Key Research and Development Program of China (2016YFD0500503 and 2018YFD0501706), the Natural Science Foundation of China Program (31802032), the Natural Science Foundation of Guangdong Province (2020A1515010062), the Technical System of Modern Agricultural Industry in Guangdong Province (2018LM1121 and 2018LM2158), the major scientific projects in general Colleges and Universities of Guangdong Province (2017KTSCX023), and Guangdong Provincial Promotion Project on Preservation and Utilization of Local Breed of Livestock and Poultry.

SUPPLEMENTARY MATERIAL

The Supplementary Material for this article can be found online at: <https://www.frontiersin.org/articles/10.3389/fmicb.2020.01014/full#supplementary-material>

FIGURE S1 | Changes in the temperature humidity index (THI) at different times of day in the cowshed during the experimental period.

FIGURE S2 | Rarefaction curves. Number of sequences (A) and number of sample (B) rarefaction curves for the sampled fecal microbiotas. Number of detected OTUs on the y-axis; number of sequences (A) and of samples (B) on the x-axis.

FIGURE S3 | Ternary plot showing an abundance comparison of the fecal microbiota among the three groups at genus-taxa and species-taxa levels.

FIGURE S4 | Correlation analyses of genus-taxa with the energy utilization rate, fecal SCFA concentrations, serum biochemical indexes, and growth performance.

REFERENCES

- Abd, A. E. A., Choi, J. H., Rahman, M. M., Kim, S. W., Tosun, A., and Shim, J. H. (2014). Residues and contaminants in tea and tea infusions: a review. Food additives & contaminants. Part A Chem. Anal. Control Expos. Risk Assess. 31, 1794–1804. doi: 10.1080/19440049.2014.958575
- Ahmad, V., Iqbal, A. M. Z., Haseeb, M., and Khan, M. S. (2014). Antimicrobial potential of bacteriocin producing *Lysinibacillus* jx416856 against foodborne bacterial and fungal pathogens, isolated from fruits and vegetable waste. *Anaerobe* 27, 87–95. doi: 10.1016/j.anaerobe.2014.04.001
- Ahsan, M. A., Katla, S. K., Islam, M. T., Hernandez-Viezas, J. A., Martinez, L. M., Diaz-Moreno, C. A., et al. (2018). Adsorptive removal of methylene blue, tetracycline and Cr (VI) from water using sulfonated tea waste. *Environ. Technol. Innovat.* 11, 23–40. doi: 10.1016/j.eti.2018.04.003
- Barker, S. B., and Summerson, W. H. (1941). The colorimetric determination of lactic acid in biological material. *J. Biol. Chem.* 138, 535–554.
- Chatterton, N. J., Watts, K. A., Jensen, K. B., Harrison, P. A., and Horton, W. H. (2006). Nonstructural carbohydrates in oat forage. *J. Nutrit.* 136:2111S. doi: 10.1093/jn/136.7.2111S
- Chemists, A. A., and Horwitz, W. (1990). *Official Methods Of Analysis*, 15th Edn, Arlington, VA: AOAC.
- Dicksved, J., Jansson, J. K., and Lindberg, J. E. (2015). Fecal microbiome of growing pigs fed a cereal based diet including chicory (*Cichorium intybus* L.) or ribwort (*Plantago lanceolata* L.) forage. *J. Anim. Sci. Biotechnol.* 6:53. doi: 10.1186/s40104-015-0054-8

Each cell contains the corresponding correlation and *P*-value. The table is color-coded by correlation according to the color legend. DE/GE, the ratio of digestible energy to gross energy; ME/GE, the ratio of metabolizable energy to gross energy; Aa, acetic acid; Pa, propionic acid; Ia, isobutyric acid; Ba, butyric acid; Iva, isovaleric acid; Va, valeric acid. HSP70, heat shock protein 70, COR: cortisol; LDH, lactate dehydrogenase; IgA, immunoglobulin G; IgG, immunoglobulin G; ALT, alanine aminotransferase; CK, creatine kinase; T-AOC, total antioxidant capacity; MDA, malondialdehyde; SOD, superoxide dismutase; GSH-PX, glutathione peroxidase; BL, body length; BOL, body oblique length; BH, body height; RL, rump length; HW, hip width.

TABLE S1 | Nutritional composition of HTRs; pH and nutrient composition of HTRs before and after fermentation; ingredients of the concentrate formula; ingredients and nutrient compositions of the total mixed rations in the three treatments.

TABLE S2A | Quality control and preprocessing of metagenomic datasets.

TABLE S2B | Sequence composition of each sample at each level in the Greengenes database.

TABLE S2C | Aligned counts at each level between different samples.

TABLE S3A | The aligned counts that were annotated at the phylum level.

TABLE S3B | The aligned percentages that were annotated at the phylum level.

TABLE S3C | The aligned counts that were annotated at the class level.

TABLE S3D | The aligned percentages that were annotated at the class level.

TABLE S3E | The aligned counts that were annotated at the order level.

TABLE S3F | The aligned percentages that were annotated at the order level.

TABLE S3G | The aligned counts that were annotated at the family level.

TABLE S3H | The aligned percentages that were annotated at the family level.

TABLE S3I | The aligned counts that were annotated at the genus level.

TABLE S3J | The aligned percentages that were annotated at the genus level.

TABLE S3K | The aligned counts that were annotated at the species level.

TABLE S3L | The aligned percentages that were annotated at the species level.

TABLE S4A | Significant differences between the CN and LC groups identified at the genus-taxa level.

TABLE S4B | Significant differences between the CN and HC groups identified at the genus-taxa level.

TABLE S5A | Significant differences between the CN and LC groups identified at the species-taxa level.

TABLE S5B | Significant differences between the CN and HC groups identified at the species-taxa level.

- Edgar, R. C. (2004). MUSCLE: multiple sequence alignment with high accuracy and high throughput. *Nucleic Acids Res.* 32, 1792–1797. doi: 10.1093/nar/gkh340
- Edgar, R. C. (2013). UPARSE: highly accurate OTU sequences from microbial amplicon reads. *Nat. Methods* 10:996. doi: 10.1038/nmeth.2604
- Edgar, R. C., Haas, B. J., Clemente, J. C., Quince, C., and Knight, R. (2011). UCHIME improves sensitivity and speed of chimera detection. *Bioinformatics* 27, 2194–2200. doi: 10.1093/bioinformatics/btr381
- Fang, J., Cao, Y., Matsuzaki, M., and Suzuki, H. (2016). Effects of apple pomace proportion levels on the fermentation quality of total mixed ration silage and its digestibility, preference and ruminal fermentation in beef cows. *Anim. Sci. J.* 87, 217–223. doi: 10.1111/asj.12410
- Gurung, M., Adhikari, B. B., Alam, S., Kawakita, H., Ohto, K., Inoue, K., et al. (2013). Adsorptive removal of Cs (I) from aqueous solution using polyphenols enriched biomass-based adsorbents. *Chem. Eng. J.* 231, 113–120. doi: 10.1016/j.cej.2013.06.028
- Haas, B. J., Gevers, D., Earl, A. M., Feldgarden, M., Ward, D. V., Giannoukos, G., et al. (2011). Chimeric 16S rRNA sequence formation and detection in Sanger and 454-pyrosequenced PCR amplicons. *Genome Res.* 21, 494–504. doi: 10.1101/gr.112730.110
- Horwitz, W. (2010). “Official methods of analysis of AOAC international,” in *Agricultural Chemicals Contaminants Drugs*, ed. W. Horwitz (Gaithersburg: AOAC International).
- Iqbal Khan, M. A., Ueno, K., Horimoto, S., Komai, F., Tanaka, K., and Ono, Y. (2007). Evaluation of the physio-chemical and microbial properties of green tea waste-rice bran compost and the effect of the compost on spinach production. *Plant Product. Sci.* 10, 391–399. doi: 10.1626/pp.s.10.391
- Kim, D. G., Lee, M. R., Yoo, J. M., Park, K. I., and Ma, J. Y. (2017). Fermented herbal formula KIOM-MA-128 protects against acute colitis induced by dextran sodium sulfate in mice. *BMC Complement. Alternat. Med.* 17:354. doi: 10.1186/s12906-017-1855-4
- Kovács, L., Kézér, F. L., Ruff, F., Jurkovich, V., and Szenci, O. (2018). Heart rate, cardiac vagal tone, respiratory rate, and rectal temperature in dairy calves exposed to heat stress in a continental region. *Intern. J. Biometeorol.* 62, 1791–1797. doi: 10.1007/s00484-018-1581-8
- Kumar, S., Bass, B. E., Bandrick, M., Loving, C. L., Brockmeier, S. L., Looft, T., et al. (2017). Fermentation products as feed additives mitigate some ill-effects of heat stress in pigs. *J. Anim. Sci.* 95, 279–290. doi: 10.2527/jas.2016.0662
- Li, D. L., Zheng, X. L., Duan, L., Deng, S. W., Ye, W., Wang, A. H., et al. (2017). Ethnobotanical survey of herbal tea plants from the traditional markets in Chaoshan, China. *J. Ethnopharmacol.* 205, 195–206. doi: 10.1016/j.jep.2017.02.040
- Liu, H. W., Tong, J. M., and Zhou, D. W. (2011). Utilization of Chinese herbal feed additives in animal production. *Agric. Sci. China* 10, 1262–1272. doi: 10.1016/S1671-2927(11)60118-1
- Mao, S., Zhang, M., Liu, J., and Zhu, W. (2015). Characterising the bacterial microbiota across the gastrointestinal tracts of dairy cattle: membership and potential function. *Sci. Rep.* 5:16116. doi: 10.1038/srep16116
- Martin, M. (2011). Cutadapt removes adapter sequences from high-throughput sequencing reads. *EMBnet J.* 17, 10–12. doi: 10.14806/embnet.17.1.200
- Naderi, N., Ghorbani, G. R., Sadeghi-Sefidmazgi, A., Nasrollahi, S. M., and Beauchemin, K. A. (2016). Shredded beet pulp substituted for corn silage in diets fed to dairy cows under ambient heat stress: Feed intake, total-tract digestibility, plasma metabolites, and milk production. *J. Dairy Sci.* 99, 8847–8857. doi: 10.3168/jds.2016-11029
- Niba, A. T., Beal, J. D., Kudi, A. C., and Brooks, P. H. (2009). Potential of bacterial fermentation as a biosafe method of improving feeds for pigs and poultry. *Afr. J. Biotechnol.* 8, 1758–1767. doi: 10.4314/ajb.v8i9.60378
- Nicolet, J. (1996). Animal mycoplasmoses: a general introduction. *Revue Sci. Techn. Off. Intern. Epizoot.* 15, 1233–1240. doi: 10.20506/rst.15.4.982
- Ozkaya, S., and Bozkurt, Y. (2008). The relationship of parameters of body measures and body weight by using digital image analysis in pre-slaughter cattle. *Archiv. Anim. Breed.* 51, 120–128. doi: 10.5194/aab-51-120-2008
- Pardau, M. D., Pereira, A. S., Apostolides, Z., Serem, J. C., and Bester, M. J. (2017). Antioxidant and anti-inflammatory properties of Ilex guayusa tea preparations: a comparison to *Camellia sinensis* teas. *Food Funct.* 8, 4601–4610. doi: 10.1039/C7FO01067B
- Park, J., Lee, J., Yeom, Z., Heo, D., and Lim, Y. H. (2017). Neuroprotective effect of *Ruminococcus albus* on oxidatively stressed SH-SY5Y cells and animals. *Sci. Rep.* 7:14520. doi: 10.1038/s41598-017-15163-5
- Presley, L. L., Wei, B., Braun, J., and Borneman, J. (2010). Bacteria associated with immunoregulatory cells in mice. *Appl. Environ. Microbiol.* 76, 936–941. doi: 10.1128/AEM.01561-09
- Quast, C., Pruesse, E., Yilmaz, P., Gerken, J., Schweer, T., Yarza, P., et al. (2012). The SILVA ribosomal RNA gene database project: improved data processing and web-based tools. *Nucleic Acids Res.* 41, D590–D596. doi: 10.1093/nar/gks1219
- Rhoads, M. L., Rhoads, R. P., VanBaale, M. J., Collier, R. J., Sanders, S. R., Weber, W. J., et al. (2009). Effects of heat stress and plane of nutrition on lactating holstein cows: i. production metabolism and aspects of circulating somatotropin. *J. Dairy Sci.* 92, 1986–1997. doi: 10.3168/jds.2008-1641
- Seelam, N. S., Katike, U., Kotha, P., Akula, H., and Obulam, V. S. R. (2018). Hypolipidemic effects of *Lysinibacillus sphaericus* fermented tomato and carrot juices in high-fat diet-fed albino Wistar rats. *J. Appl. Biol. Biotechnol.* 6, 64–70. doi: 10.7324/JABB.2018.60611
- Shan, C. H., Guo, J., Sun, X., Li, N., Yang, X., Gao, Y., et al. (2018). Effects of fermented Chinese herbal medicines on milk performance and immune function in late-lactation cows under heat stress conditions. *J. Anim. Sci.* 96, 4444–4457. doi: 10.1093/jas/sky270
- Shen, B., Tian, L., Li, F., Zhang, X., Xu, H., and Singh, S. (2017). Elemental mercury removal by the modified bio-char from waste tea. *Fuel* 187, 189–196. doi: 10.1016/j.fuel.2016.09.059
- Song, X., Luo, J., Fu, D., Zhao, X., Bunlue, K., Xu, Z., et al. (2014). Traditional Chinese medicine prescriptions enhance growth performance of heat stressed beef cattle by relieving heat stress responses and increasing apparent nutrient digestibility. *Asian Austr. J. Anim. Sci.* 27:1513. doi: 10.5713/ajas.2014.14058
- Srikandakumar, A., and Johnson, E. H. (2004). Effect of heat stress on milk production, rectal temperature, respiratory rate and blood chemistry in Holstein, Jersey and Australian Milking Zebu cows. *Trop. Anim. Health Product.* 36, 685–692. doi: 10.1023/B:TROP.0000042868.76914.a9
- Su, J., Zhu, Q., Zhao, Y., Han, L., Yin, Y., Blachier, F., et al. (2018). Dietary supplementation with chinese herbal residues or their fermented products modifies the colonic microbiota, bacterial metabolites, and expression of genes related to colon barrier function in weaned piglets. *Front. Microbiol.* 9:3181. doi: 10.3389/fmicb.2018.03181
- Sun, J., Zeng, B., Chen, Z., Yan, S., Huang, W., Sun, B., et al. (2017). Characterization of faecal microbial communities of dairy cows fed diets containing ensiled *Moringa oleifera* fodder. *Sci. Rep.* 7:41403. doi: 10.1038/srep41403
- Tuzcu, M., Sahin, N., Karatepe, M., Cikim, G., Kilinc, U., and Sahin, K. (2008). Epigallocatechin-3-gallate supplementation can improve antioxidant status in stressed quail. *Br. Poult. Sci.* 49, 643–648. doi: 10.1080/00071660802298336
- Van Keulen, J., and Young, B. A. (1977). Evaluation of acid-insoluble ash as a natural marker in ruminant digestibility studies. *J. Anim. Sci.* 44, 282–287. doi: 10.2527/jas1977.442282x
- Van Soest, P. V., Robertson, J. B., and Lewis, B. A. (1991). Methods for dietary fiber, neutral detergent fiber, and nonstarch polysaccharides in relation to animal nutrition. *J. Dairy Sci.* 74, 3583–3597. doi: 10.3168/jds.S0022-0302(91)78551-2
- Wang, H., Ji, Y., Yin, C., Deng, M., Tang, T., Deng, B., et al. (2018). Differential analysis of gut microbiota correlated with oxidative stress in sows with high or low litter performance during lactation. *Front. Microbiol.* 9:1665. doi: 10.3389/fmicb.2018.01665
- Wang, H. F., Yang, W. R., Wang, Y. X., Yang, Z. B., and Cui, Y. H. (2011). The study on the effects of Chinese herbal mixtures on growth, activity of post-ruminal digestive enzymes and serum antioxidant status of beef cattle. *Agric. Sci. China* 10, 448–455. doi: 10.1016/S1671-2927(11)60024-2
- Wang, L., Piao, X. L., Kim, S. W., Piao, X. S., Shen, Y. B., and Lee, H. S. (2008). Effects of *Forsythia suspensa* extract on growth performance, nutrient digestibility, and antioxidant activities in broiler chickens under high ambient temperature. *Poult. Sci.* 87, 1287–1294. doi: 10.3382/ps.2008-00023
- White, J. R., Nagarajan, N., and Pop, M. (2009). Statistical methods for detecting differentially abundant features in clinical metagenomic samples. *PLoS Comput. Biol.* 5:e1000352. doi: 10.1371/journal.pcbi.1000352
- Yan, F., Xue, B., Song, L., Dalecuo, J., Xiao, J., Ding, S., et al. (2016). Effect of dietary net energy concentration on dry matter intake and energy partition

- in cows in mid-lactation under heat stress. *Anim. Sci. J.* 87, 1352–1362. doi: 10.1111/asj.12561
- Yang, X., and Cui, X. (2013). Adsorption characteristics of Pb (II) on alkali treated tea residue. *Water Resour. Indust.* 3, 1–10. doi: 10.1016/j.wri.2013.05.003
- Zenewicz, L. A., Yin, X., Wang, G., Elinav, E., Hao, L., Zhao, L., et al. (2013). IL-22 deficiency alters colonic microbiota to be transmissible and colitogenic. *J. Immunol.* 190, 5306–5312. doi: 10.4049/jimmunol.130.0016
- Zeng, B., Sun, J. J., Chen, T., Sun, B. L., He, Q., Chen, X. Y., et al. (2018). Effects of *Moringa oleifera* silage on milk yield, nutrient digestibility and serum biochemical indexes of lactating dairy cows. *J. Anim. Physiol. Anim. Nutr.* 102, 75–81. doi: 10.1111/jpn.12660
- Zeng, J., Deng, G., Wang, J., Zhou, J., Liu, X., Xie, Q., et al. (2011). Potential protective immunogenicity of recombinant *Clostridium perfringens* α - β 2- β 1 fusion toxin in mice, sows and cows. *Vaccine* 29, 5459–5466. doi: 10.1016/j.vaccine.2011.05.059
- Zhong, R. Z., Tan, C. Y., Han, X. F., Tang, S. X., Tan, Z. L., and Zeng, B. (2009). Effect of dietary tea catechins supplementation in goats on the quality of meat kept under refrigeration. *Small Rumin. Res.* 87, 122–125. doi: 10.1016/j.smallrumres.2009.10.012
- Zou, C. X., Lively, F. O., Wylie, A. R. G., and Yan, T. (2016). Estimation of the maintenance energy requirements, methane emissions and nitrogen utilization efficiency of two suckler cow genotypes. *Animal* 10, 616–622. doi: 10.1017/S1751731115002268

Conflict of Interest: The authors declare that the research was conducted in the absence of any commercial or financial relationships that could be construed as a potential conflict of interest.

Copyright © 2020 Xie, Chen, Wang, Chen, Sun, He, Luo, Chen, Xi, Zhang and Sun. This is an open-access article distributed under the terms of the Creative Commons Attribution License (CC BY). The use, distribution or reproduction in other forums is permitted, provided the original author(s) and the copyright owner(s) are credited and that the original publication in this journal is cited, in accordance with accepted academic practice. No use, distribution or reproduction is permitted which does not comply with these terms.

RESEARCH

Open Access



Fermentation quality of herbal tea residue and its application in fattening cattle under heat stress

Xiaona Zhuang[†], Zujing Chen[†], Xiaohong Sun[†], Fangjun Li, Junyi Luo, Ting Chen, Qianyun Xi, Yongliang Zhang^{*} and Jiajie Sun^{*}

Abstract

Background: Herbal tea residue (HTR) is generally considered to be the waste of herbal tea beverage production while it still retains rich nutrients and active substances. The main aim of the present study was to investigate the effect of fermentation technology on improving the quality of HTRs, and focus on the fermented HTR-induced alleviation of summer heat stress in fattening cattle.

Results: In this study, the waste HTR was fermented and then fed to a total of 45 fattening cattle that were divided into 3 groups (fermented HTR replaced 0, 15, 30% of the forage component of the diet), and the feeding experiment was lasted for 40 days. The physiological indexes, growth performance and fecal microbiota of fattening cattle were evaluated and results showed that fermented HTR could effectively reduce the respiratory rate and rectal temperature of fattening cattle under heat stress, increase the daily feed intake and daily gain, and improve the antioxidant content and blood immune index. In addition, we studied the fecal microbiota composition of 6 fattening cattle in control and 30% HTR substitution groups and found fermented HTR significantly changed the composition of fecal microbiota and increased microbial diversity, and correlation analysis suggested that the bacteria were closely related to fecal SCFA levels of fattening cattle under heat stress.

Conclusions: In this study, fermented HTR replaced 30% of the forage component of the diet that can change the intestine microorganisms, maintain health and alleviate the heat stress of fattening cattle.

Keywords: Herbal tea residue, Microorganism, Fattening cattle, Fermented feed, Heat stress

Background

Herbal medicine has a long history of being used to prevent and treat diseases in China [1]. Studies have shown that drinking herbal tea can help to relieve heat in the body and the symptoms of sore throat caused by summer

heat stress [2]. Herbal tea drinks are consumed widely because of their natural ingredients, convenient drinking, and unique health benefits [3–5]. In some areas, such as Guangdong, China, drinking herbal tea has even become part of the culture [6]. More and more people are consuming herbal tea drinks, requiring large scale tea production and resulting in large amounts of HTR [7]. In the past, most of tea residues were regarded as waste and were burned or dumped into landfill [8], which was not only environmentally damaging, but also a represented a waste of resources. Fortunately, researchers are now paying attention to the resource utilization of tea residues.

*Correspondence: jiajiesun@scau.edu.cn; jiajiesun@scau.edu.cn

[†]Xiaona Zhuang, Zujing Chen and Xiaohong Sun contributed equally to this work.

Guangdong Provincial Key Laboratory of Animal Nutrition Control, Guangdong Engineering & Research Center for Woody Fodder Plants, National Engineering Research Center for Breeding Swine Industry, Guangdong Laboratory for Lingnan Modern Agriculture, South China Agricultural University, Guangzhou 510642, Guangdong, China



© The Author(s) 2021. **Open Access** This article is licensed under a Creative Commons Attribution 4.0 International License, which permits use, sharing, adaptation, distribution and reproduction in any medium or format, as long as you give appropriate credit to the original author(s) and the source, provide a link to the Creative Commons licence, and indicate if changes were made. The images or other third party material in this article are included in the article's Creative Commons licence, unless indicated otherwise in a credit line to the material. If material is not included in the article's Creative Commons licence and your intended use is not permitted by statutory regulation or exceeds the permitted use, you will need to obtain permission directly from the copyright holder. To view a copy of this licence, visit <http://creativecommons.org/licenses/by/4.0/>. The Creative Commons Public Domain Dedication waiver (<http://creativecommons.org/publicdomain/zero/1.0/>) applies to the data made available in this article, unless otherwise stated in a credit line to the data.

Researchers have found that tea residues can significantly improve the soil fertility, leading to their use as organic fertilizers [9]. In addition, tea residues have been developed as a non-conventional water adsorbent to remove water pollutants like methylene blue [10], antibiotics [11], and heavy metals, such as chromium [12], cadmium [13], copper [14], lead, zinc [15], and arsenic [16] from aqueous solutions.

Alternatively, tea residues can be used as an unconventional feed resource in animal production. Generally, during tea production, not all of the effective substances are completely dissolved, thus some tea residues still retain a good proportion of the nutrients and bioactive compounds [17]. Like tea residues, it is reported that HTR contains many residual bioactive substances, such as phenols, polysaccharides, organic acids, alkaloids, and essential oils, which have been proven to have anti-oxidant and anti-bacterial effects [18]. Moreover, tea residues also contain protein, carbohydrate, fat, fiber, vitamins, and minerals [18]. Previous studies have used tea residues as substitutes for antibiotics to help improve the gut microbial composition of grower pigs [19]. In addition, tea residues improved the abdominal fat accumulation of broiler chickens, and had a positive impact on egg yolk quality [20]. Besides, researchers demonstrated the potential of tea residues for feeding ruminants [17]. In another study, a fermented herbal residue was fed to Holstein heifers, which effectively promoted the growth and immune performance of cows under heat stress [21].

In our paper, the tested HTRs included *Plumeria rubra* flowers, Honeysuckle flowers, Chrysanthemum flowers, *Mesona chinensis* leaves, *Prunella vulgaris* leaves, *Microcos paniculata* leaves and *Liquiritia glycyrrhiza* roots. The potential feeding value of the HTRs prompted us to develop a suitable technology for animal production. Currently, to apply HTRs, problems of storage, unbalanced nutrition, and poor palatability need to

be solved. Therefore, the main aim of the present study was to investigate the effect of fermentation technology on improving the quality of HTRs, and focus on the fermented HTR-induced alleviation of summer heat stress in fattening cattle.

Results

Nutritional components and changes to the HTR after fermentation

As shown in Table S1, the HTR contained a high water content (75.10%) and the dry matter content was 24.90%. As a proportion of the dry matter content, the crude protein, crude fat, and ash contents were 13.10, 2.60, 6.69%, respectively. In addition, HTR also contained minerals, and the contents of potassium, calcium, magnesium, phosphorus, sulfur, and chlorine were 0.61, 1.14, 0.40, 0.25, 0.21, and 0.51%, respectively. The acid detergent fiber (ADF) and neutral detergent fiber (NDF) were 39.8 and 54.3%; contents of lactate acid, acetic acid, and butyric acid were 4.67, 1.58, and 0.35%, respectively; and the water soluble carbohydrate (WSC) was 3.10%. The net energy for maintenance and net energy gain of HTR were 0.79 and 0.25 Mcal/kg DM, respectively.

As shown in Table 1, the pH value of the mixture of the HTR, oat hay, and bacteria decreased from 4.95 to 3.89 after fermentation. On the basis of dry matter, the crude protein in the HTR increased by 1.07% compared with that of the unfermented HTR. The contents of NDF and ADF decreased by 5.82 and 4.32% respectively. On the basis of dry matter, the contents of lactate, acetic acid, and propionic acid increased to 6.93, 0.62 and 112.33 g/kg DM, respectively. Basal diet composition and nutritional level of bovine feeding were shown in Table S2. Compared with CN group, LC group and HC group had more abundant crude protein (11.25, 11.32 and 11.35%, respectively). In addition, compared with CN group, LC group and HC group also had more abundant crude fat

Table 1 Nutrient composition of fermented herbal tea residue for 0 and 30 days

Item	Fermentation for 0 days	Fermentation for 30 days
PH	4.95 ± 0.03	3.89 ± 0.04
Dry matter (%)	26.58 ± 0.74	24.94 ± 0.51
Crude protein (%)	8.85 ± 0.98	9.92 ± 0.82
Ash (%)	6.17 ± 0.04	6.56 ± 0.06
Neutral detergent fiber (%)	60.11 ± 1.30	54.29 ± 0.86
Acid detergent fiber (%)	34.33 ± 0.28	30.01 ± 0.36
Acetic acid (g/kg)	1.04 ± 0.01	6.93 ± 0.06
Propionic acid (g/kg)	0.02 ± 0.004	0.62 ± 0.009
Lactic acid (g/kg)	15.74 ± 0.002	112.33 ± 0.004
NEmf (MJ/kg)	5.68 ± 0.09	5.76 ± 0.11

The values were calculated as the means ± standard error of the mean (N = 6), except for dry matter, others item are based on dry matter

(3.15, 3.2 and 3.22%, respectively), calcium (0.43, 0.65 and 0.79%, respectively) and phosphorus (0.45, 0.53 and 0.48%, respectively).

Temperature and humidity index in the cowshed

The daily changes in ambient temperature and THI among the three time points is shown in Fig. S1. In general, the THI classification of heat stress is as follows: No heat stress when $\text{THI} \leq 72$; mild heat stress when $72 < \text{THI} \leq 79$; high heat stress when $79 < \text{THI} \leq 84$; and severe heat stress when $\text{THI} > 84$ [22]. During the experiment, the mean THI of the barn was 81 (range 79–84), 86 (more than 84), and 79 (range 72–79) in the morning (08:00), afternoon (15:00), and evening (22:00), respectively. The total average THI was 82, which was between $79 < \text{THI} < 84$. Therefore, we concluded that fattening cattle were in a high heat stress state during the whole period of the formal experiment.

Effects of fermented HTR on RR and RT of fattening cattle under heat stress

The daily average RR of CN group was 87.04 breaths/min, and RT was 38.84°C; RR and RT of LC group were 83.39 breaths/min and 38.75°C, respectively; and of the HC group they were 80.23 breaths/min and 38.63°C (Table 2). At three measurement times, the RR and RT of LC had no significant differences with CN group, while HC group showed significantly reduced RR at 15:00 and 22:00 ($P < 0.05$) and a reduced RT at 8:00 and 15:00 ($P < 0.05$) compared with those of the CN group. At 15:00, the RT of the HC group was significantly lower than that of the LC group ($P < 0.05$). Therefore, 30% fermented HTR replacement could effectively alleviate the RR and RT of fattening cattle under heat stress.

Table 2 Effects of fermented herbal tea residue feed on respiratory rate and rectal temperature of fattening cattle

Items	Time	CN	LC	HC
Respiratory rates (breaths/min)	8:00	87.12 ± 1.25	86.67 ± 1.12	85.00 ± 1.48
	15:00	87.50 ± 2.80 ^a	83.00 ± 2.80 ^{ab}	78.50 ± 1.00 ^b
	22:00	86.50 ± 3.20 ^a	80.50 ± 3.43 ^{ab}	77.20 ± 1.74 ^b
Rectal temperature (°C)	8:00	38.85 ± 0.04 ^a	38.75 ± 0.04 ^{ab}	38.61 ± 0.05 ^b
	15:00	38.88 ± 0.06 ^a	38.78 ± 0.05 ^{ab}	38.60 ± 0.08 ^c
	22:00	38.80 ± 0.05	38.73 ± 0.07	38.68 ± 0.07

The values were showed as the means ± standard error ($N = 15$); Different letters showed significant difference ($P < 0.05$), while the same letter or no letter showed no significant difference ($P > 0.05$)

HTR herbal tea residue, CN no herbal tea residues, the control group, LC 15% fermented HTRs replaced, the 15% replacement group, HC 30% fermented HTRs replaced, the 30% replacement group

Effects of fermented HTR on feed intake and weight gain

Compared with the CN group, the feed intake and daily gain of the LC and HC increased gradually, which correlated positively with the increase in fermented HTR replacement (Table 3). The feed intake and average daily gain of the HC group were significantly higher than those of the CN group ($P < 0.05$). The average daily gain between the CN and LC groups showed no significant differences ($P > 0.05$); however, the feed intake increased significantly in the LC group ($P < 0.05$). In addition, fermented HTR also reduced the F/G value of fattening cattle significantly ($P < 0.05$). Therefore, fermented HTR could improve the feed intake and increased the feed conversion rate of fattening cattle under heat stress, and the effect of 30% fermented HTR replacement was better than that of 15%.

Effects of fermented HTR on serum biochemical indexes

Compared with the fattening cattle fed with a basal diet, the levels of HSP70 and LDH in the LC and HC groups decreased with the increase in fermented HTR substitution ($P < 0.05$), while IL-2 level increased gradually ($P < 0.05$). Compared with that in the CN group, the level of Cor in HC group reduced significantly in serum under heat stress ($P < 0.05$), and the levels of IgG and SOD significantly increased ($P < 0.05$). Compared with that in the CN group, the LDH level in the LC group decreased significantly ($P < 0.05$), and T-AOC level increased significantly in the LC group ($P < 0.05$). IgA, IL-6, ALT, AST, MDA and T4 levels had no significant among three treatments; IgA, IL-6, ALT and AST showed an increased trend, while MDA and T4 showed a decreased trend with the increase of fermented HTR substitution (Table 4). The above results showed that fermented HTR could improve the anti-heat stress and antioxidant capacity of

Table 3 Effect of fermented herbal tea residue feed on feed intake and weight gain of fattening cattle

Items	CN	LC	HC
Initial weight (kg)	518.29 ± 27.24	521.43 ± 38.45	524 ± 34.21
Final weight (kg)	542.94 ± 26.52	550.13 ± 37.35	558.33 ± 32.55
ADG (kg/day)	0.94 ± 0.05 ^b	1.09 ± 0.09 ^{ab}	1.26 ± 0.05 ^a
Feed intake (kg/day)	12.64 ± 0.21 ^c	13.41 ± 0.21 ^b	14.27 ± 0.18 ^a
Feed conversion ratio (F/G)	13.85 ± 1.07 ^a	12.61 ± 0.53 ^b	11.64 ± 0.40 ^c

The values were calculated as the means ± standard error ($N = 15$); Different letters showed significant difference ($P < 0.05$), while the same letter or no letter showed no significant difference ($P > 0.05$)

HTR herbal tea residue; CN no herbal tea residues, the control group, LC 15% fermented HTRs replaced, the 15% replacement group, HC 30% fermented HTRs replaced, the 30% replacement group

Table 4 Analysis of serum indices in beef cattle under heat stressed between three groups

Items	CN	LC	HC
HSP70 (ng/mL)	18.67 ± 1.17 ^a	17.78 ± 0.54 ^b	16.87 ± 1.60 ^c
Cor (ng/mL)	91.55 ± 1.83 ^a	80.96 ± 0.60 ^{ab}	72.63 ± 4.22 ^b
LDH (U/L)	696.00 ± 10.65 ^a	601.00 ± 8.97 ^b	583.00 ± 3.76 ^b
IgG (ng/mL)	7.96 ± 1.16 ^b	9.62 ± 0.44 ^{ab}	12.30 ± 1.18 ^a
IgA (ng/mL)	3.57 ± 0.24	4.29 ± 0.43	4.60 ± 0.66
IL-2 (pg/mL)	308.75 ± 2.40 ^c	332.81 ± 2.16 ^b	340.47 ± 0.43 ^a
IL-6 (pg/mL)	316.17 ± 15.25	327.69 ± 4.43	336.81 ± 4.80
ALT (U/L)	27.50 ± 2.02	29.50 ± 0.87	31.00 ± 3.21
AST (U/L)	78.00 ± 6.06	84.50 ± 9.49	90.25 ± 4.94
T-AOC (mmol/L)	0.27 ± 0.03 ^b	0.36 ± 0.01 ^a	0.33 ± 0.01 ^{ab}
MDA (mmol/L)	25.21 ± 1.67	24.93 ± 0.00	23.47 ± 0.85
SOD (U/mL)	48.73 ± 2.79 ^b	51.76 ± 0.58 ^{ab}	56.43 ± 0.20 ^a
T4 (ng/mL)	33.02 ± 1.06	33.47 ± 0.36	32.46 ± 0.70

The values were showed as the means ± standard error (N = 6); Different letters showed significant difference ($P < 0.05$), while the same letter or no letter showed no significant difference ($P > 0.05$)

Cor Cortisol, LDH Lactate dehydrogenase, IgA Immunoglobulin A, IgG Immunoglobulin G, IL-2 Interleukin-2, IL-6 Interleukin-6, ALT Alanine aminotransferase, AST Aspartate aminotransferase, T-AOC Total antioxidant capacity, MDA Malondialdehyde, SOD Superoxide dismutase, T4 Thyroxine, HTR Herbal tea residue, CN no herbal tea residues, the control group, LC 15% fermented HTRs replaced, the 15% replacement group, HC 30% fermented HTRs replaced, the 30% replacement group

fattening cattle, and the effect of 30% replacement was more obvious than that of 15% replacement.

Compared with that in the CN group, 30% fermented HTR could reduce blood glucose significantly, and 15 and 30% fermented HTR replacement could increase the content of total protein and albumin significantly. The content of blood urea nitrogen (BUN), total cholesterol (T-CHO) and triglyceride (TG) had no significant among three treatments; BUN and T-CHO showed a decreased trend with the increase of fermented HTR replacement, while TG showed an increased trend (Table 5).

16S rRNA gene sequencing and annotation analysis

To study the effect of fermented HTR on intestinal microorganisms, we studied the fecal microbiota composition of 6 fattening cattle in control and 30% HTR replacement groups. We extracted the genomic DNA of 12 fecal samples from CN group and HC groups, and amplified the corresponding 16S DNA V3-V4 fragment. After sequencing, the CN group produced an average of 89,720 raw reads and the HC group produced an average of 90,069 raw reads. After splicing, the CN group produced an average of 88,745 combined reads and the average combined percentage was 98.92%. The HC group produced an average of 88,679 combined reads and the average combined percentage was 98.47%. After filtering low quality and short length fragments, the number of tag

Table 5 Effect of fermented herbal tea residue on biochemical indicators of fattening cattle during summer heat stressed

Items	CN	LC	HC
Glu (mmol/L)	2.09 ± 0.008 ^a	2.06 ± 0.03 ^{ab}	1.99 ± 0.006 ^b
TP (g/L)	67.27 ± 2.15 ^b	74.87 ± 0.67 ^a	77.25 ± 1.01 ^a
ALB (g/L)	32.23 ± 0.65 ^b	33.67 ± 0.52 ^a	36.65 ± 1.88 ^a
BUN (mmol/L)	3.35 ± 0.31	3.04 ± 0.17610	2.69 ± 0.07
T-CHO (mmol/L)	2.72 ± 0.20	2.34 ± 0.28	2.46 ± 0.02
TG (mmol/L)	0.127 ± 0.03	0.14 ± 0.01	0.15 ± 0.009

The values were showed as the means ± standard error (N = 6); Different letters showed significant difference ($P < 0.05$), while the same letter or no letter showed no significant difference ($P > 0.05$)

Glu Glucose, ALB Albumin, TP Total protein, BUN blood urea nitrogen, T-CHO Total cholesterol, TG Triglyceride, HTR Herbal tea residue, CN no herbal tea residues, the control group, LC 15% fermented HTRs replaced, the 15% replacement group, HC 30% fermented HTRs replaced, the 30% replacement group

sequences for subsequent analysis were 58,016 no-chime reads in the CN group, with an average effective rate of 64.93%, and 58,636 no-chime reads in the HC group, with an average effective rate of 65.21% (Table S3A). The CN group data generated 1451 OTUs and the HC group generated 1446 OTUs on average (Table S3B). There were 669 core OTUs in the 12 samples (Fig. 1A); with 319 unique OTUs in the CN group and 297 OTUs in the HC group, while there were 1786 shared OTUs between the two groups (Fig. 1B; Table S3C).

The relative abundance of the top 10 fecal microbiota at the phylum level is shown Fig. 1 C and D. The most abundant bacteria at the phylum level were *Firmicutes* and *Bacteroidetes* within and between the CN and HC groups. The average percentage of *Firmicutes* in HC group was 59.54%, which was significantly higher than that in the CN group (52.94%) ($P < 0.01$). The average percentage of *Bacteroidetes* in the HC group was 31.87%, which was significantly lower than that in the CN group (37.87%) ($P < 0.01$). The annotated counts and percentages at the class, order, family, genus, and species levels are shown in Table S4 and S5.

Observed species, the Shannon index, the Simpson index, Chao1, ACE, Good's coverage, and PD whole tree reflected the richness and diversity of species in the samples. The species richness of the HC group was slightly higher than that of the CN group, but there was no significant difference ($P > 0.05$) (Table 6). The PCA between the groups is shown in Fig. 2A. We found that CN and HC groups samples were separated from each other, which reflected the influence of HTR substitution on microbial community changes. Similar results were obtained and showed in Fig. 2B. The UPGMA clustering tree was shown in Fig. 2C, which confirmed the significant structural separation of the fecal microflora

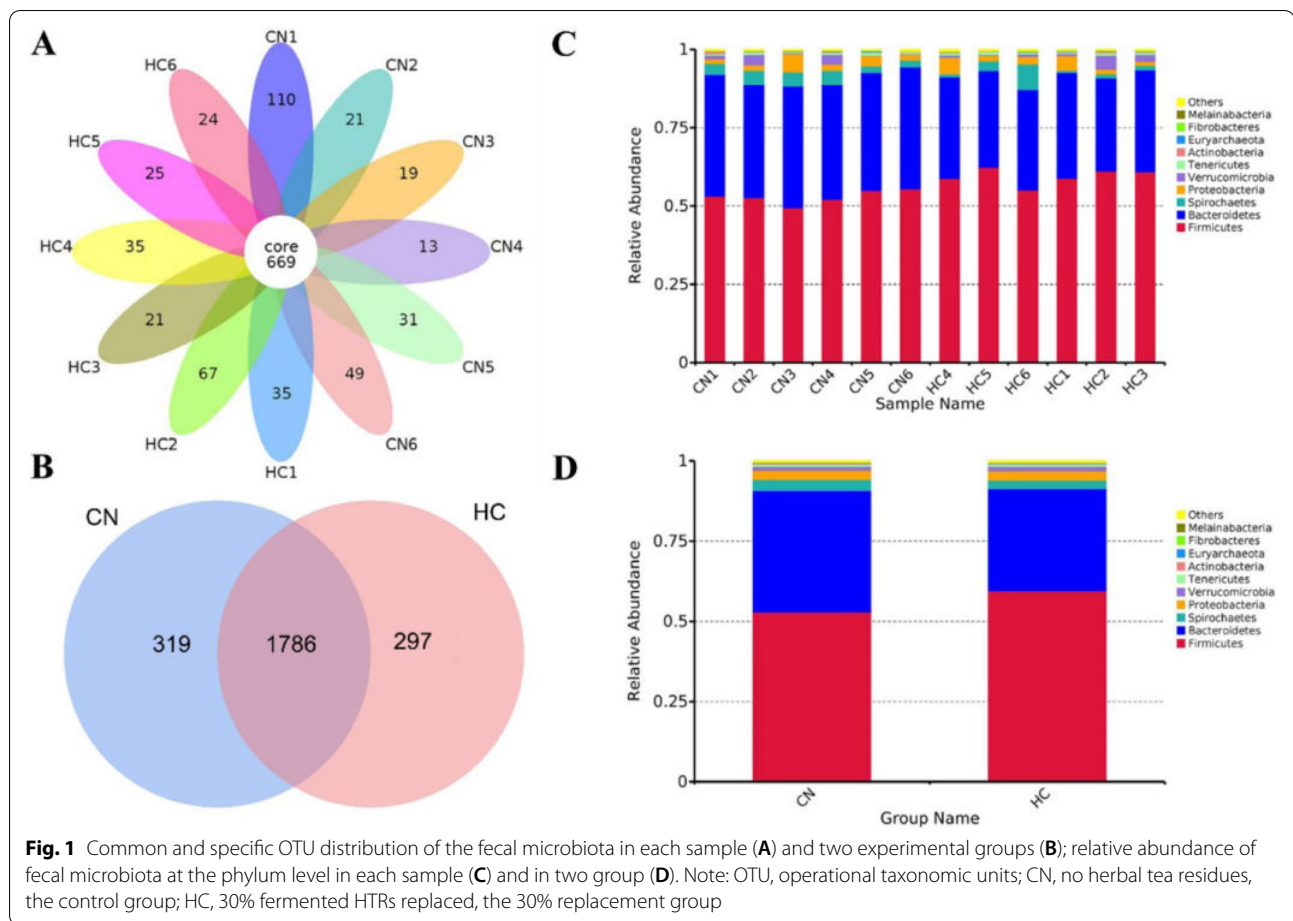


Fig. 1 Common and specific OTU distribution of the fecal microbiota in each sample (A) and two experimental groups (B); relative abundance of fecal microbiota at the phylum level in each sample (C) and in two group (D). Note: OTU, operational taxonomic units; CN, no herbal tea residues, the control group; HC, 30% fermented HTRs replaced, the 30% replacement group

Table 6 Statistical analysis of sample complexity

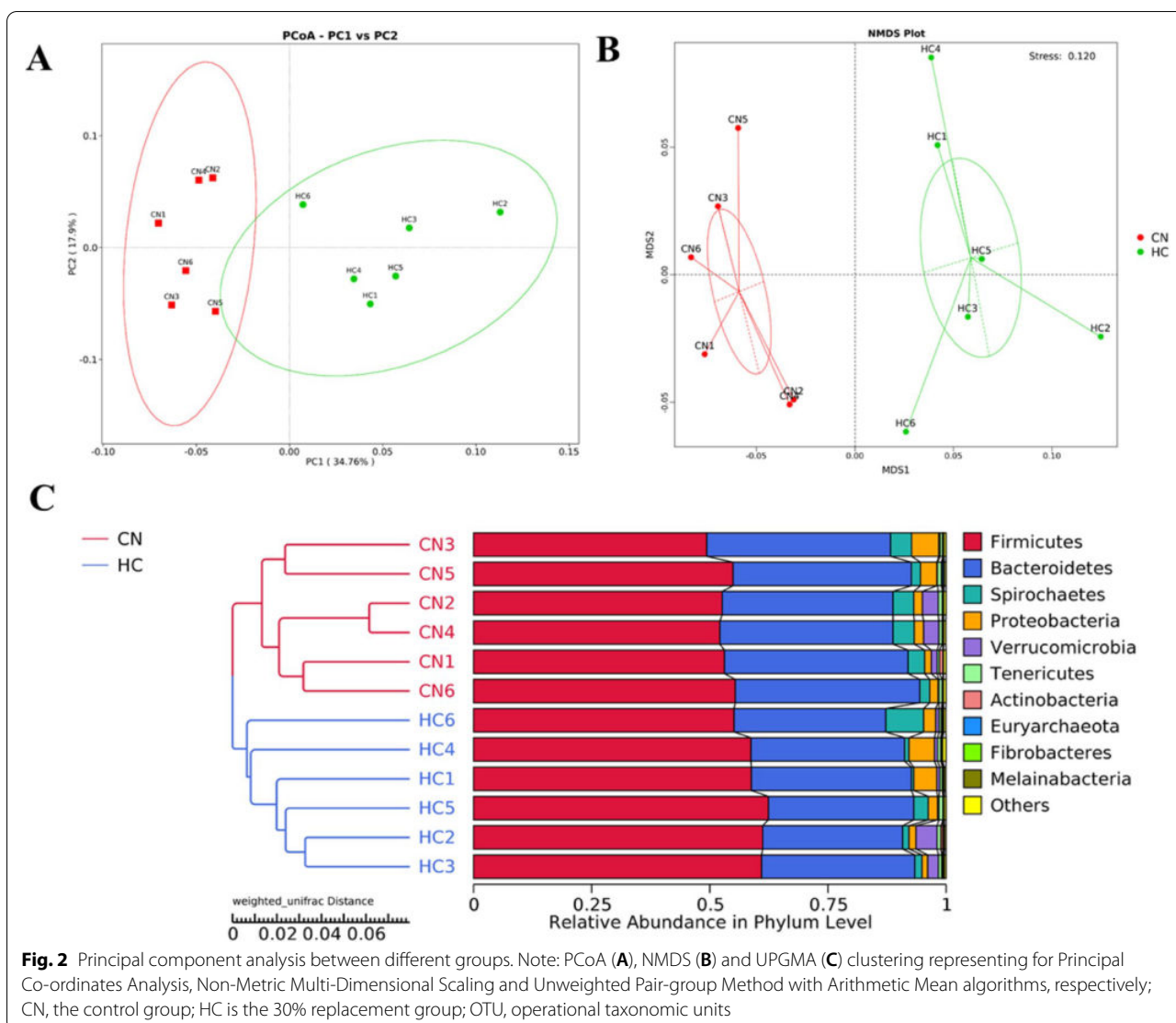
Item	CN	HC	P value
Observed species	1260.50 ± 15.1805	1265.50 ± 16.5726	0.828
Shannon	8.02 ± 0.0537	8.07 ± 0.0668	0.564
Simpson	0.99 ± 0.0006	0.99 ± 0.0010	0.568
Chao1	1316.69 ± 16.97	1319.46 ± 17.83	0.913
Ace	1321.61 ± 18.36	1320.44 ± 17.79	0.964
Goods coverage	0.99 ± 0.0001	0.99 ± 0.0001	0.334
PD whole tree	85.54 ± 2.3358	93.59 ± 2.7638	0.05

Alpha diversity reflected the richness and diversity of species in samples, and it has a variety of indicators: observed species, shannon, simpson, chao1, ace, goods coverage, PD whole tree. The higher the value of Observed species, the higher the species richness are. Shannon index evaluates the richness and evenness of species composition in the sample. The greater the value, the more abundant and evenly distributed the species are. The Chao1 and ACE indices measure species richness. Goods coverage index represents sequencing depth. PD whole tree index reflects phylogenetic diversity

HTR herbal tea residue, CN no herbal tea residues, the control group, HC 30% fermented HTRs replaced, the 30% replacement group

between the two groups by measuring the similarity of microbial communities according to the degree of their overlap.

The data in Table S6 show that the levels the *Bacteroidia* and *Clostridia* in the HC group were significantly lower and higher, respectively, than those in the CN group at the class level ($P < 0.01$), while the *Bacteroidales* and *Clostridiales* ($P < 0.01$) showed the same trend at the order level. At the family level, the *Rikenellaceae* and *Paludibacteraceae* levels were decreased in the HC group ($P < 0.01$ and $P < 0.05$), and the *Ruminococcaceae* levels were increased ($P < 0.05$). At the genus level, *Erysipelotrichaceae* levels in the HC group increased ($P < 0.01$), and *Fournierella*, *Acetobacterium*, *Anaerovorax*, *Butyrivibrio*, and *Oscillibacter* levels in the HC group were also higher than those in the CN group ($P < 0.05$), whereas, the *Alistipes* levels were lower ($P < 0.05$). At the species level, the *rumen_bacterium_NK4A214* were enriched in the HC group ($P < 0.05$). LEFSe identified 29 differentially abundant taxonomic clades in the CN and HC groups, whose LDA scores were greater than 2.0 (Fig. 3). The results showed that at the phylum level, the *Bacteroidetes*



were enriched in the CN group, while the *Fibrobacteres* and *Firmicutes* were enriched in the HC group.

Fecal SCFAs concentration and their correlation with microbiota genera

SCFAs are the main products of microbial metabolism in the intestines, and the types and quantity of SCFAs are regulated by microbial species, diet, and the environment [23]. As shown in Table 7, the SCFAs of the fecal microorganisms in the CN, LC and HC groups showed different trends. The concentration of Aa increased gradually with the increase in fermented HTR substitution, at 13.33, 13.37, and 14.82 mg/g in the three groups, respectively. The Aa content in the HC group was significantly higher than that in the CN and LC groups. The concentrations of Pa (3.29, 3.46, and 3.542 mg/g, respectively), Ba (2.35, 2.51, and 2.49 mg/g, respectively), and Va (0.09, 0.09,

and 0.10 mg/g, respectively) increased in the fermented HTR replacement groups, without statistical significance among the groups. The concentrations of Ia were 0.15, 0.13, and 0.17 mg/g, respectively, with the concentrations in HC group being significantly higher than those in the CN and LC groups. However, the concentration of Iva (0.22, 0.18, and 0.18 mg/g, respectively) in the LC and HC groups were significantly lower than those in the CN group. We also studied the correlation between SCFAs and significantly enriched fecal microbiota at the genus level. As shown in Fig. 4, there was a significant positive correlation between Aa and the relative abundance of *Acetobacterium* ($P < 0.01$), and a positive correlation with the relative abundance of *Anaerovorax* ($P = 0.05$). In addition, there was a positive correlation between Pa and the relative abundance of *Acetobacterium* ($P < 0.05$), *Erysipelotrichaceae* ($P < 0.05$), and *Fournierella* ($P < 0.05$).

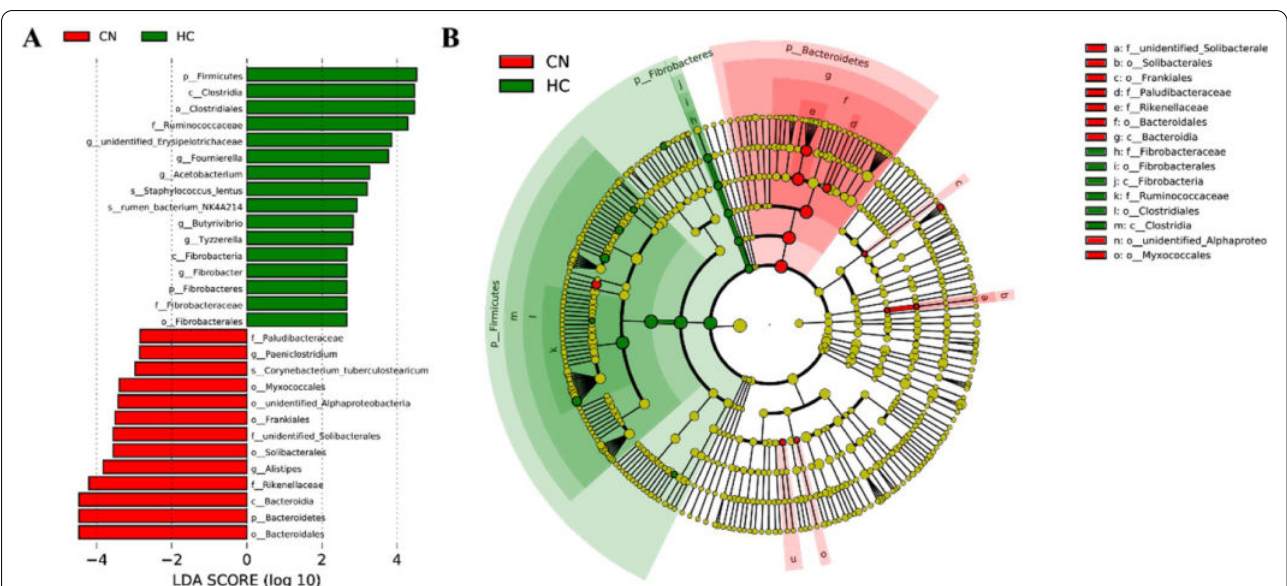


Fig. 3 Taxonomic differences of fecal microbiota between CN and HC groups derived from the LefSe method. Note: **A** LDA scores observed for individual taxa that passed the LefSe significance threshold of 4. **B** Taxonomic cladogram. Taxa with enriched levels in CN were showed in red, whereas those with enriched levels in HC were showed in green. The brightness of the respective colors is proportional to the observed effect size. CN, no herbal tea residues, the control group; HC, 30% fermented HTRs replaced, the 30% replacement group

Table 7 Effect of fermented herbal tea residue on the content of short chain fatty acids (SCFAs) in feces of fattening cattle (mg/g) (N = 6)

Item	CN	LC	HC
Acetic acid	13.33 ± 0.91 ^b	13.37 ± 1.27 ^b	14.82 ± 0.95 ^a
Propionic acid	3.29 ± 0.22	3.46 ± 0.63	3.54 ± 0.26
Isobutyric acid	0.15 ± 0.01 ^b	0.13 ± 0.01 ^b	0.17 ± 0.02 ^a
Butyric acid	2.35 ± 0.16	2.51 ± 0.22	2.49 ± 0.21
Isovaleric acid	0.22 ± 0.03 ^a	0.18 ± 0.02 ^b	0.18 ± 0.02 ^b
Valeric acid	0.09 ± 0.01	0.09 ± 0.01	0.10 ± 0.02

The values were showed as the means ± standard error (N = 6); Different letters showed significant difference (P < 0.05), while the same letter or no letter showed no significant difference (P > 0.05)
CN no herbal tea residues, the control group, LC 15% fermented HTRs replaced, the 15% replacement group, HC 30% fermented HTRs replaced, the 30% replacement group

However, there was no significant relationship between Ia, Ba, Iva, Va, and *Acetobacterium*, *Alistipes*, *Anaerovox*, *Butyrivibrio*, *Erysipelotrichaceae*, *Fournierella*, or *Oscillibacter* (P > 0.05).

Discussion

HTR is the residual water-insoluble substance produced by herbal tea beverage, which has the potential to be used as feed [21]. Like corn silage with a high NDF and Lingnin contents [17], in this experiment, HTR contained more NDF (54.30% DM) and Lingnin (8.60%

DM). Higher fiber level can enhance rumen peristalsis, and more NDF can also provide substrate and energy for roughage fermentation in rumen [24], indicating that HTR could be used as a source of ruminant roughage. To improve the palatability of HTR and solve the problem of storage, we fermented the HTR. However, the content of NDF was higher than 54% and the content of water soluble carbohydrate (WSC) was only 3.10%, which was not conducive to fermentation alone [25]. The addition of molasses increased the WSC of fermented materials [26], and oat hay helped to control the total water content at the beginning of fermentation. In addition, complex bacteria were added to help fermentation. Previous studies have shown that *Bacillus subtilis* grows strongly and can inhibit the growth of other aerobic and harmful microorganisms during the fermentation process [27]. At the same time, it can produce rich metabolites, such as organic acids and bioactive substances and during fermentation, *Bacillus subtilis* also produces a large number of enzymes [27]. Yeast is suitable for growth in acidic and humid environments containing sugar. Yeast can use monosaccharides or oligosaccharides produced in fermentation to produce alcohol and carbon dioxide, which is one of the best combination fermentation strains. *Lactobacillus* can inhibit the growth of spoilage bacteria, reduce the pH, maintain an acidic environment, and ensure the fermentation quality [28]. After fermentation, the content of lactic acid, acetic acid, and propionic acid increased, and the pH decreased to 3.89, which effectively

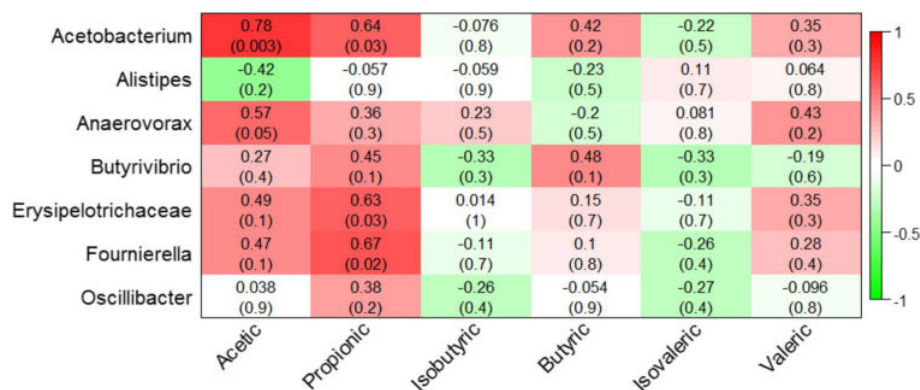


Fig. 4 Statistical analysis of correlation between genus taxa and fecal SCFA. Note: Each cell contained the corresponding correlation and P value. The table is color-coded by correlation according to the color legend (Red indicates positive correlation and green indicates negative correlation)

inhibited the reproduction of undesirable bacteria, increased the content of crude protein and decreased the content of NDF, indicating a better fermentation quality. Previous study found that green tea residue silage could be used as a protein source for lactating dairy cows to replace part of the alfalfa and soybean meal in their diet, which had no adverse effect on the performance of the dairy cows [29], suggesting that fermented HTR could be used as feed resource.

In the subtropical region of southern China, the climate is hot in summer; therefore, beef cattle are vulnerable to summer heat stress, which affects their eating and health [30]. This results in growth retardation, which affects the development of the beef cattle industry [31]. It has been reported that heat stress can reduce the intake of feed and affect the metabolism after absorption [32]. The temperature and humidity index reflects the heat stress intensity of animals by measuring the temperature and humidity index of the breeding environment [33]. Our results showed that the total average THI was 82, which was between $79 < \text{THI} < 84$. Therefore, we concluded that the fattening cattle were in a high heat stress state during the whole period of the formal experiment. RR and RT are indices used to quantify the physiological changes of animals under heat stress [34]. Replacement with fermented HTR was beneficial to reduce the RT and RR of fattening cattle in the heat stress environment, with the 30% fermented HTR having a more significant effect. This suggested that fermented HTR could alleviate heat stress symptoms of fattening cattle in summer, which is consistent with the results of other studies [35–37]. Chen found that Chinese herbal medicine could reduce significantly the RR of beef cattle under heat stress [36]. Song found that Chinese herbal medicine could reduce the RT for a certain period of time under high temperature [35].

When animals are exposed to heat stress, they eat less to reduce their heat production [37], which ultimately affects their growth and fattening.

Cor is a hormone secreted by the adrenal gland during stress. When the body is in the state of heat stress, it will stimulate the adrenal cortex to secrete Cor to adapt to the adverse environment [38]. Our results showed that in the heat stress environment, with the increase in fermented HTR in the diet, the amount of Cor secreted by the fattening cattle decreased gradually, indicating that fermented HTR could effectively alleviate the heat stress response of fattening cattle. This was consistent with the results of Song et al., who found that Chinese herbal medicine could reduce the secretion of Cor in beef cattle under heat stress [35] and this might be explained by the fact that herbal medicine active substances are retained in the HTR, which can relieve heat stress in summer. LDH participates in glycolysis. Hocking et al. found that high heat treatment can increase LDH activity [39]. In our results, LDH level decreased with the increase of fermented HTR replacement, indicating that fermented HTR could alleviate heat stress in fattening cattle.

When the animals are in the state of heat stress for a long time, the body's immunity will decline [40]. IgG is the most abundant immunoglobulin in animal organs, which can protect the body from infection, and is an important immune index under heat stress [41]. Interleukin-2 (IL-2) is a cell growth factor in the immune system of the body, and is also an important indicator of cellular immune function under heat stress [42]. Furthermore, IL-6 is a proinflammatory cytokine that is associated with an increased inflammatory response [43]. Studies have shown that HTR can enhance the immune function of the human body [44]. In the present study, we found that the levels of IgG and IL-2

in the serum of beef cattle fed with fermented HTR increased significantly, which indicated that fermented HTR could enhance the immune function of beef cattle under heat stress.

The content of MDA indirectly reflects the degree of lipid peroxidation in tissues and cells, and can be used as a surrogate for the degree of cell damage [45]. SOD is an antioxidant enzyme that can scavenge free radicals in vivo. Studies show that heat stress can inhibit the expression of SOD [46]. T-AOC represents the antioxidant capacity of the whole body. In this study, the MDA level had a decreased trend with the increase of fermented HTR replacement, and we therefore inferred that fermented HTR may be required to alleviate the cell damage caused by heat stress. T-AOC level increased significantly in 15% substitution and SOD level increased significantly in 30% substitution group, reflecting the antioxidant activity of fermented HTR, which was consistent with Chaudhary's findings [47].

In addition, some studies have suggested that to adapt to heat stress, the body needs to increase the absorption of glucose to ensure the energy supply, resulting in an increased serum glucose content [48]. In the present study, there was no significant difference in the total cholesterol level with increasing fermented HTR. However, under heat stress, the glucose level of the fattening cattle fed with the basal diet was significantly higher than that of cattle fed with the 30% fermented HTR alternative diet, suggesting that heat stress has an effect on the glucose level, which can be alleviated by fermented HTR. Compared with those of the CN group, the total protein and albumin of the fermented HTR groups increased while blood urea nitrogen showed a decreased trend, which was similar with Guo's results [49]. Guo pointed out that this might be the result of thyroid regulation, which was conducive to maintaining the body's water and salt balance, and alleviating the adverse effects of heat stress [49].

At present, there are few studies on the effect of HTR on the fecal microorganisms of fattening cattle under heat stress. Recently, a study showed that there are significant differences in the microbial composition between spring and summer, indicating that environmental temperature has an impact on the microbial community structure of feces [50]. In the present study, we found that 30% fermented HTR had a more significant effect on heat stress index of fattening cattle than 15%; therefore, we chose the CN and HC group to study the fecal microbial community of fattening cattle. According to the results of alpha diversity analysis and PCA, the fecal microbial community of heat stressed fattening cattle fed with fermented HTR was significantly different from cattle fed with the basic diet, and the microbial diversity of the HC

group increased. The most abundant bacteria in the phylum level of the CN and HC group were *Firmicutes* and *Bacteroidetes*. Li showed that under the different climates in spring and summer, the main microorganisms in cow feces were *Firmicutes* and *Bacteroidetes*; in summer, *Firmicutes* levels were higher than those in spring, while *Bacteroidetes* levels were lower than those in spring [50]. It has been reported that ruminants have a core microbial community mainly composed of *Firmicutes* and *Bacteroidetes*, which can maintain stable digestive function [51]. In our study, the feeding of fermented HTR changed the relative proportion of these two bacteria, which was consistent with Hu's study [52]. The results showed that the enrichment of *Firmicutes* in the HC group was significantly higher than that in CN group, and *Bacteroidetes* levels in HC group were significantly lower, indicating that fermented HTR had a certain effect on fecal microbial flora of fattening cattle under summer heat stress. It is reported that *Bacteroidetes* is mainly responsible for the degradation of fiber, and its degree of enrichment is related to diets with a high fiber content. By contrast, *Firmicutes* are responsible for the degradation of carbohydrates, fats, and proteins, which are related to a high calorie diet [53]. We infer that the increase of *Firmicutes* in HC group is related to the richer crude protein and crude fat in fermented HTR.

At the family taxonomic level, the *Rikenellaceae* and *Paludibacteraceae* in the HC group decreased, and the *Ruminococcaceae* increased. It has been reported that the *Rikenellaceae* increased and the *Ruminococcaceae* decreased in the intestines of mice fed with a high-fat diet, suggesting that a high calorie diet can cause changes in the intestinal microflora [54], which is contrary to the results of the HC group and might be explained by the fact that under heat stress, the fermented HTRs reduced the caloric level of the diet, alleviated the heat production during fattening, and changed the intestinal flora. At the genus taxonomic level, *Fournierella* and *Oscillibacter* are two genera of the *Ruminococcaceae*, and both showed an increasing trend in the HC group. *Acetobacterium*, *Anaerovorax*, *Butyrivibrio*, and *Erysipelotrichaceae* also increased in the HC group. A study has reported that *Butyrivibrio* is more involved in epithelium promotion, while *Erysipelotrichaceae* is more abundant at high temperatures [55]. Besides, *Alistipes* decreased in the HC group. A study suggested that *Alistipes* is the source of colorectal cancer, and its abundance is related to the severity of intestinal diseases [56], which indicates that fermented HTR is beneficial to maintain the health of fattening cattle under heat stress.

We also studied the association between fecal SCFAs and microorganisms at the genus level where changes were observed. We found that there was a significant

positive correlation between Aa and the relative abundance of *Acetobacterium* and a positive correlation between Pa and the relative abundance of *Acetobacterium*, *Erysipelotrichaceae*, and *Fournierella*. It has been reported that *Acetobacter* is mainly involved in Aa fermentation [57] and *Fournierella* can metabolize and produce Aa and Pa [58]. SCFAs are the main products of microbial metabolism in the intestines, and the types and quantity of SCFAs are regulated by microbial species, diet, and the environment [23]. Therefore, we speculated that fermented HTRs change the composition and abundance of large intestine microorganisms in fattening cattle, promote the fermentation of large intestine microorganisms, and help the body to maintain health and resist the adverse effects of heat stress.

Conclusions

After fermentation with oat hay and compound bacteria, the pH of the HTR decreased and the nutritional level increased, which was conducive to the resource utilization of HTR. In addition, fermented HTR could alleviate the heat stress of fattening cattle in summer, improve their growth performance, enhance their immune performance, help them to resist an adverse environment, and maintain their health. In addition, 30% fermented HTR replacement had an impact on the fecal microbial community of heat stressed fattening cattle, and the bacteria were closely related to the cattle's fecal SCFA levels. Based on our findings, we concluded that 30% fermented HTRs replacing *Pennisetum purpureum* grass might be advantageous for fattening cattle under heat stress. In addition, the co-fermented products also included molasses, oat hay, and mixed bacterial strains in our test, and the potential roles of these co-fermented products on heat stress should be further study.

Materials and methods

Fermentation

The HTRs used in the experiment were obtained from Heyuan Jilongxiang Biological Technology Co., LTD. (Heyuan, Guangdong, China). The molasses were purchased from Guangzhou Linong Feed Co., Ltd. (Guangzhou, Guangdong, China) and strains were purchased from Guangdong Microbial Culture Collection Center (Guangzhou, Guangdong, China). The feedstock department of Guangzhou Fengxing Dairy Co., LTD. (Guangzhou, Guangdong, China) provided the oat hay.

Based on dry matter, the tested HTR contained 20% *Mesona chinensis* leaves, 20% *Plumeria rubra* flowers, 20% *Microcos paniculata* leaves, 12% Honeysuckle flowers, 12% *Chrysanthemum* flowers, 12% *Prunella vulgaris* leaves and 4% *Liquiritia glycyrrhiza* roots in mass ratios, respectively. The nutritional components of HTR was

analyzed by E-more Technology Co., Ltd. (Ulanqab, Inner Mongolia, China). In details, HTR was grind to power in 1 mil with UDY-cyclone (UDY Corporation, Fort Collins, CO); then scanned by NIR spectroscopy with 'Feed and Forage' system (1100-2500 nm) (Thermo Scientific, Waltham, Massachusetts, US) and merged with Dairy on (<https://dairyone.com/>) database.

In this experiment, HTR and oat hay were cut into 2–3 cm pieces. Fermentation was carried out on HTR and oat hay (CP: 12.3%; NDF: 50.8%; ADF: 26.7%) with a mass ratio of 6:4 on a wet weight basis (approximately 3:7 on dry matter basis), with 2% added molasses. The mixed bacteria used for fermentation were *Saccharomyces cerevisiae* GDMCC2.167 (3×10^8 colony forming units/g), *Bacillus subtilis* GDMCC1.372 (3×10^8 colony forming units/g), *Lactobacillus plantarum* GIM1.191 (5×10^9 colony forming units/g) and *Enterococcus faecalis* GDMCC1.612 (3×10^8 colony forming units/g), with mass ratios of 250 g: 1 t, 300 g: 1 t, 300 g: 1 t, and 200 g: 1 t, respectively. The fermentation materials were mixed and stirred evenly using a feed-stuff mixer. Then the mixture was compacted to remove air and pressed into polyethylene bags (50 kg each) and sealed, and fermented for 25–30 days at room temperature. After approximately 30 days of fermentation, 20 g of fermented samples were added to 180 mL of distilled water, sealed with preservative film, and placed in a refrigerator at 4 °C for 24 h. During extraction, the solution was shaken every 30 min. After 24 h, the solution was filtered through qualitative filter paper, and a pH meter (Horiba, Tokyo, Japan) was used to determine the pH value of the filtrate. High performance liquid chromatography (HPLC) was used to determine the content of organic acids in the extract of fermented HTRs, while AOAC International guidelines [59] were used to analyze the dry matter, crude protein, NDF, ADF, and ash contents.

Experimental animals and design

This experiment was carried out in Guangzhou from July to August in 2019, and the weather is hot, rainy and humid, which usually leads to a natural heat stress and we judged whether the individuals were in the state of heat stress by using the environmental temperature and humidity index [22]. A total of 45 healthy female Simmental crossbred cattle (18 months old), balanced with body weight, were selected and divided into three treatment groups (15 cattle per group) in the same cowshed: The CN group (fed with basal diet, without fermented HTR), the LC group (fermented HTR replaced 15% of *Pennisetum purpureum* grass), and the HC group (fermented HTR replaced 30% of *Pennisetum purpureum* grass). The experiment lasted for 40 days, including a

7-day adaptation period and a 33-day formal experimental period.

The animal feeding experiment was carried out at the Yunfu benben beef cattle farm (Yunfu, Guangdong, China), and the basal diet for the experimental cattle was provided by the farm and was shown in Table S2. During the experiment, all individuals were fed at 8:00 am and 5:00 pm every day. A total mixed ration (TMR) feed mixer was used to fully mix the experimental diets, and the diet and drinking water were allowed to intake freely during the experiment.

Measurements and sampling

During the experiment, a dry and wet thermometer (Kimo Industry Co., Biarritz, France) was set at 1.5 m above the center of ground in the cowshed. The temperature, humidity, and wet bulb temperature of the cowshed were recorded at 08:00, 14:00, and 20:00 every day to calculate the daily average temperature, humidity and the temperature humidity index (THI) of the cowshed. The following formula was used to calculate the THI: $THI = (0.35 \times TDB + 0.65 \times TWB) \times 1.8 + 32$, where TDB is the dry bulb temperature and TWB is the wet bulb temperature [22].

In every 3 days, an animal thermometer (Kruuse, Langeskov, Denmark) was used to measure the rectal temperature (RT) of the experimental cattle at 08:00, 14:00, and 22:00 during the formal experimental period. When the tested cattle lay still, we counted the times of chest fluctuation in 1 min with the counter, which was recorded as respiratory rate (RR). At the beginning and end of the formal experiment, the weights of the experimental cattle were recorded after a 12-h overnight fast. The amount of TMR consumed by the experimental cattle, and that remaining unconsumed, were recorded every day. The above data were used to calculate the average daily feed intake (ADFI), average daily gain (ADG), and the feed to weight ratio (F/G). On the day before the end of the experiment, six individuals in each treatment group were randomly selected and 20 mL blood samples were taken from the tail vein, placed in a centrifuge tube, and then centrifuged immediately after being placed obliquely for 2 h. Enzyme linked immunosorbent assay (ELISA) kits were used to determine the serum levels of heat shock protein 70 (HSP70), cortisol (Cor), lactate dehydrogenase (LDH), immunoglobulin G (IgG), immunoglobulin A (IgA), alanine aminotransferase (ALT), creatine kinase (CK), total antioxidant capacity (T-AOC), malondialdehyde (MDA), superoxide dismutase (SOD), glutathione peroxidase (GSH-PX) according to the manufacturer instructions (Nanjing Jiancheng Bioengineering Research Institute, Nanjing, China).

At the end of the experiment, six animals of each group were randomly selected and 200 g feces were collected from 12 fattening cattle rectums in CN and HC groups, then put into a frozen storage tube and stored in liquid nitrogen. Approximately 100 g were used for HPLC (Actlabs, Ancaster, ON, Canada) determination of fecal volatile fatty acid contents, including acetic acid (Aa), propionic acid (Pa), isobutyric acid (Ia), butyric acid (Ba), isovaleric acid (Iva), and valeric acid (Va). The other 100 g were used to extract total genomic DNA to investigate fecal microorganisms and the total genomic DNA was extracted using CTAB/SDS method. DNA concentration and purity was monitored on 1% agarose gels. According to the concentration, DNA was diluted to 1 ng/μL using sterile water.

16S rRNA gene sequencing and annotation analysis

We amplified the V3 and V4 regions of the 16S rRNA sequence of the bovine fecal microbial communities by using a forward primer (5'-GTGCCAGCMGCCGCGG-3') and a reverse primer (5'-GGACTACHVGGGTWTCTAAT-3'), and then constructed gene fragment libraries. The paired end method was used to sequence the libraries on the Illumina Novaseq sequencing platform (Illumina, Waltham, MA, USA). High-quality tags data (clean tags) were obtained after splicing and filtering of the reads [60], and then mosaic filtering was performed to obtain effective tags for subsequent analysis. The Uparse software (Uparse v7.0.1001) [61] was used to cluster all effective tags of all samples. Sequences with $\geq 97\%$ identity were clustered into same operational taxonomic units (OTUs). Then, Silva databases and Mothur [62] were used to annotate and analyze the OTU sequences. The composition and abundance of microbial communities in each sample were counted at each taxonomic level, including kingdom, phylum, class, order, family, genus, and species. Fast multiple sequence alignment and annotation was carried out using the MUSCLE software (Version 3.8.31), and the phylogenetic relationships between different OTUs were obtained [63]. Finally, the data of each sample were homogenized, and the subsequent Alpha and Beta diversity were analyzed based on the homogenized data. The QIIME pipeline (Version 1.7.0) was used to calculate the UniFrac distance and an Unweighted Pair-group Method with Arithmetic Means (UPGMA) clustering tree was also constructed. The R software (Version 2.15.3) was used to draw Principal Component Analysis (PCA), Principal Co-ordinates Analysis (PCoA), and Non-Metric Multi-Dimensional Scaling (NMDS) maps to explore the differences of community structure among the different samples. The Linear discriminant analysis Effect Size (LEfSe) analysis was performed with a linear discriminant analysis LDA score of 2 to further analyze the differences in community structure.

Statistical analysis

One-way analysis of variance (ANOVA) and Duncan's test (SPSS 17.0, IBM Corp., Armonk, NY, USA) were used to analyze the physiological parameters, serum biochemical indices, and the fecal concentrations of short-chain fatty acids (SCFAs). The results are shown as the mean \pm standard error (SE), and $P < 0.05$ and $P < 0.01$ were used as the criteria to judge significant and extremely significant differences.

Supplementary Information

The online version contains supplementary material available at <https://doi.org/10.1186/s12917-021-03061-y>.

Additional file 1 : Figure S1. Daily changes in cowshed ambient temperature and humidity index (THI) in three time. The red line represents the daily changes of THI index at 8:00 am, the orange line represents the daily changes of THI index at 15:00 pm, and the gray line represents the daily changes of THI index at 22:00 pm. **Supplementary Tables S1–S6.**

Authors' contributions

XZ and JS conceived the report, participated in its design, performed data analysis, and drafted the manuscript; ZC, XS and FL performed in experiments. JL, TC, QX and YZ provided guidance and funding. All authors read and approved the final manuscript.

Funding

This work was supported by the Natural Science Foundation of China Program [grant numbers 31802032, 32072714]; the Natural Science Foundation of Guangdong Province [grant number 2020A1515010062]; the Science and Technology Project of Guangzhou [grant number 202002030037]; and the Key-Area Research and Development Program of Guangdong Province [2019B110209005].

This work was supported by the Natural Science Foundation of China Program [grant numbers 31802032, 32072714]; the Natural Science Foundation of Guangdong Province [grant number 2020A1515010062]; the Science and Technology Project of Guangzhou [grant number 202002030037]; and the Key-Area Research and Development Program of Guangdong Province [2019B110209005].

Availability of data and materials

The raw sequences were deposited into Sequence Read Archive (SRA) database with the BioProject accession number PRJNA699165.

Declarations

Ethics approval and consent to participate

The animal feeding experiment was carried out at the Yunfu benben beef cattle farm (Yunfu, Guangdong, China). The tested animals were housed in an open cowshed, and animals were fed individually. All animal procedures were approved by the owner of farm and the Animal Care Committee at South China Agricultural University according to the university's guidelines for animal research (2018F006).

Consent for publication

Not applicable.

Competing interests

The authors declare that they have no competing interests.

Received: 28 August 2021 Accepted: 31 October 2021

Published online: 12 November 2021

References

- Li FS, Weng JK. Demystifying traditional herbal medicine with modern approach. *Nat Plants*. 2017;3:17109.
- Chio PH, Zaroff CM. Traditional Chinese medicinal herbal tea consumption, self-reported somatization, and alexithymia. *Asia Pac Psychiatry*. 2015;7(2):127–34.
- Desideri D, Meli MA, Roselli C, Feduzi L. Alpha and gamma spectrometry for determination of natural and artificial radionuclides in tea, herbal tea and camomile marketed in Italy. *Microchem J*. 2011;98(1):170–5.
- Zhao J, Deng JW, Chen YW, Li SP. Advanced phytochemical analysis of herbal tea in China. *J Chromatogr A*. 2013;1313:2–23.
- Dalar A, Konczak I. Phenolic contents, antioxidant capacities and inhibitory activities against key metabolic syndrome relevant enzymes of herbal teas from eastern anatolia. *Ind Crop Prod*. 2013;44:383–90.
- Shen J, Shan J, Zhu X, Xu Y, Li M. Effect of Chinese herbal tea on health tested on drosophila model. *Plant Foods Hum Nutr*. 2020;75(2):305–6.
- Yang D, Liang J, Wang Y, Sun F, Tao H, Xu Q, et al. Tea waste: an effective and economic substrate for oyster mushroom cultivation. *J Sci Food Agric*. 2010;96(2):680–4.
- Kondo M, Kita K, Yokota H. Effects of tea leaf waste of green tea, oolong tea, and black tea addition on sudangrass silage quality and in vitro gas production. *J Sci Food Agric*. 2004;84(7):721–7.
- Ozdemir N, Yakupoglu T, Dengiz O. The effects of bio-solid and tea waste application into different levels of eroded soil on N, P and K concentrations. *Environ Monit Assess*. 2009;156(1–4):109–18.
- Hameed BH. Spent tea leaves: a new non-conventional and low-cost adsorbent for removal of basic dye from aqueous solutions. *J Hazard Mater*. 2009;161(2–3):753–9.
- Shang JG, Kong XR, He LL, Li WH, Liao QJH. Low-cost biochar derived from herbal residue: characterization and application for ciprofloxacin adsorption. *Int J Environ Sci Technol*. 2016;13(10):2449–58.
- Ahsan MA, Katla SK, Islam MT, Hernandez-Viezas JA, Martinez LM, Diaz-Moreno CA, et al. Adsorptive removal of methylene blue, tetracycline and Cr (VI) from water using sulfonated tea waste. *Environ Technol Innov*. 2018;11:23–40.
- Cheraghi M, Sobhanardakani S, Lorestani B, Zandipak R. Tea wastes efficiency on removal of cd(ii) from aqueous solutions. *Arch Hyg Sci*. 2016;5(3):184–91.
- Dizadji N, Anaraki NA. Adsorption of chromium and copper in aqueous solutions using tea residue. *Int J Environ Sci and Tech*. 2011;8(3):631–8.
- Wan S, Qu N, He F, Wang M, Liu G, He H. Tea waste-supported hydrated manganese dioxide (hmo) for enhanced removal of typical toxic metal ions from water. *RSC Adv*. 2015;5:88900–7.
- Lunge S, Singh S, Sinha A. Magnetic iron oxide (fe₃o₄) nanoparticles from tea waste for arsenic removal. *J Magn Magn Mater*. 2014;356:21–31.
- Hristov AN, Harper MT, Roth G, Canale C, Huhtanen P, Richard TL, et al. Effects of ensiling time on corn silage neutral detergent fiber degradability and relationship between laboratory fiber analyses and in vivo digestibility. *J Dairy Sci*. 2020;103(3):2333–46.
- Liu HW, Tong JM, Zhou DW. Utilization of chinese herbal feed additives in animal production. *Agric Sci China*. 2011;10:1262–72.
- Samanta AK, Jayaram C, Jayapal N, Sondhi N, Kolte AP, Senani S, et al. Assessment of fecal microflora changes in pigs supplemented with herbal residue and prebiotic. *PLoS One*. 2015;10(7):e0132961.
- Liu W, Rouzmehr F, Seidavi A. Effect of amount and duration of waste green tea powder on the growth performance, carcass characteristics, blood parameters, and lipid metabolites of growing broilers. *Environ Sci Pollut Res Int*. 2018;25(1):375–87.
- Xie Y, Chen Z, Wang D, Chen G, Sun X, He Q, et al. Effects of fermented herbal tea residues on the intestinal microbiota characteristics of Holstein heifers under heat stress. *Front Microbiol*. 2020;11:1014.
- Berman A. Estimates of heat stress relief needs for Holstein dairy cows. *J Anim Sci*. 2005;83(6):1377–84.
- Macfarlane S, Macfarlane GT. Regulation of short-chain fatty acid production. *Proc Nutr Soc*. 2003;62(1):67–72.
- Zou Y, Zou X, Li X, Guo G, Ji P, Wang Y, et al. Substituting oat hay or maize silage for portion of alfalfa hay affects growth performance, ruminal fermentation, and nutrient digestibility of weaned calves. *Asian-Australas J Anim Sci*. 2018;31(3):369–78.
- Smith LH. Theoretical carbohydrate requirement for alfalfa silage production. *Agron J*. 1962;54(4):291–3.

26. Thompson DN, Barnes JM, Houghton TP. Effect of additions on ensiling and microbial community of senesced wheat straw. *Appl Biochem Biotechnol*. 2005;121-124:21–46.
27. Chen KL, Kho WL, You SH, Yeh RH, Tang SW, Hsieh CW. Effects of *Bacillus subtilis* var. natto and *Saccharomyces cerevisiae* mixed fermented feed on the enhanced growth performance of broilers. *Poult Sci*. 2009;88(2):309–15.
28. Wang C, He L, Xing Y, Zhou W, Yang F, Chen X, et al. Fermentation quality and microbial community of alfalfa and stylo silage mixed with *Moringa oleifera* leaves. *Bioresour Technol*. 2019;284:240–7.
29. Kondo M, Nakano M, Kaneko A, Agata H, Kita K, Yokota H. Ensiled green tea waste as partial replacement for soybean meal and alfalfa hay in lactating cows. *Asian-Aust J Anim Sci*. 2004;17(7):960–6.
30. Hahn GL. Dynamic responses of cattle to thermal heat loads. *J Anim Sci*. 1999;77(Suppl 2):10–20.
31. St-Pierre NR, Cobanov B, Schnitkey G. Economic losses from heat stress by us livestock industries1. *J Dairy Sci*. 2003;86:52–77.
32. Belhadj Slimen I, Najar T, Ghram A, Abdrrabba M. Heat stress effects on livestock: molecular, cellular and metabolic aspects, a review. *J Anim Physiol Anim Nutr (Berl)*. 2016;100(3):401–12.
33. Zhong S, Ding Y, Wang Y, Zhou G, Guo H, Chen Y, et al. Temperature and humidity index (THI)-induced rumen bacterial community changes in goats. *Appl Microbiol Biotechnol*. 2019;103(7):3193–203.
34. da Costa AN, Feitosa JV, Montezuma PA Jr, de Souza PT, de Araújo AA. Rectal temperatures, respiratory rates, production, and reproduction performances of crossbred Girolando cows under heat stress in northeastern Brazil. *Int J Biometeorol*. 2015;59(11):1647–53.
35. Song X, Luo J, Fu D, Zhao X, Bunlue K, Xu Z, et al. Traditional chinese medicine prescriptions enhance growth performance of heat stressed beef cattle by relieving heat stress responses and increasing apparent nutrient digestibility. *Asian-Australas J Anim Sci*. 2014;27(10):1513–20.
36. Chen J, Guo K, Song X, Lan L, Liu S, Hu R, et al. The anti-heat stress effects of Chinese herbal medicine prescriptions and rumen-protected γ -aminobutyric acid on growth performance, apparent nutrient digestibility, and health status in beef cattle. *Anim Sci J*. 2020;91(1):e13361.
37. Wang J, Li J, Wang F, Xiao J, Wang Y, Yang H, et al. Heat stress on calves and heifers: a review. *J Anim Sci Biotechnol*. 2020;11:79.
38. Chanclón B, Martínez-Fuentes AJ, Gracia-Navarro F. Role of SST, CORT and ghrelin and its receptors at the endocrine pancreas. *Front Endocrinol (Lausanne)*. 2012;3:114.
39. Hocking PM, Maxwell MH, Mitchell MA. Haematology and blood composition at two ambient temperatures in genetically fat and lean adult broiler breeder females fed ad libitum or restricted throughout life. *Br Poult Sci*. 1994;35(5):799–807.
40. Dahl GE, Tao S, Laporta J. Heat stress impacts immune status in cows across the life cycle. *Front Vet Sci*. 2020;7:116.
41. Liu DY, He SJ, Liu SQ, Tang YG, Jin EH, Chen HL, et al. Daidzein enhances immune function in late lactation cows under heat stress. *Anim Sci J*. 2014;85(1):85–9.
42. Padgett DA, Glaser R. How stress influences the immune response. *Trends Immunol*. 2003;24(8):444–8.
43. Esposito G, Irons PC, Webb EC, Chapwanya A. Interactions between negative energy balance, metabolic diseases, uterine health and immune response in transition dairy cows. *Anim Reprod Sci*. 2014;144(3-4):60–71.
44. Costa LB, Luciano FB, Miyada VS, Gois FD. Herbal extracts and organic acids as natural feed additives in pig diets. *S Afr J Anim Sci*. 2013;43:181–93.
45. Tsikas D. Assessment of lipid peroxidation by measuring malondialdehyde (MDA) and relatives in biological samples: analytical and biological challenges. *Anal Biochem*. 2017;524:13–30.
46. Yang CY, Lin MT. Oxidative stress in rats with heatstroke-induced cerebral ischemia. *Stroke*. 2002;33(3):790–4.
47. Chaudhary SS, Singh VK, Upadhyay RC, Puri G, Odedara AB, Patel PA. Evaluation of physiological and biochemical responses in different seasons in Surti buffaloes. *Vet World*. 2015;8(6):727–31.
48. Sun X, Zhang H, Sheikhamadi A, Wang Y, Jiao H, Lin H, et al. Effects of heat stress on the gene expression of nutrient transporters in the jejunum of broiler chickens (*Gallus gallus domesticus*). *Int J Biometeorol*. 2015;59(2):127–35.
49. Guo K, Cao H, Zhu Y, Wang T, Hu G, Kornmatitsuk B, et al. Improving effects of dietary rumen protected γ -aminobutyric acid additive on apparent nutrient digestibility, growth performance and health status in heat-stressed beef cattle. *Anim Sci J*. 2018;89(9):1280–6.
50. Li H, Li R, Chen H, Gao J, Wang Y, Zhang Y, et al. Effect of different seasons (spring vs summer) on the microbiota diversity in the feces of dairy cows. *Int J Biometeorol*. 2020;64(3):345–54.
51. Weimer PJ. Redundancy, resilience, and host specificity of the ruminal microbiota: implications for engineering improved ruminal fermentations. *Front Microbiol*. 2015;6:296.
52. Hu X, Liu G, Li Y, Wei Y, Lin S, Liu S, et al. High-throughput analysis reveals seasonal variation of the gut microbiota composition within Forest musk deer (*Moschus berezovskii*). *Front Microbiol*. 2018;9:1674.
53. Jami E, Israel A, Kotser A, Mizrahi I. Exploring the bovine rumen bacterial community from birth to adulthood. *ISME J*. 2013;7(6):1069–79.
54. Daniel H, Gholami AM, Berry D, Desmarchelier C, Hahne H, Loh G, et al. High-fat diet alters gut microbiota physiology in mice. *ISME J*. 2014;8(2):295–308.
55. Ziętak M, Kovatcheva-Datchary P, Markiewicz LH, Ståhlman M, Kozak LP, Bäckhed F. Altered microbiota contributes to reduced diet-induced obesity upon cold exposure. *Cell Metab*. 2016;23(6):1216–23.
56. Parker BJ, Wearsch PA, Veloo ACM, Rodriguez-Palacios A. The genus *Alisipites*: gut bacteria with emerging implications to inflammation, cancer, and mental health. *Front Immunol*. 2020;11:906.
57. Kremp F, Poehlein A, Daniel R, Müller V. Methanol metabolism in the acetogenic bacterium *Acetobacterium woodii*. *Environ Microbiol*. 2018;20(12):4369–84.
58. Togo AH, Durand G, Khelaifa S, Armstrong N, Robert C, Cadoret F, et al. *Fournierella massiliensis* gen. nov., sp. nov., a new human-associated member of the family Ruminococcaceae. *Int J Syst Evol Microbiol*. 2017;67(5):1393–9.
59. Horwitz W. Official methods of analysis of AOAC International. Volume I, agricultural chemicals, contaminants, drugs/edited by William Horwitz. Gaithersburg: AOAC International; 2020.
60. Bokulich NA, Subramanian S, Faith JJ, Gevers D, Gordon JL, Knight R, et al. Quality-filtering vastly improves diversity estimates from Illumina amplicon sequencing. *Nat Methods*. 2013;10(1):57–9.
61. Edgar RC. UPARSE: highly accurate OTU sequences from microbial amplicon reads. *Nat Methods*. 2013;10(10):996–8.
62. Quast C, Pruesse E, Yilmaz P, Gerken J, Schweer T, Yarza P, et al. The SILVA ribosomal RNA gene database project: improved data processing and web-based tools. *Nucleic Acids Res*. 2013;41(Database issue):D590–6.
63. Edgar RC. MUSCLE: multiple sequence alignment with high accuracy and high throughput. *Nucleic Acids Res*. 2004;32(5):1792–7.

Publisher's Note

Springer Nature remains neutral with regard to jurisdictional claims in published maps and institutional affiliations.

Article

CircEZH2 Regulates Milk Fat Metabolism through miR-378b Sponge Activity

Dongyang Wang, Zhengjiang Zhao, Yiru Shi, Junyi Luo, Ting Chen, Qianyun Xi, Yongliang Zhang * and Jiajie Sun * 

College of Animal Science, Guangdong Provincial Key Laboratory of Animal Nutrition Control, National Engineering Research Center for Breeding Swine Industry, South China Agricultural University, Guangzhou 510642, China; wangdy960821@outlook.com (D.W.); orcsblade@163.com (Z.Z.); shiyiru00@163.com (Y.S.); luojunyi@scau.edu.cn (J.L.); allinchen@scau.edu.cn (T.C.); xqy0228@163.com (Q.X.)
* Correspondence: zhangyl@scau.edu.cn (Y.Z.); jiajiesun@scau.edu.cn (J.S.)

Simple Summary: Heat stress has seriously threatened the performance and health of dairy cows and has become one of the most important factors restricting the development of the dairy industry. In our previous study, we found that heat stress markedly altered the expression patterns of circRNAs in dairy cow's mammary gland tissue, and heat-induced circRNAs participated in the regulation of milk fat metabolism through competing endogenous RNA (ceRNA) networks. Therefore, we evaluated the roles of heat-induced circEZH2 in the regulation of milk fat metabolism in this study. In more detail, we found that circEZH2 affects the proliferation, apoptosis, and lipid metabolism of mammary gland epithelial cells, and successfully verified the targeting relationship of circEZH2-bta-miR378b-LPL and circEZH2-bta-miR378b-CD36. This experiment expands the basic data on the role of circRNA in milk fat regulation, and provides a theoretical basis for alleviating heat stress in dairy cows.



Citation: Wang, D.; Zhao, Z.; Shi, Y.; Luo, J.; Chen, T.; Xi, Q.; Zhang, Y.; Sun, J. CircEZH2 Regulates Milk Fat Metabolism through miR-378b Sponge Activity. *Animals* **2022**, *12*, 718. <https://doi.org/10.3390/ani12060718>

Academic Editors: Duy Ngoc Do and Prashanth N Suravajhala

Received: 14 January 2022

Accepted: 7 March 2022

Published: 12 March 2022

Publisher's Note: MDPI stays neutral with regard to jurisdictional claims in published maps and institutional affiliations.



Copyright: © 2022 by the authors. Licensee MDPI, Basel, Switzerland. This article is an open access article distributed under the terms and conditions of the Creative Commons Attribution (CC BY) license (<https://creativecommons.org/licenses/by/4.0/>).

Abstract: In this study, we evaluated the roles of heat-induced circEZH2 in the regulation of milk fat metabolism. CircEZH2 overexpression increased HC11 cell proliferation and decreased apoptosis. These changes were accompanied by increased expression of proliferation marker proteins (PCNA, Cyclin D, and Cyclin E) and the anti-apoptotic protein Bcl2, while expression of the pro-apoptotic proteins Bax and cleaved-caspase was reduced. SiRNA-mediated silencing of EZH2 in HC11 cells had the opposite effects. CircEZH2 overexpression promoted the uptake of a fluorescent fatty acid (Bodipy) as well as expression of the fatty acid transport-related protein CD36, lipolysis-related protein LPL, and unsaturated fatty acid metabolism-related proteins FADS1 and SCD1. Dual luciferase reporter assays verified the targeting relationship of the two ceRNA networks, circEZH2-miR378b-LPL and circEZH2-miR378b-CD36. This information provides further clarification of the role of circRNAs in milk fat regulation in addition to a theoretical basis for alleviating the effects of heat stress on milk production by dairy cows.

Keywords: circEZH2; proliferation; apoptosis; miR378b; fatty acid metabolism

1. Introduction

Milk is a natural and healthy drink, favored for its rich nutritional value, unique flavor, and outstanding health functions. As one of the major nutrients in milk [1], milk fat not only affects the flavor and nutritional value of milk, but also participates in the process of nutrient metabolism that regulates human growth and development [2]. Therefore, exploration of mechanisms regulating milk fat synthesis and fatty acid composition is an active area of research [3]. Milk fat metabolism is a complex process regulated by multiple genes as well as a series of regulatory factors [4]. Although some factors have been identified using high-throughput sequencing technology, the underlying regulatory mechanisms remain to be elucidated [5].

Circular RNAs (circRNAs) are naturally occurring, endogenous non-coding RNA (ncRNA) with a closed circular structure [6]. Numerous studies have shown that circRNAs participate in regulating the growth, development, reproduction, and health of livestock, especially in the process of animal lactation [7]. Many circRNAs that are closely related to lactation have been found in the mammary gland tissues of humans [8], dairy cows [9], sheep [10], goats [11], and sows [12]. These studies have shown that circRNAs play important regulatory roles in the development of animal mammary glands, milk secretion, and the synthesis of nutrients in milk. However, the function and mechanism of related circRNAs are still unclear.

In our previous study, we showed that heat stress markedly altered the expression patterns of circRNAs and revealed that as a competitive endogenous circRNA, circEZH2 (circular Enhancer of zeste 2 polycomb repressive complex 2 subunit) participates in the regulation of milk fat metabolism [13]. In this study, we hypothesized that the heat induced circEZH2 plays an important role in the regulation of milk fat metabolism, providing valuable insights into the mechanisms that control lactation and milk quality.

2. Materials and Methods

2.1. RNA Extraction and Real-Time Quantitative PCR

We extracted the total RNA from the HC11 mouse mammary epithelial cells using TRIzol reagent (Invitrogen, Carlsbad, CA, USA) according to the manufacturer's instructions, and then reverse-transcribed the RNA into cDNA using the PrimeScript RT Reagent Kit with gDNA Eraser (TaKaRa, Dalian, China). Real-time quantitative PCR (RT-qPCR) of related genes was carried out using the Bio-Rad CFX 96™ Real-Time Detection System and SYBR Green PCR Master Mix (TaKaRa). The formula for calculating relative gene expression was calculated using the $2^{-\Delta\Delta C_t}$ method and the primers are shown in Table S1. In more detail, qPCR data were derived from six biological replicates, and the gene *glyceraldehyde-3-phosphate dehydrogenase (GAPDH)* was used as a reference gene for normalization [9].

2.2. Identification of circRNA

To verify the structural homology of mouse and cow circEZH2, we designed a pair of divergent primers that crossed the cyclization site and a pair of convergent primers that did not cross the cyclization site. The authenticity of circEZH2 head and tail splicing was preliminarily verified by electrophoretic separation and Sanger sequencing of the PCR products. To further confirm the presence of circEZH2, we treated total RNA with RNase R enzyme at 37 °C for 10 min and analyzed the RNA expression levels of circular RNA and its linear mRNA by RT-qPCR. The primer sequences used in this experiment are shown in Table S1.

2.3. Plasmid Construction and Oligonucleotide Synthesis

To construct the circEZH2 overexpression plasmid, the full-length sequence of circEZH2 was amplified by adding *Bam*HI and *Kpn*I restriction enzyme sites and protective bases at both ends of the primers. The full-length sequence of circEZH2 was inserted into the pCD2.1-ciR vector (Genesee, Guangzhou, China) by double enzyme digestion followed by ligation with T4 DNA Ligase (TaKaRa). Based on shared miRNA regulatory elements, two pairs of circEZH2-miRNA-mRNA networks were discovered by miRanda (<http://mirtoolsgallery.tech/mirtoolsgallery/node/1055>; Accessed date: 5 May 2020): circEZH2-miR-378b-CD36 and circEZH2-miR-378b-LPL. The pmirGLO plasmid (Promega, Madison, WI, USA) was used to design the luciferase reporter constructs containing the miR-378b target sites originating from the 3'-UTR region of *lipoprotein lipase (LPL)* and *CD36* genes, and circEZH2. The wild-type (LPL-WT, CD36-WT, and circEZH2-WT), mutant (LPL-MUT, CD36-MUT, and circEZH2-MUT) and deletion (LPL-DEL, CD36-DEL, and circEZH2-DEL) sequences that contained miR-378b binding sites in *LPL*, *CD36*, and circEZH2 were designed and synthesized (Sangon Biotech, Shanghai, China), and restriction enzymes *Xba*I and

XhoI sequences were added at both ends of the sequence. Finally, these sequences were ligated into the multiple cloning regions in the 3'-UTR of the *Renilla luciferase* gene. The primer sequences used in this experiment are shown in Table S1. To further explore the function of circEZH2, we also designed and synthesized three interference sequences targeting the circEZH2 junction site, miR-378b mimics (for miRNA overexpression) and miR-378b inhibitor (for miRNA downexpression) (Genepharma, Suzhou, China) as shown in Table S1.

2.4. Cell Culture and Transfection

The HC11 mouse mammary epithelial cell line was purchased from the Chinese Collection of Authenticated Cell Cultures (Beijing, China). After resuscitation, the cells were cultured in a RPMI-1640 medium (Gibco, Grand Island, NY, USA) supplemented with 10% fetal bovine serum (FBS) (Gibco) and 10 ng/mL EGF at 37 °C under 5% CO₂; the medium was changed every 48 h. Adherent HC11 cells were released from the tissue culture flask by trypsinization and seeded into a 12-well plate (approximately 1×10^5 cells per well). After reaching confluence, the medium was replaced with EGF-free HC11 medium and the cells were cultured for a further 2 days before HC11 differentiation was induced by the addition of 5 µg/mL insulin (Sigma Adlrch, Wisconsin, WI, USA), 100 nM dexamethasone (Sigma) and 5 µg/mL prolactin (Sigma).

At 75% confluence, the stably adherent cells were transfected with plasmid or miR-378b mimics using Lipofectamine 2000 transfection reagent (Invitrogen). After 48 h, the cells were collected for further analysis; three biological replicates were prepared for each treatment.

2.5. Western Blot Analysis

HC11 cells (mouse mammary gland cells) were lysed, total proteins were extracted with Radio immunoprecipitation assay (RIPA) reagent (Thermo Scientific, Waltham, MA, USA) containing protease inhibitors, and the protein concentration was determined using the Bicinchoninic acid (BCA) protein assay kit (Nanjing Jiancheng Institute of Bioengineering, Nanjing, China). All extracted proteins were diluted with sodium dodecyl sulfate (SDS) buffer and boiled at 95 °C for 10 min. Equal amounts of proteins were separated by SDS polyacrylamide gel electrophoresis and transferred to a polyvinylidene fluoride (PVDF) membrane (Millipore, Bedford, MA, USA). Membranes were then probed with primary antibodies for the detection of CyclinD, CyclinE, PCNA, Bax, Bcl2, Caspase3, CD36, FADS1, and SCD1. The membranes were then incubated for 30 min at 37 °C with goat anti-rabbit HRP conjugate antibody (Sangon Biotech, Shanghai, China) and goat anti-mouse HRP conjugate antibody (Sangon Biotech). Finally, the protein bands were quantified by densitometry using Image J software V1.8 (National Institutes of Health, Bethesda, MD, USA). All results were expressed as target protein/internal reference protein.

2.6. Cell Proliferation Analysis

Cell proliferation was determined by Cell Counting Kit-8 (CCK-8) assay (Bioss, Woburn, MA, USA). Cells were seeded in a 96-well cell culture plate (5×10^3 cells per well), and transfected for 24 h, 48 h, and 72 h. Subsequently, the cells with CCK-8 reagent were then incubated for about 2 h. The optical density (OD) in each well was measured at 450 nm using a multifunctional microplate reader (Bio-Rad, Hercules, CA, USA).

2.7. Flow Cytometry Analysis

Two days after transfection, adherent cells were released by digestion with trypsin in the absence of EDTA (Gibco); the digestion reaction was terminated by the addition of RPMI-1640 medium containing 10% FBS. The cell suspension was then centrifuged at $2000 \times g$ for 5 min at 4 °C. The cell pellet was then washed twice with 1 mL ice-cold 1×PBS (Gibco) and resuspended in RPMI-1640 medium. After counting, Annexin V solution and propidium iodide staining solution were added to the cell suspension (MultiSciences,

Hangzhou, China) and incubated for 15 min at 20 °C in the dark. The cell samples were then fixed by incubation overnight with 70% alcohol (Damao, Tianjin, China). After washing the cell pellets with pre-chilled 5% PBS solution, 0.5 mL PI/RNase Staining buffer (Beyotime, Shanghai, China) was added to each sample, and the cells were incubated for 30 min at 37 °C in the dark. Cell cycle analysis was then performed using a CytoFLEX flow cytometer (Beckman Coulter, Miami, FL, USA).

2.8. Fluorescent Fatty Acid Uptake Assay

The HC11 cell line was digested and seeded into a 96-well plate (approximately 5×10^3 cells per well). Following stable adherence and culture to 75% confluence, the cells were transfected with the plasmid and cultured for a further 24 h. Before the assay, the cells were starved in serum-free medium for 12 h, and then incubated with Bodipy-C12 (Thermo Fisher Scientific, Bedford, MA, USA) for 5 min at 37 °C without light. After quenching the extracellular fluorescence with trypan blue reagent (Gibco), the absorbance was measured by multifunctional microplate reader and recorded using an inverted fluorescence microscope (FSM-Precision, Suzhou, China), and the value was normalized to CCK8 analysis.

2.9. Double Luciferase Activity Analysis

HeLa cells were seeded into a 96-well plate (approximately 5×10^3 cells per well) and cultured in Dulbecco's Modified Eagle Medium (DMEM) high-glucose medium at 37 °C under 5% CO₂. Following stable adherence and culture to 75% confluence, the cells were transfected with the reporter gene plasmid vector and miR-378b mimics and cultured for a further 48 h. Luciferase activity was then determined by measuring the absorbance using a multifunctional microplate reader.

2.10. Prediction of Translation Function

We used the IRESfinder software (<https://github.com/topics/iresfinder>; Accessed date: 10 October 2020) to predict the internal ribosome entry site (IRES) region of circEZH2 [14] and searched for IRES sequence activity using the circRNADb database [15]. We then used the ORF_finder software (<https://www.ncbi.nlm.nih.gov/orffinder/>; Accessed date: 10 October 2020) to predict the coding region of circEZH2, with an ORF sequence of at least 300 bp in length (allowed to span one back-splice joint) [16].

2.11. Statistical Analysis

All statistical analysis was performed using SPSS 20.0 software (SPSS Inc., Chicago, IL, USA) and graphs were generated using GraphPad Prism 5.0 software (GraphPad Software Inc., San Diego, CA, USA). Data were expressed as mean and standard deviation (mean \pm SD). The differences between treatment groups were analyzed using independent *t*-tests and *p* < 0.05 were set as the thresholds for statistical significance.

3. Results

3.1. Homology of Mouse CircEZH2 with Bovine Sequences

The mouse circEZH2 sequence was shown to consist of 899 bases encoded by 2–8 exons (Figure 1A). We used cDNA and gDNA isolated from mouse mammary epithelial HC11 cells as templates for amplification of circEZH2 with convergent primers, while successful amplification using cDNA as a template was achieved only using the divergent primers (Figure 1B,C). The circEZH2 circularization site was confirmed by Sanger sequencing (Figure 1D) and found to be similar to the homologous bovine sequence. Generally, circRNA is more resistant to external stimuli due to its ring structure. Linear RNA molecules are susceptible to exonuclease R digestion, while circRNA is resistant. Therefore, RNase R was used to identify the circRNA candidates [17]. Agarose gel electrophoresis and RT-qPCR analysis revealed that there was no significant difference in circEZH2 expression different between the RNase R-treated and mock groups, while the expression of linear parental

genes decreased significantly in the treated group (Figure 1E,F), further confirming the successful cyclization of circEZH2.

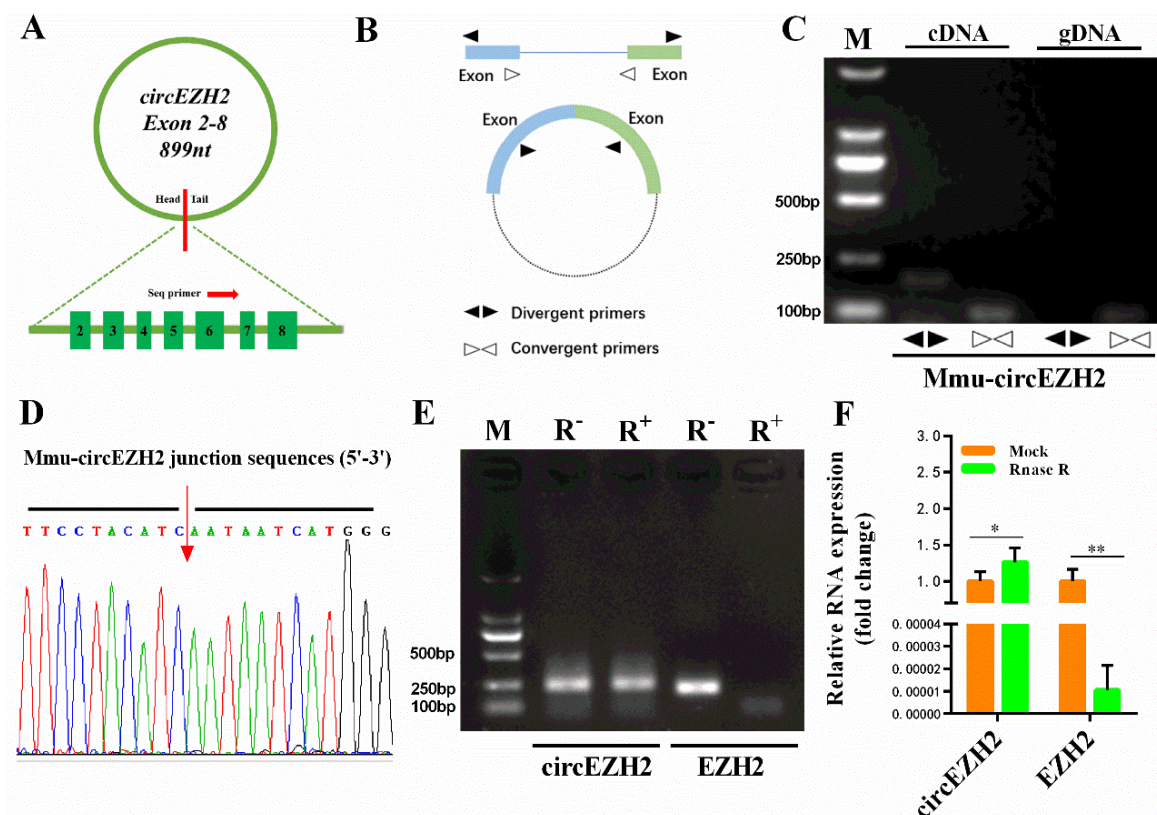


Figure 1. Validation of mouse circEZH2. (A) Schematic diagram of circEZH2. (B) Schematic diagram of divergent primer and convergent primer design. (C) Identification of circEZH2 by divergent primers and convergent primers. Divergent primers amplify circEZH2 in cDNA but not genomic DNA (gDNA). (D) Sanger sequencing results using divergent primer pairs. (E) RNase R enzyme digestion electrophoresis. (F) qRT-PCR analysis of RNA expression. Data represent means \pm standard deviation, *, $p < 0.05$; **, $p < 0.01$.

3.2. Construction of the CircEZH2 Overexpression Vector and Interference Sequences

To explore the function of circEZH2, we used specific primers to synthesize the full-length sequence of circEZH2 (Figure 2A) and ligated it into the pCD2.1-ciR vector, which also contains the green fluorescent protein (GFP) expression sequence. Successful construction of the circEZH2 overexpression plasmid (OE-circEZH2) was verified by restriction enzyme digestion (Figure 2B) and Sanger sequencing (Additional File S1). Effective transfection of HC11 cells with the empty vector and OE-circEZH2 plasmid was confirmed by detection of GFP protein expression by fluorescence microscopy (Figure 2C). Subsequently, RT-qPCR analysis showed that circEZH2 expression increased significantly in transfected HC11 cells (Figure 2D). In contrast, RT-qPCR analysis showed significant reduction in the expression of circEZH2 in HC11 cells following transfection with the three short interfering RNA (siRNA) sequences compared with the levels detected in cells transfected with the negative control (NC) (Figure 2E). Of these, circEZH2-siRNA1 (si-circEZH2) exhibited the highest interference efficiency and was used in subsequent experiments.

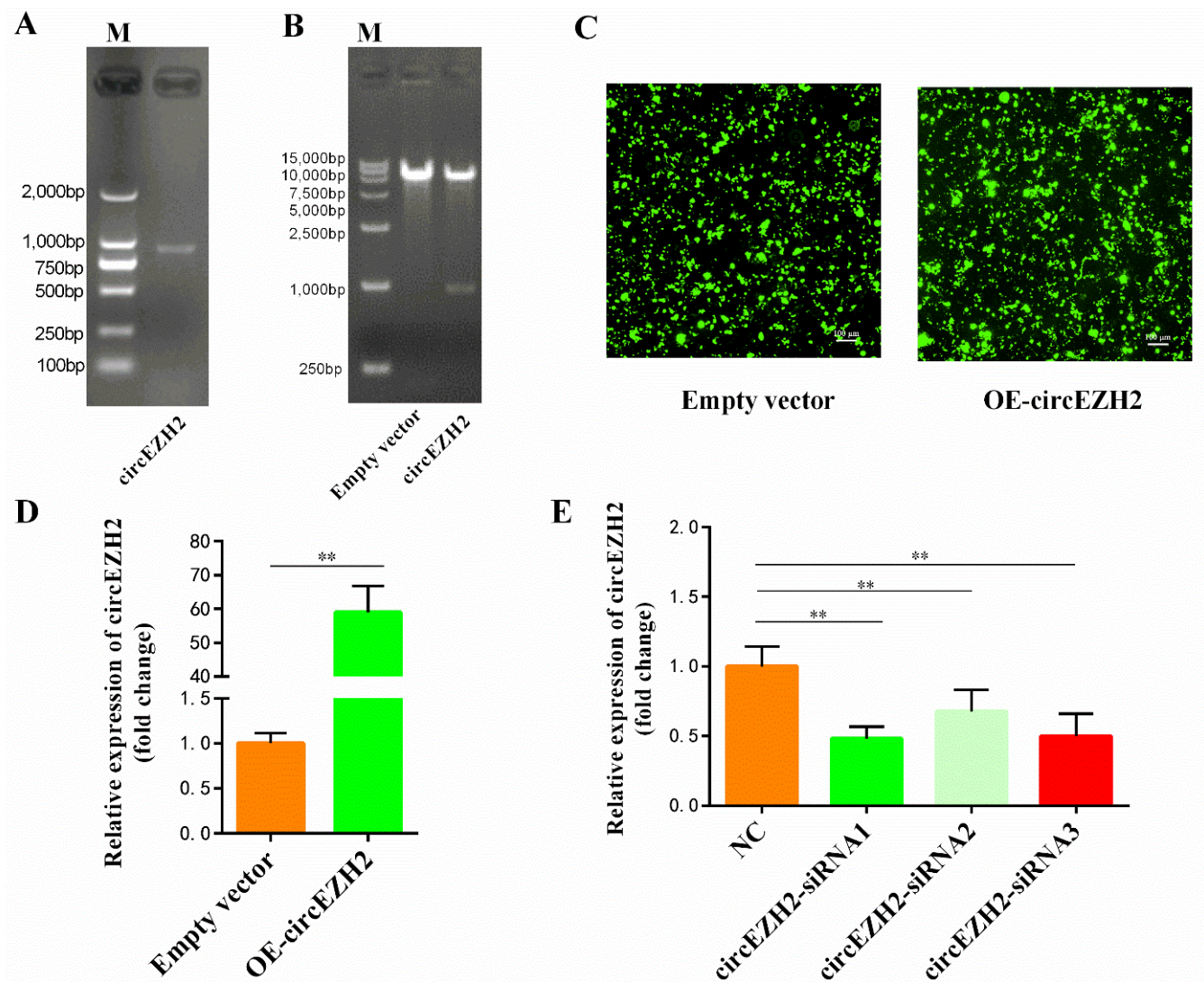


Figure 2. Construction of circEZH2 overexpression vector and interference sequence. (A) Agarose electrophoresis of full-length circEZH2. (B) Agarose electrophoresis following double enzyme digestion of circEZH2 overexpression vector and empty vector. (C) The GFP protein expression tested by fluorescence microscopy. (D) qRT-PCR analysis of the expression efficiency of the circEZH2 overexpression vector. (E) qRT-PCR analysis of the efficiency of the interference sequences. Data represent means \pm standard deviation, **, $p < 0.01$.

3.3. CircEZH2 Affects HC11 Cell Proliferation and Apoptosis

CCK8 assays were used to assess HC11 cell proliferation at 24 h, 48 h, and 72 h after transfection with the OE-circEZH2 plasmid or empty vector. The OD value of the OE-circEZH2 group was significantly higher than that of the empty plasmid group at each time-point, implying that the cell proliferation efficiency was significantly improved (Figure 3A). Flow cytometric analysis also showed that the proportion of cells in the G0/G1 phase was significantly reduced in the OE-circEZH2 group, while the proportion of cells in the S phase and G2/M phase was significantly increased (Figure 3B,C). Overexpression of circEZH2 in HC11 cells promoted the expression of the proliferation marker proteins PCNA, CyclinD, CyclinE, and the anti-apoptotic protein Bcl2, while expression of the pro-apoptotic proteins Bax and Cleaved-caspase 3 was inhibited (Figure 3D,E).

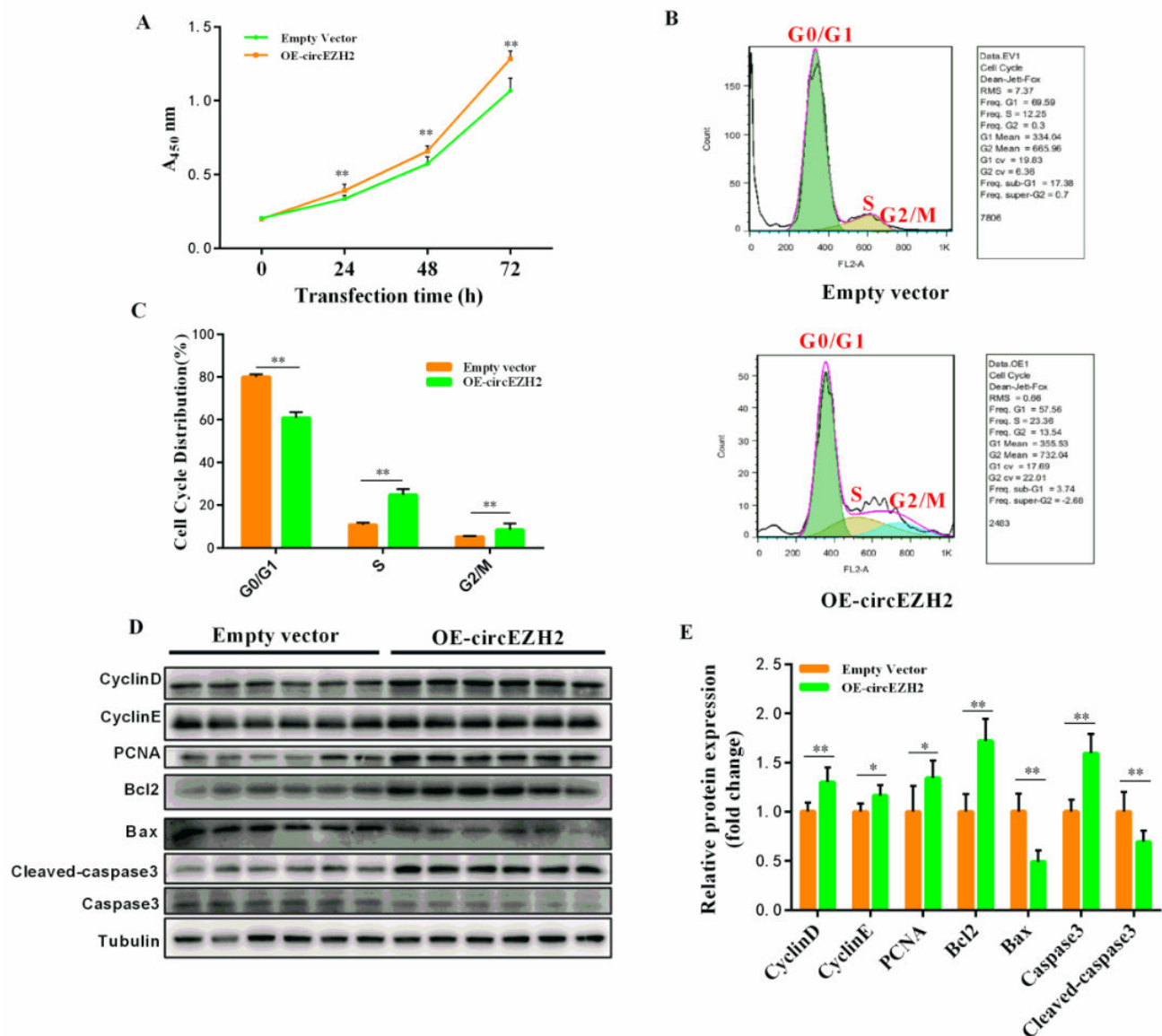


Figure 3. CircEZH2 overexpression vector affects cell proliferation and apoptosis. (A) CCK8 analysis of HC11 cell proliferation. (B) Flow cytometric analysis of cell cycle distribution. (C) Quantitative analysis of cell cycle distribution. (D) Western blot analysis of the expression of proliferation- and apoptosis-related proteins. (E) Quantitative analysis of the expression of proliferation- and apoptosis-related proteins. Data represent means \pm standard deviation, *, $p < 0.05$; **, $p < 0.01$.

The opposite results were obtained after transfecting HC11 cells with NC and si-circEZH2. CCK8 assays were used to assess HC11 cell proliferation at 24 h, 48 h, and 72 h after transfection with si-circEZH2 or NC. The OD value of the si-circEZH2 group was significantly lower than that in the NC group at each time-point (Figure 4A). Furthermore, flow cytometric cell cycle analysis revealed an increased proportion of cells in G0/G1 phase in the si-circEZH2 group, while the proportion of cells in the S phase and G2/M phase was reduced compared with the NC group (Figure 4B,C). Western blot and qRT-PCR analyses confirmed siRNA-mediated silencing of circEZH2 resulted in significantly increased expression of Bax and Cleaved-caspase 3, while the expression of PCNA, CyclinD, CyclinE, and Bcl2 was inhibited (Figure 4D,E).

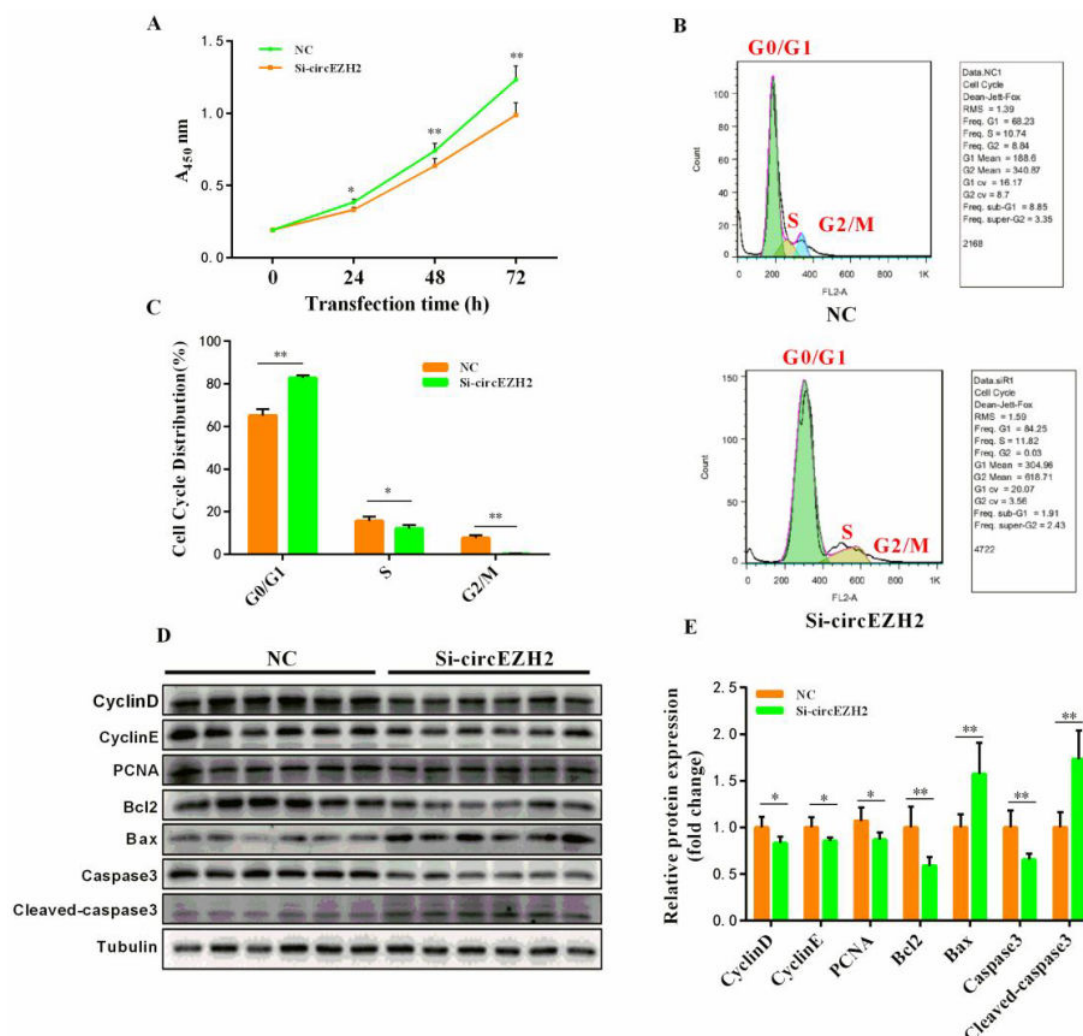


Figure 4. Silencing of circEZH2 expression affects cell proliferation and apoptosis. (A) CCK8 analysis of HC11 cell proliferation. (B) Flow cytometric analysis of cell cycle distribution (C) Quantitative analysis of cell cycle distribution. (D) Western blot analysis of the expression of proliferation- and apoptosis-related proteins. (E) Quantitative analysis of the expression of proliferation- and apoptosis-related proteins. Data represent means \pm standard deviation, *, $p < 0.05$; **, $p < 0.01$.

3.4. CircEZH2 Affects Cell Lipid Metabolism

In our previous study, we showed that heat stress reduced the total amount of oleic acid and unsaturated fatty acids in milk produced by dairy cows, and provided evidence that implicated circEZH2 in milk fat metabolism [13]. Therefore, in the current study, we further explored the role of circEZH2 in milk fat metabolism. Bodipy-C12, which is a red fluorescent derivative of lauric acid, is widely used in the study of fatty acid uptake [18], transport [19], and metabolism [20] in cells. The fluorescence intensity of HC11 cells transfected with OE-circEZH2 was significantly higher than that of the NC group (Figure 5A,B), indicating that circEZH2 overexpression significantly improved the fatty acid uptake capacity of these cells. Western blot and qRT-PCR analyses showed that circEZH2 overexpression significantly promoted the expression of fatty acid metabolism-related proteins (CD36, FADS1, LPL and SCD1) in HC11 cells (Figure 5C,D). The opposite results were obtained following siRNA-mediated silencing of circEZH2. In fluorescent fatty acid uptake assays, the red fluorescence of the si-circRNA group was significantly decreased compared with that in the NC group (Figure 5E,F). Western blot and qRT-PCR analyses confirmed that the expression of fatty acid metabolism-related proteins (CD36, FADS1, LPL and SCD1) was also inhibited (Figure 5G,H).

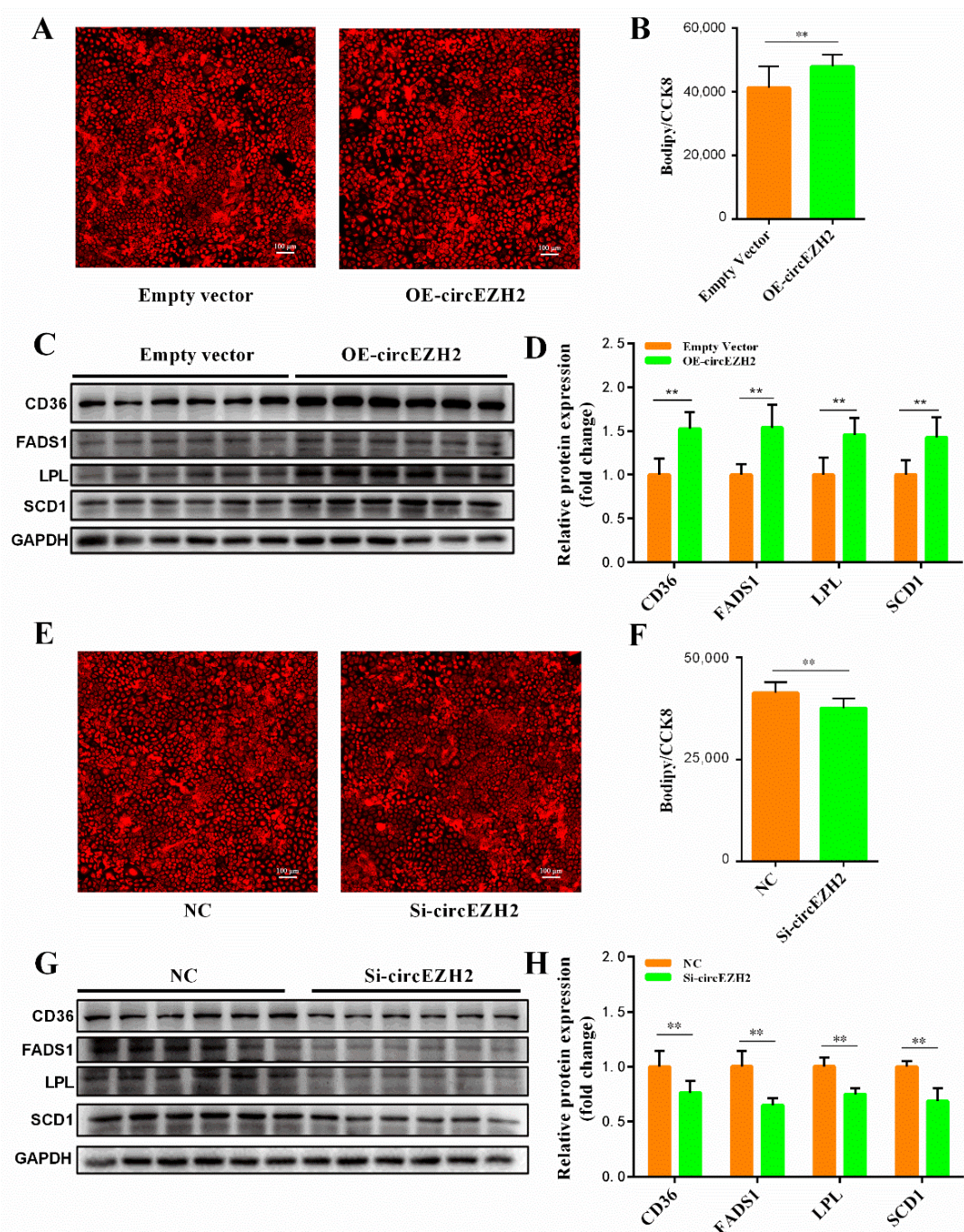


Figure 5. CircEZHZ2 affects cell lipid metabolism. (A,E) Fluorescence imaging of fatty acid uptake assay. (B,F) Quantitative analysis of fatty acid uptake. The value was normalized to CCK8 analysis. (C,G) Western blot analysis of lipid metabolism-related protein expression. (D,H) Quantitative analysis of lipid metabolism-related protein expression. Data represent means \pm standard deviation; **, $p < 0.01$.

3.5. CircEZHZ2 Relieves the Negative Effects of Heat Stress

At ambient temperatures, the expression of heat stress proteins in the cell is very low. However, when cells are subjected to heat stress, the concentration of heat stress proteins (especially HSP70) increases rapidly [21]. After exposure of HC11 cells C to 42 °C for 6 h, RT-qPCR analysis showed that *HSP70* expression increased significantly in response to heat stress (Figure 6A). Using this model, we found that circEZHZ2 expression also decreased significantly in HC11 cells exposed to heat stress (Figure 6B), which was consistent with

our previous observations in vivo [13]. Furthermore, Western blot and qRT-PCR analyses showed that heat stress resulted in decreased expression of PCNA, CyclinD, CyclinE, and Bcl2, while the expression of Bax and Cleaved-caspase increased (Figure 6C,D). Similarly, heat stress also reduced the expression of CD36, FADS1, LPL, and SCD1 proteins in HC11 cells (Figure 6E,F). However, circEZH2 overexpression increased the expression of PCNA, CyclinD, CyclinE, and Bcl2 proteins in HC11 cells under heat stress, while the expression of Bax and Cleaved-caspase 3 was inhibited (Figure 6C,D). In addition, circEZH2 overexpression increased the expression of CD36, FADS1, LPL, and SCD1 proteins in HC11 under heat stress, indicating that it effectively alleviates the adverse effects of heat stress on cell lipid metabolism (Figure 6E,F). These findings indicate that circEZH2 restores the proliferation ability and inhibits apoptosis of HC11 cells under heat stress as well as alleviating the adverse effects of heat stress on lipid metabolism.

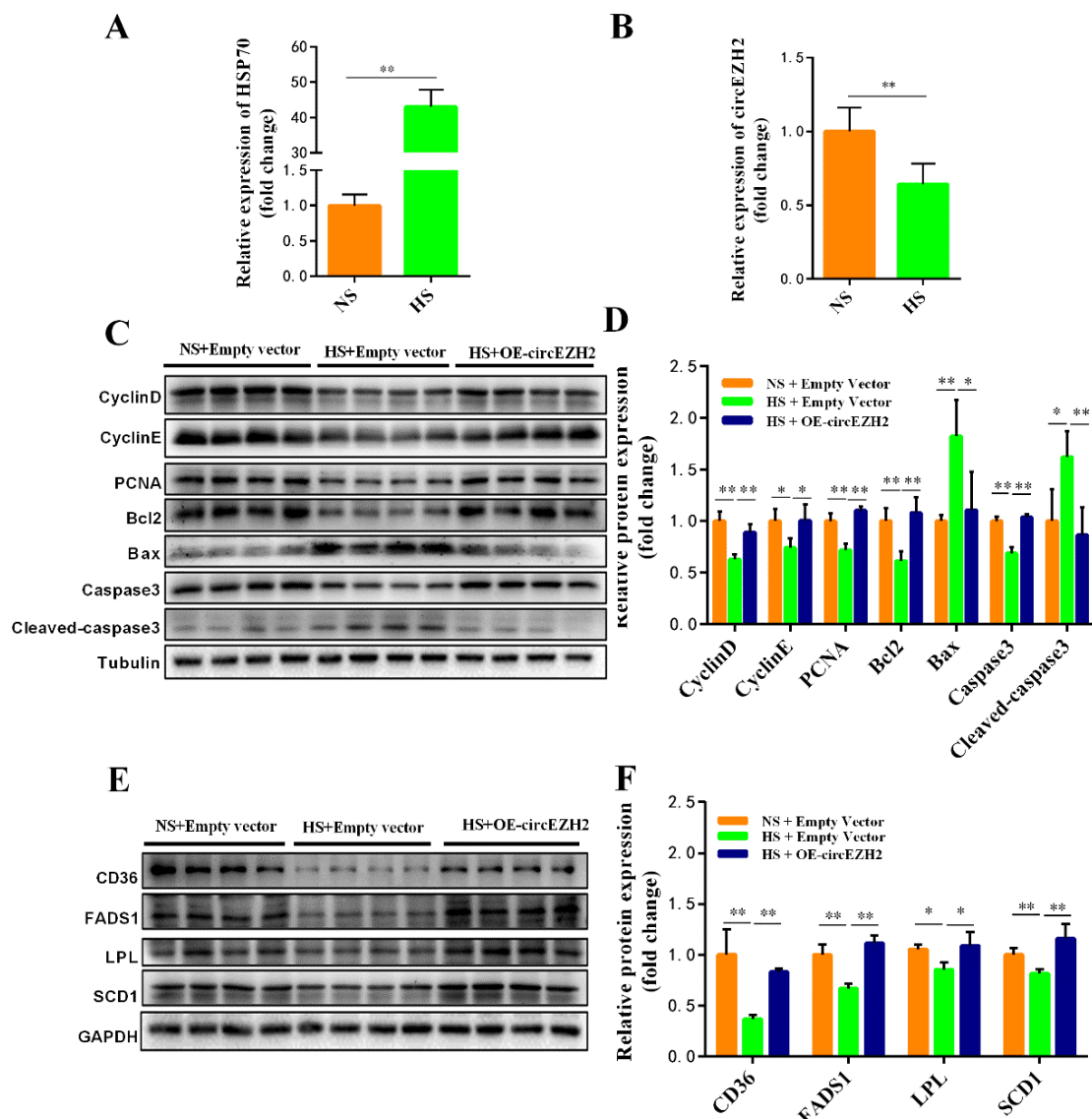


Figure 6. CircEZH2 relieves the negative effects of heat stress. (A) qRT-PCR analysis of HSP70 expression. (B) qRT-PCR analysis of circEZH2 expression. (C,D) Western blot analysis of the expression of proliferation- and apoptosis-related proteins under heat stress. (E,F) Western blot analysis of the expression of lipid metabolism-related proteins under heat stress. Data represent means \pm standard deviation, *, $p < 0.05$; **, $p < 0.01$.

3.6. Analysis of the CircEZH2 Competitive Regulatory Network

Many studies have demonstrated that circRNAs function as miRNA sponges and play an important role in regulating mRNA expression [22]. Based on shared miRNA regulatory elements, two pairs of circEZH2-miRNA-mRNA networks were discovered: circEZH2-miR-378b-CD36 and circEZH2-miR-378b-LPL (Figure 7A). We then designed and synthesized miR-378b mimics and inhibitors and used RT-qPCR to confirm the efficiency of HC11 cell transfection (Figure 7B). Compared with the NC group, the expression of LPL and CD36 proteins decreased significantly after miR-378b mimics transfection. In contrast, the expression of LPL and CD36 proteins increased significantly after treatment with miR-378b inhibitor (Figure 7C,D). Co-transfection of miR-378b mimics and circEZH2 revealed that circEZH2 effectively alleviated the inhibitory effect of miR-378b mimics on LPL and CD36 expression (Figure 7E,F), thus confirming the existence of a connection between the competitive regulatory networks.

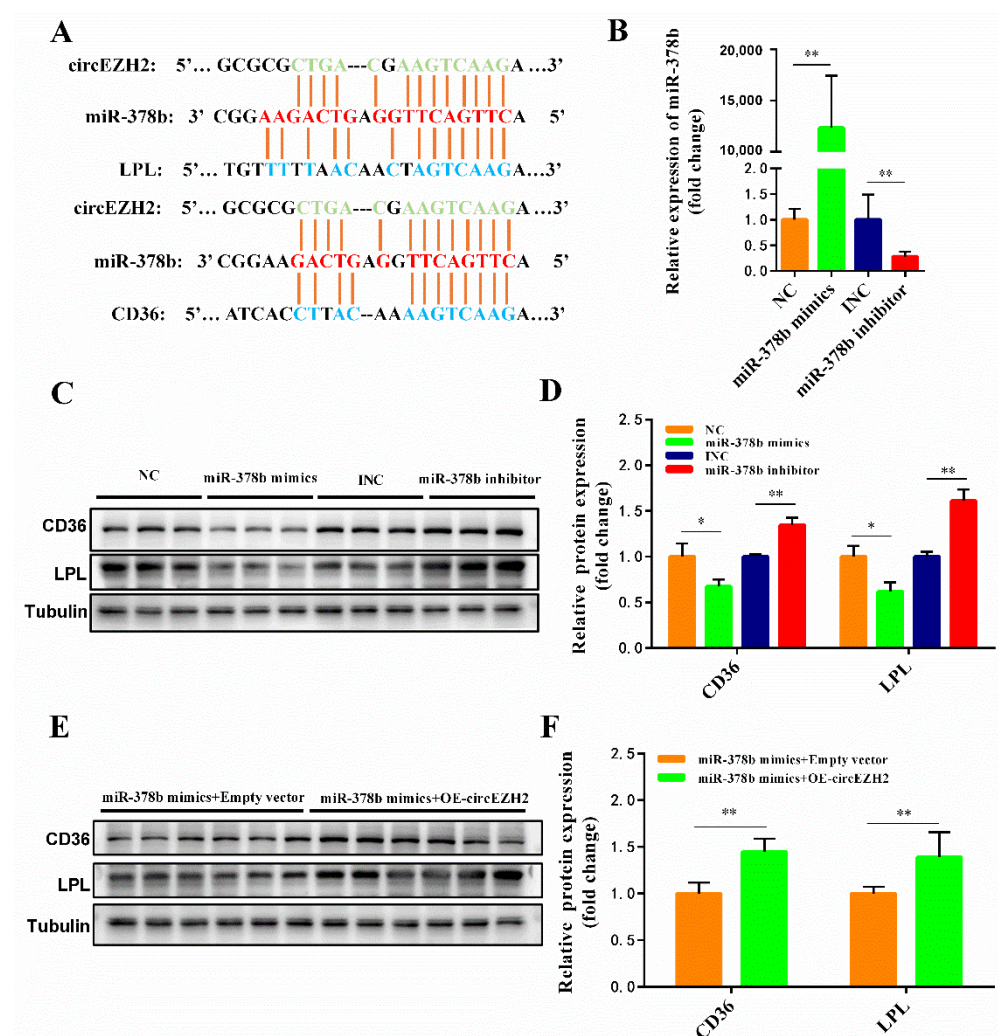


Figure 7. Prediction of circEZH2 competitive regulatory network. (A) Schematic diagram of target relationship prediction. (B) qRT-PCR analysis of the efficiency of miR-378b mimics and inhibitor. (C,D) Western blot analysis of the changes in LPL and CD36 protein expression following co-transfection with miR-378b and circEZH2. (E,F) Western blot analysis of the changes in LPL and CD36 protein expression following co-transfection with or miR-378b and circEZH2. Data represent means \pm standard deviation, *, $p < 0.05$; **, $p < 0.01$.

3.7. Verification of Target Relationship and Prediction of Translation Ability

We further confirmed the direct target relationships with dual luciferase reporter assays. We designed and synthesized wild-type, mutant, and deleted sequences for circEZH2, LPL, and CD36 that are complementary to the miR-378b sequence and ligated these sequences into the pmirGLO vector. Co-transfection of HeLa cells with the miR-378b mimics and the constructed plasmids showed that miR-378b overexpression significantly reduced the luciferase activity in the circEZH2-WT group, but had no significant effect on the luciferase activity in the circEZH2-DEL and circEZH2-MUT groups (Figure 8A). Using this system, we showed that miR-378b overexpression had similar effects on the luciferase activity of the cells with constructs expressing CD36 (Figure 8B) and LPL (Figure 8C). These results indicated that miR-378b directly regulated circEZH2, LPL and CD36 expression, and confirmed the authenticity of circEZH2-miR-378b-LPL and circEZH2-miR-378b-CD36 ceRNA networks.

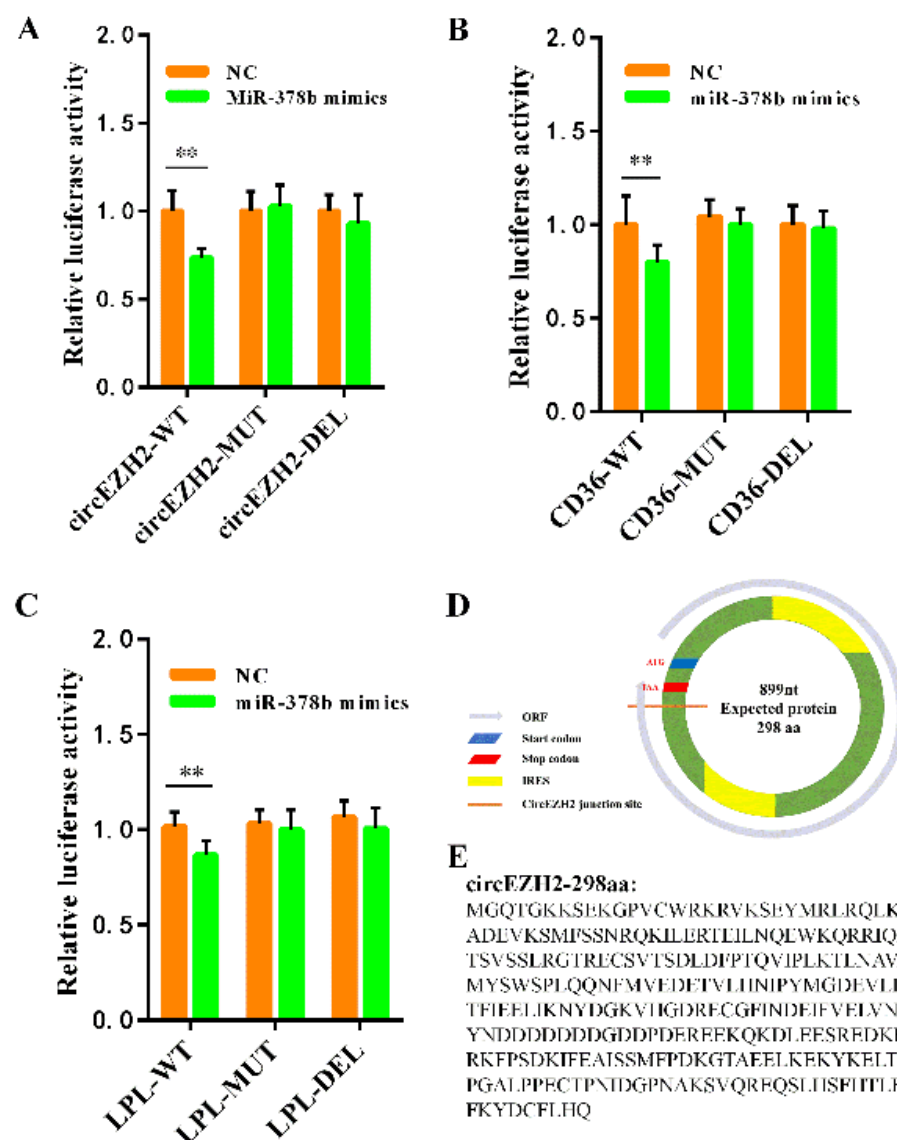


Figure 8. Verification of target relationship and prediction of translation ability. Dual luciferase reporter gene assay verifies the target relationship between miR-378b and circEZH2 (A), CD36 (B), or LPL (C). (D) Schematic diagram of circEZH2 translation potential. (E) Putative polypeptide sequence encoded by circEZH2. Data represent means \pm standard deviation, **, $p < 0.01$.

These results indicated that circEZH2 directly regulates LPL and CD36 expression via ceRNA networks, although the mechanism underlying the effects on cell proliferation, apoptosis, and unsaturated fatty acid metabolism (FADS1 and SCD1) are still unclear. It has been reported that circRNAs have many potential functions, including alternative splicing of mRNA [23], and interactions with RNA-binding proteins (RBPs) to act as a protein sponge [24]. In recent years, the functions of circRNA-encoded proteins have become a research hotspot [25]. In general, circRNAs lack a 5'-cap and canonical ORF (ORF > 100 amino acids) due to their unique loop structure. Consequently, circRNAs were always thought to be devoid of protein coding ability [26]. However, recent studies have shown that some circRNAs have translation functions and can directly recruit ribosomes to initiate translation through the internal ribosome entry site (IRES) [27]. Here, we identified two IRES fragments on the candidate circEZH2 sequence using the IRESfinder (<https://github.com/topics/iresfinder>; Accessed date: 10 October 2020). Through ORF finder software (<https://www.ncbi.nlm.nih.gov/orffinder/>; Accessed date: 10 October 2020) analysis, we found that circEZH2 has an initiation codon and terminator near the splicing site, which can form an ORF (Figure 8D). The target sequence may have coding ability and encode a 290 amino acid circEZH2 polypeptide (Figure 8E).

4. Discussion

With the intensification of the global greenhouse effect, heat stress has seriously threatened the performance and health of dairy cows. To date, some studies have indicated that the negative effects of heat stress can be alleviated through physical prevention [28] and nutritional regulation [29]. However, the molecular mechanism of cow lactation has not been fully elucidated. Mammary gland development and activation of lactation are not only regulated by hormones, growth factors, and nutrient supply [30], but also closely related to the genetic changes in the mammals [31]. In recent years, with the rapid development of bioinformatics, it has been discovered that a new type of non-coding RNAs (circRNAs) exists in large amounts in mammary gland tissue [10]. Heat stress has been shown to affect the lactation performance of animals and change the expression of circRNAs in mammary gland tissue [32]. Therefore, it is speculated that circRNAs may be involved in the process of lactation regulation [33].

Numerous circRNAs have been identified in the mammary gland tissue of dairy cows, and changes in expression have been detected during the period of lactation period [9]. Among these, circCSN1S1 expression is positively correlated with milk production and regulates casein secretion through its interaction with miR-2284 [34]. High-throughput sequencing of dairy cow mammary gland tissues in the early and peak periods of lactation revealed that a variety of circRNAs are related to milk fat metabolism and significantly increase the transcription of milk fat synthesis-related genes [35]. For example, circ09863 binds to miR-27a-3p to accelerate triglyceride (TG) accumulation and increase the proportion of unsaturated fatty acids in milk [36]. Although circRNAs have been shown to play a role in lactation, the underlying mechanism is not yet clear. Therefore, in this study, we investigated the changes in the expression of circEZH2 in mammary cells under heat stress further elucidate its role in the mechanism by which milk fats are regulated.

It has been reported that the lactation ability of mammals correlates positively with the number and viability of mammary epithelial cells [37]. Heat stress can destroy the structure of proteins [38], damage the function of cell mitochondria, inhibit proliferation and promote apoptosis of bovine mammary epithelial cells [39]. Therefore, the decrease in milk production and milk quality of dairy cows in summer is probably caused by the inhibitory effects of heat stress on the proliferation of mammary cells and the induction of apoptosis, which, in turn, reduces the number and viability of mammary epithelial cells. In this study, we found that heat stress caused a significant decrease in the expression of cell proliferation-related proteins (PCNA, CyclinD, and CyclinE) and anti-apoptotic protein (Bcl2) in HC11 cells, while the expression of apoptosis-related proteins (Bax and Cleaved-caspase) was significantly increased. These findings are consistent with those

of previous studies, and further confirm that high temperature causes serious damage to mammary gland epithelial cells [40]. In this study, we showed that circEZH2 overexpression significantly promoted cell proliferation and inhibited apoptosis, which greatly alleviated the adverse effects of heat stress in HC11 cells.

Generally, the metabolism of fatty acids in mammary gland involves a complex network of reactions, including a series of processes, such as de novo synthesis of fatty acids, uptake and transport of fatty acids, formation of triglycerides, and formation and secretion of lipid droplets, with numerous enzymes playing extremely important roles [41]. In our previous study, we found that heat stress significantly reduced the expression of *LPL*, *CD36*, *SCD1*, and *FADS1* in the mammary glands of dairy cows [13]. As a key enzyme involved in lipid metabolism, LPL hydrolyzes serum triglycerides into glycerol and free fatty acids, which are a key factor in the intake of exogenous fatty acids [42]. CD36 also plays an important role in the process of fatty acid transport. It not only promotes the transmembrane transport of fatty acids, but also regulates the rate of fatty acid uptake by cells [43]. In our previous analysis of milk components, we found that milk fat levels are significantly reduced under heat stress. We speculate that the reduction in the expression of LPL and CD36 caused by heat stress leads to a decrease in fatty acid intake. The fatty acid desaturases SCD1 and the fatty acid deoxygenase FADS1 have a marked influence on the synthesis of unsaturated fatty acids [44,45]. This was confirmed in our previous study of the fatty acid profile of milk. Heat stress causing a decrease in the expression of SCD1 and FADS1, reduced the content of decorating enzymes in the mammary gland, and significantly reduced the content of unsaturated fatty acids in milk [13]. These results were also verified in our cell studies, with heat stress found to significantly reduce the expression of LPL, CD36, SCD1, and FADS1 proteins. Furthermore, through circEZH2 overexpression and siRNA-mediated silencing, we showed that circEZH2 was positively correlated with the expression of CD36, FADS1, LPL, and SCD1. CircEZH2 overexpression also effectively alleviated the adverse effects of heat stress on fat metabolism, which successfully verified the important role of circEZH2 in lipid metabolism.

To date, most studies have shown that circRNAs can function as competitive endogenous RNAs (ceRNAs) by combining with miRNAs to perform their biological functions [46]. Therefore, to explore the mechanism underlying the role of circEZH2 in milk fat metabolism, we analyzed the targeting relationship between circEZH2-miRNA and miRNA-mRNA. We found that the 3'-UTR of *LPL* and *CD36* genes, and the base sequence of circEZH2, contained fragments that are complementary to the seed sequence of miR-378b, and predicted that these might play a novel role in endogenous competitive regulation. It has been reported that miR-378b plays a key role in the regulation of lipid metabolism in rat liver [47]. It has been reported that miR-378 can affect lipogenesis by promoting the expression of fatty acid metabolism-related genes such as *FAS* and *SCD1*, thereby increasing triglyceride production and the size of lipid droplets [48]. In contrast, it has also been speculated that miR-378 promotes lipolysis because its role in lipid metabolism is highly related to catecholamines [49]. This study also showed that miR-378b plays a unique role in lipid metabolism, possibly by regulating the uptake of fatty acids via the ceRNA network. In this study, we successfully verified the target relationship between the two ceRNA networks circEZH2-miR378b-LPL and circEZH2-miR378b-CD36 through using the dual luciferase reporter system. The regulation of these two pairs of ceRNA networks may play an important role in the milk fat metabolism under heat stress.

In general, circRNAs are enriched in miRNA-binding sites that play function as miRNA sponges [50]. However, in this study, we did not predict the miRNA that interacts with ceRNA to explain the effect of circEZH2 on cell proliferation and apoptosis and unsaturated fatty acid metabolism in HC11 cells. It is speculated that circEZH2 may perform these roles through other functions, such as encoding polypeptides or proteins [51]. Therefore, we used bioinformatics software to predict putative peptides encoded by circEZH2. This analysis indicated that circEZH2 encodes a 298 amino acid polypeptide, which may initiate translation through the IRES site; however, the specific mechanism requires further research.

5. Conclusions

We found that HC11 cell proliferation is inhibited, and apoptosis is promoted following exposure to heat stress. Lipoprotein hydrolysis, fatty acid uptake, and unsaturated fatty acid production were also significantly reduced. Thus, we conclude that the heat stress-related circEZH2 effectively alleviates the adverse effects of heat stress in HC11 cells through two ceRNA competitive regulatory networks (circEZH2-miR378b-CD36, circEZH2-miR378b-LPL) to restore cell proliferation, apoptosis, and lipid metabolism.

Supplementary Materials: The following supporting information can be downloaded at <https://www.mdpi.com/article/10.3390/ani12060718/s1>. Additional File S1: (A) Schematic diagram of the construction of the circEZH2 overexpression plasmid. (B) Sanger sequencing result after *KpnI* restriction site. (C) Sanger sequencing result after *BamHI* restriction site. Table S1: Primers for Real-time PCR and RT-PCR.

Author Contributions: All authors were involved in project conception and design. D.W. and J.S. led the laboratory assays, analyses of data, and writing of the manuscript. Y.Z. and J.S. contributed reagents, materials, and analysis tools. All authors have read and agreed to the published version of the manuscript.

Funding: This work was supported by the Natural Science Foundation of China Program [grant numbers 32072714, 31802032]; the Natural Science Foundation of Guangdong Province [grant number 2020A1515010062]; The Guangdong Basic and Applied Basic Research Foundation-Enterprise (Wens) Joint Fund [2019B1515210017]; the Science and Technology Project of Guangzhou [grant number 202002030037]. The sponsors had no role in the study design; in the collection, analysis, or interpretation of the data; in the writing of the report; or in the decision to submit the article for publication.

Institutional Review Board Statement: All procedures were performed in accordance with the procedures approved by the Institutional Animal Care and Use Committee of South China Agricultural University (Ethics Approval Code: SCAU2018F006, 13 March 2018).

Informed Consent Statement: Not applicable.

Data Availability Statement: All data are contained in the manuscript.

Conflicts of Interest: The authors declare no conflict of interest. The funding sponsors had no role in the design of the study; in the collection, analyses, and interpretation of data; in the writing of the manuscript; or in the decision to publish the results.

Abbreviations

circRNAs	circular RNAs
ceRNA	competing endogenous RNAs
EZH2	Enhancer of zeste 2 polycomb repressive complex 2 subunit
LPL	Lipoprotein lipase
PCNA	Proliferating cell nuclear antigen
siRNA	Small interfering RNA
FADS1	Fatty acid desaturase 1
SCD1	Stearoyl-Coenzyme A desaturase 1
ncRNA	non-coding RNA
RT-qPCR	Real-time quantitative PCR
UTR	Untranslated regions
EGF	Epidermal growth factor
SDS	Sodium dodecyl sulfate
PVDF	Polyvinylidene fluoride
CCK-8	Cell Counting Kit-8
EDTA	Ethylenediamine tetraacetic acid
FBS	Fetal bovine serum
PBS	Phosphate balanced normal saline

DMEM	Dulbecco's modified eagle medium
IRES	Internal ribosome entry site
ORF	Open reading frame
gDNA	genomic DNA
GFP	Green fluorescent protein
HSP70	Heat shock protein 70

References

1. Lauridsen, C. Effects of Dietary Fatty Acids on Gut Health and Function of Pigs Pre- and Post-Weaning. *J. Anim. Sci.* **2020**, *98*, 1–12. [[CrossRef](#)] [[PubMed](#)]
2. German, J.B.; Dillard, C.J. Composition, Structure and Absorption of Milk Lipids: A Source of Energy, Fat-Soluble Nutrients and Bioactive Molecules. *Crit. Rev. Food Sci. Nutr.* **2006**, *46*, 57–92. [[CrossRef](#)] [[PubMed](#)]
3. Chen, Z.; Chu, S.; Wang, X.; Fan, Y.; Zhan, T.; Arbab, A.A.I.; Li, M.; Zhang, H.; Mao, Y.; Loo, J.J.; et al. MicroRNA-106b regulates milk fat metabolism via ATP binding cassette subfamily A member 1 (ABCA1) in bovine mammary epithelial cells. *J. Agric. Food Chem.* **2019**, *67*, 3981–3990. [[CrossRef](#)]
4. Xu, B.; Gerin, I.; Miao, H.; Vu-Phan, D.; Johnson, C.N.; Xu, R.; Chen, X.W.; Cawthorn, W.P.; MacDougald, O.A.; Koenig, R.J. Multiple Roles for the Non-Coding RNA SRA in Regulation of Adipogenesis and Insulin Sensitivity. *PLoS ONE* **2010**, *5*, e14199. [[CrossRef](#)] [[PubMed](#)]
5. Ibeagha-Awemu, E.M.; Li, R.; Ammah, A.A.; Dudemaine, P.L.; Bissonnette, N.; Benchaar, C.; Zhao, X. Transcriptome adaptation of the bovine mammary gland to diets rich in unsaturated fatty acids shows greater impact of linseed oil over safflower oil on gene expression and metabolic pathways. *BMC Genom.* **2016**, *17*, 104. [[CrossRef](#)] [[PubMed](#)]
6. Jeck, W.R.; Sorrentino, J.A.; Wang, K.; Slevin, M.K.; Burd, C.E.; Liu, J.; Marzluff, W.F.; Sharpless, N.E. Circular RNAs are abundant, conserved, and associated with ALU repeats. *RNA* **2013**, *19*, 141–157. [[CrossRef](#)]
7. Zeng, B.; Chen, T.; Luo, J.; Xie, M.; Wei, L.; Xi, Q.; Sun, J.; Zhang, Y. Exploration of Long Non-coding RNAs and Circular RNAs in Porcine Milk Exosomes. *Front. Genet.* **2020**, *11*, 652. [[CrossRef](#)]
8. Yang, R.; Xing, L.; Zheng, X.; Sun, Y.; Wang, X.; Chen, J. The circRNA circAGFG1 acts as a sponge of miR-195-5p to promote triple-negative breast cancer progression through regulating CCNE1 expression. *Mol. Cancer* **2019**, *18*, 4. [[CrossRef](#)]
9. Zhang, C.; Wu, H.; Wang, Y.; Zhu, S.; Liu, J.; Fang, X.; Chen, H. Circular RNA of cattle casein genes are highly expressed in bovine mammary gland. *J. Dairy Sci.* **2016**, *99*, 4750–4760. [[CrossRef](#)]
10. Hao, Z.; Zhou, H.; Hickford, J.G.H.; Gong, H.; Wang, J.; Hu, J.; Liu, X.; Li, S.; Zhao, M.; Luo, Y. Identification and characterization of circular RNA in lactating mammary glands from two breeds of sheep with different milk production profiles using RNA-Seq. *Genomics* **2020**, *112*, 2186–2193. [[CrossRef](#)]
11. Zhu, C.; Jiang, Y.; Zhu, J.; He, Y.; Yin, H.; Duan, Q.; Zhang, L.; Cao, B.; An, X. CircRNA8220 Sponges MiR-8516 to Regulate Cell Viability and Milk Synthesis via Ras/MEK/ERK and PI3K/AKT/mTOR Pathways in Goat Mammary Epithelial Cells. *Animals* **2020**, *10*, 1347. [[CrossRef](#)] [[PubMed](#)]
12. Sun, J.; Zhang, H.; Hu, B.; Xie, Y.; Wang, D.; Zhang, J.; Chen, T.; Luo, J.; Wang, S.; Jiang, Q.; et al. Emerging Roles of Heat-Induced circRNAs Related to Lactogenesis in Lactating Sows. *Front. Genet.* **2020**, *10*, 1347. [[CrossRef](#)] [[PubMed](#)]
13. Wang, D.; Chen, Z.; Zhuang, X.; Luo, J.; Chen, T.; Xi, Q.; Zhang, Y.; Sun, J. Identification of circRNA-Associated-ceRNA Networks Involved in Milk Fat Metabolism under Heat Stress. *Int. J. Mol. Sci.* **2020**, *21*, 4162. [[CrossRef](#)] [[PubMed](#)]
14. Zhao, J.; Wu, J.; Xu, T.; Yang, Q.; He, J.; Song, X. IRESfinder: Identifying RNA internal ribosome entry site in eukaryotic cell using framed k-mer features. *J. Genet. Genom.* **2018**, *45*, 403–406. [[CrossRef](#)] [[PubMed](#)]
15. Chen, X.; Han, P.; Zhou, T.; Guo, X.; Song, X.; Li, Y. circRNADb: A comprehensive database for human circular RNAs with protein-coding annotations. *Sci. Rep.* **2016**, *6*, 34985. [[CrossRef](#)] [[PubMed](#)]
16. Kong, S.; Tao, M.; Shen, X.; Ju, S. Translatable circRNAs and lncRNAs: Driving mechanisms and functions of their translation products. *Cancer Lett.* **2020**, *483*, 59–65. [[CrossRef](#)]
17. Zganiacz, D.; Milanowski, R. Characteristics of circular ribonucleic acid molecules (circRNA). *Postepy Biochem.* **2017**, *63*, 221–232.
18. Kolahi, K.S.; Amy, V.; Thornburg, K.L. Real-time microscopic assessment of fatty acid uptake kinetics in the human term placenta. *Placenta* **2018**, *72–73*, 1–9. [[CrossRef](#)]
19. Rambold, A.S.; Cohen, S.; Lippincott-Schwartz, J. Fatty acid trafficking in starved cells: Regulation by lipid droplet lipolysis, autophagy, and mitochondrial fusion dynamics. *Dev. Cell* **2015**, *32*, 678–692. [[CrossRef](#)]
20. Xu, D.; Li, Y.; Wu, L.; Li, Y.; Zhao, D.; Yu, J.; Huang, T.; Ferguson, C.; Parton, R.G.; Yang, H.; et al. Rab18 promotes lipid droplet (LD) growth by tethering the ER to LDs through SNARE and NRZ interactions. *J. Cell Biol.* **2018**, *217*, 975–995. [[CrossRef](#)]
21. Isosaki, M.; Nakashima, T. Psychological stress induces heat shock protein 70 expression in rat aorta. *Jpn. J. Pharmacol.* **1998**, *76*, 305. [[CrossRef](#)] [[PubMed](#)]
22. Huang, C.; Shan, G. What happens at or after transcription: Insights into circRNA biogenesis and function. *Transcription* **2015**, *6*, 61–64. [[CrossRef](#)] [[PubMed](#)]
23. Barrett, S.P.; Salzman, J. Circular RNAs: Analysis, expression and potential functions. *Development* **2016**, *143*, 1838. [[CrossRef](#)] [[PubMed](#)]

24. Geng, X.; Jia, Y.; Zhang, Y.; Shi, L.; Li, Q.; Zang, A.; Wang, H. Circular RNA: Biogenesis, degradation, functions and potential roles in mediating resistance to anticarcinogens. *Epigenomics* **2020**, *12*, 267–283. [[CrossRef](#)] [[PubMed](#)]
25. Zhang, M.; Zhao, K.; Xu, X.; Yang, Y.; Yan, S.; Wei, P.; Liu, H.; Xu, J.; Xiao, F.; Zhou, H.; et al. A peptide encoded by circular form of LINC-PINT suppresses oncogenic transcriptional elongation in glioblastoma. *Nat. Commun.* **2018**, *9*, 4475. [[CrossRef](#)]
26. Godet, A.C.; David, F.; Hantelys, F.; Tatin, F.; Lacazette, E.; Garmy-Susini, B.; Prats, A.C. IRES Trans-Acting Factors, Key Actors of the Stress Response. *Int. J. Mol. Sci.* **2019**, *20*, 924. [[CrossRef](#)]
27. Xiang, L.; Li, Y.; Chen, L.L. The Biogenesis, Functions, and Challenges of Circular RNAs. *Mol. Cell* **2018**, *71*, 428–442.
28. West, J.W. Effects of heat-stress on production in dairy cattle. *J. Dairy Sci.* **2003**, *86*, 2131–2144. [[CrossRef](#)]
29. Jin, L.; Yan, S.; Shi, B.; Bao, H.; Gong, J.; Guo, X.; Li, J. Effects of vitamin A on the milk performance, antioxidant functions and immune functions of dairy cows. *Anim. Feed Sci. Technol.* **2014**, *192*, 15–23. [[CrossRef](#)]
30. Lacasse, P.; Lollivier, V.; Dessauge, F.; Bruckmaier, R.M.; Ollier, S.; Boutinaud, M. New developments on the galactopoietic role of prolactin in dairy ruminants. *Domest. Anim. Endocrin.* **2012**, *43*, 154–160. [[CrossRef](#)]
31. Cowley, F.C.; Barber, D.G.; Houlihan, A.V.; Poppi, D.P. Immediate and residual effects of heat stress and restricted intake on milk protein and casein composition and energy metabolism. *J. Dairy Sci.* **2015**, *98*, 2356–2368. [[CrossRef](#)] [[PubMed](#)]
32. Pan, T.; Sun, X.; Liu, Y.; Li, H.; Deng, G.; Lin, H.; Wang, S. Heat stress alters genome-wide profiles of circular RNAs in Arabidopsis. *Plant. Mol. Biol.* **2018**, *96*, 217–229. [[CrossRef](#)] [[PubMed](#)]
33. Dou, C.; Cao, Z.; Yang, B.; Ding, N.; Hou, T.; Luo, F.; Kang, F.; Li, J.; Yang, X.; Jiang, H.; et al. Changing expression profiles of lncRNAs, mRNAs, circRNAs and miRNAs during osteoclastogenesis. *Sci. Rep.* **2016**, *6*, 21499. [[CrossRef](#)] [[PubMed](#)]
34. Jin, W.; Ibeagha-Awemu, E.M.; Liang, G.; Beaudoin, F.; Zhao, X.; Guan, L.L. Transcriptome microRNA profiling of bovine mammary epithelial cells challenged with Escherichia coli or Staphylococcus aureus bacteria reveals pathogen directed microRNA expression profiles. *BMC Genom.* **2014**, *15*, 181. [[CrossRef](#)]
35. Lin, X.; Luo, J.; Zhang, L.; Wang, W.; Gou, D. MiR-103 controls milk fat accumulation in goat (*Capra hircus*) mammary gland during lactation. *PLoS ONE* **2013**, *8*, e79258.
36. Chen, Z.; Zhou, J.; Wang, M.; Liu, J.; Zhang, L.; Looor, J.J.; Liang, Y.; Wu, H.; Yang, Z. Circ09863 Regulates Unsaturated Fatty Acid Metabolism by Adsorbing miR-27a-3p in Bovine Mammary Epithelial Cells. *J. Agric. Food Chem.* **2020**, *68*, 8589–8601. [[CrossRef](#)]
37. Petridis, I.G.; Fthenakis, G.C. Mammary involution and relevant udder health management in sheep. *Small Rumin. Res.* **2019**, *181*, 66–75. [[CrossRef](#)]
38. Collier, R.J.; Collier, J.L.; Rhoads, R.P.; Baumgard, L.H. Invited review: Genes involved in the bovine heat stress response. *J. Dairy Sci.* **2008**, *91*, 445–454. [[CrossRef](#)]
39. Li, L.; Sun, Y.; Wu, J.; Li, X.; Luo, M.; Wang, G. The global effect of heat on gene expression in cultured bovine mammary epithelial cells. *Cell Stress Chaperon.* **2015**, *20*, 381–389. [[CrossRef](#)]
40. Pantschenko, A.G.; Woodcock-Mitchell, J.; Bushmich, S.L.; Yang, T.J. Establishment and characterization of a caprine mammary epithelial cell line (CMEC). *In Vitro Cell Dev. Biol. Anim.* **2000**, *36*, 26–37. [[CrossRef](#)]
41. Kadegowda, A.K.; Bionaz, M.; Piperova, L.S.; Erdman, R.A.; Looor, J.J. Peroxisome proliferator-activated receptor-gamma activation and long-chain fatty acids alter lipogenic gene networks in bovine mammary epithelial cells to various extents. *J. Dairy Sci.* **2009**, *92*, 4276–4289. [[CrossRef](#)] [[PubMed](#)]
42. Faulconnier, Y.; Bonnet, M.; Bocquier, F.; Leroux, C.; Chilliard, Y. Effects of photoperiod and feeding level on adipose tissue and muscle lipoprotein lipase activity and mRNA level in dry non-pregnant sheep. *Brit. J. Nutr.* **2001**, *85*, 299–306. [[CrossRef](#)] [[PubMed](#)]
43. Xu, S.; Jay, A.; Brunaldi, K.; Huang, N.; Hamilton, J.A. CD36 enhances fatty acid uptake by increasing the rate of intracellular esterification but not transport across the plasma membrane. *Biochemistry* **2013**, *52*, 7254–7261. [[CrossRef](#)] [[PubMed](#)]
44. Macciotta, N.P.; Mele, M.; Conte, G.; Serra, A.; Cassandro, M.; Zotto, R.D.; Borlino, A.C.; Pagnacco, G.; Secchiari, P. Association Between a Polymorphism at the Stearoyl CoA Desaturase Locus and Milk Production Traits in Italian Holsteins. *J. Dairy Sci.* **2008**, *91*, 3184–3189. [[CrossRef](#)]
45. Glaser, C.; Heinrich, J.; Koletzko, B. Role of FADS1 and FADS2 polymorphisms in polyunsaturated fatty acid metabolism. *Metabolism* **2010**, *59*, 993–999. [[CrossRef](#)]
46. Kulcheski, F.R.; Christoff, A.P.; Margis, R. Circular RNAs are miRNA sponges and can be used as a new class of biomarker. *J. Biotechnol.* **2016**, *238*, 42–51. [[CrossRef](#)]
47. Lu, Y.L.; Jing, W.; Feng, L.S.; Zhang, L.; Xu, J.F.; You, T.J.; Zhao, J. Effects of hypoxic exercise training on microRNA expression and lipid metabolism in obese rat livers. *J. Zhejiang Univ. Sci. B* **2014**, *15*, 820–829. [[CrossRef](#)]
48. Gerin, I.; Bommer, G.T.; McCoin, C.S.; Sousa, K.M.; Krishnan, V.; MacDougald, O.A. Roles for miRNA-378/378* in adipocyte gene expression and lipogenesis. *Am. J. Physiol. Endocrinol. Metab.* **2010**, *299*, E198–E206. [[CrossRef](#)]
49. Kulyté, A.; Lorente-Cebrián, S.; Gao, H.; Mejhert, N.; Agustsson, T.; Arner, P.; Rydén, M.; Dahlman, I. MicroRNA profiling links miR-378 to enhanced adipocyte lipolysis in human cancer cachexia. *Am. J. Physiol. Endocrinol. Metab.* **2014**, *306*, E267–E274. [[CrossRef](#)]
50. Shi, X.; Sun, M.; Liu, H.; Yao, Y.; Song, Y. Long non-coding RNAs: A new frontier in the study of human diseases. *Cancer Lett.* **2013**, *339*, 159–166. [[CrossRef](#)]
51. Yang, Y.; Fan, X.; Mao, M.; Song, X.; Wu, P.; Zhang, Y.; Jin, Y.; Yang, Y.; Chen, L.L.; Wang, Y.; et al. Extensive translation of circular RNAs driven by N⁶-methyladenosine. *Cell Res.* **2017**, *27*, 626–641. [[CrossRef](#)] [[PubMed](#)]



Effects of Herbal Tea Residue on Growth Performance, Meat Quality, Muscle Metabolome, and Rumen Microbiota Characteristics in Finishing Steers

Ling Li[†], Xiaohong Sun[†], Junyi Luo, Ting Chen, Qianyun Xi, Yongliang Zhang* and Jiajie Sun*

Guangdong Provincial Key Laboratory of Animal Nutrition Control, Guangdong Laboratory for Lingnan Modern Agriculture, National Engineering Research Center for Breeding Swine Industry, South China Agricultural University, Guangzhou, China

OPEN ACCESS

Edited by:

Robert W. Li,
Agricultural Research Service,
United States Department
of Agriculture (USDA), United States

Reviewed by:

Yury Tatiana Granja-Salcedo,
Colombian Corporation
for Agricultural Research
(AGROSAVIA), Colombia
Carmen Gallo,
Austral University of Chile, Chile

*Correspondence:

Yongliang Zhang
zhangyongliang@scau.edu.cn
Jiajie Sun
jiajiesun@scau.edu.cn

[†]These authors have contributed
equally to this work

Specialty section:

This article was submitted to
Systems Microbiology,
a section of the journal
Frontiers in Microbiology

Received: 24 November 2021

Accepted: 29 December 2021

Published: 18 January 2022

Citation:

Li L, Sun X, Luo J, Chen T, Xi Q,
Zhang Y and Sun J (2022) Effects
of Herbal Tea Residue on Growth
Performance, Meat Quality, Muscle
Metabolome, and Rumen Microbiota
Characteristics in Finishing Steers.
Front. Microbiol. 12:821293.
doi: 10.3389/fmicb.2021.821293

Herbal tea residue (HTR) contains various medicinal and nutritional components and is a potential high-quality unconventional source of roughage. In this study, a total of 30 healthy Simmental crossbred finishing steers were equally divided into two groups: CN (fed with a basic diet) and RE (HTR partly replaced *Pennisetum purpureum*). HTR did not alter the growth performance of steers but increased the net meat rate, tenderness, and water-holding capacity and increased the moisture content and oleic acid and linoleic acid concentrations in *longissimus dorsi*. It altered muscle metabolic pathways and improved rumen fermentation by increasing the propionic acid concentration and propionic acid-to-acetic acid ratio. We studied the steers' rumen microbial community composition and determined their correlation with the tested parameters. Certain rumen microorganisms were closely associated with muscle glucolipid metabolites and rumen NH₃-N and volatile fatty acid levels. Our findings suggest that, as a functional roughage source, HTR improved to a certain extent the meat quality of steers by altering the rumen microbial composition and affecting the rumen fatty acid composition and muscle glucolipid metabolism.

Keywords: feed resources, herbal tea residue, muscle metabolism, microbial diversity, beef

INTRODUCTION

Herbal tea, one of the most unique beverages, is a specialty drink developed according to the climatic characteristics of Lingnan in south China (Li et al., 2017). Herbal tea is mainly prepared by decocting Chinese herbal medicines such as herbal jelly, honeysuckle, chrysanthemum, prunella vulgaris, buzha leaf, and licorice (Zhao et al., 2013) and contains various bioactive substances such as flavonoids, organic acids, polysaccharides, alkaloids, and volatile oils (Liu et al., 2011). These substances usually have antibacterial, anti-inflammatory, antioxidant, antiviral, and immune-enhancing medicinal effects (Cao et al., 2014), because of which herbal teas are favored by people in the subtropical region of China.

Herbal tea residue (HTR) is the natural byproduct of preparing herbal tea. With the continuously increasing annual consumption of herbal tea, a large quantity of HTR is produced (Yang and Cui, 2013). To date, the main treatment methods for HTR are landfill, incineration, and stacking (Suthar and Singh, 2011), which not only waste resources but also pollute the environment

(Malkoc and Nuhoglu, 2006). It has been reported that HTR can be used as an adsorbent for heavy metal ions to reduce water pollution (Ahsan et al., 2018). HTR is also a high-quality compost material, which significantly improves the ecological characteristics of soil (Iqbal Khan et al., 2015). Moreover, HTR is essentially a type of Chinese herbal residue (CHR), which still contains a variety of nutrients and functional active substances similar to the raw materials and can be used as animal feed (Abdallah et al., 2019). A previous study suggested that adding 0.5% CHRs to duck diets improved the crude protein content and water-holding capacity of duck meat (Jin-Woo et al., 2017). Supplementation of poultry diets with 3% CHRs improved the nutritional value, sensory quality, and tenderness of meat while reducing the antioxidant status (Kim et al., 2014). Moreover, Chinese herbal feed improves the immune function of dairy cows under heat stress (Shan et al., 2018) and contributes to rumen fermentation and energy metabolism of sheep (Liang et al., 2013).

Many recent reports recommend using a small quantity of CHRs as a functional feed additive. As a type of CHR, HTR is not only rich in protein but also contains crude fiber and trace elements that ruminant require (Xie et al., 2020). Ruminants require approximately 17% dietary crude fiber content (Ding et al., 2020). We therefore hypothesized that HTR could be used as an unconventional feed material to improve growth performance and meat quality in ruminant. In this paper, the HTR was added to the diet of steers to investigate its effects on growth performance, meat quality, muscle metabolome, rumen fermentation and rumen microbial diversity.

MATERIALS AND METHODS

Animals, Experimental Design, and Treatments

This study was conducted at a large-scale steer farm in Guangxi, China. According to the principle of completely random allocation, 30 healthy Simmental crossbred steers (18 months old and approximately 480 kg per animal) were divided into two groups, namely CN group (fed with basic diet) and RE group (HTR partly replaced *Pennisetum purpureum*). Each experimental group included three replicates, and each replicate contained five animals. All steers were housed individually in an open cowshed at the same time. The basic composition and nutritional level of steer feed are shown in **Table 1**. The chemical composition of HTR was showed in **Supplementary Table 1**. In details, the HTR contained a high water content (75.10%) and the dry matter content was 24.90%. As a proportion of the dry matter content, the crude protein, crude fat, and ash contents were 13.10, 2.60, 6.69%, respectively. The acid detergent fiber and neutral detergent fiber were 39.8 and 54.3% (Zhuang et al., 2021). The experiment lasted for 67 days, including a 7-day pre-feeding period and a 60-day formal study period. During the experiment, the steers were fed regularly at 8 am and 5 pm, and water was available *ad libitum* throughout the experimental period. All animal procedures were approved by the Animal Care Committee at South China Agricultural University.

TABLE 1 | Basic diet composition and nutrient level of finishing steers.

Item	CN	RE
Ingredients		
Corn (%)	23.7	23.7
Bean curd residue (%)	15.0	15.0
<i>Pennisetum purpureum</i> (%)	60.0	10.0
Herbal tea residue (%)	0	50.0
Premix (%)	1.00	1.00
Salt (%)	0.30	0.30
Total (%)	100	100
Nutritional level		
Dry matter (%)	34.6	30.7
Crude protein (%)	9.14	9.70
r Crude fat (%)	2.05	3.00
Neutral detergent fiber (%)	71.2	68.9
Acid detergent fiber (%)	25.2	27.6
Calcium (%)	0.69	0.63
Phosphorus (%)	0.22	0.30
Net energy (MJ/kg)	5.56	5.36

The indicators were calculated on the basis of dry matter. The nutrient contents of the premix were as follows: Zinc, 70–100 mg/kg; Iron, 50–70 mg/kg; Copper, 30–45 mg/kg; Manganese, 6.25–10 mg/kg; Selenium, 0.3–0.5 mg/kg; Iodine, 0.2–1.00 mg/kg; Vitamin A, 7,000–10,000 IU/kg; Vitamin D, 40,000–90,000 IU/kg; Vitamin E, 4,000–5,000 mg/kg. Net energy was a calculated value, and others were measured values. CN, no herbal tea residues; RE, 50% HTRs replaced *Pennisetum purpureum*.

Measurements and Sampling

The average daily feed intake (ADFI) was recorded once a week, and individual steers were weighed at the beginning and end of the experiment to determine initial weight and average daily gain (ADG). On the last day of the experiment, 200 mL of rumen fluid per individual was obtained from 15 steers in each group before the morning feeding. Whole ruminal samples were collected from steers with a suction strainer (19 mm diameter; 1.5 mm mesh for its filter) and strained through four layers of cheesecloth (Gilbreath et al., 2020). One aliquot (100 mL) was used to determine volatile fatty acids (VFAs) using high-performance liquid chromatography (Actlabs, Ancaster, ON, Canada). Another aliquot (100 mL) was used to extract total genomic DNA for sequencing of rumen microorganisms.

At the end of the experiment, the feed was detained for 12 hours and weighed, and all animals were slaughtered at the same time. Then the carcass weight, eye muscle area (EMA), net meat weight (the weight of muscle and fat in the carcass after bone has been removed), dressing percentage, and net meat percentage were recorded for each animal post slaughter. Dressing percentage is the ratio of carcass weight to live weight at slaughter. Net meat percentage refers to net meat weight as a percentage of carcass weight. After the carcasses were chilled for 45 min at 4°C, the meat color were measured. Following aging for 24 h at 4°C, longissimus dorsi (LD) samples were collected between the 9th and 13th ribs from the right side of the carcasses, of which one was stored at 4°C for subsequent physical analysis, and the other one was frozen for nutrient value analysis.

Meat Quality and Nutritional Composition

The meat color [lightness (L^*), redness (a^*), and yellowness (b^*)], water-holding capacity (drip loss and cooking loss) and tenderness (shear force) were analyzed. In detail, meat color (average of three randomly selected areas on the sample) was assessed using a Minolta Chroma Meter (CR-300, Dietikon, Switzerland), applying the L^* , a^* , and b^* system (Razminowicz et al., 2006). Drip loss was determined as the weight loss after suspending meat samples ($5 \times 2 \times 3$ cm) at 4°C for 24 h. Meat samples in dry polyethylene bags were weighed and heated in a water bath at 85°C for 20 min and then cooled to room temperature (25°C) in running water. The cooked samples were dried and weighed again to calculate cooking loss, expressed as the percentage of uncooked sample weight (%). After measuring the cooking loss, the samples were stored for 24 h at 4°C . Subsequently, shear force was tested with a digital tenderness meter (C-LM3B, Tenovo, Beijing, China), and the average of nine replicates per sample was regarded as the final value (Sales et al., 2020). LD samples were also analyzed for moisture, dry matter, crude protein, crude fat, and ash according to Association of Official Analytical Chemists [AOAC] (2000). The fatty acid composition of frozen samples was measured by fatty acid methyl ester synthesis (O'Fallon et al., 2007). Amino acid levels were determined employing an automatic amino acid analyzer (L-8800; Hitachi, Tokyo, Japan) based on the method described by Yan et al. (2018).

Muscle Metabolome

Non-targeted muscle metabolomics analysis was performed by Novogene Biotechnology (Beijing, China) using LC-MS platform. Specifically, approximately 100 mg of frozen samples were ground and homogenized in 500 μL of 80% methanol containing 0.1% formic acid. The mixtures were kept in an ice bath for 5 min, and then centrifuged at $15,000 \times g$ for 10 min at 4°C . After the content of methanol in the supernatant was diluted to 53%, the mixture was centrifuged again ($15,000 \times g$ for 10 min at 4°C). Then, the supernatant (200 μL) was transferred to an LC-MS sampling vial for LC-MS analysis. Raw data were filtered and aligned by parameter (retention time, mass-to-charge ratio, and peak intensity) selection of Compound Discoverer 3.1 software (Thermo Scientific). The processed data were used to annotate the metabolites using the KEGG, HMDB and LIPID MAPS databases. Moreover, the dataset of two groups was separated with partial least squares discriminant analysis (PLS-DA). The differentially expressed metabolites between two groups are illustrated with a volcano plot.

16S rRNA Gene Sequencing and Annotation Analysis of Rumen Microorganisms

Total genomic DNA was extracted from rumen fluid samples using the SDS method, and the integrity of the extracted DNA was assessed by 1% agarose gel electrophoresis (Black and Foorde, 2007). DNA concentration was determined using Qubit Fluorometer (Invitrogen, Carlsbad, CA). 16S rRNA

genes were subsequently amplified using specific primers with barcode (Forward: 5'-GTGCCAGCMGCCGCGG-3' and Reverse: 5'-GGACTACHVGGGTWTCTAAT-3') targeting the variable regions V3-V4. The sequencing library was prepared using the gDNA samples using the Illumina TruSeq® DNA PCR-Free Sample Preparation Kit. Qubit and Real-Time PCR System were used to assess the quantity and quality of the sample library. Then, the library constructed was sequenced using NovaSeq6000 platform. Clean reads were obtained from the raw data by strict quality filtering and chimeric sequence removal (Haas et al., 2011). The effective tags of all samples were clustered, and the tags with over 97% similarity were regarded as one operational taxonomic unit (OTU) (Edgar, 2013). According to the Silva 132 database, a representative sequence for each OTU was screened for taxonomic identification based on the Mothur algorithm (Quast et al., 2013). To explore the phylogenetic relationship among different OTUs, multiple sequence alignment was performed using MUSCLE software (Version 3.8.31) (Yuan et al., 2018). All the data were normalized, and the least amount of data were considered as the standard. The subsequent alpha-diversity and beta-diversity analysis were based on the normalized data. Alpha-diversity analysis reflected the complexity and diversity of species for the samples, including the observed species, Simpson, Shannon, Chao1 and ACE indices. For beta-diversity analysis, principal coordinate analysis (PCoA) was performed to obtain the principal coordinates and visualize complex, multidimensional data. Non-metric multi-dimensional scaling (NMDS) was employed to visualize and compare the relationship of the rumen microbial community structure between the two groups. Unweighted pair group method with arithmetic means (UPGMA) clustering was conducted as a type of hierarchical clustering method to interpret the distance matrix using average linkage. Linear discriminant analysis effect size (LEfSe) method was employed to identify statistically significant biomarkers between groups.

Statistical Analysis

Growth performance, carcass characteristics, meat quality, meat nutrition level, and rumen VFA content were analyzed by the independent sample *t*-test using SPSS software 17.0 (IBM Corp., Armonk, NY, United States). The correlation analyses of rumen microbiota with the tested traits were performed using the function `cor(x, y, use = "p")` and illustrated with function `labeledHeatmap(Matrix, xLabels, yLabels)` in the R package WGCNA (Langfelder and Horvath, 2008). The data were expressed as mean \pm standard error of the mean (SEM), and statistical significance was established at $P < 0.05$.

RESULTS

Growth Performance and Carcass Characteristics

The growth performance and carcass characteristics between the two groups during the finishing phase are listed in **Table 2**. The growth performance parameters initial weight, live weight at slaughter, ADFI, and ADG did not differ between treatments

($P > 0.05$). The carcass weight, dressing percentage, net meat weight, and EMA were not significantly different between groups ($P > 0.05$), but the net meat rate was higher in the RE group than in the CN group (41.72 and 40.28%, respectively; $P < 0.05$).

Meat Quality and Nutritional Composition

The LD quality traits are presented in **Table 3**. Compared with the CN group, the RE group showed a significantly lower drip loss (5.85% vs. 4.45%, $P < 0.01$), cooking loss (29.96% vs. 27.58%, $P < 0.01$) and shear force (65.26 N vs. 48.13 N, $P < 0.01$). For meat color-related parameters (L^* , a^* , and b^*), the values of a^* and b^* were not significantly different between treatments, but the L^* value of the RE group was higher than that of CN group (34.96 and 36.91, respectively). The crude protein and crude fat contents were significantly different between groups. However, the moisture content in the CN and RE groups was 3.30 and 4.69%, respectively, indicating a significant increase ($P < 0.01$) when Simmental steers were fed with diets containing HTR. The content of crude ash was lower in the RE group than in the CN group (0.038% vs. 0.044%, $P < 0.05$; **Table 4**). The amino acid composition in LD was not significantly different

between groups (**Supplementary Table 2**). Regarding fatty acid composition (**Table 5**), the content of oleic acid (C18:1n9c) and linoleic acid (C18:2n6t) content accounted for 37.35% and 0.11% of fatty acids in the CN group and 39.74% and 0.18% of fatty acids in the RE group, respectively; their content in the RE group was significantly higher than that in the CN group ($P < 0.05$). Moreover, the ratio of ω -6/ ω -3 fatty acids in the RE group was lower than that in the CN group ($P = 0.06$).

Muscle Metabolome

A total of 774 metabolites were detected in the steer muscles, including 519 in the positive ionization mode and 255 in the negative ionization mode (**Supplementary Tables 3A,B**). The annotation results obtained using biological databases (KEGG, HMDB, LIPID MAPS) suggest that these metabolites were mainly involved in the metabolic pathways of lipid metabolism, carbohydrate metabolism, and amino acid metabolism (**Figure 1** and **Supplementary Figure 1**). A total of 21, 6, and 38 metabolites in the positive ion mode were mainly involved in lipid, carbohydrate, and amino acid metabolism pathways, whereas 18, 11, and 19 metabolites in the negative ion mode were associated with lipid, carbohydrate, and amino acid metabolism (**Supplementary Tables 3C,D**). As shown in **Supplementary Figure 2A** ($R^2Y = 0.84$, $Q^2Y = 0.56$) and **2B** ($R^2Y = 0.78$, $Q^2Y = 0.39$), the PLS-DA model revealed a clear separation between muscle metabolomes of steers fed with different diets. **Supplementary Tables 3E,F** summarize all the differential metabolites of the two groups in the positive and negative ion mode, as well as their query IDs, P -value, and fold change (FC). Based on FC threshold ≥ 2 (or ≤ 0.5) and a P -value < 0.05 ; 90 metabolites, including 30 upregulated and 32 downregulated metabolites in the positive ion mode and 19 upregulated and 9 downregulated metabolites in the negative ion mode, were significantly altered between the two groups (**Figure 2**). Moreover, we found that many differential metabolites were associated with glucose and lipid metabolism pathways. Phosphocholine, linolenic acid, and D-glucose 6-phosphate (G6p) showed significantly lower levels in the muscle in RE animals than in CN animals, whereas adenosine 5'-monophosphate (AMP), androstenedione, arachidonic acid (ARA), caprylic acid, cortisol, cortisone, docosahexaenoic acid (DHA), docosapentaenoic acid (DPA), D-glucarate, histamine,

TABLE 2 | Effects of herbal tea residue feed on the growth performance and carcass characteristics of finishing steers.

Parameter	CN	RE	P-value
Initial weight (kg)	479.87 \pm 10.99	482.53 \pm 6.95	0.24
Live weight at slaughter (kg)	542.91 \pm 11.68	547.09 \pm 7.56	0.28
Average daily feed intake (kg)	12.64 \pm 0.30	12.33 \pm 0.28	0.79
Average daily gain (kg)	1.05 \pm 0.04	1.08 \pm 0.05	0.72
Carcass weight (kg)	307.58 \pm 18.02	319.01 \pm 16.53	0.65
Dressing percentage (%)	56.54 \pm 0.90	57.26 \pm 0.46	0.49
Net meat weight (kg)	257.58 \pm 18.02	267.58 \pm 15.71	0.68
Net meat percentage (%)	40.28 \pm 0.38	41.72 \pm 0.48	0.04
Eye muscle area (cm ²)	78.82 \pm 5.03	81.70 \pm 6.09	0.72

The values were calculated as the mean \pm standard error of the mean ($N = 15$). $P < 0.05$ indicated a significant difference between the two groups; $P > 0.05$ indicated no significant difference between the two groups. CN, no herbal tea residues; RE, 50% HTR replaced *Pennisetum purpureum*.

TABLE 3 | Effects of herbal tea residue feed on the meat quality of finishing steers.

Parameter	CN	RE	P-value
Drip loss (%)	5.85 \pm 0.304	4.45 \pm 0.233	0.001
Cooking loss (%)	29.96 \pm 0.752	27.58 \pm 0.443	0.006
Shear force (N)	65.26 \pm 3.404	48.13 \pm 2.314	0.001
Meat color			
Lightness (L^*)	34.96 \pm 0.662	36.91 \pm 0.55	0.032
Redness (a^*)	18.91 \pm 0.723	18.68 \pm 0.753	0.823
Yellowness (b^*)	9.50 \pm 0.534	9.85 \pm 0.452	0.624

The values were calculated as the mean \pm standard error of the mean ($N = 15$). The shear force was calculated as the average of nine replicates per sample. $P < 0.05$ indicated a significant difference between the two groups; $P > 0.05$ indicated no significant difference between the two groups. CN, no herbal tea residue; RE, 50% HTR replaced *Pennisetum purpureum*.

TABLE 4 | Effects of herbal tea residue feed on the basic nutritional composition of beef.

Parameter	CN	RE	P-value
Moisture (%)	3.30 \pm 0.18	4.69 \pm 0.16	0.002
Crude protein (%)	86.19 \pm 1.38	88.04 \pm 1.08	0.33
Crude fat (%)	0.43 \pm 0.003	0.46 \pm 0.00	0.53
Crude ash (%)	0.044 \pm 0.001	0.038 \pm 0.002	0.04

The indicators were calculated on the basis of lyophilized samples. The values were calculated as the mean \pm standard error of the mean ($N = 15$). $P < 0.05$ indicated a significant difference between the two groups; $P > 0.05$ indicated no significant difference between the two groups. CN, no herbal tea residue; RE, 50% HTR replaced *Pennisetum purpureum*.

TABLE 5 | Effects of herbal tea residue feed on the fatty acid content of beef (g/100 g).

Fatty acid	CN	RE	P-value
Decanoic acid (C10:0)	0.07 ± 0.007	0.06 ± 0.007	0.289
Lauric acid (C12:0)	0.10 ± 0.013	0.08 ± 0.005	0.343
Myristic acid (C14:0)	2.63 ± 0.146	2.41 ± 0.150	0.332
Myristoleic acid (C14:1)	0.44 ± 0.052	0.66 ± 0.108	0.061
Pentadecanoic acid (C15:0)	0.45 ± 0.036	0.46 ± 0.052	0.830
Palmitic acid (C16:0)	26.70 ± 0.453	25.57 ± 0.516	0.123
Palmitoleic acid (C16:1)	3.44 ± 0.141	3.39 ± 0.249	0.851
Heptadecanoic acid (C17:0)	0.97 ± 0.061	1.21 ± 0.130	0.106
10-Heptadecenoic acid (C17:1)	0.65 ± 0.057	0.69 ± 0.034	0.566
Stearic acid (C18:0)	18.18 ± 0.597	17.59 ± 0.651	0.513
Oleic acid (C18:1n9c)	37.345 ± 0.536	39.74 ± 0.855	0.036
Linoleic acid (C18:2n6t)	0.11 ± 0.010	0.18 ± 0.031	0.050
Methyl linoleate (C18:2n6c)	4.27 ± 0.406	4.50 ± 0.618	0.772
α-Linolenic acid (C18:3n3)	0.40 ± 0.050	0.43 ± 0.034	0.577
Arachidic acid (C20:0)	0.15 ± 0.016	0.15 ± 0.008	0.817
11,14,17-Eicosatrienoic acid (C20:3n3)	0.59 ± 0.266	0.53 ± 0.182	0.840
Methyl arachidonic acid (C20:4n6)	1.55 ± 0.329	2.20 ± 0.794	0.454
Eicosapentaenoic acid (C20:5n3)	0.24 ± 0.068	0.25 ± 0.074	0.899
Heneicosanoic acid-methyl ester (C21:0)	0.24 ± 0.062	0.21 ± 0.038	0.696
Docosanoic acid (C22:0)	0.06 ± 0.012	0.05 ± 0.020	0.520
Methyl cis-13,16-docosadienoic acid (C22:2)	0.13 ± 0.032	0.14 ± 0.023	0.896
Nervonic acid (C24:1)	0.21 ± 0.030	0.21 ± 0.055	0.999
Saturated fatty acid (SFA)	49.57 ± 0.439	48.95 ± 0.632	0.437
Unsaturated fatty acid (UFA)	50.24 ± 0.461	51.07 ± 0.738	0.359
Omega-6 (ω-6)	7.07 ± 1.145	6.64 ± 1.373	0.811
Omega-3 (ω-3)	1.18 ± 0.360	1.27 ± 0.302	0.846
ω-6: ω-3	6.98 ± 0.358	5.99 ± 0.334	0.060

The values were calculated as the mean ± standard error of the mean ($N = 15$). $P < 0.05$ indicated a significant difference between the two groups; $P > 0.05$ indicated no significant difference between the two groups. CN, no herbal tea residue; RE, 50% HTR replaced *Pennisetum purpureum*.

lauric acid, and progesterone showed significantly higher levels in RE animals ($P < 0.05$).

NH₃-N and Volatile Fatty Acid Concentrations in Rumen Fluid

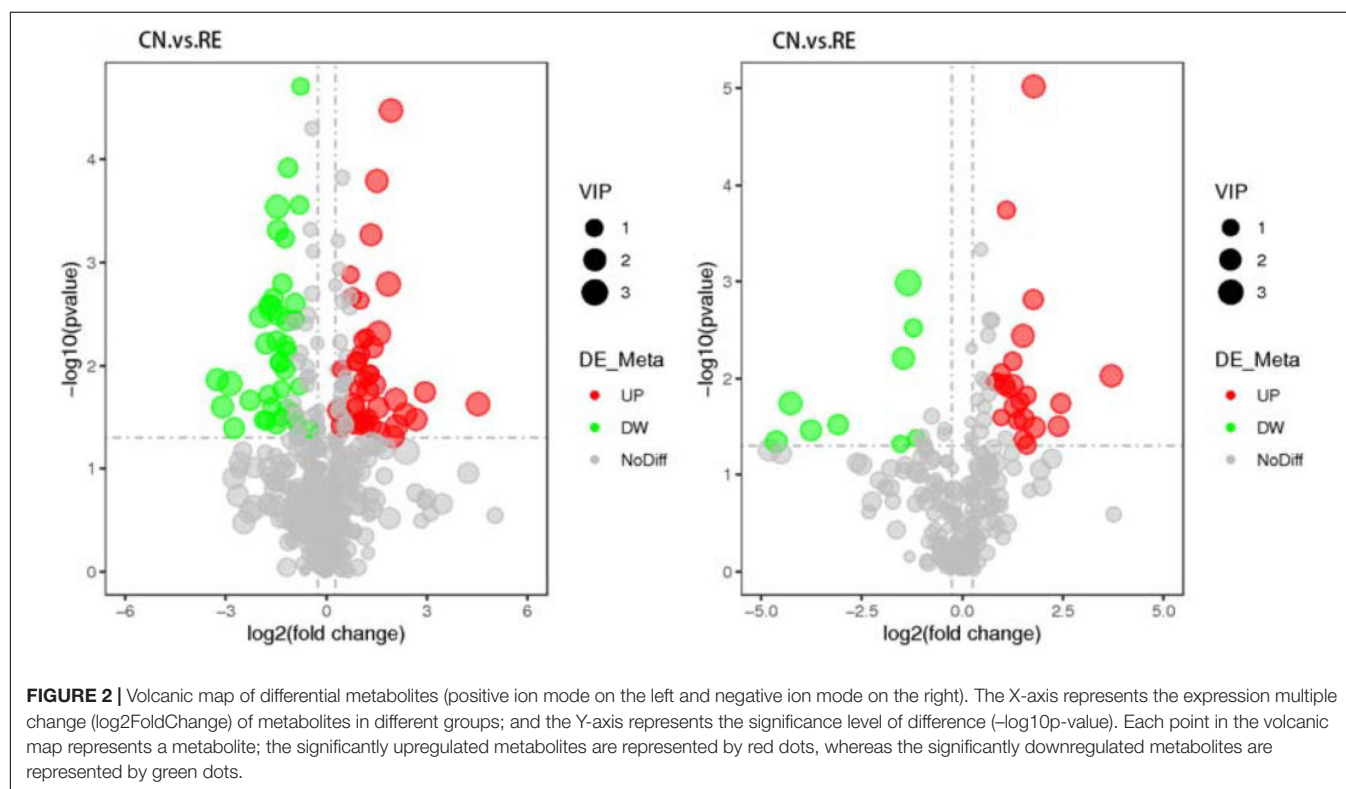
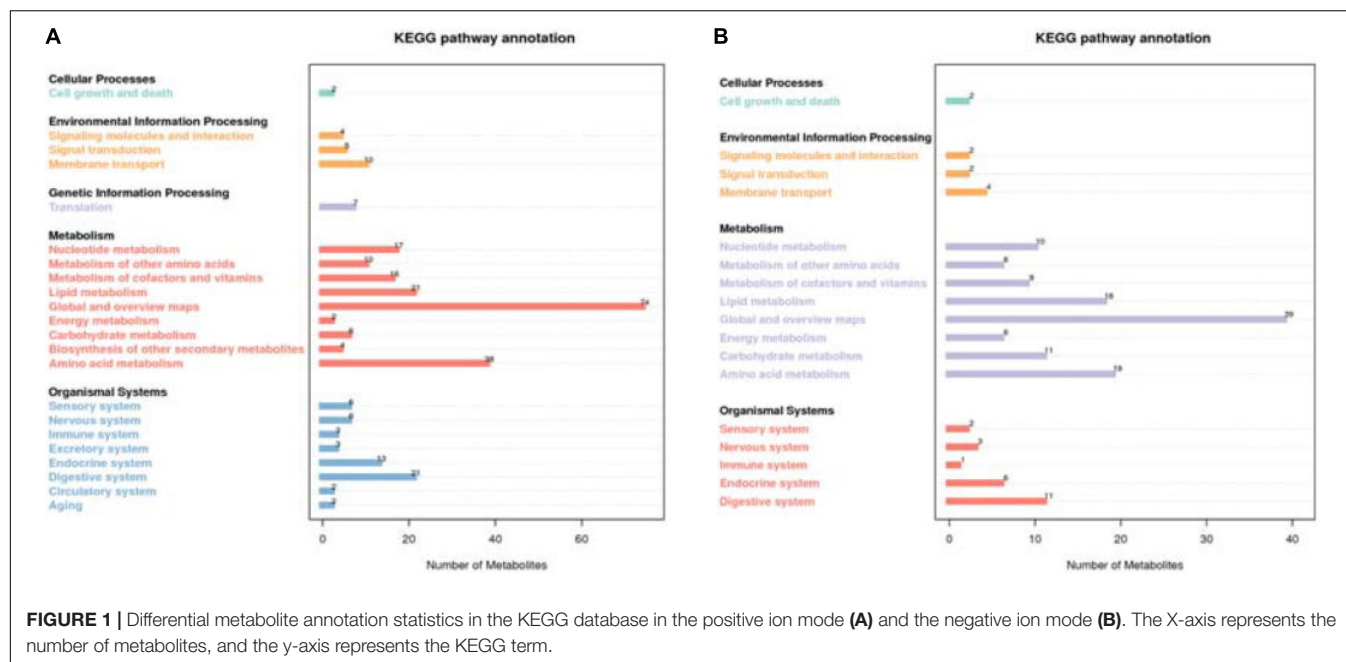
The rumen NH₃-N and VFA concentrations are listed in **Table 6**. The concentration of propionic acid in the CN and RE groups was 8.40 and 10.38 mmol/L, respectively, with the RE group showing significantly higher levels than the CN group ($P < 0.05$). The ratio of propionic acid to acetic acid levels in the RE group was also significantly higher than that in the CN group (0.22 and 0.24, respectively; $P < 0.05$). However, there were no significant differences between the CN and RE groups in the concentrations of acetic acid, isobutyric acid, butyric acid, isovaleric acid, and valeric acid ($P > 0.05$).

16S rRNA Gene Sequencing and Annotation Analysis

The high-throughput sequencing analysis generated a total of 2,442,873 raw reads. On average, each sample yielded approximately 81,429 joined tags, and more than 61.09% of the total joined tags in each sample were processed for subsequent analysis after data filtering, quality control, and chimera removal (**Supplementary Table 4A**). A total of 3,184 OTUs were identified on the basis of 97% nucleotide sequence similarity; of these, 2,611 OTUs were found across all groups and defined as core OTUs. The number of unique OTUs in the CN and RE groups was 251 and 322, respectively (**Figure 3A** and **Supplementary Table 4B**). We annotated all these OTU tags to the Silva132 database and found that 92.09% of the sequences were assigned at the phylum level, whereas 89.42, 81.88, 71.39, 30.59, and 10.27% of the annotated OTUs were assigned at the class, order, family, genus, and species levels, respectively (**Supplementary Table 4C**). Phylogenetic analysis identified the top 10 phyla from the rumen of steers using the QIIME pipeline on the basis of the OTU annotation (**Figures 3B,C**). The dominant phyla in the rumen of steers were Bacteroidetes, Firmicutes, and Euryarchaeota, accounting for 43.95, 31.45, and 7.76%, respectively. And the Firmicutes to Bacteroidetes ratio increased from 0.72 in the CN group to 1.02 in the RE group (**Supplementary Table 5A**). At the genus level, a total of 301 classifiable genera were detected, and nine genera had a relative abundance greater than 1.0%, including *Methanobrevibacter*, *Anaeroplasma*, *Bacteroidales*, *Mycoplasma*, *Candidatus Saccharimonas*, *Lachnospiraceae*, *Ruminococcaceae*, *Prevotellaceae*, and *Saccharofermentans*. The most abundant genus in the rumen of Simmental steers was *Methanobrevibacter* (4.59%) (**Supplementary Table 5B**).

Changes in Rumen Microorganisms

For the alpha-diversity analysis, we calculated the observed species index, Shannon, Simpson, Chao1, ACE, Good's coverage, PD whole tree indices for each group. Although alpha diversity in RE groups tended to decrease compared with the control, these differences did not significantly affect species level microbial diversity ($P > 0.05$; **Table 7**). The results of the PCoA and NMDS analysis between the groups are shown in **Figure 4A**. The CN and RE samples were separated from each other, which reflects the effect of HTR on the rumen microbial community. The UPGMA clustering tree (**Figure 4B**) measured the similarity in microbial communities between groups according to the degree of their overlap and confirmed the significant structural separation of the rumen microflora between the two groups. The LEfSe analysis was used to identify the biomarkers between the two groups, and 18 differentially abundant taxonomic clades were found, with a Linear Discriminant Analysis (LDA) score higher than 4. The number of biomarkers at the kingdom, phylum, class, order, family, genus and species levels were 2, 4, 5, 3, 2, 1, and 1 respectively (**Figure 5**, left). A total of 11 taxa can be used as biomarkers for CN samples, including Archaea at the kingdom level, Bacteroidetes and Euryarchaeota at the phylum level, Bacteroidia and Methanobacteriales at the class level, Bacteroidales and



Methanobacteriales at the order level, *Methanobacteriaceae* and *Rikenellaceae* at the family level, *Methanobrevibacter* at the genus level, and *Bacteroidales-bacterium-Bact-22* at the species level. A total of seven taxa can be used as biomarkers for RE samples, including Bacteria at the kingdom level; Proteobacteria and Tenericutes at the phylum level; Mollicutes, Alphaproteobacteria, and Gammaproteobacteria at the class

level, and Rickettsiales at the order level (Figure 5, right). A total of 23 genera displayed a significant difference in abundance between the CN and RE groups, including 3 upregulated and 20 downregulated genera ($FDR < 0.05$). Specifically, the abundance of *Riemerella* in the CN group and the abundance of *Rikenellaceae*, *Anaerovorax*, *Desulfovibrio*, *Papillibacter*, *Succiniclasticum*, *Veillonellaceae*, *Acetitomaculum*,

TABLE 6 | Effects of herbal tea residue feed on the rumen fermentation parameters of finishing steers.

Metabolite	CN	RE	P-value
Ammonia-N (mg/100 mL)	8.80 ± 1.053	11.43 ± 2.435	0.396
Acetic acid (mmol/L)	35.88 ± 2.660	30.58 ± 3.385	0.233
Propionic acid (mmol/L)	8.40 ± 0.343	10.38 ± 0.659	0.019
Isobutyric acid (mmol/L)	0.69 ± 0.109	0.59 ± 0.085	0.457
Butyric acid (mmol/L)	3.89 ± 0.299	3.92 ± 0.436	0.956
Isovaleric acid (mmol/L)	0.74 ± 0.145	0.64 ± 0.075	0.512
Valeric acid (mmol/L)	0.24 ± 0.043	0.19 ± 0.022	0.325
Propionic acid/Acetic acid	0.22 ± 0.007	0.24 ± 0.006	0.023

The values were calculated as the mean ± standard error of the mean (N = 15). $P < 0.05$ indicated a significant difference between the two groups; $P > 0.05$ indicated no significant difference between the two groups. CN, no herbal tea residue; RE, 50% HTR replaced *Pennisetum purpureum*.

Christensenellaceae, and *Schwartzia* in the RE group was significantly decreased ($FDR < 0.01$; Supplementary Table 5C).

Correlation of Rumen Microbiota Abundance With Volatile Fatty Acid and NH₃-N Concentration

Pearson correlation analysis was performed to further identify the relationship between the relative abundance of differential bacterial genera identified by 16S rRNA sequencing with rumen VFA and NH₃-N concentration (Supplementary Figure 3). The concentration of acetic acid, propionic acid, and butyric acid correlated negatively with the relative abundance of *Riemerella* ($P = 0.01$, $P = 0.03$, and $P = 0.03$, respectively) and *Moraxella* ($P = 0.01$, $P = 0.03$, and $P = 0.04$, respectively). The concentration of propionic acid was negatively correlated with the relative abundance of *Marvinbryantia* ($P = 0.03$). The concentration of isovaleric acid, valeric acid, and NH₃-N showed a significant positive correlation with the relative abundance of *Veillonellaceae* ($P = 0.03$, $P = 0.05$, and $P = 0.02$, respectively), *Olsenella* ($P = 0.008$, $P = 0.01$, and $P = 0.009$, respectively) and *Schwartzia* ($P = 0.01$, $P = 0.002$, and $P = 0.02$, respectively). Additionally, the concentration of isobutyric acid was most highly correlated with the relative abundance of *Olsenella* ($P = 0.002$).

Correlation Between Rumen Microbiota and Muscle Glycolipid Metabolites

We also performed a correlation analysis between differential rumen microorganisms with muscle differential glycolipid metabolites (Figure 6). The concentration of caprylic acid, DHA, DPA, glucarate, and lauric acid displayed a strong and positive correlation with relative abundance of *Moraxella* and *Riemerella*, respectively ($P < 0.01$). The concentration of linolenic acid showed a positive correlation with the relative abundance of *Acetivomaculum*, *Anaerovibrio*, *Anaerovorax*, *Blautia*, *Desulfovibrio*, *Howardella*, *Papillibacter*, *Schwartzia*, *Veillonellaceae* ($P < 0.01$) and a negative correlation with the relative abundance of *Riemerella* ($P = 0.01$). The concentration of phosphocholine was positively related to the bacterial abundance of *Anaerovibrio*, *Desulfovibrio*, *Olsenella*, *Papillibacter*,

Rikenellaceae, *Schwartzia*, and *Veillonellaceae* ($P < 0.01$). In addition, the concentration of G6P correlated strongly and positively with the relative abundance of *Schwartzia* and *Succinoclasticum* ($P < 0.01$).

DISCUSSION

HTR still retain a considerable proportion of the nutrients and bioactive compounds, which has the potential to be used as an unconventional feed resource for ruminant (Xie et al., 2020). The results of the study showed that the HTR as a part of the diet has no adverse effects on the growth performance of finishing steers, and this is in accordance with our early reports of Zhuang et al. (2021). In this study, HTR had no significant effect on carcass weight, dressing percentage and EMA of finishing steers, but significantly improved the net meat percentage. This could be the ample nutrients and active ingredients in HTR to improve the fattening degree of finishing steers (Brscic et al., 2014). Meat quality is an important economic trait of bovine husbandry. Tenderness, water-holding capacity, and color are the vital but highly variable attributes of beef quality (Modzelewska-Kapituła et al., 2018). In the present study, the meat drip loss, cooking loss, and shear force were significantly lower in the RE group than in the CN group. This finding is consistent with the findings reported by Ding et al. (2020), who showed that tea residues increased moisture content and tenderness in pork. The increase in the L* value in RE group was associated with the high moisture content of beef (Barahona et al., 2016). According to our findings, HTR could improve the meat quality of finishing steers to a certain extent.

Regarding the muscle nutrient composition, the content of C18:1n9c and C18:2n6t was higher, and the ω -6/ ω -3 ratio was slightly lower when the steers were fed with HTR. C18:1n9c, a monounsaturated fatty acid, can regulate blood lipids and lowers cholesterol (Sales-Campos et al., 2013). C18:2n6t, a type of trans-fatty acid produced by ruminants, has a potential protective effect against the development of coronary heart diseases (Salter, 2013). Moreover, a low ω -6/ ω -3 ratio in beef is more beneficial for human health as it decreases the risk of heart disease and cancer (Kang, 2004). Ahmed et al. (2016) reported that Chinese herbal medicine feed additive improved the nutritional value of pork by decreasing the ω -6/ ω -3 value. Thus, the findings suggest that the beef of the experimental group is more appropriate for human diet.

In this study, HTR did not affect within-sample diversity (species richness and evenness), however, the composition and structure of the rumen microbial community were influenced by HTR. In steers fed with HTR, the abundance of *Bacteroidetes* markedly decreased, whereas the abundance of *Firmicutes* markedly increased, and it became the most abundant phylum. In humans and mice, an increase in the *Firmicutes*-to-*Bacteroidetes* ratio has been correlated with fat deposition in tissues (Ley et al., 2006; Turnbaugh et al., 2006). In our study, the crude fat content of muscle did show an upward trend with an increasing *Firmicutes*-to-*Bacteroidetes* ratio. The abundance of the genera *Veillonellaceae*, *Schwartzia*, and *Olsenella* decreased in the rumen

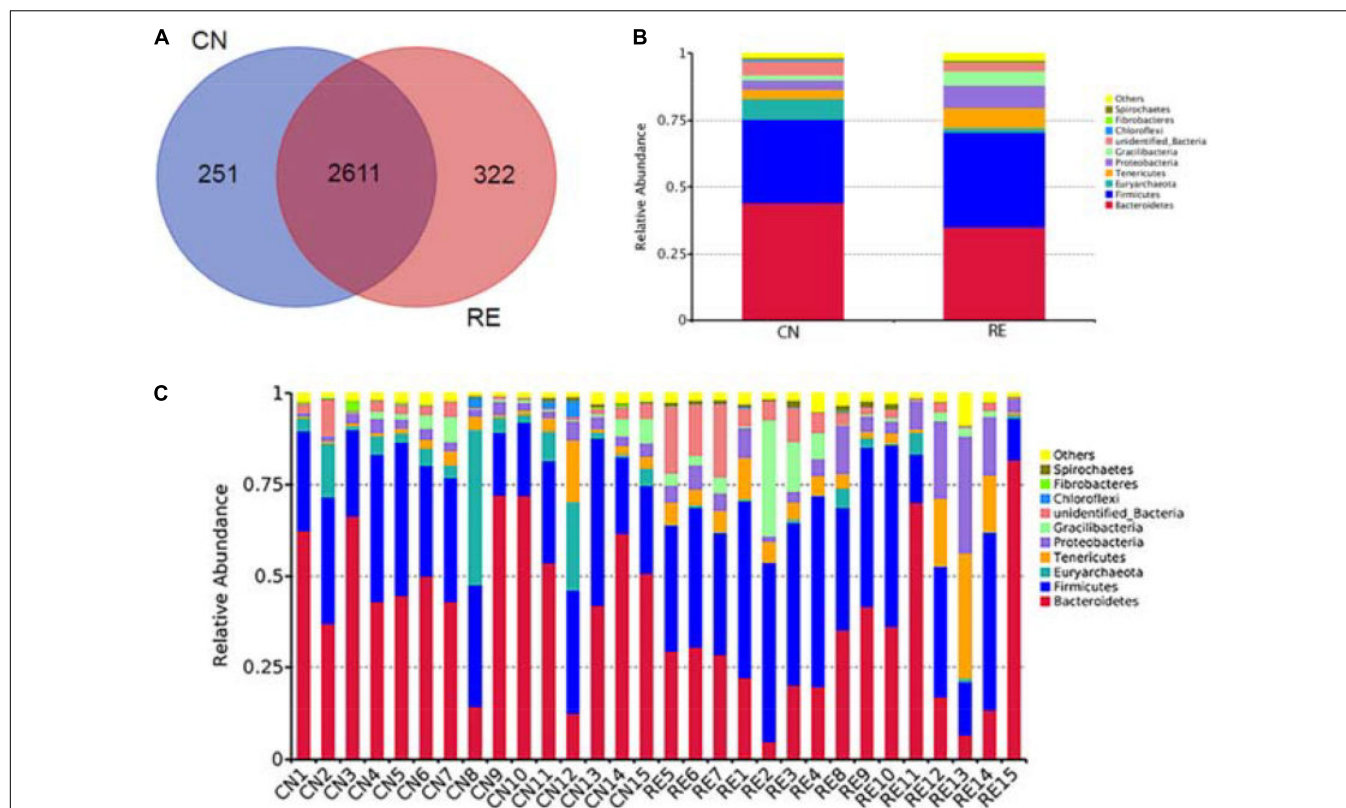


FIGURE 3 | Venn diagram representing the shared and exclusive OTUs at the 97% similarity level between rumen microbiota in the two groups **(A)**. Bar plot shows the relative abundance of rumen microbiota at the phylum level in each group **(B)** and in each sample **(C)**. OTUs, operational taxonomic units; CN, no herbal tea residue (control); RE, 50% HTR replaced *Pennisetum purpureum*.

of Simmental steers fed with HTR. Notably, these genera showed a strong positive correlation with isobutyric acid, valeric acid, and isovaleric acid concentrations. Compared with CN group, isobutyric acid, valeric acid, and isovaleric acid concentrations presented a decreasing trend in the RE group. This finding is consistent with previous findings that these bacteria were positively correlated with rumen VFAs (Kong et al., 2019; Li et al., 2019; Wang et al., 2021). Genus *Marvinbryantia* was

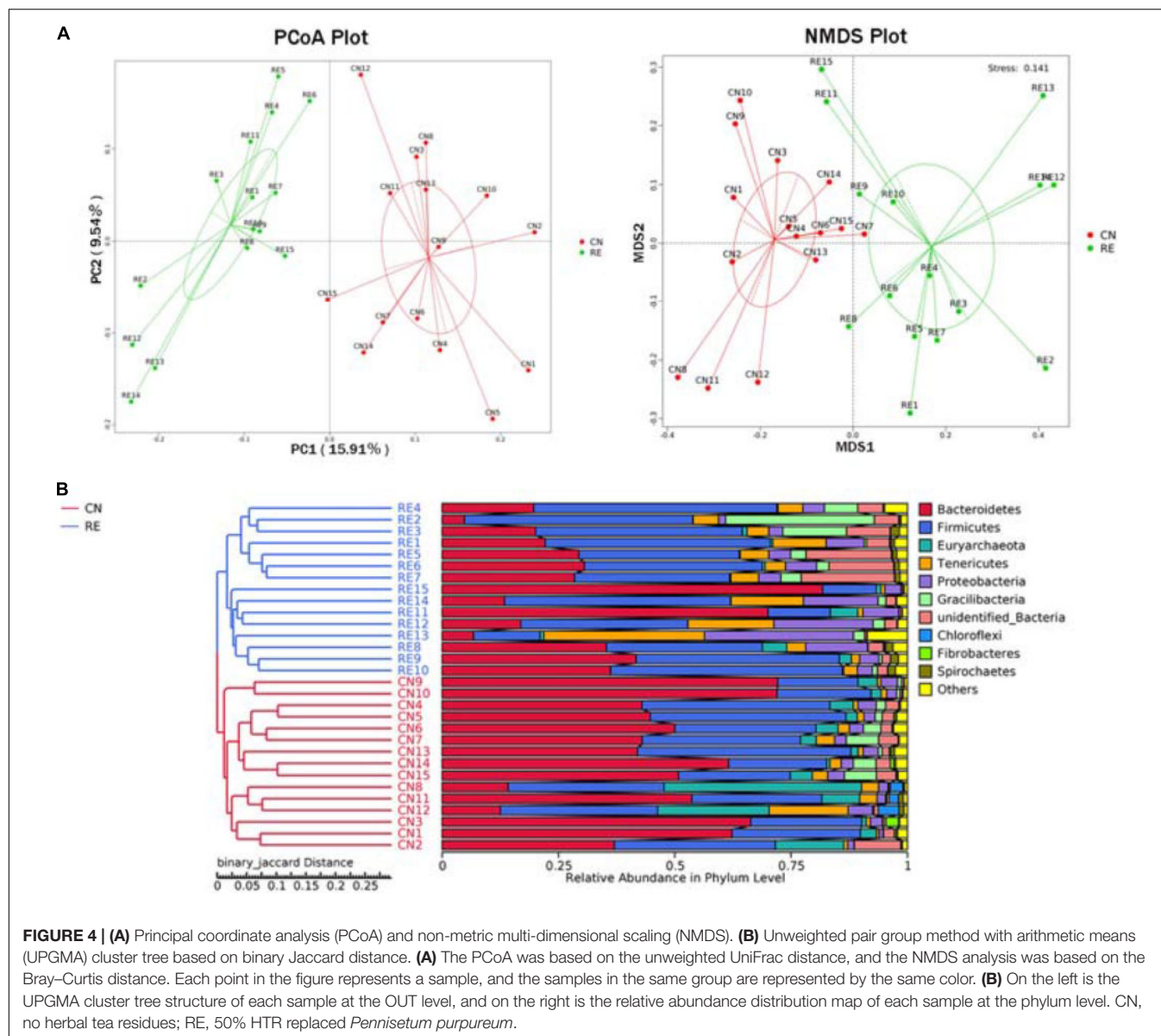
also downregulated in the RE group compared with the CN group. The relative abundance of *Marvinbryantia* correlated negatively with the concentrations of propionic acid. Wang et al. (2018) reported that *Marvinbryantia* was an inflammatory bacterium and was negatively correlated with VFA concentration. These findings suggest that HTR reduces the proliferation of inflammatory bacteria. An increase in propionic acid and propionic acid-to-acetic acid ratio was observed in this study, which is often observed as a result of enhanced digestion of fiber and the proliferation of microorganisms in the rumen and may induce changes in metabolic pathways and better rumen fermentation (Christensen et al., 2015). This finding is in agreement with the findings reported by Zhu et al. (2018) and Liang et al. (2019), who suggested that Chinese herbal mixture feed additives improved rumen fermentation, mainly by increasing the concentration of propionic acid and the ratio of propionic acid to acetic acid. Notably, propionate is the main source of glucose for ruminants (den Besten et al., 2013), which may explain the improved carcass characteristics, especially net meat percentage, observed in the RE group in the present study.

Metabolomics analysis showed that the levels of D-glucarate, caprylic acid, lauric acid, DHA, and DPA were higher in the RE group. D-glucarate is oxidized to D-glycerate by glucose oxidase. D-glycerate is a crucial component of pentose phosphate pathway (PPP), which is involved in the first step of glucose

TABLE 7 | Effects of herbal tea residue feed on the alpha diversity indices for bacteria in the ruminal samples of finishing steers.

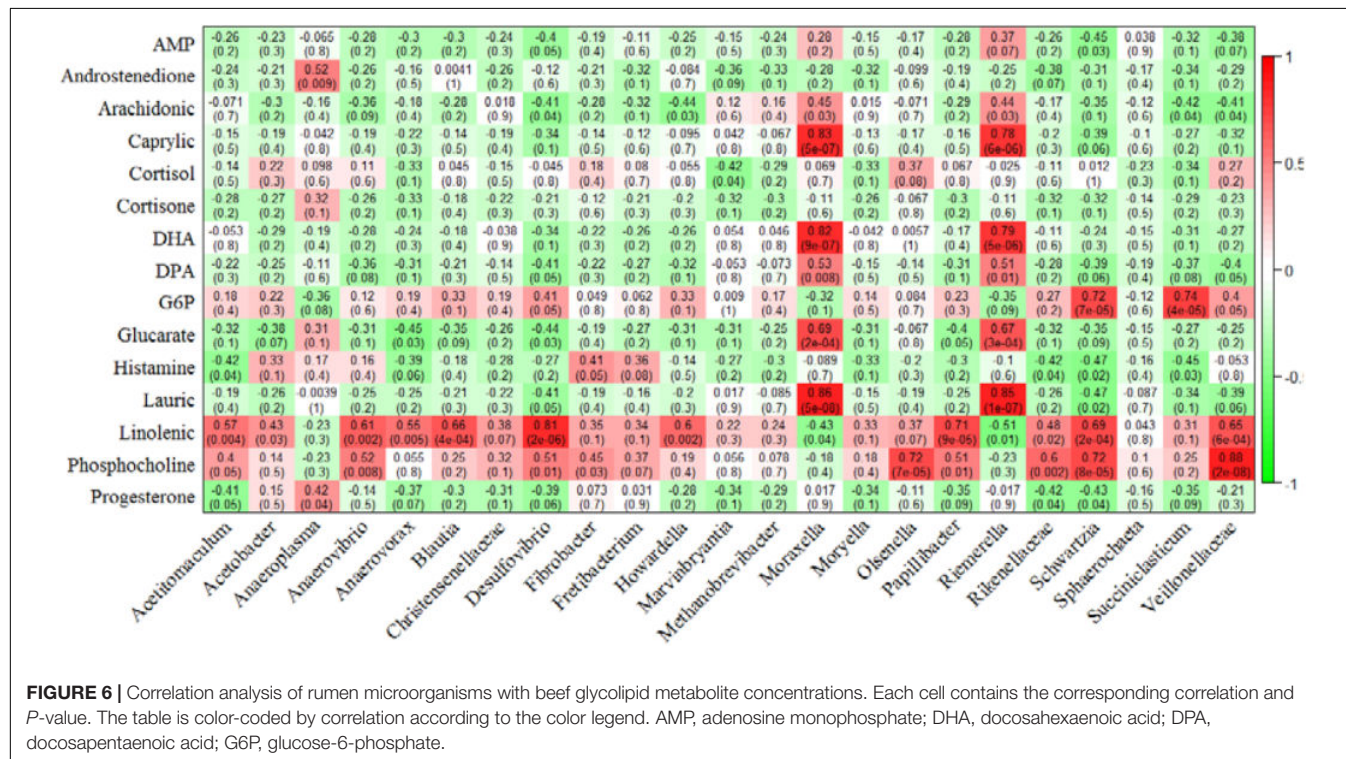
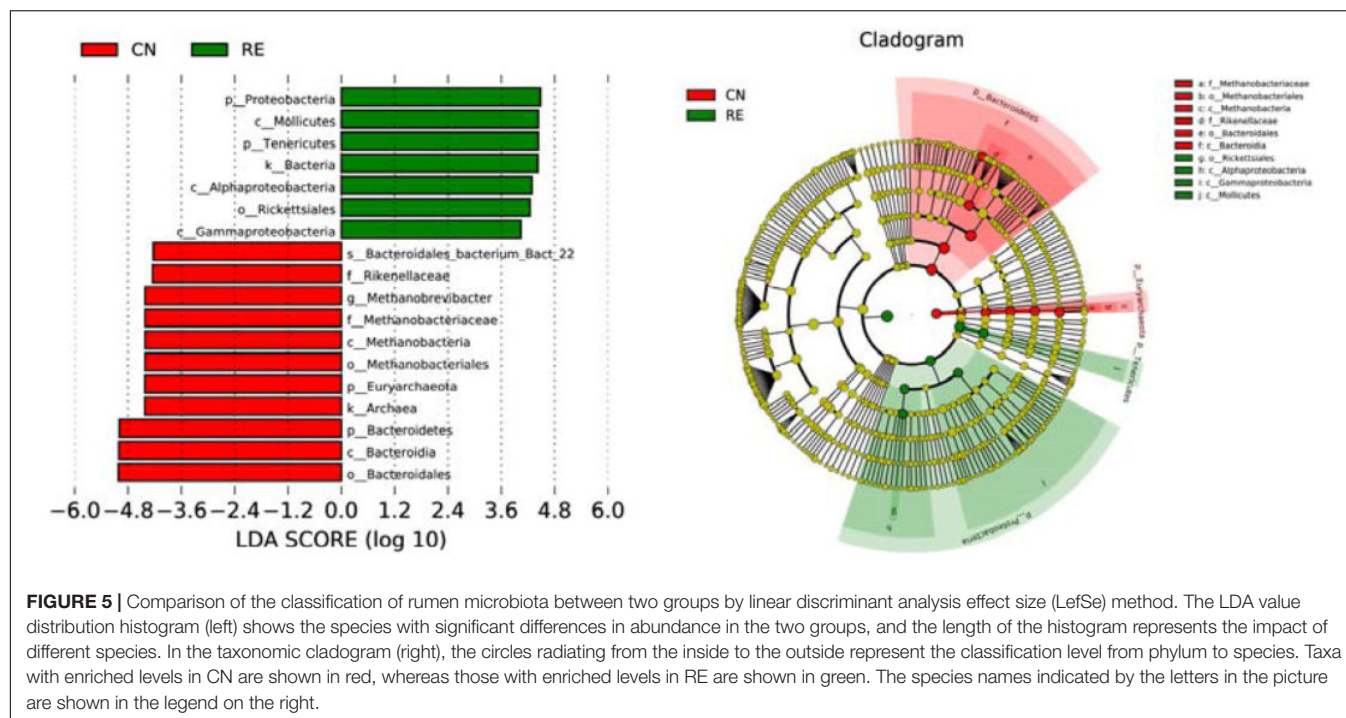
Items	CN	RE	P-value
Observed species	1179.60±50.59	1100.47±56.37	0.305
Shannon	6.81±0.28	6.61±0.28	0.634
Simpson	0.95±0.01	0.95±0.01	0.947
Chao1	1447.77±110.81	1332.69±68.89	0.385
ACE	1426.82±61.86	1353.86±64.65	0.422
Good's coverage	0.99±0.00	0.99±0.00	0.711
PD whole tree	88.93±3.96	87.41±2.90	0.759

The values were calculated as the mean ± standard error of the mean (N = 15). $P < 0.05$ indicated a significant difference between the two groups, and $P > 0.05$ indicated no significant difference between the two groups. CN, no herbal tea residue; RE, 50% HTR replaced *Pennisetum purpureum*.



metabolism in the glycolysis branch (Stincone et al., 2015). Medium-chain fatty acids (e.g., caprylic acid and lauric acid) are known to contribute to better beef flavor and odor and improve cholesterol levels (Wilson et al., 2006). DHA and DPA are the most bioactive of ω -3 polyunsaturated fatty acids (PUFAs) and play vital roles in decreasing the hepatic triglyceride content (Pirillo and Catapano, 2013), and PUFAs are known to be beneficial for human health (Russo, 2009). This is consistent with our results of the fatty acid analysis, which showed a reduction in the ω -6: ω -3 ratio. Remarkably, the abundance of *Moraxella* and *Riemerella* increased in the rumen of Simmental steers fed HTR, and the abundance of these bacteria was positively correlated with the levels of D-glucarate, caprylic acid, lauric acid, DHA, and DPA. Currently, there is no information on specific associations between these bacteria and the above muscle metabolites. In addition, the concentration

of G6P correlated strongly and positively with the relative abundance of *Succiniclasticum*, which includes starch-degrading bacteria that degrade dietary starch (Fernando et al., 2010; Huws et al., 2016). The abundance of *Anaerovibrio* and *Papillibacter* correlated positively with the concentration of linolenic acid. *Anaerovibrio* participates in the breakdown of fats and sugars (Ouattara et al., 1992; Mannelli et al., 2018). *Papillibacter* belongs to the *Ruminococcaceae* family; members of the *Ruminococcaceae* family are essential for cellulose degradation (Krause et al., 2003). The specific association of *Anaerovibrio* and *Papillibacter* with linolenic acid remains unclear and requires an in-depth investigation in the future. The present findings suggest that HTR improves muscle glucolipid metabolism and rumen fermentation by altering the microbial community composition. However, more systematic studies should be included to reveal the biological associations.



CONCLUSION

The present study showed that HTR improved meat quality to a certain extent, influenced the muscle metabolic pathways, and altered the rumen VFA concentration and rumen microbial community composition in Simmental crossbred finishing steers.

Moreover, the bacteria were closely associated with muscle glucolipid metabolites and rumen VFA levels of the steers. Our findings suggest that, as a functional roughage, HTR improves the meat quality of steers mainly by altering rumen microbial populations and then affecting rumen fatty acid composition and muscle glucolipid metabolism.

DATA AVAILABILITY STATEMENT

The original contributions presented in the study are included in the article/**Supplementary Material**, further inquiries can be directed to the corresponding author/s.

ETHICS STATEMENT

The animal study was reviewed and approved by the Animal Care Committee at South China Agricultural University.

AUTHOR CONTRIBUTIONS

LL: writing-original draft preparation. XS: investigation. JS: data curation and visualization. JL, TC, and QX: supervision. YZ and JS: conceptualization, methodology, writing-reviewing, and editing. All authors contributed to the article and approved the submitted version.

FUNDING

This work was supported by the Natural Science Foundation of China Program (Grant Nos. 31802032 and 32072714), the

Natural Science Foundation of Guangdong Province (Grant No. 2020A1515010062), the Science and Technology Project of Guangzhou (Grant No. 202002030037), and the Key-Area Research and Development Program of Guangdong Province (2019B110209005).

SUPPLEMENTARY MATERIAL

The Supplementary Material for this article can be found online at: <https://www.frontiersin.org/articles/10.3389/fmicb.2021.821293/full#supplementary-material>

Supplementary Figure 1 | Differential metabolites annotation statistics in HMDB (A) and LIPID MAPS (B) database. The left picture is the positive ion mode, and the right picture is the negative ion mode. The X-axis represents the number of metabolites, and the y-axis represents the term of HMDB or LIPID MAPS.

Supplementary Figure 2 | The PLS-DA scatter plots of each sample in positive (left) and negative (right) modes. The abscissa is the score of the sample on the first principal component; The ordinate is the score of the sample on the second principal component; R²Y represents the explanatory rate of the model, and Q²Y is used to evaluate the predictive ability of the PLS-DA model. When R²Y is greater than Q²Y, the model is well established.

Supplementary Figure 3 | Correlation analysis of rumen microorganisms with rumen volatile fatty acid concentrations. Each cell contains the corresponding correlation and P-value. The table is color-coded by correlation according to the color legend.

REFERENCES

- Abdallah, A., Zhang, P., Zhong, Q., and Sun, Z. (2019). Application of traditional chinese herbal medicine by-products as dietary feed supplements and antibiotic replacements in animal production. *Curr. Drug Metab.* 20, 54–64. doi: 10.2174/1389200219666180523102920
- Ahmed, S. T., Mun, H. S., Islam, M. M., Ko, S. Y., and Yang, C. J. (2016). Effects of dietary natural and fermented herb combination on growth performance, carcass traits and meat quality in grower-finisher pigs. *Meat Sci.* 122, 7–15. doi: 10.1016/j.meatsci.2016.07.016
- Ahsan, M. A., Katla, S. K., Islam, M. T., Hernandez-Viezas, J. A., Martinez, L. M., Diaz-Moreno, C. A., et al. (2018). Adsorptive removal of methylene blue, tetracycline and Cr(VI) from water using sulfonated tea waste. *Environ. Technol. Innov.* 11, 23–40. doi: 10.1016/j.eti.2018.04.003
- Association of Official Analytical Chemists [AOAC] (2000). *Association of Official Analytical Chemists*, 17th Edn. Gaithersburg, MD: AOAC.
- Barahona, M., Olleta, J., Sañudo, C., Albertí, P., Panea, B., Pérez-Juan, M., et al. (2016). Effects of whole linseed and rumen-protected conjugated linoleic acid enriched diets on beef quality. *Animal* 10, 709–717. doi: 10.1017/s1751731115002591
- Black, J., and Foarde, K. (2007). Comparison of four different methods for extraction of *Stachybotrys chartarum* spore DNA and verification by real-time PCR. *J. Microbiol. Methods* 70, 75–81. doi: 10.1016/j.mimet.2007.03.017
- Brsic, M., Prevedello, P., Stefani, A. L., Cozzi, G., and Gottardo, F. (2014). Effects of the provision of solid feeds enriched with protein or nonprotein nitrogen on veal calf growth, welfare, and slaughter performance. *J. Dairy Sci.* 97, 4649–4657. doi: 10.3168/jds.2013-7618
- Cao, Y., Ruan, Y., Shen, T., Huang, X., Li, M., Yu, W., et al. (2014). Astragalus polysaccharide suppresses doxorubicin-induced cardiotoxicity by regulating the PI3k/Akt and p38MAPK pathways. *Oxid. Med. Cell. Longev.* 2014:674219. doi: 10.1155/2014/674219
- Christensen, R. G., Yang, S. Y., Eun, J. S., Young, A. J., Hall, J. O., and MacAdam, J. W. (2015). Effects of feeding birdsfoot trefoil hay on neutral detergent fiber digestion, nitrogen utilization efficiency, and lactational performance by dairy cows. *J. Dairy Sci.* 98, 7982–7992. doi: 10.3168/jds.2015-9348
- den Besten, G., van Eunen, K., Groen, A. K., Venema, K., Reijngoud, D. J., and Bakker, B. M. (2013). The role of short-chain fatty acids in the interplay between diet, gut microbiota, and host energy metabolism. *J. Lipid Res.* 54, 2325–2340. doi: 10.1194/jlr.R036012
- Ding, X., Li, H., Wen, Z., Hou, Y., Wang, G., Fan, J., et al. (2020). Effects of fermented tea residue on fattening performance, meat quality, digestive performance, serum antioxidant capacity, and intestinal morphology in fatteners. *Animals* 10:185. doi: 10.3390/ani10020185
- Edgar, R. (2013). UPARSE: highly accurate OTU sequences from microbial amplicon reads. *Nat. Methods* 10, 996–998. doi: 10.1038/nmeth.2604
- Fernando, S. C., Purvis, H. T., Najar, F. Z., Sukharnikov, L. O., Krehbiel, C. R., Nagaraja, T. G., et al. (2010). Rumen microbial population dynamics during adaptation to a high-grain diet. *Appl. Environ. Microbiol.* 76, 7482–7490. doi: 10.1128/AEM.00388-10
- Gilbreath, K., Nawaratna, G., Wickersham, T., Satterfield, M., Bazer, F., and Wu, G. (2020). Metabolic studies reveal that ruminal microbes of adult steers do not degrade rumen-protected or unprotected L-citrulline. *J. Anim. Sci.* 98, skz370. doi: 10.1093/jas/skz370
- Haas, B., Gevers, D., Earl, A., Feldgarden, M., Ward, D., Giannoukos, G., et al. (2011). Chimeric 16S rRNA sequence formation and detection in Sanger and 454-pyrosequenced PCR amplicons. *Genome Res.* 21, 494–504. doi: 10.1101/gr.112730.110
- Huws, S. A., Edwards, J. E., Creevey, C. J., Rees Stevens, P., Lin, W., Girdwood, S. E., et al. (2016). Temporal dynamics of the metabolically active rumen bacteria colonizing fresh perennial ryegrass. *FEMS Microbiol. Ecol.* 92:fiv137. doi: 10.1093/femsec/fiv137
- Iqbal Khan, M. A., Ueno, K., Horimoto, S., Komai, F., Tanaka, K., and Ono, Y. (2015). Evaluation of the physio-chemical and microbial properties of green tea waste-rice bran compost and the effect of the compost on spinach production. *Plant Prod. Sci.* 10, 391–399. doi: 10.1626/pp.10.391
- Jin-Woo, H., Sun, H. C., Yon-Suk, K., Jae-Woong, L., Bo-Im, Y., Sang-Ho, M., et al. (2017). Effects of dietary supplementation of oriental herbal medicine residue and methyl sulfonyl methane on the growth performance and meat quality of ducks. *Anim. Prod. Sci.* 57, 948–957.
- Kang, J. X. (2004). Achieving balance in the omega-6/omega-3 ratio through nutrigenomics. *World Rev. Nutr. Diet.* 93, 92–98. doi: 10.1159/000081253
- Kim, Y., Lee, G., and Choi, I. (2014). Effects of dietary supplementation of red ginseng marc and α -tocopherol on the growth performance and meat quality of broiler chicken. *J. Sci. Food Agric.* 94, 1816–1821. doi: 10.1002/jsfa.6497

- Kong, C., Gao, R., Yan, X., Huang, L., and Qin, H. (2019). Probiotics improve gut microbiota dysbiosis in obese mice fed a high-fat or high-sucrose diet. *Nutrition* 60, 175–184. doi: 10.1016/j.nut.2018.10.002
- Krause, D. O., Denman, S. E., Mackie, R. I., Morrison, M., Rae, A. L., Attwood, G. T., et al. (2003). Opportunities to improve fiber degradation in the rumen: microbiology, ecology, and genomics. *FEMS Microbiol. Rev.* 27, 663–693. doi: 10.1016/S0168-6445(03)00072-X
- Langfelder, P., and Horvath, S. (2008). WGCNA: an R package for weighted correlation network analysis. *BMC Bioinformatics* 9:559. doi: 10.1186/1471-2105-9-559
- Ley, R. E., Turnbaugh, P. J., Klein, S., and Gordon, J. I. (2006). Microbial ecology: human gut microbes associated with obesity. *Nature* 444, 1022–1023. doi: 10.1038/4441022a
- Li, D., Zheng, X., Duan, L., Deng, S., Ye, W., Wang, A., et al. (2017). Ethnobotanical survey of herbal tea plants from the traditional markets in Chaoshan. *China. J. Ethnopharmacol.* 205, 195–206. doi: 10.1016/j.jep.2017.02.040
- Li, F., Li, C., Chen, Y., Liu, J., Zhang, C., Irving, B., et al. (2019). Host genetics influence the rumen microbiota and heritable rumen microbial features associate with feed efficiency in cattle. *Microbiome* 7:92. doi: 10.1186/s40168-019-0699-1
- Liang, X., Bi, X., Kamruzzaman, M., and Sano, H. (2019). Effect of Chinese herbal medicine on kinetics of plasma phenylalanine, tyrosine and whole body protein synthesis in sheep. *Anim. Sci. J.* 90, 533–538. doi: 10.1111/asj.13180
- Liang, X., Yamazaki, K., Kamruzzaman, M., Bi, X., Panthee, A., and Sano, H. (2013). Effects of Chinese herbal medicine on plasma glucose, protein and energy metabolism in sheep. *J. Anim. Sci. Biotechnol.* 4:51. doi: 10.1186/2049-1891-4-51
- Liu, H. W., Tong, J. M., and Zhou, D. W. (2011). Utilization of chinese herbal feed additives in animal production. *Agric. Sci. China* 10, 1262–1272. doi: 10.1016/S1671-2927(11)60118-1
- Malkoc, E., and Nuhoglu, Y. (2006). Removal of Ni(II) ions from aqueous solutions using waste of tea factory: adsorption on a fixed-bed column. *J. Hazard. Mater.* 135, 328–336. doi: 10.1016/j.jhazmat.2005.11.070
- Mannelli, F., Cappucci, A., Pini, F., Pastorelli, R., Decorosi, F., Giovannetti, L., et al. (2018). Effect of different types of olive oil pomace dietary supplementation on the rumen microbial community profile in Comisana ewes. *Sci. Rep.* 8:8455. doi: 10.1038/s41598-018-26713-w
- Modzelewska-Kapituła, M., Tkacz, K., Nogalski, Z., Karpińska-Tymoszczyk, M., Draszanowska, A., Pietrzak-Fiećko, R., et al. (2018). Addition of herbal extracts to the Holstein-Friesian bulls' diet changes the quality of beef. *Meat Sci.* 145, 163–170. doi: 10.1016/j.meatsci.2018.06.033
- O'Fallon, J., Busboom, J., Nelson, M., and Gaskins, C. (2007). A direct method for fatty acid methyl ester synthesis: application to wet meat tissues, oils, and feedstuffs. *J. Anim. Sci.* 85, 1511–1521. doi: 10.2527/jas.2006-491
- Quattara, A., Traore, A., and Garcia, J. (1992). Characterization of *Anaerovibrio burkinabensis* sp. nov. a lactate fermenting bacterium isolated from rice field soils. *Int. J. Syst. Bacteriol.* 42, 390–397.
- Pirillo, A., and Catapano, A. L. (2013). Omega-3 polyunsaturated fatty acids in the treatment of hypertriglyceridaemia. *Int. J. Cardiol.* 170, S16–S20. doi: 10.1016/j.ijcard.2013.06.040
- Quast, C., Pruesse, E., Yilmaz, P., Gerken, J., Schweer, T., Yarza, P., et al. (2013). The SILVA ribosomal RNA gene database project: improved data processing and web-based tools. *Nucleic Acids Res.* 41, D590–D596. doi: 10.1093/nar/gks1219
- Razminowicz, R., Kreuzer, M., and Scheeder, M. (2006). Quality of retail beef from two grass-based production systems in comparison with conventional beef. *Meat Sci.* 73, 351–361. doi: 10.1016/j.meatsci
- Russo, G. L. (2009). Dietary n-6 and n-3 polyunsaturated fatty acids: from biochemistry to clinical implications in cardiovascular prevention. *Biochem. Pharmacol.* 77, 937–946. doi: 10.1016/j.bcp.2008.10.020
- Sales, F., Bravo-Lamas, L., Realini, C., Lira, R., Aldai, N., and Morales, R. (2020). Grain supplementation of calves as an alternative beef production system to pasture-finished steers in Chilean Patagonia: meat quality and fatty acid composition. *Transl. Anim. Sci.* 4, 352–362. doi: 10.1093/tas/txz188
- Sales-Campos, H., Souza, P. R. D., Peghini, B. C., da Silva, J. S., and Cardoso, C. R. (2013). An overview of the modulatory effects of oleic acid in health and disease. *Mini Rev. Med. Chem.* 13, 201–210. doi: 10.2174/1389557511313020003
- Salter, A. M. (2013). Dietary fatty acids and cardiovascular disease. *Animal* 7, 163–171. doi: 10.1017/S1751731111002023
- Shan, C., Guo, J., Sun, X., Li, N., Yang, X., Gao, Y., et al. (2018). Effects of fermented Chinese herbal medicines on milk performance and immune function in late-lactation cows under heat stress conditions. *J. Anim. Sci.* 96, 4444–4457. doi: 10.1093/jas/sky270
- Stincone, A., Prigione, A., Cramer, T., Wamelink, M. M. C., Campbell, K., Cheung, E., et al. (2015). The return of metabolism: biochemistry and physiology of the pentose phosphate pathway. *Biol. Rev. Camb. Philos. Soc.* 90, 927–963. doi: 10.1111/brv.12140
- Suthar, S., and Singh, D. (2011). Phytotoxicity of composted herbal pharmaceutical industry wastes. *Environ. Sci. Pollut. Res. Int.* 19, 3054–3059. doi: 10.1007/s11356-012-0985-yv
- Turnbaugh, P., Ley, R., Mahowald, M., Magrini, V., Mardis, E., and Gordon, J. (2006). An obesity-associated gut microbiome with increased capacity for energy harvest. *Nature* 444, 1027–1031. doi: 10.1038/nature05414
- Wang, B., Wang, Y., Zuo, S., Peng, S., Wang, Z., Zhang, Y., et al. (2021). Untargeted and Targeted Metabolomics Profiling of Muscle Reveals Enhanced Meat Quality in Artificial Pasture Grazing Tan Lambs via Rescheduling the Rumen Bacterial Community. *J. Agric. Food Chem.* 69, 846–858. doi: 10.1021/acs.jafc.0c06427
- Wang, H., Ji, Y., Yin, C., Deng, M., Tang, T., Deng, B., et al. (2018). Differential analysis of gut microbiota correlated with oxidative stress in sows with high or low litter performance during lactation. *Front. Microbiol.* 9:1665. doi: 10.3389/fmicb.2018.01665
- Wilson, T. A., Kritchevsky, D., Kotyla, T., and Nicolosi, R. J. (2006). Structured triglycerides containing caprylic (8:0) and oleic (18:1) fatty acids reduce blood cholesterol concentrations and aortic cholesterol accumulation in hamsters. *Biochim. Biophys. Acta* 1761, 345–349. doi: 10.1016/j.bb.alip
- Xie, Y., Chen, Z., Wang, D., Chen, G., Sun, X., He, Q., et al. (2020). Effects of Fermented Herbal Tea Residues on the Intestinal Microbiota Characteristics of Holstein Heifers Under Heat Stress. *Front. Microbiol.* 11:1014. doi: 10.3389/fmicb.2020.01014
- Yan, J., Liu, P., Xu, L., Huan, H., Zhou, W., Xu, X., et al. (2018). Effects of exogenous inosine monophosphate on growth performance, flavor compounds, enzyme activity, and gene expression of muscle tissues in chicken. *Poult. Sci.* 97, 1229–1237. doi: 10.3382/ps/pex415
- Yang, X., and Cui, X. (2013). Adsorption characteristics of Pb (II) on alkali treated tea residue. *Water Resour. Ind.* 3, 1–10. doi: 10.1016/j.wri.2013.05.003
- Yuan, M., Li, D., Zhang, Z., Sun, H., An, M., and Wang, G. (2018). Endometriosis induces gut microbiota alterations in mice. *Hum. Reprod.* 33, 607–616. doi: 10.1093/humrep/dex372
- Zhao, J., Deng, J., Chen, Y., and Li, S. (2013). Advanced phytochemical analysis of herbal tea in China. *J. Chromatogr.* 1313, 2–23. doi: 10.1016/j.chroma.2013.07.039
- Zhu, Z., Song, Z. H., Cao, L. T., Wang, Y., Zhou, W. Z., Zhou, P., et al. (2018). Effects of traditional Chinese medicine formula on ruminal fermentation, enzyme activities and nutrient digestibility of beef cattle. *Anim. Sci. J.* 89, 661–671. doi: 10.1111/asj.12978
- Zhuang, X., Chen, Z., Sun, X., Li, F., Luo, J., Chen, T., et al. (2021). Fermentation quality of herbal tea residue and its application in fattening cattle under heat stress. *BMC Vet. Res.* 17:348. doi: 10.1186/s12917-021-03061-y

Conflict of Interest: The authors declare that the research was conducted in the absence of any commercial or financial relationships that could be construed as a potential conflict of interest.

Publisher's Note: All claims expressed in this article are solely those of the authors and do not necessarily represent those of their affiliated organizations, or those of the publisher, the editors and the reviewers. Any product that may be evaluated in this article, or claim that may be made by its manufacturer, is not guaranteed or endorsed by the publisher.

Copyright © 2022 Li, Sun, Luo, Chen, Xi, Zhang and Sun. This is an open-access article distributed under the terms of the Creative Commons Attribution License (CC BY). The use, distribution or reproduction in other forums is permitted, provided the original author(s) and the copyright owner(s) are credited and that the original publication in this journal is cited, in accordance with accepted academic practice. No use, distribution or reproduction is permitted which does not comply with these terms.

RESEARCH

Open Access



Identification of circRNA-associated ceRNA networks using longissimus thoracis of pigs of different breeds and growth stages

Xiaona Zhuang, Zekun Lin, Fang Xie, Junyi Luo, Ting Chen, Qianyun Xi, Yongliang Zhang* and Jiajie Sun*

Abstract

Background: Long-term artificial selection for growth rate and lean meat rate has eventually led to meat quality deterioration. Muscle fiber type is a key factor that markedly affects meat quality. circRNAs have been reported to participate in diverse biological activities, including myofiber growth and development; thus, we herein compared porcine circRNA transcriptome between oxidative and glycolytic muscle tissues.

Results: Longissimus thoracis muscle tissues were obtained from Lantang and Landrace pigs at birth (LT1D and LW1D, respectively) and 90 postnatal days (LT90D and LW90D, respectively). Hematoxylin and eosin staining and quantitative real-time PCR revealed that all structural traits of the muscle showed large variations between different breeds and growth stages. In total, 329 known miRNAs and 42,081 transcript candidates were identified; 6,962 differentially expressed transcripts were found to play a key role in myogenesis by gene ontology and Kyoto Encyclopedia of Genes and Genomes pathway analyses. In addition, 3,352 circRNAs were identified using five predicting algorithms, and 104 circRNA candidates were differentially expressed. Integrated analysis of differentially expressed miRNAs, mRNAs, and circRNAs led to the identification of 777, 855, and 22 convincing ceRNA interactions in LT1D vs. LT90D, LW1D vs. LW90D, and LT90D vs. LW90D, respectively. Finally, we identified a circRNA candidate circKANSL1L, which showed high homology between mice and pigs, and it was found to inhibit the proliferation of C₂C₁₂ cells but promote their differentiation.

Conclusions: We identified genome-wide circRNAs in 0- and 90-day-old Lantang and Landrace pigs by RNA-seq and found that circRNAs were abundant, differentially expressed, and associated with myogenesis. Our results should serve as a reference for future studies on pork quality.

Keywords: CircRNA, Meat quality, C₂C₁₂, circKANSL1L, RNA-seq

Background

Over the past few decades, modern pig breeding programs have primarily focused on the genetic improvement of economically important traits [1]. Consequently, commercial pig breeds with highly

desirable features, such as rapid growth rate [2], favorable feeding behavior [3], higher weight gain [2], lean meat content [2], excellent fertility [4], and enhanced disease resistance [5], now exist. Certain meat quality traits, such as color, marbling, tenderness, juiciness, and flavor, play an essential role in the consumer acceptance of pork; however, long-term selection has been reported to markedly affect these traits [6]. Pork quality is a complex feature that is associated with various physical and biochemical parameters, including environmental conditions, pre-slaughter handling,

*Correspondence: jiajiesun@scau.edu.cn

Guangdong Provincial Key Laboratory of Animal Nutrition Control, National Engineering Research Center for Breeding Swine Industry, Guangdong Laboratory for Lingnan Modern Agriculture, South China Agricultural University, Guangzhou 510642, Guangdong, China



© The Author(s) 2022. **Open Access** This article is licensed under a Creative Commons Attribution 4.0 International License, which permits use, sharing, adaptation, distribution and reproduction in any medium or format, as long as you give appropriate credit to the original author(s) and the source, provide a link to the Creative Commons licence, and indicate if changes were made. The images or other third party material in this article are included in the article's Creative Commons licence, unless indicated otherwise in a credit line to the material. If material is not included in the article's Creative Commons licence and your intended use is not permitted by statutory regulation or exceeds the permitted use, you will need to obtain permission directly from the copyright holder. To view a copy of this licence, visit <http://creativecommons.org/licenses/by/4.0/>. The Creative Commons Public Domain Dedication waiver (<http://creativecommons.org/publicdomain/zero/1.0/>) applies to the data made available in this article, unless otherwise stated in a credit line to the data.

slaughter procedure, energy metabolism, lipid deposition, and myofiber characteristics [7, 8]. In general, muscle fibers strongly influence meat quality, and they can be differentiated into oxidative and glycolytic types depending on contractile and metabolic properties as well as morphological traits [9].

The growth and development of myofibers involves ontogenesis during distinct embryonic stages, as well as hypertrophy and conversion in postnatal stage [10]. Such biological processes are controlled by several myogenic regulatory factors [11], signaling pathways [12], genes, and noncoding RNAs (ncRNAs) [13] via diverse mechanisms. Circular RNAs (circRNAs) are a large class of ncRNAs with covalently closed continuous loop structures, and they are produced from precursor mRNA back-splicing [14]. Recent research indicates that circRNAs play a key role in myogenesis in various organisms [15]. They are dynamically expressed and particularly abundant in muscle tissues across many species, including humans [16], monkeys [17], bovine [18], goats [19], sheep [20], pigs [21], chicken [22], and mice [23]. Although the functions of circRNAs remain largely unexplored, their most important role is to serve as miRNA sponge and promote mRNA stability or protein production [24]. In this study, we compared porcine circRNA transcriptome between oxidative and glycolytic skeletal muscles. Our core objective was to reveal circRNA-associated ceRNA

network so as to support further systematic studies of myogenesis.

Results

Muscle Fiber Type Distribution

Hematoxylin and eosin staining was performed to characterize the structural traits of longissimus thoracis between Lantang and Landrace pigs at birth (LT1D and LW1D, respectively) and 90 postnatal days (LT90D and LW90D, respectively). The number of fibers per unit area and average cross-sectional area of myofibers were determined (Fig. S1). We found that the structural traits showed large variations between different growth stages ($P < 0.01$). To explain, the number of myofibers significantly decreased between birth and 90 postnatal days ($P < 0.01$), and the average cross-sectional area of myofibers showed an obvious increase during postnatal development ($P < 0.01$). Further, Lantang pigs showed higher number of myofibers than Landrace pigs at birth ($P < 0.01$), but there were no significant differences in terms of the cross-sectional area of myofibers. In comparison with Landrace pigs, Lantang pigs showed lower number and cross-sectional area of myofibers at 90 postnatal days ($P < 0.01$). We then calculated the proportion of different muscle fiber types based on the expression of myosin heavy chain isoforms (MyHCs; Fig. 1). The proportion of MyHC I, IIa, and IIx myofibers at birth was higher than that at 90 postnatal days in both Lantang and Landrace pigs ($P < 0.01$), while the proportion of MyHC

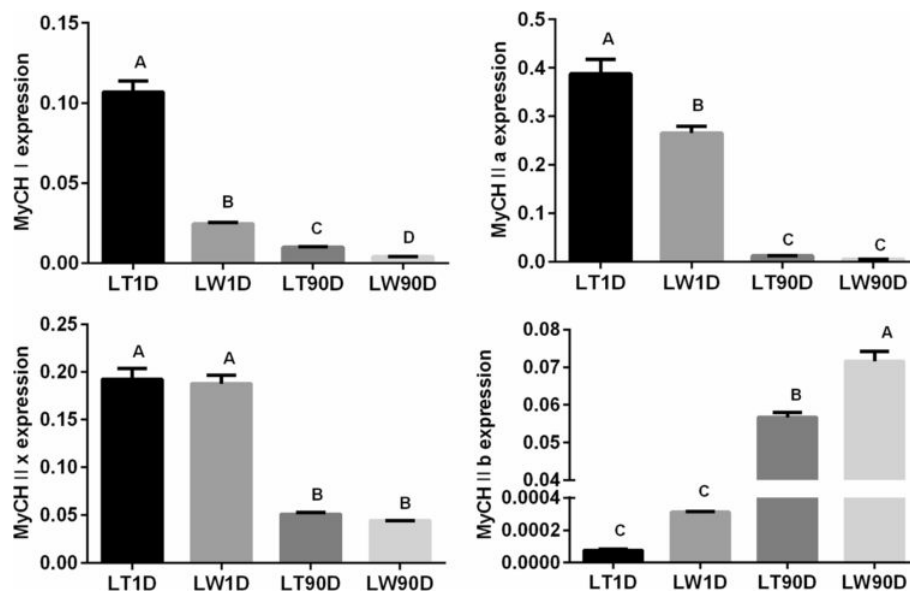


Fig. 1 Relative expression level of MyHC isoforms (I, IIa, IIx, and IIb) in Lantang and Landrace pigs at birth and 90 postnatal days. Values represent mean \pm SD of three biological replicates. LT1D, Lantang pig 1 day after birth; LW1D, Landrace pig 1 day after birth; LT90D, Lantang pig 90 days after birth; LW90D, Landrace pig 90 days after birth. Different superscripts indicate significant differences at $P < 0.01$

IIf myofibers was higher at 90 postnatal days ($P < 0.01$). At birth, the expression of MyHC I and IIa in Lantang pigs was significantly higher than that in Landrace pigs ($P < 0.01$), while the expression of MyHC IIf was higher in Landrace pigs ($P > 0.05$). Besides, at 90 postnatal days, higher amount of MyHC I was distributed in Lantang pigs ($P < 0.01$), and MyHC IIf showed the opposite trend between Lantang and Landrace pigs ($P < 0.01$).

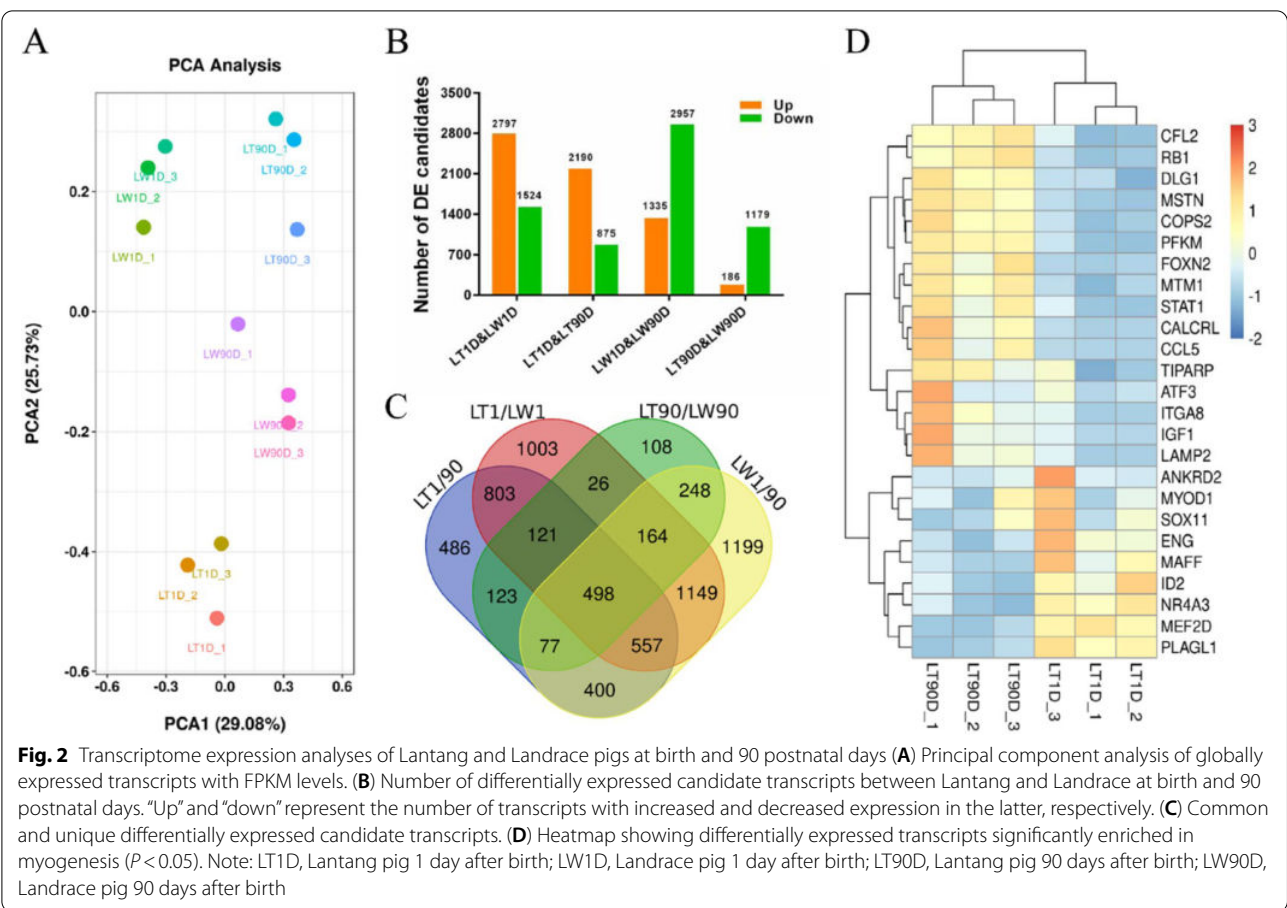
miRNA Expression Analysis

miRNA-seq generated 21.06 ± 1.32 million raw reads with a length of 49 nucleotides from each library. After filtering, approximately 18.68 ± 1.33 million clean reads were obtained, accounting for $89.12\% \pm 3.47\%$ of total raw sequences (Table S1A). The clean sequences were then annotated and assigned to 470.78 ± 86.52 thousand unique tags in each library by alignments to Rfam and porcine-specific sequences within miRBase, Repeat and Reference mRNA databases (Table S1B). We observed that only $3.16\% \pm 0.41\%$ ($11,464 \pm 415$ per library) unique reads belonged to known porcine miRNAs, and these unique reads represented $15.27\% \pm 0.69\%$ ($2,871,531 \pm 269,401$ per library) of total clean sequences. Using the miRDeep2 algorithm, 321, 311, 315, and 316 known miRNAs were identified in LT1D, LT90D, LW1D, and LW90D libraries, respectively, and 302 miRNAs were common across all samples. The 10 most highly expressed miRNAs in each library accounted for $71.26\% \pm 1.15\%$ of the total count of all identified miRNAs, and six miRNAs (miR-1, miR-206, let-7a, let-7c, miR-10b, and let-7f) were found across all libraries. Of them, ssc-miR-206 showed the highest expression level in LT1D and LW1D libraries, as well as ssc-miR-1 in LT90D and LW90D libraries. We further investigated differentially expressed miRNAs between different breeds and growth stages (Table S1C). In Lantang pigs, 89 miRNAs were differentially expressed between LT1D and LT90D libraries; 34 miRNAs were upregulated and 55 were downregulated in LT90D libraries. In Landrace pigs, 100 differentially expressed miRNAs were identified; 19 miRNAs were upregulated and 81 were downregulated in LW90D libraries. At birth, only seven miRNAs were differentially expressed between LT1D and LW1D libraries, including six up- and one downregulated miRNAs in LW1D libraries, and at 90 postnatal days, 11 miRNAs were differentially expressed between LT90D and LW90D libraries, including four up- and seven downregulated miRNAs in LW90D libraries.

Transcriptome Expression Analysis

In total, 12 muscle tissue samples obtained from Lantang and Landrace pigs at birth and 90 postnatal days (in triplicate) were subjected to Illumina sequencing after rRNA depletion, which led to the generation of

approximately 1.49 billion reads (average of 124.57 ± 0.29 million reads per sample). After quality control/trimming, 122.86 ± 0.21 million valid reads were obtained, accounting for $98.63\% \pm 0.19\%$ of raw reads in each library. On alignment of all valid reads, we found that over $84.45\% \pm 1.46\%$ clean reads could be successfully mapped to the porcine *Sscrofa11.1* reference genome, including $78.88\% \pm 1.26\%$ mapped reads with proper pair alignment (Table S2A). Transcript assemblies with StringTie revealed 138,278 isoforms across the 12 libraries, including approximately 24.98% identified candidates that completely matched Ensembl transcript regions (Table S2B). A comparison of known Ensembl transcripts revealed that 39,734, 39,909, 40,445, and 38,429 known transcripts were expressed in LT1D, LT90D, LW1D, and LW90D libraries, respectively; 42,081 transcripts existed in all libraries (Table S3A). Principal component analysis of globally expressed transcripts with fragments per kilobase of transcript per million mapped reads (FPKM) levels was performed, which showed that the differences between groups caused by breed or age were much greater than those between experimental individuals (Fig. 2A). We therefore applied the Ballgown algorithm to analyze differences in libraries between different breeds and growth stages (Fig. 2B). With normalized RPKM, there were 4,321 differentially expressed Ensembl transcripts between LT1D and LW1D libraries; 2,797 transcripts were upregulated and 1,524 were downregulated in LW1D libraries (Table S3B). Between LT1D and LT90D libraries, we detected 3,065 differentially expressed transcripts; 2,190 transcripts were upregulated and 875 were downregulated in LT90D libraries (Table S3C). Further, 4,292 differentially expressed transcripts were identified between LW1D and LW90D libraries; 1,335 transcripts were significantly upregulated and 2,957 were downregulated in LW90D libraries (Table S3D). In comparison with LW90D libraries, the expression levels of 1,365 transcripts were significantly different in LT90D libraries; 186 and 1,179 transcripts were up- and downregulated in LW90D libraries, respectively (Table S3E). In total, 6,962 unique differentially expressed transcripts were found on comparing LT1/90D, LW1/90D, LT/LW90D, and LT/LW1D, and only 498 transcripts were common (Fig. 2C). Gene ontology (GO) analysis revealed that these differentially expressed transcripts were significantly enriched ($P < 0.05$) in several biological processes associated with myogenesis, including skeletal muscle cell differentiation, muscle cell cellular homeostasis, positive regulation of smooth muscle cell proliferation, smooth muscle tissue development, muscle contraction, regulation of skeletal muscle satellite cell proliferation, and response to muscle stretch (Table S4A–D), and 25 myogenesis-related transcripts were identified between LT1D and



LT90D samples (Fig. 2D). Moreover, Kyoto Encyclopedia of Genes and Genomes (KEGG) pathway analysis revealed that several differentially expressed transcripts were involved in muscle development and growth pathways, such as mTOR signaling pathway, Wnt signaling pathway, AMPK signaling pathway, and biosynthesis of amino acids (Table S4E–H). We randomly selected 10 dysregulated mRNAs (PFKM, ANKRD2, MSTN, MYOD1, SRF, IGF1, MYBPC2, LIMCH1, PFKFB1, and MEF2D; Fig. S2A) from these myogenesis-related GO terms and signaling pathways and validated their expression levels by performing quantitative real-time PCR (RT-qPCR). Between LT1D and LW1D, RT-qPCR data revealed that the expression levels of ANKRD2, MYOD1, LIMCH1, and MEF2D were significantly upregulated in LT1D, but those of PFKM, MSTN, MYBPC2, SRF, and PFKFB1 did not show a significant change. The RT-qPCR results of MSTN, ANKRD2, and SRF were inconsistent with those of RNA-seq. According to RNA-seq data, there was no significant difference in the expression level of ANKRD2, whereas the expression levels of SRF and MSTN were significantly upregulated in LT1D and LW1D, respectively. Further, in the comparison between

LT1D and LT90D, the expression levels of ANKRD2, MYOD1, LIMCH1, and MEF2D were significantly upregulated in LT1D, and those of PFKM, MSTN, SRF, and MYBPC2 were significantly upregulated in LT90D; PFKFB1 was not significantly differentially expressed. RNA-seq did not reveal any significant differences in LIMCH1 expression between LT1D and LT90D. In the comparison between LW1D and LW90D, the expression levels of ANKRD2 and MEF2D were significantly upregulated in LT90D, and those of MSTN, SRF, MYBPC2, and PFKFB1 were significantly upregulated in LW90D; PFKM, MYOD1, and LIMCH1 expression showed no significant differences. According to RNA-seq data, the expression level of SRF was significantly upregulated in LW1D, which contradicted RT-qPCR results. In the comparison between LT90D and LW90D, the expression level of PFKM was significantly upregulated in LT90D and that of PFKFB1 was significantly upregulated in LW90D, but MSTN, MYOD1, MYBPC2, LIMCH1, ANKRD2, and SRF expression levels showed no significant differences. The results for MSTN, PFKFB1, and PFKM were inconsistent between RT-qPCR and RNA-seq. RNA-seq data indicated that the expression levels of PFKFB1 and

PFKM did not show a significant change between LT90D and LW90D, while the expression level of *MSTN* was significantly upregulated in LW90D (Fig. S2B).

Identification of circRNAs

We characterized circRNA landscape and expression by performing deep RNA-seq experiments using the 12 aforementioned muscle tissue samples. In total, 52,133 circRNA candidates were identified using five different predicting algorithms (Fig. 3A); circRNA landscape differed quite radically depending on the algorithm used. To explain, 25,295, 33,283, 10,601, 38,292, and 4,751 circRNA candidates were detected by CIRCexplorer2, circRNA_Finder, CIRI, find_circ, and MapSplice algorithms, respectively (Table S5); find_circ and MapSplice exhibited the highest and lowest level of sensitivity, respectively. Only 3,352 circRNA candidates were commonly detected by all five algorithms, and these were subjected to further analyses. These circularization events were found to be produced from 1,745 hosting transcript loci, including 712 transcripts that generated multiple circRNA candidates (Table S6). With normalized back-splice junction reads, we analyzed significant differences in circRNA candidates across four comparisons: LT/LW1D, LT1/90D, LW1/90D, and LT/LW90D (Fig. 3B). Only three differentially expressed circRNA candidates were found between LT1D and LW1D libraries, and all three of them were significantly upregulated in LW1D library. Further, 39 and 38 circRNA candidates were differentially expressed between LT1D and LT90D libraries and between LW1D and LW90D libraries, respectively (Fig. 3C). Interestingly, 24 differentially expressed circRNA candidates were differentially expressed between LT90D and LW90D libraries, and all of them were downregulated in LW90D libraries.

Construction of circRNA-associated-ceRNA Networks

The expression of circRNAs potentially plays a key role in physiological and pathological conditions by regulating endogenous RNA targets [25]. We therefore performed Pearson correlation analysis to assess the association between differentially expressed

circRNAs and mRNAs in each comparison (Fig. S3), which revealed 8, 187, 456, and 69 significant interactions in LT1D vs. LW1D, LT1D vs. LT90D, LW1D vs. LW90D, and LT90D vs. LW90D, respectively. Few circRNA candidates have been reported to directly modulate the transcription of their parent genes [26]. Herein we found that only circANKRD2, derived from exons 3 and 4 of *ANKRD2*, was positively correlated with its linear counterpart at the expression level between LW1D and LW90D, suggesting the involvement of circANKRD2 and *ANKRD2* in myogenesis. In addition, it has been found that endogenous circRNAs serve as miRNA sponges to consequently repress the function of their targets [27]. This prompted us to predict shared miRNA-binding sites between differentially expressed circRNAs and mRNAs (Table S7A–G) and further analyze circRNA-miRNA-mRNA ceRNA networks. We identified 777, 855, and 22 convincing ceRNA interactions in LT1D vs. LT90D, LW1D vs. LW90D, and LT90D vs. LW90D, respectively (Table S7H–J); the number of putative interactions per miRNA markedly varied, ranging from 1 to 51 miRNA-associated ceRNA networks. We observed that the highly expressed circKANS1L1L, circKANS1L1L_2, circKANS1L1L_3, circKANS1L1L_4, and circKANS1L1L_5 participated in 279 ceRNA transcriptional regulatory axes, including a total of 27 unique myo-miRNAs and 30 special myogenes. As evident from Fig. 3D, LT1D and LT90D comparison revealed 31 up–down–up regulation patterns: circKANS1L1L, circKANS1L1L_2, and circKANS1L1L_3 were upregulated in LT90D and could sponge miR-128, miR-130a, miR-133b, miR-142-3p, miR-19a, miR-19b, miR-432-5p, miR-7142-3p, and miR-885-5p to significantly upregulate *ATF3*, *CFL2*, *COPS2*, *DLG1*, *ITGA8*, *MSTN*, *MYOD1*, *PFKM*, and *TIPARP* expression (Table S7H). On the contrary, 14 down–up–down regulation patterns were identified on comparing LW1D and LW90D: circKANS1L1L_4 was downregulated in LW90D and could sponge miR-130a, miR-19a, miR-19b, miR-299, miR-376a-3p, miR-487b, and miR-493-5p to significantly downregulate *ACTN2*, *COPS2*, *FBXO40*, *FOXN2*, *MYBPC1*, *SCN7A*, *TPM3*, and *TPM4* expression (Table S7I).

(See figure on next page.)

Fig. 3 Identification of circRNA candidates using five predicting algorithms (A) Common circRNA candidates identified by all five algorithms. (B) Number of differentially expressed circRNAs between Lantang and Landrace pigs at birth and 90 postnatal days. “Up” and “down” represent the number of circRNAs with increased and decreased expression in the latter, respectively. (C) Heatmap showing differentially expressed circRNAs. (D) 31 up–down–up regulation patterns of circRNA-miRNA-mRNA correlation networks between LT1D and LT90D comparison. Solid circles represent circRNAs, triangles represent miRNAs, and squares represent coding genes. Red represents upregulation and green represents downregulation in Lantang pigs. Color depth represents $-\log(\text{FDR value}, 2)$, and a darker color represents greater significant. Size represents $\log(\text{mean FPKM level in LT1D}, 10)$, and a bigger size represents greater expression in Lantang pigs at birth. Note: LT1D, Lantang pig 1 day after birth; LW1D, Landrace pig 1 day after birth; LT90D, Lantang pig 90 days after birth; LW90D, Landrace pig 90 days after birth

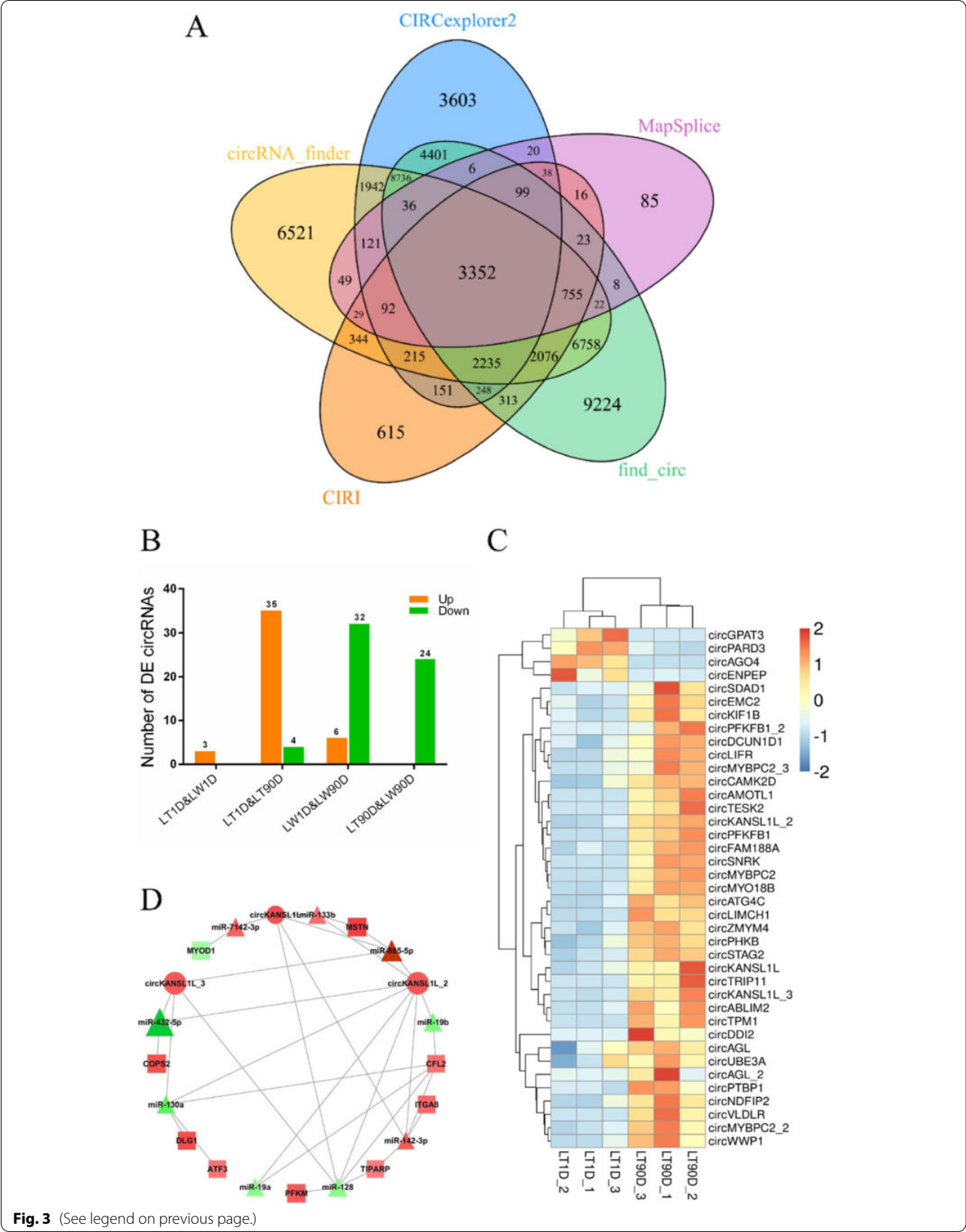


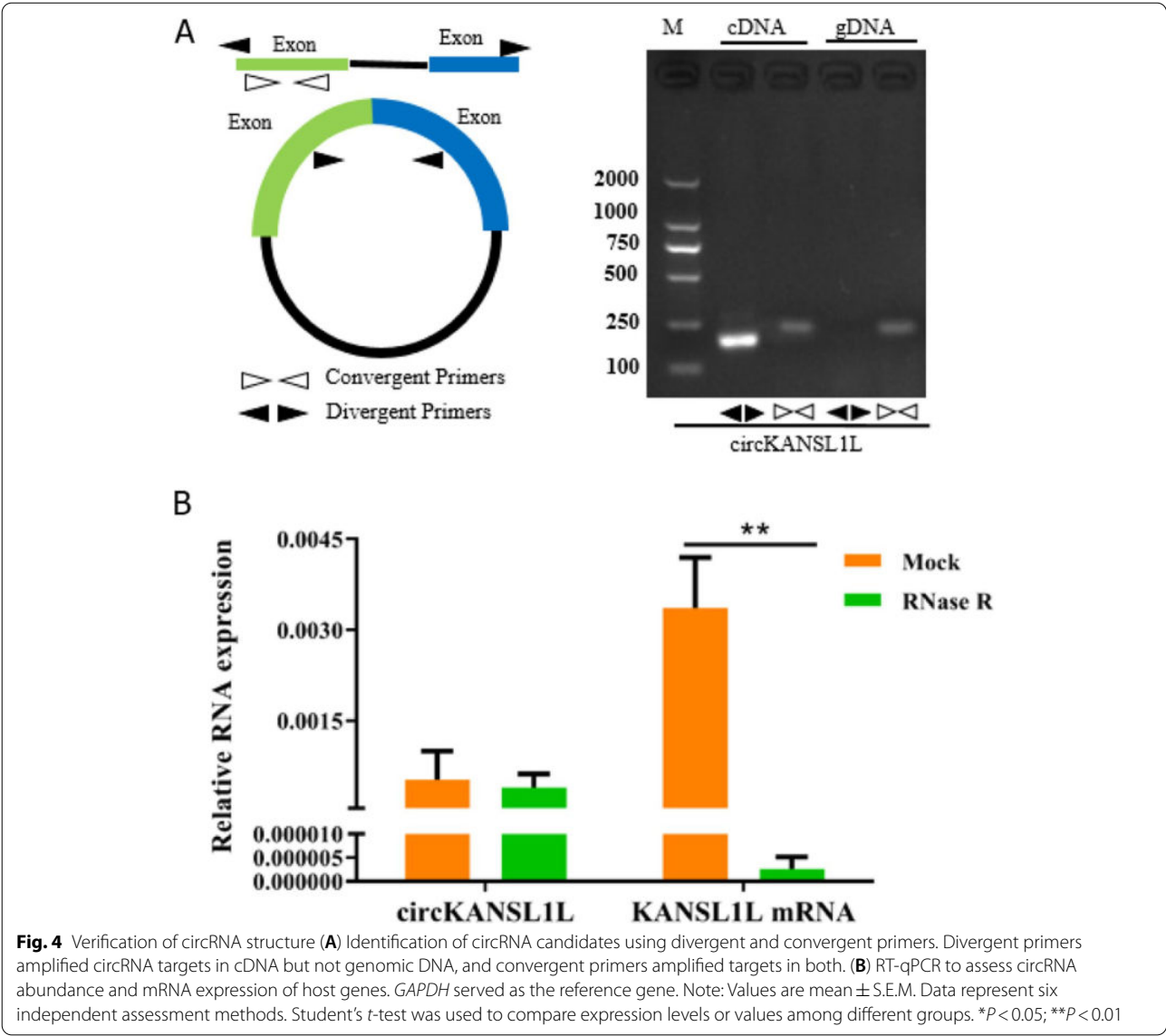
Fig. 3 (See legend on previous page.)

Characterization of Myogenesis-related circRNAs

To verify the circular structure of circRNAs, differentially and highly expressed circRNA candidates that were correlated with myogenes were selected for further analyses. cDNA was amplified using a pair of divergent primers, which led to the identification of nine circRNAs: circP-FKFB1, circKANSL1L-3, circLIMCH1, circKANSL1L, circ4082, circKANSL1L-2, circMYBPC2, circMYBPC2-2, and circNR1H3 (Fig. S4A). Sanger sequencing further verified their head–tail junction structure (Fig. S4B).

Furthermore, on comparing the homology of the nine aforementioned circRNAs, we found that circKANSL1L sequence showed high homology between

mice and pigs based on NCBI blastn suite (Fig. S5). To further verify their structure, we analyzed them in C₂C₁₂ cells using divergent and convergent primers (Fig. 4). Convergent primers could successfully amplify both cDNA and genomic DNA, but divergent primers could only amplify cDNA (Fig. 4A). On RNase R digestion and RT-qPCR of the circRNAs and hosting mRNA, we found that there was no significant change in circRNA expression levels between the RNase R treatment and control groups. However, the mRNA expression level of the hosting gene was significantly different ($P < 0.01$, Fig. 4B). These findings further suggested that the structure of circKANSL1L was indeed circular.



Inhibition of C₂C₁₂ Cell Proliferation by circKANS1L

To elucidate the role of circKANS1L in myogenesis, we constructed the overexpression plasmid OE-circKANS1L and designed the knockdown gene si-circKANS1L, and RT-qPCR was performed to verify their effects. We found that OE-circKANS1L and

si-circKANS1L significantly increased and decreased the expression of circKANS1L in C₂C₁₂ cells, but the expression of the host gene KANS1L was unaffected (Fig. 5A).

Besides, RT-qPCR was performed to assess the relative expression levels of the cell proliferation-related genes PCNA, Cyclin D1, and Cyclin E. After circKANS1L

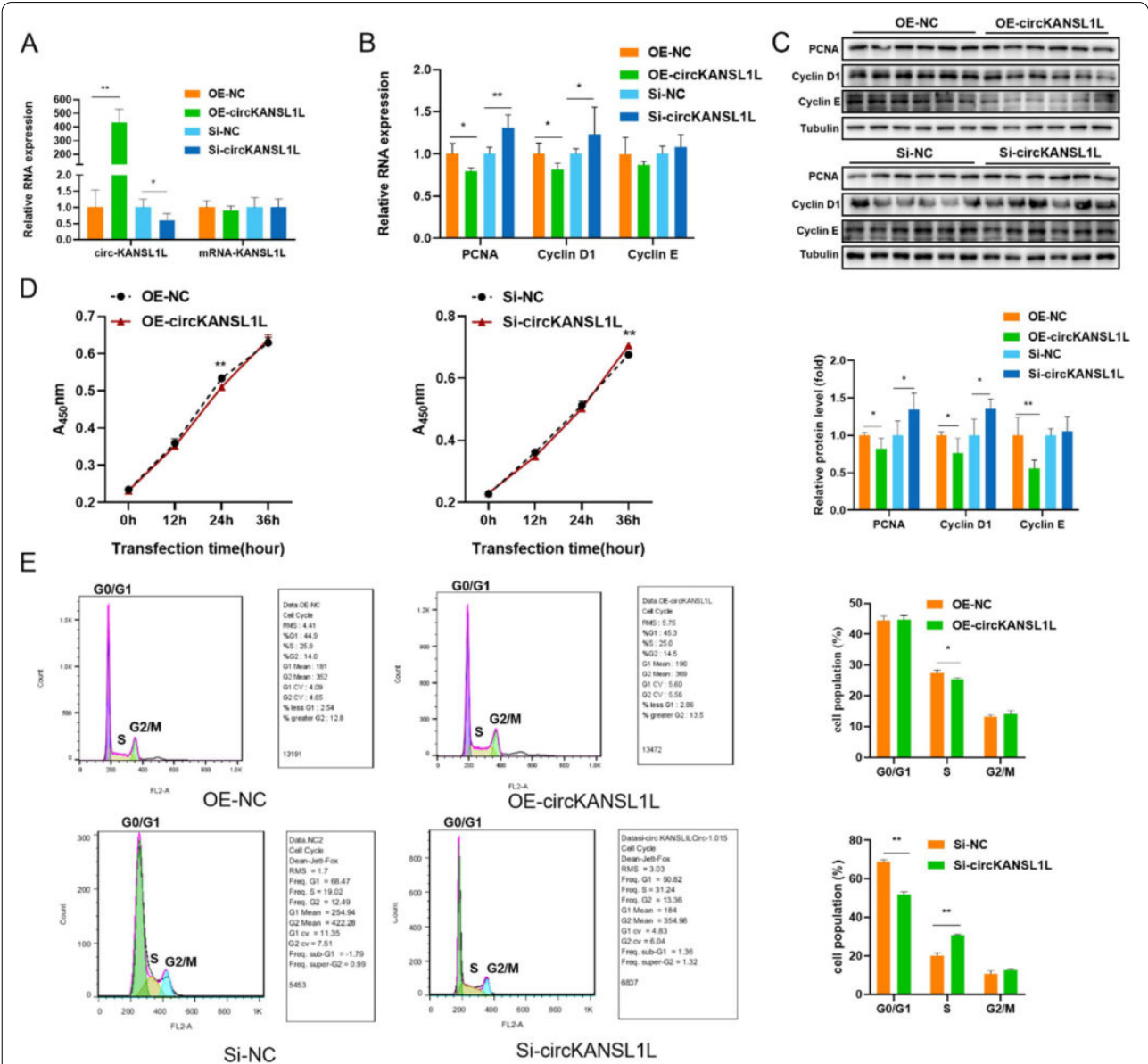


Fig. 5 Inhibition of C₂C₁₂ cell proliferation by circKANS1L (A) Relative expression of circKANS1L and mRNA-KANS1L in C₂C₁₂ cells following circKANS1L overexpression or inhibition. GAPDH served as the reference gene. (B) Relative RNA and (c, above panel) protein levels of cell proliferation-related genes in C₂C₁₂ cells following circKANS1L overexpression or inhibition. (C, below panel) PCNA, CyclinD1, and CyclinE band intensities quantified by Image J and normalized against internal reference Tubulin. (D) Growth curve of C₂C₁₂ cells following circKANS1L overexpression and inhibition. (E) Cell cycle analysis of C₂C₁₂ cells following circKANS1L overexpression or inhibition. Note: Values are mean ± S.E.M. Data represent six independent assessment methods. Student's t-test was used to compare expression levels or values among different groups. *P < 0.05; **P < 0.01

overexpression, the expression level of PCNA ($P < 0.05$) and Cyclin D1 ($P < 0.05$) significantly decreased in C_2C_{12} cells and that of Cyclin E showed the same trend ($P > 0.05$). After circKANS1L1 knockdown, the expression level of PCNA ($P < 0.01$) and Cyclin D1 ($P < 0.05$) significantly increased in C_2C_{12} cells and that of Cyclin E also increased, but the change was not significant ($P > 0.05$; Fig. 5B). When circKANS1L1 expression was upregulated, the protein expression levels of PCNA ($P < 0.05$), Cyclin D1 ($P < 0.01$), and Cyclin E ($P < 0.01$) significantly decreased, and when circKANS1L1 expression was downregulated, the protein expression levels of PCNA ($P < 0.05$) and Cyclin D1 ($P < 0.05$) significantly increased and that of Cyclin E also increased, but the change was not significant ($P > 0.05$; Fig. 5C), these results were consistent with RT-qPCR results. On transfecting C_2C_{12} cells with empty vector and OE-circKANS1L1, cell proliferation was measured by Cell Counting Kit-8 (CCK-8) assay at 0, 12, 24, and 36 h. In comparison with the empty vector group, after circKANS1L1 overexpression, absorbance (450 nm) significantly decreased at 24 h ($P < 0.01$); however, after circKANS1L1 knockdown, absorbance (450 nm) significantly increased at 36 h ($P < 0.01$; Fig. 5D). In addition, our cell cycle analysis

showed that when circKANS1L1 was overexpressed, cells were arrested in the G1 phase, and the number of cells entering the S phase was significantly lower than that in the control group ($P < 0.05$). circKANS1L1 knockdown promoted the progression of C_2C_{12} cells to the S and G2 phases ($P < 0.01$, Fig. 5E). Altogether, these results indicated that circKANS1L1 inhibited the proliferation of C_2C_{12} cells.

Enhancement of C_2C_{12} Cell Differentiation by circKANS1L1

RT-qPCR was performed to assess the relative expression levels of MYF5, MYOD1, Myogenin (MYOG), and MyHC (Fig. 6A). circKANS1L1 overexpression significantly increased the expression levels of MYF5 ($P = 0.06$), MYOD1 ($P < 0.05$), MYOG ($P < 0.05$), and MyHC ($P < 0.05$), while circKANS1L1 knockdown significantly decreased their expression levels ($P < 0.05$ for all). Western blotting was performed to detect MYOD1, MYOG and MyHC protein expression levels (Fig. 6B). The results showed the same trend as RT-qPCR results, and the data were significant (MYOD1, $P < 0.05$; MYOG, $P < 0.01$; MyHC, $P < 0.05$). We also assessed RNA expression levels of MyHC I and MyHC IIb. CircKANS1L1

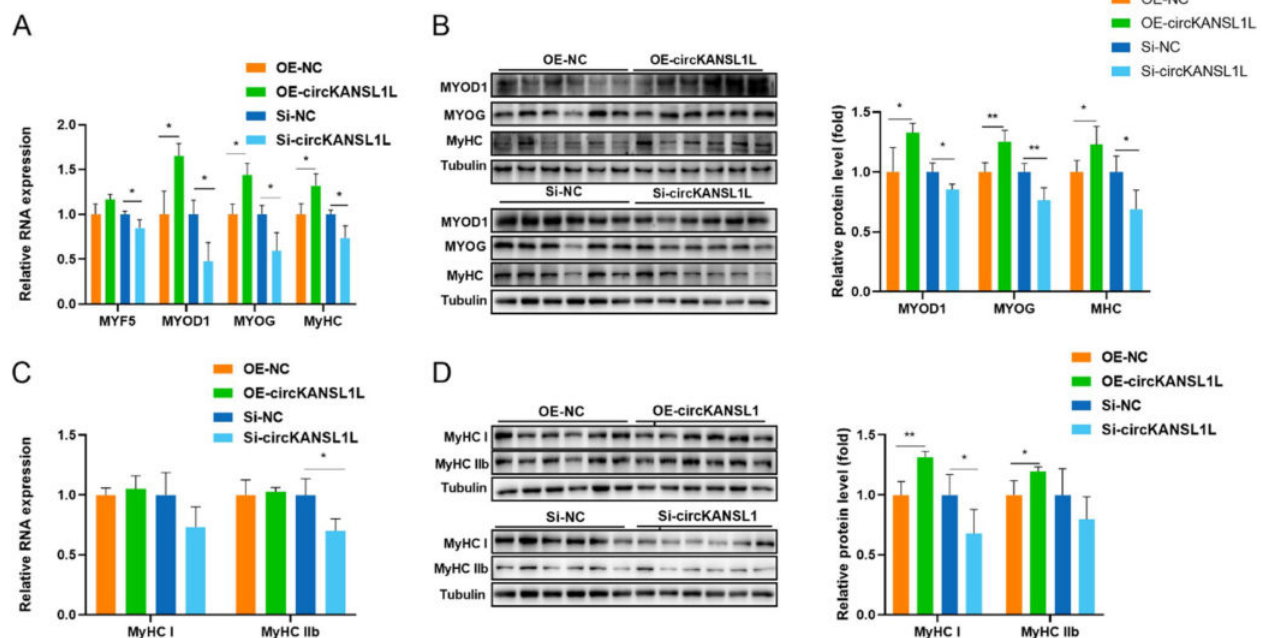


Fig. 6 Enhancement of C_2C_{12} cell differentiation by circKANS1L1. **(A)** Relative RNA levels of muscle cell differentiation marker genes in C_2C_{12} cells following circKANS1L1 overexpression or inhibition. GAPDH served as the reference gene. **(B)** Protein levels of MYOG and MyHC in C_2C_{12} cells following circKANS1L1 overexpression or inhibition (left panels). MYOG and MyHC band intensities were quantified by Image J and normalized against GAPDH (right panels). **(C)** Relative RNA levels of MyHC I and IIb in C_2C_{12} cells following circKANS1L1 overexpression or inhibition. **(D)** Protein levels of MyHC I and IIb in C_2C_{12} cells following circKANS1L1 overexpression or inhibition (left panels). MyHC I and IIb band intensities were quantified by Image J and normalized against GAPDH (right panels). Values are mean \pm S.E.M. Data represent six independent assessment methods. Student's *t*-test was used to compare expression levels or values among different groups. * $P < 0.05$; ** $P < 0.01$

overexpression promoted MyHC I and MyHC IIb expression, while circKANSL1L knockdown inhibited MyHC I and MyHC IIb expression, but the results were insignificant (Fig. 6C). Protein expression levels showed a consistent trend with RNA expression levels (Fig. 6D). When circKANSL1L expression was upregulated, the protein expression levels of MyHC I ($P < 0.01$) and MyHC IIb ($P < 0.05$) significantly increased, and when circKANSL1L expression was downregulated, the protein expression levels of MyHC I ($P < 0.05$) significantly decreased and MyHC IIb decreased but not significantly ($P > 0.05$), indicating that circKANSL1L has a regulatory effect on muscle fiber type differentiation; further studies are nevertheless warranted.

Discussion

The demand for better meat quality is exponentially increasing among consumers each year, with tenderness, color, water-holding capacity, and flavor of meat being key factors [28]. However, the long-term artificial selection for growth rate and lean meat rate has led to the deterioration of meat quality [29, 30]. Accordingly, several studies focusing on effective strategies to improve meat quality have been reported. Muscle fiber type is evidently a pivotal factor affecting meat quality [31], as it influences the color, water-holding capacity, tenderness, and flavor of meat [32]. Muscle fibers occupy 75%–90% of the total muscle volume [33]. According to the contractile and metabolic properties and morphological traits of muscles, muscle fibers can be differentiated into oxidative and glycolytic types [9]. The proportions of these different muscle fibers reportedly affect meat quality [34]. Larzul et al. (1997) reported that a decrease in the proportion of glycolytic fiber is beneficial to meat tenderness, color, and water-holding capacity [35]. However, it is notable that various factors influence the proportion and distribution of muscle fiber types [33], such as breed, genotype, feeding, slaughter method, chilling, and storage conditions [7, 8].

Landrace pigs (lean type pigs) and Lantang pigs (obese type pigs) have great differences in meat quality, such as fat content, meat color and tenderness [36, 37]. Therefore, in this study, longissimus thoracis muscle tissues were collected from Landrace pigs and Lantang pigs at birth and 90 postnatal days. Through hematoxylin and eosin staining and RT-qPCR, we found that species as well as age affected the distribution of muscle fiber types. There were considerable differences in oxidative and glycolytic muscle tissues between different species and growth stages, and this finding was consistent with that of Zhao et al. [38]. Therefore, these two types of porcine muscle tissues can be reliably used to comprehend the mechanism underlying muscle development and

phenotypic differences [40]. In addition, RNA-seq analysis revealed that some differentially expressed genes between Lantang and Landrace pigs at birth and 90 postnatal days were significantly enriched in myogenesis, and RT-qPCR revealed a small but specific set of these differentially expressed genes with inconsistent expression measurements to RNA-seq analysis. In general, these genes were typically lower expressed, smaller and had fewer exons [41].

With the development of sequencing technology, an increasing number of studies have indicated that ncRNAs play a regulatory role in myogenesis [40, 42, 43]. circRNAs are a type of covalently closed circular RNAs [14], and miRNAs are a class of short ncRNAs with a length of approximately 22 bp [43]. Although the functions of circRNAs remain largely unexplored, they serve as miRNA sponges [24] and ultimately affect mRNA expression [44]. For example, circLMO7 regulates the expression of HDAC4 mRNA by adsorbing miR-378a-3p [27], thereby inhibiting myogenic differentiation. circFRFR4 binds to miR-107 to competitively regulate Wnt3a expression and promote bovine myoblast differentiation [18], and circFUT10 directly binds to miR-133a to regulate myoblast differentiation [45]. Moreover, circHUWE1 targets AKT3 by adsorbing miR-29b, consequently promoting myoblast proliferation and inhibiting cell differentiation [46], and circZFP609 can sponge miR-194-5p to sequester its inhibition on BCLAF1 so as to repress myogenic differentiation [47]. Further, circHIPK3 has been reported to regulate myoblast proliferation and differentiation through the miR-7/TCF12 pathway [48]. Some studies have also shown that circRNAs, such as circZNF609 [49] and circFAM188B [50], play a role in myogenesis directly by translating proteins. Therefore, we explored circRNA transcriptome using oxidative and glycolytic muscle tissues obtained from pigs of different growth stages and revealed circRNA-associated ceRNA networks for further systematic studies of myogenesis. Our experiments led to the identification of differentially expressed miRNAs, mRNAs, and circRNAs between different pig breeds and growth stages. By GO and KEGG pathway analyses, we established a potential molecular signaling pathway for differentially expressed mRNAs, which was related to muscle development. Next, we performed Pearson correlation analysis to study the interaction between circRNAs and mRNA, and finally, a circRNA-miRNA-mRNA ceRNA network related to muscle growth and development was identified. We noticed that circKANSL1L, which was differentially expressed in Lantang pigs at birth and 90 postnatal days, showed a high expression level and participated in pairs of circRNA-miRNA-mRNA networks. It seems that these network pairs play a crucial role in myogenesis. Altogether, our

findings provide a new direction for studying muscle formation and a theoretical basis for improving meat quality.

In general, PCNA is involved in DNA synthesis and DNA damage repair [51], and Cyclin D1 and Cyclin E are regulatory factors of cell cycle progression [52]; all of them reflect the growth rate and state of cells. Our results showed that circKANSL1L decreased the expression level of PCNA, Cyclin D1, and Cyclin E in C₂C₁₂ cells, eventually inhibiting their proliferation. Elnour et al. also used PCNA and Cyclin D1 as marker genes to evaluate the state of cell proliferation, and they found that circMYL1 inhibited the proliferation of bovine primary myoblasts by sponging miR-2400 [53]. Our cell cycle analysis and CCK-8 assay results also indicated that circKANSL1L decreased the proliferation rate of C₂C₁₂ cells. Li et al. found that circFUT10 inhibited myoblast proliferation by blocking cells in the G1/G0 phase [45]. Myf5, MyoD1, and MyoG, as core myogenic regulators, play a key role in myogenesis [54, 55]. The transcription factor MYOG is involved in the regulation of myocyte fusion and is essential for the growth of muscle fibers and proliferation of muscle nuclei [56]. MyHC is the basic unit of myosin, and its expression level indicates the differentiation process of myoblasts [57]. In the present study, circKANSL1L overexpression was found to enhance RNA expression levels of MYF5, MYOD1, MYOG, and MyHC. At the same time, protein expression levels of MYOG and MyHC were detected using Western blotting, and the obtained results showed the same trend as RNA expression levels, further confirming that circKANSL1L promoted the differentiation of C₂C₁₂ cells. Several studies have reported that circRNAs are involved in muscle fiber differentiation. Shen et al. determined the expression levels of MYOD1, MYOG, and MyHC to report that circTMTTC1 inhibited the differentiation of chicken skeletal muscle satellite cells into myotubes by sponging miR-128-3p [58]. Ouyang et al. found that circSVIL overexpression upregulated the mRNA and protein levels of MYOG and MHC, suggesting that circSVIL promoted myoblast differentiation [59]. To summarize, an increasing number of circRNAs are being reported to play a biological role in myogenesis, and our results should serve as a reference.

Conclusions

To conclude, RNA-seq was performed to identify genome-wide circRNAs in 0- and 90-day-old Lantang pigs and Landrace pigs, which revealed that circRNAs were abundant, differentially expressed, and involved in myogenesis. We also identified a novel circRNA, circKANSL1L, which was found to inhibit the proliferation of C₂C₁₂ cells but promote their differentiation.

Methods

Tissue Preparation

Landrace (lean type) and Lantang (fat type) pigs were obtained from Banling breeding farm (Xinfeng County, Shaoguan City, Guangdong Province, China). Five body weight- and sex-balanced piglets of each breed were humanely slaughtered at birth and at 3 months of age (i.e., 10 pigs of each breed); subsequently, 20 longissimus thoracis muscle tissues were immediately collected and snap-frozen in liquid nitrogen for further analyses. In addition, any anesthesia or euthanizing agent was not used in our study.

Muscle Fiber Characteristics

After carcass bleeding, a part of the muscle tissue was cut into approximately 0.5 × 0.5 × 1.0 cm pieces, which were then immediately fixed in 4% paraformaldehyde for 24 h. The samples were then immersed in xylene-alcohol (1:1, v/v), infiltrated, and embedded in paraffin. Cross-sections were prepared at 3-μm thickness, stained with hematoxylin and eosin, viewed under a microscope, and photographed (200 × and 400 × magnification). The number of myofibers and total cross-sectional areas were subsequently assessed using Image-Pro Plus v6.0 (Media Cybernetics Inc., Rockville, MD, USA). In addition, relative expression levels of MyHC isoforms (I, IIa, IIx, and IIb) were analyzed by RT-qPCR, with *GAPDH* serving as the reference gene.

Library Preparation and RNA-seq

Total RNA was extracted from the tissue samples using TRIzol (Takara, Dalian, China). RNA quantity and purity were determined using an Agilent 2100 Bioanalyzer and the RNA 6000 Nano LabChip Kit (Agilent, Santa Clara, USA). For miRNA-seq library construction, RNA fragments of 18–30 nucleotides were separated and enriched by 15% polyacrylamide gel electrophoresis, and proprietary indexed adapters were then ligated to 5'- and 3'-termini. Subsequently, reverse transcription was performed, followed by low-cycle PCR, to obtain sufficient products for Illumina sequencing. For RNA-seq library construction, approximately 10 μg of total RNA per sample was used to deplete rRNA, according to the instructions of the Epicentre Ribo-Zero Gold Kit (Illumina, San Diego, USA), which was followed by TRIzol extraction. The rRNA-depleted RNAs were then fragmented and reverse-transcribed to obtain cDNA libraries using the RNA Library Prep Kit (Illumina). Finally, paired-end sequencing was performed on an Illumina HiSeq4000 platform (LC Sciences, Hangzhou, China).

Primary Analysis

We first used FastQC v0.11.9 (<http://www.bioinformatics.babraham.ac.uk/projects/fastqc/>) to evaluate the preliminary quality of raw sequences and then Cutadapt v2.6 [60] to filter low quality reads and bases contaminated with adapters. Using the SOAP algorithm [61], filtered reads from miRNA-seq libraries were aligned and annotated against porcine mRNA (ftp://ftp.ensembl.org/pub/release-96/fasta/sus_scrofa/cdna/) and CDS (ftp://ftp.ensembl.org/pub/release-96/fasta/sus_scrofa/cds/), Rfam v14.2 (<http://rfam.xfam.org/>), RepeatMasker (<http://www.repeatmasker.org>), and miRBase v22.1 (<http://www.mirbase.org/>). The types and abundance distribution of known porcine miRNAs were further analyzed and counted using miRDeep2 package v2.0.0.8 with the Perl script 'quantifier.pl' [62]. The edgeR package v3.30.3 (<https://bioconductor.org/packages/edgeR/>) [63] was then used to identify differentially expressed miRNAs with FDR < 0.05. In addition, clean reads from RNA-seq libraries were mapped to the *Sscrofa11.1* reference genome (ftp://ftp.ensembl.org/pub/release-94/fasta/sus_scrofa/dna/) using HISAT2 v2.1.0, and StringTie v2.0.6 was used to assemble and quantify transcripts in each library [64]. mRNA expression levels were measured and normalized as FPKM, and Ballgown v2.20.0 [64] was used to identify and compare differentially expressed transcripts and produce tables and plots. To predict circRNA candidates, we used five different algorithms: CIRCexplorer2 [65], circRNA_Finder [66], CIRI [67], find_circ [68], and MapSplice [69]. Only circRNA candidates that were identified by all of them were further analyzed. The expression levels of circRNA candidates were calculated with back-splice junction reads, and the edgeR algorithm was applied to examine their differential expression (FDR < 0.05). Finally, biological processes (GO terms) and KEGG pathway analyses [70] were performed using DAVID (<https://david.ncifcrf.gov/>).

Cell Culture

The mouse myoblast cell line C₂C₁₂ was purchased from American Type Culture Collection. The cells were grown in a growth medium [GM, Dulbecco's modified Eagle's medium (DMEM; Gibco, Grand Island, NY, United States) + 10% fetal bovine serum (Gibco) + 1% penicillin–streptomycin (Invitrogen, Carlsbad, CA, United States)] and induced to differentiate in a differentiation medium [DM, DMEM + 2% horse serum (Gibco) + 1% penicillin–streptomycin (Invitrogen)] when they reached 90% confluence. The cells were cultured in a humidified incubator at 37 °C and 5% CO₂.

RT-qPCR

Total RNA was isolated from the muscle tissue samples and C₂C₁₂ cells using TRIzol, and cDNA was synthesized from RNA using the PrimeScript™ RT Reagent Kit with gDNA Eraser (Takara), according to manufacturer instructions. Genomic DNA was extracted from C₂C₁₂ cells using a kit (Sangon, Shanghai, China). To verify the circular structure of circRNAs, we designed a pair of convergent and divergent primers and verified their head-to-tail splicing using PCR and Sanger sequencing (Sangon). The primer sequences used in the experiment are listed in Table S8. Moreover, 2 µg total RNA from C₂C₁₂ cells was incubated with 3 U/µL ribonuclease R (RNase R) at 37 °C for 10 min; total RNA without RNase R (i.e., mock control) was also incubated under the same conditions. Gene expression levels were determined using the 2^{−ΔΔCT} method. *GAPDH* served as the reference gene.

Vector Construction and RNA Oligonucleotides

To synthesize the full-length linear sequence of circKANS_L1L, a primer was designed using Primer 5.0. This sequence was amplified using C₂C₁₂ cDNA and subsequently cloned into pCD2.1-ciR (Genesee Biotech, Guangzhou, China) using the KpnI and BamHI (Takara) restriction sites (OE-circKANS_L1L). The empty vector was used as the negative control (OE-NC). siRNAs targeting circKANS_L1L junction sites (si-circKANS_L1L) and negative control (si-NC) were designed and synthesized by GenePharma Co., Ltd. (Shanghai, China).

Transfection

C₂C₁₂ cells were transfected with OE-circKANS_L1L, OE-NC, si-circKANS_L1L, and si-NC using Lipofectamine 2000 (Invitrogen, Carlsbad, CA), according to manufacturer instructions, when they reached approximately 60% confluence. si-RNA transfection mix (20 pmol si-circKANS_L1L or si-NC + 50 µL serum-free DMEM) or plasmid DNA transfection mix (1 µg OE-circKANS_L1L or 1 µg OE-NC plasmid DNA + 50 µL serum-free DMEM) was prepared for each well, incubated at room temperature for 20 min, and subsequently diluted with transfection medium (1 µL lip 2000 + 50 µL serum-free DMEM). This mix was then added to each well, and the medium was replaced to GM after 6 h. The cells were harvested for protein and RNA analyses after 48 h to study cell proliferation. Further, the medium was switched to DM after 48 h, and the cells were collected for protein and RNA analyses at 96 h to study cell differentiation.

CCK-8 Assay

CCK-8 (EZBioscience, Roseville, MN) assay was used to evaluate cell proliferation. Approximately 10^4 cells were seeded in 96-well plates. After they adhered to the wall, they were transfected with OE-circKANS1L, OE-NC, si-circKANS1L, or si-NC. Six hours after transfection was recorded as 0 h. CCK-8 was added at 0, 12, 24, and 36 h, followed by incubation for 1 h. Absorbance was then measured at 450 nm using a microplate reader (Thermo Fisher Scientific, Waltham, MA).

Flow Cytometric Cell Cycle Analysis

C₂C₁₂ cells were transfected with OE-circKANS1L, OE-NC, si-circKANS1L, and si-NC. After 48 h, the cells were collected, fixed with 75% ethanol, and stored overnight at -20°C . They were then resuspended in 500 μL PI/RNase staining buffer solution (BD Biosciences, Franklin Lakes, NJ) and incubated at 37°C for 30 min. A BD Accuri C6 flow cytometer and FACSDiVa software (BD Biosciences) were used to perform flow cytometric analysis.

Western Blotting

The cells were lysed using RIPA lysis buffer (Solarbio Life Sciences, Beijing, China) to obtain proteins, which were then separated by 10% sodium dodecyl sulfate–polyacrylamide gel electrophoresis, transferred to a 0.45-mm polyvinylidene fluoride membrane (Sigma, St. Louis, MO), and sealed with 5% skim milk for 2 h at room temperature. The cells transfected for 48 h were incubated overnight at 4°C with the following primary antibodies: PCNA, Cyclin D1, Cyclin E, and Tubulin (ZenBio, Chengdu, China). Further, the cells transfected and differentiated for 96 h were incubated overnight with following primary antibodies: MYOG, MyHC, Tubulin (ZenBio), MyHC I, MyHC IIb, and GAPDH (ABclonal, Wuhan, China). After washing with Tris-buffered saline with Tween 20, the secondary antibody goat anti-rabbit IgG-HRP or goat anti-mouse IgG-HRP (Biorworld, Minneapolis, MN) was added, followed by incubation at room temperature for 1 h. Finally, enhanced chemiluminescence luminous fluid (Solarbio Life Sciences) was used for band visualization.

Statistical Analysis

The comparative analysis of two groups was performed using unpaired independent *t*-test, and multiple comparative analysis was performed with one-way ANOVA. SPSS 20.0 (SPSS Inc., Chicago, IL) was used for statistical analyses. $P < 0.05$ and $P < 0.01$ indicated different and statistically different, respectively.

Abbreviations

ncRNA: Noncoding RNAs; circRNAs: Circular RNAs; MyHCs: Myosin heavy chain isoforms; mTOR: Mammalian target of rapamycin; AMPK: Adenosine 5'-monophosphate-activated protein kinase; CDS: Coding sequence; DAVID: The Database for Annotation, Visualization and Integrated Discovery; KEGG: Kyoto Encyclopedia of Genes and Genomes.

Supplementary Information

The online version contains supplementary material available at <https://doi.org/10.1186/s12864-022-08515-7>.

Additional file 1. 12864_2022_8515_MOESM1_ESM.pdf.

Additional file 2. 12864_2022_8515_MOESM2_ESM.pdf.

Additional file 3. 12864_2022_8515_MOESM3_ESM.pdf.

Additional file 4. 12864_2022_8515_MOESM4_ESM.pdf.

Additional file 5. 12864_2022_8515_MOESM5_ESM.pdf.

Additional file 6. 12864_2022_8515_MOESM6_ESM.xlsx.

Additional file 7. 12864_2022_8515_MOESM7_ESM.xlsx.

Additional file 8. 12864_2022_8515_MOESM8_ESM.xlsx.

Additional file 9. 12864_2022_8515_MOESM9_ESM.xlsx.

Additional file 10. 12864_2022_8515_MOESM10_ESM.xlsx.

Additional file 11. 12864_2022_8515_MOESM11_ESM.xlsx.

Additional file 12. 12864_2022_8515_MOESM12_ESM.xlsx.

Additional file 13. 12864_2022_8515_MOESM13_ESM.xlsx.

Acknowledgements

We thank the High Performance Computing center of South China Agricultural University for providing computational resources in this work.

Authors' contributions

XZ and JS gathered samples, conceived the study, participated in its design, performed data analysis, and drafted the manuscript. ZL and FX performed the experiments. JL, TC, QX, and YZ provided guidance and funding. All authors have read and approved the final manuscript.

Funding

This work was supported by the Science and Technology Innovation Strategy projects of Guangdong Province [grant numbers 2018B020203002], the Natural Science Foundation of China Program [grant numbers 31802032, 32072714]; the Natural Science Foundation of Guangdong Province [grant number 2020A1515010062]; the Science and Technology Project of Guangzhou [grant number 202002030037]. The sponsors had no role in the study design; in the collection, analysis, and interpretation of the data; in the writing of the report; and in the decision to submit the article for publication.

Availability of data and materials

The raw sequences were deposited into Sequence Read Archive (SRA) database with the BioProject accession number PRJNA778795 (<https://www.ncbi.nlm.nih.gov/bioproject/PRJNA778795/>).

Declarations

Ethics approval and consent to participate

Our study was carried out in compliance with the ARRIVE guidelines, and any anesthesia or euthanizing agent was not used in our study. All experimental animal procedures complied with the laboratory animal management and welfare regulations approved by the Ethics Committee of South China Agricultural University, Guangdong Province, China. This study was approved by the Ethics Committee of South China Agricultural University, Guangdong Province, China.

Consent for publication

Not applicable.

Competing interests

The authors declare that they have no competing interests.

Received: 28 August 2021 Accepted: 29 March 2022

Published online: 11 April 2022

References

1. Merks JW. One century of genetic changes in pigs and the future needs. *BSAP Occasional Publication*. 2000;27:8–19. <https://doi.org/10.1017/S1463981500040498>.
2. Chen P, Baas TJ, Mabry JW, Dekkers JC, Koehler KJ. Genetic parameters and trends for lean growth rate and its components in US Yorkshire Duroc Hampshire and Landrace pigs. *J Anim Sci*. 2002;80(8):2062–70. <https://doi.org/10.2527/2002.8082062x>.
3. Labroue F, Gueblez R, Sellier P. Genetic parameters of feeding behaviour and performance traits in group-housed Large White and French Landrace growing pigs. *Genet sel evol*. 1997;29(4):451. <https://doi.org/10.1186/1297-9686-29-4-451>.
4. Broekhuijsen ML, Šostarić E, Feitsma H, Gadella BM. Application of computer-assisted semen analysis to explain variations in pig fertility. *J Anim Sci*. 2012;90(3):779–89. <https://doi.org/10.2527/jas.2011-4311>.
5. Rowland RR, Lunney J, Dekkers J. Control of porcine reproductive and respiratory syndrome (PRRS) through genetic improvements in disease resistance and tolerance. *Front Genet*. 2012;3:260. <https://doi.org/10.3389/fgene.2012.00260>.
6. Schwab CR, Baas TJ, Stalder KJ, Mabry JW. Effect of long-term selection for increased leanness on meat and eating quality traits in Duroc swine. *J Anim Sci*. 2006;84(6):1577–83. <https://doi.org/10.2527/2006.8461577x>.
7. Rosenvold K, Andersen HJ. Factors of significance for pork quality—a review. *Meat Sci*. 2003;64(3):219–37. [https://doi.org/10.1016/S0309-1740\(02\)00186-9](https://doi.org/10.1016/S0309-1740(02)00186-9).
8. Bonneau M, Lebret B. Production systems and influence on eating quality of pork. *Meat Sci*. 2010;84(2):293–300. <https://doi.org/10.1016/j.meatsci.2009.03.013>.
9. Lee SH, Joo ST, Ryu YC. Skeletal muscle fiber type and myofibrillar proteins in relation to meat quality. *Meat Sci*. 2010;86(1):166–70. <https://doi.org/10.1016/j.meatsci.2010.04.040>.
10. Lefaucheur L. Myofiber typing and pig meat production. *Slov Vet Res*. 2001;38(1):5–28.
11. Zanolu N, Gailly P. Skeletal muscle hypertrophy and regeneration: interplay between the myogenic regulatory factors (MRFs) and insulin-like growth factors (IGFs) pathways. *Cell Mol Life Sci*. 2013;70(21):4117–30. <https://doi.org/10.1007/s00018-013-1330-4>.
12. Eggerman MA, Glass DJ. Signaling pathways controlling skeletal muscle mass. *Crit Rev Biochem Mol Biol*. 2014;49(1):59–68. <https://doi.org/10.3109/10409238.2013.857291>.
13. Sun J, Xie M, Huang Z, Li H, Chen T, Sun R, Wang J, Xi Q, Wu T, Zhang Y. Integrated analysis of non-coding RNA and mRNA expression profiles of 2 pig breeds differing in muscle traits. *J Anim Sci*. 2017;95(3):1092–103. <https://doi.org/10.2527/jas.2016.0867>.
14. Ashwal-Fluss R, Meyer M, Pamudurti NR, Ivanov A, Bartok O, Hanan M, et al. circRNA biogenesis competes with pre-mRNA splicing. *Mol Cell*. 2014;56(1):55–66. <https://doi.org/10.1016/j.molcel.2014.08.019>.
15. Zhang P, Chao Z, Zhang R, Ding R, Wang Y, Wu W, et al. Circular RNA Regulation of Myogenesis Cells. 2019;8(8):885. <https://doi.org/10.3390/cells8080885>.
16. Maass PG, Glazar P, Memczak S, Dittmar G, Hollfinger I, Schreyer L, et al. A map of human circular RNAs in clinically relevant tissues. *J Mol Med (Berl)*. 2017;95(11):1179–89. <https://doi.org/10.1007/s00109-017-1582-9>.
17. Abdelmohsen K, Panda AC, De S, Grammatikakis I, Kim J, Ding J, et al. Circular RNAs in monkey muscle age-dependent changes. *Aging (Albany NY)*. 2015;7(11):903–10. <https://doi.org/10.18632/aging.100834>.
18. Wei X, Li H, Yang J, Hao D, Dong D, Huang Y, et al. Circular RNA profiling reveals an abundant circLMO7 that regulates myoblasts differentiation and survival by sponging miR-378a-3p. *Cell Death Dis*. 2017;8(10):e3153. <https://doi.org/10.1038/cddis.2017.541>.
19. Ling Y, Zheng Q, Zhu L, Xu L, Sui M, Zhang Y, et al. Trend analysis of the role of circular RNA in goat skeletal muscle development. *BMC Genomics*. 2020;21(1):220. <https://doi.org/10.1186/s12864-020-6649-2>.
20. Cao Y, You S, Yao Y, Liu ZJ, Hazi W, Li CY, et al. Expression profiles of circular RNAs in sheep skeletal muscle. *Asian-Australas J Anim Sci*. 2018;31(10):1550–7. <https://doi.org/10.5713/ajas.17.0563>.
21. Hong L, Gu T, He Y, Zhou C, Hu Q, Wang X, et al. Genome-Wide Analysis of Circular RNAs Mediated ceRNA Regulation in Porcine Embryonic Muscle Development. *Front Cell Dev Biol*. 2019;7:289. <https://doi.org/10.3389/fcell.2019.00289>.
22. Ouyang H, Chen X, Wang Z, Yu J, Jia X, Li Z, et al. Circular RNAs are abundant and dynamically expressed during embryonic muscle development in chickens. *DNA Res*. 2018;25(1):71–86. <https://doi.org/10.1093/dnares/dsx039>.
23. Song Z, Liu Y, Fang X, Xie M, Ma Z, Zhong Z, et al. Comprehensive analysis of the expression profile of circRNAs and their predicted protein-coding ability in the muscle of mdx mice. *Funct Integr Genomics*. 2020;20(3):397–407. <https://doi.org/10.1007/s10142-019-00724-w>.
24. Li X, Yang L, Chen LL. The Biogenesis, Functions, and Challenges of Circular RNAs. *Mol Cell*. 2018;71(3):428–42. <https://doi.org/10.1016/j.molcel.2018.06.034>.
25. Hansen TB, Jensen TI, Clausen BH, Bramsen JB, Finsen B, Damgaard CK, et al. Natural RNA circles function as efficient microRNA sponges. *Nature*. 2013;495(7441):384–8. <https://doi.org/10.1038/nature11993>.
26. Zhang C, Wu H, Wang Y, Zhu S, Liu J, Fang X, et al. Circular RNA of cattle casein genes are highly expressed in bovine mammary gland. *J Dairy Sci*. 2016;99(6):4750–60. <https://doi.org/10.3168/jds.2015-10381>.
27. Panda AC. Circular RNAs Act as miRNA Sponges. *Adv Exp Med Biol*. 2018;1087:67–79. https://doi.org/10.1007/978-981-13-1426-1_6.
28. Listrat A, Lebret B, Louveau I, Astruc T, Bonnet M, Lefaucheur L, et al. How Muscle Structure and Composition Influence Meat and Flesh Quality. *ScientificWorldJournal*. 2016;2016:3182746. <https://doi.org/10.1155/2016/3182746>.
29. Cameron ND, Nute GR, Brown SN, Enser M, Wood JD. Meat quality of Large White pig genotypes selected for components of efficient lean growth rate. *Anim*. 1999;68(1):115–27. <https://doi.org/10.1017/S1357729800050141>.
30. Liu Y, Yang X, Jing X, He X, Wang L, Liu Y, et al. Transcriptomics Analysis on Excellent Meat Quality Traits of Skeletal Muscles of the Chinese Indigenous Min Pig Compared with the Large White Breed. *Int J Mol Sci*. 2017;19(1):21. <https://doi.org/10.3390/ijms19010021>.
31. Karlsson AH, Klont RE, Fernandez X. Skeletal muscle fibres as factors for pork quality. *Livestock Production Science*. 1999;60:255–69. [https://doi.org/10.1016/S0301-6226\(99\)00098-6](https://doi.org/10.1016/S0301-6226(99)00098-6).
32. Maltin CA, Warkup CC, Matthews KR, Grant CM, Porter AD, Delday MI. Pig muscle fibre characteristics as a source of variation in eating quality. *Meat Sci*. 1997;47(3–4):237–48. [https://doi.org/10.1016/S0309-1740\(97\)00055-7](https://doi.org/10.1016/S0309-1740(97)00055-7).
33. Lefaucheur L. A second look into fibre typing—relation to meat quality. *Meat Sci*. 2010;84(2):257–70. <https://doi.org/10.1016/j.meatsci.2009.05.004>.
34. Lefaucheur L, Milan D, Ecolan P, Le Callennec C. Myosin heavy chain composition of different skeletal muscles in Large White and Meishan pigs. *J Anim Sci*. 2004;82(7):1931–41. <https://doi.org/10.2527/2004.8271931x>.
35. Larzul C, Lefaucheur L, Ecolan P, Gogué J, Talmant A, Sellier P, et al. Phenotypic and genetic parameters for longissimus muscle fiber characteristics in relation to growth, carcass, and meat quality traits in large white pigs. *J Anim Sci*. 1997;75(12):3126–37. <https://doi.org/10.2527/1997.75123126x>.
36. Zhang J, Chai J, Luo Z, He H, Chen L, Liu X, Zhou Q. Meat and nutritional quality comparison of purebred and crossbred pigs. *Anim Sci J*. 2018;89(1):202–10. <https://doi.org/10.1111/asj.12878>.
37. Wang XQ, Yang WJ, Yang Z, Shu G, Wang SB, Jiang QY, et al. The differential proliferative ability of satellite cells in Lantang and Landrace pigs. *PLoS One*. 2012;7(3):e32537. <https://doi.org/10.1371/journal.pone.0032537>.
38. Zhao X, Mo D, Li A, Gong W, Xiao S, Zhang Y, et al. Comparative analyses by sequencing of transcriptomes during skeletal muscle development between pig breeds differing in muscle growth rate and fatness. *PLoS ONE*. 2011;6(5):e19774. <https://doi.org/10.1371/journal.pone.0019774>.
40. Everaert C, Luybaert M, Maag J, Cheng QX, Dinger ME, Hellemans J, et al. Benchmarking of RNA-sequencing analysis workflows using whole-transcriptome RT-qPCR expression data. *Sci Rep*. 2017;7(1):1559. <https://doi.org/10.1038/s41598-017-01617-3>.

41. Zhou R, Wang YX, Long KR, Jiang AA, Jin L. Regulatory mechanism for lncRNAs in skeletal muscle development and progress on its research in domestic animals. *Yi Chuan*. 2018;40(4):292–304. <https://doi.org/10.16288/jyczz.17-358>.
42. Das A, Das A, Das D, Abdelmohsen K, Panda AC. Circular RNAs in myogenesis. *Biochim Biophys Acta Gene Regul Mech*. 2020;1863(4): 194372. <https://doi.org/10.1016/j.bbaggm.2019.02.011>.
43. Bartel DP. MicroRNAs: genomics, biogenesis, mechanism, and function, which are widely expressed in organisms and play a role in biological regulation. *Cell*. 2004;116(2):281–97. [https://doi.org/10.1016/S0092-8674\(04\)00045-5](https://doi.org/10.1016/S0092-8674(04)00045-5).
44. Panda AC. Circular RNAs Act as miRNA Sponges. *Adv Exp Med Biol*. 2018;1087:67–79. https://doi.org/10.1007/978-981-13-1426-1_6.
45. Li H, Wei X, Yang J, Dong D, Hao D, Huang Y, et al. circFGFR4 Promotes Differentiation of Myoblasts via Binding miR-107 to Relieve Its Inhibition of Wnt3. *Mol Ther Nucleic Acids*. 2018;11:272–83. <https://doi.org/10.1016/j.omtn.2018.02.012>.
46. Li H, Yang J, Wei X, Song C, Dong D, Huang Y, et al. CircFUT10 reduces proliferation and facilitates differentiation of myoblasts by sponging miR-133a. *J Cell Physiol*. 2018;233(6):4643–51. <https://doi.org/10.1002/jcp.26230>.
47. Yue B, Wang J, Ru W, Wu J, Cao X, Yang H, et al. The Circular RNA circHUWE1 Sponges the miR-29b-AKT3 Axis to Regulate Myoblast Development. *Mol Ther Nucleic Acids*. 2020;19:1086–97. <https://doi.org/10.1016/j.omtn.2019.12.039>.
48. Wang Y, Li M, Wang Y, Liu J, Zhang M, Fang X, et al. A Zfp609 circular RNA regulates myoblast differentiation by sponging miR-194-5p. *Int J Biol Macromol*. 2019;121:1308–13. <https://doi.org/10.1016/j.jbiomac.2018.09.039>.
49. Gao M, Li X, Yang Z, Zhao S, Ling X, Li J, et al. circHIPK3 regulates proliferation and differentiation of myoblast through the miR-7/TCF12 pathway. *J Cell Physiol*. 2021. <https://doi.org/10.1002/jcp.30363>.
50. Legnini I, Di Timoteo G, Rossi F, Morlando M, Briganti F, Sthandier O, et al. Circ-ZNF609 Is a Circular RNA that Can Be Translated and Functions in Myogenesis. *Mol Cell*. 2017;66(1):22–37.e9. <https://doi.org/10.1016/j.molcel.2017.02.017>.
51. Yin H, Shen X, Zhao J, Cao X, He H, Han S, et al. Circular RNA CircFAM188B Encodes a Protein That Regulates Proliferation and Differentiation of Chicken Skeletal Muscle Satellite Cells. *Front Cell Dev Biol*. 2020;8: 522588. <https://doi.org/10.3389/fcell.2020.522588>.
52. Kumari P, Sundaram R, Manohar K, Vasudevan D, Acharya N. Interdomain connecting loop and J loop structures determine cross-species compatibility of PCNA. *J Biol Chem*. 2021;297(1): 100911. <https://doi.org/10.1016/j.jbc.2021.100911>.
53. Wianny F, Real FX, Mummery CL, Van Rooijen M, Lahti J, Samarut J, et al. G1-phase regulators, cyclin D1, cyclin D2, and cyclin D3: up-regulation at gastrulation and dynamic expression during neurulation. *Dev Dyn*. 1998;212(1):49–62. [https://doi.org/10.1002/\(SICI\)1097-0177\(199805\)212:1%3C49::AID-AJA5%3E3.0.CO;2-2](https://doi.org/10.1002/(SICI)1097-0177(199805)212:1%3C49::AID-AJA5%3E3.0.CO;2-2).
54. Elnour IE, Wang X, Zhansaya T, Akhatayeva Z, Khan R, Cheng J, et al. Circular RNA circMYL1 Inhibit Proliferation and Promote Differentiation of Myoblasts by Sponging miR-2400. *Cells*. 2021;10(1):176. <https://doi.org/10.3390/cells10010176>.
55. Sassoon DA. Myogenic regulatory factors: dissecting their role and regulation during vertebrate embryogenesis. *Dev Biol*. 1993;156(1):11–23. <https://doi.org/10.1006/dbio.1993.1055>.
56. Wright WE, Sassoon DA, Lin VK. Myogenin a factor regulating myogenesis has a domain homologous to MyoD. *Cell*. 1989;56(4):607–17. [https://doi.org/10.1016/0092-8674\(89\)90583-7](https://doi.org/10.1016/0092-8674(89)90583-7).
57. Ganassi M, Badodi S, Wanders K, Zammit PS, Hughes SM. Myogenin is an essential regulator of adult myofibre growth and muscle stem cell homeostasis. *Elife*. 2020;9: e60445. <https://doi.org/10.7554/eLife.60445>.
58. Parry DJ. Myosin heavy chain expression and plasticity: role of myoblast diversity. *Exerc Sport Sci Rev*. 2001;29(4):175–9. <https://doi.org/10.1097/00003677-200110000-00008>.
59. Shen X, Liu Z, Cao X, He H, Han S, Chen Y, et al. Circular RNA profiling identified an abundant circular RNA circTMTC1 that inhibits chicken skeletal muscle satellite cell differentiation by sponging miR-128-3p. *Int J Biol Sci*. 2019;15(10):2265–81. <https://doi.org/10.7150/ijbs.36412>.
60. Ouyang H, Chen X, Li W, Li Z, Nie Q, Zhang X. Circular RNA circSVIL Promotes Myoblast Proliferation and Differentiation by Sponging miR-203 in Chicken. *Front Genet*. 2018;9:172. <https://doi.org/10.3389/fgene.2018.00172>.
61. Martin M. Cutadapt removes adapter sequences from high-throughput sequencing reads. *EMBnet J*. 2011;17(1):10–2. <https://doi.org/10.14806/ej.17.1.200>.
62. Li R, Li Y, Kristiansen K, Wang J. SOAP: short oligonucleotide alignment program. *Bioinformatics*. 2008;24(5):713–4. <https://doi.org/10.1093/bioinformatics/btn025>.
63. Friedländer MR, Mackowiak SD, Li N, Chen W, Rajewsky N. miRDeep2 accurately identifies known and hundreds of novel microRNA genes in seven animal clades. *Nucleic Acids Res*. 2012;40(1):37–52. <https://doi.org/10.1093/nar/gkr688>.
64. Robinson MD, McCarthy DJ, Smyth GK. edgeR: a Bioconductor package for differential expression analysis of digital gene expression data. *Bioinformatics* (Oxford, England). 2010;26(1):139–40. <https://doi.org/10.1093/bioinformatics/btp616>.
65. Pertea M, Kim D, Pertea GM, Leek JT, Salzberg SL. Transcript-level expression analysis of RNA-seq experiments with HISAT, StringTie and Ballgown. *Nat Protoc*. 2016;11(9):1650–67. <https://doi.org/10.1038/nprot.2016.095>.
66. Zhang XO, Dong R, Zhang Y, Zhang JL, Luo Z, Zhang J, et al. Diverse alternative back-splicing and alternative splicing landscape of circular RNAs. *Genome Res*. 2016;26(9):1277–87. <https://doi.org/10.1101/gr.202895.115>.
67. Fu X, Liu R. CircrnaFinder: A tool for identifying circular RNAs using RNA-Seq data. The 6th International Conference on Bioinformatics and Computational Biology (BICOB-2014). 2014.
68. Gao Y, Wang J, Zhao F. CIRI: an efficient and unbiased algorithm for de novo circular RNA identification. *Genome Biol*. 2015;16(1):4. <https://doi.org/10.1186/s13059-014-0571-3>.
69. Memczak S, Jens M, Elefsinioti A, Torti F, Krueger J, Rybak A, et al. Circular RNAs are a large class of animal RNAs with regulatory potency. *Nature*. 2013;495(7441):333–8. <https://doi.org/10.1038/nature11928>.
70. Wang K, Singh D, Zeng Z, Coleman SJ, Huang Y, Savich GL, et al. Map-Splice: accurate mapping of RNA-seq reads for splice junction discovery. *Nucleic Acids Res*. 2010;38(18): e178. <https://doi.org/10.1093/nar/gkq622>.
71. Kanehisa M, Sato Y, Kawashima M, Furumichi M, Tanabe M. KEGG as a reference resource for gene and protein annotation. *Nucleic Acids Res*. 2016;44(D1):D457–62. <https://doi.org/10.1093/nar/gkv1070>.

Publisher's Note

Springer Nature remains neutral with regard to jurisdictional claims in published maps and institutional affiliations.

Ready to submit your research? Choose BMC and benefit from:

- fast, convenient online submission
- thorough peer review by experienced researchers in your field
- rapid publication on acceptance
- support for research data, including large and complex data types
- gold Open Access which fosters wider collaboration and increased citations
- maximum visibility for your research: over 100M website views per year

At BMC, research is always in progress.

Learn more biomedcentral.com/submissions





Article

The Characteristic Function of Blood-Derived Exosomes and Exosomal circRNAs Isolated from Dairy Cattle during the Dry Period and Mid-Lactation

Yiru Shi [†], Zhengjiang Zhao [†], Xiao He, Junyi Luo, Ting Chen, Qianyun Xi, Yongliang Zhang ^{*} and Jiajie Sun ^{*ID}

Guangdong Provincial Key Laboratory of Animal Nutrition Control, College of Animal Science, South China Agricultural University, Guangzhou 510642, China; shiyiru00@163.com (Y.S.); zhengjiangzhao0314@163.com (Z.Z.); hexiao_0408@163.com (X.H.); luojunyi@scau.edu.cn (J.L.); allinchen@scau.edu.cn (T.C.); xiqianyun_scau@163.com (Q.X.)

^{*} Correspondence: zhangyl@scau.edu.cn (Y.Z.); jiajiesun@scau.edu.cn (J.S.); Tel.: +86-139-2515-8841 (J.S.)

[†] These authors contributed equally to this work.

Abstract: Exosomes are key mediators of intercellular communication. They are secreted by most cells and contain a cargo of protein-coding genes, long noncoding RNAs (lncRNAs), and circular RNAs (circRNAs), which modulate recipient cell behavior. Herein, we collected blood samples from Holstein cows at days 30 (mid-lactation) and 250 (dry period) of pregnancy. Prolactin, follicle-stimulating hormone, luteinizing hormone, estrogen, and progesterone levels showed an obvious increase during D250. We then extracted exosomes from bovine blood samples and found that their sizes generally ranged from 100 to 200 nm. Further, Western blotting validated that they contained CD9, CD63, and TSG101, but not calnexin. Blood-derived exosomes significantly promoted the proliferation of mammary epithelial cells, particularly from D250. This change was accompanied by increased expression levels of proliferation marker proteins PCNA, cyclin D, and cyclin E, as detected by EdU assay, cell counting kit-8 assay, and flow cytometric cell cycle analysis. Moreover, we treated mammary epithelial cells with blood-derived exosomes that were isolated from the D30 and D250 periods. And RNA-seq of two groups of cells led to the identification of 839 differentially expressed genes that were significantly enriched in KEGG signaling pathways associated with apoptosis, cell cycle and proliferation. In bovine blood-derived exosomes, we found 12,747 protein-coding genes, 31,181 lncRNAs, 9374 transcripts of uncertain coding potential (TUCP) candidates, and 460 circRNAs, and 32 protein-coding genes, 806 lncRNAs, 515 TUCP candidates, and 45 circRNAs that were differentially expressed between the D30 and D250 groups. We selected six highly expressed and four differentially expressed circRNAs to verify their head-to-tail splicing using PCR and Sanger sequencing. To summarize, our findings improve our understanding of the key roles of blood-derived exosomes and the characterization of exosomal circRNAs in mammary gland development.

Keywords: exosomes; mammary gland development; lactation; circular RNA; Sanger sequencing



Citation: Shi, Y.; Zhao, Z.; He, X.; Luo, J.; Chen, T.; Xi, Q.; Zhang, Y.; Sun, J. The Characteristic Function of Blood-Derived Exosomes and Exosomal circRNAs Isolated from Dairy Cattle during the Dry Period and Mid-Lactation. *Int. J. Mol. Sci.* **2023**, *24*, 12166. <https://doi.org/10.3390/ijms241512166>

Academic Editor: Brad Freking

Received: 26 June 2023

Revised: 21 July 2023

Accepted: 26 July 2023

Published: 29 July 2023



Copyright: © 2023 by the authors. Licensee MDPI, Basel, Switzerland. This article is an open access article distributed under the terms and conditions of the Creative Commons Attribution (CC BY) license (<https://creativecommons.org/licenses/by/4.0/>).

1. Introduction

Exosomes are nanoscale extracellular vesicles of endocytic origin [1] that are shed by most cell types and circulate in bodily fluids, such as blood [2], urine [3], saliva [4], and breast milk [5]. Exosomal contents comprise various growth factors, proteins, lipids, and nucleic acids [1]. In recent years, an increasing number of studies have attempted to understand the function of exosomes in mediating pathological and physiological processes [6]. Notably, studies on exosomes have been increasing remarkably in the recent years, especially following the discovery of functional miRNAs in exosomes [7]. The mammary gland, a dynamic organ that develops primarily in the adult, undergoes extensive expansion during puberty, followed by cycles of growth and regression with each estrus

cycle and every pregnancy–lactation–involution cycle [8]. The complex regulation of mammary gland development has been extensively studied at the genetic [9], physiological [10], and morphological levels [8]. Exosomes evidently play a key role in different stages of mammary gland development; in particular, they are associated with the proliferation and differentiation of mammary gland cells [11].

Protein molecules or lipid ligands on exosomes directly activate receptors on the surface of target cells, generating signaling complexes and activating intracellular signaling pathways [12,13], or exosomes fuse with the plasma membrane of target cells or are endocytosed into cells, delivering their contents (i.e., proteins, lipids, and nucleic acids) and, consequently, regulating cell function and biological behavior [14]. Numerous circular RNAs (circRNAs) are enriched and stable in exosomes; they are detectable in blood and milk, and involved in intercellular information exchange [15]. In addition, circRNAs, as a novel class of endogenous noncoding RNAs, play a vital role in gene expression regulation, impacting many key physiological processes [16]. With the development of deep RNA sequencing (RNA-seq) technologies and novel bioinformatic approaches, recent studies have reported a large number of endogenous circRNAs that are abundant, stable, and ubiquitously expressed, with some circRNAs having unique roles [17,18]. The expression of circRNAs is closely related to the growth and development of the mammary gland in humans [19], rats [20], and sheep [21]. Furthermore, in dairy cattle, circRNAs are apparently involved in gene expression [22] and cell proliferation [23] in the mammary gland.

Herein, we determined the expression profile of exosomal circRNAs in bovine blood between the dry period (day 250 of pregnancy, D250) and mid-lactation stage (day 30 of pregnancy, D30) and attempted to identify circRNA candidates related to mammary gland development. Our findings should improve our understanding of the chief roles of blood-derived exosomes and circRNA candidates in mammary gland development and also provide a basis for the selection of circRNA candidates for more detailed functional studies for future research.

2. Results

2.1. Analysis of Blood-Derived Exosomes

We measured PRL, FSH, LH, E2, and PROG levels in blood of dairy cattle at D30 and D250. Relative to D30, blood FSH and PROG levels were highly significantly elevated at D250 ($p < 0.01$), while blood E2 level was significantly elevated ($p < 0.05$). In contrast, blood PRL and LH levels showed no significant differences between these groups (Figure 1A).

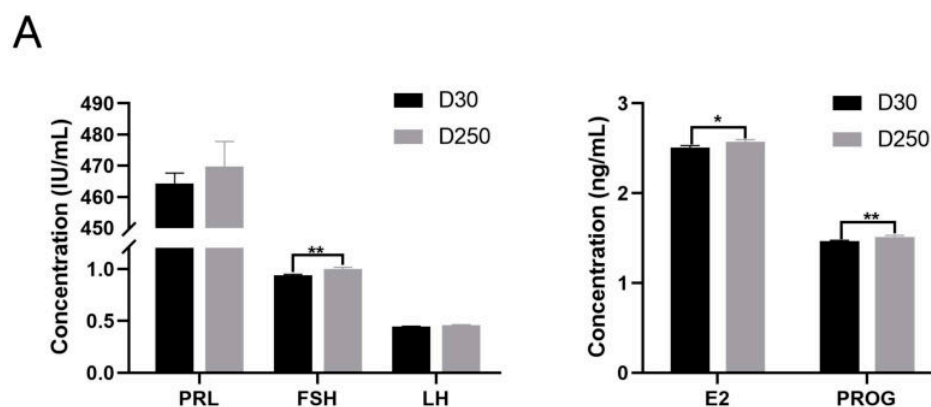


Figure 1. Cont.

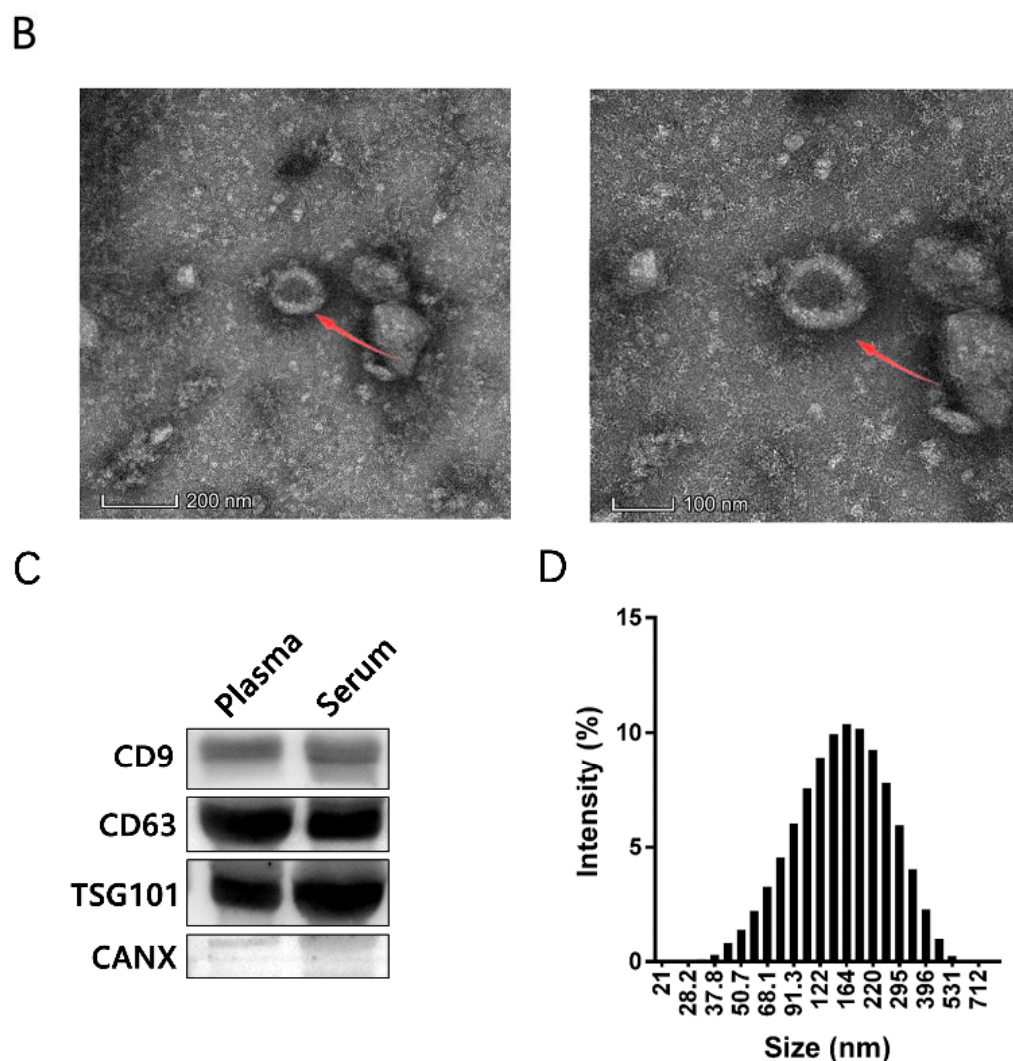


Figure 1. Identification of exosomes in bovine blood. (A) Hormone levels measured in blood from dairy cattle on D30 and D250. (B) Transmission electron microscopy images of blood-derived exosomes. Arrows point toward bovine blood-derived exosomes. (C) Exosome-specific markers CD9, CD63, and TSG101 and the non-exosomal marker calnexin detected by Western blotting. (D) Size distribution of blood-derived exosomes measured by Zetasizer Nano analysis. The asterisks above the graph bar indicate statistically significant differences according to Student's *t*-test (* $p < 0.05$, ** $p < 0.01$). Mean relative expression levels, standard error and *p*-values were calculated using the software SPSS 17.0.

Blood-derived exosomes were identified and characterized by transmission electron microscopy, Zetasizer Nano analysis, and Western blotting. Consistent with previously reported results [24], transmission electron microscopy demonstrated that the size of the isolated particles ranged from 100 to 200 nm (Figure 1B). Western blotting revealed that these particles contained CD9 (motility-related protein-1), CD63 (LAMP-3, lysosome-associated membrane protein-3), and TSG101 (tumor susceptibility gene 101 protein) but not calnexin (Figure 1C), confirming successful isolation of exosomes from blood samples. On Zetasizer Nano analysis, a broad peak was observed, corresponding to the mean particle size of 160 nm (range, 40–400 nm) (Figure 1D).

2.2. Blood-Derived Exosomes Promote MAC-T Cell Proliferation

Western blotting showed that blood-derived exosomes promoted the expression of the proliferation marker proteins PCNA (proliferating cell nuclear antigen), cyclin D (cyclin protein D1), and cyclin E (cyclin protein E) (Figure 2A) in MAC-T cells. PCNA and cyclin

E expression levels in the D30 and D250 groups were significantly higher than those in the negative control (NC) group. Further, cyclin D expression level in the D250 group was higher than that in the NC and D30 groups. EdU assay revealed that the fluorescence intensity of MAC-T cells treated with blood-derived exosomes was elevated; the intensity in the D250 group was higher than that in the D30 group (Figure 2B). CCK-8 assay was used to assess MAC-T cell proliferation at 12 h, 24 h, 36 h, and 48 h after treatment with PBS or blood-derived exosomes isolated from the D30 and D250 periods. The D250 and D30 groups showed significantly higher optical density values than the NC group, implying that the proliferation efficiency of MAC-T cells was significantly improved (Figure 2C). Flow cytometric cell cycle analysis showed that the proportion of cells in the S and G2/M phases was significantly higher in the D30 and D250 groups (Figure 2D). These results indicated that blood-derived exosomes isolated from the D30 and D250 periods promoted MAC-T cell proliferation, with those isolated from the D250 period having a more prominent effect.

2.3. RNA-Seq Analysis of MAC-T Cells Treated with Blood-Derived Exosomes

We constructed six cDNA libraries from MAC-T cells treated with blood-derived exosomes isolated from the D30 and D250 periods, and each library generated approximately 40.41 ± 3.06 million raw reads. After quality correction, each library comprised approximately 40.20 ± 3.07 million clean reads, accounting for 99.47% original reads (Table S2A). After removing all reads that mapped to a rRNA database, 39.95 ± 3.07 million remaining reads were subjected to assembly and gene abundance analyses (Table S2B). We compared all valid reads to the bovine reference genome and found that approximately $97.28\% \pm 0.21\%$ valid reads could be successfully mapped to the genome (Table S2C). The distribution of total mapped reads in the reference genome was calculated; the exon region accounted for 86.21% of total mapped reads (Table S2D). These findings validated the successful construction of libraries and also their suitability for subsequent analyses. In total, 407 novel transcripts were identified across all six libraries (Table S2E), and transcript abundance was quantified using FPKM values (Table S2F). We also performed principal component analysis with FPKM values of the identified candidates and observed that differences between the D30 and D250 groups were much larger than those between experimental individuals (Figure 3A). In comparison with D250 libraries, we identified 839 significantly differentially expressed genes (Table S2G, Figure 3B), including 395 up- and 444 downregulated genes, in D30 libraries (Figure 3C). Differentially expressed transcripts were found to participate in 290 KEGG signaling pathways (Table S2H), including TNF signaling pathway, IL-17 signaling pathway, HIF-1 signaling pathway, and apoptosis (Figure 3D). KEGG pathway genes were subjected to gene set enrichment analysis (Table S2I); genes in the KO04668_TNF signaling pathway showed significant enrichment (Figure 3E).

2.4. Transcriptome Expression Analysis of Bovine Blood-Derived Exosomes

Overall, 96.32 ± 0.85 and 101.80 ± 1.97 million clean reads were obtained from the D30 and D250 groups, respectively (Table S3A). Clean reads were aligned to the bovine reference genome, and 63.87 ± 6.21 million ($64.42\% \pm 5.19\%$) reads were successfully mapped to the genome (Table S3B). Approximately 2.05 ± 0.25 million clean reads that matched Ensembl protein-coding regions, accounting for $7.65\% \pm 0.96\%$ clean reads in each library (Table S3C). In total, 53,302 assembled transcripts were identified across all libraries (Table S3D), including 31,003 novel lncRNAs and 9374 TUCP candidates. As evident from these results, annotation to the bovine reference genome was associated with poor outcomes, considering that a large number of novel transcripts needed more systematic annotation; besides, 31,181 lncRNA candidates, including 178 known lncRNAs, were identified after excluding annotation transcripts with protein-coding potentials (Figure 4A), and the expression levels of lncRNA candidates were much higher than those of the majority of mRNA molecules (Figure 4B). Further, we performed structural characterization by assessing exon size, fragment length, and open reading frame (ORF) length between

lncRNAs and mRNAs (Figure 4C), as well as between mRNAs and TUCP candidates (Figure 4D). Consistent with the results of a previous study [25], the length of novel and annotated lncRNAs and their ORFs was shorter than that of mRNAs; moreover, lncRNAs contained fewer exons. However, the structural characteristics of TUCPs were similar to those of mRNAs.

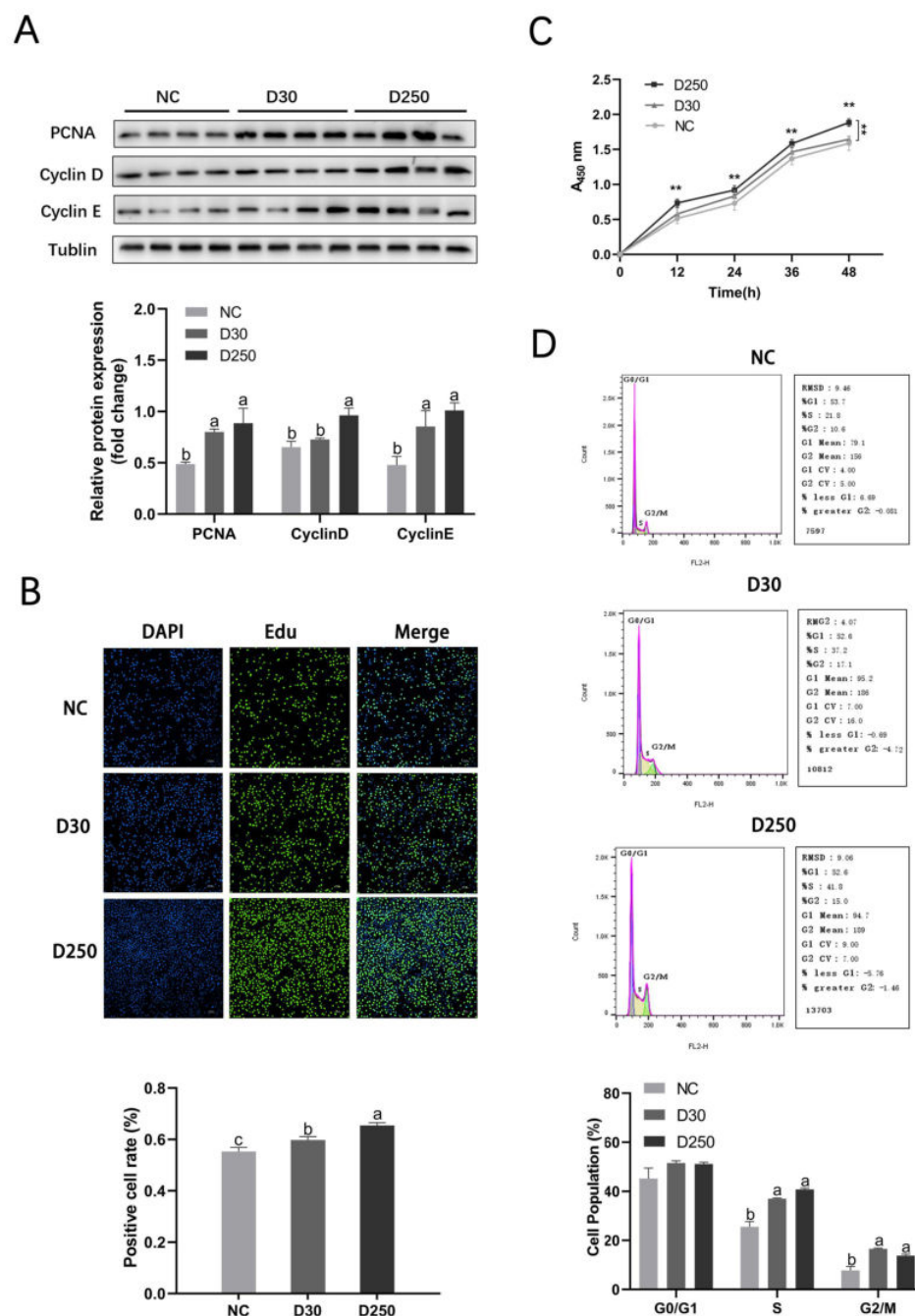


Figure 2. Proliferation of MAC-T cells induced by blood-derived exosomes in vitro. (A) Western blotting showing the expression levels of cell proliferation-related proteins in the NC, D30, and D250 groups. (B) EdU assay with MAC-T cells. (C) CCK-8 assay with MAC-T cells treated with PBS or blood-derived exosomes isolated from the D30 and D250 periods. (D) Flow cytometric cell cycle analysis. The asterisks above the graph bar indicate statistically significant differences according to Student's *t*-test (** $p < 0.01$). The different lowercase letters above the graph bar indicate statistically significant differences between two groups. Mean relative expression levels, standard error and *p*-values were calculated using the software SPSS 17.0.

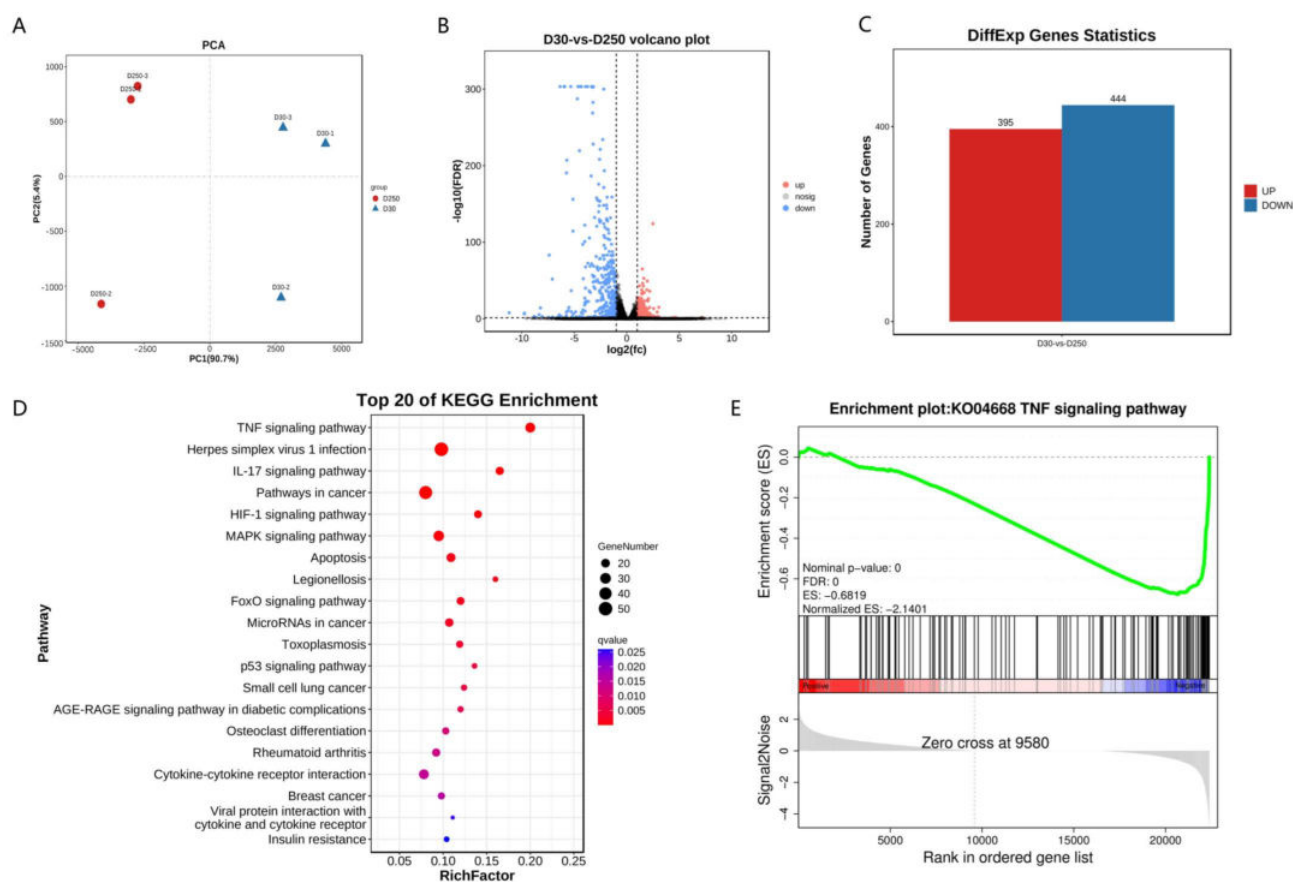


Figure 3. Functional enrichment analysis. (A) Principal component analysis based on whole transcripts in MAC-T cells treated with blood-derived exosomes isolated from the D30 and D250 periods. (B) Volcano plot showing significantly differentially expressed genes. (C) Statistics pertaining to differentially expressed genes. (D) KEGG pathway enrichment analysis of differentially expressed genes. (E) Gene set enrichment analysis plot for the KO04668_TNF signaling pathway.

2.5. Functional Enrichment Analysis of Differentially Expressed Transcripts in Bovine Blood-Derived Exosomes

We performed principal component analysis using FPKM values of all identified transcripts and found that differences caused by the physiological states of the mammary gland between the groups were much larger than those between experimental individuals (Figure 5A). With normalized FPKM, 32 differentially expressed Ensembl transcripts were found between D30 and D250 libraries (Table S3E), including 22 up- and 10 down-regulated transcripts in the D250 group (Figure 5B). In addition, 806 differentially expressed lncRNA candidates were identified between the D30 and D250 groups (Table S3F), as well as 515 TUCP candidates (Table S3G). GO enrichment analysis indicated that differentially expressed Ensembl transcripts were significantly enriched in translation, ribosome assembly, and various snoRNA metabolic processes in the biological process category (Figure 5C; Table S3H). Furthermore, KEGG pathway enrichment analysis showed that these transcripts were significantly enriched in ribosome, regulation of actin cytoskeleton, RNA degradation, and RNA transport (Figure 5D; Table S3I).

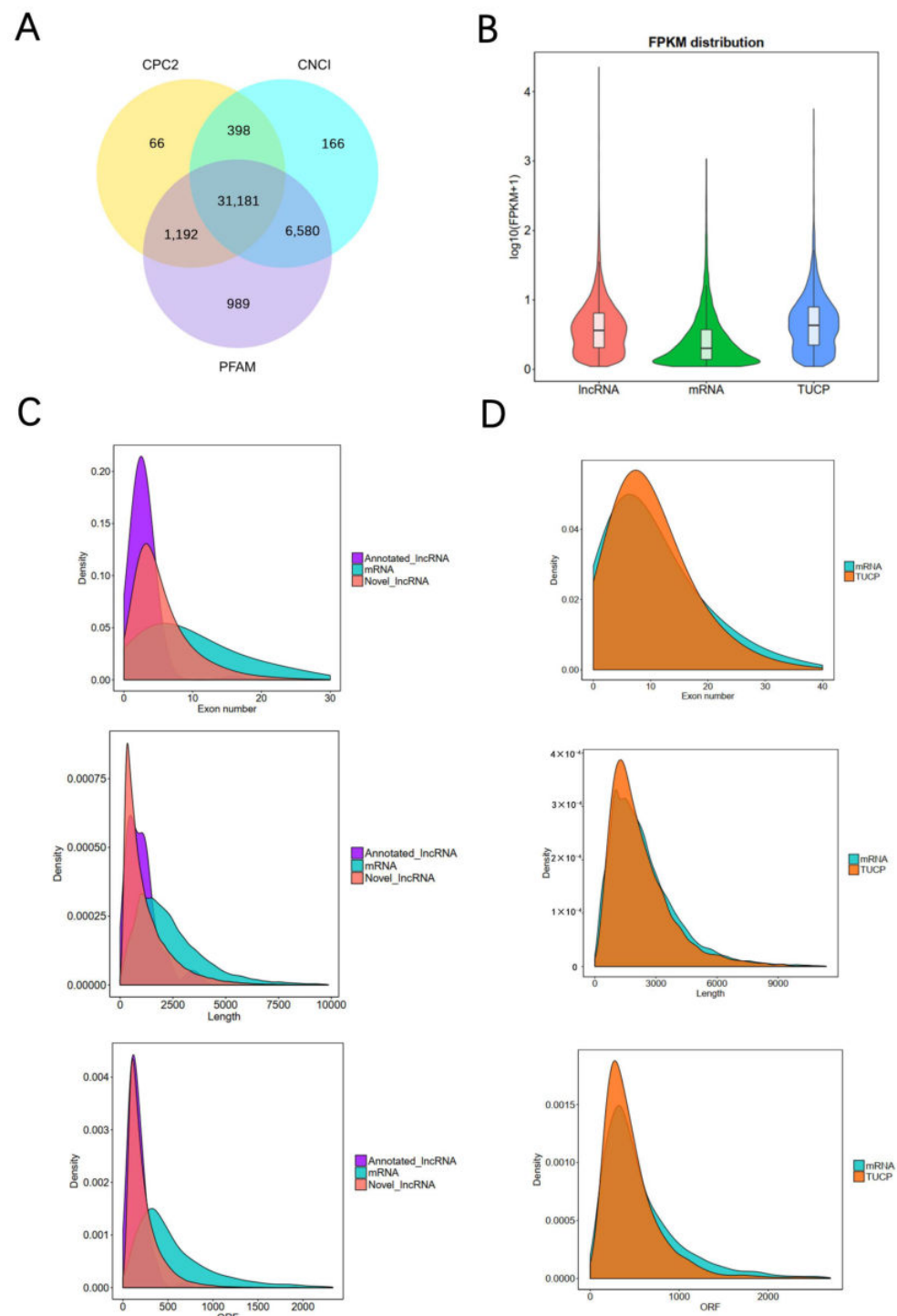


Figure 4. Identification and characterization of lncRNAs in bovine blood-derived exosomes. (A) Selection of lncRNAs in bovine blood-derived exosomes using CPC, Pfam-scan, and CNCI; 31,181 novel lncRNAs were identified after eliminating putative protein-coding transcripts. (B) Expression level of mRNA, TUCP, and lncRNA based on $\log_{10}(\text{FPKM} + 1)$. (C) Distribution of exon density in lncRNAs and mRNAs, distribution of lncRNA and mRNA length, and distribution of ORF density in lncRNAs and mRNAs. (D) Distribution of exon density in TUCP and mRNAs, distribution of TUCP and mRNAs length, and distribution of ORF density in TUCP and mRNAs.

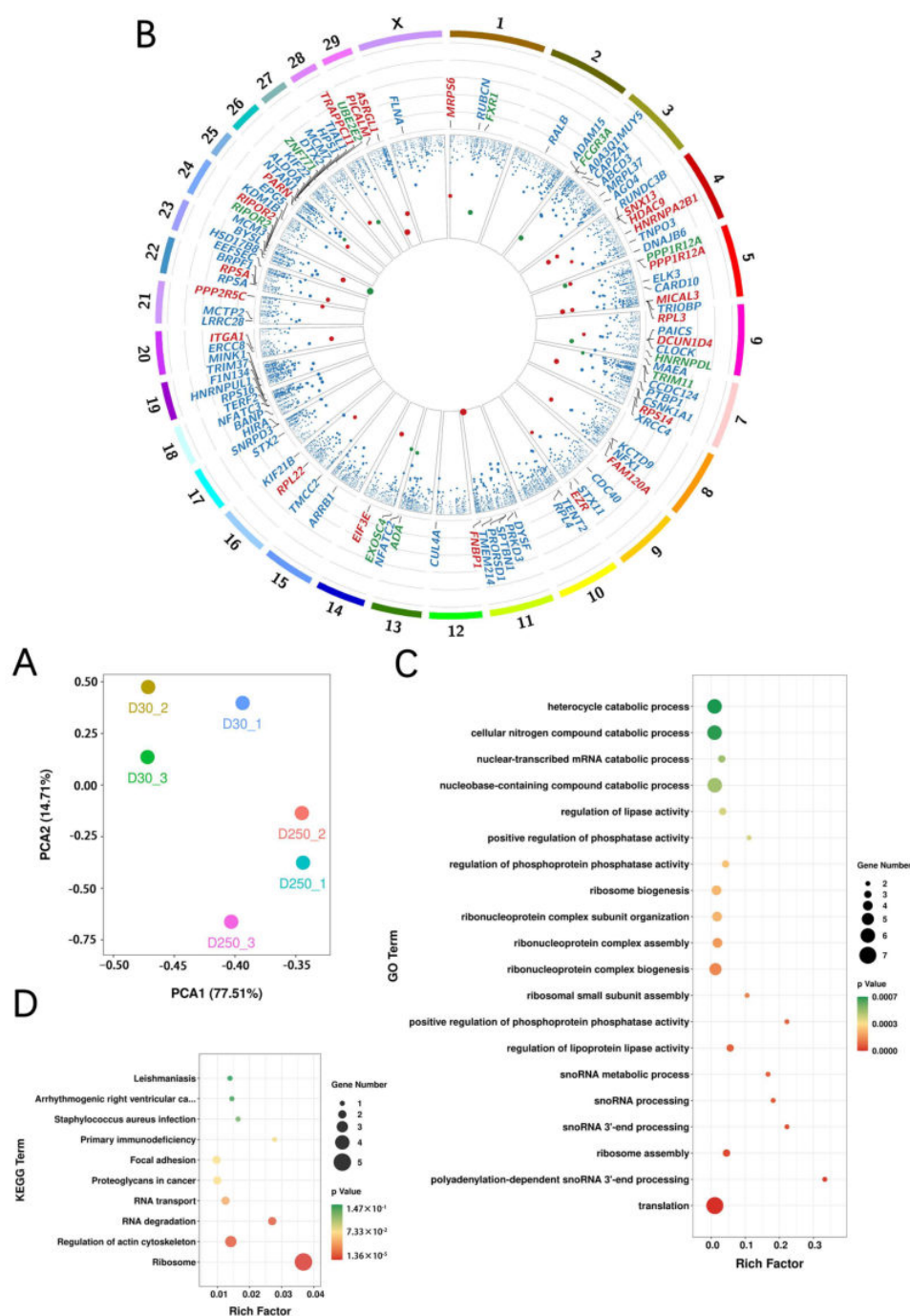


Figure 5. Cluster and enrichment analyses of exosomal transcripts. **(A)** Principal component analysis of whole transcripts in blood-derived exosomes isolated from the D30 and D250 periods. **(B)** Circos plot showing gene distribution on the chromosomes. **(C)** GO annotation analysis. **(D)** KEGG pathway enrichment analysis of neighboring gene functions.

2.6. Identification of circRNAs in Bovine Blood-Derived Exosomes

circRNA profiles were explored in bovine blood-derived exosomes. Overall, 460 circRNAs were identified in RNA-seq data using the find_circ and CIRI2 algorithms (Table S4A). Further, 256 circularization events were from exon regions, while 101 and 103 circularization events were from intergenic and intron regions, respectively (Table S4A). These events were found to originate from 324 hosting transcript loci, including 49 transcripts that generated multiple circRNA candidates. With normalized back-splice junction reads, we analyzed significant differences in circRNA candidates between D30 and D250 libraries (Table S4B).

Forty-five circRNA candidates were differentially expressed (Figure 6A): 19 up- and 26 downregulated circRNAs were found in D250 libraries (Figure 6B). GO and KEGG pathway enrichment analyses were performed on hosting transcripts of the identified circRNA candidates (Table S4C,D). GO annotation indicated that hosting transcripts of significantly expressed circRNAs mainly participated in chromatin remodeling, peptidyl-serine phosphorylation, integrin-mediated signaling pathway, positive regulation of cytokinesis, and androgen receptor signaling pathway in the biological process category (Figure 6C). In addition, KEGG pathway enrichment analysis showed that these hosting transcripts participated in GnRH signaling pathway, ubiquitin mediated proteolysis, adherens junction, focal adhesion, regulation of actin cytoskeleton, Rap1 signaling pathway, and FoxO signaling pathway (Figure 6D).

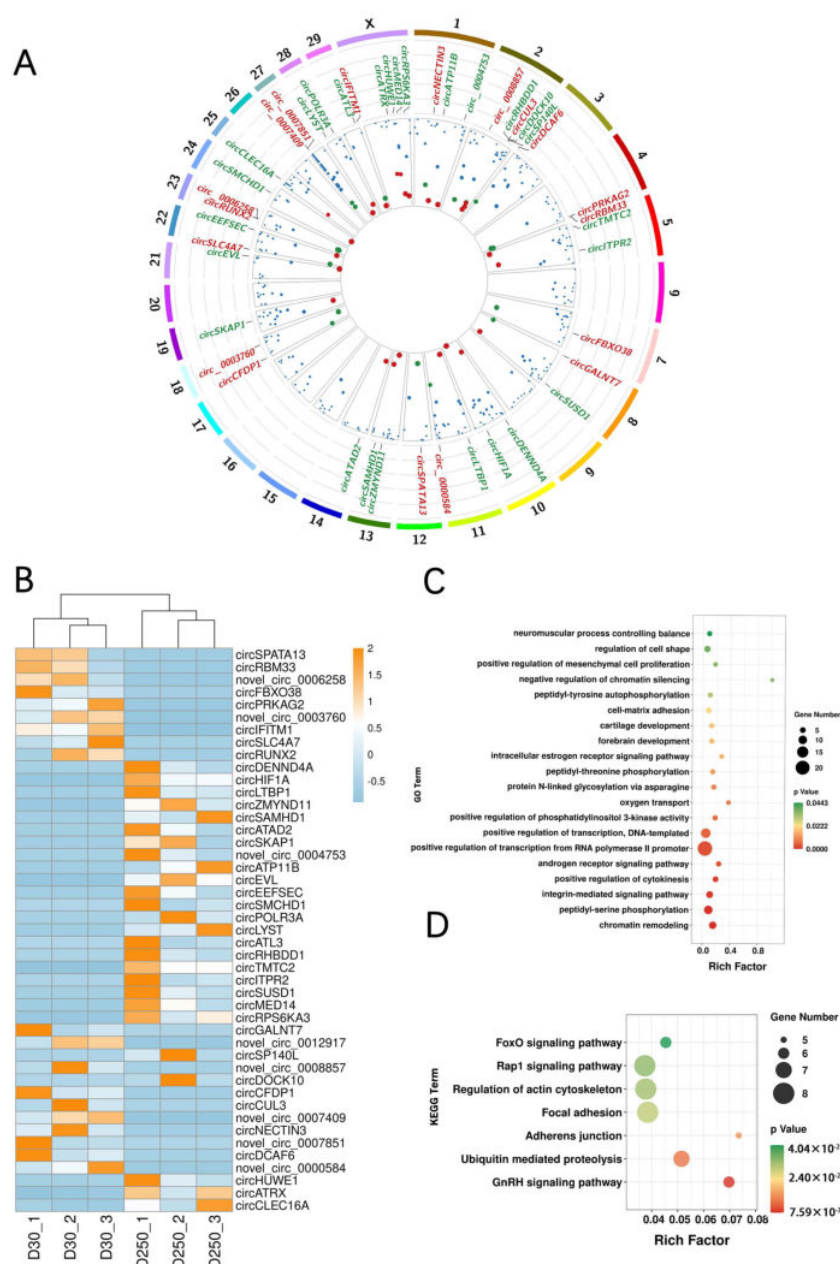


Figure 6. Cluster and enrichment analyses of bovine blood-derived exosomal circRNAs. (A) Circos plot showing the distribution of bovine blood-derived exosomal circRNAs on the chromosomes. (B) Heatmap of differentially expressed circRNAs between the D30 and D250 groups. (C) GO and (D) KEGG pathway enrichment analyses.

2.7. RT-qPCR Analysis and Authentication of Blood-Derived Exosomal circRNAs

RT-qPCR was performed to validate the expression of 13 differentially expressed candidates between the D30 and D250 groups. As with our sequencing results, the expression level of all Ensembl transcripts, except RIPOR2 and FCGR3A, in the D250 group was higher than that of those in the D30 group. EIF3E and MRPS6 expression level in the D250 group was significantly upregulated than that in the D30 group ($p < 0.05$). Further, HDAC9 and RPL3 expression level in the D250 group was extremely higher than that in the D30 group ($p < 0.01$) (Figure 7A).

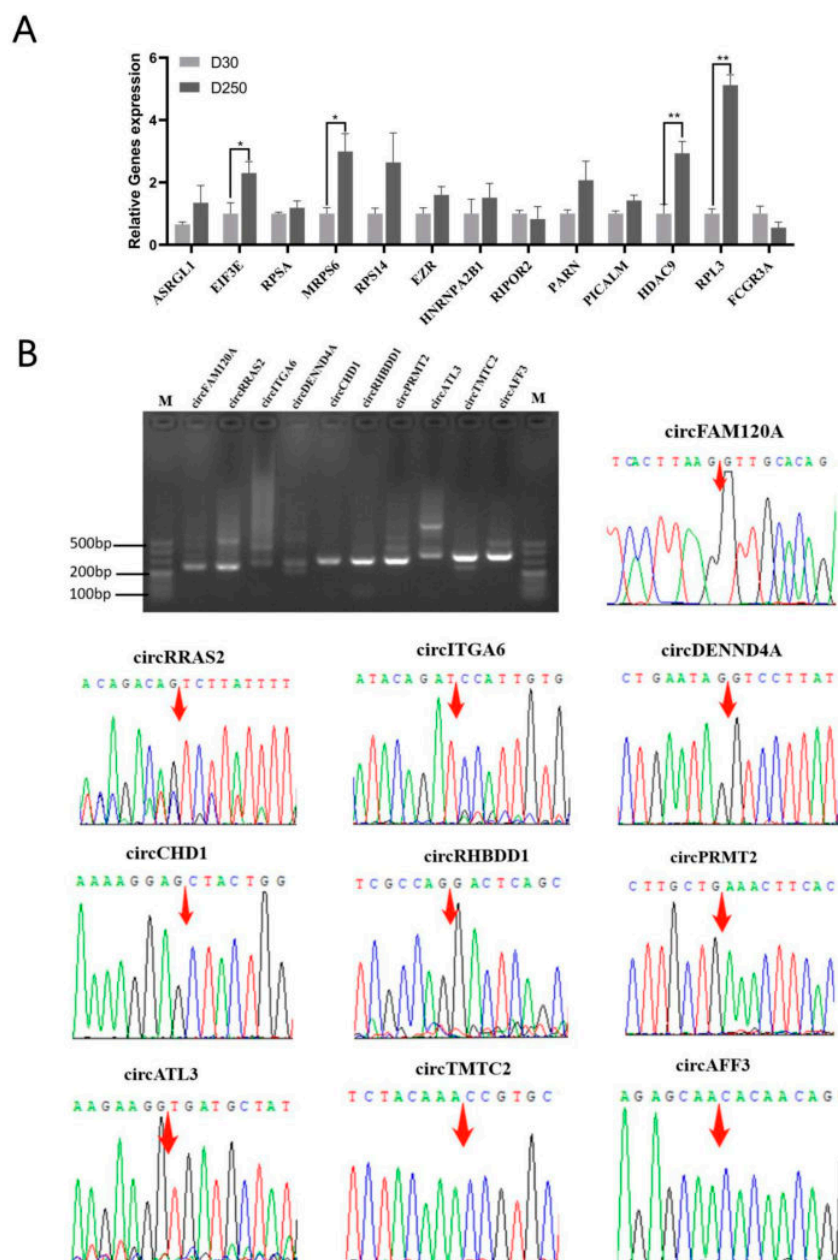


Figure 7. Validation of the presence of few selected blood exosomal circRNAs. (A) Relative expression levels of genes in blood-derived exosomes isolated from the D30 and D250 periods. (B) RT-qPCR amplifiers derived from circRNAs using divergent primers for bovine blood-derived exosome RNA; head-to-tail splice junctions for circRNAs were confirmed by DNA sequencing and are marked with a red arrow on the chromatograms. The asterisks above the graph bar indicate statistically significant differences according to Student's *t*-test (* $p < 0.05$, ** $p < 0.01$). Mean relative expression levels, standard error and *p*-values were calculated using the software SPSS 17.0.

To validate the authenticity of the identified circRNAs, 10 circRNAs were subjected to RT-qPCR and Sanger sequencing. RT-qPCR successfully detected all circRNA candidates, and DNA sequencing confirmed the presence of head-to-tail splice junctions, as indicated by RNA-seq analyses (Figure 7B).

3. Discussion

The mammary gland is essential for lactation and responds to hormonal changes occurring during pregnancy and after birth [26]. Hormones, growth factors [27], and nutrient availability [28] closely control its development and functions [29]. During pregnancy, PROG, E2, cortisol, placental lactogen, and insulin must work in harmony to prepare this gland for lactation [30]. The initial growth of the lactiferous ductal system is dependent on E2, whereas growth hormone and cortisol have a synergistic effect [31]. Further, in the course of pregnancy, the increased levels of PRL, placental lactogen, E2, and PROG favor the development of the milk secretory alveolar apparatus [32]. In humans, serum PRL levels begin to linearly increase upon direct E2 stimulation during the first trimester of pregnancy [33]. Herein, we collected blood samples and measured serum concentrations of PRL, FSH, LH, E2, and PROG. As previously reported, hormone levels in the D250 group were generally higher than those in the D30 group. During a bovine lactation, the dry period is required to facilitate cell turnover in the bovine mammary gland to optimize milk yield in the next lactation [34]. It is notable that the aforementioned hormones can potentially inhibit mammary gland degeneration [35].

Mammary gland development is influenced by several noncoding RNAs and functional genes [36,37]. Exosomes are present in blood [38,39], and noncoding RNAs [40,41] and protein-coding genes [42] have been identified from exosomes. Exosomes play a key role in development [43], immunity [44], tissue homeostasis [45], cancer [46], and neurodegenerative diseases [47]. Nevertheless, the role of bovine blood-derived exosomes in regulating mammary gland development remains unclear. Exosome-encapsulated microRNAs reportedly function as circulating biomarkers for breast cancer [48], and serum-derived exosomal lncRNAs have therapeutic effects on breast cancer [49]. Moreover, exosomes are implicated in mammary gland development [50]. In this study, we collected blood samples from dairy cattle in D250 and D30, followed by isolation and identification of blood-derived exosomes. We treated MAC-T cells with these exosomes to explore their effects on the mammary gland. Our data indicated that blood-derived exosomes play an important role in mammary gland development by promoting the proliferation of MAC-T cells. Further, sequencing analyses of MAC-T cells treated with blood-derived exosomes from D250 and D30 revealed the participation of significantly differentially expressed genes in important biological processes, including cell proliferation, TNF signaling pathway [51], IL-17 signaling pathway [52], HIF-1 signaling pathway [53], apoptosis [54], FoxO signaling pathway [55], and p53 signaling pathway [56]. These functions may be regulated by cargo in blood-derived exosomes, such as functional proteins, metabolites, and nucleic acids, which play intercellular communication roles upon transfer to recipient cells [57].

Exosomes have a diverse composition of genetic material [58], including several circRNAs that are enriched and stable in them [15]. Therefore, we performed deep sequencing to comprehensively explore the profile of bovine blood-derived exosomal circRNAs, which led to the identification of 31,181 lncRNAs and 460 circRNAs. On comparing genomic features between lncRNAs and mRNAs, our results were consistent with those previously reported [59,60]. Cargo selection into exosomes is a regulated, non-random process; previous studies have indicated that RNAs are selectively encapsulated into exosomes [61]. In this study, we found that relative to mRNAs, lncRNAs encapsulated in bovine blood-derived exosomes were expressed at higher levels, which suggests that they play a comparatively crucial role in physiological function [62]. The circular structure of circRNAs makes them more stable than other RNA types [16]. Many circRNAs are conserved in mammals and have potential biological functions [63]. Of the 460 identified circRNAs, 45 were differentially expressed between the D250 and D30 groups. circRNAs were re-

cently suggested to play a key role in dairy cattle immunity, development, and disease [64]. Herein, functional enrichment analyses showed that hosting transcripts of the identified circRNA candidates participated in cell cycle and proliferation, Rap1 signaling pathway, focal adhesion, regulation of actin cytoskeleton, and FoxO signaling pathway. Based on our findings, we suggest that these predicted circRNAs enveloped in blood-derived exosomes are an attractive regulatory element in cell proliferation and mammary gland development.

To the best of our knowledge, this is the first study to identify circRNAs in bovine blood-derived exosomes, although their presence in human serum exosomes [65], porcine milk exosomes [24], and bovine milk exosomes [66] has been reported previously. Our results present comprehensive information on the expression profiles of circRNAs in bovine blood-derived exosomes and should considerably enrich the transcript genomic database of dairy cattle.

To conclude, we successfully isolated and verified blood-derived exosomes from dairy cattle, and these exosomes were found to promote MAC-T cell proliferation, particularly those from D250. We compared exosomal RNA expression in bovine blood between the D250 and D30 groups and found numerous lncRNAs and circRNAs in blood-derived exosomes. Functional enrichment analyses revealed that hosting transcripts of the identified circRNA candidates were significantly enriched in various key processes, including apoptosis, cell cycle, and proliferation. Our findings improve our understanding of the important roles of blood-derived exosomes and the characterization of circRNA candidates in mammary gland development.

4. Materials and Methods

4.1. Animals and Management

We selected six healthy mastitis-free Holstein cows from the Wenshi Dinghu dairy farm (Zhaoqing, China). Three cows were in D30, while the other three were in D250. Approximately 200 mL blood samples from each cow were collected via the tail vein, and serum concentrations of prolactin (PRL), follicle-stimulating hormone (FSH), luteinizing hormone (LH), estrogen (E2), and progesterone (PROG) were measured using ELISA kits (Jiancheng Bioengineering Institute, Nanjing, Jiangsu, China). All experiments were performed in accordance with the procedures approved by the Institutional Animal Care and Use Committee of the South China Agricultural University (ethics approval code: SCAU2018F006, 13 March 2018).

4.2. Exosome Isolation

Milk exosomes were separated, as previously described [25]. Briefly, blood samples obtained from dairy cattle were centrifuged at $3000 \times g$ and 4°C for 15 min; the supernatant thus obtained was filtered through a $0.22\text{-}\mu\text{m}$ filter (Millipore, Billerica, MA, USA) to obtain a clear fraction. This fraction was then ultracentrifuged at $120,000 \times g$ and 4°C for 3 h using an SW70Ti rotor (Beckman Coulter Instruments, Fullerton, CA, USA), and the pellets were re-suspended in PBS to obtain exosome solutions. These solutions were stored at -80°C for further analyses.

4.3. Transmission Electron Microscopy and Particle Size Analysis

Approximately 10 mL purified exosomal fractions were analyzed under a transmission electron microscope (Talos F200S 1604154S, Hillsboro, OR, USA). Samples were placed on formvar-coated copper grids for 2 min, briefly washed with ultrapure water, negatively stained with 1% uranyl acetate, and then observed by transmission electron microscopy. Size distribution was measured using Zetasizer Nano ZS-90 (Malvern, Great Malvern, UK).

4.4. Western Blotting Analysis of Exosomal Biomarkers

To confirm the presence of bovine blood-derived exosomes, three exosomal biomarkers (tumor susceptibility gene 101 protein (TSG101), CD9, and CD63) were subjected to Western blotting. Exosomal protein content was assayed using the Pierce[®] BCA Protein Assay Kit

(Jiancheng Institute of Bioengineering, Nanjing, China). Proteins (20 µg) were first separated by 10% sodium dodecyl sulfate–polyacrylamide gel electrophoresis and then transferred to a polyvinylidene difluoride membrane (Millipore, Bedford, MA, USA). After blocking with 5% skimmed milk for 2 h, the membranes were incubated overnight at 4 °C with calnexin, TSG101, CD9, and CD63 antibodies (ZenBio, Chengdu, China). Subsequently, they were incubated with the secondary antibody horseradish peroxidase-conjugated goat anti-rabbit IgG (Sangon Biotech, Shanghai, China) for 1 h at 25 °C. Finally, enhanced chemiluminescence luminous fluid (Solarbio Life Sciences, Beijing, China) was used for band visualization; protein bands were quantified by densitometry using ImageJ v1.8 (National Institutes of Health, Bethesda, MD, USA).

4.5. MAC-T Cell Culture

The bovine mammary epithelial cell line MAC-T was purchased from the Chinese Collection of Authenticated Cell Cultures (Beijing, China). Cells were cultured in Dulbecco's modified Eagle's medium (Gibco, Grand Island, NY, USA) containing 10% fetal bovine serum (Gibco) and 1% penicillin–streptomycin (Invitrogen, Carlsbad, CA, USA) in a humidified incubator at 37 °C and 5% CO₂.

4.6. Western Blotting Analysis of MAC-T Cells

MAC-T cells were lysed, and total proteins were extracted using radioimmunoprecipitation assay reagent (Thermo Scientific, Waltham, MA, USA) containing protease inhibitors. All extracted proteins were diluted with sodium dodecyl sulfate buffer and boiled at 95 °C for 10 min. Equal amounts of proteins were separated by sodium dodecyl sulfate–polyacrylamide gel electrophoresis and transferred to a polyvinylidene fluoride membrane (Millipore, Bedford, MA, USA). After blocking with 5% skimmed milk for 2 h at room temperature, the membranes were probed with primary antibodies to detect cyclin D, cyclin E, and proliferating cell nuclear antigen (PCNA) (ZenBio), followed by incubation with goat anti-rabbit HRP conjugate antibody for 30 min at 37 °C (Sangon Biotech). Finally, enhanced chemiluminescence luminous fluid (Solarbio Life Sciences) was used for band visualization; protein bands were quantified by densitometry using ImageJ v1.8 (National Institutes of Health).

4.7. EdU Assay

MAC-T cells were seeded in 6-well culture plates at a density of 1×10^5 cells/well and treated with PBS or blood-derived exosomes isolated from the D30 and D250 periods (50 µg/mL) for 24 h. Subsequently, EdU staining was performed, according to the manufacturer instructions (Beyotime Biotechnology, Shanghai, China).

4.8. Cell Counting Kit-8 (CCK-8) Assay

MAC-T cells were seeded in a 96-well culture plate (1×10^3 cells per well) and treated with PBS or blood-derived exosomes isolated from the D30 and D250 periods (50 µg/mL). The end of 3 h of treatment was recorded as 0 h. CCK-8 reagent (EZBioscience, Roseville, MN) was added at 0 h, 12 h, 24 h, 36 h, and 48 h, followed by incubation for approximately 1 h. Optical density of each well was then measured at 450 nm using a multifunctional microplate reader (Thermo Fisher Scientific, Waltham, MA, USA).

4.9. Flow Cytometric Cell Cycle Analysis

MAC-T cells were treated with PBS or blood-derived exosomes isolated from the D30 and D250 periods (50 µg/mL). After 48 h, cells were collected, fixed in 75% ethanol, and stored overnight at −20 °C. They were then resuspended in 500 µL PI/RNase staining buffer (BD Biosciences, Franklin Lakes, NJ, USA) and incubated at 37 °C for 30 min. Flow cytometric cell cycle analysis was performed on the BD Accuri™ C6 flow cytometer and FACSDiVa software v9.0 (BD Biosciences).

4.10. RNA Extraction and Sequencing of MAC-T Cells Treated with Blood-Derived Exosomes

Cells were seeded in a 6-well culture plate (1×10^5 cells/well) and treated with blood-derived exosomes at D30 and D250 (50 $\mu\text{g}/\text{mL}$) for 48 h. TRIzol (Invitrogen) was used for total RNA extraction from MAC-T cells, according to the manufacturer's instructions. Subsequently, eukaryotic mRNA was enriched by oligo-dT beads. This enriched mRNA was then fragmented into short segments using a fragmentation buffer and reverse transcribed into cDNA using the NEBNext[®] Ultra RNA Library Prep Kit (New England Biolabs, Ipswich, MA, USA). The resulting cDNA library was sequenced using Illumina Novaseq 6000 by Gene Denovo Biotechnology Co., Ltd. (Guangzhou, China).

Raw reads obtained on sequencing were further filtered by fastq (v0.18.0) [67] to obtain high-quality clean reads; this process involved removing reads containing adapters, reads containing > 10% unknown nucleotides, and low-quality reads containing > 50% low-quality (Q value ≤ 20) bases. Bowtie2 v2.2.8 [68] was used for mapping reads to a rRNA database, and unmapped reads were subjected to further analyses. An index of bovine reference genome (*bosTau* 9) was built, and the remaining clean reads were aligned to this reference genome using Hisat2 v2.0.4 [69]. The mapped reads were assembled by StringTie v1.3.1 and annotated with Ensembl transcript regions in a reference-based approach [70]. For each transcription region, a fragment per kilobase of transcript per million mapped reads (FPKM) value was calculated to quantify its expression abundance using RSEM [71], and differential expression analysis was performed by DESeq2 [72]. Transcripts with false discovery rate < 0.05 and absolute fold change ≥ 2 were considered to be differentially expressed. Further, Kyoto Encyclopedia of Genes and Genomes (KEGG) pathway enrichment analysis was performed to identify significantly enriched metabolic or signal transduction pathways for differentially expressed genes and to compare differentially expressed genes with the whole genome background. We also performed gene set enrichment analysis to identify whether a set of genes in specific KEGG pathways showed significant differences in two groups [73].

4.11. Blood-Derived Exosomal RNA Preparation and Sequencing

We used TRIzol (Invitrogen) to extract total RNA from blood-derived exosomes, as per the manufacturer's instructions. To remove genomic DNA, RNA samples were treated with DNase I (Takara, Dalian, China). RNA samples with RNA integrity number ≥ 7.5 were further analyzed. In each experimental group, two randomly selected samples were mixed in equal quantities to derive one sequenced pool. The Ribo-Zero[™] rRNA Removal Kit (Illumina, San Diego, CA, USA) was used to remove rRNA from RNA libraries, and the remaining RNA fragments were reverse transcribed to cDNA using the RNA-seq Library Preparation Kit (Illumina). Finally, paired-end sequencing of the libraries was performed on an Illumina HiSeq[™] 4000 sequencer (LC Bio, Hangzhou, China).

4.12. Transcriptome Analysis of Blood-Derived Exosomes

Raw reads were processed using in-house Perl scripts. Clean reads were obtained by eliminating reads containing adapters, reads containing > 10% unknown nucleotides, and low-quality reads containing > 50% low-quality (Q value ≤ 20) bases. Further, Q20, Q30, and GC contents were calculated. The index of the reference genome was built using Bowtie2 v2.2.8, and paired-end clean reads were aligned to the reference genome (*bosTau* 9) using Hisat2 v2.0.4 [68]. The mapped reads were assembled by StringTie v1.3.1 and annotated with Ensembl transcript regions in a reference-based approach [70]. Transcript expression levels were measured and normalized as FPKM. Ballgown v2.20.0 [74] was used to compare differentially expressed transcripts and generate tables and plots.

4.13. Identification of Unannotated Transcripts and circRNA Candidates

To identify novel long noncoding RNAs (lncRNAs) and transcripts of uncertain coding potential (TUCP), we followed these steps: (1) unannotated transcripts with one exon were deleted; (2) unannotated transcripts with a length of <200 bp were removed;

(3) unannotated transcripts that overlapped with the exon region of database-annotated RNAs were removed using Cuffcompare [75] (meanwhile, transcripts overlapped with known lncRNA exon regions in the database as annotated lncRNAs); (4) unannotated transcripts with FPKM < 0.5 were eliminated; and (5) unannotated transcripts that did not pass the protein-coding-score test were removed using CPC [76], CNCI [77], and Pfam-scan [78]. Transcripts that passed the size and abundance filters of our pipeline and with a Pfam domain hit were defined as TUCP set transcripts [79].

To identify circRNAs, RNA-seq data were analyzed using the find_circ [80] and CIRI2 [81] algorithms. circRNA candidates identified by both these algorithms were subjected to further evaluation. The expression levels of circRNA candidates were calculated with back-splice junction reads, followed by normalization with the TMM algorithm. The edgeR package v3.30.3 [82] was then used to identify differentially expressed circRNAs with false discovery rate < 0.05.

4.14. Functional Enrichment Analysis of Differentially Expressed Transcripts and circRNA-Hosting Genes

Differentially expressed transcripts and circRNA-hosting genes were subjected to gene ontology (GO) enrichment analysis with the Goseq R package [83], and KEGG pathway enrichment analysis was conducted using KOBAS [84].

4.15. RT-qPCR

Total RNA was extracted from bovine blood-derived exosomes by TRIzol (Invitrogen), and 500 ng total RNA was reverse transcribed using a kit (Vazyme, Nanjing, China) to obtain cDNA. Primer Premier 5.0 was used to design quantitative primers for differentially expressed transcripts between the D30 and D250 groups. Primer sequences are listed in Table S1A. The external reference was cel-miR-39-3p (RiboBio, Guangzhou, China). The reaction mixture comprised 1 µL cDNA, 0.5 µL of upstream and downstream primers, 10 µL SYBR Green Real-Time PCR Master Mix (Vazyme, Nanjing, China), and 8 µL ddH₂O. The cycling conditions were as follows: pre-denaturation at 95 °C for 10 min, followed by 40 cycles at 95 °C for 15 s, 60 °C for 15 s, and 72 °C for 40 s. After amplification, the dissociation curve was analyzed. Relative quantification was performed using the $2^{-\Delta\Delta CT}$ method.

4.16. Validation of circRNAs by Sanger Sequencing

To verify the circular structure of circRNAs, we designed a pair of divergent primers and verified their head-to-tail splicing using PCR and Sanger sequencing. Primer sequences are listed in Table S1B. PCR was performed on a Bio-Rad system (Bio-RAD, Hercules, CA, USA) in a 20 µL reaction volume containing 2 µL cDNA, 7 µL nuclease-free water, 1 mM of each primer, and 10 µL of 2× Tap Master Mix (Vazyme). The cycling conditions were as follows: 95 °C for 3 min, followed by 30 cycles at 95 °C for 30 s, 30 s at the corresponding annealing temperature, and 72 °C for 30 s, and final elongation at 72 °C for 10 min. PCR products of 10 randomly selected circRNAs (six highly expressed and four differentially expressed) were confirmed by agarose gel electrophoresis.

4.17. Statistical Analysis

Values represent mean ± SEM. Data were analyzed using SPSS 17.0 (SPSS Inc., Chicago, IL, USA). One-way ANOVA was used to analyze the function of exosomes in MAC-T cells subjected to EdU assay, CCK-8 assay, and flow cytometric cell cycle analysis. We used *t*-tests to compare hormone levels in blood samples collected from the D30 and D250 groups, as well as relative gene expression in exosomes. *p* < 0.05 indicated statistically significant values, and *p* < 0.01 indicated extremely significant values. GraphPad Prism v8.0 was used to construct charts.

Supplementary Materials: The following supporting information can be downloaded at: <https://www.mdpi.com/article/10.3390/ijms241512166/s1>.

Author Contributions: Conceptualization, J.S. and Y.Z.; investigation, Y.S., Z.Z. and X.H.; writing—original draft preparation, Y.S.; writing—review and editing, J.S. and J.L.; visualization, J.S. and Q.X.; supervision, J.S. and T.C.; funding acquisition, J.S. All authors have read and agreed to the published version of the manuscript.

Funding: This work was supported by the Natural Science Foundation of China Program (grant number 32072714) and the National Key Research and Development Program of China (grant number 2022YFD1300905). The funders had no role in the study's design, data collection and analysis, decision to publish, or preparation of the manuscript.

Institutional Review Board Statement: Not applicable.

Informed Consent Statement: Not applicable.

Data Availability Statement: Not applicable.

Conflicts of Interest: The authors declare no conflict of interest.

References

1. Braicu, C.; Tomuleasa, C.; Monroig, P.; Cucuianu, A.; Berindan-Neagoe, I.; Calin, G.A. Exosomes as divine messengers: Are they the Hermes of modern molecular oncology. *Cell Death Differ.* **2015**, *22*, 34–45. [\[CrossRef\]](#) [\[PubMed\]](#)
2. Muller, L.; Hong, C.; Stolz, D.B.; Watkins, S.C.; Whiteside, T.L. Isolation of biologically-active exosomes from human plasma. *J. Immunol. Methods* **2014**, *411*, 55–65. [\[CrossRef\]](#) [\[PubMed\]](#)
3. Elsharkawi, F.; Elsabah, M.; Shabayek, M.; Khaled, H. Urine and Serum Exosomes as Novel Biomarkers in Detection of Bladder Cancer. *Asian Pac. J. Cancer Prev.* **2019**, *20*, 2219–2224. [\[CrossRef\]](#) [\[PubMed\]](#)
4. Mi, B.; Chen, L.; Xiong, Y.; Yan, C.; Xue, H.; Panayi, A.C.; Liu, J.; Hu, L.; Hu, Y.; Cao, F.; et al. Saliva exosomes-derived UBE2O mRNA promotes angiogenesis in cutaneous wounds by targeting SMAD6. *J. Nanobiotechnol.* **2020**, *18*, 68. [\[CrossRef\]](#) [\[PubMed\]](#)
5. Munagala, R.; Aqil, F.; Jeyabalan, J.; Gupta, R.C. Bovine milk-derived exosomes for drug delivery. *Cancer Lett.* **2016**, *371*, 48–61. [\[CrossRef\]](#) [\[PubMed\]](#)
6. Kalluri, R.; Lebleu, V.S. The biology, function, and biomedical applications of exosomes. *Science* **2020**, *367*, eaau6977. [\[CrossRef\]](#) [\[PubMed\]](#)
7. Valadi, H.; Ekström, K.; Bossios, A.; Sjöstrand, M.; Lee, J.J.; Lötvall, J.O. Exosome-mediated transfer of mRNAs and microRNAs is a novel mechanism of genetic exchange between cells. *Nat. Cell Biol.* **2007**, *9*, 654–659. [\[CrossRef\]](#) [\[PubMed\]](#)
8. Watson, C.J.; Khaled, W.T. Mammary development in the embryo and adult: New insights into the journey of morphogenesis and commitment. *Development* **2020**, *147*, dev169862. [\[CrossRef\]](#)
9. Silanikove, N. Natural and abrupt involution of the mammary gland affects differently the metabolic and health consequences of weaning. *Life Sci.* **2014**, *102*, 10–15. [\[CrossRef\]](#) [\[PubMed\]](#)
10. Jaswal, S.; Jena, M.K.; Anand, V.; Jaswal, A.; Kancharla, S.; Kolli, P.; Mandadapu, G.; Kumar, S.; Mohanty, A.K. Critical Review on Physiological and Molecular Features during Bovine Mammary Gland Development: Recent Advances. *Cells* **2022**, *11*, 3325. [\[CrossRef\]](#) [\[PubMed\]](#)
11. Lin, M.C.; Chen, S.Y.; He, P.L.; Luo, W.T.; Li, H.J. Transfer of Mammary Gland-forming Ability Between Mammary Basal Epithelial Cells and Mammary Luminal Cells via Extracellular Vesicles/Exosomes. *J. Vis. Exp.* **2017**, *3*, e55736. [\[CrossRef\]](#)
12. Théry, C.; Zitvogel, L.; Amigorena, S. Exosomes: Composition, biogenesis and function. *Nat. Rev. Immunol.* **2002**, *2*, 569–579. [\[CrossRef\]](#)
13. Yáñez-Mó, M.; Siljander, P.R.M.; Andreu, Z.; Bedina Zavec, A.; Borràs, F.E.; Buzas, E.I.; Buzas, K.; Casal, E.; Cappello, F.; Carvalho, J.; et al. Biological properties of extracellular vesicles and their physiological functions. *J. Extracell. Vesicles* **2015**, *4*, 27066. [\[CrossRef\]](#) [\[PubMed\]](#)
14. O'Brien, K.; Breyne, K.; Ughetto, S.; Laurent, L.C.; Breakefield, X.O. RNA delivery by extracellular vesicles in mammalian cells and its applications. *Nat. Rev. Mol. Cell. Biol.* **2020**, *21*, 585–606. [\[CrossRef\]](#)
15. Li, Y.; Zheng, Q.; Bao, C.; Li, S.; Guo, W.; Zhao, J.; Chen, D.; Gu, J.; He, X.; Huang, S. Circular RNA is enriched and stable in exosomes: A promising biomarker for cancer diagnosis. *Cell Res.* **2015**, *25*, 981–984. [\[CrossRef\]](#) [\[PubMed\]](#)
16. Liu, C.; Chen, L. Circular RNAs: Characterization, cellular roles, and applications. *Cell* **2022**, *185*, 2016–2034. [\[PubMed\]](#)
17. Jeck, W.R.; Sorrentino, J.A.; Wang, K.; Slevin, M.K.; Burd, C.E.; Liu, J.; Marzluff, W.F.; Sharpless, N.E. Circular RNAs are abundant, conserved, and associated with ALU repeats. *RNA* **2013**, *19*, 141–157. [\[CrossRef\]](#) [\[PubMed\]](#)
18. Qu, S.; Yang, X.; Li, X.; Wang, J.; Gao, Y.; Shang, R.; Sun, W.; Dou, K.; Li, H. Circular RNA: A new star of noncoding RNAs. *Cancer Lett.* **2015**, *365*, 141–148. [\[CrossRef\]](#)
19. Xu, T.; Wu, J.; Han, P.; Zhao, Z.; Song, X. Circular RNA expression profiles and features in human tissues: A study using RNA-seq data. *BMC Genom.* **2017**, *18* (Suppl. S6), 680. [\[CrossRef\]](#) [\[PubMed\]](#)
20. Zhang, C.; Wu, H.; Wang, Y.; Zhao, Y.; Fang, X.; Chen, C.; Chen, H. Expression Patterns of Circular RNAs from Primary Kinase Transcripts in the Mammary Glands of Lactating Rats. *J. Breast Cancer* **2015**, *18*, 235–241. [\[CrossRef\]](#) [\[PubMed\]](#)

21. Wang, J.; Zhou, H.; Hickford, J.G.H.; Hao, Z.; Gong, H.; Hu, J.; Liu, X.; Li, S.; Shen, J.; Ke, N.; et al. Identification and characterization of circular RNAs in mammary gland tissue from sheep at peak lactation and during the nonlactating period. *J. Dairy Sci.* **2021**, *104*, 2396–2409. [[CrossRef](#)] [[PubMed](#)]
22. Zhang, C.; Wu, H.; Wang, Y.; Zhu, S.; Liu, J.; Fang, X.; Chen, H. Circular RNA of cattle casein genes are highly expressed in bovine mammary gland. *J. Dairy Sci.* **2016**, *99*, 4750–4760. [[CrossRef](#)] [[PubMed](#)]
23. Liu, J.; Zhang, M.; Li, D.; Li, M.; Kong, L.; Cao, M.; Wang, Y.; Song, C.; Fang, X.; Chen, H.; et al. Prolactin-Responsive Circular RNA circHIPK3 Promotes Proliferation of Mammary Epithelial Cells from Dairy Cow. *Genes* **2020**, *11*, 336. [[CrossRef](#)] [[PubMed](#)]
24. Zeng, B.; Chen, T.; Xie, M.; Luo, J.; He, J.; Xi, Q.; Sun, J.; Zhang, Y. Exploration of long noncoding RNA in bovine milk exosomes and their stability during digestion in vitro. *J. Dairy Sci.* **2019**, *102*, 6726–6737. [[CrossRef](#)] [[PubMed](#)]
25. Chen, S.; Zhou, Y.; Chen, Y.; Gu, J. fastp: An ultra-fast all-in-one FASTQ preprocessor. *Bioinformatics* **2018**, *34*, i884–i890. [[CrossRef](#)] [[PubMed](#)]
26. Langmead, B.; Salzberg, S.L. Fast gapped-read alignment with Bowtie 2. *Nat. Methods* **2012**, *9*, 357–359. [[CrossRef](#)] [[PubMed](#)]
27. Kim, D.; Langmead, B.; Salzberg, S.L. HISAT: A fast spliced aligner with low memory requirements. *Nat. Methods* **2015**, *12*, 357–360. [[CrossRef](#)]
28. Pertea, M.; Pertea, G.M.; Antonescu, C.M.; Chang, T.C.; Mendell, J.T.; Salzberg, S.L. StringTie enables improved reconstruction of a transcriptome from RNA-seq reads. *Nat. Biotechnol.* **2015**, *33*, 290–295. [[CrossRef](#)]
29. Li, B.; Dewey, C.N. RSEM: Accurate transcript quantification from RNA-Seq data with or without a reference genome. *BMC Bioinform.* **2011**, *12*, 323. [[CrossRef](#)]
30. Love, M.I.; Huber, W.; Anders, S. Moderated estimation of fold change and dispersion for RNA-seq data with DESeq2. *Genome Biol.* **2014**, *15*, 550. [[CrossRef](#)] [[PubMed](#)]
31. Subramanian, A.; Tamayo, P.; Mootha, V.K.; Mukherjee, S.; Ebert, B.L.; Gillette, M.A.; Paulovich, A.; Pomeroy, S.L.; Golub, T.R.; Lander, E.S.; et al. Gene Set Enrichment Analysis: A Knowledge-Based Approach for Interpreting Genome-Wide Expression Profiles. *Proc. Natl. Acad. Sci. USA* **2005**, *102*, 15545–15550. [[CrossRef](#)] [[PubMed](#)]
32. Pertea, M.; Kim, D.; Pertea, G.M.; Leek, J.T.; Salzberg, S.L. Transcript-level expression analysis of RNA-seq experiments with HISAT, StringTie and Ballgown. *Nat. Protoc.* **2016**, *11*, 1650–1667. [[CrossRef](#)] [[PubMed](#)]
33. Trapnell, C.; Roberts, A.; Goff, L.; Pertea, G.; Kim, D.; Kelley, D.R.; Pimentel, H.; Salzberg, S.L.; Rinn, J.L.; Pachter, L. Differential gene and transcript expression analysis of RNA-seq experiments with TopHat and Cufflinks. *Nat. Protoc.* **2012**, *7*, 562–578. [[CrossRef](#)] [[PubMed](#)]
34. Kong, L.; Zhang, Y.; Ye, Z.; Liu, X.; Zhao, S.; Wei, L.; Gao, G. CPC: Assess the protein-coding potential of transcripts using sequence features and support vector machine. *Nucleic Acids Res.* **2007**, *35*, W345–W349. [[CrossRef](#)]
35. Sun, L.; Luo, H.; Bu, D.; Zhao, G.; Yu, K.; Zhang, C.; Liu, Y.; Chen, R.; Zhao, Y. Utilizing sequence intrinsic composition to classify protein-coding and long non-coding transcripts. *Nucleic Acids Res.* **2013**, *41*, e166. [[CrossRef](#)]
36. Finn, R.D.; Bateman, A.; Clements, J.; Coghill, P.; Eberhardt, R.Y.; Eddy, S.R.; Heger, A.; Hetherington, K.; Holm, L.; Mistry, J.; et al. Pfam: The protein families database. *Nucleic Acids Res.* **2013**, *42*, D222–D230. [[CrossRef](#)] [[PubMed](#)]
37. Cabili, M.N.; Trapnell, C.; Goff, L.; Koziol, M.; Tazon-Vega, B.; Regev, A.; Rinn, J.L. Integrative annotation of human large intergenic noncoding RNAs reveals global properties and specific subclasses. *Gene Dev.* **2011**, *25*, 1915–1927. [[CrossRef](#)] [[PubMed](#)]
38. Memczak, S.; Jens, M.; Elefsinioti, A.; Torti, F.; Krueger, J.; Rybak, A.; Maier, L.; Mackowiak, S.D.; Gregersen, L.H.; Munschauer, M.; et al. Circular RNAs are a large class of animal RNAs with regulatory potency. *Nature* **2013**, *495*, 333–338. [[CrossRef](#)]
39. Gao, Y.; Zhang, J.; Zhao, F. Circular RNA identification based on multiple seed matching. *Brief. Bioinform.* **2018**, *19*, 803–810. [[CrossRef](#)]
40. Robinson, M.D.; McCarthy, D.J.; Smyth, G.K. edgeR: A Bioconductor package for differential expression analysis of digital gene expression data. *Bioinformatics* **2009**, *26*, 139–140. [[CrossRef](#)]
41. Young, M.D.; Wakefield, M.J.; Smyth, G.K.; Oshlack, A. Gene ontology analysis for RNA-seq: Accounting for selection bias. *Genome Biol.* **2010**, *11*, R14. [[CrossRef](#)] [[PubMed](#)]
42. Mao, X.; Cai, T.; Olyarchuk, J.G.; Wei, L. Automated genome annotation and pathway identification using the KEGG Orthology (KO) as a controlled vocabulary. *Bioinformatics* **2005**, *21*, 3787–3793. [[CrossRef](#)] [[PubMed](#)]
43. Zeng, B.; Chen, T.; Luo, J.; Xie, M.; Wei, L.; Xi, Q.; Sun, J.; Zhang, Y. Exploration of Long Non-Coding RNAs and Circular RNAs in Porcine Milk Exosomes. *Front. Genet.* **2020**, *11*, 652. [[CrossRef](#)] [[PubMed](#)]
44. Jena, M.K.; Jaswal, S.; Kumar, S.; Mohanty, A.K. Molecular mechanism of mammary gland involution: An update. *Dev. Biol.* **2019**, *445*, 145–155. [[CrossRef](#)]
45. Jeong, W.; Bae, H.; Lim, W.; Bazer, F.W.; Lee, H.; Song, G. The functional effects and mechanisms by which fibroblast growth factor 2 (FGF2) controls bovine mammary epithelial cells: Implications for the development and functionality of the bovine mammary gland1. *J. Anim. Sci.* **2017**, *95*, 5365–5377. [[CrossRef](#)]
46. Baldi, A.; Cheli, F.; Pinotti, L.; Pecorini, C. Nutrition in mammary gland health and lactation: Advances over eight Biology of Lactation in Farm Animals meetings1. *J. Anim. Sci.* **2008**, *86*, 3–9. [[CrossRef](#)] [[PubMed](#)]
47. Blum, J.W.; Baumrucker, C.R. Colostral and milk insulin-like growth factors and related substances: Mammary gland and neonatal (intestinal and systemic) targets. *Domest. Anim. Endocrinol.* **2002**, *23*, 101–110. [[CrossRef](#)]
48. Macias, H.; Hinck, L. Mammary gland development. *Wiley Interdiscip. Rev. Dev. Biol.* **2012**, *1*, 533–557. [[CrossRef](#)] [[PubMed](#)]

49. Galoiu, S. *Yen and Jaffe's Reproductive Endocrinology: Physiology, Pathophysiology and Clinical Management*, 7th ed.; Saunders: Philadelphia, PA, USA, 2015.
50. Djiane, J.; Durand, P. Prolactin-progesterone antagonism in self-regulation of prolactin receptors in the mammary gland. *Nature* **1977**, *266*, 641–643. [\[CrossRef\]](#)
51. Jaffe, R.B.; Yuen, B.H.; Keye, W.J.; Midgley, A.J. Physiologic and pathologic profiles of circulating human prolactin. *Am. J. Obstet. Gynecol.* **1973**, *117*, 757–773. [\[CrossRef\]](#)
52. Collier, R.J.; Annen-Dawson, E.L.; Pezeshki, A. Effects of continuous lactation and short dry periods on mammary function and animal health. *Animal* **2012**, *6*, 403–414. [\[CrossRef\]](#) [\[PubMed\]](#)
53. Accorsi, P.A.; Pacioni, B.; Pezzi, C.; Forni, M.; Flint, D.J.; Seren, E. Role of prolactin, growth hormone and insulin-like growth factor 1 in mammary gland involution in the dairy cow. *J. Dairy Sci.* **2002**, *85*, 507–513. [\[CrossRef\]](#) [\[PubMed\]](#)
54. Chen, Z.; Liang, Y.; Lu, Q.; Nazar, M.; Mao, Y.; Aboragah, A.; Yang, Z.; Loo, J.J. Cadmium promotes apoptosis and inflammation via the circ08409/miR-133a/TGFB2 axis in bovine mammary epithelial cells and mouse mammary gland. *Ecotoxicol. Environ. Saf.* **2021**, *222*, 112477. [\[CrossRef\]](#) [\[PubMed\]](#)
55. Briata, P.; Caputo, L.; Zapparoli, E.; Marcaccini, E.; Passalacqua, M.; Brondolo, L.; Bordo, D.; Rossi, A.; Nicoletti, C.; Bucci, G.; et al. LncRNAEPR-induced METTL7A1 modulates target gene translation. *Nucleic Acids Res.* **2022**, *50*, 7608–7622. [\[CrossRef\]](#) [\[PubMed\]](#)
56. Song, Y.; Wang, B.; Zhu, X.; Hu, J.; Sun, J.; Xuan, J.; Ge, Z. Human umbilical cord blood-derived MSCs exosome attenuate myocardial injury by inhibiting ferroptosis in acute myocardial infarction mice. *Cell Biol. Toxicol.* **2021**, *37*, 51–64. [\[CrossRef\]](#)
57. Zhang, X.; Takeuchi, T.; Takeda, A.; Mochizuki, H.; Nagai, Y. Comparison of serum and plasma as a source of blood extracellular vesicles: Increased levels of platelet-derived particles in serum extracellular vesicle fractions alter content profiles from plasma extracellular vesicle fractions. *PLoS ONE* **2022**, *17*, e270634. [\[CrossRef\]](#)
58. Geng, T.; Song, Z.; Xing, J.; Wang, B.; Dai, S.; Xu, Z. Exosome Derived from Coronary Serum of Patients with Myocardial Infarction Promotes Angiogenesis Through the miRNA-143/IGF-IR Pathway. *Int. J. Nanomed.* **2020**, *15*, 2647–2658. [\[CrossRef\]](#)
59. Li, P.; Xu, Z.; Liu, T.; Liu, Q.; Zhou, H.; Meng, S.; Feng, Z.; Tang, Y.; Liu, C.; Feng, J.; et al. Circular RNA Sequencing Reveals Serum Exosome Circular RNA Panel for High-Grade Astrocytoma Diagnosis. *Clin. Chem.* **2022**, *68*, 332–343. [\[CrossRef\]](#)
60. Lasser, C.; Alikhani, V.S.; Ekstrom, K.; Eldh, M.; Paredes, P.T.; Bossios, A.; Sjostrand, M.; Gabrielsson, S.; Lotvall, J.; Valadi, H. Human saliva, plasma and breast milk exosomes contain RNA: Uptake by macrophages. *J. Transl. Med.* **2011**, *9*, 9. [\[CrossRef\]](#)
61. Sharma, P.; Mesci, P.; Carromeu, C.; McClatchy, D.R.; Schiapparelli, L.; Yates, J.R.; Muotri, A.R.; Cline, H.T. Exosomes regulate neurogenesis and circuit assembly. *Proc. Natl. Acad. Sci. USA* **2019**, *116*, 16086–16094. [\[CrossRef\]](#)
62. Robbins, P.D.; Morelli, A.E. Regulation of immune responses by extracellular vesicles. *Nat. Rev. Immunol.* **2014**, *14*, 195–208. [\[CrossRef\]](#) [\[PubMed\]](#)
63. Takahashi, A.; Okada, R.; Nagao, K.; Kawamata, Y.; Hanyu, A.; Yoshimoto, S.; Takasugi, M.; Watanabe, S.; Kanemaki, M.T.; Obuse, C.; et al. Exosomes maintain cellular homeostasis by excreting harmful DNA from cells. *Nat. Commun.* **2017**, *8*, 15287. [\[CrossRef\]](#)
64. Paskeh, M.D.A.; Entezari, M.; Mirzaei, S.; Zabolian, A.; Saleki, H.; Naghdi, M.J.; Sabet, S.; Khoshbakht, M.A.; Hashemi, M.; Hushmandi, K.; et al. Emerging role of exosomes in cancer progression and tumor microenvironment remodeling. *J. Hematol. Oncol.* **2022**, *15*, 83. [\[CrossRef\]](#) [\[PubMed\]](#)
65. Jarmalavičiūtė, A.; Pivoriūnas, A. Exosomes as a potential novel therapeutic tool against neurodegenerative diseases. *Pharmacol. Res.* **2016**, *113*, 816–822. [\[CrossRef\]](#)
66. Joyce, D.P.; Kerin, M.J.; Dwyer, R.M. Exosome-encapsulated microRNAs as circulating biomarkers for breast cancer. *Int. J. Cancer* **2016**, *139*, 1443–1448. [\[CrossRef\]](#)
67. Han, M.; Gu, Y.; Lu, P.; Li, J.; Cao, H.; Li, X.; Qian, X.; Yu, C.; Yang, Y.; Yang, X.; et al. RETRACTED ARTICLE: Exosome-mediated lncRNA AFAP1-AS1 promotes trastuzumab resistance through binding with AUF1 and activating ERBB2 translation. *Mol. Cancer* **2020**, *19*, 26. [\[CrossRef\]](#) [\[PubMed\]](#)
68. Hendrix, A.; Hume, A.N. Exosome signaling in mammary gland development and cancer. *Int. J. Dev. Biol.* **2011**, *55*, 879–887. [\[CrossRef\]](#)
69. Zhang, R.; Xue, T.; Shao, A.; Lang, Y.; Qin, C.; Zhao, M.; Kuang, Y.; Yu, Z.; Geng, Y.; Zhao, C.; et al. Bclaf1 regulates c-FLIP expression and protects cells from TNF-induced apoptosis and tissue injury. *EMBO Rep.* **2022**, *23*, e52702. [\[CrossRef\]](#)
70. Li, Y.; Chang, L.H.; Huang, W.Q.; Bao, H.W.; Li, X.; Chen, X.H.; Wu, H.T.; Yao, Z.Z.; Huang, Z.Z.; Weinberg, S.E.; et al. IL-17A mediates pyroptosis via the ERK pathway and contributes to steroid resistance in CRSwNP. *J. Allergy Clin. Immunol.* **2022**, *150*, 337–351. [\[CrossRef\]](#)
71. Wang, J.Z.; Zhu, W.; Han, J.; Yang, X.; Zhou, R.; Lu, H.C.; Yu, H.; Yuan, W.B.; Li, P.C.; Tao, J.; et al. The role of the HIF-1 α /ALYREF/PKM2 axis in glycolysis and tumorigenesis of bladder cancer. *Cancer Commun.* **2021**, *41*, 560–575. [\[CrossRef\]](#)
72. Zhang, Q.; Wu, X.; Zhang, H.; Wu, Q.; Fu, M.; Hua, L.; Zhu, X.; Guo, Y.; Zhang, L.; You, Q.; et al. Protein Phosphatase 5-Recruiting Chimeras for Accelerating Apoptosis-Signal-Regulated Kinase 1 Dephosphorylation with Antiproliferative Activity. *J. Am. Chem. Soc.* **2022**, *145*, 1118–1128. [\[CrossRef\]](#)
73. Pauta, M.; Rotllan, N.; Fernández-Hernando, A.; Langhi, C.; Ribera, J.; Lu, M.; Boix, L.; Bruix, J.; Jimenez, W.; Suárez, Y.; et al. Akt-mediated foxo1 inhibition is required for liver regeneration. *Hepatology* **2016**, *63*, 1660–1674. [\[CrossRef\]](#)
74. Ghosh, M.; Saha, S.; Bettke, J.; Nagar, R.; Parrales, A.; Iwakuma, T.; van der Velden, A.W.M.; Martinez, L.A. Mutant p53 suppresses innate immune signaling to promote tumorigenesis. *Cancer Cell* **2021**, *39*, 494–508. [\[CrossRef\]](#) [\[PubMed\]](#)

75. Gurung, S.; Perocheau, D.; Touramanidou, L.; Baruteau, J. The exosome journey: From biogenesis to uptake and intracellular signalling. *Cell Commun. Signal.* **2021**, *19*, 47. [[CrossRef](#)] [[PubMed](#)]
76. Abels, E.R.; Breakefield, X.O. Introduction to Extracellular Vesicles: Biogenesis, RNA Cargo Selection, Content, Release, and Uptake. *Cell. Mol. Neurobiol.* **2016**, *36*, 301–312. [[CrossRef](#)]
77. Ren, H.; Wang, G.; Chen, L.; Jiang, J.; Liu, L.; Li, N.; Zhao, J.; Sun, X.; Zhou, P. Genome-wide analysis of long non-coding RNAs at early stage of skin pigmentation in goats (*Capra hircus*). *BMC Genom.* **2016**, *17*, 67. [[CrossRef](#)]
78. Ma, Q.; Li, L.; Tang, Y.; Fu, Q.; Liu, S.; Hu, S.; Qiao, J.; Chen, C.; Ni, W. Analyses of long non-coding RNAs and mRNA profiling through RNA sequencing of MDBK cells at different stages of bovine viral diarrhea virus infection. *Res. Vet. Sci.* **2017**, *115*, 508–516. [[CrossRef](#)]
79. Skog, J.; Wurdinger, T.; van Rijn, S.; Meijer, D.H.; Gainche, L.; Sena-Esteves, M.; Curry, W.J.; Carter, B.S.; Krichevsky, A.M.; Breakefield, X.O. Glioblastoma microvesicles transport RNA and proteins that promote tumour growth and provide diagnostic biomarkers. *Nat. Cell Biol.* **2008**, *10*, 1470–1476. [[CrossRef](#)] [[PubMed](#)]
80. Grammatikakis, I.; Lal, A. Significance of lncRNA abundance to function. *Mamm. Genome* **2022**, *33*, 271–280. [[CrossRef](#)]
81. Rybak-Wolf, A.; Stottmeister, C.; Glažar, P.; Jens, M.; Pino, N.; Giusti, S.; Hanan, M.; Behm, M.; Bartok, O.; Ashwal-Fluss, R.; et al. Circular RNAs in the Mammalian Brain Are Highly Abundant, Conserved, and Dynamically Expressed. *Mol. Cell* **2015**, *58*, 870–885. [[CrossRef](#)]
82. Raza, S.; Wijayanti, D.; Pant, S.D.; Abdelnour, S.A.; Hashem, N.M.; Amin, A.; Wani, A.K.; Prakash, A.; Dawood, M.; Zan, L. Exploring the physiological roles of circular RNAs in livestock animals. *Res. Vet. Sci.* **2022**, *152*, 726–735. [[CrossRef](#)] [[PubMed](#)]
83. Pan, B.; Qin, J.; Liu, X.; He, B.; Wang, X.; Pan, Y.; Sun, H.; Xu, T.; Xu, M.; Chen, X.; et al. Identification of Serum Exosomal has-circ-0004771 as a Novel Diagnostic Biomarker of Colorectal Cancer. *Front. Genet.* **2019**, *10*, 1096. [[CrossRef](#)] [[PubMed](#)]
84. Wang, Y.; Li, D.; Wang, Y.; Li, M.; Fang, X.; Chen, H.; Zhang, C. The landscape of circular RNAs and mRNAs in bovine milk exosomes. *J. Food Compos. Anal.* **2019**, *76*, 33–38. [[CrossRef](#)]

Disclaimer/Publisher’s Note: The statements, opinions and data contained in all publications are solely those of the individual author(s) and contributor(s) and not of MDPI and/or the editor(s). MDPI and/or the editor(s) disclaim responsibility for any injury to people or property resulting from any ideas, methods, instructions or products referred to in the content.

RESEARCH

Open Access



The difference of intestinal microbiota composition between Lantang and Landrace newborn piglets

Ling Li¹, Shuai Li¹, Junyi Luo¹, Ting Chen¹, Qianyun Xi¹, Yongliang Zhang^{1*} and Jiajie Sun^{1*}

Abstract

Background The early development of intestinal microbiota plays a fundamental role in host health and development. To investigate the difference in the intestinal microbial composition between Lantang and Landrace newborn piglets, we amplified and sequenced the V3-V4 region of 16 S rRNA gene in jejunal microbiota of Lantang and landrace newborn.

Results The findings revealed that the dominant phyla in the jejunum of Lantang piglets were Firmicutes, Actinobacteria and Bacteroidetes, while the dominant phyla of Landrace is Proteobacteria and Fusobacteria. Specifically, *Corynebacterium_1*, *Lactobacillus*, *Rothia*, *Granulicatella*, *Corynebacteriales_unclassified*, *Corynebacterium*, *Globicatella* and *Actinomycetales_unclassified* were found to be the dominant genera of Lantang group, while *Clostridium_sensu_stricto_1*, *Escherichia-Shigella*, *Actinobacillus* and *Bifidobacterium* were the dominant genera of Landrace. Based on the functional prediction of bacteria, we found that bacterial communities from Lantang samples had a significantly greater abundance pathways of fatty acid synthesis, protein synthesis, DNA replication, recombination, repair and material transport across membranes, while the carrier protein of pathogenic bacteria was more abundant in Landrace samples.

Conclusions Overall, there was a tremendous difference in the early intestinal flora composition between Landang and Landrace piglets, which was related to the breed characteristics and may be one of the reasons affecting the growth characteristics. However, more further extensive studies should be included to reveal the underlying relationship between early intestinal flora composition in different breeds and pig growth characteristics.

Keywords Breeds, Newborn piglets, Jejunal microbiota, High throughput sequencing

*Correspondence:

Yongliang Zhang
zhangyl@scau.edu.cn
Jiajie Sun
jiajiesun@scau.edu.cn

¹College of Animal Science, Guangdong Provincial Key Laboratory of Animal Nutrition Control, National Engineering Research Center for Breeding Swine Industry, South China Agricultural University, Guangzhou, Guangdong 510642, China



© The Author(s) 2023. **Open Access** This article is licensed under a Creative Commons Attribution 4.0 International License, which permits use, sharing, adaptation, distribution and reproduction in any medium or format, as long as you give appropriate credit to the original author(s) and the source, provide a link to the Creative Commons licence, and indicate if changes were made. The images or other third party material in this article are included in the article's Creative Commons licence, unless indicated otherwise in a credit line to the material. If material is not included in the article's Creative Commons licence and your intended use is not permitted by statutory regulation or exceeds the permitted use, you will need to obtain permission directly from the copyright holder. To view a copy of this licence, visit <http://creativecommons.org/licenses/by/4.0/>. The Creative Commons Public Domain Dedication waiver (<http://creativecommons.org/publicdomain/zero/1.0/>) applies to the data made available in this article, unless otherwise stated in a credit line to the data.

Background

Lantang (a Chinese indigenous lardtype breed) and Landrace (a typical lean breed) pigs show obvious differences in stress resistance, production, growth performances and meat quality characteristics [1]. In general, Lantang has high reproductive rate, strong adaptability and good meat quality [2]; Landrace is well-known for fast growing rate and lean meat percentage but low ability of resistance to disease [3]. The molecular mechanism underlying these phenotype differences has been well studied, and a growing body of evidence has also unraveled important roles of the gut microbiome in immune function [4], organ development [5], host metabolism [6] and colonization resistance to enteric pathogens [7].

Accumulating information about porcine gastrointestinal tract microorganisms has been acquired since the expansive application of “omics analysis” [8, 9]. Emerging studies deemed that the gut of newborns is short of microorganisms before birth, but will rapidly arise a distinct shift from a basically sterile state to an extremely dense microbial population [10, 11]. The colonization and succession of gut microbe in the early postpartum period facilitates immune maturation and have long-term impacts on the healthy growth and development of newborns [12]. In addition to many assorted environmental factors, the influence of breeds on the composition of early intestinal flora in piglets cannot be ignored [13].

The importance of the intestinal microbiota for early growth in pigs have been extensively studied, but fewer studies have investigated the possible association between breeds and early intestinal microbial composition of piglets [14]. Therefore, the major aim of this study was to investigate the jejunal microflora of newborn between Lantang and Landrace, and to compare the characteristics of intestinal microflora involved in pig breeds.

Result

16 S rRNA sequencing and annotation

By high-throughput sequencing analysis, a total of 1,677,229 raw reads were generated from Landrace and Lantang libraries. Each library produced an average of approximately 83,861 joined tags (minimum=80,032 and maximum=87,907), and more than 90.47% valid reads from each sample were processed for further analysis (Table S1). Based on the obtained feature OTU, a total of 666 convincing candidates were identified (Table S2A); and only 115 candidates were shared across two groups, while 202 and 349 were identified uniquely in the Landrace and Lantang groups, respectively (Fig. 1A). All OTU candidates were annotated with the SILVA database to evaluate the microbial diversity in the jejunum of two breeds using the QIIME2 pipeline, which detected a total

of 16 taxonomic phyla (Table S2B). In details, the dominant phyla in the jejunum of piglets were Firmicutes, Proteobacteria, Actinobacteria, Bacteroidetes and Fusobacteria, accounting for 70.25%, 29.15%, 0.53%, 0.03% and 0.02%, respectively. And the proportion of Firmicutes (84.58% vs. 55.92%), Actinobacteria (0.10% vs. 0.06%) and Bacteroidetes (0.05% vs. 0.01%) were greater in the jejunum of Lantang piglets than in Landrace, while Proteobacteria (14.31% vs. 43.98%) and Fusobacteria (0.01% vs. 0.02%) were lower in the jejunum of Lantang piglets (Figure S1). The number of 37 classes, 73 orders and 130 families were detected, of which four classes, six orders and seven families had a relative abundance greater than 1.0% (Table S2C, D, E). At the genus level, a total of 257 classifiable genera were identified (Table S2F), and seven genera had a relative abundance greater than 1.0%, including *Lactobacillus*, *Clostridium_sensu_stricto_1*, *Escherichia-Shigella*, *Veillonella*, *Burkholderia-Caballeronia-Paraburkholderia*, *Streptococcus* and *Actinobacillus* (Fig. 1B). Among them, *Lactobacillus*, *Burkholderia-Caballeronia-Paraburkholderia* and *Streptococcus* were found to be more abundant in the jejunum of Lantang piglets, while *Clostridium_sensu_stricto_1*, *Escherichia-Shigella*, *Veillonella*, and *Actinobacillus* are more abundant of Landrace. Among the 391 species detected (Table S2G), the most abundant species in the jejunum of Lantang was *Lactobacillus_sp_L-YJ*, and the most abundant species of Landrace was *Clostridium_sensu_stricto_1_unclassified* (Fig. 1C). In addition, the tree of species evolution was constructed according to the multi-sequence alignment results of feature sequences (Fig. 1D). We drew a conclusion that functional diversity of bacterial communities were represented mainly by a clade of Firmicutes, Proteobacteria, Actinobacteria and Bacteroidetes. In details, *Helicobacter* and *ruminococcaceae_ucg-005* from Firmicutes have a correlative evolutionary relationship, and *Gastranaerophilales_unclassified* is closely related to the evolution of Actinobacteria.

The difference of intestinal microbiota composition between two breeds

The Observed species, Shannon, Simpson, Chao1, and Goods_coverage indices between two groups were calculated to compare the jejunum microbial alpha-diversity of the two breeds (Table 1). There was an increasing trend of Observed species ($P=0.08$) and Chao1 ($P=0.09$) diversity indices in the Lantang group compared with those of the Landrace group, and the Simpson diversity index exhibited a significant increase in the Landrace ($P=0.02$). For the beta-diversity, the PCA (Fig. 2A), PCoA (Fig. 2B) and NMDS (Figure S2) analysis showed Lantang and Landrace samples could be separated absolutely into two groups, which reflected the differences in early jejunum microbial community composition between

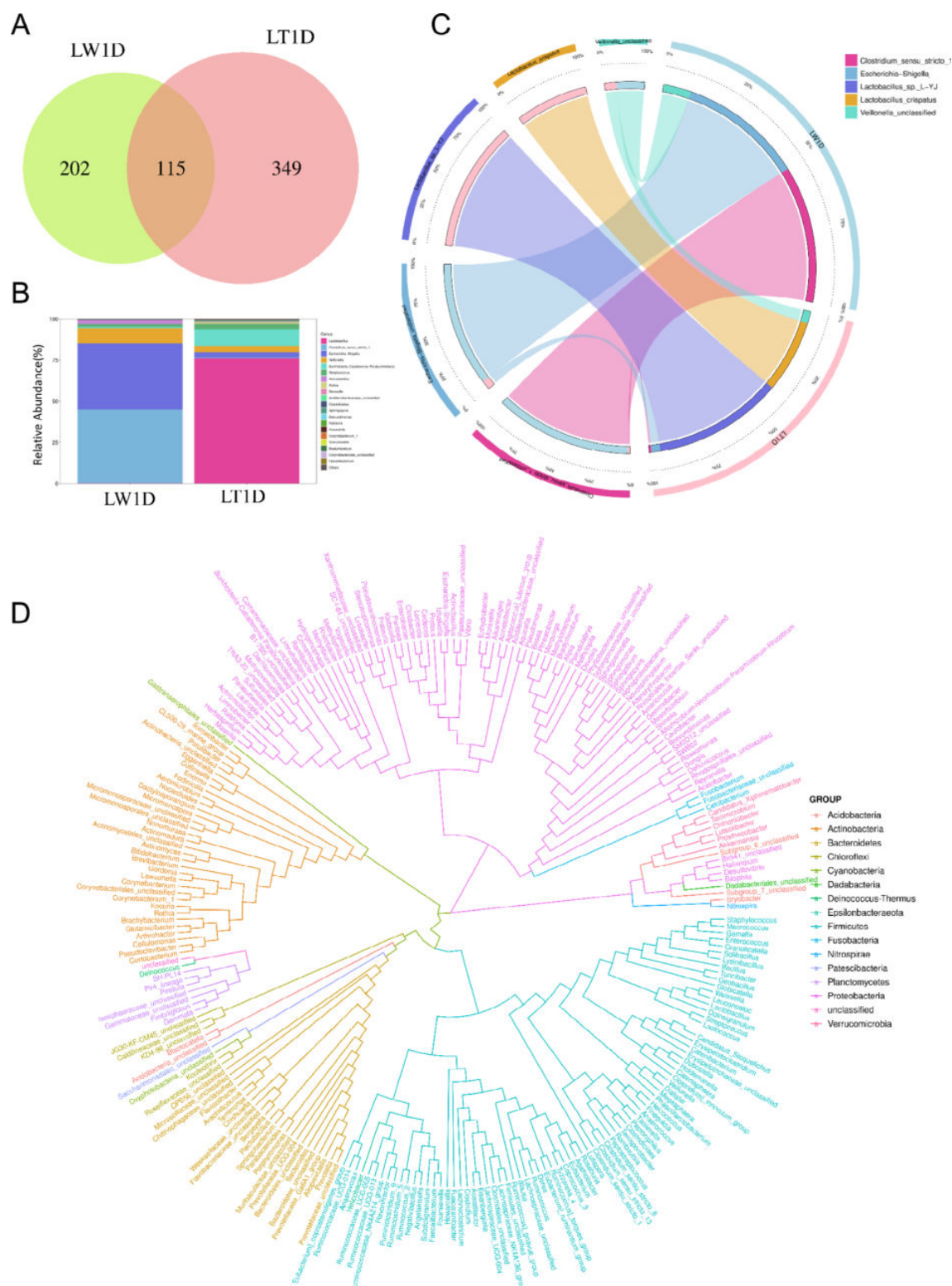


Fig. 1 16 S rRNA gene sequencing and annotation analysis **(A)** Venn diagram. Venn diagram representing the shared and exclusive OTUs at the 97% similarity level between Jejunal microbiota in the two groups **(B)** Stacked bar chart. Bar plot shows the relative abundance of jejunal microbiota at the genus level in each group **(C)** Circos. The left half of circos is the top5 relative abundance species and their corresponding abundance information; the right half is the grouping information displays according to groups, and the wider the width, the higher the abundance **(D)** Phylogenetic tree. Different colors represent different phyla and different branches represent different genus levels. The closer the distance between the two species, the closer the evolutionary relationship between them Note: OTUs, operational taxonomic units; LWID, Lantang piglets; LTID, Landrace piglets

Table 1 Microbial diversity indices of the jejunal microbiome

Item	LW1D	LT1D	P value
Observed species	78.20±8.64	113.30±16.87	0.08
Shannon	2.86±0.03	2.59±0.22	0.25
Simpson	0.77±0.01	0.65±0.05	0.02
Chao1	80.38±8.97	115.55±17.42	0.09
Goods_coverage	0.99±0.00	0.99±0.00	1.00

Note: The values were calculated as the mean±standard error of the mean. $P<0.05$ indicated a significant difference between the two groups. LW1D, Lantang piglets; LT1D, Landrace piglets

different breeds of piglets. And the cluster tree revealed the significant structural separation of jejunal microflora between the two breeds (Figure S3). Subsequently, LefSe algorithm was employed to identify statistically significant biomarkers among the two groups. A total of 117 differentially abundant taxonomic clades were found, with a Linear Discriminant Analysis (LDA) score higher than 3. The number of biomarkers at the phylum, class, order, family, genus and species levels were 4, 9, 15, 20, 26, and 43, respectively. Among them, 14 genera can be used as biomarkers for Lantang samples, including *Lactobacillus*, *Burkholderia-Caballeronia-Paraburkholderia*, *Streptococcus*, *Novosphingobium*, *Subgroup_6_unclassified*, *Rothia*, *Weissella*, *Pseudoclavibacter*, *Subgroup_7_unclassified*, *Acidobacteria_unclassified*, *Rhizobacter*, *Actinomycetales_unclassified*, *Howardella*, *Pseudomonas*, while 12 genera can be used as biomarkers for Landrace samples, including *Actinobacillus*, *Lysobacter*, *Micromonospora*, *Lachnospiraceae_UCG-004*, *Lachnospiraceae_NK4A136_group*, *Rhodospirillales_unclassified*, *Faecalibacterium*, *Bifidobacterium*, *Clostridiales_unclassified*, *Citrobacter*, *Clostridium_sensu_stricto_1*, *Escherichia-Shigella* (Figure S4). According to the sample species abundance table, we found 5, 5, 11, 16, 12 and 28 significantly different microorganisms at the phylum, class, order, family, genus and species levels, respectively (Table S3). The difference analysis results displayed that the significantly differential microorganisms were mainly classified to the phyla of Firmicutes and Actinobacteria in Lantang group and the phyla of Proteobacteria and Firmicutes in Landrace group (Fig. 2C). Specifically, the dominant genera of Lantang group were *Corynebacterium_1*, *Lactobacillus*, *Rothia*, *Granulicatella*, *Corynebacteriales_unclassified*, *Corynebacterium*, *Globicatella* and *Actinomycetales_unclassified*, while the dominant genera of Landrace were *Clostridium_sensu_stricto_1*, *Escherichia-Shigella*, *Actinobacillus* and *Bifidobacterium*.

In general, the relationship between different microbial groups plays a considerable role in revealing some biological significance. The reticulum network contained a node representing *Lactobacillus*. Its neighbors formed five mutually exclusive clusters: *Burkholderia-Caballeronia-Paraburkholderia* was positively correlated

with *Lactobacillus*, and the other negatively correlated with *Lactobacillus*, consisting mainly of members of the *Escherichia-Shigella*, *Clostridium_sensu_stricto_1*, *Actinobacillus* and *Veillonella*. The genus of *Clostridium_sensu_stricto_1* was positively related to *Escherichia-Shigella*, *Actinobacillus* and *Veillonella*, and negatively related to *Burkholderia-Caballeronia-Paraburkholderia*. The genus of *Escherichia-Shigella* was observed to be positively correlated with *Actinobacillus* and *Veillonella*, and negatively correlated with *Burkholderia-Caballeronia-Paraburkholderia* (Figure S5).

Molecular function of bacterial microbiota

PICRUSt2 software was employed to predict the functionality of the microorganism using the 16 S rRNA gene data. We found Abundant gene families were identified in all samples; of these, many of these genes play novel roles in glycolysis, fatty acid metabolism, amino acid metabolism, DNA replication and repair and pathogenicity (Table S4A and S4B). Prediction of these function revealed significant differences between the jejunal microbe of the two breeds. There were 4,231 and 2,718 differential functional features of the jejunal microbiome between the two breeds in the KO and COG database, respectively (Table S4C and S4D). We provided a visual representation of the top 30 secondary classification Clusters of KO pathways (Fig. 2D). The abundance of seven functional annotations in the Lantang group was higher than that in the Landrace group, including “cfa; cyclopropane-fatty-acyl-phospholipid synthase [EC:2.1.1.79]”, “acpP; acyl carrier protein”, “hupB; DNA-binding protein HU-beta”, “groEL, HSPD1; chaperonin GroEL”, “RP-S21, MRPS21, rpsU; small subunit ribosomal protein S21”, “groES, HSPE1; chaperonin GroES” and “ABC.PA.P; polar amino acid transport system permease protein”. The abundance of other 23 functional annotations was higher in the Landrace group, such as “terC; tellurite resistance protein TerC”, “kdgT; 2-keto-3-deoxygluconate permease”. For the COG pathways, only four functional annotations were higher in the Lantang group than in the Landrace group, which were the “Na⁺/H⁺-antiporter NhaD or related arsenite permease”, “Co-chaperonin GroES (HSP10)”, “Uracil-DNA glycosylase” and “Cyclopropane fatty-acyl-phospholipid synthase and related methyltransferases” (Figure S6).

Discussion

In this study, clustering analysis revealed that the Firmicutes, Actinobacteria and Bacteroidetes were the dominant phyla in Lantang piglets, while Proteobacteria and Fusobacteria were the dominant phyla in Landrace. In agreement with previous results, pig breed affects the proportion of Firmicutes and Bacteroidetes, which are higher in Chinese indigenous pig breeds than in foreign

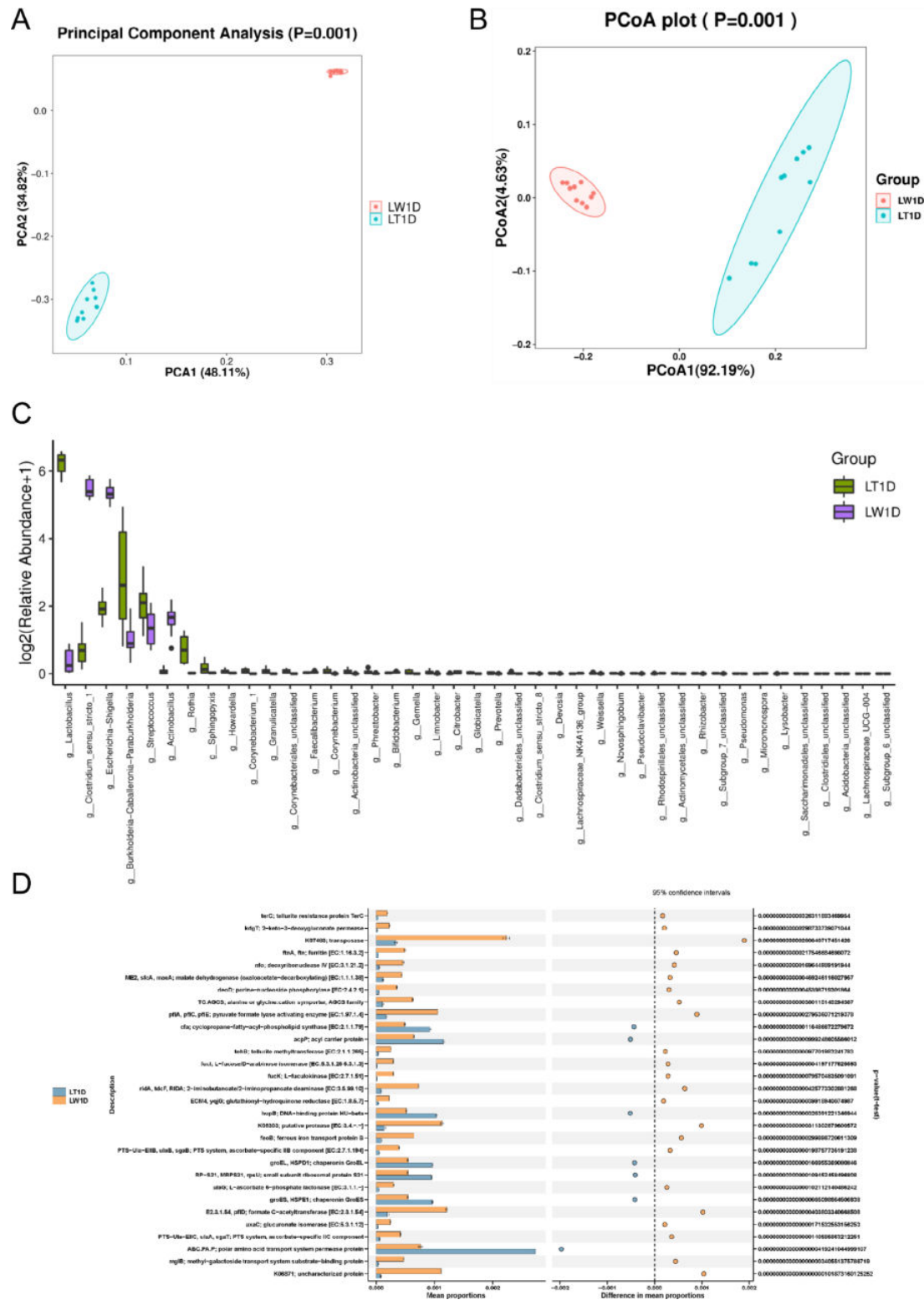


Fig. 2 Microbial diversity in the jejunum of the two breeds **(A)** Principal Component Analysis (PCA). The same group is displayed as a circle graph with 95% confidence interval. The farther the distance between two samples, the greater the difference of microbial composition and structure between samples **(B)** Principal coordinate analysis (PCoA). The PCoA is based on the weighted UniFrac distance **(C)** Barplot difference analysis. The barplot shows microorganisms with significant differences at the genus level ($P < 0.05$ is defined as significantly different species) **(D)** Functional prediction STAMP difference analysis. The analysis results show the top 30 differential classification Clusters between the two group in KO function pathways ($P < 0.05$, 95% confidence interval) Note: LW1D, Lantang piglets; LT1D, Landrace piglets

breeds [14]. Firmicutes, Actinobacteria and Bacteroidetes are the main energy-producing bacteria in the gut, decomposing various kinds of non-digestible polysaccharides and fermentating the resulting monosaccharides into SCFA, primarily acetate, propionate and butyrate, as well as other organic acids [15]. Additionally, the proportion of Firmicutes and Bacteroidetes have been attributed to energy metabolism and immune regulation [16–18]. However, there is increasing evidence that Proteobacteria is related to the dysbiosis and metabolic disorders [19, 20]. Fusobacteria has been supposed in the proinflammatory signature and disease of the body [21–23]. Hermann-Bank et al. [24] found that the number of Fusobacteria bacteria was doubled in piglets experiencing diarrhea.

Different pig breeds may exhibit their unique microbial diversity [25]. In this study, the PCA, PCoA and NMDS analysis indicated that Lantang and Landrace samples are mainly gathered into two different regions. This result corroborates the report of Yang et al. [14], who observed that the pig breeds affected the composition of intestinal microbiota, and the composition is different with different breeds, especially between Chinese indigenous breeds and foreign breeds. Genetic background is closely related to the intestinal microbial taxa and characteristics of the host [26].

Among the differential microbes of jejunum between the two breeds, *Corynebacterium_1*, *Lactobacillus*, *Rothia*, *Granulicatella*, *Corynebacteriales_unclassified*, *Corynebacterium*, *Globicatella* and *Actinomycetales_unclassified* was found to be more abundant in the jejunum of Lantang piglets, while *Clostridium_sensu_stricto_1*, *Escherichia-Shigella*, *Actinobacillus* and *Bifidobacterium* were more abundant of Landrace. *Corynebacterium_1*, *Rothia*, *Corynebacteriales_unclassified*, *Corynebacterium* and *Actinomycetales_unclassified* are all from phylum Actinobacteria. Binda et al. [20] suggested that Actinobacteria are absolute participants in preserving intestinal barrier homeostasis. Moreover, *Rothia* breaks down protein in feed and helps the digestion and absorption of nutrients in the intestine [27]. *Lactobacillus* is a major systematic group in the proximal gastrointestinal tract of several mammals [28, 29], which can metabolize carbohydrates to produce lactic acid, the end product [30, 31]. Previous studies reported that some species of *Lactobacillus* could be transferred from the mother to the intestines of piglets via faeces or breast milk, so as to prevent and treat diarrhea [32]. Consistent with the findings of predecessors, the abundance of *Clostridium_sensu_stricto_1* and *Escherichia-Shigella* are high in suckling Landrace piglets, and they have been proved to be potential causative agents of diarrhea [33–35]. *Actinobacillus* equal as a primary pathogen in breeding sows and piglets [36]. The capacity to efficiently use mucus is

a typical feature of *Bifidobacterium*, an intestinal genus that maintaining healthy intestines and preventing disease [37]. Furthermore, we found that *Burkholderia-Caballeronia-Paraburkholderia* was positively correlated with *Lactobacillus*, and the other negatively correlated with *Lactobacillus*, consisting mainly of members of the *Escherichia-Shigella*, *Clostridium_sensu_stricto_1*, *Actinobacillus* and *Veillonella*. *Burkholderia-Caballeronia-Paraburkholderia* shows a unique spectrum of antimicrobial activity and inhibited carbapenem-resistant Gram-negative bacterial pathogens [38]. The importance of *Veillonella* in mammal infections is uncertain, and they are generally considered to be of low virulence [39]. The results showed that the predominant species of Lantang group was genus of *Lactobacillus*, while the Landrace group were genera of *Clostridium_sensu_stricto_1* and *Escherichia-Shigella*. We believe that the difference of the above microorganism might be one of the reasons why Lantang pigs are resistant to rough feeding and have strong adaptability, while Landrace pigs have weak physique and poor resistance to stress.

Furthermore, bacterial communities from Lantang samples had a significantly greater abundance pathways of fatty acid synthesis, protein synthesis, DNA replication, recombination, repair and material transport across membranes. Previous studies have revealed that the *cfa* gene encodes cyclopropane fatty acyl phospholipid synthase, which converts unsaturated fatty acids to their cyclopropane form [40]. The cyclopropane fatty acids in cell membrane is momentous for bacteria to adapt to the rapidly changing environment [41, 42]. In mammals, Acyl carrier protein (ACP) is a universal and highly conserved carrier of acyl intermediates during fatty acid synthesis [43]. DNA-binding protein HU-beta are involved in DNA replication, recombination and DNA repair [44]. Chaperone proteins, as an indispensable part of the protein-folding mechanism of bacterial cells, help maintain cellular homeostasis [45, 46], may also offset the harmful effects of mutations [47]. Tokuriki et al. [48] showed that chaperonin GroEL/GroES promotes the evolution of recombinant proteins. Small subunit ribosomal protein S21 also plays an important role in protein synthesis [49]. The ABC transporter system promotes the absorption of nutrients by bacteria [50], excretes substances that are not conducive to cell growth out of the cell, and also participates in signal transduction, protein secretion and antigen presentation in eukaryotes [51]. However, the abundance of “terC; tellurite resistance protein TerC” and “kdgT; 2-keto-3-deoxygluconate permease” functional annotation was higher in the Landrace group than Lantang group. Some studies have shown that the tellurite resistance gene operon is widely spread among pathogenic bacterial species [52]. And 2-keto-3-deoxygluconate permease is considered as a carrier protein for

the fermentation of gluconate via 2-keto-3-deoxygluconate in many *Clostridium* bacteria [53]. Moreover, the relative abundance of “Na⁺/H⁺ antiporter” and “Uracil-DNA glycosylase” functional annotation in the Lantang group was found to be higher than that in the Landrace group. The Na⁺/H⁺ antiporters play a primary role in the maintenance of intracellular pH homeostasis and dynamic balance of cellular Na⁺, and in the regulation of cell volume [54]. The Uracil-DNA glycosylase for the removal of Uracil formed by incorrect input or mutation during DNA repair [55, 56]. The functional responses of jejunum microbiome of the above two breeds was significantly different. It is reasonable to assume that the difference of early microbial composition are one of the reasons for the different growth characteristics of Lantang and Landrace.

Conclusion

Our findings revealed that there were tremendous differences in the early intestinal microflora composition between Lantang and Landrace newborn piglets due to breed characteristics. Furthermore, we found that these differences might be associated with growth characteristics of different breeds via the functional prediction of bacteria. However, more further extensive studies should be included to reveal the underlying relationship between early y intestinal flora composition in different breeds and pig growth characteristics.

Materials and methods

Sampling

All piglets were collected from a large-scale pig farm (Xinfeng County, Shaoguan City, Guangdong Province, China). After the sows farrowed, 10 healthy and pure-bred Lantang and Landrace male piglets (the piglets had no contact with the external environment and did not take breast milk) were slaughtered and digesta of jejunum were collected immediately; subsequently, a total of 10 intestinal contents in each breed were snap-frozen in liquid nitrogen and stored at -80 °C for further analysis. The experiment were approved and conducted under the supervision of the Animal Care Committee of South China Agricultural University.

DNA extraction, PCR amplification and sequencing

Microbial genomic DNA was extracted from intestinal digesta using cetyltrimethylammonium bromide (CTAB) method, and the integrity of genomic DNA was assessed by 1% agarose gel electrophoresis and quantified with NanoDrop 8000 spectrophotometer (Thermo Fisher Scientific, Waltham, MA). According to the concentration, DNA was diluted to 1 ng/μL using sterile water. The intestinal bacterial 16 S rRNA gene was amplified by polymerase chain reaction (PCR) with specific

primers (341 F: 5'-CCTACGGGNGGCWGCAG-3'; 805R: 5'-GACTACHVGGGTATCTAATCC-3') targeting V3-V4 variable region [57]. After amplification, the products were purified by AMPure XT beads (Beckman Coulter, Danvers, MA) and quantified by Qubit (Invitrogen, Carlsbad, CA). The libraries were pooled subsequently at equal molar ratios, and sequenced on Illumina NovaSeq platform (LC Sciences, Hangzhou, China).

Bioinformatics analysis

The quality control and chimeric sequence filtering were carried out to obtain high-quality clean reads by fqtrim (<http://ccb.jhu.edu/software/fqtrim/index.shtml>) and Vsearch softwares (<https://github.com/torognes/vsearch>). The clean tags of all samples were then clustered, and the tags with over 97% similarity were regarded as one operational taxonomic unit (OTU). According to SILVA (release 132) classifier, the feature sequences were annotated and normalized into different taxonomic levels [58]. Alpha diversity is applied in analyzing complexity of species diversity for a sample through 5 indices, including Chao1, Observed species, Goods coverage, Shannon, Simpson, and all these indices in our samples were calculated with QIIME2 [59]. For beta-diversity analysis, principal component analysis (PCA) was employed to reveal the simple rules under the intricate data background. Principal coordinate analysis (PCoA) and non-metric multi-dimensional scaling (NMDS) were performed to visualize the relationship between the samples. Unweighted pair group method with arithmetic means (UPGMA) is commonly considered as a method that effectively demonstrating good grouping and sample repeatability. Mann-Whitney U test was utilized for species difference test, and linear discriminant analysis effect size (LEfSe) was employed to find the biomarkers between different groups [60]. SparCC was performed to calculate the abundance of the top 30 microorganisms at the genus level, and the network diagram and correlation heat map were drawn based on the correlation and significance *P* value between the two dominant bacteria groups [61]. The PICRUST2 was performed to predict the potential molecular functions of bacterial communities by obtaining the abundance of each predicted functional trait corresponding to normalized feature [62, 63]. These predictions are pre-calculated for genes in databases including KEGG Orthology (KO) and Clusters of Orthologous Groups (COG).

Statistical analysis

The results of alpha-diversity and bacterial phenotype prediction were statistically analyzed by the T-test using SPSS software 17.0 (IBM Corp., Armonk, NY). All other statistical analyses were completed in R software (v3.4.4). Data were expressed as mean ± standard error

of the mean (SEM), with $P < 0.05$ considered as statistical significance.

Supplementary Information

The online version contains supplementary material available at <https://doi.org/10.1186/s12917-023-03642-z>.

Figure S1 Stacked bar chart. Bar plot shows the relative abundance of jejunal microbiota at the phylum level in each group. **Figure S2** Non-metric multi-dimensional scaling (NMDS). The NMDS analysis was based on the Bray–Curtis distance. Each point in the figure represents a sample, and the samples in the same group are represented by the same color. **Figure S3** On the left is the UPGMA cluster tree structure of each sample at the OTU level, and on the right is the relative abundance distribution map of each sample at the genus level. **Figure S4** Comparison of the classification of rumen microbiota between two groups by linear discriminant analysis effect size (LefSe) method. The LDA value distribution histogram (left) shows the species with significant differences in abundance in the two groups, and the length of the histogram represents the impact of different species. In the taxonomic cladogram (right), the circles radiating from the inside to the outside represent the classification level from phylum to species. **Figure S5** Sparcc network diagram and heat map. Different nodes in the network diagram represent different dominant genera. The connection between nodes indicates that there is correlation between the two genera. The thickness of the line indicates the strength of the correlation, and the size of the node indicates the number of other bacteria associated with the bacterium. **Figure S6** Functional prediction STAMP difference analysis. The analysis results show the top 30 differential classification Clusters between the two group in COG function pathways ($P < 0.05$, 95% confidence interval).

Tables S1 Quality control and preprocessing of metagenomic datasets.

Tables S2 (A) Sequence composition of each sample at each level based on the SILVA and NT-16S database. (B) The aligned percentages that annotated at Phylum level. (C) The aligned percentages that annotated at Class level. (D) The aligned percentages that annotated at Order level. (E) The aligned percentages that annotated at Family level. (F) The aligned percentages that annotated at Genus level. (G) The aligned percentages that annotated at Species level.

Tables S3 (A) Differences between two groups identified at Phylum-taxa level. (B) Differences between two groups identified at Class-taxa level. (C) Differences between two groups identified at Order-taxa level. (D) Differences between two groups identified at Family-taxa level. (E) Differences between two groups identified at Genus-taxa level. (F) Differences between two groups identified at Species-taxa level.

Tables S4 (A) Function prediction results in the COG database. (B) Function prediction results in the KO database. (C) Differential functional prediction analysis of each sample in the COG databases. (D) Differential functional prediction analysis of each sample in the KO database.

Acknowledgements

The research was supported by the Natural Science Foundation of China (32072714), Guangdong Basic and Applied Basic Research Foundation (2020A1515010062) and the Science and Technology Project of Guangzhou (202002030037).

Authors' contributions

Ling Li: Writing-Original draft preparation; Shuai Li: Investigation; Jiajie Sun: Data curation and Visualization; Junyi Luo, Ting Chen and Qianyun Xi: Supervision; Yongliang Zhang and Jiajie Sun: Conceptualization, Methodology, Writing- Reviewing and Editing. All authors read and approved the final manuscript.

Funding

This work was supported by the Natural Science Foundation of China Program [grant numbers 32072714]; Guangdong Basic and Applied Basic Research Foundation [grant number 2020A1515010062]; the Science and Technology Project of Guangzhou [grant number 202002030037]. The sponsors had no

role in the study design; in the collection, analysis, and interpretation of the data; in the writing of the report; and in the decision to submit the article for publication.

Data Availability

The raw sequences were deposited into Sequence Read Archive (SRA) database with the BioProject accession number PRJNA876404 (https://www.ncbi.nlm.nih.gov/sra?LinkName=bioproject_sra_all&from_uid=876404).

Declarations

Ethical approval and consent

All piglets were collected from a large-scale pig farm (Xinfeng County, Shaoguan City, Guangdong Province, China). All animal procedures were approved by the owner of farm and the Animal Care Committee at South China Agricultural University according to the university's guidelines for animal research (2018F006), and all methods were performed in accordance with the relevant guidelines and regulations.

All methods were reported in accordance with ARRIVE guidelines (<https://arriveguidelines.org>).

Consent to publish

Not applicable.

Competing interests

The authors declare no competing interests.

Received: 15 November 2022 / Accepted: 12 July 2023

Published online: 27 September 2023

References

1. Yu K, Shu G, Yuan F, Zhu X, Gao P, Wang S, et al. Fatty acid and transcriptome profiling of longissimus dorsi muscles between pig breeds differing in meat quality. *Int J Biol Sci*. 2013;9(1):108–18.
2. Cheng P, Wang Y, Liang J, Wu Y, Wright A, Liao X. Exploratory analysis of the Microbiological potential for efficient utilization of Fiber between Lantang and Duroc Pigs. *Front Microbiol*. 2018;9:1342.
3. Miao ZG, Wang LJ, Xu ZR, Huang JF, Wang YR. Developmental changes of carcass composition, meat quality and organs in the Jinhua pig and landrace. *Animal*. 2009;3(3):468–73.
4. Belkaid Y, Hand TW. Role of the microbiota in immunity and inflammation. *Cell*. 2014;157(1):121–41.
5. Lahiri S, Kim H, Garcia-Perez I, Reza MM, Martin KA, Kundu P, et al. The gut microbiota influences skeletal muscle mass and function in mice. *Sci Transl Med*. 2019;11:502.
6. Gomes AC, Hoffmann C, Mota JF. The human gut microbiota: metabolism and perspective in obesity. *Gut Microbes*. 2018;9(4):308–25.
7. Haak BW, Prescott HC, Wiersinga WJ. Therapeutic potential of the gut microbiota in the Prevention and Treatment of Sepsis. *Front Immunol*. 2018;9:2042.
8. De Rodas B, Youmans BP, Danzeisen JL, Tran H, Johnson TJ. Microbiome profiling of commercial pigs from farrow to finish. *J Anim Sci*. 2018;96(5):1778–94.
9. Wang X, Tsai T, Deng F, Wei X, Chai J, Knapp J, et al. Longitudinal investigation of the swine gut microbiome from birth to market reveals stage and growth performance associated bacteria. *Microbiome*. 2019;7(1):109.
10. de Goffau MC, Lager S, Sovio U, Gaccioli F, Cook E, Peacock SJ, et al. Human placenta has no microbiome but can contain potential pathogens. *Nature*. 2019;572(7769):329–34.
11. Gresse R, Chaucheyras Durand F, Dunière L, Blanquet-Diot S, Forano E. Microbiota Composition and Functional Profiling throughout the gastrointestinal tract of Commercial Weaning Piglets. *Microorganisms*. 2019;7(9).
12. Liu H, Zeng X, Zhang G, Hou C, Li N, Yu H, et al. Maternal milk and fecal microbes guide the spatiotemporal development of mucosa-associated microbiota and barrier function in the porcine neonatal gut. *BMC Biol*. 2019;17(1):106.
13. Holman DB, Brunelle BW, Trachsel J, Allen HK. Meta-analysis to define a core microbiota in the Swine Gut. *mSystems*. 2017;2(3).

14. Bergamaschi M, Tiezzi F, Howard J, Huang YJ, Gray KA, Schillebeeckx C, et al. Gut microbiome composition differences among breeds impact feed efficiency in swine. *Microbiome*. 2020;8(1):110.
15. Samuel BS, Gordon JL. A humanized gnotobiotic mouse model of host-archaeal-bacterial mutualism. *Proc Natl Acad Sci U S A*. 2006;103(26):10011–6.
16. Jandhyala SM, Talukdar R, Subramanyam C, Vuyyuru H, Sasikala M, Nageshwar Reddy D. Role of the normal gut microbiota. *World J Gastroenterol*. 2015;21(29):8787–803.
17. Gibiino G, Lopetuso LR, Scalfadiferri F, Rizzatti G, Binda C, Gasbarrini A. Exploring Bacteroidetes: metabolic key points and immunological tricks of our gut commensals. *Dig Liver Dis*. 2018;50(7):635–9.
18. Tseng CH, Wu CY. The gut microbiome in obesity. *J Formos Med Assoc*. 2019;118(Suppl 1):3–59.
19. Shin NR, Whon TW, Bae JW. Proteobacteria: microbial signature of dysbiosis in gut microbiota. *Trends Biotechnol*. 2015;33(9):496–503.
20. Binda C, Lopetuso LR, Rizzatti G, Gibiino G, Cennamo V, Gasbarrini A, Actinobacteria. A relevant minority for the maintenance of gut homeostasis. *Dig Liver Dis*. 2018;50(5):421–8.
21. Strauss J, Kaplan GG, Beck PL, Rioux K, Panaccione R, Devinney R, et al. Invasive potential of gut mucosa-derived *Fusobacterium nucleatum* positively correlates with IBD status of the host. *Inflamm Bowel Dis*. 2011;17(9):1971–8.
22. Kostic AD, Chun E, Robertson L, Glickman JN, Gallini CA, Michaud M, et al. *Fusobacterium nucleatum* potentiates intestinal tumorigenesis and modulates the tumor-immune microenvironment. *Cell Host Microbe*. 2013;14(2):207–15.
23. Bashir A, Miskeen AY, Hazari YM, Asrafuzzaman S, Fazili KM. *Fusobacterium nucleatum*, inflammation, and immunity: the fire within human gut. *Tumour Biol*. 2016;37(3):2805–10.
24. Hermann-Bank ML, Skovgaard K, Stockmarr A, Strube ML, Larsen N, Kongsted H, et al. Characterization of the bacterial gut microbiota of piglets suffering from new neonatal porcine diarrhoea. *BMC Vet Res*. 2015;11:139.
25. Pajarillo EA, Chae JP, Balolong MP, Kim HB, Seo KS, Kang DK. Pyrosequencing-based analysis of fecal microbial communities in three purebred pig lines. *J Microbiol*. 2014;52(8):646–51.
26. Xiao Y, Li K, Xiang Y, Zhou W, Gui G, Yang H. The fecal microbiota composition of boar Duroc, Yorkshire, Landrace and Hampshire pigs. *Asian-Australasian J Anim Sci*. 2017;30(10):1456–63.
27. Wei G, Darwish G, Oppenheim FG, Schuppan D, Helmerhorst EJ. Commensal bacterium *Rothia aeria* degrades and detoxifies Gluten via a highly effective subtilisin enzyme. *Nutrients*. 2020;12(12).
28. Fuller R, Brooker BE. Lactobacilli which attach to the crop epithelium of the fowl. *Am J Clin Nutr*. 1974;27(11):1305–12.
29. Fuller R, Barrow PA, Brooker BE. Bacteria associated with the gastric epithelium of neonatal pigs. *Appl Environ Microbiol*. 1978;35(3):582–91.
30. Aguirre M, Collins MD. Lactic acid bacteria and human clinical infection. *J Appl Bacteriol*. 1993;75(2):95–107.
31. Bağder Elmaci S, Tokatli M, Dursun D, Özçelik F, Şanlıbaba P. Phenotypic and genotypic identification of lactic acid bacteria isolated from traditional pickles of the Çubuk region in Turkey. *Folia Microbiol (Praha)*. 2015;60(3):241–51.
32. Jost T, Lacroix C, Braegger CP, Rochat F, Chassard C. Vertical mother-neonate transfer of maternal gut bacteria via breastfeeding. *Environ Microbiol*. 2014;16(9):2891–904.
33. Wei J, Goldberg MB, Burland V, Venkatesan MM, Deng W, Fournier G, et al. Complete genome sequence and comparative genomics of *Shigella flexneri* serotype 2a strain 2457T. *Infect Immun*. 2003;71(5):2775–86.
34. Konstantinov SR, Awati AA, Williams BA, Miller BG, Jones P, Stokes CR, et al. Post-natal development of the porcine microbiota composition and activities. *Environ Microbiol*. 2006;8(7):1191–9.
35. Han C, Dai Y, Liu B, Wang L, Wang J, Zhang J. Diversity analysis of intestinal microflora between healthy and diarrheal neonatal piglets from the same litter in different regions. *Anaerobe*. 2019;55:136–41.
36. Thompson AB, Postey RC, Snider T, Pasma T. *Actinobacillus equuli* as a primary pathogen in breeding sows and piglets. *Can Vet J*. 2010;51(11):1223–5.
37. Turrioni F, Duranti S, Bottacini F, Guglielmetti S, Van Sinderen D, Ventura M. *Bifidobacterium bifidum* as an example of a specialized human gut commensal. *Front Microbiol*. 2014;5:437.
38. Depoorter E, De Canck E, Coenye T, Vandamme P. *Burkholderia* bacteria produce multiple potentially novel molecules that inhibit carbapenem-resistant gram-negative bacterial pathogens. *Antibiot (Basel)*. 2021;10(2).
39. Vesth T, Ozen A, Andersen SC, Kaas RS, Lukjancenko O, Bohlin J, et al. Veillonella, Firmicutes: microbes disguised as Gram negatives. *Stand Genomic Sci*. 2013;9(2):431–48.
40. Grogan DW, Cronan JE Jr. Cyclopropane ring formation in membrane lipids of bacteria. *Microbiol Mol Biol Rev*. 1997;61(4):429–41.
41. Muñoz-Rojas J, Bernal P, Duque E, Godoy P, Segura A, Ramos JL. Involvement of cyclopropane fatty acids in the response of *Pseudomonas putida* KT2440 to freeze-drying. *Appl Environ Microbiol*. 2006;72(1):472–7.
42. Shabala L, Ross T. Cyclopropane fatty acids improve *Escherichia coli* survival in acidified minimal media by reducing membrane permeability to H⁺ and enhanced ability to extrude H⁺. *Res Microbiol*. 2008;159(6):458–61.
43. Byers DM, Gong H. Acyl carrier protein: structure-function relationships in a conserved multifunctional protein family. *Biochem Cell Biol*. 2007;85(6):649–62.
44. Le Treut G, Képès F, Orland H. Phase behavior of DNA in the Presence of DNA-Binding proteins. *Biophys J*. 2016;110(1):51–62.
45. Houry WA. Chaperone-assisted protein folding in the cell cytoplasm. *Curr Protein Pept Sci*. 2001;2(3):227–44.
46. Lin Z, Rye HS. GroEL-mediated protein folding: making the impossible, possible. *Crit Rev Biochem Mol Biol*. 2006;41(4):211–39.
47. Rutherford SL, Lindquist S. Hsp90 as a capacitor for morphological evolution. *Nature*. 1998;396(6709):336–42.
48. Tokuriki N, Tawfik DS. Chaperonin overexpression promotes genetic variation and enzyme evolution. *Nature*. 2009;459(7247):668–73.
49. Van Duin J, Wijnands R. The function of ribosomal protein S21 in protein synthesis. *Eur J Biochem*. 1981;118(3):615–9.
50. Theodoulou FL, Kerr ID. ABC transporter research: going strong 40 years on. *Biochem Soc Trans*. 2015;43(5):1033–40.
51. Ponte-Sucre A. Availability and applications of ATP-binding cassette (ABC) transporter blockers. *Appl Microbiol Biotechnol*. 2007;76(2):279–86.
52. Turkovicova L, Smidak R, Jung G, Turna J, Lubec G, Aradska J. Proteomic analysis of the TerC interactome: novel links to tellurite resistance and pathogenicity. *J Proteom*. 2016;136:167–73.
53. Bender R, Andreesen JR, Gottschalk G. 2-keto-3-deoxygluconate, an intermediate in the fermentation of gluconate by clostridia. *J Bacteriol*. 1971;107(2):570–3.
54. Cui Y, Cheng B, Meng Y, Li C, Yin H, Xu P, et al. Expression and functional analysis of two NhaD type antiporters from the halotolerant and alkaliphilic *Halomonas* sp. Y2. *Extremophiles*. 2016;20(5):631–9.
55. Jacobs AL, Schär P. DNA glycosylases: in DNA repair and beyond. *Chromosoma*. 2012;121(1):1–20.
56. Krokan HE, Bjørås M. Base excision repair. *Cold Spring Harb Perspect Biol*. 2013;5:a012583.
57. Behrendt L, Larkum AW, Trampe E, Norman A, Sørensen SJ, Kühl M. Microbial diversity of biofilm communities in microniches associated with the didemnid ascidian *Lissoclinum patella*. *Isme j*. 2012;6(6):1222–37.
58. Quast C, Priesse E, Yilmaz P, Gerken J, Schweer T, Yarza P, et al. The SILVA ribosomal RNA gene database project: improved data processing and web-based tools. *Nucleic Acids Res*. 2013;41(Database issue):D590–596.
59. Li B, Zhang X, Guo F, Wu W, Zhang T. Characterization of tetracycline resistant bacterial community in saline activated sludge using batch stress incubation with high-throughput sequencing analysis. *Water Res*. 2013;47(13):4207–16.
60. Segata N, Izard J, Waldron L, Gevers D, Miropolsky L, Garrett WS, et al. Metagenomic biomarker discovery and explanation. *Genome Biol*. 2011;12(6):R60.
61. Friedman J, Alm EJ. Inferring correlation networks from genomic survey data. *PLoS Comput Biol*. 2012;8(9):e1002687.
62. Langille MG, Zaneveld J, Caporaso JG, McDonald D, Knights D, Reyes JA, et al. Predictive functional profiling of microbial communities using 16S rRNA marker gene sequences. *Nat Biotechnol*. 2013;31(9):814–21.
63. Douglas GM, Beiko RG, Langille MG. Predicting the functional potential of the Microbiome from marker genes using PICRUSt. *Methods Mol Biol*. 2018;1849:169–77.

Publisher's Note

Springer Nature remains neutral with regard to jurisdictional claims in published maps and institutional affiliations.



动物营养学报
Chinese Journal of Animal Nutrition
ISSN 1006-267X, CN 11-5461/S

《动物营养学报》网络首发论文

题目: 凉茶渣对育肥猪生长性能、胴体性状和肉品质的影响
作者: 谢月琴, 孙小红, 汪东阳, 陈郭平, 罗君谊, 陈婷, 习欠云, 张永亮, 孙加节
收稿日期: 2019-04-15
网络首发日期: 2019-08-06
引用格式: 谢月琴, 孙小红, 汪东阳, 陈郭平, 罗君谊, 陈婷, 习欠云, 张永亮, 孙加节. 凉茶渣对育肥猪生长性能、胴体性状和肉品质的影响[J/OL]. 动物营养学报. <http://kns.cnki.net/kcms/detail/11.5461.S.20190805.1024.056.html>



网络首发: 在编辑部工作流程中, 稿件从录用到出版要经历录用定稿、排版定稿、整期汇编定稿等阶段。录用定稿指内容已经确定, 且通过同行评议、主编终审同意刊用的稿件。排版定稿指录用定稿按照期刊特定版式(包括网络呈现版式)排版后的稿件, 可暂不确定出版年、卷、期和页码。整期汇编定稿指出版年、卷、期、页码均已确定的印刷或数字出版的整期汇编稿件。录用定稿网络首发稿件内容必须符合《出版管理条例》和《期刊出版管理规定》的有关规定; 学术研究成果具有创新性、科学性和先进性, 符合编辑部对刊文的录用要求, 不存在学术不端行为及其他侵权行为; 稿件内容应基本符合国家有关书刊编辑、出版的技术标准, 正确使用和统一规范语言文字、符号、数字、外文字母、法定计量单位及地图标注等。为确保录用定稿网络首发的严肃性, 录用定稿一经发布, 不得修改论文题目、作者、机构名称和学术内容, 只可基于编辑规范进行少量文字的修改。

出版确认: 纸质期刊编辑部通过与《中国学术期刊(光盘版)》电子杂志社有限公司签约, 在《中国学术期刊(网络版)》出版传播平台上创办与纸质期刊内容一致的网络版, 以单篇或整期出版形式, 在印刷出版之前刊发论文的录用定稿、排版定稿、整期汇编定稿。因为《中国学术期刊(网络版)》是国家新闻出版广电总局批准的网络连续型出版物(ISSN 2096-4188, CN 11-6037/Z), 所以签约期刊的网络版上网络首发论文视为正式出版。

凉茶渣对育肥猪生长性能、胴体性状和肉品质的影响

谢月琴 孙小红 汪东阳 陈郭平 罗君谊 陈 婷 习欠云 张永亮* 孙加节*
(华南农业大学动物科学学院, 广东省动物营养调控重点实验室, 国家生猪种业工程技术中心, 广州 510642)

摘 要: 为研究凉茶渣对育肥猪生长性能、胴体性状和肉品质的影响, 试验选取 78 头健康、体重 90 kg 左右的“杜×长×大”三元杂交育肥猪, 随机分为 2 组, 每组 3 个重复, 每个重复 13 头。对照组饲喂基础饲料, 试验组(凉茶渣组)饲喂在基础饲料中添加 4% 凉茶渣粉的饲料。试验预试期 7 d, 正试期 31 d。结果表明: 1) 与对照组相比, 饲料添加 4% 凉茶渣粉对育肥猪终末体重、平均日增重、平均日采食量以及料重比无显著影响($P>0.05$)。2) 与对照组相比, 凉茶渣组育肥猪胴体重和眼肌面积分别提高了 10.98% 和 21.88% ($P<0.05$)。3) 与对照组相比, 凉茶渣组育肥猪肉色的亮度值、剪切力和滴水损失分别降低了 11.58%、26.83% 和 42.21% ($P<0.05$), 肉色的红度值和大理石纹评分分别提高了 16.88% 和 53.46% ($P<0.05$)。4) 育肥猪肌肉中干物质、粗蛋白质、粗脂肪和粗灰分含量在 2 组间无显著差异($P>0.05$)。5) 与对照组相比, 凉茶渣组育肥猪肌肉中谷氨酸、丙氨酸、精氨酸、组氨酸、异亮氨酸、亮氨酸、脯氨酸、丝氨酸和天冬氨酸的含量显著提高($P<0.05$), 分别提高了 4.88%、12.83%、0.91%、6.65%、8.50%、6.06%、14.23%、15.85% 和 3.02%; 饱和脂肪酸月桂酸、肉豆蔻酸、十七酸和硬脂酸的含量显著下降($P<0.05$), 分别降低了 26.67%、14.71%、21.43% 和 16.17%; 不饱和脂肪酸棕榈烯酸、油酸、花生四烯酸、亚麻酸、花生三烯酸和芥酸的含量显著提高($P<0.05$), 分别提高了 24.34%、6.61%、43.14%、12.71%、58.33% 和 40.00%; 肌苷酸含量显著提高了 11.27% ($P<0.05$)。由此可见, 在育肥猪饲料中添加 4% 凉茶渣粉不仅可以显著提高育肥猪胴体性状, 改善猪肉品质, 而且对生长性能无负面影响。

关键词: 凉茶渣; 固废污染; 育肥猪; 生长性能; 肉品质

中图分类号: S816.7

文献标识码: A

文章编号: 1006-267X(2019)11-0000-00

凉茶具有清热解毒的功效, 深受我国南方地区群众青睐, 但凉茶渣固废污染却日益严重。据初步统计, 目前仅广东地区主要凉茶生产企业, 日均可产生约 680 t 固废茶渣, 焚烧、填埋和堆肥等传统处理不仅造成严重环境压力, 还会浪费大量可利用中药资源。近年来, 随着我国畜牧业迅速发展, 草本饲料和粮食类饲料资源已不能完全满足我国畜牧业生产需求^[1], 开发新型非粮饲料资源已成为当前研究热点之一。王老吉凉茶是由凉

粉草、鸡蛋花、金银花、菊花、夏枯草、布渣叶和甘草等 7 种中草药煎制而成, 凉茶渣固废与原药材具有相似的营养与活性成分^[2], 经过我们前期测定发现凉茶渣平均含 20.55% 干物质、28.83% 粗纤维、9.78% 粗蛋白质、3.52% 粗脂肪和 6.68% 粗灰分等营养成分(除干物质外, 其余指标均为半干基础), 而且多糖、黄酮、生物碱与矿物质等活性成分含量丰富, 是优质饲料和功能性饲料开发资源。

因此, 本试验旨在研究育肥猪饲料中添加王

收稿日期: 2019-04-15

基金项目: 广东省农业技术研发项目(2018LM2158); 广东省现代农业产业技术体系(2017LM1121); 2018 年生猪调出大县奖励资金(省级统筹部分)项目

作者简介: 谢月琴(1994—), 女, 贵州铜仁人, 硕士研究生, 动物营养与饲料科学专业。E-mail: 791312265@qq.com

* 通信作者: 张永亮, 教授, 博士生导师, E-mail: zhangyl@scau.edu.cn; 孙加节, 副教授, 硕士生导师, E-mail: jiajiesun@scau.edu.cn

老吉凉茶渣粉对育肥猪生长性能、胴体性状和肉品质的影响,为缓解我国饲料资源紧缺、开发新型功能性饲料和解决凉茶渣固废污染做出积极探索,促进形成中药与饲料行业供需新模式。

1 材料与方法

1.1 试验材料

王老吉凉茶渣由广州王老吉大健康有限责任公司提供,将凉茶渣烘至半干再粉碎,密封备用。

1.2 试验设计与饲料

试验采用单因素随机分组设计,选用 78 头体重 90 kg 左右且健康的“杜×长×大”三元杂育肥猪,随机分为 2 个组,每组 3 个重复,每个重复 13 头。试验采用玉米-豆粕型全价饲料,参照 NRC (1998) 和我国《猪饲养标准》(NY/T 65—2004) 生长育肥猪营养需要,并结合所在猪场生产实际配制成粉状饲料,基础饲料组成及营养水平见表 1。对照组饲喂基础饲料,试验组(凉茶渣组)饲喂在基础饲料中添加 4% 凉茶渣粉的饲料。试验预试期 7 d,正试期 31 d。

1.3 饲养管理

试验猪舍采用半敞开式建筑模式,水泥地面圈养,在整个试验期,试验猪可以自由采食和饮水,猪舍进行定期消毒,每天清扫圈舍,保持圈内清洁干爽,舍内自然通风。

1.4 测定指标与方法

1.4.1 生长性能

分别于试验开始和结束的当天晨饲前逐栏称重,记录初始体重和终末体重,计算平均日增重;同时试验期间每天记录采食量,试验结束后结算各组消耗饲料,计算平均日采食量;根据平均日增重和平均日采食量计算料重比。

1.4.2 胴体性状

饲养试验结束后,从每个重复中选取体重相近的 2 头肥育母猪,每组 6 头,共 12 头。在禁食 12 h 后称量宰前活重,随后进行屠宰。屠宰流程严格按照我国《生猪屠宰操作规程》(GB/T 17236—2008) 进行。随后参照《瘦肉型种猪性能测定技术规程》(GB 8467—1987) 测量胴体重、眼肌面积和背膘厚,计算屠宰率。

1.4.3 肉品质及风味指标

猪屠宰后取背最长肌测定猪肉 pH、肉色、大理石纹评分、滴水损失、蒸煮损失、剪切力和瘦肉

率,测定方法参照张伟力^[3-6]介绍的方法进行。将背最长肌肉样,剁碎混合均匀,-20℃冷冻保存备用,用冷冻干燥机冷冻干燥,经测初水分后,制成风干样品,测定其肌肉中的干物质、粗蛋白质、粗脂肪、粗灰分、氨基酸、脂肪酸以及肌苷酸等含量。

表 1 基础饲料组成及营养水平(风干基础)

Table 1 Composition and nutrient levels of the basal diet (air-dry basis)

项目 Items	含量 Content
原料 Ingredients	
玉米 Corn	65
豆粕 Soybean meal	10
膨化大豆 Expanded soybean	5
菜籽粕 Rapeseed meal	5
豆油 Soybean oil	5
米糠 Rice bran	5
石粉 Limestone	1
预混料 Premix ¹⁾	4
合计 Total	100
营养水平 Nutrient levels ²⁾	
粗蛋白质 CP	14.44
钙 Ca	0.52
磷 P	0.47
蛋氨酸 Met	0.55
赖氨酸 Lys	0.95
消化能 DE/(MJ/kg)	13.67

¹⁾ 预混料为每千克饲料提供 The premix provided the following per kg of the diet: VA 10 800 IU,VB₁ 10 mg,VB₂ 20 mg,VB₁₂ 20 mg,VD₃ 3 000 IU,VE 80 mg,VK₃ 2 mg,生物素 biotin 200 mg,D-泛酸 D-pantothenic acid 15 mg,烟酸 nicotinic acid 10 mg,Cu (as copper sulfate) 25 mg,Fe (as ferrous sulfate) 90 mg,Mn (as manganese sulfate) 15 mg,Zn (as zinc sulfate) 100 mg。

²⁾ 消化能为计算值,其余为实测值。DE was a calculated value,while the others were measured values.

1.5 数据统计分析

所得数据首先运用 Excel 2007 软件进行初步的整理和计算,然后采用 SPSS 17.0 统计软件进行组间 t 检验分析,以 P<0.05 为差异显著性标准,结果数据用平均值±标准误表示。

2 结果

2.1 凉茶渣对育肥猪生长性能的影响

由表 2 可见,2 组间育肥猪终末体重、平均日

增重、平均日采食量以及料重比均无显著差异($P>0.05$)。

表 2 凉茶渣对育肥猪生长性能的影响

Table 2 Effects of herbal tea residue on growth performance of finishing pigs

项目 Items	对照组 Control group	凉茶渣组 Herbal tea residue group
初始体重 IBW /kg	91.79±1.65	92.68±1.46
终末体重 FBW /kg	112.94±1.72	114.15±1.43
平均日增重 ADG /(kg/d)	0.68±0.01	0.70±0.01
平均日采食量 ADFI/(kg/d)	2.70±0.04	2.68±0.05
料重比 F/G	3.94±0.06	3.89±0.07

同行数据肩标无字母或相同字母表示差异不显著($P>0.05$) ,不同字母表示差异显著($P<0.05$)。下表同。
In the same row , values with no letter or the same letter superscripts mean no significant difference ($P>0.05$) , while with different letter superscripts mean significant difference ($P<0.05$) . The same as below.

2.2 凉茶渣对育肥猪胴体性状的影响

由表 3 可见 ,与对照组相比 ,凉茶渣组育肥猪胴体重显著提高($P<0.05$) ,提高了 10.98%; 2 组间育肥猪屠宰率无显著差异($P>0.05$)。与对照组

相比 ,凉茶渣组育肥猪眼肌面积显著提高($P<0.05$) ,提高了 21.88%; 2 组间育肥猪背膘厚度无显著差异($P>0.05$)。

表 3 凉茶渣对育肥猪胴体性状的影响

Table 3 Effects of herbal tea residue on carcass traits of finishing pigs

项目 Items	对照组 Control group	凉茶渣组 Herbal tea residue group
胴体重 Carcass weight/kg	79.86±1.73 ^b	88.63±2.88 ^a
屠宰率 Slaughter rate/%	71.01±0.22	70.24±2.84
眼肌面积 Loin-eye area/cm ²	62.16±4.06 ^b	75.76±5.43 ^a
背膘厚度 Backfat thickness/mm	26.78±2.42	27.85±1.35

2.3 凉茶渣对育肥猪肉品质的影响

由表 4 可见 ,育肥猪背最长肌肉中干物质、粗蛋白质、粗脂肪和粗灰分含量在 2 个组间差异不显著($P>0.05$)。由表 5 可见 ,凉茶渣组育肥猪背最长肌肉色的亮度值、剪切力和滴水损失显著降低($P<0.05$) ,分别降低了 11.58%、26.83% 和 42.21%; 肉色的红度值和大理石纹评分显著提高($P<0.05$) ,分别提高了 16.88% 和 53.46%。
pH_{45 min}、pH_{24 h}、肉色黄度值、蒸煮损失在 2 个组间差异不显著($P>0.05$)。由表 6 可见 ,凉茶渣粉组育肥猪背最长肌中谷氨酸、丙氨酸、精氨酸、组氨酸、异亮氨酸、亮氨酸、脯氨酸、丝氨酸和天冬氨酸的含量显著提高($P<0.05$) ,分别提高了 4.88%、12.83%、0.91%、6.65%、8.50%、6.06%、14.23%、15.85% 和 3.02% ,其他的氨基酸在 2 个组间无显著差异($P>0.05$)。由表 7 可见 ,凉茶渣组育肥猪

背最长肌中月桂酸、肉豆蔻酸、十七酸和硬脂酸的含量显著降低($P<0.05$) ,分别降低了 26.67%、14.71%、21.43% 和 16.17%; 棕榈烯酸、油酸、花生四烯酸、亚麻酸、花生三烯酸和芥酸的含量显著提高($P<0.05$) ,分别提高了 24.34%、6.61%、43.14%、12.71%、58.33% 和 40.00%; 其他脂肪酸含量在 2 个组间无显著差异($P>0.05$)。由表 8 可见 ,凉茶渣粉组育肥猪背最长肌中肌苷酸的含量显著提高($P<0.05$) ,提高了 11.27%。

3 讨 论

3.1 凉茶渣对育肥猪生长性能的影响

目前 ,虽然在饲料中添加王老吉凉茶渣在家禽、牛、羊以及猪等领域尚还没有研究报道 ,但是茶渣的应用研究报道很多。凉茶渣属于茶渣的一种 ,同样都是含有较高的纤维和多种多样的功能

活性物质。最早的一项研究表明将 3% 的茶渣添加搭配猪的饲料可以显著提高猪的平均日增重,缩短出栏时间,降低饲料成本^[7]。而且茶渣作为猪的新型饲料还能够显著促进肌肉增加和加快生长速度,降低料重比,且对猪的生理功能无负面影响^[8]。杨红初等^[9]在每千克育肥猪饲料中添加 10~40 g 的茶渣茶末,均能够促进育肥猪的生长,而且可以显著提高育肥猪的平均日增重及饲料报酬,以添加 40 g 效果最佳。徐瑞等^[10]为了研究茶

渣对育肥猪的生长性能的影响,在育肥猪饲料中添加 2% 的茶渣,结果发现其可以显著提高育肥猪的平均日采食量,显著降低料重比。本研究结果与上述研究结果基本相符,凉茶渣组育肥猪的平均日增重有上升趋势,料重有下降趋势,但均未达到显著水平,可能是由于替代比例较高,降低了基础营养水平,但因含有有益活性物质,弥补了部分生长性能,所以与对照组增重等仍然相当。

表 4 凉茶渣对育肥猪肌肉营养物质含量的影响

Table 4 Effects of herbal tea residue on muscle nutrient contents of finishing pigs %

项目 Items	对照组 Control group	凉茶渣组 Herbal tea residue group
干物质 DM	23.94±0.57	25.60±0.61
粗蛋白质 CP	19.34±1.13	20.54±1.80
粗脂肪 CF	3.56±0.34	3.96±0.79
粗灰分 Ash	1.04±0.18	1.10±0.13

表 5 凉茶渣对育肥猪肉品质的影响

Table 5 Effects of herbal tea residue on meat quality of finishing pigs

项目 Items	对照组 Control group	凉茶渣组 Herbal tea residue group
pH _{45 min}	6.12±0.13	6.09±0.05
pH _{24 h}	5.55±0.03	5.54±0.04
肉色 Meat color		
亮度 L*	56.73±1.69 ^a	50.16±1.82 ^b
红度 a*	9.48±0.31 ^b	11.08±0.27 ^a
黄度 b*	6.24±0.25	5.54±0.38
剪切力 Shear force/kgf	6.82±0.58 ^a	4.99±0.18 ^b
滴水损失 Drip loss/%	4.88±0.44 ^a	2.82±0.27 ^b
蒸煮损失 Cooking loss/%	34.72±0.32	34.76±1.32
大理石纹评分 Marbling score	2.17±0.12 ^b	3.33±0.34 ^a

表 6 凉茶渣对育肥猪肌肉氨基酸组成的影响

Table 6 Effects of herbal tea residue on muscle amino acid composition of finishing pigs mg/kg

项目 Items	对照组 Control group	凉茶渣组 Herbal tea residue group
谷氨酸 Glu	307.83±3.03 ^b	322.84±3.83 ^a
甘氨酸 Gly	228.04±2.19	232.39±1.27
丙氨酸 Ala	274.12±2.44 ^b	309.29±3.57 ^a
精氨酸 Arg	7 055.71±11.05 ^b	7 119.63±8.96 ^a
组氨酸 His	154.14±1.92 ^b	164.39±3.48 ^a
苏氨酸 Thr	85.02±1.00	86.57±1.44

续表 6

项目 Items	对照组 Control group	凉茶渣组 Herbal tea residue group
缬氨酸 Val	104.22±1.58	104.72±1.82
蛋氨酸 Met	113.82±0.68	112.01±0.63
异亮氨酸 Ile	106.87±0.92 ^b	115.95±0.90 ^a
亮氨酸 Leu	151.98±2.21 ^b	161.19±1.97 ^a
苯丙氨酸 Phe	130.98±0.85	135.23±2.53
赖氨酸 Lys	151.86±1.67	147.39±2.85
脯氨酸 Pro	288.13±3.34 ^b	329.14±0.90 ^a
丝氨酸 Ser	125.71±2.24 ^b	145.63±1.81 ^a
酪氨酸 Tyr	135.52±1.66	140.37±1.37
天冬氨酸 Asp	304.34±3.17 ^b	313.52±0.84 ^a
半胱氨酸 Cys	No hit	No hit

No hit 表示半胱氨酸含量<21.80 mg/kg ,显示未检测出。
No hit indicated cystine content<21.80 mg/kg , indicating no detection.

表 7 凉茶渣对育肥猪肌肉脂肪酸组成的影响
Table 7 Effects of herbal tea residue on muscle fatty acid composition of finishing pigs %

项目 Items	对照组 Control group	凉茶渣组 Herbal tea residue group
葵酸 C10:0	0.12±0.01	0.11±0.01
月桂酸 C12:0	0.15±0.01 ^a	0.11±0.01 ^b
肉豆蔻酸 C14:0	1.36±0.07 ^a	1.16±0.03 ^b
棕榈酸 C16:0	25.21±0.22	24.58±0.31
十七酸 C17:0	0.14±0.01 ^a	0.11±0.01 ^b
硬脂酸 C18:0	14.29±0.22 ^a	11.98±0.43 ^b
花生酸 C20:0	0.18±0.01	0.19±0.01
山嵛酸 C22:0	0.52±0.02	0.53±0.02
棕榈烯酸 C16:1	2.26±0.04 ^b	2.81±0.05 ^a
十七烯酸 C17:1	0.16±0.01	0.15±0.01
油酸 C18:1n9c	42.05±0.35 ^b	44.83±0.29 ^a
亚油酸 C18:2n6c	11.22±0.39	11.16±0.24
花生四烯酸 C20:4n6	0.51±0.02 ^b	0.73±0.06 ^a
亚麻酸 C18:3n3	1.18±0.02 ^b	1.33±0.03 ^a
花生三烯酸 C20:3n3	0.12±0.00 ^b	0.19±0.02 ^a
芥酸 C22:1n9	0.10±0.00 ^b	0.14±0.01 ^a

表 8 凉茶渣对育肥猪肌肉肌苷酸和吲哚含量的影响
Table 8 Effects of herbal tea residue on contents of inosinic acid and indole in muscle of finishing pigs

项目 Items	对照组 Control group	凉茶渣组 Herbal tea residue group
肌苷酸 IMP/(mg/kg)	1 018.80±20.95 ^b	1 133.58±39.02 ^a
吲哚 Indole/(μg/kg)	No hit	No hit

No hit 表示吲哚含量<100 μg/kg ,显示未检测出。
No hit indicated indole content<100 μg/kg , indicating no detection.

3.2 凉茶渣对育肥猪胴体性状的影响

屠宰率、瘦肉率、眼肌面积、背膘厚度是评价猪胴体性状的重要指标。有研究表明,在育肥猪饲料中添加 1% 茶叶渣,发现育肥猪的增重、胴体含瘦肉率显著提高,而背膘厚则显著降低^[11]。陈伟等^[12]在 30 kg 左右的健康仔猪饲料中添加 2% 茶末饲喂至出栏,结果发现出栏猪的瘦肉率、后腿比例和眼肌面积都显著提高。马帮军^[13]在育肥猪饲料中添加 1%~3% 茶粉后发现育肥猪的背膘厚度显著降低。本研究结果与前人的研究结果基本一致,凉茶渣组育肥猪的胴体重和眼肌面积显著提高,分别提高了 10.98% 和 21.88%,这可能是因为茶渣中的甘草具有盐皮质激素样作用,可促进生长激素的分泌,从而促进肌肉的生长,提高育肥猪胴体重和眼肌面积^[14]。

3.3 凉茶渣对育肥猪肉品质的影响

影响猪肉品质的因素很多,随着人们生活水平的提高,消费者对猪肉品质的要求也越来越高。短期来看,可以通过调整饲养营养水平或使用新型饲料来改善猪肉品质。一般猪肉品质的评定指标有猪肉 pH、肉色、嫩度、滴水损失、大理石纹评分和蒸煮损失,此外还有常规营养物质以及风味物质氨基酸、脂肪酸、肌苷酸和吲哚含量等。其中,肌肉 pH 会直接影响肌肉的嫩度、肉色、大理石纹评分、滴水损失以及蒸煮损失^[15]。研究表明,屠宰后 45 min 的 pH<5.9 时,可以评定为 PSE 肉;屠宰后 24 h 的 pH>6.5 时,可评判为 DFD 肉^[16]。而本试验的 pH 不管是 45 min 还是 24 h 均在正常范围内,并且对照组和试验组没有显著差异。肉色评定指标包括亮度、红度和黄度值,其中红度是影响肌肉颜色的主要因素,红度越高,肌肉品质质量越佳,而亮度和黄度是衡量肉色的辅助性指标,亮度和黄度越低则肉品质越差^[17]。有研究表明在育肥猪饲料中根据猪的体重添加 1.0 和 2.0 g/kg 茶粉,结果发现试验组猪肉的黄度值显著低于对照组,红度值显著高于对照组^[18]。在本试验中,与对照组相比,凉茶渣组肉色的红度值显著提高,肉色的亮度值显著降低,黄度值也有所降低,但未达到显著水平。这说明了凉茶渣是可以改善猪肉的肉色,提高肉品质,这与前人的研究结果一致。有关凉茶渣对肉品质的影响目前尚未见报道,但这可能是由于茶渣中的有效成分增强了肌肉中肌红蛋白的表达和机体的抗氧化能力,从而有效防止肌红蛋白或氧合肌红蛋白氧化成正铁肌红蛋白,进

而改善肉色。肌肉嫩度是食肉口感的重要指标之一,又称剪切力。有试验表明,肌肉的嫩度直接影响人们的口感,嫩度越高则口感越好,而滴水损失、蒸煮损失、大理石纹评分及剪切力直接影响嫩度的高低,进而影响口感^[19]。蔡海莹等^[20]研究表明,在育肥猪饲料中添加 2% 的茶渣,结果发现肉色和大理石纹评分均显著高于对照组,且剪切力和滴水损失显著低于对照组,说明在育肥猪的饲料中添加 2% 的茶渣可提高育肥猪猪肉的色泽、嫩度和保水性能。而且有研究表明,每千克饲料添加 400 mg 茶多酚可以显著提高猪肉品质,并且在猪肉货架期可以增强猪肉抗氧化、稳定猪肉色和系水力的作用^[21]。本试验中,凉茶渣组育肥猪肌肉剪切力和滴水损失显著降低,分别降低了 26.83% 和 42.21%,并且大理石纹评分显著提高,与前人的研究结果一致,表明凉茶渣可以提高嫩度和保水能力,进而改善肉品质。分析可能与凉茶渣中所包含的 7 种中草药中的活性成分有关,如金银花的主要成分黄酮、绿原酸。肌肉中的常规营养物质包括水分、干物质、粗蛋白质、粗脂肪、粗灰分等。在本试验中,饲料添加 4% 凉茶渣粉对育肥猪肌肉中干物质、粗蛋白质、粗脂肪和粗灰分含量无显著影响。

控制猪肉风味的因素有很多,典型的有氨基酸、脂肪酸、肌苷酸以及吲哚的含量。有研究表明在体重为 30 kg 左右的健康仔猪饲料中添加 2% 的茶叶粉末,结果发现 16 种常见氨基酸和必需氨基酸含量均高于对照组,而且鲜味氨基酸和芳香族氨基酸也均高于对照组^[22]。在本试验中,饲料添加 4% 凉茶渣粉显著提高了育肥猪背最长肌中谷氨酸、丙氨酸、精氨酸、组氨酸、异亮氨酸、亮氨酸、脯氨酸、丝氨酸和天冬氨酸的含量,分别提高了 4.88%、12.83%、0.91%、6.65%、8.50%、6.06%、14.23%、15.85% 和 3.02%,与前人的研究结果一致。有研究表明,在体重为 28 kg 左右的三元杂猪饲料中添加 400 mg/kg 茶多酚能在一定程度上改变猪肌肉中脂肪酸组成,而且指出这可能与茶多酚可以阻止不饱和脂肪酸氧化有关,但试验没有显示与其添加水平的高低有关^[23]。而在本试验中,凉茶渣组较对照组相比,育肥猪背最长肌中的月桂酸、肉豆蔻酸、十七酸和硬脂酸的含量显著降低,分别降低了 26.67%、14.71%、21.43% 和 16.17%;棕榈烯酸、油酸、花生四烯酸、亚麻酸、花生三烯酸和芥酸的含量显著提高,分别提高了 24.

34%、6.61%、43.14%、12.71%、58.33%和 40.00% , 与前人的研究结果不一致,可能的原因是本研究中的凉茶渣所含的活性物质种类较多,如凉粉草富含酚酸类活性物质、夏枯草含有三萜和黄酮类、菊花富含多糖等,相对于单一的茶多酚来说,凉茶渣的功能更强,因此阻止不饱和脂肪酸氧化的能力更强。

次黄嘌呤核苷酸又称为鲜味素和肌苷酸,是决定口感的重要因素,有研究表明在猪饲料中添加茶渣能显著提高猪肉中肌苷酸的含量,增加鲜味^[24];另外在肉仔鸡饲料中添加 1% 茶渣、茶末,结果发现肉鸡的肉质显著变嫩,肉色显著提高,而且维生素 A 和维生素 E 含量均显著增加^[25]。在本试验中,饲料添加 4% 凉茶渣粉显著提高了育肥猪背最长肌中肌苷酸的含量,提高了 11.27% ,与前人的研究结果基本一致。这表明凉茶渣可以提高猪肉中鲜味物质的含量,改善肉品质。有研究表明,用添加茶渣、茶末的饲料饲喂育肥猪,可显著降低腥味物质吡啶的含量,进而改善猪肉胴体的腥味^[26]。而在本试验中,育肥猪肌肉吡啶含量在试验组和对照组中均没有达到检测标品的最低值,无具体数值。

4 结 论

① 饲料添加凉茶渣粉对育肥猪生长性能无负面影响。

② 饲料添加凉茶渣粉可以提高育肥猪胴体重和眼肌面积,进而改善胴体性状。

③ 饲料添加凉茶渣粉可以降低育肥猪肉色的亮度值、剪切力和滴水损失,提高肉色的红度值和大理石纹评分,进而改善猪肉品质。

④ 饲料添加凉茶渣粉可以提高育肥猪肌肉中谷氨酸、丙氨酸、精氨酸、组氨酸、异亮氨酸、亮氨酸、脯氨酸、丝氨酸和天冬氨酸以及棕榈烯酸、油酸、花生四烯酸、亚麻酸、花生三烯酸、芥酸和肌苷酸的含量,降低月桂酸、肉豆蔻酸、十七酸和硬脂酸的含量,进而改善猪肉的风味。

参考文献:

- [1] 聂琳,彭杰,常军,等.木本饲料的研究进展[J].中国农学通报,2012,28(17):1-4.
- [2] 贺颖颖,罗燕玉,林朝展,等.王老吉凉茶化学成分研究[J].中药材,2018,41(4):889-893.
- [3] 张伟力.猪肉质测定的采样与前处理[J].养猪,2002(1):30-31.

- [4] 张伟力.猪肉肉色与酸度测定方法[J].养猪,2002(2):33-34.
- [5] 张伟力.猪肉系水力测定方法[J].养猪,2002(3):25-26.
- [6] 张伟力.猪肉质地与风味测定[J].养猪,2002(4):33-35.
- [7] 孙克年.茶叶在养殖业中的应用[J].江西饲料,1999(6):28-29.
- [8] 王彤,刘显军.茶多酚对猪肉品质影响的研究综述[J].现代畜牧兽医,2013(6):21-22.
- [9] 杨红初,石新林.茶叶末对肥育猪生产性能和肉质的影响[J].养猪,2010(3):9-10.
- [10] 徐瑞,王改琴,郭本成,等.茶叶渣对育肥猪生产性能及猪肉品质的影响[J].黑龙江畜牧兽医,2017(10):73-75.
- [11] 孙克年.茶叶在提升畜禽产品品质生产中的应用[J].中国饲料添加剂,2016(5):5-8.
- [12] 陈伟,燕志宏,陶林,等.饲料中添加茶末对育肥猪胴体性状的影响[J].黑龙江畜牧兽医,2014(24):28-29.
- [13] 马帮军.含茶饲料对猪胴体品质的影响[D].硕士学位论文.合肥:安徽农业大学,2015.
- [14] 高雪丽,王亚静,陈复生.甘草功能特性研究进展[J].粮食与油脂,2016,29(10):1-4.
- [15] TU F L, LIAO C M, LIN K J. Effects of supplemental Chinese traditional herbal medicine complex on the growth performance, carcass characteristics, and meat quality of male Holstein calves [J]. Journal of Applied Animal Research, 2014, 42(2): 222-227.
- [16] 何叶如.几种绿色饲料添加剂对生长肥育猪的生产性能、消化机能和猪肉品质的研究[D].硕士学位论文.兰州:甘肃农业大学,2003.
- [17] 孙建广.发酵乳酸杆菌对生长肥育猪生长性能和肉品质的影响[D].硕士学位论文.长沙:湖南农业大学,2009.
- [18] 冯尚连,姜红进,朱建津,等.日粮添加超微粉碎茶粉对育肥猪生长性能及肉品质的影响[J].饲料研究,2013(12):54-56.
- [19] 陈润生.猪生产学[M].北京:中国农业出版社,1995.
- [20] 蔡海莹,朱建和,张晓,等.日粮中添加茶多酚对肥育猪肉品质的影响[J].中国畜牧杂志,2007,43(9):27-30.
- [21] 王玉龙,费兆生.茶叶提取物对肉猪生产性能、肌肉品质及肌肉抗氧化指标的影响[J].畜牧与兽医,2014,46(12):50-52.
- [22] 陈伟,刘忠伟,燕志宏,等.饲料中添加茶叶粉末对育肥猪肉肉质性状的影响[J].江苏农业科学,2014,42(8):190-192.
- [23] 蔡海莹.茶多酚和维生素 E 对肥育猪生产性能及其肉品质的影响[D].硕士学位论文.合肥:安徽农业大学,2006.

- [24] 佐野满昭, 孙希琪. 茶添加到家畜饲料中的利用效果 [J]. 农业新技术新方法译丛, 1996(2): 32-33.
- [25] SARKER M S K, YIM K J, KO S Y, et al. Green tea level on growth performance and meat quality in finishing pigs [J]. Pakistan Journal of Nutrition, 2010, 9 (1): 10-14.
- [26] 曾光辉, 汪海峰. 茶多酚的生理功能及其在畜牧生产中的应用研究进展 [J]. 浙江畜牧兽医, 2010, 35 (3): 12-13.

Effects of Herbal Tea Residue on Growth Performance, Carcass Traits and Meat Quality of Finishing Pigs

XIE Yueqin SUN Xiaohong WANG Dongyang CHEN Guoping LUO Junyi CHEN Ting
XI Qianyun ZHANG Yongliang* SUN Jiajie*

(National Pig Breeding Engineering Technology Center, Key Laboratory of Animal Nutrition Control in Guangdong, College of Animal Science, South China Agricultural University, Guangzhou 510642, China)

Abstract: This experiment was conducted to study the effects of herbal tea residue on growth performance, carcass traits and meat quality of finishing pigs. A total of 78 cross-bred (Duroc×Landrace×Yorkshire) finishing pigs with a similar initial weight of 90 kg were selected and randomly allotted into 2 groups with 3 replicates per group and 13 pigs per replicate. Pigs in the control group were fed a basal diet, and the others in the experimental group were fed the basal diet supplemented with 4% herbal tea residue powder. The pre-experimental period lasted for 7 days, and the experimental period lasted for 31 days. The results showed as follows: 1) compared with the control group, dietary 4% herbal tea residue powder had no significant effects on the final body weight, average daily gain, average daily feed intake and feed-to-gain ratio of finishing pigs ($P>0.05$). 2) Compared with the control group, the carcass weight and loin-eye area of finishing pigs in the experimental group were increased 10.98% and 21.88%, respectively ($P<0.05$). 3) Compared with the control group, the brightness value of flesh color, shear force and drip loss in muscle of finishing pigs in the experimental group were decreased by 11.58%, 26.83% and 42.21% ($P<0.05$), respectively, and the redness value of flesh color and marbling score were increased by 16.88% and 53.46% ($P<0.05$), respectively. 4) There were no significant differences in contents of dry matter, crude protein, crude fat and ash in muscle of finishing pigs between the two groups ($P>0.05$). 5) Compared with the control group, the contents of glutamic acid, alanine, arginine, histidine, isoleucine, leucine, proline, serine and aspartic acid in muscle of finishing pigs in the experimental group were increased by 4.88%, 12.83%, 0.91%, 6.65%, 8.50%, 6.06%, 14.23%, 15.85% and 3.02% ($P<0.05$), respectively; contents of saturated fatty acids such as lauric acid, myristic acid, heptadecanoic acid and stearic acid were decreased by 26.67%, 14.71%, 21.43% and 16.17% ($P<0.05$), respectively; contents of unsaturated fatty acids such as palmitoleic acid, oleic acid, arachidonic acid, linolenic acid, eicosatrienoic acid and erucic acid were increased by 24.34%, 6.61%, 43.14%, 12.71%, 58.33% and 40.00% ($P<0.05$), respectively; and the inosinic acid content was increased significantly by 11.27% ($P<0.05$). In conclusion, dietary 4% herbal tea residue can not only increase the carcass traits, but also improve the meat quality, and has no negative effects of finishing pigs. [Chinese Journal of Animal Nutrition, 2019, 31(11)]

Key words: herbal tea residue; solid waste pollution; finishing pigs; growth performance; meat quality

* Corresponding authors: ZHANG Yongliang, professor, E-mail: zhangyl@scau.edu.cn; SUN Jiajie, associate professor, E-mail: jiajiesun@scau.edu.cn

Dietary supplementation with *Moringa oleifera* and mulberry leaf affects pork quality from finishing pigs

Zujing Chen | Yueqin Xie | Junyi Luo | Ting Chen | Qianyun Xi | Yongliang Zhang | Jiajie Sun 

College of Animal Science, Guangdong Engineering & Research Center for Woody Fodder Plants, Guangdong Provincial Key Laboratory of Animal Nutrition Control, National Engineering Research Center for Breeding Swine Industry, Guangdong Laboratory for Lingnan Modern Agriculture, South China Agricultural University, Guangzhou, China

Correspondence

Yongliang Zhang and Jiajie Sun, College of Animal Science, Guangdong Engineering & Research Center for Woody Fodder Plants, Guangdong Provincial Key Laboratory of Animal Nutrition Control, National Engineering Research Center for Breeding Swine Industry, Guangdong Laboratory for Lingnan Modern Agriculture, South China Agricultural University, Guangzhou, China. Emails: zhangyl@scau.edu.cn; jiajiesun@scau.edu.cn

Funding information

The National Key Research and Development Program of China, Grant/Award Number: 2016YFD0500503; Technical System of Modern Agricultural Industry in Guangdong Province, Grant/Award Number: 2018LM1121 and 2018LM2158; Science and Technology Innovation Strategy Projects of Guangdong Province, Grant/Award Number: 2018B020203002

Abstract

Moringa oleifera and *Morus alba* leaves are nutritious non-traditional feed ingredients containing bioactive substances. This study was to evaluate the potential application of dietary *Moringa* and *Morus* leaf powder on the growth traits, carcass characteristics and meat quality of finishing pigs. *Moringa* did not alter growth performance or carcass characteristics, but it decreased meat b^* value, increased *MyHCIIa* and decreased *MyHCIIx* mRNA levels, and increased CP and concentrations of Ala, Thr, Ile, Lys and Pro in longissimus thoracis. *Morus* increased final BW, ADFI and ADG, decreased F/G ratio, improved slaughter weight, carcass weight, carcass yield and meat a^* value, and decreased shear force, drip loss, *MyHCIIx* and *MyHCIIb* mRNA levels, and increased *MyHCI* and *MyHCIIa* mRNA levels. *Morus* also increased CP, Glu, Gly, Ala, Arg, Ile, Phe, Pro, Ser, Tyr and Asp, and C16:1, C18:1n9c, C20:4n6, C18:3n3, C20:3n3, C22:1n9 and n-3 PUFA, but decreased C12:0 and C16:0. In summary, *Morus* improved the parameters and held great potential as an unconventional feed crop.

KEYWORDS

finishing pigs, meat quality, *Moringa oleifera*, mulberry, myofibres

1 | INTRODUCTION

With improvements in pig rearing technology, modern pig production has successfully met the growing requirement for cheap meat products. But, with the increase in lean meat percentage and carcass yield, problems such as reduced flavour and poor taste of pork have gradually emerged. Thus, it is really critical to study how to improve pork quality. Recent studies show that

the quality of pork can be improved by adding dietary supplements. For instance, dietary supplementation with natural or fermented herb combinations can reduce the back fat thickness of pigs and improve the quality of pig meat (Ahmed, Mun, Islam, Ko, & Yang, 2016), and other dietary additives such as ramie powder, linseed and plant extracts can have a positive effect (Li et al., 2018; Okrouhlá, Stupka, Čítek, Šprysl, & Brzobohatý, 2013; Rossi et al., 2013).

Zujing Chen and Yueqin Xie contributed equally to this work.

Moringa oleifera is a shrub that has been mainly grown in tropical and subtropical regions. *Moringa oleifera* leaves (MOL) have been regarded as an unconventional feed because of its unique nutritional characteristics, which have aroused the attention of researchers (Meesse, Getye, Berihun, & Banerjee, 2013; Nkukwana et al., 2014). MOL contains vitamins and minerals that are also present at levels above those in most conventional feed ingredients (Tesfaye, Animut, Urge, & Dessie, 2013). MOL also contains 84.60 g/kg polyunsaturated fatty acids (PUFAs) (Saini, Shetty, & Giridhar, 2014). In recent years, large-scale cultivation of this plant species has been initiated, and uses for the protein-rich product are being sought.

Mulberry (*Morus alba* L.) has also been mainly grown in subtropical regions. Currently, mulberry leaves have attracted the attention of researchers because it contains many kinds of bioactive substances including 1-deoxynojirimycin (Kimura et al., 2007) and flavonoids (Chen & Li, 2007), which enhanced antioxidant capacity (Arabshahi-Delouee & Urooj, 2007) and improved lipid and glucose metabolism (Sun, Yamasaki, Katsube, & Shiwaku, 2015). Currently, mulberry leaves are mostly found on the market in the form of nutritional supplements (Toyinbo et al., 2012). But the information about the effects of mulberry leaves on pork quality was really rare.

Recently, Klont and Brocks (1998) reported that meat quality was mainly associated with the traits of muscle fibres. The types of muscle fibre include slow-oxidative type I, fast oxido-glycolytic type IIa and fast glycolytic types IIx and IIb, which are more closely associated with the pH, colour and tenderness of pork (Lefaucheur, Ecolan, Plantard, & Gueguen, 2002). Interest in *M. oleifera* and mulberry as diet components for animal production is increasing, but most previous studies have focused mainly attention to the growth trait. The effects on pork quality, nutrient composition and muscle fibre characteristics have been neglected. This research was designed to evaluate the influence of dietary MOL powder (MOLP) and mulberry leaf powder (MLP) supplementation on the growth traits, carcass characteristics, meat quality, fatty acid (FA) element, the content of amino acid and inosine monophosphate (IMP), and muscle fibre characteristics of finishing pigs. We therefore hypothesized that dietary MOLP and MLP inclusion may be beneficial to meat quality traits of animals, and the evaluation and application were carried out subsequently in finishing pigs.

2 | MATERIALS AND METHODS

2.1 | Preparation of MOLP and MLP

Moringa oleifera leaves powder was obtained from Yangjiang Magic Plus Biotechnology Co., Ltd., and MLP was provided by Henan Sangyuan Agricultural Technology Co., Ltd. Mulberry and *M. oleifera* were harvested after 90 days of growth. The harvested Mulberry and *M. oleifera* were dried, smashed, sieved and packaged. Nutritive value was provided by the above two companies and summarized in File S1.

2.2 | Animals and diets

117 crossbred barrows (Duroc × Landrace × Yorkshire) (balanced for initial body weight, BW: 93.30 ± 1.60 kg) were randomly divided into three treatment groups (three replicates in each group, 13 pigs per replicate): control group (fed a basic diet); 4% MLP group (4% MLP replaced wheat bran); and 4% MOLP group (4% MOLP replaced wheat bran). Diets meet the nutritional requirements for pigs according to the Ministry of Agriculture of the People's Republic of China (2004). The nutrient component of three treated diets was displayed in File S2. The FA and amino acid compositions of the diets were presented in File S3 and S4 respectively. The feeding experiment lasted for 7-day adaptation period and a 31-day experimental period. The weight of the pig at the starting and end of experiments and the depletion of feed was determined weekly throughout the experiment.

2.3 | Carcass traits

On the last experimental day, feed was withheld for 12 hr, and six randomly selected pigs (two pigs per replicate) in each treatment were transported over a distance of approximately 13 km (20 min) from farm to abattoir. Then, a total of 18 pigs in three different treated groups were slaughtered, scalded, dehaired and eviscerated after a 10-hr rest period in the lairage where they had free access to water by the method of Zhu et al. (2019). Within 45 min after evisceration in chilling conditions of 12–15°C, the carcasses were weighed for calculation of the dressing percentage. The average back fat thickness was determined opposite the last lumbar vertebra and the first and last rib, and the loin eye area was determined in the last rib. Then, muscle samples were sampled from longissimus thoracis (LT) muscle and stored for further pork quality analysis.

2.4 | Meat quality measurements and muscle chemical analysis

The pH, meat colour involving lightness, redness and yellowness, cooking loss and shearing force of LT were determined under the way of Stein et al. (2006) and Rossi et al. (2013). In details, meat colour was assessed with a CR-300 Chroma Meter (Minolta Camera Co., Ltd.), and the instrument was calibrated using the white calibration plate (Calibration Plate CR-A43; Minolta Cameras). The colorimeter had an 8-mm measuring area and was illuminated with a pulsed Xenon arc lamp (Illuminati C). The subjective marbling score of the LT was determined on the 10th-rib using the guidelines of the National Pork Producers Council (NPPC, 1991). The pH was measured using a pH star (Model 5000; SFK Technology) equipped with a puncture-type combination pH electrode (LoT406-M6-DXK-S7/25; Mettler-Toledo, GmbH). The pH probe was calibrated using two buffers (pH 4.6 and 7.0), and calibration was monitored between

samples. Shearing force was tested with a crosshead speed of 200 mm/min and a 5-kN load cell calibrated to read over a range of 0–100 N, and six replicates of each sample were measured to calculate the average value. Then, LT samples were analysed for nutrients including dry matter (DM), crude protein (CP) and ash according to AOAC methods (AOAC, 1990). The IMP and FA content were measured under the way of Li et al. (2014). Briefly, approximately 5 g of muscle tissues was pulverized in liquid nitrogen and homogenized with chloroform: methanol (2:1, vol/vol) to extract the lipids, as well as fodder samples. The FAs were then methylated to methyl esters using BF₃ in methanol and analysed by gas chromatography coupled with flame ionization detection (GC-FID; Shimadzu GC-2010 Plus, Shimadzu Corp.) using a 100% cyanopropyl polysiloxane capillary column (SP 2560; 100 m, 0.25 mm i.d., and 0.20-μm film thickness; Supelco Inc.). Results of FA content were presented as the percentage of total FAs detected. And amino acids were measured using automatic amino acid analyser (Hitachi Ltd.) based on the method of Yan et al. (2018).

2.5 | RNA extraction and RT-PCR

Total RNA from LT samples was extracted using Trizol reagent based on the instructions of manufacturers and monitored the concentration of RNA using the NanoDrop 2000. Then, mRNA was converted to cDNA using a TaKaRa kit (TaKaRa Co., Ltd.). Quantitative real-time PCR was performed in a 96-well optical plate at 95°C for 10 min followed by 40 cycles at 95°C for 15 s, 60°C for 60 s and 72°C for 30 s. The primers of RT-PCR are displayed in File S5, and GAPDH was used as a control. The primers were designed using Premier 5.0 (Premier Biosoft). The relative expression of gene was calculated under the way of Livak and Schmittgen (2001).

2.6 | Statistical analyses

All data were displayed as the mean ± SE and analysed using Statistical Product and Service Solutions (SPSS) version 18.0.

One-way ANOVA with Tukey's multiple comparison procedure was performed to evaluate the significance of the main effects ($p < .05$). Data regarded to growth performance, carcass traits and meat quality of finishing pigs were analysed using a mixed model. In this model, each replicate was included as random effects, as well as different treatments (Control group, 4% MOLP group, and 4% MLP group were included as fixed effects).

3 | RESULTS

3.1 | Growth performance

Feed intake and growth performance results are displayed in Table 1. Supplementation with 4% MOLP had no effect on final BW, ADFI, ADG or F/G values in experimental periods ($p > .05$), whereas 4% MLP not only increased final BW ($p < .05$), ADFI ($p < .01$) and ADG ($p < .01$), but lowered the F/G ratio ($p < .05$). Initial BW was not significantly different among the three groups ($p = .60$).

3.2 | Carcass traits

Table 2 shows the effect of dietary supplementation with 4% MOL or MLP on carcass traits of finishing pigs. MOLP had not affected slaughter weight, carcass weight, carcass yield, loin eye area or average back fat depth ($p > .05$). By contrast, 4% MLP significantly increased slaughter weight ($p < .05$), carcass weight ($p < .01$) and carcass yield ($p < .05$), but MLP had no significant influence on loin eye area or average back fat depth ($p > .05$).

3.3 | Meat quality

Although neither 4% MOLP nor 4% MLP altered the pH at 45 min, 4% MOLP significantly decreased pH at 24 hr ($p < .01$). The b* value of meat decreased ($p < .05$) when 4% MOLP was included in the diet, but no difference was observed for L* value, a* value, shearing force,

TABLE 1 Effects of MOLP and MLP on growth performance of finishing pigs

Items	Control	4% MOLP	4% MLP	p-value
Initial BW (kg)	91.79 ± 1.65	93.44 ± 1.35	93.80 ± 1.51	.60
Final BW (kg)	112.94 ± 1.72 ^b	113.80 ± 1.36 ^{ab}	118.12 ± 1.65 ^a	.05
ADFI (kg)	2.69 ± 0.04 ^b	2.76 ± 0.01 ^b	2.87 ± 0.01 ^a	<.01
ADG (kg)	0.68 ± 0.01 ^b	0.66 ± 0.02 ^b	0.76 ± 0.02 ^a	<.01
F/G	3.94 ± 0.06 ^{ab}	4.12 ± 0.11 ^a	3.75 ± 0.09 ^b	.02

Note: Values are means ± SE ($n = 39$). In the same row, values with no letter or the same letter superscripts represent no significant difference ($p > .05$), while different small letter superscripts represent significant differences ($p < .05$). The same applies below.

Abbreviations: ADFI, average daily feed intake; ADG, average daily gain; BW, body weight; F/G, ratio of feed intake to gain; MLP, mulberry leaf powder; MOLP, *Moringa oleifera* leaves powder.

^{a, b} Values that differ significantly at $P < .05$.

Items	Control	4% MOLP	4% MLP	p-value
Carcass weight (kg)	79.86 ± 1.73 ^b	81.47 ± 0.67 ^b	87.76 ± 0.92 ^a	<.01
Carcass yield (%)	71.01 ± 0.22 ^b	70.05 ± 0.65 ^b	73.82 ± 1.23 ^a	.02
Loin eye area (cm ²)	62.16 ± 4.06	64.11 ± 2.60	65.63 ± 2.37	.73
Average back fat depth (cm)	26.78 ± 2.42	27.75 ± 0.94	26.86 ± 2.68	.94

Note: Values are means ± SE (n = 6).

Abbreviations: MLP, mulberry leaf powder; MOLP, *Moringa oleifera* leaves powder.

^{a,b} Values that differ significantly at *P* < .05.

TABLE 2 Effects of MOLP and MLP on carcass traits of finishing pigs

Items	Control	4% MOLP	4% MLP	p-value
pH _{45 min}	6.12 ± 0.13	6.13 ± 0.05	6.08 ± 0.07	.93
pH _{24 hr}	5.55 ± 0.03 ^a	5.38 ± 0.02 ^b	5.56 ± 0.04 ^a	<.01
L* (lightness)	56.73 ± 1.69	51.33 ± 3.02	50.96 ± 1.12	.12
a* (redness)	9.48 ± 0.31 ^b	9.86 ± 0.66 ^{ab}	11.09 ± 0.33 ^a	.05
b* (yellowness)	6.24 ± 0.25 ^a	5.14 ± 0.35 ^b	6.08 ± 0.24 ^a	.03
Shear force (N)	62.81 ± 15.05 ^a	60.39 ± 19.53 ^a	46.72 ± 11.22 ^b	<.01
Drip loss (%)	4.88 ± 0.44 ^a	4.40 ± 0.34 ^a	2.82 ± 0.27 ^b	<.01
Cooking loss (%)	34.72 ± 0.32	34.26 ± 0.47	35.40 ± 0.50	.20
Marbling score	2.17 ± 0.12	2.50 ± 0.22	2.67 ± 0.33	.38

Note: Values are means ± SE (n = 6), while the values of shear force from six biological replicates with each measurement repeated three times.

Abbreviations: MLP, mulberry leaf powder; MOLP, *Moringa oleifera* leaves powder.

^{a,b} Values that differ significantly at *P* < .05.

TABLE 3 Effects of MOLP and MLP on meat quality of finishing pigs

dripping loss, cooking loss or marbling score (*p* > .05). L*, b*, marbling score and cooking loss were not altered by the addition of 4% MLP to the diet, but the a* value of meat was decreased (*p* < .05), as well as shear force and drip loss (*p* < .01; Table 3).

3.4 | MyHC expression levels

As shown in Figure 1, 4% MOLP did not affect the levels of MyHCIIb or MyHCIIb mRNAs (*p* > .05), but it obviously increased (*p* < .05) MyHCIIa and decreased (*p* < .05) MyHCIIx levels in LT. Meanwhile, 4% MLP did significantly up-regulate (*p* < .05) the levels of MyHCIIa and MyHCIIa, and it down-regulated (*p* < .05) MyHCIIx and MyHCIIb levels. Furthermore, 4% MLP induced higher mRNA expression levels for MyHCIIa, MyHCIIa and MyHCIIx than 4% MOLP (*p* < .05), but MyHCIIb mRNA expression levels were not significantly different between 4% MOLP or MLP groups (*p* > .05).

3.5 | Muscle chemical composition

Supplementation of 4% MOLP or MLP did not affect DM, IMF and IMP content in LT samples from finishing pigs (*p* > .05). While CP content was significantly decreased (*p* < .01) in 4% MLP groups,

there were no significant differences between Control and 4% MOLP groups (Table 4).

The content of amino acid of LT muscle is shown in File S6. Supplementation with 4% MLP significantly increased (*p* < .05) the level of Ala, Thr, Ile, Lys and Pro, but there were no obviously changes (*p* > .05) in the profiles of other amino acids in response to 4% MOLP supplementation in the diet. Furthermore, 4% MLP markedly increased (*p* < .05) the concentration of Glu, Gly, Ala, Arg, Ile, Phe, Pro, Ser, Tyr and Asp, but not affected the content of other amino acids (*p* > .05). Additionally, 4% MLP increased of Glu, Gly, Arg, Phe, Pro, Ser, Tyr and Asp levels to a greater extent than 4% MOLP.

Supplementation with 4% MOLP had no significant effect on most FAs but it did reduce the concentration of C17:1 (*p* < .01) and C20:4n6 (*p* < .01). However, 4% MLP obviously affected the FA composition of pork. In details, the concentrations of C16:1, C18:1n9c, C20:4n6, C18:3n3, C20:3n3, C22:1n9 and n-3 PUFA were increased (*p* < .05) in meat from pigs fed with 4% MLP diet, while concentrations of C12:0 and C16:0 were decreased (*p* < .05). Consequently, the level of total unsaturated fatty acids (TUFAs) was higher (*p* < .01) in meat from pigs fed the 4% MLP diet than pigs fed the control or 4% MOLP diets. By contrast, 4% MLP were reduced (*p* < .01) the level of total saturated fatty acids (TSFAs). In addition, the ratio of n-6/n-3 was markedly decreased (*p* < .01) when 4% MLP was added to the diet (File S7).

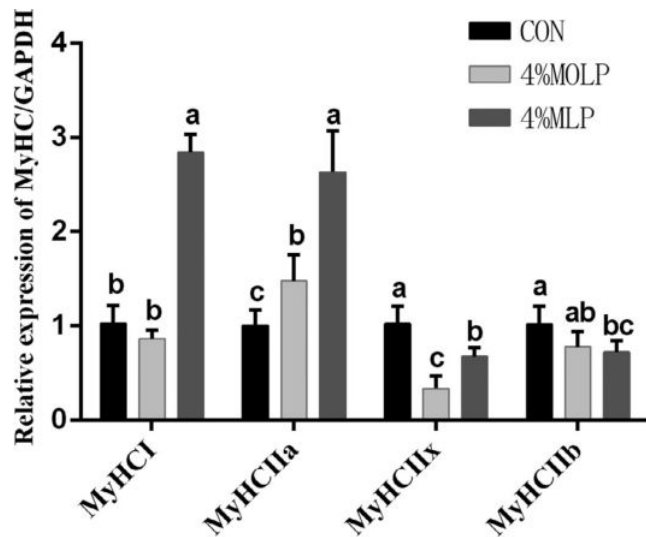


FIGURE 1 Effect of dietary supplementation with 4% *Moringa oleifera* leaves powder (MOLP) or mulberry leaf powder (MLP) on longissimus dorsi myosin heavy chain (MyHC) isoform mRNA levels in finishing pigs. Expression levels of MyHCI, MyHCIIa, MyHCIIx and MyHCIIb mRNAs were normalized against GAPDH as an internal control. Results are means \pm SEM ($n = 6$). ^{a-c}Values with different letters indicate significant differences among all treatments ($p < .05$)

4 | DISCUSSION

4.1 | Growth traits

In this study, 4% MOLP supplementation had not affected ($p > .05$) the final BW, ADFI, ADG or F/G values, consistent with the finding of Serem et al. (2017). However, Mukumbo et al. (2015) reported that diet supplemented with MOLP can increase feed intake of finishing pigs. Differences in the response to MOLP supplementation between studies might be associated with differentiation in the amount of leaf components in extracts. Therefore, more studies are needed to establish the most appropriate amount of MOLP in finishing pig diet. By contrast, 4% MLP not only increased ($p < .05$) final BW, ADFI and ADG values, but also yielded a higher ($p < .05$) F/G ratio than the 4% MOLP diet. A possible reason is that MOLP

contains higher levels of CF and NDF than MLP, resulting in lower growth performance of pigs.

4.2 | Carcass characteristics

Information on the effects of MOLP on carcass characteristics of finishing pigs is scarce. In the present study, 4% MOLP supplementation had not affected slaughter weight, carcass weight, carcass yield, loin eye area or average back fat depth ($p > .05$). Therefore, MOLP had not affected the carcass traits of finishing pigs. According to Zhu et al. (2019), carcass weight, carcass yield and average back fat thickness gradually decreased with increasing MLP level, and 4% MLP significantly increased slaughter weight ($p < .05$), carcass weight ($p < .01$) and carcass yield ($p < .05$), by 6.06%, 9.89% and 3.96%, respectively, compared with the control group, inconsistent with our current results. However, the specific molecular mechanism is unclear. In addition, in the present work, 4% MLP resulted in higher carcass weight and carcass yield than 4% MOLP, possibly because MLP contains less CF and NDF, making nutrients easier to digest and absorb, resulting in superior carcass traits.

4.3 | Meat quality

The pork in this experiment is normal meat because of initial pH above 5.8 and final pH below 6.0, in agreement with Warner, Kauffman, and Greaser (1997). In the present study, 4% MOLP had a tiny and subtle effect on pork quality, except for pH_{24 hr} and b* value; and shearing force, dripping loss, cooking loss and marbling score were similar to control groups, consistent with Zhang et al. (2019). This could be because the balance of isonitrogenous and isoenergetic in diets was adjusted. However, addition of 4% MLP to the diet significantly increased the a* value of meat ($p < .05$) and decreased shearing force and dripping loss ($p < .01$), consistent with Zhu et al. (2019) who observed increased a* value, and lower shearing force and dripping loss with MLP supplementation. This is most likely due to the fact that it contains quercetin,

TABLE 4 Effects of MOLP and MLP on nutrient composition in LT of finishing pigs

Items	Control	4% MOLP	4% MLP	p-value
DM (%)	23.94 \pm 0.57	23.27 \pm 0.89	21.91 \pm 0.93	.23
CP (%)	19.34 \pm 1.13 ^a	19.16 \pm 1.04 ^a	18.07 \pm 0.79 ^b	<.01
Ash %	1.04 \pm 0.18 ^a	0.72 \pm 0.04 ^b	0.84 \pm 0.09 ^{ab}	.026
IMF (%)	3.56 \pm 0.06	3.39 \pm 0.38	3.00 \pm 0.21	.35
IMP (mg/kg)	1,018.80 \pm 20.95	1,074.94 \pm 13.27	1,106.42 \pm 33.92	.10

Note: Values are means \pm SE ($n = 6$).

Abbreviations: CP, crude protein; DM, dry matter; IMF, intramuscular fat; IMP, inosinemonphosphate; LT, longissimus thoracis; MLP, mulberry leaf powder; MOLP, *Moringa oleifera* leaves powder.

^{a, b} Values that differ significantly at $P < .05$.

which has strong antioxidative activity and high water-holding capacity.

4.4 | MyHC expression levels

Muscle fibre type is known to determine meat quality. Herein, we investigated mRNA expression in type I, IIa, IIb and IIx muscle fibres, as typically carried out in myofibre research. We found that 4% MOLP significantly increased MyHCIIa and decreased MyHCIIx expression levels in LT, whereas 4% MLP not only significantly increased ($p < .05$) MyHCI and MyHCIIa levels, but also decreased ($p < .05$) MyHCIIx and MyHCIIb levels. Furthermore, 4% MLP induced greater expression of MyHCI, MyHCIIa and MyHCIIx than 4% MOLP. Previous study has pointed out that the effect of carcass weight on muscle fibre characteristics was greatly subtle and small (Choe & Kim, 2014). Therefore, this result is not because of differences in body weight. Hamill et al. (2012) reported that muscle fibres and IMF were greatly correlated with tenderness of meat. Choi and Kim (2009) suggested that type I fibre have smaller diameters, lower in shear force and better tenderness traits compared with the type IIb fibres. Maltin et al. (1998) reported early that content of intramuscular fat is actively associated with content of Type I fibre. In this study, 4% MLP significantly increased content of IMF and meat colour a^* value, and decreased shear force and drip loss, consistent with myofibre characteristics. This may reflect biological substances present in MLP. One study found that resveratrol increased MyHCI and MyHCIIa mRNA expression (He & Lu, 2013; Price et al., 2012). However, the underlying mechanism of the effects of MOLP on changes in muscle fibre type remains unclear because there is no information on the effects of MOLP and the biological substances within it on mRNA expression levels of muscle fibres in finishing pigs. Based on the above results, this may be related to its rich and diverse active substances, and the biological functions and specific mechanism of MOLP needs further research.

4.5 | Muscle chemical composition

In this study, neither 4% MOLP nor MLP affected DM, IMF or IMP content in LT samples from finishing pigs, indicating minimal influence on muscle chemical composition. However, 4% MOLP and MLP increased the content of CP. Zhang et al. (2019) observed that there were no differences in the pork chemical composition when provided MOLP into finishing pigs, but the mechanism by which MOLP affects meat chemical composition was not clear (Zhang et al., 2019). In addition, research on the effect of MLP on the chemical composition of pork has not been reported. Therefore, future research is necessary to investigate how MOLP and MLP regulate changes in chemical composition of pork.

4.6 | Amino acid profile

In the present study, 4% MOLP not only not negatively affected the amino acid content of pork, but also significantly increased the concentration of Ala, Thr, Ile, Lys and Pro, consistent with Zhang et al. (2019). However, there is no information on the effect of MLP on the amino acid profile of pork. We found that dietary supplementation with 4% MLP markedly increased the concentration of Glu, Gly, Ala, Arg, Ile, Phe, Pro, Ser, Tyr and Asp. Moreover, 4% MLP enhanced levels of Glu, Gly, Arg, Phe, Pro, Ser, Tyr and Asp than did 4% MOLP. Thus, feeding pigs with MLP positively affected the amino acid content of pork, but the specific regulatory mechanism is still unknown.

4.7 | FA composition

In this study, although 4% MOL reduced the abundance of C17:1 and C20:4n6, it had no impact on TSFA, TUFA, n-3 PUFA, n-6 PUFA and the ratio of n-6/n-3. Therefore, there was no negative effect on the composition of FAs, similar to the findings of Mukumbo et al. (2015). However, 4% MLP obviously affected the composition of FA in pork. Concentrations of C16:1, C18:1n9c, C20:4n6, C18:3n3, C20:3n3, C22:1n9 and n-3 PUFA were elevated, while C12:0 and C16:0 were decreased. Consequently, TUFA levels were higher than in meat from control and 4% MOLP animals, while the concentration of TSFA was decreased. In addition, the n-6/n-3 ratio was markedly decreased. This pork may be preferable for human nutrition. Mukumbo et al. (2015) discovered that feeding MLP to rabbits can lower levels of saturated fats and increase PUFAs in meat, consistent with the results of the present study. Currently, there was no information on the influence of dietary MLP on the FA composition of finishing pigs. Based on our study, the research indicates that MLP has a positive effect overall.

5 | CONCLUSIONS

In this study, 4% MOLP had no detrimental effects on growth traits, carcass characteristics, meat quality and the composition of FAs of finishing pigs, and it significantly increased expression of MyHCIIa and decreased expression of MyHCIIx mRNA in LT. Supplementation with 4% MOLP markedly increased the content of CP and the concentration of Ala, Thr, Ile, Lys and Pro in LT. Inclusion of 4% MLP in the diet of finishing pigs not only promoted the growth performance, as indicated by higher final BW, ADFI and ADG values, and lower F/G ratio, but also improved carcass traits, as indicated by higher slaughter weight, carcass weight and carcass yield. Furthermore, it made better the quality of pork including higher redness and mRNA expression levels of oxidative-type fibres, and lower shearing force, dripping loss and mRNA expression levels of glycolytic muscle fibres. Moreover, 4% MLP supplementation improved meat flavour,

as indicated by increased CP content, concentrations of amino acids and TUFAs, and decreased concentrations of TSFAs. This meat may be preferable for human nutrition. In total, supplementation with a moderate amount of MOLP or MLP to finishing pigs may be beneficial. MLP appears to be more beneficial than MOLP under the same conditions.

ACKNOWLEDGEMENTS

This work was supported by grants from The National Key Research and Development Program of China (2016YFD0500503), the Technical System of Modern Agricultural Industry in Guangdong Province (2018LM1121, 2018LM2158) and the Science and Technology Innovation Strategy Projects of Guangdong Province (2018B020203002).

CONFLICT OF INTEREST

None of the authors declare any conflicts of interests.

ANIMAL WELFARE STATEMENT

This experiment was conducted in accordance with the guidelines of the Department of College of Animal Science, South China Agricultural University, China. The study was approved by the Ethics Committee of Local Experimental Animals Care Committee and conducted in accordance with the guidelines of South China Agricultural University, China (No. 201004152). All efforts were made to minimize animal suffering.

ORCID

Jiajie Sun  <https://orcid.org/0000-0003-1992-154X>

REFERENCES

- Ahmed, S. T., Mun, H. S., Islam, M. M., Ko, S. Y., & Yang, C. J. (2016). Effects of dietary natural and fermented herb combination on growth performance, carcass traits and meat quality in grower-finisher pigs. *Meat Science*, 122, 7–15. <https://doi.org/10.1016/j.meatsci.2016.07.016>
- AOAC. (1990). *Official methods of analysis*. Washington, DCAssociation of Official Analytical Chemists.
- Arabshahi-Delouee, S., & Urooj, A. (2007). Antioxidant properties of various solvent extracts of mulberry (*Morus indica* L.) leaves. *Food Chemistry*, 102, 1233–1240. <https://doi.org/10.1016/j.foodchem.2006.07.013>
- Chen, J., & Li, X. (2007). Hypolipidemic effect of flavonoids from mulberry leaves in triton WR-1339 induced hyperlipidemic mice. *Asia Pacific Journal of Clinical Nutrition*, 16, 290.
- Choe, J. H., & Kim, B. C. (2014). Association of blood glucose, blood lactate, serum cortisol levels, muscle metabolites, muscle fiber type composition, and pork quality traits. *Meat Science*, 97, 137–142. <https://doi.org/10.1016/j.meatsci.2014.01.024>
- Choi, Y. M., & Kim, B. C. (2009). Muscle fiber characteristics, myofibrillar protein isoforms, and meat quality. *Livestock Science*, 122. <https://doi.org/10.1016/j.livsci.2008.08.015>
- Hamill, R. M., McBryan, J., McGee, C., Mullen, A. M., Sweeney, T., Talbot, A., ... Davey, G. C. (2012). Functional analysis of muscle gene expression profiles associated with tenderness and intramuscular fat content in pork. *Meat Science*, 92(4), 440–450. <https://doi.org/10.1016/j.meatsci.2012.05.007>
- He, H., & Lu, Y. H. (2013). Comparison of inhibitory activities and mechanisms of five mulberry plant bioactive components against α -glucosidase. *Journal of Agricultural and Food Chemistry*, 61, 8110–8119. <https://doi.org/10.1021/jf4019323>
- Kimura, T., Nakagawa, K., Kubota, H., Kojima, Y., Goto, Y., Yamagishi, K., ... Miyazawa, T. (2007). Food-grade mulberry powder enriched with 1-deoxynojirimycin suppresses the elevation of postprandial blood glucose in humans. *Journal of Agricultural and Food Chemistry*, 55(14), 5869–5874. <https://doi.org/10.1021/jf062680g>
- Klont, R., & Brocks, L. (1998). Eikelenboom G. Muscle fibre type and meat quality. *Meat Science*, 49, S219–S229.
- Lefcaucheur, L., Ecolan, P., Plantard, L., & Gueguen, N. (2002). New insights into muscle fiber types in the pig. *Journal of Histochemistry & Cytochemistry*, 50, 719–730. <https://doi.org/10.1177/002215540205000513>
- Li, Y., Li, F., Lin, B., Kong, X., Tang, Y., & Yin, Y. (2014). Myokine IL-15 regulates the crosstalk of co-cultured porcine skeletal muscle satellite cells and preadipocytes. *Molecular Biology Reports*, 41, 7543–7553. <https://doi.org/10.1007/s11033-014-3646-z>
- Li, Y., Liu, Y., Li, F., Lin, Q., Dai, Q., Sun, J., ... Yin, Y. (2018). Effects of dietary ramie powder at various levels on carcass traits and meat quality in finishing pigs. *Meat Science*, 143, 52–59. <https://doi.org/10.1016/j.meatsci.2018.04.019>
- Livak, K. J., & Schmittgen, T. D. (2001). Analysis of relative gene expression data using real-time quantitative PCR and the $2^{-\Delta\Delta CT}$ method. *Methods*, 25, 402–408. <https://doi.org/10.1006/meth.2001.1262>
- Maltin, C. A., Sinclair, K. D., Warriss, P. D., Grant, C. M., Porter, A. D., Delday, M. I., & Warkup, C. C. (1998). The effects of age at slaughter, genotype and finishing system on the biochemical properties, muscle fibre type characteristics and eating quality of bull beef from suckled calves. *Animal Science*, 66, 341–348. <https://doi.org/10.1017/S1357729800009462>
- Meesse, A., Getye, Y., Berihun, K., & Banerjee, S. (2013). Effect of feeding graded levels of *Moringa stenopetala* leaf meal on growth performance, carcass traits and some serum biochemical parameters of Koekoek chickens. *Livestock Science*, 157, 498–505. <https://doi.org/10.1016/j.livsci.2013.08.012>
- Ministry of Agriculture of the People's Republic of China. (2004). *Feeding standard of swine* (GB, NY/T 65-2004). Beijing, China: China Agriculture Press.
- Mukumbo, F., Maphosa, V., Hugo, A., Nkukwana, T., Mabusela, T., & Muchenje, V. (2015). Effect of moringa oleifera leaf meal on finisher pig growth performance, meat quality, shelf life and fatty acid composition of pork. *South African Journal of Animal Science*, 44, 388–400. <https://doi.org/10.4314/sajas.v44i4.9>
- Nkukwana, T. T., Muchenje, V., Pieterse, E., Masika, P. J., Mabusela, T. P., Hoffman, L. C., & Dzama, K. (2014). Effect of *Moringa oleifera* leaf meal on growth performance, apparent digestibility, digestive organ size and carcass yield in broiler chickens. *Livestock Science*, 161, 139–146. <https://doi.org/10.1016/j.livsci.2014.01.001>
- NPPC. (1991). *Procedures to evaluate market hogs*. Des Moines, IANational Pork Producers Council.
- Okrouhlá, M., Stupka, R., Čítek, J., Šprysl, M., & Brzobohatý, L. (2013). Effect of dietary linseed supplementation on the performance, meat quality, and fatty acid profile of pigs. *Czech Journal of Animal Science*, 58, 279–288. <https://doi.org/10.17221/6826-CJAS>
- Omidiran, M. O., Baiyewu, R. A., Ademola, I. T., Fakorede, O. C., Toyinbo, E. O., Adewumi, O. J., & Adekunle, E. A. (2012). Phytochemical analysis, nutritional composition and antimicrobial activities of white mulberry (*Morus alba*). *Pakistan Journal of Nutrition*, 11, 456–460. <https://doi.org/10.3923/pjn.2012.456.460>
- Price, N. L., Gomes, A. P., Ling, A. J. Y., Duarte, F. V., Martin-Montalvo, A., North, B. J., ... Sinclair, D. A. (2012). SIRT1 is required for AMPK activation and the beneficial effects of resveratrol on mitochondrial function. *Cell Metabolism*, 15, 675–690. <https://doi.org/10.1016/j.cmet.2012.04.003>

- Rossi, R., Pastorelli, G., Cannata, S., Tavaniello, S., Maiorano, G., & Corino, C. (2013). Effect of long-term dietary supplementation with plant extract on carcass characteristics meat quality and oxidative stability in pork. *Meat Science*, 95, 542–548. <https://doi.org/10.1016/j.meatsci.2013.05.037>
- Saini, R. K., Shetty, N. P., & Giridhar, P. (2014). GC-FID/MS analysis of fatty acids in Indian cultivars of *Moringa oleifera*: Potential sources of PUFA. *Journal of the American Oil Chemists' Society*, 91, 1029–1034. <https://doi.org/10.1007/s11746-014-2439-9>
- Serem, J. K., Wahome, R. G., Gakuya, D. W., Kiama, S. G., Gitao, G. C., & Onyango, D. W. (2017). Growth performance, feed conversion efficiency and blood characteristics of growing pigs fed on different levels of *Moringa oleifera* leaf meal. *Journal of Veterinary Medicine and Animal Health*, 9, 327–333.
- Stein, H. H., Everts, A. K., Sweetser, K. K., Peters, D. N., Maddock, R. J., Wulf, D. M., & Pedersen, C. (2006). The influence of dietary field peas (*Pisum sativum* L.) on pig performance, carcass quality, and the palatability of pork. *Journal of Animal Science*, 84, 3110–3117.
- Sun, X., Yamasaki, M., Katsube, T., & Shiwaku, K. (2015). Effects of quercetin derivatives from mulberry leaves: Improved gene expression related hepatic lipid and glucose metabolism in short-term high-fat fed mice. *Nutrition Research and Practice*, 9, 137–143. <https://doi.org/10.4162/nrp.2015.9.2.137>
- Tesfaye, E., Animut, G., Urge, M., & Dessie, T. (2013). *Moringa olifera* leaf meal as an alternative protein feed ingredient in broiler ration. *International Journal of Poultry Science*, 12, 289–297. <https://doi.org/10.3923/ijps.2013.289.297>
- Warner, R. D., Kauffman, R. G., & Greaser, M. L. (1997). Muscle protein changes post mortem in relation to pork quality traits. *Meat Science*, 45, 339–352. [https://doi.org/10.1016/S0309-1740\(96\)00116-7](https://doi.org/10.1016/S0309-1740(96)00116-7)
- Yan, J., Liu, P., Xu, L., Huan, H., Zhou, W., Xu, X., & Shi, Z. (2018). Effects of exogenous inosine monophosphate on growth performance, flavor compounds, enzyme activity, and gene expression of muscle tissues in chicken. *Poultry Science*, 97, 1229–1237. <https://doi.org/10.3382/ps/pex415>
- Zeng, Z., Jiang, J.-J., Yu, J., Mao, X.-B., Yu, B., & Chen, D.-W. (2019). Effect of dietary supplementation with mulberry (*Morus alba* L.) leaves on the growth performance, meat quality and antioxidative capacity of finishing pigs. *Journal of Integrative Agriculture*, 18, 143–151. [https://doi.org/10.1016/S2095-3119\(18\)62072-6](https://doi.org/10.1016/S2095-3119(18)62072-6)
- Zhang, T., Si, B., Tu, Y., Cui, K., Zhou, C., & Diao, Q. (2019). Effect of including different levels of moringa (*Moringa oleifera*) leaf meal in the diet of finishing pigs: Performance, pork quality, fatty acid composition, and amino acid profile. *Czech Journal of Animal Science*, 64, 141–149. <https://doi.org/10.17221/204/2018-CJAS>

SUPPORTING INFORMATION

Additional supporting information may be found online in the Supporting Information section.

How to cite this article: Chen Z, Xie Y, Luo J, et al. Dietary supplementation with *Moringa oleifera* and mulberry leaf affects pork quality from finishing pigs. *J Anim Physiol Anim Nutr*. 2020;00:1–8. <https://doi.org/10.1111/jpn.13450>

RESEARCH ARTICLE

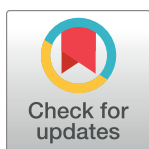
Effects of fermented feeds and ginseng polysaccharides on the intestinal morphology and microbiota composition of Xuefeng black-bone chicken

Yueqin Xie[☯], Jie Liu[☯], Huan Wang, Junyi Luo, Ting Chen, Qianyun Xi, Yongliang Zhang*, Jiajie Sun[✉]*

College of Animal Science, Guangdong Provincial Key Laboratory of Animal Nutrition Control, Guangdong Laboratory for Lingnan Modern Agriculture, South China Agricultural University, Guangzhou, Guangdong, China

☯ These authors contributed equally to this work.

* zhangyl@scau.edu.cn (YZ); jiajiesun@scau.edu.cn (JS)



OPEN ACCESS

Citation: Xie Y, Liu J, Wang H, Luo J, Chen T, Xi Q, et al. (2020) Effects of fermented feeds and ginseng polysaccharides on the intestinal morphology and microbiota composition of Xuefeng black-bone chicken. PLoS ONE 15(8): e0237357. <https://doi.org/10.1371/journal.pone.0237357>

Editor: Michael H. Kogut, USDA-Agricultural Research Service, UNITED STATES

Received: April 30, 2020

Accepted: July 23, 2020

Published: August 11, 2020

Peer Review History: PLOS recognizes the benefits of transparency in the peer review process; therefore, we enable the publication of all of the content of peer review and author responses alongside final, published articles. The editorial history of this article is available here: <https://doi.org/10.1371/journal.pone.0237357>

Copyright: © 2020 Xie et al. This is an open access article distributed under the terms of the [Creative Commons Attribution License](https://creativecommons.org/licenses/by/4.0/), which permits unrestricted use, distribution, and reproduction in any medium, provided the original author and source are credited.

Data Availability Statement: All relevant data are within the paper and its Supporting Information files.

Abstract

Fermented feeds contain abundant organic acids, amino acids, and small peptides, which improve the nutritional status as well as the morphology and microbiota composition of the intestine. Ginseng polysaccharides exhibit several biological activities and contribute to improving intestinal development. Here, Xuefeng black-bone chickens were fed a basal diet fermented by *Bacillus subtilis*, *Saccharomyces cerevisiae*, *Lactobacillus plantarum*, and *Enterococcus faecium*, with or without ginseng polysaccharides. The 100% microbially fermented feed (Fe) and 100% microbially fermented feed and ginseng polysaccharide (FP) groups showed significantly increased villus height and villus height to crypt depth ratio, and decreased crypt depth in the jejunum. In the 100% complete feed and ginseng polysaccharide (Po) group, the villus height to crypt depth ratio was significantly increased, crypt depth was reduced, and villus height remained unaffected. Next, we studied the intestinal microbial composition of 32 Xuefeng black-bone chickens. A total of 10 phyla and 442 genera were identified, among which *Firmicutes*, *Proteobacteria*, and *Bacteroidetes* were the most dominant phyla. At the genus level, *Sutterella* and *Asteroleplasma* abundance increased and decreased, respectively, in the FP and Po groups. *Sutterella* abundance was positively correlated to villus height and villus height to crypt depth ratio, and negatively correlated to crypt depth, and *Asteroleplasma* abundance was positively correlated to crypt depth and negatively correlated to villus height to crypt depth ratio. At the species level, the FP group showed significantly increased *Bacteroides_vulgatus* and *Eubacterium_tortuosum* and decreased *Mycoplasma_gallinarum* and *Asteroleplasma_anaerobium* abundance, and the Po group showed significantly increased *Mycoplasma_gallinarum* and *Asteroleplasma_anaerobium* abundance. Moreover, bacterial abundance was closely related to the jejunum histomorphology. *Asteroleplasma_anaerobium* abundance was positively correlated with crypt depth and negatively correlated with villus height to crypt depth ratio. *Mycoplasma_gallinarum* abundance was positively correlated to villus height, and *Bacteroides_vulgatus* and *Eubacterium_tortuosum* abundance was positively correlated with villus height to crypt

Funding: This study was supported by the Technical System of Modern Agricultural Industry in Guangdong Province [2018LM1121, 2018LM2158].

Competing interests: The authors have declared that no competing interests exist.

depth ratio and negatively correlated with crypt depth. Therefore, fermented feeds with ginseng polysaccharides may be used as effective alternatives to antibiotics for improving intestinal morphology and microbial composition.

Introduction

It is well known that antibiotic growth promoters are added to animal feed for livestock growth promotion. However, the overuse of antibiotics has led to antibiotic resistance in animal microbial populations and raises the risk of transfer of antibiotic resistance genes to the human microbiota [1], thereby posing a threat to global public health. Hence, the use of antibiotics in animal feeds has been prohibited in many countries [2], which has led to a decline in animal production and an increase in the risk of food-borne infections in consumers due to higher rates of infections in livestock [3]. In order to solve the problems associated with the ban of antibiotics in livestock production, researchers are working towards finding new alternatives to antibiotics, such as the use of feed fermented by microbes. In general, the basal diet that fermented with probiotics has been extensively studied due to its benefits of increasing nutrient bioavailability and nutritional value [4]. Many researchers have reported that the use of probiotics for feed fermentation improves growth performance [4], meat quality [5], ileal amino acid digestibility [6], and immune function [7] in broilers. Other alternatives include addition of biological and functional additives to the diet, such as moringa, mulberry, Chinese herbal medicine, tea polyphenol, dietary fiber, and ginseng polysaccharides. Among them, ginseng polysaccharides, due to their high content of polysaccharides, peptides, saponins, and other active substances, can be used as functional feed additives to promote food intake [8], improve immunity [9], and decrease the amount of abdominal fat and serum cholesterol [10] in broilers. Therefore, if ginseng polysaccharide is mixed with microbially fermented feed, it may have a positive impact on the development of new alternative antibiotics. To date, however, no studies have focused on evaluating the effect of the combined use of these two substances in livestock and poultry diet. Xuefeng black-bone chicken is the most famous native breed in the Hunan province of China. It is greatly favored by people because its meat contains high contents of protein, vitamins, and amino acids [11], which has led to its increased demand. However, its slow growth, long feeding period, and risk of disease during the breeding process largely limits the development of the Xuefeng black-bone chicken industry. In the present study, we aimed to investigate the effect of feed fermented by microbes and ginseng polysaccharide on Xuefeng black-bone chicken intestinal morphology and microflora population. Our findings not only help solve the problems associated with the ban of antibiotics in livestock production, but also contribute to the development of new, effective alternatives to antibiotics, and provide a new scheme for improving intestinal health in Xuefeng black-bone chicken.

Materials and methods

Chickens, diet, and experimental design

For microbial fermentation of feed, the basal diet was mixed with probiotics, including *Bacillus subtilis* (5×10^8 colony forming units/g), *Saccharomyces cerevisiae* (5×10^7 colony forming units/g), *Lactobacillus plantarum* (3×10^8 colony forming units/g), and *Enterococcus faecium* (5×10^8 colony forming units/mL) (inoculum proportion = 1:1:3:3 v/v, inoculum size = 3% v/

v, moisture = 45% w/v, and temperature = $35 \pm 1^\circ\text{C}$). Additionally, molasses (2%) was added and mixed thoroughly using a feed-stuff mixer. The fermented feed was kept in a polyethylene bag with a one-way air valve during the fermentation process, and fermented by anaerobic fermentation for 20 days. The probiotic strains were obtained from the probiotics collection of Guangdong Institute Microbiology (Guangzhou, China).

Xuefeng black-bone chicken, a native breed of China, has excellent quality of meat with high contents of protein, vitamins, and amino acids, and hence was selected for this experiment. A total of 400 Xuefeng black-bone chickens (one-day-old and balanced for body weight) were used in a completely randomized design for a 7-d adaptation period and a 150-d experimental period. The chickens were randomly divided into 4 groups (4 replicates per group and 25 chickens in each replicate): 100% complete feed group (Cn group), 100% microbially fermented feed group (Fe group), 100% complete feed and ginseng polysaccharide (200 g/t) group (Po group), and 100% microbially fermented feed and ginseng polysaccharide group (FP group). In our paper, the Ginseng polysaccharides were extracted from the roots of ginseng with hot water, precipitated by 80% ethanol and deproteinated based on our previous method [12]. Their nutritional requirements were met according to the National Research Council feeding standards (NRC, 1994) and basic diet formulations and nutrient composition are shown in S1 Table. Chickens were raised in floor pens, and placed into separate floor pens with 20 individuals per pen. All birds received feed and fresh water *ad libitum* throughout the experiment. Feed was removed from the pen 24 hours before sampling. All animal procedures were approved by the Animal Care Committee at South China Agricultural University, and the experimental individuals were anaesthetized prior to exsanguination according to the University's guidelines for animal research.

Data collection and sampling

On day 150, 2 broiler chickens were randomly selected from each pen (8 broiler chickens/treatment) and euthanized with an overdose of CO_2 [13]. The intestinal tract was immediately removed. Tissue samples of the jejunum were obtained and gently flushed with 0.9% saline to remove the intestinal contents and fixed in 10% formalin for histomorphological analysis. Subsequently, the jejunum contents (8 broiler chickens/treatment) were collected in sterile 1.5 mL tubes and stored at -80°C until DNA isolation.

Intestinal histomorphology

The intestinal samples were processed according to the method of Thompson et al. [14]. In brief, the intestinal samples were dehydrated with increasing concentrations of ethanol, cleared with xylene (Surgipath Medical Industries, Richmond, IL), and embedded in paraffin wax (Thermo Fisher Scientific, Kalamazoo, MC). Cross sections ($5\ \mu\text{m}$) were stained with hematoxylin and eosin (GeneCopoeia, Rockville, MD). The stained sections were dehydrated with ethanol, cleared with xylene, and mounted with DPX mountant based on the method of Jiang et al. [15]. ImageJ software (National Institutes of Health, USA) was used to determine the morphometric measurements of villus height and crypt depth of the jejunum using an Olympus BX40 F-3 microscope (Olympus Cooperation, Tokyo, Japan) attached to a digital video camera (Q-imaging, 01-MBF-200R-CLR-12, SN: Q32316, Canada) [16].

DNA extraction, 16S rRNA gene sequencing, and annotation analysis

Total genomic DNA from the jejunum contents was extracted using QIAamp DNA Stool Mini Kit (Qiagen, Hilden, Germany) according to the specifications of the manufacturers. The DNA samples were tested for integrity using 1% agarose gel electrophoresis and their concentration

was determined using a Qubit fluorometer (Invitrogen, Carlsbad, CA). Based on the concentration, the DNA sample was diluted to 1 ng/ μ L using sterile water. The V3–V4 regions of the 16S ribosomal DNA genes were amplified by PCR based on the method of Sun et al. [17]. Sequencing libraries were generated using an Illumina MiSeq Reagent Kit (Illumina, San Diego, CA) on an Illumina MiSeq Sequencer. Single-end reads were assigned to samples based on their unique barcode in the adaptor sequence. Quality filtering of the raw reads was performed to obtain high-quality clean reads according to the Cutadapt quality controlling process [18]. The reads were compared with the reference database [19] using the UCHIME algorithm [20] to detect chimeric sequences [21], and clean reads were finally obtained using the Uparse software (Uparse v7.0.1001) [22]. Sequences with $\geq 97\%$ similarity were assigned to the same operational taxonomic units (OTU). For each representative OTU, the Silva Database was used to annotate taxonomic information based on the Mothur algorithm [19]. To study the phylogenetic relationships between different OTU, multiple sequence alignment was performed using the MUSCLE software (Version 3.8.31) [23]. Alpha diversity was applied to analyze the complexity of species diversity within groups, including the Observed-species, Chao1, ACE, and Shannon indices. Beta diversity analysis was used to evaluate differences between groups using non-metric multi-dimensional scaling. Two different complementary analyses, analysis of similarity and multiresponse permutation procedure, were used to determine significant differences between jejunum microbiota in their response to fermented diets with or without ginseng polysaccharide. All these indices were calculated using the quantitative insights into microbial ecology pipeline (version 1.7.0) and displayed using the R software (version 2.15.3).

Statistical analysis

The experimental design included a completely randomized design. All data, including villus height, crypt depth, and the ratio of villus height to crypt depth were analyzed using one-way ANOVA and Duncan's test with SPSS version 17.0 (IBM Corp., Armonk, NY). The R software was used to perform MetaStat analysis to determine differences in the relative abundance of fecal microbiomes [24]. The *P* values indicated the significant differences at the levels of $P < 0.05$. The correlation analyses of microbiota composition with the intestinal morphology were tested by the cor function (*x*, *y*, use = "p") (<http://127.0.0.1:1153/library/stats/html/cor.html>), and illustrated with a function-labelled Heatmap (Matrix, xLabels, yLabels) in the R package WGCNA (<http://127.0.0.1:1153/library/stats/html/cor.html>).

Results

Histomorphological measurements of the intestine

The effects of fermented feed and ginseng polysaccharide on the villus height, crypt depth, and the ratio of villus height to crypt depth of the jejunum of Xuefeng black-bone chicken were evaluated, as shown in Fig 1. The villus height was significantly increased in the Fe and FP groups ($P < 0.05$) but not in the Po group compared to that in the Cn group ($P > 0.05$). The crypt depth was significantly decreased ($P < 0.05$) in the Fe, Po, and FP groups compared with that in the Cn group. However, no significant differences in crypt depth were observed between the Fe, Po, and FP groups ($P > 0.05$). The ratio of villus height to crypt depth was significantly higher ($P < 0.05$) in the Fe, Po, and FP groups compared with that in the Cn group. However, no differences in villus height to crypt depth ratio were observed between the Po and FP groups ($P > 0.05$) while higher than those in the Fe group ($P < 0.05$).

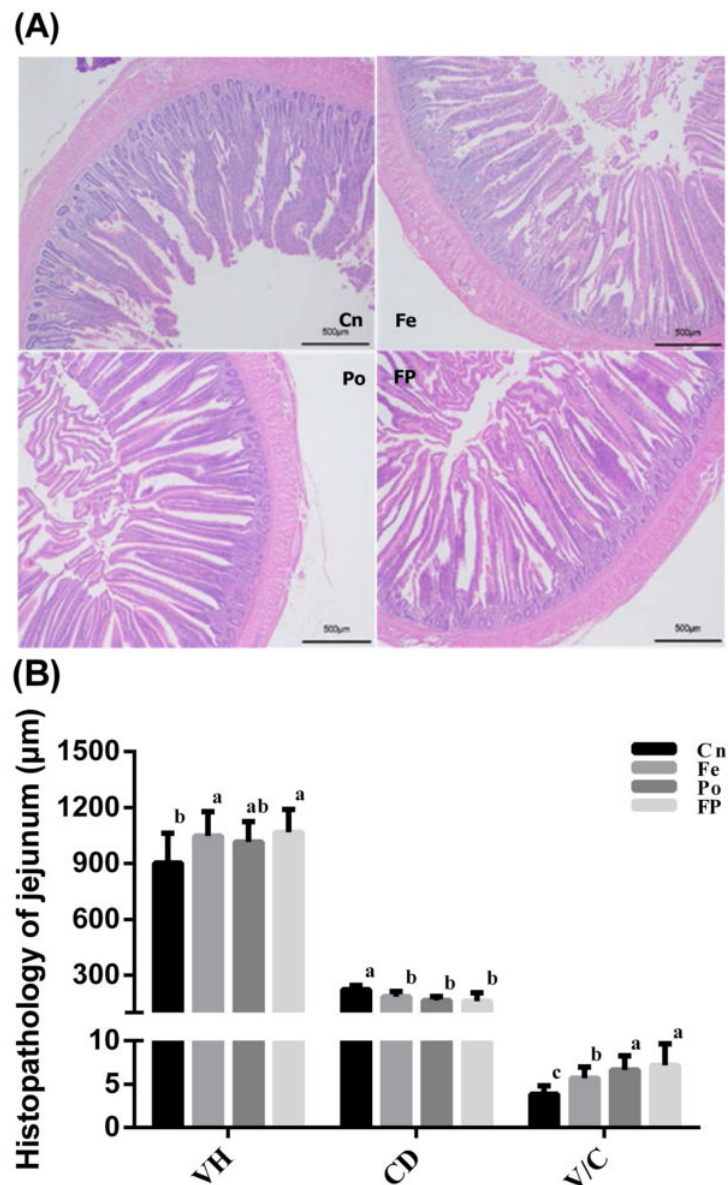


Fig 1. Effects of dietary treatment on villus height, crypt depth, and the ratio of villus height to crypt depth in the jejunum of broiler chickens. Treatments with different letters are significantly different at $P < 0.05$. Data were obtained from transmission electron microscopy, and were means of 10 birds (2 bird from each pen). Cn, 100% complete feed group; Fe, 100% microbial fermented feed group; Po, 100% complete feed and ginseng polysaccharide group; FP, 100% microbial fermented feed and ginseng polysaccharide group. VH, villus height; CD, crypt depth; V/C, the ratio of villus height to crypt depth.

<https://doi.org/10.1371/journal.pone.0237357.g001>

16S rRNA gene sequencing and annotation analysis

After DNA extraction, the hypervariable V3–V4 regions of the 16S ribosomal DNA were enriched in each sample, and subsequent high-throughput analysis generated a total of 2,886,390 raw reads. On an average, each sample produced approximately 90,200 joined tags, which were assembled using PandaSeq v2.8 (min = 77,322, max = 99,325). Over $77.65\% \pm$

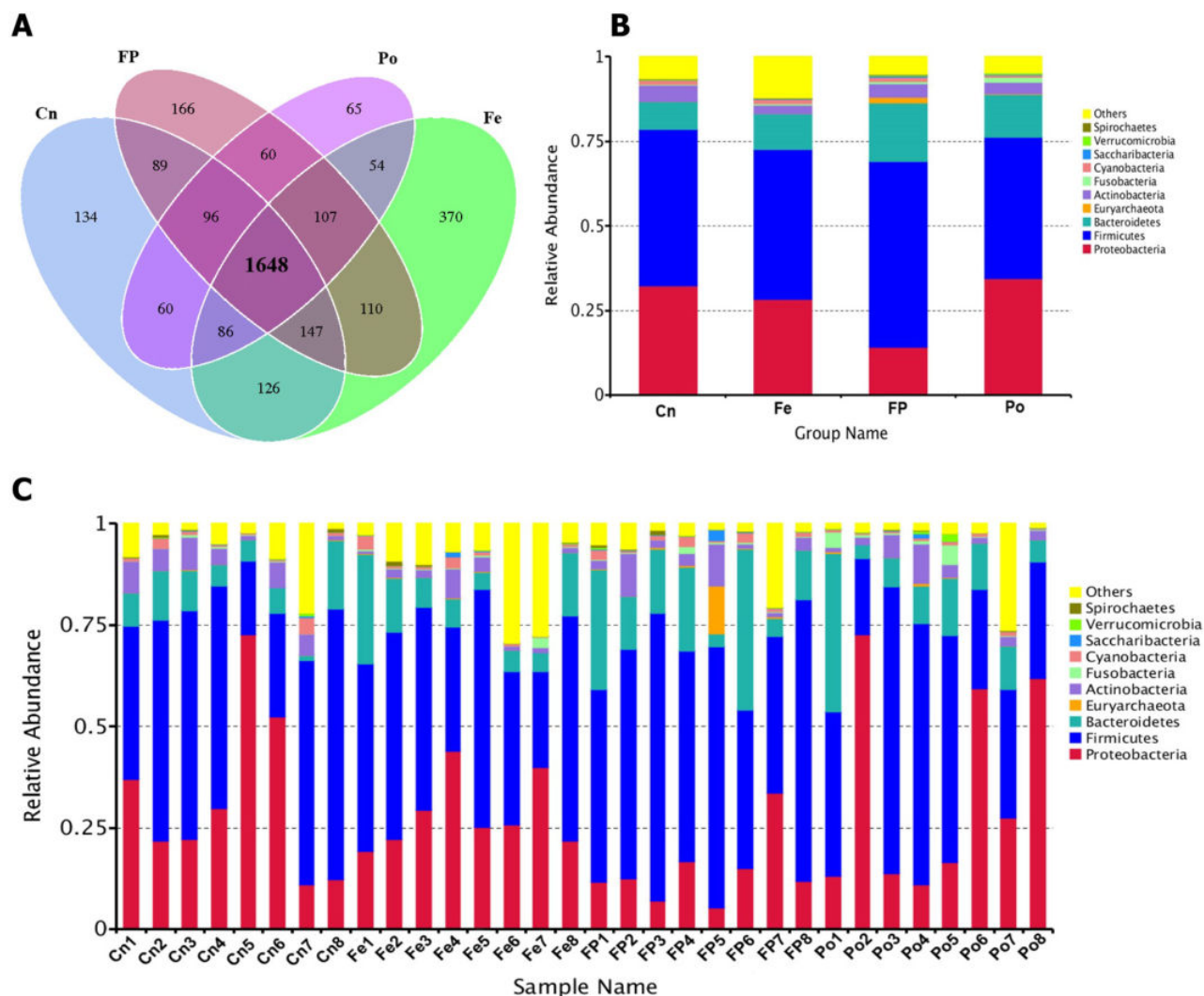


Fig 2. Venn Graph representation of the shared and exclusive OTUs at the 97% similarity level among the three groups of fecal microbiota (A). Bar plots analysis shows relative abundance of fecal microbiota at the phylum level in each group (B) and in each sample (C).

<https://doi.org/10.1371/journal.pone.0237357.g002>

4.33% of the total joined tags from each sample passed quality control and were processed for further analysis (S2 Table). OTU clustering of the high-quality tags yielded 3,318 unique OTU candidates at 97% sequence similarity, and 1,648 candidates that were shared across all samples were defined as core OTU. The core OTU comprised approximately 49.67% of the total candidates, while only 134, 166, 65 and 370 OTU were identified uniquely in the Cn, FP, Po, and Fe groups (Fig 2A and S3 Table). Additionally, the microbial diversity in the jejunum contents of broiler chickens was assessed using quantitative insights into microbial ecology pipeline based on the OTU annotation, which identified the top 10 phyla (Fig 2B and 2C). The most abundant phylum in the jejunum contents of Xuefeng black-bone chicken was *Firmicutes*, which accounted for approximately 46.75% of all sequences, followed by *Proteobacteria* (27.36%) and *Bacteroidetes* (12.20%) (S4 and S5 Tables). At the class level, a total of 59 classes were detected, and 9 classes, including *Clostridia*, *Gammaproteobacteria*, *Bacteroidia*, *Epsilonproteobacteria*, *Bacilli*, *Alphaproteobacteria*, *unidentified_Actinobacteria*, *Deltaproteobacteria*,

and *Melainabacteria* had a relative abundance greater than 1.0%. The most abundant class in the jejunum contents of Xuefeng black-bone chicken was *Clostridia* (40.21%) (S6 and S7 Tables). At the order level, we detected 11 orders with a relative abundance greater than 1.0% (S8 and S9 Tables). Specifically, the most abundant order in the jejunum contents of Xuefeng black-bone chicken was *Clostridiales*, which accounted for approximately 39.73% of all sequences, followed by *Bacteroidales* (11.69%), *Campylobacteriales* (7.12%), *Enterobacteriales* (6.17%), *Lactobacillales* (4.64%), *Oceanospirillales* (4.62%), *Alteromonadales* (1.87%), *Rhizobiales* (1.73%), *Desulfovibrionales* (1.53%), *Bifidobacteriales* (1.29%), and *Caulobacteriales* (1.04%). At the family level, among the 189 families detected, 17 families, including *Ruminococcaceae*, *Lachnospiraceae*, *Helicobacteraceae*, *Enterobacteriaceae*, *Peptostreptococcaceae*, *Halomonadaceae*, *Bacteroidaceae*, *Lachnospiraceae*, *Rikenellaceae*, *Christensenellaceae*, *Shewanellaceae*, *Prevotellaceae*, *Desulfovibrionaceae*, *Clostridiales_vadinBB60_group*, *Bifidobacteriaceae*, *Caulobacteraceae*, and *Enterococcaceae* had a relative abundance greater than 1.0%. The most abundant family in the jejunum contents of Xuefeng black-bone chicken was *Ruminococcaceae* (19.23%) (S10 and S11 Tables). Among the 442 genera detected, 18 genera, including *Helicobacter*, *Serratia*, *Romboutsia*, *Bacteroides*, *Halomonas*, *Lactobacillus*, *Ruminococcaceae_UCG-010*, *Christensenellaceae_R-7_group*, *Rikenellaceae_RC9_gut_group*, *Shewanella*, *Lachnoclostridium*, *Ruminococcaceae_UCG-005*, *Enterococcus*, *Faecalibacterium*, *Eubacterium_coprostanoligenes_group*, *Desulfovibrio*, *Ruminococcaceae_UCG-014*, and *Ruminococcaceae_NK4A214_group* had a relative abundance greater than 1.0% (S12 and S13 Tables). At the species level, among the 216 species detected, 3 species, including *Serratia_marcescens*, *Bacteroides_barnesi*, and *Shewanella_algae* had a relative abundance greater than 1.0%. The most abundant species in the jejunum contents of Xuefeng black-bone chicken was *Serratia_marcescens* (4.93%) (S14 and S15 Tables).

Microbial diversity in the jejunum contents of Xuefeng black-bone chicken

We compared the alpha-diversity (within-sample diversity or estimate of species richness and evenness) of each sample with differing sequence counts or sampling efforts. Rarefaction curve analysis indicated that the number of sequences and sequencing depth were sufficient for this study (S1 Fig). We further used observed species, Chao1, ACE, and Shannon indices to evaluate the diversity of jejunum content of Xuefeng black-bone chicken among the different groups (Fig 3). Specifically, observed species, Chao 1, ACE, and the Shannon diversity index indicated a significant decrease in the diversity of jejunum content of the Po group compared with that of the Cn, Fe, and FP groups ($P = 0.007$, $P = 0.071$, $P = 0.003$, and $P = 0.003$, respectively). For beta diversity analysis, the relationship between the microbial communities in the jejunum of chickens fed different diets was assessed by non-metric multi-dimensional scaling, as shown in Fig 4. There were overlaps between the Cn and Fe groups, but the microbial communities of the FP and Po groups formed a distinct cluster separated from those of the Cn group. In addition, pairwise analysis of similarity [25] suggested that there were highly significant differences between the Cn and Fe groups (global $R = 0.139$, $P = 0.045$), the Cn and FP groups (global $R = 0.239$, $P = 0.004$), the Cn and Po groups (global $R = 0.253$, $P = 0.005$), the Fe and FP groups (global $R = 0.387$, $P = 0.003$), the Fe and Po groups (global $R = 0.436$, $P = 0.004$), and the FP and Po groups (global $R = 0.165$, $P = 0.05$) (Table 1). We also performed a multiresponse permutation procedure [26] in within- and between-group populations. The differences for between-group homogeneity were higher than those for within-group with an A value > 0 , and the change degree reached a significant level between the Cn and Fe groups ($P = 0.031$), the Cn and FP groups ($P = 0.018$), the Cn and Po groups ($P = 0.01$), the Fe and FP

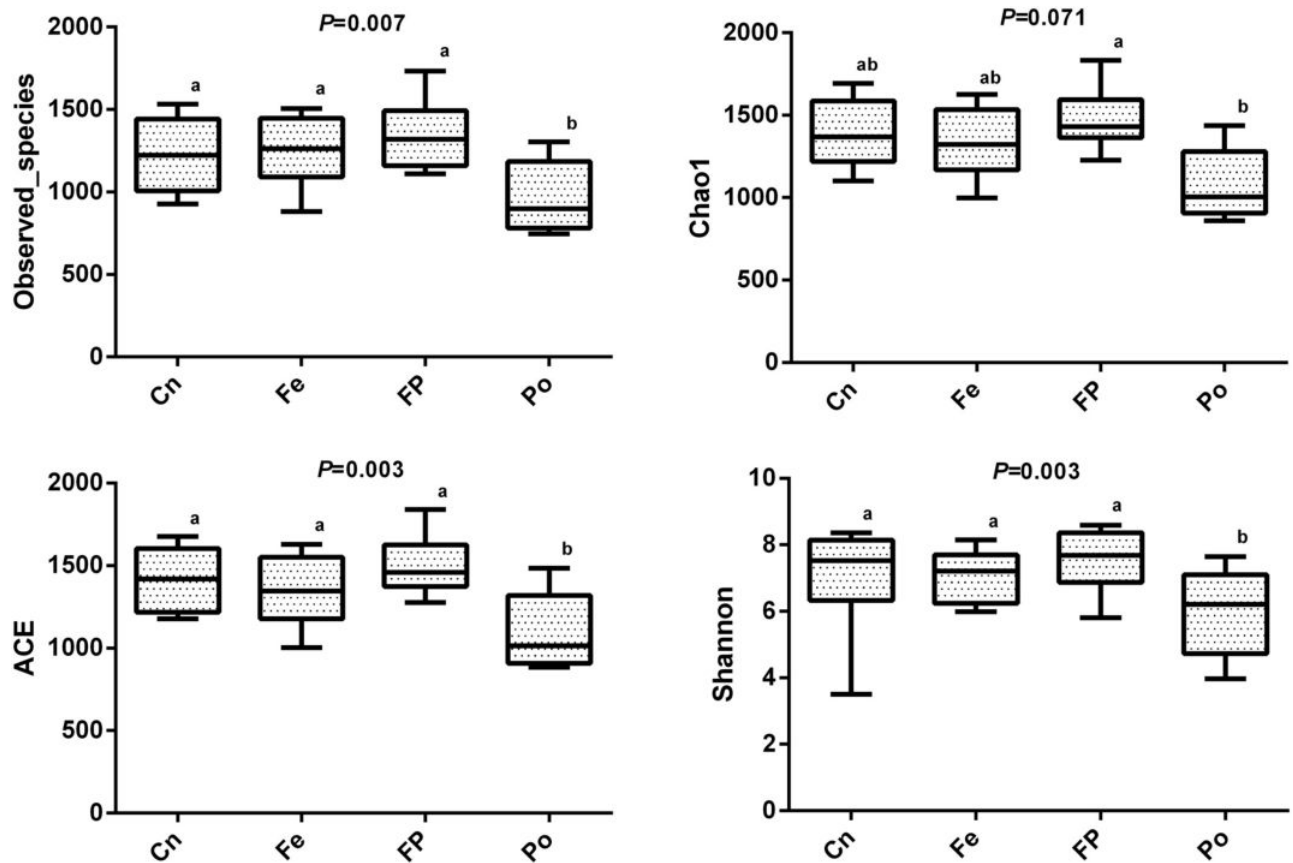


Fig 3. Microbial diversity indices in the fecal microbiome. Summary of four measures of α -diversity (observed species, Chao 1 index, ACE and Shannon).

<https://doi.org/10.1371/journal.pone.0237357.g003>

groups ($P = 0.009$), the Fe and Po groups ($P = 0.004$), and the FP and Po groups ($P = 0.038$) (Table 1).

Anosim, analysis of similarity; MRPP, multiresponse permutation procedure. The R-value ranged from -1 to 1, and an R-value > 0 that showed the significant differences in the between-group population compared with those in the within-group population, as well as A-value (analysed by MRPP). The P values indicated the significant differences at the levels of $P < 0.05$ or $P < 0.01$.

Alternative diets changed the intestinal microbiota composition

Differences in the microbial composition (relative abundance) of the jejunum microbiomes between the Cn and FP groups and the Cn and Po groups were evaluated by the MetaStat method using Fisher's exact test [24]. A total of 19 genera displayed a significant difference in relative abundance between the Cn and FP groups. Among them, the abundance of *Ureaplasma*, *Synechococcus*, *Coprococcus_1*, *Fonticella*, *Butyricoccus*, *Elusimicrobium*, *Sutterella*, *Anaerostipes*, *Faecalitalea*, *Thalassospira*, and *Bacteroides* was increased, and that of *Sporolactobacillus*, *Bacillus*, *Halomonas*, *Aquamicrobium*, *Devosia*, *Microbacterium*, *Asteroleplasma*, and *Shewanella* was decreased in the FP group (S16 Table). Compared with that in the Cn group, the relative abundance of 4 genera, including *Thermoplasmatales*, *Odoribacter*,

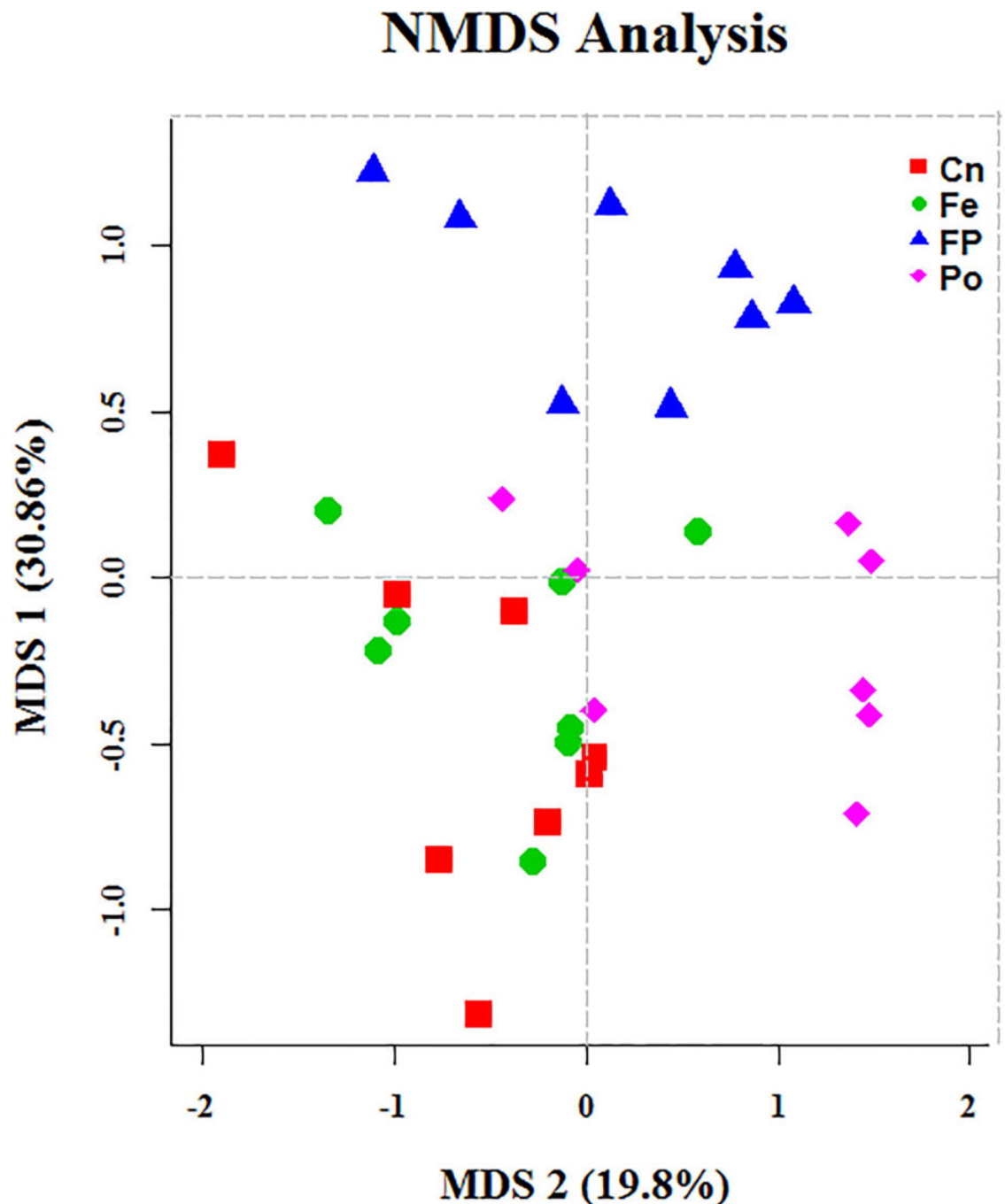


Fig 4. First two dimensions from the (non-metric) multi-dimensional scaling (NMDS) of the Bray-Curtis dissimilarity matrix. Each point in the figure represents a sample, the distance between points indicates the degree of difference, and the samples in the same group are represented by the same color.

<https://doi.org/10.1371/journal.pone.0237357.g004>

Erysipelotrichaceae_UCG-003, and *Sutterella* was significantly increased, and that of 7 genera, including *Bacillus*, *Coprococcus_2*, *Sporolactobacillus*, *Alkaliphilus*, *Aequorivita*, *Asteroleplasma*, and *Sphingobacterium* was significantly decreased in the Po group (S17 Table). At the species level, a total of 8 species displayed a significant difference in relative abundance

Table 1. Significant differences in community structure in the jejunal microbiota of between different groups.

Group	Anosim		MRPP			
	R value	P value	A value	Observed delta	Expected delta	P value
Cn-Fe	0.139	0.045	0.024	0.607	0.622	0.031
Cn-FP	0.239	0.004	0.033	0.618	0.639	0.018
Cn-Po	0.253	0.005	0.036	0.632	0.655	0.01
Fe-FP	0.387	0.003	0.057	0.584	0.619	0.009
Fe-Po	0.436	0.004	0.069	0.597	0.642	0.004
FP-Po	0.165	0.05	0.028	0.608	0.626	0.038

<https://doi.org/10.1371/journal.pone.0237357.t001>

between the Cn and FP groups. Among them, the abundance of *Clostridiales_bacterium_NK3B98*, *Lactobacillus_phage_Sal3*, *Bacteroides_vulgatus*, and *Eubacterium_tortuosum* was increased, and that of *Mycoplasma_gallinarum*, *Acinetobacter_lwoffii*, *Gallibacterium_anatis*, and *Asteroleplasma_anaerobium* was decreased (S18 Table). A total of 6 species displayed a significant difference in relative abundance between the Cn and Po groups. Among them, the abundance of *Methanogenic_archaeon_CH1270*, *Clostridiales_bacterium_60-7e*, and *Lactobacillus_phage_Sal3* was increased, and that of *Mycoplasma_gallinarum*, *Asteroleplasma_anaerobium*, and *Brevundimonas_diminuta* was decreased (S19 Table).

Correlation between intestinal microbiota and histomorphology of jejunum

To further identify the genera that significantly correlated with the jejunum histomorphology, we performed Pearson's correlation test. Results showed that the villus height of the jejunum of Xuefeng black-bone chicken displayed a strong positive correlation with the relative abundance of *Coprococcus_1*, *Odoribacter*, and *Butyricicoccus* ($P = 0.02$, $P = 0.01$, and $P = 0.05$, respectively) and a negative correlation with that of *Coprococcus_2* ($P = 0.008$) (Fig 5). The crypt depth of the

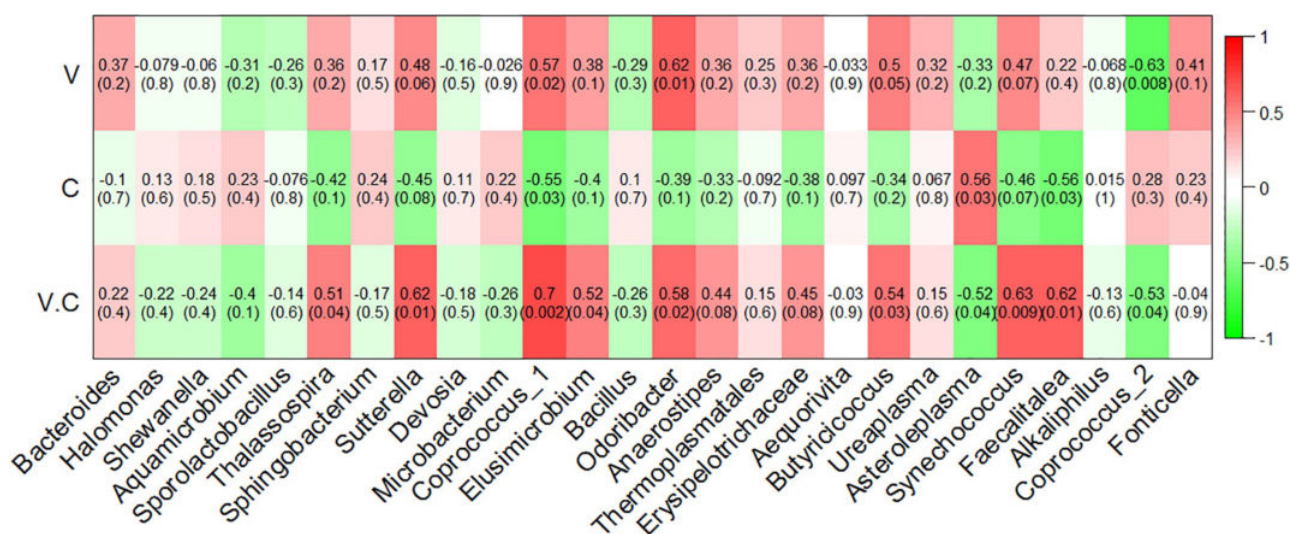


Fig 5. Correlation analyses of genera taxa with the villus height, crypt depth, and the ratio of villus height to crypt depth in the jejunum of broiler chickens. Each cell contains the corresponding correlation and P-value. The table is color-coded by correlation according to the color legend. V, the villus height; C, the crypt depth; V.C, the ratio of villus height to crypt depth.

<https://doi.org/10.1371/journal.pone.0237357.g005>

jejunum of Xuefeng black-bone chicken showed a positive correlation with the relative abundance of *Asteroleplasma* ($P = 0.03$), and a negative correlation with that of *Coproccoccus_1* ($P = 0.03$) and *Faecalitalea* ($P = 0.03$) (Fig 5). The relative abundance of *Thalassospira*, *Sutterella*, *Coproccoccus_1*, *Elusimicrobium*, *Odoribacter*, *Butyricicoccus*, *Synechococcus*, and *Faecalitalea* was positively correlated with the ratio of villus height to crypt depth of the jejunum of Xuefeng black-bone chicken ($P = 0.04$, $P = 0.01$, $P = 0.002$, $P = 0.04$, $P = 0.02$, $P = 0.03$, $P = 0.009$, and $P = 0.01$, respectively). However, the ratio of villus height to crypt depth was negatively correlated with the relative abundance of *Asteroleplasma* ($P = 0.04$) and *Coproccoccus_2* ($P = 0.04$) (Fig 5). At the species level, the villus height of the jejunum of Xuefeng black-bone chicken showed a slight positive correlation with the relative abundance of *Clostridiales_bacterium_60-7e* ($P = 0.07$) and a negative correlation with that of *Mycoplasma_gallinarum* ($P = 0.04$) (S2 Fig). The crypt depth of the jejunum of Xuefeng black-bone chicken was positively correlated with the relative abundance of *Asteroleplasma_anaerobium* ($P = 0.03$), and negatively correlated with that of *Bacteroides_vulgatus* ($P = 0.05$) and *Eubacterium_tortuosum* ($P = 0.03$) (S2 Fig). The ratio of villus height to crypt depth showed a positive correlation with the relative abundance of *Bacteroides_vulgatus* ($P = 0.01$) and *Eubacterium_tortuosum* ($P = 0.01$), and a negative correlation with that of *Asteroleplasma_anaerobium* ($P = 0.04$) (S2 Fig).

Discussion

The primary function of the small intestine is the digestion and absorption of nutrients by the intestinal mucosa [27]. Its function is closely related to the villus height, crypt depth, and villus height to crypt depth ratio. A previous study reported that changes in the intestinal morphology, such as increased villus height and villus height to crypt depth ratio, and shallow crypts indicate enhanced digestion and absorption in the small intestine [28]. Consistent with our findings, several studies have shown that dietary supplementation of fermented feed with probiotics significantly improves intestinal morphology [29], and increases the villus height, crypt depth, and villus height to crypt depth ratio in the jejunum of broilers [30, 31]. In this study, we demonstrated that the Fe group displayed significantly increased villus height and villus height to crypt depth ratio, and decreased crypt depth in the jejunum ($P < 0.05$). This may be caused by fermentation of metabolites, including organic acids, amino acids, small peptides, and other substances, which improves the nutritional status of the intestine as well as intestinal morphology [32]. Additionally, we found that the Po group displayed slightly increased villus height, significantly increased villus height to crypt depth ratio, and significantly reduced crypt depth. This finding is in agreement with the results of Zahran et al. [32], who showed that dietary supplementation of astragalus polysaccharides caused a significant increase in the intestinal villus height in tilapia fish. Wang et al. [33] demonstrated that Sargassum fusiforme polysaccharides affect intestinal parameters, such as the ratio of villus height to crypt depth in mice. This may be caused by polysaccharides that are herbal plants with important biological activities to improve intestinal development [34]. Interestingly, in our study, compared to the Cn group, the FP group showed increased villus height, shallow crypt depth, and higher villus height to crypt depth ratio in the jejunum ($P < 0.05$). However, there is currently no information on the effect of fermented feed and ginseng polysaccharides on the intestinal structure of broiler chickens, and hence, further research is required.

Next, we characterized the microbial composition of the intestinal contents of 32 Xuefeng black-bone chickens. A total of 2,245,803 high quality valid tags were obtained across all samples, and the sequence size of each sample ranged from 49,767 to 80,545, which was greater than that reported in previous studies on broilers [35]. The Chao1 index indicated

that this sequencing depth was sufficient for further analysis. Cluster analysis revealed that *Firmicutes* was the most dominant phyla among the total sequences. This finding is consistent with that of a study conducted by Wu et al. [36]. However, the functions of the phyla require further research. Additionally, in this study, the composition and structure of the gut microbial community was altered in the FP and Po groups. At the genus level, the FP and Po groups displayed significantly increased abundance of *Sutterella* and decreased abundance of *Asteroleplasma*. Interestingly, we found that the bacterial abundance of *Sutterella* was positively correlated to the villus height and villus height to crypt depth ratio, and negatively correlated to the crypt depth. In contrast, the bacterial abundance of *Asteroleplasma* was positively correlated to the crypt depth and negatively correlated to the villus height to crypt depth ratio. A previous study reported that the members of the genus *Sutterella* are widely prevalent in the human gastrointestinal tract, and their deficiency alters the colonic microbiota, resulting in disruption of the normal function of the colonic epithelium and inflammatory bowel disease [37, 38]. Min et al. [39] reported that an increase in the abundance of *Asteroleplasma* resulted in intestinal inflammation and other colonic epithelium diseases. At the species level, we discovered that the FP group showed significantly increased abundance of *Bacteroides_vulgatus* and *Eubacterium_tortuosum* and decreased abundance of *Mycoplasma_gallinarum* and *Asteroleplasma_anaerobium*. However, the abundance of *Mycoplasma_gallinarum* and *Asteroleplasma_anaerobium* was increased in the Po group, which may be because the combined effect of polysaccharides and fermented feeds is stronger than that of polysaccharides alone. Additionally, we found that the bacterial abundance of *Mycoplasma_gallinarum* was negatively correlated with the intestinal villus height. The crypt depth was positively correlated with the relative abundance of *Asteroleplasma_anaerobium*, and negatively correlated with that of *Bacteroides_vulgatus* and *Eubacterium_tortuosum*. However, the ratio of villus height to crypt depth was positively correlated with the relative abundance of *Bacteroides_vulgatus* and *Eubacterium_tortuosum*, and negatively correlated with that of *Asteroleplasma_anaerobium*. A previous study showed that an increase in the abundance of *Asteroleplasma_anaerobium* resulted in loss of pyruvate kinase activity, which slows glucose metabolism, thus hindering intestinal development, and an increase in the abundance of *Mycoplasma_gallinarum* resulted in intestinal inflammation and respiratory disease [40]. Previous studies have also reported that the relative abundance of *Bacteroides_vulgatus* is negatively correlated with inflammatory bowel disease [41]. Waidmann et al. [42] showed that an abundance of *Bacteroides_vulgatus* protected against *Escherichia coli*-induced colitis in gnotobiotic interleukin-2-deficient mice. Additionally, Tadayon et al. [43] reported that deficiency of *Eubacterium_tortuosum* caused suppurative inflammation of the intestine. Based on the above findings, we proposed a hypothesis that FP and Po might improve intestinal morphology by altering the microbial communities. However, further in-depth research is needed to confirm this hypothesis.

Conclusions

The results of the present study indicated that the Fe, FP, or Po groups showed improved intestinal morphology, including increased villus height and villus height to crypt depth ratio, and decreased crypt depth of the jejunum of Xuefeng black-bone chicken. Additionally, we also compared the intestinal microbial composition of Xuefeng black-bone chicken among the FP and Po groups. Moreover, they are closely related to the histomorphological characteristics of chicken jejunum, including villus height, crypt depth, and villus height to crypt depth ratio. Therefore, a combination of ginseng polysaccharides and microbial

fermented feeds or ginseng polysaccharide alone can be used as a new, effective alternative to antibiotics for improving intestinal morphology. However, further in-depth research is required to reveal the underlying mechanisms.

Supporting information

S1 Fig. Rarefaction curves. Number of sequences (A) and number of sample (B) rarefaction curves for the sampled jejunum microbiotas. Number of detected OTUs on the y-axis; number of sequences (A) and of samples (B) on the x-axis.

(PDF)

S2 Fig. Correlation analyses of species taxa with the villus height, crypt depth, and the ratio of villus height to crypt depth in the jejunum of broiler chickens.

(PDF)

S1 Table. Basic diet formulations and nutrient composition.

(DOCX)

S2 Table. Quality control and preprocessing of metagenomic datasets.

(XLSX)

S3 Table. Sequence composition of each sample at each level in the Greengenes database.

(XLSX)

S4 Table. The aligned counts that were annotated at the phylum level.

(XLSX)

S5 Table. The aligned percentages that were annotated at the phylum level.

(XLSX)

S6 Table. The aligned counts that were annotated at the class level.

(XLSX)

S7 Table. The aligned percentages that were annotated at the class level.

(XLSX)

S8 Table. The aligned counts that were annotated at the order level.

(XLSX)

S9 Table. The aligned percentages that were annotated at the order level.

(XLSX)

S10 Table. The aligned counts that were annotated at the family level.

(XLSX)

S11 Table. The aligned percentages that were annotated at the family level.

(XLSX)

S12 Table. The aligned counts that were annotated at the genus level.

(XLSX)

S13 Table. The aligned percentages that were annotated at the genus level.

(XLSX)

S14 Table. The aligned counts that were annotated at the species level.

(XLSX)

S15 Table. The aligned percentages that were annotated at the species level.
(XLSX)

S16 Table. Significant differences between the Cn and FP groups identified at the genus-taxa level.
(XLSX)

S17 Table. Significant differences between the Cn and Po groups identified at the genus-taxa level.
(XLSX)

S18 Table. Significant differences between the Cn and FP groups identified at the species-taxa level.
(XLSX)

S19 Table. Significant differences between the Cn and Po groups identified at the species-taxa level.
(XLSX)

Author Contributions

Data curation: Jiajie Sun.

Formal analysis: Jiajie Sun.

Investigation: Jie Liu, Huan Wang.

Project administration: Junyi Luo, Ting Chen, Qianyun Xi, Yongliang Zhang, Jiajie Sun.

Supervision: Jiajie Sun.

Writing – original draft: Yueqin Xie, Jiajie Sun.

Writing – review & editing: Jiajie Sun.

References

1. Mingmongkolchai S, Panbangred W. Bacillus probiotics: an alternative to antibiotics for livestock production. *Journal of Applied Microbiology*. 2018; 124: 1334–1346. <https://doi.org/10.1111/jam.13690> PMID: [29316021](#)
2. Castanon JIR. History of the use of antibiotic as growth promoters in European poultry feeds. *Poultry science*. 2007; 86: 2466–2471. <https://doi.org/10.3382/ps.2007-00249> PMID: [17954599](#)
3. Cheng G, Hao H, Xie S, Wang X, Dai M, Huang L, et al. Antibiotic alternatives: the substitution of antibiotics in animal husbandry? *Frontiers in Microbiology*. 2014; 5: 69–83. <https://doi.org/10.3389/fmicb.2014.00069> PMID: [24624122](#)
4. Yun W, Lee DH, Choi YI, Kim IH, Cho JH. Effects of supplementation of probiotics and prebiotics on growth performance, nutrient digestibility, organ weight, fecal microbiota, blood profile, and excreta noxious gas emissions in broilers. *Journal of Applied Poultry Research*. 2017; 26: 584–592. <https://doi.org/10.3382/japr/pfx033>
5. Park SH, Choi JS, Jung DS, Auh JH, Choi YI. Effects of complex probiotics and antibiotics on growth performance and meat quality in broilers. *Korean journal for food science of animal resources*. 2010; 30: 504–511. <https://doi.org/10.5851/kosfa.2010.30.3.504>
6. Zhang ZF, Kim IH. Effects of multistrain probiotics on growth performance, apparent ileal nutrient digestibility, blood characteristics, cecal microbial shedding, and excreta odor contents in broilers. *Poultry science*. 2014; 93: 364–370. <https://doi.org/10.3382/ps.2013-03314> PMID: [24570458](#)
7. Jamshidparvar A, Javandel F, Seidavi A, Blanco FP, Marín ALM, Ramírez CA, et al. Effects of golpar (*Heracleum persicum* Desf.) and probiotics in drinking water on performance, carcass characteristics, organ weights, blood plasma constituents, and immunity of broilers. *Environmental science and pollution research*. 2017; 24: 23571–23577. <https://doi.org/10.1007/s11356-017-9983-4> PMID: [28852951](#)

8. Wang J, Li Y, Luo P, Chen Y, Xi Q, Wu H, et al. Oral supplementation with ginseng polysaccharide promotes food intake in mice. *Brain and Behavior*. 2019; 9: e01340. <https://doi.org/10.1002/brb3.1340> PMID: [31392839](#)
9. Akhter KF, Mumin MA, Lui EM, Charpentier PA. Fabrication of fluorescent labeled ginseng polysaccharide nanoparticles for bioimaging and their immunomodulatory activity on macrophage cell lines. *International Journal of Biological Macromolecules Structure Function & Interactions*. 2018; 109: 254–262.
10. Yan L, Meng QW, Lee JH, Wang JP, Kim IH. Effects of dietary wild-ginseng adventitious root meal on growth performance, blood profiles, relative organ weight and meat quality in broiler chickens. *Asian Australasian Journal of Animal sciences*. 2010; 24: 258–263. <https://doi.org/10.5713/ajas.2011.10222>
11. Zhao X, Wang Y, Ren Z, Zhang Z, Luo Y, Zhang C. Effect of Probiotics Substituted for Antibiotics on the Performance of Broilers. *China Poultry*. 2011; 33: 29–31.
12. Liu XL, Xi QY, Yang L, Li HY, Jiang QY, Shu G, et al. The effect of dietary Panax ginseng polysaccharide extract on the immune responses in white shrimp, *Litopenaeus vannamei*. *Fish & shellfish immunology*. 2011; 30(2): 495–500. <https://doi.org/10.1016/j.fsi.2010.11.018> PMID: [21129487](#)
13. Thompson KL, Applegate TJ. Feed withdrawal alters small-intestinal morphology and mucus of broilers. *Poultry science*. 2006; 85: 1535–1540. <https://doi.org/10.1093/ps/85.9.1535> PMID: [16977838](#)
14. Jiang RR, Zhao GP, Chen JL, Zheng MQ, Zhao JP, Li P, et al. Effect of dietary supplemental nicotinic acid on growth performance, carcass characteristics and meat quality in three genotypes of chicken. *Journal of animal physiology and animal nutrition*. 2011; 95: 137–145. <https://doi.org/10.1111/j.1439-0396.2010.01031.x> PMID: [20666866](#)
15. Jiang S, Mohammed AA, Jacobs JA, Cramer TA, Cheng HW. Effect of synbiotics on thyroid hormones, intestinal histomorphology, and heat shock protein 70 expression in broiler chickens reared under cyclic heat stress. *Poultry Science*. 2019; <https://doi.org/10.3382/ps/pez571>
16. Samuel KG, Wang J, Yue HY, Wu SG, Zhang HJ, Duan ZY, et al. Effects of dietary gallic acid supplementation on performance, antioxidant status, and jejunum intestinal morphology in broiler chicks. *Poultry Science*. 2017; 96: 2768–2775. <https://doi.org/10.3382/ps/pex091> PMID: [28521034](#)
17. Sun J, Zeng B, Chen Z, Yan S, Huang W, Sun B, et al. Characterization of faecal microbial communities of dairy cows fed diets containing ensiled *Moringa oleifera* fodder. *Scientific Reports*. 2017; 7: 41403. <https://doi.org/10.1038/srep41403> PMID: [28134261](#)
18. Martin M. Cutadapt removes adapter sequences from high-throughput sequencing reads. *EMBnet Journal*. 2011; 17: 10–12. <https://doi.org/10.14806/ej.17.1.200>
19. Quast C, Pruesse E, Yilmaz P, Gerken J, Schweer T, Yarza P, et al. The SILVA ribosomal RNA gene database project: improved data processing and web-based tools. *Nucleic Acids Research*. 2012; 41: D590–D596. <https://doi.org/10.1093/nar/gks1219> PMID: [23193283](#)
20. Edgar RC, Haas BJ, Clemente JC, Quince C, Knight R. UCHIME improves sensitivity and speed of chimera detection. *Bioinformatics*. 2011; 27: 2194–2200. <https://doi.org/10.1093/bioinformatics/btr381> PMID: [21700674](#)
21. Haas BJ, Gevers D, Earl AM, Feldgarden M, Ward DV, Giannoukos G, et al. Chimeric 16S rRNA sequence formation and detection in Sanger and 454-pyrosequenced PCR amplicons. *Genome Research*. 2011; 21: 494–504. <https://doi.org/10.1101/gr.112730.110> PMID: [21212162](#)
22. Edgar RC. UPARSE: highly accurate OTU sequences from microbial amplicon reads. *Nature Methods*. 2013; 10: 996. <https://doi.org/10.1038/nmeth.2604> PMID: [23955772](#)
23. Edgar RC. MUSCLE: multiple sequence alignment with high accuracy and high throughput. *Nucleic Acids Research*. 2004; 32: 1792–1797. <https://doi.org/10.2460/ajvr.69.1.82> PMID: [18167091](#)
24. White JR, Nagarajan N, Pop M. Statistical methods for detecting differentially abundant features in clinical metagenomic samples. *PLoS Computational Biology*. 2009; 5: e1000352. <https://doi.org/10.1371/journal.pcbi.1000352> PMID: [19360128](#)
25. Clarke KR, Ainsworth M. A method of linking multivariate community structure to environmental variables. *Marine Ecology Progress Series*. 1993; 92: 205–205. <https://doi.org/10.3354/meps092205>
26. Xia Y, Sun J. Hypothesis testing and statistical analysis of microbiome. *Genes & diseases*. 2017; 4: 138–148. <https://doi.org/10.1016/j.gendis.2017.06.001> PMID: [30197908](#)
27. Montagne L, Pluske JR, Hampson DJ. A review of interactions between dietary fibre and the intestinal mucosa, and their consequences on digestive health in young non-ruminant animals. *Animal Feed Science and Technology*. 2003; 108: 95–117. [https://doi.org/10.1016/s0377-8401\(03\)00163-9](https://doi.org/10.1016/s0377-8401(03)00163-9)
28. Pirarat N, Pinpimai K, Endo M, Katagiri T, Ponpornpisit A, Chansue N, et al. Modulation of intestinal morphology and immunity in Nile tilapia (*Oreochromis niloticus*) by *Lactobacillus rhamnosus* GG. *Research in Veterinary Science*. 2011; 91: e92–e97. <https://doi.org/10.1016/j.rvsc.2011.02.014> PMID: [21536310](#)

29. Jayaraman S, Thangavel G, Kurian H, Mani R, Mukkalil R, Chirakkal H. *Bacillus subtilis* PB6 improves intestinal health of broiler chickens challenged with *Clostridium perfringens*-induced necrotic enteritis. *Poultry Science*. 2013; 92: 370–374. <https://doi.org/10.3382/ps.2012-02528> PMID: 23300303
30. Aliakbarpour HR, Chamani M, Rahimi G, Sadeghi AA, Qujeq D. The *Bacillus subtilis* and lactic acid bacteria probiotics influences intestinal mucin gene expression, histomorphology and growth performance in broilers. *Asian-Australasian Journal of Animal Sciences*. 2012; 25: 1285–1293. <https://doi.org/10.5713/ajas.2012.12110> PMID: 25049692
31. Long SF, Xu YT, Pan L, Wang QQ, Wang CL, Wu JY, et al. Mixed organic acids as antibiotic substitutes improve performance, serum immunity, intestinal morphology and microbiota for weaned piglets. *Animal Feed Science and Technology*. 2018; 235: 23–32. <https://doi.org/10.1016/j.anifeedsci.2017.08.018>
32. Zahran E, Risha E, AbdelHamid F, Mahgoub HA, Ibrahim T. Effects of dietary *Astragalus polysaccharides* (APS) on growth performance, immunological parameters, digestive enzymes, and intestinal morphology of Nile tilapia (*Oreochromis niloticus*). *Fish & Shellfish Immunology*. 2014; 38: 149–157. <https://doi.org/10.1016/j.fsi.2014.03.002> PMID: 24657260
33. Wang W, Lu JB, Wang C, Wang CS, Zhang HH, Li CY, et al. Effects of *Sargassum fusiforme* polysaccharides on antioxidant activities and intestinal functions in mice. *International Journal of Biological Macromolecules*. 2013; 58: 127–132. <https://doi.org/10.1016/j.ijbiomac.2013.03.062> PMID: 23567289
34. Liu HW, Tong JM, Zhou DW. Utilization of Chinese herbal feed additives in animal production. *Agricultural Sciences in China*. 2011; 10: 1262–1272.
35. Wu W, Xiao Z, An W, Dong Y, Zhang B. Dietary sodium butyrate improves intestinal development and function by modulating the microbial community in broilers. *PloS One*. 2018; 13: e0197762. <https://doi.org/10.1371/journal.pone.0197762> PMID: 29795613
36. Hiiipala K, Kainulainen V, Kalliomäki M, Arkkila P, Satokari R. Mucosal prevalence and interactions with the epithelium indicate commensalism of *Sutterella* spp. *Frontiers in Microbiology*. 2016; 7: 1706. <https://doi.org/10.3389/fmicb.2016.01706> PMID: 27833600
37. Wang L, Christophersen CT, Sorich MJ, Gerber JP, Angley MT, Conlon MA. Increased abundance of *Sutterella* spp. and *Ruminococcus torques* in feces of children with autism spectrum disorder. *Molecular Autism*. 2013; 4: 42. <https://doi.org/10.1186/2040-2392-4-42> PMID: 24188502
38. Min BR, Perkins D, Wright C, Dawod A, Min BJ, Terrill TH, et al. Effects of feeding two different tannin-containing diets on ruminal fermentation profiles and microbial community changes in meat goats. *Agriculture, Food and Analytical Bacteriology*. 2015; 5: 153–165.
39. Hackmann TJ, Ngugi DK, Firkins JL, Tao J. Genomes of rumen bacteria encode atypical pathways for fermenting hexoses to short-chain fatty acids. *Environmental Microbiology* 2017; 19: 4670–4683. <https://doi.org/10.1111/1462-2920.13929> PMID: 28892251
40. Kleven SH. Mycoplasmas in the etiology of multifactorial respiratory disease. *Poultry Science*. 1998; 77: 1146–1149. <https://doi.org/10.1093/ps/77.8.1146> PMID: 9706080
41. Fujita H, Eishi Y, Ishige I, Saitoh K, Takizawa T, Arima T, et al. Quantitative analysis of bacterial DNA from *Mycobacteria* spp., *Bacteroides vulgatus*, and *Escherichia coli* in tissue samples from patients with inflammatory bowel diseases. *Journal of Gastroenterology*. 2002; 37: 509–516. <https://doi.org/10.1007/s005350200079> PMID: 12162408
42. Waidmann M, Bechtold O, Frick JS, Lehr HA, Schubert S, Dobrindt U, et al. *Bacteroides vulgatus* protects against *Escherichia coli*-induced colitis in gnotobiotic interleukin-2-deficient mice. *Gastroenterology*. 2003; 125: 162–177. [https://doi.org/10.1016/s0016-5085\(03\)00672-3](https://doi.org/10.1016/s0016-5085(03)00672-3) PMID: 12851881
43. Tadayon RA, Cheema AH, Muhammed SI. Microorganisms associated with abscesses of sheep and goats in the south of Iran. *American Journal of Veterinary Research*. 1980; 41: 798–802. <https://doi.org/10.1007/s10592-007-9378-z> PMID: 6996545



Article

Identification of circRNA-Associated-ceRNA Networks Involved in Milk Fat Metabolism Under Heat Stress

Dongyang Wang [†], Zujing Chen [†], Xiaona Zhuang, Junyi Luo, Ting Chen, Qianyun Xi, Yongliang Zhang ^{*} and Jiajie Sun ^{*}

College of Animal Science, Guangdong Provincial Key Laboratory of Animal Nutrition Control, Guangdong Engineering & Research Center for Woody Fodder Plants, National Engineering Research Center for Breeding Swine Industry, South China Agricultural University, Guangzhou 510642, Guangdong, China; wangdy@stu.scau.edu.cn (D.W.); zujingchen@scau.edu.cn (Z.C.); zhuangxn@stu.scau.edu.cn (X.Z.); luojunyi@scau.edu.cn (J.L.); allinchen@scau.edu.cn (T.C.); xqy0228@scau.edu.cn (Q.X.)

^{*} Correspondence: zhangyl@scau.edu.cn (Y.Z.); jiajiesun@scau.edu.cn (J.S.)

[†] These authors contributed equally to this work.

Received: 7 May 2020; Accepted: 9 June 2020; Published: 11 June 2020



Abstract: Summer temperatures are generally high in Southern China, and cows are likely to suffer a heat stress reaction. Heat stress will have a negative impact on the performance of dairy cows; however, the mechanism by which high temperature affects lactation is not clear. CircRNA is a type of non-coding RNA discovered in recent years, which performs a crucial function in many biological activities. However, the effects of circRNA on lactation function of dairy cows under heat stress is unknown. The present study aimed to explore the expression levels of circRNA in the mammary gland tissue of cows under heat stress. Firstly, we collected blood and milk samples of summer and winter cows and evaluated lactation performance using serum indicators, milk production, and milk composition. Incorporating the calculation of the temperature and humidity index, we conformed the heat stress status of cows in summer. Heat stress increased the concentration of HSP70 and decreased the concentration of SOD and PRL. Heat stress not only reduced milk yield but also affected milk quality, with milk lactose and milk protein decreasing with increased temperature. The analysis of the fatty acid composition in summer milk found significantly reduced concentrations of unsaturated fatty acids, especially long-chain unsaturated fatty acids. Sequencing of the cow's mammary gland transcriptome revealed that compared to the appropriate temperature (ST) group, the heat stress (HS) group had a total of 2204 upregulated and 3501 downregulated transcripts. GO enrichment and KEGG pathway analysis showed that these genes were mainly related to milk fat metabolism. In addition, 19 upregulated and 19 downregulated circRNA candidates were found in response to heat stress. We used Pearson's test to establish the correlation of circRNA-mRNA and identified four pairs of circRNA-miRNA networks between four circRNAs, six miRNAs, and the CD36 gene. In this study, we revealed the possible role of circRNAs in lactation of dairy cows and identified that circRNA-miRNA-mRNA networks might exist in the cow's mammary glands, providing valuable experience for dairy lactation and milk quality.

Keywords: heat stress; milk fat; ceRNA; CD36

1. Introduction

As global temperatures rise [1], the hotter climate has become one of the main challenges for agriculture in this century, which affects the survival, growth, and reproduction of animals [2]. Their increased generation of metabolic heat means that high-yielding animals are extremely susceptible

to heat stress in summer [3], which has caused huge economic losses to the livestock industry (about 2 billion per year in the United States) [4].

As one of the best foods for humans, milk has extremely high nutritional value. It not only contains most nutrients but also is a good source of many essential amino acids [5]. Dairy cows are intrinsically heat-tolerant; however, they can be susceptible to heat stress, which could result in significant decreases in milk production and milk quality [6]. Most studies have found that heat stress is associated with a decline in milk quality [7]. There has been a decrease in milk yield by 40% and in milk protein content by 4.8% in cows exposed to heat stress [8]. Compared with other seasons, milk protein content in summer reduces by 6% [7].

These large losses have resulted in extensive studies on the effects of heat stress on lactating cows [9]. According to the traditional concept, the reduced production performance of dairy cows during heat stress is closely related to decreased feed intake [10,11]. However, a series of recent studies have shown that the reduction in nutritional intake during heat stress accounts for only 35 to 50% of the reduction in milk synthesis [12,13]. Heat stress might directly affect milk production through unknown mechanisms unrelated to reduced intake, which might affect the expression of lactation genes by regulating hormone levels in cows [14]. Heat stress might increase the body's gluconeogenesis, in which the catabolism of amino acids occurs to provide energy, and the supply of protein synthesis precursors is inadequate, which leads to a reduction in the content of milk protein [15,16].

Previously, changes in hormones [17] and their cellular levels [18] were believed to explain the effect of heat stress on the performance of dairy cows. Few studies have focused on the changes of ncRNA. CircRNA is a type of ncRNA discovered in recent years. It exists in large amounts in animals and plays an important role in the growth and development of animals [19,20]. CircRNA can act as miRNA sponges to regulate the transcription and splicing of parent genes and can be converted into peptides or proteins [21]. Increasing evidence shows that circRNA is involved in the most basic process of cells [22], and that heat stress can affect circRNA biosynthesis [23]; however, little is known about how circRNA regulates milk synthesis under heat stress. In the present study, we focused on the changes in circRNA levels of the mammary gland in lactating cows under heat stress and further explored the potential mechanism of circRNA-mediated regulation of milk synthesis in mammary tissue.

2. Results

2.1. The Performances of Dairy Cows under Heat Stress

We conducted the study during December 2018 and August 2019, respectively. In the two experimental groups, there was a difference between the THI index formed by ambient temperature and humidity ($p < 0.01$). The THI index in winter was significantly lower than 72, while the THI index in summer was significantly higher than 72 (Figure 1A). By measuring the physiological indicators of the cows, we observed that their respiration rate in summer was increased ($p < 0.01$; Figure 1B), and their rectal temperature in summer was higher than that in winter ($p < 0.01$; Figure 1B). The changes in stress-related hormone levels in the serum of dairy cows are shown in Figure 1C. The results showed that the serum level of HSP70 was higher in the heat stress (HS) group than in the appropriate temperature (ST) group ($p < 0.01$), and there was no significant change in IgG levels. However, the levels of SOD and PRL in the serum of dairy cows in summer decreased compared with those in winter ($p < 0.05$; Figure 1C). Table 1 shows the effect of the environment on milk performance. Compared with those in winter, in summer, the milk production of cows and the levels of milk proteins, fat, and lactose all decreased significantly, and somatic cell numbers in milk increased significantly. The fatty acid profile of milk showed that the levels of C18:1n9c fatty acids and unsaturated fatty acids were significantly decreased in summer compared with those in winter (Table S1).

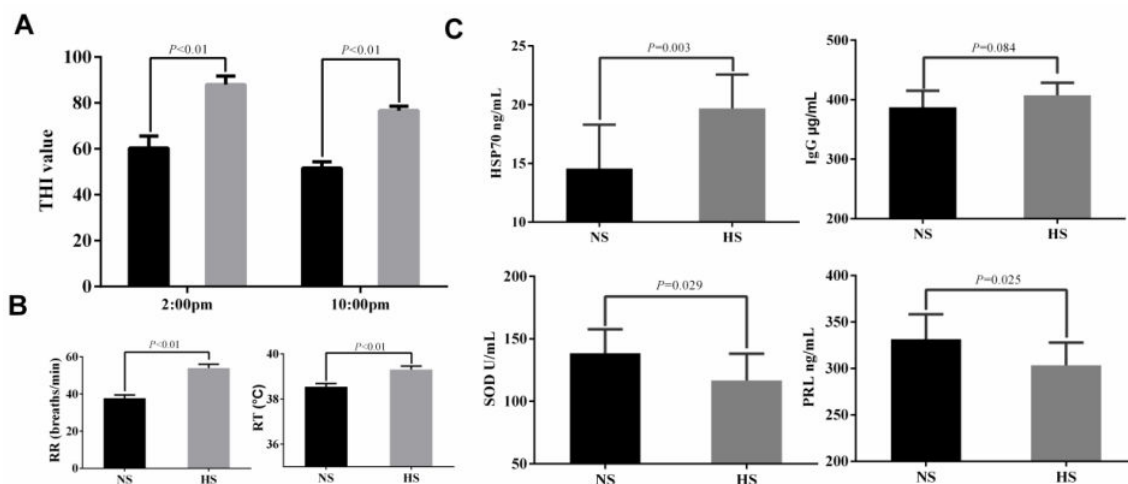


Figure 1. Heat stress-related indicators were identified during the experimental period. (A) changes in the temperature-humidity index at different times; (B) respiratory rate and rectal temperature of cows; (C) analysis of serum biochemical indices between different groups. ST, the appropriate temperature group; HS, heat stress group. Black histograms represent NS, and grey histograms represent HS.

Table 1. Milk yield and composition in dairy cows.

Item	NS	HS
Milk yield kg/day	22.83 ± 0.2251 ^A	19.06 ± 0.1643 ^B
Protein %	3.46 ± 0.0336 ^A	3.30 ± 0.0329 ^B
Fat %	3.71 ± 0.0352 ^A	3.55 ± 0.0253 ^B
Lactose %	4.69 ± 0.0292 ^a	4.58 ± 0.0318 ^b
Somatic cell counts 10 ⁴ /mL	30.47 ± 0.5833 ^B	37.83 ± 0.7445 ^A

ST, the appropriate temperature group; HS, heat stress group. a and b denote values that differ significantly at $p < 0.05$, and A and B denote values that differ significantly at $p < 0.01$.

2.2. RNA Sequencing and Transcript Analysis

We constructed six cDNA libraries from cow mammary tissue collected during summer and winter, and each RNA-seq library produced approximately 110.69 ± 5.11 million raw reads. After quality correction, each library contained approximately 103.14 ± 4.69 million effective reads, accounting for approximately 93.19% of the original reads. We compared all valid reads to the *Bos taurus* reference genome and found that about $83.79 \pm 1.24\%$ of the valid reads could be successfully mapped to the genome, with $79.53 \pm 1.82\%$ proper pair alignments in the six libraries (Table S2A). These results proved the successful construction of this library and confirmed its suitability for the subsequent analysis of the sequencing results. Among the candidate transcripts from all the libraries, there were 153,575 unigenes in six mammary libraries, including 33.48% of the transcripts that completely matched the Ensembl known regions (Table S2B). For the annotated transcripts, we identified a total of 38,434 candidates, and 29,718 unigenes were expressed in all tissues (Table S2C). Additionally, *CSN1S1*, *CSN2*, *CSN1S2*, *PAEP*, *CSN3*, *LALBA*, *RPLP1*, *RPL37*, *EEF1A1*, and *COX1* were the top 10 highly expressed genes across the libraries, which are well-known as having key functions in the lactation process. We then performed principal component analysis (PCA) using the FPKM values of the identified transcripts (Figure 2A), and the results showed that the differences caused by environmental factors between the groups were much larger than those between the experimental individuals. To filter out false-positive results, we only retained transcripts that were expressed in at least three libraries. Finally, the study retained 20,277 tags for further analysis (Table S3A). Compared with the ST population, we identified 5705 significantly differently expressed transcripts, including 2204 upregulated transcripts and 3501 downregulated transcripts in HS libraries vs. the ST libraries (Figure 2B). GO enrichment analysis of the differentially expressed transcripts showed that these candidates were significantly enriched in the biological process

of lipid metabolism-related functions (Table S3B), including ‘fatty acid beta-oxidation’, ‘fatty acid biosynthetic process’, ‘fatty acid beta-oxidation using acyl-CoA dehydrogenase’, ‘fatty acid metabolic process’, ‘lipid transport’, and ‘lipid homeostasis’ (Figure 2C). Among the differentially expressed transcripts, we identified 5428 genes that participated in 77 KEGG signaling pathways (Table S3C), including ‘prolactin signaling pathway’, ‘fatty acid metabolism’, ‘biosynthesis of unsaturated fatty acids’, and ‘PPAR signaling pathway’ (Figure 2C,D). Thus, the GO enrichment and KEGG pathway analysis provided some hints for the variabilities of milk fat content in cows under heat stress.

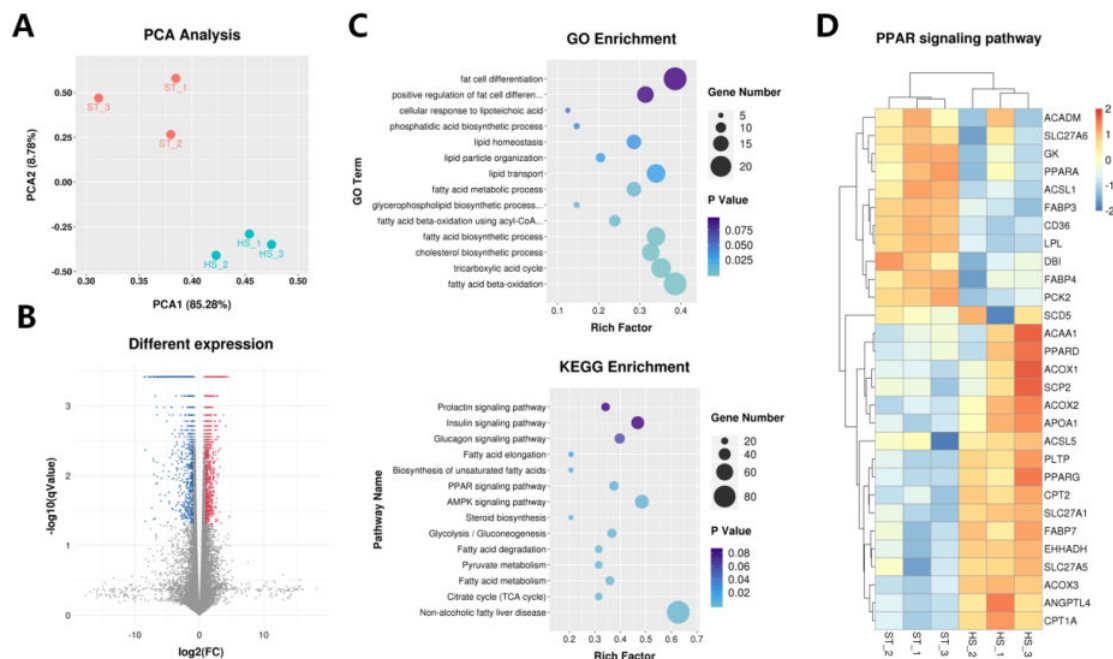


Figure 2. Transcriptome analysis of the mammary gland of dairy cows under heat stress. (A) principal component analysis of the whole transcripts in the mammary gland of dairy cows under heat stress; (B) volcano plot, showing significantly differentially expressed genes; (C) GO and KEGG analysis of differentially expressed genes; (D) heatmap, displaying the lactation-related gene identified in PPAR signaling pathway. ST, the appropriate temperature group; HS, heat stress group.

2.3. Identification of circRNAs

Based on anti-splicing reads generated from high-throughput RNA sequencing datasets, researchers have developed several tools to identify circular RNAs. In this paper, we used five different circular RNA prediction algorithms, which identified 61,175 unique circRNAs in the six libraries. A comparison of the prediction results demonstrated differences in the outputs of the five algorithms. Find_circ predicted the most circRNA types ($n = 44,330$), and MapSplice predicted the fewest ($n = 7719$). CIRCexplorer2, CircRNA_finder, and CIRI identified 27,565, 38,358, and 15,220 circRNAs, respectively (Table S4). To eliminate the possible errors in the algorithms, further analyses only used candidate circRNAs predicted by all five algorithms ($n = 2950$) (Figure 3A). These circularization events were produced from 1350 host loci, including 1600 transcripts that generated more than one circRNA (Table S5). Of the 2950 identified circRNAs, only 38 were differentially expressed between ST and HS individuals. Compared with the ST group, 19 circRNA candidates were upregulated, and 19 were downregulated (Figure 3B).

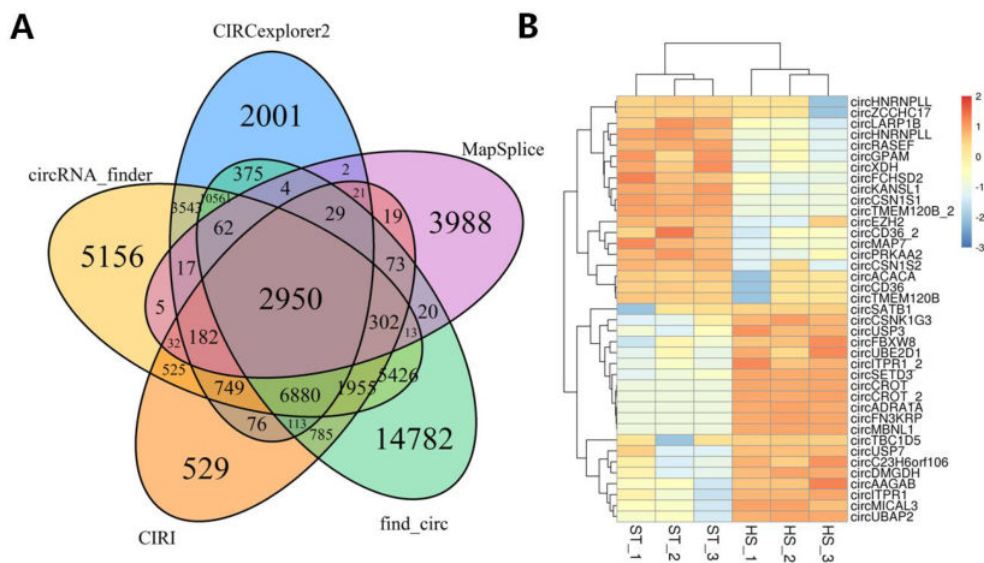


Figure 3. CircRNAome analysis of the mammary gland of dairy cows under heat stress. (A) Common circRNA candidates identified by all five approaches; (B) Heatmap, showing significantly differentially expressed circRNA candidates. ST, the appropriate temperature group; HS, heat stress group.

2.4. Functional Interactions between circRNAs and mRNAs

To discover the interactions between circRNA and mRNA expression, we firstly performed Pearson's tests on the 38 differentially expressed circRNAs and 29 PPAR pathway genes (Figure 2D). This analysis identified 255 significantly positively correlated circRNA-mRNA interactions with $p < 0.05$ and $R > 0.8$ (Table S6). In general, miRNAs play an important role in the processes of circRNA and mRNA interactions [21]. Among data deposited at the NCBI, we collected 23 bovine mammary gland libraries and identified 861 miRNAs (Table S7A). Next, we selected the 242 mammary-enriched miRNA candidates that were expressed in all libraries for further analysis (Table S7B). We then evaluated the putative interactions between differentially expressed circRNAs and PPAR pathway-related genes from this study for competitive binding with shared mammary-special miRNAs using the miRanda algorithm (<http://www.microrna.org/microrna/home.do>), with energies of ≤ -20.0 kcal/mol and no mismatch in the seed region. The analysis identified 427 circRNA-miRNA interactions (Table S8A) and 732 mRNA-miRNA interactions (Table S8B). Subsequently, we constructed 890 circRNA-miRNA-mRNA networks (Table S8C). Generally, almost all long-chain fatty acids are considered to be derived from diet digestion and absorption [24], and the expression levels of cluster of differentiation 36 (CD36) and solute carrier family 27 (SLC27) are stimulated for fatty acid uptake and transport during lactation [25]. In the present study, the expression levels of CD36 and SLC27A6 decreased significantly in response to heat stress. Moreover, CD36 expression was significantly and positively associated with the expression of 14 different circRNA candidates, while SLC27A6 was associated with eight candidates (Table S6). We constructed circRNA-miRNA-CD36 (SLC27A6) networks by pairing the shared miRNA recognition sequences. In detail, circRNA-miRNA-CD36 included 10 circRNAs (*circZCCHC17*, *circFCHSD2*, *circCD36_2*, *circMAP7*, *circKANSL1*, *circHNRNPLL*, *circCD36*, *circHNRNPLL_1*, *circRASEF*, and *circLARP1B*) and 16 miRNAs (miR-450b, miR-500, miR-6516, miR-2284a, miR-2284g, miR-2284y, miR-2285av, miR-2285cf, miR-2285cp, miR-2285cr, miR-2285db, miR-11986b, miR-345-3p, miR-502b, miR-218, and miR-378b), and the circRNA-miRNA-SLC27A6 network only contained *circCSN1S2* and miR-223 (Table S9).

2.5. Characterization of circRNA

To prove the circular structure of circRNA, we selected five highly expressed candidates (*circACACA*, *circCSN1S1*, *circEZH2*, *circPRKAA2*, and *circTMEM120B_2*) and 11 unique circRNAs that

were positively correlated with *CD36* and *SLC27A6* expression for further analysis. We designed a pair of divergent primers and convergent primers and then used cDNA or genomic DNA (gDNA) as a template for amplification. Generally, amplification was successful for both cDNA and gDNA templates using the convergent primers for the tested circRNAs. However, amplification using the divergent primers was successful for only nine candidates in cDNA but not genomic DNA (Figure 4A). We verified the junction sequences of the nine putative circRNAs using Sanger sequencing (Table S10A). Next, quantitative real-time reverse transcription PCR (qRT-PCR) analysis of the nine circRNAs and their parent genes was carried out, and we found that the expression levels of the circRNA candidates were not significantly changed between RNase R treated and mock groups. However, the mRNA expression levels of the host genes and *GAPDH* were different (Additional file 10B; Figure 4B). In addition, the results showed that these nine circRNA candidates were consistent between RT-qPCR and sequencing analysis between ST and HS groups (Table S11), suggesting that our estimation of abundance was accurate. In detail, the expression of these circRNAs was significantly downregulated in the HS group, except for *circKANSL1* and *circTMEM120B_2*. These two circRNAs showed to descend in the HS group, but no significant levels were detected.

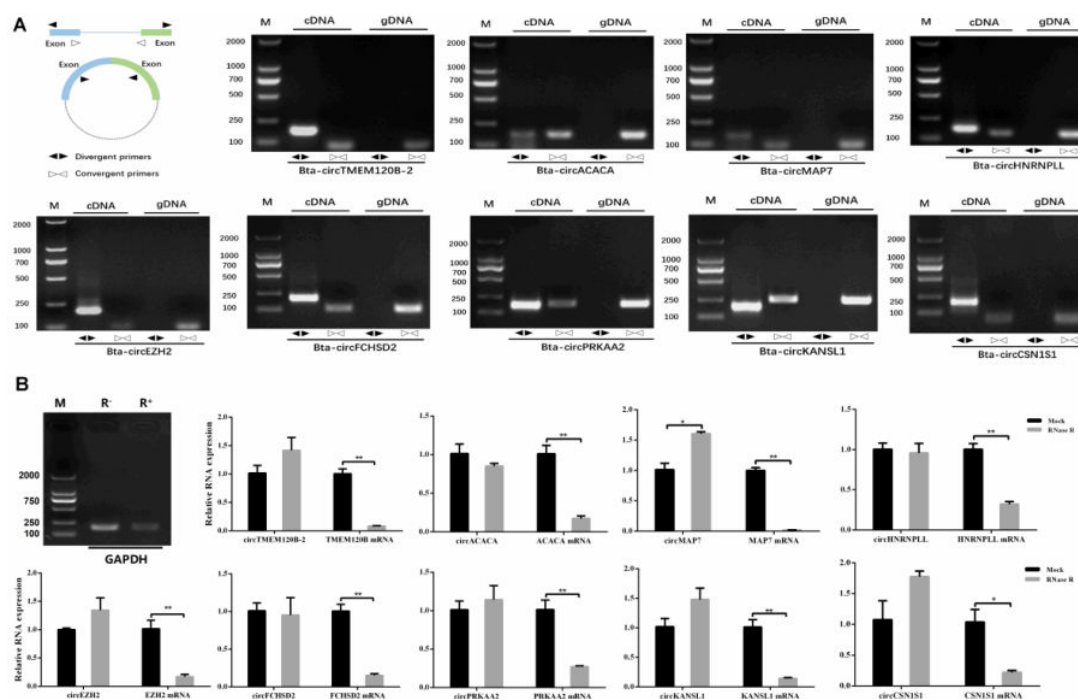


Figure 4. Characterization of circRNA candidates. (A) identification of circRNA candidates by divergent and convergent primers; Divergent primers amplify circRNA candidates in cDNA but not genomic DNA, and convergent primers amplify targets in both cDNA and genomic DNA. (B) RT-qPCR for the abundance of circRNA and their hosting mRNA treated with RNase R.

3. Discussion

As a typical heat-resistant animal, the appropriate feeding temperature for dairy cows is 5–25 °C. During the summer in southern China, the temperature is much higher, and cows are extremely sensitive to changes in warm environments because of their high metabolic rate. Therefore, cows are particularly vulnerable to heat stress [13]. Numerous studies have shown that THI can effectively identify whether cows are under heat stress. Usually, THI = 72 is used as a threshold for judging the heat stress status of cows. When THI is higher than 72, cows develop heat stress [26]. In the present study, the THI index in summer was higher than 72, indicating that the cows were in the state of heat stress. The THI index was lower than 72 in winter, and the cows were in good condition. As a constant temperature animal, cows need to control their body temperature within a certain range to maintain

normal metabolism; however, the balance of the body is disturbed by external factors, such as heat stress. When cows are in a heat stress state, the main way to reduce the adverse effects of heat stress is to accelerate heat dissipation to maintain their heat balance [27]. Cows increase heat dissipation mainly by increasing their respiration rate. When the heat cannot be dissipated completely, the cows' rectal temperature will increase [28]. Therefore, rectal temperature and the respiratory rate can be used as direct indicators to evaluate heat stress in dairy cows [29]. In the present study, the respiratory rate and rectal temperature in summer were significantly higher than those in winter, confirming that the cows were suffering from heat stress in summer.

Heat stress proteins exist widely in various tissues, and their expression level is low under normal conditions [30]. As an important molecular chaperone, HSP70 has anti-apoptosis, anti-oxidation, cell proliferation promotion, and immune regulatory functions [31]. When heat stress occurs, HSP70 can protect its tissue cells from the damage caused by adverse stress stimulation by increasing its synthesis, thus playing an important role in stress tolerance and protection [32]. Previous studies have found that heat stress can increase HSP70 levels in goats [33], chickens [34], and fruit flies [35], which is similar to the results in the present study. When the human body is in a state of heat stress, cell metabolism is accelerated, respiratory function is enhanced, and a large amount of reactive oxygen species is produced in the body [36]. Under normal circumstances, the free radicals metabolized by the body will be neutralized by the antioxidant system [37]. However, previous studies have found that heat stress can reduce the antioxidant capacity of the body, generating oxidative stress [38,39] and reducing immune function [40,41]. These results are consistent with the results of SOD reduction in this experiment. However, there was no significant change in IgG levels in this experiment, which might be caused by the self-regulation of chronic heat stress. Studies have found that heat stress reduces the serum concentration of PRL in dairy cows [42]. PRL is essential in mammary development and lactation [43]. Consistent with previous studies, our data showed that PRL levels in dairy cows decreased significantly under heat stress.

In the present study, we found that heat stress had a significant effect on milk yield. The output per cow in winter was as high as 22.83 ± 0.2251 kg/day, while during the heat stress period in summer, this was reduced markedly to 19.06 ± 0.1643 kg/day. Ravagnolo and Misztal [44] and Kadzere et al. [3] reported similar results. Under heat stress, cows' milk yield decreases by 10–30% [45]. Habeeba et al. analyzed the milk production of cows at ambient temperatures of 20, 30, and 40 °C and found that the milk yield at 30 and 40 °C decreased significantly by 14.7% and 55%, respectively [46]. Heat stress not only affects the milk yield of dairy cows but also changes its composition. With the increased temperature, the contents of milk yield and milk protein of dairy cows decrease rapidly [47]. Beede and Sheare found a negative correlation between milk fat levels and ambient temperature [48]. Goat milk has shown a similar trend, with a significant negative correlation between ambient temperature and the milk's physicochemical properties [49]. With the increase of ambient temperature, our study found that cows were in a state of heat stress and the levels of milk lactose, fat, and protein all declined, which was similar to the results of previous studies [50–52]. Excessive oxygen free radicals produced by the body during heat stress easily oxidize unsaturated fatty acids (especially polyunsaturated fatty acids); therefore, the content of saturated fatty acids in milk increases, while the content of unsaturated fatty acids decreases [53]. Our study found similar results, and in pig milk, Christon et al. found that high temperatures could negatively affect the metabolism of polyunsaturated fatty acids [54].

A previous study has found that under heat stress, the dry matter intake and milk production of dairy cows are correlated significantly and negatively with THI [55,56]. Energy intake changes during heat stress have long been considered to be responsible for the decrease in milk quality during heat stress. However, recent studies have shown that the reduction of nutrient intake accounts for only 35–50% of the reduction in heat-induced milk synthesis [17]. The remainder might be caused by the non-matching of genetically-regulated nutrients in the body during heat stress [57]. Therefore, in the current study, we used RNA-Seq to investigate the potential molecular mechanisms underlying the

changes in cow milk synthesis under heat stress. The sequencing results identified 38,431 unique Ensembl genes that were expressed in the mammary tissue of lactating dairy cows, among which lactation-related genes were highly expressed. Similar results were obtained previously in cows [58], goats [59], and humans [60]. In addition, we focused on identifying differentially expressed genes in response to high ambient temperature. GO analysis indicated that these genes participated in the biological process of milk fat metabolism, but their expression levels decreased with the onset of heat stress. KEGG analysis showed that differentially expressed genes, such as *CD36*, *PPARG*, *SCD*, and *SLC27*, were rich in PPAR signaling pathways and played an important role in fatty acid absorption, de novo synthesis, triglyceride synthesis, and milk fat droplet secretion [61]. In many mammals, mammary tissue is one of the organs with the strongest fatty acid metabolism [62]. Generally, fatty acid metabolism in the mammary gland involves a more complex network [63]. Among the above-mentioned factors, *CD36*, as an important fatty acid uptake protein, shows a gradually increasing expression level during lactation, reaching its peak at the zenith of lactation [25]. *PPARG* is a core factor that regulates fatty acid metabolism during lactation [25]. *SCD* is a protease bound to the endoplasmic reticulum, which catalyzes saturated fatty acids to unsaturated fatty acids, thereby directly affecting the composition of fatty acids in milk [64]. Through the identification of dairy cow transcripts, we found that *SLC27* expression was the highest among genes related to fatty acid metabolism [25]. In the present study, changes in the composition of fatty acids in milk also verified the roles of these genes in milk production under heat stress.

CircRNAs, as a type of non-coding RNAs that exist widely in mammals, have attracted increased attention recently [65]. Many studies have shown that circRNAs can act as competitive endogenous RNAs (ceRNAs) to regulate miRNAs and mRNAs, thereby exerting their biological functions [66]. Recently, a study on the mammary gland of dairy cows has shown that a circRNA derived from the *CSN1S1* gene is highly expressed in the mammary gland, contains many miR-2284 family binding sites, and might serve as a miR-2284 sponge to regulate casein translation [67]. To explore the regulatory effect of circRNAs on lactation of dairy cows under heat stress, we performed a circRNAome analysis on the mammary tissue of cows between the ST and HS groups, in which five algorithms identified 2950 circRNAs, 38 of which were differentially expressed. Pearson's test was used to identify circRNA-mRNA correlations, which identified 255 positive correlations. The expression levels of *CD36* and *SLC27A6* genes have extremely important effects on the uptake of long-chain fatty acids [68]; therefore, based on the ceRNA theory, we focused on the circRNA candidates positively related to *CD36* and *SLC27A6*. Considering their covalent closed-loop structure [69], we finally identified 11 circRNAs through the design of divergent and convergent primers, Rnase R digestion, and Sanger sequencing. Next, we performed a Pearson correlation analysis on the circRNA-miRNA and miRNA-mRNA interactions. Based on their shared miRNA regulatory elements, we found four pairs of circRNA-miRNA-mRNA networks: circFCHSD2-miR6516-*CD36*; circHNRNPLL-miR11986b-*CD36*; circKANSL1- miR345 and miR502b and miR6516-*CD36*; circMAP7-miR11986b and miR345-*CD36*. These four pairs of circRNA-miRNA-mRNA might play an important role in the milk fat metabolism of dairy cows under heat stress. The construction of the ceRNA network provides a new direction for research into bovine lactation and provides a theoretical basis for improving the performance of cow milk production in the future.

In summary, we found that heat stress, which has brought huge economic losses to the dairy industry, had a negative effect on milk quality with increasing ambient temperature. Heat stress markedly altered the expression patterns of circRNAs in dairy cow's mammary gland tissue. These heat-induced circRNAs participated in the regulation of milk fat metabolism through ceRNA networks. Our results provided a new theoretical basis to study the function of circRNAs in dairy cows in response to heat stress.

4. Materials and methods

4.1. Experimental Design and Sample Collection

We conducted the experiment at a dairy farm in Guangzhou, Guangdong Province, China. We selected 60 cows balanced for their lactation stage and parity and divided them into two groups, each group containing 30 animals. One group was assessed during December 2018 (the appropriate temperature (ST) group). The other group was assessed in the summer (August) 2019 and termed the heat stress (HS) group. Table S12 showed the composition and nutritional level of the feed. All cows were fed the same commercial formula diet and raised under the same management conditions. We obtained the temperature and relative humidity data of the cowshed at 14:00 and 22:00 every day using five thermometers and hygrometers placed in the center and around the cowshed to calculate the THI. In the course of the experiment, we measured the rectal temperature and respiration rate of each cow from 10:00 to 11:30 and 16:00 to 17:30 on two consecutive days each week. We obtained the rectal temperature by leaving the animal thermometer in the rectum for 3 min. The breathing rate was based on the up and down movement of the chest and abdomen within 1 min by visual inspection. During the test period, each cow's milk production was recorded daily. We collected fresh milk samples every 10 days and used to determine the milk composition. Three days before the end of the experiment, we collected blood samples via tail vein blood collection, and we detected the concentrations of SOD, IgG, HSP70, and PRL in serum using ELISA kits (Nanjing Jiancheng Bioengineering Institute, Nanjing, Jiangsu, China).

In each group, six animals that were balanced for milk yield were chosen randomly, and percutaneous biopsies from each cow were obtained from the right rear quarter of the mammary gland. The mammary glands were washed with diethyl pyrocarbonate (DEPC)-treated PBS, excess tissue and fat were removed, and the glands were cut into small pieces, placed in cryopreservation tubes, marked, and stored in liquid nitrogen as samples for RNA extraction. All procedures were performed in accordance with the procedures approved by the Institutional Animal Care and Use Committee of South China Agricultural University (Ethics Approval Code: SCAU2018F006, 13 March 2018).

4.2. RNA Preparation and Sequencing

In accordance with the manufacturer's instructions, we used the Trizol reagent (Invitrogen, Carlsbad, CA, USA) to extract the total RNA from the mammary tissue. To remove genomic DNA from each RNA sample, we used DNase I (Takara, Dalian, Liaoning, China). Only RNA samples with suitable RNA electrophoresis results ($28S/18S \geq 1.0$) and RNA integrity number (RIN) ≥ 7.5 could be analyzed further. In each experimental group, we used 5 μ g of each RNA sample and mixed in pairs to prepare a total of three RNA pools. A Ribo-ZeroTM rRNA Removal Kit (Illumina, San Diego, CA, USA) was used to remove the ribosomal RNA from the RNA libraries, and the remaining RNA fragments were reverse transcribed using an RNA-seq Library Preparation Kit (Illumina) to form the final cDNA. Finally, we used an Illumina HiSeq 4000 sequencer (LC Bio, Hangzhou, Zhejiang, China) for paired-end sequencing of the libraries.

4.3. Bioinformatic Analysis

We first used FastQC v0.11.9 (<http://www.bioinformatics.babraham.ac.uk/projects/fastqc/>) to quickly evaluate the quality of the raw sequencing data to ensure the accuracy of subsequent analysis. Then, we used Cutadapt to filter the data, which can remove the reads that contain low-quality data and bases contaminated by the Adapter v2.10 [70]. We compared the filtered data with the *Bos taurus* reference genome downloaded from the Ensembl Genome website using TopHat v2.1.1 (<http://ccb.jhu.edu/software/tophat/index.shtml>). We then used Cufflinks v2.2.1 (<http://cole-trapnell-lab.github.io/cufflinks/cuffdiff/index.html>) to assemble the transcripts of the TopHat alignments, estimate the abundance of target transcripts, and detect the differential expression between samples [71]. In this study, we used five algorithms to predict circRNA: MapSplice [72], find_circ [73],

circRNA_Finder [74], CIRI [75], and CIRCexplorer2 [76]. To eliminate the possible errors in the algorithm, only circRNA candidates identified by all five algorithms were processed for further analysis. After the above preliminary analysis, we evaluated the expression level of all coding genes in the library using FPKM and calculated the expression abundance of circRNA using the number of splice junctions [77]. Then, we used Cuffdiff v2.2.1 [71] to compare the expression levels of coding transcripts and used the edgeR package v3.11 [78] to calculate the differentially expressed circRNA between the ST and the HS groups, with a q value of < 0.05 . Finally, to evaluate the main functional pathways of the differentially expressed genes, the GO terms and KEGG pathway analysis were performed using DAVID gene functional classification (<https://david.ncifcrf.gov/>), and obvious enrichment results were obtained with p values < 0.05 . In addition, we downloaded 23 miRNA-seq data sets for bovine mammary glands from the gene expression omnibus (GEO) database (<https://www.ncbi.nlm.nih.gov/gds/>) with the accession numbers PRJNA542496, PRJNA482122, and PRJNA248657. We then used the miRDeep2 program [79] to further analyze the miRNA libraries by BLAST searching against bovine miRBase annotation (<http://www.mirbase.org/>) to identify mammary-specific miRNA candidates.

4.4. Validation of circRNAs

In accordance with the manufacturer's instructions, we used Trizol reagent (Invitrogen) to extract the total RNA from mammary tissues. Subsequently, we used a PrimeScript RT Reagent Kit with gDNA Eraser (Takara, Dalian, Liaoning, China) to reverse transcribe RNA to cDNA. To verify the circular structure of the circRNA, we designed a pair of convergent and divergent primers and verified their head-to-tail splicing using PCR and Sanger sequencing. Then, we performed RNase R treatment, in which 2 μ g of total RNA was incubated with 3 U/ μ g RNase R at 37 °C for 10 min. As a control, another 2 μ g total RNA was incubated with RNase-free water under the same conditions. After treatment with RNase R, we detected the RNA expression levels of circRNAs and their linear mRNA using quantitative real-time PCR (qPCR). We used *GAPDH* (glyceraldehyde 3-phosphate dehydrogenase) as an internal reference for data analysis. Table S13 shows the primer sequences used in the present study.

Supplementary Materials: Supplementary materials can be found at <http://www.mdpi.com/1422-0067/21/11/4162/s1>.

Author Contributions: All authors were involved in project conception and design. D.Y.W. and J.J.S. led the laboratory assays, analyses of data, and writing of the manuscript. Y.L.Z. and J.J.S. contributed reagents, materials, and analysis tools. All authors have read and agreed to the published version of the manuscript.

Funding: This work was supported by the National Key Research and Development Program of China (2016YFD0500503), the Natural Science Foundation of China Program (31802032), the Natural Science Foundation of Guangdong Province (2020A1515010062), the Science and Technology Project of Guangzhou (202002030037), the Major Scientific Projects of Colleges and Universities of Guangdong Province (2017KTSCX023), and the projects of Guangdong Provincial Promotion Project on Preservation and Utilization of Local Breed of Livestock and Poultry.

Conflicts of Interest: The authors declare no conflict of interest. The founding sponsors had no role in the design of the study; in the collection, analyses, and interpretation of data; in the writing of the manuscript, and in the decision to publish the results.

Abbreviations

HSP70	Heat shock protein 70
SOD	Superoxide dismutase
PRL	Prolactin
GO	Gene ontology
KEGG	Kyoto Encyclopedia of Genes and Genomes
ncRNA	Non-coding RNAs
THI	Temperature-humidity index
FPKM	Fragments Per Kilobase of transcript per Million
CoA	Coenzyme A
PPAR	Peroxisome proliferative activated receptor
PPARG	Peroxisome proliferative activated receptor, gamma
SCD	Stearoyl-CoA desaturase

References

1. Luber, G.; McGeehin, M. Climate change and extreme heat events. *Am. J. Prev. Med.* **2008**, *35*, 429–435. [[CrossRef](#)] [[PubMed](#)]
2. Nardone, A.; Ronchi, B.; Lacetera, N.; Ranieri, M.S.; Bernabucci, U. Effects of climate changes on animal production and sustainability of livestock systems. *Livest. Sci.* **2010**, *130*, 57–69. [[CrossRef](#)]
3. Kadzere, T.C.; Murphy, M.R.; Silanikove, N.; Maltz, E. Heat stress in lactating dairy cows: A review. *Livest. Prod. Sci.* **2002**, *77*, 59–91. [[CrossRef](#)]
4. Carabaño, J.M.; Logar, B.; Bormann, J.; Minet, J.; Vanrobays, M.-L.; Díaz, C.; Tychon, B.; Gengler, N.; Hammami, H. Modeling heat stress under different environmental conditions. *J. Dairy Sci.* **2016**, *99*, 3798–3814. [[CrossRef](#)]
5. Borad, G.S.; Kumar, A.; Singh, A.K. Effect of processing on nutritive values of milk protein. *Crit. Rev. Food Sci. Nutr.* **2017**, *57*, 3690–3702. [[CrossRef](#)]
6. Hill, L.D.; Wall, E. Dairy cattle in a temperate climate: The effects of weather on milk yield and composition depend on management. *Animal* **2015**, *9*, 138–149. [[CrossRef](#)]
7. Bernabucci, U.; Basirico, L.; Morera, P.; Dipasquale, D.; Vitali, A.; Cappelli, F.P.; Calamari, L. Effect of summer season on milk protein fractions in Holstein cows. *J. Dairy Sci.* **2015**, *98*, 1815–1827. [[CrossRef](#)]
8. Rhoads, L.M.; Rhoads, R.P.; Vanbaale, M.J.; Collier, R.J.; Sanders, S.R.; Weber, W.J.; Crooker, B.A.; Baumgard, L.H. Effects of heat stress and plane of nutrition on lactating Holstein cows: I. Production, metabolism, and aspects of circulating somatotropin. *J. Dairy Sci.* **2009**, *92*, 852–864. [[CrossRef](#)]
9. Pierre St, N.R.; Cobanov, B.; Schnitkey, G. Economic losses from heat stress by US livestock industries. *J. Dairy Sci.* **2003**, *86*, E52–E77. [[CrossRef](#)]
10. Fuquay, J.W. Heat stress as it affects animal production. *J. Anim. Sci.* **1981**, *52*, 164–174. [[CrossRef](#)]
11. West, W.J.; Mullinix, B.G.; Bernard, J.K. Effects of hot, humid weather on milk temperature, dry matter intake, and milk yield of lactating dairy cows. *J. Dairy Sci.* **2003**, *86*, 232–242. [[CrossRef](#)]
12. Wheelock, B.J.; Rhoads, R.P.; Vanbaale, M.J.; Sanders, S.R.; Baumgard, L.H. Effects of heat stress on energetic metabolism in lactating Holstein cows. *J. Dairy Sci.* **2010**, *93*, 644–655. [[CrossRef](#)]
13. Bernabucci, U.; Biffani, S.; Buggiotti, L.; Vitali, A.; Lacetera, N.; Nardone, A. The effects of heat stress in Italian Holstein dairy cattle. *J. Dairy. Sci.* **2014**, *97*, 471–486. [[CrossRef](#)] [[PubMed](#)]
14. Leroy, L.J.; Rizos, D.; Sturmey, R.; Bossaert, P.; Gutierrez-Adan, A.; van Hoeck, V.; Valckx, S.; Bols, P.E. Intrafollicular conditions as a major link between maternal metabolism and oocyte quality: A focus on dairy cow fertility. *Reprod. Fertil. Dev.* **2012**, *24*, 1. [[CrossRef](#)] [[PubMed](#)]
15. Cowley, C.F.; Barber, D.G.; Houlihan, A.V.; Poppi, D.P. Immediate and residual effects of heat stress and restricted intake on milk protein and casein composition and energy metabolism. *J. Dairy Sci.* **2015**, *98*, 2356–2368. [[CrossRef](#)] [[PubMed](#)]
16. Li, M.; Tian, S.Z.H.; Zhou, X.; Zhang, Y.; Li, S.; Yang, H.; Zheng, N.; Wang, J. Metabolic responses and “omics” technologies for elucidating the effects of heat stress in dairy cows. *Int. J. Biometeorol.* **2017**, *61*, 1149–1158.
17. Vujanac, I.; Kirovski, D.; Šamanc, H.; Prodanovic, R.; Lakic, N.; Adamovic, M.; Valcic, O. Milk production in high-yielding dairy cows under different environment temperatures. *Large Anim. Rev.* **2012**, *18*, 31–36.

18. Zielniok, K.; Sobolewska, A.; Gajewska, M. Mechanisms of autophagy induction by sex steroids in bovine mammary epithelial cells. *J. Mol. Endocrinol.* **2017**, *59*, 29–48. [[CrossRef](#)]
19. Zhang, C.; Wu, H.; Wang, Y.; Zhao, Y.; Fang, X.; Chen, C.; Chen, H. Expression patterns of circular RNAs from primary kinase transcripts in the mammary glands of lactating rats. *J. Mammary Cancer* **2015**, *18*, 235–241. [[CrossRef](#)]
20. Wang, Y.; Li, D.; Wang, Y.; Li, M.; Fang, X.; Chen, H.; Zhang, C. The landscape of circular RNAs and mRNAs in bovine milk exosomes. *J. Food Compos. Anal.* **2019**, *76*, 33–38. [[CrossRef](#)]
21. Li, X.; Yang, L.; Chen, L. The Biogenesis, Functions, and Challenges of Circular RNAs. *Mol. Cell* **2018**, *71*, 428–442. [[CrossRef](#)] [[PubMed](#)]
22. Patop, L.I.; Kadener, S. circRNAs in Cancer. *Curr. Opin. Genet. Dev.* **2018**, *48*, 121–127. [[CrossRef](#)] [[PubMed](#)]
23. Pan, T.; Sun, X.; Liu, Y.; Li, H.; Deng, G.; Lin, H.; Wang, S. Heat stress alters genome-wide profiles of circular RNAs in Arabidopsis. *Plant Mol. Biol.* **2018**, *96*, 217–229. [[CrossRef](#)] [[PubMed](#)]
24. Palmquist, D.L. Milk Fat: Origin of Fatty Acids and Influence of Nutritional Factors Thereon. In *Advanced Dairy Chemistry Volume 2: Lipids*; Springer: Boston, MA, USA, 2006; pp. 43–92.
25. Bionaz, M.; Loor, J.J. ACSL1, AGPAT6, FABP3, LPIN1, and SLC27A6 Are the Most Abundant Isoforms in Bovine Mammary Tissue and Their Expression is affected by stage of lactation. *J. Nutr.* **2008**, *138*, 1019–1024. [[CrossRef](#)] [[PubMed](#)]
26. Min, L.; Cheng, J.B.; Shi, B.L.; Yang, H.J.; Zheng, N.; Wang, J.Q. Effects of heat stress on serum insulin, adipokines, AMP-activated protein kinase, and heat shock signal molecules in dairy cows. *J. Zhejiang Univ. Sci. B* **2015**, *16*, 541–548. [[CrossRef](#)] [[PubMed](#)]
27. Bellagi, R.; Martin, B.; Chassaing, C.; Najjar, T.; Pomies, D. Evaluation of heat stress on tarentaise and holstein cow performance in the mediterranean climate. *Int. J. Biometeorol.* **2017**, *61*, 1371–1379. [[CrossRef](#)]
28. Preez, J.H.D. Parameters for the determination and evaluation of heat stress in dairy cattle in South Africa. *Onderstepoort J. Vet. Res.* **2001**, *67*, 263–271.
29. Dikmen, S.; Hansen, P.J. Is the temperature-humidity index the best indicator of heat stress in lactating dairy cows in a subtropical environment. *J. Dairy Sci.* **2009**, *92*, 109–116. [[CrossRef](#)]
30. Park, J.C.; Seo, Y.S. Heat Shock Proteins: A Review of the Molecular Chaperones for Plant Immunity. *Plant Pathol. J.* **2015**, *31*, 323–333. [[CrossRef](#)] [[PubMed](#)]
31. Morimoto, I.R.; Sarge, K.D.; Abravaya, K. Transcriptional regulation of heat shock genes. A paradigm for inducible genomic responses. *J. Biol. Chem.* **1992**, *267*, 21987.
32. Sabirzhanov, B.; Stoica, B.A.; Hanscom, M.; Piao, C.S.; Faden, A.I. Over-expression of HSP70 attenuates caspase-dependent and caspase-independent pathways and inhibits neuronal apoptosis. *J. Neurochem.* **2012**, *123*, 542–554. [[CrossRef](#)] [[PubMed](#)]
33. Dangi, S.S.; Gupta, M.; Dangi, S.K.; Chouhan, V.S.; Maurya, V.P.; Kumar, P.; Singh, G.; Sarkar, M. Expression of HSPs: An adaptive mechanism during long-term heat stress in goats (*Capra hircus*). *Int. J. Biometeorol.* **2015**, *59*, 1095–1106. [[CrossRef](#)] [[PubMed](#)]
34. Xu, J.; Tang, S.; Yin, B.; Sun, J.R.; Song, E.B.; Bao, E.D. Co-enzyme Q10 and acetyl salicylic acid enhance Hsp70 expression in primary chicken myocardial cells to protect the cells during heat stress. *Mol. Cell. Biochem.* **2017**, *435*, 73–86. [[CrossRef](#)] [[PubMed](#)]
35. Sarup, P.; Dahlggaard, J.; Norup, A.M.; Rgensen, K.T.J.; Hebsgaard, M.B.; Loeschcke, V. Down Regulation of Hsp70 Expression Level Prolongs the Duration of Heat-Induced Male Sterility in *Drosophila buzzatii*. *Funct. Ecol.* **2004**, *18*, 365–370. [[CrossRef](#)]
36. Sun, L.L.; Gao, S.T.; Wang, K.; Xu, J.C. Effects of source on bioavailability of selenium, antioxidant status, and performance in lactating dairy cows during oxidative stress-inducing conditions. *J. Dairy Sci.* **2018**, *102*, 1–9. [[CrossRef](#)]
37. Yasui, T.; Mcart, J.A.A.; Ryan, C.M.; Gilbert, R.O.; Nydam, D.V.; Valdez, F.; Griswold, K.E.; Overton, T.R. Effects of chromium propionate supplementation during the periparturient period and early lactation on metabolism, performance, and cytological endometritis in dairy cows. *J. Dairy Sci.* **2014**, *97*, 6400–6410. [[CrossRef](#)]
38. Song, J.H.; Xue, Q.L.; Bing, S.Z.; Jun, G.W. Response of the Photosynthesis and Antioxidant Systems to High-Temperature Stress in *Euonymus japonicus* Seedlings. *For. Sci.* **2010**, *56*, 172–180.

39. Zhang, J.F.; Weng, X.G.; Wang, J.F.; Zhou, D.; Zhang, W.; Zhai, C.C.; Hou, Y.X.; Zhu, Y.H. Effects of temperature-humidity index and chromium supplementation on antioxidant capacity, heat shock protein 72, and cytokine responses of lactating cows. *J. Anim. Sci.* **2014**, *92*, 3026–3034. [\[CrossRef\]](#)
40. Caroprese, M.; Marzano, A.; Entrican, G.; Wattegedera, S.; Albenzio, M.; Sevi, A. Immune response of cows fed polyunsaturated fatty acids under high ambient temperatures. *J. Dairy Sci.* **2009**, *92*, 2796–2803. [\[CrossRef\]](#)
41. Tao, S.; Monteiro, A.P.A.; Thompson, I.M.; Hayen, M.J.; Dahl, G.E. Effect of late-gestation maternal heat stress on growth and immune function of dairy calves. *J. Dairy Sci.* **2012**, *95*, 7128–7136. [\[CrossRef\]](#)
42. Tao, S.; Bubolz, J.W.; Amaral, B.C.D.; Thompson, I.M.; Hayen, M.J.; Johnson, S.E.; Dahl, G.E. Effect of heat stress during the dry period on mammary gland development. *J. Dairy Sci.* **2011**, *94*, 5976–5986. [\[CrossRef\]](#) [\[PubMed\]](#)
43. Lacasse, P.; Lollivier, V.; Dessauge, F.; Bruckmaier, R.M.; Ollier, S.; Boutinaud, M. New developments on the galactopoietic role of prolactin in dairy ruminants. *Domest. Anim. Endocrinol.* **2012**, *43*, 154–160. [\[CrossRef\]](#) [\[PubMed\]](#)
44. Ravagnolo, O.; Misztal, I. Genetic component of heat stress in dairy cattle, parameter estimation. *J. Dairy Sci.* **2000**, *83*, 2126–2130. [\[CrossRef\]](#)
45. Segnalini, M.; Nardone, A.; Bernabucci, U.; Vitali, A.; Ronchi, B.; Lacetera, N. Dynamics of the temperature-humidity index in the Mediterranean basin. *Int. J. Biometeorol.* **2011**, *55*, 253–263. [\[CrossRef\]](#) [\[PubMed\]](#)
46. Habeeb, A.A.G.; Tarabany, A.; Atta, M. Negative effects of heat stress on growth and milk production off arm animals. *J. Anim. Husb. Dairy Sci.* **2018**, *2*, 1–12.
47. Hammami, H.; Bormann, J.; Hamdi, N.M.; Montaldo, H.H.; Gengler, N. Evaluation of Heat Stress Effects on Production Traits and Somatic Cell Score of Holsteins in a Temperate Environment. *J. Dairy Sci.* **2013**, *96*, 1844–1855. [\[CrossRef\]](#)
48. Beede, K.D.; Sheare, J.K. Nutritional Management of Dairy Cattle During Hot Weather. IV. *Agri-Practice* **1991**, *12*, 5–13.
49. Chornobai, A.C.; Damasceno, J.C.; Visentainer, J.V.; Matsushita, M. Physical-chemical composition of in natura goat milk from cross Saanen throughout lactation period. *Arch. Latinoam. Nutr.* **1999**, *49*, 283–286.
50. Umberto, B.; Nicola, L.; Bruno, R.; Alessandrol, N. Effects of the hot season on milk protein fractions\rin Holstein cows. *Anim. Res.* **2002**, *51*, 25–33.
51. Rhoads, R.E.; Grudzien-Nogalska, E. Translational regulation of milk protein synthesis at secretory activation. *J. Mammary Gland Biol. Neoplasia* **2007**, *12*, 283–292. [\[CrossRef\]](#)
52. Shwartz, G.; Rhoads, M.L.; Vanbaale, M.J.; Rhoads, R.P.; Baumgard, L.H. Effects of a supplemental yeast culture on heat-stressed lactating Holstein cows. *J. Dairy Sci.* **2009**, *92*, 935–942. [\[CrossRef\]](#) [\[PubMed\]](#)
53. Goode, F.H.; Webster, N.R. Free radicals and antioxidants in sepsis. *Crit. Care Med.* **1993**, *21*, 1770–1776. [\[CrossRef\]](#) [\[PubMed\]](#)
54. Christon, R.; Saminadin, G.; Lionet, H.; Racon, B. Dietary fat and climate alter food intake, performance of lactating sows and their litters and fatty acid composition of milk. *Anim. Sci.* **1999**, *69*, 353–365. [\[CrossRef\]](#)
55. Gao, T.S.; Guo, J.; Quan, S.Y.; Nan, X.M.; Fernandez, M.V.S.; Baumgard, L.H.; Bu, D.P. The effects of heat stress on protein metabolism in lactating Holstein cows. *J. Dairy Sci.* **2017**, *100*, 5040–5049. [\[CrossRef\]](#) [\[PubMed\]](#)
56. Garner, B.J.; Douglas, M.; Williams, S.R.O.; Wales, B. Responses of dairy cows to short-term heat stress in controlled-climate chambers. *Anim. Prod. Sci.* **2017**, *57*, 1233–1241. [\[CrossRef\]](#)
57. Collier, J.R.; Collier, J.L.; Rhoads, R.P.; Baumgard, L.H. Invited review: Genes involved in the bovine heat stress response. *J. Dairy Sci.* **2008**, *91*, 445–454. [\[CrossRef\]](#)
58. Wickramasinghe, S.; Rincon, G.; Islas-Trejo, A.; Medrano, F.J. Transcriptional profiling of bovine milk using RNA sequencing. *BMC Genomics* **2012**, *13*, 45. [\[CrossRef\]](#)
59. Shi, H.; Zhu, J.; Luo, J.; Cao, W.; Shi, H.; Yao, D.; Li, J.; Sun, Y.; Xu, H.; Yu, K.; et al. Genes regulating lipid and protein metabolism are highly expressed in mammary gland of lactating dairy goats. *Funct. Integr. Genom.* **2015**, *15*, 309–321. [\[CrossRef\]](#)
60. Lemay, G.D.; Ballard, A.O.; Hughes, A.M.; Morrow, L.A.; Horseman, D.N.; Nommsen-Rivers, A.L. RNA sequencing of the human milk fat layer transcriptome reveals distinct gene expression profiles at three stages of lactation. *PLoS ONE* **2013**, *8*, e67531. [\[CrossRef\]](#)

61. Bionaz, M.; Loor, J.J. Gene networks driving bovine milk fat synthesis during the lactation cycle. *BMC Genom.* **2008**, *9*, 366–370. [\[CrossRef\]](#)
62. Chong, M.B.; Reigan, P.; Mayle-Combs, K.D.; Orlicky, D.J.; Mcmanaman, J.L. Determinants of adipophilin function in milk lipid formation and secretion. *Trends Endocrinol. Metab.* **2011**, *22*, 211–217. [\[CrossRef\]](#) [\[PubMed\]](#)
63. Kadegowda, G.A.K.; Bionaz, M.; Piperova, L.S.; Erdman, R.A.; Loor, J.J. Peroxisome proliferator-activated receptor- γ activation and long-chain fatty acids alter lipogenic gene networks in bovine mammary epithelial cells to various extents. *J. Dairy Sci.* **2009**, *92*, 4276–4289. [\[CrossRef\]](#) [\[PubMed\]](#)
64. Macciotta, P.N.P.; Mele, M.; Conte, G.; Serra, A.; Cassandro, M.; Cassandro, R.; Zotto, R.D.; Borlino, A.C.; Pagnacco, G.; Secchiari, P. Association Between a Polymorphism at the Stearoyl CoA Desaturase Locus and Milk Production Traits in Italian Holsteins. *J. Dairy Sci.* **2008**, *91*, 3184–3189. [\[CrossRef\]](#) [\[PubMed\]](#)
65. Du, W.W.; Yang, W.; Chen, Y.; Wu, Z.K. Foxo3 circular RNA promotes cardiac senescence by modulating multiple factors associated with stress and senescence responses. *Eur. Heart J.* **2017**, *38*, 1402–1412. [\[CrossRef\]](#) [\[PubMed\]](#)
66. Kulcheski, R.F.; Christoff, A.P.; Margis, R. Circular RNAs are miRNA sponges and can be used as a new class of biomarker. *J. Biotechnol.* **2016**, *238*, 42–51. [\[CrossRef\]](#)
67. Zhang, C.; Wu, H.; Wang, Y.; Zhu, S.; Liu, J.; Fang, X.; Chen, H. Circular RNA of cattle casein genes are highly expressed in bovine mammary gland. *J. Dairy Sci.* **2016**, *99*, 4750–4760. [\[CrossRef\]](#) [\[PubMed\]](#)
68. Xu, S.; Jay, A.; Brunaldi, K.; Huang, N.; Hamilton, J.A. CD36 Enhances Fatty Acid Uptake by Increasing the Rate of Intracellular Esterification but Not Transport across the Plasma Membrane. *Biochemistry* **2013**, *52*, 7254–7261. [\[CrossRef\]](#) [\[PubMed\]](#)
69. Qu, S.; Yang, X.; Li, X.; Wang, J.; Gao, Y.; Shang, R.; Sun, W.; Dou, K.; Li, H. Circular RNA: A new star of noncoding RNAs. *Cancer Lett.* **2015**, *3201565*, 141–148. [\[CrossRef\]](#) [\[PubMed\]](#)
70. Martin, M. Cutadapt removes adapter sequences from high-throughput sequencing reads. *Embnet J.* **2011**, *17*, 10–12. [\[CrossRef\]](#)
71. Trapnell, C.; Roberts, A.; Goff, L.; Pertea, G.; Kim, D.; Kelley, D.R.; Pimentel, H.; Salzberg, S.L.; Rinn, J.L.; Pachter, L. Differential gene and transcript expression analysis of RNA-seq experiments with TopHat and Cufflinks. *Nat. Protoc.* **2012**, *7*, 562. [\[CrossRef\]](#)
72. Wang, K.; Singh, D.; Zeng, Z.; Coleman, S.J.; Coleman, S.J.; Huang, Y.; Savich, G.L.; He, X.; Mieczkowski, P.; Grimm, S.A.; et al. MapSplice: Accurate mapping of RNA-seq reads for splice junction discovery. *Nucleic Acids Res.* **2010**, *38*, e178. [\[CrossRef\]](#) [\[PubMed\]](#)
73. Memczak, S.; Jens, M.; Elefsinioti, A.; Torti, F.; Krueger, J.; Rybak, A.; Maier, L.; Mackowiak, S.D.; Gregersen, L.H.; Munschauer, M.; et al. Circular RNAs are a large class of animal RNAs with regulatory potency. *Nature* **2013**, *495*, 333. [\[CrossRef\]](#) [\[PubMed\]](#)
74. Fu, X.; Liu, R. CircRNAFinder: A tool for identifying circular RNAs using RNA-Seq data. In Proceedings of the 6th International Conference on Bioinformatics and Computational Biology, BICOB, Las Vegas, NV, USA, 4–6 April 2014.
75. Gao, Y.; Wang, J.; Zhao, F. CIRI: An efficient and unbiased algorithm for de novo circular RNA identification. *Genome Biol.* **2015**, *16*, 4. [\[CrossRef\]](#) [\[PubMed\]](#)
76. Zhang, O.X.; Dong, R.; Zhang, Y.; Zhang, J.L.; Luo, Z.; Zhang, J.; Chen, L.L.; Yang, L. Diverse alternative back-splicing and alternative splicing landscape of circular RNAs. *Genome Res.* **2016**, *26*, 1277–1287. [\[CrossRef\]](#) [\[PubMed\]](#)
77. Zhang, O.X.; Wang, H.B.; Zhang, Y.; Lu, X.; Chen, L.L.; Yang, L. Complementary sequence-mediated exon circularization. *Cell* **2014**, *159*, 134–147. [\[CrossRef\]](#) [\[PubMed\]](#)
78. Robinson, D.M.; McCarthy, D.J.; Smyth, G.K. EdgeR: A Bioconductor package for differential expression analysis of digital gene expression data. *Bioinformatics* **2010**, *26*, 139–140. [\[CrossRef\]](#) [\[PubMed\]](#)
79. Friedländer, R.M.; Mackowiak, S.D.; Li, N.; Chen, W.; Rajewsky, N. Mirdeep2 accurately identifies known and hundreds of novel microrna genes in seven animal clades. *Nucleic Acids Res.* **2012**, *40*, 37–52. [\[CrossRef\]](#)



蓝塘猪与长白猪背最长肌全基因组 DNA 甲基化分析

林泽堃, 谢芳, 罗君谊, 陈婷, 习欠云, 张永亮, 孙加节

(华南农业大学 动物科学学院 国家生猪种业工程技术研究中心, 广东 广州 510642)

【摘要】【目的】分析蓝塘猪与长白猪背最长肌组织全基因组 DNA 甲基化水平, 筛选 2 个猪品种的差异甲基化基因(DMG), 为优质肉猪选育提供理论依据。【方法】利用全基因组亚硫酸氢盐测序(WGBS)技术, 分析 1 日龄雄性蓝塘猪与长白猪背最长肌组织全基因组 DNA 的甲基化水平、差异甲基化区域(DMR)和 DMG, 并对 DMG 进行 GO 注释, 揭示蓝塘猪与长白猪差异甲基化基因的功能。【结果】蓝塘猪和长白猪样本测序获得的原始序列数量分别为 300 005 805 和 300 012 190 条, 有效序列数量分别为 210 334 070 和 210 758 564 条, 有效序列与猪参考基因组的比对成功率分别为 70.11% 和 70.25%, Bisulfite 转化率分别为 98.54% 和 98.36%。蓝塘猪全基因组范围内胞嘧啶(C)的甲基化率为 4.07%, 其中 CG、CHG 和 CHH 中胞嘧啶的甲基化率分别为 74.50%, 1.74% 和 1.51%; 长白猪全基因组范围内胞嘧啶的甲基化率为 4.44%, 其中 CG、CHG 和 CHH 中胞嘧啶的甲基化率分别为 76.92%, 2.13% 和 1.87%。共检测出 13 126 个差异性甲基化区域, 总长度为 3 357 954 bp, 含有 78 234 个胞嘧啶。68.50% 的差异性甲基化区域分布在基因间区, 25.74% 分布在内含子, 1.89% 分布在外显子, 1.85% 分布在上游 2 kb 区域, 1.78% 分布在下游 2 kb 区域, 0.24% 分布在 CpG 岛。甲基化差异基因显著富集于凋亡过程的负调控、细胞迁移的正调控等 24 个 GO 条目, 其中 FAM135B、NR1H2、ID4、ZFPM2、FOXO1 等 5 个基因与蓝塘猪和长白猪的脂肪代谢相关, 长白猪 FAM135B、NR1H2、ZFPM2 和 FOXO1 的表达水平高于蓝塘猪, 而 ID4 略低于蓝塘猪。【结论】明确了蓝塘猪和长白猪背最长肌组织全基因组 DNA 的甲基化情况, 为深入研究 2 个猪种肉质差异的分子机制提供了基础数据。

【关键词】 蓝塘猪; 长白猪; 背最长肌; DNA 甲基化; 肉品质

【中图分类号】 S828.2

【文献标志码】 A

【文章编号】 1671-9387(2023)06-0001-10

Whole genome-wide DNA methylation of longissimus dorsi muscle in Lantang and Landrace pigs

LIN Zekun, XIE Fang, LUO Junyi, CHEN Ting, XI Qianyun, ZHANG Yongliang, SUN Jiajie

(National Engineering Research Center for Breeding Swine Industry, College of Animal Science, South China Agricultural University, Guangzhou, Guangdong 510642, China)

Abstract:【Objective】This study analyzed the genome-wide DNA methylation levels of the longissimus dorsi muscle tissue of Lantang and Landrace pigs and screened out differentially methylated gene (DMG) between the two breeds to provide basis for the selection and breeding of high-quality pork pigs.【Method】Whole genome bisulfite sequencing (WGBS) technology was used to analyze the methylation level, differentially methylated region (DMR) and DMG of whole genome DNA of longissimus dorsi muscle tissue in 1-day-old male Lantang and Landrace pigs, and the DMG was annotated by GO to reveal the function of di-

【收稿日期】 2022-04-04

【基金项目】 国家自然科学基金项目(32072714, 32072812, 31872435, 32072814); 广东省自然科学基金项目(2020A1515010062); 广州市科技项目(202002030037)

【作者简介】 林泽堃(1997—), 男, 福建漳州人, 在读硕士, 主要从事动物生物化学研究。E-mail: 1078466285@qq.com

【通信作者】 张永亮(1966—), 男, 河北黄骅人, 教授, 博士, 博士生导师, 主要从事动物生物化学研究。E-mail: zhangyl@scau.edu.cn

孙加节(1984—), 男, 江苏盐城人, 副教授, 博士, 博士生导师, 主要从事动物生物化学研究。

E-mail: jiajiesun@scau.edu.cn

fferential methylation genes.【Result】 The number of original sequences was 300 005 805 and 300 012 190 for Lantang and Landrace pigs and the number of effective sequences was 210 334 070 and 210 758 564, respectively. Their successful ratios of effective sequence to pig reference genome were 70.11% and 70.25%, and Bisulfite conversion rates were 98.54% and 98.36%, respectively. The genome-wide methylation rate of cytosine (C) in the whole genome of Lantang pigs was 4.07%, and the methylation rates of C in CG, CHG and CHH were 74.50%, 1.74% and 1.51%, respectively. The genome-wide methylation rate of C in Landrace pigs was 4.44%, and the methylation rates of C in CG, CHG and CHH were 76.92%, 2.13% and 1.87%, respectively. A total of 13 126 DMR were detected, with 3 357 954 bp length and 78 234 cytosines. About 68.50% of DMR were distributed in intergenic region, 25.74% in introns, 1.89% in exons, 1.85% in upstream 2 kb region, 1.78% in downstream 2 kb region and 0.24% in CpG island. DMGs function was significantly enriched in 24 GO genes, including negative regulation of apoptotic process and positive regulation of cell migration. Among them, *FAM135B*, *NR1H2*, *ID4*, *ZFPM2* and *FOXO1* genes were related to fat metabolism in Lantang and Landrace pigs. The expression levels of *FAM135B*, *NR1H2*, *ZFPM2* and *FOXO1* in Landrace pigs were higher than those in Lantang pigs, while the expression levels of *ID4* in Lantang pigs were slightly higher than that in Landrace pigs.【Conclusion】 The genome-wide DNA methylation of longissimus dorsi muscle tissues of Lantang and Landrace pigs was clarified, which provided basic data for in-depth study of molecular mechanism of meat quality differences between the two breeds.

Key words: Lantang pig; Landrace pig; longissimus dorsi muscle; DNA methylation; meat quality

DNA 甲基化是一种主要的表观遗传机制,在基因表达、胚胎发育、细胞分化和基因印迹等生物学过程中发挥着重要的调控作用^[1-2]。这种 DNA 修饰可通过增强或降低蛋白质与 DNA 相互作用的亲和性来调节转录因子的募集,从而影响基因的激活或抑制^[1,3]。DNA 高甲基化会抑制基因表达,而低甲基化则会促进基因转录^[4]。DNA 甲基化由 DNA 甲基转移酶(DNA methyltransferases, DNMTs)催化,通常发生在胞嘧啶的 5' 碳位置上,大多数的甲基化胞嘧啶位于鸟嘌呤附近被称为 CpG 岛的位点上。CpG 位点通常位于启动子的上游或基因体内,其中 70%~80% 发生了甲基化^[5]。在极少数情况下,甲基化也发生在 CHG 和 CHH 三核苷酸位点(H 代表除 G 外的任何核苷酸)^[6]。DNMTs 家族有 5 个成员,即 DNMT1、DNMT2、DNMT3a、DNMT3b 和 DNMT3L,但只有 DNMT1、DNMT3a 和 DNMT3b 具有 DNA 甲基转移酶活性^[7]。

目前,检测基因组 DNA 甲基化的方法很多,包括亚硫酸氢盐测序(bisulfite sequencing, BS)、简化表观亚硫酸氢盐测序(reduced representation bisulfite-sequencing, RRBS)、甲基化 DNA 免疫沉淀测序(MeDIP-seq)、甲基结合域测序(MBD-seq, MethylCap-seq)等技术^[8-9]。BS 和 RRBS 原理是利用亚硫酸氢盐对基因组 DNA 进行处理,将未发生甲基化的胞嘧啶脱氨基变成尿嘧啶,而发生了甲基化的

胞嘧啶不发生反应,从而将甲基化状态的差异转化为 DNA 序列的差异,这种差异可以通过 PCR 方法检测^[1]。BS 和 RRBS 方法具有高度单链特异性,可降低 DNA 的复杂性,从而降低后续分析的难度,基于此可以通过比较亚硫酸氢盐处理和未处理测序样本,从而发现甲基化位点^[10-11]。

生猪产业是我国畜牧业的支柱产业,猪肉产品是城乡居民肉类消费的主要品种,消费量约占肉类消费总量的 2/3,同时我国也是世界上最大的猪肉生产国,产量占全球一半以上。目前,国内商品猪品种主要是从国外引进的瘦肉型猪种及其杂交后代。长白猪作为典型的瘦肉型品种,原产于丹麦,具有生长速度快、胴体瘦肉率与饲料转化率高等优点^[12],但是肉质不如我国地方猪种,而且体质较弱,抗逆性差。蓝塘猪是中国华南地区典型的脂肪型猪品种,原产于广东省紫金县蓝塘乡,具有早熟易肥、肉质细嫩等优点^[13]。肌肉脂肪(intramuscular fat, IMF)含量和脂肪酸组成是重要的肉质性状,对色泽、嫩度、保水力、多汁性和风味等具有重要作用,IMF 含量越高,猪肉品质越好^[14]。IMF 含量不仅取决于前体脂肪细胞转化为成熟 IMF 细胞的数量,还取决于 IMF 细胞内脂滴和肌细胞内脂滴的沉积量^[15]。近年来,随着消费者对猪肉品质要求的提高,培育肉质优良的猪种已成为当务之急。

本研究利用全基因组亚硫酸氢盐测序(whole

genome bisulfite sequencing, WGBS) 技术, 绘制了 1 日龄雄性蓝塘猪与长白猪的背最长肌全基因组 DNA 甲基化图谱, 旨在揭示 2 猪种脂肪代谢相关基因甲基化修饰的差异, 进而为优质肉猪的选育提供基础数据。

1 材料与方法

1.1 材料

1 日龄蓝塘猪(LT)与长白猪(LW), 购自广东省新丰县板岭原种猪场(广东, 韶关), 每个品种 3 头小公猪, 屠宰后取背最长肌组织 200 g, 用锡箔纸包裹后置于液氮中冷冻后, 于-80 ℃冰箱中保存备用。

DNeasy Blood & Tissue Kit 试剂盒, QIAGEN 公司; EZ DNA Methylation Gold™ 试剂盒, Zymo Research 公司; RNAiso Plus、SYBR Premix Ex Taq II 和 PrimeScript RT Master Mix Kit, TaKaRa 公司。

Covaris S-2 超声波 DNA 破碎仪, Covaris; Qubit 荧光定量 PCR 仪, Invitrogen; Bio-Rad CFX96 Real-Time PCR 检测系统, Bio-Rad; Agilent 2100-Bioanalyzer, Agilent。

1.2 2 种猪全基因组 DNA 文库构建与测序

采用 DNeasy Blood & Tissue Kit 试剂盒提取猪背最长肌 DNA, 每个品种取 3 个样本用等量 DNA 构建 DNA 池。用 Covaris S-2 超声波 DNA 破碎仪处理基因组 DNA, 将其打断为 200~300 bp 的片段, 对打断后的 DNA 片段进行末端修复(末端加 A 碱基)后, 连接测序接头序列。使用 EZ DNA Methylation Gold™ 试剂盒对 DNA 片段进行亚硫酸氢盐处理, 脱盐处理后用 2% 的琼脂糖凝胶电泳选择片段并切胶回收。

文库构建完成后, 使用 Qubit 荧光定量 PCR 仪测定 DNA 文库浓度, 并使用 Agilent 2100Bioanalyzer 检测 DNA 文库质量, 将合格的 DNA 文库用于 Illumina 测序。测序由深圳市恒创基因科技有限公司完成。

1.3 数据分析

1.3.1 参考序列比对 对测序获得的原始序列进行过滤, 去除测序接头和低质量数据后得到有效序列。将过滤后的数据与猪参考基因组(ftp://ftp.ensembl.org/pub/release-94/fasta/sus_scrofa/dna/)进行比对, 计算每个样品的比对成功率和 Bisulfite 转化率。数据过滤标准为: ①序列含有接头; ②序列中 N 碱基的比例超过序列总长度的 5%;

③序列中质量值小于 5 碱基的比例超过序列总长度的 50%。如果某条序列符合以上 3 个条件中的任何一个, 则去除该序列。数据比对参数为: 采用 BSMAP 软件将有效序列与猪参考基因组进行比对, 比对模式为 map to 2 forward strands, i. e. BSW(++) and BSC(-+).

1.3.2 测序深度统计 甲基化 C 碱基在基因组上的分布类型主要包含 CG、CHG 和 CHH 3 种形式, 其中 H 代表 A 或 T 或 C 碱基。甲基化 C 碱基数目与基因组总碱基数目的比值即为该位点的测序深度, 计算 CG、CHG 和 CHH 3 种序列环境下甲基化 C 碱基的测序深度, 绘制有效测序深度累积分布图。

1.3.3 甲基化水平计算 对于每个甲基化 C 碱基, 甲基化水平按如下公式进行计算: 全基因组 C 碱基甲基化水平 = 基因组中 C 碱基发生甲基化的位点数/全基因组中 C 碱基总数 × 100%; CG、CHG 和 CHH 3 种序列环境中 C 碱基甲基化水平 = 各类型甲基化 C 碱基(mCG、mCHG 和 mCHH)的序列数/各类型序列总数 × 100%。例如, mCG 所占比例 = mCG 序列数/CG 序列总数, 在一定程度上反映了特定品种全基因组甲基化的特点。

1.3.4 CG、CHG 和 CHH 中甲基化 C 附近碱基的序列特征分析 对包括甲基化 C 碱基在内的共 9 bp 碱基统计作图(上下游各 4 bp), 比较不同序列环境下甲基化 C 碱基上下游的序列特征, 为甲基化预测提供依据。

1.3.5 不同基因组功能元件甲基化水平分析 在全基因组水平上, 对 C 碱基在基因功能元件(上游 2 kb 区域、外显子、内含子、下游 2 kb 区域、基因间区和 CpG 岛)上的甲基化修饰水平进行统计并作图, 再将每个基因的各个功能区域划分为相同单位长度, 计算每个单位长度的平均甲基化水平并绘制成折线图。

1.3.6 差异甲基化基因功能富集分析 甲基化主要通过基因启动子区域调控基因表达。本试验选取基因启动子上游 2 kb 区域以及外显子差异甲基化区域的基因进行 GO 功能富集分析, GO 富集采用在线软件 DAVID(<https://david.ncifcrf.gov/>)进行分析。

1.4 实时荧光定量 PCR(RT-qPCR)

采用 RNAiso Plus 提取猪背最长肌组织总 RNA, 利用 PrimeScript RT Master Mix Kit 及随机六聚体引物(random hexamer primer)合成 cDNA。以猪 GAPDH 基因作为参考基因, 采用 RT-qPCR

法检测候选基因 *FAM135B*(序列相似家族 135 成员 B)、*NR1H2*(核受体亚家族 1 组 H 成员 2)、*ID4*(DNA 结合抑制因子 4)、*ZFPM2*(锌指蛋白 FOG 家族成员 2)、*FOXO1*(叉头盒蛋白 O1)的相对表达水平。在 Bio-Rad CFX96 Real-Time PCR 检测系

统上,使用 SYBR Premix Ex *Taq* II 按照说明进行 RT-qPCR,每个 RNA 样品进行 3 个重复,使用 $2^{-\Delta\Delta C_t}$ 法计算 mRNA 的相对表达水平。试验所有引物均利用 Primer Premier 5.0 软件进行设计,引物信息详见表 1。

表 1 RT-qPCR 引物序列及其产物信息

Table 1 Sequences and product information of RT-qPCR primers

基因 Gene	引物序列(5'→3') Sequence of primers (5'→3')	产物大小/bp Product size
<i>FAM135B</i>	F:TTAGCTTCATCGGCCACTCC;R:CGCAGATCAGCATTATCCCT	232
<i>NR1H2</i>	F:GCTCATCGCCATCAACATCTTCTC;R:AAAGCGGCAGCTTCTTGTC	240
<i>ID4</i>	F:GAGATCCTGCCGCACGTTATCG;R:TGCTGTCGCCCTGCTTGTTACAC	199
<i>ZFPM2</i>	F:CTCAGCACGAAGACGGTCAC;R:GGAGCCTGGGTAGAGCCATT	145
<i>FOXO1</i>	F:ACCGCTTTACAAGTGCCTCTGC;R:GCTCAATGAACATGCCATCCAA	148
<i>GAPDH</i>	F:CTGCCGCTGGAGAAACCT;R:GCTGTAGCCAAATTCATTGTCG	226

2 结果与分析

2.1 猪背最长肌基因组测序数据比对分析

由表 2 可知,蓝塘猪样本测序获得原始序列 300 005 805 条,有效序列 210 334 070 条,有效序列与猪参考基因组的比对成功率为 70.11%,Bisulfite

转化率为 98.54%;长白猪样本测序获得原始序列 300 012 190 条,有效序列 210 758 564 条,有效序列与猪参考基因组的比对成功率为 70.25%,Bisulfite 转化率为 98.36%。该结果表明,测序质量较好,亚硫酸氢盐处理成功。

表 2 蓝塘猪(LT)和长白猪(LW)背最长肌全基因组测序数据统计

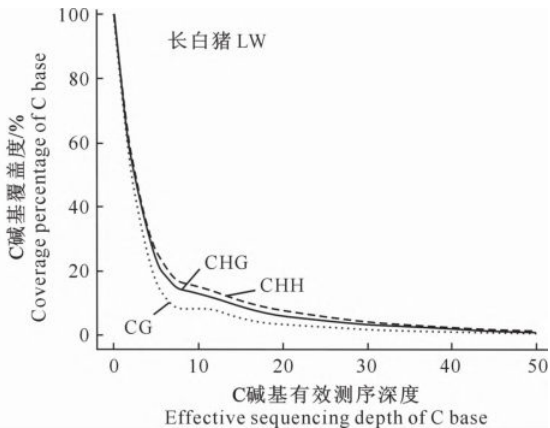
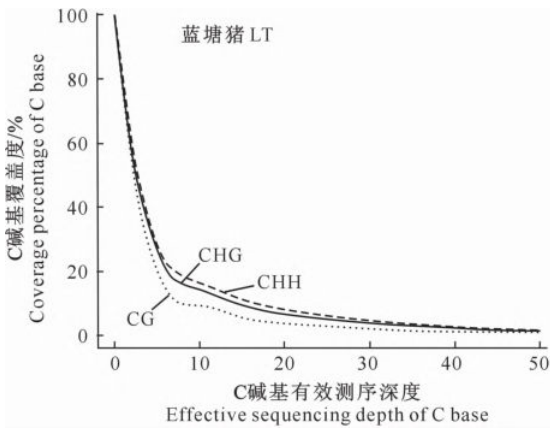
Table 2 Whole genome sequencing data of longissimus dorsi muscle of Lantang (LT) and Landrace (LW) pigs

样本 Sample	原始序列/条 Raw reads	有效序列/条 Alignment reads	比对成功率/% Alignment rate	Bisulfite 转化率/% Conversion rate of Bisulfite
蓝塘猪 LT	300 005 805	210 334 070	70.11	98.54
长白猪 LW	300 012 190	210 758 564	70.25	98.36

2.2 猪背最长肌基因组甲基化 CG、CHG 和 CHH 的测序深度统计

3 种主要类型 C 碱基有效测序深度的累积分布(基于有效数据计算)见图 1。由图 1 可知,蓝塘猪和长白猪在相同有效测序深度下甲基化 C 碱基的

累积分布基本一致,随着有效测序深度的增加,C 碱基的覆盖度降低;由于 CHH 与 CHG 形式 C 碱基总数较少,其覆盖度变化趋势较为一致,均略高于 CG。



H 代表 A 或 T 或 C 碱基。下同

H represents A, T or C base. The same below

图 1 蓝塘猪(LT)和长白猪(LW)背最长肌全基因组甲基化 CG、CHG 和 CHH 有效测序深度的累积分布
Fig.1 Cumulative distribution of effective sequencing depth of methylated CG,CHG and CHH across whole genomes of longissimus dorsi muscle of Lantang (LT) and Landrace (LW) pigs

2.3 猪背最长肌基因组 C 碱基甲基化水平分析

全基因组甲基化水平可以反映基因组甲基化图谱的总体特征,蓝塘猪和长白猪背最长肌基因组 C 碱基的甲基化水平如表 3 所示。由表 3 可知,蓝塘猪和长白猪全基因组范围内 C 位点的甲基化率分

别为 4.07%和 4.44%;CG 位点的甲基化率最高,分别为74.50%和 76.92%;CHG 和 CHH 位点的甲基化率较低,其中 CHG 位点分别为 1.74%和2.13%,CHH 位点分别为 1.51%和 1.87%。

表 3 蓝塘猪(LT)和长白猪(LW)背最长肌全基因组 C、CG、CHG 和 CHH 的平均甲基化水平

Table 3 Average methylation levels of C,CG,CHG and CHH across whole genome of longissimus dorsi muscle of Lantang (LT) and Landrace (LW) pigs

样本 Sample	C	CG	CHG	CHH
蓝塘猪 LT	4.07	74.50	1.74	1.51
长白猪 LW	4.44	76.92	2.13	1.87

表 4 显示,在蓝塘猪中,甲基化的 CG、CHG 和 CHH 分别占 60.08%,9.70%和 30.23%;在长白猪中,甲基化的 CG、CHG 和 CHH 分别占 52.93%,

11.33%和 35.73%。与蓝塘猪相比,长白猪甲基化 CG 的比例降低了 7.15%,甲基化 CHG 和 CHH 的比例分别上升了 1.63%和 5.50%。

表 4 蓝塘猪(LT)和长白猪(LW)背最长肌全基因组甲基化 CG、CHG 和 CHH 的数量及比例

Table 4 Number and proportion of different distribution types of methylated CG,CHG and CHH across whole genome of longissimus dorsi muscle of Lantang (LT) and Landrace (LW) pigs

样本 Sample	CG		CHG		CHH	
	甲基化数 No. of mCG	甲基化 CG 占总 CG 的比例/% Ratio of mCG to total CG	甲基化数 No. of mCHG	甲基化 CHG 占总 CHG 的比例/% Ratio of mCHG to total CHG	甲基化数 No. of mCHH	甲基化 CHH 占总 CHH 的比例/% Ratio of mCHH to total CHH
蓝塘猪 LT	10 745 361	60.08	1 734 665	9.70	5 406 370	30.23
长白猪 LW	10 024 646	52.93	2 145 842	11.33	6 767 376	35.73

CG、CHG 和 CHH 甲基化水平在不同物种间甚至同一物种不同细胞类型间均存在差异。由图 2 可知,在甲基化水平较低时,蓝塘猪和长白猪 2 种猪 CG 的比例明显低于 CHG 和 CHH,但随着甲基化

水平的增加,CG 的比例逐渐高于 CHG 和 CHH;CG 所占的比例随着甲基化水平的升高而逐渐增大,CHG 和 CHH 所占的比例随着甲基化水平的升高先增加再减少。

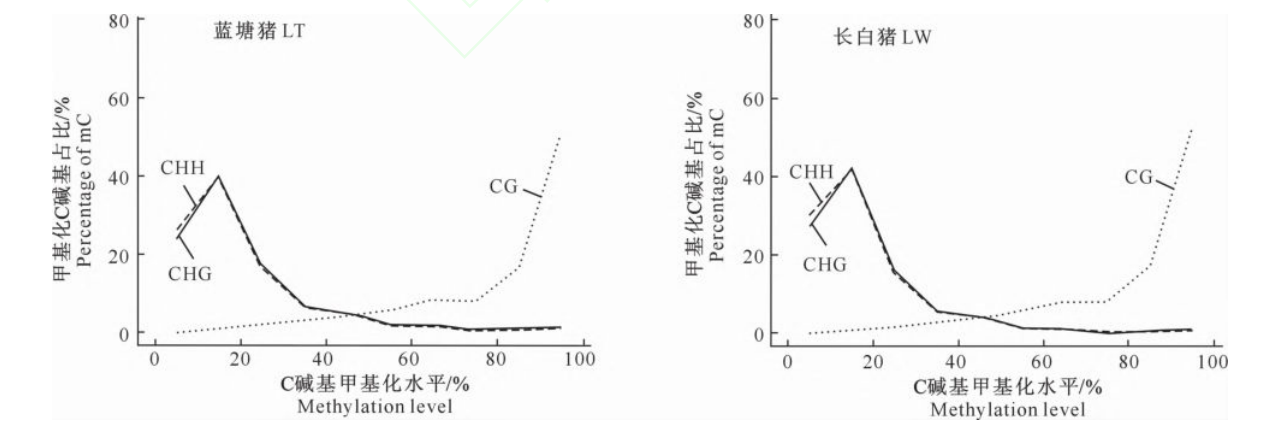


图 2 蓝塘猪(LT)和长白猪(LW)背最长肌全基因组甲基化胞嘧啶的甲基化水平

Fig. 2 Methylation level of methylated cytosine across whole genome of longissimus dorsi muscle of Lantang (LT) and Landrace (LW) pigs

2.4 CG、CHG 和 CHH 附近碱基的序列特征分析

分析 CG 和非 CG 位点甲基化 C 附近碱基的分布情况,统计不同甲基化模式出现的概率。结果(图 3)显示,蓝塘猪和长白猪 CG、CHG 位点的甲基化

无明显区别;而 CHH 位点的甲基化在蓝塘猪中第一位 H 以 A 最多,C 次之,而在长白猪中第一位 H 以 A 最多,T 次之。

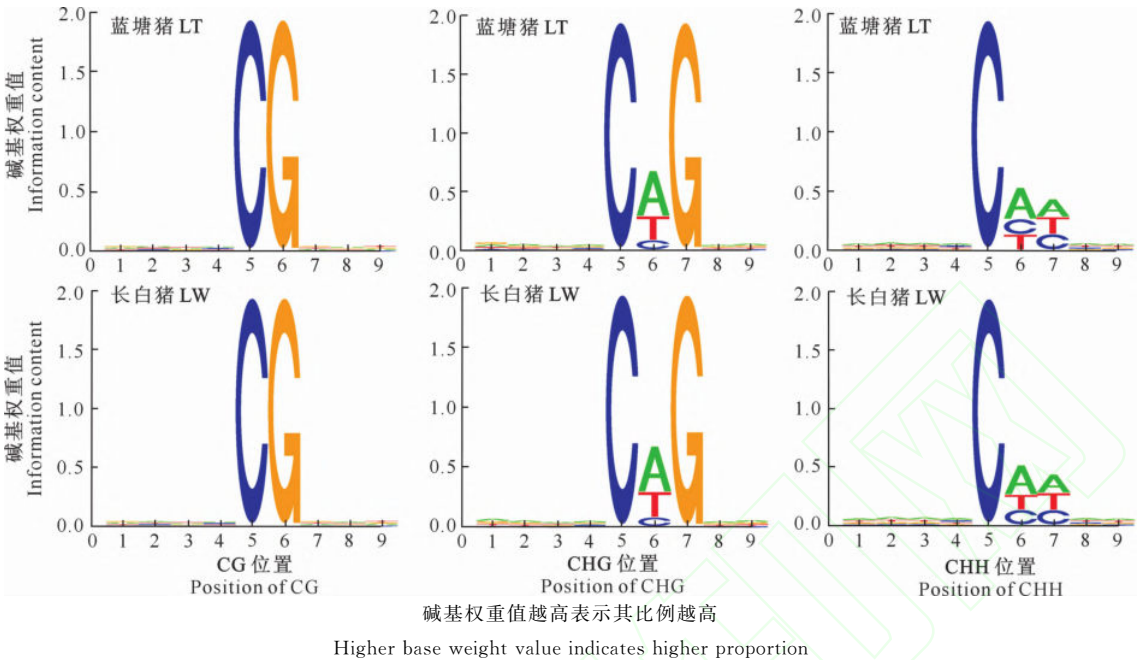


图 3 蓝塘猪(LT)和长白猪(LW)背最长肌全基因组 CG、CHG 和 CHH 中甲基化 C 附近碱基的序列特征
Fig. 3 Sequence characterization of bases near methylated C in CG,CHG and CHH across whole genome of longissimus dorsi muscle of Lantang (LT) and Landrace (LW) pigs

2.5 猪背最长肌全基因组不同功能元件的甲基化水平分析

基因组功能元件分为上游 2 kb 区域、外显子、内含子、下游 2 kb 区域、基因间区和 CpG 岛,分别

统计蓝塘猪和长白猪基因组各功能元件中 CG、CHG 和 CHH 的平均甲基化水平,结果(图 4)表明,2 种猪基因组功能元件的平均甲基化水平相似。

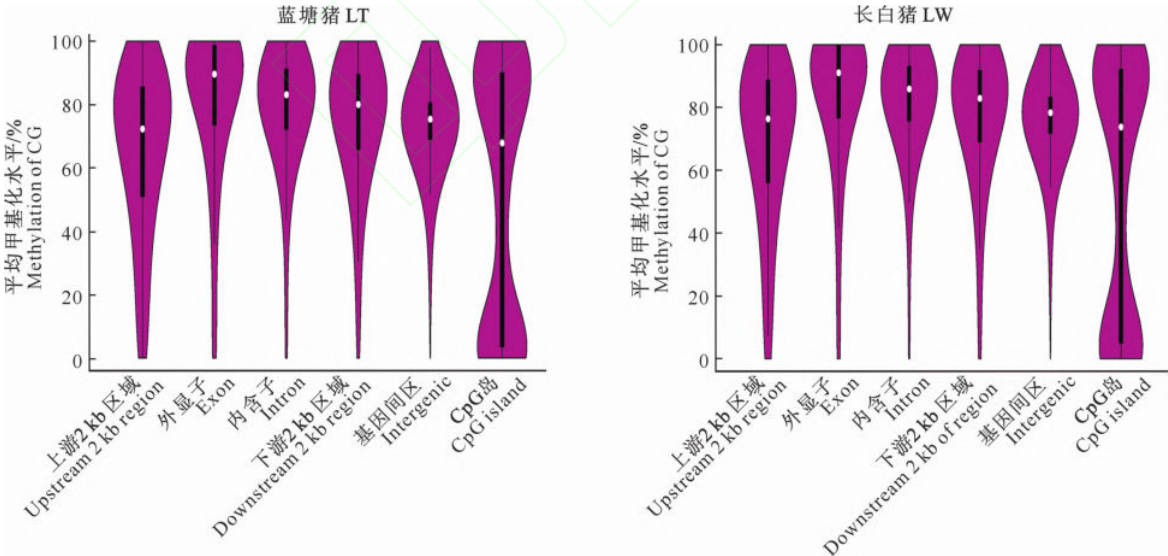


图 4 蓝塘猪(LT)和长白猪(LW)背最长肌全基因组功能元件的平均甲基化水平
Fig. 4 Average methylation levels of functional elements across whole genome of longissimus dorsi muscle of Lantang (LT) and Landrace (LW) pigs

分析 DNA 甲基化水平在不同功能区的分布特点,有助于从全基因组水平了解不同区域 DNA 甲基化修饰的作用。本试验分析了 2 种猪背最长肌全基因组上游 2 kb 区域、外显子、内含子和下游 2 kb 区域 DNA 甲基化的分布,结果(图 5)表明,在不同

的基因组功能元件区域,蓝塘猪和长白猪 DNA 甲基化水平的分布相似,CG 的甲基化水平高于 CHG 和 CHH;CG 中外显子和内含子的甲基化水平较高,且高于侧翼区域(上游 2 kb 区域和下游 2 kb 区域)。

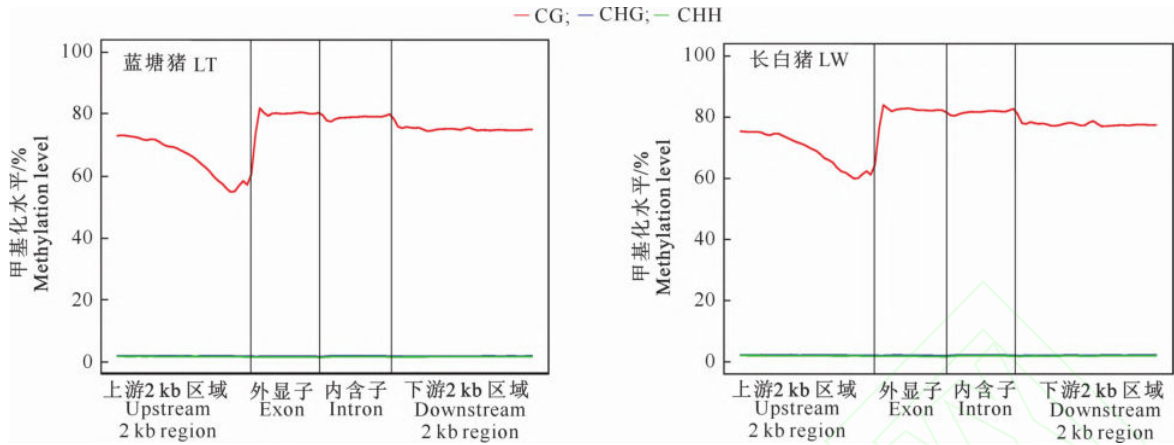


图 5 蓝塘猪(LT)和长白猪(LW)背最长肌全基因组不同功能元件区域甲基化水平的分布

Fig. 5 Horizontal distribution of methylation in different functional element regions across whole genome of longissimus dorsi muscle of Lantang (LT) and Landrace (LW) pigs

2.6 猪背最长肌全基因组差异甲基化分析

对蓝塘猪和长白猪进行全基因组差异甲基化分析,在 2 猪种基因组相同位置上寻找至少 5 个 CG 位点,分析 CG 位点甲基化水平的差异,确定差异甲基化区域(differential methylation region, DMR),最终共检测出 13 126 个 DMR,其总长度为 3 357 954 bp,含有 78 234 个胞嘧啶。将 DMR 注释到基因组功能元件上,统计 DMR 在基因组功能元件上的分布,结果表明,DMR 在基因间区、内含子、外显子、上游 2 kb 区域、下游 2 kb 区域和 CpG 岛的分布分别为 68.50%,25.74%,1.89%,1.85%,1.78%和 0.24%,可见大部分 DMR 位于基因间区和内含子上。

2.7 猪背最长肌全基因组的 GO 富集分析

由于上游区域和外显子区域包含着与基因转录

起始和表达调控有关的许多元件,因此选取上游区域和外显子区域进行 GO 富集分析,结果见图 6 和图 7。

由统计分析结果(图 6 和图 7)可知,上游区域高甲基化基因参与的生物学过程有 RNA 聚合酶 II 启动子对转录的正调控、基因表达的正调控等;外显子区域高甲基化基因参与的生物学过程有凋亡过程的负调控、细胞迁移的正调控等。结合脂代谢相关基因的功能,鉴别到 5 个蓝塘猪与长白猪肌间脂肪相关的候选基因为 *FAM135B*、*NR1H2*、*ID4*、*ZF-PM2*、*FOXO1*。其中,*FAM135B* 和 *NR1H2* 显著富集于细胞脂代谢过程,而 *ID4*、*ZFPM2* 和 *FOXO1* 显著富集于脂肪细胞分化的负调控。

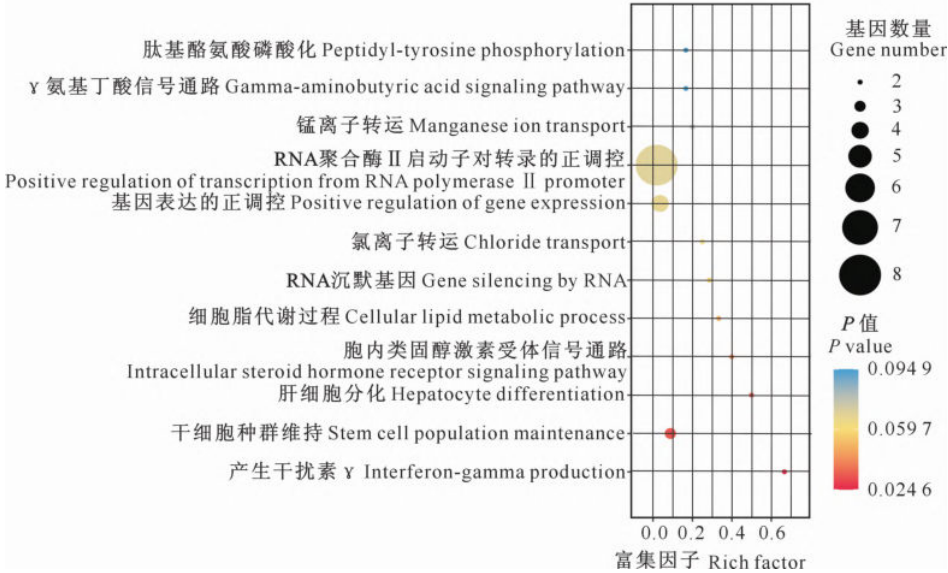


图 6 蓝塘猪(LT)和长白猪(LW)背最长肌全基因组上游区域差异甲基化基因的 GO 富集分析

Fig. 6 GO enrichment analysis of differential methylated genes in upstream region across whole genome of longissimus dorsi muscle of Lantang (LT) and Landrace (LW) pigs

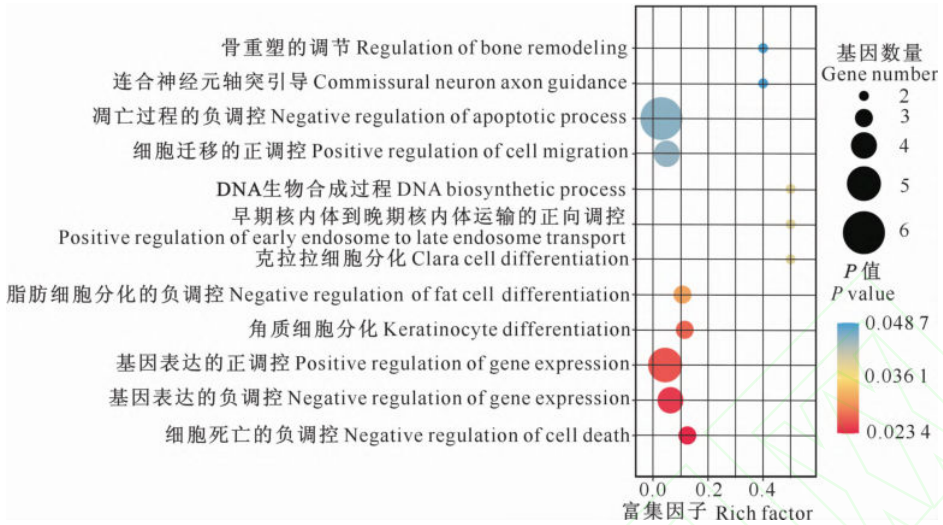
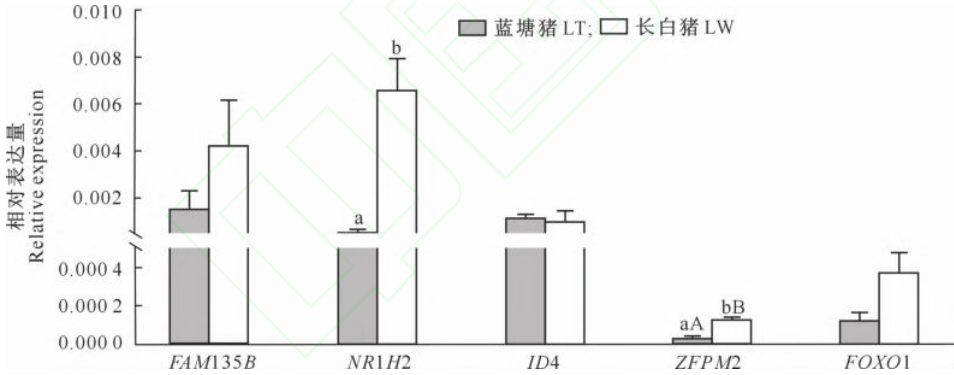


图 7 蓝塘猪(LT)和长白猪(LW)背最长肌全基因组外显子区域差异甲基化基因的 GO 富集分析
Fig. 7 GO enrichment analysis of differential methylated genes in exon region across whole genome of longissimus dorsi muscle of Lantang (LT) and Landrace (LW) pigs

2.8 2 种猪肌间脂肪相关候选基因的鉴定

通过实时荧光定量 PCR(RT-qPCR),检测上述候选基因在蓝塘猪和长白猪背最长肌中的表达情

况。结果(图 7)显示,长白猪 *FAM135B*、*NR1H2*、*ZFPM2* 和 *FOXO1* 的表达水平高于蓝塘猪,而 *ID4* 的表达水平略低于蓝塘猪。



图柱上标不同小写和大写字母表示 2 个猪种相比差异显著($P<0.05$)或极显著($P<0.01$)。有效重复数 $n=3$
Different lowercase and capital letters on the column indicate significant difference ($P<0.05$) or extremely significant difference ($P<0.01$) between two pig breeds. The effective number of replications $n=3$

图 8 蓝塘猪(LT)和长白猪(LW)肌间脂肪相关候选基因的 RT-qPCR 验证

Fig. 8 RT-qPCR validation of intermuscular fat related candidate genes in Lantang (LT) and Landrace (LW) pigs

3 讨 论

DNA 甲基化在基因表达和细胞功能的调控中起着重要作用^[10]。越来越多的研究表明,DNA 甲基化可以调控猪的生长发育等生物过程。Hao 等^[16]通过 WGBS 绘制出热应激猪与非热应激猪之间的 DNA 甲基化图谱,在两组猪之间共鉴定出 57 147 个差异甲基化区域,对应于 1 422 个差异甲基化基因 (differentially methylated gene, DMG)。Yang 等^[9]利用甲基化 DNA 免疫沉淀测序技术对 3 个猪种(通城猪、长白猪和五指山猪)血白细胞的全

基因组 DNA 甲基化谱进行了研究,结果显示通城猪与长白猪、通城猪与五指山猪、长白猪与五指山猪的差异甲基化基因分别为 2 807,2 969 和 5 547 个,3 个对比组共有 868 个 DMG,在发育和代谢相关的生物过程和途径中显著富集。Yang 等^[17]通过整合分析了 3 个不同猪种(通城猪、长白猪和五指山猪)全基因组 DNA 甲基化、mRNA、lncRNA 和 miRNA 谱,系统地对骨骼肌进行了比较分析,发现 DMG 与脂质代谢、氧化应激和肌肉发育显著相关。

Zheng 等^[18]通过深度测序技术,对巴马香猪和大白猪的背最长肌和大白猪睾丸的 20 个甲基化组

和转录组数据进行评估,发现 DNA 甲基化修饰在不同的品种和组织中发挥着重要的调控作用,甚至导致表型发生质的变化。Chen 等^[19]使用全基因组亚硫酸氢盐测序对长白猪、杜洛克猪和大白猪的胞嘧啶甲基化水平进行了分析,结果发现 3 个商品猪品种的精子特异性低甲基化区域(hypomethylated regions, HMRs)均高度保守。品种特异性 HMR 与每个品种的表型变化和经济复杂性状有关。Wang 等^[20]对 30 头青峪猪和 31 头长白猪进行了 RRBS 测序,分析了全基因组差异甲基化 DNA,鉴定出 5 个与猪肉质性状和适应性有关的基因。Wang 等^[21]对 60~400 日龄的莱芜猪背最长肌进行了全基因组转录组和甲基组分析,发现了一组参与肌间脂肪沉积的候选基因和转录因子。Wang 等^[22]对成华猪和大白猪肌肉组织进行了 RRBS 测序,鉴定出与猪肌肉发育和肉质性状相关的 6 个关键基因组区域和 8 个关键 DMG。Zhang 等^[23]对 18, 21 和 28 日龄的五指山猪进行 WGBS 测序,发现在小型猪中肌原性基因的早期去甲基化有助于成肌细胞的早期终末分化。Zhang 等^[25]采用 RRBS 法分析了初生仔猪骨骼肌中成脂和成肌前体全基因组 DNA 的甲基化水平,共鉴定出 11 361 个差异甲基化区域,主要位于基因间区和内含子中,此外还鉴定出 153 个具有不同 DNA 甲基化和表达水平的成脂前体和成肌前体基因。基因组 DNA 甲基化测序技术已经十分成熟,近年来针对猪的各种性状进行了大量的 DNA 甲基化分析,为未来猪种的选育提供新的思路。

本研究只探讨了公猪全基因组的甲基化水平,关于母猪全基因组的甲基化水平尚有待进一步研究。在雄性蓝塘猪和长白猪背最长肌全基因组范围内,C 位点的平均甲基化率约为 4%,CG 位点的平均甲基化率最高,CHG 位点和 CHH 位点的平均甲基化率较低,表明雄性蓝塘猪和长白猪的甲基化主要发生在 CG 位点上,与此前报道的结果^[16,24-25]一致,这提示在不同猪种中甲基化方式存在保守性。分析 DMRs 在不同基因元件上的分布情况,发现 DMRs 在基因间区和内含子的分布为 68.50%和 25.74%,表明大部分 DMRs 位于基因间区和内含子上,这与此前报道的结果^[17,23,25]一致,说明基因间区和内含子区在整个基因组中占比较高,因此大多数的甲基化出现在这 2 个位点中。

本研究通过基因功能 GO 的富集分析,鉴别到 5 个候选基因(*FAM135B*、*NR1H2*、*ID4*、*ZFPM2*

和 *FOXO1*)与脂代谢相关。*FAM135B* 可促进颗粒蛋白(granulin, GRN)的分泌,GRN 是一种在上皮细胞、免疫细胞、软骨细胞和神经细胞中高表达的分泌性生长因子^[26]。*NR1H2* 也被称为肝脏 X 受体(LXRs),是脂质激活的核受体,对胆固醇的生物合成和代谢以及胆汁酸的分泌发挥调节作用,并可控制细胞死亡和增殖平衡^[27];同时也是肝脏新生脂肪生成的关键调节因子,可增强脂肪酸生物合成和极低密度脂蛋白(VLDL)的分泌^[28]。Murad 等^[29]证实,与野生型同窝小鼠相比,*ID4* 纯合子缺失的小鼠(*ID4*^{-/-})身体脂肪减少,体质量增加也少得多。与野生型小鼠相比,*ID4*^{-/-}鼠中分离的小鼠胚胎成纤维细胞的成脂潜能降低,证明 *ID4* 在脂肪细胞分化中具有重要作用。*ZFPM2* 也被称为 GATA 伴侣蛋白 2(the friend of GATA 2, FOG2),与 GATA 蛋白的 N 端锌指相互作用,能够控制脂肪细胞的增殖和分化^[30];张潇飞等^[31]发现,干扰 *ZFPM2* 能显著促进鸡前体脂肪细胞的增殖。Nakae 等^[32]发现,FOXO1 在脂肪中的主要作用是抑制脂肪生成;在末端分化过程中,被激活的 FOXO1 与 PPAR γ 启动子结合,通过竞争性抑制功能性 PPAR γ /视黄醇类 X 受体(retinoid X receptor, RXR)/DNA 复合物的形成,并抑制 PPAR γ 的转录活性,从而抑制脂肪生成和脂肪细胞分化^[33-34]。庞卫军^[35]研究证实,抑制内源 FOXO1 的表达可导致猪前体脂肪细胞成脂能力和成肌细胞成肌能力增强。因此,本研究所鉴定到的候选基因可能通过 DNA 甲基化的调控,在猪的脂肪代谢与合成过程中发挥重要作用,但其具体机制还有待进一步研究。

4 结 论

本研究利用 WGBS 绘制了蓝塘猪与长白猪背最长肌全基因组的 DNA 甲基化图谱,共检测出 13 126 个差异甲基化区域,其中胞嘧啶总数目为 73 234 个,总长度为 3 357 954 bp。差异甲基化基因显著富集于细胞凋亡过程的负调控、细胞迁移的正调控等 24 个 GO 条目,并鉴别到 5 个与蓝塘猪和长白猪脂肪相关的差异基因(*FAM135B*、*NR1H2*、*ID4*、*ZFPM2*、*FOXO1*),该研究结果为深入探究蓝塘猪和长白猪脂肪组成差异的分子机制奠定了基础。

404 参考文献

[1] Pajares M J, Palanca-Ballester C, Urtasun R, et al. Methods for

- analysis of specific DNA methylation status [J]. *Methods*, 2021, 187: 3-12.
- [2] Moore L D, Le T, Fan G. DNA methylation and its basic function [J]. *Neuropsychopharmacology*, 2013, 38(1): 23-38.
 - [3] Adusumalli S, Mohd Omar M F, Soong R, et al. Methodological aspects of whole-genome bisulfite sequencing analysis [J]. *Brief Bioinform*, 2015, 16(3): 369-379.
 - [4] Wang X, Kadarmideen H N. Genome-wide DNA methylation analysis using next-generation sequencing to reveal candidate genes responsible for boar taint in pigs [J]. *Anim Genet*, 2019, 50(6): 644-659.
 - [5] Zhang X, Nie Y, Cai S, et al. Earlier demethylation of myogenic genes contributes to embryonic precocious terminon differentiation of myoblasts in miniature pigs [J]. *FASEB J*, 2019, 33(8): 9638-9655.
 - [6] Weyrich A, Schüllermann T, Heeger F, et al. Whole genome sequencing and methylome analysis of the wild guinea pig [J]. *BMC Genomics*, 2014, 15(1): 1036-1048.
 - [7] Stachecka J, Lemanska W, Noak M, et al. Expression of key genes involved in DNA methylation during *in vitro* differentiation of porcine mesenchymal stem cells (MSCs) into adipocytes [J]. *Biochem Biophys Res Commun*, 2020, 522(3): 811-818.
 - [8] Choi M, Lee J, Le M T, et al. Genome-wide analysis of DNA methylation in pigs using reduced representation bisulfite sequencing [J]. *DNA Res*, 2015, 22(5): 343-355.
 - [9] Yang Y L, Zhou R, Mu Y L, et al. Genome-wide analysis of DNA methylation in obese, lean, and miniature pig breeds [J]. *Sci Rep*, 2016, 6: 30160-30172.
 - [10] Bibikova M, Fan J B. Genome-wide DNA methylation profiling [J]. *Wiley Interdiscip Rev Syst Biol Med*, 2010, 2(2): 210-223.
 - [11] Campagna M P, Xavier A, Lechner-Scott J, et al. Epigenome-wide association studies: current knowledge, strategies and recommendations [J]. *Clin Epigenetics*, 2021, 13(1): 214-238.
 - [12] Sun J, Xie M, Huang Z, et al. Integrated analysis of non-coding RNA and mRNA expression profiles of 2 pig breeds differing in muscle traits [J]. *J Anim Sci*, 2017, 95(3): 1092-1103.
 - [13] 王艳明. 中国优良地方猪种及其种质特性 [J]. *畜牧与饲料科学*, 2009, 30(4): 162-165.
Wang Y M. Excellent local pig breeds in China and their germplasm characteristics [J]. *Animal Husbandry and Feed Science*, 2009, 30(4): 162-165.
 - [14] Du J, Xu Y, Zhang P, et al. MicroRNA-125a-5p affects adipocytes proliferation, differentiation and fatty acid composition of porcine intramuscular fat [J]. *Int J Mol Sci*, 2018, 19(2): 501-515.
 - [15] Sun Y, Cai R, Wang Y, et al. A newly identified lncRNA LncIMF4 controls adipogenesis of porcine intramuscular preadipocyte through attenuating autophagy to inhibit lipolysis [J]. *Animals*, 2020, 10(6): 926-941.
 - [16] Hao Y, Cui Y, Gu X. Genome-wide DNA methylation profiles changes associated with constant heat stress in pigs as measured by bisulfite sequencing [J]. *Sci Rep*, 2016, 6: 27507-27520.
 - [17] Yang Y, Liang G, Niu G, et al. Comparative analysis of DNA methylome and transcriptome of skeletal muscle in lean-, obese-, and mini-type pigs [J]. *Sci Rep*, 2017, 7: 39883-33897.
 - [18] Zheng M, Xiao S, Guo T, et al. DNA methylomic homogeneity and heterogeneity in muscles and testes throughout pig adulthood [J]. *Aging*, 2020, 12(24): 25412-25431.
 - [19] Chen S, Liu S, Mi S, et al. Comparative analyses of sperm DNA methylomes among three commercial pig breeds reveal vital hypomethylated regions associated with spermatogenesis and embryonic development [J]. *Front Genet*, 2021, 12: 740036-740047.
 - [20] Wang K, Wu P, Wang S, et al. Differential DNA methylation analysis reveals key genes in Chinese Qingyu and Landrace pigs [J]. *Genome*, 2021, 65(1): 1-8.
 - [21] Wang Y, Ma C, Sun Y, et al. Dynamic transcriptome and DNA methylome analyses on longissimus dorsi to identify genes underlying intramuscular fat content in pigs [J]. *BMC Genomics*, 2017, 18(1): 780-798.
 - [22] Wang K, Wu P, Wang S, et al. Genome-wide DNA methylation analysis in Chinese Chenghua and Yorkshire pigs [J]. *BMC Genom Data*, 2021, 22(1): 21-30.
 - [23] Zhang X, Sun W, He L, et al. Global DNA methylation pattern involved in the modulation of differentiation potential of adipogenic and myogenic precursors in skeletal muscle of pigs [J]. *Stem Cell Res Ther*, 2020, 11(1): 536-551.
 - [24] 郭添福, 张志燕, 陈冬, 等. 不同性别大白猪肌肉全基因组高分辨率单碱基甲基化差异分析 [J]. *畜牧兽医学报*, 2018, 49(11): 2326-2339.
Guo T F, Zhang Z Y, Chen D, et al. High resolution and single base genome-wide methylation variance analysis of muscle of large white pigs with different sexes [J]. *Acta Veterinaria et Zootechnica Sinic*, 2018, 49(11): 2326-2339.
 - [25] 徐盼, 仲德, 马政, 等. 基于全基因组差异甲基化分析鉴别影响苏姜猪体重的候选基因 [J]. *中国畜牧兽医*, 2021, 48(8): 2889-2900.
Xu P, Zhong D, Ma Z, et al. Identification of candidate genes for body weight in Sujang pigs based on genome-wide differential methylation analysis [J]. *China Animal Husbandry & Veterinary Medicine*, 2021, 48(8): 2889-2900.
 - [26] Ruan D, Zhuang Z, Ding R, et al. Weighted single-step GWAS identified candidate genes associated with growth traits in a Duroc pig population [J]. *Genes*, 2021, 12(1): 117-132.
 - [27] Handschin C, Meyer U A. Regulatory network of lipid-sensing nuclear receptors: roles for *CAR*, *PXR*, *LXR*, and *FXR* [J]. *Arch Biochem Biophys*, 2005, 433(2): 387-396.
 - [28] Wang B, Tontonoz P. Liver X receptors in lipid signalling and membrane homeostasis [J]. *Nat Rev Endocrinol*, 2018, 14(8): 452-463.
 - [29] Murad J M, Place C S, Ran C, et al. Inhibitor of DNA binding

- 4 (*ID4*) regulation of adipocyte differentiation and adipose tissue formation in mice [J]. *J Biol Chem*, 2010, 285 (31): 24164-24173.
- [30] Jack B H, Crossley M. GATA proteins work together with friend of GATA (FOG) and C-terminal binding protein (CTBP) co-regulators to control adipogenesis [J]. *J Biol Chem*, 2010, 285 (42): 32405-32414.
- [31] 张潇飞, 宋 鹤, 刘 静, 等. 鸡 miR-17-92 基因簇靶基因 *ZFPM2* 的鉴定及功能分析 [J]. *遗传*, 2017, 39(4): 333-345.
Zhang X F, Song H, Liu J, et al. Identification and analysis of *ZFPM2* as a target gene of miR-17-92 cluster in chicken [J]. *Hereditas*, 2017, 39(4): 333-345.
- [32] Nakae J, Kitamura T, Kitamura Y, et al. The forkhead transcription factor *FoxO1* regulates adipocyte differentiation [J]. *Dev Cell*, 2003, 4(1): 119-129.
- [33] Chen J, Lu Y, Tian M, et al. Molecular mechanisms of *FoxO1* in adipocyte differentiation [J]. *J Mol Endocrinol*, 2019, 62 (3): 239-253.
- [34] Homan E P, Brandão B B, Softic S, et al. Differential roles of *FOXO* transcription factors on insulin action in brown and white adipose tissue [J]. *J Clin Invest*, 2021, 131 (19): e143328.
- [35] 庞卫军. 猪 *FoxO1* 基因 cDNA 的克隆及对前体脂肪细胞和成肌细胞分化的调控作用 [D]. 陕西杨凌: 西北农林科技大学, 2007.
Pang W J. Cloning of porcine *FoxO1* gene and its regulation during cloning of porcine *FoxO1* gene and its regulation during preadipocyte and myoblast differentiation [D]. Yangling, Shaanxi: Northwest A&F University, 2007.



动物营养学报
Chinese Journal of Animal Nutrition
ISSN 1006-267X, CN 11-5461/S

《动物营养学报》网络首发论文

题目: 凉茶渣替代象草对育肥牛空肠组织形态、屏障功能以及菌群结构的影响
作者: 李玲, 孙小红, 连旭, 罗君谊, 陈婷, 习欠云, 张永亮, 孙加节
收稿日期: 2021-07-14
网络首发日期: 2021-10-21
引用格式: 李玲, 孙小红, 连旭, 罗君谊, 陈婷, 习欠云, 张永亮, 孙加节. 凉茶渣替代象草对育肥牛空肠组织形态、屏障功能以及菌群结构的影响[J/OL]. 动物营养学报. <https://kns.cnki.net/kcms/detail/11.5461.S.20211020.1043.038.html>



网络首发: 在编辑部工作流程中, 稿件从录用到出版要经历录用定稿、排版定稿、整期汇编定稿等阶段。录用定稿指内容已经确定, 且通过同行评议、主编终审同意刊用的稿件。排版定稿指录用定稿按照期刊特定版式(包括网络呈现版式)排版后的稿件, 可暂不确定出版年、卷、期和页码。整期汇编定稿指出版年、卷、期、页码均已确定的印刷或数字出版的整期汇编稿件。录用定稿网络首发稿件内容必须符合《出版管理条例》和《期刊出版管理规定》的有关规定; 学术研究成果具有创新性、科学性和先进性, 符合编辑部对刊文的录用要求, 不存在学术不端行为及其他侵权行为; 稿件内容应基本符合国家有关书刊编辑、出版的技术标准, 正确使用和统一规范语言文字、符号、数字、外文字母、法定计量单位及地图标注等。为确保录用定稿网络首发的严肃性, 录用定稿一经发布, 不得修改论文题目、作者、机构名称和学术内容, 只可基于编辑规范进行少量文字的修改。

出版确认: 纸质期刊编辑部通过与《中国学术期刊(光盘版)》电子杂志社有限公司签约, 在《中国学术期刊(网络版)》出版传播平台上创办与纸质期刊内容一致的网络版, 以单篇或整期出版形式, 在印刷出版之前刊发论文的录用定稿、排版定稿、整期汇编定稿。因为《中国学术期刊(网络版)》是国家新闻出版广电总局批准的网络连续型出版物(ISSN 2096-4188, CN 11-6037/Z), 所以签约期刊的网络版上网络首发论文视为正式出版。

凉茶渣替代象草对育肥牛空肠组织形态、屏障功能以及菌群结构的影响

李玲 孙小红 连旭 罗君谊 陈婷 习欠云 张永亮* 孙加节*

(华南农业大学动物科学学院, 广东省动物营养调控重点实验室, 广州 510642)

摘要: 本试验旨在研究凉茶渣替代象草对育肥牛空肠组织形态、屏障功能以及菌群结构的影响。选取 120 头健康且体重相近的西门塔尔杂交肉牛, 随机分为 2 个组, 分别为对照组(饲喂基础饲料)、试验组(50%凉茶渣替代部分象草), 每组 3 个重复, 每个重复 20 头。试验期共 67 d, 包括 7 d 的预试期, 60 d 的正试期。在试验期结束后, 采集试验牛血液、空肠组织、空肠内容物, 通过苏木精-伊红(HE)染色测量空肠绒毛高度、隐窝深度; 通过酶联免疫吸附测定(ELISA)试剂盒检测血清中炎症因子、D-乳酸(D-Lac)以及二胺氧化酶(DAO)浓度; 通过荧光定量 PCR 测定空肠紧密连接蛋白基因闭合小环蛋白-1(ZO-1)、闭锁蛋白(Occludin)、闭合蛋白-1(Claudin-1)的 mRNA 表达水平; 利用 16S rDNA 高通量测序分析空肠菌群结构。结果表明: 1) 与对照组相比, 试验组育肥牛空肠绒毛高度显著增加($P<0.05$), 血清中 D-Lac 浓度显著降低($P<0.05$), 空肠紧密连接蛋白 ZO-1 的 mRNA 表达水平显著上调($P<0.05$)。2) 在门水平上, 对照组和试验组厚壁菌门(Firmicutes)相对丰度分别为 85.79%、76.96%, 拟杆菌门(Bacteroidetes)相对丰度分别为 0.54%、3.11%。在属水平上, 对照组和试验组之间罗姆布茨菌属(Romboutsia)、罗斯氏菌属(Rothia)、布劳特氏菌属(Blautia)等相对丰度表现出显著差异($P<0.05$)。3) Pearson 相关性分析表明, 空肠绒毛高度与 Blautia、Rothia、短波单胞菌属(Brevundimonas)、四球虫属(Tetrasphaera)相对丰度呈显著正相关($P<0.05$), 相关系数为 0.46~0.57; 血清中 D-Lac 浓度与 Romboutsia、土孢杆菌属(Terrisporobacter)相对丰度呈显著正相关($P<0.05$), 相关系数分别为 0.56、0.62; 空肠紧密连接蛋白 ZO-1 的 mRNA 表达水平与梭菌属(Solobacterium)相对丰度呈显著负相关($P<0.05$), 相关系数为 -0.50。由此可见, 饲料中添加 50%凉茶渣作为功能性粗饲料对育肥牛空肠绒毛高度、屏障功能有积极的影响, 凉茶渣可能通过改变空肠菌群组成和相对丰度, 进而影响空肠组织形态与屏障功能, 最终促进肠道健康。

关键词: 凉茶渣; 育肥牛; 空肠; 组织形态; 屏障功能; 空肠菌群

中图分类号: S823

文献标识码: A

凉茶主要由凉粉草、鸡蛋花、金银花、菊花、夏枯草、布渣叶和甘草等 7 种植物性中草药煎制而成, 凉茶渣成分与其原材料相近^[1], 主要包含 7 种酚酸类物质、6 种黄酮苷类物质、3 种皂苷类物质

以及 1 种甾醇类物质^[2], 具有清热排毒、抗菌消炎的功效^[3-4]。据初步统计, 目前仅广东地区主要凉茶生产企业, 日均可产生约千吨固废凉茶渣, 采用焚烧、填埋的方式进行处理, 不仅加剧环境污染, 更是对中草药资源的严重浪费。如将凉茶渣作为

收稿日期: 2021-07-14

基金项目: 国家重点研发计划(2018YFD0501700); 广东省重点研发计划(2019B110209005); 广东省现代农业技术体系(2018LM1121, 2018LM2158)

作者简介: 李玲(1997—), 女, 河南信阳人, 硕士研究生, 从事动物营养组学研究。E-mail: 1350979603@qq.com

* 通信作者: 张永亮, 教授, 博士生导师, E-mail: zhangyl@scau.edu.cn; 孙加节, 副教授, 硕士生导师, E-mail: jiajiesun@scau.edu.cn

非常规饲料资源进行开发,对缓解我国饲料资源紧缺将有很大益处^[5]。试验表明,凉茶渣作为后备奶牛功能性粗饲料,能够部分缓解机体夏季热应激^[6]。

肠道微生物群是一个稳定且复杂的生态系统,可以通过形成菌膜、促进肠道上皮细胞增殖分化等方式保护肠道健康^[7]。因此,本文将凉茶渣作为育肥牛非常规粗饲料资源进行利用,探究其对育肥牛空肠组织形态、屏障功能以及菌群结构的影响,为凉茶渣饲料化利用提供技术数据。

1 材料与方法

1.1 试验设计及饲养管理

凉茶渣主要营养成分含量(除干物质外,其余指标均为干物质基础)^[6]:干物质 20.55%,中性洗涤纤维 61.22%,酸性洗涤纤维 40.29%,粗蛋白质 9.78%,粗脂肪 3.52%,粗灰分 6.68%。

试验采用单因素随机分组设计,选用 120 头约 18 月龄、体况良好且体重 $[(487\pm29)\text{ kg}]$ 相近的西门塔尔杂交育肥牛,随机分为 2 个组,分别为对照组(CN 组,饲喂基础饲料)、试验组(RE 组,50%凉茶渣替代部分象草),每组 3 个重复,每个重复 20 头牛。预试期 7 d,正试期 60 d。根据育肥肉牛现阶段营养需要与所在养殖场生产实际配制饲料,试验饲料组成及营养水平见表 1。饲料均由饲料搅拌机混合均匀,每天 08:00 和 17:00 定时喂料,自由饮水。牛舍每天清扫,定期进行消毒,保持清爽整洁。

表 1 试验饲料组成及营养水平(干物质基础)

Table 1 Composition and nutrient levels of experimental diets (DM basis) %

项目 Items	组别 Groups	
	CN	RE
原料 Ingredients		
玉米 Corn	23.7	23.7
象草 <i>Pennisetum purpureum</i>	60.0	10.0
凉茶渣 Herbal tea residue		50.0
豆腐渣 Bean curd residue	15.0	15.0
食盐 NaCl	0.3	0.3
预混料 Premix ¹⁾	1.0	1.0
合计 Total	100.0	100.0
营养水平 Nutrient levels ²⁾		
干物质 DM	34.55	30.65

续表 1

项目 Items	组别 Groups	
	CN	RE
粗蛋白质 CP	9.14	9.70
粗脂肪 CF	2.05	3.00
钙 Ca	0.69	0.63
磷 P	0.22	0.30
中性洗涤纤维 NDF	71.16	68.86
酸性洗涤纤维 ADF	25.23	27.57
净能 NE/(MJ/kg)	5.56	5.36

1) 预混料为每千克饲料提供 The premix provided the following per kg of diets: Ca 150~160 mg, Zn 70.00~100 mg, Fe 50.00~70.00 mg, Cu 30.00~30.20 mg, Mn 6.25~10.00 mg, Se 31.25~35.00 mg, I 0.2~1.00 mg, VA 70 000~10 000 IU, VD 40 000~90 000 IU, VE 46.75~50.00 mg。

2) 净能为计算值,其余为实测值。NE was a calculated value, while the others were measured values.

1.2 样品采集

试验期结束前 1 天,每组随机选取 10 头牛进行尾静脉采血,采取的血液在离心管中静置 2 h,4 000 r/min 离心 10 min,分离出的血清于 -20 ℃ 保存备用。试验牛屠宰前隔夜禁食 16 h,每组随机选取 10 头,立即分离出肠道,分别取空肠组织、空肠内容物于离心管中,液氮速冻后放入 -80 ℃ 冰箱冻存备用。

1.3 空肠组织切片染色

将空肠组织放入 4% 多聚甲醛溶液中固定 24 h 后,用 0.01 mol/L 磷酸盐缓冲液(PBS)溶液冲洗,再用浓度递增的乙醇脱水,二甲苯清洗,并包埋在石蜡中;切片后展平放置于载玻片上,再烘干;苏木精-伊红(HE)染色后用乙醇脱水,用二甲苯使切片透明,并用封固剂封固。使用 Imager 软件测量空肠绒毛高度和隐窝深度。

1.4 血清免疫指标

血清中肿瘤坏死因子- α (TNF- α)、白细胞介素-6(IL-6)、白细胞介素-10(IL-10)、转化生长因子- β (TGF- β)、D-乳酸(D-Lac)、二胺氧化酶(DAO)浓度采用南京建成生物工程研究所酶联免疫吸附测定(ELISA)试剂盒进行检测,操作过程严格按照试剂盒说明书进行。

1.5 荧光定量 PCR(qRT-PCR)

取黄豆粒儿大小的空肠组织块并剪碎,用 Trizol 裂解法提取空肠组织样品 RNA,并按照反转

录试剂盒操作步骤合成 cDNA。参照武笑天等^[8]的引物序列,对肠道紧密连接蛋白闭合小环蛋白-1(zonula occludens-1, ZO-1)、闭锁蛋白(Occludin)、闭合蛋白-1(Claudin-1)进行 qRT-PCR 分析,引物购买于生工生物工程(上海)股份有限公司。

1.6 16S rRNA 基因测序及注释分析

采用十二烷基硫酸钠(SDS)方法对空肠内容物基因组 DNA 进行提取,利用琼脂糖凝胶电泳判断检测 DNA 的纯度和浓度。对 16S rDNA 的 V3~V4 设计带 Barcode 的特异引物,利用高效高保真酶进行 PCR,确保扩增效率和准确性。文库构建、上机测序与操作分类单元(operational taxonomic units, OTUs)聚类 and 物种注释,以及后续的组内 Alpha 多样性分析、组间 Beta 多样性分析及 Pearson 相关性分析由诺禾致源生物公司完成。

1.7 数据统计分析

空肠组织形态及血清免疫指标等试验数据采用 Excel 2010 进行初步整理,然后利用 SPSS V17.0 软件进行独立样本 t 检验,以 $P<0.05$ 为差异显著性标准。利用 MetaStat 分析,在属水平上做 2 组间空肠微生物的置换检验(permutation test),得到 P 值,然后对 P 值进行修正,得到错误发现率(false discovery rate, FDR)值,以 $FDR<0.05$ 为菌群差异显著性标准^[9]。

2 结 果

2.1 凉茶渣对育肥牛空肠组织形态与屏障功能的影响

空肠组织 HE 染色结果见图 1-A。由图 1-B 可见,空肠绒毛高度和隐窝深度测量结果表明,与 CN 组相比,RE 组的空肠绒毛高度显著增加($P<0.05$),空肠隐窝深度无显著差异($P>0.05$)。由图 1-C 可见,血清中 D -Lac 和 DAO 浓度检测结果表明,与 CN 组相比,RE 组的血清中 D -Lac 浓度显著降低($P<0.05$),血清中 DAO 浓度有所下降,但差异不显著($P>0.05$)。由图 1-D 可见,血清中炎症因子 $TNF-\alpha$ 、IL-6、IL-10、 $TGF-\beta$ 浓度检测结果表明,与 CN 组相比,RE 组血清中 IL-6 和 $TNF-\alpha$ 浓度均有所下降,但差异不显著($P>0.05$)。由图 1-E 可见,为了进一步研究凉茶渣对肠道屏障功能的作用,利用 RT-qPCR 检测肠道紧密连接蛋

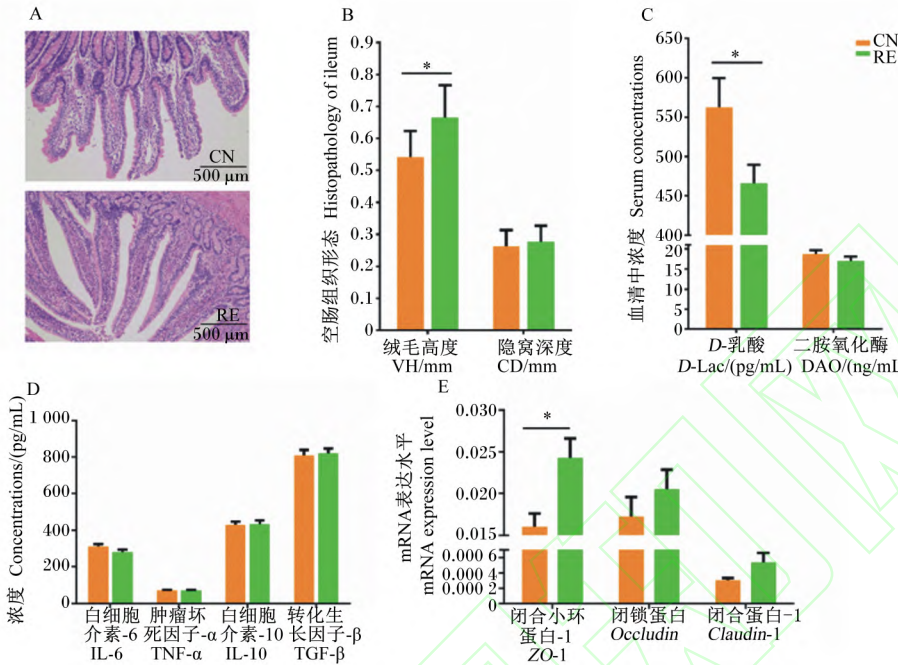
白 ZO-1、Occludin、Claudin-1 的 mRNA 表达水平,与 CN 组相比,RE 组的空肠紧密连接蛋白 ZO-1 的 mRNA 表达水平显著上调($P<0.05$),Occludin、Claudin-1 的 mRNA 表达水平均上调,但差异不显著($P>0.05$)。

2.2 凉茶渣对育肥牛空肠菌群的影响

2.2.1 OTUs 聚类 and 物种注释

根据 Barcode 序列拆分出各样本数据,使用 FLASH(<http://ccb.jhu.edu/software/FLASH/>)对每个样本的 reads 进行拼接,平均每个样本得到原始 Tags 序列 $85\,403\pm2\,052$ 条,参照 Qiime(http://qiime.org/scripts/split_libraries_fastq.html)质量控制流程,每个样品获得 Effective Tags 序列($54\,589\pm1\,327$)条。利用 Uparse 软件(<http://www.drive5.com/uparse/>)对所有样本的全部 Effective Tags 进行聚类,默认以 97% 的一致性将序列聚类成为 OTUs,共得出 3 999 个有效 OTUs 片段,其中 2 组样品共有 1 835 个 OTUs, CN 和 RE 组中特有的 OTUs 数量分别为 1 057 和 1 107 个(图 2-A)。根据物种注释结果,确定了 20 个样本中最大相对丰度排名前 10 的物种(图 2-B),其中相对丰度最大的 2 个菌门是厚壁菌门(Firmicutes)和变形菌门(Proteobacteria),分别为 81.37% 和 8.00%。CN 和 RE 组厚壁菌门相对丰度分别为 85.79%、76.96%,变形菌门相对丰度分别为 4.44%、11.57%;另外, CN 和 RE 组拟杆菌门相对丰度差别较大,分别为 0.54% 和 3.11%。即 RE 组厚壁菌门相对丰度较 CN 组有所减少,变形菌门、拟杆菌门相对丰度较 CN 组有所增加,但优势菌群在门水平上没有发生改变。且与 CN 组相比,RE 组中厚壁菌门与拟杆菌门的比值(F/B)有所降低。

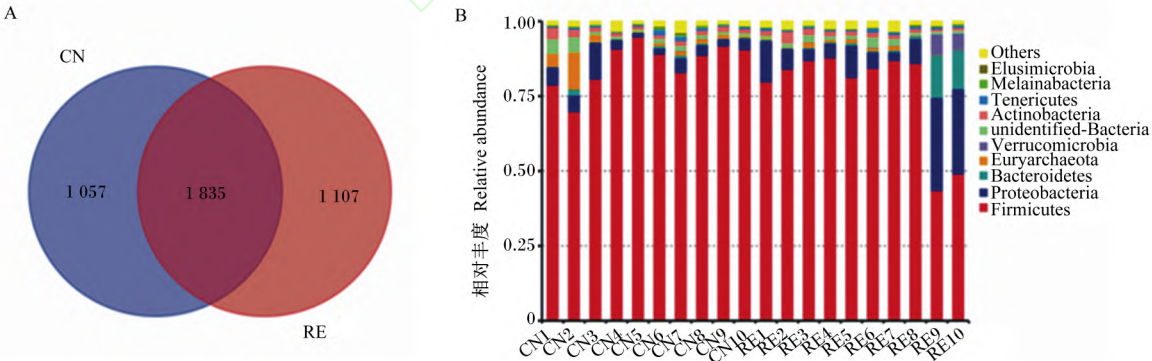
由图 3 可见,物种丰度聚类分析表明,在属水平上, CN 组和 RE 组之间表现出显著差异的前 10 个菌属分别是罗姆布茨菌属(Romboutsia)、假丁酸弧菌(Pseudobutyrvibrio)、柠檬酸杆菌(Limnobacter)、黑水仙菌属(Melainabacteria)、艰难杆菌属(Mogibacterium)、马文伯里安菌(Marvinbryantia)、丁酸麻球菌属(Butyricicoccus)、罗斯氏菌属(Rothia)、布劳特氏菌属(Blautia)。另外,与 CN 组相比,RE 组 Rothia、Blautia 相对丰度显著增加($P<0.05$), Romboutsia 相对丰度显著减少($P<0.05$)。



A: 空肠组织 HE 染色 HE staining of jejunum tissue; B: 凉茶渣对育肥牛空肠绒毛高度和隐窝深度的影响 effects of herbal tea residue on villus height and crypt depth of jejunum of fattening cattle; C: 凉茶渣对育肥牛血清中 *D*-Lac 与 DAO 浓度的影响 effects of herbal tea residue on concentrations of *D*-Lac and DAO in serum of fattening cattle; D: 凉茶渣对育肥牛血清免疫因子浓度的影响 effects of herbal tea residue on serum immune factor concentration of fattening cattle; E: 凉茶渣对育肥牛空肠紧密连接蛋白基因表达的影响 effect of herbal tea residue on gene expression of tight junction proteins in jejunum of fattening cattle.
* : 差异显著 significant difference ($P<0.05$) ; CN: 对照组 control group; RE: 试验组 experimental group. 下图同 the same as below .

图 1 凉茶渣对育肥牛空肠组织形态与屏障功能的影响

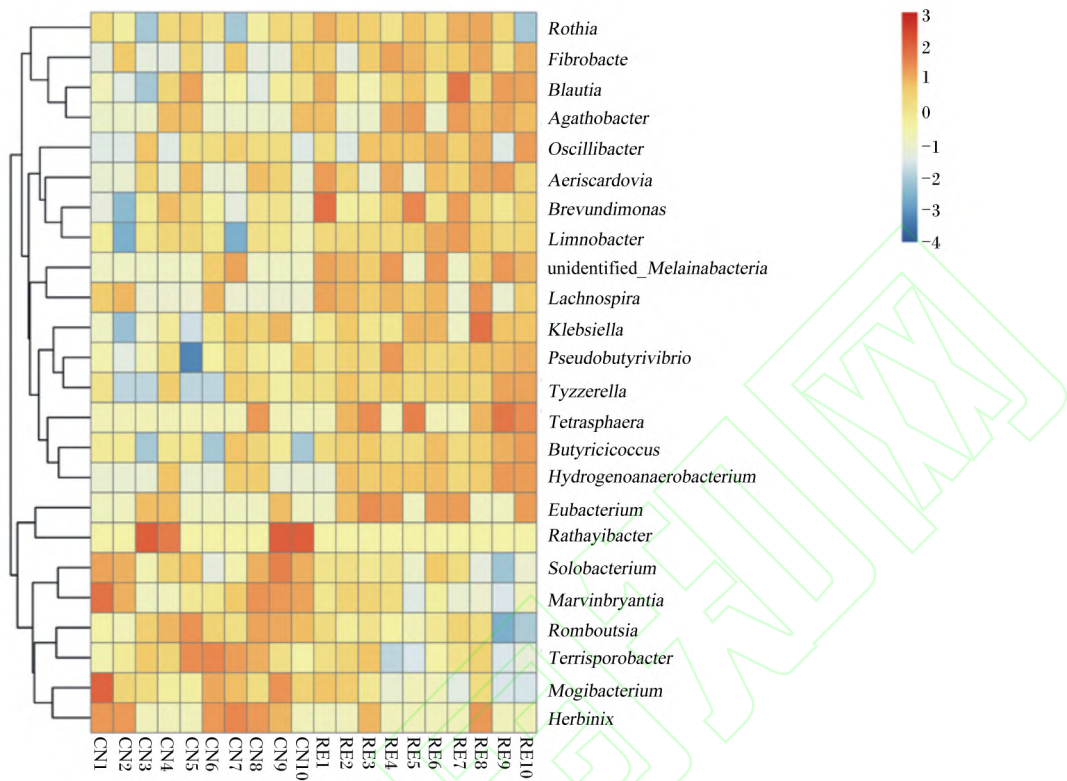
Fig.1 Effects of herbal tea residue on morphology and barrier function of jejunum of fattening cattle



A: 各组基于 OTUs 的韦恩图统计 Venn diagram statistics of each group based on OTUs; B: 每个样品在门水平上的物种相对丰度柱形统计 column statistics of species relative abundance of each sample at phylum level. Firmicutes: 厚壁菌门; Proteobacteria: 变形菌门; Bacteroidetes: 拟杆菌门; Euryarchaeota: 广古菌门; Verrucomicrobia: 疣微菌门; unidentified-Bacteria: 未分类菌门; Actinobacteria: 放线菌门; Tenericutes: 柔壁菌门; Melainabacteria: 黑水仙菌门; Elusimicrobia: 迷踪菌门; Others: 其他。

图 2 空肠菌群在门水平上的相对丰度

Fig.2 Relative abundance of jejunal flora at phylum level



Rothia: 罗斯氏菌属; *Fibrobacte*: 纤维杆菌属; *Blautia*: 布劳特氏菌属; *Agathobacter*: 无杆菌属; *Oscillibacter*: 颤螺旋菌属; *Aeriscardovia*: 气斯卡多维亚氏菌属; *Brevundimonas*: 短波单胞菌属; *Limnobacter*: 柠檬酸杆菌属; *unidentified_Melainabacteria*: 未分类黑水仙菌属; *Lachnospira*: 毛螺菌属; *Klebsiella*: 克雷伯氏菌属; *Pseudobutyrvibrio*: 假丁酸弧菌; *Tyzzerella*: 泰泽雷拉菌属; *Tetrasphaera*: 四球虫属; *Butyricoccus*: 丁蓖麻球菌属; *Hydrogenoanaerobacterium*: 氢厌氧小杆属; *Eubacterium*: 真杆菌属; *Rathayibacter*: 鸭舌草杆菌属; *Solobacterium*: 梭菌属; *Marvinbryantia*: 马文伯里安菌属; *Romboutsia*: 罗姆布茨菌属; *Terrisporobacter*: 土孢杆菌属; *Mogibacterium*: 艰难杆菌属; *Herbinix*: 赫宾尼菌属。

图 3 每个样品的物种相对丰度聚类热图

Fig.3 Cluster statistical chart of species relative abundance of each samples

2.2.2 空肠菌群多样性研究

由图 4-A 可见,RE 组的 Observed_species 指数显著高于 CN 组 ($P<0.05$) ,表明 RE 组物种数目显著高于 CN 组 ,但是 CN 组和 RE 组之间 Shannon、Simpson、Chao1 指数均无显著差异 ($P>0.05$) 。Beta 多样性分析是对不同组间样品的微生物群落构成进行比较分析 ,其中 Anosim 分析是一种非参数检验 ,用来检验组间的差异是否显著大于组内差异 ,从而判断分组是否有意义^[10] 。由图 4-B 可见 ,Anosim 分析得出 $R = 0.159$, $P = 0.011$, R 值大于 0 小于 1 ,且 P 值小于 0.05 ,表明组间差异水平显著大于组内。

2.3 空肠菌群与其组织形态、屏障功能相关性分析

为了进一步鉴定与空肠组织形态、屏障功能

显著相关的菌属 ,进行了 Pearson 相关性分析 ,此分析指 2 个变量之间的线性相关性 ,相关系数越接近 1 表明 2 个变量之间越相关。由图 5 可见 ,空肠绒毛高度与 *Blautia*、*Brevundimonas*、*Rothia*、*Tetrasphaera* 相对丰度呈显著正相关 ($P<0.05$) ,相关系数范围为 0.46 ~ 0.57; 血清中 *D*-Lac 浓度与 *Romboutsia*、*Terrisporobacter* 相对丰度呈显著正相关 ($P<0.05$) ,相关系数分别为 0.56、0.62; 血清中 DAO 浓度与 赫宾尼菌属 (*Herbinix*)、*Terrisporobacter* 相对丰度呈显著正相关 ($P<0.05$) ,相关系数分别为 0.60、0.52; 血清中 IL-6 浓度与气斯卡多维亚氏菌属 (*Aeriscardovia*) 相对丰度呈显著正相关 ($P=0.05$) ,相关系数为 -0.44; 血清中 IL-10 浓度与 *Mogibacterium* 相对丰度呈显著负相关 ($P<$

蛋白 *Occludin* 的 mRNA 表达水平与 *Herbinix* 相对丰度呈显著负相关 ($P<0.05$) 相关系数为-0.46。

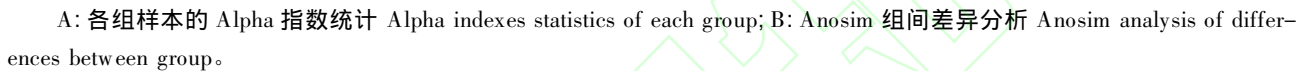


Fig.4 Alpha and Beta diversity analysis of jejunal flora

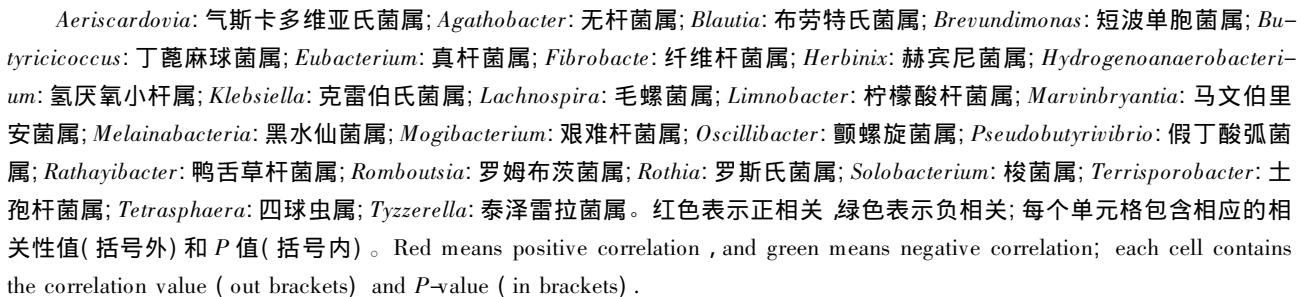


Fig.5 Correlation between differential intestinal flora at genus level and related indexes

3 讨 论

3.1 凉茶渣对育肥牛空肠组织形态与屏障功能的影响

空肠是动物对饲料营养成分进行消化与吸收的主要部位,其消化吸收作用主要依赖于肠上的环形皱襞、肠绒毛及绒毛表面的柱状上皮细胞等结构^[11]。肠绒毛的存在极大地增加了小肠与食物的接触面积,绒毛高度越高,其消化吸收面积就越大;肠隐窝是肠上皮在绒毛根部下陷至固有层而形成的管状腺,肠隐窝深度代表细胞的生成率,隐窝越浅细胞成熟度越好,分泌功能越好。所以肠绒毛高度和隐窝深度是衡量动物消化吸收能力的 2 个重要指标^[12-13],同时也是肠道机械屏障的依托结构。研究表明,饲料中添加 4% 的中草药显著增加了大鼠后段小肠的绒毛高度,对小肠形态与功能的生长发育具有促进作用^[14];另外在饲料中添加中草药能够调理肠道,显著提高肉牛的表现消化率^[15]。在本试验中,饲喂凉茶渣的育肥牛空肠绒毛高度显著升高,与前人的研究结果一致。因此推测,凉茶渣在一定程度上能够改变空肠组织形态,进而提高其消化吸收能力。

肠道的屏障功能主要依靠相邻肠道上皮细胞之间的紧密连接结构,对于动物健康至关重要, Occludins、Claudins、ZO-1 这 3 种紧密连接蛋白是紧密连接结构中的关键部分^[16-18]。D-Lac 主要来自肠道,完整的肠黏膜可以防止 D-Lac 通过门脉循环进入血液^[19],当肠道屏障功能受损时,肠道中大量的 D-Lac 会被释放到血液循环中^[20]。DAO 是一种细胞内酶,在哺乳动物小肠绒毛上皮中具有高活性,肠黏膜损伤后,血清 DAO 浓度会增加^[21]。因此血清中的 D-Lac 和 DAO 浓度可以反映肠道屏障功能是否受损。研究表明,中草药饲料添加剂能够改善热应激肉牛的肠道炎症,修复肠道受损^[15];中药渣能通过刺激 ZO-1 的表达来增强断奶仔猪肠上皮细胞的屏障功能,改善肠道环境^[22]。在本试验中,饲喂凉茶渣的育肥牛血清中 D-Lac 浓度显著降低,空肠 ZO-1 的 mRNA 表达水平显著上调,与前人的研究结果一致。这表明凉茶渣能增强育肥牛空肠的屏障功能,改善肠道环境。

3.2 凉茶渣对育肥牛空肠菌群结构的影响

肠道菌群是机体肠道微生物的集合体,不仅

参与机体消化和吸收营养物质的过程,而且能够抵抗病原菌的侵入,对机体健康具有至关重要的作用^[23]。影响肠道菌群组成和多样性因素很多,主要包括饮食、环境和年龄,其中饮食在影响肠道菌群结构中尤为重要^[24-26]。本研究结果中,OTUs 聚类分析发现 CN 和 RE 组中特有的 OTUs 数量分别为 1 057 和 1 107 个,表明饲料中添加凉茶渣使育肥牛空肠菌群物种数目有所增加。

根据物种注释结果,20 个样本中最丰富的 2 个菌门是厚壁菌门和变形菌门,RE 组厚壁菌门相对丰度较 CN 组有所减少,拟杆菌门、变形菌门相对丰度有所增加,且 RE 组厚壁菌门与拟杆菌门的比值有所降低。研究表明,牛肠道中的主要有益微生物是厚壁菌门和拟杆菌门^[27],厚壁菌门内的瘤胃球菌可通过发酵纤维二糖和纤维素产生甲酸与乙酸^[28],拟杆菌门的细菌可利用葡萄糖发酵产生乙酸、琥珀酸等^[29]。厚壁菌门与拟杆菌门的比值是反映肠道菌群紊乱的重要指标,其升高对动物健康是不利的^[30-31]。同时,厚壁菌门与拟杆菌门的比值也与机体的胖瘦程度有关,肥胖机体肠道菌群中厚壁菌门与拟杆菌门的比值更高^[32]。变形菌门中包括很多病原菌,数量过多时会引发肠道炎症,但本试验结果表明 RE 组血清炎症因子浓度与 CN 组并无显著差异。此外,瘤胃酸中毒时期,瘤胃中厚壁菌门相对丰度增加,拟杆菌门相对丰度下降^[33]。上述分析说明凉茶渣在一定程度上会影响肉牛的育肥效果,但是牛体内脂肪沉积过多会导致内分泌功能紊乱,无法正常供应机体所需的糖分^[34]。因此从总体而言,凉茶渣能够维持育肥牛肠道菌群稳态,减少疾病的发生。

在属水平上,与 CN 组相比,RE 组 *Rothia*、*Blautia* 相对丰度显著增加,*Romboutsia* 相对丰度显著减少。*Blautia* 是一种有益菌,其产生的丁酸酯可通过免疫调节来增强抗菌作用^[35]; *Rothia* 能够降解饲料中的蛋白质,有助于肠道对营养物质的消化吸收^[36],而 *Romboutsia* 是肠道菌群失衡的生物标志物^[37]。这说明凉茶渣能够使育肥牛空肠菌群有益菌数量增加,有害菌数量减少,改善肠道稳态。

Alpha 多样性分析反映了样品物种丰富度和多样性,RE 组的 Observed_species 指数显著高于 CN 组,表明 RE 组菌群物种数目显著高于 CN 组。对于 Beta 多样性分析,Anosim 方法得出 $R =$

0.159 $P=0.011$,表明组间微生物群落结构差异显著。Alpha、Beta 多样性分析结果说明凉茶渣能够使育肥牛肠道菌群组成和相对丰度发生显著变化。

3.3 育肥牛空肠菌群与其组织形态、屏障功能的相关性

众多研究结果表明肠道菌群影响其组织形态和功能^[38-39] ,而且肠道菌群的代谢产物对肠道健康也有重要的影响 ,比如代谢产物短链脂肪酸可以促进肠上皮细胞的增殖和分化 ,增加 ZO-1 和 Occludin 的 mRNA 表达水平 ,增强肠道屏障功能^[40] 。Pearson 相关性分析结果中 ,空肠绒毛高度与 *Blautia*、*Brevundimonas*、*Rothia*、*Tetrasphaera* 相对丰度呈显著正相关。*Blautia* 可能是通过代谢产物丁酸酯的抗菌作用减少肠道炎症^[35] ,从而促进绒毛增长;*Rothia* 可能是通过降解饲料蛋白为绒毛增长提供能量^[36] 。血清中 D-Lac 浓度与 *Romboutsia*、*Terrisporobacter* 相对丰度呈显著正相关 ,DAO 浓度与 *Herbinix*、*Terrisporobacter* 相对丰度呈显著正相关。*Romboutsia* 是肠道菌群失衡的生物标志物^[37] ,*Terrisporobacter* 与肠道炎症有关^[41] ,从侧面论证了血清中 D-Lac 和 DAO 浓度可以反映肠道屏障功能是否受损。此外 ,肠道菌群的变化还使动物血清中炎症因子浓度、紧密连接蛋白基因的 mRNA 表达水平发生相应变化。这部分结果说明空肠菌群能通过自身或代谢产物对其组织形态、炎症反应、屏障功能产生一定程度的影响。

4 结 论

凉茶渣替代象草能够改变育肥牛空肠组织形态 ,增强空肠屏障功能 ,改善空肠菌群组成和相对丰度 ,促进肠道健康。

参考文献:

- [1] 刘主洁.王老吉凉茶的化学成分分析及质量评价研究[D].硕士学位论文.广州:广州中医药大学,2016.
LIU Z J. Chemical components analysis and quality control of Wanglaoji herbal tea [D]. Master's Thesis. Guangzhou: Guangzhou University of Chinese Medicine, 2016. (in Chinese)
- [2] 贺颖颖,罗燕玉,林朝展,等.王老吉凉茶化学成分研究[J].中药材,2018,41(4):889-893.
HE Y Y, LUO Y Y, LIN C Z, et al. Chemical constituents from Wanglaoji herbal tea [J]. Journal of Chinese Medicinal Materials, 2018, 41(4): 889-893. (in Chinese)
- [3] LI D L, ZHENG X L, DUAN L, et al. Ethnobotanical survey of herbal tea plants from the traditional markets in Chaoshan, China [J]. Journal of Ethnopharmacology, 2017, 205: 195-206.
- [4] RAHMAN I U, AFZAL A, IQBAL Z, et al. Herbal teas and drinks: folk medicine of the Manoor Valley, Lesser Himalaya, Pakistan [J]. Plants, 2019, 8(12): 581.
- [5] AJILA C M, BRAR S K, VERMA M, et al. Bio-processing of agro-byproducts to animal feed [J]. Critical Reviews in Biotechnology, 2012, 32(4): 382-400.
- [6] XIE Y Q, CHEN Z J, WANG D Y, et al. Effects of fermented herbal tea residues on the intestinal microbiota characteristics of Holstein heifers under heat stress [J]. Frontiers in Microbiology, 2020, 11: 1014.
- [7] 张萌萌,姜宁,张爱忠.肠道微生物对肠道屏障功能完整性的维护机制研究概况[J].微生物学通报,2020,47(3):933-940.
ZHANG M M, JIANG N, ZHANG A Z. Maintenance mechanism of intestinal barrier function integrity by intestinal microbes [J]. Microbiology, 2020, 47(3): 933-940. (in Chinese)
- [8] 武笑天,温翌,李锐瑞,等.叶酸和维生素 B₁₂ 对产蛋鸡生产性能、小肠屏障功能及相关基因表达的影响[J].动物营养学报,2021,33(5):2616-2630.
WU X T, WEN Z, LI R R, et al. Effects of folic acid and vitamin B₁₂ on performance, small intestinal barrier function and related gene expression of laying hens [J]. Chinese Journal of Animal Nutrition, 2021, 33(5): 2616-2630. (in Chinese)
- [9] PAULSON J N, POP M, BRAVO H C. Metastats: an improved statistical method for analysis of metagenomic data [J]. Genome Biology, 2011, 12(Suppl. 1): P17.
- [10] CHAPMAN M G, UNDERWOOD A J. Ecological patterns in multivariate assemblages: information and interpretation of negative values in ANOSIM tests [J]. Marine Ecology Progress Series, 1999, 180: 257-265.
- [11] 陈耀星,崔燕.动物解剖学与组织胚胎学[M].北京:中国农业出版社,2019.
CHEN Y X, CUI Y. Animal anatomy and histology [M]. Beijing: China Agriculture Press, 2019. (in Chinese)
- [12] 王娇,杨宝钰,阿依古丽·艾买尔,等.甜高粱与苜蓿混合青贮对肉羊消化道组织形态的影响[J].饲料

- 工业 2021 42(7): 54-60.
- WANG J ,YANG B Y ,AIMAIER A Y G L ,et al. Effects of sweet sorghum and alfalfa silage mixtures on digestive tissue morphology in meat sheep [J]. Feed Industry 2021 42(7): 54-60.(in Chinese)
- [13] WOYENGO T A ,KIARIE E ,NYACHOTI C M. Metabolizable energy and standardized ileal digestible amino acid contents of expeller-extracted canola meal fed to broiler chicks [J]. Poultry Science ,2010 ,89 (6): 1182-1189.
- [14] 王凤英. 中草药结合 α -酮戊二酸对断奶大鼠消化道生长发育的影响 [D]. 硕士学位论文. 乌鲁木齐: 新疆农业大学 2004.
- WANG F Y. The effects of Chinese herbs combined with α -ketoglutarate on the small intestinal morphology and physiology in weaned rats [D]. Master's Thesis. Urumqi: Xinjiang Agricultural University 2004.(in Chinese)
- [15] CHEN J ,GUO K ,SONG X Z ,et al. The anti-heat stress effects of Chinese herbal medicine prescriptions and rumen-protected γ -aminobutyric acid on growth performance ,apparent nutrient digestibility ,and health status in beef cattle [J]. Animal Science Journal , 2020 91(1): e13361.
- [16] HUANG S W ,FU Y J ,XU B ,et al. Wogonoside alleviates colitis by improving intestinal epithelial barrier function via the MLCK/pMLC2 pathway [J]. Phyto-medicine 2020 68: 153179.
- [17] ZEISEL M B ,DHAWAN P ,BAUMERT T F. Tight junction proteins in gastrointestinal and liver disease [J]. Gut 2019 68(3): 547-561.
- [18] KAWANO M ,MIYOSHI M ,OGAWA A ,et al. *Lactobacillus gasseri* SBT2055 inhibits adipose tissue inflammation and intestinal permeability in mice fed a high-fat diet [J]. Journal of Nutritional Science 2016 , 5: e23.
- [19] GAO M ,JIANG Y ,XIAO X F ,et al. Protective effect of pioglitazone on sepsis-induced intestinal injury in a rodent model [J]. The Journal of Surgical Research , 2015 ,195(2): 550-558.
- [20] DUZGUN A P ,GULGEZ B ,OZMUTLU A ,et al. The relationship between intestinal hypoperfusion and serum d-lactate levels during experimental intra-abdominal hypertension [J]. Digestive Diseases and Sciences , 2006 51(12): 2400-2403.
- [21] HONZAWA Y ,NAKASE H ,MATSUURA M ,et al. Clinical significance of serum diamine oxidase activity in inflammatory bowel disease: importance of evaluation of small intestinal permeability [J]. Inflammatory Bowel Diseases 2011 ,17(2): E23-E25.
- [22] SU J Y ,ZHU Q ,ZHAO Y ,et al. Dietary supplementation with Chinese herbal residues or their fermented products modifies the colonic microbiota ,bacterial metabolites and expression of genes related to colon barrier function in weaned piglets [J]. Frontiers in Microbiology 2018 9: 3181.
- [23] SHREINER A B ,KAO J Y ,YOUNG V B. The gut microbiome in health and in disease [J]. Current Opinion in Gastroenterology 2015 31(1): 69-75.
- [24] MA Q T ,LI Y Q ,LI P F ,et al. Research progress in the relationship between type 2 diabetes mellitus and intestinal flora [J]. Biomedicine & Pharmacotherapy , 2019 ,117: 109138.
- [25] MA N ,TIAN Y A ,WU Y ,et al. Contributions of the interaction between dietary protein and gut microbiota to intestinal health [J]. Current Protein & Peptide Science 2017 ,18(8): 795-808.
- [26] SARESELLA M ,MENDOZZI L ,ROSSI V ,et al. Immunological and clinical effect of diet modulation of the gut microbiome in multiple sclerosis patients: a pilot study [J]. Frontiers in Immunology 2017 8: 1391.
- [27] WANG H ,JI Y C ,YIN C ,et al. Differential analysis of gut microbiota correlated with oxidative stress in sows with high or low litter performance during lactation [J]. Frontiers in Microbiology 2018 9: 1665.
- [28] GAGEN E J ,PADMANABHA J ,DENMAN S E ,et al. Hydrogenotrophic culture enrichment reveals rumen *Lachnospiraceae* and *Ruminococcaceae* acetogens and hydrogen-responsive *Bacteroidetes* from pasture-fed cattle [J]. FEMS Microbiology Letters ,2015 ,362 (14): fnv104.
- [29] NAKAYAMA J ,YAMAMOTO A ,PALERMO-CONDE L A ,et al. Impact of westernized diet on gut microbiota in children on Leyte island [J]. Frontiers in Microbiology 2017 8: 197.
- [30] 许杰 ,王伊龙 ,王拥军. 肠道菌群与高血压 [J]. 中国卒中杂志 2017 ,12(2): 175-178.
- XU J ,WANG Y L ,WANG Y J. Gut microbiome and hypertension [J]. Chinese Journal of Stroke ,2017 ,12 (2): 175-178.(in Chinese)
- [31] LI J ,ZHAO F Q ,WANG Y D ,et al. Gut microbiota dysbiosis contributes to the development of hypertension [J]. Microbiome 2017 5(1): 14.
- [32] TURNBAUGH P J ,LEY R E ,MAHOWALD M A ,et

- al. An obesity-associated gut microbiome with increased capacity for energy harvest[J]. *Nature* ,2006 , 444(7122) : 1027–1031.
- [33] PLAIZIER J C ,LI S ,TUN H M ,et al. Nutritional models of experimentally-induced subacute ruminal acidosis (SARA) differ in their impact on rumen and hindgut bacterial communities in dairy cows[J]. *Frontiers in Microbiology* ,2017 ,7: 2128.
- [34] 孙鹏.奶牛酮病的发生原因、临床特征、诊断及防治措施[J]. *现代畜牧科技* ,2021(3) : 78–79.
- SUN P. Causes ,clinical features ,diagnosis and control measures of ketosis in dairy cows[J]. *Modern Animal Husbandry Science & Technology* ,2021(3) : 78–79. (in Chinese)
- [35] BERNI CANANI R ,SANGWAN N ,STEFKA A T ,et al. *Lactobacillus rhamnosus* GG-supplemented formula expands butyrate-producing bacterial strains in food allergic infants [J]. *The ISME Journal* ,2016 ,10(3) : 742–750.
- [36] WEI G X ,DARWISH G ,OPPENHEIM F G ,et al. Commensal bacterium *Rothia aeria* degrades and detoxifies gluten via a highly effective subtilisin enzyme [J]. *Nutrients* ,2020 ,12(12) : 3724.
- [37] MANGIFESTA M ,MANCABELLI L ,MILANI C ,et al. Mucosal microbiota of intestinal polyps reveals putative biomarkers of colorectal cancer [J]. *Scientific Reports* ,2018 ,8(1) : 13974.
- [38] KELLER M ,MAZUCH J ,ABRAHAM U ,et al. A circadian clock in macrophages controls inflammatory immune responses [J]. *Proceedings of the National Academy of Sciences of the United States of America* , 2009 ,106(50) : 21407–21412.
- [39] 尉浩斌 张小丹 李苏宜.肠屏障功能损伤机制及其临床检测方法研究现状[J]. *肿瘤代谢与营养电子杂志* ,2020 ,7(4) : 407–414.
- WEI H B ,ZHANG X D ,LI S Y. Research status of the mechanism of intestinal barrier function injury and its clinical detection methods [J]. *Electronic Journal of Metabolism and Nutrition of Cancer* ,2020 ,7(4) : 407–414. (in Chinese)
- [40] BACH KNUDSEN K E ,LÆRKE H N ,HEDEMAN M S ,et al. Impact of diet-modulated butyrate production on intestinal barrier function and inflammation [J]. *Nutrients* ,2018 ,10(10) : 1499.
- [41] CAI C X ,ZHANG Z X ,MORALES M ,et al. Feeding practice influences gut microbiome composition in very low birth weight preterm infants and the association with oxidative stress: a prospective cohort study [J]. *Free Radical Biology & Medicine* ,2019 ,142: 146–154.

Effects of Herbal Tea Residue on Ileum Morphology , Barrier Function and Flora Structure of Fattening Cattle

LI Ling SUN Xiaohong LIAN Xu LUO Junyi CHEN Ting XI Qianyun

ZHANG Yongliang* SUN Jiajie*

(Key Laboratory of Animal Nutrition Control in Guangdong , College of Animal Science , South China Agricultural University , Guangzhou 510642 , China)

Abstract: This experiment was conducted to study the effects of herbal tea residue on ileum morphology , barrier function and flora structure of fattening cattle. A total of 120 healthy Simmental crossbred beef cattle with similar body weight were randomly divided into two groups: control group (fed a basal diet) and experimental group (50% herbal tea residue replaced part of elephant grass) , with 3 replicates in each group and 20 heads in each replicate. The experimental period lasted for 67 days , including 7 days of pre feeding period and 60 days of formal experimental period. At the end of the experimental period , the blood , jejunal tissue and jejunal contents were collected , and the villus height and crypt depth of jejunum were measured by hematoxylin-eosin (HE) staining; the concentrations of inflammatory factors , *D*-lactic acid (*D*-Lac) and diamine oxidase (DAO) in serum were measured by enzyme-linked immunosorbent assay (ELISA) kit; the mRNA expression levels of tight junction proteins of zonula occludens-1 (*ZO*-1) , *Occludin* and *Claudin*-1 in jejunum were determined by fluorescence quantitative PCR; the 16S rDNA high-throughput sequencing was used to analyze the structure of jejunal flora. The results showed as follows: 1) compared with the control group , the jejunal villi height of the experimental group was significantly increased ($P<0.05$) , the serum *D*-Lac concentration was significantly decreased ($P<0.05$) , and the mRNA expression level of tight junction protein *ZO*-1 in jejunum was significantly up-regulated ($P<0.05$) . 2) At the phylum level , the *Firmicutes* relative abundances in the control group and the experimental group were 85.79% and 76.96% , respectively , and the *Bacteroidetes* relative abundances were 0.54% and 3.11% , respectively. At the genus level , the relative abundances of *Romboutsia* , *Rothia* and *Blautia* showed significant differences between the control group and the experimental group ($P<0.05$) . 3) Pearson correlation analysis displayed that the jejunal villi height showed significant positive correlations with the relative abundances of *Blautia* , *Brevundimonas* , *Rothia* and *Tetrasphaera* ($P<0.05$) , and the correlation coefficients ranged from 0.46 to 0.57; the serum *D*-Lac concentration showed significant positive correlations with the relative abundances of *Romboutsia* and *Terrisporobacter* ($P<0.05$) , and the correlation coefficients were 0.56 and 0.62 , respectively; the mRNA expression level of tight junction protein *ZO*-1 in jejunum showed a significant negative correlation with the relative abundances of *Solobacterium* ($P<0.05$) , and correlation coefficient was -0.50. In conclusion , adding 50% herbal tea residue as functional roughage in the diet has positive effects on the jejunal villus height and barrier function of fattening cattle , the herbal tea residue may affect intestinal tissue morphology and barrier function by changing the composition and relative abundance of jejunal flora , and ultimately promote the intestinal health. [Chinese Journal of Animal Nutrition , 2022 , 34(2)

Key words: herbal tea residue; fattening cattle; jejunum; tissue morphology; barrier function; jejunal flora

* Corresponding authors: ZHANG Yongliang , professor , E-mail: zhangyl@scau.edu.cn; SUN Jiajie , associate professor , E-mail: jiajiesun@scau.edu.cn



Effect of miR-493-5p on proliferation and differentiation of myoblast by targeting ANKRD17

Xiaona Zhuang¹ · Fang Xie¹ · Zekun Lin¹ · Junyi Luo¹ · Ting Chen¹ · Qianyun Xi¹ · Yongliang Zhang¹ · Jiajie Sun¹

Received: 6 December 2022 / Accepted: 20 April 2023

© The Author(s), under exclusive licence to Springer-Verlag GmbH Germany, part of Springer Nature 2023

Abstract

The hypertrophy and conversion of postnatal muscle fibers largely determine the yield and quality of meat, which is closely related to the economic value of pigs. MicroRNA (miRNA), as a kind of endogenous noncoding RNA molecule, is widely involved in myogenesis of livestock and poultry. The longissimus dorsi tissues of Lantang pigs at 1 and 90 days (LT1D and LT90D) were collected and profiled by miRNA-seq. We found 1871 and 1729 miRNA candidates in LT1D and LT90D samples, and 794 miRNAs were shared. We identified 16 differentially expressed miRNAs between two tested groups and explored the function of miR-493-5p in myogenesis. The miR-493-5p promoted the proliferation and inhibited the differentiation of myoblasts. Using GO and KEGG analyses of 164 target genes of miR-493-5p, we found that *ATP2A2*, *PPP3CA*, *KLF15*, *MED28*, and *ANKRD17* genes were related to muscle development. RT-qPCR detection showed that the expression level of *ANKRD17* was highly expressed in LT1D libraries, and the double luciferase report test preliminarily proved that miR-493-5p and *ANKRD17* have a directly targeting relationship. We established miRNA profiles for the longissimus dorsi tissues of 1-day-old and 90-day-old Lantang pigs and found that miR-493-5p was differentially expressed and associated with myogenesis by targeting *ANKRD17* gene. Our results should serve as a reference for future studies on pork quality.

Keywords MiRNA · Muscle · C₂C₁₂ · miR-493-5p · RNA-seq

Introduction

The yield and quality of pork are the key indicators to measure the economic traits of pigs. Over the past few decades, the excessive pursuit of growth rate in pig breeding has led to the decline of meat quality (Schwab et al. 2006). In general, muscle fiber is the basic unit of muscle, whose number does not increase after birth (Moss 1968). The growth potential of postnatal muscle mainly focuses on the hypertrophy and conversion of muscle fibers (Paredes et al. 2013), which

has an important impact on meat quality, such as meat tenderness, water power, and color (Ashmore 1974; Joo et al. 2013). Myofiber types are divided into oxidation and fermentation types (Lefaucheur 2010). Oxidation fibers include types I and IIa and mainly rely on aerobic metabolism, and the diameter is small (Peter et al. 1972). Oxidized muscle fibers are rich in oxidized myoglobin, thus making pork with bright red color (Karlsson et al. 1999). Fermentative muscle fibers include type IIx and type IIb fibers, and the diameter of fermentative fibers is large (Larzul et al. 1997); and the main breathing mode is anaerobic fermentation (Schiaffino and Reggiani 1996), which is related to water holding capacity of pork (Lawrie 1970; Bowker et al. 2005). Therefore, muscle fiber development is an important entry point to study muscle development.

The growth and development of muscle fibers involve complex molecular mechanism (Anakwe et al. 2002; Borycki et al. 1999; Swoap et al. 2000). With the progress of biological sequencing technology, the function of noncoding genes in muscle development has been gradually excavated. MicroRNA (miRNA) is a kind of endogenous noncoding small-RNA fragments containing 22–24 nucleotide bases

Xiaona Zhuang and Fang Xie contributed equally to this article. Yongliang Zhang and Jiajie Sun are co-corresponding authors.

✉ Yongliang Zhang
zhangyl@scau.edu.cn

✉ Jiajie Sun
jjajiesun@scau.edu.cn

¹ College of Animal Science, Guangdong Provincial Key Laboratory of Animal Nutrition Control, National Engineering Research Center for Breeding Swine Industry, South China Agricultural University, Guangzhou 510642, Guangdong, China

(Ambros 2004). They mainly target 3' untranslated region (UTR) of coding genes through base complementarity, affecting their translation and original biological function (Macfarlane and Murphy 2010; Bartel 2009; Filipowicz et al. 2008). It is reported that a number of miRNAs are widely involved in the proliferation and differentiation of livestock and poultry muscle fibers (Luo et al. 2014; Zhao et al. 2016a; Zhu et al. 2019).

In general, the conversion of muscle fiber types is mainly concentrated in the early 3 months after birth (Wank et al. 2006), and the proportion of type IIb fibers in the longissimus dorsi of pigs increased obviously (Lefaucheur and Vigneron 1986). In order to explore the potential miRNAs involved in this biological process, we selected the longissimus dorsi tissues of 1-day-old and 90-day-old Lantang pigs and screened the differentially expressed miRNA candidates through high-throughput sequencing. Among them, miR-493-5p was found to inhibit the proliferation of myoblasts and promote their differentiation by targeting *ANKRD17* gene, revealing the potential mechanism and function of miR-493-5p in myogenesis. Our objective was to identify miRNA candidates regulating the development of muscle fibers and provide theoretical data for pig breeding.

Result

miRNA expression analysis

To identify the differentially expressed miRNAs of LT1D and LT90D, we constructed LT1D and LT90D miRNA libraries with three replicates in each stage. We obtained 20.56 ± 1.76 million raw reads from each sample. After filtering, approximately 17.03 ± 1.66 million clean reads were obtained, and $92.87 \pm 0.54\%$ clean reads were mapped successfully to porcine genome. A total of 2806 miRNAs were finally found in LT1D and LT90D, including 525 known porcine miRNAs and 2282 novel miRNAs (Table S1A). Among them, 1871 miRNA candidates were expressed in LT1D, 1729 were expressed in LT90D, and 794 miRNAs were shared across two stages (Fig. 1a). We assessed the top 10 highly expressed miRNA species, and ssc-miR-1, ssc-miR-206, ssc-miR-10b, ssc-miR-378, ssc-miR-26a, ssc-let-7a, ssc-let-7f-5p, and ssc-let-7i-5p were shared between LT1D and LT90D libraries (Table S1B). PCA analysis found that the miRNA expression of LT1D and LT90D was clustered with growth stages (Fig. 1b). There were 16 differentially expressed (DE) miRNAs between LT1D and LT90D libraries ($FDR < 0.05$, Table S1B). Compared with LT90D, LT1D contained 9 miRNAs with significantly up-regulated expression and 7 miRNAs with significantly down-regulated expression (Fig. 1c). In detail, miR-novel-769, miR-novel-1656, miR-novel-1314,

miR-novel-1844, ssc-miR-885-5p, ssc-miR-935, and ssc-miR-7134-5p were identified as highly expressed in LT90D, while miR-novel-100, miR-novel-1295, miR-novel-2124, miR-novel-2117, miR-novel-1133, ssc-miR-18a, ssc-miR-493-5p, ssc-miR-432-5p, and ssc-miR-545-5p were identified as having low expression in LT90D (Fig. 1d).

miR-493-5p promotes C2C12 proliferation

We synthesized miR-493-5p mimics and inhibitor and verified the overexpression and knockdown efficiency of miR-493-5p by RT-qPCR (Fig. 2a). Compared with the control group, miR-493-5p mimics and inhibitor significantly increased and knocked down the expression level of miR-493-5p ($P < 0.01$), indicating the effect of miR-493-5p mimics and inhibitor that can be used for subsequent experiments. Then, C₂C₁₂ cells were transfected with miR-493-5p mimics and inhibitor, and the relative expression levels of cell proliferation-related genes such as *PCNA*, *cyclin D1* and *cyclin E* were evaluated by RT-qPCR. The expression levels of *PCNA* ($P < 0.05$) and *cyclin D1* ($P < 0.01$) increased significantly in over-expressed cells, while the expression level of *cyclin E* did not change significantly ($P > 0.05$). After knockdown of miR-493-5p, the expression levels of *PCNA* ($P < 0.05$) and *cyclin D1* ($P < 0.05$) in C₂C₁₂ cells decreased significantly, and the decrease in level of *cyclin E* was not significant ($P > 0.05$) (Fig. 2b). After transfection with miR-493-5p mimics, the protein expression levels of *PCNA* ($P < 0.05$) and *cyclin E* ($P < 0.05$) increased significantly, while the increased level of *cyclin D1* was not significant ($P > 0.05$). When the expression of miR-493-5p was down-regulated, the protein expression levels of *PCNA* ($P < 0.05$) and *cyclin D1* ($P < 0.05$) decreased significantly, while the protein expression level of *cyclin E* also decreased but not significantly ($P > 0.05$) (Fig. 2c, c', and d). The trends were consistent with the results of RT-qPCR, indicating that miR-493-5p promoted the proliferation of muscle cells. CCK-8 assay was performed on C₂C₁₂ cells that were transfected with miR-493-5p mimics and inhibitor (Fig. 2e and f).

Compared with the control group, the absorbance (450 nm) of miR-493-5p mimic treatments increased significantly at 24 h ($P < 0.05$), and the absorbance (450 nm) of inhibitor group decreased significantly at 36 h ($P < 0.05$), indicating that miR-493-5p improved the proliferation efficiency of C₂C₁₂ cells and promoted cell proliferation. When miR-493-5p was highly expressed, the number of cells entering S phase is significantly higher than that in the control group ($P < 0.01$; Fig. 3a, a', and 3b), indicating that cells are rich in DNA replication phase. When the expression of miR-493-5p was knocked down, the cells were blocked in G₀/G₁ phase and G₂/M phase, and the cells in DNA replication phase decreased significantly ($P < 0.05$, Fig. 3c, c', and d).

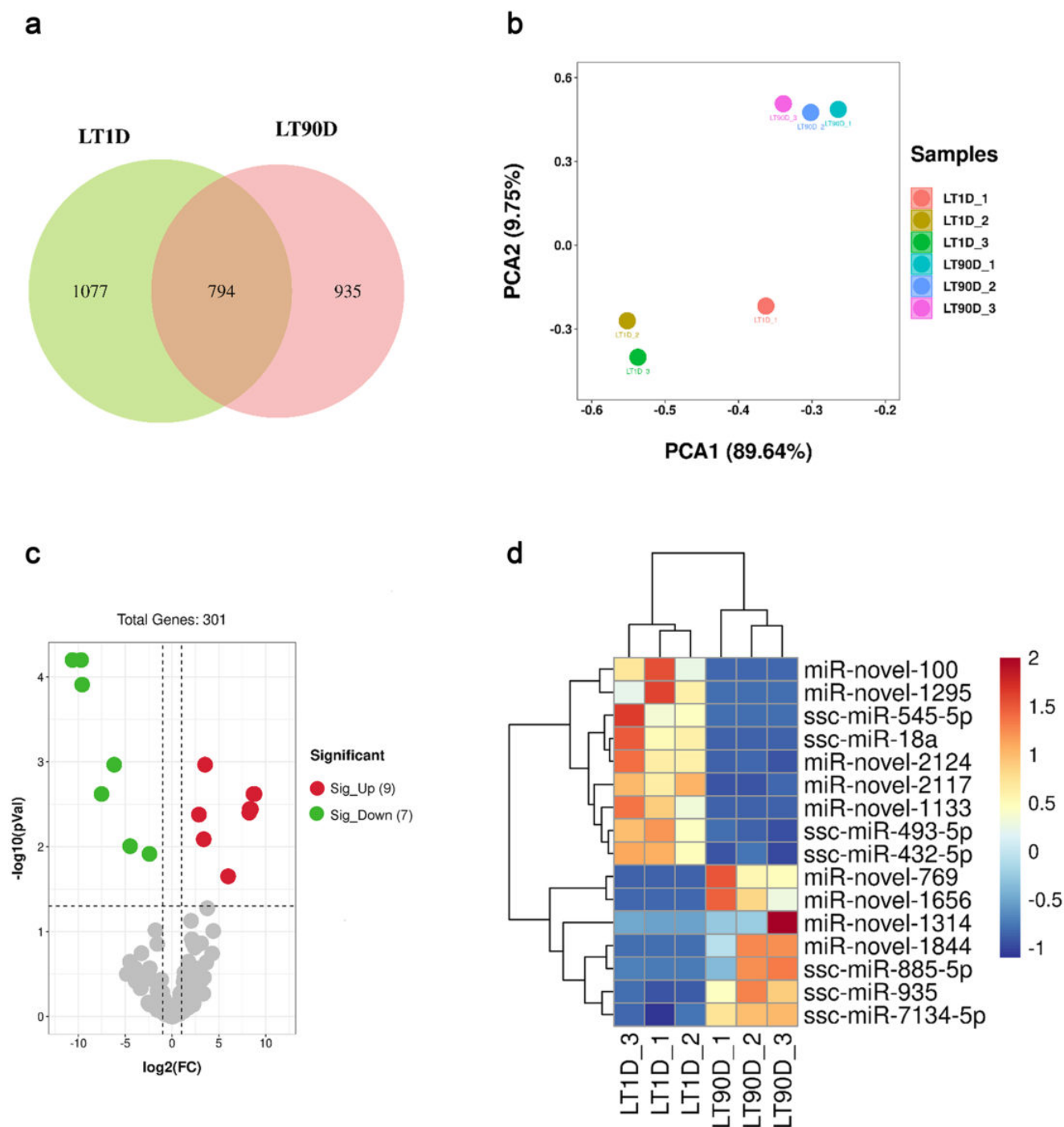


Fig. 1 miRNA expression analysis between Lantang pigs aged 1 and 90 days. **a** Common candidate miRNAs identified in LT1D and LT90D, **b** principal component analysis (PCA) of miRNAs with FPKM levels, **c** volcanic map showing differentially expressed

miRNA between LT1D and LT90D, and **d** heat map showing differentially expressed miRNAs between LT1D and LT90D. Note: LT1D, Lantang pig 1 day after birth; LT90D, Lantang pig 90 days after birth

The results of EdU analysis are shown in Fig. 4. The rate of cells with DNA replication activity in C_2C_{12} cells transfected with miR-493-5p mimics was significantly higher than that in the control group ($P < 0.05$, Fig. 4a–a'''),

while the rate of cells with DNA replication activity in C_2C_{12} cells transfected with miR-493-5p inhibitor was significantly lower than that in the control group ($P < 0.05$, Fig. 4b–b'''). Quantitative analysis of proportion of C_2C_{12}

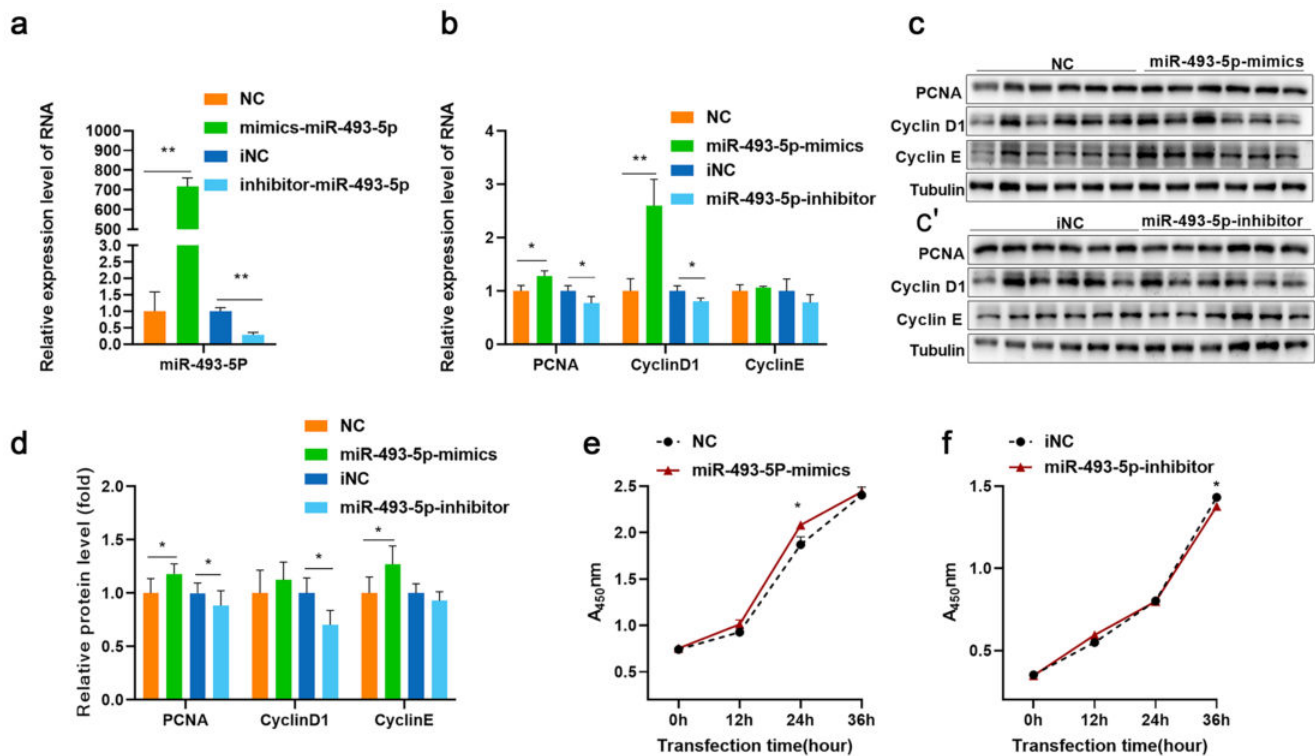


Fig. 2 Enhancement of C₂C₁₂ cell proliferation by miR-493-5p **a** RT-qPCR analysis of the expression efficiency of miR-493-5p mimics and inhibitor, **b** RT-qPCR analysis of the expression of proliferation-related genes, **c**, **c'** Western blot analysis of the expression of proliferation-related proteins, **d** quantitative analysis of the expression of

proliferation-related proteins, **e** growth curve of C₂C₁₂ cells following miR-493-5p mimics, and **f** growth curve of C₂C₁₂ cells following miR-493-5p inhibitor. Note: data are represented as mean \pm SEM. $n=6$; *, $P<0.05$; **, $P<0.01$

cells with replication activity following miR-493-5p mimics and inhibitor is showed in Fig. 4c.

miR-493-5p inhibits differentiation

To further study the effect of miR-493-5p on C₂C₁₂ differentiation, the relative expression levels of differentiation marker genes *Myf5*, *MyoD1*, *MyoG*, and *MyHC* were detected by RT-qPCR analysis. The miR-493-5p mimics significantly decreased the expression level of *MyHC* ($P<0.05$), while *Myf5*, *MyoD1*, and *MyoG* decreased but not significantly ($P>0.05$). miR-493-5p inhibitor significantly promoted the expression level of *MyoG* ($P<0.05$), and the levels of *Myf5*, *MyoD1*, and *MyoG* were increased but not significantly ($P<0.05$) (Fig. 5a). The effects of miR-493-5p mimics and inhibitor on the expression levels of *MyoD1*, *MyoG*, and *MyHC* proteins were detected by Western blot (Fig. 5b, b'), and the results showed the same trend as the results of RT-qPCR. Compared with the control group, miR-493-5p mimics significantly inhibited the protein expression levels of *MyoD1* and *MyoG* ($P<0.05$, Fig. 5c), and miR-493-5p inhibitor significantly promoted the protein expression levels of *MyoD1* and

MyoG ($P<0.05$, Fig. 5c); *MyHC* showed the same trend as *MyoD1* and *MyoG*, but the result was not significant. In addition, we also evaluated the RNA expression levels of *MyHC I* and *MyHC IIb*. The miR-493-5p mimics significantly inhibited the expression of *MyHC IIb* ($P<0.05$), while miR-493-5p inhibitor significantly promoted the expression of *MyHC I* ($P<0.01$, Fig. 5d). The results of Western blot showed that the protein expression levels of *MyHC I* ($P<0.05$) and *MyHC IIb* ($P<0.01$) decreased significantly when miR-493-5p was highly expressed; when the expression of miR-493-5p was inhibited, the protein expression level of *MyHC I* increased significantly ($P<0.05$), and *MyHC IIb* showed no significant difference ($P>0.05$) (Fig. 5e, e', and 5f), indicating that miR-493-5p inhibited the expression of *MyHC I* and *MyHC IIb*. *MyHC* immunofluorescence staining was performed.

Compared with the control group, miR-493-5p mimics significantly reduced the proportion of *MyHC* positive fibers ($P<0.01$, Fig. 6a–a'''), and miR-493-5p inhibitor significantly increased the proportion of *MyHC*-positive fibers ($P<0.05$, Fig. 6b–b'''). Quantitative analysis of proportion of C₂C₁₂ cells with *MyHC* fluorescence activity following miR-493-5p mimics and inhibitor is shown in Fig. 6c.

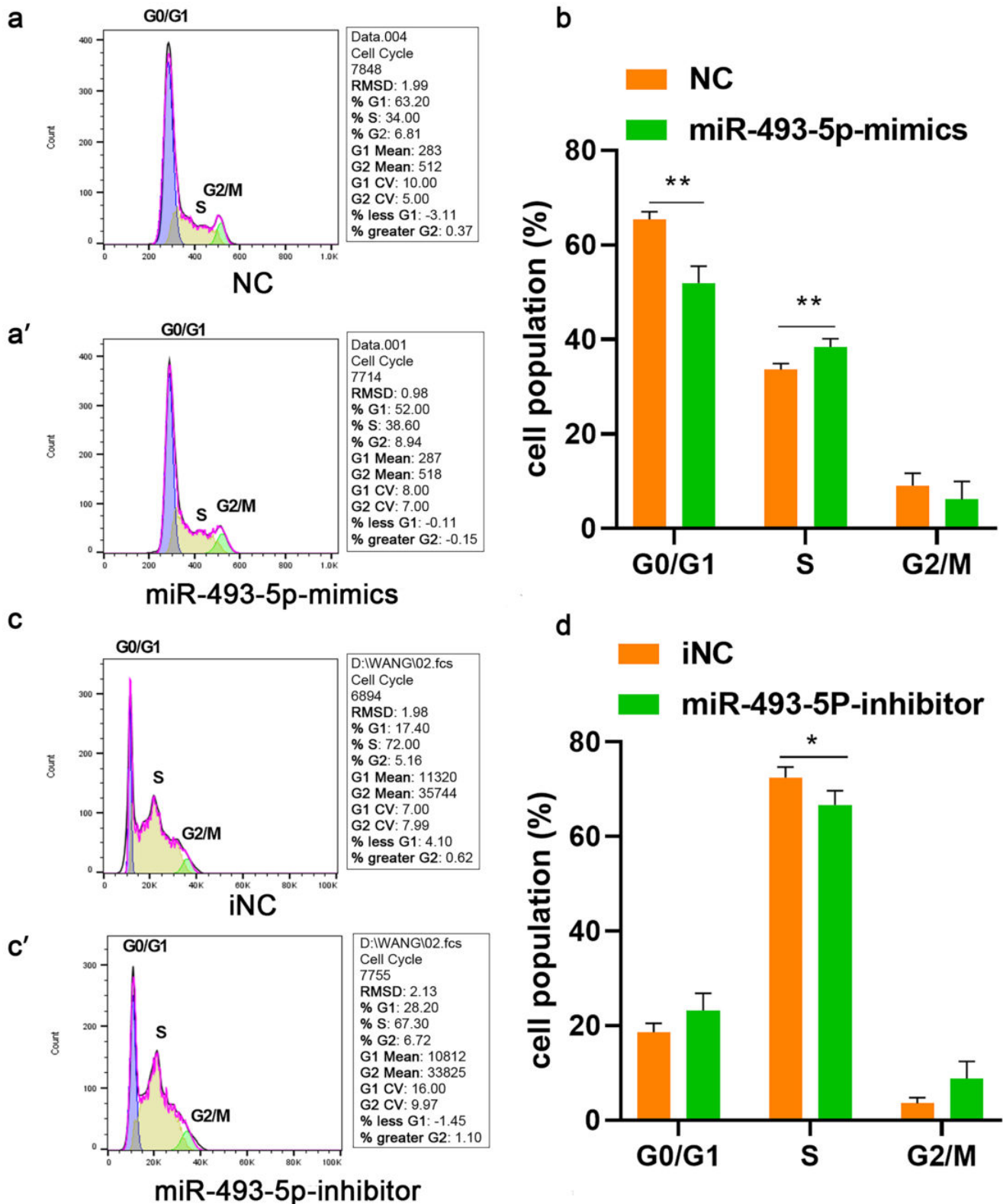


Fig. 3 Enhancement of C_2C_{12} cell cycle process by miR-493-5p. **a**, **a'** Cell cycle analysis of C_2C_{12} cells following miR-493-5p mimics, **b** quantitative analysis of C_2C_{12} cell cycle distribution following miR-493-5p mimics, **c**, **c'** cell cycle analysis of C_2C_{12} cells following miR-

493-5p inhibitor, and **d** quantitative analysis of C_2C_{12} cell cycle distribution following miR-493-5p inhibitor. Note: data are represented as mean \pm SEM. $n=4$; *, $P<0.05$; **, $P<0.01$

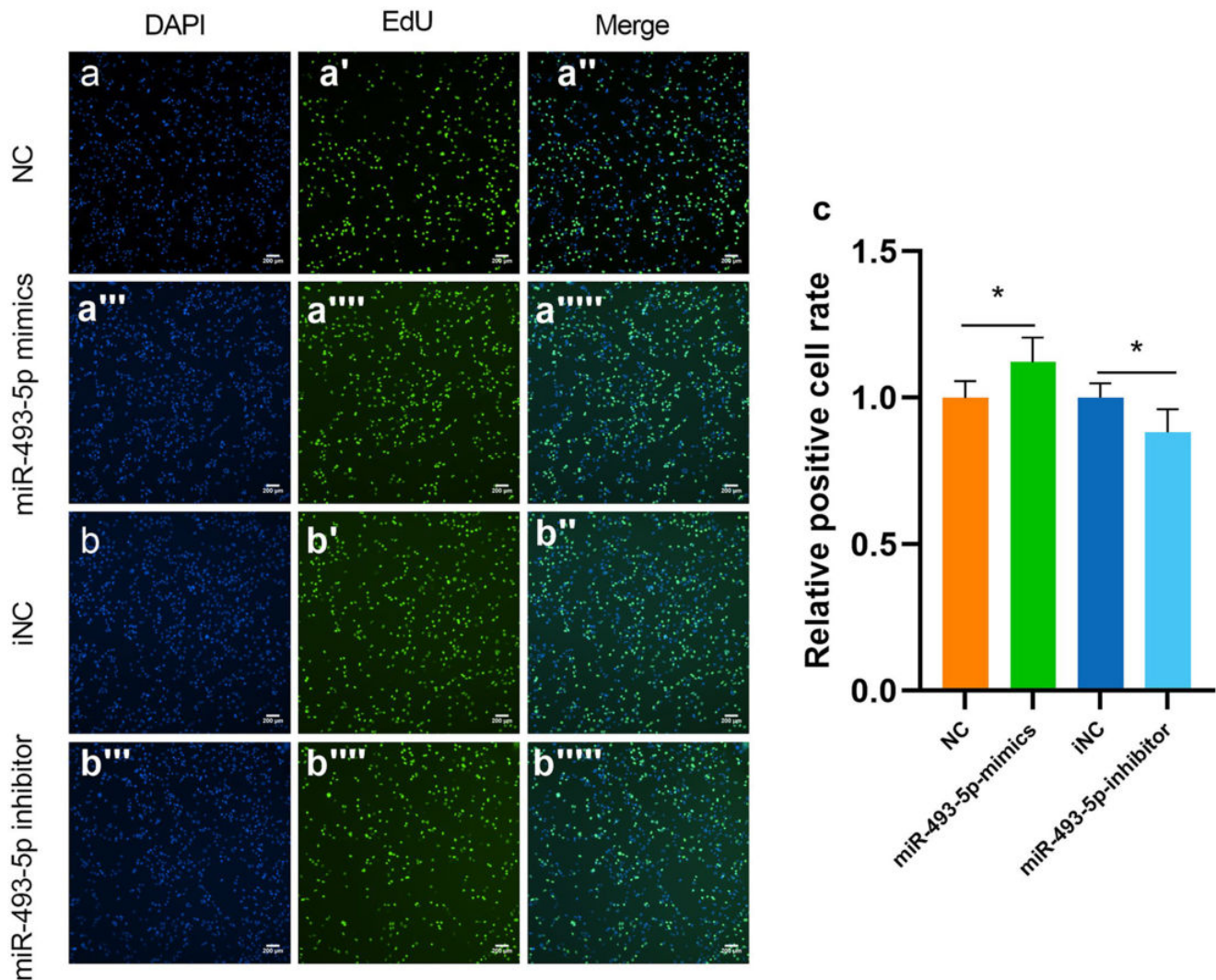


Fig. 4 Enhancement of the C₂C₁₂ cell proliferation activity by miR-493-5p. **a–a''''** Edu analysis of C₂C₁₂ cell DNA replication activity following miR-493-5p mimics, **b–b''''** Edu analysis of C₂C₁₂ cell DNA replication activity following miR-493-5p inhibitor, and **c** quan-

titative analysis of proportion of C₂C₁₂ cells with replication activity following miR-493-5p mimics and inhibitor. Note: data are represented as mean \pm SEM. $n=6$; *, $P<0.05$; **, $P<0.01$

miR-493-5p has a target relationship with ANKRD17

To identify the potential function of miR-493-5p, target prediction was performed using miRanda software, and a total of 184 putative target sites were identified (Table S1C). GO and KEGG pathway analyses showed that potential targets of miR-493-5p were mainly related to muscle development such as cardiac muscle hypertrophy and smooth muscle cell differentiation (Table S1D and S1E, Fig. 7a and 7b). RT-qPCR detection of myogenic targets showed that the expression level of *MED28* and *ANKRD17* increased significantly in LT90D compared with LT1D, and that there were no significant differences in the expression levels of *ATP2A2*, *PPP3CA*,

and *KLF15* (Fig. 7c). The interaction target between *ANKRD17* and miR-493-5p was predicted successfully (Fig. 7d), and we also designed three double luciferase vectors for *ANKRD17* target sequences, namely, *ANKRD17*pmirGLO-Wt, pmirGLO-Mut, and pmirGLO-Del. We co-transfected the above three vectors with miR-493-5p mimics into 293 T cells and detected the changes in double luciferase activity. By co-transfection of miR-493-5p and pmirGLO-Wt, the ratio of Firefly/Renilla luciferase activity decreased significantly compared with the control group ($P<0.05$), while the pmirGLO-Mut and pmirGLO-Del groups did not change significantly, indicating that there was direct interaction between miR-493-5p and *ANKRD17*.

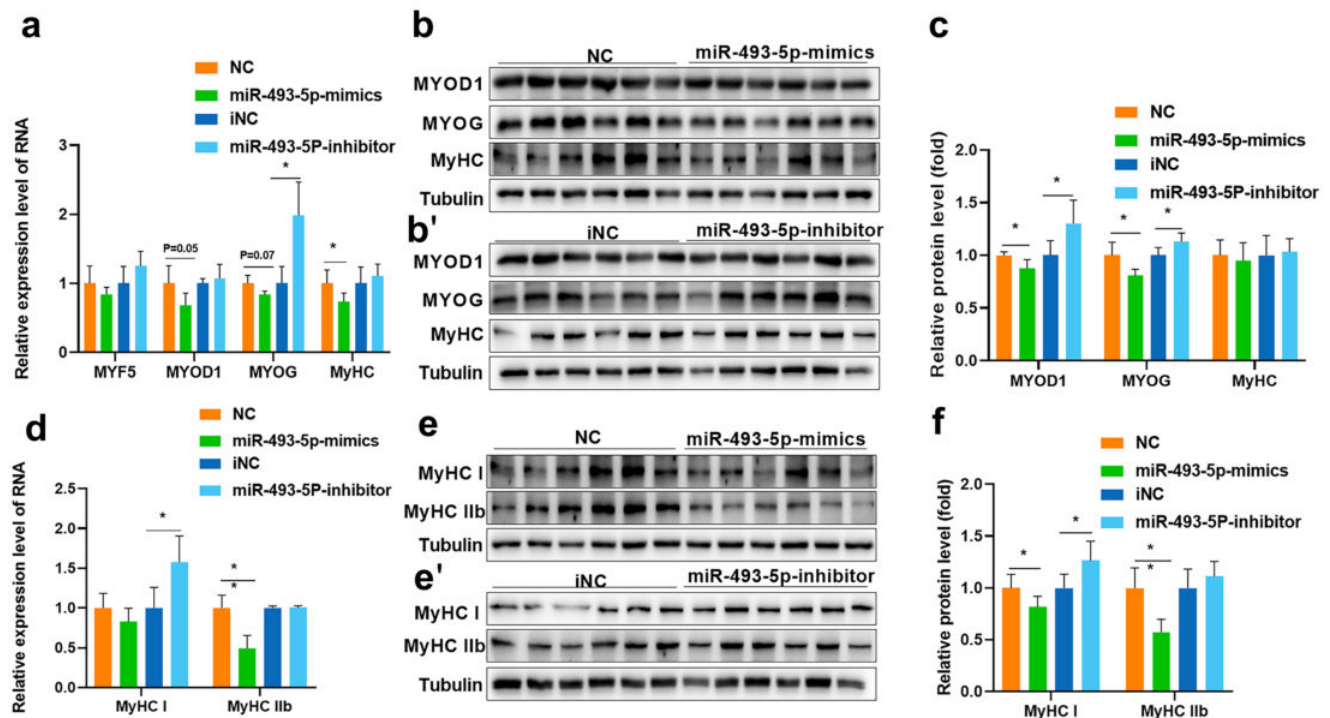


Fig. 5 Inhibition of C_2C_{12} cell differentiation by miR-493-5p. **a** RT-qPCR analysis of the expression of differentiation marker genes, **b**, **b'** Western blot analysis of the expression of differentiation marker proteins, **c** quantitative analysis of the expression of differentiation marker proteins, **d** RT-qPCR analysis of the expression of MyHC

I and MyHC IIb; **e**, **e'** Western blot analysis of the expression of MyHC I and IIb proteins, **f** quantitative analysis of the expression of MyHC I and IIb proteins. Note: data are represented as mean \pm SEM. $n=6$; *, $P<0.05$; **, $P<0.01$

Discussion

Myofiber hyperplasia in pigs is basically completed at 90 days of pregnancy (Wigmore and Stickland 1983), and the number of postnatal muscle fibers basically does not increase (Moss 1968). Therefore, the hypertrophy and transformation of postnatal muscle fibers are the main research fields (Schiaffino et al. 2013; Pearson 1990; Brummer et al. 2013). In the early stage after birth, the proportion of oxidized muscle fibers gradually decreased and the proportion of enzymatic muscle fibers increased (Wank et al. 2006). This process was accompanied by the increase in muscle volume and the decrease in meat quality (Chang et al. 2003). In details, *Pax7* gene regulates early muscle development (Lagha et al. 2005); MyoD family controls myogenic differentiation (Hasty et al. 1993); myostatin can inhibit muscle development (Gao et al. 2020). In addition to the above transcription factors, noncoding miRNAs are also widely involved in the regulation of muscle development (Horak et al. 2016; Zhuang et al. 2022). In this paper, the muscles of Lantang were selected to study the miRNA expression from birth to early postnatal period. We found that the expression levels of *ssc-miR-1*, *ssc-miR-206*, *ssc-miR-10b*, *ssc-miR-378*, *ssc-miR-26a*, *ssc-let-7a*, *ssc-let-7f-5p*,

and *ssc-let-7i-5p* were highly expressed in LT1D and LT90D libraries. Among them, miR-1 and miR-206 are muscle-specific miRNA molecules (Mitchelson and Qin 2015) which play a regulatory role in the differentiation of skeletal muscle cells (Sun et al. 2010; Kim et al. 2006). MiR-26a is abundant in skeletal muscle and promotes myogenic differentiation and skeletal muscle regeneration (Dey et al. 2012). miR-378 can regulate autophagy and apoptosis of muscle cells and maintain muscle homeostasis (Li et al. 2018). miR-10b plays a regulatory role in the proliferation of vascular smooth muscle (Yu et al. 2015). Tewari et al. found that miR-10b is highly expressed in 10-month-old bovine skeletal muscle, indicating the potential biological function of miR-10b in skeletal muscle (Tewari et al. 2021). Let-7 family is involved in cell differentiation (Tolonen et al. 2014), in which let-7a regulates myocardial hypertrophy (Zhou et al. 2017) and smooth muscle cell proliferation (Lin et al. 2020). Hu et al. reported that let-7i-5p is involved in regulating cardiomyocyte proliferation and affecting the process of cardiomyocyte cycle (Hu et al. 2019).

We excavated 16 differentially expressed miRNAs, and the expression of miR-432-5p was significantly down-regulated at 90 days, which was similar to previous study (Chen et al. 2020). They compared the miRNA

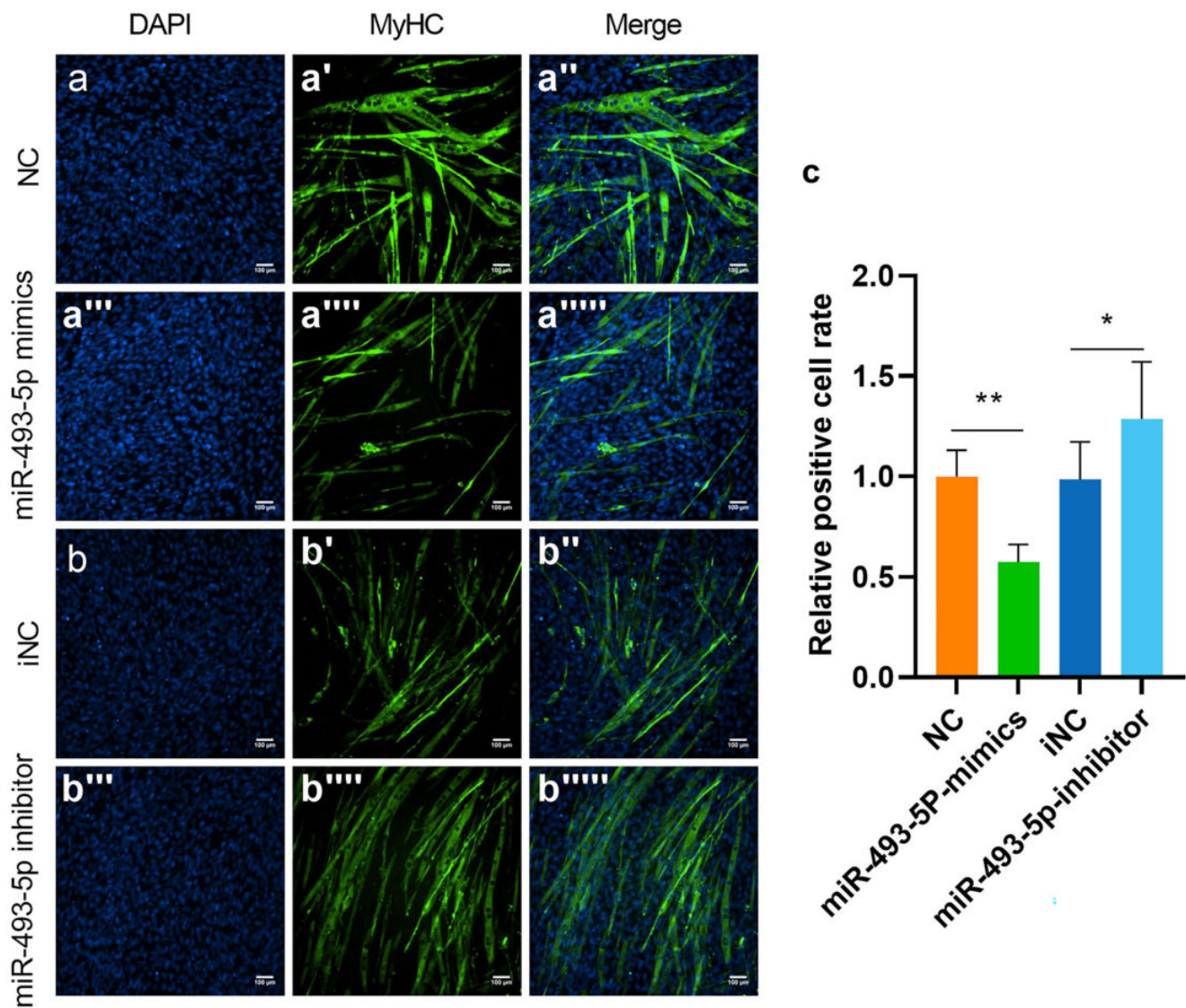


Fig. 6 Inhibition of C₂C₁₂ cell myotube differentiation by miR-493-5p. **a–a'''** Immunofluorescence imaging of MyHC in C₂C₁₂ myotubes following miR-493-5p mimics, **b–b'''** immunofluorescence imaging of MyHC in C₂C₁₂ myotubes following miR-493-5p

inhibitor, and **c** quantitative analysis of proportion of C₂C₁₂ cells with MyHC fluorescence activity following miR-493-5p mimics and inhibitor. Note: data are represented as mean \pm SEM. $n = 3$; *, $P < 0.05$; **, $P < 0.01$

expression in the longissimus dorsi of Rongchang pigs between 35 and 287 days after birth and found that the expression of miR-432-5p was down-regulated in adulthood (Chen et al. 2020). miR-novel-1656 is homologous with hsa-mir-378a-3p, and it is involved in myoblast proliferation and differentiation in skeletal muscle development (Wei et al. 2016). miR-novel-2117 is homologous with hsa-miR-377-3p, and miR-377-3p is mainly related to cancer progression (Zhang et al. 2020) and vascular smooth muscle proliferation and migration (Wang et al. 2020). This study explored the function of miR-493-5p in skeletal muscle. Several studies have indicated that miR-493-5p has antitumor properties in various cancer

types. For instance, epigenetic silencing of miR-493-5p was regarded as a marker of some advanced cancers, and miR-493-5p upregulation can effectively impede the growth and migration of tumor cells (Zhao et al. 2016b). Although miR-493-5p has been widely studied in inhibiting the proliferation of cancer cells such as liver cancer and breast cancer (Zhao et al. 2016b; Gailhouste et al. 2019), a recent study found that the overexpression of miR-493-5p promoted the growth of cholangiocarcinoma tumor cells in vitro (Toshida et al. 2022). It shows that miR-493-5p has more biological functions that need further exploration. Our data imply that miR-493-5p may act as a regulator of muscle development.

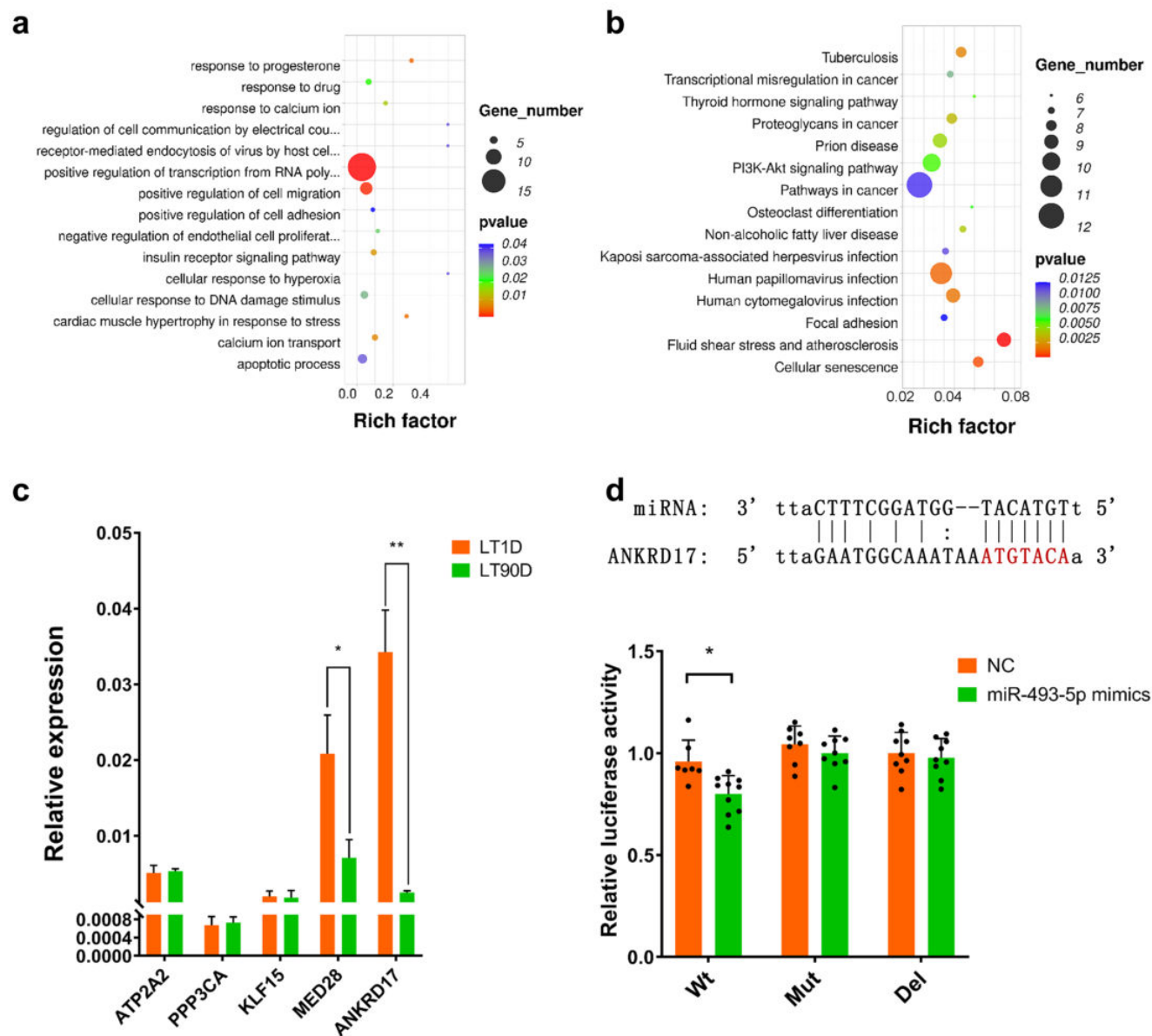


Fig. 7 Analysis of candidate target genes downstream of miR-493-5p. **a** GO analysis of candidate target genes downstream of miR-493-5p, **b** KEGG analysis of candidate target genes downstream of miR-493-5p, **c** expression of candidate target genes downstream of miR-

493-5p in longissimus dorsi muscle of LT1D and LT90D, and **d** targeting sites and double luciferase test results between miR-493-5p and ANKRD17. Note: LT1D, Lantang pig 1 day after birth; LT90D, Lantang pig 90 days after birth; *, $P < 0.05$; **, $P < 0.01$

In general, *PCNA*, *cyclin D1* and *cyclin E* are marker genes of cell proliferation, and *PCNA* is involved in DNA synthesis (Kumari et al. 2021) and cell cycle regulation (Zhang et al. 1993). *Cyclin D1* is an important regulator of the early to metaphase process of cell G1 (Fu et al. 2004). *Cyclin E* mainly controls the transformation of G1 and S phases of cell cycle and promotes the process of cell cycle (Möröy and Geisen 2004). MiR-493-5p mimics increased the expression levels of *PCNA*, *cyclin D1* gene, and protein in C_2C_{12} cells. Knocking down of miR-493-5p showed the

opposite trend, indicating that miR-493-5p can promote the proliferation of C_2C_{12} cells. CCK-8 experiment, flow cytometry, and Edu results further proved the promoting effect of miR-493-5p on cell proliferation. Myogenic regulatory factors (MRFs), including *Myf5*, *MyoD1*, *MyoG*, and *MRF4*, play myogenic regulatory roles in myoblasts (Asfour et al. 2018). MRF promotes differentiation and sarcomere assembly by blocking the cell cycle of precursor cells (Buckingham and Rigby 2014). In the early stage of myoblastic differentiation, *Myf5* and *MyoD1* can jointly

promote the early differentiation of myoblasts (Braun et al. 1992). *MyoG* is an advanced factor regulating the terminal differentiation of myoblasts, participates in the regulation of myocyte fusion, and is very important for muscle fiber growth and myonuclear proliferation (Ganassi et al. 2020). Myosin heavy chain (*MyHC*) is the basic unit of myosin, and the expression level of *MyHC* indicates the differentiation process of myoblasts (Parry 2001). In this study, miR-493-5p mimics inhibited the levels of *Myf5*, *MyoD1*, *MyoG*, and *MyHC*, and the down-regulation of miR-493-5p showed the opposite results, which proved that miR-493-5p could inhibit the differentiation of C₂C₁₂ cells. The results of cellular immunofluorescence experiment on *MyHC* gene further proved that miR-493-5p could inhibit C₂C₁₂ muscle fiber differentiation. This experiment also detected the effect of miR-493-5p on the gene and protein expression of *MyHC I* and *Iib*. MiR-493-5p inhibited the expression of *MyHC I* and *Iib* proteins, indicating that miR-493-5p inhibited the formation of myotubes (Parry 2001).

In general, miRNA negatively regulates the expression of downstream target genes by binding with 3' UTR (Filipowicz 2005). We therefore predicted the downstream target genes of miR-493-5p and conducted function enrichment analysis. Through target prediction, we found 184 potential target genes interacting with miR-493-5p. GO functional annotation found that *ATP2A2*, *PPP3CA*, *KLF15*, *MED28*, and *ANKRD17* were related to muscle development. RT-qPCR found that *MED28* and *ANKRD17*, as potential target genes of miR-493-5p, were also significantly differentially expressed between LT1D and LT90D. The double luciferase experiment finally verified the target relationship between *ANKRD17* and miR-493-5p. It is reported that *ANKRD17* is involved in the development of mouse liver (Watt et al. 2001), promotes the differentiation of vascular smooth muscle cells (Hou et al. 2009), and is also a downstream effector of *cyclin E*, which is directly involved in the cell cycle regulation of DNA replication (Deng et al. 2009). Therefore, our paper preliminarily proves that there is a target relationship between miR-493-5p and *ANKRD17* in myogenesis.

Materials and methods

Sample collection

The pigs were obtained from Banling farm (Xinfeng town, Shaoguan City, Guangdong Province, China). Five male pigs of Lantang breed balanced with body weight were humanely slaughtered at birth (LT1D) and 3 months (LT90D). A total of 10 longissimus samples were immediately collected and stored in liquid nitrogen until further analysis.

Library preparation and miRNA-seq analysis

For total RNA extraction, three longissimusdorsi tissues were randomly selected in each growth stage and homogenized in TRIzol reagents (Takara, Dalian, China), and the RNA quantity and purity were further determined by Agilent 2100 bioanalyzer (Agilent, Santa Clara, CA, USA) and RNA 6000Nano LabChip Kit (Agilent, Santa Clara, CA, USA) with RNA integrity number (RIN) value of > 7.0. Next, the RNA fragments with the length of 18–30nt were separated and enriched by 15% polyacrylamide gel electrophoresis (PAGE), and the proprietary indexed adapters were then ligated to 5' and 3' termini, respectively. A reverse transcription reaction followed by low cycle PCR was performed to obtain sufficient products for Illumina sequencing. The preliminary quality control analysis of Fastq files was carried out using FastQC software (<https://github.com/s-andrews/FastQC>). After trimming adaptor sequences and removal of reads with poly A and reads smaller than 18 nt by FASTX-Toolkit (http://hannonlab.cshl.edu/fastx_toolkit), clean reads were further mapped with *Sscrofa11.1* reference genome and counted by miRDeep2 package v2.0.0.8 with a Perl script “miRDeep2.pl” (Friedländer et al. 2012). Then, the edgeR package v3.30.3 (<https://bioconductor.org/packages/edgeR/>) was used to find the differentially expressed miRNAs with FDR < 0.05. A search for miRNA target genes was performed using the miRanda software (John et al. 2004), and gene ontology (GO) terms and Kyoto Encyclopedia of Genes and Genomes (KEGG) pathway analyses were performed using DAVID software (<https://david.ncifcrf.gov/>).

RNA extraction and RT-qPCR

TRIzol (Takara, Dalian, China) was used to extract the total RNA of the samples, and the reverse transcription was carried out using PrimeScript™ RT reagent kit with gDNA Eraser (Takara, Dalian, China). Quantitative reverse transcription PCR (RT-qPCR) was performed using Bio-Rad CFX 96™ Real Time Detection System (Agilent Technologies, Santa Clara, CA, USA) and SYBR Green PCR Master Mix (Takara, Dalian, China) in a 20-μl reaction. The cycle conditions were as follows: 95 °C for 30 s followed by 40 cycles of 95 °C for 10 s, 60 °C for 10 s, and 68 °C for 20 s. The primer sequences are listed in Table S1F, and the specificity and efficiency of primers were checked with melt curve analysis. The tested miRNA and mRNA used *U6* and *GAPDH* as internal parameters control, respectively, and 2^{−ΔΔC_t} method was used to process the data in the experiment.

Cell culture and transfection

The myoblast cell line C₂C₁₂ used in this experiment was purchased from the Chinese Collection of Authenticated Cell Cultures (Beijing, China). The cells were cultured in

humidified incubators at 37 °C and 5% CO₂. In the proliferation stage, the cells grew in growth medium (GM, DMEM; GIBCO, Grand Island, NY, USA) + 10% fetal bovine serum (GIBCO, Grand Island, NY, USA) + 1% penicillin streptomycin (Invitrogen, Carlsbad, CA, USA). In the differentiation stage, the cells were induced by differentiation medium (DM, DMEM; GIBCO, Grand Island, NY, USA) + 2% horse serum (GIBCO, Grand Island, NY, USA) + 1% penicillin streptomycin (Invitrogen, Carlsbad, CA, USA). Cells were transfected when cell confluence reached approximately 60%, and miR-493-5p mimics and inhibitor were transfected with Lipofectamine 2000 (Invitrogen, Carlsbad, CA, USA). Cells were harvested for protein and RNA analysis after 48 h to study cell proliferation or switched to DM culturing for 96 h to study cell differentiation.

Western blot

The cells were lysed in RIPA lysis buffer (Solarbio, Beijing, China) to collect cell total protein. The protein was separated by SDS-PAGE, transferred to polyvinylidene fluoride (PVDF) membrane (Millipore, Bedford, MA, USA), and sealed with 5% skim milk for 2 h at room temperature. In the proliferative stage, the protein samples were detected by anti *PCNA* (cat.: 200,947-2E1, dilution ratio: 1/2000), *cyclin D1* (cat.: 380,999, dilution ratio: 1/2000), *cyclin E* (cat.: 340,298, dilution ratio: 1/2000), and *Tubulin* (cat.: R23453, dilution ratio: 1/5000) (ZenBio, Chengdu, China), and the proteins in differentiation stage were detected by anti *MyoD1* (cat.: 252,249, dilution ratio: 1/1000), *MyoG* (cat.: 382,257, dilution ratio: 1/1000) (ZenBio, Chengdu, China), *MyHC* (cat.: MAB4470, dilution ratio: 1/2000) (R&D Systems, Minneapolis, USA), *MyHC I* (cat.: A7564, dilution ratio: 1/2000), *MyHC IIb* (cat.: A15293, dilution ratio: 1/2000) (ABclonal, Wuhan, China), and *Tubulin*. All the antibodies used had good specificity.

Cell counting kit-8 (cck-8)

The cells were inoculated into 96-well cell plates, and miR-493-5p mimics and inhibitor were transfected into cells according to the transfection procedure. After transfection, the cell proliferation was detected by cck-8 (EZBioscience, Roseville, MN, USA) at 0, 12, 24, and 36 h.

Flow cytometry

C₂C₁₂ cells transfected with miR-493-5p mimics and inhibitor for 48 h were collected, fixed in 70% ethanol, and stored at −20 °C. The cells were resuspended with PI/RNase staining buffer (BD Biosciences, Franklin Lakes, NJ, USA) and cultured in dark at 37 °C for 30 min. Finally, the cell cycles

were analyzed by BD Accuri C6 flow cytometer (BD Biosciences, Franklin Lakes, NJ, USA) and FACSDiVa software (BD Biosciences, Franklin Lakes, NJ, USA).

Edu experiment

The cells were inoculated into 48-well plates and transfected with miR-493-5p mimics and inhibitor. After 48 h, Beyo-click™ Edu-488 Kit (Biyuntian Biotechnology, Shanghai, China) was used for cell proliferation detection. Finally, the fluorescence inverted microscope (Nikon, Tokyo, Japan) was used to take photos, and the image was analyzed by Image J software (Media Cybernetics, Bethesda, MD, USA).

Double Luciferase reporter

Wild type (Wt), deletion (Del), and mutant (Mut) fragments containing binding sites of miR-493-5p in the 3' untranslated region (UTR) of *ANKRD17* gene were synthesized and connected with pmirGLO vector (Promega, Madison, WI, USA) to construct pmirGLO-Wt, pmirGLO-Del, and pmirGLO-Mut vectors, respectively. 293 T cells were inoculated on 96-well plates, and pmirGLO-Wt, pmirGLO-Del, and pmirGLO-Mut vectors were co-transfected with miR-493-5p mimics into 293 T cells. After 48 h of culture, the activity of Luciferase was detected by Dual-Glo® Reagent and Dual-Glo® Stop & Glo Reagent (Promega, Madison, WI, USA).

Cellular immunofluorescence

C₂C₁₂ cells were inoculated on 12-well plates, transfected with miR-493-5p mimics and inhibitor, and then cultured until 96 h of differentiation. The cells were fixed with 4% paraformaldehyde for 60 min incubated with 0.4% TritonX-100 at room temperature for 30 min, and finally blocked with 5% goat serum for 60 min. *MyHC* primary antibody (cat.: MAB4470, dilution ratio: 1/2000) (R&D Systems, Minneapolis, USA) was incubated at 4 °C overnight, the corresponding fluorescent labeled secondary antibody was incubated at room temperature for 1 h, and DAPI was incubated at room temperature for 5 min. Finally, the fluorescence inverted microscope (Nikon, Tokyo, Japan) equipped with an RGB digital camera was used for microscopic examination, while the images were taken at ×20 objectives. The ImageJ software (Media Cybernetics, Bethesda, MD, USA) was used to analyze images and statistics.

Data statistics

The SPSS v17.0 software (SPSS Inc., Chicago, IL, USA) was used for statistical analysis of the data. Independent sample

t-test was used for the numerical comparison between the two treatment groups. $P < 0.05$ indicated that the difference was significant and marked with *; $P < 0.01$ indicated that the difference was very significant and marked with **.

Conclusions

We established the miRNA expression profiles of porcine longissimus dorsi tissues at 1 day old and 90 days old, and screened differentially expressed miRNA candidates. We also identified a DE miRNA candidate, miR-493-5p, which was found to promote the proliferation of myoblasts and inhibit their differentiation by targeting *ANKRD17* gene, revealing the potential mechanism and function of miR-493-5p in muscle development.

Supplementary Information The online version contains supplementary material available at <https://doi.org/10.1007/s00441-023-03777-3>.

Author contribution XZ and JS gathered samples, conceived the study, participated in its design, performed data analysis, and drafted the manuscript; FX and ZL performed the experiments; JL, TC, QX, and YZ provided guidance and funding. All authors have read and approved the final version of the manuscript.

Funding This work was supported by the Natural Science Foundation of China Program [grant numbers 31802032, 32072714] and the Guangdong Chimelong Philanthropic Foundation [CLPF2021007Z]. The sponsors had no role in the study design, in the collection, analysis, and interpretation of the data, in the writing of the report, and in the decision to submit the article for publication.

Availability of data and materials All data are contained in the manuscript.

Declarations

Ethics approval and consent to participate All procedures were performed in accordance with the procedures approved by the Institutional Animal Care and Use Committee of South China Agricultural University (ethics approval code: SCAU2018F006, March 13, 2018). All methods were carried out in accordance with relevant guidelines and regulations. All methods are reported in accordance with ARRIVE guidelines (<https://arriveguidelines.org>) for the reporting of animal experiments.

Competing interests The authors declare no conflict of interest. The funding sponsors had no role in the design of the study, in the collection, analyses, and interpretation of data, in the writing of the manuscript, or in the decision to publish the results.

References

- Ambros V (2004) The functions of animal microRNAs. *Nature* 431(7006):350–355. <https://doi.org/10.1038/nature02871>
- Anakwe K, Robson L, Hadley J, Buxton P, Church V, Allen S et al (2002) 16 Wnt regulation of limb muscle differentiation. *J Anat* 201(5):421
- Asfour HA, Allouh MZ, Said RS (2018) Myogenic regulatory factors: the orchestrators of myogenesis after 30 years of discovery. *Exp Biol Med* (Maywood) 243(2):118–128. <https://doi.org/10.1177/1535370217749494>
- Ashmore CR (1974) Phenotypic expression of muscle fiber types and some implications to meat quality. *J Anim Sci* 38(5):1158–1164. <https://doi.org/10.2527/jas1974.3851158x>
- Bartel DP (2009) MicroRNAs: target recognition and regulatory functions. *Cell* 136(2):215–233. <https://doi.org/10.1016/j.cell.2009.01.002>
- Borycki AG, Li J, Jin F, Emerson CP, Epstein JA (1999) Pax3 functions in cell survival and in pax7 regulation. *Development* 126(8):1665–1674. <https://doi.org/10.1242/dev.126.8.1665>
- Bowker BC, Swartz DR, Grant AL, Gerrard DE (2005) Myosin heavy chain isoform composition influences the susceptibility of actin-activated S1 ATPase and myofibrillar ATPase to pH inactivation. *Meat Sci* 71(2):342–350. <https://doi.org/10.1016/j.meatsci.2005.04.014>
- Braun T, Rudnicki MA, Arnold HH, Jaenisch R (1992) Targeted inactivation of the muscle regulatory gene Myf-5 results in abnormal rib development and perinatal death. *Cell* 71(3):369–382. [https://doi.org/10.1016/0092-8674\(92\)90507-9](https://doi.org/10.1016/0092-8674(92)90507-9)
- Brummer H, Zhang MY, Piddoubny M, Medler S (2013) Hybrid fibers transform into distinct fiber types in maturing mouse muscles. *Cells Tissues Organs* 198(3):227–236. <https://doi.org/10.1159/000355280>
- Buckingham M, Rigby PW (2014) Gene regulatory networks and transcriptional mechanisms that control myogenesis. *Dev Cell* 28(3):225–238. <https://doi.org/10.1016/j.devcel.2013.12.020>
- Chang KC, da Costa N, Blackley R, Southwood O, Evans G, Plastow G et al (2003) Relationships of myosin heavy chain fibre types to meat quality traits in traditional and modern pigs. *Meat Sci* 64(1):93–103. [https://doi.org/10.1016/s0309-1740\(02\)00208-5](https://doi.org/10.1016/s0309-1740(02)00208-5)
- Chen X, Zhao C, Dou M, Sun Y, Yu T, Pang W et al (2020) Deciphering the miRNA transcriptome of Rongchang pig longissimus dorsi at weaning and slaughter time points. *J Anim Physiol Anim Nutr (berl)* 104(3):954–964. <https://doi.org/10.1111/jpn.13314>
- Deng M, Li F, Ballif BA, Li S, Chen X, Guo L et al (2009) Identification and functional analysis of a novel cyclin e/cdk2 substrate ankrd17. *J Biol Chem* 284(12):7875–7888. <https://doi.org/10.1074/jbc.M807827200>
- Dey BK, Gagan J, Yan Z, Dutta A (2012) miR-26a is required for skeletal muscle differentiation and regeneration in mice. *Genes Dev* 26(19):2180–2191. <https://doi.org/10.1101/gad.198085.112>
- Filipowicz W (2005) RNAi: the nuts and bolts of the RISC machine. *Cell* 122(1):17–20. <https://doi.org/10.1016/j.cell.2005.06.023>
- Filipowicz W, Bhattacharyya SN, Sonenberg N (2008) Mechanisms of post-transcriptional regulation by microRNAs: are the answers in sight? *Nat Rev Genet* 9(2):102–114. <https://doi.org/10.1038/nrg2290>
- Friedländer MR, Mackowiak SD, Li N, Chen W, Rajewsky N (2012) miRDeep2 accurately identifies known and hundreds of novel microRNA genes in seven animal clades. *Nucleic Acids Res* 40(1):37–52. <https://doi.org/10.1093/nar/gkr688>
- Fu M, Wang C, Li Z, Sakamaki T, Pestell RG (2004) Minireview: cyclin D1: normal and abnormal functions. *Endocrinology* 145(12):5439–5447. <https://doi.org/10.1210/en.2004-0959>
- Gailhouste L, Liew LC, Yasukawa K, Hatada I, Tanaka Y, Kato T et al (2019) MEG3-derived miR-493-5p overcomes the oncogenic feature of IGF2-miR-483 loss of imprinting in hepatic cancer cells. *Cell Death Dis* 10(8):553. <https://doi.org/10.1038/s41419-019-1788-6>

- Ganassi M, Badodi S, Wanders K, Zammit PS, Hughes SM (2020) Myogenin is an essential regulator of adult myofibre growth and muscle stem cell homeostasis. *Elife* 9:e60445. <https://doi.org/10.7554/eLife.60445>
- Gao L, Yang M, Wei Z, Gu M, Yang L, Bai C et al (2020) MSTN mutant promotes myogenic differentiation by increasing demethylase TET1 expression via the SMAD2/SMAD3 pathway. *Int J Biol Sci* 16(8):1324–1334. <https://doi.org/10.7150/ijbs.40551>
- Hasty P, Bradley A, Morris JH, Edmondson DG, Venuti JM, Olson EN et al (1993) Muscle deficiency and neonatal death in mice with a targeted mutation in the myogenin gene. *Nature* 364(6437):501–506. <https://doi.org/10.1038/364501a0>
- Horak M, Novak J, Bienertova-Vasku J (2016) Muscle-specific microRNAs in skeletal muscle development. *Dev Biol* 410(1):1–13. <https://doi.org/10.1016/j.ydbio.2015.12.013>
- Hou SC, Chan LW, Chou YC, Su CY, Chen X, Shih YL et al (2009) Ankrd17, an ubiquitously expressed ankyrin factor, is essential for the vascular integrity during embryogenesis. *FEBS Lett* 583(17):2765–2771. <https://doi.org/10.1016/j.febslet.2009.07.025>
- Hu Y, Jin G, Li B, Chen Y, Zhong L, Chen G et al (2019) Suppression of miRNA let-7i-5p promotes cardiomyocyte proliferation and repairs heart function post injury by targeting CCND2 and E2F2. *Clin Sci (lond)* 133(3):425–441. <https://doi.org/10.1042/CS20181002>
- John B, Enright AJ, Aravin A, Tuschl T, Sander C (2004) Marks DS. Human microRNA targets. *PLoS biology* 2(11):e363. <https://doi.org/10.1371/journal.pbio.0020363>
- Joo ST, Kim GD, Hwang YH, Ryu YC (2013) Control of fresh meat quality through manipulation of muscle fiber characteristics. *Meat Sci* 95(4):828–836. <https://doi.org/10.1016/j.meatsci.2013.04.044>
- Karlsson AH, Klont RE, Fernandez X (1999) Skeletal muscle fibres as factors for pork quality. *Livest Prod Sci* 60(2–3):255–269. 52. [https://doi.org/10.1016/S0301-6226\(99\)00098-6](https://doi.org/10.1016/S0301-6226(99)00098-6)
- Kim HK, Lee YS, Sivaprasad U, Malhotra A, Dutta A (2006) Muscle-specific microRNA miR-206 promotes muscle differentiation. *J Cell Biol* 174(5):677–687. <https://doi.org/10.1083/jcb.200603008>
- Kumari P, Sundaram R, Manohar K, Vasudevan D, Acharya N (2021) Interdomain connecting loop and J loop structures determine cross-species compatibility of PCNA. *J Biol Chem. Epub ahead of print* 297(1):100911. <https://doi.org/10.1016/j.jbc.2021.100911>
- Lagha M, Rocancourt D, Relaix F (2005) Origine du muscle squelettique: rôles de Pax3/Pax7-dependent population of skeletal muscle progenitor cells. *Med Sci (paris)* 21(10):801–803. <https://doi.org/10.1051/medsci/20052110801>
- Larzul C, Lefaucheur L, Ecolan P, Gogué J, Talmant A, Sellier P et al (1997) Phenotypic and genetic parameters for longissimus muscle fiber characteristics in relation to growth, carcass, and meat quality traits in large white pigs. *J Anim Sci* 75(12):3126–3137. <https://doi.org/10.2527/1997.75123126x>
- Lawrie RA (1970) Muscle differentiation in relation to meat quality. *Community Health (bristol)* 1(4):192–197. <https://doi.org/10.1021/bi201322c>
- Lefaucheur L (2010) A second look into fibre typing-relation to meat quality. *Meat Sci* 84(2):257–270. <https://doi.org/10.1016/j.meatsci.2009.05.004>
- Lefaucheur L, Vigneron P (1986) Post-natal changes in some histochemical and enzymatic characteristics of three pig muscles. *Meat Sci* 16(3):199–216. [https://doi.org/10.1016/0309-1740\(86\)90026-4](https://doi.org/10.1016/0309-1740(86)90026-4)
- Li Y, Jiang J, Liu W, Wang H, Zhao L, Liu S et al (2018) microRNA-378 promotes autophagy and inhibits apoptosis in skeletal muscle. *Proc Natl Acad Sci U S A* 115(46):E10849–E10858. <https://doi.org/10.1073/pnas.1803377115>
- Lin SL, Duan H, Wang S, Li JJ (2020) Overexpression of Lin28B promoted the proliferation of adenomyotic smooth muscle cells of the junctional zone via regulating Let-7a. *Reprod Sci* 27(5):1156–1163. <https://doi.org/10.1007/s43032-019-00107-3>
- Luo W, Wu H, Ye Y, Li Z, Hao S, Kon L, et al (2014) The transient expression of miR-203 and its inhibiting effects on skeletal muscle cell proliferation and differentiation. *Cell Death Dis* 5(7):e1347. <https://doi.org/10.1038/cddis.2014.289>
- Macfarlane LA, Murphy PR (2010) MicroRNA: biogenesis, function and role in cancer. *Curr Genomics* 11(7):537–561. <https://doi.org/10.2174/138920210793175895>
- Mitchelson KR, Qin WY (2015) Roles of the canonical myomiRs miR-1, -133 and -206 in cell development and disease. *World J Biol Chem* 6(3):162–208. <https://doi.org/10.4331/wjbc.v6.i3.162>
- Möröy T, Geisen C (2004) Cyclin E. *Int J Biochem Cell Biol* 36(8):1424–1439. <https://doi.org/10.1016/j.biocel.2003.12.005>
- Moss FP (1968) The relationship between the dimensions of the fibres and the number of nuclei during normal growth of skeletal muscle in the domestic fowl. *Am J Anat* 122(3):555–563. <https://doi.org/10.1002/aja.1001220308>
- Paredes SP, Kalbe C, Jansman AJ, Verstegen MW, van Hees HM, Lösel D et al (2013) Predicted high-performing piglets exhibit more and larger skeletal muscle fibers. *J Anim Sci* 91(12):5589–5598. <https://doi.org/10.2527/jas.2013-6908>
- Parry DJ (2001) Myosin heavy chain expression and plasticity: role of myoblast diversity. *Exerc Sport Sci Rev* 29(4):175–179. <https://doi.org/10.1097/00003677-200110000-00008>
- Pearson AM (1990) Muscle growth and exercise. *Crit Rev Food Sci Nutr* 29(3):167–196. <https://doi.org/10.1080/10408399009527522>
- Peter JB, Barnard RJ, Edgerton VR, Gillespie CA, Stempel KE (1972) Metabolic profiles of three fiber types of skeletal muscle in guinea pigs and rabbits. *Biochemistry* 11(14):2627–2633. <https://doi.org/10.1021/bi00764a013>
- Schiaffino S, Reggiani C (1996) Molecular diversity of myofibrillar proteins: gene regulation and functional significance. *Physiol Rev* 76(2):371–423. <https://doi.org/10.1152/physrev.1996.76.2.371>
- Schiaffino S, Dyar KA, Ciciliot S, Blaauw B, Sandri M (2013) Mechanisms regulating skeletal muscle growth and atrophy. *FEBS J* 280(17):4294–4314. <https://doi.org/10.1111/febs.12253>
- Schwab CR, Baas TJ, Stalder KJ, Mabry JW (2006) Effect of long-term selection for increased leanness on meat and eating quality traits in Duroc swine. *J Anim Sci* 84(6):1577–1583. <https://doi.org/10.2527/2006.8461577x>
- Sun Y, Ge Y, Drnevich J, Zhao Y, Band M, Chen J (2010) Mammalian target of rapamycin regulates miRNA-1 and follistatin in skeletal myogenesis. *J Cell Biol* 189(7):1157–1169. <https://doi.org/10.1083/jcb.200912093>
- Swoap SJ, Hunter RB, Stevenson EJ, Felton HM, Kansagra NV, Lang JM et al (2000) The calcineurin-NFAT pathway and muscle fiber-type gene expression. *Am J Physiol Cell Physiol* 279(4):C915–C924. <https://doi.org/10.1152/ajpcell.2000.279.4.C915>
- Tewari RS, Ala U, Accornero P, Baratta M, Miretti S (2021) Circulating skeletal muscle related microRNAs profile in Piedmontese cattle during different age. *Sci Rep* 11(1):15815. <https://doi.org/10.1038/s41598-021-95137-w>
- Tolonen AM, Magga J, Szabó Z, Viitala P, Gao E, Moilanen AM, et al (2014) Inhibition of Let-7 microRNA attenuates myocardial remodeling and improves cardiac function postinfarction in mice. *Pharmacol Res Perspect*. 2(4):e00056. <https://doi.org/10.1002/prp2.56>
- Toshida K, Itoh S, Harada N, Morinaga A, Yugawa K, Tomiyama T, et al (2022) Cancer-associated fibroblasts promote tumor cell growth via miR-493-5p in intrahepatic cholangiocarcinoma. *Cancer Sci. Epub ahead of print*. <https://doi.org/10.1111/cas.15644>
- Wang H, Wei Z, Li H, Guan Y, Han Z, Wang H, et al (2020) MiR-377-3p inhibits atherosclerosis-associated vascular smooth muscle cell proliferation and migration via targeting neuropilin2. *Biosci Rep* 40(6). <https://doi.org/10.1042/BSR20193425>
- Wank V, Fischer MS, Walter B, Bauer R (2006) Muscle growth and fiber type composition in hind limb muscles during postnatal

- development in pigs. *Cells Tissues Organs* 182(3–4):171–181. <https://doi.org/10.1159/000093966>
- Watt AJ, Jones EA, Ure JM, Peddie D, Wilson DI, Forrester LM (2001) A gene trap integration provides an early in situ marker for hepatic specification of the foregut endoderm. *Mech Dev* 100(2):205–215. [https://doi.org/10.1016/s0925-4773\(00\)00530-x](https://doi.org/10.1016/s0925-4773(00)00530-x)
- Wei X, Li H, Zhang B, Li C, Dong D, Lan X et al (2016) miR-378a-3p promotes differentiation and inhibits proliferation of myoblasts by targeting HDAC4 in skeletal muscle development. *RNA Biol* 13(12):1300–1309. <https://doi.org/10.1080/15476286.2016.1239008>
- Wigmore PM, Stickland NC (1983) Muscle development in large and small pig fetuses. *J Anat* 137(Pt 2):235–245. <https://doi.org/10.1007/BF00305930>
- Yu X, Li Z, Chen G, Wu WK (2015) MicroRNA-10b induces vascular muscle cell proliferation through Akt pathway by targeting TIP30. *CurrVascPharmacol* 13(5):679–686. <https://doi.org/10.2174/1570161113666150123112751>
- Zhang H, Xiong Y, Beach D (1993) Proliferating cell nuclear antigen and p21 are components of multiple cell cycle kinase complexes. *Mol Biol Cell* 4(9):897–906. <https://doi.org/10.1091/mbc.4.9.897>
- Zhang XY, Dong XM, Wang FP (2020) MiR-377-3p inhibits cell metastasis and epithelial-mesenchymal transition in cervical carcinoma through targeting SGK3. *Eur Rev Med Pharmacol Sci* 24(9):4687–4696. https://doi.org/10.26355/eurrev_202005_21156
- Zhao Q, Kang Y, Wang HY, Guan WJ, Li XC, Jiang L et al (2016a) Expression profiling and functional characterization of miR-192 throughout sheep skeletal muscle development. *Sci Rep* 6:30281. <https://doi.org/10.1038/srep30281>
- Zhao L, Feng X, Song X, Zhou H, Zhao Y, Cheng L et al (2016b) miR-493-5p attenuates the invasiveness and tumorigenicity in human breast cancer by targeting FUT4. *Oncol Rep* 36(2):1007–1015. <https://doi.org/10.3892/or.2016.4882>
- Zhou X, Sun F, Luo S, Zhao W, Yang T, Zhang G et al (2017) Let-7a is an antihypertrophic regulator in the heart via targeting calmodulin. *Int J Biol Sci* 13(1):22–31. <https://doi.org/10.7150/ijbs.16298>
- Zhu L, Hou L, Ou J, Xu G, Jiang F, Hu C et al (2019) MiR-199b represses porcine muscle satellite cells proliferation by targeting JAG1. *Gene* 691:24–33. <https://doi.org/10.1016/j.gene.2018.12.052>
- Zhuang X, Lin Z, Xie F, Luo J, Chen T, Xi Q et al (2022) Identification of circRNA-associated ceRNA networks using longissimus thoracis of pigs of different breeds and growth stages. *BMC Genomics* 23(1):294. <https://doi.org/10.1186/s12864-022-08515-7>

Publisher's Note Springer Nature remains neutral with regard to jurisdictional claims in published maps and institutional affiliations.

Springer Nature or its licensor (e.g. a society or other partner) holds exclusive rights to this article under a publishing agreement with the author(s) or other rightsholder(s); author self-archiving of the accepted manuscript version of this article is solely governed by the terms of such publishing agreement and applicable law.

非编码 RNA 对猪骨骼肌发育的影响

林泽堃, 庄晓娜, 罗君谊, 陈 婷, 习欠云, 张永亮, 孙加节*

(华南农业大学动物科学学院, 国家生猪种业工程技术研究中心, 广州 510642)

摘 要: 骨骼肌发育与猪肉产量和品质密切相关, 且受到各种因素的影响。近年来, 非编码 RNA(non-coding RNA, ncRNA) 对骨骼肌发育的影响已成为新的研究热点之一。ncRNA 主要包括微小 RNA(miRNA)、长链非编码 RNA(long non-coding RNA, lncRNA) 和环状 RNA(circular RNA, circRNA), 是一类不具有编码蛋白功能的 RNA, 最初被认为只是在转录或转录后水平调控基因的表达, 但随着研究的深入, 越来越多的 ncRNA 被证实参与骨骼肌细胞增殖、分化与凋亡等生物过程, 其中 miRNA 可通过与靶基因互补序列结合发挥功能; lncRNA 与 circRNA 主要作为分子海绵竞争性结合 miRNA, 解除其对靶基因的抑制作用。作者主要从 ncRNA 介绍及 miRNA、lncRNA 和 circRNA 对猪骨骼肌发育的影响等进行综述, 并就 ncRNA 对猪骨骼肌生长发育的研究进行了展望。

关键词: 非编码 RNA; 猪; 骨骼肌发育; 微小 RNA; 长链非编码 RNA; 环状 RNA

中图分类号: Q752

文献标识码: A

Doi: 10.16431/j.cnki.1671-7236.2021.10.010

开放科学(资源服务)标识码(OSID):



Effects of Non-coding RNAs on Skeletal Muscle Development in Pigs

LIN Zekun, ZHUANG Xiaona, LUO Junyi, CHEN Ting, XI Qianyun,

ZHANG Yongliang, SUN Jiajie*

(National Engineering Research Center for Breeding Swine Industry, College of Animal Science, South China Agricultural University, Guangzhou 510642, China)

Abstract: Skeletal muscle development is closely related to pork yield and quality, which is affected by various factors. In recent years, the influence of non-coding RNA (ncRNA) on skeletal muscle development has become one of the new research hotspot. ncRNA mainly include microRNA (miRNA), long non-coding RNA (lncRNA) and circular RNA (circRNA), which were a class of RNAs that do not have the function of encoding a protein. Initially, they were thought to only regulate gene expression at the transcriptional and post-transcriptional level. However, with the deepening of research, more and more non-coding RNAs have been confirmed to be involved in various biological processes, such as proliferation, differentiation and apoptosis of skeletal muscle cells. In details, miRNAs affect the function of the targeted mRNAs by binding to the complementary sequences of their target mRNA. lncRNA and circRNA can act as molecular sponges of miRNA to weaken the inhibitory effect of miRNA on targets. Therefore, the author mainly reviews ncRNA introduction, and the effects of miRNA, lncRNA and circRNA on the development of porcine skeletal muscle, and put forward the prospect of ncRNA on the growth

收稿日期: 2021-04-23

基金项目: 广东省科技创新战略专项(2018B020203002); 国家自然科学基金(31802032、32072714); 广东省自然科学基金(2020A1515010062); 广州市科技项目(202002030037)

作者简介: 林泽堃(1997-), 男, 福建漳州人, 硕士, 研究方向: 动物营养组学, E-mail: michaelinzk@gmail.com

*** 通信作者:** 孙加节, 博士, 副教授, 研究方向: 动物营养组学与饲料生物技术, E-mail: jiajiesun@scau.edu.cn

and development of porcine skeletal muscle.

Key words: ncRNA; pigs; skeletal muscle development; miRNA; lncRNA; circRNA

骨骼肌纤维占动物机体总重的 35%~65%,肌纤维数目在动物出生前基本固定,分娩后肌纤维体积肥大,与畜禽产肉性状密切相关^[1]。同时,肉品质也是家畜重要的经济性状,主要由肌肉颜色、pH、持水性、嫩度、肌间脂肪和风味物质含量等因素决定,骨骼肌纤维类型的组成对这些因素有重要的影响^[2]。近年来,越来越多的证据表明,非编码 RNA(non-coding RNA, ncRNA)广泛参与骨骼肌细胞增殖分化的调控以及一系列后续肌生成过程。因此,研究 ncRNA 特性与功能对猪肉增产和肉品质改善具有重要意义。作者主要从 ncRNA 介绍及微小 RNA(microRNA, miRNA)、长链非编码 RNA(long non-coding RNA, lncRNA)和环状 RNA(circular RNA, circRNA)对猪骨骼肌发育的影响等几个部分展开综述。

1 ncRNA

随着 RNA 高通量测序技术的发展,目前已经在不同物种和组织中鉴定出大量 ncRNA。长期以来,ncRNA 被认为是没有编码潜能的 RNA 分子,是垃圾核酸序列^[3]。尽管人们普遍认为大多数遗传信息是由蛋白质编码基因进行处理的,但这并非意味着这些 ncRNA 没有功能。研究表明,哺乳动物和其他复杂生物体的大多数基因组实际上存在大量 ncRNA,其中许多 ncRNA 被选择性地剪接或加工成较小的产物^[4]。一般而言,ncRNA 主要包括 miRNA、lncRNA、circRNA 等,它们通过多种形式直接或间接参与调控骨骼肌发生过程,如卫星细胞活化、增殖、分化和自我更新等^[5-6]。

1.1 miRNA

miRNA 是在植物、动物和一些病毒中发现的小 ncRNA 分子,约包含 22 个核苷酸,miRNA 可抑制信使 RNA(messenger RNA, mRNA)转录或翻译,在转录后水平调控基因表达^[7-8]。一般而言,miRNA 结合靶 mRNA 3' 端非翻译区(3'-untranslated regions, 3'-UTR),并诱导形成 RNA 进而诱导沉默复合体(RNA-induced silencing complex, RISC),导致靶 mRNA 降解以终止蛋白质翻译^[9]。miRNA 在概念和机制上都与 RNA 干扰(RNA interference, RNAi)和小干扰 RNA(small interference RNA, siRNA)相似,可以直接抑制靶基

因。通常只有极少数的 miRNA 与它们的 mRNA 靶点几乎完全互补,在这种情况下,被靶向的 mRNA 可以被直接切割和降解^[10]。然而在大多数情况下,miRNA 与其靶基因之间的序列互补位点位于 miRNA 的 5' 端由 2~8 个核苷酸组成的种子序列(seed region)上,这导致 mRNA 活性被抑制^[11]。研究表明,miRNA 是由独立基因的 RNA 聚合酶 II(Pol II)特异性转录本或蛋白质编码基因的内含子加工而成。在经典通路中,初级前体 miRNA(pri-miRNA)的处理过程分为两个步骤:由核糖核酸酶 III(RNase III)家族的 2 个成员 Drosha 和 Dicer 催化,在 dsRNA 结合蛋白(dsRBPs)配合作用下被切割成成熟 miRNA 和前体 miRNA(pre-miRNA);成熟的 miRNA 双链最终被加载到 RISC 中,其中一个选定的 miRNA 链(-5p 或-3p)与 Argonaute(AGO)蛋白结合,引导复合物到达其靶 mRNA 上发挥作用^[8]。AGO 蛋白是 RISC 的核心组分,大多数物种表达多种 AGO 同源物,如哺乳动物中的 AGO1~AGO4,苍蝇中的 dAGO1 和 dAGO2,秀丽隐杆线虫中的 ALG-2^[12]。同时, pri-miRNA 的编辑除了影响 miRNAs 对靶点的作用外,也是调节特定 miRNA 生物合成和成熟的重要机制^[12]。

1.2 lncRNA

长度>200 nt 的 ncRNA 通常被称为 lncRNA,位于细胞核或细胞质中,很少编码蛋白质。像 mRNA 一样,lncRNA 相对稳定,经常被剪接,且都有 5' 端帽状结构和 3' 端的 Poly(A)尾巴,大多数 lncRNA 由 RNA 聚合酶 II 转录^[3,10,13-14]。lncRNA 的功能机制多种多样,包括充当蛋白支架、诱饵、引导信号传递等,可以通过基因组靶向、顺反调节或反义干扰发挥功能^[10,15]。研究表明,一些 lncRNA 实际上编码小蛋白^[16]。目前,根据转录本的长度,lncRNA 可分为普通 lncRNA、长基因间非编码 RNA(long-intergenic non-coding RNA, lincRNA)和非常长的基因间非编码 RNA(very long intergenic non-coding RNA, vlincRNA)^[17];根据 lncRNA 在基因组中的位置,可分为基因间长链非编码 RNA(intergenic lncRNA)、反义长链非编码 RNA(antisense lncRNA)、正义长链非编码 RNA(sense lncRNA)、内含子长链非编码 RNA(intronic lncRNA)和双向长链非编码 RNA(bidirectional

lncRNA)^[18]。lncRNA 发挥作用的方式大致可分为转录水平调控、转录后调控和其他水平三大类^[19]。转录水平调控是 lncRNA 通过转录干扰和染色质重塑来调节基因转录。转录后调控又可分为两种转录后调控机制,即剪接调控和翻译控制,参与剪接调控的 lncRNA 可能通过与 mRNA 序列结合或调节剪接因子,或直接与 mRNA 序列杂交以阻断剪接而发挥作用;而参与翻译控制的 lncRNA 可能通过结合翻译因子或核糖体发挥作用,可以结合翻译起始因子 4A(eukaryotic translation initiation factor 4A, eIF4A)、Poly(A)结合蛋白(Poly(A) binding protein, PABP)等因子,通过阻断所需复合物的组装来抑制翻译起始。除了转录水平调控和转录后调控外, lncRNA 还可通过其他机制发挥作用,如蛋白质定位、端粒复制、RNA 干扰和翻译调控等^[19]。

1.3 circRNA

Sanger 等^[20]在 1976 年研究马铃薯纺锤块茎病时发现存在着某种未包被的感染性 RNA 分子,这是人类首次发现 circRNA,当时科学家们发现有一种类病毒可以感染植物并可导致其死亡。之后,1979 年 Hsu 等^[21]首次通过电子显微镜观察到真核细胞中有 circRNA 的存在。circRNA 由前体 mRNA 反向剪接产生,形成共价闭合的环状结构,没有 5'端帽状结构和 3'端的 Poly(A)尾巴。通常, circRNA 被认为是低丰度和剪接错误,且在真核生物中表现出细胞和组织特异性模式^[22-24]。circRNA 分为 4 类:外显子环状 RNA(exonic circRNA, ecircRNA)、内含子环状 RNA(intronic circRNA, ciRNA)、外显子-内含子环状 RNA(exon-intron circRNA, EIciRNA)和基因间环状 RNA(intergenic circRNA, icircRNA)^[25]。哺乳动物外显子 circRNA 产生的方式有两种:第一种被称为错误剪接或直接反剪接,是指外显子的干扰作用致使外显子以不规则的顺序剪接,并将中间 RNA 环化;第二种被称为套索中间机制或外显子跳跃机制,涉及到外显子跳跃产生的套索内的剪接^[26-27],二者都涉及到由典型的剪接体形成的反向剪接(backsplice)。研究发现, circRNA 可通过充当 miRNA 和 RNA 结合蛋白的海绵,发挥竞争性内源性 RNA(competitive endogenous RNA, ceRNA)的作用来调控基因表达^[9]。近年来也有研究证明, circRNA 可以翻译成蛋白质^[28],而 circRNA 的环状结构必然意味着其拥有一种不依赖帽子结构的内部机制来启动翻译。编码蛋白质的 circRNA 包含开放阅读框(open

reading frame, ORF)、内部核糖体进入位点(internal ribosome entry site, IRES)或 N⁶-甲基腺苷(N⁶-methyladenosine, m⁶A)甲基化修饰^[29-30]。

2 miRNA 对猪骨骼肌发育的影响

尽管对 miRNA 的认识不断增加,但人们注意到并非所有的 miRNA 都广泛表达,即一些 miRNA 以组织特异性的方式表达,如优先表达于肌肉的 miRNA 被称为 myomiR,目前已被证实的 myomiR 有: miR-1、miR-133a、miR-133b、miR-206、miR-208a、miR-208b、miR-486 和 miR-499^[31]。越来越多的 miRNA 被证实参与了骨骼肌细胞增殖、分化和自我更新的过程。

2.1 miRNA 在猪肌肉组织中的表达规律

He 等^[32]通过对梅山猪和大白猪 miRNA 转录组进行差异表达分析发现,一些与肌生成相关的 miRNAs(miR-133、miR-1、miR-206 和 miR-148a)在梅山猪中高度表达,而其他 miRNAs(let-7 家族、miR-214 和 miR-181)在大白猪中高度表达,表明调节肌肉发育的主要 miRNA 在两个猪品种之间存在差异。Xie 等^[33]利用含有 ZFN 编辑 MSTN 功能丧失突变(MSTN^{-/-}, MKO)的梅山猪,对来自 MKO 和野生型(MWT)猪的骨骼肌样品进行转录组测序和 miRNA 测序,结果发现,与 MWT 猪相比, MKO 猪中有 200 个基因和 4 个 miRNAs 被显著上调,而 238 个基因和 5 个 miRNAs 被显著下调。GO 功能和 KEGG 通路富集表明,差异表达的 miRNA 及其靶基因参与了骨骼肌生长和发育的信号途径,如 AMPK、mTOR 和 TGF- β 。Mai 等^[34]通过对猪不同肌肉发育阶段 miRNA 的表达模式进行全面研究,结果发现, miRNA 是产前和产后肌肉发育的关键调控因子,其功能在骨骼肌发育的不同阶段具有特异性。Xie 等^[35]通过对蓝塘猪和长白猪骨骼肌发育不同阶段进行 miRNA 差异表达分析,结果表明,肌源性 miRNA 可能在胚胎阶段的肌纤维形成和出生后阶段的肌肉肥大过程中调控肌原纤维基因,导致不同品种的肌肉生产存在明显差异。

2.2 miRNA 在骨骼肌细胞增殖分化中的作用

近年来发现了多种参与骨骼肌细胞增殖分化的 miRNAs。miR-208b 通过靶向 e-蛋白家族成员转录因子 12(TCF12)促进肌源性细胞增殖,抑制其分化^[36]; miR-423-5p 是一种潜在的肌生成调节因子,在成肌细胞增殖和分化过程中发挥负向调控作用^[37]; miR-34c 在体外可抑制猪骨骼肌卫星细胞增

殖,促进分化,在体内抑制猪肌肉发育^[38];miR-501-3p 通过抑制靶基因 *FOS* 的表达,抑制了 C2C12 细胞的增殖,促进了 C2C12 细胞的分化^[39];miR-27b 通过靶向 *MDFI* 促进猪骨骼肌卫星细胞的生成^[40];miR-432 通过靶向肌细胞中的 *E2F3* 和 *P55PIK* 抑制肌细胞生成^[41];miR-323-3p 通过靶向 *Smad2* 抑制成肌细胞增殖,促进成肌细胞分化^[42];miR-195/497 可以通过抑制 *HMGA1-Id3* 通路来促进肌细胞分化^[43];miR-1 通过靶向猪 *CNN3* 基因调控骨骼肌发育^[44];miR-499-5p 可能通过下调 *pSox6* 基因的表达促进氧化肌纤维的形成^[2];miR-696 通过抑制 *CNTFR α* 基因的表达来抑制 C2C12 细胞增殖和分化^[45];猪肌管中过表达 miR-152 可促进慢肌纤维的形成,而抑制 miR-152 的表达则效果相反^[46];miR-199b 通过靶向 *JAG1* 抑制猪骨骼肌卫星细胞的增殖^[7];猪骨骼肌卫星细胞中过表达或抑制 miR-143-3p 可诱导慢肌纤维基因和 *MYH7* 蛋白表达量的增加或减少^[47];miRNA-23a 通过抑制 *MEF2c* 表达降低慢肌纤维类型组成,这是影响肉质的潜在表观遗传调控机制^[48];miR-208b 可通过靶向抑制 *Mettl8* 从而影响不同肌纤维类型的转化^[49];miR-378b-3p 通过介导 *HDAC3/MEF2D/PGC-1 α* 信号通路促进慢肌或氧化型纤维的形成^[50]。目前,miRNA 在骨骼肌细胞增殖分化过程中的作用机制研究较多,这些研究均表明了 miRNA 的调控机制具有复杂性与多样性。

3 lncRNA 对猪骨骼肌发育的影响

研究表明,lncRNA 在众多发育过程中发挥着关键的作用,包括成肌细胞分化、脂肪发生、细胞周期和细胞增殖^[51]。从机制上讲,lncRNA 可作为竞争性内源性 RNA 或 miRNA 分子海绵来影响 miRNA 靶基因的表达,从而参与肌肉发育和脂质代谢的调控^[52]。H19 是最早发现的 lncRNA,它可以在胚胎生长过程中招募组蛋白修饰标记物来抑制印迹基因的转录,并调节参与骨骼肌分化和再生的 miRNA^[53]。

3.1 lncRNA 在猪肌肉组织中的表达规律

Huang 等^[54]利用约克夏猪和藏猪的转录组数据,分析 lncRNA 在 2 个品种猪骨骼肌发育差异中的可能作用,共获得了 138 个差异表达 lncRNAs (DELs),并对其潜在靶基因 (PTGs) 进行了预测,GO 功能和 KEGG 通路分析结果显示,PTGs 参与了与肌肉发育相关的多个生物学过程和通路;对

DELs 的数量性状位点 (QTL) 进行预测表明,大部分 QTL 与肌肉发育相关;根据肌肉发育相关的 PTGs (MDRPTGs) 与相应的 DELs 的表达水平构建了共表达网络,结果显示,DELs 的表达与相应的 MDRPTGs 显著相关,且多个 MDRPTGs 参与了肌肉纤维肥大的关键调控通路,即 *IGF-1-Akt-mTOR* 通路。Tan 等^[55]研究了 3 个不同发育阶段青峪猪基因表达水平,包括最大生长速率的拐点 (MGI)、逐渐增加阶段到快速增加阶段的拐点 (GRI) 以及最大生长速度的拐点 (RSI),通过 Ribo-Zero RNA 测序在这 3 个阶段共鉴定出 14 530 个 mRNAs 和 11 970 个 lncRNAs,在 GRI 与 MGI、RSI 与 MGI 的关系中共鉴定出 645、323 个差异表达基因和 696、760 个差异表达 lncRNAs;功能富集分析表明,参与免疫系统发育和能量代谢的基因(主要涉及氨基酸、碳水化合物和脂质)分别在 GRI 和 MGI 阶段富集,而参与脂质代谢的基因在 RSI 阶段富集。

3.2 lncRNA 在骨骼肌细胞增殖分化中的作用

研究 lncRNA 与其他分子(如 miRNA)的相互作用,可为猪骨骼肌细胞增殖分化的机制研究提供参考。研究发现,H19 长链非编码 RNA 在骨骼肌分化和再生中具有关键的反式调节功能,该功能是由 H19 吸附的 miRNA 介导^[56];MyHC II A/X-AS 作为 miR-130b 的海绵,可调控 MyHC II X 的表达和快速肌纤维表型^[1];AK143003 可以作为负调控因子调控肌肉分化^[54];lncRNA-SYISL 一方面可通过招募 PRC2 抑制 *p21* 基因表达,导致无法退出细胞周期,从而促进成肌细胞增殖,另一方面可引导 PRC2 抑制肌肉特异性基因,如 *MyoG* 和 *MyH4* 的表达,从而抑制成肌细胞的分化^[53]。Li 等^[57]研究揭示了 lncRNA-MSTRG. 59589 可以诱导 *PALLD* 表达水平的升高,促进猪骨骼肌卫星细胞的分化;lncRNA-MSTRG. 42019 可能参与调节骨骼肌的生长和发育,并参与骨骼肌纤维转化^[58]。H19 可能作为一个支架,将 *TDP43* 招募到 *MyoD* 的启动子上,从而激活 *MyoD* 的转录,导致猪骨骼肌卫星细胞的分化;H19 还可通过两种不同的途径调控 *PSC* 分化,一方面,H19 作为 miR-140-5p 的海绵抑制猪骨骼肌卫星细胞的分化,从而调节 *Sox4* 的解抑制,另一方面,H19 通过直接与 *DBN1* 结合调控 *PSC* 猪骨骼肌卫星细胞分化^[59-60]。程晓芳^[61]研究表明,lncRNA-MEG3 通过吸附 miR-423-5p 调控 *SRF* 来促进骨骼肌卫星细胞的分化。lncMGPF 作为 miR-135a-5p 的海绵,可减弱 miR-135a-5p 对 *MEF2C* 的

抑制作用,从而增加 *MEF2C* 基因的表达,在肌肉的生长和再生中起着重要的正向调节作用^[62]。*lncRNA-Neat1* 通过招募 *Ezh2* 增加 *H3k27me3* 在 *p21* 启动子上的结合水平,抑制 *p21* 表达,促进成肌细胞增殖^[63]。*lncRNA-MAR1* 作为 *miR-487b* 海绵,可调控 *Wnt5a* 蛋白,促进肌肉的分化和再生^[64]。*linc-YY1* 在 C2C12 成肌细胞或肌肉卫星细胞中功能的增加或丧失会改变肌源性分化^[65]。此外,*lncRNATCONS_00791383* 可能促进猪骨骼肌卫星细胞的增殖和分化^[66]。*lncRNA-MEG3* 中的 4 个 SNPs 在脂肪型和瘦肉型猪中形成了 2 个有利的单倍型 (CCCA 和 TTCC),从而影响了 *lncRNA-MEG3* 的转录。不同 *MEG3* 单倍型过表达通过失活 *PI3K/Akt* 和 *MAPK/ERK1/2* 通路抑制肌卫星细胞的增殖,*lncRNA-MEG3* 单倍型的上调可通过 *JAK2/STAT3* 途径促进肌卫星细胞的分化^[67]。*lnc-ADAMTS9* 可以通过抑制 *ERK/MAPK* 信号通路促进成肌前体细胞的增殖和分化^[68]。从上述内容可以看出,*lncRNA* 主要作用方式是通过海绵作用吸附 *miRNA*,从而对靶向的 *miRNA* 进行调控。

4 circRNA 对猪骨骼肌发育的影响

最近研究表明,circRNA 在骨骼肌生成过程中发挥着重要作用,可以作为竞争性内源性 RNA 或分子海绵特异性吸附 *miRNA*,进而影响其靶向的 mRNA^[69-70]。目前,已有超过 100 种 circRNAs 被报道可以抑制 *miRNA* 与靶 mRNA 的结合,从而调控骨骼肌细胞生长、增殖、分化和衰老等各种生物过程^[71]。此外,circRNA 还可以通过 IRES 来启动翻译,circZNF609 能够翻译成一种由 IRES 驱动蛋白,并对肌生成具有调控作用^[28]。

4.1 circRNA 在猪肌肉组织中的表达规律

Hong 等^[72]通过对杜洛克猪妊娠后 33、65 和 90 d 胎儿肌肉 circRNA 表达谱进行分析,结果显示,超过 5 000 个 circRNAs 在胎儿肌肉发育中特异性表达。Sun 等^[73]通过对长白猪和蓝塘猪背最长肌中的整体表达情况进行分析,共鉴定出 22 469 个编码转录本,其中与长白猪相比只有 547 个候选 circRNAs 在蓝塘猪中差异表达,包括 461 个上调和 86 个下调。Li 等^[22]使用 RNA-Seq 技术构建了猪的快速收缩的股二头肌 (*biceps femoris*, Bf) 和慢收缩的比鱼肌 (*soleus*, Sol) 的 circRNA 表达谱,并鉴

定出 16 342 个不同的 circRNAs 候选基因,其中存在 242 个差异表达的 circRNAs,包括 105 个上调和 137 个下调,且它们是潜在的调节骨骼肌纤维转化的候选 circRNAs。Liang 等^[74]分析贵州小型猪的 9 个器官和 3 块骨骼肌中的 circRNA 表达,共鉴定出 5 934 个 circRNAs,其中 149 个 circRNAs 可能与肌肉生长相关,并发现它们的宿主基因显著参与肌肉发育、收缩、染色质修饰、阳离子稳态和 ATP 水解偶联质子运输。Shen 等^[75]对生长曲线拐点 (最大生长速率) 猪氧化型和酵解型骨骼肌中 *lncRNA* 和 circRNA 的表达进行了全基因组多样性分析,共鉴定出 911 个差异 *lncRNAs* 和 137 个差异 circRNAs,它们可能与糖酵解过程、氧化还原过程、ATP 代谢和纤维类型的转变有关,还发现了 circRNA290-miR27b-Foxj3 和 circRNA9210-miR-23a-MEF2C 是 2 个相互竞争的 ceRNA 网络,与肌肉纤维型转换密切相关。近年来研究人员通过对 circRNA 的表达谱进行分析,发现存在大量的与骨骼肌细胞增殖分化相关的 circRNA,暗示 circRNA 在骨骼肌细胞增殖分化的过程中发挥着重要的作用。

4.2 circRNA 在骨骼肌细胞增殖分化中的作用

Li 等^[76]研究发现, circFUT10 通过直接与 *miR-133a* 结合并抑制 *miR-133a* 活性来调控成肌细胞的分化和存活; *MyoD* 可以激活 circRNA *CDR1as* 转录, *CDR1as* 通过海绵 *miR-7* 增加 *IGF1R* 水平,随后激活肌生成^[77]。circHIPK3 能够促进 C2C12 成肌细胞的分化^[78]; circHUWE1 通过海绵介导 *miR-29b* 并靶向 *Akt3*,促进成肌细胞增殖,减少细胞凋亡和分化,间接激活 *Akt* 信号通路^[79]; circMYLK4 可促进猪慢肌纤维的发育,并抑制猪骨骼肌卫星细胞分化^[80]; circZfp609 可以作为 *miR-194-5p* 的海绵来阻止其对 *BCLAF1* 的抑制,从而抑制肌源性分化^[81]; circHIPK3 作为竞争性内源 RNA,其过表达可增加 *TCF12* 的表达,从而逆转 *miR-7* 对 C2C12 细胞增殖分化的调控^[82] (表 1)。目前,有关 circRNA 对猪骨骼肌调控机制的研究还相对匮乏,当前的研究主要集中在对猪骨骼肌进行高通量测序,以及利用生物信息学等方式对测序结果进行筛选与分析,并预测其中的 circRNA 的作用方式,构建出竞争性调控网络。

表 1 参与骨骼肌细胞增殖分化的 circRNAs

Table 1 circRNAs involved in skeletal muscle cell proliferation and differentiation

circRNAs	作用方式 Mode of action	生物学功能 Biological function	参考文献 References
circFUT10	吸附 miR-133a	调控成肌细胞的分化	Li 等 ^[76]
circCDR1as	吸附 miR-7,并增加 IGF-1R 水平	激活肌生成	Li 等 ^[77]
circHIPK3	吸附 miR-124 和 miR-379	促进成肌细胞的分化	Yao 等 ^[78]
circHUWE1	吸附 miR-29b,靶基因为 <i>Akt3</i>	促进成肌细胞增殖,抑制凋亡和分化	Yue 等 ^[79]
circMYLK4	显著升高了慢肌相关基因 <i>MyHC I</i> 等的表达	促进猪慢肌纤维的发育,抑制猪骨骼肌卫星细胞分化	曹海港 ^[80]
circZfp609	吸附 miR-194-5p,靶基因为 <i>BCLAF1</i>	抑制肌源性分化	Wang 等 ^[81]
circHIPK3	吸附 miR-7,增加 <i>TCF12</i> 基因表达	调控成肌细胞增殖分化	Gao 等 ^[82]

5 小 结

骨骼肌为猪体内重要的组织,也是人们日常食用肉制品的来源。近年来,随着高通量测序技术和生物信息学的进步,越来越多的 ncRNA 被发现,且不少 ncRNA 参与到骨骼肌的增殖分化调控过程中。因此,研究 ncRNA 并了解其在骨骼肌发育的调控作用对于畜牧生产过程尤为重要。现今 miRNA 与 lncRNA 对于骨骼肌发育的研究较多,技术也较为成熟, circRNA 作为新发现的 ncRNA,调控机制尚不明确,主要的作用是充当 ceRNA。作者对 ncRNA 在猪肌肉发育中的作用进行总结,但 ncRNA 对于骨骼肌发育的调控作用还需深度发掘,摸清 ncRNA 与基因之间的调控模式,可为进一步挖掘 ncRNA 调控骨骼肌发育的机制提供线索。

参考文献 (References):

- [1] DOU M, YAO Y, MA L, et al. The long noncoding RNA MyHC II A/X-AS contributes to skeletal muscle myogenesis and maintains the fast fiber phenotype[J]. *Journal of Biological Chemistry*, 2020, 295(15):4937-4949.
- [2] WANG X Y, CHEN X L, HUANG Z Q, et al. microRNA-499-5p regulates porcine myofiber specification by controlling Sox6 expression[J]. *Animal*, 2017, 11(12):2268-2274.
- [3] KAIKKONEN M U, ADELMAN K. Emerging roles of non-coding RNA transcription[J]. *Trends in Biochemical Sciences*, 2018, 43(9):654-667.
- [4] MATTICK J S, MAKUNIN I V. Non-coding RNA[J]. *Human Molecular Genetics*, 2006, 15(1):R17-R29.
- [5] 白凤庭,李 林,陈军豪,等. 非编码 RNA 与骨骼肌发育研究进展[J]. *中国畜牧兽医*, 2020, 47(11):

3584-3594.

BAI F T, LI L, CHEN J H, et al. Research progression on non-coding RNA and skeletal muscle development[J]. *China Animal Husbandry & Veterinary Medicine*, 2020, 47(11):3584-3594. (in Chinese)

- [6] ZHAO Y, CHEN M, LIAN D, et al. Non-coding RNA regulates the myogenesis of skeletal muscle satellite cells injury repair and diseases[J]. *Cells*, 2019, 8(9):988.
- [7] ZHU L, HOU L, OU J, et al. miR-199b represses porcine muscle satellite cells proliferation by targeting JAG1[J]. *Gene*, 2019, 691:24-33.
- [8] SOUSA M, DOLICKA D, GJORGJEVA M, et al. Deciphering miRNAs' action through miRNA editing[J]. *International Journal of Molecular Sciences*, 2019, 20(24):6249.
- [9] IQBAL A, PING J, ALI S, et al. Role of microRNAs in myogenesis and their effects on meat quality in pig—A review[J]. *Asian Australasian Journal of Animal Sciences*, 2020, 33(12):1873-1884.
- [10] WEI J W, HUANG K, YANG C, et al. Non-coding RNAs as regulators in epigenetics (review)[J]. *Oncology Reports*, 2017, 37(1):3-9.
- [11] MOHR A M, MOTT J L. Overview of microRNA biology[J]. *Seminars in Liver Disease*, 2015, 35(1):3-11.
- [12] KROL J, LOEDIGE I, FILIPOWICZ W. The widespread regulation of microRNA biogenesis, function and decay[J]. *Nature Reviews Genetics*, 2010, 11(9):597-610.
- [13] GIL N, ULITSKY I. Regulation of gene expression by cis-acting long non-coding RNAs[J]. *Nature Reviews Genetics*, 2020, 21(2):102-117.
- [14] MARCHESE F P, RAIMONDI I, HUARTE M. The multidimensional mechanisms of long noncoding RNA function[J]. *Genome Biology*, 2017, 18(1):206.

- [15] QUINN J J, CHANG H Y. Unique features of long non-coding RNA biogenesis and function[J]. *Nature Reviews Genetics*, 2016, 17(1): 47-62.
- [16] KOPP F, MENDELL J T. Functional classification and experimental dissection of long noncoding RNAs[J]. *Cell*, 2018, 172(3): 393-407.
- [17] ST LAURENT G, WAHLESTEDT C, KAPRANOV P. The landscape of long noncoding RNA classification[J]. *Trends in Genetics*, 2015, 31(5): 239-251.
- [18] JARROUX J, MORILLON A, PINSKAYA M. History, discovery, and classification of lncRNAs[J]. *Advances in Experimental Medicine and Biology*, 2017, 1008: 1-46.
- [19] MA L, BAJIC V B, ZHANG Z. On the classification of long non-coding RNAs[J]. *RNA Biology*, 2013, 10(6): 925-933.
- [20] SANGER H L, KLOTZ G, RIESNER D, et al. Viroids are single-stranded covalently closed circular RNA molecules existing as highly base-paired rod-like structures[J]. *Proceedings of the National Academy of Sciences of the United States of America*, 1976, 73(11): 3852-3856.
- [21] HSU M, COCAPRADOS M. Electron microscopic evidence for the circular form of RNA in the cytoplasm of eukaryotic cells[J]. *Nature*, 1979, 280(5720): 339-340.
- [22] LI B, YIN D, LI P, et al. Profiling and functional analysis of circular RNAs in porcine fast and slow muscles[J]. *Frontiers in Cell and Developmental Biology*, 2020, 8: 322.
- [23] LUO H, LV W, TONG Q, et al. Functional non-coding RNA during embryonic myogenesis and postnatal muscle development and disease[J]. *Frontiers in Cell and Developmental Biology*, 2021, 9: 628339.
- [24] JECK W R, SORRENTINO J A, WANG K, et al. Circular RNAs are abundant, conserved, and associated with ALU repeats[J]. *RNA*, 2013, 19(2): 141-157.
- [25] MENG S, ZHOU H, FENG Z, et al. circRNA: Functions and properties of a novel potential biomarker for cancer[J]. *Molecular Cancer*, 2017, 16(1): 94.
- [26] JECK W R, SHARPLESS N E. Detecting and characterizing circular RNAs[J]. *Nature Biotechnology*, 2014, 32(5): 453-461.
- [27] 谢月琴, 陈 婷, 罗君谊, 等. circRNA 作用机制及其对动物肌肉发育的影响[J]. *中国畜牧兽医*, 2018, 45(8): 2270-2275.
- XIE Y Q, CHEN T, LUO J Y, et al. Mechanism of circRNA and its effect on development of animal muscles[J]. *China Animal Husbandry & Veterinary Medicine*, 2018, 45(8): 2270-2275. (in Chinese)
- [28] LEGNINI I, DI TIMOTEO G, ROSSI F, et al. circ-ZNF609 is a circular RNA that can be translated and functions in myogenesis[J]. *Molecular Cell*, 2017, 66(1): 22-37.
- [29] 郑 婷, 甘麦邻, 沈林园, 等. circRNA 及其调控动物骨骼肌发育研究进展[J]. *遗传*, 2020, 42(12): 1178-1191.
- ZHENG T, GAN M L, SHEN L Y, et al. circRNA on animal skeletal muscle development regulation[J]. *Hereditas*, 2020, 42(12): 1178-1191. (in Chinese)
- [30] DIALLO L H, TATIN F, DAVID F, et al. How are circRNAs translated by non-canonical initiation mechanisms? [J]. *Biochimie*, 2019, 164: 45-52.
- [31] HORAK M, NOVAK J, BIENERTOVA-VASKU J. Muscle-specific microRNAs in skeletal muscle development[J]. *Developmental Biology*, 2016, 410(1): 1-13.
- [32] HE D, ZOU T, GAI X, et al. microRNA expression profiles differ between primary myofiber of lean and obese pig breeds[J]. *PLoS One*, 2017, 12(7): e0181897.
- [33] XIE S, LI X, QIAN L, et al. An integrated analysis of mRNA and miRNA in skeletal muscle from myostatin-edited Meishan pigs[J]. *Genome*, 2019, 62(5): 305-315.
- [34] MAI M, JIN L, TIAN S, et al. Deciphering the microRNA transcriptome of skeletal muscle during porcine development[J]. *PeerJ*, 2016, 4: e1504.
- [35] XIE S, CHEN L, ZHANG X, et al. An integrated analysis revealed different microRNA-mRNA profiles during skeletal muscle development between Landrace and Lantang pigs[J]. *Scientific Reports*, 2017, 7(1): 2516.
- [36] FU L, WANG H, LIAO Y, et al. miR-208b modulating skeletal muscle development and energy homeostasis through targeting distinct targets[J]. *RNA Biology*, 2020, 17(5): 743-754.
- [37] GE J, ZHU J, XIA B, et al. miR-423-5p inhibits myoblast proliferation and differentiation by targeting Sufu[J]. *Journal of Cell Biochemistry*, 2018, 119(9): 7610-7620.
- [38] HOU L, XU J, LI H, et al. miR-34c represses muscle development by forming a regulatory loop with Notch1[J]. *Scientific Reports*, 2017, 7(1): 9346.
- [39] HOU L, ZHU L, LI H, et al. miR-501-3p forms a feedback loop with FOS, MDFI, and MyoD to regulate C2C12 myogenesis[J]. *Cells*, 2019, 8(6): 573.
- [40] HOU L, XU J, JIAO Y, et al. miR-27b promotes

- muscle development by inhibiting MDFI expression[J]. *Cell Physiology Biochemistry*, 2018, 46(6): 2271-2283.
- [41] MA M, WANG X, CHEN X, et al. microRNA-432 targeting E2F3 and P55PIK inhibits myogenesis through PI3K/Akt/mTOR signaling pathway[J]. *RNA Biology*, 2017, 14(3): 347-360.
- [42] QIN J, SUN Y, LIU S, et al. microRNA-323-3p promotes myogenesis by targeting Smad2[J]. *Journal of Cell Biochemistry*, 2019, 120(11): 18751-18761.
- [43] QIU H, ZHONG J, LUO L, et al. Regulatory axis of miR-195/497 and HMGA1-Id3 governs muscle cell proliferation and differentiation[J]. *Internal Journal Biology Science*, 2017, 13(2): 157-166.
- [44] TANG Z, LIANG R, ZHAO S, et al. CNN3 is regulated by microRNA-1 during muscle development in pigs[J]. *Internal Journal Biology Science*, 2014, 10(4): 377-385.
- [45] WANG H, SHI L, LIANG T, et al. miR-696 regulates C2C12 cell proliferation and differentiation by targeting CNTFR α [J]. *Internal Journal Biology Science*, 2017, 13(4): 413-425.
- [46] ZHANG Y, YAN H, ZHOU P, et al. microRNA-152 promotes slow-twitch myofiber formation via targeting uncoupling protein-3 gene[J]. *Animals (Basel)*, 2019, 9(9): 669.
- [47] ZUO J, WU F, LIU Y, et al. microRNA transcriptome profile analysis in porcine muscle and the effect of miR-143 on the MYH7 gene and protein[J]. *PLoS One*, 2015, 10(4): e0124873.
- [48] SHEN L, CHEN L, ZHANG S, et al. microRNA-23a reduces slow myosin heavy chain isoforms composition through myocyte enhancer factor 2C (MEF2C) and potentially influences meat quality[J]. *Meat Science*, 2016, 116: 201-206.
- [49] 李 想. miR-208b 通过抑制 Mettl8 表达调控骨骼肌纤维类型转化[D]. 北京: 中国农业科学院, 2020.
- LI X. miR-208b regulates skeletal muscle fiber types conversion by inhibiting Mettl8 expression[D]. Beijing: Chinese Academy of Agricultural Sciences, 2020. (in Chinese)
- [50] 张 勇. microRNA-378b-3p 对猪骨骼肌纤维类型转化的调节作用及其机制[D]. 雅安: 四川农业大学, 2018.
- ZHANG Y. The role of microRNA-378b-3p in regulating porcine skeletal muscle fiber type conversion and its mechanism[D]. Ya'an: Sichuan Agricultural University, 2018. (in Chinese)
- [51] YANG Y, LIANG G, NIU G, et al. Comparative analysis of DNA methylome and transcriptome of skeletal muscle in lean-, obese-, and mini-type pigs[J]. *Scientific Reports*, 2017, 7: 39883.
- [52] JIN J J, LV W, XIA P, et al. Long noncoding RNA SYISL regulates myogenesis by interacting with polycomb repressive complex 2[J]. *Proceedings of the National Academy of Sciences of the United States of America*, 2018, 115(42): E9802-E9811.
- [53] GUO Y, WANG J, ZHU M, et al. Identification of MyoD-responsive transcripts reveals a novel long non-coding RNA (lncRNA-AK143003) that negatively regulates myoblast differentiation[J]. *Scientific Reports*, 2017, 7(1): 2828.
- [54] HUANG Z, LI Q, LI M, LI C. Transcriptome analysis reveals the long intergenic noncoding RNAs contributed to skeletal muscle differences between Yorkshire and Tibetan pig[J]. *Scientific Reports*, 2021, 11(1): 2622.
- [55] TAN Y, GAN M, SHEN L, et al. Profiling and functional analysis of long noncoding RNAs and mRNAs during porcine skeletal muscle development[J]. *Internal Journal of Molecular Sciences*, 2021, 22(2): 503.
- [56] DEY B K, PFEIFER K, DUTTA A. The H19 long noncoding RNA gives rise to microRNAs miR-675-3p and miR-675-5p to promote skeletal muscle differentiation and regeneration[J]. *Genes & Development*, 2014, 28(5): 491-501.
- [57] LI L, CHENG X, CHEN L, et al. Long noncoding ribonucleic acid MSTRG. 59589 promotes porcine skeletal muscle satellite cells differentiation by enhancing the function of PALLD[J]. *Frontiers in Genetics*, 2019, 10: 1220.
- [58] LI R, LI B, JIANG A, et al. Exploring the lncRNAs related to skeletal muscle fiber types and meat quality traits in pigs[J]. *Genes (Basel)*, 2020, 11(8): 883.
- [59] LI J, ZHAO W, LI Q, et al. Long non-coding RNA H19 promotes porcine satellite cell differentiation by interacting with TDP43[J]. *Genes (Basel)*, 2020, 11(3): 259.
- [60] LI J, SU T, ZOU C, et al. Long non-coding RNA H19 regulates porcine satellite cell differentiation through miR-140-5p/SOX4 and DBN1[J]. *Frontiers in Cell and Developmental Biology*, 2020, 8: 518724.
- [61] 程晓芳. lncRNA-MEG3 调控猪骨骼肌卫星细胞分化的机制研究[D]. 武汉: 华中农业大学, 2020.
- CHENG X F. Mechanisms of lncRNA-MEG3 in regulating the differentiation of porcine satellite

- cells[D]. Wuhan: Huazhong Agricultural University, 2020. (in Chinese)
- [62] LV W, JIN J, XU Z, et al. lncMGPF is a novel positive regulator of muscle growth and regeneration[J]. *Journal of Cachexia Sarcopenia Muscle*, 2020, 11(6): 1723-1746.
- [63] WANG S, ZUO H, JIN J, et al. Long noncoding RNA Neat1 modulates myogenesis by recruiting Ezh2[J]. *Cell Death Disease*, 2019, 10(7): 505.
- [64] ZHANG Z K, LI J, GUAN D, et al. A newly identified lncRNA MAR1 acts as a miR-487b sponge to promote skeletal muscle differentiation and regeneration[J]. *Journal of Cachexia Sarcopenia Muscle*, 2018, 9(3): 613-626.
- [65] ZHOU L, SUN K, ZHAO Y, et al. Linc-YY1 promotes myogenic differentiation and muscle regeneration through an interaction with the transcription factor YY1[J]. *Nature Communication*, 2015, 6: 10026.
- [66] 李倩倩, 李 龙, 黄子莹, 等. 猪 lncRNA TCONS_00791383 对骨骼肌卫星细胞增殖分化的影响[J]. 畜牧兽医学报, 2020, 51(6): 1177-1186.
- LI Q Q, LI L, HUANG Z Y, et al. Effect of pig lncRNA TCONS_00791383 on the proliferation and differentiation of skeletal muscle satellite cells[J]. *Acta Veterinaria et Zootechnica Sinica*, 2020, 51(6): 1177-1186. (in Chinese)
- [67] YANG R, LIU Y, CHENG Y, et al. Effects and molecular mechanism of single-nucleotide polymorphisms of MEG3 on porcine skeletal muscle development[J]. *Frontiers in Genetics*, 2021, 12: 607910.
- [68] WANG L, HE T, ZHANG X, et al. Global transcriptomic analysis reveals lnc-ADAMTS9 exerting an essential role in myogenesis through modulating the ERK signaling pathway[J]. *Journal Animal Science Biotechnology*, 2021, 12(1): 4.
- [69] YUE B, WANG J, SONG C, et al. Biogenesis and ceRNA role of circular RNAs in skeletal muscle myogenesis[J]. *International Journal of Biochemistry Cell Biology*, 2019, 117: 105621.
- [70] ZHANG P, CHAO Z, ZHANG R, et al. Circular RNA regulation of myogenesis[J]. *Cells*, 2019, 8(8): 885.
- [71] DAS A, DAS A, DAS D, et al. Circular RNAs in myogenesis[J]. *Biochimica et Biophysica Acta (BBA)-Gene Regulatory Mechanisms*, 2020, 1863(4): 194372.
- [72] HONG L, GU T, HE Y, et al. Genome-wide analysis of circular RNAs mediated ceRNA regulation in porcine embryonic muscle development[J]. *Frontiers in Cell and Developmental Biology*, 2019, 7: 289.
- [73] SUN J, XIE M, HUANG Z, et al. Integrated analysis of non-coding RNA and mRNA expression profiles of 2 pig breeds differing in muscle traits[J]. *Journal of Animal Science*, 2017, 95(3): 1092-1103.
- [74] LIANG G, YANG Y, NIU G, et al. Genome-wide profiling of *Sus scrofa* circular RNAs across nine organs and three developmental stages[J]. *DNA Research*, 2017, 24(5): 523-535.
- [75] SHEN L, GAN M, TANG Q, et al. Comprehensive analysis of lncRNAs and circRNAs reveals the metabolic specialization in oxidative and glycolytic skeletal muscles[J]. *International of Journal Molecular Science*, 2019, 20(12): 2855.
- [76] LI H, YANG J, WEI X, et al. circFUT10 reduces proliferation and facilitates differentiation of myoblasts by sponging miR-133a[J]. *Journal of Cell Physiology*, 2018, 233(6): 4643-4651.
- [77] LI L, CHEN Y, NIE L, et al. MyoD-induced circular RNA CDR1as promotes myogenic differentiation of skeletal muscle satellite cells[J]. *Biochimica et Biophysica Acta (BBA)-Gene Regulatory Mechanisms*, 2019, 1862(8): 807-821.
- [78] YAO R, YAO Y, LI C, et al. circ-HIPK3 plays an active role in regulating myoblast differentiation[J]. *International Journal of Biological Macromolecules*, 2020, 155: 1432-1439.
- [79] YUE B, WANG J, RU W, et al. The circular RNA circHUWE1 sponges the miR-29b-Akt3 axis to regulate myoblast development[J]. *Molecular Therapy-Nucleic Acids*, 2020, 19: 1086-1097.
- [80] 曹海港. 猪骨骼肌纤维类型关键 circRNAs 的筛选及 circMYLK4 的功能研究[D]. 杨凌: 西北农林科技大学, 2019.
- CAO H G. Screening of key circRNAs in skeletal muscle fiber types of pigs and functional study of circMYLK4[D]. Yangling: Northwest A&F University, 2019. (in Chinese)
- [81] WANG Y, LI M, WANG Y, et al. A Zfp609 circular RNA regulates myoblast differentiation by sponging miR-194-5p[J]. *International Journal of Biological Macromolecules*, 2019, 121: 1308-1313.
- [82] GAO M, LI X, YANG Z, et al. circHIPK3 regulates proliferation and differentiation of myoblast through the miR-7/TCF12 pathway[J]. *Journal of Cell Physiology*, 2021, 10: 1-13.

(责任编辑 晋大鹏)

非编码 RNA 调控猪肌间脂肪沉积的研究进展

谢 芳, 罗君谊, 陈 婷, 习欠云, 张永亮, 孙加节[✉]

(华南农业大学动物科学学院, 国家生猪种业工程技术研究中心, 广州 510642)

摘 要: 肌间脂肪含量与肉品质密切相关, 决定着猪肉的风味、多汁性和嫩度等感官指标, 因此, 提高肌间脂肪沉积量对改善肉品质有重要作用。肌间脂肪沉积是一个复杂的生物学过程, 受多种调控因子和成脂相关信号通路的影响, 其中非编码 RNA(non-coding RNA, ncRNA) 对猪肌间脂肪沉积的调控作用引起了研究者的广泛关注。ncRNA 是一类不编码蛋白质的 RNA 分子, 在细胞增殖、分化、凋亡等多种生物学过程中发挥着调控作用。近年来研究表明, ncRNA 中微小 RNA(microRNA, miRNA)、长链非编码 RNA(long non-coding RNA, lncRNA) 和环状 RNA(circular RNA, circRNA) 均是肌间脂肪沉积的潜在调节因子, 参与调控动物脂肪沉积过程。作者概述了 ncRNA 的生物学特性, 介绍了肌间脂肪细胞的来源, 总结了现阶段 ncRNA 在猪肌间脂肪沉积中的研究进展, 以期为猪肉品质改良提供基础数据。

关键词: 非编码 RNA; 猪; 肌间脂肪; 肉品质

中图分类号: Q752

文献标识码: A

Doi: 10.16431/j.cnki.1671-7236.2023.10.027

开放科学(资源服务)标识码(OSID):



Research Progress on Non-coding RNA Regulating Intermuscular Fat Deposition in Pig

XIE Fang, LUO Junyi, CHEN Ting, XI Qianyun, ZHANG Yongliang, SUN Jiajie[✉]

(National Engineering Research Center for Breeding Swine Industry, College of Animal Science, South China Agricultural University, Guangzhou 510642, China)

Abstract: The content of intermuscular fat is closely related to meat quality, which determines sensory indicators such as flavor, juiciness, and tenderness of pork. Therefore, increasing intermuscular fat deposition plays an important role in improving meat quality. Intermuscular fat deposition is a complex biological process influenced by multiple regulatory factors and lipogenesis-related signaling pathways, among which the role of non-coding RNA (ncRNA) has attracted much attention from researchers. ncRNA is a class of RNA molecules that do not encode proteins, and plays a regulatory role in cell proliferation, differentiation, apoptosis and other biological processes. Recent studies have shown that microRNA (miRNA), long non-coding RNA (lncRNA) and circular RNA (circRNA) are potential regulators of intermuscular fat deposition and are involved in the regulation of fat deposition in animals. The authors summarized the biological characteristics of ncRNA, introduced the origin of intermuscular fat cells, and summarized the current research progress of ncRNA in pig intermuscular fat deposition, in order to provide basic data for pork quality improvement.

Key words: non-coding RNA; pig; intermuscular fat; meat quality

动物脂肪组织按其分布部位可分为皮下脂肪(subcutaneous fat)、内脏脂肪(visceral fat)、肌内脂肪(intramuscular fat)和肌间脂肪(intermuscular fat),其中皮下脂肪含量最高,有隔热、贮存能量的作用;内脏脂肪包裹在腹腔脏器周围,主要对各脏器起支撑、保护作用^[1];肌内脂肪位于肌外膜、肌内膜和肌束膜上,肌间脂肪分布在肌纤维束之间,二者对改善肉品质均有重要作用^[2]。肌间脂肪含量是评估肉品质的关键指标,与猪肉的嫩度、风味、多汁性和大理石花纹密切相关^[3]。猪肌间脂肪沉积对肉的感官品质和胴体性状具有重要调控作用,因而肌间脂肪沉积成为动物生产领域的研究热点。肌间脂肪沉积是一个复杂的生物学过程,受转录因子、蛋白质编码基因、非编码 RNA(non-coding RNA, ncRNA)等因素调节^[4-6]。近年来,随着高通量测序在畜牧业研究中的广泛应用,越来越多研究表明,ncRNA 参与动物脂肪沉积调控,并在肌间脂肪沉积过程中发挥重要功能。然而,目前对猪肌间脂肪沉积的机制研究主要集中在脂肪细胞分化及脂质合成相关编码基因的表达水平上,对 ncRNA 调控猪肌间脂肪沉积的作用机制研究较少。因此,作者主要阐述了 ncRNA 在猪肌间脂肪沉积中的研究进展,为 ncRNA 对猪前体脂肪细胞增殖、分化的调控机制研究提供数据支撑。

1 ncRNA 概述

ncRNA 是一类不编码蛋白质的表观遗传学调节因子,其根据核苷酸序列长短主要分为短链 ncRNA 和长链 ncRNA(long non-coding RNA, lncRNA),短链 ncRNA 是长度 <200 nt 的 ncRNA,如微小 RNA(microRNA, miRNA)、小干扰 RNA(small interfering RNA, siRNA)、核小 RNA(small nuclear RNA, snRNA)等;lncRNA 是长度 >200 nt 的 ncRNA;另还有一种结构特殊的 ncRNA—环状 RNA(circular RNA, circRNA)^[7]。作者概述了研究中常见的 3 种 ncRNA: miRNA、lncRNA、circRNA。

miRNA 是一类由 18~23 个核苷酸组成的 ncRNA,在转录后水平上调节多种生物学过程中相关基因表达^[8]。miRNA 与其靶基因的相互作用受多种因素调节,如 miRNA 的亚细胞定位、miRNA 和靶 mRNA 的丰度、miRNA 与靶 mRNA 相互作用的亲和力等^[9]。一般认为 miRNA 与靶 mRNA 序列中的 3'-端非编码区(3'-UTR)相互作用诱导靶

mRNA 降解和抑制蛋白质合成^[9]。但也有研究发现,在特定条件下,miRNA 与 5'-UTR、基因启动子、编码序列相互作用,可激活翻译或调节转录^[9-11]。由此可见,miRNA 是调节基因表达的重要因子,参与转录和翻译过程,有助于维持 mRNA 的稳定性。此外,单个 miRNA 可靶向数百个 mRNA,参与调节整个蛋白质网络,而 1 个 mRNA 则由几个 miRNA 调控,导致 miRNA 和其他因子可能竞争特定 RNA 上的结合位点^[11-12]。lncRNA 主要分布于细胞核,在染色质区域富集^[13]。早期研究发现,lncRNA 被认为不编码蛋白质,其加工特性与 mRNA 相似,主要由 RNA 聚合酶 II(RNA polymerase II, Pol II)进行转录、剪接、加帽和多聚腺苷酸化^[14-15],但最近一项研究发现,lncRNA 可与核糖体互作编码蛋白质或多肽^[16]。与 mRNA 的作用机制相比,lncRNA 表达水平较低,物种间序列保守性较差,但其具有较强的组织或细胞类型特异性^[14]。lncRNA 与其亚细胞定位、序列和二级结构密切相关,主要与蛋白质、RNA、DNA 之间相互作用,调节染色质状态和基因的转录活性,进而影响 RNA 剪接、稳定性和翻译^[17]。另外,lncRNA 还可作为 miRNA 的海绵,通过吸附 miRNA 影响 mRNA 丰度,调节蛋白质编码基因的转录和翻译^[18]。circRNA 是一种由 mRNA 反向剪接而成的闭合 ncRNA,主要存在于细胞质中,相较于线性 RNA 分子,其缺乏 5'-末端帽子结构和 3'-末端 poly(A)尾巴结构,对核糖核酸外切酶有较强抗性^[19]。早在 20 世纪 70 年代至 20 世纪 90 年代,研究者已经发现了几种 circRNA,但直到高通量测序技术的普及, circRNA 丰度和功能才逐渐被关注。circRNA 具有多种生物学功能,包括调控基因表达、竞争性结合 miRNA、编码蛋白质等^[20]。目前,已报道数千个含有 miRNA 结合位点的 circRNA,表明 circRNA 可充当 miRNA 的海绵吸附 miRNA,发挥竞争性内源 RNA(competing endogenous RNA, ceRNA)的功能,参与细胞增殖、分化、凋亡、基因转录以及信号转导^[21]。

2 肌间脂肪细胞来源

肌间脂肪沉积主要通过脂肪细胞增殖和分化实现,在早期胚胎发育时期,脂肪细胞以增殖为主,其数量在出生前已基本固定,出生后主要依赖脂肪细胞体积增大及分化,生长发育期的肌间脂肪沉积量由脂滴大小决定^[22]。一般而言,肌间脂肪细胞主要

来源于纤维/脂肪形成祖细胞 (fibro-adipogenic progenitors, FAPs), FAPs 是一种非肌源性的间充质干细胞亚群,兼具成脂分化能力及成纤维分化潜能的前体细胞^[23-25]。FAPs 的分化能力受环境影响,胰岛素是细胞成脂分化的关键调节因子,可促进 FAPs 分化成富含脂质的脂肪细胞^[23],而转化生长因子- β (transforming growth factor- β , TGF- β) 可诱导 FAPs 分化为表达胶原蛋白 I 型的成纤维细胞^[26]。研究显示,肌肉中的 FAPs 主要是由中胚层特异性表达奇跳相关转录因子 1 (odd-skipped related transcription factor1, OSR1) 的肌肉间质结缔组织细胞分化而成^[27], FAPs 增殖和成脂分化潜能与大理石花纹相关,且 FAPs 数量在肌间脂肪含量不同的肌肉组织中存在差异^[25]。肌肉中的 FAPs 主要位于肌束膜内,肌束膜是肌间脂肪细胞生成的主要场所,因而 FAPs 增殖有利于肌间脂肪沉积。在动物生产中,肌间脂肪沉积直接影响大理石花纹评分和肉质风味、嫩度、多汁性等感官品质^[3]。因此,促进 FAPs 增殖使其分化为成熟的脂肪细胞,调节脂肪组织中的脂质沉积,对改善肉品质有重要意义。

大量研究表明,仅肌肉中的 FAPs 可特异性表达骨髓肌血小板源性生长因子受体 α (PDGFR α),其可能是肌间脂肪形成过程中祖细胞的潜在生物标志物^[23-24]。Uezumi 等^[23]通过体外试验以 CD31-CD45-SM/C-2.6-PDGFR α ⁺ 为标志物分选小鼠肌肉组织中的细胞群,发现只有 PDGFR α ⁺ 标识的细胞群具有成脂分化能力。此外, FAPs 对维持肌肉稳态、神经肌肉完整性和肌肉再生能力至关重要,其在正常情况下数量较少,但在急性肌肉损伤后会迅速增殖,并迁移至萎缩的肌纤维周围释放多种营养因子,激活卫星细胞增殖并诱导其分化,从而促进肌肉再生^[28]。研究者通过对小鼠注射心脏毒素或甘油诱导肌肉损伤后发现,产生的脂肪细胞主要来源于 PDGFR α ⁺ 和 FAPs 细胞群,表明 PDGFR α ⁺ 和 FAPs 是骨骼肌损伤后生成脂肪细胞的主要来源^[29]。Sun 等^[30]对 180 日龄瘦肉型猪和脂肪型猪背最长肌进行 PDGFR α ⁺ 细胞检测,发现后者背最长肌的肌纤维间隙中含有更多的 PDGFR α ⁺ 细胞。PDGFR α ⁺ 和 FAPs 作为脂肪细胞的主要来源,其增殖、成脂分化潜能与脂肪沉积密切相关。研究发现,脂肪含量在不同动物、品种、部位等方面存在差异,外源营养因子和药物添加可扩大 FAPs 池,诱导前体脂肪细胞向成熟脂肪细胞转化,促进脂肪沉积^[31]。

3 ncRNA 对猪肌间脂肪沉积的影响

3.1 miRNA 调控脂肪沉积

探究脂肪组织中 ncRNA 的表达差异可为提高猪肉适口性提供新的思路。大量研究表明,脂肪细胞分化由特定的基因网络调节,miRNA 作为潜在影响因素,在脂肪沉积中发挥直接或间接的调控作用。刘慧莹^[32]通过构建数字基因表达谱,利用生物信息学分析筛选出了 44 个与脂肪含量相关的 miRNA,并鉴定出了高、低脂肪组之间有 8 个显著差异表达的 miRNA。研究者对金华猪和长白猪脂肪沉积相关的 miRNA 进行分析发现,2 个品种猪之间有 220 个差异表达 miRNA^[33]。另有研究发现,以高、低脂肪约克夏猪为模型进行 miRNA 深度测序,鉴定出 268 个成熟的 miRNA (已知 70 个,保守 162 个,特异 36 个),其中 miR-365-3p 的 mRNA 表达量在低脂肪组中上调,在高脂肪组中下调,推测 miR-365-3p 可能对脂肪前体细胞成脂分化具有调控作用^[34]。

miRNA 调控脂肪沉积受到多种基因影响,包括 KLF 家族 (krüppel-like factors, KLF)、过氧化物酶体增殖物激活受体 (peroxisome proliferator-activated receptor, PPAR)、长链脂酰辅酶 A 合成酶 (long-chain acyl-CoA synthetase, ACSL) 家族等。KLF 家族成员基因存在于真核生物中,可调节富含 GC 和 CACCC 启动子的基因表达,在调控脂肪细胞生成、分化中发挥重要作用^[35]。Du 等^[36]发现,miR-125a-5p 过表达可提高周期蛋白依赖性激酶 2 (cyclin-dependent kinases, CDK2)、CDK3 和细胞周期蛋白 B (Cyclin B) 等增殖相关基因的表达水平,促进猪前体脂肪细胞增殖,且过表达 miR-125a-5p 还显著抑制转录调节因子 CCAAT 增强子结合蛋白 α (CCAAT/enhancer binding protein α , C/EBP α)、脂肪酸结合蛋白 4 (adipocyte fatty acid-binding protein 4, FABP4) 等成脂相关基因的表达水平,进一步研究显示 KLF13 是 miR-125a-5p 的直接靶基因,抑制猪前体脂肪细胞分化。过表达 miR-206 可抑制猪前体脂肪细胞增殖和分化,其分子机制是 miR-206 直接靶向 StAR 相关脂质转移结构域 7 (STAR related lipid transfer domaincontaining 7, STARD7) 降低 Cyclin B 和 Cyclin E 的表达,同时 miR-206 通过靶向 KLF4 抑制 PPAR γ 、脂肪酸合酶 (fatty acid synthase, FAS) 和脂肪细胞蛋白 2 (adipocyte protein 2, aP2) 等成脂相关基因的表达^[37]。在二花脸猪背最长肌中,肌间脂肪含量与

KLF3 呈负相关,过表达 KLF3 会导致 *PPAR γ* 、*C/EBP α* 、*FABP4* 等成脂相关基因表达下调,研究进一步证实了 miR-32-5p 通过靶向负调控 KLF3,促进猪前体脂肪细胞分化^[38]。*PPAR γ* 作为 PPAR 家族中对脂肪细胞最具特异性的成员,是脂肪前体细胞分化的关键调节因子,参与脂肪生成和调节脂质代谢过程^[39]。miR-130a 在二花脸猪前体脂肪细胞的分化时期表达量下调,直接靶向 *PPAR γ* 的 3'-UTR 区抑制猪前体脂肪细胞的分化^[40]。研究者发现 miR-34a 通过靶向 *PDGFR α* 阻遏 ERK 信号通路,抑制猪前体脂肪细胞分化^[30]。也有研究发现,通过荧光素酶报告基因检测到猪前体脂肪细胞中 miR-34a 的靶基因为 *ACSL4*,并发现 miR-34a 作用于 *ACSL4* 会显著降低 *PPAR γ* 和固醇调节元件结合蛋白-1c (sterol regulatory element binding transcription factor 1, *SREBP*) 的表达水平,从而抑制猪前体脂肪细胞的分化^[41]。*ACSL4* 是 *ACSL* 家族中的一种同工酶,*ACSL* 家族作为脂质合成的关键酶,在 ATP 供能的前提下催化游离脂肪酸生成脂酰辅酶 A,参与脂肪酸 β 氧化和甘油三酯合成^[42]。在约克夏猪前体脂肪细胞中,miR-26a-5p 与 *ACSL3* 表达水平呈负相关,研究进一步证实了 miR-26a-5p 靶向负调控 *ACSL3*,抑制前体脂肪细胞的成脂分化^[43]。乙酰辅酶 A 羧化酶 α (acetyl-CoA carboxylases alpha, *ACACA*) 是脂肪酸生物合成的关键限速酶,在脂肪细胞合成及脂质代谢过程中起重要作用^[44]。研究显示,*ACACA* 表达与大理石花纹评分和脂肪沉积呈正相关,在猪原代脂肪细胞中,过表达 miR-451 会显著降低 *ACACA* 表达水平,抑制脂质沉积^[45]。另外,miR-146a-5p 可能是一个新型的脂肪沉积调控因子,其通过 TGF- β 和 AKT/mTORC1 信号通路参与前体脂肪细胞增殖、分化。一方面,miR-146a-5p 通过靶向 SMAD 家族成员 4 (SMAD family member 4, *SMAD4*) 可诱导 TGF- β 信号通路负调控前体脂肪细胞增殖;另一方面,miR-146a-5p 可靶向 TNF 受体关联因子 6 (TNF receptor associated factor 6, *TRAF6*) 介导 AKT/mTORC1 信号通路抑制成脂分化^[46]。以上研究表明,miRNA 与猪肌间脂肪沉积显著相关,但其具体作用机制仍有待后期进一步深入研究。

3.2 lncRNA 调控脂肪沉积

lncRNA 是动物脂肪组织的重要调控因子,广泛参与脂肪生成和脂质代谢过程。lncRNA 表达谱在表型不同的脂肪组织和脂肪细胞中存在差异。

Huang 等^[47] 通过高通量测序获得了莱芜猪和大白猪脂肪组织 lncRNA 表达谱,鉴定出 55 个差异表达 lncRNA,其中 XLOC-046142、XLOC-015408、XLOC-015408 在脂肪沉积中起重要调控作用。Wang 等^[48] 通过对高、低脂肪莱芜猪背最长肌进行高通量测序发现,二者之间共有 17 个差异表达 lncRNAs。Tan 等^[49] 在贵州从江猪不同分化阶段(第 0、4、8 天)的前体脂肪细胞中,分别鉴定到 479、192、126 个差异表达 lncRNA,并通过靶基因和组织表达谱分析确定了与脂肪沉积密切相关的 lncRNA (TCONS-00012086 和 TCONS-00007245)。Yang 等^[50] 对比了 7 个脂肪型本地猪种和瘦肉型约克夏猪的 lncRNA 差异表达谱发现,一个本地猪种脂肪组织中共存在 9 114 个差异表达 lncRNAs,其中 LTCONS-00073280 与肌间脂肪含量相关,LTCONS-00101781、LTCONS-00037879、LTCONS-00088260 和 LTCONS-00128343 可通过调节背膘厚度影响脂肪沉积。

八眉猪和约克夏猪背最长肌的前体脂肪细胞 RNA 测序鉴定中发现 lncIMF 4 与脂肪形成有关,体外试验研究表明,敲低 lncIMF 4 可提高增殖相关基因 *Cyclin B*、*Cyclin D*、*Cyclin E* 的 mRNA 和蛋白表达水平,且显著提高 *PPAR γ* 、*C/EBP α* 、*SREBP-1* 等成脂相关基因表达水平,促进前体脂肪细胞增殖和分化^[51]。孟珊等^[52] 发现,lncRNA-6617 在马身猪前体脂肪细胞的早期成脂分化过程中特异性高表达,且敲低 lncRNA-6617 可抑制前体脂肪细胞分化,表现为 *C/EBP α* 、*PPAR γ* 、*aP2* 等成脂关键基因表达下调。目前已有研究证实,lncRNA 可直接海绵化 miRNA,减少 miRNA 与 mRNA 的结合率,从而影响 miRNA 靶基因的表达水平。功能预测分析发现,lncIMF 2 与脂质代谢相关,在猪前体脂肪细胞中过表达 lncIMF 2 可显著促进 *Cyclin B*、*Cyclin D*、*Cyclin E*、*PPAR γ* 、*aP2* 表达,其分子机制是 lncIMF 2 通过与 miR-217 相互作用促进猪前体脂肪细胞的增殖和分化^[53]。Wang 等^[54] 发现 IMF lnc1 与脂肪沉积相关,其通过结合 miR-199a-5p 提高窖蛋白-1 (caveolin-1, *CAV-1*) 表达水平,进而通过 cAMP 通路促进猪前体脂肪细胞的分化。以上研究表明,lncRNA 不仅能通过调节特异基因的表达影响脂肪沉积,还可作为 miRNA 的海绵吸附 miRNA 参与调控前体脂肪细胞的增殖、分化。然而,目前有关 lncRNA 对猪肌间脂肪沉积的作用网络和具体机制报道较少,还需进一步研究。

3.3 circRNA 调控脂肪沉积

与 miRNA、lncRNA 相似,不同肌间脂肪含量肌肉组织中 circRNA 的表达存在差异。Li 等^[55]通过高通量测序探究了高、低脂肪莱芜猪中 circRNA 表达谱的差异,并鉴定出 105 个差异表达 circRNA。比较确山黑猪和大白猪背最长肌转录组测序数据发现,二者共存在 62 个差异表达 circRNA^[56]。李媛等^[57]从莱芜猪和大白猪脂肪组织的 circRNA 表达谱中共鉴定出 181 个差异表达 circRNA,其中 circ-0002807、circ-0009352 可能参与调控脂肪沉积。circRNA 已被证实参与调节脂质代谢和脂肪沉积,但其调控肌间脂肪沉积的作用机制尚不清晰,目前的研究主要集中在 circRNA 可直接与 miRNA 结合发挥调节脂肪生成的功能。有研究报道,大白猪和莱芜猪背最长肌组织高通量测序共鉴定出 283 个差异表达 circRNA,通过 circRNA-miRNA 共表达网络分析发现了 2 个关键 circRNA(circRNA-23437、circRNA-08840)均含有 miR-370 结合位点,且通过 circRNA-miRNA-mRNA 网络影响烯脂酰辅酶异构酶 1(enoyl-coenzyme isomerase1,EC11)表达,从而参与调控脂肪沉积^[58]。Li 等^[59]采用 RNA 测序对

高、低脂肪猪背最长肌进行分析发现,两组之间有 336 个差异表达 circRNA,通过构建 circRNA-miRNA 相互作用网络鉴定出与脂肪含量呈正相关的 circRNA、circPPARA。进一步研究表明,过表达 circPPARA 可显著提高 *C/EBPα*、*PPARγ*、脂滴包被蛋白(perilipin-1, PLIN1)等成脂相关基因的表达,生物学功能分析显示,circPPARA 通过海绵作用吸附 miR-429 发挥 ceRNA 功能,促进猪前体脂肪细胞分化和抑制其增殖。miR-149-5p 与脂肪生成相关,miR-149-5p 可靶向抑制与脂质代谢相关的 CREB 转录激活因子 1(CREB regulated transcription coactivator 1, CRTC1)和 CRTC2 表达,进而促进前体脂肪细胞增殖和抑制其分化,circSETBP1 可通过 miR-149-5p 解除其对 CRTC1 和 CRTC2 的抑制作用,促进猪前体脂肪细胞分化,抑制细胞增殖^[60]。

综上所述,ncRNA 主要通过调控相关靶基因和信号通路影响脂肪沉积,其作为肌间脂肪沉积的重要调控元件,与猪前体脂肪细胞的增殖、分化紧密相关。表 1 总结了近年来研究报道的参与猪脂肪沉积的相关 ncRNA。

表 1 参与猪脂肪沉积的 ncRNAs
Table 1 ncRNAs involved in fat deposition in pigs

非编码 RNAs ncRNAs	靶基因 Target genes	生物学功能 Biological function	参考文献 References
miR-125a-5p	/	促进前体脂肪细胞增殖	Du 等 ^[36]
miR-206	<i>KLF13</i>	抑制前体脂肪细胞分化	Xu 等 ^[37]
	<i>STARD7</i>	抑制前体脂肪细胞增殖	
miR-32-5p	<i>KLF4</i>	抑制前体脂肪细胞分化	Liu 等 ^[38]
	<i>KLF3</i>	促进前体脂肪细胞分化	
miR-130a	<i>PPARγ</i>	抑制前体脂肪细胞分化	Wei 等 ^[40]
miR-34a	<i>PDGFRα</i>	抑制前体脂肪细胞分化	Sun 等 ^[30]
miR-34a	<i>ACSL4</i>	抑制前体脂肪细胞分化	Wang 等 ^[41]
miR-26a-5p	<i>ACSL3</i>	抑制前体脂肪细胞分化	Ding 等 ^[43]
miR-451	<i>ACACA</i>	抑制脂质沉积	Gan 等 ^[45]
miR-146a-5p	<i>SMAD4</i>	抑制前体脂肪细胞增殖	Zhang 等 ^[46]
miR-146a-5p	<i>TRAF6</i>	抑制前体脂肪细胞分化	Zhang 等 ^[46]
lncIMF 4	/	抑制前体脂肪细胞增殖、分化	Sun 等 ^[51]
lncRNA-6617	/	促进前体脂肪细胞分化	孟珊等 ^[52]
lncIMF 2	miR-217	促进前体脂肪细胞增殖、分化	Yi 等 ^[53]
IMF1nc1	miR-199a-5p	促进前体脂肪细胞分化	Wang 等 ^[54]
circPPARA	miR-429	促进前体脂肪细胞分化,抑制前体脂肪细胞增殖	Li 等 ^[59]
circSETBP1	miR-149-5p	促进前体脂肪细胞分化,抑制前体脂肪细胞增殖	Liu 等 ^[60]

/,文献未提及
/,Not mentioned in the literature

4 小 结

以往国内外对猪的选育侧重于提高瘦肉率和生长速度,而忽视猪肉肌间脂肪含量变化,导致肉的口感和品质下降,因而在降低猪皮下脂肪含量的同时,提高肌间脂肪沉积量成为今后的重要研究方向。猪肉品质受水分、氨基酸、脂肪含量等多种因素的影响,其中肌间脂肪含量是影响肉品质的关键因子,适当提高肌间脂肪沉积量对生产优质猪肉有重要作用。已有研究证实,ncRNA 在脂肪沉积过程中发挥调节作用,但目前 ncRNA 在猪肌间脂肪沉积中的研究仍处于起步阶段,尽管利用高通量测序技术和生物信息学筛选鉴定出大量与调控猪肌间脂肪沉积的 ncRNA,但相关研究主要集中在 miRNA 方面,而对于 lncRNA 和 circRNA 的研究报道有限。当前的研究多集中在发现和鉴定猪肌间脂肪沉积相关组织中的 ncRNA,而对 ncRNA 靶基因及信号通路的挖掘与验证研究较少,致使 ncRNA 调控肌间脂肪沉积的分子机制仍不完全清晰。通过完善 miRNA、lncRNA 和 circRNA 在肌间脂肪沉积过程中的作用网络和调控机制,将为改善肉品质研究提供新思路。

参考文献 (References):

[1] SCHUMACHER M, DELCURTO-WYFFELS H, THOMSON J, et al. Fat deposition and fat effects on meat quality—A review[J]. *Animals (Basel)*, 2022, 12(12):1550.

[2] 杨茜梓,胡睿智,贺建华,等. 影响猪肌间脂肪沉积的主要因素及潜在调控机理[J]. *动物营养学报*, 2021, 33(3):1266-1276.

YANG X Z, HU R Z, HE J H, et al. Main factors affecting porcine intermuscular fat deposition and potential regulation mechanism[J]. *Chinese Journal of Animal Nutrition*, 2021, 33 (3): 1266-1276. (in Chinese)

[3] MILLER R. Drivers of consumer liking for beef, pork, and lamb; A review[J]. *Foods*, 2020, 9(4):428.

[4] LIU S, HUANG J, WANG X, et al. Transcription factors regulate adipocyte differentiation in beef cattle[J]. *Animal Genetics*, 2020, 51(3):351-357.

[5] MUÑOZ M, GARCÍA-CASCO J M, CARABALLO C, et al. Identification of candidate genes and regulatory factors underlying intramuscular fat content through longissimus dorsi transcriptome analyses in heavy Iberian pigs[J]. *Frontiers in Genetics*, 2018, 9:608.

[6] LI Q, HUANG Z, ZHAO W, et al. Transcriptome analysis reveals long intergenic non-coding RNAs

contributed to intramuscular fat content differences between Yorkshire and Wei pigs[J]. *International Journal of Molecular Sciences*, 2020, 21(5):1732.

[7] PALAZZO A F, LEE E S. Non-coding RNA: What is functional and what is junk? [J]. *Frontiers in Genetics*, 2015, 6:2.

[8] KATARIA P, SURELA N, CHAUDHARY A, et al. miRNA: Biological regulator in host-arasite interaction during malaria infection[J]. *International Journal of Environmental Research and Public Health*, 2022, 19(4):2395.

[9] O'BRIEN J, HAYDER H, ZAYED Y, et al. Overview of microRNA biogenesis, mechanisms of actions, and circulation[J]. *Frontiers in Endocrinology*, 2018, 9:402.

[10] XIAO M, LI J, LI W, et al. microRNAs activate gene transcription epigenetically as an enhancer trigger[J]. *RNA Biology*, 2017, 14(10):1326-1334.

[11] CORREIA DE SOUSA M, GJORGJIEVA M, DOLICKA D, et al. Deciphering miRNAs' action through miRNA editing[J]. *International Journal of Molecular Sciences*, 2019, 20(24):6249.

[12] GJORGJIEVA M, SOBOLEWSKI C, DOLICKA D, et al. miRNAs and NAFLD: From pathophysiology to therapy[J]. *Gut*, 2019, 68(11):2065-2079.

[13] MA T, JIA H, JI P, et al. Identification of the candidate lncRNA biomarkers for acute kidney injury: A systematic review and meta-analysis [J]. *Expert Review of Molecular Diagnostics*, 2021, 21(1):77-89.

[14] DENIZ E, ERMAN B. Long noncoding RNA (lincRNA), a new paradigm in gene expression control[J]. *Functional & Integrative Genomics*, 2017, 17(2-3):135-143.

[15] ZUCKERMAN B, RON M, MIKL M, et al. Gene architecture and sequence composition underpin selective dependency of nuclear export of long RNAs on NXF1 and the TREX complex[J]. *Molecular Cell*, 2020, 79(2):251-267.

[16] DUTTA A, LI H, ABOUNADER R. Cryptic lncRNA-encoded ORFs: A hidden source of regulatory proteins[J]. *The Journal of Clinical Investigation*, 2023, 133(5):e167271.

[17] STATELLO L, GUO C J, CHEN L L, et al. Gene regulation by long non-coding RNAs and its biological functions[J]. *Nature Reviews Molecular Cell Biology*, 2021, 22(2):96-118.

[18] WANG L X, WAN C, DONG Z B, et al. Integrative

- analysis of long noncoding RNA (lncRNA), microRNA (miRNA) and mRNA expression and construction of a competing endogenous RNA (ceRNA) network in metastatic melanoma[J]. *Medical Science Monitor*, 2019, 25: 2896-2907.
- [19] GAO Y, WANG S, MA Y, et al. Circular RNA regulation of fat deposition and muscle development in cattle[J]. *Veterinary Medicine and Science*, 2022, 8(5): 1-10.
- [20] HUANG A, ZHENG H, WU Z, et al. Circular RNA-protein interactions: Functions, mechanisms, and identification[J]. *Theranostics*, 2020, 10 (8): 3503-3517.
- [21] THOMAS L F, SAETROM P. Circular RNA are depleted of polymorphisms at microRNA binding sites[J]. *Bioinformatics*, 2014, 30(16): 2243-2246.
- [22] PAULA M, ALLISON J, HANG H, et al. Transcriptional regulation of adipogenesis[J]. *Comprehensive Physiology*, 2017, 7(2): 635-674.
- [23] UEZUMI A, FUKADA S, YAMAMOTO N, et al. Mesenchymal progenitors distinct from satellite cells contribute to ectopic fat cell formation in skeletal muscle[J]. *Nature Cell Biology*, 2010, 12: 143-152.
- [24] UEZUMI A, FUKADA S, YAMAMOTO N, et al. Identification and characterization of PDGFR α ⁺ mesenchymal progenitors in human skeletal muscle[J]. *Cell Death and Disease*, 2014, 5: e1186.
- [25] LI X, FU X, YANG G, et al. Review: Enhancing intramuscular fat development *via* targeting fibro-adipogenic progenitor cells in meat animals[J]. *Animal*, 2020, 14(2): 312-321.
- [26] GONZALEZ D, CONTRERAS O, REBOLLEDO D L, et al. ALS skeletal muscle shows enhanced TGF- β signaling, fibrosis and induction of fibro/adipogenic progenitor markers[J]. *PLoS One*, 2017, 12 (5): e0177649.
- [27] JURGEN S, VALLECILLO G P, VOM H, et al. Odd skipped-related 1 (Osr1) identifies muscle-interstitial fibro-adipogenic progenitors (FAPs) activated by acute injury[J]. *Stem Cell Research*, 2018, 32: 8-16.
- [28] JOE A W, YI L, NATARAJAN A, et al. Muscle injury activates resident fibro/adipogenic progenitors that facilitate myogenesis[J]. *Nature Cell Biology*, 2010, 12: 153-163.
- [29] KOPINKE D, ROBERSON E C, REITER J F, et al. Ciliary Hedgehog signaling restricts injury-induced adipogenesis[J]. *Cell*, 2017, 170(2): 340-351.
- [30] SUN Y M, QIN J, LIU S G, et al. PDGFR α regulated by miR-34a and FoxO1 promotes adipogenesis in porcine intramuscular preadipocytes through ERK signaling pathway[J]. *International Journal of Molecular Sciences*, 2017, 18(11): 2424.
- [31] LI X, FU X, YANG G, et al. Review: Enhancing intramuscular fat development *via* targeting fibro-adipogenic progenitor cells in meat animals[J]. *Animal*, 2020, 14(2): 312-321.
- [32] 刘慧莹. 猪肌内脂肪沉积相关 miRNA 的鉴定及其功能研究[D]. 武汉: 华中农业大学, 2014.
- LIU H Y. Identification and function study of miRNA associated with porcine intramuscular fat deposition[D]. Wuhan: Huazhong Agricultural University, 2014. (in Chinese)
- [33] MIAO Z, SHAN W, WANG Y, et al. Comparison of microRNAs in the intramuscular adipose tissue from Jinhua and Landrace pigs[J]. *Journal of Cellular Biochemistry*, 2019, 120(1): 192-200.
- [34] SUN Y, WANG S, LIU H, et al. Profiling and characterization of miRNAs associated with intramuscular fat content in Yorkshire pigs[J]. *Animal Biotechnology*, 2020, 31(3): 1-8.
- [35] PROSDOCIMO D A, SABEH M K, JAIN M K. Kruppel-like factors in muscle health and disease[J]. *Trends in Cardiovascular Medicine*, 2015, 25 (4): 278-287.
- [36] DU J, XU Y, ZHANG P, et al. microRNA-125a-5p affects adipocytes proliferation, differentiation and fatty acid composition of porcine intramuscular fat[J]. *International Journal of Molecular Sciences*, 2018, 19(2): 1-3.
- [37] XU K, JI M, HUANG X, et al. Differential regulatory roles of microRNAs in porcine intramuscular and subcutaneous adipocytes[J]. *Journal of Agricultural and Food Chemistry*, 2020, 68(13): 3954-3962.
- [38] LIU H C, WEI W, LIN W M, et al. miR-32-5p regulates lipid accumulation in intramuscular fat of Erhualian pigs by suppressing KLF3[J]. *Lipids*, 2021, 56(3): 279-287.
- [39] ZHANG X, YOUNG H A. PPAR and immune system—What do we know? [J]. *International Immunopharmacology*, 2002, 2(8): 1029-1044.
- [40] WEI W, SUN W, HAN H, et al. miR-130a regulates differential lipid accumulation between intramuscular and subcutaneous adipose tissues of pigs *via* suppressing PPAR γ expression[J]. *Gene*, 2017, 636: 23-29.
- [41] WANG W, LI X, DING N, et al. miR-34a regulates adipogenesis in porcine intramuscular adipocytes by

targeting ACSL4[J]. *BMC Genetics*, 2020, 21 (1): 1-11.

[42] MASHEK D G, BORNFELDT K E, COLEMAN R A, et al. Revised nomenclature for the mammalian long-chain acyl-CoA synthetase gene family[J]. *Journal of Lipid Research*, 2004, 45(10):1958-1961.

[43] DING N, WANG W, TENG J, et al. miR-26a-5p regulates adipocyte differentiation via directly targeting ACSL3 in adipocytes[J]. *Adipocyte*, 2023, 12(1):1-10.

[44] SHI X, LIU S, METGES C C, et al. C/EBP-beta drives expression of the nutritionally regulated promoter 1A of the acetyl-CoA carboxylase- α gene in cattle[J]. *Biochimica et Biophysica Acta- Gene Regulatory Mechanisms*, 2010, 1799(8):561-567.

[45] GAN M, SHEN L, FAN Y, et al. ssc-miR-451 regulates porcine primary adipocyte differentiation by targeting ACACA[J]. *Animals*, 2020, 10(10):1891.

[46] ZHANG Q, CAI R, TANG G, et al. miR-146a-5p targeting SMAD4 and TRAF6 inhibits adipogenesis through TGF- β and AKT/mTORC1 signal pathways in porcine intramuscular preadipocytes[J]. *Journal of Animal Science and Biotechnology*, 2021, 12(1):1-16.

[47] HUANG W, ZHANG X, LI A, et al. Genome-wide analysis of mRNAs and lncRNAs of intramuscular fat related to lipid metabolism in two pig breeds[J]. *Cellular Physiology & Biochemistry*, 2018, 50(6):2406-2422.

[48] WANG L, XIE Y, CHEN W, et al. Identification and functional prediction of long noncoding RNAs related to intramuscular fat content in Laiwu pigs[J]. *Animal Bioscience*, 2022, 35(1):115-125.

[49] TAN L, CHEN Z, TENG M, et al. Genome-wide analysis of mRNAs, lncRNAs, and circRNAs during intramuscular adipogenesis in Chinese Guizhou Congjiang pigs[J]. *PLoS One*, 2022, 17(1):e0261293.

[50] YANG X M, LIANG Y, ZHONG Z J, et al. Comparison of long non-coding RNAs in adipose and muscle tissues between seven indigenous Chinese and the Yorkshire pig breeds[J]. *Animal Genetics*, 2021, 52(5):645-655.

[51] SUN Y, CAI R, WANG Y, et al. A newly identified lncRNA lncIMF 4 controls adipogenesis of porcine intramuscular preadipocyte through attenuating autophagy to inhibit lipolysis[J]. *Animals (Basel)*, 2020, 10(6):926.

[52] 孟 珊, 杨 阳, 李睿霄, 等. lncRNA-6617 调控猪肌肉前体脂肪细胞分化的筛选与功能研究[J]. *畜牧兽医学报*, 2022, 53(6):1712-1722.

MENG S, YANG Y, LI R X, et al. Screening and functional study of lncRNA-6617 regulating porcine intramuscular preadipocytes differentiation[J]. *Chinese Journal of Animal and Veterinary Sciences*, 2022, 53(6):1712-1722. (in Chinese)

[53] YI X, HE Z, TIAN T, et al. lncIMF 2 promotes adipogenesis in porcine intramuscular preadipocyte through sponging miR-217[J]. *Animal Biotechnology*, 2023, 34(2):268-279.

[54] WANG J, CHEN M Y, CHEN J F, et al. lncRNA IMF1nc1 promotes porcine intramuscular adipocyte adipogenesis by sponging miR-199a-5p to up-regulate CAV-1[J]. *BMC Molecular and Cell Biology*, 2020, 21(1):1-16.

[55] LI J, ZHAO X, WANG Y, et al. Comprehensive analysis of differentially expressed mRNAs, lncRNAs and circRNAs related to intramuscular fat deposition in Laiwu pigs[J]. *Genes*, 2022, 13(8):1349.

[56] QI K, LIU Y, LI C, et al. Construction of circRNA-related ceRNA networks in longissimus dorsi muscle of Queshan Black and Large White pigs[J]. *Molecular Genetics & Genomics*, 2022, 297(1):101-112.

[57] 李 媛, 张秀秀, 黄万龙, 等. 大白猪和莱芜猪肌肉脂肪组织 circRNAs 的鉴定与分析[J]. *畜牧兽医学报*, 2018, 49(7):1343-1353.

LI A, ZHANG X X, HUANG W L, et al. Identification and analysis of circRNAs in intramuscular adipose tissues between Large White and Laiwu pigs[J]. *Chinese Journal of Animal and Veterinary Sciences*, 2018, 49 (7): 1343-1353. (in Chinese)

[58] YOUSUF S, LI A, FENG H, et al. Genome-wide expression profiling and networking reveals an imperative role of IMF-associated novel circRNAs as ceRNA in pigs[J]. *Cells*, 2022, 11(17):2638.

[59] LI B, HE Y, WU W, et al. Circular RNA profiling identifies novel circPPARA that promotes intramuscular fat deposition in pigs[J]. *Journal of Agricultural and Food Chemistry*, 2022, 70 (13): 4123-4137.

[60] LIU Y, DOU Y, QI K, et al. circSETBP1 acts as a miR-149-5p sponge to promote intramuscular fat deposition by regulating CRTCs[J]. *Journal of Agricultural and Food Chemistry*, 2022, 70 (40): 12841-12851.

doi :10.3969/j.issn.2095-3887.2019.03.013

综述 与 专论

茶及其副产品在畜禽养殖中的应用

孙小红, 谢月琴, 罗君谊, 陈婷, 习欠云, 张永亮, 孙加节

(华南农业大学动物科学学院, 广东省动物营养调控重点实验室, 广州 510642)

摘要 我国茶资源丰富, 且其富含多种独特的营养成分, 可以调节畜禽机体的生理功能, 在畜禽养殖应用中无残留、无毒副作用, 能从根本上满足人们对畜禽产品品质安全的需求, 从而改善和提高人们的生活水平。为此, 文章就茶及其副产物的生物学特征和营养水平进行介绍, 并综述其作为饲料资源对畜禽自身的生长发育、畜产品品质的影响, 以及在畜禽养殖上的保健作用, 旨在为茶及其副产物作为新型饲料资源的开发应用提供参考。

关键词 茶; 茶副产品; 营养成分; 新型畜禽饲料资源

中图分类号: S816

文献标志码: A

文章编号: 2095-3887(2019)03-0051-05

The Application of Tea and its by-products in Livestock and Poultry Breeding

Sun Xiaohong, Xie Yueqin, Luo Junyi, Chen Ting, Xi Qianyun, Zhang Yongliang, Sun Jiajie

(College of Animal Science, South China Agricultural University,

Guangdong Provincial Key Laboratory of Animal Nutrition Control, Guangzhou 510642, China)

Abstract : There are rich tea resources in China. The nutritional ingredients of tea are rich and particular. The ingredients can regulate physiological functions of livestock and poultry. Because of no residue, no toxic and side effect, tea can be used as fodder to meet the people's requirement for the product quality safe of livestock and poultry. So, in this paper, the biological characteristics and nutritional value of tea and its by-products were introduced. From the point of fodder, effects of tea and its by-products on animal growth and product quality as well as health care function were reviewed in livestock and poultry breeding so as to use tea and its by-products as the new fodder resource.

Keywords tea; by-product of tea; nutritional ingredient; new fodder resource

茶叶是一种价格低廉, 来源广泛, 营养丰富且全面的天然植物, 我国茶叶的产量居世界首位, 其副产品资源丰富。根据刘丽芳^[1]报道, 2016 年中国茶园种植面积 293.3 万 hm^2 , 茶叶产量约 250 万 t。目前, 茶叶的用途除了作为普通饮品外, 还广泛应用于各项食品加工业。茶叶及相关的茶产品的生产、销售也在逐年增加, 但如何处理茶叶加工过程中产生的大量废茶和茶渣, 给生产茶叶的企业带来了新的难题。据不完全统计^[2], 在生产茶叶时, 每生产 1 t 红茶可产生 30~50 kg 的副产品, 每吨绿茶可产生 30 kg 的副产品。把这些废茶和茶渣用作肥料和燃料是其中一种出路, 若用在畜牧业中则更具

价值。因此, 利用茶叶副产品生产更为廉价的饲料原料, 是极其具有现实意义的研究课题。

1 茶副产品的营养成分及生物学特性

茶叶作为我国人民日常生活的饮品原料, 其有效活性物质的利用率不高。有研究对茶副产品中含有的粗蛋白质、粗纤维、氨基酸、维生素、茶多酚和咖啡碱等营养成分进行了研究^[3-4], 发现茶叶及其副产品中含有丰富的营养成分, 此结果可为茶叶及其副产品的开发利用提供理论依据。

由于茶叶中含有较多的茶多酚、茶碱等独特的活性成分, 所以饮茶不仅有广泛抗炎症、抗衰老、抗突变、抗生物氧化、降低血脂和胆固醇以及清除体内自由基的作用^[5]; 用茶副产品作为饲料原料饲喂动物, 能使动物的中枢神经兴奋, 增强机体血液循环, 具有强心利尿等作用。茶叶及其副产品中含有的独特生物学活性成

收稿日期: 2019-02-27

基金项目: 国家重点研发计划(2018YFD0501706)

作者简介: 孙小红(1994-), 女, 硕士, 主要从事饲料生物合成关键技术研究。

通信作者: 孙加节, 副教授, 博士, 主要从事饲料生物技术研究。

分及在动物体内的整体生理调节功能与绿色环保特征,完全符合当今消费者对畜产品质量的要求,使茶叶及其副产品作为畜禽的饲料原料或添加剂具有很大的潜在发展市场^[6]。

2 茶及其副产品在动物饲料中的应用

2.1 茶及其副产品在猪饲料中的应用

随着人们生活水平的提高和健康、环保意识的增强,人们对畜禽产品品质的要求也逐渐提高,对畜禽养殖过程中使用抗生素时产生的耐药性和残留等毒副作用也越来越重视。在备受关注的状态下,研究者对茶叶可治疗和预防畜禽疾病的保健功能进行了研究,发现用茶饲料饲喂畜禽可治疗畜禽的某些疾病和增强机体抗病能力,因此,茶饲料有望被开发成无残留、无毒副作用的药剂,满足人们对畜产品品质的要求。早在 1997 年,日本研究人员开展了以茶养猪试验,将茶叶用作饲料添加剂添加在白猪的饲料中,进行饲喂直至屠宰,然后分析猪肉品质,结果表明,试验组的猪肉中所含的次黄嘌呤核苷酸比一般猪肉多,而次黄嘌呤核苷酸是决定口感的重要因素^[7],同时猪肉中维生素 E 的含量是一般猪肉的 3 倍,因此猪肉中的腥味大幅度下降。也有研究采用茶多酚饲喂生长育肥猪,结果显示,茶多酚具有提高育肥猪平均日增重和胴体长度的效果,且推荐添加量为 0.1%~0.3% 时综合效果最为适宜^[8-9]。茶叶及其副产物的利用不仅在育肥猪上有报道,在仔猪上也有相关研究。在仔猪的日粮中添加 1% 茶多酚可显著改善氧化应激,提高仔猪的生长性能和免疫功能^[10]。日粮中添加一定量的茶多酚可有效地改善畜禽的肌肉品质,提高肌肉中水分的含量,使猪肉品质变得鲜嫩^[11]。茶及其副产物添加在畜禽日粮中还有降低血脂和胆固醇的作用。Suzuki 等^[12]通过在去势猪的基础日粮中添加绿茶末研究了茶叶对猪肉胆固醇的影响,发现猪肉中胆固醇的含量明显降低,这一试验结果与日本一试验场^[13]的试验结果相似。另外,添加 1%~2% 茶粉饲料对猪可起到明显的降血脂作用^[14]。研究发现^[15-16],用茶多酚复合添加剂饲喂育肥猪,对育肥猪的平均日增重和净增重有显著的提高作用。用茶及其副产品饲喂猪,还具有抗氧化作用。王玉龙等^[17]研究表明,在肉猪的饲料中添加 500 g/t 的茶叶提取物能够明显改善肌肉中抗氧化指标。总结以上的研究报道得出,将适量茶及其副产物添加到猪的基础饲料中,不仅在一定程度上改善猪肉的风味和肉品质,还能提高育肥猪的生长性能和抗氧化功能。

2.2 茶及其副产品在禽类饲料中的应用

日本永田农业研究报告表明,用 0.1%~10.0% 的茶粉饲喂鸡 20~30 d,可提高鸡的产蛋率,且产下的蛋无腥味,耐收藏,蛋重增加,蛋白澄清透明,蛋黄嫩黄明亮,鸡的平均体重也有所增加。Biswas 等^[18]以 18 日龄的肉鸡为试验动物,发现饲喂绿茶粉后可以提高鸡的饲喂效率。在试验组鸡的饲料中添加茶渣,6 周后鸡的平均重量虽然低于对照组鸡,但死亡率却低于对照组鸡(死亡率 21.4%)^[19]。茶副产品中富含维生素 A 和胡萝卜素,用 1% 左右的茶渣粉饲料饲喂鸡,可使蛋壳颜色加深,皮肤颜色呈橘红色^[20]。佐野满昭等^[21]用秋末无商品价值的茶渣作为鸡日粮,结果发现饲喂茶渣饲料对鸡肉品质有显著的影响,维生素含量明显增加,其中维生素 A 和维生素 E 的含量较饲喂基础日粮的鸡分别增加 1.3~1.5 倍和 2.2~2.4 倍。刘德义等^[22]用含量为 0.25% 的茶多酚添加在鸡日粮中,结果显示添加茶多酚对鸡法氏囊的发育有一定程度的影响,进而增强鸡的体液免疫功能。王晓方等^[23]将 1 000 mg/kg 茶多酚添加在鸡的基础日粮中,发现茶多酚可降低鸡的平均日采食量。另外,Murugesan 等^[24]研究发现,废黑茶在加工发酵过程中会产生废茶真菌生物,将这种发酵产物添加在雏仔鸡的日粮中,有提高肉鸡的生产性能和胴体品质的功能。由以上研究可以看出,在鸡的日粮中添加茶副产品对鸡的生长性能、免疫功能等具有一定的促进作用,对于蛋鸡能改善其鸡蛋品质,提高产蛋量,对肉鸡的肉品质也有明显的提高作用,且还可降低鸡的死亡率,提高雏鸡的生产性能和胴体品质,增强鸡的体液免疫功能,帮助机体维持在健康稳定的状态。

2.3 茶及其副产品在奶牛饲料中的应用

目前,茶及茶副产品饲喂反刍动物的研究报告尚不多见。然而,刘红云等^[25]研究表明,茶及茶副产品中赖氨酸、蛋氨酸、组氨酸和亮氨酸等反刍动物所必需的氨基酸含量丰富,分别为赖氨酸 1.75%、蛋氨酸 0.54%、组氨酸 0.83% 和苯丙氨酸 1.26%。斯里兰卡佩拉德尼亚大学科研人员发现,茶饮料茶渣(速溶茶渣)中尚含有很高的营养成分,且氨基酸的组成与鱼粉蛋白质相似,可以直接将速溶茶渣用作奶牛和水牛犊的优质饲料^[26]。早在 20 世纪 80 年代,国内对茶副产品用作牛饲料进行了研究。李英爱等^[27]研究发现,当茶渣在日粮中占干物质的 7%~9% 且干物质中粗蛋白的含量为 34.77% 时,对茶蛋白质在瘤胃中具有双重保护作用,可增加反刍动物的采食量,提高动物生产性能,因此认为茶渣是饲

喂泌乳牛和生长犊牛较好的饲料。赖建辉等^[28]和陈祥麟^[29]研究发现,用茶叶渣和茶粉饲喂奶牛,发现茶叶渣和茶粉中含有丰富且全面的营养成分,可提高奶牛的日平均产奶量,节约饲养成本,增加养殖户的收入。这一研究结果与张兴华等^[30]用一定浓度的茶饲料饲喂奶牛的研究结果相似。日本报道,从小牛 7 日龄开始每天饲喂绿茶提取物 35 g,饲喂一年至分娩前,发现实验组的奶牛肠胃中有益微生物菌群的数量增加,细菌数量没有明显的变化,产奶量提高,小牛期缩短。另外,饲喂茶粉的奶牛胃肠道中硫化物、氨等显著减少^[31]。由上述研究结果可知,适量茶及其副产品添加到奶牛饲料中能改善奶牛肠道微生物的菌群数量,提高奶牛乳产量和乳品质。

2.4 茶及其副产品在羊饲料中的应用

苑文珠^[32]的试验结果表明,用茶皂素饲喂羊,可提高羊的日增重和饲料转化率。2009 年 Zhong 等^[33]以公羊为研究对象,在公羊的日粮中添加适量的茶渣可以有效地抑制脂质氧化,减少鲜肉的滴水损失,提高山羊肉色的稳定性和冷藏肉的品质。同年,乔金玲等^[34]以公羊为研究对象,发现适当浓度的绿茶提取物可以作为保鲜剂用于肉制品的贮藏。潘发明等^[35]以绵羊为试验对象,发现在羊的饲料中添加茶渣,茶渣中的单宁可以降低饲料的体外瘤胃蛋白降解率,并且对饲料中的蛋白质具有很好的保护作用。Kondo 等^[36]在青贮饲料中添加绿茶渣饲喂山羊,山羊对干物质的摄入量没有显著差异,但粗蛋白质消化率显著增加并增加了氮摄入量,而不影响尿液和粪便中氮的排泄,从而提高了氮的保留率。Xu 等^[37]把绿茶粉发酵 120 d 后,在阉割羊全混合日粮中加入 10% 的发酵绿茶粉代替等量的谷物成分,结果显示,饲喂发酵绿茶粉可使阉割羊体内的尿氮和瘤胃氨氮含量明显减少。总结以上的研究报道,饲料中添加适量茶叶及其副产物可以提高山羊对粗蛋白质的利用率和生长性能,有效抑制脂质的氧化,并可改善胴体品质。

2.5 茶及其副产品在水产动物饲料中的应用

我国作为世界上第一水产养殖大国,水产养殖业年总产值达几千亿元,因此,对于优质鱼饲料的需求巨大。汪水平等^[38]用 1% 茶粉饲喂草鱼,发现饲喂茶粉可提高草鱼的增重率,且肠炎显著降低。徐奇友等^[39]报道,在日粮中添加茶多酚可改善虹鳟鱼的非特异性免疫和肌肉品质,且添加量为 50~100 mg/kg 时效果最佳。张云等^[40]提出,茶黄素可作为免疫增强剂应用在水产养殖中。黄亮^[41]的试验结果表明,茶叶能显著提高草鱼

鱼体干重率以及鱼体蛋白含量和干物质含量,鱼体脂肪含量有下降的趋势。朱全芬等^[42]的研究结果表明,将一种含茶皂素 70%、pH 值 6~7、含水率 5% 的茶皂素制剂按照 3 mL/L 水的浓度投入虾池中,95% 的鱼被杀死,且在 266.7 hm² 虾池实际应用时,虾的产量每 0.07 m² 增加 42 kg,增值 700 元。总结以上研究结果可知,水产动物饲料中添加适量茶及其副产物可以提高鱼类的生长性能以及增重率,降低肠炎的发生率,改善鱼类的非特异性免疫和肌肉品质,降低鱼的脂肪含量,提高鱼体干物质的含量,且茶及其副产物在虾养殖的应用中可以用于清池。

2.6 茶及其副产品在兔饲料中的应用

李海利等^[43]以产于福建的茶渣为原料,测得茶渣中含有 18% 的粗蛋白质和 28% 的粗纤维,以 10%~20% 的添加量添加到生长肉兔的饲料中,效果良好,是家兔良好的饲料资源。另外,在肉兔精料中添加一定比例的茶末,可使肉兔的增重率提高 12.7%,饲料利用率提高 8.5%,成活率提高 26.5%,且推荐添加量为 1.5% 时综合效果最佳^[44]。宫爱华等^[45]以家兔为试验动物,在家兔的饮水中分别添加 0.2% 和 0.4% 的茶多酚,结果显示家兔血清中总胆固醇含量明显降低,高密度脂蛋白升高。Miyamura 等^[46]研究发现,兔口服茶水,体内中低密度脂蛋白和主动脉内膜脂肪的沉积量有下降趋势,对高胆固醇症和动脉粥样硬化有抑制作用。邱燕祥^[47]在家兔的日粮和饮水中分别加入 0.4% 和 0.8% 的茶多酚,饲喂 8 周,结果显示,茶多酚能够有效降低家兔的血脂水平,具有一定的血脂代谢调节作用。总结以上研究结果可以看出,将茶及其副产物添加到兔饲料中可以提高兔的生长性能、饲料利用率以及成活率,降低机体的总胆固醇含量和血脂水平,并可以调节血脂代谢。

3 展望

我国茶资源丰富,在茶叶加工过程中产生大量的废茶和茶渣,截止到目前为止,已经有很多关于茶资源应用现状的报告,将茶副产品开发研制为畜禽饲料用于生产,可以充分发挥茶以及茶副产品的营养特性和药用作用,且无残留、无毒副作用,把茶叶作为绿色饲料添加剂添加到畜禽饲料中可提高茶业资源的利用率。茶叶在畜禽饲料应用中具有很大的潜在市场,它不仅能增加茶叶及其副产品的价值,还对畜禽业、饲料业的发展也具有积极作用。总之,将茶副产品研发成一种质优价廉、营养全面且丰富的新型饲料原料,将其变废为宝,具有重大的现实意义。

参考文献

- [1] 刘丽芳.国内外茶叶产业发展情况[J].农学学报,2018,8(3):87-92.
- [2] 吴慧敏,杨江帆,叶乃兴.茶渣、茶末对蛋鸡生产性能及鸡蛋品质的影响研究进展[J].亚热带农业研究,2015,11(3):212-215.
- [3] 李勤建.畜禽绿色饲料添加剂的研究与应用[J].河南畜牧兽医,2001(4):28-29.
- [4] 李勤建.畜禽绿色饲料添加剂的研究与应用[J].河南畜牧兽医(综合版),2001,22(4):28-29.
- [5] Park Y H, Han D W, Suh H. Protective effects of green tea polyphenol against reactive oxygen species-induced oxidative stress in cultured rat calvarial osteoblast [J]. Cell Biology & Toxicology, 2003, 19(5):325-337.
- [6] 张士康.全价利用跨界开发——中国茶产业优化突破有效路径探索[J].茶世界,2010(11):34-35,38-39.
- [7] 陈晓虹.以茶养猪可使猪肉味更佳[J].饲料研究,1999(5):42.
- [8] 姚波,屠幼英,王春花.茶多酚作为育肥猪天然肉质改良剂的应用研究[J].饲料工业,2015,36(20):12-14.
- [9] 王晓方,常文环,张姝,等.不同饲料添加剂对肉鸡生长性能、胴体品质、肌肉脂肪和肌苷酸含量的影响[J].中国家禽,2014,36(3):24-29.
- [10] 李永义,段绪东,赵娇,等.茶多酚对氧化应激仔猪生长性能和免疫功能的影响[J].中国畜牧杂志,2011,47(15):53-57.
- [11] 刘晓华,郝卫华,夏瑜,等.茶多酚对肉仔鸡生产性能、屠宰性能及肉品质的影响[J].现代畜牧兽医,2004(12):9-11.
- [12] Suzuki K, Kadowaki H, Hino M. The influence of green tea in pig feed on meat production and quality[J]. Japanese Journal of Swine Science, 2002, 39(2):59-65.
- [13] 许甲平,李吕木.茶多酚在饲料生产中的应用[J].兽药与饲料添加剂,2009,14(4):16-17.
- [14] 活泼,黄光荣,张晓晖,等.非水溶性茶叶蛋白降血脂作用的研究[J].茶叶科学,2005(2):95-99.
- [15] 徐坤,李明元,马娜.茶多酚对生长育肥猪生长性能和肉质的影响研究[J].粮食与饲料工业,2009(4):43-44.
- [16] 晁娅梅,陈代文,余冰,等.茶多酚对育肥猪生长性能、抗氧化能力、胴体品质和肉品质的影响[J].动物营养学报,2016,28(12):3996-4005.
- [17] 王玉龙,费兆生.茶叶提取物对肉猪生产性能、肌肉品质及肌肉抗氧化指标的影响[J].畜牧与兽医,2014,46(12):50-52.
- [18] Biswas M A H, Wakita M. Comparison of two dietary factors green tea powder feeding and feed restriction influencing laying performance and egg quality in hens [J]. Bulletin of the Faculty of Biore-sources- Mie University (Japan), 2001, 25:55-61.
- [19] 曲路.用绿茶副产品喂鸡效果明显[J].畜牧兽医科技信息,2002(1):26-26.
- [20] 王素霞.茶饲料开发前景广阔[J].江西饲料,2006(1):22-23.
- [21] 佐野满昭,孙希琪.茶添加到家畜饲料中的利用效果[J].农业新技术新方法译丛,1996(2):32-33.
- [22] 刘德义,郭子建,陈会良.茶多酚对固始鸡免疫器官发育的影响[J].中国饲料,2008(2):26-27.
- [23] 王晓方,常文环,张姝,等.不同饲料添加剂对肉鸡生长性能、胴体品质、肌肉脂肪和肌苷酸含量的影响[J].中国家禽,2014,36(3):24-29.
- [24] Murugesan G S, Sathishkumar M, Swaminathan K. Supplementation of waste tea fungal biomass as a dietary ingredient for broiler chicks [J]. Bioresource Technology, 2005, 96(16):1743-1748.
- [25] 刘红云,梁慧玲.茶渣用作饲料的研究[J].饲料研究,2004(9):19-20.
- [26] 侍丽君.茶叶在饲料添加剂中的应用[J].新疆畜牧业,2015(11):15-16,35.
- [27] 李英.茶渣——反刍家畜的优质蛋白饲料[J].饲料研究,1983(6):31.
- [28] 赖建辉,刘中秋,田超,等.乌龙茶用作奶牛饲料添加剂的初步效果[J].茶叶科学,1994(1):79.
- [29] 陈祥麟.茉莉花渣喂奶牛效果好[J].福建畜牧兽医,1994(1):19.
- [30] 张兴华,汤建卫,陈阿芳.茶多酚在奶牛生产中的应用效果[J].中兽医学杂志,2006(4):5-7.
- [31] 李荣林,周维仁,申爱华.茶叶及其提取物在畜牧和饲料中的应用[J].粮食与饲料工业,2002(7):30-31.
- [32] 苑文珠.茶皂素对湖羊生产性能及瘤胃发酵的影响[D].杭州:浙江大学,2002.
- [33] Zhong R Z, Tan C Y, Han X F. Effect of dietary tea catechins supplementation in goats on the quality of meat kept under refrigeration [J]. Small Ruminant Research, 2009, 87(1):122-125.
- [34] 乔金玲,胡永金,曹振辉,等.绿茶提取物对冷却羊肉保鲜作用的影响[J].食品科学,2009,30(12):289-292.
- [35] 潘发明,李发弟,郝正里,等.茶渣单宁含量对绵羊养分消化利用与氮代谢参数的影响[J].畜牧兽医学报,2012,43(1):71-81.
- [36] Kondo M, Kita K, Yokota H. Feeding value to goats of whole-crop oat ensiled with green tea waste [J]. Animal Feed Science & Technology, 2004, 113(1):71-81.
- [37] Chuncheng Xu, Yimin Cai, Naoko Moriya. Influence of replacing brewers' grains with green tea grounds on feed intake, digestibility and ruminal fermentation characteristics of wethers[J]. Animal Science Journal, 2010, 79(2):226-233.
- [38] 汪水平,王文娟.茶饲料及其应用[J].饲料博览,2002(12):38-40.
- [39] 徐奇友,李婵,许红,等.茶多酚对虹鳟生长性能、生化指标和非特异性免疫指标的影响[J].动物营养学报,2008(5):547-553.
- [40] 张云,温小波,宁丽军,等.茶黄素的生理作用及其在水产动物生产中的应用[J].广东饲料,2011,20(1):27-29.
- [41] 黄亮.6种茶叶对草鱼与斑点叉尾鮰鱼鱼体生化成分及几项免疫指标的影响[D].合肥:安徽农业大学,2015.
- [42] 朱全芬,夏春华,樊兴士,等.茶皂素的鱼毒活性及其应用的研究——茶皂素的溶血性与鱼毒作用[J].茶叶科学,1993(1):69-78.

牧业建设奠定了坚实的基础。

3.2 优化结构,规模经营

一是在充分利用新村搬迁产生的弃耕地、撂荒地的同时,以土地流转的方式大力发展饲草种植业,流转区域内产业结构明显优化,普遍呈现出土地产出效益提高、农民综合收入提高、产业综合生产能力增强的良好态势。二是加快省级现代农牧业示范园区建设,引进种养业产业化企业入驻园区,积极鼓励标准化规模养殖场、农民专业合作社、家庭农牧场加快推进畜牧业产业化发展转型升级,带动了全省畜牧业加速发展。三是以“公司+基地+农户”“公司+中介+农户”等畜牧业产业化经营模式,优化调整畜群结构,积极推广优良种畜。四是发展订单草业,打造饲草品牌。在动员养殖户种植饲草的基础上,积极协调养殖企业、饲草加工企业发展订单饲草业。饲草生产基本形成了“饲草加工企业带头、养殖基地或合作社带动、农户参与、上下联动、规模化经营”的格局,产、供、销一体化路子初步形成。五是初步建立了牧草良种扩繁基地,逐步建立了育、繁、推一体化的牧草良种繁育体系,提高了种子专业化生产水平和综合生产能力^[5]。

3.3 因地制宜,合理规划

一是按照产业化经营的要求,加强品种创新和应用技术创新,推进草产品品牌化、规模化、标准化、科技化发展,经充分论证、多次试验,选配了产量高、适应能力强、经济效益好的燕麦、黑麦作为高海拔旱地的主要种植品种。二是根据饲草产业发展实际确定规模化养殖基地,适度增加畜群数量,种养结合发展草食畜牧业。三是发挥合作社的连接带动作用。通过加大牲畜养殖户、饲草种植户、农机服务组织和牧草加工厂有机捆绑形式,形成了产业化体系,使机具拥有者与种植户互惠互利,切实带动了闲置农机租赁业的发展,促进了农机装备结构的优化,有效提高了全县饲草的市场竞

争力。

3.4 完善服务,不断创新

一是发挥基层草原站技术支撑作用,建立了饲草料产业发展技术推广服务体系,利用农技推广示范县项目进行科技指导及服务。大力开展农牧民种植技术、机械化收储、牧草良种推广、饲草微贮、青贮等技术培训,增加了科技含量、提高了产出效益。二是不断创新服务形式,鼓励和支持科技人员参与饲草料生产加工和科技示范点建设,开展科技服务、技术开发和技术咨询,面向农牧民提供产前、产中、产后技术服务。三是以农信通等平台为依托,积极向养殖户、养殖场、饲草加工企业、饲草种植大户发布县内外、省内外饲草价格、需求等信息。

4 结束语

通过对湟源县主要农作物种植产业进行的定向调研,对主要农作物产业之间的经济成本进行了对比核算,在全面了解和掌握该县各种种植产业的投入产出情况的同时,也总结了饲草产业发展不足之处和值得肯定的做法。调研成果为青海省牧业草畜联动试点、粮改饲发展草食畜牧业试点、饲草产业长足发展决策提供真实有效的数据资料。

参考文献

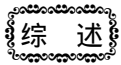
- [1] 邓艳芳,杜文华,乔安海,等.青海省草地资源开发战略布局探讨[J].安徽农业科学,2016(13):127-128.
- [2] 范月君,侯向阳,杨予海,等.旱区旱作人工草地高效用水及生态环境效应[J].青海畜牧兽医杂志,2018(3):32-35.
- [3] 康维海.青海公布第二次土地调查数据青海省耕地面积 882 万亩[J].青海国土经略,2014(1):49.
- [4] 星景花.青海省生态旅游开发条件分析及对策研究[J].经济师,2009(5):199-200.
- [5] 邓艳芳,乔安海,杜文华.青海省牧草良种繁育体系现状及建设方向[J].中国畜牧兽医文摘,2016(8):225-226.

(上接第 54 页)

- [43] 李海利,谷子林,刘亚娟,等.茶渣饲料资源开发研究进展[J].中国养兔,2013(4):11-13,34.
- [44] 王素霞.茶饲料的开发和利用[J].饲料世界,2006(3):20-21.
- [45] 宫爱华,荣文平,赵秀兰,等.茶多酚对家兔血脂的影响[J].实用医药杂志,2003(8):596-597.
- [46] Miyamura, Mitsuhiko Moriyama, Hironori Murata, et al. Inhibitory

effects of “Goishi-tea” as a post-fermented-tea on dietary-induced hypercholesterolemia and atherosclerosis in rabbits [J]. Cheminform, 2008, 39(46):1037-1044.

- [47] 邱燕祥.茶多酚对家兔血脂影响的观察研究[J].中国医药导报,2013,10(11):14-15,18.



夏季热应激对肉牛养殖的影响及防控措施

林婉, 孙小红, 罗君谊, 陈婷, 习欠云, 张永亮, 孙加节*

(华南农业大学动物科学学院 广东省动物营养调控重点实验室 广东 广州 510642)

摘要:动物健康生产受许多因素的影响,近年来随着全球变暖,温热环境逐渐成为影响畜牧业发展的重要和关键因素之一。虽然肉牛生产受到热应激的影响没有奶牛显著,但这种影响也不容小觑。本文综述影响肉牛养殖的环境因素,并阐述温湿度指数在肉牛健康养殖中的评定方法,以及热应激对肉牛生产性能、生理机能、免疫指标、繁殖性能和肉品质方面的影响。最后,提出缓解热应激对肉牛生产影响的有效策略,这些策略包括物理预防、肉牛耐热性的品种选育以及营养调控等。

关键词:热应激;肉牛;健康养殖

中图分类号:S823;S815 **文献标识码:**A **文章编号:**1001-9111(2019)05-0058-04

热应激是指动物受到超过机体调节能力的过高温度刺激时发生的非特异性生理反应。一项结合温度和湿度的指数(temperature-humidity index, THI)一直被用来评估牛的热应激。该技术是为了评估湿热环境对牛生产的影响而开发的,在畜牧业中得到了广泛的应用。一般通过干湿球温度计的读数进行THI的计算: $THI = 0.72 \times (\text{干球读数} + \text{湿球读数}) + 40.6$ 。A. Berman^[1]等报道,牛舍的THI值小于74时,牛只处于舒适的环境状态,当牛舍的THI值为75~78时,牛只处于轻度热应激状态下,THI值为79~83为高度热应激,84以上为严重热应激。肉牛处于热应激的状态下会表现为食欲减退,体温升高,心跳呼吸加快,鼻镜干燥,烦躁不安,严重时引发热射病可在数小时内死亡;生理状态上会出现抗氧化能力降低,内分泌系统紊乱;在生产性能方面,处于热应激状态下的肉牛对饲料中的营养物质消化率降低,进而降低生产性能。预测热应激的发生并做出相应的防控措施,可以减轻热应激对动物健康和生产性能的影响。肉牛属于恒温动物,正常肉牛的体温在38.5~39.5℃,与其他恒温动物相似,肉牛对自身体温的调节是借助传导、对流、辐射进行散热,利用出汗、喘息、皮肤蒸发等进行去湿。因此肉牛的适宜饲养温度通常在10~25℃,最佳的生长温

度则在15~18℃。在我国南方地区,环境高温持续时间长达6个多月,温度高且多雨潮湿,极端气温甚至超过40℃,当环境温度达到或接近牛的体温时,环境中较高的相对湿度会减少牛体的热蒸发量,影响机体的降温能力,导致体温上升。同时,高湿环境下从呼吸道和机体表面的热蒸发量也很低,导致机体散热状况不佳,因此,南方地区夏季普遍存在的热应激已成为限制肉牛健康养殖的关键因素。

1 夏季热应激对肉牛的影响

1.1 热应激与肉牛的生产性能和生理机能

肉牛属于恒温动物,对自身体温的调节是借助体表将体内代谢产生的热量散失,以此来保持与周围环境的热平衡。当牛舍的环境温度接近或者高于肉牛自身的温度时,肉牛会出现直肠温度升高、呼吸频率加快等症状,所以热应激会对肉牛的生理功能造成损伤^[2],直肠温度和呼吸频率被用来评价恒温动物生理状况的重要指标,也是评价热感受性的指标,可以用来评估畜禽热应激的影响程度。Beatty等证明肉牛处于热应激状态下会出现体温升高、呼吸频率加快、食欲下降等症状^[3];Hendricks等研究表明当牛舍的环境温度从29℃上升到31℃时,育成牛的直肠温由37.8℃上升到38℃,呼吸频率由

收稿日期:2019-06-03 修回日期:2019-06-23

基金项目:国家重点研发计划项目“南方湿热条件下优质肉牛高效安全养殖技术应用与示范”(2018YFD0501706);广东省农业技术研发项目(2018LM2158);广东省现代农业产业技术体系项目(2017LM1121)

作者简介:林婉(1997—),女,海南琼海人,本科生,主要从事畜禽健康养殖研究。E-mail: 1546672987@qq.com

* 通讯作者:孙加节(1984—),男,江苏盐城人,博士,副教授,硕士生导师,主要从事动物营养组学研究。E-mail: jiajiesun@scau.edu.cn

20.5 次/min 升高到 21.8 次/min^[4];此外,张瑞光等研究表明热应激造成肉牛呼吸频率增加可使肉牛血液中 CO₂ 和 H⁺ 浓度下降,血液 pH 值上升,肉牛容易出现呼吸性碱中毒现象^[5]。

在热应激的状态下,肉牛的饮水量增加,采食量下降,引起肉牛日增重显著降低^[6]。Moore 等^[7]研究秦川牛发现,肉牛在持续热应激下(温度达到 39℃)可引起肉牛的精料采食量比温度在 25℃时平均下降 0.5 kg,干草采食量平均下降 1.1 kg。另有研究^[8-9]报道,轻度热应激下,动物采食量下降,消化率可能会稍有上升,持续热应激时,肉牛瘤胃微生物因温度偏高或 pH 值异常影响到微生物的活力,对养分的消化率显著下降。血液中的激素水平是反应牛在经受高热环境影响下的重要生理指标,也是一种潜在的指示剂^[10],肉牛在热应激状态下采食量下降,体内的激素水平受到应影响,发生变化,主要表现为肉牛血清生长激素水平降低,胰岛素样生长因子 II (IGF - II) 的水平急剧上升,皮质醇分泌增加,甲状腺激素分泌下降,个体的生长速度也随之放缓。Stowell 等^[11]结果表明,肉牛在热应激短暂的刺激下,血清中部分激素水平会增加,而在长期热应激条件下,部分激素水平会降到最低。受温热环境的影响,牛血浆中的甲状腺素(T₄)和三碘甲状腺原氨酸(T₃)水平也会显著下降^[12]。

1.2 热应激与肉牛的免疫指标

在炎热的夏季,机体的体液免疫和细胞免疫均会受到热应激的影响,动物机体抵抗疾病的能力下降,使机体对疾病的易感性增加^[13]。有报道^[14-15]证明,慢性应激使固有免疫和适应性免疫应答受到抑制或功能障碍,急性应激反应会导致可变的免疫抑制或免疫调节。在热应激环境下,机体中儿茶酚胺浓度升高,进而影响 IL α 和 IL - 1 β 对免疫系统产生负作用^[16]。另外,儿茶酚胺和糖皮质激素共同作用,可引起细胞因子 Th1 和 Th2 的变化,进一步使起细胞免疫收到抑制,导致 Th2 介导的体液免疫应答发生转移^[17]。

1.3 热应激与肉牛的繁殖性能

环境温度过高可能会降低肉牛两性的繁殖效率。在雌性动物发情周期中,热应激通过改变孕酮、黄体生成素和促卵泡激素的分泌来影响卵母细胞的生长^[18]。此外,热应激可能会使肉牛卵泡中雌二醇分泌减少,导致发情不明显,降低肉牛生育能力^[19-21]。在夏季,肉牛的怀孕率从 27% 下降到 20%^[22-23]。Roy 和 Prakash 报道,在高温环境下小母牛发情周期血浆孕酮较低,泌乳素浓度较高。以上研究结果得出,在炎热的夏季,泌乳素和孕酮水平与

肉牛的繁殖性能直接相关,高泌乳素可能导致肉牛不育,热应激还与牛胚胎发育受损和胚胎死亡率增加有关^[24-25]。此外,怀孕期间的牛在热应激的状态下,减缓胎儿的生长,增加流产。

在公牛中,精液浓度、每次射精精子数和运动细胞数在夏季低于冬季和春季^[26]。据报道^[27],暴露在较高的环境温度下会导致公牛精液质量下降,这可以通过降低活动精子的比例、减少精子产量以及增加异常和老化精子的比例来证明。

1.4 热应激与肉牛的肉品质

肉牛通常生活在简易的牛棚,不仅特别容易受到极端环境条件的影响,而且还容易受到气候迅速变化的影响。特别是肥壮的牛(皮下脂肪起到隔热作用,减缓散热)、毛发浓密的牛(隔热效果更好)和深色皮毛的牛(黑色和暗红色牛)对热非常敏感^[28-29]。动物健康与动物福利动物委员会表明,相对湿度在 80% 以下的 30.8℃和相对湿度在 80% 以上的 27.8℃是肉牛干物质采食量和饲料消化率容易受到不良影响的阈值温度^[30]。Mitlohner 等人报道,在热应激条件下饲养的奶牛,干物质采食量和平均日增重、胴体体重减轻、脂肪厚度降低和疾病发生率增加^[31]。此外,Kadim 等^[32]发现炎热季节平均气温(37.7 \pm 1.4)℃和相对湿度(48.8 \pm 7.6)%对牛肉品质有较强的负面影响。黄涛等^[33]以锦江黄牛为试验动物发现,处于高温状态下的肉牛,牛肉的肌肉剪切力、滴水损失显著提高,肉色 a 值显著下降。

2 预防热应激环境对肉牛的影响措施

为减少热应激给畜牧业带来负面影响,有必要采取适当的措施,尽可能减少热应激给肉牛带来的负面影响,或使其适应热应激的管理方法。物理预防、肉牛的品种选育以及营养调控等是预防热应激环境对肉牛影响的有效措施。

2.1 物理措施预防热应激

养牛场可通过物理防护措施来改变肉牛畜舍环境,如:可以加强牛舍通风条件、在通风条件良好的地方建造半开放型牛舍,搭建牛舍顶棚时设置隔热层,在牛舍周围、隔离带局部利用树荫等方式避免阳光直射等降低牛舍的环境温度和湿度以便缓解肉牛在夏季的热应激症状。也可以在基于对流、传导原理下,进行牛体热量辐射和蒸发,可以在高温的牛舍安装吊扇吹风,给牛体洒水,通过蒸发牛体热量来降温^[34-37]。Aggarwal 等^[38]报道,给水牛淋浴能显著降低水牛的体表和直肠温度、呼吸频率,可以降低水牛对热应激的反应。张政等^[39]报道,牛舍中安装风机

喷雾系统,同样能使肉牛的呼吸频率、直肠温度降低,提高养殖业的经济效益。另外,在夏季,适当降低饲养密度,保证牛舍的卫生,充足的饮水,也能够预防肉牛出现热应激症状^[40]。

2.2 品种选育预防热应激

动物的生存依赖于饲养管理,可是,在长期的热应激过程中,饲养管理不能完全消除热应激给动物带来的抑制作用,通过遗传选择等方法,培育耐热性高、热适应性强的肉牛是缓解气候热应激的最有效的方法。个别品种与品种之间,甚至同一品种与品种内的个体之间的耐热性存在着相当大的差异。在热带地区,自然选择的过程有利于出现具有高度抗热应激能力的品种。但是,在相似的实验条件下比较,本土热带品种的生产力普遍低于外来畜禽品种^[41]。然而,在非常恶劣的条件下(炎热的气候/营养不良),使用本土品种可能是提高生产水平的最成功办法。利用本地品种的耐热性,可以将商业品种与外来品种杂交,利用特定的能力来提高性能水平^[42]。该技术已成功地应用于肉牛和肉鸡,以提高耐热性。研究^[43]表明,不同品种的肉牛杂交所产生的肉牛热适应性不同,以安格斯牛与其他品种牛杂交得到的牛热适应能力高的品种风险低。

2.3 营养调控预防热应激

在炎热的环境下,动物为减少机体增热和散热负担,势必会减少饲料摄入量,在热应激期间,牛营养需求发生变化,这导致需要重新制定日粮,以便在热应激状态下提高牛的采食量和生产性能。如减少纤维摄入量以使瘤胃正常运作,增加补充脂肪和精料喂量,以避免代谢紊乱,在高温条件下,牛的能量摄入有限,增加能量摄入的常见方法是增加饲料中精料的含量。据报道,当饮食中含有 14%~17% 的酸洗涤纤维时,一些在热应激期间的干物质采食量的减少可以被预防。低纤维、高发酵的碳水化合物饮食可以在高温条件下刺激能量摄入,为了避免代谢紊乱,维持瘤胃正常功能,不应将酸洗涤纤维和中洗涤纤维分别降低到日粮干物质的 18% 和 28% 以下。另外,还可以在饲料中添加维生素 E 或微量元素 Zn 等,提高牛的免疫功能,对热应激动物的生产性能产生有益的影响。此外,热应激引起的热调节反应也可能影响矿物质需要量。血液酸碱平衡受到过度通气的干扰,导致呼吸性碱中毒,降低肉牛的生长速度。矿物质治疗是治疗呼吸性酸中毒的有效手段。通过提供 1.0% 的碳酸氢钠喂养的热应激牛的生产得到了提高^[44]。其他饲料添加剂如烟酸、共轭亚油酸等均能减弱高温对反刍动物生长性能的影响。

在我国,中草药在肉牛生产中产上抗热应激的应用,已经有了有力的理论支持。中草药源于天然物质,富含维生素与微量元素,有助于促进机体生长和增加耐热应激的能力。有报道^[45]证明,在夏季高温湿热环境下在肉牛的饲料中加藿香、黄柏、苍术和石膏等,有降低肉牛体温和呼吸频率,提高消化酶活性,改善肉牛的育肥性能的效果。同样,在夏季高温高湿条件下,用藿香、苍术、黄芪和石膏等按照一定配制比例添加在肉牛的饲料中能降低肉牛的体温、腹泻率,提高饲料养分消化率,调节蛋白质的合成与脂质的代谢,增强机体免疫能力,对缓解肉牛的热应激有一定的作用^[46-47]。

3 总 结

热应激对热带地区动物生产性能产生了负面影响,给畜牧业造成了重大经济损失。随着全球变暖加剧,环境热应激将日趋严重。目前环境管理方面的重大进展以及改变饲养策略,都可以减弱热应激对动物性能的影响,同时从品种间和品种内的遗传变异程度来看,选择耐热性是可行的。就目前而言,需要更多的科技工作者来更好地预测实际条件下热应激对肉牛生产力的影响,这对缓解和预防炎热气候下热应激对肉牛生产水平的影响至关重要。

参考文献:

- [1] Berman A. Estimates of heat stress relief needs for Holstein dairy cows[J]. Journal of Animal Science 2005 83(6): 1377-1384.
- [2] Busby D, Loy D. Heat stress in feedlot cattle: Producer survey results[J]. Beef Research Report 1997 1(1): 1-12.
- [3] Beatty D T, Barnes A, Taylor E, et al. Physiological responses of *Bos taurus* and *Bos indicus* cattle to prolonged continuous heat and humidity[J]. Journal of Animal Science 2006 84(4): 972.
- [4] Hendricks K E, Hansen P J. Can programmed cell death be induced in post-ejaculatory bull and stallion spermatozoa? [J]. Theriogenology 2009 71(7): 1138-1146.
- [5] 张瑞光, 吴晓鸣, 鲍若虹, 等. 热应激与非热应激期福安水牛生理和抗氧化指标分析[J]. 江西农业学报, 2010, 22(11): 136-138.
- [6] Curtis A K, Scharf B, Eichen P A, et al. Relationships between ambient conditions, thermal status, and feed intake of cattle during summer heat stress with access to shade[J]. Journal of Thermal Biology 2017 63: 104-111.
- [7] Moore K L, Johnston D J, Graser H U, et al. Genetic and phenotypic relationships between insulin-like growth factor-1 (IGF-1) and net feed intake, fat, and growth traits in Angus beef cattle[J]. Australian Journal of Agricultural Research 2005 56(3): 211-218.
- [8] 宋小珍, 付戴波, 瞿明仁, 等. 热应激对肉牛血清内分泌激素含量、抗氧化酶活性及生理生化指标的影响[J]. 动物营养学报, 2012 24(12): 2485-2490.
- [9] 李建国, 桑润滋, 张正珊, 等. 热应激对中国荷斯坦牛血液生化指标及产奶性能的影响[J]. 中国畜牧杂志, 1999(2): 25-26.

- [10] Fisher A D ,Roberts N ,Bluett S J ,et al. Effects of shade provision on the behaviour ,body temperature and milk production of grazing dairy cows during a New Zealand summer[J]. New Zealand Journal of Agricultural Research 2008 ,51(2) :99-105.
- [11] Stowell R R ,Gooch C A ,Inglis S. Performance of tunnel ventilation for freestall dairy facilities as compared to natural ventilation with supplemental cooling fans [C]// Livestock environment VI: Proceedings of the 6th international symposium 2001. American Society of Agricultural and Biological Engineers 2001.
- [12] Strickland J T ,Bucklin R A ,Nordstedt R A ,et al. Sprinkler and fan cooling system for dairy cows in hot ,humid climates[J]. Applied Engineering in Agriculture ,1989 ,5(2) :231-236.
- [13] Eitam H ,Brosh A ,Orlov A ,et al. Caloric stress alters fat characteristics and Hsp70 expression in milk somatic cells of lactating beef cows [J]. Cell Stress and Chaperones ,2009 ,14 (2) :173-182.
- [14] Mishra A ,Hooda O K ,Singh G ,et al. Influence of induced heat stress on HSP70 in buffalo lymphocytes [J]. Journal of Animal Physiology and Animal Nutrition 2011 ,95(4) :540-544.
- [15] Löhre B ,Viergutz T ,Kanitz W ,et al. Hydroperoxides in circulating lipids from dairy cows: Implications for bioactivity of endogenous-oxidized lipids [J]. Journal of Dairy Science 2005 ,88(5) :1708-1710.
- [16] Bernabucci U ,Lacetera N ,Baumgard L H ,et al. Metabolic and hormonal acclimation to heat stress in domesticated ruminants [J]. Animal 2010 ,4(7) :1167-1183.
- [17] E Paula L A C ,Andrzejewski J ,Julian D ,et al. Oxygen and steroid concentrations in preovulatory follicles of lactating dairy cows exposed to acute heat stress [J]. Theriogenology ,2008 ,69(7) :805-813.
- [18] Ronchi B ,Stradaoli G ,Supplizi A V ,et al. Influence of heat stress or feed restriction on plasma progesterone ,oestradiol-17 β , LH ,FSH ,prolactin and cortisol in Holstein heifers [J]. Livestock Production Science 2001 ,68(2/3) :231-241.
- [19] Biggers B G ,Geisert R D ,Wetteman R P ,et al. Effect of heat stress on early embryonic development in the beef cow [J]. Journal of Animal Science ,1987 ,64(5) :1512-1518.
- [20] De Rensis F ,Scaramuzzi R J. Heat stress and seasonal effects on reproduction in the dairy cow: A review [J]. Theriogenology ,2003 ,60(6) :1139-1151.
- [21] Amundson J L ,Mader T L ,Rasby R J ,et al. Environmental effects on pregnancy rate in beef cattle [J]. Journal of Animal Science ,2006 ,84(12) :3415-3420.
- [22] Chebel R C ,Santos J E P ,Reynolds J P ,et al. Factors affecting conception rate after artificial insemination and pregnancy loss in lactating dairy cows [J]. Animal Reproduction Science 2004 ,84(3/4) :239-255.
- [23] Lucy M C. Reproductive loss in farm animals during heat stress [C]// Proceedings 15th conference on biometeorology and aerobiology. Citeseer 2002.
- [24] Bényei B ,Gáspárdy A ,Barros C. Changes in embryo production results and ovarian recrudescence during the acclimatisation to the semiarid tropics of embryo donor Holstein-Friesian cows raised in a temperate climate [J]. Animal Reproduction Science 2001 ,68(1/2) :57-68.
- [25] Hansen P J. Exploitation of genetic and physiological determinants of embryonic resistance to elevated temperature to improve embryonic survival in dairy cattle during heat stress [J]. Theriogenology 2007 ,68:242-249.
- [26] Nichi M ,Bols P E J ,Zuge R M ,et al. Seasonal variation in semen quality in *Bos indicus* and *Bos taurus* bulls raised under tropical conditions [J]. Theriogenology 2006 ,66(4) :822-828.
- [27] Meyerhoeffer D C ,Wettemann R P ,Coleman S W ,et al. Reproductive criteria of beef bulls during and after exposure to increased ambient temperature [J]. Journal of Animal Science ,1985 ,60(2) :352-357.
- [28] Brown-Brandl T M ,Eigenberg R A ,Nienaber J A. Heat stress risk factors of feedlot heifers [J]. Livestock Science 2006 ,105(1/3) :57-68.
- [29] Gaughan J B ,Mader T L ,Holt S M ,et al. Assessing the heat tolerance of 17 beef cattle genotypes [J]. International Journal of Biometeorology 2010 ,54(6) :617-627.
- [30] Hahn G L ,Mader T L ,Harrington J A ,et al. Living with climatic variability and potential global change: Climatological analyses of impacts on livestock performance [C]// Proceedings of the 16th international congress on biometeorology. Kansas City 2002: 45-49.
- [31] Mitlöhner F M ,Galyean M L ,McGlone J J. Shade and water misting effects on behavior ,physiology ,performance ,and carcass traits of heat-stressed feedlot cattle [J]. Journal of Animal Science 2001 ,79(9) :2327-2335.
- [32] Kadim I T ,Mahgoub O ,Al-Ajmi D S ,et al. The influence of season on quality characteristics of hot-boned beef *m. longissimus thoracis* [J]. Meat Science 2004 ,66(4) :831-836.
- [33] 黄涛. 金银花提取物对夏季高温条件下肉牛骨骼肌纤维形态和肌肉品质的影响 [D]. 南昌: 江西农业大学 2015.
- [34] Wu Z H ,Liu M ,Zhang L B ,et al. Effect of orifice schemes on air supply and cooling performance of wet curtain fan-fiber duct in beef cattle barn [J]. Transactions of the Chinese Society of Agricultural Engineering 2016 ,32(24) :212-217.
- [35] Gaughan J B ,Mader T L. Body temperature and respiratory dynamics in un-shaded beef cattle [J]. International Journal of Biometeorology 2014 ,58(7) :1443-1450.
- [36] Boyd B M ,Shackelford S D ,Hales K E ,et al. Effects of shade and feeding zilpaterol hydrochloride to finishing steers on performance ,carcass quality ,heat stress ,mobility ,and body temperature [J]. Journal of Animal Science 2015 ,93(12) :5801-5811.
- [37] 丁丽 ,范明杰 ,王慧军. 吹风对缓解肉牛热应激的影响 [J]. 山东畜牧兽医 2014 ,35(9) :18-19.
- [38] Aggarwal A ,Singh M. Changes in skin and rectal temperature in lactating buffaloes provided with showers and wallowing during hot-dry season [J]. Tropical Animal Health & Production 2008 ,40(3) :223-228.
- [39] 张政 ,牛欢 ,颜培实. 喷雾吹风系统在南方肉牛舍应用效果 [J]. 畜牧与兽医 2016 ,48(2) :31-35.
- [40] 王福丽 ,安文福. 肉牛热应激的临床症状和防治措施 [J]. 现代畜牧科技 2016(8) :161.
- [41] Renaudeau D ,Huc E ,Noblet J. Acclimation to high ambient temperature in Large White and Caribbean Creole growing pigs [J]. Journal of Animal Science 2007 ,85(3) :779-790.
- [42] Falconer D S ,Mackay T. Introduction to quantitative genetics [M]. 4th ed. Harlow ,UK: Longmans ,1996.

(下转第74页)

州区肉牛养殖急需解决的问题。

参考文献:

- [1] 朱立泽. 甘肃省武威市凉州区肉牛产业的发展现状与分析思考[J]. 中国牛业科学 2015 41(4):74-76.
- [2] 许国军. 凉州区发展现代肉牛产业的战略思考[J]. 中兽医学杂志 2014(9):76.
- [3] 陈福斌,党武吉. 凉州区畜牧业发展面临的问题与对策[J]. 中兽医学杂志 2015(9):162-164.
- [4] 梁天军. 凉州区肉牛产业发展模式研究[J]. 中国畜禽种业, 2010(11):12-13.
- [5] 王亚萍,简勇,邓琼. 肉牛养殖模式的影响因素及现状分析[J]. 农业开发与装备 2016(11):196.

Investigation and Evaluation of Shelter Cattle Breeding Model in Liangzhou District

LIU Hu-jun, LIU Shu-juan, WAN Xiang*, LIU Guang-wu,

ZHANG Wei-xing, ZHANG Zhong, LIU Kai-lin, LI Jing-jing, DU Juan

(Gansu Desert Control Research Institute, State Key Laboratory of Desertification and Aeolian Sand Disaster
Gansu(Ministry of State Key Laboratory breeding base) Lanzhou 730070)

Abstract: Cattle raising was a traditional industry in Liangzhou district of Wuwei city, and a benefit way to increase farmers' income. The cattle companies and farmers were visited and field observation. The results of observation showed that 66.67% of cattle raising was households, and the leading farmers played an extremely important role in local cattle farming. The number of cattle between 5 and 30 was an effective quantity for farmers who raise cattle by themselves' technologies. The coexistence of various cattle breeding modes was suitable for local economic conditions. The trend of cattle breeding was being standardized and systematized in Liangzhou district. It was urgent to solve the problem of improving the cattle breeding environment by shortening the treatment process of manure in the cattle farm.

Key words: Liangzhou district; cattle breeding; model; benefit

(上接第 61 页)

- [43] Hay K E, Morton J M, Mahony T J, et al. Associations between animal characteristic and environmental risk factors and bovine respiratory disease in Australian feed-lot cattle[J]. Preventive Veterinary Medicine 2016, 125(2):66-74.
- [44] 孙科业,石传林,张娜. 炎夏日粮中添加小苏打对泌乳牛生产性能的影响[J]. 黑龙江畜牧兽医, 2002(10):23-24.
- [45] 王文娟,汪水平,左福元,等. 中药复方对夏季肉牛的影响: I. 育肥性能、生理指标及血清激素水平和酶活性[J]. 畜牧兽医学报 2010 41(10):1260-1267.
- [46] 宋小珍,付戴波,瞿明仁,等. 中草药复方添加剂对高温环境下肉牛体温和腹泻率的影响[J]. 中国饲料, 2012(15):27-30.
- [47] 付戴波,瞿明仁,宋小珍,等. 中药复方添加剂对热应激条件下锦江黄牛血液生化指标的影响[J]. 饲料工业 2012 33(7):48-50.

Effects of Heat Stress on Beef Cattle Production and Control Measures

LIN Wan, SUN Xiao-hong, LUO Jun-yi, CHEN Ting,

XI Qian-yun, ZHANG Yong-liang, SUN Jia-jie*

(College of Animal Science, South China Agricultural University, Guangdong Provincial Key Laboratory of
Animal Nutrition Control, Guangzhou, Guangdong 510642)

Abstract: Animal health production is affected by many factors. With global warming, warm environment has gradually become one of the important and key factors affecting the development of animal husbandry. Although the effect of heat stress on beef cattle production was not as significant as that of cows, it was also not to be underestimated. The purpose of this paper was to review the environmental factors affecting beef cattle production and to elaborate the assessment method of temperature and humidity index, as well as the effects of heat stress on the performance and physiological functions, immune index, reproductive performance and meat quality of beef cattle. Finally, effective strategies were proposed to mitigate the impact of heat stress on beef cattle production, including physical prevention, breed selection of beef cattle heat tolerance and nutritional regulation.

Key words: heat stress; beef cattle; healthy breeding

茶渣资源再利用研究概况

谢月琴,罗君谊,陈 婷,习欠云,张永亮,孙加节

(华南农业大学动物科学学院/广东省动物营养调控重点实验室,广州 510642)

摘要:为了探寻茶渣的再利用情况,本研究综述了国内外近几年对茶渣再利用的研究。结论是无论在国外还是国内茶渣在工业和农业领域的再利用趋于饱和,但是在畜牧领域的研究甚少,还尚存在较大的研究空间。因此,今后还需把研究方向朝向畜牧行业。本研究首先简要地概括了茶渣的来源和成分,随后详细地阐述了茶渣在工业、农业和畜牧业3个领域的应用概况,着重介绍了茶渣作为动物饲料在畜牧业方面的研究,最后以茶渣现有的研究为基础,提出了王老吉茶渣作为反刍动物饲料的应用展望,希望对茶渣的开发提供有价值的参考依据。

关键词:茶渣;资源再利用;成分;肥料;饲料

中图分类号:S816

文献标志码:A

论文编号:casb18060083

Reuse of Tea Residue Resources: A Review

Xie Yueqin, Luo Junyi, Chen Ting, Xi Qianyun, Zhang Yongliang, Sun Jiajie

(College of Animal Science, South China Agricultural University/Guangdong Key Laboratory of Animal Nutrition Control, Guangzhou 510642)

Abstract: The paper aims to explore the reuse of tea residues. We reviewed the researches on the reuse of tea residues in recent years at home and abroad, found that the reuse of tea residues tended to be saturated in industrial and agricultural fields, but there was little research in the field of animal husbandry, and the research direction could be adjusted to animal husbandry in the future. We briefly summarized the sources and compositions of tea residues, and then elaborated the applications of tea residues in 3 fields of industry, agriculture and animal husbandry, focusing on the researches of tea residues as animal feed in animal husbandry; finally, based on the existing researches on tea residues, we put forward the prospects of applying Wanglaoji tea residues as ruminant animal feed to provide a reference for the development and utilization of Wanglaoji tea residues in the future.

Keywords: tea residue; resource reuse; composition; fertilizer; feed

0 引言

随着人们对茶饮料的需求增加,以及茶叶加工技术的不断发展,茶饮料的生产规模逐渐扩大,而大量的茶渣也就随之产生。徐明喜等^[1]报道中国每年排放的茶渣量达到16万t,因此,茶渣的处理成了非常棘手的问题。面对大量的茶渣,若随意丢弃不仅会对环境造成较大的负面影响,而且也会导致严重的资源浪费。因此,如何处理这些资源浪费的问题已经成为人们重

视和关注的焦点。

根据现有的文献报道,目前对于茶渣再利用的研究主要是:制作生物吸附剂^[2],制作有机无机复合肥^[3]以及通过微生物固体发酵后用作动物饲料^[4]。前两者的研究报道较多,后者用作动物饲料的研究较少,主要原因是茶渣中含有一些难处理的抗营养因子如单宁、多酚和草酸。另外,还大量难消化的粗纤维。王老吉凉茶是茶饮料的一种,有清热降火的功效,有研究表

基金项目:广东省自然科学基金(2016A030310449、2016A030313413)。

第一作者简介:谢月琴,女,1994年出生,贵州铜仁市人,硕士,研究方向:动物功能基因组学。通信地址:555110 贵州省石阡县龙塘镇新场村黄家坟组,E-mail:791312265@qq.com。

通讯作者:孙加节,男,1984年出生,江苏盐城人,副教授,博士,研究方向:动物肉品质调控机制。通信地址:510642 广东省广州市天河区五山街 华南农业大学,E-mail:jiajiesun@scau.edu.cn,214465654@qq.com。

收稿日期:2018-06-20,修回日期:2019-02-25。

明,王老吉凉茶可以提高小鼠的免疫功能^[5]和增强抗氧化应激能力^[6],但是用作反刍动物饲料尚未有研究。

综合前人的研究进展以及本实验室的研究基础,笔者拟对王老吉凉茶渣进行微生物固态发酵来改善凉茶渣的适口性,消除抗营养因子,降低粗纤维含量,提高茶渣中养分的利用率,随后探讨发酵后的凉茶渣对夏季泌乳牛的产奶性能、免疫性能和抗热应激能力的影响。但是,此项目存在许多薄弱环节,首先是研究尚有空白,导致研究基础不够牢固,而且凉茶渣中的药用成分自带苦味,这会直接影响适口性,再者就是凉茶渣的水分高达80%,不易贮存。因此,启动本研究,拟解决以下几个关键问题:改善凉茶渣的适口性,提高茶渣中养分的利用率,提高凉茶渣药用价值,确定适用剂量,解决贮存困难并探究发酵后的茶渣对夏季泌乳牛的产奶性能、抗免疫能力和缓解热应激能力的影响,以期为后续凉茶渣的开发和利用提供实质性的研究依据和参考价值。

1 茶渣的成分

茶叶中含有丰富的营养成分,然而,茶作为一种比较传统的饮料,人们所饮用的物质只占茶叶的少部分。因此,在茶渣里还保留着很多有效并且可以利用的成分。李娟等^[7]发现,茶渣中的氨基酸组成比较丰富;Krishnapillai^[8]发现,茶渣中含具有药用价值的成分,如茶多酚,咖啡碱等功能性物质。除此之外,还有报道^[9]说明茶渣中含有丰富的纤维素、半纤维素、木质素以及一些微量元素。因此,不管是在畜牧产业还是工业,茶渣都具有很高的开发潜力。而从广东某公司取得的凉茶渣,经过本实验室测定发现,常规营养成分也很丰富,粗纤维含量高达28.83%,粗蛋白含量为9.78%,粗灰分含量为6.69%,酸性洗涤纤维为45.29%,中性洗涤纤维含量为61.22%,由此可见,凉茶渣的开发潜力并不弱于茶渣。接下来本实验将会继续测定凉茶渣中的药用成分含量以及开展后续的相关研究。

2 茶渣的应用研究现状

2.1 用于制备吸附剂

由于茶渣中含有丰富的纤维成分,其中一种就是膳食纤维,这种膳食纤维是一种具有吸附功能的活性成分,有研究报道^[10]活这种活性成分可能是茶渣含有吸附功能的主要原因,但是未开展相关的实验来证明茶渣的吸附功能。随着开发技术的不断更新,用茶渣为原料制作吸附剂的研究已经成为国内外研究者的关注焦点。最早证明茶渣具有吸附重金属功能是在2000年,李明静等^[11]用信阳茶渣为原料来研究对重金

属Au的吸附作用,研究表明信阳原茶与茶残渣对金属Au都有很强的吸附作用,让人惊讶的是,茶渣的吸附重金属功能要远远高于原茶。此研究成果打开了茶渣吸附功能研究的新篇章,这引起国内外研究人员的高度重视,因此,对茶渣吸附重金属功能的研究越来越多,成为当时的研究热点。

在2006年,Murugesan等^[12]发现经过FeCl₃预处理的茶渣可以吸附地下水中的As元素,除此之外,还发现茶渣对Cr^[13],Ni^[14],Mn^[15],Cu^[16],Pb和Cd^[17]以及Hg^[18]等重金属也有着同样的吸附功能。茶渣的吸附功能不仅仅如此,有研究表明茶渣除了可以吸附重金属以外还可以吸附放射性物质以及一些有机染料。最早发现茶渣可以吸附放射性物质是在2009年,Eroglu^[19]团队发现红茶的茶渣可以有效的除去废弃水中的放射性物质Ti,接着次年又发现红茶渣还可以吸附Ga^[20]。在2011年,日本科学家Gurung^[21]研究团队发现通过浓硫酸处理过的绿茶渣可以高效的吸附废水中的放射性物质Cs。对于茶渣吸附有机染料的研究最初是在2009年,由Uddin等^[22]发现茶渣可以高效地去除水体中的有机染料亚甲蓝,并且2011年Giahi等^[23]探究了茶渣对亚甲蓝吸附的数量和吸附率。诸如此类的研究还有很多,如最新的研究发现,经过磺化处理后的茶渣可以有效的吸附水中的亚甲蓝,四环素和Cr(VI)^[24]。从现有的研究进展来看,有着来源广泛且成本低价的茶渣来制作物美价廉的吸附剂是当下环境发展的不二之选,由此可见,茶渣在治理环境和节约资源两个方面都有着非常可观的开发前景。

2.2 用于种植农作物

最先用茶渣制备有机肥的研究是在2003年,由国内研究者夏会龙的团队^[25]发现用茶渣可以有效的改善土壤的有机含量以及增加一些微生物的数目。接着国外也有研究表明,茶渣中的单宁可以明显的改善土壤的生态特性^[26]。2012年,茶渣被称为是一种高质量的堆肥原料,这已经被国外研究者Pant等^[27]证实,他发现以茶渣作为堆肥原料的各项堆肥指标要高于用家禽粪便为原料的堆肥指标。由于有研究证明茶渣可以很明显的改善土壤的特性,所以茶渣逐渐被广泛的应用到大棚种植业,并且也获得了较好的结果。如孙志栋等^[28]用茶渣作为肥料可以增加大棚番茄种植的产量,他在葡萄种植方面也证实了茶渣肥料的优越性^[29]。2010年周菁清等^[30]研究表明,茶渣肥料可以显著的加快玉米的生长速度。另外,茶渣含有纤维等含量丰富的营养成分,并且还含有较多的矿物质,可以满足培养食用菌的养分。用茶渣来栽培食用菌不但可以解决资

源浪费的问题,而且又为栽培食用菌所需的养分提供了充足的来源。最近研究发现,用茶渣来栽培蘑菇也获得了可观的收益。另外,有研究表明用原料为50%茶渣肥料栽培姬菇^[31]、杏鲍菇^[32]都能取得较好的经济效益,类似的研究还有用王老吉茶渣栽培双孢蘑菇,发现其产量、品质以及经济效益都显著提高^[33]。

2.3 用于制备动物饲料

由于茶渣含有较高的营养成分和多种有效的药用成分,因此茶渣被认为是一种理想的饲料资源。随着开发技术的进步,茶渣用作饲料应用在养牛、养羊、养猪、养鸡以及兔等各个领域。据调查,用作反刍动物饲料、家禽饲料的研究到目前为止非常少,用作家畜饲料研究相对较多,用作家畜饲料的研究对象主要是育肥猪。国内对茶渣用作牛饲料的研究最早是在20世纪80年代,李英^[34]发现干物质占比为7%~10%的茶渣可以增强蛋白质过瘤胃能力,可能的原因是茶渣中的多酚类物质对茶蛋白具有保护作用,可以减少茶蛋白在瘤胃中发酵,进而提高生产性能,是反刍动物的优质蛋白饲料。时隔10年之余,茶渣开始用作羊饲料,是Zhong等^[35]在2009年用公羊位研究对象,在日粮中添加适宜的茶渣可以有效的抑制脂质氧化,提高冷藏肉的品质。在此之后潘发明^[36]以绵羊为研究对象,发现添加茶渣单宁可以降低饲料的体外瘤胃蛋白降解率,而且对饲料中的蛋白质具有很好的保护效果。茶渣饲料在养牛和养羊方面的研究为零,但是在家畜和家禽方面的研究越来越多。首先,用作猪饲料的研究最早也是在20世纪90年代,由高凤仙等^[37]用茶渣代替日粮中的某些成分对育肥猪的生长性能以及肉品质虽然没有显著的差异,但是也没有负面影响;而孙克年^[38]在猪的日粮中添加茶渣可以提高育肥猪的饲料利用率,缩短育肥猪的上市时间,从而提高经济效益;万玉春^[39]的研究结果与之相符。

接着有研究发现,添加茶渣可以提高猪肉的抗氧化能力,延长猪肉的保存时间和稳定肉色^[40]。最新的研究表明在肥育猪的日粮中添加1%茶渣与1%的中草药使得育肥猪日增重增加7.41%,采食量提高4.62%,料肉比下降1.94%,除此之外,肥育猪的免疫功能显著性增强,肉品质显著性提高以及腹泻率显著降低等极其可观的应用效果^[41]。在家禽方面的研究最早也是在90年代,舒庆龄等^[42]用2%糖化过的茶渣喂肉用鸡,发现其日增重显著增加,育肥效果明显。之后有研究者开始把研究对象从肉鸡转变为蛋鸡,吴慧敏^[43]在蛋鸡的日粮中添加1%和2%的茶渣观察蛋鸡的生产性能和免疫功能,首先是生产性能方面的效果,发现其产蛋

数和蛋重显著增加,并且添加2%茶渣组对降低破蛋数的效果非常好,添加2%的茶渣可以显著性的降低料蛋比。免疫机能方面,1%茶渣可以显著提高血清中的GSH-Px、T-SOD、lgA、lgM含量,同时可以显著性的降低血清中的胆固醇含量。

在这些动物中茶渣的应用方式大致为2种:一种是用作饲料添加剂直接添加,以上笔者所介绍的研究均为直接添加。随着开发技术的不断推进,研究者们利用微生物发酵的方式对茶渣饲料进行运用,有研究表明,茶渣经过不同的微生物发酵后其营养成分会有所增加。如刘姝等^[44]以茶渣为原料,利用霉菌以及微生物发酵进行发酵,发现粗蛋白质和可溶性物质的含量显著增加,并且其营养含量已经完全满足仔猪配合日粮的需求。吴慧敏^[43]对茶渣发酵效果也进行了相关的研究,她发现茶渣发酵后喂蛋鸡可以显著提高总蛋重,极显著提高蛋黄的色泽度,鸡蛋中胆固醇含量降低,V_A含量显著提高,并且添加0.5%、1%的发酵茶渣,蛋鸡血清中的GSH-Px、T-SOD含量显著提高,添加2%发酵茶渣显著提高lgA、lgM、lgG含量。

3 展望

虽然产生凉茶渣的数量在成倍增加,但是根据现有的研究报告,凉茶渣用于开发饲料的研究极其少。实际上,茶渣无论是经过发酵还是不发酵都存在着非常可观的利用价值。首先,凉茶渣中含有较高的粗纤维,这刚好可以满足反刍动物的消化特征,维持反刍动物的基本需求。其次,凉茶渣中还含有较多的蛋白,适当处理便可以达到家禽的理想蛋白水平,从而改善肉品质。

另外,重要的是茶渣中含有多种可利用的中药成分,如有抗氧化功能的多酚和咖啡碱、改善肉品质的氨基酸以及抑制瘤胃原虫生长的皂素等多种活性物质。然而在实际生产上,用凉茶渣来饲喂鸡、鸭、牛、羊等动物的研究尚为不多,这充分说明了茶渣的药用价值并没有很好的应用到养殖产业。笔者认为在现有的基础上研制出适合于不同生长阶段、不同品种动物的凉茶渣饲料可能会是将来畜牧行业的研究热点之一。而本实验室即将开展的实验就是广州王老吉大健康产业有限公司提供的凉茶渣,经微生物发酵后饲喂泌乳牛或肉牛是否会发挥其实质性的作用,如生产性能是否提高,血液中抗氧化能力、抗免疫能力以及缓解热应激的能力是否增强。根据调查,与凉茶相关的研究比较少。但是有研究表明,凉茶可以增加脾脏NK细胞数,提高NK细胞杀伤活性,还可以显著提高MDA含量、提高细胞内ORAC水平^[5]。

此外,张梦娇等^[6]研究发现,王老吉凉茶对高脂膳食引起的氧化应激损伤有一定的保护作用。但是到现阶段为止,对凉茶渣的研究为零,因此在实验过程中可能会存在比较多的薄弱环节,首先是缺乏研究基础,无论是剂量还是适用任意阶段的奶牛或肉牛,另外凉茶渣中的药用成分略有苦味,这会直接影响适口性,进而影响动物的偏好性,最终导致生产性能降低,再者就是凉茶渣的水分非常高,达80%以上,不易贮存。因此,本实验室即将开展的实验的目的就是解决这几个问题,优化添加剂量,改善凉茶渣的适口性,提高药用价值,解决凉贮存困难。

笔者认为,如果上述涉及到的问题得到解决,那么凉茶渣开发成动物饲料应用到养殖行业具有非常广阔的发展前景。因此,笔者认为有必要通过各种技术对凉茶渣的回收利用进行深入研究,为提升废弃茶渣的利用价值和效率、降低养殖业的生产成本、延长农业畜牧业产业链以及提高经济效益提供坚实的技术支撑和研究基础。

参考文献

- [1] 徐明喜,王东升,陈莉莉,等.不同茶渣有机肥用量对H60甘蓝产量和品质的影响[J].蔬菜,2017(2):26-27.
- [2] 李明静,陈映霞,何建英,等.信阳废次茶残渣对Au(Ⅲ)的吸附研究[J].化学研究,2000,11(2):40-42.
- [3] Pant A P, Radovich T J K, Hue N V, et al. Biochemical properties of compost tea associated with compost quality and effects on pak choi growth[J].Scientia Horticulturae,2012,148(01):138-146.
- [4] 李英.茶渣——反刍家畜的优质蛋白饲料[J].饲料研究,1983(6):31.
- [5] 何蓉蓉,栗原博,宝丽,等.王老吉凉茶对应激小鼠免疫机能及体内过氧化状态的影响[J].中国实验方剂学杂志,2008(2):38-42.
- [6] 张梦娇,杨杏芬,赵敏,等.王老吉凉茶对高脂膳食喂养小鼠氧化应激状态的影响[J].华南预防医学,2014,40(1):78-81.
- [7] 李娟,活泼,杨海燕.茶叶中非水溶性蛋白质提取工艺及功能性质的研究[J].浙江农业科学,2006,1(2):150-153.
- [8] Krishnapillai S. Effect of waste tea (tea fluff) on growth of young tea plants (*Camellia sinensis* L.) [J].Cancer Research,1981,69(8):3347-3355.
- [9] 谢枫,金玲莉,涂娟,等.茶废弃物综合利用研究进展[J].中国农学通报,2015,31(1):140-145.
- [10] 艾仄宜,张洁,杨晓萍,等.茶叶非水溶性膳食纤维的提取及其理化特性研究[J].食品科学,2010,31(8):121-124.
- [11] 李明静,何建英,李桂莲,等.信阳废次茶残渣对Au(Ⅲ)的吸附研究[J].化学研究,2000,11(2):40-42.
- [12] Murugesan G S, Sathishkumar M, Swaminathan K. Arsenic removal from groundwater by pretreated waste tea fungal biomass [J].Bioresource Technology,2006,97(3):483-487.
- [13] Albadarin A B, Mangwandi C, Walker G M, et al. Influence of solution chemistry on Cr(VI) reduction and complexation onto date-pits/tea- waste biomaterials[J].Journal of Environmental Management,2013,114(2):190-201.
- [14] Panneerselvam P, Morad N, Tan K A. Magnetic nanoparticle (Fe₃O₄) impregnated onto tea waste for the removal of nickel(II) from aqueous solution[J].Journal of Hazardous Materials,2011,186(1):160.
- [15] Khajeh M, Barkhordar A. Modelling of solid- phase tea waste extraction for the removal of manganese from food samples by using artificial neural network approach[J].Food Chemistry,2013,141(2):712-717.
- [16] 崔晓宁,侯伟华,杨晓萍,等.茶叶纤维对Cu²⁺的吸附性能研究[J].茶叶科学,2010,30(4):259-262.
- [17] 张军科,郝庆菊,江长胜,等.废弃茶叶渣对废水中铅(Ⅱ)和镉(Ⅱ)的吸附研究[J].中国农学通报,2009,25(4):256-259.
- [18] Shen B, Tian L, Li F, et al. Elemental mercury removal by the modified bio-char from waste tea[J].Fuel,2017(187):189-196.
- [19] Eroglu H, Yaptıcı S, Nuhoglu C, et al. An environmentally friendly process; adsorption of radionuclide Tl-201 on fibrous waste tea[J]. Journal of Hazardous Materials,2009,163(2/3):607.
- [20] Eroglu H, Varoglu E, Yaptıcı S, et al. An environmentally friendly batch bioadsorption study of the radionuclides 67 Ga from aqueous solutions by fibrous tea waste[J].Chemical Engineering Journal, 2010,165(2):563-572.
- [21] Gurung M, Adhikari B B, Alam S, et al. Adsorptive removal of Cs (I) from aqueous solution using polyphenols enriched biomass-based adsorbents[J].Chemical Engineering Journal,2013,231(17):113-120.
- [22] Uddin M T, Islam M A, Mahmud S, et al. Adsorptive removal of methylene blue by tea waste[J].Journal of Hazardous Materials, 2009,164(1):53-60.
- [23] Masoud Giahi, Roohan Rakhshae, Bagherinia M. Removal of methylene blue by tea wastages from the synthesis waste waters[J]. Chinese Chemical Letters,2011,22(2):225-228.
- [24] Ahsan M A, Katla S K, Islam M T, et al. Adsorptive removal of methylene blue, tetracycline and Cr(VI) from water using sulfonated tea waste[J].Environmental Technology & Innovation, 2018,11:23-40.
- [25] 夏会龙.茶渣复混肥对茶园土壤的生态效应[J].污染防治技术, 2003(z2):76-78,120.
- [26] Kraus T E C, Zasoski R J, Dahlgren R A. Fertility and pH effects on polyphenol and condensed tannin concentrations in foliage and roots [J].Plant & Soil, 2004,262(1/2):95-109.
- [27] Pant A P, Radovich T J K, Hue N V, et al. Biochemical properties of compost tea associated with compost quality and effects on pak choi growth[J].Scientia Horticulturae,2012(148):138-146.
- [28] 孙志栋,吴海军,施旭辉,等.茶渣肥在大棚番茄生产上应用效果初报[J].耕作与栽培,2009(5):48,51.
- [29] 孙志栋,张松强,陈惠云,等.茶渣有机无机活性肥改良大棚葡萄土壤初步研究[J].中国农学通报,2010,26(4):178-181.

- [30] 周菁清,郑小龙,周璐萍,等. 茶渣有机肥及其对植物生长的影响[J]. 云南化工,2010,37(5):17-19.
- [31] 苗人云,谭伟,周洁,等. 茶渣作为主料栽培姬菇的研究[J]. 西南农业学报,2016,29(1):164-168.
- [32] 谭伟,苗人云,周洁,等. 杏鲍菇茶渣栽培基质配方优化研究[J]. 中国食用菌,2016,35(3):23-28.
- [33] 柯丽娜,袁滨,张志鸿,等. 王老吉茶渣栽培双孢蘑菇的综合评价[J]. 北方园艺,2018(6):134-138.
- [34] 李英. 茶渣——反刍家畜的优质蛋白饲料[J]. 饲料研究,1983(6):31.
- [35] Zhong R Z, Tan C Y, Han X F, et al. Effect of dietary tea catechins supplementation in goats on the quality of meat kept under refrigeration[J]. Small Ruminant Research,2009,87(1):122-125.
- [36] 潘发明,李发弟,郝正里,等. 茶渣单宁含量对绵羊养分消化利用与氮代谢参数的影响[J]. 畜牧兽医学报,2012,43(1):71-81.
- [37] 高凤仙,田科雄,王继成. 速溶茶渣饲用价值研究 I. 速溶茶渣对育肥猪的饲养效果[J]. 湖南农业大学学报:自然科学版,1998(6):46-48.
- [38] 孙克年. 茶叶在养殖业中的应用[J]. 江西饲料,1999(6):28-29.
- [39] 万玉春. 速溶茶渣对育肥猪的饲养效果[J]. 河南畜牧兽医:综合版,2000(5):47.
- [40] 王玉龙,费兆生. 茶叶提取物对肉猪生产性能、肌肉品质及肌肉抗氧化指标的影响[J]. 畜牧与兽医,2014,46(12):50-52.
- [41] 童勤. 茶渣与中草药对猪生长、肉质和腹泻等性能的影响[D]. 长沙:湖南农业大学,2016.
- [42] 舒庆龄,赵和涛. 茶渣饲养肉用鸡效果研究[J]. 安徽农业科学,1995(4):355-356.
- [43] 吴慧敏. 茶渣、茶末对蛋鸡生产性能及鸡蛋品质的影响研究[D]. 福州:福建农林大学,2016.
- [44] 刘姝,涂国全. 茶渣经微生物固体发酵成饲料的初步研究[J]. 江西农业大学学报,2001,23(1):130-133.

调控乳蛋白合成信号通路的研究进展

汪东阳, 谢月琴, 罗君谊, 陈婷, 习欠云, 张永亮, 孙加节

(华南农业大学动物科学学院, 国家生猪种业工程技术研究中心, 广州 510642)

中图分类号: S8-1 文献标识码: A 文章编号: 1004-4264 (2020) 05-0006-06

DOI: 10.19305/j.cnki.11-3009/s.2020.05.002



微信扫描二维码

听独家语音介绍

与作者在线交流

开放科学(资源服务)
标识码(OSID)

摘要: 本文概述了JAK-STAT、mTOR和GCN2-eIF2a信号通路的组成, 以及其在乳蛋白合成过程中进行的调控作用和机理, 对近些年来关于JAK-STAT、mTOR以及GCN2-eIF2a信号通路的相关研究进展进行了综述, 为乳蛋白合成信号通路的研究提供了理论基础。

关键词: 乳蛋白; JAK-STAT; mTOR; GCN2-eIF2a

随着科学技术的发展和生活水平的提高, 人们对膳食营养的要求也不断上升。牛奶作为天然的食物, 一直以来都是人们摄取营养物质的首选^[1]。乳蛋白作为牛奶中重要的营养物质, 不仅含有各种必需氨基酸, 还可以调节生理平衡, 抵抗高血压并增加机体自身免疫力, 其在牛乳中的含量已成为衡量乳品质的重要指标^[2]。

如何有效提高乳品中的蛋白含量一直是当前的研究热点。在研究的早期, 认为通过增加奶牛日粮中的蛋白质含量包括过瘤胃蛋白的水平, 可以增加小肠中的可利用氨基酸的含量, 最终达到提高乳蛋白的目的^[3,4]。但是日粮中的蛋白质含量不可能无损耗, 而且随着日粮中蛋白质含量的增加, 机体吸收的效率反而会降低, 过量地添加日粮蛋白质大部分都会随着粪尿排放掉^[5], 并不能有效地提升乳品质。关于如何提高乳品质, 在动物体内外已经开展了大量的研究, 但是关于细胞分子方面的产

生机制依旧不太清楚。

伴随着细胞生物学和分子生物学的迅猛发展, 对如何调控乳蛋白合成的研究已逐步转移到相关基因的表达和联系上^[6]。如今已经可以通过对细胞分子水平的研究从一定程度上阐述奶牛的营养调控机制, 为提高奶牛产乳量和乳品质提供理论依据。目前, 利用分子生物学手段对与乳蛋白合成相关的信号通路进行研究已经成为乳品研究领域的一个重要方向。而且关于乳蛋白合成机制的研究已经取得了一定的进展, 但关于信号通路如何具体影响乳蛋白合成的机制仍在进一步研究中。本文综合乳蛋白合成的信号通路, 综述了其对于乳蛋白合成的调节作用及最新研究进展, 旨在为提高奶牛生产效率提供理论基础。

1 乳蛋白合成信号通路

随着研究的深入, 发现关于乳蛋白的合成通路主要有以下三条: 在基因水平上调控转录的JAK-STAT信号通路; 调控蛋白质翻译的mTOR信号通路; 检测体内氨基酸水平的GCN2-eIF2a信号通路。

1.1 JAK-STAT信号通路

收稿日期: 2019-09-17

基金项目: 国家重点研发计划(2016YFD0500503); 广东省普通高校省级特色创新类项目(2017KTSCX023)。

作者简介: 汪东阳(1996-), 男, 安徽人, 硕士, 主要从事动物营养学及饲料资源开发利用的研究。

通讯作者: 孙加节, 副教授, 博士, 研究方向为动物营养与生化。

JAK作为一种与细胞因子受体相连的酪氨酸蛋白激酶,在生物体内信号传递中发挥重要作用^[7]。在哺乳动物体内,目前为止共发现其有四个家族成员(JAK1~3和TYK2),他们都具有相似的JAK分子结构^[8]。JAK分子内包含了7个结构域:JH1是位于羧基末尾的激酶区,其具有催化作用,且序列呈现高度保守;JH2与激酶的功能相关,其是可以抑制活性的假激酶区,具有间接的催化作用;JH6和JH7是受体结合区;其他区域也在细胞因子与其受体结合时发挥了一定的作用^[9]。

STAT是重要的泌乳信号传导及转录激活因子,其共有6个家族成员(STAT1~6),作为JAK的靶蛋白,被JAK活化后的STAT蛋白会形成二聚体,并将信号传递进细胞核,从而调控特定基因的表达。STAT蛋白一般包括一个与其活化密切相关的酪氨酸残基、可以与细胞因子受体相结合的SH2结构域、与DNA相结合的结构域、转录激活区等重要功能片段^[10]。

信号传导从细胞外因子与对应的跨膜受体的结合时开始,受体上含有JAK,当配体与受体相结合后会使得JAK空间结构发生变化,JH1远离具有抑制活性能力的JH2,JAK被激活,随后具有酪氨酸激酶活性的JAK会磷酸化STAT上的酪氨酸残基和SH2结构域,活化的STAT蛋白立即形成二聚体,然后进入细胞核与靶基因相结合,调节其转录^[11]。

当前在乳腺组织中研究最多的还是JAK2-STAT5,这是蛋白合成在转录水平的重要信号通路^[12]。通过对小鼠乳腺的研究也证实了催乳素确实可以激活JAK2,继而磷酸化STAT5,进而调控体内多种乳蛋白基因转录,最终提高了乳蛋白的分泌量^[13]。有研究对乳腺上皮细胞中的STAT5a基因的表达进行抑制,发现这会导致细胞内酪蛋白基因转录mRNA丰度的下降,若对STAT5a基因进行过表达则会提高酪蛋白基因转录mRNA丰度^[14]。通过对转基因动物的试验发现,在乳清酸性蛋白基因和乳球蛋白基因的启动子附近发现含有STAT5的GAS特异序列,其是促进这些乳蛋白分泌所必需的位点^[15]。

通过研究发现,同一种或者不同种细胞外因子都有可能产生不同效果,其可能激活不同的JAK激酶,并磷酸化不同的STAT蛋白,导致乳蛋白组成和其含量的变化^[16]。有报道发现,其他激素也可作用于JAK-STAT通路,进而调控乳蛋白的合成^[17]。通过对泌乳早期的奶牛

进行试验,发现通过注射胰岛素可增加其产奶量和乳蛋白水平^[18]。同时发现,生长激素、胰岛素样生长因子等其他泌乳因子也会对奶牛乳腺中乳蛋白基因的表达产生调控作用^[19]。

细胞因子信号抑制因子(SOCS)是JAK-STAT信号通路的负调控子^[20]。SOCS3作为一个关键性调节细胞因子的信号分子,可能参与各种细胞过程。通过试验发现,对SOCS3的过表达和抑制都可以调控JAK-STAT信号通路的活性并显著改变乳蛋白的合成,SOCS3是JAK-STAT信号通路的抑制剂^[21]。在乳腺细胞中,SOCS3不仅可以抑制STAT5,还可以封闭酪蛋白基因的表达^[22]。

JAK-STAT信号通路是一条复杂的信号传导途径,即使最近这些年在JAK-STAT分子结构、调控机制和机理上的研究已产生了丰硕的成果,但仍有许多方面需进一步研究,正确认识JAK-STAT信号通路对生产优质奶方面起着极为重要的基础作用。

1.2 mTOR信号通路

mTOR作为哺乳动物雷帕霉素靶蛋白,属于磷酸肌醇激酶,在机体细胞中广泛分布,其不仅仅是一种重要的信号传递因子,更在细胞生长和蛋白质的合成过程中发挥重要的作用^[23]。mTOR包含有两种复合物:mTORC1和mTORC2^[24],其结构和功能各不相同。mTORC1在激素和生长因子的作用下,对蛋白质的合成、细胞生长增殖等过程进行调控^[25];而mTORC2则主要对肌动蛋白骨架结构的构建功能进行调控。

1.2.1 mTOR上游信号通路

1.2.1.1 PI3K-Akt

磷脂酰肌醇3-激酶(PI3K)包含一个p85调节亚基和一个p110催化亚基。P85亚基氨基端不仅包含一个SH3结构域,而且还有能与SH3结构域结合的脯氨酸富集区;P110亚基具有和蛋白激酶相似的序列,且其本身含有Ser/Thr蛋白激酶的特征,还具有磷脂酰肌醇激酶的特征^[16]。AKT又被称为蛋白激酶B(PKB),其也是属于Ser/Thr蛋白激酶的一种^[26]。AKT由氨基末端的调节区(PH)、中间的酶活性区、羧基末端的调节区(HM)以及负责将PH区与激酶活性区相连接的铰链区组成^[27]。激素、生长因子等通过其与受体的结合,可以将细胞内的胰岛素受体酶解物(IRS1)激活,从而将

PI3K激活, 然后进一步作用于Akt, 活化后的Akt可以直接作用于mTOR。

1.2.1.2 LKB1-AMPK

LKB1是一种Ser/Thr蛋白激酶, 其结构包括氨基调节区、羧基调节区以及激酶区。氨基调节区含有一个核定位序列, 使LKB1定位于细胞核中^[28]。LKB1可以通过磷酸化增强AMPK的活性, 进而负反馈调控乳蛋白翻译的启动过程^[29]。

AMPK为异源三聚体复合物, 由 α 、 β 、 γ 三个亚基组成, α 亚基包含催化域和上游激酶结合域, 主要负责催化功能; γ 亚基含有和ATP、ADP和AMP的结合位点, 主要负责与核苷酸的结合; β 亚基上含有 α 亚基和 γ 亚基的结合位点, 主要负责AMPK信号通路的组合连接^[30]。

AMPK作为机体内部的能量感受器, 可以准确感受细胞内能量和营养物质的变化, 能在细胞水平, 甚至机体整体水平上调控代谢能量平衡^[31,32]。AMPK对细胞内AMP浓度的变化较为敏感, 当感受到细胞内AMP的浓度升高时, 促使其被磷酸化, 从而被激活^[33]。激活的AMPK不仅能抑制ATP的消耗, 储存能量, 而且还能刺激产能的分解代谢, 生成更多的ATP。泌乳时, 乳腺需要提供大量能量, AMPK信号通路此时便发挥重要的作用。当AMPK感受到体内能量不足时, 即开启生成ATP的代谢途径, 同时活化的AMPK可对mTOR及其效应器进行抑制^[34], 并激活eEF2激酶, 增加eEF2的磷酸化, 进而抑制蛋白质的合成, 降低ATP的损耗, 维持能量平衡^[35]; 当体内的能量充足时, ATP即可转化为ADP促进乳蛋白的生成^[36]。

AMPK作为应激性蛋白激酶, 其被激活大多发生在应激条件下, 除AMP/ATP以外, 瘦素、氨基酸等对AMPK均有调节作用^[37]。研究发现, 将必需氨基酸添加到奶牛乳腺上皮细胞中可增加ATP水平, 抑制AMPK的激活^[38]。在乳腺上皮细胞中添加乙酸、葡萄糖等能量物质可影响AMPK信号通路进而调控乳蛋白的合成^[39]。

1.2.2 mTOR下游信号通路

mTOR下游信号通路的直接作用底物是真核细胞翻译起始因子结合蛋白-1 (4EBP1) 和核糖体蛋白S6激酶 (S6K) ^[40], 它们在蛋白质翻译过程中发挥着重要作用。mTOR被激活后, 可通过磷酸化4EBP1和S6K1使

其活化, S6K1是一种能控制核糖体转录的激酶, 活化后可以促进蛋白质的翻译及表达^[41], eIF4E可特异性识别并夹住mRNA5'端的帽子结构, 促进翻译的起始, 而4EBP1是一种翻译起始抑制子, 未磷酸化的4EBP1易与eIF4E结合, 并抑制其活性, 当4EBP1被磷酸化后, 活化的4EBP1从eIF4E脱离下来, 翻译起始正常形成^[42,43]。mTOR可通过抑制4EBP1的同时激活S6K^[44], 调控翻译的起始和蛋白质的合成^[45]。

研究发现, mTOR信号通路协调乳蛋白合成翻译过程, 且氨基酸在其中发挥着重要的作用^[46]。将适量的氨基酸混合物添加到乳腺组织培养液中可提升50%左右的乳蛋白含量^[47]。Moshel等^[48]和Appuhany等^[49]通过对乳腺上皮细胞的培养试验发现, 亮氨酸和异亮氨酸可以通过mTOR信号通路磷酸化S6K1和4EBP1, 从而促进乳蛋白的合成。Mahmood等^[50]发现, 通过向培养的奶牛乳腺上皮细胞中添加一定浓度的赖氨酸和蛋氨酸后, 可以激活mTOR信号通路的表达^[51]。除氨基酸以外, 小肽也可以通过mTOR信号通路调控乳蛋白的合成。Yang等^[52]将蛋氨酸替换成蛋氨酸-蛋氨酸二肽添加到奶牛乳腺组织中, 发现mTOR通路上的关键基因表达显著增加, 从而促进乳蛋白的合成。Menzies等^[53]的试验结果表明, 胰岛素作用于mTOR信号通路后, 通过4EBP1加快了调节翻译的速度, 进而协调乳蛋白合成速度。Hayashi等^[54]将生长激素注射到奶牛乳腺组织中, 发现生长激素可以通过mTOR途径改变酪蛋白mRNA的起始和翻译, 显著增加牛奶的产量。

1.3 GCN2-eIF2a信号通路

蛋白质合成的过程中其所需氨基酸不可替代, 并必不可少, 因此动物体内必须要有一个监管机制, 有效地监督是否缺乏某种氨基酸^[55], 以避免合成肽链过程中的失败^[56]。在一般性调控中, 阻遏蛋白激酶2 (GCN2) 发挥着重要的作用, 它对空载tRNA具有极高的结合性^[57], 能有效感知各种氨基酸的缺乏和不足^[58]。当氨基酸的含量充足时, 氨基酸与特定的tRNA相连接, 当氨基酸含量不足时, 则GCN2易与空载tRNA相结合从而被激活^[59]。

活化后的GCN2可以磷酸化真核翻译起始抑制因子eIF2a^[60], 通过eIF2a磷酸化引起的翻译起始阻碍来抑制全局蛋白翻译的速率^[61], 从而降低细胞内氨基酸的消

耗量。GCN2还会激活转录因子4 (ATF4)，其是机体中控制适应性功能的相关基因的重要调控子，通过增强某些特定基因的转录，同时促进多巴胺的释放、抑制采食氨基酸失衡饲料^[62]，进而缓解氨基酸缺乏的危害。Timosenko等^[63]发现，营养均衡的培养基细胞中几乎无ATF4，然而当色氨酸或谷氨酰胺缺乏时，ATF4的表达显著增加，且氨基酸转运体的表达也增加，此时再把细胞的ATF4敲除后，也不会影响氨基酸转运体的变化。当敲除肠上皮细胞中的GCN2基因，则会降低氨基酸缺乏时的自噬反应^[64]。缺乏氨基酸会导致GCN2的激活进而引起自噬基因的转录，机体内部通过自噬反应循环利用体内的氨基酸，以弥补氨基酸总量上的不足。

2 展望

提高乳产量和乳质量是奶牛行业一直追求的目标，但仅靠简单地引进高产品种，提升日粮蛋白质水平已不能满足要求。随着细胞分子学的发展，乳蛋白合成信号通路已经成为当前泌乳生物学研究的重点。在乳腺中蛋白质的合成极其复杂，不同环境、不同生理状态下，JAK-STAT、mTOR和GCN2-eIF2a等信号通路在乳蛋白合成过程中均发挥重要作用。全面了解奶牛乳腺蛋白质合成信号通路分子的机理，有助于对奶牛乳腺中乳蛋白的合成进行分析，可为合理调控营养供给、为提高家畜的生产效率提供一定的依据。本文对与乳蛋白合成相关的信号通路进行了综述，希望能为后续的相关研究有一些参考作用，对奶牛的生产产生一定的影响。

参考文献

- [1] 史琳琳,赵锋,高学军,等. 乳蛋白合成信号通路的研究进展[J]. 中国畜牧兽医, 2013, 40(1):130-135.
- [2] 杨金勇. 蛋氨酸、赖氨酸及其二肽对奶牛乳腺上皮细胞酪蛋白 α 基因表达的影响[D]. 杭州:浙江大学, 2006.
- [3] 杨金波,文斯敏,赵瑞. 反刍动物蛋白质及氨基酸营养研究进展[J]. 广东饲料, 2010, 19(6):33-37.
- [4] Sinclair K D, Garnsworthy P C, Mann G E, et al. Reducing dietary protein in dairy cow diets: implications for nitrogen utilization, milk production, welfare and fertility[J]. Animal An International Journal of Animal Bioscience, 2014, 8(2):262-274.
- [5] Appuhamy J A, Bell A L, Nayananjali W A, et al. Essential amino acids regulate both initiation and elongation of mRNA translation independent of insulin in MAC-T cells and bovine mammary tissue slices[J]. Journal of Nutrition, 2011, 141(6):1209-1215.
- [6] 曹洋,艾阳,张源淑. 乳蛋白合成的信号通路营养调控[J]. 畜牧与兽医, 2014, 46(6):133-136.
- [7] Holdorf A D, Lee K H, Burack W R, et al. Regulation of Lck activity by CD4 and CD28 in the immunological synapse[J].

Nature Immunology, 2002, 3(3):259.

- [8] Musso T, Johnston J A, Linnekin D, et al. Regulation of JAK3 expression in human monocytes: phosphorylation in response to interleukins 2, 4, and 7[J]. Journal of Experimental Medicine, 1995, 181(4):1425.
- [9] Clifford L, O'Sullivan L A, Trengove M C, et al. Evolution of JAK-STAT pathway components: mechanisms and role in immune system development[J]. Plos One, 2012, 7(3):e32777.
- [10] Wang Y, Levy D E. Comparative evolutionary genomics of the STAT family of transcription factors[J]. JAK-STAT, 2012, 1(1):23-36.
- [11] Villarino A V, Kanno Y, Ferdinand J R, et al. Mechanisms of Jak/STAT signaling in immunity and disease[J]. Journal of Immunology, 2015, 194(1):21-27.
- [12] Liu X, Robinson G W, Wagner K U, et al. Stat5a is mandatory for adult mammary gland development and lactogenesis[J]. Genes & Development, 1997, 11(2):179.
- [13] Watson C J, Burdon T G. Prolactin signal transduction mechanisms in the mammary gland: the role of the Jak/Stat pathway[J]. Rev Reprod, 1996, 1(1):1-5.
- [14] 王立娜. 氨基酸与STAT5A基因互作对奶牛乳腺上皮细胞泌乳的调节作用及机理[D]. 哈尔滨:东北农业大学, 2014.
- [15] Oliver C H, Watson C J. Making milk: A new link between STAT5 and Akt1[J]. Jakstat, 2013, 2(2):e23228.
- [16] 史琳琳. 奶牛乳腺上皮细胞JAK2-STAT5和mTOR信号通路协同调控乳蛋白合成[D]. 哈尔滨:东北农业大学, 2013.
- [17] Bionaz M, Loo J J. Gene networks driving bovine mammary protein synthesis during the lactation cycle[J]. Bioinform Biol Insights, 2011, 2011(5):83-98.
- [18] Molento C F M, Block E, Cue R I, et al. Effects of insulin, recombinant bovine somatotropin, and their interaction on insulin-like growth factor-I secretion and milk protein production in dairy cows[J]. Journal of Dairy Science, 2002, 85(4):738-747.
- [19] Yang J, Kennelly J J, Baracos V E. The activity of transcription factor Stat5 responds to prolactin, growth hormone, and IGF-I in rat and bovine mammary explant culture[J]. Journal of Animal Science, 2000, 78(12):3114-3125.
- [20] 曹洋,艾阳,张源淑. 乳蛋白合成的信号通路营养调控[J]. 畜牧与兽医, 2014, 46(6):133-136.
- [21] Yu-Ling H, Feng Z, Chao-Chao L, et al. SOCS3-mediated blockade reveals major contribution of JAK2/STAT5 signaling pathway to lactation and proliferation of dairy cow mammary epithelial cells in vitro[J]. Molecules, 2013, 18(10): 12987-13002.
- [22] Barclay J L, Anderson S T, Waters M J, et al. SOCS3 as a tumor suppressor in breast cancer cells, and its regulation by PRL[J]. International Journal of Cancer, 2010, 124(8):1756-1766.
- [23] Kimball S R, Jefferson L S. New functions for amino acids: effects on gene transcription and translation[J]. American Journal of Clinical Nutrition, 2006, 83(2):500S.
- [24] Dario B, Tsung-Ming Y, Morgan J R, et al. Mammalian target of rapamycin contributes to the acquired apoptotic resistance of human mesothelioma multicellular spheroids[J]. Journal of Biological Chemistry, 2008, 283(19):13021-13030.
- [25] 余婕,晏向华. 氨基酸调节哺乳动物雷帕霉素靶蛋白复合体1信号通路的分子机制[J]. 动物营养学报, 2015, 27(7):2012-2017.

- [26] Martelli A M, Faenza I, Billi A M, et al. Intracellular 3' -phosphoinositide metabolism and Akt signaling: New mechanisms for tumorigenesis and protection against apoptosis[J]. Cellular Signalling, 2006, 18(8):1101-1107.
- [27] Franke T F. Intracellular signaling by Akt: bound to be specific[J]. Science Signaling, 2008, 1(24):e29.
- [28] 张霞,孙琳琳,钟殿胜. LKB1-AMPK-mTOR信号传导通路在肿瘤中的研究进展[J]. 中国肺癌杂志, 2011, 14(08): 685-688.
- [29] 高海娜. 必需氨基酸通过mTOR信号通路调控乳蛋白合成研究进展[C]. 中国陕西西安: 2014.
- [30] Biplab D, Jeong Sun J, Yo S, et al. The AMPK β 2 subunit is required for energy homeostasis during metabolic stress[J]. Molecular & Cellular Biology, 2012, 32(14):2837.
- [31] Hardie D. AMPK and Raptor: matching cell growth to energy supply[J]. Molecular Cell, 2008, 30(3):214-226.
- [32] Zhang B B, Zhou G, Cai L. AMPK: An Emerging Drug Target for Diabetes and the Metabolic Syndrome[J]. Cell Metabolism, 2009, 9(5):407-416.
- [33] Mihaylova M M, Shaw R J. The AMPK signalling pathway coordinates cell growth, autophagy and metabolism[J]. Nature Cell Biology, 2011, 13(9):1016-1023.
- [34] Park S H, Gammon S R, Knippers J D, et al. Phosphorylation-activity relationships of AMPK and acetyl-CoA carboxylase in muscle. [J]. Journal of Applied Physiology, 2002, 92(6):2475-2482.
- [35] D Grahame H. AMPK--sensing energy while talking to other signaling pathways[J]. Cell Metabolism, 2014, 20(6):939-952.
- [36] Gowans G J, Hawley S A, Ross F A, et al. AMP is a true physiological regulator of AMP-activated protein kinase by both allosteric activation and enhancing net phosphorylation[J]. Cell Metabolism, 2013, 18(4):556-566.
- [37] D Grahame H, Ross F A, Hawley S A. AMPK: a nutrient and energy sensor that maintains energy homeostasis[J]. Nat Rev Mol Cell Biol, 2012, 13(4):251-262.
- [38] Appuhamy J A D R, Nayananjali W A, England E M, et al. Effects of AMP-activated protein kinase (AMPK) signaling and essential amino acids on mammalian target of rapamycin (mTOR) signaling and protein synthesis rates in mammary cells[J]. Journal of Dairy Science, 2014, 97(1):419-429.
- [39] Burgos S A, Dai M, Cant J P. Nutrient availability and lactogenic hormones regulate mammary protein synthesis through the mammalian target of rapamycin signaling pathway[J]. Journal of Dairy Science, 2010, 93(1):153-161.
- [40] Avruch J, Long X, Ortiz-Vega S, et al. Amino acid regulation of TOR complex 1. [J]. AJP Endocrinology & Metabolism, 2009, 296(4):E592-E602.
- [41] 陈洪菊,屈艺,母得志. mTOR信号通路的生物学功能[J]. 生命的化学. 2010, 30(4):555-561.
- [42] Lamming D W, Cummings N E, Rastelli A L, et al. Restriction of dietary protein decreases mTORC1 in tumors and somatic tissues of a tumor-bearing mouse xenograft model[J]. Oncotarget, 2015, 6(31):31233-31240.
- [43] Adiel C, Hall M N. An amino acid shuffle activates mTORC1[J]. Cell, 2009, 136(3):399-400.
- [44] Goberdhan D I, Wilson C, Harris A. Amino Acid Sensing by mTORC1: Intracellular Transporters Mark the Spot[J]. Cell Metabolism, 2016, 23(4):580-589.
- [45] Duan Y, Li F, Tan K, et al. Key mediators of intracellular amino acids signaling to mTORC1 activation[J]. Amino Acids, 2015, 47(5):857-867.
- [46] Kimball S R, Jefferson L S. Role of amino acids in the translational control of protein synthesis in mammals[J]. Seminars in Cell & Developmental Biology, 2005, 16(1):21-27.
- [47] Burgos S A, Dai M, Cant J P. Nutrient availability and lactogenic hormones regulate mammary protein synthesis through the mammalian target of rapamycin signaling pathway[J]. Journal of Dairy Science, 2010, 93(1):153-161.
- [48] Yana M, Rhoads R E, Itamar B. Role of amino acids in translational mechanisms governing milk protein synthesis in murine and ruminant mammary epithelial cells[J]. Journal of Cellular Biochemistry, 2010, 98(3):685-700.
- [49] Appuhamy J A D R, Nayananjali W A, England E M, et al. Effects of AMP-activated protein kinase (AMPK) signaling and essential amino acids on mammalian target of rapamycin (mTOR) signaling and protein synthesis rates in mammary cells[J]. Journal of Dairy Science, 2014, 97(1):419-429.
- [50] Xuemei N, Dengpan B, Xiyan L, et al. Ratio of lysine to methionine alters expression of genes involved in milk protein transcription and translation and mTOR phosphorylation in bovine mammary cells[J]. Physiological Genomics, 2014, 46(7):268-275.
- [51] Xiaodong L, Lena S, Hong X, et al. Human receptors for sweet and umami taste[J]. Proceedings of the National Academy of Sciences of the United States of America, 2002, 99(7):4692-4696.
- [52] Yang J X, Wang C H, Xu Q B, et al. Methionyl-Methionine Promotes α -s1 Casein Synthesis in Bovine Mammary Gland Explants by Enhancing Intracellular Substrate Availability and Activating JAK2-STAT5 and mTOR-Mediated Signaling Pathways[J]. Journal of Nutrition, 2015, 145(8):1748-1753.
- [53] Menzies K K, Lefèvre C, Macmillan K L, et al. Insulin regulates milk protein synthesis at multiple levels in the bovine mammary gland[J]. Functional & Integrative Genomics, 2009, 9(2):197-217.
- [54] Hayashi A A, Nones K, Roy N C, et al. Initiation and elongation steps of mRNA translation are involved in the increase in milk protein yield caused by growth hormone administration during lactation[J]. Journal of Dairy Science, 2009, 92(5):1889-1899.
- [55] Sophie F, Iadh M, Gildas B, et al. Tryptophan depletion and the kinase GCN2 mediate IFN- γ -induced autophagy[J]. Journal of Immunology, 2012, 189(6):2954-2964.
- [56] Alejo E, Comb W C, Sabatini D M. Nutrient-sensing mechanisms and pathways[J]. Nature, 2015, 517(7534):302.
- [57] 黄鑫. 核因子 κ B1调控奶牛乳腺上皮细胞乳合成和细胞增殖的作用机理[D]. 哈尔滨:东北农业大学, 2017.
- [58] 何流琴,周锡红,李铁军,等. 氨基酸信号对mTOR和GCN2通路的影响研究进展[J]. 生命科学, 2016, 11:1398-1404.
- [59] Sebastian L, Jinwei Z, Stefan R, et al. Interaction between the tRNA-binding and C-terminal domains of Yeast Gcn2 regulates kinase activity in vivo[J]. Plos Genetics, 2015, 11(2):e1004991.
- [60] Tsalikis J, Croitoru D O, Philpott D J, et al. Nutrient sensing and metabolic stress pathways in innate immunity[J]. Cellular Microbiology, 2013, 15(10):1632-1641.
- [61] Deval C, Talvas J, Chaveroux C, et al. Amino-acid limitation

- induces the GCN2 signaling pathway in myoblasts but not in myotubes[J]. Biochimie, 2008, 90(11):1716-1721.
- [62] Bjordal M, Arquier N, Kniazeff J, et al. Sensing of Amino Acids in a Dopaminergic Circuitry Promotes Rejection of an Incomplete Diet in Drosophila[J]. Cell, 2014, 156(3):510-521.
- [63] Timosenko E, Ghadbane H, Silk J D, et al. Nutritional Stress Induced by Tryptophan-Degrading Enzymes Results in ATF4-Dependent Reprogramming of the Amino Acid Transporter Profile in Tumor Cells[J]. Cancer Research, 2016, 76(21): 6193.
- [64] Ravindran R, Loebbermann J, Nakaya H I, et al. The amino acid sensor GCN2 controls gut inflammation by inhibiting inflammasome activation[J]. Nature, 2016, 531(7595):523-527.

Research Progress in Regulating the Signal Pathway of Milk Protein Synthesis

WANG Dong-yang, XIE Yue-qin, LUO Jun-yi, CHEN Ting, XI Qian-yun, ZHANG Yong-liang, SUN Jia-jie
(College of Animal Science, South China Agricultural University, National Engineering Research Center for Breeding Swine Industry, Guangzhou 510642)

Abstract: This review makes an introduction on the composition of milk protein synthesis about JAK-STAT, mTOR and GCN2-eIF2a signaling pathways, the regulatory roles and mechanisms of the milk protein synthesis on these signaling pathways. The research progress on JAK-STAT, mTOR and GCN2-eIF2a signaling pathways in recent years was reviewed, providing a theoretical basis for the research on milk protein synthesis signaling pathway.

Key words: Milk protein; JAK-STAT; mTOR; GCN2-eIF2a 

好 书 速 递

《中国奶业年鉴（2018卷）》

出版时间：2019年10月 定价：580.00



《中国奶业年鉴》是反映我国奶业发展情况的综合性年刊，也是农业农村部年鉴系列中的一部重要产业年鉴，2002年经农业农村部（原农业部）批准由中国奶业协会组织编纂，已经连续出版十六卷，其中2012卷、2017卷分别获第五届年鉴编纂出版质量评比综合二等奖、第六届年鉴编纂出版质量评比综合一等奖。2018卷为第十七卷本。

《中国奶业年鉴》自出版发行以来，客观记述了我国奶业的发展历程，反映了奶业生产的实际情况，为行业管理部门制定规划、政策和实施决策提供了依据，为奶业生产经营者提供了技术和数据支持，为广大消费者提供了市场和信息引导，是中国奶业发展的编年史册，也是奶业行业发展的公报。

行业数据主要采用国家统计局、海关总署、国家发展和改革委员会的统计数据，部分数据资料由农业农村部畜牧兽医局、全国畜牧总站和中国奶业协会等单位提供。2018卷所刊载资料一般截至2017年年底，部分时效性较强的资料不限于2017年。

购书方式：

联系电话：010-62673004

将书款直接汇款到下列帐号：

账 户 名：北京四而博达广告有限公司

账 号：0200006109200118951

开户银行：中国工商银行北京清河镇支行

汇款时请注明汇款人姓名和联系方式，以便邮寄图书。

Advances in the Evaluation and Application of Nutritionally Valuable Woody Feeding Plants

Xie Y^{1*}, Chen Z^{2#}, He Q², Luo J¹, Chen T¹, Xi Q¹, Zhang Y^{1*}, Sun J^{1*}

¹College of Animal Science, Guangdong Provincial Key Laboratory of Animal Nutrition Control, National Engineering Research Center for Breeding Swine Industry, South China Agricultural University, Guangzhou, Guangdong 510642, China

²College of Forestry and Landscape Architecture, Guangdong Engineering & Research Center for Woody Fodder Plants, South China Agricultural University, Guangzhou, Guangdong 510642, China

#authors contributed equally to this work

*Corresponding author: Zhang Y and Sun J, College of Animal Science, Guangdong Provincial Key Laboratory of Animal Nutrition Control, National Engineering Research Center for Breeding Swine Industry, South China Agricultural University, Guangzhou, Guangdong 510642, China, E-mail: zhangyl@scau.edu.cn, jjajiesun@scau.edu.cn

Received Date: October 24, 2020 Accepted Date: November 25, 2020 Published Date: November 27, 2020

Citation: Xie Y (2020) Advances in the Evaluation and Application of Nutritionally Valuable Woody Feeding Plants. J Food Nutr 6: 1-8.

Abstract

This review presents the current status of woody feed resources in China. *Morus alba*, *Moringa*, and *Broussonetia papyrifera* were evaluated with respect to their nutritional value, and their impact on the performance and product quality of herbivores, monogastric and aquatic animals. Feed resources are becoming increasingly scarce in China, and therefore woody forage, as an alternative feed resource, is attracting increasing attention. Woody forage is abundant in nutrients and natural active substances as well as being of high nutritional and feeding value, thereby enhancing the health of livestock and poultry, while improving the quality and flavor of the resulting product. In short, the development of woody plants has many advantages, increasing the feeding and economic value, but also helping solve the problem of feed shortages. The development and utilization of woody plants as a feed resource is therefore of great significance in promoting the stable development of animal husbandry.

Keywords: Woody forage; *Morus alba*; *Moringa*; *Broussonetia papyrifera*; Nutritional value; Feeding effect

Introduction

Woody feed, also known as ‘woodgrass’ or ‘woody forage’, refers to young shoots and leaves, flowers, fruit, seeds and their by-products of woody plants with feeding value that can be used not only for direct grazing, but also for collecting, cutting, and processing [1]. In China, economic development is causing an increase in living standards, thereby increasing the demand for eggs, milk and meat, which is leading to a sharp increase in the development of animal husbandry. Not only is this having a direct effect on grassland areas, which are continually shrinking, but it is also leading to a reduction in the area of grassland occupied by livestock, creating imbalance between livestock and available land. As a result, herb and grain feed resources are no longer able to meet the demands of livestock production.

At present, China is facing a shortage of total feed resources, with a lack of grain-based energy feeds, a severe shortage of protein feeds. Moreover, the supply and demand relationship is currently characterized by a lack of concentrated, protein and green feed, and insufficient overall amounts of feed in general [2,3]. Meanwhile, woody feed resources are particularly rich in nutrients, especially the branches and leaves, which have a high crude protein, amino acid and mineral content [4]. They are therefore an important feeding supplement for ruminant livestock. According to recent reports, China’s existing forest area covers approximately 147.2 million hectares [5]. Meanwhile, the annual average fodder and leaf feed requirements of animal are approximately 500 million tons, while only about 300 million tons are available [6]. The development of woody feed resources is therefore important in helping alleviate feed shortages in the livestock industry, thereby ensuring the stable development of animal husbandry in China.

In this review, we report the current status of woody feed resources in China. To do so, *Morus alba*, *Moringa*, and *Broussonetia papyrifera*, all of which are important woody crops, were evaluated with respect to their nutritional value, and their impact on the performance and product quality of herbivores, monogastric and aquatic animals.

The application status of woody plant feed in China and overseas

Because woody plants are rich in nutrients, they are widely used as a nitrogen source for ruminants. As a result, large amounts of woody plant species are cultivated in parts of Africa, America, Asia and Australia, most of which are used as a protein resource in cow and goat feed. In Africa, the most abundant

and widely used species is *Calliandra calothyrsus*. The earliest research on *C. calothyrsus* was conducted in 2003, revealing high palatability as well as increases in milk quality and an average yield increase of 1.5 L per day when added to cattle feed [7]. In addition, supplementation with *C. calothyrsus* was also found to improve nitrogen retention in cattle fed a low-protein diet [8]. *Albizia lebbeck* is another important woody feed in western Africa, and although abundantly available is poorly valorized [9]. Recent research suggests that *A. lebbeck* could be used as a protein concentrate in dietary supplements to combat widespread malnutrition [10]. Moreover, it also possesses hepatoprotective and antioxidant activity [11] and the platelet anti-aggregation activity *in vitro* [12]. Similar plants include *Bauhinia purpurea* linn and *Cratylia argentea* Benth, both of which are planted widely across North America. Studies have also shown that they can improve the quality and absorption rate of feed as well as the digestibility of crude protein [13,14]. In Asia, 13 species of woody plants are widely used in ruminant feeding systems; namely, *Areca catechu*, *Acacia nilotica*, *A. sieberiana*, *Manihot esculenta*, *Erythrina variegata*, *Ficus exasperata*, *F. bengalensis*, *F. religiosa*, *Gliricidia sepium*, *Artocarpus heterophyllus*, *Albizia lebbeck*, *Prosopis juliflora*, *P. glandulosa*, *Cajanus cajan* and *Tamarindus indica* [15]. A large number of woody feed plants are cultivated in Australia such as *Chamaecytisus proliferus*, *Leucaena leucocephala* and *Atriplex* spp., all of which are used mainly to feed cattle, providing sustainable high productivity [16]. Thus, overall, the development and application of woody plants is relatively widespread around the world.

In China, woody feed cultivation is among the most abundant and the most widely used. Because China has a long standing tradition of woody feed application [17], it is in an excellent situation for the development of new woody feed resources. Due to the complex diversity of woody forage plants, they can be roughly divided into six types according to their appearance: conifer arbor, broadleaf arbor, shrub, semi-shrub, woody cane-brake and bamboo [1]. Of the numerous woody feed resources, research in China tends to have focused on the nutritional and feeding value of *M. alba*, *Moringa* and *B. papyrifera*. The following provides a summary of these studies.

Nutritional Value

Nutritional value of *Morus alba*

The chemical composition of mulberry leaves is extremely complex, and is affected by a number of factors, such as genetic and physiological characteristics as well as the climate, soil and cultivation conditions [18]. In order to meet the de-

mand for specialized edible mulberry varieties, factor analysis was applied to comprehensively evaluate the nutritional quality of leaves from different mulberry germplasms and varieties [19], and the nutritional composition of mulberry is listed in Table 1 [19]. In addition to the basic nutrients, mulberry also possesses indispensable trace elements, while the leaves are rich in protein and contain at least 17 kinds of amino acid, the most abundant of which are glutamic and aspartic acid (13.7 and 12.3%, respectively). Research also illustrates, in addition, that essential amino acids in mulberry leaves account for 32.61% of the requirements of animals [20]. The amino acid contents of mulberry leaves are listed in Table 2 [20].

Table 1: The nutritional composition of mulberry (*Morus alba*) leaves (air-dry basis) [19].

Nutritional component	Content (% / mg/g)
Moisture	61.74-79.30%
Crude protein	13.61-24.97%
Carbohydrate	3.99-17.44%
Ash	0.09-0.23%
Ca	1.05-4.33%
P	0.16-0.62%
S	0.12-0.32%
Mg	0.11-0.45%
Fe	135.29-314.66 mg /g
Mn	18.65-124.75 mg /g
Zn	17.95-45.86 mg /g
Cu	6.85-25.81 mg /g

Table 2: Amino acid contents of mulberry (*Morus alba*) leaves (dry matter basis) (Wang et al., 2015).

Item	Content (mg/g)
Ile	10.0
Leu	27.0
Lys	25.1
Met	9.8
Phe	22.3
Thr	16.6
Val	13.1
Asp	43.8
Ser	19.0
Gly	23.0
Ala	26.1
Glu	48.9
Cys	3.4
Tyr	15.4
His	9.2
Arg	25.9
Pro	18.8

Mulberry leaves are therefore an exceptional source of protein and worth developing as a woody feed resource. Re-

search also suggests that mulberry leaves contain a wide variety of fatty acids, mainly palmitic, linolenic, linoleic, stearic, oleic, arachidic, palmitoleic, behenic and cerotic acid, which account for 26.87, 22.99, 13.40, 6.99, 3.17, 3.43, 3.05, 2.93 and 1.63% of the total, respectively [21]. Mulberry leaves were also found to contain abundant secondary metabolites such as flavonoids, alkaloids and polyphenols [22,23,24], all of which possess numerous bioactivities. The most abundant are flavonoids such as astragalin and quercetin, both of which possess antioxidant activity [25]. The effect of total flavonoids from mulberry leaves on sugar metabolism, antioxidative enzyme and albumin glycosylation activity in diabetic rats was also examined, revealing a decrease in blood glucose and lipid peroxide and an increase in plasma superoxide dismutase activity (SOD) as well as inhibition of albumin glycosylation [26]. With the increasing number of diabetic patients, human studies are focusing on the effects of 1-deoxynojirimycin [27,28], fagomine, and other alkaloids from mulberry leaves [29]. For example, research suggests that 1-deoxynojirimycin, a natural α -glycosidase inhibitor, can reduce increases in postprandial blood glucose and maintain stable blood-sugar levels [30]. Mulberry leaf is therefore of high pharmaceutical value with potential as a natural health care product. However, studies on the effect of bioavailable substances in mulberry leaves on the health of livestock and poultry have yet to be carried out. In animal husbandry, the prospect of mulberry application should therefore be considerable.

Nutritional value of Moringa

The nutritional characteristics of Moringa are also rich, not only the leaves but also the stems, pods and seeds. The most notable features are its high protein and low fiber content. It was previously revealed that Moringa leaf powder had a crude protein content close to 28% and a true protein content of up to 81.3% [31]. Moreover, Moringa leaves were found to contain 14 to 17 fatty acids, of which linolenic acid accounts for 57% [32]. The nutritional composition of Moringa is shown in Table 3 [31,32]. As shown, it contains at least 17 kinds of amino acid, representing a total content of 20.49%. Of these, glutamic and aspartic acid are most abundant, accounting for 14.52% of the total. In addition, Moringa contains five essential amino acids including lysine and threonine, both of which are lacking in animal staple diet [33]. The amino acid content of *Moringa oleifera* is given in Table 4 [33]. Moringa is therefore a potentially good source of protein. Moringa leaves also contain large amounts of vitamins and minerals (Table 5; 34], which were previously shown to overcome the negative effects of iron deficiency in rats [35].

Table 3: Nutritional composition of *Moringa oleifera* leaves (dry matter basis) (Liu and Guo-Hua, 2004; Sánchez-Machado et al., 2010) [31,32].

Nutritional component	Content (%)
Crude protein	27.6
Crude fat	8.65
Crude fiber	7.12
Total starch	5.65
Total sugar	15.12
Total flavonoids	1.09
Linolenic acid	56.87
Palmitic acid	23.28
Linoleic acid	6.11
Oleic acid	5.12
Arachidonate	0.21

Table 4: Amino acid contents of *Moringa oleifera* leaves (dry matter basis) (Rao, 2007) [33].

Item	Content (%)
Glu	3.05
Asp	3.05
Phe	2.00
Leu	1.47
Val	1.34
Lys	1.23
Arg	1.07
Ala	1.06
Ile	1.04
Thr	0.95
Ser	0.90
Gly	0.82
Pro	0.82
Tyr	0.54
Met	0.45
His	0.36
Cys	0.34

Table 5: Vitamin and mineral contents of *Moringa oleifera* leaves (dry matter basis) (Ding, 2014) [34].

Item	Content (mg/kg)
VE	1130.0
Pantothenic acid	891.0
β-carotene	603.0
VC	368.0
VB ₂	19.0
K	15505
Ca	16920
P	5651
Mg	3243
Fe	164.8
Al	133.
Cu	77.6

Item	Content (mg/kg)
Mn	62.5
Zn	47.6
Se	0.6

Moringa also contains a number of active substances such as flavonoids, polysaccharides and polyphenols. According to Tumer et al. (2015), isothiocyanate from Moringa leaves is not only rich in content, but also has a very strong antioxidant capacity. Moringa leaves also contain quercetin, kaempferol, chlorogenic acid and zeatin, all of which have anti-oxidant [36,37], anti-tumor [38] and anti-bacterial effects [39]. Moringa is therefore of potential use as a natural multi-functional health supplement. Saponins, meanwhile, are an inert substance and non-toxic to animals. According to a report, the contents of tannins, trypsin inhibitor, nitrate and oxalic acid in Moringa are very low at 20.7mg/g, 1.45 TIU/g, 17 mg/g and 10.5 mg/g, respectively [40]. Based on these findings, the potential wide-spread use of Moringa as a feed resource should therefore be considered.

Nutritional value of *Broussonetia papyrifera*

B. papyrifera leaves are rich in protein, vitamins, carbohydrates, trace elements, and various amino acids, notably the leaves. The crude protein content is twice that of wheat and three times that of corn and rice, while the crude fat content is twice that of rice and wheat. The only plant with a higher content is soybean; however, the content of nitrogen-free extract is higher in *B. papyrifera* [41]. Table 6 compares the nutritional value of *B. papyrifera* leaves with alfalfa and soybean meal [41]. Zhou [42] previously analyzed the amino acid composition of *B. papyrifera* leaves and found approximately 16 kinds of amino acid, the content of which varied depending on the plant part (Table 7). As shown, seven essential amino acids were found.

Table 6: Nutritional composition of *Broussonetia papyrifera* leaves, alfalfa and soybean meal (air-dry basis) (Tu et al., 2009).

Content (% / mg/kg)			
Item	<i>B. papyrifera</i> leaves	Alfalfa	Soybean meal
Moisture	9.1%	13.0%	11.0%
Crude protein	26.1%	19.1%	44.2%
Crude fat	5.2%	2.3%	1.9%
NDF	15.9%	36.7%	13.6%
ADF	13.0%	25.0%	9.6%
Ash	15.4%	7.6%	6.1%
Ca	3.4%	1.4%	0.3%
Total P	0.2%	0.5%	0.6%
Cu	8.3 mg/kg	9.7 mg/kg	23.5 mg/kg
Fe	247.1 mg/kg	3.6 mg/kg	181.0 mg/kg

Content (% / mg/kg)			
Item	<i>B. papyrifera</i> leaves	Alfalfa	Soybean meal
Mn	50.3 mg/kg	30.7 mg/kg	27.4 mg/kg
Zn	62.9 mg/kg	16.0 mg/kg	45.4 mg/kg
Mg	62.3 mg/kg	3600.0 mg/kg	2700.0 mg/kg

Table 7: Total amino acid content and composition of different parts of the *Broussonetia papyrifera* plant (dry matter basis) (Zhou, 2005).

Content (g /100g)				
Item	Leaves	Aggregate fruit	Male inflorescence	Fruit
Asp	2.55	2.84	2.08	1.50
Thr	1.07	0.39	0.29	0.36
Ser	0.80	0.38	0.46	0.40
Glu	3.13	1.37	3.41	2.18
Gly	1.55	0.73	0.98	1.05
Ala	1.65	0.51	0.43	0.54
Val	1.63	0.57	1.08	0.68
Met	0.41	0.06	0.15	0.09
Ile	1.42	0.47	0.72	0.54
Leu	2.50	0.70	1.06	0.91
Tyr	0.87	0.47	0.33	0.40
Phe	1.43	0.50	0.41	0.58
Lys	1.49	0.58	1.14	0.76
His	0.57	0.29	0.34	0.34
Arg	1.50	1.30	2.65	1.74
Pro	1.57	0.65	0.31	0.30
Cys	0.08	0.04	0.04	0.07

As shown in Tables 6 and 7, *B. papyrifera* leaves also have a high protein content, making them a potentially high-quality plant protein feed. However, they also contain anti-nutritional factors such as tannins. Tannins affect the digestion and absorption of nutrients mainly in combination with other substances in the diet (enzymes, sugars, proteins and metal ions), which can result in precipitation, thereby reducing the overall nutritional value. Processing of *B. papyrifera* leaves is therefore needed prior to potential use as a feed resource.

Feeding Effect

Feeding effect of *Morus alba*

At present, Mulberry leaves are widely used in poultry breeding. Different studies have shown that the addition of mulberry leaf powder to chicken feed has differing effects on laying performance, but a significant effect on overall egg quality [43]. A previous study examined the effect of adding 2.5, 5, 7.5 and 10% mulberry feed to the basic diet of China Agricultural University dwarf layers, revealing significant improvements in yolk

color, the Haugh unit and egg shell thickness as well as indexes of egg shape and egg shell strength at amounts of 7.5 and 10.0% [44]. Study also examined the effect of adding 3, 6, 9 and 12% mulberry leaf powder to the diet of roman layers, and revealed significant increases in yolk color and reductions in damage to the shell [45]. At lower levels, the more powder that was added, the more significant the effect; however, at over 9%, a negative impact on egg production, average egg weight and feed efficiency was observed. Similarly, Wu et al. (2014) added 2, 4, 6 and 8% mulberry powder to the basal diet of Luoman brown layers and revealed a significant ameliorating effect on yolk color; however, at 8%, a significant decrease in total protein, globulin and albumin was observed ($P < 0.05$) along with a significant decrease in food consumption and egg production ($P < 0.01$). They therefore concluded that mulberry, as a protein feed resource, should not exceed 4% of the basal diet of laying hens. Mulberry leaf powder was also found to be beneficial in terms of muscle quality in broiler hens [46]. Addition of 5% mulberry leaves significantly improved the quality of breast muscle by increasing the content of polyunsaturated fatty acids and decreasing the content of saturated fatty acids and the omega 6 to omega 3 ratio. Moreover, Lan et al. (2012) reported that addition of 5% mulberry leaves to the broiler diet reduced the abdominal fat rate. Adding mulberry leaf powder to fowl diet was also found to reduce the phenomenon of feather pecking and decrease the ammonia content in fowl feces, thereby reducing environmental pollution [47].

In swine, addition of mulberry leaf powder to the diet of pigs was found to have a significant effect on pork quality and flavor [48]. Adding 10-15% forage mulberry to the basal diet of finisher pigs did not affect growth performance, and moreover, improved pork quality by slowing down the decrease in muscle pH after slaughter, increasing the fat, polyunsaturated fatty acid, total amino acid and linoleic acid content in the muscle, and decreasing the back fat thickness and content of saturated fatty acids. Meanwhile, another study revealed that basal diet containing 10% mulberry leaves had no effect on the growth rate of finisher pigs, but decreased the leaf lard percentage and back fat thickness, and increased the contents of inosinic acid and fat in the muscle, [49]. Moreover, the mechanism behind these effects was found to be the regulation of fat metabolism and deposition via regulation of sucrose, lipase and glucose-metabolizing enzyme activity in the liver. In addition, mulberry leaf powder was also found to have an important effect on growth performance, meat quality and serum biochemical indexes in finisher pigs [50]. For example, a significant decrease in the average daily gain and significant increase in the ratio of feed to gain was observed in 'Duroc × Yorkshire × Landrace' finisher pigs fed diet containing 15%

mulberry leaf powder in [51]. Moreover, at levels of 5, 10 and 15%, SOD activity and the urea nitrogen content increased significantly along with a significant decrease in the malondialdehyde content in the serum, thereby improving the overall antioxidant performance of the muscle. Furthermore, adding mulberry leaf powder to the diet of breeding sow was also found to have a significant impact on reproductive performance [51].

In herbivores, mulberry leaves can improve rumen fermentation efficiency and digestibility. For example, according to Huyen et al. [52], increasing levels of mulberry leaf pellets (MUP) at a rate of 600g mulberry leaf pellets/head/day, which can improve the apparent digestibility of dry matter, organic matter, crude protein, neutral detergent fiber and acid detergent fiber, and increase in total volatile fatty acid, acetate and butyrate concentrations and the acetate to propionate ratio with a linear. Studies also suggest that the addition of mulberry leaves after silage to the diet of beef cattle can significantly increase the fatty acid content of the meat, including that of arachidate and behenate [53]. Furthermore, addition of mulberry leaf flavonoids to the diet of calves had important effects on energy and nitrogen metabolism, rumen microbial protein synthesis and rumen fermentation [54]. An increase in the metabolizable energy rate and nitrogen biological value of pre-weaning calves, decrease in fecal energy and total excrete nitrogen, increase in the metabolizability of gross energy and utilization of nitrogen in post-weaning calves as well as improvements in rumen fermentation were also observed. Moreover, addition of mulberry leaf powder to the diet of Xiangdong black goats had similar effects, such as an increase in total volatile fatty acids and acetic acid contents, and a significant increase in the ratio of acetic to propionic acid [55]. Dietary supplementation with mulberry leaf powder therefore has significant beneficial effects on rumen fermentation. Mulberry leaves can also promote growth of herbivores to a certain extent, reducing the cost of feeding, and thereby improving economic efficiency. In general, mulberry leaf powder has the potential to reduce the feed gain ratio, while increasing dry matter intake, daily gain, and milk production and performance.

Moreover, in aquatic animals, with the shortage of fishmeal resources and increasing prices, the search is on for an alternative plant feed source. Mulberry leaf powder could therefore be added to aquatic feed as a protein source; however, its crude fiber content is high, and there are a number of anti-nutritional that could have negative effects on aquatic animals when added to excess. Chen et al. (2015) revealed no effects on growth when 40% fish meal was replaced with fermented mulberry leaf protein in a low fish meal diet (fish meal content: 5%), while 80% inhibited growth, but effectively reduced blood glucose and lipid

contents. Moreover, Shen et al. (2016) confirmed these results, revealing that a low level of fermented mulberry leaf powder had no effect on growth of Tilapia, while high levels inhibited growth, but decreased serum lipid and blood glucose levels, and enhanced the antioxidant ability in hyperlipidemic Tilapia with in a dose-dependent manner. Overall, therefore, mulberry leaf powder could be added to aquatic animal feed, but not at excessive quantities.

Meanwhile, according to Hou [56], rex rabbit fed a diet supplemented with 10% mulberry leaf powder had a lower ratio of feed to weight gain, with an increase in amino acids in the muscles, improving overall flavor and meat quality. Since mulberry leaves have a high protein content, Jiao et al. (2016) also investigated its potential use as rabbit protein fodder, revealing no effect on the daily gain, feed intake or feed weight ratio. Mulberry leaf powder could therefore completely replace alfalfa as protein fodder for growing rabbits.

Feeding effect of Moringa

As mentioned above, Moringa is rich in nutrients and can therefore be used as feed for broiler and laying hens. Research on the application of Moringa in animal husbandry is therefore increasing. A study has shown that up to 15% Moringa leaf powder could be incorporated into the broiler diet without adverse effects on haematological and serum biochemical indices; however, up to 20% caused a significant increase in the uric acid concentration [57]. Moreover, Kumar et al. (2017) examined the effect of *M. oleifera* leaf meal on growth performance as well as the lipid profile and meat fatty acid composition of Vanaraja chicken, revealing a significant decrease in total cholesterol and triglyceride levels, and significant improvements in the fatty acid composition. Furthermore, addition of *M. oleifera* leaves also enhanced the ability of broiler hens to resist heat stress [58] and improved the meat quality and antioxidant capacity [59]. Moreover, *M. oleifera* leaf was also found to have a vital effect on performance, egg quality, plasma parameters and organ histopathological indices in laying hens [60]. Dietary supplementation with 5% *M. oleifera* leaf also improved yolk color and protein absorption without adverse effects on laying performance or egg quality [60]. Moreover, dietary supplementation with 8% was found to significantly decrease the concentration of low density lipoprotein and total cholesterol [61]. Thus, Moringa leaf powder has no negative effects on production performance, egg quality, the nutritional composition of the yolk or serum biochemical indexes in laying hens, while improving yolk color and decreasing blood fat. These findings are therefore highly significant in terms of the development of new feed resources.

In swine, research on Moringa is currently focused on finisher pigs. Cross-bred (Duroc × Landrace × Yorkshire) finisher pigs fed a basal diet supplemented with 3, 6 and 9% Moringa leaf showed a significant increase in final body weight, carcass straight length, serum SOD activity and average daily gain, with a significant decrease in the ratio of feed to gain, back fat thickness and serum malondialdehyde [62]. In addition, 5% Moringa oleifera leaf meal to finisher pig feed had no negative effect on feed conversion efficiency, carcass or meat quality traits, and even improved shelf life [63]. However, Moringa leaf powder was also found to have a negative effect on the growth performance of finisher pigs when the concentration was too high [64]. Meanwhile, in Mong Cai pigs, addition of Moringa leaf powder not only had no negative effect on growth, but also has maintained nitrogen balance, thereby improving the digestion and utilization of nitrogen [65]. According to these findings, Moringa-based meal could constitute an important protein source in the diet of growing pigs.

In herbivores, Moringa can also be used as high-quality roughage in dairy cow farming, mainly as green fodder and silage. *Moringa oleifera*, both fresh and ensiled, was previously compared with Elephant grass as the main feedstuff of dairy cows [66]. Accordingly, fresh Moringa treatment was found to increase the grassy flavor and aroma of the milk, while ensiled Moringa increased the digestibility of both protein and fiber. Meanwhile, the partial replacement of alfalfa hay and maize silage with *M. oleifera* silage had no negative effects on milk yield, in vivo nutrient apparent digestibility or serum biochemical indexes in lactating cows, thereby reducing feeding costs and increasing economic efficiency [67]. Due to its high protein content, it was also found that Moringa leaf meal could replace soybean meal in the dairy cow diet with no significant effect on milk composition or the organoleptic characteristics of the milk [68]. A study also revealed that milk yield, 4% fat corrected milk and energy corrected milk increased significantly in dairy cows fed *M. oleifera* [69]. More importantly, replacement of 50% alfalfa with *M. oleifera* leaves and peduncles was found to have an important impact on production performance, and plasma biochemical, antioxidant and immune indexes in lactating dairy cows [70]. It has also been shown that 15% Moringa leaf powder to the diet can increase milk yield and energy corrected milk and feed intake, while enhancing nutrient digestibility and ruminal fermentation in goats [71]. An increase in growth performance in goats was also observed, with improvements in carcass quality and flavor [72]. These studies all confirm that Moringa leaf powder can be used as a high-quality protein feed resource for ruminants.

However, in aquatic animals, Moringa application is very rare because of its anti-nutritional factors such as polyphenols,

tannins, saponins and phytic acid, all of which have a negative effect on the growth and health of fish. However, studies also suggest that dietary supplementation with *M. oleifera* leaves significantly improves growth performance and increases the muscle protein profile, potentially improving the quality of fish and increasing aquaculture yield [73]. Thus, the use of Moringa as aquatic animal feed requires further attention.

Feeding effect of *Broussonetia papyrifera*

As mentioned above, *B. papyrifera* leaves are rich in protein, amino acids, vitamins and various trace elements, making them a good source of unconventional feed. A number of studies have reported that mulberry leaves could replace the basic diet of broiler hens, with no significant effect on yield. For example, adding fermented *B. papyrifera* leaves not only had no adverse effects on growth of AA broilers, but also increased the pH of the muscles and the content of IMP + HxR, thereby improving meat quality [74]. *B. papyrifera* leaves have also been shown to be suitable for laying hens. For example, Li [75] examined the effects on production performance, egg quality, serum biochemical parameters and immunity, revealing significant increases in yolk color, and the relative weight and thickness of the shell. Moreover, expression of IL-2 mRNA in the spleen was also significantly improved; that is, the Th1 immune response was promoted.

In swine, *B. papyrifera* leaves have mainly been used in growing and finisher pigs, with few reports on sows and weaned piglets. The leaves are rich in nutrients, but the fiber content is high and the protein structure is complicated, hindering digestion and resulting in nutrient loss if fed directly to monogastric animals. As a result, *B. papyrifera* leaves need to be processed prior to use. For example, studies have shown that adding fermented leaves to the diet can significantly reduce the thickness of the backfat and significantly increase the average daily gain of growing pigs as well as the content of free amino acids and sodium glutamate in the muscles, deepening the color of the meat [76]. It is well known that pork taste has a direct positive correlation with intramuscular fat content and meat flavor. Addition of *B. papyrifera* leaf powder could therefore have a positive effect on fat deposition in growing pigs, and therefore, taste of the final product. *B. papyrifera* leaves were also fed to growing pigs by fermentation, with improvements in both the quality and feed efficiency, as well as a positive weight gain effect [77].

In contrast, few reports have documented the application of *B. papyrifera* leaves in cattle and sheep diets. However, one study revealed that cow feed containing the leaves of *B. papyrifera* had no effect on milk production, milk fat or milk protein, but reduced economic costs [74]. In addition, positive effects on growth

performance and the blood profile of West African Dwarf sheep were revealed [78]. Thus, while application of *B. papyrifera* leaves in herbivore diets remains limited, it could potentially replace expensive feeds, thereby reducing farming costs.

Conclusions

The findings of this review suggest that alternative resources such as *Morus alba*, *Moringa* and *Broussonetia papyrifera* could be used in animal feed, while maintaining productivity and the quality of meat, eggs and milk. Although research on the feeding value of woody plants in China has achieved fruitful results, and has since been applied to animal husbandry, resulting in economic, ecological and social gains, China's livestock and poultry feed conversion efficiency rates remain low because of continuing problems with the development, production and utilization of woody feed. To maximize the economic benefits, it is therefore necessary to fully understand the feed values, while developing further technologies aimed at actively realizing the production and application of woody feed. Comprehensive evaluation is therefore important to fully exploit the feeding value of woody plants. Moreover, the utilization value of woody plants is also significantly higher than that of herbaceous feed plants, and therefore, combined with existing feed resources in agriculture production, forestry, animal husbandry and other sideline industries, could aid further economic and ecological benefits.

Acknowledgments

This work was supported by grants from the National Key Research and Development Program of China [2018YFD0501706], and Technical System of Modern Agricultural Industry in Guangdong Province [2018LM1121, 2018LM2158].

References

1. Jing DB, Pei J, Kou LI, Zhang ZW, Zhang CG, et al. (2003) The exploration, manufacture and application of feeding xylophyta resources. *Acta Pratacultural Sci* 12: 7-13.
2. Yue Gao HU, Zhi Jian LI, Zhao HH, Zeng ZH (2000) The status and production of green feed, and progress in its research. *Journal of Natural Resources* 2000: 194-6.
3. Nie L, Peng J, Chang J, Liu X (2012) Research Status and Progress of Woody Fodder Plants. *Chinese Agricultural Science Bulletin* 28: 1-4.
4. Papanastasis VP, Yiakoulaki MD, Decandia M, Dini-Papanastasi O (2008) Integrating woody species into livestock feeding in the Mediterranean areas of Europe. *Animal Feed Science & Technology* 140: 1-17.
5. Daowei XU, Liu J, Hong W, Zhongsheng HE (2017) Distribution balance on forest ecology and wild plants nature reserves in China. *J Fujian Agri Forestry University*.
6. Li M, Zi X, Zhou H (2011a) Research advance on woody forage in China. *China Feed* 2011: 34-8.
7. Kingamkono M, Lyamchai C (2003) Sensitisation and dissemination of *Calliandra calothyrsus* in Marangu, Mshiri, Masai villages in Moshi Rural District, Tanzania.
8. Korir D, Goopy JP, Gachui C, Butterbachbahl K (2016) Supplementation with *Calliandra calothyrsus* improves nitrogen retention in cattle fed low-protein diets. *Anim Prod Sci* 56: 619-26.
9. Larbi A, Smith JW, Kurdi IO, Adekunle IO, Raji AM, et al. (1996) Feed value of multipurpose fodder trees and shrubs in West Africa: edible forage production and nutritive value of *Millettia thonningii* and *Albizia lebbek*. *Agrofor Syst* 33: 41-50.
10. Khan LH, Varshney VK (2017) Chemical Utilization of *Albizia lebbek* Leaves for Developing Protein Concentrates as a Dietary Supplement. *J Dietary Supplements* 15: 386-97.
11. Sokkar NM, Elhawary SM, Slem AM, Talaat Z, Sokkar NM, et al. (2016) The Phenolic Composition of the Hepatoprotective and Antioxidant Fractions of *Albizia lebbek* L. *Quím Nova* 39.
12. El-Gamal AA, Abd-El-Halim ME, Kalil AT, Basudan OA, Al-Rehaily AJ, et al. (2010) A novel β -lactam derivative, albactam from the flowers of *Albizia lebbek* with platelets anti-aggregatory activity in vitro. *Pak J Pharm Sci* 28: 745-53.

13. Jank L, Valle CBD, Carvalho PDF, Reynolds SG, Frame J (2005) New grasses and legumes: advances and perspectives for the tropical zones of Latin America. Grasslands Developments Opportunities Perspectives, Science Publishers, USA.
14. Sánchez NR, Spörndly E, Ledin I (2006) Effect of feeding different levels of foliage of *Moringa oleifera* to creole dairy cows on intake, digestibility, milk production and composition. *Livestock Science* 101: 24-31.
15. Speedy A, Pugliese PL (1992) Legume trees and other fodder trees as protein sources for livestock. Proceedings. Fao Animal Production & Health Paper.
16. Lefroy E (2002) Forage Trees and Shrubs in Australia: Their Current Use and Future Potential, Australia.
17. Tang Y, Chen KM, Xie JS, Chen JZ (2002) Role and Potential of Woody Fodder Development and Its Potential in Soil Conservation. *Research of Soil & Water Conservation* 9: 150-4.
18. Liu J, Xiao GS, Liao ST, Zou YX, Gao YC, et al. (2011) Nutrients Analysis and Quality Evaluation of Mulberry Leaves from different Sources. *Modern Food Sci Technol* 27: 1520-6.
19. Zheng S, Zeng W, Han L, Liu C, Maode YU, et al. (2017) Comprehensive Evaluation of Nutritional Quality of Leaves from 45 Mulberry Germplasms and Varieties 38: 159-63.
20. Wang F, Qiao L, Zhang Q, Shen B (2015) Amino Acid Composition and Nutritional Evaluation of Mulberry Leaves. *Food Science* 36: 225-8.
21. Zhou Y (2004) Analysis of fatty acids in mulberry leaves by GC-MS. *Guangxi Sciences* 2004: 116-20.
22. Hirayama C, Wasano KN (2007) Differential effects of sugar-mimic alkaloids in mulberry latex on sugar metabolism and disaccharidases of Eri and domesticated silkworms: Enzymatic adaptation of *Bombyx mori* to mulberry defense. *Insect Biochem Mol Biol* 37: 1348-58.
23. Tallini LR, Pedrazza GPR, Bordignon SADL, Costa ACO, Steppe M, et al. (2015) Analysis of flavonoids in *Rubus erythroides* and *Morus nigra* leaves extracts by liquid chromatography and capillary electrophoresis. *Revista Brasileira De Farmacognosia* 25: 219-27.
24. Nchez-Salcedo SÁ, Tassotti EM, Del M, Hernã RD, MartãNez NF, et al. (2016) (Poly)phenolic fingerprint and chemometric analysis of white (*Morus alba* L.) and black (*Morus nigra* L.) mulberry leaves by using a non-targeted UHPLC-MS approach. *Food Chemistry* 212: 250-5.
25. Kim SY, Gao JJ, Lee WC, Ryu KS, Lee KR, et al. (1999) Antioxidative flavonoids from the leaves of *Morus alba*. *Archives Pharma Res* 22: 81-5.
26. Xiang-Rong LI, Xiao F, Ling-Ying YU (2005) Effect of flavonoids from mulberry leaves on antioxidative enzyme and albumin glycosylation in diabetic rat. *Journal of Zhejiang University* 2005: 88-91.
27. Li YG, Ji DE, Zhong S, Lv ZQ, Lin TB, et al. (2011b) Hybrid of 1-deoxynojirimycin and polysaccharide from mulberry leaves treat diabetes mellitus by activating PDX-1/insulin-1 signaling pathway and regulating the expression of glucokinase, phosphoenolpyruvate carboxykinase and glucose-6-phosphatase in alloxan. *J Ethnopharmacol* 134: 961-70.
28. Xu B, Zhang DY, Liu ZY, Zhang Y, Liu L, et al. (2015) Rapid determination of 1-deoxynojirimycin in *Morus alba* L. leaves by direct analysis in real time (DART) mass spectrometry. *J Pharm Biomed Anal* 114: 447-54.
29. Yang Z, Wang Y, Wang Y, Zhang Y (2012) Bioassay-guided screening and isolation of α -glucosidase and tyrosinase inhibitors from leaves of *Morus alba*. *Food Chemistry* 131: 617-25.
30. Kimura T, Nakagawa K, Kubota H, Kojima Y, Goto Y, et al. (2007) Food-grade mulberry powder enriched with 1-deoxynojirimycin suppresses the elevation of postprandial blood glucose in humans. *J Agri Food Chem* 55: 5869-74.
31. Liu CF, Guo-Hua LI (2004) Nutritional Value of Drumstick Tree Leaves. *Trop Agric Sci Technol* 2004: 27-9.
32. Sánchez-Machado DI, Núñez-Gastélum JA, Reyes-Moreno C, Ramírez-Wong B, López-Cervantes J (2010) Nutritional Quality of Edible Parts of *Moringa oleifera*. *Food Analytical Methods* 3: 175-80.
33. Rao Z (2007) Study on nutrients of *moringa oleifera*. *Modern Instruments* 13: 18-20.
34. Ding YQ (2014) Determination of mineral elements in *Moringaoleifera* leaves by microwave digestion and ICP-OES method. *Fujian Agri Sci Technol* 45: 11-4.
35. Saini RK, Manoj P, Shetty NP, Srinivasan K, Giridhar P (2014) Dietary iron supplements and *Moringa oleifera* leaves influence the liver hepcidin messenger RNA expression and biochemical indices of iron status in rats. *Nutrition Research* 34: 630-8.
36. Verma AR, Vijayakumar M, Mathela CS, Rao CV (2009) In vitro and in vivo antioxidant properties of different fractions of *Moringa oleifera* leaves. *Food & Chemical Toxicology* 47: 2196-201.

37. Ndhlala AR, Rofhiwa M, Bhekumthetho N, Abdelgadir HA, Plooy CP, et al. (2014) Antioxidant, antimicrobial and phytochemical variations in thirteen *Moringa oleifera* Lam. cultivars. *Molecules* 19: 10480-94.
38. Jung IL (2014) Soluble extract from *Moringa oleifera* leaves with a new anticancer activity. *Plos One* 9: e95492.
39. Ping-Hsien C, Chi-Wei L, Jia-Ying C, Murugan M, Bor-Jinn S, et al. (2007) Anti-fungal activity of crude extracts and essential oil of *Moringa oleifera* Lam. *Bioresour Technol* 98: 232-6.
40. Teixeira EM, Carvalho MR, Neves VA, Silva MA, Arantespereira L (2014) Chemical characteristics and fractionation of proteins from *Moringa oleifera* Lam. leaves. *Food Chemistry* 147: 51-4.
41. Tu Y, Diao QY, Zhang R, Yan GL, Xiong W (2009) Analysis on feed nutritive value of hybrid *Broussonetia papyrifera* leaf. *Pratacultural Science* 13: 30-4.
42. Zhou F (2005) Amino acids analysis of the leaves, flowers and fruits of *Broussonetia papyrifera*. *Journal of Pharmaceutical Practice* 2005: 154-6.
43. Zhang X, Zhu J, Li H, Yan H, Jiang G (2018b) Effects of mulberry leaf powder on performance of laying hens, egg quality and Haugh unit during the storage process. *Feed Industry* 39: 32-5.
44. Zhang XM, Ren FZ, Ke-Shan GE (2007) Effects of Mulberry Leaves on Performance of Hen Laying and Eggs Quality. *Food Science* 2007: 89-91.
45. Liu XM, Zeng YH (2011) Effects of Adding Mulberry-leaf Powder to Feed on Laying Performance of Layers and Egg Quality. *Human Agri Sci* 2011: 132-6.
46. Margareta O, Diana CR, Maria CG, Mariana R, Tatiana P, et al. (2015) Effect of dietary mulberry (*Morus alba*) leaves on performance parameters and quality of breast meat of broilers. *Indian Journal of Animal Sciences* 85: 291-5.
47. Zhang NF, Diao QY, Wang HY, Huang WM, An FG, et al. (2009) Effects of mulberry leaf on production performance and egg quality of layers. *China Poultry* 31: 19-22.
48. Yang J, Cao HZ, Tong-Zhou LI, Hai-Yan BU, Hou XF, et al. (2015) Nutritional value of forage mulberry for growing-finishing pigs. *Chinese Journal of Veterinary Science* 35: 1371-4.
49. Yougui LI (2012) Effects of Dietary Mulberry Leaf on Growth Performance, Fat Metabolism and Meat Quality of Finishing Pigs. *Chinese Journal of Animal Nutrition* 24: 1805-11.
50. Song Q, Wei Q, Zou Z, Zhou Q, Liu L, et al. (2016) Effects of Mulberry Leaf Powder on Growth Performance, Meat Quality and Serum Biochemical Indexes in Finishing Pigs. *Chinese Journal of Animal Nutrition* 28: 541-7.
51. Zeng Z, Bing YU, Jie YU, Chen D (2018) Nutritional Value of Mulberry Leaf and Its Application in Animal Production. *Chinese Journal of Animal Nutrition* 30: 468-75.
52. Huyen NT, Wanapat M, Navanukraw C (2012) Effect of Mulberry leaf pellet (MUP) supplementation on rumen fermentation and nutrient digestibility in beef cattle fed on rice straw-based diets. *Anim Feed Sci Technol* 175: 8-15.
53. Jeon BT (2012) Effects of mulberry (*Morus alba* L) silage supplementation on the haematological traits and meat compositions of Hanwoo (*Bos taurus coreanae*) steer. *Afr J Agric Res* 7: 662-8.
54. Yang C, Diao Q, Peibin QU, Bingwen SI, Junnan MA, et al. (2016) Effects of *Candida tropicalis* and Mulberry Leaf Flavonoids on Nutrient Metabolism and Rumen Fermentation of Calves. *Chinese Journal of Animal Nutrition* 28: 224-34.
55. Hao-Bang LI, Zeng P, Sheng LI, Zhou CS, Lei H, et al. (2016) Effects of Mulberry Leaves Powder on Rumen Fermentation Parameters for Xiangdong Black Goat. *J Domest Anim Ecol* 37: 19-25.
56. Hou Q, Tao L, Zhao W, Li L (2016) Production Performance of Rex Rabbit Feeding on Diets Containing Different Proportions of Mulberry Leaf Powder. *Sci Sericulture* 42: 500-6.
57. Lateef T, Adetayo A, Kudirat A, Murisiku O (2016) Effect of Moringa Leaf Meal Supplementation on Haematological and Serum Biochemical Profile of Broiler Chicken.
58. Hassan HMA, El-Moniary MM, Hamouda Y, El-Daly EE, Youssef AW, et al. (2016) Effect of Different Levels of *Moringa oleifera* Leaves Meal on Productive Performance, Carcass Characteristics and Some Blood Parameters of Broiler Chicks Reared Under Heat Stress Conditions. *Asian J Anim Vet Adv* 11: 60-6.
59. Karthivashan G, Arulselvan P, Alimon AR, Safinar II, Fakurazi S (2015) Competing role of bioactive constituents in *Moringa oleifera* extract and conventional nutrition feed on the performance of Cobb 500 broilers. *Biomed Res Int* 1-13.
60. Lu W, Wang J, Zhang HJ, Wu SG, Qi GH (2016) Evaluation of *Moringa oleifera* leaf in laying hens: effects on laying performance, egg quality, plasma biochemistry and organ histopathological indices. *Italian J Anim Sci* 15: 1-8.

61. Xi Q, Zeng B, Lan W, Sun B, Chen X, et al (2015) Effects of moringa oleifera leaf powder on production performance, egg quality and serum biochemical indexes of laying hens. *Feed Industry* 36: 10-5.
62. Zhang T, Zhang B, Bingwen SI, Zhang N, Yan TU, et al. (2018a) Effects of Moringa Leaf on Growth Performance, Slaughter Performance, Antioxidant Function and Meat Quality of Finishing Pigs. *Chinese Journal of Animal Nutrition* 30: 255-61.
63. Mukumbo FE, Maphosa V, Hugo A, Nkukwana TT, Mabusela TP, et al. (2015) Effect of Moringa oleifera leaf meal on finisher pig growth performance, meat quality, shelf life and fatty acid composition of pork. *South African Journal of Animal Science* 44: 388.
64. Ruckli A, Bee G (2016) Moringa oleifera as an alternative protein source to soybean meal in pig production. *J Anim Sci* 94: 60-60.
65. Ly J, Samkol P, Phiny C, Bustamante D (2016) Balance of nitrogen (n) in pigs fed with Moringa Oleifera foliage meal. *Civic Exchange*.
66. Mendieta-Araica B, Spörndly E, Reyes-Sánchez N, Spörndly R (2011a) Feeding Moringa oleifera fresh or ensiled to dairy cows--effects on milk yield and milk flavor. *Tropical Animal Health & Production* 43: 1039-47.
67. Zeng B, Sun JJ, Chen T, Sun BL, He Q, et al. (2017) Effects of Moringa oleifera silage on milk yield, nutrient digestibility and serum biochemical indexes of lactating dairy cows. *Journal of Animal Physiology & Animal Nutrition* 102: 75-81.
68. Mendieta-Araica B, Spörndly R, Reyes-Sánchez N, Spörndly E (2011b) Moringa (Moringa oleifera) leaf meal as a source of protein in locally produced concentrates for dairy cows fed low protein diets in tropical areas. *Livestock Science* 137: 10-7.
69. Cohenzinder M, Leibovich H, Vaknin Y, Sagi G, Shabtay A, et al. (2016) Effect of feeding lactating cows with ensiled mixture of Moringa oleifera, wheat hay and molasses, on digestibility and efficiency of milk production. *Anim Feed Sci Technol* 211: 75-83.
70. Zhang X, Lin C, Yang LI, Wang Y, Gao H, et al. (2017) Effects of Moringa oleifera Leaves and Peduncles on Production Performance, and Plasma Biochemical, Antioxidant and Immune Indexes in Dairy Cows. *Chinese Journal of Animal Nutrition* 29: 628-35.
71. Kholif AE, Gouda GA, Morsy TA, Salem AZM, Lopez S, et al. (2015) Moringa oleifera leaf meal as a protein source in lactating goat's diets: Feed intake, digestibility, ruminal fermentation, milk yield and composition, and its fatty acids profile. *Small Rumin Res* 129: 129-37.
72. Moyo B, Masika PJ, Muchenje V (2012) Effect of supplementing crossbred Xhosa lop-eared goat castrates with Moringa oleifera leaves on growth performance, carcass and non-carcass characteristics. *Tropical Animal Health & Production* 44: 801-9.
73. Sirimongkolvorakul S, Jiraungkoorskul W, Kosai P, Inwisai T (2015) Effect of Feeding Different Levels of Moringa oleifera on Growth Performance and Potential Role in Muscle Proteins in Fish *Puntius altus*. *Walailak Journal of Science & Technology* 12: 565-71.
74. Li L, Wang Z, You J, Yang J, Guo X (2018) Research advances on the application of broussonetia papyrifera leaves for livestock and poultry. *Feed Industry* 39: 24-6.
75. Yanzhi LI, Qian LI, Wang Y, Hou H, Shi W, et al. (2010) Effects of Leaves of Broussonetia papyrifera on Production Performance and Egg Quality of Layers. *China Poultry* 32: 26-9.
76. Yang QC, Chen SH, Liu Y, University GO, Center MB (2014) The Effect of Broussonetiapapyrifera Leaf on the Production Performance, Meat Quality and Apparent Digestibility of Fattening Pigs. *Journal of Henan Agricultural Sciences* 43: 133-7.
77. Tao XW, Liu ZJ, Zhang QX, Min LL, Zhou MY (2006) The Fermentation Process of Broussonetia Papyrifera Vent'leaf and its Feeding Experiment on Growing-Finishing Pigs. *Journal of Wuhan Polytechnic University* 2006: 5-7.
78. Alhassan O (2011) Effects of supplementation with leaves of Paper Mulberry (Broussonetia Papyrifera) on growth performance and blood indices of West African Dwarf Sheep (Djallonké) fed Napier Grass Basal Diet, Faculty of Agriculture, College of Agriculture and Natural Resources, Ghana.

Submit your manuscript to a JScholar journal and benefit from:

- ✦ Convenient online submission
- ✦ Rigorous peer review
- ✦ Immediate publication on acceptance
- ✦ Open access: articles freely available online
- ✦ High visibility within the field
- ✦ Better discount for your subsequent articles

Submit your manuscript at
<http://www.jscholaronline.org/submit-manuscript.php>

DOI:10.16720/j.cnki.tcyj.2023.032

环境应激对圈养野生动物繁殖性能的影响

李方俊¹, 曹思广¹, 张鹏², 杨汉东², 孙加节^{1*}

(1. 华南农业大学动物科学学院, 广东 广州 510642; 2. 广东长隆集团有限公司, 长隆动植物研创院, 广东 广州 511430)

摘要: 野生动物在人工圈养过程中受到多种环境应激源的干扰, 导致其行为和生理处于应激状态, 各种形式的环境应激可干扰野生动物生殖, 包括生理、配子功能和生物体行为等, 这些应激通常会降低动物繁殖的成功率。本文综述了环境中几种常见的应激对动物繁殖性能的影响, 阐明环境应激对圈养野生动物繁殖性能潜在的影响, 为圈养野生动物的饲养管理提供理论依据。

关键词: 环境应激; 圈养野生动物; 繁殖性能

中图分类号: S865 文献标识码: A

Effects of Environmental Stress on Reproductive Performance of Captive Wild Animals

LI Fangjun¹, CAO Siguang¹, ZHANG Peng², YANG Handong², SUN Jiajie^{1*}

(1. College of Animal Science, South China Agricultural University, Guangzhou 510642, China; 2. Guangdong Chimelong Group Co., Ltd, Chimelong Institute of Flora and Fauna Conservation, Guangzhou 511430, China)

Abstract: In the process of captivity, wild animals are disturbed by a variety of stressors in the environment, resulting in their behavior and physiological stress state. These stressors have a great impact on the production performance, behavior expression, and reproductive performance of wild animals. Various forms of environmental stress can interfere with many different aspects of reproduction in wildlife, including physiology, gamete function, and organismal behavior. These stresses often reduce the reproductive success of the animal. In this article, we review the impact of several common stresses on animal reproduction in the environment and indirectly clarify the potential impact of environmental stress on the reproductive performance of wild animals, which would provide the theoretical basis for the feeding management of wild animals.

Keywords: environmental stress; captive wild animal; reproductive performance

动物园圈养野生动物生活在人为环境中, 即使圈养环境尽可能模拟野生动物的野外生存环境, 但在实际的圈养中, 大多数野生动物仍属于异地饲养, 圈养地的自然环境和气候条件与动物的野外原始生存环境不同, 自然野性与圈养环境产生了冲突, 不可避免地产生多种干扰野生动物生存的因素, 而这些因素导致野生动物产生应激^[1]。有些应激对动物的影响是非常严重的, 不仅会对野生动物的生产性能、行为表达和繁殖性能等产生负面影响; 还可以造成动物精神紧张、内分泌

失调、免疫力下降, 诱发各种应激性疾病, 严重的还会造成动物死亡, 造成巨大损失^[2]。本文主要综述了圈养环境中几种常见的应激(热应激、冷应激、噪音应激、光照应激和饲养密度等)对动物繁殖性能影响的研究进展, 为圈养野生动物的饲养管理提供参考。

1 应激概述

应激是 1936 年由加拿大著名病理生理学家 Hans Selye 首先提出, 认为应激是指机体对外界或内部各种刺激所产生的非特异性应答反应的总和。应激的实质

收稿日期: 2022-11-09

基金项目: 广东长隆慈善基金会项目 (CLPF2021007Z); 广东长隆集团野生动物保育技术项目 (F110020220303)

作者简介: 李方俊 (1997-), 男, 广东茂名, 硕士研究生, 主要从事动物生物化学研究。

*通讯作者: 孙加节 (1984-), 男, 江苏盐城人, 博士, 副教授, 硕士生导师, 主要从事动物生物化学研究。

是机体的防御机能克服刺激源的不良作用,保持体内在极端情况下的稳态平衡^[3]。总体讲,典型的应激发生过程为动物受到强烈的应激源刺激后,通过神经系统、内分泌系统、免疫系统和代谢调节,力图使机体的生命活动恢复到一个新的相对稳定的正常功能状态,它包括惊恐反应或动员阶段、适应或抵抗阶段和衰竭阶段3个阶段^[3-5]。应激反应分为劣性应激和良性应激两类,劣性应激是指动物受到长时间的应激时,超过其自身耐受力,进而使动物受到危害,甚至死亡,也称为病理性应激;良性应激是指当动物受到刺激时,提高机体抵抗刺激的能力,对于动物而言有一定积极作用,也称为生理应激或自然应激^[4,6,7]。根据应激反应的作用时间,又可分为急性应激和慢性应激,其中机体受突然刺激发生的应激称为急性应激(单一的、交替的和时间有限的暴露),长期持续性的紧张状态引起慢性应激(交替的和延长的暴露)^[4,7]。

2 环境应激对动物繁殖性能的影响

2.1 热应激对繁殖性能的影响

热应激会降低雄性动物的繁殖力。动物暴露于高环境温度对生理和生殖功能有不利影响^[8]。一年中温暖月份的高环境温度或实验性暴露于热应激会降低受孕率、生育力和胚胎发育^[9]。阴囊温度缺乏体温调节可导致睾丸体温过高,从而导致生殖器热应激。热应激对精子发生有害,并导致精子质量下降。研究表明,在热应激状态下,会降低动物附睾重量、阴囊宽度和周长,并降低血浆中睾酮的浓度和精子性激素受体 mRNA 表达水平;降低精液量、精子活力、精子代谢活性、精子浓度和进行性运动,在性行为上,提高射精的总时间以及射精的坐骑次数^[10-12]。热应激还会破坏机体生殖器官的氧化平衡引起氧化应激,导致睾丸生殖细胞凋亡升高^[13]。Mahdivand 等^[14]研究结果显示,与对照组相比,热应激(43 °C,持续 20 min/d)处理大鼠的精子浓度、精子活力百分比、正常形态的精子百分比显著降低,精子丙二醛(MDA)水平、精子畸形指数(SDI)和畸形精子指数(TZI)显著增加,观察到具有染色质异常的精子百分比和精子 DNA 损伤显著增加;对大鼠的试管婴儿结果显示,在热应激处理组中,观察到受精卵和双细胞胚胎、囊胚期和孵化胚胎的数量显著降低以及停滞胚胎百分比显著增加。这表明热应激可能通过精子脂质过氧化升高以及精子数量和质量降低而对体外受精结果产生不利影响。

雌性动物的卵细胞分化、发育、受精卵着床、妊娠、

分娩、繁殖行为和性机能及第二性征等由于热应激影响可能出现障碍;同时,生殖器官也会受到影响^[15]。Sejian 等^[16]研究表明,在热应激(42 °C,持续 6 h/d)条件下 Malpura 母羊血浆中雌二醇的含量显著降低。Li 等^[17]则报道,妊娠母猪热应激饲养(28~32 °C)降低了母乳总蛋白含量和催乳素水平;两组仔猪出生时体重相似,但热应激组断奶年龄时体重显著降低。同样,Liu 等^[18]在研究热应激对初产母猪妊娠后期姿势转变和繁殖性能的影响,发现妊娠期间热应激(28~32 °C)饲养可使分娩持续时间延长,对照组(18~22 °C)仔猪平均体重在第 10 天和断奶时显著高于热应激组。此外,Han 等^[19]研究报道,与对照组(22 ± 2 °C)相比,热应激组(温度为 38 °C,湿度为 45%~60%,持续 2 h/d)母鼠的间情期显著延长,血清雌二醇(E2)和孕酮(P)显著降低,并且子宫上皮高度显著降低;高环境温度可诱发母鼠明显的子宫结构紊乱(细胞核变形,染色质散射和分泌细胞数量减少)。研究表明,在热应激的状态下,能缩短母羊的发情期和妊娠期^[20];降低母羊胎重和蛋白质、RNA 和 DNA 总含量^[21]以及母羊哺乳期的产奶量^[22]。Romo-Barron 等^[23]在系统评价和 Mate 分析热应激对母羊繁殖性能和生理的影响时,发现热应激使母羊发情持续时间减少了 7.09 h,在热应激怀孕母羊中,胎盘和胎儿体重分别减少 183.62 g 和 1 665.18 g。此外,Fabris 等^[24]研究显示,与对照组相比,热应激显著降低了奶牛的产奶量和牛奶中乳糖的含量。综上所述,热应激主要通过改变雌性动物的繁殖周期、性激素水平、母体产奶量和母乳营养成分含量,以干扰卵细胞的成熟分化,诱发生殖器官结构紊乱,影响胎儿的发育,降低幼仔的断奶体重和成活率等,进而导致雌性动物繁殖性能的降低。

引起动物热应激的因素除了环境中的温度外,还主要受到环境中湿度的影响,动物在温度和湿度较高的环境下比较容易发生热应激。这两者通过间接或直接来影响动物生理性能,而且也会影响动物的繁殖性能。通常用温湿度指数(THI)的高低来反映动物热应激程度。当 THI ≤ 72 时,没有热应激;当 72 < THI ≤ 79 时,表示动物处于轻度热应激状态;当 79 < THI ≤ 84 时,表示动物处于中度热应激状态;当 THI > 84 时为严重热应激状态^[25]。研究显示,奶牛精子的活力和体外生育能力受到荷兰气候条件的影响,与在低 THI (38~55)下收集的样本相比,在较高 THI (60~81)下获得的精子样本的活力降低,导致囊胚发育减少和孵化延迟^[26]。Amitha 等^[27]在研究热应激对马拉巴里山羊

不同繁殖相关基因表达模式的影响时,发现与棚内舒适的环境 THI(69.9 ~ 74.9)相比,棚外高的环境 THI(73.5~86.5)引起的热应激显著影响促卵泡激素受体(*FSHR*)、促黄体生成素受体(*LHR*)、雌激素受体 α (*ESR α*)、前列腺素 F 2α (*PGF 2α*)和环氧合酶-2(*COX-2*)的表达模式,进而对山羊的生殖效率产生不利影响。此外,山羊在交配期间直到妊娠前 45 d 的热应激 THI(85 \pm 3)缩短了怀孕时间,并倾向于减少孩子的窝重^[20]。

2.2 冷应激对繁殖性能的影响

大量研究证实,低温对动物繁殖性能和生殖系统有不良影响。研究表明,小母牛处于冷应激(平均日最低气温小于 4℃)与受孕率降低和胎儿流产增加有关^[28]。亚热带气候的环境冷胁迫会降低中国西南土产山羊的出生体重和存活率,且提高新生儿死亡率^[29]。寒冷暴露可导致生殖细胞凋亡增加和哺乳动物生殖能力降低^[30,31]。Wang 等^[32]研究表明,在受冷应激(以 20 min/d 在 0~1℃的冰水中游泳)刺激的大鼠中,冷应激不仅可以延长发情周期并降低睾丸激素、雌二醇和黄体酮水平,而且冷应激还可能导致生理性生殖器官功能障碍,对血液流变学和微循环产生不利影响。Xu 等^[33]在研究冷应激对雌性大鼠生殖功能的影响时,发现冷应激(在 -10℃下,每天 4 h,持续 2 周)可导致雌性大鼠发情周期不规则和卵巢形态的一些改变;冷应激可能通过改变血清黄体生成素(LH)水平和增加黄体生成素受体(LHR)表达来损害卵巢功能。此外,寒冷引起的应激可导致动物精子的凋亡,降低睾丸激素水平和精子质量,破坏睾丸细胞抗氧化防御系统和活性氧(ROS)产生之间的平衡,从而引起氧化应激。Juárez-Rojas 等^[34]报道,在 15℃冷水中浸泡 15 min/d 的慢性应激会导致大鼠睾酮减少,这与睾丸生殖细胞(主要是圆形精子细胞和初级精母细胞)的损失和退化有关,从而破坏精子发生。也有研究数据表明,15℃冷水浸泡 15 min/d 的急性和慢性应激最终导致大鼠睾丸生殖细胞凋亡,在急性应激中,凋亡生殖细胞和生精小管的百分比在应激暴露后的第 1 h 时内增加,在 24 h 达到峰值,在慢性应激期间,在所有试验时间(20 d、40 d 和 50 d)观察到凋亡生殖细胞生精小管百分比显著增加;冷水浸泡诱导的慢性冷应激导致大鼠的全身和睾丸重量降低,还导致附睾精子活力和精子数量以及精子总活力和进行性运动的减少^[35]。此外,García-Díaz 等^[36]结果显示,活性氧(ROS)仅在大鼠急性冷应激(15℃冷水浸泡 15 min/d)后 6 h 增加,而抗氧化酶、脂质过氧化(LPO)

和精子参数的活性和表达在睾丸中未被改变。慢性冷应激后,睾丸绝对重量下降;此外,ROS 产量和 LPO 分别在 20 d、40 d 和 50 d 增加;超氧化物歧化酶(SOD)和谷胱甘肽过氧化物酶(GSH-Px)的活性在整个慢性胁迫期间下降,过氧化氢酶(CAT)的活性在 40 d 和 50 d 时降低,在 20 d 时增加;精子活动能力、精子活力和精子数量下降,而异常精子随着慢性压力而增加。这表明急性冷应激下不会影响大鼠睾丸中的抗氧化状态,而冷水浸泡的慢性压力会显著改变氧化还原状态并损害各种睾丸功能,可见睾丸对持续冷应激的适应性较弱。

2.3 噪音对繁殖性能的影响

在各种环境应激源中,噪音应激是最广泛和最危险的天然应激源,对身体产生有害的生理、心理和形态学影响。噪音应激也会降低生殖功能,在暴露于高频噪音的情况下,会降低妊娠率并增加新生儿死亡率和致畸性^[37]。郝苏平^[38]研究报道,100 dB 噪音环境可导致绝大多数妊娠小鼠流产,妊娠剖检后子宫内无胎儿,无法计算死胎数。2003 年 4 月 20 日上午,齐齐哈尔市龙沙公园的驼鹿因商业广场开业时燃放的礼炮及礼花噪音而产生应激,导致流产^[39]。长期暴露于噪音环境中对雄性动物的生育能力产生负面影响,其基础是增强发病应激诱导的细胞凋亡过程并抑制精子发生的动力学^[40]。Rasmussen 等^[41]报道,暴露于适度至高水平的噪音中,通过减少出生的幼崽数量和增加死产幼崽的数量,显著降低了小鼠的繁殖效率。此外,Farzadinia 等^[42]结果表明,噪音应激降低了 115 dB 噪音强度处理组大鼠的睾酮水平,同时增加了促肾上腺皮质激素和皮质醇水平。睾丸组织切片显示,与对照组相比,生精小管的平均直径和生发上皮的厚度减小,间质组织面积与睾丸组织总面积比值也显著增加。以上研究表明,噪音压力可能对雄性动物生育能力产生负面影响。另有研究指出,暴露于 90~130 dB 噪声环境中的大鼠睾丸细胞凋亡和坏死的发生率增加,而且这些细胞的活力在睾丸中降低^[43],说明噪声应激可通过增加凋亡和坏死细胞对睾丸组织的细胞产生负面影响。Bisong 等^[44]研究表明,处于 90~120 dB、8 h/d 的噪音环境中显著降低大鼠精子数量、活力、运动性和快速进行性向前运动,而非运动性精子的百分比在噪音应激中显著增加;噪音应激组的血清睾酮、促卵泡激素和黄体生成素显著下降;睾丸组织学显示许多生精小管中的生殖细胞丢失,附睾组织学显示,噪音应激组中的精子密度降低,可见噪音应激可通过抑制激素分泌损害睾丸功能。

2.4 光照对繁殖性能的影响

明暗节律的交替引起动物的一系列生理、生化和代谢变化,也改变了动物的生长发育以及摄食、迁徙和繁殖等行为活动。昼长的变化是季节性繁殖动物生殖激活的重要线索,以确保母体投资最大的时间与有利的环境条件相吻合。然而,夜间的人造光有可能干扰对这种自然线索的感知。事实上,有证据表明,人造光可以作为一种慢性应激源,通过下丘脑-垂体-肾上腺轴抑制鸟类性激素的产生^[45]。暴露于环境光污染也会改变野生动物的繁殖时间。例如,环境光水平被用作许多动物繁殖过程时间的提示,可能会被光污染破坏。Dominoni等^[46]研究报道,黑鸟(*Turdus merula*)在夜间暴露于人造光1年后,鸟类性腺的季节性发育和血浆睾酮浓度的增加都相应提前,并且在暴露的第2年后,性腺根本没有显示出季节性发育以及血浆睾酮水平在整个繁殖期保持较低水平。此外,夜间人造光已被证明会延迟 Tammar 小袋鼠(*Macropus eugenii*)的分娩^[47],这可能是由褪黑激素的抑制介导的。Li等^[48]研究结果表明,在短时间(小于2周)光照条件下,24 h光照处理导致小鼠卵泡总数减少,昼夜节律相关基因下调。此外,在光照24 h后,还检测到血清性激素水平的变化,其中黄体生成素(LH)、卵泡刺激素(FSH)和雌二醇(E₂)的浓度升高,但孕酮(P)的浓度降低。24 h光照增加了DNA损伤和修复相关基因的表达,TUNEL和RAD51阳性细胞的数量,这表明短时间24 h光照增加了小鼠DNA损伤和细胞凋亡,从而影响了卵巢的发育。Ogo等^[49]则报道,恒定光周期(24 h光照)导致大鼠后代雄鼠睾丸激素水平、附睾重量和附睾精子数、生精小管直径、支持细胞数和正常精子数下降。在恒定光周期组中,还观察到睾丸组织病理学损伤和体视学改变,说明怀孕期间暴露在连续光照下会导致雄性后代成年期发育受损。

2.5 饲养密度对繁殖性能的影响

过高的饲养密度对动物的生长发育、行为习性及其繁殖性能均有不利的影响。例如,在高放养密度下饲养家禽会降低性激素水平,延缓卵巢发育,并导致卵泡闭锁,导致产卵性能差^[50]。高密度饲养(143 cm²/只)的日本鹌鹑显示出生育力、孵化率、产量和免疫力参数的下降^[51],同样,高放养密度(15只/m²)可降低卵巢发育和成熟速度,导致山麻鸭饲养期间繁殖性能延迟^[52]。过高的密度产生的拥挤应激导致了动物对资源的竞争,如食物、水或配偶,这反过来导致高皮质醇水平和攻击

行为,免疫反应降低或繁殖减少^[53]。Shang等^[54]发现,高密度(0.4只/m²)增加了发育期根田鼠(*Microtus oeconomus*)的粪便皮质酮代谢物(FCM)水平,降低了繁殖。高密度对发育期根田鼠繁殖的负面影响部分是通过其对发育期田鼠FCM水平的积极影响来实现的。也有研究表明,高密度的马鹿(*Cervus elaphus hispanicus*)种群与怀孕率大幅下降有关^[55]。此外,有研究发现,受拥挤应激的克里奥尔山羊(*Capra hircus*)的性行为减少:受应激雌性克里奥尔山羊的趋近、甩尾、排尿和阴道分泌物和侧腹收缩减少;雄克里奥尔山羊的肛门生殖器嗅探、舔舐、咩咩叫、坐骑尝试和坐骑减少。与对照动物相比,应激克里奥尔山羊的皮质醇水平更高;与对照雌性相比,应激雌性克里奥尔山羊在卵泡期和黄体期的雌二醇和黄体酮水平分别显著降低;在繁殖前和繁殖期间,应激雄性克里奥尔山羊的睾丸激素水平均低于对照组^[56],表明应激克里奥尔山羊的肾上腺轴被激活,高的皮质醇水平可能导致雌性雌二醇水平和雄性睾丸酮水平降低以及生殖行为表达中断。Hou等^[57]报道,长期高密度(初始放养密度8.6 kg/m³,最终密度为49.3 kg/m³)饲养导致虹鳟鱼(*Oncorhynchus mykiss*)卵黄蛋白原合成过程中下丘脑促性腺激素释放激素-1(GnRh-1)、垂体卵泡刺激素(FSH)、卵巢卵泡刺激素受体(FSHR)和血清雌二醇(E₂)降低,下丘脑促性腺激素释放激素-2(GnRh-2)和血清多巴胺升高,可见,虹鳟鱼下丘脑-垂体-性腺(HPG)轴可能在密集饲养条件下受到抑制。Hou等^[58]研究显示,高初始放养密度(8.6 kg/m³)虹鳟鱼卵巢发育较迟缓,卵黄原积累较少。高密度养殖虹鳟鱼血清E₂、er α mRNA表达量显著降低,er β mRNA表达量呈升高趋势,当密度接近50 kg/m³时,卵巢er β 2 mRNA表达明显增加。综上可见,高密度诱导的er β mRNA表达增加导致了er α mRNA表达减少和卵黄发生。因此,高密度的卵巢发育会受到阻碍。

2.6 环境改变对繁殖性能的影响

早期研究报道,对母羊进行8 h的长途运输应激不仅增加了皮质类固醇的平均血浆浓度,而且显著阻断了8只母羊中有5只的发情表达,并延迟了发情的表达^[59]。将雌性梅花鹿和其所生梅花仔鹿母子分开,隔离饲养,分群后母子均终日频繁叫唤,烦躁不安,在圈舍不断跑动寻找母鹿;与此同时,母子食欲均显著减损,严重时采食量仅为正常水平的10.9%^[60]。陈晶^[61]研究报道,苏州动物园野生动物在搬迁后对繁殖状况有负面影响,特别是短期搬迁应激后明显抑制野生动

物繁殖育幼,如怀孕动物个数和出生动物个数都明显降低,且新出生的幼崽死亡率比较高,母兽不带出生幼崽或咬伤幼崽的比往常概率高。姜清漪^[62]的研究表明,车速约 80 km/h 持续 6 h 的道路运输应激导致蛋鸡卵巢上有多数闭锁卵泡,各级卵泡数量减少,卵泡周围出血,大量炎性细胞浸润,并且显著降低蛋鸡卵巢组织中 FSHR、催乳素受体 (PRLR)、雌二醇受体 (E2R)、LHR 和 PR 的 mRNA 表达水平。这说明运输应激能抑制蛋鸡卵泡的发育,并诱导蛋鸡卵巢性激素分泌紊乱,进而影响蛋鸡生殖性能。Melchert 等^[63]研究表明,分娩时将母马转移到新环境中推迟了小马驹排出体外的时间。孙丽萍^[64]在研究长途运输应激对妊娠动物的影响时,发现长途运输 (1 000 km, 时间约 15 h) 应激会造成妊娠中期母鼠活胎率的显著下降和死胎率的明显增加。此外,刘佳佳^[65]在研究运输应激对动物繁殖性能的影响时,发现在初情期前进行运输应激 (1 000 km, 时间约 14 h),可导致小鼠初情期提前,发情周期缩短,影响卵泡正常发育,减少成熟卵泡数量;在性成熟前进行运输应激,可影响小鼠体成熟后泌乳性能,降低仔鼠断奶窝重;在性成熟后运输应激,可抑制小鼠体成熟后卵巢排卵功能,减少排卵数,降低产仔数,并影响母鼠泌乳性能,减少仔鼠断奶窝重。结果表明,运输应激影响小鼠繁殖和泌乳性能,且其影响程度和影响类别与发生应激时小鼠所处生理时期有关。

3 小结

野生动物圈养在人为环境里,与其野外自然环境相比,人造圈养环境的环境丰容大幅降低,使生活在其中的野生动物极易受到各种环境应激源的影响而产生应激反应。如不同季节和气候所引起的温度变化,会使动物产生热应激和冷应激;园内游客参观和周围环境的噪音导致的应激;夜间人造光照引起光照节律动物的不适;与野外自然环境相比圈养的环境使动物的饲养密度提高,让动物的生长活动受到限制,导致其无法主动地避开有害环境,从而引起动物的慢性应激;不同动物园间的引种交配和外借展览时的运输和环境改变都会引起动物的应激等。这些应激通常会影响动物繁殖的各个阶段,降低动物的繁殖成功率。因此,对于野生动物圈养过程中避免发生环境应激应重视预防措施,如环境温度过高和过低时,要及时采取防暑降温和防寒保暖措施;要提供繁殖时期动物足够的活动空间并提高其环境丰容,保持其生存环境的安静;对于新引进的动物,尽量给动物以安静的环境,使动物

逐渐适应新环境时再进行繁殖交配;在其日粮中添加抗应激添加剂 (如维生素制剂、电解质、氨基酸和中草药制剂等) 以减少环境应激对圈养野生动物繁殖性能的不良影响,提高圈养野生动物的繁殖力和物种丰富度,更好地保护野生动物的种质资源。

参 考 文 献

- [1] 井霞. 圈养野生动物的应激反应及应对措施[J]. 今日畜牧兽医, 2021, 37(10): 38-39+42.
- [2] 张永宾, 伊霞, 王海锋. 应激对圈养野生动物的影响及防治措施[J]. 黑龙江畜牧兽医, 2015, (9): 229-231.
- [3] 姚勤. 动物应激及防治[J]. 芜湖职业技术学院学报, 2006, 8(4): 76-77.
- [4] 刘强. 动物应激与炎症的生理机制与临床症状[J]. 养殖技术顾问, 2012(7): 153.
- [5] 张红梅, 季新宇. 集约化畜牧业生产中动物应激及控制[J]. 中国畜牧业, 2021(7): 77.
- [6] 苗玉涛. 动物应激问题及其在畜牧兽医实践中的意义[J]. 农家参谋, 2018(1): 116.
- [7] 宋金山. 关于动物应激综合征的发生和治疗[J]. 中国动物保健, 2017, 19(4): 59-60.
- [8] TAKAHASHI M. Heat stress on reproductive function and fertility in mammals[J]. Reproductive Medicine and Biology, 2011, 11(1): 37-47.
- [9] YAERAM J, SETCHELL B P, MADDOCKS S. Effect of heat stress on the fertility of male mice in vivo and in vitro[J]. Reproduction, Fertility and Development, 2006, 18(6): 647-653.
- [10] KIM M K, CHA K M, HWANG S Y, et al. Pectinase-treated *Panax ginseng* protects heat stress-induced testicular damage in rats[J]. Reproduction, 2017, 153(6): 737-747.
- [11] MAURYA V P, SEJIAN V, KUMAR D, et al. Impact of heat stress, nutritional restriction and combined stresses (heat and nutritional) on growth and reproductive performance of Malpura rams under semi-arid tropical environment[J]. Journal of Animal Physiology and Animal Nutrition, 2016, 100(5): 938-946.
- [12] SABÉS-ALSINA M, TALLO-PARRA O, MOGAS M T, et al. Heat stress has an effect on motility and metabolic activity of rabbit spermatozoa[J]. Animal Reproduction Science, 2016, 173: 18-23.
- [13] MAHDIVAND N, SHALIZAR-JALALI A, NEJATI V, et al. Adaptogenic potential of royal jelly in reproductive system of heat stress-exposed male rats[J]. Journal of Thermal Biology, 2021, 96: 102827.
- [14] MAHDIVAND N, NAJAFI G, NEJATI V, et al. Royal jelly protects male rats from heat stress-induced reproductive failure[J]. Andrologia, 2019, 51(3): e13213.
- [15] 曾菊英. 热应激对动物繁殖性能的影响研究进展[J]. 中国畜牧兽医文摘, 2012, 28(7): 58-59+61.
- [16] SEJIAN V, SINGH A K, SAHOO A, et al. Effect of mineral

- mixture and antioxidant supplementation on growth, reproductive performance and adaptive capability of Malpura ewes subjected to heat stress[J]. *Journal of Animal Physiology and Animal Nutrition*, 2014, 98(1): 72-83.
- [17] LI Y, FAN G, LIU Y, et al. Heat stress during late pregnancy of sows influences offspring longissimus dorsi muscle growth at weaning[J]. *Research in Veterinary Science*, 2021, 136: 336-342.
- [18] LIU L, TAI M, YAO W, et al. Effects of heat stress on posture transitions and reproductive performance of primiparous sows during late gestation[J]. *Journal of Thermal Biology*, 2021, 96: 102828.
- [19] HAN J, YANG D, LIU Z, et al. The damage effect of heat stress and psychological stress combined exposure on uterus in female rats[J]. *Life Sciences*, 2021, 286: 120053.
- [20] COLOMA-GARCÍA W, MEHABA N, LLONCH P, et al. Prenatal heat stress effects on gestation and postnatal behavior in kid goats[J]. *PloS One*, 2020, 15(2): e0220221.
- [21] EARLY R J, MCBRIDE B W, VATNICK I, et al. Chronic heat stress and prenatal development in sheep: II. placental cellularity and metabolism[J]. *Journal of Animal Science*, 1991, 69(9): 3610-3616.
- [22] HOOPER H B, DOS SANTOS SILVA P, DE OLIVEIRA S A, et al. Long-term heat stress at final gestation: physiological and heat shock responses of Saanen goats[J]. *International journal of biometeorology*, 2021, 65(12): 2123-2135.
- [23] ROMO-BARRON C B, DIAZ D, PORTILLO-LOERA J J, et al. Impact of heat stress on the reproductive performance and physiology of ewes: a systematic review and meta-analyses[J]. *International Journal of Biometeorology*, 2019, 63(7): 949-962.
- [24] FABRIS T F, LAPORTA J, SKIBIEL A L, et al. Effect of heat stress during early, late, and entire dry period on dairy cattle[J]. *Journal of Dairy Science*, 2019, 102(6): 5647-5656.
- [25] 高民, 杜瑞平, 温雅丽. 热应激对奶牛生产的影响及应对策略[J]. *畜牧与饲料科学*, 2011, 32(Z1): 59-62.
- [26] LLAMAS LUCÉ Ñ O N, DE SOUZA RAMOS ANGRIMANI D, DE CÁSSIA BICUDO L, et al. Exposing dairy bulls to high temperature-humidity index during spermatogenesis compromises subsequent embryo development in vitro[J]. *Theriogenology*, 2020, 141: 16-25.
- [27] AMITHA J P, KRISHNAN G, BAGATH M, et al. Heat stress impact on the expression patterns of different reproduction related genes in Malabari goats[J]. *Theriogenology*, 2019, 131: 169-176.
- [28] CHEBEL R C, BRAGA F A, DALTON J C. Factors affecting reproductive performance of Holstein heifers[J]. *Animal Reproduction Science*, 2007, 101(3-4): 208-224.
- [29] LUO N, WANG J, HU Y, et al. Cold and heat climatic variations reduce indigenous goat birth weight and enhance pre-weaning mortality in subtropical monsoon region of China[J]. *Tropical animal Health and Production*, 2020, 52(3): 1385-1394.
- [30] FARAONE-MENNELLA M R, FERONE A, MARINO L, et al. Poly (ADP-ribosyl) ation of proteins and germ cell development in hypertrophic rat testes[J]. *Molecular and Cellular Biochemistry*, 2009, 323(1-2): 119-129.
- [31] NABENISHI H, YAMAZAKI A. Impaired reproduction in Japanese Black cattle under cold environmental conditions[J]. *Reproduction in Domestic Animals*, 2017, 52(3): 371-375.
- [32] WANG D, CHENG X, FANG H, et al. Effect of cold stress on ovarian & uterine microcirculation in rats and the role of endothelin system[J]. *Reproductive Biology and Endocrinology*, 2020, 18(1): 29.
- [33] XU T, LI X, YANG L, et al. Impact of cold exposure on the reproductive function in female rats[J]. *BioMed Research International*, 2018: 3674906.
- [34] JUÁREZ-ROJAS L, VIGUERAS-VILLASE OR R M, CASILLAS F, et al. Gradual decrease in spermatogenesis caused by chronic stress[J]. *Acta Histochemica*, 2017, 119(3): 284-291.
- [35] JUÁREZ-ROJAS A L, GARCÍA-LORENZANA M, ARAGÓN-MARTÍNEZ A, et al. Intrinsic and extrinsic apoptotic pathways are involved in rat testis by cold water immersion-induced acute and chronic stress[J]. *Systems Biology in Reproductive Medicine*, 2015, 61(4): 211-221.
- [36] GARCÍA-DÍAZ E C, GÓMEZ-QUIROZ L E, ARENAS-RÍOS E, et al. Oxidative status in testis and epididymal sperm parameters after acute and chronic stress by cold-water immersion in the adult rat[J]. *Systems Biology in Reproductive Medicine*, 2015, 61(3): 150-160.
- [37] SWAMI C G, RAMANATHAN J, CHARAN JEGANATH C. Noise exposure effect on testicular histology, morphology and on male steroidogenic hormone[J]. *The Malaysian Journal of Medical Sciences*, 2007, 14(2): 28-35.
- [38] 郝苏平. 中药对动物噪音应激诱导流产的安胎作用及机理[D]. 河北: 河北农业大学, 2012.
- [39] 白晓洁, 王文锋, 车桂翠. 几种环境因子对驼鹿应激影响的观察研究[J]. *中国畜禽种业*, 2008, 4(17): 77-80.
- [40] JALALI M, HEMADI M, SAKI G, et al. Study of spermatogenesis fetal testis exposed noise stress during and after natal period in rat[J]. *Pakistan Journal of Biological Sciences*, 2013, 16(19): 1010-1015.
- [41] RASMUSSEN S, GLICKMAN G, NORINSKY R, et al. Construction noise decreases reproductive efficiency in mice[J]. *Journal of the American Association for Laboratory Animal Science*, 2009, 48(4): 363-370.
- [42] FARZADINIA P, BIGDELI M, AKBARZADEH S, et al. Effect of noise pollution on testicular tissue and hormonal assessment in rat[J]. *Andrologia*, 2016, 48(9): 869-873.
- [43] HEMADI M, SAKI G, RAJABZADEH A, et al. The effects of honey and vitamin E administration on apoptosis in testes of rat exposed to noise stress[J]. *Journal of Human Reproductive Sciences*, 2013, 6(1): 54-58.
- [44] BISONG S A, UKOH I E, NNA V U, et al. Vitamin E attenuates nicotine- and noise-induced reproductive impairment in

- male albino Wistar rats[J]. *Andrologia*, 2018, 50(7): e13050.
- [45] RUSS A, REITEMEIER S, WEISSMANN A, et al. Seasonal and urban effects on the endocrinology of a wild passerine[J]. *Ecology and Evolution*, 2015, 5(23): 5698-5710.
- [46] DOMINONI D M, QUETTING M, PARTECKE J. Long-term effects of chronic light pollution on seasonal functions of European blackbirds (*Turdus merula*)[J]. *PloS One*, 2013, 8(12): e85069.
- [47] ROBERT K A, LESKU J A, PARTECKE J, et al. Artificial light at night desynchronizes strictly seasonal reproduction in a wild mammal[J]. *Proceedings Biological Sciences*, 2015, 282(1816): 20151745.
- [48] LI Y, CHENG S, LI L, et al. Light-exposure at night impairs mouse ovary development via cell apoptosis and DNA damage[J]. *Bioscience Reports*, 2019, 39(5): BSR20181464.
- [49] OGO F M, SIERVO G E M L, DE MORAES A M P, et al. Extended light period in the maternal circadian cycle impairs the reproductive system of the rat male offspring[J]. *Journal of Developmental Origins of Health and Disease*, 2021, 12(4): 595-602.
- [50] KRAUSE E T, SCHRADER L. Suggestions to derive maximum stocking densities for layer pullets[J]. *Animals*, 2019, 9(6): 348.
- [51] EL-TARABANY M S. Impact of cage stocking density on egg laying characteristics and related stress and immunity parameters of Japanese quails in subtropics[J]. *Journal of Animal Physiology and Animal Nutrition*, 2016, 100(5): 893-901.
- [52] JIANG D L, ZHOU X L, XU Y L, et al. Effects of stocking density on ovarian development and maturation during the rearing period in Shan-ma ducks[J]. *Poultry Science*, 2022, 101(5): 101809.
- [53] VAS J, CHOJNACKI R, KJØREN M F, et al. Social interactions, cortisol and reproductive success of domestic goats (*Capra hircus*) subjected to different animal densities during pregnancy[J]. *Applied Animal Behaviour Science*, 2013, 147(1): 117-126.
- [54] SHANG G, DU S, YANG Y, et al. Is negative density-dependent reproduction regulated by density-induced stress in roosters two field experiments[J]. *Ecology and Evolution*, 2022, 12(5): e8927.
- [55] RODRIGUEZ-HIDALGO P, GORTAZAR C, TORTOSA F S, et al. Effects of density, climate, and supplementary forage on body mass and pregnancy rates of female red deer in Spain[J]. *Oecologia*, 2010, 164(2): 389-398.
- [56] DÍAZ PACHECO M, VARGAS ROMERO J, ROJAS-MAYA S, et al. Effects of crowding and water restriction stress on creole goat reproduction in the Oaxacan Sierra Mixteca, Mexico[J]. *Reproduction in Domestic Animals*, 2018, 53(6): 1386-1395.
- [57] HOU Z S, WEN H S, LI J F, et al. Hypothalamus-pituitary-gonad axis of rainbow trout (*Oncorhynchus mykiss*) during early ovarian development and under dense rearing condition[J]. *General and Comparative Endocrinology*, 2016, 236: 131-138.
- [58] HOU Z S, WEN H S, LI J F, et al. Expression of estrogen receptors in female rainbow trout (*Oncorhynchus mykiss*) during first ovarian development and under dense rearing condition[J]. *General and Comparative Endocrinology*, 2018, 259: 1-11.
- [59] EHNERT K, MOBERG G P. Disruption of estrous behavior in ewes by dexamethasone or management-related stress [J]. *Journal of Animal Science*, 1991, 69(7): 2988-2994.
- [60] 韦旭斌, 王水琴, 李养贤, 等. 圈养鹿主要应激原及其致病性研究[J]. *特产研究*, 1999(2): 1-5.
- [61] 陈晶. 苏州动物园搬迁中动物应激的发生及对策[D]. 江苏: 苏州大学, 2017.
- [62] 姜清漪. 运输应激对蛋鸡卵巢损伤及生产性能的影响[D]. 哈尔滨: 东北农业大学, 2018.
- [63] MELCHERT M, AURICH C, AURICH J, et al. External stress increases sympathoadrenal activity and prolongs the expulsive phase of foaling in pony mares[J]. *Theriogenology*, 2019, 128: 110-115.
- [64] 孙丽萍. 奶牛精液品质和抗病及抗运输应激的分子机制研究[D]. 武汉: 华中农业大学, 2013.
- [65] 刘佳佳. 水牛泌乳性状全基因组关联分析与运输应激对繁殖性能的影响及其分子机制研究[D]. 武汉: 华中农业大学, 2017.



Exploration of long noncoding RNA in bovine milk exosomes and their stability during digestion in vitro

Bin Zeng,* Ting Chen,* Mei-Ying Xie, Jun-Yi Luo, Jia-Jian He, Qian-Yun Xi, Jia-Jie Sun,† and Yong-Liang Zhang†

Guangdong Provincial Key Laboratory of Animal Nutrition Control, National Engineering Research Center for Breeding Swine Industry, College of Animal Science, South China Agricultural University, Guangzhou, 510642, China

ABSTRACT

Previous studies have demonstrated that bovine milk contains mRNA and microRNA that are largely encapsulated in milk-derived exosomes. However, little information is available about long noncoding RNAs (lncRNA) in bovine milk. Increasing evidence suggests that lncRNA are of particular interest given their key role in gene expression and development. We performed a comprehensive analysis of lncRNA in bovine milk exosomes by RNA sequencing. We used a validated human in vitro digestion model to investigate the stability of lncRNA encapsulated in bovine milk exosomes during the digestion process. We identified 3,475 novel lncRNA and 6 annotated lncRNA. The lncRNA shared characteristics with those of other mammals in terms of length, exon number, and open reading frames. However, lncRNA showed higher expression than mRNAs. We selected 12 lncRNA of high-expression abundance and identified them by PCR. Gene ontology (GO) enrichment and Kyoto Encyclopedia of Genes and Genomes (KEGG) pathway analyses showed that lncRNA regulate immune function, osteoblastogenesis, neurodevelopment, reproduction, cell proliferation, and cell-cell communication. We also investigated the 12 lncRNA using quantitative real-time PCR to reveal their expression profiles in milk exosomes during different stages of lactation (colostrum 2 d, 30 d, 150 d, and 270 d); their resulting expression levels in milk exosomes showed variations across the stages. A digestion experiment showed that bovine milk exosome lncRNA was resistant to in vitro digestion with different digestive juices, including saliva, gastric juice, pancreatic juice, and bile juice. Taken together, these results show for the first time that cow milk contains lncRNA, and that

their abundance varied at different stages of lactation. As expected, bovine milk exosomal lncRNA were stable during in vitro digestion. These findings provide a basis for further understanding of the physiological role of milk lncRNA.

Key words: bovine, milk exosomes, long noncoding RNA, stability

INTRODUCTION

Milk has been identified as a rich source of vital nutrients contributing to health (Admyre et al., 2007). It contains a diverse mixture of components, including nutrients, milk fat globules, growth factors, immune cells, antibodies, cytokines, and antimicrobial peptides that play a pivotal role in infant development (Savino and Liguori, 2008; Dieterich et al., 2013). The beneficial effects of milk include decreased risk of sudden infant death syndrome, reduced risk of neonatal infection, and more optimal metabolic development throughout childhood (Hauck et al., 2011). Bovine milk is widely used as a dairy product, especially in infant formula, and it is an important material in the food industry.

Recently, increasing attention has been given to milk-derived exosomes, which are small, lipid-bilayer membrane vesicles. Exosome cargos include proteins, lipids, DNA, and various RNA species. Emerging evidence has shown that exosomal RNA participate in many regulated pathways, including cellular growth, antiviral activity, and insulin sensitivity (Vlassov et al., 2012; Nabat et al., 2017; Ying et al., 2017). Milk-derived exosomes have been found in humans, cows, pigs, and rats (Chen et al., 2014; Izumi et al., 2015; Hock et al., 2017), and are involved in multiple biological processes. Previous studies have reported that bovine milk contains microRNAs (miRNA; Chen et al., 2010) and mRNAs (Izumi et al., 2015). As well, expression levels of exosomal miRNA were different between bovine colostrum and mature milk. Bovine milk exosomes (BME) contain more immune-related miRNA in colostrum than in mature milk (Izumi et al., 2012; Sun et al., 2013b). Long noncoding RNA (lncRNA) are those longer than 200 nucleotides.

Received January 6, 2019.

Accepted April 1, 2019.

*These authors contributed equally to this work.

†Corresponding authors: jiajiesun@scau.edu.cn and zhangyl@scau.edu.cn

They have received much attention in the past several years, and have been found to play important functional roles in almost all biological processes, including transcriptional regulation, epigenetic gene regulation, and disease (Batista and Chang, 2013; Karlsson et al., 2016). For example, exosome-transmitted lncRNA *PTENP1* suppresses bladder cancer progression in vitro and in vivo (Zheng et al., 2018). However, few reports are available on bovine milk lncRNA and their profiles in different lactation periods.

The literature has clearly indicated that milk exosomal RNA can be taken up by human macrophages and intestinal cells (Izumi et al., 2015; Wolf et al., 2015) and are permeable to the intestinal barrier in vitro (Rani et al., 2017). Indeed, BME and their RNA cargos in the tissues of mice (Manca et al., 2018) are bioactive in attenuating arthritis (Arntz et al., 2015) and regulating skeletal muscle growth and development (Mobley et al., 2017; Leiferman et al., 2018). However, it is a harsh journey for breast milk RNA to play a role in infant development and maturation (Tomé-Carneiro et al., 2018), and whether exosomal RNA can resist digestive processes remains controversial (Title et al., 2015).

In this study, we confirmed that lncRNA were present in BME. We also identified the abundance of 12 lncRNA at different periods of lactation using quantitative real-time PCR analyses. We also examined the resistance of BME lncRNA to different digestive processes in vitro. Our findings may provide a better understanding of bovine milk in terms of molecular events and physiological functions.

MATERIALS AND METHODS

Milk Sample Preparation and Milk Exosome Isolation

Milk samples that conformed to Chinese national quality standards were collected from FengXing farm in southern China (Guangdong). Milk from 8 healthy Holstein cows (50 to 100 d in lactation) was mixed in equal amounts to construct a pooled milk sample. We used the pooled milk sample for lncRNA sequencing and in vitro digestion. Milk samples in 4 different lactation periods were collected from 24 healthy Holstein cows at 2 d (colostrum, 6 cows), 30 d (6 cows), 150 d (6 cows), and 270 d (6 cows) postpartum. All milk samples were frozen immediately and kept at -30°C until use. Milk exosomes were separated as previously described (Zhou et al., 2012). Briefly, raw bovine milk samples (40 mL) were subjected to 2 successive centrifugations at $2,000$ and $12,000 \times g$ at 4°C for 30 min to remove milk fat globules and cellular debris. The resulting supernatant was filtered through a $0.45\text{-}\mu\text{m}$

filter to obtain a clear whey fraction. Then, the clear whey fraction was prepared for ultracentrifugation at $160,000 \times g$ for 2 h by an SW70Ti rotor (Optima XPN-100; Beckman Coulter Instruments, Fullerton, CA), and the pellets were resuspended in 2 mL of PBS and passed through a $0.22\text{-}\mu\text{m}$ filter to obtain exosome solutions. The exosome solutions were stored at -80°C for further analysis.

RNA Extraction and lncRNA Sequencing

We extracted total RNA from BME samples using Trizol reagent (Invitrogen, Carlsbad, CA) according to the manufacturer's protocol. Total RNA was used as input material for the construction of a cDNA library. The sample was prepared as previously described (Ma et al., 2017). The library was constructed using a NEBNext Ultra Directional RNA Library Prep Kit for Illumina (New England Biolabs Inc., Ipswich, MA) after the removal of ribosomal RNA using an Epicenter Ribo-zero rRNA Removal Kit (Epicenter, Madison, WI). Library sequencing was performed on an Illumina HiSeq 4000 platform (Illumina Inc., San Diego, CA) and 150-bp paired-end reads were generated at the Novogene Bioinformatics Institute (Beijing, China).

Sequence Data Analysis

First, we processed raw reads in fastq format through in-house perl scripts. Then, we obtained clean reads by removing low-quality reads and those containing adapters and poly-N from the raw data. At the same time, Q20, Q30, and GC content of the clean data were calculated. The Q20 and Q30 content represent the percentage of bases with Phred value greater than 20 and 30 in the total bases, respectively. All of the subsequent analyses were performed using high-quality data (mapped reads). An index of the reference genome was built using bowtie2 v2.2.8 and paired-end clean reads were aligned to the reference genome using HISAT2 v2.0.4 (Langmead and Salzberg, 2012). The mapped reads were assembled by StringTie (v1.3.1) software in a reference-based approach (Pertea et al., 2016).

We used 3 types of coding potential analysis software, CNCI (v2; Sun et al., 2013a), CPC (0.9-r2; Kong et al., 2007), and Pfam-scan (v1.3; Bateman et al., 2004), to distinguish mRNA from lncRNA. The intersecting results of each software were defined, and those that were determined to be noncoding were designated as candidate lncRNA. We used Cufflink (v2.1.1) to calculate fragments per kilobase million (FPKM) for both lncRNA and coding genes (Trapnell et al., 2010). The transcript expression levels (FPKM value) were expressed as fragments per kilobase of transcript per

million mapped reads values. Target genes located in *cis* to lncRNA were predicted, based on the assumption that lncRNAs regulate their neighboring regions. Coding genes 100 kb upstream and downstream of all lncRNAs were searched, and their functional roles were analyzed. We implemented gene ontology (GO) enrichment analysis of lncRNA target genes using the GOSec R package (Young et al., 2010), in which gene length bias was corrected; GO terms with a corrected *P*-value of <0.05 were considered significantly enriched. In the identified Kyoto Encyclopedia of Genes and Genomes (KEGG) pathways, we conducted statistical enrichment of target genes using KOBAS software (Mao et al., 2005).

LncRNA Identification by PCR

Total RNA from bovine milk exosome samples was extracted using Trizol reagent (Invitrogen) according to the manufacturer's protocol and cDNA was synthesized using a reverse transcription kit (PrimeScript RT Reagent Kit with gDNA Eraser; TaKaRa, Dalian, China) using 500 ng of total RNA according to the manufacturer's instructions (<https://www.takarabio.com/search-results?term=RR047A>). The PCR was performed on C1000 Touch Thermal Cycler (Bio-Rad, Hercules, CA) in a final 20- μ L volume reaction containing 2 μ L of cDNA, 7 μ L of nuclease-free water, 1 mM each primer and 10 μ L of 2 \times Tap Master Mix (Vazyme, Nanjing, China). The PCR program was as follows: 5 min at 95°C, 35 cycles of 30 s at 95°C, 30 s at the cor-

responding annealing temperature and 72°C for 30 s, followed by 72°C for 10 min. The primers were designed using Primer 5.0 (Supplemental Table S1; <https://doi.org/10.3168/jds.2019-16257>). We confirmed the PCR products of 12 lncRNA by agarose gel and sequencing.

Digestion In Vitro

Milk was digested in vitro as described previously (Kopf-Bolanz et al., 2012). All chemicals and enzymes for in vitro digestion were purchased from Sigma-Aldrich (St. Louis, MO). Briefly, using a table concentrator at 37°C, 2.25 mL of cow milk was initially mixed with 3 mL of salivary juice and incubated for 5 min; then, 6 mL of gastric juice was added to incubate for 60 min; finally, 6 mL of pancreatic juice plus 3 mL of bile juice were added to incubate for 60 min. As a negative normal saline control (undigested), 2.25 mL of milk mixed with 18 mL of normal saline went through the same procedure for in vitro digestion. Whey fraction and exosomes isolation were carried out as in Milk Sample Preparation and Milk Exosome Isolation, above. The digested conditions are shown in Figure 1.

Transmission Electron Microscopy and Particle Size Analysis

Purified exosomal fractions of 10 μ L were analyzed by transmission electron microscopy (TEM; JEM-2000EX; Jeol, Tokyo, Japan). Samples were placed on formvar-coated copper grids for 2 min, washed briefly

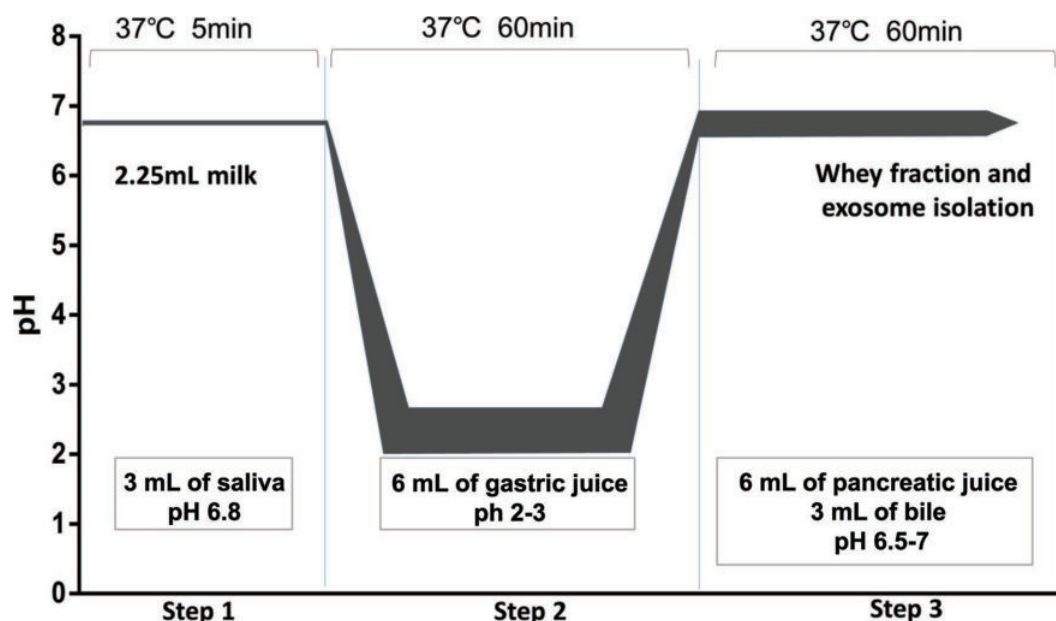


Figure 1. Incubation times and conditions during in vitro digestion of milk.

in ultrapure water, negatively stained with 1% uranyl acetate, and observed. Size distribution was determined by the Zetasizer (Malvern Panalytical, Malvern, UK) at 25°C.

BCA Protein Assay, SDS-PAGE and Western Blot Analyses

We assayed all protein content using the Pierce BCA Protein Assay Kit (ThermoScientific, Waltham, MA) according to the manufacturer's instructions (<https://www.thermofisher.com/order/catalog/product/23225?SID=srch-srp-23225>), and SDS-PAGE (10%) was used to separate proteins. Equal amounts of proteins (20 µg) from milk whey samples (undigested and in vitro digested) were run on the gel, and stained with 0.1% Coomassie Brilliant Blue R-250. To confirm exosomes from undigested and in vitro-digested milk, we used 2 positive markers (CD9 and CD63) for Western blots. The proteins were separated by SDS-PAGE and transferred to a polyvinylidene difluoride membrane (Millipore, Billerica, MA). After blocking with 5% skim milk for 2 h, the membranes were incubated overnight at 4°C with specific antibodies against CD9 and CD63 (1:1,000; Sangon Biotech, China). We applied horseradish peroxidase-conjugated goat anti-rabbit IgG (H⁺L; 1:50,000; Jackson ImmunoResearch, West Grove, PA) as a secondary antibody for 1 h at room temperature. The proteins were measured using a FluorChem M Fluorescent Imaging System (ProteinSimple, Santa Clara, CA).

lncRNA Expression Analysis

We extracted total RNA from exosomes isolated from normal saline control (undigested) milk, in vitro-digested milk, and bovine milk from 4 different periods of lactation using Trizol reagent (Invitrogen) according to the manufacturer's protocol. We synthesized cDNA using a reverse transcription kit (PrimeScript RT Reagent Kit with gDNA Eraser; TaKaRa) using 500 ng of total RNA according to the manufacturer's instructions (<https://www.takarabio.com/search-results?term=RR047A>). We used SYBR Green qRT-PCR Master Mix reagent (Promega, Madison, WI) sense and anti-sense primers for real-time quantitative PCR. We performed quantitative real-time PCR analysis using the CFX96 Real-Time PCR Detection System (Bio-Rad). We normalized lncRNA levels in BME against a synthesized exogenous reference λpolyA + RNA (TaKaRa; Gilsbach et al., 2006). According to the instructions (<https://www.takarabio.com/search-results?term=3789>), we added synthetic λpolyA + RNA (1.8×10^8 copies) to 1.2 mL of denatured sample (all BME sam-

ples with equal protein concentration and equal volume were mixed with Trizol reagent). Next, total RNA was extracted according to the instructions provided with the Trizol reagent. The expression of indicated genes was normalized to exogenous reference control using the $2^{-\Delta\Delta Ct}$ method.

Statistical Analysis

Quantitative real-time PCR was performed in triplicate. All data were expressed as means \pm standard error of the mean (SEM). Data were analyzed using SPSS 17.0 (SPSS Inc., Chicago, IL). One-way ANOVA followed by Tukey's multiple comparison was used to compare the lncRNA levels in exosomes isolated from bovine milk in different periods of lactation. We used *t*-tests to compare lncRNA level in exosomes isolated from undigested milk and in vitro-digested milk. We considered *P*-values <0.05 to be statistically significant.

RESULTS

Identification of lncRNA in BME Using RNA-seq

For RNA-seq data, we obtained 72,899,916 raw reads and 68,824,548 clean reads after removing low-quality sequences and adaptor sequences. Data output quality and mapped reads information are shown in Supplemental Tables S2 and S3, respectively (<https://doi.org/10.3168/jds.2019-16257>). Based on structural and noncoding functional characteristics of lncRNA, we identified 3,475 novel lncRNA after filtering out annotation transcripts (Figure 2A-B; detailed information shown in Supplemental Files S1 and S2, <https://doi.org/10.3168/jds.2019-16257>), including 86.3% (2,998) long intergenic noncoding RNA, 4.1% (141) antisense lncRNA, and 9.7% (336) intronic lncRNA (Figure 2C). We detected 6 annotated lncRNA in BME (<http://asia.ensembl.org/index.html>), with detailed information shown in Supplemental Files S3 and S4 (<https://doi.org/10.3168/jds.2019-16257>).

Genomic Features of lncRNA in Bovine Milk Exosomes

We analyzed gene structures and expression levels for comparison between lncRNA and mRNA. In agreement with a previous study (Trapnell et al., 2010), lncRNA (novel and annotated lncRNA) are shorter than protein-coding transcripts (Figure 2D), and their genes tend to contain fewer exons (Figure 2E). Most of the mRNA had longer open reading frames than lncRNA (Figure 2F), but our findings showed higher expression of lncRNA than mRNA in BME (Figure 2G).

Identification of lncRNA by PCR Analysis

To verify the sequencing results, we randomly selected 12 lncRNA from the top 20 expression levels in sequencing for PCR amplification. The product sizes of all selected lncRNA were fully matched (Figure 3A). Sequencing of 12 lncRNA amplified products showed that 7 lncRNA were fully matched and 5 had 1 to 3

mismatched nucleotides when compared with RNA sequencing (Supplemental Table S4; <https://doi.org/10.3168/jds.2019-16257>).

GO and KEGG Annotation of lncRNA

Recent studies have suggested that lncRNA may act in *cis* and affect the gene expression of their chromo-

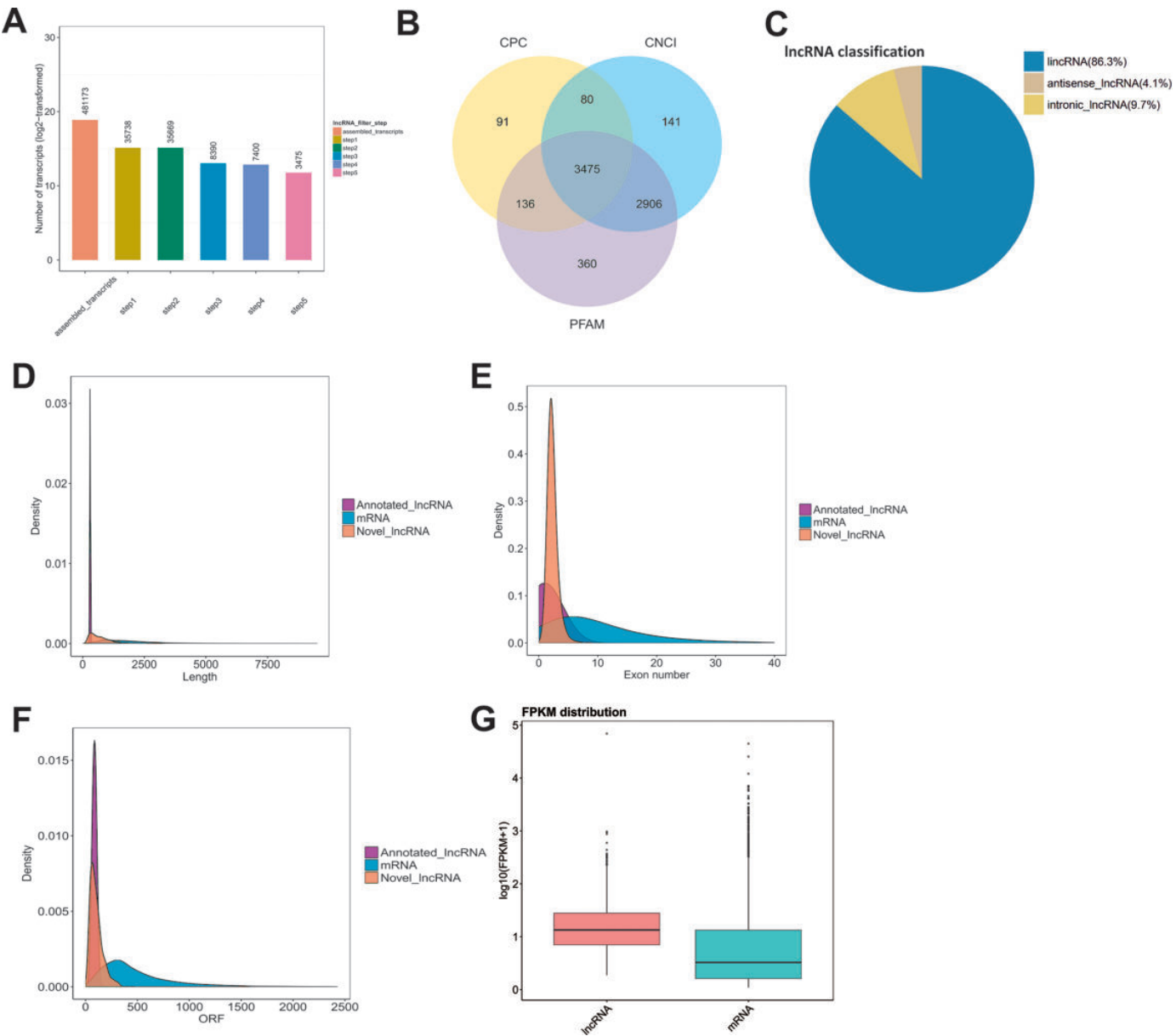


Figure 2. Identification and characterization of long noncoding RNA (lncRNA) in bovine milk exosomes. (A, B) Selection of lncRNA in bovine milk exosomes using CPC, Pfam and CNCI software; 3,475 novel lncRNA were identified after the removal of putative protein-coding transcripts; (C) distribution of the 3 types of lncRNA; (D) distribution of lncRNA and mRNA length; (E) distribution of the density of exons in lncRNA and mRNA; (F) distribution of the density of open reading frames (ORF) in lncRNA and mRNA; (G) expression level of mRNA and lncRNA based on log₁₀(FPKM + 1). FPKM = fragments per kilobase million. The upper edge of the boxes is the upper quartile, and the lower edge is the lower quartile. The midline is the median. The whiskers are the maximum or minimum. The dots are outlier values. CPC = coding potential calculator; CNCI = coding-noncoding index; PFAM = protein families; ORF = open reading frames.

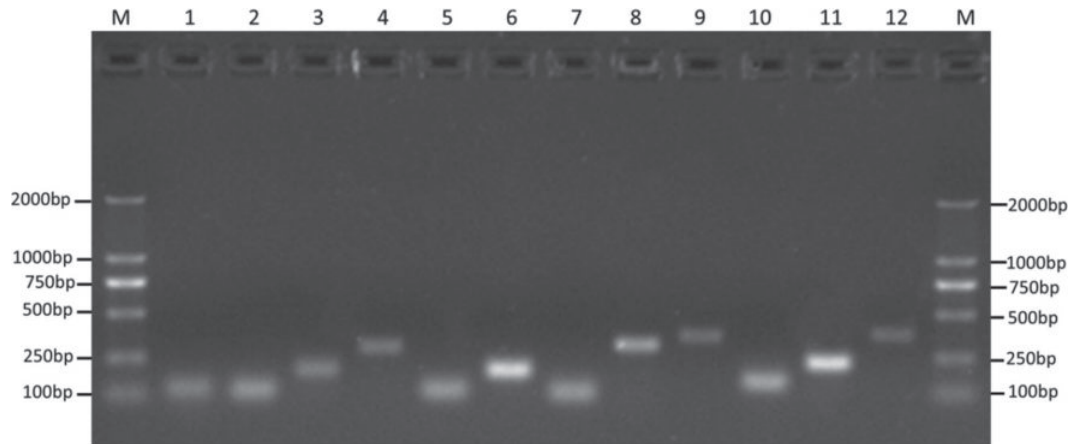


Figure 3. Identification of long noncoding RNA (LNC) PCR product size by agarose gel electrophoresis. Lane M: marker; lanes 1 to 12, respectively: ENSBTAT00000065829 (119 bp), LNC_001182 (112 bp), LNC_001285 (195 bp), LNC_002259 (298 bp), LNC_001989 (111 bp), LNC_001183 (189 bp), LNC_002066 (101 bp), LNC_002229 (306 bp), LNC_001972 (362 bp), LNC_002303 (144 bp), LNC_001965 (227 bp), LNC_001442 (359 bp).

somal neighborhood, 100 kb upstream and downstream (Ørom et al., 2010). To investigate the relationship of lncRNA and their neighboring coding genes, we identified BME lncRNA that corresponded to 3,025 protein-coding genes (detailed information shown in Supplemental File S5; <https://doi.org/10.3168/jds.2019-16257>). Our GO annotation indicated that the predicted target genes were significantly enriched in antigen processing and presentation, positive regulation of type I interferon production, negative regulation of tumor necrosis factor production, thymus development, osteoblast differentiation, embryonic cranial skeleton morphogenesis, neuron projection development, response to progesterone, androgen receptor binding, cell division, cell-cell adhesion, and extracellular exosome terms (Figure 4A). Our KEGG pathway analysis showed that lncRNA target genes were significantly enriched in ribosomes, the neurotrophin signaling pathway, the FcεRI signaling pathway, and the gonadotropin-releasing hormone signaling pathway. Regulation of the actin cytoskeleton, vascular endothelial growth factor signaling pathway, intestinal immune network for IgA production, hypoxia-inducible factors-1 signaling pathway and FcγR-mediated phagocytosis were also enriched (Figure 4B). These findings suggested that BME lncRNA could regulate fetal growth, development, immune system, and reproduction.

LncRNA Expression in BME in 4 Lactation Periods

Previous studies have indicated that miRNA demonstrate different expression patterns between colostrum and mature milk. To examine whether lncRNA expression levels are diverse in different lactation periods,

we selected 12 high-expressed lncRNA and compared expression levels in 4 periods (d 2 colostrum, d 30, 150, and 270 of lactation) using quantitative real-time PCR. As shown in Figure 5, expression levels of the 12 lncRNA varied during different lactation stages. Expression levels of LNC_001182 and LNC_002303 were higher in colostrum than in mature milk. However, levels of LNC_001442 were higher in the mid- and late-lactation periods (150 and 270 d) than in colostrum and early lactation (30 d). Notably, expression of 4 lncRNA (LNC_001965, LNC_001183, LNC_001989, and LNC_002066) was higher in the mid-lactation period (150 d) than in colostrum and early lactation (30 d). The expression levels of other selected lncRNA (LNC_001285, LNC_002259, LNC_001972, LNC_002229, and ENSBTAT00000065829) remained unchanged in colostrum and the other 3 lactation periods. These results implied that different expression patterns were present and might be related to their function in milk.

Characterization of Milk Protein, Exosome Stability, and lncRNA Components After In Vitro Digestion

Milk exosomes were stable, maintaining their characteristic features and lncRNA components in simulated human in vitro digestion. Our SDS-PAGE analysis showed that most of the milk proteins, including abundant casein fractions and β-lactoglobulin, were digested by the different juices (Figure 6A). We further characterized exosomes isolated from undigested and in vitro-digested milk using transmission electron microscopy and Zetasizer analyses and found that the morphology (Figure 6B and C) and size (Figure 6D) of in vitro-

digested milk exosomes did not change significantly compared with undigested milk exosomes. Moreover, positive common surface markers CD9 and CD63 were present in both undigested and in vitro-digested milk exosomes (Figure 6E). We used agarose gel to verify the

RNA stability of milk exosomes after in vitro digestion, and results showed that the in vitro digestion process did not change RNA stability (Figure 6F). Quantitative real-time PCR analysis showed that the levels of the 12 lncRNA did not change after in vitro digestion

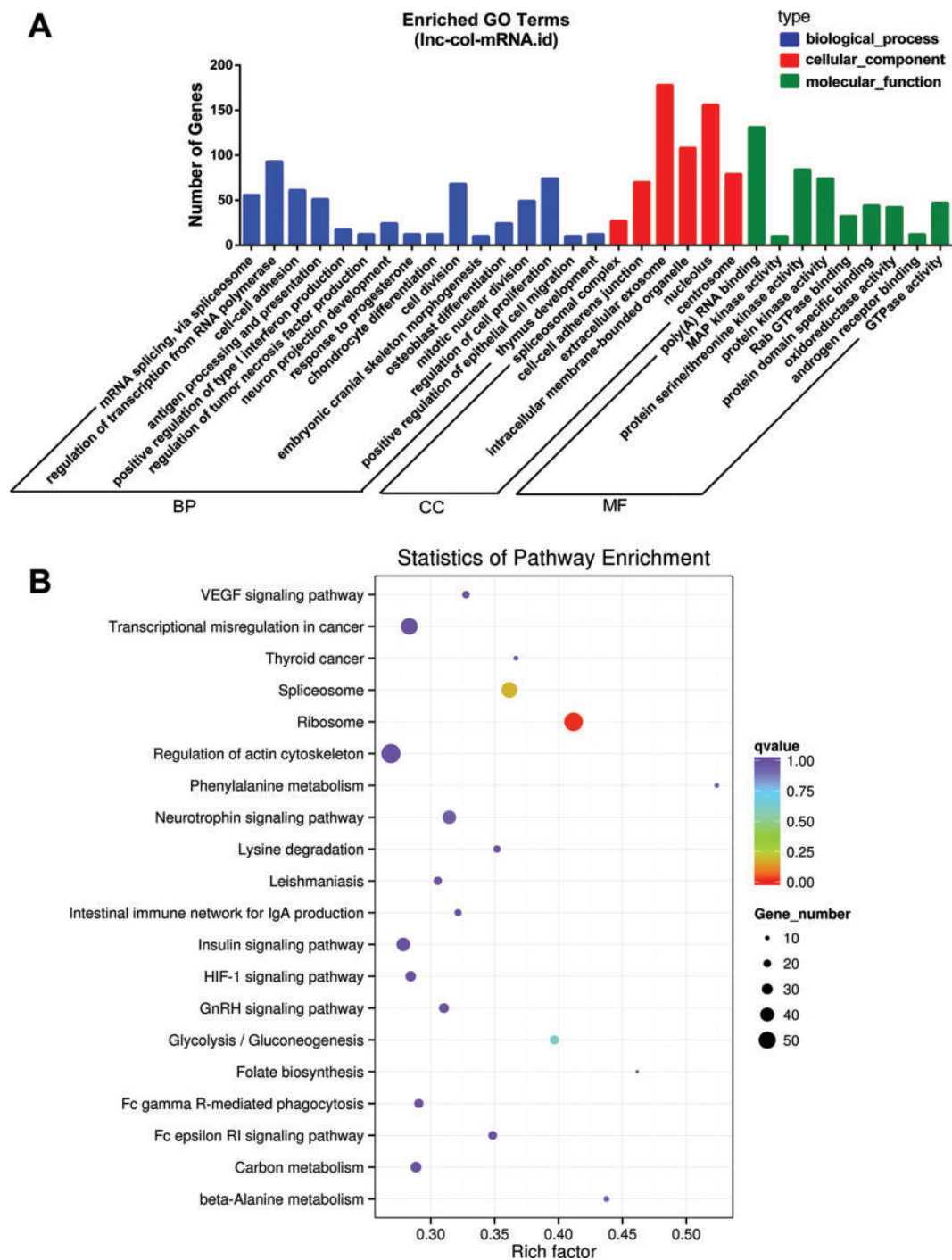


Figure 4. Cluster analysis and enrichment analysis of bovine milk exosome long noncoding RNA (lncRNA). (A) Gene ontology (GO) annotation analysis. (B) Kyoto Encyclopedia of Genes and Genomes (KEGG) enrichment analysis of neighboring gene functions. BP = biological process; CC = cellular component; MF = molecular function.

(Figure 7). Taken together, these results indicate that the digestive process did not affect the characteristic features or lncRNA components of the milk exosomes.

DISCUSSION

In the present study, we explored a comprehensive BME lncRNA expression profile via deep sequencing. We identified 3,481 lncRNA in BME. Comparison of the genomic features of lncRNA and mRNA revealed

that our observations coincided with recent studies (Ren et al., 2016; Ma et al., 2017). Moreover, the PCR product sequence of 12 lncRNA in BME was basically matched (Dohm et al., 2008). To the best of our knowledge, this is the first work to report lncRNA in exosomes from bovine milk, although previous studies have confirmed the presence of mRNA and miRNA in BME (Chen et al., 2010; Izumi et al., 2015). Our results provide supplemental evidence for future research into bovine milk RNA.

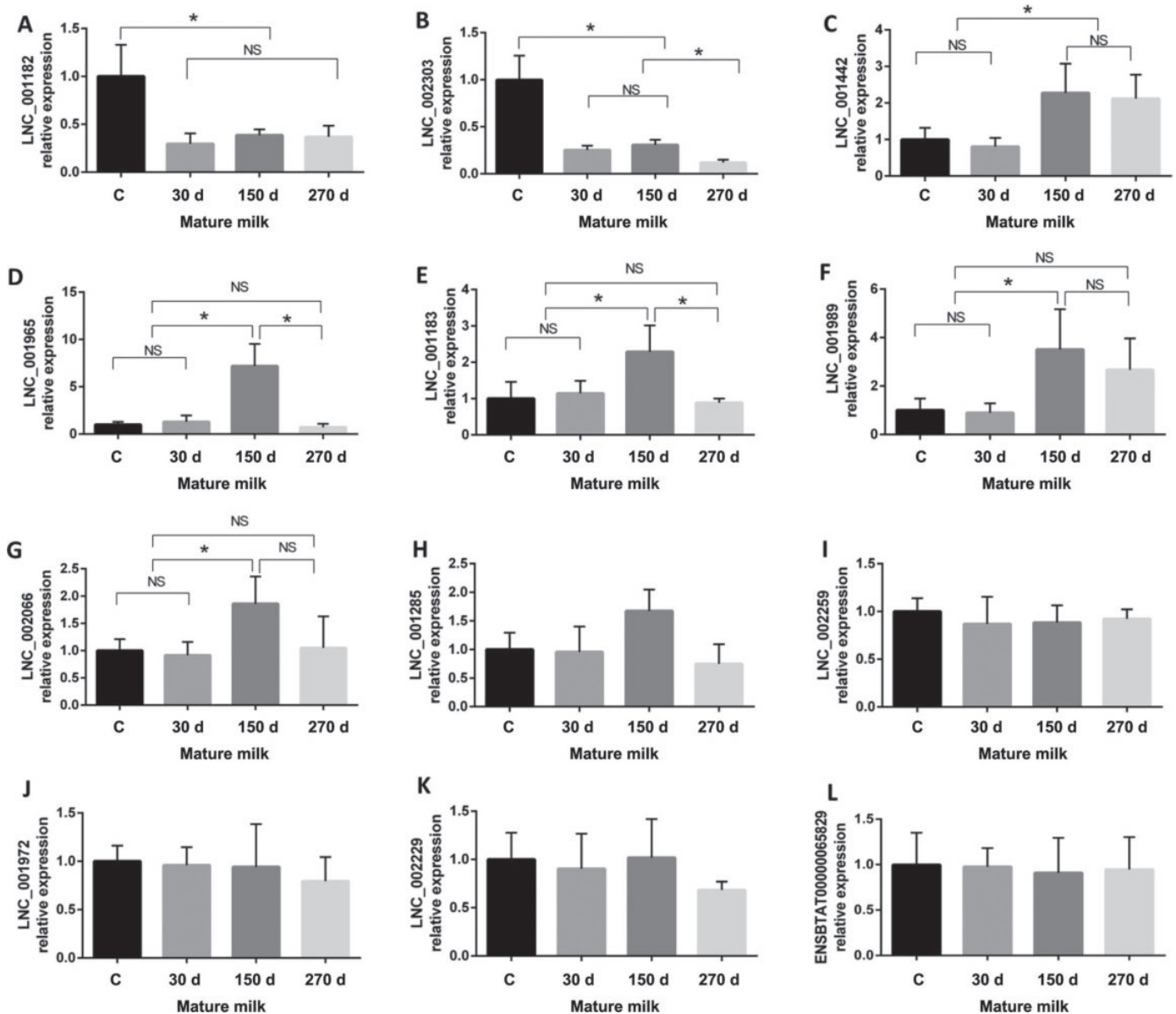


Figure 5. Quantitative real-time PCR analysis of selected long noncoding RNA (lncRNA; LNC) with normalization. To measure the expression levels of lncRNA in equal volumes and protein contents of exosomes from 4 periods of lactation milk (C = colostrum; 30, 150, and 270 d = mature milk from different stages of lactation), quantitative PCR data obtained were normalized to a synthesized exogenous reference λ polyA + RNA. The expression of indicated genes was normalized to an exogenous reference control using $2^{-\Delta\Delta Ct}$ method. Values are mean \pm SEM ($n = 6$). * $P < 0.05$.

Breast milk is the optimal food for infants and will never be fully equivalent to artificial substitutes (Sobti et al., 2002). Traditionally, immunoglobulins and non-nutritional bioactive factors in milk have been considered the main regulated immunity substance. More recently, scientific interest in the modulating function of milk exosomal RNA has increased. Exosomes are of particular interest, because the cargo of sorting in exosomes is a regulated, nonrandom process, and exosomes play essential roles in cell-to-cell communication. Previous studies have indicated that RNA are selectively encapsulated into exosomes (Skog et al., 2008). We found that lncRNA encapsulated in BME were expressed at higher levels than mRNA. Functional analysis showed that BME lncRNA target genes were enriched in many biological processes that are essential for the growth and development of infants. The BME lncRNA have been predicted to be involved in antigen processing and presentation, the regulation of interferon and tumor

necrosis factor production, thymus development, and the FcεRI signaling pathway, which are associated with immune response (Kawakami and Galli, 2002). Emerging diverse mechanisms for lncRNA have demonstrated their effect on innate and adaptive immunity (Aune and Spurlock, 2016). Izumi et al. (2015) have suggested that cargos in BME, particularly RNA, are delivered to circulating immune cells in humans. Arntz et al. (2015) have reported that oral administration of bovine milk-derived exosomes attenuate autoimmune and inflammatory diseases, possibly because BME contains many immunoregulatory RNA. It was also revealed by GO and KEGG analysis that osteoblast differentiation, embryonic cranial skeleton morphogenesis, and regulation of actin cytoskeleton were enriched. A previous study (Oliveira et al., 2016) found that BME increase osteocyte number and woven bone formation, contributing to altered osteoblast differentiation and bone matrix formation in mice, and increased osteoblast differentia-

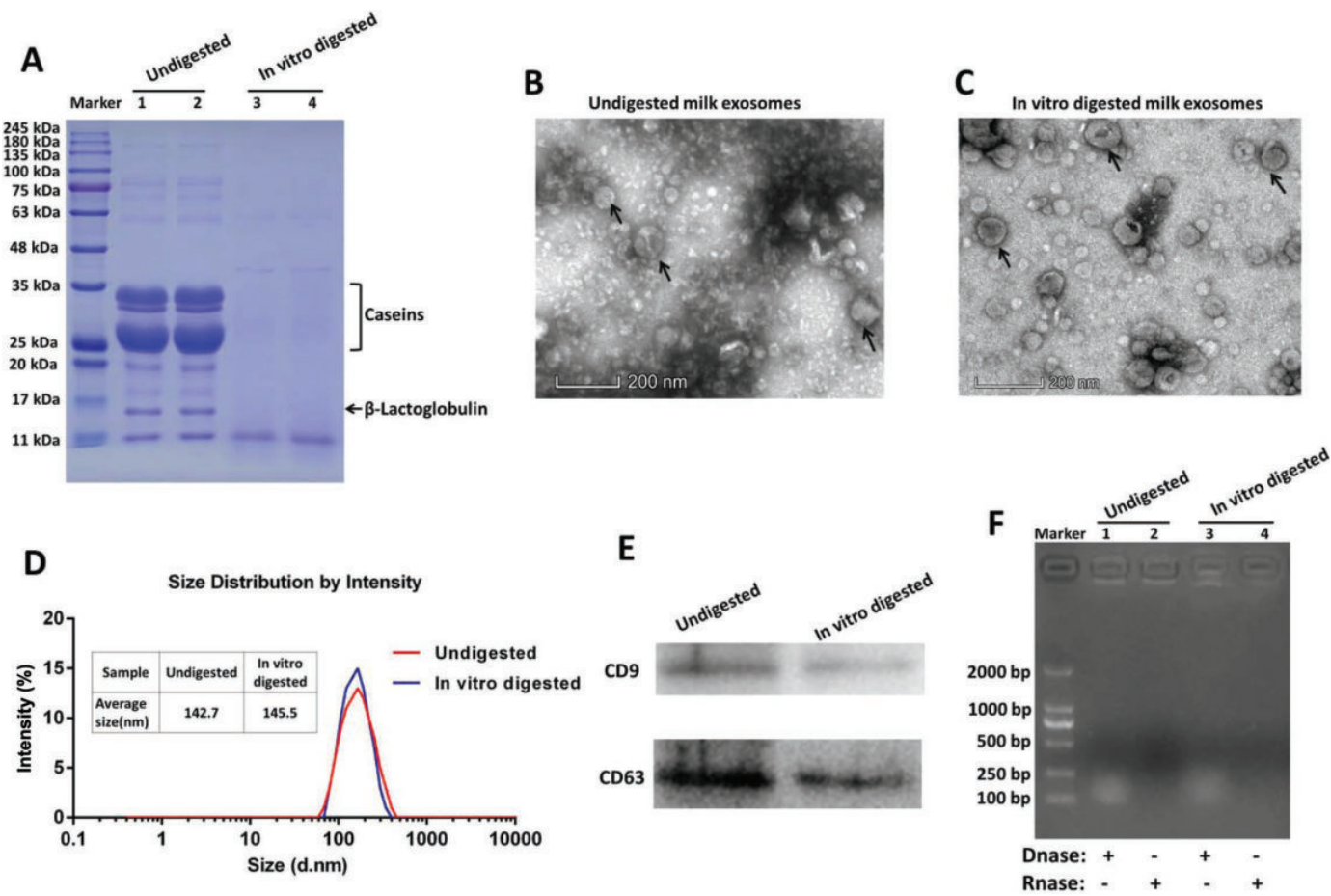


Figure 6. (A) Sodium dodecyl sulfate-PAGE (10%) analysis; equal amounts of protein (20 μg) isolated from undigested and in vitro-digested milk were loaded onto the gel and stained with 0.1% Coomassie Brilliant Blue R-250; (B) transmission electron microscopy analysis of undigested milk exosomes (indicated by arrows) and (C) in vitro-digested milk exosomes; (D) size distribution analysis of undigested and in vitro-digested milk exosomes; (E) bovine milk exosome proteins from undigested and in vitro-digested milk resolved by SDS-PAGE, and analyzed by Western blot (2 positive markers, CD9 and CD63); (F) agarose gel analysis of RNA extracted from undigested and in vitro-digested milk exosomes.

tion in human bone marrow-derived mesenchymal stem cells. We know that BME also regulate skeletal muscle development. Mobley et al. (2017) reported that bovine whey protein contains exosomes capable of stimulating an anabolic response in skeletal muscle cells. Leiferman et al. (2018) obtained bovine milk exosome- and RNA-depleted (ERD) diets by ultrasound (ultrasonication leads to >98% depletion of RNA cargos in exosomes, >20% decrease in exosome count) and found that BME and their RNA cargos have moderate effects on skeletal muscle in mice. In our study, functional analysis showed that BME lncRNA target genes were also enriched in neurodevelopment and reproduction, which included neuron projection development, response to progesterone, androgen receptor binding, the neurotrophin signaling pathway, the gonadotropin-releasing hormone signaling pathway, and the vascular endothelial growth factor signaling pathway. More recently, Zempleni et al. (2019) reviewed milk-derived exosomes, mentioning much of their unpublished data. The ERD and exosome- and RNA-sufficient (ERS) diets are used to assess various phenotypes from dietary depletion of BME in mice. Mice fed an ERD diet exhibited a loss of spatial learning and memory, and a loss in fecundity compared with ERS controls. Hepatic levels of purine metabolites

were substantially higher in mice fed the ERD diet than in ERS controls. The litter size produced by ERS breeders was twice that of the litter size of ERD breeders (Zempleni et al., 2019). Based on our findings and those of other teams, we suggest that the abundant lncRNA in BME may be absorbed by infants and play an important role in their growth and development. Milk not only provides nutrition, but also can serve as important information transfer for infants, and lncRNA are potential regulatory molecules in bovine milk.

In this study, the profile of lncRNA in BME from different lactation periods showed diverse expression. We found that expression of LNC_001182 and LNC_002303 were higher in colostrum than in mature milk. Earlier studies (Izumi et al., 2012; Sun et al., 2013b) provided strong evidence that related to immune development were significantly higher in colostrum than in mature milk. Our results show that LNC_001182 and LNC_002303 could be involved in the regulation organ or immune system development in newborn calves, but further research is needed to describe the detailed mechanisms. We found that 4 lncRNA (LNC_001965, LNC_001183, LNC_001989, and LNC_002066) had higher expression in mid-lactation milk (150 d) than in colostrum and early-lactation milk (30 d). These

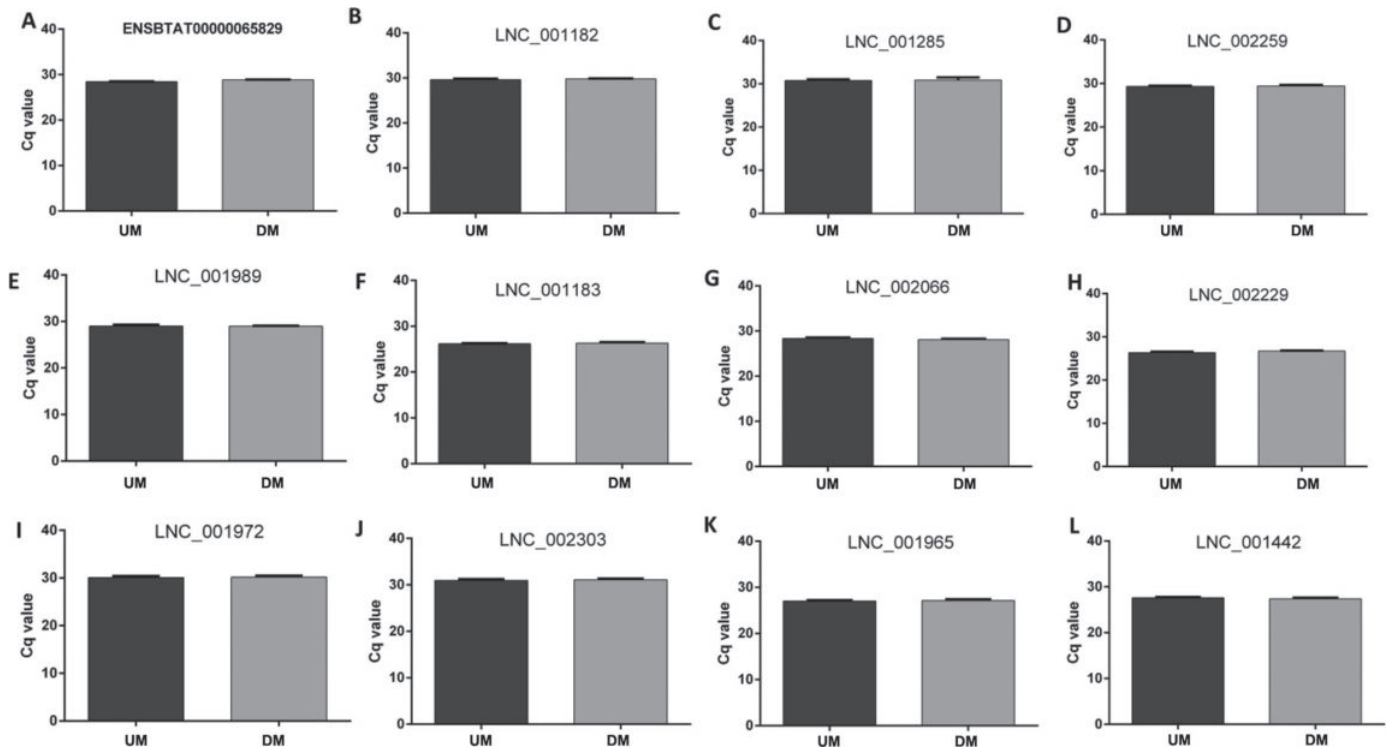


Figure 7. Analysis of abundant long noncoding RNA (lncRNA; LNC) present in undigested (UM) and in vitro-digested (DM) milk exosomes. Equal amounts of the exosomal RNA (500 ng) from undigested and in vitro-digested milk were used to synthesize cDNA. Real-time PCR of abundant lncRNA was done using the SYBR Green kit. The y-axis indicates cycle quantification (C_q) values obtained after real-time PCR. Values are mean \pm SEM ($n = 3$).

findings suggest that the levels of these lncRNA may change to accommodate infants' development requirements and the regulation of lactation (Yang et al., 2018). We also identified 5 lncRNA (LNC_001285, LNC_002259, LNC_001972, LNC_002229 and ENSBTAT00000065829) that were present at stable levels in milk from all lactation periods. As Chen et al. (2010) have reported, stable RNA expression levels can serve as an internal "standard" or "biomarker" for quality control of milk, but more research is needed to validate these findings.

Studies have assessed the stability of milk exosomes and whether their contents can survive various digestive conditions, such as low pH, different temperatures, and digestion in vitro (Izumi et al., 2012; Rani et al., 2017). In the present study, we used a validated in vitro digestion model (Kopf-Bolan et al., 2012) and proved that milk exosomes and their lncRNA were stable and could resist digestive processes. According to the absence of the major caseins and β -lactoglobulin in the digested samples, we confirmed that the in vitro digestion process for bovine milk was efficient, and that results were consistent with human digestive processes for macronutrient decomposition (Kopf-Bolan et al., 2012). Excitingly, exosomal morphology and size showed no significant difference between undigested and in vitro-digested milk. The positive surface markers for milk exosomes, CD9 and CD63, were still present after digestion in vitro. These results confirmed that BME remained intact during the digestion process. More importantly, RNA extracted from in vitro-digested milk exosomes remained undigested (Figure 6F). Real-time PCR revealed that in vitro digestion did not change the levels of BME lncRNA. Thus we concluded that exosomal lncRNA in bovine milk were stable after in vitro digestive processes. Previous reports have demonstrated that milk exosomal miRNA were stable after undergoing RNase treatment, low pH treatment, and in vitro digestion in bovines (Izumi et al., 2012; Rani et al., 2017) and humans (Liao et al., 2017). The reason that milk exosomes and encapsulated lncRNA survive the harsh digestive processes is the protective shielding effect of the exosomal lipid-bilayer membrane, along with its embedded proteins (Théry et al., 2002; Rani et al., 2017). Survival of milk exosomal lncRNA forms a basis for their further biological activity in their recipients.

CONCLUSIONS

The present study is the first to explore BME lncRNA profiles by high-throughput sequencing. We have demonstrated that bovine milk contained lncRNA, and that most of them participated in immunity, develop-

ment, and reproduction. Bovine milk exosomal lncRNA exhibited various expression patterns during different periods of lactation, representing special mechanisms for adapting to infants' development needs. We also found that milk exosomal lncRNA were stable in the harsh environment of the human digestive system in vitro. These results contribute to an increased understanding of the roles of lncRNA in BME, and build a foundation for future studies to evaluate the role of milk lncRNA in infants.

ACKNOWLEDGMENTS

This work was supported by grants from the National Key Research and Development Program of China (2016YFD0500503, 2016YFD0501205), the Natural Science Foundation of China program (31802156, 31472163, and 31872435), and the Key Project of Guangdong Provincial Nature Science Foundation (2018B030311015, 2016A030313413).

REFERENCES

- Admyre, C., S. M. Johansson, K. R. Qazi, J.-J. Filen, R. Lahesmaa, M. Norman, E. P. A. Neve, A. Scheynius, and S. Gabrielsson. 2007. Exosomes with immune modulatory features are present in human breast milk. *J. Immunol.* 179:1969–1978.
- Arntz, O. J., B. C. H. Pieters, M. C. Oliveira, M. G. A. Broeren, M. B. Bennink, M. de Vries, P. L. E. M. van Lent, M. I. Koenders, W. B. van den Berg, P. M. van der Kraan, and F. A. J. van de Loo. 2015. Oral administration of bovine milk derived extracellular vesicles attenuates arthritis in two mouse models. *Mol. Nutr. Food Res.* 59:1701–1712.
- Aune, T. M., and C. F. Spurlock III. 2016. Long non-coding RNAs in innate and adaptive immunity. *Virus Res.* 212:146–160.
- Bateman, A., L. Coin, R. Durbin, R. D. Finn, V. Hollich, S. Griffiths-Jones, A. Khanna, M. Marshall, S. Moxon, E. L. L. Sonnhammer, D. J. Studholme, C. Yeats, and S. R. Eddy. 2004. The Pfam protein families database. *Nucleic Acids Res.* 32:D138–D141.
- Batista, P. J., and H. Y. Chang. 2013. Long noncoding RNAs: Cellular address codes in development and disease. *Cell* 152:1298–1307.
- Chen, T., Q.-Y. Xi, R.-S. Ye, X. Cheng, Q.-E. Qi, S.-B. Wang, G. Shu, L.-N. Wang, X.-T. Zhu, Q.-Y. Jiang, and Y.-L. Zhang. 2014. Exploration of microRNAs in porcine milk exosomes. *BMC Genomics* 15:100.
- Chen, X., C. Gao, H. Li, L. Huang, Q. Sun, Y. Dong, C. Tian, S. Gao, H. Dong, D. Guan, X. Hu, S. Zhao, L. Li, L. Zhu, Q. Tan, J. Zhang, K. Zen, and C.-Y. Zhang. 2010. Identification and characterization of microRNAs in raw milk during different periods of lactation, commercial fluid, and powdered milk products. *Cell Res.* 20:1128–1137.
- Dieterich, C. M., J. P. Felice, E. O'Sullivan, and K. M. Rasmussen. 2013. Breastfeeding and health outcomes for the mother-infant dyad. *Pediatr. Clin. North Am.* 60:31–48.
- Dohm, J. C., C. Lottaz, T. Borodina, and H. Himmelbauer. 2008. Substantial biases in ultra-short read data sets from high-throughput DNA sequencing. *Nucleic Acids Res.* 36:e105.
- Gilsbach, R., M. Kouta, H. Bonisch, and M. Brüss. 2006. Comparison of in vitro and in vivo reference genes for internal standardization of real-time PCR data. *Biotechniques* 40:173–177.
- Hauck, F. R., J. M. D. Thompson, K. O. Tanabe, R. Y. Moon, and M. M. Vennemann. 2011. Breastfeeding and reduced risk of sudden infant death syndrome: A meta-analysis. *Pediatrics* 128:103–110.

- Hock, A., H. Miyake, B. Li, C. Lee, L. Ermini, Y. Koike, Y. Chen, P. Maattanen, A. Zani, and A. Pierro. 2017. Breast milk-derived exosomes promote intestinal epithelial cell growth. *J. Pediatr. Surg.* 52:755–759.
- Izumi, H., N. Kosaka, T. Shimizu, K. Sekine, T. Ochiya, and M. Takase. 2012. Bovine milk contains microRNA and messenger RNA that are stable under degradative conditions. *J. Dairy Sci.* 95:4831–4841.
- Izumi, H., M. Tsuda, Y. Sato, N. Kosaka, T. Ochiya, H. Iwamoto, K. Namba, and Y. Takeda. 2015. Bovine milk exosomes contain microRNA and mRNA and are taken up by human macrophages. *J. Dairy Sci.* 98:2920–2933.
- Karlsson, O., R. S. Rodosthenous, C. Jara, K. J. Brennan, R. O. Wright, A. A. Baccarelli, and R. J. Wright. 2016. Detection of long non-coding RNAs in human breastmilk extracellular vesicles: Implications for early child development. *Epigenetics* 11:721–729.
- Kawakami, T., and S. J. Galli. 2002. Regulation of mast-cell and basophil function and survival by IgE. *Nat. Rev. Immunol.* 2:773–786.
- Kong, L., Y. Zhang, Z.-Q. Ye, X.-Q. Liu, S.-Q. Zhao, L. Wei, and G. Gao. 2007. CPC: Assess the protein-coding potential of transcripts using sequence features and support vector machine. *Nucleic Acids Res.* 35:W345–W349.
- Kopf-Bolanz, K. A., F. Schwander, M. Gijs, G. Vergeres, R. Portmann, and L. Egger. 2012. Validation of an in vitro digestive system for studying macronutrient decomposition in humans. *J. Nutr.* 142:245–250.
- Langmead, B., and S. L. Salzberg. 2012. Fast gapped-read alignment with Bowtie 2. *Nat. Methods* 9:357–359.
- Leiferman, A., J. Shu, R. Grove, J. Cui, J. Adamec, and J. Zemleni. 2018. A diet defined by its content of bovine milk exosomes and their RNA cargos has moderate effects on gene expression, amino acid profiles and grip strength in skeletal muscle in C57BL/6 mice. *J. Nutr. Biochem.* 59:123–128.
- Liao, Y., X. Du, J. Li, and B. Lonnerdal. 2017. Human milk exosomes and their microRNAs survive digestion in vitro and are taken up by human intestinal cells. *Mol. Nutr. Food Res.* 61.
- Ma, Q., L. Li, Y. Tang, Q. Fu, S. Liu, S. Hu, J. Qiao, C. Chen, and W. Ni. 2017. Analyses of long non-coding RNAs and mRNA profiling through RNA sequencing of MDBK cells at different stages of bovine viral diarrhea virus infection. *Res. Vet. Sci.* 115:508–516.
- Manca, S., B. Upadhyaya, E. Mutai, A. T. Desaulniers, R. A. Cedarberg, B. R. White, and J. Zemleni. 2018. Milk exosomes are bioavailable and distinct microRNA cargos have unique tissue distribution patterns. *Sci. Rep.* 8:11321.
- Mao, X., T. Cai, J. G. Olyarchuk, and L. Wei. 2005. Automated genome annotation and pathway identification using the KEGG Orthology (KO) as a controlled vocabulary. *Bioinformatics* 21:3787–3793.
- Mobley, C. B., P. W. Mumford, J. J. McCarthy, M. E. Miller, K. C. Young, J. S. Martin, D. T. Beck, C. M. Lockwood, and M. D. Roberts. 2017. Whey protein-derived exosomes increase protein synthesis and hypertrophy in C2C12 myotubes. *J. Dairy Sci.* 100:48–64.
- Nabet, B. Y., Y. Qiu, J. E. Shabason, T. J. Wu, T. Yoon, B. C. Kim, J. L. Benci, A. M. DeMichele, J. Tchou, J. Marcotrigiano, and A. J. Minn. 2017. Exosome RNA unshielding couples stromal activation to pattern recognition receptor signaling in cancer. *Cell* 170:352–366.e13.
- Oliveira, M. C., O. J. Arntz, E. N. B. Davidson, P. L. E. M. van Lent, M. I. Koenders, P. M. van der Kraan, W. B. van den Berg, A. V. M. Ferreira, and F. A. J. van de Loo. 2016. Milk extracellular vesicles accelerate osteoblastogenesis but impair bone matrix formation. *J. Nutr. Biochem.* 30:74–84.
- Ørom, U. A., T. Derrien, M. Beringer, K. Gumireddy, A. Gardini, G. Bussotti, F. Lai, M. Zytnicki, C. Notredame, Q. Huang, R. Guigo, and R. Shiekhattar. 2010. Long Noncoding RNAs with Enhancer-like Function in Human Cells. *Cell* 143:46–58.
- Pertea, M., D. Kim, G. M. Pertea, J. T. Leek, and S. L. Salzberg. 2016. Transcript-level expression analysis of RNA-seq experiments with HISAT, StringTie and Ballgown. *Nat. Protoc.* 11:1650–1667.
- Rani, P., M. Vashisht, N. Golla, S. Shandilya, S. K. Onteru, and D. Singh. 2017. Milk miRNAs encapsulated in exosomes are stable to human digestion and permeable to intestinal barrier in vitro. *J. Funct. Foods* 34:431–439.
- Ren, H., G. Wang, L. Chen, J. Jiang, L. Liu, N. Li, J. Zhao, X. Sun, and P. Zhou. 2016. Genome-wide analysis of long non-coding RNAs at early stage of skin pigmentation in goats (*Capra hircus*). *BMC Genomics* 17:67.
- Savino, F., and S. A. Liguori. 2008. Update on breast milk hormones: Leptin, ghrelin and adiponectin. *Clin. Nutr.* 27:42–47.
- Skog, J., T. Wuerdinger, S. van Rijn, D. H. Meijer, L. Gainche, M. Sena-Esteves, W. T. Curry Jr., B. S. Carter, A. M. Krichevsky, and X. O. Breakefield. 2008. Glioblastoma microvesicles transport RNA and proteins that promote tumour growth and provide diagnostic biomarkers. *Nat. Cell Biol.* 10:1470–1476.
- Sobti, J., G. P. Mathur, A. Gupta, and World Health Organization. 2002. WHO's proposed global strategy for infant and young child feeding: A viewpoint. *J. Indian Med. Assoc.* 100:502–504.
- Sun, L., H. Luo, D. Bu, G. Zhao, K. Yu, C. Zhang, Y. Liu, R. Chen, and Y. Zhao. 2013a. Utilizing sequence intrinsic composition to classify protein-coding and long non-coding transcripts. *Nucleic Acids Res.* 41:e166.
- Sun, Q., X. Chen, J. Yu, K. Zen, C.-Y. Zhang, and L. Li. 2013b. Immune modulatory function of abundant immune-related microRNAs in microvesicles from bovine colostrum. *Protein Cell* 4:197–210.
- Théry, C., L. Zitvogel, and S. Amigorena. 2002. Exosomes: Composition, biogenesis and function. *Nat. Rev. Immunol.* 2:569–579.
- Title, A. C., R. Denzler, and M. Stoffel. 2015. Uptake and function studies of maternal milk-derived microRNAs. *J. Biol. Chem.* 290:23680–23691.
- Tomé-Carneiro, J., N. Fernandez-Alonso, C. Tomas-Zapico, F. Visioli, E. Iglesias-Gutierrez, and A. Davalos. 2018. Breast milk microRNAs harsh journey towards potential effects in infant development and maturation. Lipid encapsulation can help. *Pharmacol. Res.* 132:21–32.
- Trapnell, C., B. A. Williams, G. Pertea, A. Mortazavi, G. Kwan, M. J. van Baren, S. L. Salzberg, B. J. Wold, and L. Pachter. 2010. Transcript assembly and quantification by RNA-Seq reveals unannotated transcripts and isoform switching during cell differentiation. *Nat. Biotechnol.* 28:511–515.
- Vlassov, A. V., S. Magdaleno, R. Setterquist, and R. Conrad. 2012. Exosomes: Current knowledge of their composition, biological functions, and diagnostic and therapeutic potentials. *Biochim. Biophys. Acta* 1820:940–948.
- Wolf, T., S. R. Baier, and J. Zemleni. 2015. The intestinal transport of bovine milk exosomes is mediated by endocytosis in human colon carcinoma Caco-2 cells and rat small intestinal IEC-6 Cells. *J. Nutr.* 145:2201–2206.
- Yang, B., B. Jiao, W. Ge, X. Zhang, S. Wang, H. Zhao, and X. Wang. 2018. Transcriptome sequencing to detect the potential role of long non-coding RNAs in bovine mammary gland during the dry and lactation period. *BMC Genomics* 19:605.
- Ying, W., M. Riopel, G. Bandyopadhyay, Y. Dong, A. Birmingham, J. B. Seo, J. M. Ofrecio, J. Wollam, A. Hernandez-Carretero, W. Fu, P. Li, and J. M. Olefsky. 2017. Adipose tissue macrophage-derived exosomal miRNAs can modulate in vivo and in vitro insulin sensitivity. *Cell* 171:372–384.e12.
- Young, M. D., M. J. Wakefield, G. K. Smyth, and A. Oshlack. 2010. Gene ontology analysis for RNA-seq: Accounting for selection bias. *Genome Biol.* 11:R14 (J).
- Zemleni, J., S. Sukreet, F. Zhou, D. Wu, and E. Mutai. 2019. Milk-derived exosomes and metabolic regulation. *Annu. Rev. Anim. Biosci.* 7:245–262.
- Zheng, R., M. Du, X. Wang, W. Xu, J. Liang, W. Wang, Q. Lv, C. Qin, H. Chu, M. Wang, L. Yuan, J. Qian, and Z. Zhang. 2018. Exosome-transmitted long non-coding RNA PTENP1 suppresses bladder cancer progression. *Mol. Cancer* 17:143.
- Zhou, Q., M. Li, X. Wang, Q. Li, T. Wang, Q. Zhu, X. Zhou, X. Wang, X. Gao, and X. Li. 2012. Immune-related MicroRNAs are abundant in breast milk exosomes. *Int. J. Biol. Sci.* 8:118–123.

RESEARCH ARTICLE

Plant MIR156 regulates intestinal growth in mammals by targeting the Wnt/ β -catenin pathway

Meng Li,^{1*} Ting Chen,^{1*} Ran Wang,² Jun-Yi Luo,¹ Jia-Jian He,¹ Rui-Song Ye,¹ Mei-Ying Xie,¹ Qian-Yun Xi,¹ Qing-Yan Jiang,¹ Jia-Jie Sun,^{1*} and Yong-Liang Zhang^{1*}

¹Guangdong Provincial Key Laboratory of Animal Nutritional Regulation, National Engineering Research Center for Breeding Swine Industry, Guangdong Provincial Key Laboratory of Agro-Animal Genomics and Molecular Breeding, College of Animal Science, South China Agricultural University, Guangzhou, China; and ²College of Forestry and Landscape Architecture, South China Agricultural University, Guangzhou, China

Submitted 28 January 2019; accepted in final form 12 May 2019

Li M, Chen T, Wang R, Luo JY, He JJ, Ye RS, Xie MY, Xi QY, Jiang QY, Sun JJ, Zhang YL. Plant MIR156 regulates intestinal growth in mammals by targeting the Wnt/ β -catenin pathway. *Am J Physiol Cell Physiol* 317: C434–C448, 2019. First published June 5, 2019; doi:10.1152/ajpcell.00030.2019.—MicroRNAs (miRNAs) are important negative regulators of genes involved in physiological and pathological processes in plants and animals. Recent studies have shown that miRNAs might regulate gene expression among different species in a cross-kingdom manner. However, the specific roles of plant miRNAs in animals remain poorly understood and somewhat. Herein, we found that plant MIR156 regulates proliferation of intestinal cells both in vitro and in vivo. Continuous administration of a high plant miRNA diet or synthetic MIR156 elevated MIR156 levels and inhibited the Wnt/ β -catenin signaling pathway in mouse intestine. Bioinformatics predictions and luciferase reporter assays indicated that MIR156 targets Wnt10b. In vitro, MIR156 suppressed proliferation by downregulating the Wnt10b protein and upregulating β -catenin phosphorylation in the porcine jejunum epithelial (IPEC-J2) cell line. Lithium chloride and an MIR156 inhibitor relieved this inhibition. This research is the first to demonstrate that plant MIR156 inhibits intestinal cell proliferation by targeting Wnt10b. More importantly, plant miRNAs may represent a new class of bioactive molecules that act as epigenetic regulators in humans and other animals.

intestine; MIR156; proliferation; Wnt

INTRODUCTION

MicroRNAs (miRNAs) are involved in multiple physiological and pathological processes (4), and they negatively regulate gene expression by targeting the 3'-untranslated region (UTR) of mRNAs (23). MiRNAs perform remarkably similar functions in plants (36). In humans and other animals, endogenous miRNAs are believed to be transported in blood and delivered to recipient cells to mediate repression of critical mRNA targets (1, 63). In offspring, the expression and functions of endogenous miRNAs are mediated by maternal nutrition (6), and maternal miRNAs are transferred through the mammalian placenta and directly regulate fetal gene expres-

sion, thereby influencing fetal development (35a). In addition, various studies have shown that exogenous miRNAs can diffuse through body fluid via cross-kingdom delivery (38, 79, 82). Plant miRNAs are reportedly resistant to the harsh acidic gastric environment, different temperature conditions, and nuclease enzymes, although their ability to survive passage through the intestinal tract varies among individuals (8, 38, 61a). They can be associated with Argonaute protein 2 (Ago2) (82) or packaged into secreted exosomes (82) or exosome-like nanoparticles (ELNs) (48) to exert cross-kingdom regulatory effects on physiological processes across different species. Bioinformatics predictions indicated that plant miRNAs can regulate specific human and animal gene expression (51), and subsequent studies suggested that plant miRNAs might be useful for treating human diseases. Oral administration of plant miRNAs can suppress influenza viruses (84), tumor growth (12), and atherosclerosis (27), and plant miRNAs in beebread can even regulate honeybee caste development (86). Surprising, naturally occurring trans-species miRNAs were only recently discovered. *Cuscuta campestris* miRNAs are induced through the haustorium to target and reduce accumulation of mRNAs, such as F-box/RNI-like superfamily protein (TIR1) and sieve element occlusion amino-terminus protein 1 (SEOR1), in host plants (54). This finding provides new evidence that food-derived miRNAs may offer strategies for preventing human diseases and nutritional therapies to aid animal development.

However, the potential scope of plant miRNAs detected in mammalian specimens remains controversial, and the real source of foreign miRNAs from dietary consumption has been questioned (9, 71, 72). Although miRNAs from many exogenous organisms have been found in body fluids of humans and other animals, the cross-kingdom action of plant-derived miRNAs through dietary intake in regulating mammalian gene expression has not been proven unequivocally (9). In some studies, plant miRNAs were not detected in body fluids and organs of animals fed with corresponding plant materials (9, 47). Other studies have shown that levels of some miRNAs are too low for effective delivery of diet-derived miRNAs to recipient animals (44, 57) and therefore are unavailable to regulate biological processes. On the other hand, a recent study revealed that plant material contamination contributes to the observation of plant miRNAs in animal small RNA (sRNA)

* M. Li and T. Chen contributed equally to this work; J.-J. Sun and Y.-L. Zhang contributed equally to this work as co-senior authors.

Address for reprint requests and other correspondence: Y.-L. Zhang, College of Animal Science, South China Agricultural Univ., 483 Wushan Rd., Guangzhou 510642, China (e-mail: zhangyl@scau.edu.cn).

data sets (83). Liang et al. (40) explained that selection of plant miRNAs, the method of RNA extraction, and the proper internal controls may interfere with miRNA detection. More evidence is clearly needed to prove that exogenous miRNAs can be absorbed and subsequently regulate specific animal genes.

The intestine plays an important role in nutrient digestion, absorption, metabolism, and immunity. A healthy intestine is critical if a varied diet is consumed. Numerous studies link miRNAs to development (46), nutrient metabolism (35), intestinal barrier function (61), and disease progression (53) in the intestine. One potential regulatory target for intestine growth is the Wnt signaling pathway. The Wnt/ β -catenin signaling cascade is involved in the regulation of stem cell activity (11), cell proliferation (49), and cell survival in the gastrointestinal epithelium (18). In a canonical Wnt signaling pathway, the Wnt ligand forms a complex with its corresponding receptors (65) and eventually stabilizes β -catenin by suppressing its phosphorylation through inhibiting glycogen synthase kinase (GSK)-3 β (34). Subsequently, β -catenin accumulates and enters the nucleus where it interacts with T-cell factor (TCF) and lymphoid enhancing factor (LEF) transcription factors to activate transcription of the β -catenin-TCF/LEF-1 transcription complex (37). The β -catenin complex drives the transcriptions of a large number of targets, such as cyclin D1, proliferating cell nuclear antigen (PCNA), and cellular-myelocytomatosis viral oncogene (c-Myc) (21, 85). Numerous studies have revealed that miRNA-mediated gene regulation is interconnected with the Wnt/ β -catenin signaling pathway (59).

Crops have provided a large proportion of the food consumed by humans and domestic animals for thousands of years. Crop plants contain both nutritional components and agents that regulate metabolism in humans and other animals. MIR156, one of the most conserved miRNAs in plants, is highly expressed in various crops including soybean (57a), wheat (58), and maize (17). MIR156 is a master regulator of the juvenile phase, controlling juvenile development in maize by targeting *teosinte glume architecture1* (*tga1*) (13), and repressing SQUAMOSA-promoter binding-like (SPL) transcription factors in *Arabidopsis* and rice (76, 78). Previous studies showed that maize-derived miRNAs can cross the gastrointestinal tract in pigs and they have the potential to regulate mammalian gene expression (42).

We hypothesized that MIR156 might be adsorbed and play an important role in interspecific communication, and bioinformatics analysis predicted that MIR156 may target Wnt10b. In the present study, we explored whether MIR156, a plant miRNA, can serve as a mediator of the Wnt signaling pathway and thereby influence animal intestinal tract development. We detected maize MIR156 in the mouse intestine and found that it affected intestinal tract development. Moreover, MIR156 regulated IPEC-J2 cell proliferation by targeting Wnt10b in vitro. This study demonstrated for the first time that plant miRNAs can influence the growth of intestinal epithelial cells and the development of the intestinal tract. Similar to vitamins, minerals, and other essential nutrients derived from food sources, plant miRNAs may also serve as important functional components and contribute to structure and function in animals.

MATERIALS AND METHODS

In Vivo Analyses

Animal experiments and diets. All animal experiments and sample collections were carried out according to the guidelines of Guangdong Province on the Review of Welfare and Ethics of Laboratory Animals, approved by the Guangdong Province Administration Office of Laboratory Animals (GPAOLA). The procedures referred to the protocols of SCAU-AEC-2010-0416 approved by the Animal Ethics Committee of South China Agricultural University (SCAU). All animal experiments were carried out on C57BL/6 male mice with a 12-h light-dark cycle in a pathogen-free animal feeding facility at SCAU. Twelve weanling C57BL/6 male mice were divided into two groups (6 mice per group) at 21 days old. Mice had free access to a maize diet or maize starch diet for 30 days. To deliver different levels of exogenous maize miRNAs to recipient mice, the maize diet group was fed with chow diet (enriched with 39.1% maize), and the maize starch group was fed the maize starch diet but with the same quantity of maize starch instead of maize. We ensured nutritional balance for both diets. Mice were killed by cervical dislocation after 30 days, and intestine tissue was collected and stored at -80°C until use. We evacuated mice intestine as much as possible by fasting for 12 h to eliminate chymus before mice were killed. The intestine was vertically opened and washed with phosphate-buffered saline (PBS) solution to exclude sample contamination by luminal contents for total RNA extraction.

In another animal experiment, 12 weanling C57BL/6 male mice were divided into 2 groups (6 mice per group) at 21 days old. Synthetic MIR156 (a single-stranded methylated MIR156) or NC (a single-stranded methylated nucleotide sequence) was administered orally (300 pmol each) to mice fed the maize starch diet for 7 days. Body weight was then measured, and tissues were collected and stored as described above.

In situ hybridization. In situ hybridization (ISH) was performed as previously described (14). The MIR156 detection probe was obtained from Servicebio (Wuhan, Hubei, China). As with conventional miRNA and mRNA ISH, tissue was fixed by overnight immersion in 4% paraformaldehyde (PFA) in PBS to generate paraffin sections. Dehydrated paraffin sections were digested by proteinase K for 25 min at 37°C . Hybridization was performed with digoxigenin (DIG)-labeled MIR156 probe 5'-GTGCTCACTCTCTTCTGTCA-3' and Wnt10b mRNA probe 5'-CY3-CGTTACCACCTGGCGTCCCCAC-CCT-CY3-3'. Anti-DIG-AP or anti-DIG-488 was used as secondary antibodies. Images were captured using an XSP-C204 microscope (Chongguang, Chongqing, China) and IR-DIC imaging on an upright Nikon Eclipse ci microscope (Nikon, Tokyo, Japan) at a magnification of $\times 200$.

Intestinal histomorphology. For paraffin sections, fresh intestine tissues were fixed in 10% neutral buffered formalin, embedded in paraffin, and cut into horizontal sections of 6 μm in thickness. Sections were stained with hematoxylin and eosin using standard pathological procedures as previously reported (24). Villus height and crypt depth were observed under a light microscope (Nikon) at a magnification of $\times 40$ and $\times 100$.

RNA isolation. Maize materials and diets were extracted for RNA using the cetyltrimethyl ammonium bromide (CTAB) method. Frozen ground samples of 200 mg were incubated in 0.9 ml CTAB reagent at 65°C for 10 min with vigorous shaking several times, and 1 pmol of synthetic cel-miR-39-3p was added to each sample and vortexed to perform RNA isolation. The supernatant was obtained by ultracentrifugation at 7,000 rpm for 5 min, and one-third volume of KAc (5 M, pH 4.8) was added and incubated at 0°C for 30 min. An equal volume of chloroform/isoamyl alcohol (24:1, vol/vol) was added to the supernatant and mixed completely. The mixture was centrifuged at 12,000 rpm for 10 min at 4°C , except for bud samples, which were centrifuged for 20 min. The supernatant was transferred to a new tube containing 500 μl phenol water (pH 5.2), and the above step was

repeated. The supernatant was then transferred to a new tube containing an equal volume of isopropyl alcohol and incubated at 0°C for 30 min. RNA was acquired by centrifugation at 12,000 rpm for 10 min at 4°C, and an equal volume of ethanol was added to wash RNA. Total RNA was extracted from animal intestine tissue samples using TRIzol Reagent (Invitrogen, Carlsbad, CA) according to the manufacturer's instructions. Synthetic cel-miR-39-3p (1 pmol) was added to each sample and vortexed for RNA isolation. RNA concentration determined by an ND-2000 Nanodrop Spectrophotometer (NanoDrop Technology, Wilmington, DE). RNA integrity was examined by 1% agarose gel electrophoresis. Qualified RNAs were used for further PCR and real-time quantitative PCR (qPCR) analyses.

PCR and qPCR analyses. Total RNA (1 µg) was reverse transcribed to cDNA using M-MLV-R transcriptase (Promega, Madison, WI) with OligodT18 (for mRNA) or a specific stem-loop RT primer (for miRNA). Samples were amplified by PCR using complementary primers. Control miRNAs such as synthetic cel-miR-39-3p were spiked as loading controls (22), and a no template (NT) negative control was included. Plant miRNAs were reverse transcribed to cDNA using Mir-X miRNA and a First-Strand Synthesis Kit (TaKaRa Bio, Dalian, Liaoning, China) according to the protocol. PCR products (10 µl) were examined on a 2% agarose gel to assess maize miRNAs in maize materials, diets, and mice intestine tissue. To quantify miRNAs and mRNAs, cDNA was diluted fivefold with ddH₂O and qPCR (20 µl) was performed on a Bio-Rad CFX Manager 3.1 instrument (Applied Biosystems, Waltham, MA) with U6 (miRNA control) or β-actin (mRNA control) as internal controls. Reactions contained 2 µl cDNA, 10 µl 2× GoTaq QPCR Master Mix (Promega), and 0.4 µl of each primer (10 µM). The thermal profile of real-time PCR involved an initial denaturation step at 95°C for 5 min, followed by 40 cycles at 94°C for 15 s, 15 s at the corresponding annealing temperature (T_m), extension at 72°C for 30 s, followed by a quick denaturation at 95°C for 10 s, plus a slow ramp from T_m to 95°C to generate a melting curve to confirm the specificity of the amplified product. An NT negative control was included for each miRNA and mRNA, and all reactions were performed in triplicate. The 2^{-ΔC_t} method was employed to quantify and normalize the expression data. Absolute quantifications were performed as previously described (28). A standard curve was generated by dilution of known quantities of a synthesized MIR156 (miDETECTM miRNA qRT-PCR Standard RNA; RiboBio, Guangzhou, Guangdong, China) to determine the content of miRNAs in maize materials and diets. Synthetic miRNAs (RiboBio) were diluted to different concentrations (10 fM to 10⁵ fM) and subjected to both RT-PCR and stem-loop qRT-PCR. The logarithmic values of these miRNA concentrations (x-axis) were plotted against C_T values (y-axis). Detection quality and efficiency were validated using the diluted synthetic MIR156 templates and their standard curves. The miRNAs, mRNA primers, and specific stem-loop RT primers were designed with Premier Primer 5.0 (Premier Software; Supplemental Table S4; see Supplemental Data: <https://doi.org/10.6084/m9.figshare.8175509>).

Western blot analysis. Total protein was isolated from intestine tissues using RIPA buffer with 1 nM phenylmethylsulfonyl fluoride (PMSF) and quantified with a BCA Total Protein Assay Kit (Thermo Fisher, Waltham, MA). The protein suspension (20 µg) was supplemented with β-mercaptoethanol, boiled for 10 min, resolved by 5 or 10% sodium dodecyl sulfate polyacrylamide gel electrophoresis (SDS-PAGE), and transferred to a polyvinylidene difluoride membrane. Wnt10b, β-catenin, cyclin D1, and c-Myc were detected with primary antibodies anti-human Wnt10b (1:500; D162612; Sangon Biotech, Shanghai, China), anti-human β-catenin (1:500; D260137; Sangon Biotech), anti-p-β-catenin (serine 33; 1:500; D155098; Sangon Biotech), anti-human cyclin D1 (1:2,000; 2922; Cell Signaling Technology, Danvers, MA) and anti-human c-Myc (1:1,000; D199941; Sangon Biotech), followed by rabbit horseradish peroxidase-linked IgG secondary antibody (1:50,000; BS10002/3; Bioworld Technology). β-Actin (1:5,000; BS6007M; Bioworld Technology) served as a

control. Band intensities were measured using ImageJ and were normalized against β-actin.

Northern blotting analysis. Oligonucleotide probes complementary to mature MIR156 were end labeled with DIG (Servicebio). Total RNA was extracted from intestine using TRIzol Reagent (Invitrogen) according to the manufacturer's instructions. Synthetic oligonucleotides (1 pmol) were loaded as positive controls. Spike-in control miRNAs such as synthetic cel-miR-39-3p (22) (DIG-labeled cel-miR-39-3p 5'-CAAGCTGATTTACACCCGGTGA-3') were included as loading controls. We then added 1 pmol of synthetic cel-miR-39-3p prepared in TRIzol to each sample and vortexed to perform RNA isolation. Total RNA (100 µg) was fractionated by PAGE using a 15% denaturing polyacrylamide gel and then transferred onto a nylon membrane (Hybond N+; Amersham Biosciences) by electroblotting at 250 mA in 1× Tris-borate-EDTA (TBE) buffer for 1.5 h. The membrane was cross linked for 10 min and dried. A prehybridization step was performed by incubating the membrane with 5 ml of DIG Easy Hyb (Roche) preheated to 50°C for 30 min at 50°C in a standard rotating hybridization oven. The DIG-labeled probe was added directly to the DIG Easy Hyb, and the membrane was incubated overnight at 50°C with rotation in a hybridization oven. After hybridization, the membrane was washed twice for 5 min at room temperature in 2× saline-sodium citrate (SSC) and 0.5% SDS and then twice for 15 min at 68°C in 0.5× SSC and 0.5% SDS. Anti-DIG-AP was used as the secondary antibody. The membrane was wrapped in plastic, incubated at 37°C for 10 min with CSPD (Roche) and detected with FluorChem M (ProteinSimple).

In Vitro Analyses

Cell culture and transfection of cells with MIR156. IPEC-J2 cells were seeded at a density of 1 × 10⁵ cells in 12-well plates overnight (70–80% confluency) and transfected for 6 h the following day using Lipofectamine 2000 (Invitrogen) according to the manufacturer's instructions. The treatment groups were as follows: mimics group (single-stranded methylated MIR156, 20 pmol, MIR156 mimics), NC (single-stranded methylated nucleotide sequence, 20 pmol, normal control), inhibitor group (single-stranded methylated MIR156 antisense, 20 pmol, MIR156 inhibitor), i-NC (single-stranded methylated MIR156 antisense control, 20 pmol, inhibitor normal control), mimics + inhibitor (20 pmol MIR156 mimics + 40 pmol MIR156 inhibitor), NC + NaCl (20 pmol NC + 10 mM NaCl, negative control), mimics + NaCl (20 pmol mimics + 10 mM NaCl, positive control), mimics + lithium chloride (LiCl; 20 pmol mimics + 10 mM LiCl). LiCl and NaCl reagents were added to the culture medium at 8 h after transfection. Cells were harvested at 24 h or 48 h after transfection for cell counting, real-time PCR, Western blotting, and immunocytofluorescence analyses. Cells were incubated with 1 nM calyculin A for 30 min before harvesting for detection of β-catenin protein phosphorylation by Western blotting.

Dual-luciferase reporter assay. Based on the predicted miRNA-mRNA binding sequences, normal sequences bearing an MIR156 seed binding site or with the Wnt10b 3'-UTR site deleted were generated by two complementary chemically synthesized primers (Sangon Biotech) as follows: wt-Wnt10b-3'-UTR-sense (TCGAGCAGCCTTTC-GCTCTGACTTCTGTCCACGGGTCAATCTTGGCCT), wt-Wnt10b-3'-UTR-antisense (CTAGAGGCCAAGATTGACCCGTGGACAGAGTCAGAGCGAAAGGCTGC), del-Wnt10b-3'-UTR-sense (TCGAGCAGCCTTTCGCTCTGACACGGGTCAATCTTGGCCT), and del-Wnt10b-3'-UTR-antisense (CTAGAGGCCAAGATTGACCCGTGTC-AGAGCGAAAGGCTGC).

The complementary oligonucleotides were resuspended at a 1:1 ratio (1 µg/µl each) in annealing buffer (10 mM Tris pH 7.5–8.0, 50 mM NaCl, and 1 mM EDTA) and heated at 95°C for 10 min to denature secondary structure. The temperature was then gradually lowered to room temperature. Annealed products were cloned into the pmirGLO vector (Promega) downstream from the firefly lu-

ciferase coding region (between XhoI and XbaI sites). HeLa cells were seeded in 96-well cell culture plates (3.5×10^4 cells/well) and cultured in RPMI 1640 (Life Technologies, Grand Island, NY) with 10% fetal bovine serum. The next day, cells were transfected with recombinant pmirGLO-3'-UTR vector (100 ng/well) mixed with their corresponding MIR156 mimics or NC (3 pmol/well; RiboBio) for 6 h using Lipofectamine 2000 (Life Technologies). Cells were harvested at 24 h after transfection, and luciferase activity was detected by a dual luciferase reporter assay system (Promega) according to the manufacturer's recommendations. Normalized firefly luciferase activity (firefly luciferase activity/*Renilla* luciferase activity) for each construct was compared with that of the pmirGLO vector.

5-Ethynyl-2'-deoxyuridine incorporation assay. Cell proliferation was assessed by a Cell-Light EdU Apollo 488 In Vitro Imaging Kit (RiboBio) according to the manufacturer's instructions. IPEC-J2 cells were incubated with 1:1,000 5-ethynyl-2'-deoxyuridine (EdU) diluted in culture solution for 2 h at 37°C before harvesting. After several washes, cells were fixed with 4% PFA (pH 7.4) for 30 min and incubated with glycine (2 mg/ml) for 5 min. Fixed cells were washed with 0.5% Triton X-100 (diluted in PBS) for 10 min, followed by staining with Apollo buffer (RiboBio) for 30 min at room temperature in the dark. Cells were then incubated with Hoechst 33342 dye at room temperature for 30 min in the dark. Finally, images were captured using fluorescent microscopy and IR-DIC imaging on an Eclipse FN-1 upright microscope (Nikon) at a magnification of $\times 100$.

Immunocytofluorescence detection of Wnt10b and β -catenin in IPEC-J2 cells. For immunocytofluorescence staining, IPEC-J2 cells were fixed with 4% PFA and permeabilized in PBS solution containing 0.5% Triton X-100. Wnt10b and β -catenin were detected with anti-Wnt10b (1:1,000; bs-3662R; Bioss) and anti- β -catenin (1:1,000; bs-1165R; Bioss) respectively, followed by goat-anti-rabbit FITC secondary antibody (1:1,000; Bioss) for 30 min at room temperature in the dark. Cells were incubated with DAPI (1:2,000; H-1200; Vector Laboratories) at room temperature for 30 min in the dark. Images were captured using fluorescence microscopy on an Eclipse FN-1 instrument (Nikon) at a magnification of $\times 200$. Fluorescence intensity was quantified by NIS-Elements (Nikon).

Statistical Analyses

Least significant difference tests were used for multiple comparisons, and *t*-tests were employed for pairwise comparisons ($P < 0.05$ was considered statistically significant). Data are presented as the means \pm SD, and all analyses were performed using GraphPad Prism Software 6.0.

RESULTS

Plant MIR156 Is Absorbed by Mouse Intestine Tissues

MIR156 is highly conserved and expressed throughout the plant kingdom (52, 64) and is present at highest levels in sera from Chinese subjects (82). Herein, we detected abundant MIR156 by PCR (Fig. 1A, top) and Northern blotting (Fig. 1A, bottom) in mouse intestine tissue following consumption of a maize diet and maize starch diet. qPCR revealed that MIR156 was more abundant in maize than maize starch (Fig. 1C), as well as in maize diet than maize starch diet (Fig. 1D). It showed that maize diet with high maize miRNA levels and maize starch diet with low maize miRNA levels. Furthermore, qPCR and ISH further confirmed that the abundance of MIR156 in intestinal tissue was much lower in mice fed a maize starch diet than a maize diet (Fig. 1, E and F). These results suggest that maize MIR156 can be absorbed and may participate in the regulation of intestinal development.

Mouse Intestine Development Is Affected by Maize miRNAs

miRNAs are widely expressed in crops such as maize (81). However, miRNA components may be lost during starch processing since embryos are removed. Herein, we selected several miRNAs that are highly expressed in maize (MIR156, MIR319a-3p, MIR166a-3p, MIR167e-5p, MIR168a-5p, MIR159a-5p, and MIR396c-5p) for PCR analysis. All seven miRNAs were detectable in maize but not maize starch, including MIR156 (Fig. 2A), which suggests that starch processing decreased the abundance of plant miRNAs. Similar results were obtained in diet analysis (Fig. 2B). Next, we discovered a remarkable difference between maize diet-fed mice and maize starch diet-fed mice after 30 days, even though energetic and nutrition balance was identical in both (Supplemental Tables S1 and S2 and Supplemental Fig. S1; see Supplemental Data: <https://doi.org/10.6084/m9.figshare.8175509>). In the maize starch diet group, mouse body weight and intestine weight were increased dramatically, in contrast with the maize diet group (Fig. 2, C and D). Hematoxylin and eosin staining of paraffin sections showed that the maize starch diet significantly increased the villus height:crypt depth ratio in the duodenum, compared with the maize diet group (Fig. 2, E and F). Moreover, the maize diet significantly reduced the expression of Cdx2 mRNA (Fig. 2G), an intestine-specific transcription factor involved in intestinal development, differentiation and maintenance of the intestinal phenotype in the nuclei of epithelial cells (56). These results suggest that miRNAs might act as regulators of intestinal development in mouse.

MIR156 Affects Intestine Development by Targeting the Wnt/ β -Catenin Pathway In Vivo

The Wnt/ β -catenin signaling pathway regulates intestinal development. In the mice intestine, both qPCR and Western blotting revealed that both Wnt10b and β -catenin were significantly elevated in following consumption of a maize starch diet (Fig. 3). Cyclin D1 and c-Myc expression were also significantly elevated in the intestine of mice receiving a maize starch diet (Fig. 3). These results suggest an intriguing role for exogenous plant miRNAs in regulating canonical Wnt activity in intestine.

We next explored whether MIR156 is also involved in regulatory processes related to canonical Wnt activity. Synthetic MIR156 was delivered intragastrically to mice, and Northern blotting further confirmed that MIR156 was indeed absorbed by intestinal cells in vivo, while MIR156 was not detectable in the NC group (Fig. 4A). On day 7 after administration, MIR156 levels in mice intestine were elevated (Fig. 4B), while Cdx2 mRNA levels were significantly reduced (Fig. 4C), even though body weight and feed intake did not change significantly (Supplemental Fig. S2; see Supplemental Data: <https://doi.org/10.6084/m9.figshare.8175509>). Wnt10b, β -catenin, and cyclin D1 expression was significantly inhibited in the intestine of mice receiving MIR156 mimics (Fig. 4, C–E). More importantly, double immunofluorescence histochemical analysis revealed more MIR156 in intestinal crypt cells of mice receiving MIR156 mimics, accompanied by decreased Wnt10b mRNA levels (Fig. 4F), which indicates that MIR156 is absorbable and degrades Wnt10b mRNA in intestinal cells. These results provide direct evidence that

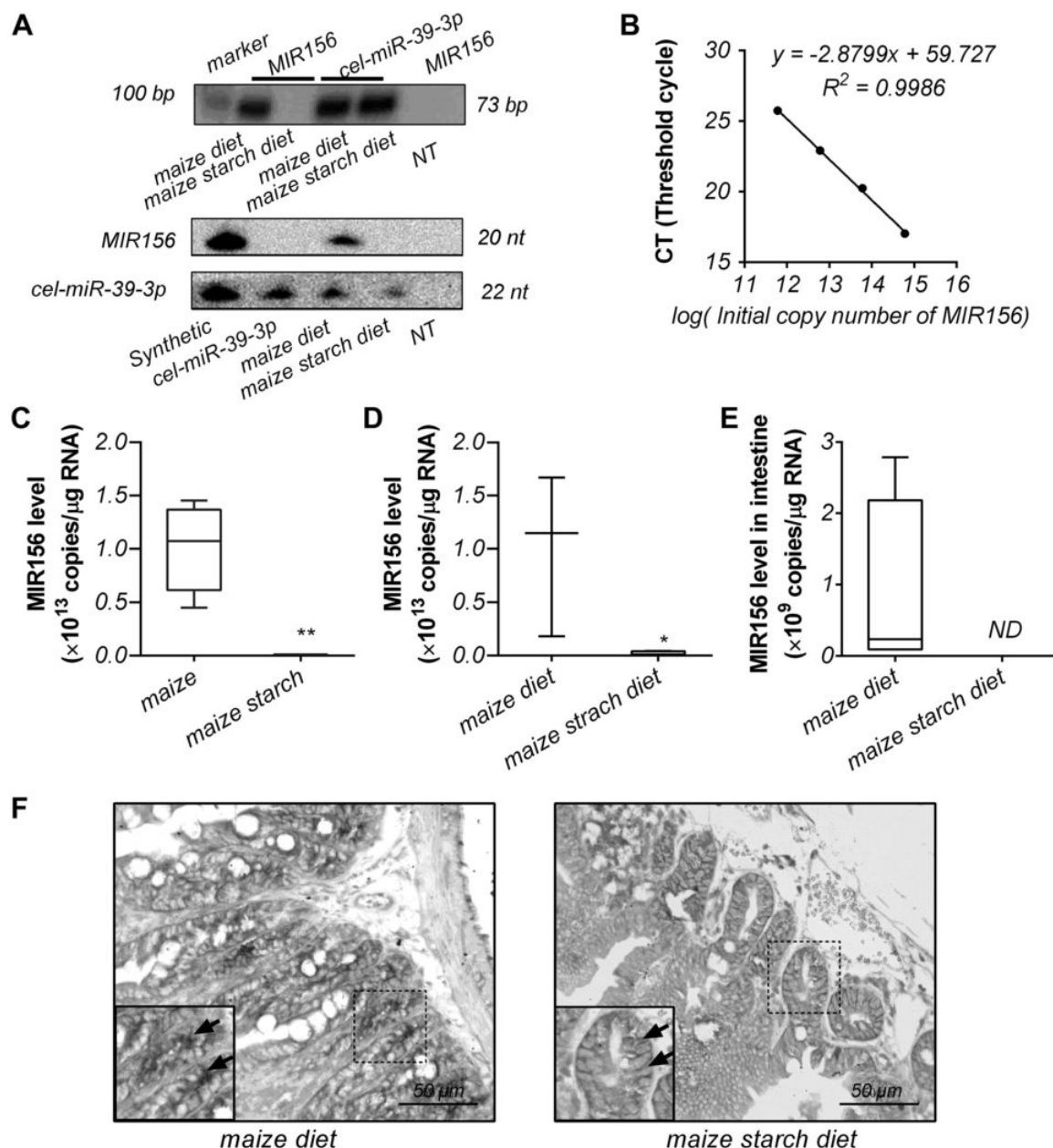


Fig. 1. Maize MIR156 can pass through the mouse intestinal tract and enter the intestine. **A**: MIR156 levels in the intestine of mice fed a maize diet or maize starch diet detected by PCR with gel analysis (top) and Northern blotting (bottom; $n = 1$). For PCR, spike-in cel-miR-39-3p served as a positive control, and no template (NT) served as a negative control. Markers = a 2,000-bp DNA ladder. For Northern blotting, synthetic miRNA served as a positive control, and NT and spike-in synthetic cel-miR-39-3p (without template for RNA isolation) served as negative controls. **B**: MIR156 standard curve ($n = 4$). **C** and **D**: absolute levels of MIR156 in maize materials (**C**) and diets (**D**) detected by real-time quantitative PCR ($n = 6$; t -tests; * $P < 0.05$, ** $P < 0.01$). **E**: absolute levels of MIR156 in intestines of mice fed a maize diet or maize starch diet detected by real-time quantitative PCR ($n = 6$); ND, not detectable. **F**: representative in situ hybridization images of intestines of mice fed a maize diet (left) or maize starch diet (right) for detection of MIR156. Positive staining of the bottom of intestinal villi is shown (scale bar = 50 μ m; $n = 1$).

maize MIR156 is absorbed and can regulate intestine development.

MIR156 Targets *Wnt10b*

In plants, the MIR156 family controls plant growth, development, and morphology by targeting SPL transcription factors (76). To identify targets of MIR156 in mammals, miRanda was employed, and the results showed that MIR156 may potentially target *Wnt10b*, a key molecule in

the Wnt/ β -catenin pathway (31, 43, 66). A putative binding site conserved among various species was located in *Wnt10b* (Fig. 5A). To explore this further, a partial *Wnt10b* normal 3'-UTR sequence and a sequence in which the MIR156 binding site is deleted were cloned into a luciferase reporter plasmid (Fig. 5A). HeLa cells were transfected with the reporter plasmids along with synthetic MIR156 mimics or NC. The results showed that MIR156 significantly reduced luciferase activity and deletion of the MIR156 bind-

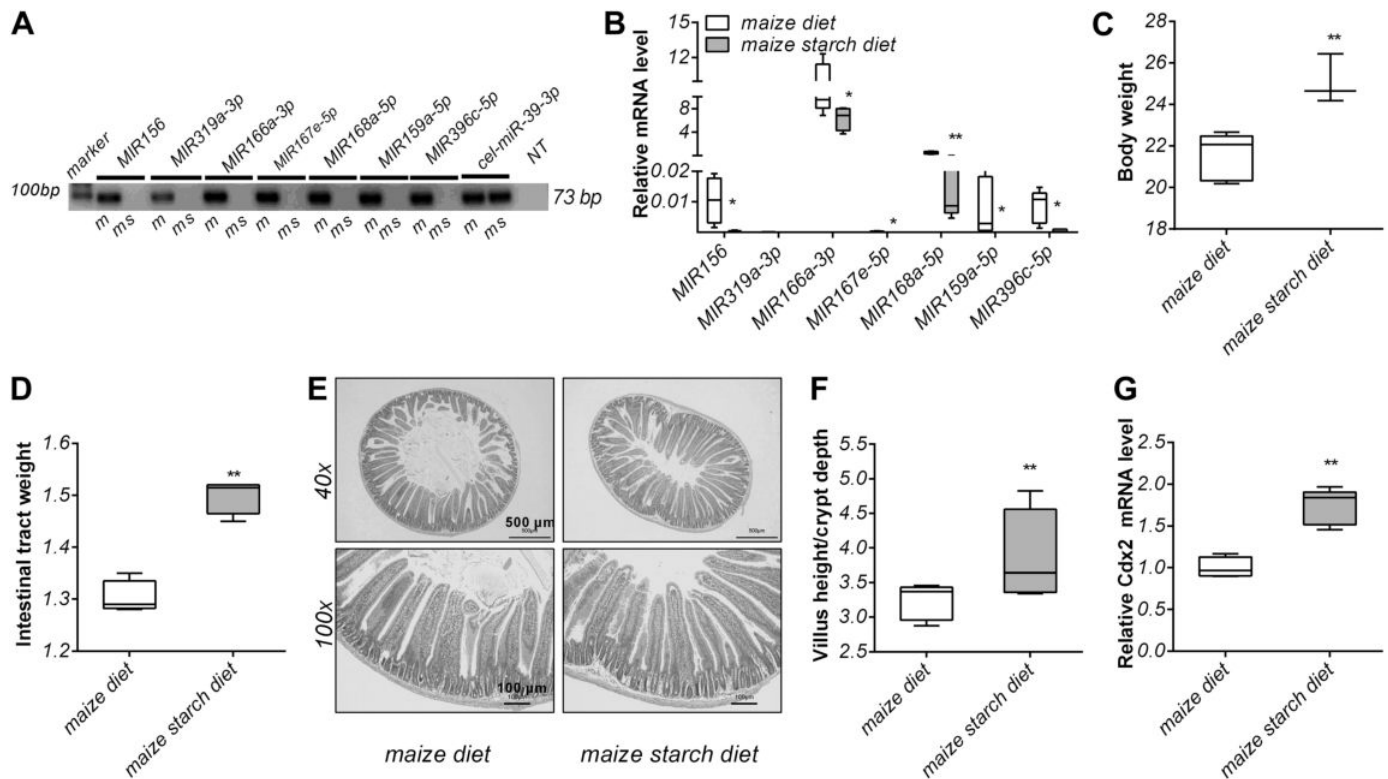


Fig. 2. Mouse intestine development is affected by maize miRNAs. **A**: detection of miRNAs in maize and maize starch by PCR with gel analysis ($n = 1$). Spike-in synthetic cel-miR-39-3p served as a positive control, and no template (NT) served as a negative control; m, maize; ms, maize starch. Markers = a 2,000-bp DNA ladder. **B**: relative levels of MIR156, MIR319a-3p, MIR166a-3p, MIR167e-5p, MIR168a-5p, MIR159a-5p, and MIR396c-5p in maize diet and maize starch diet detected by real-time quantitative PCR (normalized against spike-in cel-miR-39-3p; $n = 6$). **C** and **D**: body weight (**C**) and intestinal tract weight (**D**) changes in mice fed a maize diet or maize starch diet for 30 days ($n = 6$). **E**: the maize starch diet group display improved duodenum morphology (villus height and crypt depth) compared with the maize diet group based on microscopy observations. Scale bar = 500 μm (top) and 100 μm (bottom; $n = 5$). **F**: statistical analysis showing a significant increase in villus height: crypt depth ratio in the duodenum of the maize starch diet group ($n = 6$). **G**: real-time quantitative PCR analysis of Cdx2 mRNA levels in mouse intestine for maize diet and maize starch diet groups (normalized against β -actin; $n = 6$). Statistical significance was determined by t -tests; * $P < 0.05$, ** $P < 0.01$.

ing site diminished this reduction (Fig. 5B). These results indicate that MIR156 can target Wnt10b.

Synthetic MIR156 Suppresses Proliferation of IPEC-J2 Cells In Vitro

We next tested whether MIR156 regulated the growth of intestine epithelial cells in vitro. Cell counting showed that

MIR156 significantly reduced the number of IPEC-J2 cells, while its inhibitor did not affect cell number and relieved the inhibitory effects of MIR156 mimics (Fig. 6A), presumably because MIR156 is not present in the animal genome (83). The number of cells was significantly reduced at 24 h, and the proliferation ability decreased over time following transfection with MIR156 mimics (Fig. 6B). Furthermore, this proliferation

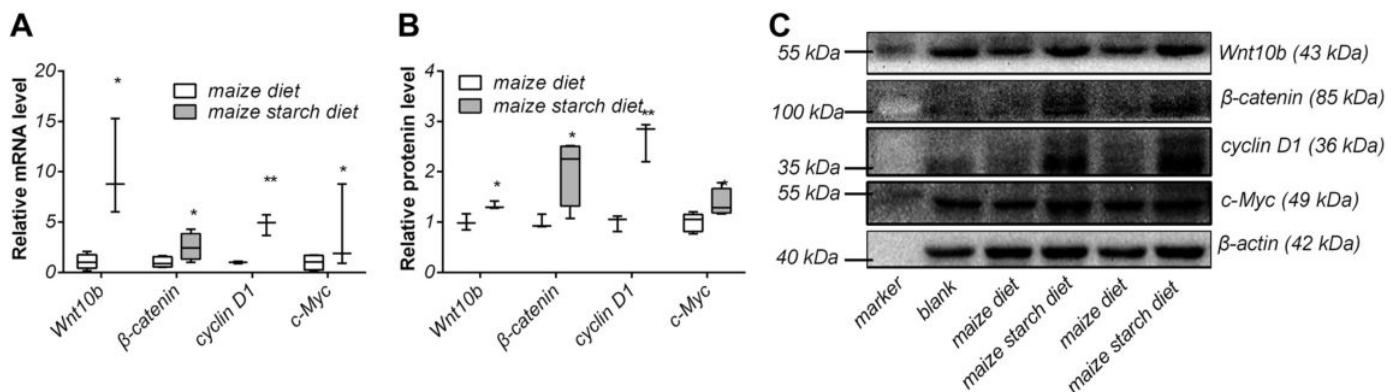


Fig. 3. Plant miRNAs regulate the Wnt/ β -catenin pathway. **A**: real-time quantitative PCR analysis of Wnt10b, β -catenin, cyclin D1, and c-Myc mRNA levels in mice intestine after maize diet or maize starch diet feeding (normalized against β -actin; $n = 6$). **B** and **C**: Western blotting analysis of Wnt10b, β -catenin, cyclin D1, and c-Myc protein expression in mouse intestine after maize diet or maize starch diet feeding ($n = 6$). Statistical significance was determined by t -tests; * $P < 0.05$, ** $P < 0.01$.

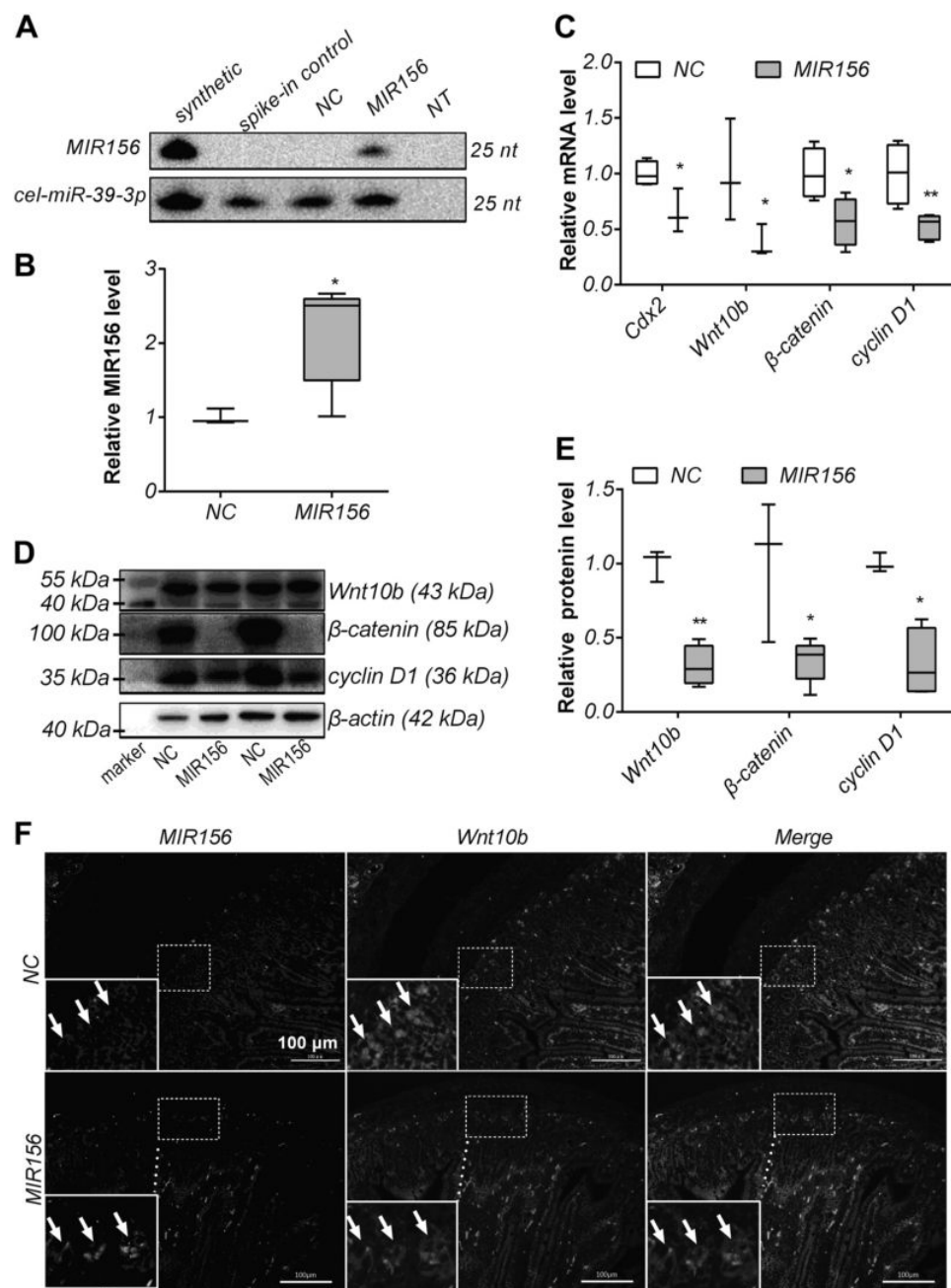


Fig. 4. Synthetic MIR156 regulates the Wnt/ β -catenin pathway in vivo. Weanling C57BL/6 male mice (21 days old) were orally administered 300 pmol synthetic MIR156 (a single-stranded methylated MIR156) or normal control (NC; a single-stranded methylated nucleotide sequence) for 7 days. **A**: MIR156 in mice intestine detected by Northern blotting. Spike-in synthetic cel-miR-39-3p (1 pmol) served as positive control, and no template (NT) served as a negative control. **B**: MIR156 in mouse intestine detected by real-time quantitative PCR (normalized against mouse U6; $n = 6$). **C**: real-time quantitative PCR analysis of Cdx2, Wnt10b, β -catenin, and cyclin D1 mRNA expression in mice intestine (normalized against β -actin; $n = 6$). **D** and **E**: Western blotting analysis of Wnt10b, β -catenin, and cyclin D1 protein expression in mouse intestine ($n = 4$). **F**: representative images of intestines of mice fed with MIR156 or NC for detection of MIR156 and Wnt10b mRNA. Scale bar = 100 μ m ($n = 2$). Statistical significance was determined by t -tests; * $P < 0.05$, ** $P < 0.01$.

inhibitory effect of MIR156 was dose dependent (Fig. 6D), as was the accumulation of MIR156 in IPEC-J2 cells (Fig. 6C). Additionally, transfection of 10 pmol/ml mimic led to 1.21×10^{12} copies/cell in IPEC-J2 cells, which was sufficient to inhibit cell proliferation (Fig. 6D and Supplemental Table S3; see Supplemental Data: <https://doi.org/10.6084/m9.figshare.8175509>). EdU incorporation assays further confirmed the above results (Fig. 6E). Therefore, MIR156 in the intestine can inhibit intestine epithelial cell proliferation.

MIR156 Inhibits Intestinal Epithelial Cell Proliferation by Targeting Wnt10b

To determine whether MIR156 inhibits enterocyte cell growth by targeting Wnt10b, IPEC-J2 cells were transfected

with synthetic MIR156 mimics, which led to a remarkable increase in MIR156 in cells (Fig. 7A). MIR156 mimics reduced Wnt10b mRNA abundance (Fig. 7B) and protein levels (Fig. 7, D and E). As expected, Wnt10b mRNA abundance and protein levels did not significantly increase after treatment with MIR156 inhibitor (Fig. 7, B, D, and E), since there was no endogenous MIR156 in IPEC-J2 cells (Fig. 7A). Additionally, β -catenin abundance declined at both mRNA (Fig. 7C) and protein (Fig. 7, D and F) levels. More interestingly, Western blotting results revealed that β -catenin phosphorylation at serine 33 was elevated by MIR156 mimics (Fig. 7G). These results indicate that MIR156 mimics probably stimulate degradation of β -catenin. Immunocytofluorescence staining showed that the fluorescence intensities of both Wnt10b and β -catenin

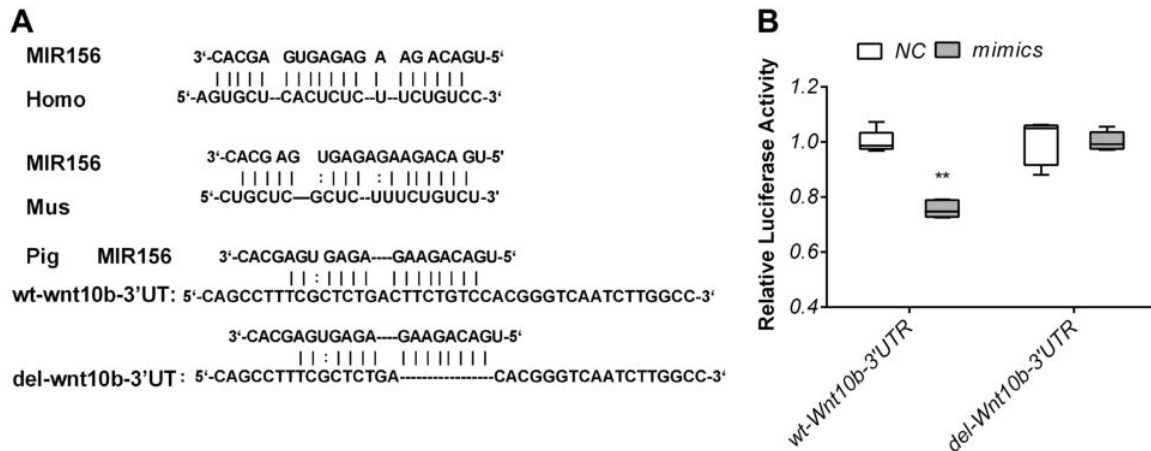


Fig. 5. MIR156 targets Wnt10b. *A*: prediction of MIR156 targets in the Wnt10b 3'-untranslated region. Black and two-dotted labels represent paired and G:U paired bases for normal and deleted Wnt10b 3'-UTR, respectively. Note that the potential binding site of MIR156 in the Wnt10b 3'-UTR is highly conserved across species. *B*: HeLa cells were transfected with each of the constructed plasmids, together with MIR156 mimics (a single-stranded methylated MIR156) or normal control (NC; a single-stranded methylated nucleotide sequence). MIR156 mimics significantly decreased luciferase activity, while the decrease was diminished in the deleted group (firefly luciferase activity/*Renilla* luciferase activity; $n = 5$). Statistical significance was determined by *t*-tests; ** $P < 0.01$.

proteins were reduced in MIR156-treated IPEC-J2 cells (Fig. 7, *H–K*). It is well known that the Wnt/ β -catenin pathway is essential in the regulation of cell growth and differentiation. We also examined several proliferation-related genes (cyclin D1, PCNA, and c-Myc) by qPCR, and compared with the NC group, MIR156 mimics significantly reduced their expression (Fig. 8, *A–C*). Moreover, Western blotting showed that MIR156 mimics significantly reduced cyclin D1 and c-Myc protein levels and these reductions could be counteracted by inhibitors (Fig. 8*D*). These results suggest that MIR156 exerts its functions through the Wnt/ β -catenin pathway and inhibits intestinal epithelial cell proliferation.

MIR156 Inhibits Proliferation via the Wnt/ β -Catenin Pathway

To further confirm whether MIR156 inhibits enterocyte cell growth via the Wnt/ β -catenin signaling pathway, lithium chloride (LiCl), an inhibitor of GSK3- β that mimics Wnt signaling by stabilizing β -catenin (15), was applied to determine the role of MIR156 in regulating the Wnt/ β -catenin pathway. LiCl significantly increased the number of IPEC-J2 cells compared with NaCl, and more importantly, LiCl restored inhibition of the number of IPEC-J2 cells by MIR156 (Fig. 9*A*). Detection of β -catenin in IPEC-J2 cells using fluorescence microscopy confirmed that MIR156 inhibited β -catenin expression, while LiCl increased β -catenin in the presence of MIR156 (Fig. 9*F*). Furthermore, downregulation of the expression of Cdx2, cyclin D1, c-Myc, and PCNA by MIR156 mimics was also counteracted by LiCl (Fig. 9, *B–E*). Taken together, these results further indicate that MIR156 inhibits the Wnt/ β -catenin signaling pathway.

DISCUSSION

Whether plant miRNAs play a role in cross-kingdom regulation of gene expression has drawn much attention in recent years. Plant miRNAs can be absorbed by humans and other animals (12, 82), and they are resistant to acidification mimicking the gastrointestinal tract environment (38, 82). After being orally administered to animals, plant miRNAs face

various major challenges before absorption, including the harsh acidic gastric environment, nuclease enzymes, pancreatic secretions, degradative enzymes, the gut flora, and cellular barriers (50). The stability of miRNAs is higher than that of mRNAs (33), presumably because miRNAs can associate with high-density lipoproteins (63) or argonaute proteins (1) or be encapsulated in exosomes (20). Plant miRNAs are processed and packaged into secreted exosomes or ELNs by cells other than colonic epithelial Caco-2 cells (30). Furthermore, plant miRNAs are 2'-*O*-methyl modified on their terminal nucleotides to protect against attenuating enzymes such as exonucleases (80). A proportion of miRNAs can survive the harsh acidic gastric environment (40, 41), and MIR2911 is highly stable in honeysuckle decoctions (84). Some plant miRNAs have been detected in human body fluids (40), and significant quantities of common plant miRNAs have also been detected in human sera of healthy donors (mean Solexa reads/total mammalian miRNAs >0.005) (82), which suggests that absorption is affected by the dosage of plant miRNAs consumed.

In the present study, food-derived mature plant miRNAs, including MIR156, were successfully detected in mice after feeding, indicating stability in the small intestines in mammals. ISH was used to confirm the existence of MIR156 in the mice intestine, and Northern blotting provided direct evidence that MIR156 could be absorbed by intestinal cells *in vivo*, while it was not detectable in mice fed a maize starch diet. These results demonstrated that accumulation of plant miRNAs in animals is possible through food intake (82).

MIR156 is a conserved and highly expressed miRNA throughout the plant kingdom. In miRBase (<http://www.mirbase.org/>), there are 314 miRNAs sharing identical seed sequences, including 167 miRNAs with the UGACAGAA-GAGAGUGAGCAC sequence found in MIR156. These miRNAs have been found in from 42 plants including soybean (57*a*), wheat (58), and maize (17), which together account for a significant proportion of the diets of humans and other animals. We found that MIR156 was abundant in maize but scarce in maize starch. Similarly, MIR156 was more abundant in the maize diet than maize starch diet (Fig. 1). This suggests

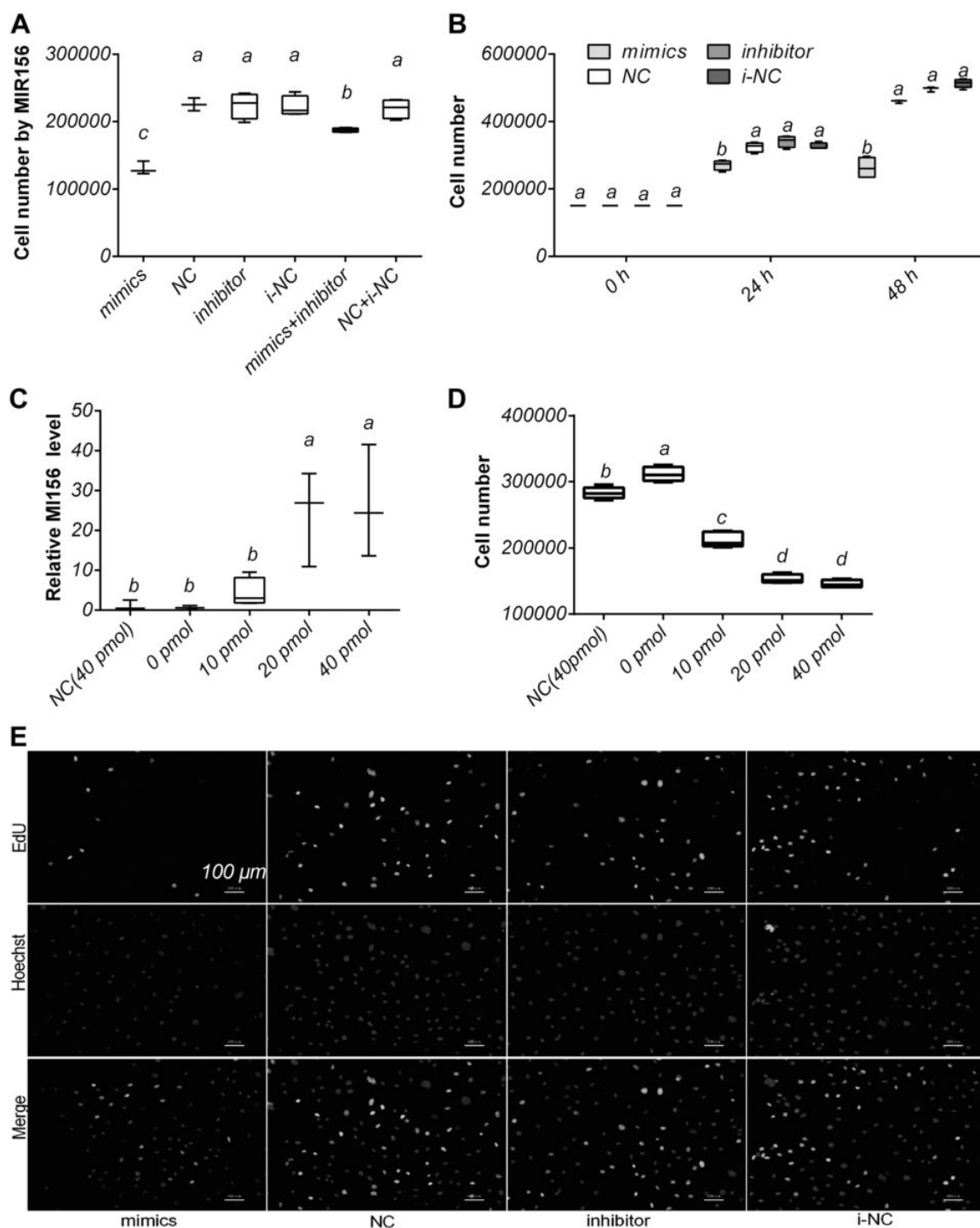


Fig. 6. Synthetic MIR156 suppresses proliferation of IPEC-J2 cell. **A** and **B**: IPEC-J2 cell proliferation after transfection with MIR156 mimics/NC/inhibitor/i-NC/mimics + inhibitor/NC + i-NC. Cell counting was performed to evaluate cell proliferation ($n = 6$). **C**: MIR156 relative expression showing a dose-dependent effect after treatment with MIR156 mimics (normalized against U6; $n = 6$). **D**: cell counting of IPEC-J2 cells transfected with the indicated dose of MIR156 ($n = 6$). **E**: representative images following immunofluorescence staining to assess incorporation of ethynyl-2'-deoxyuridine (EdU) in IPEC-J2 cells after treatment with MIR156 mimics/NC/inhibitor/i-NC for 24 h. The MIR156 treatment group shows weaker fluorescence intensity based on EdU fluorescence microscopy (scale bars = 100 μ m, $n = 6$). MIR156 mimics, a single-stranded methylated MIR156; NC, a single-stranded methylated nucleotide sequence; inhibitor, a single-stranded methylated MIR156 antisense sequence; i-NC, a single-stranded methylated MIR156 antisense control. Statistical significance was determined by least significant difference tests. The same superscripts denote nonsignificant differences ($P > 0.05$), and different superscripts denote significant differences ($P < 0.05$).

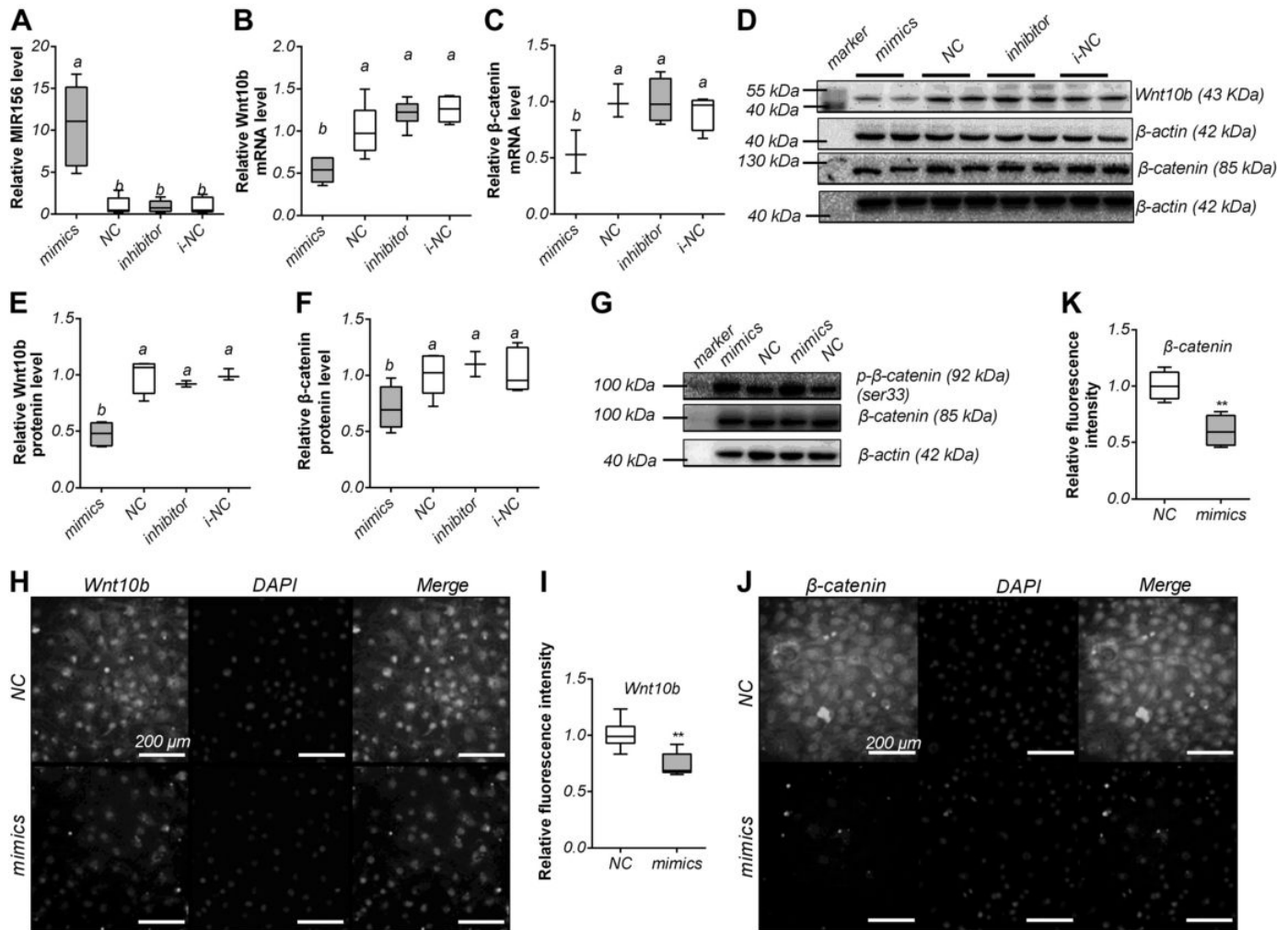


Fig. 7. MIR156 inhibits IPEC-J2 cell proliferation via the Wnt/ β -catenin pathway. **A**: real-time quantitative PCR analysis of relative MIR156 levels after cotransfection with MIR156 mimics/NC/inhibitor/i-NC [normalized against U6; $n = 6$; least significant difference (LSD) tests]. **B** and **C**: real-time quantitative PCR analysis of relative Wnt10b (**B**) and β -catenin (**C**) mRNA levels after transfection with MIR156 mimics/NC/inhibitor/i-NC (normalized against β -actin; $n = 6$; LSD tests). **D–F**: Western blotting evaluation of Wnt10b and β -catenin protein expression following transfection with MIR156 mimics/NC/inhibitor/i-NC, respectively ($n = 6$; LSD tests). **G**: Western blotting evaluation of β -catenin phosphorylation (serine 33) and β -catenin expression after transfection with MIR156 mimics or NC ($n = 4$; LSD tests). **H** and **J**: immunocytofluorescence staining showing that MIR156 reduces Wnt10b (**H**) and β -catenin (**J**) levels, and DAPI staining of nucleic acids. **I** and **K**: quantification of Wnt10b (**I**) and β -catenin (**K**) fluorescence intensity was performed using NIS-Elements (scale bars = 200 μ m; $n = 3$; t -tests). MIR156 mimics, a single-stranded methylated MIR156; NC, a single-stranded methylated nucleotide sequence; inhibitor, a single-stranded methylated MIR156 antisense sequence; i-NC, a single-stranded methylated MIR156 antisense control. The same superscripts denote nonsignificant differences ($P > 0.05$), and different superscripts denote significant differences ($P < 0.05$); $**P < 0.01$.

that maize miRNAs may be removed during starch and soybean pulp processing. In addition, soybean pulp and wheat bran account for a smaller proportion of the diet than maize. Thus replacement of maize by maize starch in formula feed is a practical way to minimize plant miRNAs in feed. Similarly, negligible MIR156 quantities were detected in maize starch diet and in the intestines of mice fed a maize starch diet. To address whether animal intestine development is regulated by dietary miRNAs, weanling mice were fed with or without maize diet. Maize MIR156 was present at significantly higher levels in gut tissue of mice fed with the maize diet, and both body weight and intestinal tract weight were decreased significantly. These results showed that deprivation of maize miRNAs can promote intestine development.

Dietary miRNAs from plants may serve as highly affordable and powerful regulatory factors (42). The present study pro-

vides the first evidence that plant miRNAs may exert cross-kingdom regulatory effects on animal gut development. In vitro experiments on IPEC-J2 cells clearly demonstrated retarded cell proliferation upon addition of synthetic MIR156 harboring plant-specific 2'-*O*-methylation. This study also revealed that the effective concentration needed for MIR156 to inhibit IPEC-J2 cell proliferation was 10^6 copies per cell, far surpassing the 100 copies per cell threshold concentration (5). The growth inhibitory effect of MIR156 was dose dependent in IPEC-J2 cells. Thus we conclude that exogenous miRNA may act as a regulatory factor in vivo.

The Wnt/ β -catenin signaling cascade is involved in the regulation of stem cell activity, cell proliferation, and cell survival in the gastrointestinal epithelium. Herein, expression of key molecules in the Wnt/ β -catenin pathway was compared in vivo between maize and maize starch diet groups. Express-

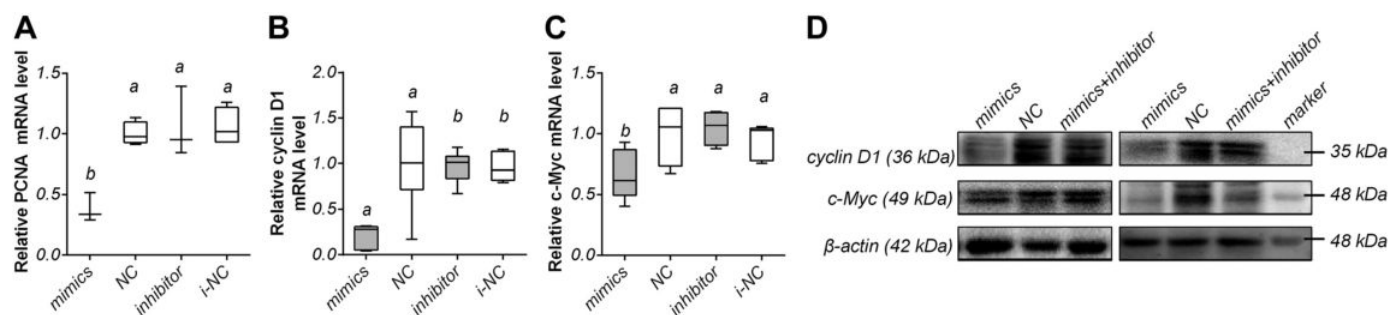


Fig. 8. MIR156 suppresses PCNA, c-Myc, and cyclin D1 expression. A–C: real-time quantitative PCR analysis of relative mRNA levels for PCNA (A), cyclin D1 (B), and c-Myc (C) following transfection with MIR156 mimics/NC/inhibitor/i-NC, respectively (normalized against β -actin; $n = 6$). D: Western blotting evaluation of cyclin D1 and c-Myc expression after transfection with MIR156 mimics/NC/mimics + inhibitor ($n = 4$). MIR156 mimics, a single-stranded methylated MIR156; NC, a single-stranded methylated nucleotide sequence; inhibitor, a single-stranded methylated MIR156 antisense sequence; i-NC, a single-stranded methylated MIR156 antisense control. Statistical significance was determined by least significant difference tests. The same superscripts denote nonsignificant differences ($P > 0.05$), and different superscripts denote significant differences ($P < 0.05$).

sion of Wnt10b and β -catenin was significantly decreased in the maize group compared with the maize starch group, as demonstrated by Western blotting and confocal immunofluorescence analyses. Moreover, expression of cyclin D1 and c-Myc showed a sharp decline in the maize diet group. These results were further confirmed by another *in vivo* experiment in which mice received synthetic MIR156 orally. More MIR156 was detected in the intestine of mice receiving MIR156, while Wnt10b mRNA levels were lower in intestinal crypt cells, indicating that MIR156 may regulate gene expression after being absorbed. These findings suggest that maize miRNAs may regulate the Wnt signaling pathway in the intestine. Moreover, we found that more than one miRNA mediated the Wnt signaling pathway by bioinformatics analysis and MIR156 is the most abundant plant miRNA in maize and human serum (27, 82). Therefore, we assumed that MIR156 may also be involved in regulating the Wnt signaling pathway. To test this hypothesis, we carried out luciferase reporter assays and *in vitro* tests and confirmed that MIR156 can target Wnt10b and influence its expression *in vitro*, demonstrating that maize miRNAs can promote degradation of their target mRNAs (42).

Drosophila Wnt has been shown to bind various Wnt receptors, including frizzled homologs and LRP5/6 at the cell surface, and stabilize cytoplasmic β -catenin (23a). In the Wnt-off state, β -catenin is phosphorylated by GSK-3 β at serine 33, serine 37, and threonine 41, and phosphorylation triggers β -catenin-mediated cross talk between signaling pathways and β -catenin-independent downstream signaling from Wnt (74). We examined Wnt signaling activity in IPEC-J2 cells by determining β -catenin levels and observed that β -catenin expression was inhibited by MIR156 at both mRNA and protein levels. Meanwhile, β -catenin phosphorylation at serine 33 was elevated in cells transfected with MIR156 mimics, indicating that MIR156 may stimulate degradation of β -catenin since phosphorylated β -catenin is reported to be an inactive form (62). Downregulation of PCNA, cyclin D1, and c-Myc caused by MIR156 indicates negative effects of MIR156 on intestinal cell proliferation. On the other hand, LiCl, an activator of the Wnt/ β -catenin pathway (15), relieved the inhibitory effects of MIR156 on cell proliferation, as well as on β -catenin expression, which further confirmed that MIR156 regulates cell proliferation via the Wnt/ β -catenin pathway. Together, the evidence shows the MIR156 can inhibit cell proliferation by influencing the Wnt/ β -catenin pathway.

Whether plant miRNAs exert cross-kingdom regulatory functions in humans and other animals remains controversial. Plant miRNAs may be associated with Ago2 (82) or packaged into secreted exosomes (82) or ELNs (48) to exert cross-kingdom regulatory effects on physiological processes across different species, and oral administration of plant miRNAs can suppress influenza viruses (84) and tumor growth (12). In particular, the transport mechanism of exogenous miRNAs remains a mystery. Previous studies showed that molecules containing both single- and double-stranded dsRNA, such as hairpin RNAs and pre-microRNAs, can be transported by systemic RNA interference deficiency (SID)-1 in *Caenorhabditis elegans* (55, 67), and SID-2 also selectively transports dsRNA (45). SID-2 is only required for environmental RNAi, and SID-1 is responsible for subsequent transport of molecules mediating RNAi silencing throughout the body (45). We found that these are expressed in the intestine of mouse and pig (data not shown). Toll-like receptor 7 (TLR7) is a transmembrane endosomal protein that plays an essential role in identifying nonself molecules, viral ssRNAs, and synthetic nucleic acid analogs in organisms. TLR7 expression is widely distributed in murine dendritic cells subsets (19). Mouse spleen mRNA and some short ssRNA oligonucleotides (of the type used to make short interfering dsRNAs) are also recognized by TLR7 (16). These studies indicate that exogenous short- and long-stranded RNAs, as well as single- and double-stranded RNAs, can be transported by transport proteins. A recent study found that plant miRNAs can be packaged into ELNs to regulate host colitis and gut bacteria (30, 48, 60). It is speculated that plant miRNAs may be recognized by these transport proteins or ELNs. In the present study, mouse experiments involving deprivation of maize MIR156 using maize starch or addition of synthetic MIR156 were performed alongside *in vitro* experiments on IPEC-J2 cells. Both sets of results consistently suggest that plant MIR156 is transported into animal intestines, but the specific mechanisms of miRNA selection and transport require further research.

The potential effects of dietary miRNA uptake are exciting, and accumulated evidence demonstrates generalized dietary miRNAs transfer and gene regulation in mammals. However, this remains controversial, and test methods, effective biological concentrations, choice of experimental subjects, and the origin of dietary miRNAs have all been questioned (57, 60a, 83). Experimental conditions clearly need to be optimized, and

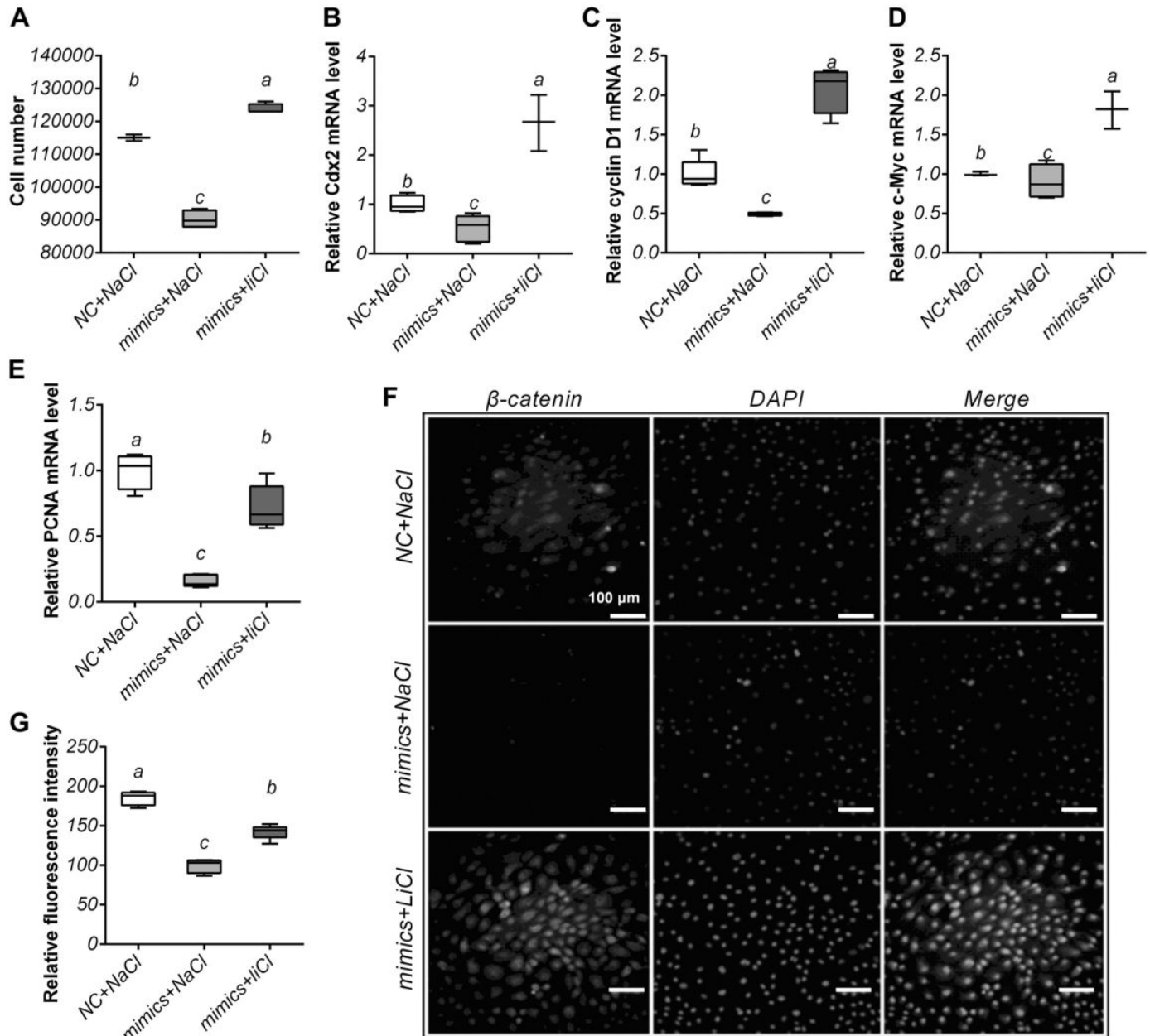


Fig. 9. Lithium chloride (LiCl) relieves inhibition by MIR156. MIR156 mimics (a single-stranded methylated MIR156) or NC (a single-stranded methylated nucleotide sequence) were transfected and incubated with 10 mM LiCl or NaCl and cell proliferation was measured at 8 h. **A**: cell counting to assess cell proliferation ($n = 6$). **B–E**: real-time quantitative PCR analysis of Cdx2, cyclin D1, c-Myc, and PCNA mRNA levels (normalized against β -actin; $n = 6$). **F**: β -catenin expression assessed by immunocytofluorescence (scale bars = 100 μ m; $n = 3$) and nucleic acid staining with DAPI. **G**: fluorescence intensities were measured using NIS-Elements. Statistical significance was determined by least significant difference tests. The same superscripts denote nonsignificant differences ($P > 0.05$), and different superscripts denote significant differences ($P < 0.05$).

more comprehensive research directions should be followed in future dietary miRNA studies. The use of a single method such as next-generation sequencing or nonspecific amplification by qPCR is one factor potentially limiting the accuracy of data related to dietary miRNAs (38a). In one previous animal feeding study, exogenous miRNAs were not transferred to animal blood, and it was concluded that exogenous miRNAs originated from technical artifacts rather than dietary intake (54). In our research, addition to qRT-PCR amplification, we used the gold standard method of Northern blotting for detection of diet-derived MIR156 in intestinal tissues. Furthermore,

ISH and fluorescence ISH results revealed greater MIR156 expression in intestinal crypt cells than at the mucosal surface in mice receiving the maize diet or MIR156 mimics. These results provide direct evidence that maize MIR156 can be absorbed, rather than simply adhered.

In vitro experiments showed that the Wnt pathway is not influenced by the MIR156 inhibitor that can inhibit endogenous miRNAs to recover expression of target genes. This result excluded contamination from endogenous miRNAs from animal sources. Intake of plant miRNAs results in gradual accumulation with functional consequences; miRNAs present at

low levels (<100 copies per cell) do not significantly repress target-containing transcripts (5). In another study, MIR168a was measured at 853 copies per cell in liver cells, comparable to endogenous mammalian miRNAs (82), indicating that diet-derived exogenous miRNAs can reach effective biological concentration in vivo. Differences in dietary intake can result in different concentrations of a specific miRNA in blood and tissues due to variability in absorption, distribution, metabolism, and elimination. Further progress and enthusiasm in this field will clearly depend on reaching a consensus regarding methods and controls.

Many abundant animal miRNAs share 100% identity across species; therefore, endogenous upregulation cannot be distinguished from influx of exogenous miRNAs (70). Witwer considered that inaccuracies can result from contamination (69, 70) and confirmation bias (68), and Witwer and Hirschi (72) considered that inaccuracies can result in technical artifacts. Luckily, plant miRNAs in animals can be accurately measured due to sequence differences between plant and animal miRNAs and specific 2'-O-methylation at the 3'-end of plant miRNAs. Milk feeding results showed that plasma sequencing data contained no miR-29b or miR-200c reads and no intake-consistent mapping of uniquely bovine miRNAs (3). The conservation of sequences among animal miRNAs makes it even more difficult to distinguish dietary animal miRNAs from endogenous miRNAs. In milk, some miRNAs may escape detection. The results of digital droplet PCR experiments indicated that all or most low-level signals were due to non-specific amplification (73). In a subsequent attempt to validate this research, dietary uptake of miR168a was found to be minimal, as was downregulation of LDLRAP1 by MIR168a after rice feeding (9). Several critical issues must be carefully considered, including the selection of appropriate miRNAs, accurate normalization, suitable RNA isolation methods, and minimizing sequencing bias (9, 39, 39a). Thus miRNA abundance is not the sole determinant of dietary miRNA uptake, and certain miRNAs enriched in foods may remain undetectable. Due to the possible selective absorption of dietary miRNAs, randomly picking one or two plant miRNAs to measure dietary miRNA uptake in animals is likely to be highly unrealistic. These issues remain to be addressed in the future. Therefore, the effects of exogenous miRNAs may not be as pronounced as has been suggested (71). However, absorption of dietary miRNAs clearly does occur, and potential effects on consumers must be considered. Despite some obvious challenges, extracellular RNA communication is a novel and important field of miRNA research with a probable bright future.

In conclusion, this study provides new evidence that diet-derived plant miRNAs can engage in cross-kingdom gene regulation in humans and other animals. Since maize is widely consumed by both humans and domesticated animals, MIR156 in maize may represent a key factor affecting intestinal development and health. Plant miRNAs should therefore be considered a new class of nutrients. We also provide the first evidence that plant MIR156 suppresses intestinal cell proliferation by targeting Wnt10b.

ACKNOWLEDGMENTS

We thank the Laboratory of Animal Center of Guangdong for providing C57BL/6 mice, and we thank Dr. Qi-En Qi (Fujian Aonong Bio-Technology

Group) and Dr. Chang-Song Liu (China Oil and Foodstuffs, Beijing, China) for providing maize material.

GRANTS

This study was supported by National Key Research and Development Program of China Grant 2016YFD0500503; Natural Science Foundation of China Program Grants 31802156, 31872435, and 31802037; and Natural Science Foundation of Guangdong Provincial Key Program Grant 2018B030311015.

DISCLOSURES

No conflicts of interest, financial or otherwise, are declared by the authors.

AUTHOR CONTRIBUTIONS

M.L., Q.-Y.J., J.-J.S., and Y.-L.Z. conceived and designed research; M.L., R.W., J.-J.H., and M.-Y.X. performed experiments; M.L., T.C., J.-J.H., R.-S.Y., and M.-Y.X. analyzed data; M.L., T.C., and J.-J.H. interpreted results of experiments; M.L. and T.C. prepared figures; M.L. and T.C. drafted manuscript; M.L., T.C., R.W., J.-Y.L., R.-S.Y., Q.-Y.X., and Y.-L.Z. edited and revised manuscript; M.L., T.C., R.W., J.-Y.L., J.-J.H., R.-S.Y., M.-Y.X., Q.-Y.X., Q.-Y.J., J.-J.S., and Y.-L.Z. approved final version of manuscript.

REFERENCES

- Arroyo JD, Chevillet JR, Kroh EM, Ruf IK, Pritchard CC, Gibson DF, Mitchell PS, Bennett CF, Pogosova-Agadjanyan EL, Stirewalt DL, Tait JF, Tewari M. Argonaute2 complexes carry a population of circulating microRNAs independent of vesicles in human plasma. *Proc Natl Acad Sci USA* 108: 5003–5008, 2011. doi:10.1073/pnas.1019055108.
- Auerbach A, Vyas G, Li A, Halushka M, Witwer K. Uptake of dietary milk miRNAs by adult humans: a validation study. *F1000 Res* 5: 721, 2016. doi:10.12688/f1000research.8548.1.
- Bartel DP. MicroRNAs: genomics, biogenesis, mechanism, and function. *Cell* 116: 281–297, 2004. doi:10.1016/S0092-8674(04)00045-5.
- Brown BD, Gentner B, Cantore A, Colleoni S, Amendola M, Zingale A, Baccarini A, Lazzari G, Galli C, Naldini L. Endogenous microRNA can be broadly exploited to regulate transgene expression according to tissue, lineage and differentiation state. *Nat Biotechnol* 25: 1457–1467, 2007. doi:10.1038/nbt1372.
- Casas-Agustench P, Iglesias-Gutiérrez E, Dávalos A. Mother's nutritional miRNA legacy: nutrition during pregnancy and its possible implications to develop cardiometabolic disease in later life. *Pharmacol Res* 100: 322–334, 2015. doi:10.1016/j.phrs.2015.08.017.
- Chen X, Ba Y, Ma L, Cai X, Yin Y, Wang K, Guo J, Zhang Y, Chen J, Guo X, Li Q, Li X, Wang W, Zhang Y, Wang J, Jiang X, Xiang Y, Xu C, Zheng P, Zhang J, Li R, Zhang H, Shang X, Gong T, Ning G, Wang J, Zen K, Zhang CY. Characterization of microRNAs in serum: a novel class of biomarkers for diagnosis of cancer and other diseases. *Cell Res* 18: 997–1006, 2008. doi:10.1038/cr.2008.282.
- Chen X, Zen K, Zhang CY. Reply to lack of detectable oral bioavailability of plant microRNAs after feeding in mice. *Nat Biotechnol* 31: 967–969, 2013. doi:10.1038/nbt.2741.
- Chiacchiera F, Rossi A, Jammula S, Pionti A, Scelfo A, Ordóñez-Morán P, Huelsken J, Koseki H, Pasini D. Polycomb complex PRC1 preserves intestinal stem cell identity by sustaining Wnt/β-catenin transcriptional activity. *Cell Stem Cell* 18: 91–103, 2016. doi:10.1016/j.stem.2015.09.019.
- Chin AR, Fong MY, Somlo G, Wu J, Swiderski P, Wu X, Wang SE. Cross-kingdom inhibition of breast cancer growth by plant miR159. *Cell Res* 26: 217–228, 2016. doi:10.1038/cr.2016.13.
- Chuck G, Cigan AM, Saeteurn K, Hake S. The heterochronic maize mutant Corngrass1 results from overexpression of a tandem microRNA. *Nat Genet* 39: 544–549, 2007. doi:10.1038/ng2001.
- Deo M, Yu JY, Chung KH, Tippens M, Turner DL. Detection of mammalian microRNA expression by in situ hybridization with RNA oligonucleotides. *Dev Dyn* 235: 2538–2548, 2006. doi:10.1002/dvdy.20847.
- Derksen PW, Tjin E, Meijer HP, Klok MD, MacGillivray HD, van Oers MH, Lokhorst HM, Bloem AC, Clevers H, Nusse R, van der Neut R, Spaargaren M, Pals ST. Illegitimate WNT signaling promotes proliferation of multiple myeloma cells. *Proc Natl Acad Sci USA* 101: 6122–6127, 2004. doi:10.1073/pnas.0305855101.

16. Diebold SS, Kaisho T, Hemmi H, Akira S, Reis e Sousa C. Innate antiviral responses by means of TLR7-mediated recognition of single-stranded RNA. *Science* 303: 1529–1531, 2004. doi:10.1126/science.1093616.
17. Ding D, Wang Y, Han M, Fu Z, Li W, Liu Z, Hu Y, Tang J. MicroRNA transcriptomic analysis of heterosis during maize seed germination. *PLoS One* 7: e39578, 2012. doi:10.1371/journal.pone.0039578.
18. Dorfman T, Pollak Y, Sohotnik R, Coran AG, Bejar J, Sukhotnik I. Enhanced intestinal epithelial cell proliferation in diabetic rats correlates with β -catenin accumulation. *J Endocrinol* 226: 135–143, 2015. doi:10.1530/JOE-14-0725.
19. Edwards AD, Diebold SS, Slack EM, Tomizawa H, Hemmi H, Kaisho T, Akira S, Reis e Sousa C. Toll-like receptor expression in murine DC subsets: lack of TLR7 expression by CD8 α^+ DC correlates with unresponsiveness to imidazoquinolines. *Eur J Immunol* 33: 827–833, 2003. doi:10.1002/eji.200323797.
20. Gallo A, Tandon M, Alevizos I, Illei GG. The majority of microRNAs detectable in serum and saliva is concentrated in exosomes. *PLoS One* 7: e30679, 2012. doi:10.1371/journal.pone.0030679.
21. Gavert N, Ben-Ze'ev A. β -Catenin signaling in biological control and cancer. *J Cell Biochem* 102: 820–828, 2007. doi:10.1002/jcb.21505.
22. Gupta SK, Bang C, Thum T. Circulating microRNAs as biomarkers and potential paracrine mediators of cardiovascular disease. *Circ Cardiovasc Genet* 3: 484–488, 2010. doi:10.1161/CIRCGENETICS.110.958363.
23. Ha M, Kim VN. Regulation of microRNA biogenesis. *Nat Rev Mol Cell Biol* 15: 509–524, 2014. doi:10.1038/nrm3838.
- 23a. He X, Semenov M, Tamai K, Zeng X. LDL receptor-related proteins 5 and 6 in Wnt/ β -catenin signaling: arrows point the way. *Development* 131: 1663–1677, 2004. doi:10.1242/dev.01117.
24. Hochstim CJ, Choi JY, Lowe D, Masood R, Rice DH. Biofilm detection with hematoxylin-eosin staining. *Arch Otolaryngol Head Neck Surg* 136: 453–456, 2010. doi:10.1001/archoto.2010.62.
27. Hou D, He F, Ma L, Cao M, Zhou Z, Wei Z, Xue Y, Sang X, Chong H, Tian C, Zheng S, Li J, Zen K, Chen X, Hong Z, Zhang CY, Jiang X. The potential atheroprotective role of plant MIR156a as a repressor of monocyte recruitment on inflamed human endothelial cells. *J Nutr Biochem* 57: 197–205, 2018. doi:10.1016/j.jnutbio.2018.03.026.
28. Hou YH, Jeyaraj A, Zhang X, Wei CL. Absolute quantification of microRNAs in green tea (*Camellia sinensis*) by stem-loop quantitative real-time PCR. *J Sci Food Agric* 97: 2975–2981, 2017. doi:10.1002/jsfa.8137.
30. Ju S, Mu J, Dokland T, Zhuang X, Wang Q, Jiang H, Xiang X, Deng ZB, Wang B, Zhang L, Roth M, Welti R, Mobley J, Jun Y, Miller D, Zhang HG. Grape exosome-like nanoparticles induce intestinal stem cells and protect mice from DSS-induced colitis. *Mol Ther* 21: 1345–1357, 2013. doi:10.1038/mt.2013.64.
31. Ju W, Ogawa A, Heyer J, Nierhof D, Yu L, Kucherlapati R, Shafritz DA, Böttinger EP. Deletion of Smad2 in mouse liver reveals novel functions in hepatocyte growth and differentiation. *Mol Cell Biol* 26: 654–667, 2006. doi:10.1128/MCB.26.2.654-667.2006.
33. Jung M, Schaefer A, Steiner I, Kempkensteffen C, Stephan C, Erbersdobler A, Jung K. Robust microRNA stability in degraded RNA preparations from human tissue and cell samples. *Clin Chem* 56: 998–1006, 2010. doi:10.1373/clinchem.2009.141580.
34. Kim SE, Huang H, Zhao M, Zhang X, Zhang A, Semenov MV, MacDonald BT, Zhang X, Garcia Abreu J, Peng L, He X. Wnt stabilization of β -catenin reveals principles for morphogen receptor-scaffold assemblies. *Science* 340: 867–870, 2013. doi:10.1126/science.1232389.
35. Lesjak M, Hoque R, Balesaria S, Skinner V, Debnam ES, Srai SK, Sharp PA. Quercetin inhibits intestinal iron absorption and ferroportin transporter expression in vivo and in vitro. *PLoS One* 9: e102900, 2014. doi:10.1371/journal.pone.0102900.
- 35a. Li J, Zhang Y, Li D, Liu Y, Chu D, Jiang X, Hou D, Zen K, Zhang CY. Small non-coding RNAs transfer through mammalian placenta and directly regulate fetal gene expression. *Protein Cell* 6: 391–396, 2015. doi:10.1007/s13238-015-0156-2.
36. Li C, Zhang B. MicroRNAs in control of plant development. *J Cell Physiol* 231: 303–313, 2016. doi:10.1002/jcp.25125.
37. Li VS, Ng SS, Boersma PJ, Low TY, Karthaus WR, Gerlach JP, Mohammed S, Heck AJR, Maurice MM, Mahmoudi T, Clevers H. Wnt signaling through inhibition of β -catenin degradation in an intact Axin1 complex. *Cell* 149: 1245–1256, 2012. doi:10.1016/j.cell.2012.05.002.
38. Liang G, Zhu Y, Sun B, Shao Y, Jing A, Wang J, Xiao Z. Assessing the survival of exogenous plant microRNA in mice. *Food Sci Nutr* 2: 380–388, 2014. doi:10.1002/fsn3.113.
- 38a. Liang H, Zen K, Zhang J, Zhang CY, Chen X. New roles for microRNAs in cross-species communication. *RNA Biol* 10: 367–370, 2013. doi:10.4161/ma.23663.
39. Liang H, Fu Z, Chen X, Zen K, Zhang CY. Reply to Dr. Witwer's letter to the editor. *J Nutr Biochem* 26: 1686–1687, 2015. doi:10.1016/j.jnutbio.2015.09.005.
- 39a. Liang H, Zhang S, Fu Z, Wang Y, Wang N, Liu Y, Zhao C, Wu J, Hu Y, Zhang J, Chen X, Zen K, Zhang CY. Effective detection and quantification of dietetically absorbed plant microRNAs in human plasma. *J Nutr Biochem* 26: 505–512, 2015. doi:10.1016/j.jnutbio.2014.12.002.
40. Liang H, Zhang S, Fu Z, Wang Y, Wang N, Liu Y, Zhao C, Wu J, Hu Y, Zhang J, Chen X, Zen K, Zhang CY. Effective detection and quantification of dietetically absorbed plant microRNAs in human plasma. *J Nutr Biochem* 26: 505–512, 2015. doi:10.1016/j.jnutbio.2014.12.002.
41. Liu S, da Cunha AP, Rezende RM, Cialic R, Wei Z, Bry L, Comstock LE, Gandhi R, Weiner HL. The host shapes the gut microbiota via fecal microRNA. *Cell Host Microbe* 19: 32–43, 2016. doi:10.1016/j.chom.2015.12.005.
42. Luo Y, Wang P, Wang X, Wang Y, Mu Z, Li Q, Fu Y, Xiao J, Li G, Ma Y, Gu Y, Jin L, Ma J, Tang Q, Jiang A, Li X, Li M. Detection of dietetically absorbed maize-derived microRNAs in pigs. *Sci Rep* 7: 645, 2017. doi:10.1038/s41598-017-00488-y.
43. MacDonald BT, Tamai K, He X. Wnt/ β -catenin signaling: components, mechanisms, and diseases. *Dev Cell* 17: 9–26, 2009. doi:10.1016/j.devcel.2009.06.016.
44. Masood M, Everett CP, Chan SY, Snow JW. Negligible uptake and transfer of diet-derived pollen microRNAs in adult honey bees. *RNA Biol* 13: 109–118, 2016. doi:10.1080/15476286.2015.1128063.
45. McEwan DL, Weisman AS, Hunter CP. Uptake of extracellular double-stranded RNA by SID-2. *Mol Cell* 47: 746–754, 2012. doi:10.1016/j.molcel.2012.07.014.
46. McKenna LB, Schug J, Vourekas A, McKenna JB, Bramswig NC, Friedman JR, Kaestner KH. MicroRNAs control intestinal epithelial differentiation, architecture, and barrier function. *Gastroenterology* 139: 1654–1664, 2010. doi:10.1053/j.gastro.2010.07.040.
47. Micó V, Martín R, Lasunción MA, Ordovás JM, Daimiel L. Unsuccessful detection of plant microRNAs in beer, extra virgin olive oil and human plasma after an acute ingestion of extra virgin olive oil. *Plant Foods Hum Nutr* 71: 102–108, 2016. doi:10.1007/s1130-016-0534-9.
48. Mu J, Zhuang X, Wang Q, Jiang H, Deng ZB, Wang B, Zhang L, Kakar S, Jun Y, Miller D, Zhang HG. Interspecies communication between plant and mouse gut host cells through edible plant derived exosome-like nanoparticles. *Mol Nutr Food Res* 58: 1561–1573, 2014. doi:10.1002/mnfr.201300729.
49. Myant KB, Cammareri P, McGhee EJ, Ridgway RA, Huels DJ, Cordero JB, Schwitala S, Kalna G, Ogg EL, Athineos D, Timpson P, Vidal M, Murray GI, Gretchen FR, Anderson KI, Sansom OJ. ROS production and NF- κ B activation triggered by RAC1 facilitate WNT-driven intestinal stem cell proliferation and colorectal cancer initiation. *Cell Stem Cell* 12: 761–773, 2013. doi:10.1016/j.stem.2013.04.006.
50. O'Neill MJ, Bourre L, Melgar S, O'Driscoll CM. Intestinal delivery of non-viral gene therapeutics: physiological barriers and preclinical models. *Drug Discov Today* 16: 203–218, 2011. doi:10.1016/j.drudis.2011.01.003.
51. Pirro S, Minutolo A, Galgani A, Potestà M, Colizzi V, Montesano C. Bioinformatics prediction and experimental validation of microRNAs involved in cross-kingdom interaction. *J Comput Biol* 23: 976, 2016. doi:10.1089/cmb.2016.0059.
52. Poethig RS. Small RNAs and developmental timing in plants. *Curr Opin Genet Dev* 19: 374–378, 2009. doi:10.1016/j.gde.2009.06.001.
53. Schaefer JS, Attumi T, Opekun AR, Abraham B, Hou J, Shelby H, Graham DY, Streckfus C, Klein JR. MicroRNA signatures differentiate Crohn's disease from ulcerative colitis. *BMC Immunol* 16: 5, 2015. doi:10.1186/s12865-015-0069-0.
54. Shahid S, Kim G, Johnson NR, Wafula E, Wang F, Coruh C, Bernal-Galeano V, Phifer T, dePamphilis CW, Westwood JH, Axtell MJ. MicroRNAs from the parasitic plant *Cuscuta campestris* target host messenger RNAs. *Nature* 553: 82–85, 2018. doi:10.1038/nature25027.
55. Shih JD, Hunter CP. SID-1 is a dsRNA-selective dsRNA-gated channel. *RNA* 17: 1057–1065, 2011. doi:10.1261/ma.2596511.

56. Silberg DG, Swain GP, Suh ER, Traber PG. Cdx1 and cdx2 expression during intestinal development. *Gastroenterology* 119: 961–971, 2000. doi:10.1053/gast.2000.18142.
57. Snow JW, Hale AE, Isaacs SK, Baggish AL, Chan SY. Ineffective delivery of diet-derived microRNAs to recipient animal organisms. *RNA Biol* 10: 1107–1116, 2013. doi:10.4161/rna.24909.
- 57a. Song QX, Liu YF, Hu XY, Zhang WK, Ma B, Chen SY, Zhang JS. Identification of miRNAs and their target genes in developing soybean seeds by deep sequencing. *BMC Plant Biol* 11: 5, 2011. doi:10.1186/1471-2229-11-5.
58. Sun F, Guo G, Du J, Guo W, Peng H, Ni Z, Sun Q, Yao Y. Whole-genome discovery of miRNAs and their targets in wheat (*Triticum aestivum* L.). *BMC Plant Biol* 14: 142, 2014. doi:10.1186/1471-2229-14-142.
59. Sun X, He Y, Huang C, Ma TT, Li J. Distinctive microRNA signature associated of neoplasms with the Wnt/ β -catenin signaling pathway. *Cell Signal* 25: 2805–2811, 2013. doi:10.1016/j.cellsig.2013.09.006.
60. Teng Y, Ren Y, Sayed M, Hu X, Lei C, Kumar A, Hutchins E, Mu J, Deng Z, Luo C, Sundaram K, Sriwastva MK, Zhang L, Hsieh M, Reiman R, Haribabu B, Yan J, Jala VR, Miller DM, Van Keuren-Jensen K, Merchant ML, McClain CJ, Park JW, Egilmez NK, Zhang HG. Plant-derived exosomal microRNAs shape the gut microbiota. *Cell Host Microbe* 24: 637–652.e8, 2018. doi:10.1016/j.chom.2018.10.001.
- 60a. Tosar JP, Rovira C, Naya H, Cayota A. Mining of public sequencing databases supports a non-dietary origin for putative foreign miRNAs: underestimated effects of contamination in NGS. *RNA* 20: 754–757, 2014. doi:10.1261/rna.044263.114.
61. Tran L, Greenwood-Van Meerveld B. Age-associated remodeling of the intestinal epithelial barrier. *J Gerontol A Biol Sci Med Sci* 68: 1045–1056, 2013. doi:10.1093/gerona/glt106.
- 61a. Turchinovich A, Weiz L, Langheinz A, Burwinkel B. Characterization of extracellular circulating microRNA. *Nucleic Acids Res* 39: 7223–7233, 2011. doi:10.1093/nar/gkr254.
62. Varisli L, Ozturk BE, Akyuz GK, Korkmaz KS. HN1 negatively influences the β -catenin/E-cadherin interaction, and contributes to migration in prostate cells. *J Cell Biochem* 116: 170–178, 2015. doi:10.1002/jcb.24956.
63. Vickers KC, Palmisano BT, Shoucri BM, Shamburek RD, Remaley AT. Corrigendum: microRNAs are transported in plasma and delivered to recipient cells by high-density lipoproteins. *Nat Cell Biol* 17: 423–433, 2014. doi:10.1038/ncb3074.
64. Wang X, Elling AA, Li X, Li N, Peng Z, He G, Sun H, Qi Y, Liu XS, Deng XW. Genome-wide and organ-specific landscapes of epigenetic modifications and their relationships to mRNA and small RNA transcriptomes in maize. *Plant Cell* 21: 1053–1069, 2009. doi:10.1105/tpc.109.065714.
65. Weise A, Bruser K, Elfert S, Wallmen B, Wittel Y, Wöhrle S, Hecht A. Alternative splicing of Tcf712 transcripts generates protein variants with differential promoter-binding and transcriptional activation properties at Wnt/ β -catenin targets. *Nucleic Acids Res* 38: 1964–1981, 2010. doi:10.1093/nar/gkp1197.
66. Wend P, Wend K, Krum SA, Miranda-Carboni GA. The role of WNT10B in physiology and disease. *Acta Physiol (Oxf)* 204: 34–51, 2012. doi:10.1111/j.1748-1716.2011.02296.x.
67. Winston WM, Molodowitch C, Hunter CP. Systemic RNAi in *C. elegans* requires the putative transmembrane protein SID-1. *Science* 295: 2456–2459, 2002. doi:10.1126/science.1068836.
68. Witwer KW. Alternative miRNAs? Human sequences misidentified as plant miRNAs in plant studies and in human plasma. *F1000 Res* 7: 244, 2018. doi:10.12688/f1000research.14060.1.
69. Witwer KW. Contamination or artifacts may explain reports of plant miRNAs in humans. *J Nutr Biochem* 26: 1685–1685, 2015. doi:10.1016/j.jnutbio.2015.09.004.
70. Witwer KW. Diet-responsive mammalian miRNAs are likely endogenous. *J Nutr* 144: 1880–1881, 2014. doi:10.3945/jn.114.202523.
71. Witwer KW. XenomiRs and miRNA homeostasis in health and disease: evidence that diet and dietary miRNAs directly and indirectly influence circulating miRNA profiles. *RNA Biol* 9: 1147–1154, 2012. doi:10.4161/rna.21619.
72. Witwer KW, Hirschi KD. Transfer and functional consequences of dietary microRNAs in vertebrates: concepts in search of corroboration: negative results challenge the hypothesis that dietary xenomiRs cross the gut and regulate genes in ingesting vertebrates, but important questions persist. *BioEssays* 36: 394–406, 2014. doi:10.1002/bies.201300150.
73. Witwer KW, McAlexander MA, Queen SE, Adams RJ. Real-time quantitative PCR and droplet digital PCR for plant miRNAs in mammalian blood provide little evidence for general uptake of dietary miRNAs: limited evidence for general uptake of dietary plant xenomiRs. *RNA Biol* 10: 1080–1086, 2013. doi:10.4161/rna.25246.
74. Wu D, Pan W. GSK3: a multifaceted kinase in Wnt signaling. *Trends Biochem Sci* 35: 161–168, 2010. doi:10.1016/j.tibs.2009.10.002.
76. Wu G, Park MY, Conway SR, Wang JW, Weigel D, Poethig RS. The sequential action of miR156 and miR172 regulates developmental timing in Arabidopsis. *Cell* 138: 750–759, 2009. doi:10.1016/j.cell.2009.06.031.
78. Xie K, Wu C, Xiong L. Genomic organization, differential expression, and interaction of SQUAMOSA promoter-binding-like transcription factors and microRNA156 in rice. *Plant Physiol* 142: 280–293, 2006. doi:10.1104/pp.106.084475.
79. Yang J, Farmer LM, Agyekeum AA, Elbaz-Younes I, Hirschi KD. Detection of an abundant plant-based small RNA in healthy consumers. *PLoS One* 10: e0137516, 2015. doi:10.1371/journal.pone.0137516.
80. Yu B, Yang Z, Li J, Minakhina S, Yang M, Padgett RW, Steward R, Chen X. Methylation as a crucial step in plant microRNA biogenesis. *Science* 307: 932–935, 2005. doi:10.1126/science.1107130.
81. Zhang B, Pan X, Anderson TA. Identification of 188 conserved maize microRNAs and their targets. *FEBS Lett* 580: 3753–3762, 2006. doi:10.1016/j.febslet.2006.05.063.
82. Zhang L, Hou D, Chen X, Li D, Zhu L, Zhang Y, Li J, Bian Z, Liang X, Cai X, Yin Y, Wang C, Zhang T, Zhu D, Zhang D, Xu J, Chen Q, Ba Y, Liu J, Wang Q, Chen J, Wang J, Wang M, Zhang Q, Zhang J, Zen K, Zhang CY. Exogenous plant MIR168a specifically targets mammalian LDLRAP1: evidence of cross-kingdom regulation by microRNA. *Cell Res* 22: 107–126, 2012. doi:10.1038/cr.2011.158.
83. Zhang Y, Wiggins BE, Lawrence C, Petrick J, Ivashuta S, Heck G. Analysis of plant-derived miRNAs in animal small RNA datasets. *BMC Genomics* 13: 381, 2012. doi:10.1186/1471-2164-13-381.
84. Zhou Z, Li X, Liu J, Dong L, Chen Q, Liu J, Kong H, Zhang Q, Qi X, Hou D, Zhang L, Zhang G, Liu Y, Zhang Y, Li J, Wang J, Chen X, Wang H, Zhang J, Chen H, Zen K, Zhang CY. Honeysuckle-encoded atypical microRNA2911 directly targets influenza A viruses. *Cell Res* 25: 39–49, 2015. doi:10.1038/cr.2014.130.
85. Zhu G, Wang Y, Huang B, Liang J, Ding Y, Xu A, Wu W. A Rac1/PAK1 cascade controls β -catenin activation in colon cancer cells. *Oncogene* 31: 1001–1012, 2012. doi:10.1038/ncr.2011.294.
86. Zhu K, Liu M, Fu Z, Zhou Z, Kong Y, Liang H, Lin Z, Luo J, Zheng H, Wan P, Zhang J, Zen K, Chen J, Hu F, Zhang CY, Ren J, Chen X. Plant microRNAs in larval food regulate honeybee caste development. *PLoS Genet* 13: e1006946, 2017. doi:10.1371/journal.pgen.1006946.

RESEARCH ARTICLE

Open Access



Genomewide analysis of circular RNA in pituitaries of normal and heat-stressed SOWS

Haojie Zhang[†], Baoyu Hu[†], Jiali Xiong, Ting Chen, Qianyun Xi, Junyi Luo, Qingyan Jiang, Jiajie Sun^{*} and Yongliang Zhang^{*}

Abstract

Background: As a newly characterized type of noncoding RNA, circular RNA (circRNA) has been shown to have functions in diverse biological processes of animals. It has been reported that several noncoding RNAs may regulate animals' response to heat stress which can be easily induced by hyperthermia in summer. However, the expression and functions of circRNAs in the pituitary of sows and whether they participate in heat stress adaption are still unclear.

Results: In this study, we found that high temperature over the thermoneutral zone of sows during the summer increased the serum heat shock protein 70 (HSP70) level, decreased the superoxide dismutase (SOD) vitality and prolactin (PRL) concentration, and induced heat stress in sows. Then, we explored circRNA in the pituitary of heat-stressed and normal sows using RNA sequencing and bioinformatics analysis. In total, 12,035 circRNAs were detected, with 59 circRNAs differentially expressed, including 42 up-regulated and 17 down-regulated circRNAs in pituitaries of the heat-stressed sows. Six randomly selected circRNAs were identified through reverse transcription PCR followed by DNA sequencing and other 7 randomly selected differentially expressed circRNAs were verified by quantitative real-time PCR analysis. The predicted target genes regulated by circRNAs through sponging microRNAs (miRNAs) were enriched in metabolic pathway. Furthermore, the predicted circRNA-miRNA-mRNA interactions showed that some circRNAs might sponge miRNAs to regulate pituitary-specific genes and heat shock protein family members, indicating circRNA's roles in pituitary hormone secretion and heat stress response.

Conclusions: Our results provided a meaningful reference to understand the functions of circRNA in the porcine pituitary and the mechanisms by which circRNA may participate in animals' response to heat stress.

Keywords: Hyperthermia, Noncoding RNA, Pituitary, Profiling, Sows

Background

Circular RNA (circRNA) is a class of noncoding RNA (ncRNA), and numerous circRNAs are formed by head-to-tail splicing of exons [1] during transcription. CircRNAs were first observed in eukaryotes [2], but they were usually considered as useless byproducts [3] with low abundance and uncertain functions. Recently, with the rapid development of high-throughput sequencing technologies and

bioinformatics, circRNAs have received significant attention. Most circRNAs originate from protein-coding genes and consist of complete exons [4]. The biological functions of circRNAs are being identified, and several studies have indicated that circRNA may act as sponges of microRNA (miRNA), sequestering and competitively suppressing miRNA activity [5, 6]. Besides, some intronic RNAs mainly located in the nucleus may interact with RNA polymerase II to influence gene transcription [7]. Some circRNAs containing ribosome entry sites may be translated into proteins [8]. Up to now, knowledge about the pig circRNAs is relatively limited comparing to mice and humans. Although several circRNAs have been discovered in pig muscles [9],

* Correspondence: jiajiesun@scau.edu.cn; zhangyl@scau.edu.cn

[†]Haojie Zhang and Baoyu Hu contributed equally to this work. Guangdong Province Key Laboratory of Animal Nutritional Regulation, National Engineering Research Center for Breeding Swine Industry, College of Animal Science, South China Agricultural University, Wushan Road, Tianhe District, Guangzhou, Guangdong 510642, People's Republic of China



© The Author(s). 2019 **Open Access** This article is distributed under the terms of the Creative Commons Attribution 4.0 International License (<http://creativecommons.org/licenses/by/4.0/>), which permits unrestricted use, distribution, and reproduction in any medium, provided you give appropriate credit to the original author(s) and the source, provide a link to the Creative Commons license, and indicate if changes were made. The Creative Commons Public Domain Dedication waiver (<http://creativecommons.org/publicdomain/zero/1.0/>) applies to the data made available in this article, unless otherwise stated.

brains [10], and other common tissues [11], the information about circRNAs in the pig pituitary is little known.

The mammalian pituitary is an important endocrine organ that modulates the stress response, metabolic homeostasis, growth, reproduction, and lactation [12]. These critical functions of the pituitary are mainly regulated by 6 different hormones that secreted by 5 specialized cell types within the anterior pituitary [13]. Recently, various ncRNAs such as miRNA and long noncoding RNA (lncRNA) in the pituitary have been identified to participate in some biological processes [14, 15]. Circular RNA in the pituitary of sheep have been analyzed and indicated to have functions in embryo pituitary development and endocrine regulation [16]. Therefore, circRNAs may be the new regulatory factors during the endocrine regulation in pigs and other mammalian animals.

High temperature has profound effects on sows ingestion, reproduction, lactation, and metabolism [17]. Especially in the south of China, high temperatures last half a year, which easily cause heat stress and negatively influences sow health and performance. Recent studies have found the expression alteration of ncRNAs in the mammalian heat stress response and indicated that ncRNAs may be novel regulators during heat stress [18]. In homeothermic animals, such as rat and mice, heat stress altered miRNAs expression patterns in the rat small intestine [19] and increased the expression of miR-1, miR-21, and miR-24 in the mice heart to generate a cardioprotective phenotype resistant to I/R injury [20]. Heat stress may also manipulate miRNA levels by affecting the enzymes that involved in miRNAs' biogenesis [21]. Besides, heat stress could alter lncRNAs expression. Two lncRNA species including B2 RNA in mice and Alu RNA in humans accumulate at relatively low levels during normal cellular growth, however, their abundance transiently increases by as much as 40-fold under certain conditions of heat stress [22, 23]. Since circRNAs are also non-coding RNAs and could function as a type of ceRNA capable of sequestering miRNA activity, it is reasonable to speculate that circRNAs may vary their expression and play a role in response to heat stress. In addition, it has reported that heat stress could affect circRNAs expression and biogenesis in plants [24, 25]. However, little attention has been focused on circRNAs' alteration and function in animals during heat stress. In this study, we researched the circRNA expression profiles in the anterior pituitaries of sows obtained in winter, when the temperature was in the thermoneutral zone, and summer, when the temperature was high. The results of our study may help to better understand the roles of circRNAs in the regulation of the pituitary function and the response to heat stress.

Methods

Animals and experiment design

This study used 12 healthy sows (Landrace), which were purchased from the Guangzhou thoroughbred farm (Guangzhou, Guangdong, P. R. China). Six sows were obtained during the winter months of 2017, with a moderate average temperature ($19.6 \pm 0.41^\circ\text{C}$), and designated the thermoneutral (TN) group. Another 6 sows were obtained during the summer months of 2017, with a high average temperature ($30.2 \pm 0.40^\circ\text{C}$), and designated the heat stress (HS) group. The body weight (in the range of 250 ± 10 kg) and parity (between 5 and 7) were balanced in the 2 test groups. The sows consume the same diet in summer and winter months.

Sample collection

Incubate the pig with an endotracheal tube (30 cm length, 8 mm ID) and anesthetize pig with isoflurane (4.5% of tidal volume by mask) [26]. Then, the pigs were euthanized by exsanguination under a surgical plane of the isoflurane anesthesia [27]. The anterior pituitaries were carefully dissected and stored at -80°C until further processing. The blood samples were collected in clean tubes and centrifuged at $3000 \times g$ for 20 min at 4°C after a room temperature clotting. The supernatant of the blood was separated and stored at -30°C for preservation. All animal experimentation complied with the laboratory animal management and welfare regulations approved by Standing Committee of Guangdong People's Congress (Guangzhou), China.

Serum assays

The activity of serum total superoxide dismutase (SOD) was measured by a SOD assay kit following the instructions of the manufacturer. The levels of serum heat shock protein 70 (HSP70), cortisol, and prolactin (PRL) were quantified using a HSP70 ELISA assay kit, cortisol ELISA assay kit, and PRL ELISA assay kit, respectively, following the instructions of the manufacturer. Nanjing Jiancheng Bioengineering Institute (Nanjing, P. R. China) provided all the commercial assay kits.

Total RNA extraction and sequencing

Three pituitary samples of each group, including the TN group and the HS group, were selected. Following the protocol of the manufacturer, we used Trizol Reagent (Invitrogen, Carlsbad, CA) to isolate total RNA of the 6 samples. The RNA quantity and quality were assessed using an RNA 6000 Nano Lab-Chip Kit and Agilent 2100 Bioanalyzer (Agilent Technologies, Inc., Santa Clara, CA) with an RNA integrity number > 7.0 . Then, ribosomal RNA was depleted from the total RNA following the instructions of the Epicentre Ribo-Zero Magnetic Gold Kit (Illumina, Inc.). After the depletion of rRNA,

the remaining RNAs were digested with RNase R (Epicentre, Madison, WI) at 37 °C for 10 min and further were reverse transcribed to construct the cDNA library using the mRNA-Seq Sample Preparation Kit (Illumina, Inc). Finally, the Illumina HiSeq 4000 platform were used to sequence the libraries with 150-bp paired-end reads at LC Sciences in Hangzhou, P. R. China.

Circular RNA identification and differential expression analysis

Firstly, raw reads were filtered using Cutadapt [28] by removing the adaptor contaminating reads and low-quality reads. Then, the remaining reads were multi-mapped to the Sscrofa10.2 genome using Bowtie 2 and TopHat2 [29, 30]. Extract the unmapped reads and continue to use TopHat-Fusion [31] to map the genome. The mapped reads were first reassembled to circRNA using CIRCexplorer2 [32, 33]; then, both the TopHat-Fusion and CIRCexplorer2 were used to identify the back-splicing reads in unmapped reads. Finally, a circRNA can be confirmed if it has at least 1 back-splicing read. The expression level of circRNA was quantified as fragments per kilobase of transcripts per million mapped reads (FPKM) using StringTie [34]. Only circRNA with 2 or more back-splicing reads were kept. Significantly differentially expressed circRNA were identified with the P -value < 0.05 and $|\log_2(\text{fold change})| \geq 0.585$ between the two groups.

PCR analysis, DNA sequencing, and quantitative real-time PCR validation

Total RNA was extracted from anterior pituitaries of the sows using Trizol Reagent (Invitrogen). Then, the PrimeScript RT Reagent Kit with gDNA Eraser (Takara, Dalian, P. R. China) was used to synthesize cDNA for circRNA. Polymerase chain reaction was conducted using specific primers for different circRNA. The circRNA primers sequences were provided in Additional file 1: Table S1. We used agarose gel electrophoresis and DNA sequencing to confirm the PCR products. Furthermore, the PCR products sequences, the pig reference genome and RNA sequencing data were compared by the software DNAMAN (Lynnon Biosoft, San Ramon, CA). Polymerase chain reaction was done using the designed primers and cDNA template. The PCR conditions were 94 °C denaturation for 5 min, 40 cycles at 94 °C for 10 s, 54 to 60 °C for 15 s, and 72 °C for 30 s. We randomly chose 7 differentially expressed circRNAs and used qRT-PCR to confirm the results of RNA-seq. The qRT-PCR was conducted on a Bio-Rad CFX96 Real-Time Detection System (Bio-Rad Laboratories, Inc., Hercules, CA) with the GoTaq qPCR Master Mix (Promega, Madison, WI, USA). The relative expression levels of circRNA were calculated using the $2^{-\Delta\Delta Ct}$ method. Porcine GAPDH was used as an internal

control. All the quantitative PCR reactions were assayed with 6 biological replicates. The primers of qRT-PCR were also provided in Additional file 1: Table S1.

Construction of predicted competing endogenous RNA networks and enrichment analysis

In order to explore circRNAs' sponge function of miRNAs, putative interaction targets between the miRNAs and the differentially expressed circRNAs or the mRNAs were predicted by miRanda [35] and RNAhybrid [36]. Only alignments with energies less than -20 kcal/mol and no mismatch in the seed region were retained for further analysis. There were three steps to construct the competing endogenous RNA interaction networks. First, differentially expressed circRNAs in heat stress and all pig miRNAs and mRNAs candidates were chose. The sequences of all pig miRNAs and mRNA transcripts were respectively obtained from miRbase (<http://mirbase.org/pub/mirbase/22.1/>, accessed October 2018) and UCSC (<http://genome.ucsc.edu/cgi-bin/hgTables>). Second, circRNA-miRNA and miRNA-mRNA negative interactions were predicted by miRanda and RNAhybrid analyses, and the common target interactions obtained by the two analyses were retained. Third, the potential interactions between circRNAs and miRNAs or mRNAs were established and the visualized circRNA-miRNA-mRNA network was constructed by Cytoscape 3.5.1 [37]. Besides, the probability (based on the shared miRNAs) for each ceRNA pair was calculated according to the previous report [38–40].

For enrichment analysis, we used DAVID software [41] to make Gene Ontology (GO) analysis and KEGG pathway enrichment of the genes that predicted to be regulated by the differentially expressed circRNAs. GO terms and KEGG pathways for which $P < 0.05$ were considered significantly enriched.

Statistical analysis

The temperature and humidity of the swine pen in the winter and summer months were recorded every day in this study. The average daily temperature and humidity were determined using the recording data. The formula: $THI = [(1.8 \times T) + 32] - [0.55 \times (1 - RH)] \times (1.8 \times T - 26)$ was used to calculate the average THI (temperature humidity index), in which T and RH respectively represent the air temperature in degrees Celsius and the relative humidity in percent [42]. Statistical analyses were performed by the SPSS software. Differences between groups were determined using an independent 2-sample t-test and considered statistically significant at $P < 0.05$. All the data are presented as the means \pm standard error.

Results

Environmental indicators and the effect of high temperature on serum hormones and the antioxidant index

The average temperature and humidity were 19.6 ± 0.41 °C and $67.2\% \pm 0.01$, respectively, from December 2016 to January 2017, and the average temperature and humidity were 30.2 ± 0.40 °C and $75.3\% \pm 0.02$, respectively, from June 2017 to July 2017. This data was used to calculate the THI, which characterizes the environmental conditions of the pen. The THI during winter was about 65.6 and was 82.5 during summer, which was well above 72. We then measured the alteration of serum HSP70, PRL, cortisol, and SOD vitality in the two groups. The SOD vitality of serum in the HS group was lower comparing with the TN group (Fig. 1a). At the same time, the level of the heat stress-sensitive protein HSP70 increased significantly in the HS group (Fig. 1b). We also found that high temperature reduced the level of cortisol (Fig. 1c) and PRL (Fig. 1d) in the HS group. The results above indicated that sows obtained in summer suffered from heat stress.

Abundance and characteristics of circular RNA in the sow pituitary

In order to explore the circRNA expression profiles of the sow pituitary under heat stress, we used RNA-seq analyses to characterize the circRNA from 6 normal anterior pituitaries of the sows obtained during warm

seasons (TN group) and hot seasons (HS group). From these 2 data sets, a total of 12,035 unique circRNAs were detected and 1616 of these candidates had at least 2 head-to-tail splicing reads (Fig. 2a). Meanwhile, 3 circRNAs (circRNA2294, circRNA1646 and circRNA2869) contained more than 100 back-splice reads in all the samples. For all pituitary samples, the detected circRNAs located in all the pig chromosomes and the chromosome 1 had the largest number of circRNAs (Fig. 2b). The host genes of the detected circRNAs were also analyzed and we found that multiple circRNAs could derive from a single gene (Fig. 2c). A striking example is that CHD2 may generate 53 distinct circRNAs. In addition, we further examined the number of circRNA exons and discovered that more than 95% of circRNAs are composed of multiple exons whereas only 4.3% are a single exon (Fig. 2d). The detailed information about the total detected circRNA was presented in Additional file 2: Table S2 and Additional file 11.

Identification of circular RNA in the sow pituitary

In order to identify the detected circRNAs in the RNA-seq results, 6 circRNAs were randomly selected and amplified by PCR with the designed divergent primers (Fig. 3a). The gel electrophoresis results showed that each circRNA had a single band at the expected location (Fig. 3b). Then, the DNA sequencing results were used to compare with the normal DNA sequences to confirm

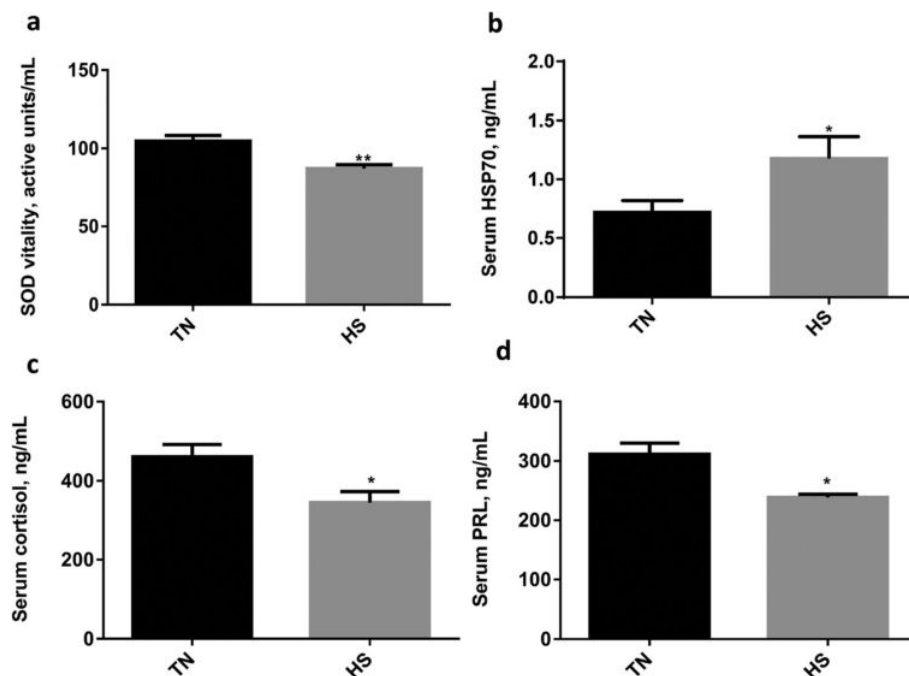


Fig. 1 The influence of heat stress on hormones and the antioxidative index. **a** The superoxide dismutase (SOD) vitality of sow serum in the thermoneutral (TN) and heat stress (HS) groups and (**b–d**) the level of heat shock protein 70 (HSP70), cortisol, and prolactin (PRL) of sow serum in the TN and HS groups. Values are expressed as means and SEM. $n = 6$; * $P < 0.05$; ** $P < 0.01$ (t-test)

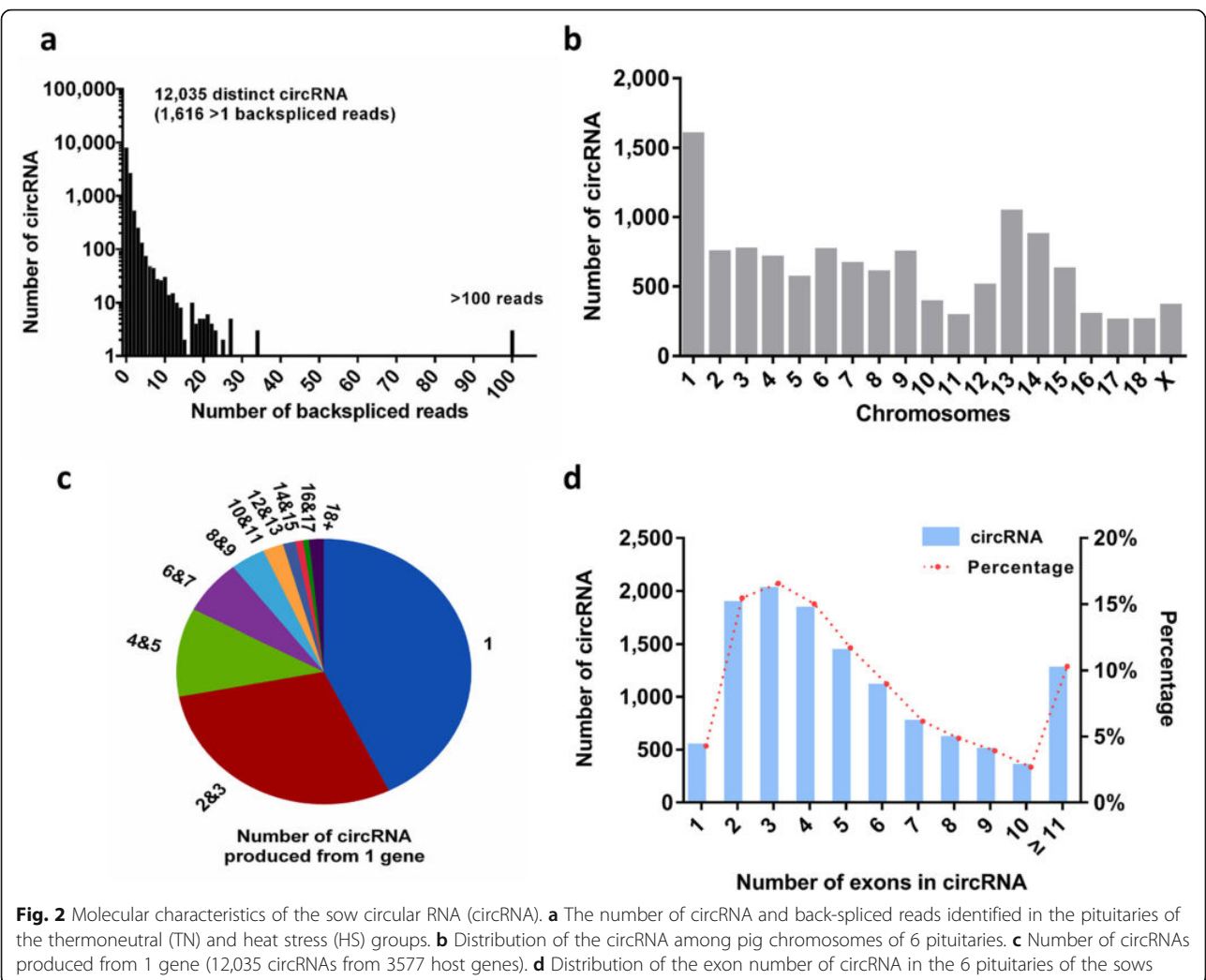


Fig. 2 Molecular characteristics of the sow circular RNA (circRNA). **a** The number of circRNA and back-spliced reads identified in the pituitaries of the thermoneutral (TN) and heat stress (HS) groups. **b** Distribution of the circRNA among pig chromosomes of 6 pituitaries. **c** Number of circRNAs produced from 1 gene (12,035 circRNAs from 3577 host genes). **d** Distribution of the exon number of circRNA in the 6 pituitaries of the sows

the back-splicing junctions (Fig. 3c). Finally, we successfully identified these six circular RNAs.

Analysis and validation of differentially expressed circular RNA

We used FPKM as the metric for the circRNA expression level. Only circRNAs with 2 or more back-splice reads within single samples were kept. The differentially expressed circRNA were screened with the $|\log_2(\text{fold change})| \geq 0.585$ and $P < 0.05$. Thus, we identified 59 differentially expressed circRNAs in the sow pituitary between the TN and HS groups (Additional file 3: Table S3). Among them, there were 42 up-regulated and 17 down-regulated circRNAs (Fig. 4a). Then, other 7 circRNAs were randomly chosen for qRT-PCR validation. The results showed the expression of circRNA8068 significantly decreased in the HS group, and the expressions of other selected circRNAs significantly increased in the HS group ($P < 0.05$), except circRNA6541 and circRNA2600, which were highly expressed in the HS

group, but has no significant difference ($P > 0.05$). The results showed a consistency between qRT-PCR and deep sequencing analysis (Fig. 4b), suggesting that the identified circRNA had a true differential expression in vivo.

Target miRNA or gene prediction of differentially expressed circRNAs and enrichment analysis

Circular RNAs were proved to have ‘sponge’ functions on miRNAs and further indirectly regulate mRNAs expression [1, 5]. Here, we predicted the potential interactions between all pig miRNAs and pig mRNAs or the differentially expressed circRNAs according to the mi-Randa and RNAhybrid pipeline. In the constructed potential circRNA–miRNA–mRNA associations, there were 110 miRNAs interacted with 10,598 mRNA transcripts and 51 differentially expressed circRNAs (Additional file 4: Table S4). In order to learn the potential functions of the differentially expressed circRNAs in the pituitary, we used GO and KEGG

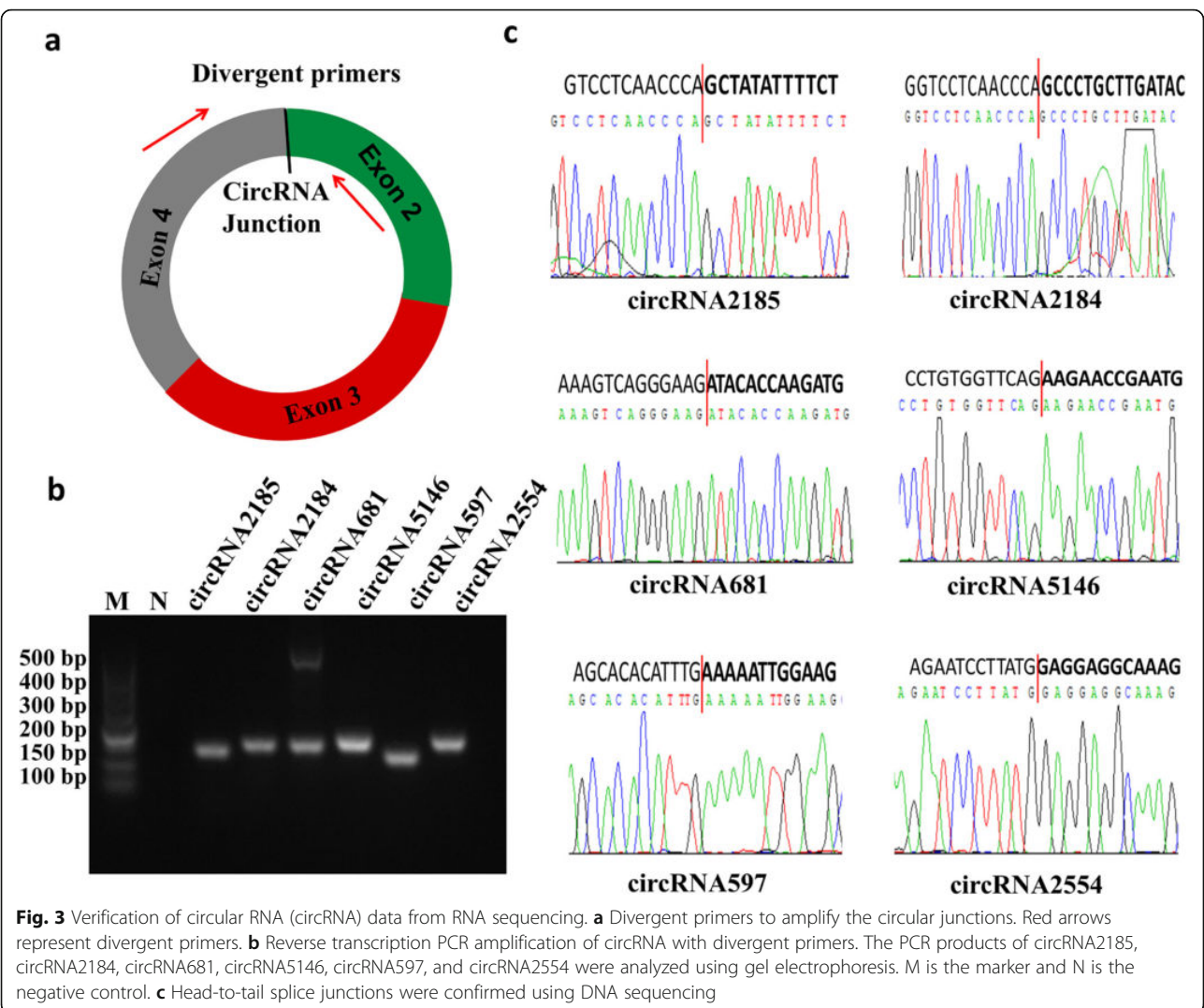


Fig. 3 Verification of circular RNA (circRNA) data from RNA sequencing. **a** Divergent primers to amplify the circular junctions. Red arrows represent divergent primers. **b** Reverse transcription PCR amplification of circRNA with divergent primers. The PCR products of circRNA2185, circRNA2184, circRNA681, circRNA5146, circRNA597, and circRNA2554 were analyzed using gel electrophoresis. M is the marker and N is the negative control. **c** Head-to-tail splice junctions were confirmed using DNA sequencing

pathway enrichment analyses to analyze enrichment of the 10,598 mRNA transcripts. In the text, only the top 20 GO categories of three differential ontologies (Fig. 5a) and the top 20 enriched pathways from the KEGG enrichment analysis are shown (Fig. 5b). The results showed that the enriched GO terms were mainly associated with metabolic process, organic substance metabolic process, cellular metabolic process, and regulation of response to stimulus ($P < 0.05$, Additional file 5: Table S5). In addition, the KEGG pathways were mainly enriched in metabolic pathways, carbon metabolism, insulin signaling pathway and TNF signaling pathway ($P < 0.05$, Additional file 6: Table S6). Which may also indicate that circRNAs have functions in metabolic process.

CeRNA networks construction and conservation analysis
 Since pig pituitary circRNAs differentially expressed under heat stress, we further focused on the pituitary

functional genes as well as the heat stress regulated genes, screened effective information from the previous circRNA-miRNA-mRNA network (Additional file 4: Table S4) and established 2 networks which had potential functions in regulating pituitary (Fig. 6a and Additional file 7: Table S7-A) and heat stress (Fig. 6b and Additional file 7: Table S7-B). In the networks, one node represented one gene, the edge connected by 2 genes represented a tight regulatory relationship. In Fig. 6, one network showed that 22 circRNAs could sponge 19 miRNAs to regulate 5 pituitary-specific genes including follicle-stimulating beta polypeptide (FSHB), PRL, growth hormone 1 (GH1), growth hormone releasing hormone receptor (GHRHR), and Chromogranin A CGA (Fig. 6a). Another network indicated that 42 circRNAs could sponge 48 miRNAs to regulate several 11 members of the HSP family, including HSF1, HSF4, HSF5, HSPA4, HSPA9, HSPB7, HSPB8, HSP13, HSPA12A, HSP90AB1 and HSPBP1 (Fig. 6b). Taken together, based on the analysis of differentially expressed circRNAs in pig

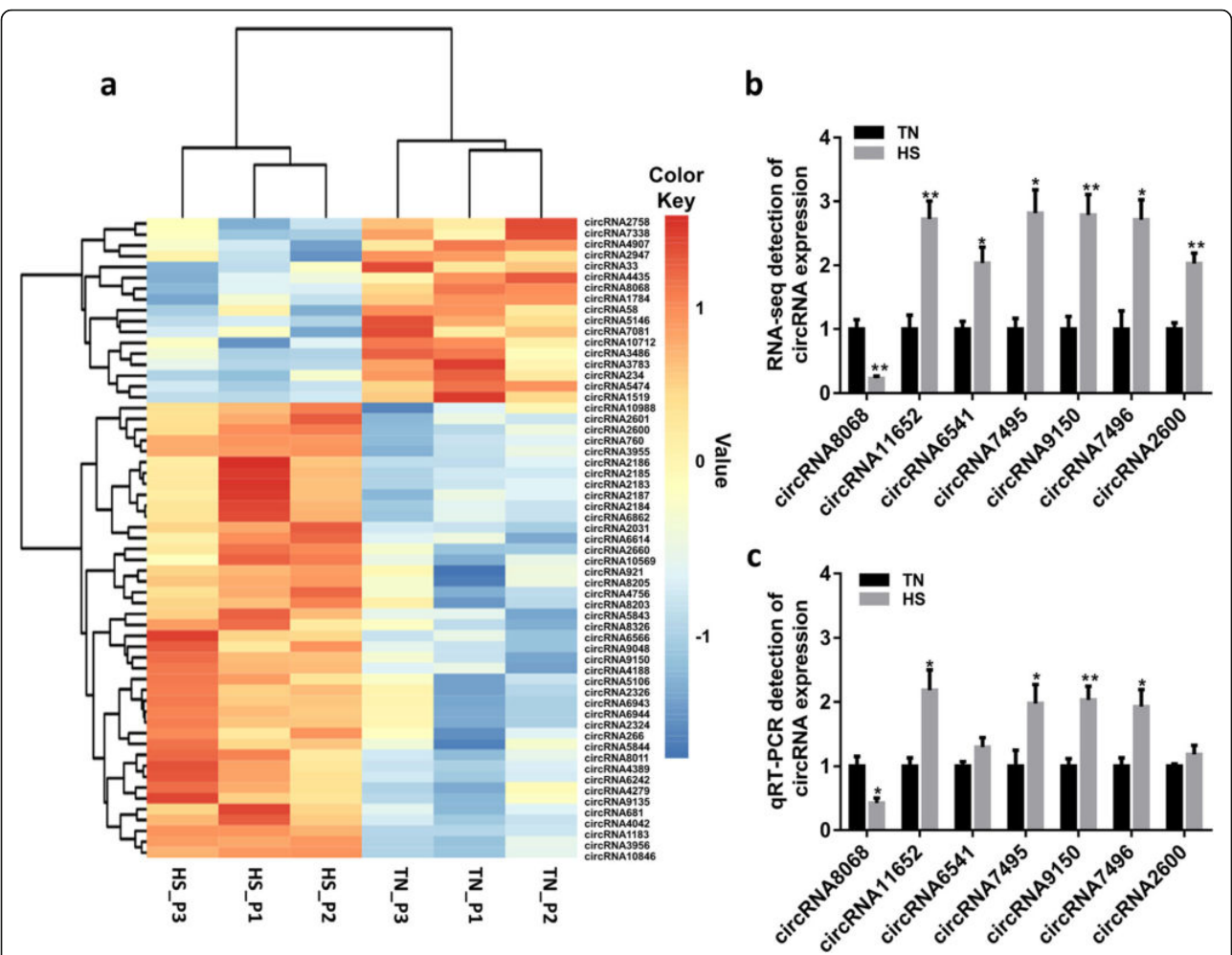


Fig. 4 Analysis and validation of differentially expressed circular RNA (circRNA). **a** The heat map of the circRNA that were differentially expressed between the thermoneutral (TN) group and the heat stress (HS) group. Blue represents low expression, and orange represents high expression ($P < 0.05$). **b** Expression of differentially expressed circRNA was determined with data from RNA sequencing (RNA-seq; 3 samples each group). **c** Expression of differentially expressed circRNA was determined using quantitative real-time PCR (qRT-PCR; 6 samples each group). Values are expressed as means and SEM. * $P < 0.05$; ** $P < 0.01$ (t-test). HS_P1 = heat stress_pituitary 1; HS_P2 = heat stress_pituitary 2; HS_P3 = heat stress_pituitary 3; TN_P1 = thermoneutral _pituitary 1; TN_P2 = thermoneutral _pituitary 2; TN_P3 = thermoneutral _pituitary 3

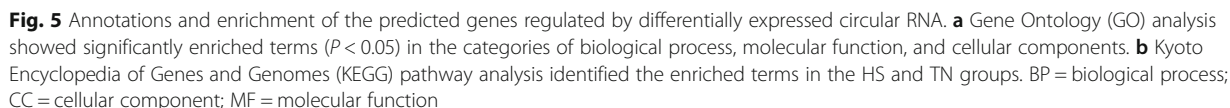
pituitary under heat stress, we found that 42 ceRNA pairs (Additional file 8: Table S8-A) may regulate pituitary-specific genes and 154 ceRNA pairs (Additional file 8: Table S8-B) may be involved in heat stress.

Our study also searched pig orthologous circRNAs from human or mouse. We compared pig circRNAs to human and mouse circRNAs with clear one to one orthologs (<http://asia.ensembl.org/biomart/martview/>) [11]. We found 68.51% of pig pituitary circRNAs have human orthologs, whereas 54.94% of pig pituitary circRNAs have mouse orthologs (Additional file 9: Table S9-A and Table S9-B). Then, we performed sequence blast analysis of the potentially conserved pig pituitary circRNAs with human or mouse circRNAs from the datasets in circbase (<http://www.circbase.org/>). Blast analysis suggested that 4903 (4903/12035 = 40.74%) and

1732 (1732/12035 = 14.39%) pig pituitary circRNAs have orthologs in humans and mice respectively (Additional file 9: Table S9-C and Table S9-D). Finally, we looked for the conserved ceRNA pairs related to pituitary specific genes or heat stress genes by checking for the conservation of miRNA-target interactions (Additional file 10: Table S10-(A-C)) from humans and mice. We identified 10 ceRNA interactions in pig pituitary were conserved with humans (Additional file 10: Table S10-D). Whereas there were no conserved ceRNA interactions related to pituitary specific genes and heat stress among pigs and mice.

Discussion

During the summer, high temperature exceeds the upper limit of the thermoneutral zone will induce heat stress in the sows. For lactating sows, this thermoneutral zone



hormone levels of the sows [46]. The SOD vitality was reduced in the HS group, indicating the sows' impaired antioxidant activity under heat stress. HSP70 is a universal marker of heat stress, and its expression rapidly increased when animals were subjected to heat stress [47, 48]. Similarly, the serum HSP70 level in the HS group also increased significantly relative to TN group in our study (Fig. 1b). In addition, the serum PRL level of the sow was significantly reduced under high temperature

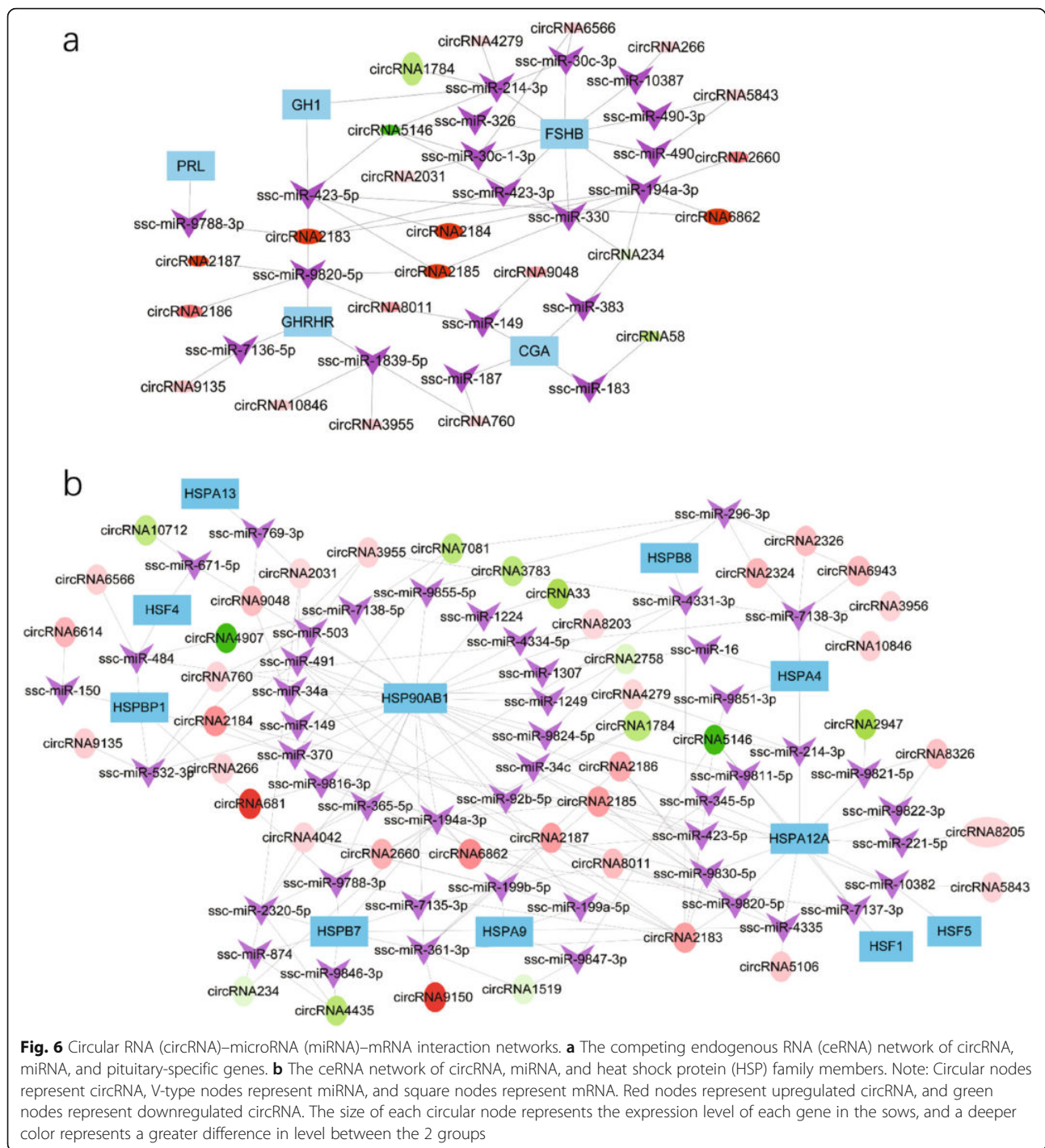


(Fig. 1d), which is accordance with former researches [49]. It is widely believed that the heat or other climatic stress can activate the hypothalamic–pituitary–adrenal axis and accompanying with an increased level of glucocorticoid (mainly cortisol) in the serum [50]. However, there was a decline in the serum cortisol level in our study (Fig. 1c). It has been reported that cortisol levels increased in the early stage of heat stress and then

decreased as the heat stress continued [51]. The different alteration of cortisol concentrations may be depended on whether the heat stress is acute or chronic [52]. In this study, sows were in chronic heat stress during the summer months. As cortisol is the hormone that regulate thermogenesis, the decreased cortisol level in heat stress is benefit for reducing the metabolic heat production [50].

Previous RNA sequencing results indicated that humans [53, 54], mice [55, 56] and rats [57, 58] have abundant circRNAs. Recently, circRNAs have also been identified in several pig tissues [10, 11]. But there is no information about circRNAs in the pig pituitary. So our study was the first to explore the circRNA expression profile of the pig pituitary, and we identified 12,035 circRNAs in the pig pituitary using high-throughput sequencing. Similarly, 10,226 circRNAs were identified in sheep pituitary, and some of these were involved in hormone secretion regulation [16]. Therefore, the abundance of circRNA in pig pituitary may also indicate that circRNAs have crucial functions in the pig pituitary.

High environmental temperature during summer seasons makes sows easily subjected to heat stress, which further induces a decrease in food intake, milk yield, and reproductive efficiency as well as an alteration of endocrine status [17, 59, 60]. Studies have reported that circRNAs have functions during heat stress in plants [24]. While, the role of circRNA in mammalian animals is little known. Therefore, we analyzed the circRNA expression changes in the sow pituitary between normal and heat stress conditions. It has been reported that heat stress alters the circRNA size and the exons numbers in *Arabidopsis* species [24]. In our study, we did not observe these obvious alterations except the different expression level of circRNA, indicating that natural high temperature may not affect circRNA biogenesis in animals. Based on the bioinformatics analysis, we identified 59 circRNAs that were differentially expressed between the 2 groups. Circular RNA can, in theory, regulate cellular stress both positively and negatively [61]. For instance, circFOXO3 promotes cardiac senescence under oxidative stress and serum starvation [62]. CircRasGEF1B regulates the antimicrobial response [63]. So, we speculated that circRNAs may be the new regulators of the heat stress response.

Researches have reported that circRNA can sponge miRNA to further regulate gene expression. For an instance, CDR1as/ciRS-7 and Sry performed the sponge function in human and mouse brain development, respectively [1, 5]. In order to explore the 59 differentially expressed circRNAs' function as ceRNA on gene regulation, we predicted target miRNA of the screened circRNA using miRanda and RNAhybrid, and created a ceRNA network containing differentially expressed circRNAs, previously reported pig miRNAs, and their target mRNAs. From the circRNA-miRNA interaction, we found that various circRNAs interact with different pituitary-related miRNAs (Additional file 4: Table S4), such as miR-128 [64], miR-132 [65], miR-16 [65, 66], miR-361-3p [67], and let-7c [68]. In addition, we also observed that a single circRNA could sponge several different miRNAs with various target sites. For example,

circRNA5146 contained potential binding sites for 17 pig miRNAs (Additional file 4: Table S4), which may indicate its strong role in sponging miRNAs.

The pituitary is an important endocrine organ modulating animal growth, development, metabolism, and sexual function through a variety of pituitary hormones [69]. There were 32 pituitary-specific genes that had been reported in the Tissue Specific Genes Database (TiSGeD) database [70]. In our study, after analyzing all the circRNA-miRNA-gene interactions, we were surprised to discover that several differentially expressed circRNAs could regulate 5 of the pituitary-specific genes through miRNAs (Fig. 6a). The results indicated that these circRNAs may play important roles in secretion of hormones, including FSHB, GH1, and PRL, which could be a possible regulatory mechanism of the endocrine status alteration during heat stress. Also, it is notable that circRNA2183 was predicted to regulate GH1 and PRL through miR-423-5p and miR-9788-3p, respectively, and regulate FSHB through miR-423-3p and miR-194a-3p. CircRNA5146 was predicted to regulate GH1 through miR-423-5p and miR-214-3p, and FSHB through miR-30c-1-3p, miR-30c-3p, miR-326, miR-330 and miR-423-5p. Therefore, circRNA2183 and circRNA5146, as potential ceRNAs, may be central regulators of pituitary gland function. Since many investigations pointed out that the HSP and HSF are the key players in animals' heat stress response [71]. We also found that the circRNAs expressed differentially between the TN and HS group could regulate HSP and HSF by interacting with miRNAs (Fig. 6b). So the circRNA-mediated network may contribute to the response and adaptation to heat stress. Certainly, all the potential interplay among genes, miRNAs, and circRNAs need further experimental analysis.

Studies have reported that some circRNAs are evolutionarily conserved among humans and mice [72, 73]. In our study, we found several pig pituitary circRNAs were also conserved with humans and mice (Additional file 9: Table S9). We identified 68.51% of pig pituitary circRNAs have human orthologs, whereas 54.94% of pig pituitary circRNAs have mouse orthologs with one-to-one orthologs analysis. A previous research has also reported that circRNAs on pig nine organs (not include pituitary) are modestly conserved with humans and mice [11]. However, our circRNAs results of one-to-one orthologs analysis were relatively higher than that of previous report, which may be related to tissue specificity. For the conservation analysis of ceRNA interactions, we identified 10 ceRNA interactions in pig pituitary were conserved with humans (Additional file 10: Table S10-D). Whereas there were no conserved ceRNA interactions related to pituitary specific genes or heat stress among pigs and mice.

To explore the function of differentially expressed circRNAs, the interrelated genes within the circRNA-mediated network (Additional file 4: Table S4) were imported to the GO Consortium and KEGG pathways for annotation analysis. The predicted genes that would be regulated by the differentially expressed circRNAs between the HS group and the TN group were enriched in GO terms associated with the metabolic process, organic substance metabolic process, cellular metabolic process, and regulation of response to stimulus. In addition, the metabolic pathways were enriched in the KEGG pathway analysis. An impact of circRNA on metabolic pathway would be of great interest because high temperature widely affects the metabolism of pigs [74, 75]. In summary, the results of our analysis suggested that the circRNA may participate in the metabolic regulation of pigs under heat stress.

Conclusion

Our study is the first to analyze the circRNA expression profile in sow pituitary and identify the differentially expressed circRNAs in pituitary of sows under heat stress. These results suggested the sow pituitary has abundant circRNAs and the differentially expressed circRNAs may play functions on hormone synthesis and stress response by regulating the specific pituitary genes and heat stress-related genes. Besides, the target genes of the differentially expressed circRNAs were enriched in biological process such as metabolic process and regulation of response to stimulus. Therefore, our study provided a reference for investigating the functions of circRNAs in pituitary regulation and heat stress response.

Supplementary information

Supplementary information accompanies this paper at <https://doi.org/10.1186/s12864-019-6377-7>.

Additional file 1: Table S1. Primer sequence for circRNAs and housekeeping genes.

Additional file 2: Table S2. The information of total detected circRNAs.

Additional file 3: Table S3. The information of differentially expressed circRNAs.

Additional file 4: Table S4. The total interaction relationships among miRNAs, mRNAs and the differentially expressed circRNAs.

Additional file 5: Table S5. GO annotation enrichment analysis.

Additional file 6: Table S6. KEGG pathway enrichment analysis.

Additional file 7: Table S7. A. The interactions among miRNAs, pituitary specific genes and the differentially expressed circRNAs. B. The interactions among miRNAs, heat stress related genes and the differentially expressed circRNAs.

Additional file 8: Table S8. A. The *p*-value of each ceRNA interactions related to pituitary specific genes. B. The *p*-value of each ceRNA interactions related to heat stress genes.

Additional file 9: Table S9. A. Orthologous circRNAs among pigs and humans with one to one orthologs analysis. B. Orthologous circRNAs among pigs and mice with one to one orthologs analysis. C. Orthologous

circRNAs among pigs and humans with blast analysis. D. Orthologous circRNAs among pigs and mice with blast analysis.

Additional file 10: Table S10. A. The interactions of miRNA- pituitary specific genes or heat stress related genes and miRNA-differentially expressed circRNAs in pig pituitary. B. Converged miRNA-gene and miRNA-circRNA interactions in humans. C. Converged miRNA-gene and miRNA-circRNA interactions in mice. D. Converged ceRNA interactions among pigs and humans.

Additional file 11. The sequences of total detected circRNAs.

Abbreviations

ceRNA: Competing endogenous RNA; circRNA: circular RNA; GO: Gene Ontology; HSP70: Heat shock protein 70; KEGG: Kyoto Encyclopedia of Genes and Genomes; miRNA: microRNA; ncRNA: noncoding RNA; PRL: prolactin; qRT-PCR: Quantitative real time PCR; SOD: Superoxide dismutase; THI: Temperature humidity index

Acknowledgements

We would thank LC Sciences (Hangzhou, China) for conducting the whole-genome circRNA sequencing.

Authors' contributions

YZ, JS, and HZ conceived and designed the experiments. HZ and BH performed the experiments and analyzed the data. HZ, JX, TC, QX, JL and QJ contributed reagents, materials, and analysis tools. HZ wrote the paper. YZ, JS, JL and HZ revised the paper. All authors read and approved the final manuscript.

Funding

The research was funded by the Chinese National Key Scientific Project (2016YFD0500503) and the National Natural Science Foundation of China (no. 31472163). The funders were not involved in the study design or collection, analysis, or interpretation of data.

Availability of data and materials

The datasets generated and/or analyzed during the current study are available in the NCBI Sequence Read Archive (SRA) repository with the accessions SRP199497, BioProject accession number PRJNA544777. Additional datasets supporting the conclusions of this article are included within the manuscript and its additional files.

Ethics approval and consent to participate

All animal experimentation complied with the laboratory animal management and welfare regulations approved by Standing Committee of Guangdong People's Congress (Guangzhou), China.

Consent for publication

Not applicable.

Competing interests

The authors declare that they have no competing interests.

Received: 8 April 2019 Accepted: 8 December 2019

Published online: 23 December 2019

References

- Memczak S, Jens M, Elefsinioti A, Torti F, Krueger J, Rybak A, Maier L, Mackowiak SD, Gregersen LH, Munschauer M, et al. Circular RNAs are a large class of animal RNAs with regulatory potency. *Nature*. 2013;495(7441):333–8.
- Hsu MT, Coca-Prados M. Electron microscopic evidence for the circular form of RNA in the cytoplasm of eukaryotic cells. *Nature*. 1979;280(5720):339–40.
- Cocquerelle C, Mascres B, Hetuin D, Bailleul B. Mis-splicing yields circular RNA molecules. *FASEB J*. 1993;7(1):155–60.
- Pamudurti NR, Bartok O, Jens M, Ashwal-Fluss R, Stottmeister C, Ruhe L, Hanan M, Wylter E, Perez-Hernandez D, Ramberger E. Translation of CircRNAs. *Mol Cell*. 2017;66(1):9–21.
- Hansen TB, Jensen TI, Clausen BH, Bramsen JB, Finsen B, Damgaard CK, Kjems J. Natural RNA circles function as efficient microRNA sponges. *Nature*. 2013;495(7441):384–8.

6. Zheng Q, Bao C, Guo W, Li S, Jie C, Bing C, Luo Y, Lyu D, Yan L, Shi G. Circular RNA profiling reveals an abundant circHIPK3 that regulates cell growth by sponging multiple miRNAs. *Nat Commun*. 2016;7:11215.
7. Li Z, Huang C, Bao C, Chen L, Lin M, Wang X, Zhong G, Yu B, Hu W, Dai L. Exon-intron circular RNAs regulate transcription in the nucleus. *Nat Struct Mol Biol*. 2015;22(3):256–64.
8. Quan G, Li J. Circular RNAs: biogenesis, expression and their potential roles in reproduction. *J Ovarian Res*. 2018;11(1):9.
9. Sun J, Xie M, Huang Z, Li H, Chen T, Sun R, Wang J, Xi Q, Wu T, Zhang Y. Integrated analysis of non-coding RNA and mRNA expression profiles of 2 pig breeds differing in muscle traits. *J Anim Sci*. 2017;95(3):1092.
10. Venø MT, Hansen TB, Venø ST, Clausen BH, Grebing M, Finsen B, Holm IE, Kjems J. Spatio-temporal regulation of circular RNA expression during porcine embryonic brain development. *Genome Biol*. 2015;16(1):245.
11. Liang G, Yang Y, Niu G, Tang Z, Li K. Genome-wide profiling of Sus scrofa circular RNAs across nine organs and three developmental stages. *DNA Res*. 2017;24(5):523–35.
12. Zhu X, Gleiberman AS, Rosenfeld MG. Molecular physiology of pituitary development: signaling and transcriptional networks. *Physiol Rev*. 2007;87(3):933.
13. Brinkmeier ML, Davis SW, Carninci P, Macdonald JW, Kawai J, Ghosh D, Hayashizaki Y, Lyons RH, Camper SA. Discovery of transcriptional regulators and signaling pathways in the developing pituitary gland by bioinformatic and genomic approaches. *Genomics*. 2009;93(5):449–60.
14. Ye RS, Li M, Qi QE, Cheng X, Chen T, Li CY, Wang SB, Shu G, Wang LN, Zhu XT, et al. Comparative anterior pituitary miRNA and mRNA expression profiles of Bama minipigs and landrace pigs reveal potential molecular network involved in animal postnatal growth. *PLoS One*. 2015;10(7):e0131987.
15. Han DX, Sun XL, Fu Y, Wang CJ, Liu JB, Jiang H, Gao Y, Chen CZ, Yuan B, Zhang JB. Identification of long non-coding RNAs in the immature and mature rat anterior pituitary. *Sci Rep*. 2017;7(1):17780.
16. Li CY, Li XY, Ma QM, Zhang XY, Cao Y, Yao Y, You S, Wang DW, Quan RZ, Hou XX, et al. Genome-wide analysis of circular RNAs in prenatal and postnatal pituitary glands of sheep. *Sci Rep*. 2017a;7:16143.
17. Williams AM, Safranski TJ, Spiers DE, Eichen PA, Coate EA, Lucy MC. Effects of a controlled heat stress during late gestation, lactation, and after weaning on thermoregulation, metabolism, and reproduction of primiparous sows. *J Anim Sci*. 2013;91(6):2700–14.
18. Place RF, Noonan EJ. Non-coding RNAs turn up the heat: an emerging layer of novel regulators in the mammalian heat shock response. *Cell Stress Chaperones*. 2014;19(2):159–72.
19. Yu J, Liu F, Yin P, Zhu X, Cheng G, Wang N, Lu A, Luan W, Zhang N, Li J. Integrating miRNA and mRNA expression profiles in response to heat stress-induced injury in rat small intestine. *Funct Integr Genomics*. 2011;11(2):203–13.
20. Chang Y, Xiaoyin W, Kukreja RC. Endogenous microRNAs induced by heat-shock reduce myocardial infarction following ischemia-reperfusion in mice. *FEBS Lett*. 2008;582(30):4137–42.
21. Oshlag JZ, Devasthanam AS, Tomasi TB. Mild hyperthermia enhances the expression and induces oscillations in the dicer protein. *Int J Hyperth*. 2013;29(1):51–61.
22. Liu WM, Chu WM, Choudary PV, Schmid CW. Cell stress and translational inhibitors transiently increase the abundance of mammalian SINE transcripts. *Nucleic Acids Res*. 1995;23(10):1758–65.
23. Li TH, Spearow J, Rubin CM, Schmid CW. Physiological stresses increase mouse short interspersed element (SINE) RNA expression in vivo. *Gene*. 1999;239(2):367–72.
24. Pan T, Sun X, Liu Y, Li H, Deng G, Lin H, Wang S. Heat stress alters genome-wide profiles of circular RNAs in Arabidopsis. *Plant Mol Biol*. 2018;96(3):1–1.
25. Zhou R, Yu X, Xu LP, Wang YL, Zhao LP, Zhao TM, Yu WG. Genome-wide identification of circular RNAs in tomato seeds in response to high temperature. *Bio plantarum*. 2018;63:97–103.
26. Jantzen AE, Lane WO, Gage SM, Haseltine JM, Galinat LJ, Jamiolkowski RM, Lin FH, Truskey GA, Achneck HE. Autologous endothelial progenitor cell-seeding technology and biocompatibility testing for cardiovascular devices in large animal model. *J Vis Exp*. 2011;55:e3197.
27. Laber K, Newcomer CE, Decelle T, Everitt JJ, Guillen J, Bronstad A. Recommendations for addressing harm-benefit analysis and implementation in ethical evaluation - report from the AALAS-FELASA working group on harm-benefit analysis - part 2. *Lab Anim-UK*. 2016;50(1 Suppl):21–42.
28. Martin M. Cutadapt removes adapter sequences from high-throughput sequencing reads. *EMBnet J*. 2011;17(1):10–2.
29. Langmead B, Salzberg SL. Fast gapped-read alignment with bowtie 2. *Nat Methods*. 2011;9(4):357–9.
30. Kim D, Pertea G, Trapnell C, Pimentel H, Kelley R, Salzberg SL. TopHat2: accurate alignment of transcriptomes in the presence of insertions, deletions and gene fusions. *Genome Biol*. 2013;14(4):R36.
31. Kim D, Salzberg SL. TopHat-fusion: an algorithm for discovery of novel fusion transcripts. *Genome Biol*. 2011;12(8):R72.
32. Zhang XO, Wang HB, Zhang Y, Lu X, Chen LL, Yang L. Complementary sequence-mediated exon circularization. *Cell*. 2014;159(1):134–47.
33. Zhang XO, Dong R, Zhang Y, Zhang JL, Luo Z, Zhang J, Chen LL, Yang L. Diverse alternative back-splicing and alternative splicing landscape of circular RNAs. *Genome Res*. 2016;26(9):1277–87.
34. Pertea M, Pertea GM, Antonescu CM, Chang TC, Mendell JT, Salzberg SL. StringTie enables improved reconstruction of a transcriptome from RNA-seq reads. *Nat Biotechnol*. 2015;33(3):290–5.
35. Betel D, Koppal A, Agius P, Sander C, Leslie C. Comprehensive modeling of microRNA targets predicts functional non-conserved and non-canonical sites. *Genome Biol*. 2010;11(8):R90.
36. Jan K, Marc R. RNAhybrid: microRNA target prediction easy, fast and flexible. *Nucleic Acids Res*. 2006;34:451–4.
37. Shannon P, Markiel A, Ozier O, Baliga NS, Wang JT, Ramage D, Amin N, Schwikowski B, Ideker T. Cytoscape: a software environment for integrated models of biomolecular interaction networks. *Genome Res*. 2003;13(11):2498–504.
38. Shao Li D, Suman G, Rituparno S, Jayprokas C, Sandro B. InCeDB: Database of human long noncoding RNA acting as competing endogenous RNA. *PLoS One*. 2014;9(6):e98965.
39. Sarver AL, Subramanian S. Competing endogenous RNA database. *Bioinformatics*. 2012;8(15):731–3.
40. Li JH, Liu S, Zhou H, Qu LH, Yang JH. Starbase v2.0: decoding miRNA-ceRNA, miRNA-ncRNA and protein-RNA interaction networks from large-scale clip-seq data. *Nucleic Acids Res*. 2014;42:92–7.
41. Huang DW, Sherman BT, Lempicki RA. Systematic and integrative analysis of large gene lists using DAVID bioinformatics resources. *Nat Protoc*. 2009;4(1):44–57.
42. Wegner K, Lambertz C, Das G, Reiner G, Gauly M. Effects of temperature and temperature-humidity index on the reproductive performance of sows during summer months under a temperate climate. *Anim Sci J*. 2016;87(11):1334–9.
43. Black JL, Mullan BP, Lorsch ML, Giles LR. Lactation in the sow during heat stress. *Livestock Prod Sci*. 1993;35(1–2):153–70.
44. Bahashwan S. Effect of cold and hot seasons on fat, protein and lactose of Dhofari cow's milk. *Net J Agric Sci*. 2014;2(1):47–9.
45. Montilla R, Isabel S. The effects of heat stress in redox balance and inflammatory signaling in porcine skeletal muscle, MS thesis. Ames: Iowa State University; 2013.
46. Farmer C, Knight C, Flint D. Mammary gland involution and endocrine status in sows: effects of weaning age and lactation heat stress. *Can J Anim Sci*. 2007;87(1):35–43.
47. Khazzaka A, Figwer P, Poirel MT, Serran M, Franck M. Hsp70 response in pigs is affected by their halothane genotypes after heat stress. *J Therm Biol*. 2006;31(8):605–10.
48. Yu J, Bao E. Effect of acute heat stress on heat shock protein 70 and its corresponding mRNA expression in the heart, liver, and kidney of broilers. *Asian-Australas J Anim Sci*. 2008;21(8):1116–26.
49. Farmer C, Devillers N, Widowski T, Massé D. Impacts of a modified farrowing pen design on sow and litter performances and air quality during two seasons. *Livest Sci*. 2006;104(3):303–12.
50. Aggarwal A, Upadhyay R. Heat Stress and Hormones. In: Heat stress and animal productivity. New Delhi: Springer; 2013a. p. 27–52.
51. Abilay TA, Mitra R, Johnson HD. Plasma cortisol and total progesterone levels in Holstein steers during acute exposure to high environmental temperature (42°C) conditions. *J Anim Sci*. 1975;41(1):113–7.
52. Christison GI, Johnson HD. Cortisol turnover in heat-stressed cow. *J Anim Sci*. 1972;35(5):1005–10.
53. Guo JU, Agarwal V, Guo H, Bartel DP. Expanded identification and characterization of mammalian circular RNAs. *Genome Biol*. 2014;15(7):409.
54. Xu T, Jing W, Ping H, Zhao Z, Song X. Circular RNA expression profiles and features in human tissues: a study using RNA-seq data. *BMC Genomics*. 2017;18(Suppl 6):680.

55. Gruner H, Cortés-López M, Cooper DA, Bauer M, Miura P. CircRNA accumulation in the aging mouse brain. *Sci Rep*. 2016;6:38907.
56. Jia W, Xu B, Wu J. Circular RNA expression profiles of mouse ovaries during postnatal development and the function of circular RNA epidermal growth factor receptor in granulosa cells. *Metabolism*. 2018;85:192–204.
57. Zhang CL, Wu H, Wang YH, Zhao YL, Fang XT, Chen CF, Chen H. Expression patterns of circular RNAs from primary kinase transcripts in the mammary glands of lactating rats. *J Breast Cancer*. 2015;18(3):235–41.
58. Li L, Guo J, Chen Y, Chang C, Xu C. Comprehensive circRNA expression profile and selection of key circRNAs during priming phase of rat liver regeneration. *BMC Genomics*. 2017;18(1):80.
59. Sevi A, Caroprese M. Impact of heat stress on milk production, immunity and udder health in sheep: a critical review. *Small Ruminant Res*. 2012; 107(1):1–7.
60. Aggarwal A, Upadhyay R. Heat Stress and Milk Production. 2013. In: Heat stress and animal productivity. New Delhi: Springer; 2013b. p. 53–77.
61. Fischer JW, Leung AK. CircRNAs: a regulator of cellular stress. *Circ Rev in Biochem Mol*. 2017;52(2):220–33.
62. Du WW, Yang W, Chen Y, Wu ZK, Foster FS, Yang Z, Li X, Yang BB. Foxo3 circular RNA promotes cardiac senescence by modulating multiple factors associated with stress and senescence responses. *Eur Heart J*. 2016;38(18):1402.
63. Ng WL, Marinov GK, Liao ES, Lam YL, Lim YY, Ea CK. Inducible RasGEF1B circular RNA is a positive regulator of ICAM-1 in the TLR4/LPS pathway. *RNA Biol*. 2016;13(9):861–71.
64. Palumbo T, Faucz FR, Azevedo M, Xekouki P, Iliopoulos D, Stratakis CA. Functional screen analysis reveals miR-26b and miR-128 as central regulators of pituitary somatomammotrophic tumor growth through activation of the PTEN/AKT pathway. *Oncogene*. 2013;32(13):1651–9.
65. Wang R, Liang H. MiR-132, miR-15a and miR-16 synergistically inhibit pituitary tumor cell proliferation, invasion and migration by targeting Sox5. *Cancer Lett*. 2015;356(2):568–78.
66. Wang DW, Wang YQ, Shu HS. MiR-16 inhibits pituitary adenoma cell proliferation via the suppression of ERK/MAPK signal pathway. *Eur Rev Med Pharmacol Sci*. 2018;22(5):1241–8.
67. Ye RS, Li M, Li CY, Qi QE, Chen T, Cheng X, Wang S, Shu G, Wang LN, Zhu XT, et al. MiR-361-3p regulates FSH by targeting FSHB in a porcine anterior pituitary cell model. *Reproduction*. 2016;153(3):341–49.
68. Qi QE, Xi QY, Ye RS, Chen T, Cheng X, Li CY, Zhu XT, Shu G, Wang LN, Jiang QY, et al. Alteration of the miRNA expression profile in male porcine anterior pituitary cells in response to GHRH and CST and analysis of the potential roles for miRNAs in regulating GH. *Growth Hormon IGF Res*. 2015; 25(2):66–74.
69. Ooi GT, Tawadros N, Escalona RM. Pituitary cell lines and their endocrine applications. *Mol Cell Endocrinol*. 2004;228(2):1–21.
70. Xiao SJ, Zhang C, Zou Q, Ji ZL. TiSGeD: a database for tissue-specific genes. *Bioinformatics*. 2010;26(9):1273–5.
71. Dangi SS, Gupta M, Dangi SK, Chouhan VS, Maurya VP, Kumar P, Singh G, Sarkar M. Expression of HSPs: an adaptive mechanism during long-term heat stress in goats (*Capra hircus*). *Int J Biometeorol*. 2015;59(8):1095–106.
72. Rybak-Wolf A, Stottmeister C, Glazar P, Jens M, Pino N, Giusti S, Hanan M, Behm M, Bartok O, Ashwal-Fluss R, et al. Circular RNAs in the mammalian brain are highly abundant, conserved, and dynamically expressed. *Mol Cell*. 2015;58(5):870–85.
73. Jeck WR, Sorrentino JA, Wang K, Slevin MK, Burd CE, Liu JZ, Marzluff WF, Sharpless NE. Circular RNAs are abundant, conserved, and associated with ALU repeats. *RNA*. 2013;19(2):141–57.
74. Pearce SC, Gabler NK, Ross JW, Escobar J, Patience JF, Rhoads RP, Baumgard LH. The effects of heat stress and plane of nutrition on metabolism in growing pigs. *J Anim Sci*. 2013;91(5):2108–18.
75. Fernandez MVS, Johnson JS, Abuajamieh M, Stoakes SK, Seibert JT, Cox L, Kahl S, Elsasser TH, Ross JW, Isom SC. Effects of heat stress on carbohydrate and lipid metabolism in growing pigs. *Physiol Rep*. 2015;3(2):e12315.

Publisher's Note

Springer Nature remains neutral with regard to jurisdictional claims in published maps and institutional affiliations.

Ready to submit your research? Choose BMC and benefit from:

- fast, convenient online submission
- thorough peer review by experienced researchers in your field
- rapid publication on acceptance
- support for research data, including large and complex data types
- gold Open Access which fosters wider collaboration and increased citations
- maximum visibility for your research: over 100M website views per year

At BMC, research is always in progress.

Learn more biomedcentral.com/submissions





Porcine milk exosome miRNAs protect intestinal epithelial cells against deoxynivalenol-induced damage

Mei-Ying Xie^{a,b,c,1}, Ting Chen^{a,c,d,e,1}, Qian-Yun Xi^{a,c,d,e}, Lian-Jie Hou^a, Jun-Yi Luo^{a,c}, Bin Zeng^{a,c}, Meng Li^{a,c}, Jia-Jie Sun^{a,c,d,e,*}, Yong-Liang Zhang^{a,c,d,e,*}

^a College of Animal Science, South China Agricultural University, 483 Wushan Road, Tianhe District, Guangzhou, Guangdong 510642, China

^b Collaborative Innovation Center of Plant Pest Management and Bioenvironmental Health Application Technology, Guangdong Eco-Engineering Polytechnic, 297 Guangshan First Road, Tianhe District, Guangzhou, Guangdong 510520, China

^c Guangdong Province Key Laboratory of Animal Nutritional Regulation, 483 Wushan Road, Tianhe District, Guangzhou, Guangdong 510642, China

^d National Engineering Research Center for Breeding Swine Industry, 483 Wushan Road, Tianhe District, Guangzhou, Guangdong 510642, China

^e Guangdong Engineering & Research Center for Woody Fodder Plants, 483 Wushan Road, Tianhe District, Guangzhou, Guangdong 510642, China

ARTICLE INFO

Keywords:

Porcine milk exosomes
Deoxynivalenol
miRNA
Proliferation and apoptosis
Tight junctions

ABSTRACT

Porcine milk exosomes play an important role in mother-infant communication. Deoxynivalenol (DON) is a toxin which causes serious damage to the animal intestinal mucosa. Our previous study showed porcine milk exosomes facilitate mice intestine development, but the effects of these exosomes to antagonize DON toxicity is unclear. Our *in vivo* results showed that milk exosomes attenuated DON-induced damage on the mouse body weight and intestinal epithelium growth. In addition, these exosomes could reverse DON-induced inhibition on cell proliferation and tight junction proteins (TJs) formation and reduce DON-induced cell apoptosis. *In vitro*, exosomes up-regulated the expression of miR-181a, miR-30c, miR-365-5p and miR-769-3p in IPEC-J2 cells and then down-regulated the expression of their targeting genes in p53 pathway, ultimately attenuating DON-induced damage by promoting cell proliferation and TJs and by inhibiting cell apoptosis. In conclusion, porcine milk exosomes could protect the intestine against DON damage, and these protections may take place through the miRNAs in exosomes. These results indicated that the addition of miRNA-enriched exosomes to feed or food could be used as a novel preventative measure for necrotizing enterocolitis.

1. Introduction

Breast milk nutrition is critical for the stimulation and maintenance of infant gastrointestinal (GI) tract growth [1]. In mammalian nutrition, the GI tract is the first physiological step to bring nutrients to cells and plays a crucial role in the growth and health of infants [2]. Exosomes in general are small (40–100 nm) membrane vesicles found in human and animal milk, blood, urine and amniotic fluid, secreted by donor cells to deliver to recipient cells [3]. Proteins, mRNAs, microRNAs (miRNAs), DNAs and lipids can be encapsulated in exosomes for protection against degradation, so as to be transported to cells to exert specific functions [4]. Milk exosomes contribute to the stimulation of developmental changes, modulations in absorptive epithelium renewal, and gut repair in the neonatal intestine after birth [5,6]. Emerging data showed that milk exosomes could enter human and rat intestinal cells, human endothelial cells and immune cells by endocytosis [7–9], and accumulate

in peripheral tissues [10,11].

MiRNAs are about 22 nucleotides long with complementary sequences in the 3'-untranslated regions (3'UTR) in mRNA [12]. They silence genes by destabilizing mRNA or inhibiting mRNA translation, and have been implicated in numerous physiologic and pathologic conditions including cancer, inflammatory disease and metabolic syndromes [13,14]. Our earlier research showed that several miRNAs in porcine milk exosomes participated in the p53 signaling pathway, which is a central regulator of proliferation and apoptosis [15]. Milk exosome miR-125b has been found to target and inactivate p53 [16], and several miRNAs abundant in milk exosomes, such as miR-30d, miR-25, and miR-504, have been proved to attenuate p53 signaling [17]. Distinct species of miRNAs in bovine milk exosomes also demonstrated unique distribution profiles and are mainly accumulated in the intestinal mucosa, spleen, liver, heart or brain [18]. Moreover, *in vitro* digestion have no pronounced effects on the expression of milk

* Corresponding authors at: College of Animal Science, South China Agricultural University, 483 Wushan Road, Guangzhou 510642, China.

E-mail addresses: jiajiesun@scau.edu.cn (J.-J. Sun), zhangyl@scau.edu.cn (Y.-L. Zhang).

¹ These authors contributed equally to this work.

exosome miRNAs [19]. These data suggested that milk exosome miRNAs may have fundamental effects on infant health and development, and investigations into milk exosomes may be a potential approach to better understand lactation physiology, milk composition, and its new functions.

Studies on mycotoxins increased awareness of the vulnerable structures of the intestine and the impairment of intestinal integrity [20]. The initial interaction of mycotoxins occurs in the intestinal epithelial cells, which are repeatedly exposed to these toxins and become a main area of high mycotoxin concentration [21]. DON is the most prominent example of mycotoxins associated with the impairment of intestinal integrity, which is first recognized for its immune modulatory and pro-inflammatory activities [22]. Its toxicological effects mainly concern the immune system and the GI tract [23]. DON could lead to adverse effects on the transmembrane TJ, such as the expressions of occludin (OCLN), junctional adhesion molecules (JAMs), Claudins (CLDNs), and cytoplasmic scaffolding proteins such as Zonula occludens (ZO) [24]. CLDNs, OCLN, and ZO-1 have been shown to be influenced by DON in porcine intestinal epithelial cells [25,26], and CLDNs are the most susceptible TJ regarding DON exposure in human intestinal epithelial cells [27].

To our knowledge, there is no published reports has been demonstrated the milk exosomes could reverse the toxin-induced damage to GI-tract cells. In this study, we will demonstrated the porcine milk exosomes protection mechanism on DON-induced intestine damage *in vivo* and *in vitro*. This study provided new evidence for protecting the neonatal intestine tract against damages by transporting breast milk exosomes to offspring. Add miRNAs-enriched exosomes to infant formula may be used as a novel preventative measure for intestinal damage.

2. Materials and methods

2.1. Preparation of exosomes

Porcine milk exosomes were separated and identified according to previously described methods [28]. Fresh porcine milk was collected after parturition from healthy lactating Landrace female pigs between 0 and 5 days after breeding in the breeding farm of the Livestock Research Institute (Guangzhou, China). Approximately 50 mL of fresh porcine milk was centrifuged at $2000 \times g$ for 30 min at 4°C to remove mammary gland-derived cells and milk fat globules (MFGs). Defatted samples were then subjected to centrifugation at $12,000 \times g$ for 30 min at 4°C to remove residual MFGs, casein, and other debris. From the supernatant, the membrane fractions were prepared by ultracentrifugation at $110,000 \times g$ for 2 h using an SW41T rotor (Beckman Coulter Instruments, Fullerton, CA) for three times, and the sediment was filtered through a $0.22 \mu\text{m}$ filter to prepare the exosomes solution. The identification of porcine milk exosomes was performed using transmission electron microscopy (TEM). Approximately 4.5 g exosomes containing 200 mg protein could be collected from about 50 mL porcine milk. The exosomes concentration was quantified and described as μg of total protein/mL of Dulbecco's modified Eagle's medium (DMEM/F12) (*in vitro* trial) or saline (*in vivo* trial). For *in vitro* trial, we dissolved the porcine milk exosomes into a solution at a concentration of 0.018 mg protein per microliter and added to the cells at a concentration of 0.562 mg protein per square centimeter. For *in vivo* trial, we dissolved the porcine milk exosomes into a solution at a concentration of 0.074 mg protein per microliter and treated each mouse with 200 μL porcine milk exosomes.

2.2. Animals

Twenty-four 18-day-old specific-pathogen-free (SPF) healthy male Kunming mice were housed under a 12 h light and 12 h dark photocycle (7 am and 7 pm, 25°C and 70–80% humidity) and were purchased from

the Animal Experimental Center of Guangdong Province. These mice were randomly divided into four groups ($n = 8$): the control group (control), the porcine milk exosomes (Exos), the saline + DON group (Saline + DON) and the porcine milk exosomes + DON group (Exos + DON). In the first three weeks of the trial, 200 μL of porcine milk exosomes were administered orally by gavage to the Exos group and Exos + DON group daily, while the control group and Saline + DON group were administered the same volume of saline each day. In the fourth week, we administered only 200 μL of DON (Deoxynivalenol; Sigma Chemical Inc., St. Sigma-D0156-5MG; USA) suspended in saline at a concentration of 2.5 mg/kg body weight to the mice of Saline + DON group and the Exos + DON group orally by gavage daily for 7 days. The control group continued to receive 200 μL of saline and the Exos group 200 μL of porcine milk exosomes. The body weight (BW) and feed intake (FI) of the mice were analyzed every week. Four weeks later, the mice were sacrificed to collect blood samples and intestinal tissues for further examinations. All animals used in this study were approved by the College of Animal Science, South China Agricultural University. All experiments were conducted following 'the instructive notions with respect to caring for laboratory animals' issued by the Ministry of Science and Technology of the People's Republic of China. The dietary components are shown in Table 1.

2.3. Hematoxylin-eosin staining (H&E)

The mice jejunum tissues (3–5 cm) were fixed in 4% formaldehyde at room temperature for 24 h and stained with hematoxylin and eosin according to standard pathological procedures, as previously reported [29]. The villus height and crypt depth of the jejunum were measured under a light microscope (Nikon, Tokyo, Japan) at a magnification of $40 \times$ or $100 \times$. Up to six villi and crypts from the same jejunum section were visualized.

2.4. IPEC-J2 cells culture

IPEC-J2 cells (intestinal porcine enterocytes isolated from the jejunum of a neonatal unsuckled piglet) were a kind gift from Professor Chen Daiwen at Sichuan Agricultural University and cell line passage number is 6. Cells were cultured in DMEM/F-12 (1:1) (Invitrogen, Life Technologies, Carlsbad, CA, USA), supplemented with 10% fetal bovine serum (FBS; GIBCO) and 5 ng/mL EGF (PeproTech, Rocky Hill, NJ, USA), at 37°C in a humidified atmosphere that contained 5% CO_2 . Cells formed a confluent monolayer within 2 days and were then used in experiments.

2.5. Cell viability tested by methylthiazolyldiphenyl-tetrazolium bromide (MTT) assay

IPEC-J2 cells were seeded in 96-well plates at a density of $2.5 \times 10^4/\text{cm}^2$ and assigned to the DMEM group (control), the porcine milk exosomes (Exos), the DON + DMEM group (DON) and the

Table 1
Composition of basal diets (%; as-fed basis).

Material	Ratio (g/kg)	Nutrient	Mass ratio %	Energy ratio %
Casein $\geq 88\%$	200	Protein	26.2	20
L-Cystine	3	Carbohydrate	26.3	20
Maltodextrin	125	Fat	34.9	60
Sucrose	68.8	Total	87.4	100
Cellulose	50			
Soybean oil	25			
Lard	245			
Mineral AIN-93	35			
Vitamin AIN-93	10			
Choline chloride	2.5			

Table 2
Primary antibodies.

Primary antibody	From
rabbit anti- β -actin	AP0060, Bioworld
rabbit anti-Beta catenin	bs-1165R, Bioss antibodies
rabbit anti-AKT	GTx121937, GeneTex
rabbit anti-phospho-AKT	Ser473, GTx128414, GeneTex
rabbit anti-p53	D120082, BBI Life Science antibody
rabbit anti-p21	#2947, Cell Signaling Technology
rabbit anti-CCND1	#2978, Cell Signaling Technology
rabbit anti-ZO-1	GTx108592, GeneTex
rabbit anti-OCN	D121068, BBI Life Science antibody
rabbit anti-CLDN	bs-1428R, Bioss antibodies
rabbit anti-CD95/FAS	bs-6477R, Bioss antibodies
rabbit anti-PAI1/SERPINE1	bs-1704R, Bioss antibodies

DON + porcine milk exosomes group (Exos + DON). After 12 h, 10 μ L of DMEM was added to the control group and DON group. The Exos group and the Exos + DON group were added 10 μ L porcine milk exosomes. After 24 h of incubation, the DON group and Exos + DON group were treated with 1.6, 3.2, 6.4, 12.8 μ g/mL DON for 12 h. The control group continued to incubate for 12 h. After all treatments were completed, 10 μ L of MTT solution (5 mg/mL) was added to each cell culture for cell viability testing. MTT assays were performed according to the manufacturer's protocol (Beyotime Biotechnology, Shanghai, China).

2.6. Cell proliferation tested by Edu assay

IPEC-J2 cells were seeded in 96-well plates at a density of 2.5×10^4 /cm² and the treated method was as same as MTT assays. At the end of the treatment, IPEC-J2 cells used for Edu were labeled by Cell-Light™ Edu Apollo®488 In Vitro Imaging Kit (RiboBio, Guangzhou, China) according to the manufacturer's protocol. Then the Edu positive IPEC-J2 cells were observed using a Nikon TE2000-U inverted microscope (Nikon Instruments, Tokyo, Japan) and counted by Image Pro Plus (Media Cybernetics, Inc., Silver Spring, MD, USA).

2.7. Cell counting

IPEC-J2 cells were seeded in 12-well plates at a density of 2.5×10^4 /cm² and the treated method was as same as MTT assays, but the cells were treated with 300 μ L porcine milk exosomes or PBS per well for 24 h instead of 10 μ L. After 24 h incubation, the PBS + DON group and exosomes + DON group were treated with 1.6 μ g/ml DON for 12 h. The PBS group and PBS + DON group continued to incubate with PBS for 12 h. At the end of the DON treatment, IPEC-J2 cells were digested by trypsin used for cell counting.

Table 3
PCR primer sequences and amplification parameters.

Gene name	Forward primer sequence (5'-3')	Reversed primer sequence (5'-3')
β -catenin	CCAGCACCATGAAGATCAAGAT	ACATCTGCTGGAAGGTGGAC
Akt	AACAAGGTGACGGGAGAAGTG	GGAAGAGGAATGCCAGTGAG
CCND1	CGCCCTCCGTATCTTACT	CGCACTTCTGCTCCTCAC
TP53	TACCACCATCCACTACAACCTCA	CTCCAGGACAGGCACAAA
p21	GAAGAGGGCTACAGGCACCA	CGTTCACAGGCGAAGTCA
Fas	GATTTACCTGTATCGCTGGACC	AGCAGAATGGACCCCTCAGC
SERPINE1	CTACTTCTTCAGGCTGTTCGG	AGGAGTGGTGAGTGCTTTT
ZO-1	CCTCCTGAGTTTGATAGTGGC	TCTCTCGGCAGACCTTGAA
OCN	GCACCCAGCAACGACATA	CACATCACGATAACGAGCATA
CLDN	CGGATGGCTGTCAATTGGG	CACTGGAAGGCGAAGGTTTT
U6	CTCGCTTCGGCAGCACA	AACGCTTCACGAATTTCGCT
miR-181a	AACTCCAGCTGGGAACATTCAACGCTGTGG	TGGTGTCTGGAGTCG
miR-30c	AACTCCAGCTGGGTGTAAACATCCTACACT	TGGTGTCTGGAGTCG
miR-365-5p	AACTCCAGCTGGGGAGGGACTTT CAGGGGC	TGGTGTCTGGAGTCG
miR-769-3p	AACTCCAGCTGGGCTGGGATCTCTG GGGTC	TGGTGTCTGGAGTCG

2.8. Western blot (WB) assay

RIPA lysis buffer was used to extract IPEC-J2 cell proteins according to the assay kit protocol (Biotek, Beijing, China). Briefly, 1 mM PMSF was added to the RIPA lysis buffer, and 200 μ L of this mixture was added to the cells. Then samples were centrifuged at 10,000 \times g for 10 min, and the supernatant was subjected to further analysis. Proteins were stored at -80°C . Protein samples (25 μ g) were measured by the BCA assay [5] according to the manufacturer's protocol, separated using 10–15% SDS-PAGE and then electroblotted to polyvinylidene fluoride, incubated with specific and HRP-conjugated secondary antibodies, and detected with an enhanced chemiluminescence kit (Roche) using FluorChem M (ProteinSimple). Protein concentrations were determined using the Pierce BCA Protein Assay Kit (Thermo Fisher, Waltham, MA, USA) and Image J software was used for gray scan analysis. Antibodies used for WB were shown in Table 2.

2.9. RNA extraction, reverse transcription and quantitative real-time polymerase chain reaction (qRT-PCR)

IPEC-J2 cells were harvested after treatment and then used for the following RNA extraction. Total RNA was first digested with DNase I (Promega, Madison, WI, USA), and 2 μ g of total RNA was reverse transcribed with oligo (dT). The cDNA was diluted 5-fold with ddH₂O, and PCR was performed on a Bio-Rad system (Hercules, CA, USA) in a final 20 μ L reaction containing 2 μ L of PCR cDNA, 10 μ L of 2 \times PCR Mix (Roche, Basel, Switzerland) and 5 mM of each primer. The real-time PCR thermal profile was as follows: 5 min at 95 $^\circ\text{C}$; 40 cycles of 30 s at 94 $^\circ\text{C}$, 30 s at the corresponding annealing temperature (T_m) and 30 s at 72 $^\circ\text{C}$; 10 min at 72 $^\circ\text{C}$. The miRNAs were quantitatively detected according to the protocol of the Mir-X miRNA First Strand Synthesis Kit (Takara Bio Company, Dalian, China). The relative expressions of mRNAs and miRNAs were normalized to β -actin or U6 levels using the $2^{-\Delta\Delta\text{Ct}}$ method [30]. $2^{-\Delta\Delta\text{Ct}}$ is defined as the ratio of the relative mRNA levels of the target gene between the experimental group and the control group. Primers were designed using Primer Premier 5 according to the mouse and pig gene sequences obtained from NCBI. The primers used for PCR are shown in Table 3.

2.10. Immunofluorescence (IF)

IPEC-J2 cells were seeded in 12-well plates at a density of 2.5×10^4 /cm². After treatment as in the cell counting assay, the cells were incubated in freshly prepared 4% paraformaldehyde-neutral PBS at room temperature for 10 min followed by incubation in 0.5% Triton X-100 for 5 min and then 5% normal serum for one hour. Afterwards, the cells were incubated overnight in rabbit anti-Beta catenin (bs-

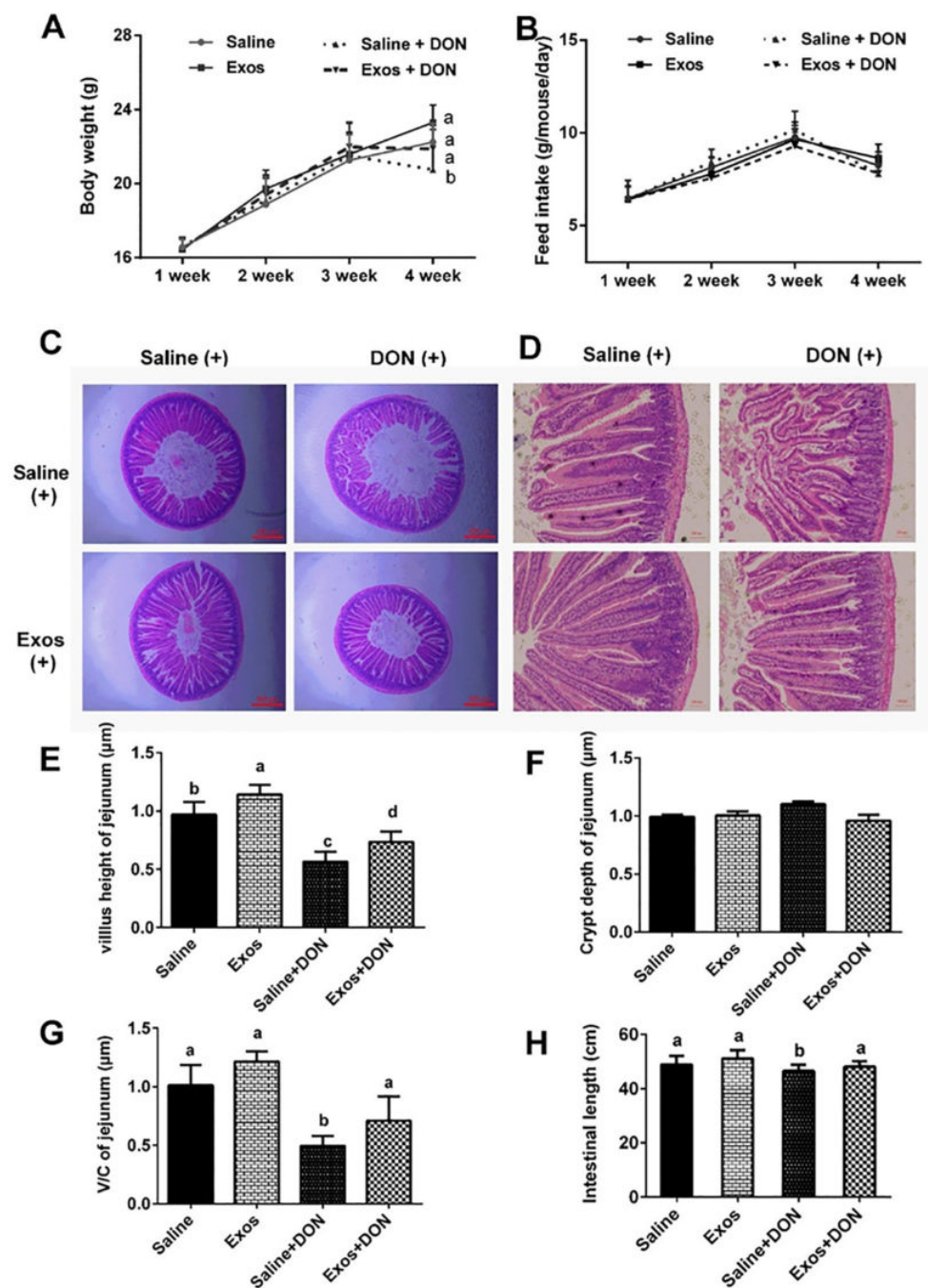


Fig. 1. Effects of porcine milk exosomes on the growth and jejunum development of mice. (A) Body weight of mice with different treatments ($n = 8$). (B). Feed intake of mice with different treatments ($n = 8$). (C). Microscopy observation of the whole jejunum morphology (magnification $40\times$, Scale bar = $500\ \mu\text{m}$) by H&E staining ($n = 8$). (D). Microscopy observation of one part of jejunum morphology (magnification $100\times$, Scale bar = $200\ \mu\text{m}$) by H&E staining ($n = 8$). (E). Statistical analyses of villi heights of jejunum ($n = 8$). (F). Statistical analyses of crypt depths of jejunum ($n = 8$). (G). Statistical analyses of V/C values of the jejunum ($n = 8$). (H). Intestinal length of Kunming mice after different treatments ($n = 8$). The results are presented as the mean \pm S.E.M. Bars with different letter indicate they are statistically significantly different ($p < 0.05$).

1165R, Bioss antibodies) or rabbit anti-CLDN (bs-0790R, Bioss antibodies) at 4°C . Then, the cells were washed with PBS three times and incubated in FITC secondary antibody (1:2000, bs-0295G, Bioss) for 1 h. Fluorescence was observed using a Nikon Eclipse Ti-s microscope with Nis-Elements BR software (Nikon Instruments, Tokyo, Japan). The cell nuclei were stained with DAPI (Beyotime, Jiangsu, China). More than six fields of view from each group were captured.

2.11. Bioinformatics analysis and dual-luciferase reporter assay

The target gene prediction was conducted using the software miRTargets 1.2 in conjunction with the TargetScan, MicroCosm, Pictar and miRDB databases [31]. The 3' UTR sequences of *Fas*, *Tp53* and *SERPINE1* were synthesized and inserted into a pmirGLO vector (Ambion, Carlsbad, CA, USA) to construct the pmirGLO-*Fas*-3'UTR, pmirGLO-*Tp53*-3'UTR and pmirGLO-*SERPINE1*-3'UTR plasmids. For

the dual-luciferase reporter assay, HEK-293T cells (3×10^4 cells per well) were seeded in 48-well culture plates and co-transfected with the 3' UTR dual-luciferase reporter of the target gene (partial 3'UTR containing the indicated miRNA-binding sites, 200 ng) and miRNA mimic or NC duplexes (30 nM) for 48 h using the Lipofectamine 3000 reagent (Invitrogen, Carlsbad, CA, USA). The activities of the firefly and Renilla luciferases were determined using a Dual-Luciferase Reporter Assay System (Promega, Madison, WI, USA), and the activity of firefly luciferase was normalized to that of Renilla luciferase.

2.12. MiRNA transfection

IPEC-J2 cells were seeded in 6-well plates at a density of 2.5×10^4 /cm². Cells were transfected with pCDNA3.1-*Fas* and 30 nM miR-181a mimics or control by Lipofectamine 3000, according to the manufacturer's instructions. Transfection efficiency was tested by quantitative

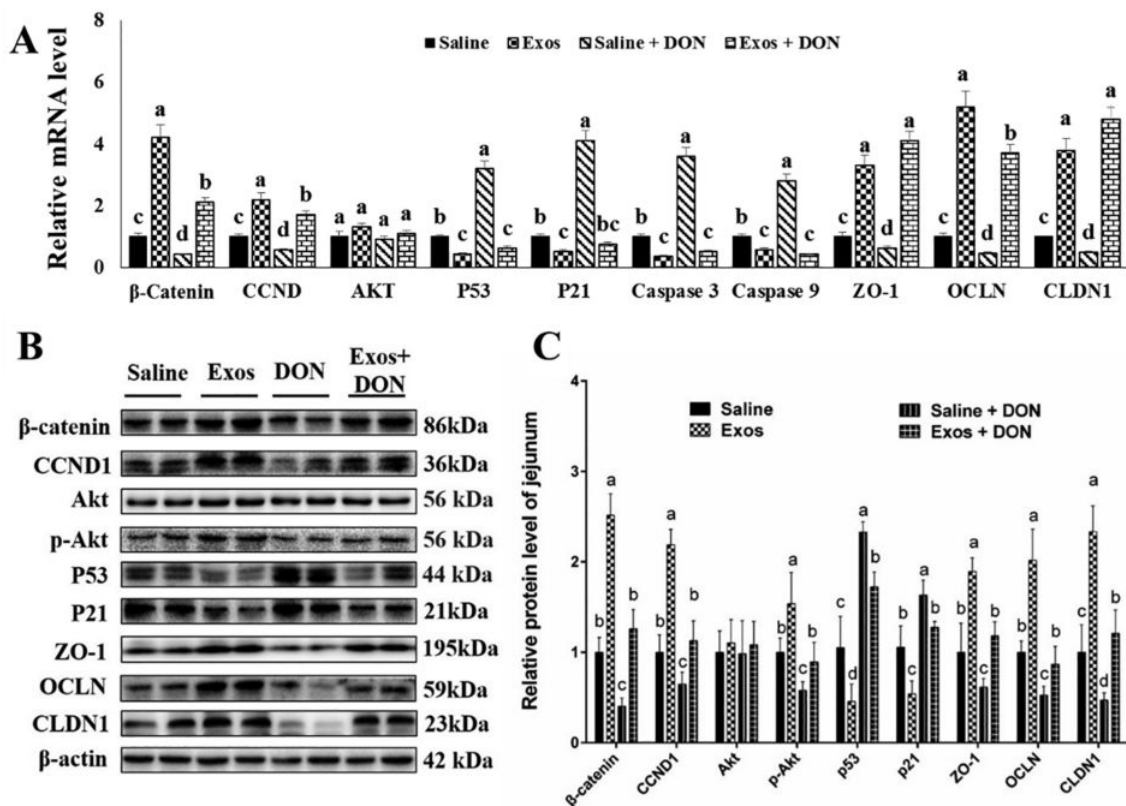


Fig. 2. Effects of porcine milk exosomes on cell proliferation, apoptosis and tight junction-related protein in jejunal mucosa. (A) The detection of cell proliferation, apoptosis and tight junction-related gene mRNA level by qRT-PCR ($n = 6$). (B) The detection of cell proliferation, apoptosis and tight junction-related proteins ($n = 6$). (C) Grayscale scanning statistics of cell proliferation, apoptosis and tight junction-related proteins ($n = 6$). The results are presented as the mean \pm S.E.M. Bars with different letter indicate they are statistically significantly different ($p < 0.05$).

real-time polymerase chain reaction (qRT-PCR) after each transfection. We transfected IPEC-J2 cells with miR-181a mimics when the cells reached approximately 80% confluency. The medium was replaced with new growth medium 6 h later, and the cells were incubated in the growth medium for an additional 24 h before subsequent examinations. The transfection of miR-30c, miR-365-5p, and miR-769-3p were similar, and the transfection of pCDNA3.1-*Tp53* and pCDNA3.1-*SERPINE1* were similar.

2.13. Statistical analysis

All data are expressed as the mean \pm standard error of the mean (S.E.M.) of three independent experiments. Our data is a normal distribution, and the homogeneity of data between each treatment group is equal under the SPSS analysis. In Fig. 6B-6E the unpaired Student's *t*-test was used for *p*-value calculations, where * is $p < 0.05$; and ** is $p < 0.01$. The data of the remaining results are in a normal distribution; and homogeneity of data between each treatment group is equal by SPSS analysis. Significant differences between treatment groups were determined by one-way ANOVA (SPSS v18.0, IBM Knowledge Center, Chicago, IL, USA). Bars with different letter indicate they are statistically significantly different ($P < 0.05$).

3. Results

3.1. Milk exosomes attenuate DON-induced damage to mouse small intestine

To assess the effects of porcine milk exosomes on DON-induced damage to small intestine *in vivo*, we examined the changes of BW, FI, small intestine length and histomorphology of intestinal villi of

Kunming mice. The results showed that the BW loss of Exos + DON group mice was lower ($p < 0.05$) than Saline + DON group mice, and was restored to the normal level, indicating that exosomes relieved the decrease of BW caused by DON (Fig. 1A). The FI of mice in these four groups showed no difference ($p > 0.05$) (Fig. 1B). Interestingly, H&E results showed that the mice administered with porcine milk exosomes promoted the development of jejunum and protected jejunum morphology from DON-induced damage, while the mice administered with saline and DON led to brittle intestinal villi (Fig. 1C and D). Statistical results of villi heights, crypt depth and V/C values (the ratio of villus heights to Crypt depth) of jejunum showed that porcine milk exosomes increased ($p < 0.05$) villi heights and V/C values, and reduced ($p < 0.05$) the DON-induced damage (Fig. 1C-G). Moreover, the average length of the whole intestine in the saline + DON group was shorter ($p < 0.05$) relative to the control, while the mice with addition of milk exosomes neutralized ($p < 0.05$) this adverse effect (Fig. 1H).

3.2. Milk exosomes relieve DON-induced proliferation inhibition, apoptosis and TJ-related proteins in jejunum tissue

Additionally, to further verify how porcine milk exosomes reduce DON-induced damage in intestinal cells, we determined proliferation, apoptosis and TJ-related protein related gene expressions in the jejunum tissue. Western blot and qRT-PCR showed that compared with the control condition, DON treatment decreased ($p < 0.05$) the expression of proliferation-related gene β -catenin and cyclin D1 (CCND1), as well as the phosphorylation level of Akt ($p < 0.05$), while porcine milk exosomes could attenuate ($p < 0.05$) these effects. Moreover, porcine milk exosomes decreased ($p < 0.05$) the apoptosis-related gene p53, p21, Caspase 3 and Caspase 9 expression compared with the Saline + DON group. In addition, DON treatment decreased

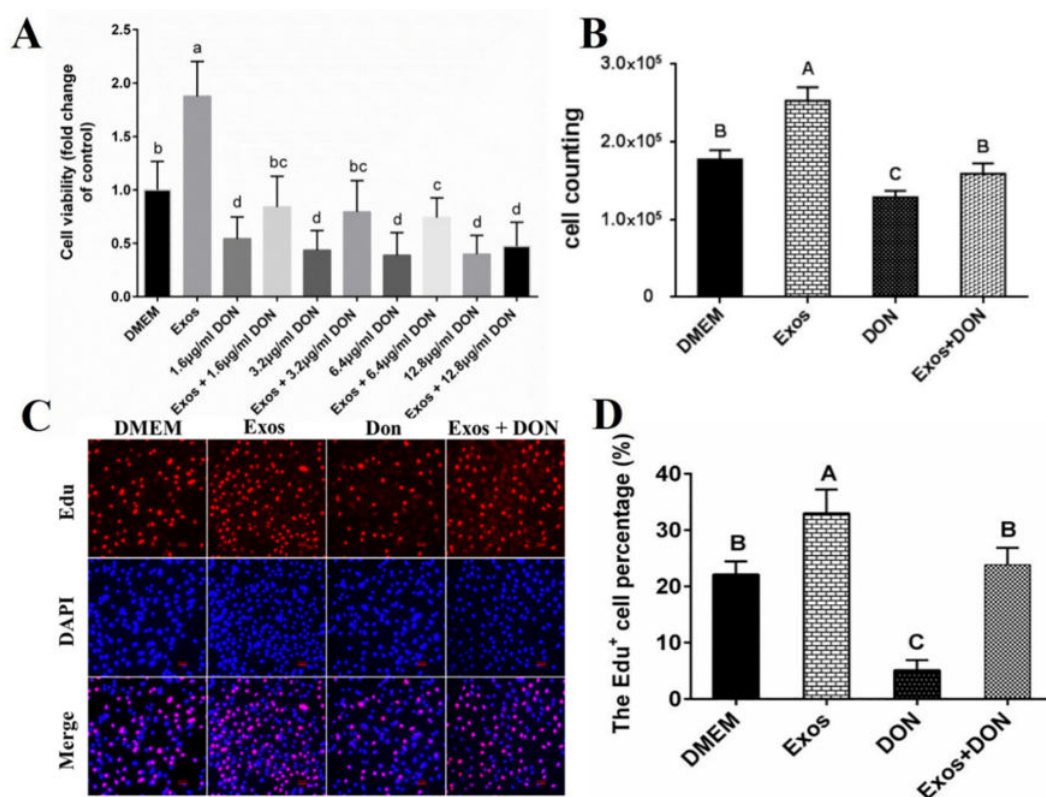


Fig. 3. Effects of porcine milk exosomes on IPEC-J2 cells proliferation. (A) a. Cell viability of IPEC-J2 cells under different treatments ($n = 12$). (B). Cell counting of IPEC-J2 cells ($n = 12$). (C). Edu staining of IPEC-J2 cells (magnification 40 \times , scale bar = 500 μ m) ($n = 6$). (D). Statistical results of Edu staining data ($n = 6$). Results were presented as mean \pm S.E.M. Bars with different lowercase letter indicate they are statistically significantly different ($p < 0.05$). Bars with different uppercase letter indicate they are statistically significantly different ($p < 0.01$).

($p < 0.05$) the levels of TJ-related gene ZO-1, OCLN, and CLDN1 expression, and porcine milk exosomes could attenuate ($p < 0.05$) these effects (Fig. 2 A-C). These results indicated that porcine milk exosomes could relieve DON-induced damage in small intestine by regulating proliferation, apoptosis and TJ-related gene expression.

3.3. Milk exosomes attenuate DON-induced inhibition of proliferation and viability in IPEC-J2 cells

To further demonstrate whether porcine milk exosomes could reduce DON-induced injury in intestinal cells, *in vitro* tests were conducted on IPEC-J2 cells. MTT assays showed that IPEC-J2 cell viability was reduced ($p < 0.05$) in the groups treated with 1.6, 3.2, 6.4 and 12.8 μ g/mL DON compared with the control group, while exosomes increased ($p < 0.05$) cell viability and attenuated ($p < 0.05$) the damage caused by DON when the concentration of DON was lower than 12.8 μ g/mL (Fig. 3A). Then we set the dose of DON used in all subsequent cell test at 1.6 μ g/mL. We counted the total cell numbers after different treatments, and in accordance with the MTT results, compared with the control group, porcine milk exosomes increased ($p < 0.01$) cell number, and DON reduced ($p < 0.01$) IPEC-J2 cell number, while exosomes attenuated ($p < 0.01$) the reduction (Fig. 3B). Furthermore, Edu assays were used to confirm the MTT and cell counting results above by analyzing the percentage of Edu-positive cells. Results showed the percentage of Edu-positive fluorescent cells in DON group was lower ($p < 0.01$) compared with the control group, while exosomes increased ($p < 0.01$) the Edu-positive fluorescent cells and revived ($p < 0.01$) the inhibited effects caused by DON to the normal level. (Fig. 3C and D).

3.4. Milk exosomes relieve DON-induced inhibition of proliferation and apoptosis-related proteins in IPEC-J2 cells

Since Wnt, Akt and p53 pathways are closely related to cell proliferation and apoptosis, we examined the expressions of related genes. Results showed that compared with the control condition, 1.6 μ g/mL DON could decrease ($p < 0.05$) the mRNA levels of β -catenin, CCND1 and Akt, while milk exosomes increased ($p < 0.05$) these mRNA levels and relieved DON-induced inhibition. Moreover, DON increased ($p < 0.05$) the mRNA levels of *Tp53* and its downstream genes *Fas*, *SERPINE1* and *p21*, while exosomes reduced ($p < 0.05$) these mRNA levels and relieved these DON-induced promotion (Fig. 4A). Then, we visualized β -catenin by immunofluorescence, and found that β -catenin fluorescence intensity was increased in the exosome group ($p < 0.05$) and decreased in the DON group ($p < 0.05$) compared with the control condition, while milk exosomes could attenuate ($p < 0.05$) the reduction of fluorescence intensity caused by DON (Fig. 4B and C). Similarly, western blot results confirmed the qRT-PCR results. The results showed that milk exosomes relieved ($p < 0.05$) the inhibition of β -catenin and CCND1 protein levels and the phosphorylation level of Akt caused by DON. Meanwhile, milk exosomes relieved ($p < 0.05$) the promotion of p53 and p21 protein level caused by DON (Fig. 4D and E). These alterations by porcine milk exosomes were fully consistent with the *in vivo* trial. All these results indicated that porcine milk exosomes may protect intestinal cells against DON by regulating the proliferation and apoptosis-related proteins.

3.5. Porcine milk exosomes relieve DON-induced dysregulation of the expression of TJ-related genes in IPEC-J2 cells

Since DON could destroy the intestinal barrier which is essential to

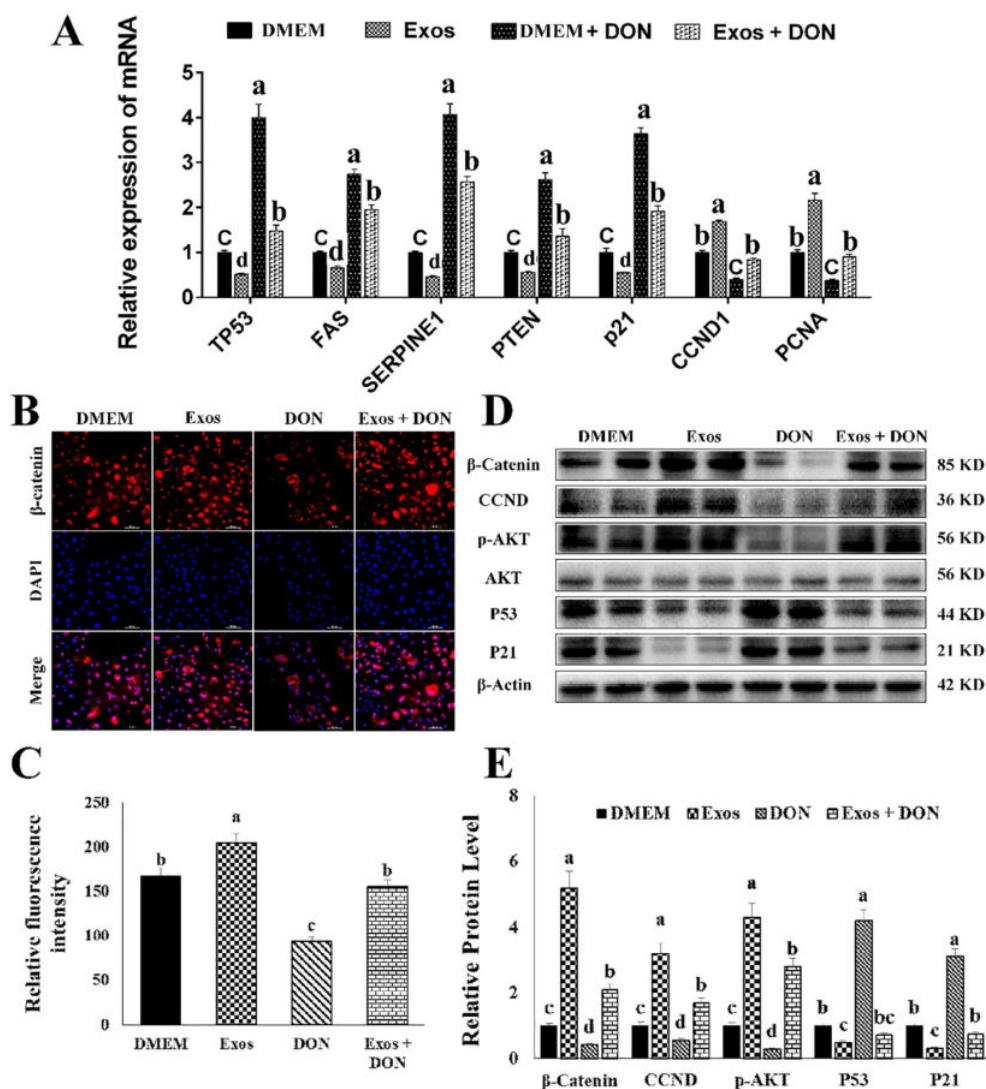


Fig. 4. Effects of porcine milk exosomes on apoptosis and cell proliferation-related genes. (A) Relative mRNA level of apoptosis and proliferation-related genes ($n = 12$). (B). Immunofluorescence assay for β -catenin protein (magnification $200\times$, scale bar = $100\ \mu\text{m}$) ($n = 3$). (C). Statistical results of β -catenin immunofluorescence results ($n = 3$). (D). Western blot of apoptosis and proliferation-related genes ($n = 6$). (E). Grayscale scanning statistics of apoptosis and proliferation-related proteins ($n = 6$). Results were presented as mean \pm S.E.M. Bars with different lowercase letter indicate they are statistically significantly different ($p < 0.05$).

intestine functions, we assayed the expression of TJ-related genes in IPEC-J2 cells. qRT-PCR results showed that compared with the control condition, $1.6\ \mu\text{g/mL}$ DON could decrease ($p < 0.05$) the mRNA levels of *ZO-1*, *OCN* and *CLDN1*, while milk exosomes increased ($p < 0.05$) these mRNA levels and relieved the DON-induced inhibition. (Fig. 5A). Then, we visualized CLDN1 by immunofluorescence, found that CLDN1 fluorescence intensity was increased in the exosomes group ($p < 0.05$) and decreased in the DON group ($p < 0.05$) compared with the control condition, while milk exosomes could attenuate ($p < 0.05$) the reduction of fluorescence intensity caused by DON (Fig. 5B and C). Similarly, western blot results confirmed the qRT-PCR results. The results showed that milk exosomes relieved ($p < 0.05$) the inhibition of *ZO-1*, *OCN* and *CLDN1* caused by DON (Fig. 5D and E). These alterations by porcine milk exosomes are fully consistent with the *in vivo* trial. All these results indicated that porcine milk exosomes may protect intestinal cells against DON partly by strengthening the intestinal barrier.

3.6. Validation of the targets of exosome miRNAs related to the p53 pathway by dual luciferase assay

To explore the function of miRNAs in porcine milk exosomes, bioinformatics analyses was used. Results indicated that some miRNAs (such as miR-181a, miR-30c, miR-365-5p and miR-769-5p) were highly expressed in exosomes which may target mRNAs in p53 pathway. Then we detected these miRNAs level in the porcine milk exosomes treated IPEC-J2 cells by qRT-PCR. Regardless of the presence or absence of DON (12 h), the levels of miR-181a, miR-30c, miR-365-5p and miR-769-5p were all up-regulated ($p < 0.05$) after 24 h of exosomal treatment (Fig. 6A). We used a dual-luciferase reporter system to verify the predicted interactions between miR-181a and *Fas*, miR-30c and *SERPINE1*, miR-365-5p and *Tp53*, and miR-769-3p and *SERPINE1*. The relative luciferase activity was decreased ($p < 0.01$) in HEK-293T cells co-transfected with miR-181a mimics and wild-type pmirGLO-*Fas*-3'UTR, miR-30c mimics and wild-type pmirGLO-*SERPINE1*-3'UTR, miR-365-5p mimics and wild-type pmirGLO-*Tp53*-3'UTR, or miR-769-3p mimics and wild-type pmirGLO-*SERPINE1*-3'UTR, compared with control HEK-293 T cells. However, luciferase activity remained

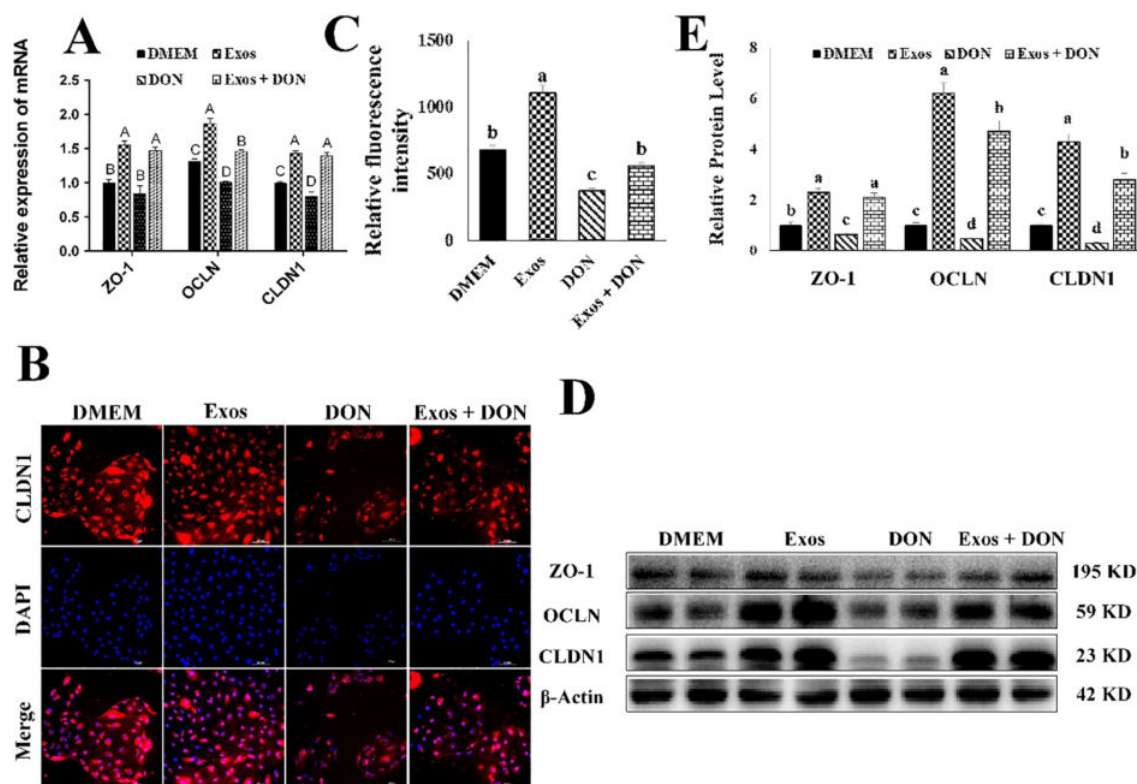


Fig. 5. Effects of porcine milk exosomes on tight junction-associated protein in IPEC-J2 cells. (A) Relative mRNA levels of tight junction-associated genes ($n = 6$). (B) Immunofluorescence assay for CLDN1 protein (magnification $200\times$, scale bar = $100\text{ }\mu\text{m}$) ($n = 3$). (C) Statistical results of CLDN1 immunofluorescence results ($n = 3$). (D) Western blot of tight junction-associated protein ($n = 6$). (E) Grayscale scanning statistics of tight junction-associated proteins ($n = 6$). Results were presented as mean \pm S.E.M. Bars with different lowercase letter indicate they are statistically significantly different ($p < 0.05$).

unchanged ($p > 0.05$) in when cells were transfected with mutated pmirGLO-*Fas*-3'UTR, pmirGLO- *SERPINE1*-3'UTR, pmirGLO- *Tp53*-3'UTR, pmirGLO- *SERPINE1*-3'UTR or pmirGLO (Fig. 6B-E). These results provided direct evidence for the targets of the miRNAs. Furthermore, compared with the control condition, the overexpression of miR-181a, miR-30c, miR-365-5p, and miR-769-3p by mimic transfection decreased ($p < 0.05$) the expression of the corresponding targets with or without DON treatment, as evidenced by both qRT-PCR (Fig. 6F-I) and Western blot analysis (Fig. 6J). Moreover, DON increased ($p < 0.05$) p21 protein level compared with the control, and miRNAs decreased ($p < 0.05$) p21 protein level when overexpressing of miR-181a, miR-30c, and miR-365-5p respectively, with or without DON treatment. However, miR-769-3p could not decrease ($p < 0.05$) p21 protein level with or without DON treatment (Fig. 6J). These results provided preliminary evidence that porcine milk exosomes may exert their regulations in IPEC-J2 cells proliferation and apoptosis by miRNAs inhibiting the p53 pathway.

4. Discussion

Chronic dietary exposure to DON causes adverse effects in human and livestock, including impaired body weight gain, damaged intestine, suppressed immunoreaction and even overt disease and death [32]. Small changes in the barrier function can lead to exposures to luminal antigens in an early phase of life and may induce disordered immunological responses and clinical diseases such as allergies [33]. Previous study showed that feed containing 2.0 mg/kg or more DON significantly reduced the body weight gain of mice, and the feed consumption significantly decreased when the mice ingested a diet containing 25 mg/kg DON [34]. Our previous data showed that there is no DON existence in porcine milk exosomes. In our study, we assessed the effect of an oral exposure of DON at a dosage of 2.5 mg/kg , and the

body weight of mice was significantly reduced.

Many studies indicated that milk exosomes facilitate the maturational effects of various biological systems in infants and even regulate endogenous genes expression in animals [35]. Our previous study provided strong evidence that porcine milk exosomes containing 0.125 , 0.25 , 0.5 or $1.0\text{ }\mu\text{g}$ total RNA facilitated both intestinal cell proliferation and intestinal tract development [5]. In this study, we added porcine milk exosomes with a concentration of $0.018\text{ mg}/\mu\text{L}$ protein to IPEC-J2 cell and fed milk exosomes with 14.8 mg protein to mice. Corresponding to our hypothesis, gavage milk exosomes attenuated the toxicity induced by DON in infant mice and IPEC-J2 cells, including weight loss and cell viability reduction caused by DON.

Human and rat mucosal cells have the ability to absorb bovine milk exosomes, and the intestinal transport of bovine milk exosomes is mediated by endocytosis [7]. MiRNAs encapsulated in milk exosomes could survive *in vitro* digestion and are taken up by human intestinal cells [36] and the endogenous synthesis of miRNAs does not compensate for dietary microRNA deficiency [37]. Furthermore, exogenous miRNAs can pass through the gastrointestinal tract, enter the peripheral bloodstream and accumulate in tissues, exerting gene regulations in mammals [38,39]. Similarly, our results showed that porcine milk exosomes increased the levels of their encapsulated miRNAs in IPEC-J2 cells, meanwhile decreasing the target gene expression of these miRNAs. The regulatory mechanisms of exosome proteins and mRNAs need further study, even though exosome miRNAs are believed to be the most significant molecules and are widely studied in the field of exosome-induced signal transmissions [9,40].

DON is known to interfere with the expression of tight junction proteins in porcine intestinal cells [41], and impair the intestinal tight junction network causing an inflammatory response [42]. This decrease in intestinal epithelial barrier leads to a variety of diseases [43]. Evidence in different human cells as well as IPEC-J2 cells has shown that

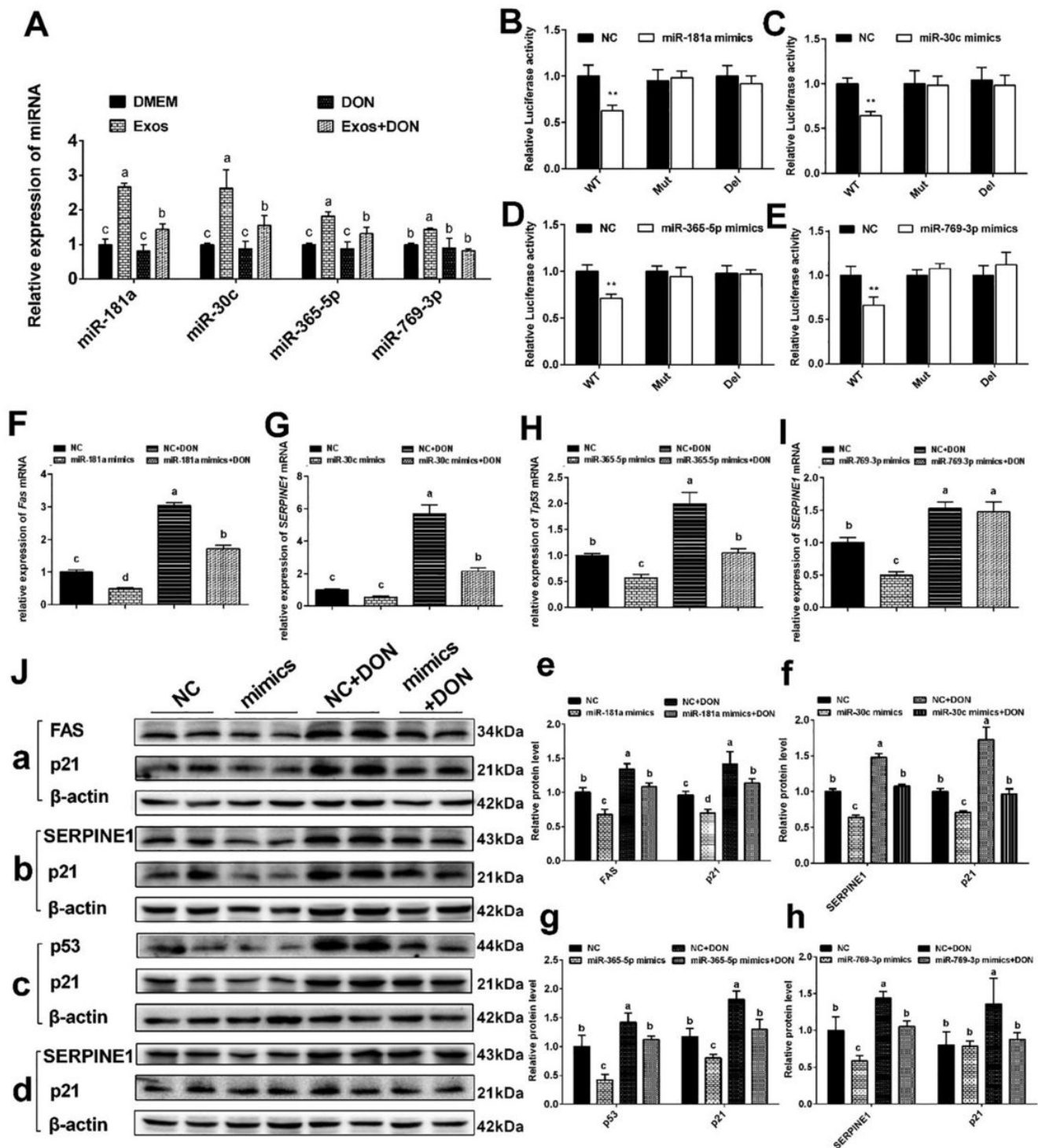


Fig. 6. Effect of porcine milk exosomes on miRNAs and genes in cells and dual luciferase assay. (A) miR-181a, miR-30c, miR-365-5p and miR-769-3p levels in IPEC-J2 cells (n = 6). (B). Targeting relationship between miR-181a and *Fas* gene detected by dual luciferase reporter system (n = 8). (C). Targeting relationship between miR-30c and *SERPINE1* gene detected by dual luciferase reporter system (n = 8). (D) Targeting relationship between miR-365-5p and *TP53* gene detected by dual luciferase reporter system (n = 8). (E) Targeting relationship between miR-769-3p and *SERPINE1* gene detected by dual luciferase reporter system (n = 8). (F) The change of *Fas* mRNA level with miR-181a or NC treatments (n = 6). (G) The change of *SERPINE1* mRNA level with miR-30c or NC treatments (n = 6). (H) The change of *TP53* mRNA level with miR-365-5p or NC treatments (n = 6). (I) The change of *SERPINE1* mRNA level with miR-769-3p or NC treatments (n = 6). (J). a. The detection of FAS and p21 proteins when transfected miR-181a in IPEC-J2 cells (n = 6). b. The detection of SERPINE1 and p21 proteins when transfected miR-30c in IPEC-J2 cells (n = 6). c. The detection of p53 and p21 proteins when transfected miR-365-5p in IPEC-J2 cells (n = 6). d. The detection of SERPINE1 and p21 proteins when transfected miR-769-3p in IPEC-J2 cells (n = 6). e. Grayscale scanning statistics of FAS and p21 proteins of fig. J-a (n = 6). f. Grayscale scanning statistics of SERPINE1 and p21 proteins of fig. J-b (n = 6). g. Grayscale scanning statistics of p53 and p21 proteins of fig. J-c (n = 6). h. Grayscale scanning statistics of SERPINE1 and p21 proteins of fig. J-d (n = 6). Results were presented as mean \pm S.E.M. ** $p < 0.01$. Bars with different lowercase letter indicate they are statistically significantly different ($p < 0.05$).

DON induces a concentration- and time-dependent drop in transepithelial electrical resistance values [44]. Research has shown that different TJs are up-regulated in the intestine, whereas in the jejunum, the mRNA expression of certain TJs (CLDN4, OCLN, ZO-1 and ZO-2) are down-regulated [45]. Consistent with this research, *ZO-1*, *CLDN1* and *OCLN* mRNA and protein levels in IPEC-J2 cells and the small intestines tissue were significantly decreased during continuous DON exposures in our study, but could be significantly rescued by porcine milk exosomes. To avoid the exosomes specific effect to IPEC-J2 cell, IEC-6 cell line was also used in our study. We have obtained similar results in these two cell lines. In order to illustrate the results more clearly, we only show the IPEC-J2 related results in this manuscript. Both *in vitro* and *in vivo* experiments strongly indicated that milk exosomes were able to effectively prevent the destruction of TJs and the damage to intestinal epithelial cells induced by DON.

In addition to the intestinal barrier, intestinal cell proliferation and apoptosis are the basis of intestinal growth and development [46]. P53 is a tumor suppressor protein and a transcription factor which can be activated by many forms of cellular stress, such as DNA damage [47,48]. The p53 protein is the main negative regulator of the cell cycle by regulating the expression of p21, which participates in the cell cycle by controlling cyclin-dependent protein kinase activity [49]. Our results indicated porcine milk exosomes relieved DON-induced damage by down-regulating p53 and p21 and up-regulating p-AKT and β -catenin protein levels, while DON inhibited these protein expressions. MiR-181a, miR-30c, miR-365-5p and miR-769-3p highly expressed in porcine milk exosomes under the existence of DON significantly decreased the protein levels of their target genes which were involved in the p53 pathway. These results suggested that milk exosome miRNAs may functionally interact with p53 pathway to attenuate DON-induced damage.

To the best of our knowledge, this is the first report to verify that porcine milk exosomes protect intestinal epithelial cells against DON-induced damage by regulating cell proliferation and TJs. Milk exosome miRNAs may contribute to this regulation. Since food and feed contamination with DON is a common event, our findings provide a new understanding to attenuate the DON contamination and are meaningful to the digestive tract and the health of newborns.

Declaration of Competing Interest

The authors declare that they have no known competing financial interests or personal relationships that could have appeared to influence the work reported in this paper.

Acknowledgements

This study was supported by grants from the National Natural Science Foundation of China (No. 31802156, 31872435, 31802037); National Key Research and Development Program of China (2016YFD0500503) and Natural Science Foundation of Guangdong provincial key Program (2018B030311015).

Author contributions

M. Xie and T. Chen are the main contributors of the study. M. Xie completed the *in vitro* and *in vivo* experiments, data collection and analysis, and manuscript writing. T. Chen contributed to the study design and data interpretation. Q. Xi, L. Hou and J. Luo contributed to the manuscript writing and contributed to the conduct of the study. B. Zeng and M. Li participated in the sample collections, and helped to facilitate the process of experiment. Y. Zhang had primary responsibility for the final content of the study, contributed to the experimental design, data interpretation and manuscript writing. J. Sun helped Y. Zhang in finishing the work. All authors read and approved the final manuscript.

References

- [1] F. Savino, S. Benetti, S.A. Liguori, M. Sorrenti, L. Cordero, Di Montezemolo, Advances on human milk hormones and protection against obesity, *Cell. Mol. Biol. (Noisy-le-grand)* 59 (1) (2013) 89–98.
- [2] P. Guilloteau, R. Zabielski, H.M. Hammon, C.C. Metges, Nutritional programming of gastrointestinal tract development. Is the pig a good model for man? *Nutr. Res. Rev.* 23 (1) (2010) 4–22.
- [3] S. Mathivanan, H. Ji, R.J. Simpson, Exosomes: extracellular organelles important in intercellular communication, *J. Proteomics* 73 (10) (2010) 1907–1920.
- [4] C. Lasser, V.S. Alikhani, K. Ekstrom, M. Eldh, P.T. Paredes, A. Bossios, et al., Human saliva, plasma and breast milk exosomes contain RNA: uptake by macrophages, *J. Transl. Med.* 9 (2011) 9.
- [5] T. Chen, M.Y. Xie, J.J. Sun, R.S. Ye, X. Cheng, R.P. Sun, et al., Porcine milk-derived exosomes promote proliferation of intestinal epithelial cells, *Sci. Rep.* 6 (2016) 33862.
- [6] N.F. Sheard, W.A. Walker, The role of breast milk in the development of the gastrointestinal tract, *Nutr. Rev.* 46 (1) (1988) 1–8.
- [7] T. Wolf, S.R. Baier, J. Zemleni, The intestinal transport of bovine milk exosomes is mediated by endocytosis in human colon carcinoma caco-2 cells and rat small intestinal IEC-6 cells, *J. Nutr.* 145 (10) (2015) 2201–2206.
- [8] R.J. Kusuma, S. Manca, T. Friemel, S. Sukreet, C. Nguyen, J. Zemleni, Human vascular endothelial cells transport foreign exosomes from cow's milk by endocytosis, *Am. J. Physiol.-Cell Phys.* 310 (10) (2016) C800–C807.
- [9] H. Izumi, M. Tsuda, Y. Sato, N. Kosaka, T. Ochiya, H. Iwamoto, et al., Bovine milk exosomes contain microRNA and mRNA and are taken up by human macrophages, *J. Dairy Sci.* 98 (5) (2015) 2920–2933.
- [10] R. Munagala, F. Aqil, J. Jeyabalan, R.C. Gupta, Bovine milk-derived exosomes for drug delivery, *Cancer Lett.* 371 (1) (2016) 48–61.
- [11] S. Manca, D. Giraud, J. Zemleni, Bioavailability and Biodistribution of Fluorophore-labeled exosomes from cow's milk after intravenous and oral administration in C57Bl/6J mice, *FASEB J.* 30 (2016).
- [12] K. Chen, N. Rajewsky, The evolution of gene regulation by transcription factors and microRNAs, *Nat. Rev. Genet.* 8 (2) (2007) 93–103.
- [13] L. Vojtech, S. Woo, S. Hughes, C. Levy, L. Ballweber, R.P. Sauteraud, et al., Exosomes in human semen carry a distinctive repertoire of small non-coding RNAs with potential regulatory functions, *Nucleic Acids Res.* 42 (11) (2014) 7290–7304.
- [14] K.M. Danielson, S. Das, Extracellular vesicles in heart disease: excitement for the future? *Exosomes Microvesicles* 2 (1) (2014).
- [15] T. Chen, Q.Y. Xi, R.S. Ye, X. Cheng, Q.E. Qi, S.B. Wang, et al., Exploration of microRNAs in porcine milk exosomes, *BMC Genom.* 15 (2014) 100.
- [16] M.T.N. Le, N. Shyh-Chang, S.L. Khaw, L.Z. Chin, C. Teh, J. Tay, E. O'Day, et al., Conserved regulation of p53 network dosage by microRNA-125b occurs through evolving miRNA-target gene pairs, *PLoS Genet.* 7 (9) (2011).
- [17] B.C. Melnik, Milk disrupts p53 and DNMT1, the guardians of the genome: implications for acne vulgaris and prostate cancer, *Nutr. Metab. (Lond.)* 14 (2017) 55.
- [18] S. Manca, B. Upadhyaya, E. Mutai, A.T. Desaulniers, R.A. Cederberg, B.R. White, et al., Milk exosomes are bioavailable and distinct microRNA cargos have unique tissue distribution patterns, *Sci. Rep.-UK* 8 (2018).
- [19] S. Kahn, Y. Liao, X. Du, W. Xu, J. Li, B. Lonnerdal, Exosomal MicroRNAs in milk from mothers delivering preterm infants survive *in vitro* digestion and are taken up by human intestinal cells, *Mol. Nutr. Food Res.* 62 (11) (2018) e1701050.
- [20] P. Pinton, I.P. Oswald, Effect of deoxynivalenol and other type B trichothecenes on the intestine: a review, *Toxins* 6 (5) (2014) 1615–1643.
- [21] B. Grenier, T.J. Applegate, Modulation of intestinal functions following mycotoxin ingestion: meta-analysis of published experiments in animals, *Toxins (Basel)* 5 (2) (2013) 396–430.
- [22] J.J. Pestka, Deoxynivalenol: mechanisms of action, human exposure, and toxicological relevance, *Arch. Toxicol.* 84 (9) (2010) 663–679.
- [23] J.J. Pestka, A.T. Smolinski, Deoxynivalenol: toxicology and potential effects on humans, *J. Toxicol. Environ. Health B Crit. Rev.* 8 (1) (2005) 39–69.
- [24] H. Chiba, M. Osanai, M. Murata, T. Kojima, N. Sawada, Transmembrane proteins of tight junctions, *Bba-Biomembranes* 1778 (3) (2008) 588–600.
- [25] M.J. Gu, S.K. Song, S.M. Park, I.K. Lee, C.H. Yun, *Bacillus subtilis* protects porcine intestinal barrier from deoxynivalenol via improved zonula occludens-1 expression, *Asian Aust. J. Anim.* 27 (4) (2014) 580–586.
- [26] K.H. Ling, M.L.Y. Wan, H. El-Nezami, M. Wang, Protective capacity of resveratrol, a natural polyphenolic compound, against deoxynivalenol-induced intestinal barrier dysfunction and bacterial translocation, *Chem. Res. Toxicol.* 29 (5) (2016) 823–833.
- [27] P. Pinton, C. Braicu, J.P. Nougayrede, J. Laffitte, I. Taranu, I.P. Oswald, Deoxynivalenol impairs porcine intestinal barrier function and decreases the protein expression of claudin-4 through a mitogen-activated protein kinase-dependent mechanism, *J. Nutr.* 140 (11) (2010) 1956–1962.
- [28] T. Chen, Q.Y. Xi, R.S. Ye, X. Cheng, Q. Qi, S.B. Wang, et al., Exploration of microRNAs in porcine milk exosomes, *BMC Genom.* 15 (1) (2014) 100.
- [29] C.J. Hochstim, J.Y. Choi, D. Lowe, R. Masood, D.H. Rice, Biofilm detection with hematoxylin-eosin staining, *Arch. Otolaryngol. Head Neck Surg.* 136 (5) (2010) 453–456.
- [30] L. Hou, J. Shi, L. Cao, G. Xu, C. Hu, C. Wang, Pig has no uncoupling protein 1, *Biochem. Biophys. Res. Commun.* 487 (4) (2017) 795–800.
- [31] A. Krek, D. Grun, M.N. Poy, R. Wolf, L. Rosenber, E.J. Epstein, et al., Combinatorial microRNA target predictions, *Nat. Genet.* 37 (5) (2005) 495–500.
- [32] W.L. Bryden, Mycotoxin contamination of the feed supply chain: implications for animal productivity and feed security, *Anim Feed Sci Tech* 173 (1–2) (2012)

- 134–158.
- [33] P. Akbari, S. Braber, S. Varasteh, A. Alizadeh, J. Garssen, J. Fink-Gremmels, The intestinal barrier as an emerging target in the toxicological assessment of mycotoxins, *Arch. Toxicol.* 91 (3) (2017) 1007–1029.
 - [34] J.H. Forsell, M.F. Witt, J.H. Tai, R. Jensen, J.J. Pestka, Effects of 8-week exposure of the B6C3F1 mouse to dietary deoxynivalenol (vomitoxin) and zearalenone, *Food Chem. Toxicol.* 24 (3) (1986) 213–219.
 - [35] J.Y. Mu, X.Y. Zhuang, Q.L. Wang, H. Jiang, Z.B. Deng, B.M. Wang, et al., Interspecies communication between plant and mouse gut host cells through edible plant derived exosome-like nanoparticles, *Mol. Nutr. Food Res.* 58 (7) (2014) 1561–1573.
 - [36] Y.L. Liao, X.G. Du, J. Li, B. Lonnerdal, Human milk exosomes and their microRNAs survive digestion in vitro and are taken up by human intestinal cells, *Mol. Nutr. Food Res.* 61 (11) (2017).
 - [37] S.R. Baier, C. Nguyen, F. Xie, J.R. Wood, J. Zemleni, MicroRNAs are absorbed in biologically meaningful amounts from nutritionally relevant doses of cow milk and affect gene expression in peripheral blood mononuclear cells, HEK-293 kidney cell cultures, and mouse livers, *J. Nutr.* 144 (10) (2014) 1495–1500.
 - [38] L. Zhang, D. Hou, X. Chen, D. Li, L. Zhu, Y. Zhang, et al., Exogenous plant MIR168a specifically targets mammalian LDLRAP1: evidence of cross-kingdom regulation by microRNA, *Cell Res.* 22 (1) (2012) 107–126.
 - [39] Y. Zhang, B.E. Wiggins, C. Lawrence, J. Petrick, S. Ivashuta, G. Heck, Analysis of plant-derived miRNAs in animal small RNA datasets, *BMC Genom.* 13 (2012) 381.
 - [40] A. Gajos-Michniewicz, M. Duechler, M. Czyz, MiRNA in melanoma-derived exosomes, *Cancer Lett.* 347 (1) (2014) 29–37.
 - [41] K.C. Ehrlich, K.W. Daigle, Protein synthesis inhibition by 8-oxo-12,13-epoxy-trichothecenes, *Biochim. Biophys. Acta, Mol. Cell. Res.* 923 (2) (1987) 206–213.
 - [42] P. Akbari, S. Braber, H. Gremmels, P.J. Koelink, K.A. Verheijden, J. Garssen, et al., Deoxynivalenol: a trigger for intestinal integrity breakdown, *FASEB J.* 28 (6) (2014) 2414–2429.
 - [43] A. Springler, S. Hessenberger, G. Schatzmayr, E. Mayer, Early activation of MAPK p44/42 is partially involved in DON-induced disruption of the intestinal barrier function and tight junction network, *Toxins* 8 (9) (2016).
 - [44] A.K. Diesing, C. Nossol, P. Panther, N. Walk, A. Post, J. Klues, et al., Mycotoxin deoxynivalenol (DON) mediates biphasic cellular response in intestinal porcine epithelial cell lines IPEC-1 and IPEC-J2, *Toxicol. Lett.* 200 (1–2) (2011) 8–18.
 - [45] A. Alizadeh, S. Braber, P. Akbari, J. Garssen, J. Fink-Gremmels, Deoxynivalenol impairs weight gain and affects markers of gut health after low-dose, short-term exposure of growing pigs, *Toxins (Basel)* 7 (6) (2015) 2071–2095.
 - [46] E.A. Reznikov, S.S. Comstock, C. Yi, N. Contractor, S.M. Donovan, Dietary bovine lactoferrin increases intestinal cell proliferation in neonatal piglets, *J. Nutr.* 144 (9) (2014) 1401–1408.
 - [47] L. Wu, A.J. Levine, Differential regulation of the p21/WAF-1 and mdm2 genes after high-dose UV irradiation: p53-dependent and p53-independent regulation of the mdm2 gene, *Mol. Med.* 3 (7) (1997) 441–451.
 - [48] C. Prives, P.A. Hall, The p53 pathway, *J. Pathol.* 187 (1) (1999) 112–126.
 - [49] S. Waga, G.J. Hannon, D. Beach, B. Stillman, The p21 inhibitor of cyclin-dependent kinases controls DNA replication by interaction with PCNA, *Nature* 369 (6481) (1994) 574–578.

Biological Characteristics and Roles of Noncoding RNAs in Milk-Derived Extracellular Vesicles

Bin Zeng, Ting Chen, Jun-Yi Luo, Lin Zhang, Qian-Yun Xi, Qing-Yan Jiang, Jia-Jie Sun, and Yong-Liang Zhang

Guangdong Provincial Key Laboratory of Animal Nutrition Control, National Engineering Research Center for Breeding Swine Industry, Guangdong Laboratory for Lingnan Modern Agriculture, College of Animal Science, South China Agricultural University, Guangzhou, China

ABSTRACT

Extracellular vesicles (EVs) have diverse roles in the transport of proteins, lipids, and nucleic acids between cells, and they serve as mediators of intercellular communication. Noncoding RNAs (ncRNAs) that are present in EVs, including microRNAs, long noncoding RNAs, and circular RNAs, have been found to participate in complex networks of interactions and regulate a wide variety of genes in animals. Milk is an important source of nutrition for humans and other mammals. Evidence suggests that milk-derived EVs contain abundant ncRNAs, which are stable and can be transported to the offspring and other consumers. Current data suggest a strong link between milk EV ncRNAs and many biological processes, and these ncRNAs have been drawing increasing attention and might play an epigenetic regulatory role in recipients, though further research is still necessary to understand their precise roles. The present review introduces basic information about milk EV ncRNAs, summarizes their expression profiles, biological characteristics, and functions based on current knowledge, and discusses their biological roles, indeterminate issues, and perspectives. Our goal is to provide a deeper understanding of the physiological effects of milk EV ncRNAs on offspring and to provide a reference for future research in this field. *Adv Nutr* 2020;00:1–14.

Keywords: extracellular vesicles, exosome, milk, microRNAs, long noncoding RNAs, circular RNAs

Introduction

Breast milk is the perfect nutrition for infants, as a result of millions of years of finetuning to the requirements of growing mammals. Breast milk is rich in proteins, lipids, and carbohydrates, which are the primary source of nutrition for infants (1). Dairy products are also full of nutrients for people of different ages. Immunoglobulins and nonnutritional

bioactive factors in milk are generally considered as the main functional substances in organismic regulation. However, in 2007 Valadi et al. (2) reported a new mechanism of gene communication between cells, namely, through transport of exosomal RNAs. In the same year, Admyre et al. (3) found exosomes—small extracellular vesicles (sEVs)—in milk. In 2012, Zhang et al. (4) reported that exogenous plant (rice) microRNAs (miRNAs) in food can regulate the expression of target genes in mammals. Since then, scientific studies on milk-derived exosomes and their RNA cargoes have been drawing much attention.

Exosomes, defined as a subtype of extracellular vesicles (EVs), originate from late endosomes (5, 6). Several proteins, including tetraspanins (CD9, CD63, and CD81), endosomal sorting complex required for transport (ESCRT), tumor susceptibility gene 101 (*TSG101*), ALG-2-interacting protein X (Alix), and heat stress protein 70 (HSP70) are often used as “exosome markers” (6, 7). EVs play an important role as mediators in cell-to-cell communication by transporting cargoes from donor to recipient cells (8). Among EV cargoes, noncoding RNAs (ncRNAs) are of particular interest. They participate in complex interactions with other nucleic acids and proteins, and they often have wide-reaching effects on cell biology and regulate a majority of genes in mammals in

Supported by the National Key Research and Development Program grant 2016YFD0500503 (to Y-LZ); the Natural Science Foundation of China grants 32072812 (to Y-LZ), 31802156 (to TC) and 31802032 (to J-JS); and the Key Project of Guangdong Provincial Nature Science Foundation grant 2018B030311015 (to Q-YX).

Author disclosures: The authors report no conflicts of interest.

BZ and TC contributed equally to this work.

Address correspondence to J-JS (e-mail: Jiajieking@126.com) or Y-LZ (e-mail: zhangyl@scau.edu.cn).

Abbreviations used: AF, Alexa Fluor; Alix, ALG-2-interacting protein X; BCAA, branched-chain amino acid; *Bach2*, BTB domain and CNC homolog 2; circRNA, circular RNA; *CRNDE*, Colorectal neoplasia differentially expressed; *DANCR*, Differentiation antagonizing non-protein coding RNA; DNMT, DNA methyltransferase; ESCRT, Endosomal sorting complex required for transport; EV, extracellular vesicle; *FAS*, TNF receptor superfamily member 6; *FOXp3*, forkhead box P3; *GASS*, Growth arrest specific transcript 5; *Hmg2*, High mobility group AT-hook 2; HSP70, Heat stress protein 70; IEC, intestinal epithelial cell; Igf2bp1, insulin-like growth factor 2 binding protein 1; IPEC-J2, Epithelial cells of porcine small intestine; lncRNA, long noncoding RNA; Mdr, multiple drug resistance; miRNA, microRNA; *Mitf*, Melanocyte inducing transcription factor; ncRNA, noncoding RNA; p53/Tp53, protein 53; RNase, ribonuclease; *SERPINE1*, Serine proteinase inhibitor, member 1; sEV, small extracellular vesicle; siRNA, short interfering RNA; *SRA1*, Steroid receptor RNA activator 1; T2DM, type 2 diabetes mellitus; *TSG101*, Tumor susceptibility gene 101; *Wnt1*, Wnt family member 1; *ZFAS1*, Zinc finger NFX1-type antisense RNA 1.

an epigenetic way (9–13). It has been reported that sEVs in breast milk from many mammals, including human (14), cow (15), pig (16), panda (17), sheep (18), rat (19), and wallaby (20), also contain abundant ncRNAs. The particle size of milk exosomes mainly ranges from 100 to 200 nm, and the positive markers, CD9, CD63, CD81, HSP70, TSG101, and Alix, can also be detected (21–23). The exosomal lipid membrane helps to protect milk-derived RNAs against degradation by ribonucleases (RNases) (15), low pH, and digestive enzymes *in vitro* (21, 24), and thereby protects the important functions of milk EV-encapsulated RNAs in the communication from mother to child. Importantly, unlike other exosomes, milk exosomes can transport their cargoes to the progeny and even to other species (25), leading to mother-child or interspecies communication.

Increasing evidence has clearly indicated that milk exosomal RNAs can be taken up by cells, are permeable to the intestinal barrier, and enter the blood circulation, although this phenomenon has been controversial in past years (26, 27). *In vitro* experiments have shown that milk exosome-derived RNAs can be absorbed by intestinal and immune cells (24, 28). Bovine milk exosomes and their RNA cargo could enter the blood circulation of the milk consumer and distribute into various tissues in mice after application of labeled bovine milk exosomes (25, 29). Endothelial cells transport milk exosomes by endocytosis, and this is an important step in the delivery of exosomes and their RNA cargo to peripheral tissues (30, 31). Recent articles have strengthened the evidence that bovine milk exosomes and RNAs play an important role in purine metabolism, fecundity, and intestinal immune responses (32, 33).

Based on these studies, it is extremely likely that EV-derived ncRNAs in breast milk, serving as a type of biomolecular software, are important for the epigenetic regulation of genes and developmental processes in newborn infants and have significant regulatory effects. Here, we summarize the composition, biological characteristics, and functions of milk EV ncRNAs based on current knowledge, and discuss the questions and perspectives of milk EV ncRNAs for future research. This review will benefit our understanding and research of milk EV ncRNAs, their physiological functions, and the underlying molecular events.

Current State of Knowledge

Isolation of milk EV RNAs

Although most of the milk RNA is contained inside sEVs such as exosomes, other components of milk also contain RNAs. Milk RNA concentrations differ between different milk fractions, such as milk cells, the lipid fraction, and whey (34). Milk cells that contain RNA include somatic cells, originating from breast epithelial cells, and white blood cells, which are involved in inflammation (35, 36). Milk RNAs are also found in milk lipids (36, 37). Isolation of milk exosomes is a prerequisite for obtaining milk exosomal RNA. Fractional centrifugation combined with supercentrifugation or an exosome extraction reagent is a common and effective

method for the separation of milk exosomes from fresh milk (22, 38, 39). However, isolation of EVs from breast milk is influenced by sample collection and storage procedures. It has been reported that the storage of unprocessed breast milk at -80°C or 4°C causes cell death in breast milk, leading to contamination of the breast milk EV population by storage-induced EVs (40). Therefore, for EV isolation, fractional centrifugation steps (to remove fat, deposited cells, and debris) should be performed prior to freezing, to reduce the number of apoptotic bodies contaminating the sample.

Studies have reported that milk exosomal RNA from human (41), cow (15), pig (42), and panda (17), contains very little 18S and 28S ribosomal RNA, but many small RNA molecules. This suggests that the RNAs in milk exosomes are specific, and different from those in eukaryotic cells. To date, there is no established endogenous RNA control in milk exosomal RNA research. To normalize the ncRNA expression data obtained by qPCR, synthetic/exogenous RNA is usually added as a control (15, 21). The RNA concentration in milk exosomes shows variations across different stages of lactation and among different species. The RNA concentration in colostrum is significantly higher than that in mature milk (15). After normalization to protein concentrations, the total RNA concentration in porcine milk exosomes is 50–100 times higher than that in bovine milk exosomes (Bin Zeng, Ting Chen, Yongliang Zhang, unpublished results). These data suggest that the milk EV RNA concentration is possibly programmed to meet the requirements of different species and different growth stages of mammals.

The Landscape of ncRNAs in Milk EVs

MicroRNAs

The best-studied ncRNA is the miRNA, which is evolutionarily conserved and involved in posttranscriptional regulation of gene expression. Mature miRNAs are ~22 nucleotides long and hybridize with complementary sequences in the 3'-untranslated regions in mRNAs, thus silencing genes by destabilizing mRNAs or preventing translation (43). Chen et al. (44) have identified miRNAs in raw milk, commercial fluid milk, and powdered milk products. miRNAs have also been found in bovine milk-derived EVs (45). miRNAs have been verified to be present in milk EVs of many mammalian species by deep sequencing or microarray analysis. Interestingly, van Herwijnen et al. (46), combining their own research with published studies, reported that miRNAs abundantly present in milk-derived EVs are conserved among mammals. Here, 12 studies in total, including human, cow, pig, panda, and sheep, are selected to compare the top 10 most abundant miRNAs (Table 1). Six miRNAs are identified in high abundance in all 5 examined species, namely, miRNA-148a (miR-148a), let-7a, let-7b, let-7f, miR-30a, and miR-30d (Table 1, which flags these miRNAs as abundant in 5 species' milk EVs). Note that miR-148a always ranks in the top 4. Furthermore, we also identified miRNAs that are abundant in milk EVs from 2 or 3 species. For example, miR-21 and miR-200c are in the top 10 most

TABLE 1 Top 10 most abundant miRNAs detected in milk extracellular vesicles from different species and studies¹

Top 10 ranked miRNA	Species and lactation period									
	Human (2 mo)	Human (3 mo)	Human (6–8 mo)	Human (3–9 mo)	Cow (Not provided)	Cow (Not provided)	Cow (3 mo)	Pig (0–28 d)	Pig (1–5 d)	Pig 3–4 wk
1	miR-148a*	miR-148a*	miR-22	miR-30d*	miR-148a*	miR-2478	miR-30a*	miR-148a*	miR-193a	Let-7a*
2	miR-30b	miR-22	miR-30d*	miR-148a*	Let-7a*	miR-1777b	miR-148a*	miR-30a*	miR-423	miR-30a*
3	Let-7*	miR-30d*	miR-181a	miR-200a	Let-7b*	miR-1777a	miR-141	miR-25b	miR-320	miR-191
4	miR-146b	Let-7b*	miR-148a*	miR-200c	Let-7b*	Let-7b*	miR-22	miR-182	miR-181a	miR-21
5	miR-29a	miR-200a	miR-30b	Let-7a*	miR-99a	miR-1224	miR-26a	miR-30d*	miR-30a*	miR-30d*
6	Let-7a*	Let-7a*	miR-141	miR-200b	Let-7*	miR-2412	miR-186	miR-574	miR-378	Let-7*
7	miR-141	Let-7*	miR-92a	miR-21	Let-7c	miR-2305	miR-182	miR-30c	miR-191	Let-7c
8	miR-182	miR-146b	miR-26a	Let-7b*	Let-7a*	Let-7a*	miR-181a	miR-200c	Let-7a*	miR-200c
9	miR-200a	miR-24	miR-375	Let-7f*	miR-26a	miR-200c	miR-191	miR-191	Let-7*	Let-7g
10	miR-378	miR-21	miR-30a*	miR-30a*	miR-30d*	miR-141	miR-27b	Let-7a*	Let-7c	miR-320
Reference	(14)	(47)	(24)	(46)	(48)	(28)	(49)	(50)	(16)	(46)
										(17)
										(18)

¹d, days; miRNA, microRNA; mo, month; wk, week.
*miRNAs abundant in 5 species' milk extracellular vesicles.

abundant miRNAs in humans, cows, and pigs. miR-141 is in the top 10 most abundant miRNAs in humans and cows. In addition, miR-200a, miR-30b, and miR-146b are only in the top 10 most abundant miRNAs in humans, whereas miR-191 is only in the top 10 in pigs. The high abundance of these miRNAs in milk EVs indicates that they might play a relatively important role in physiological function through milk EVs. As shown in Table 1, miRNA profiles in milk EVs of the same species were different in different studies. The possible causes of this phenomenon are differences in nutrient concentrations, breed, lactation number, lactation period, sample treatments, and sequencing analysis.

Furthermore, many factors, including sample collection at lactation period, disease, and change of nutrition and environment, could also underlie the varied concentrations of milk EV miRNAs. The concentrations of 7 immune-related miRNAs (miR-24, miR-30d, miR-93, miR-106a, miR-181a, miR-200a, and miR-451) in human colostrum EVs are higher than in mature milk EVs (51). The expression patterns of miRNAs in pig (42) or panda (17) milk EVs are distinct across the lactation period. Cai et al. (48) and Sun et al. (49) reported that miR-142-5p and miR-223 in bovine milk EVs are upregulated upon *Staphylococcus aureus* infection. These miRNAs are potential biomarkers for early detection of bacterial infection in mammary glands. Quan et al. (52) partly replaced alfalfa hay with whole cotton seed and soybean hull (nonforage fiber source) in the feed formula of cows and identified 9 differently expressed miRNAs (4 upregulated and 5 downregulated) in milk EVs. Moreover, miR-142, miR-135, and miR-320a in milk exosomes are found to be most responsive to group relocation of cows (53).

However, research is lacking on the profound biological roles of miRNAs that are highly expressed and relatively conserved in mammalian milk EVs, as well as those whose concentrations change under the influence of different factors. Future studies should focus on these aspects.

Long noncoding RNAs and circular RNAs

Long noncoding RNAs (lncRNAs) are >200 nucleotides in length and lack protein-coding capacity. They comprise a heterogeneous class of intergenic transcripts, enhancer RNAs, and sense or antisense transcripts that overlap other genes. lncRNAs have been proposed to carry out transcriptional regulation in cis or trans, organize nuclear domains, and regulate proteins and RNAs (54). Circular RNAs (circRNAs) are classified as a new type of endogenous ncRNAs, and they are different from common linear RNAs. They are characterized by covalently closed loops without 5' or 3' polarities (13). Recent studies have demonstrated that circRNAs can adhere to miRNAs by stable complementary binding and serve as miRNA sponges to regulate gene expression (55). lncRNAs and circRNAs have received much attention in recent years, and they have been found to play important functional roles in numerous biological processes across every branch of life, including transcriptional regulation, epigenetic gene regulation, and disease (56, 57). To

date, there have been few reports of lncRNAs and circRNAs in milk EVs. Karlsson et al. (41) used qRT-PCR to analyze 87 lncRNAs, which had been previously reported to be important for developmental processes, in human breast milk EVs. Results revealed the presence of 55 lncRNAs in EVs from ≥ 1 of the analyzed individual breast milk samples ($n = 30$). Among these, 5 lncRNAs [Colorectal neoplasia differentially expressed (*CRNDE*), Differentiation antagonizing non-protein coding RNA (*DANCR*), Growth arrest specific transcript 5 (*GAS5*), Steroid receptor RNA activator 1 (*SRA1*), and Zinc finger NFX1-type antisense RNA 1 (*ZFAS1*)] were detected in 90–100% of the breast milk samples. Our previous work identified 3475 novel lncRNAs and 6 annotated lncRNAs in bovine milk EVs by RNA sequencing, and lncRNAs showed higher expression levels than mRNAs (21). lncRNAs in bovine milk EVs are also varied across different stages of lactation, as revealed by qRT-PCR analysis. Expression levels of LNC_0,01182 and LNC_0,02303 are higher in colostrum than in mature milk. Conversely, levels of LNC_0,01442 are higher in the mid- and late lactation periods (150 and 270 d) than in colostrum (2 d) and early lactation (30 d). circRNAs have also been found in bovine milk EVs. Wang et al. (58) reported 2059 distinct circRNAs identified in milk EVs by high-throughput RNA sequencing, most of them specifically expressed either in colostrum or in mature milk EVs. In porcine milk EVs, 3205 lncRNAs were identified, but only 61 circRNAs were found (59). Here, we have collated the detailed information (location in the genome) of the top 20 most abundant lncRNAs/circRNAs in bovine and porcine milk EVs (Table 2).

In general, lncRNAs and circRNAs are less conserved in different species than miRNAs, and the biological functions of most of them are unknown. Thus, it is more difficult to research lncRNAs and circRNAs in milk EVs. The establishment and gradual improvement of the ncRNA database will be helpful in the exploration and analysis of lncRNAs and circRNAs in milk EVs.

The biogenesis, stability, and uptake of ncRNAs in milk-derived EVs

To date, there is no direct and convincing evidence about the source of RNA in milk EVs. Alsaweed et al. (60) used TaqMan OpenArrays to compare human milk RNAs with those in mammary epithelium cells, maternal peripheral blood mononuclear cells, and plasma, and suggested that milk miRNAs primarily originate from mammary epithelia, whereas the maternal circulation makes a smaller contribution. Based on previous reports, we summarized the top 15 most abundant miRNAs in the mammary gland (lactating period) and in milk EVs from 3 mammals (Table 3). Interestingly, the results from different studies show that the top 15 most abundant miRNAs in the bovine or porcine mammary gland share 10 common members with the top 15 most abundant miRNAs in their milk EVs. Also, there are 9 common miRNAs between ovine mammary glands and ovine milk EVs (Table 3, which flags miRNAs

abundant in both mammary glands and milk EVs). Le Guillou et al. (61) conducted a comparative analysis of the miRNome between milk and lactating mammary glands. Results showed that of 487 annotated miRNAs in lactating mammary glands, 433 (88.9%) were detected in milk. Sixteen miRNAs are present in the top 30 of both the lactating mammary gland and the milk. These results suggest that endogenous synthesis in the lactating mammary gland is likely to be one source of miRNAs in milk EVs, but much more work is needed to confirm this. Analysis of ncRNAs in milk EVs and mammary glands from the same individual is a useful strategy. ncRNAs in milk can exist in other forms. Immunoprecipitation assays have shown that miRNAs in porcine milk are bound to proteins, including argonaute 2 (Ago2), nucleophosmin 1 (NPM1), and HDLs (Ting Chen, Bin Zheng, Delin Lin, Yongliang Zhang, unpublished results). In addition, milk fat globules, immune cells, and nonimmune milk cells, such as milk epithelial cells and milk stem cells, might all be sources of milk RNAs (51, 62, 63).

Many studies indicate that miRNAs in milk EVs are very stable and resistant to harsh conditions, including low pH, RNase digestion, and freeze-thaw cycles, because the lipid bilayer acts as a protective covering (15, 64, 65). Milk ncRNAs are packaged in EVs, allowing them to avoid degradation in the gastrointestinal tract. Our previous study also demonstrated that lncRNAs in bovine milk EVs are resistant to in vitro digestion with different digestive juices, including saliva, gastric juice, pancreatic juice, and bile (21). However, milk EV ncRNAs could be degraded by the addition of detergent (1% Triton X-100) (15), bacterial fermentation (66), milk processing (67), microwave heating (68), and ultrasound treatment (69). Notably, when milk EVs were heated to 100°C for 10 min, the encapsulated miRNAs and lncRNAs could still be detected by PCR, despite the fact that heating resulted in degradation of the majority of ncRNAs (Bin Zeng, Ting Chen, Yongling Zhang, unpublished results). This result provides a physiological basis for the absorption of milk EV ncRNAs in the intestine. Moreover, the comparison of RNA stability between milk EVs and other EVs (nonfood sources) upon treatment with various digestive juices will likely shed more light on the generality and characteristics of milk EVs.

EV uptake is linked to multiple mechanisms and endocytic pathways, including clathrin-dependent endocytosis and clathrin-independent pathways such as caveolin-mediated uptake, macropinocytosis, phagocytosis, and lipid raft-mediated internalization (70). A recent assay revealed that the membrane fusion of exosomes could be enhanced at pH 6.0 (71). Indeed, it seems likely that a heterogeneous population of EVs can gain entry into a cell via >1 route. Evidence has suggested that the entry of milk miRNAs into recipient cells is mediated by endocytosis and depends on cell and exosome surface glycoproteins (30, 31). It has been experimentally demonstrated that bovine milk EV miRNAs could be taken up by human macrophages (28), and human milk exosomes and their miRNAs could be taken up by human intestinal crypt-like cells (24). Zemleni's team (72)

TABLE 2 Detailed genetic information of top 20 most abundant lncRNAs/circRNAs in bovine and porcine milk EVs¹

Top 20	lncRNA ID Bovine milk EV (50–100 d)	lncRNA ID Porcine milk EV (3 d)	circRNA ID Bovine milk EV (2 d)	circRNA ID Bovine milk EV (90 d)	circRNA ID Porcine milk EV (3 d)
1	Chr10: 42,863,856/42,864,152	AEMK02000696.1: 79,195/97,543	Chr3: 638,422/739,656	Chr8: 100,351,443/100,353,491	Chr14: 121,316,587/121,320,413
2	Chr26: 17,917,472/17,972,241	Chr7: 10,867,838/10,868,358	Chr6: 87,270,299/87,276,280	Chr6: 87,152,488/87,157,921	Chr15: 77,234,645/77,283,482
3	Chr6: 77,982,100/77,982,100	AEMK02000407.1: 82,569/83,800	Chr5: 41,157,982/41,297,645	Chr6: 87,145,048/87,150,953	Chr1: 119,487,613/119,500,634
4	Chr6: 77,983,357/77,986,216	AEMK02000603.1: 28,188/36,155	Chr6: 109,933,165/110,018,362	Chr26: 46,866,552/46,926,465	Chr9: 7,476,477/7,481,586
5	Chr8: 74,783,032/74,789,504	AEMK02000358.1: 14,710/22,171	Chr16: 58,714,416/58,733,499	Chr6: 87,181,195/87,186,019	Chr10: 29,037,749/29,038,934
6	Chr27: 43,452,486/43,560,243	AEMK02000665.1: 68,696/81,137	Chr14: 65,829,343/65,832,220	Chr3: 680,930/739,656	Chr15: 60,407,129/60,414,442
7	GJ058845.1: 24/1211	Chr4: 101,819,215/101,872,430	Chr3: 51,745,964/51,792,200	Chr4: 79,458,313/79,618,721	Chr1: 216,148,994/216,177,064
8	Chr8: 61,266,610/61,284,332	Chr5: 42,366,339/42,372,651	Chr1: 155,995,947/156,077,037	Chr5: 118,108,657/118,281,103	Chr1: 5,503,064/5,507,316
9	Chr2: 100,162,502/100,165,205	AEMK02000495.1: 152,240/153,686	Chr18: 15,677,553/15,769,596	Chr2: 63,170,683/63,228,633	Chr1: 45,173,523/45,175,843
10	Chr20: 70,185,321/70,185,894	Chr9: 42,551,562/42,617,514	Chr5: 38,456,047/38,485,210	Chr11: 25,674,108/25,745,152	Chr3: 93,174,831/93,179,511
11	Chr6: 19,792,457/19,802,292	AEMK02000328.1: 317,535/358,163	Chr10: 79,243,596/79,335,928	Chr29: 25,303,168/25,338,898	Chr18: 54,393,585/54,404,485
12	Chr26: 17,969,399/17,971,287	Chr14: 109,907,139/109,967,090	Chr14: 73,650,350/73,691,478	Chr13: 19,157,964/19,330,999	Chr10: 69,201,375/69,235,186
13	Chr8: 620,509/6,207,288	AEMK02000301.1: 78,258/97,242	Chr6: 20,604,830/20,700,712	Chr4: 92,833,700/92,950,401	Chr17: 13,008,091/13,031,589
14	GJ058260.1: 2/1519	AEMK02000135.1: 3328/8711	Chr17: 7,077,165/7,125,454	Chr3: 102,324,607/102,362,801	Chr1: 1,654,691/1,663,793
15	Chr8: 61,266,453/61,284,374	AEMK02000205.1: 16,230/24,313	Chr12: 11,730,279/11,824,957	Chr6: 70,427,322/70,515,551	Chr7: 113,369,840/113,371,752
16	Chr6: 19,799,937/19,802,292	Chr5: 61,105,793/61,114,297	Chr14: 4,513,617/4,527,572	Chr16: 58,714,416/58,733,499	Chr8: 18,861,487/18,879,156
17	Chr8: 6,205,093/6,207,288	AEMK02000220.1: 71,39/8444	Chr10: 45,489,842/45,610,796	Chr4: 105,645,266/105,685,635	Chr12: 59,319,171/59,331,703
18	GJ058260.1: 2/1519	Chr6: 62,037,122/62,045,112	Chr11: 40,550,350/40,623,558	Chr17: 10,435,130/10,463,829	Chr18: 10,283,698/10,300,806
19	GJ058845.1: 69/1107	AEMK02000220.1: 15,348/18,156	Chr10: 93,250,197/93,310,748	Chr26: 43,911,446/43,954,980	Chr18: 54,260,018/54,270,584
20	Chr6: 17,938,105/17,939,902	Chr4: 46,447,193/46,450,808	Chr9: 95,143,978/95,207,141	Chr13: 7,280,480/7,331,583	Chr1: 263,932,774/263,940,366
Reference	(21)	(59)	(58)	(58)	(59)

¹Chr, chromosome; circRNA, circular RNA; d, days; EV, extracellular vesicle; ID, identity document; lncRNA, long noncoding RNA.

TABLE 3 Top 15 most abundant miRNAs detected in mammary glands and milk EVs from different studies and species¹

Top 15 ranked miRNAs	Cow		Pig		Sheep	
	Mammary glands	Milk EVs	Mammary glands	Milk EVs	Mammary glands	Milk EVs
1	Let-7a*	miR-148a*	miR-21*	Let-7a*	miR-143*	miR-148a*
2	Let-7f*	Let-7a*	miR-30a*	miR-30a*	Let-7b*	Let-7b*
3	Let-7b*	Let-7b*	Let-7a*	miR-191*	Let-7a*	Let-7a*
4	Let-7g*	miR-21*	miR-200c*	miR-21*	miR-378	miR-21*
5	miR-26a*	miR-99a	Let-7f*	miR-30d*	miR-148a*	Let-7c*
6	Let-7c*	Let-7f*	miR-191*	Let-7f*	Let-7f*	Let-7i
7	miR-21*	Let-7c*	miR-30d*	Let-7c*	miR-30a*	miR-26a
8	miR-103	miR-200c*	Let-7c*	miR-200c*	Let-7c*	Let-7f*
9	miR-29a	miR-26a*	miR-200b	Let-7g*	miR-146b	miR-125b
10	miR-30a*	miR-30d	miR-30c*	miR-320	miR-21*	miR-143*
11	miR-26b	Let-7g*	Let-7g*	miR-99a	miR-103	miR-30a*
12	miR-200c*	miR-30a*	miR-375	miR-30c*	miR-200c	miR-27a
13	miR-148a*	miR-200a	miR-24	miR-92a	miR-30d	miR-127
14	miR-1	miR-151	miR-26a	miR-425	miR-126	miR-181a
15	Let-7i	miR-423	miR-186	miR-20a	Let-7g*	Let-7g*
Reference	(73)	(48)	(74)	(46)	(75)	(18)

¹ EV, extracellular vesicle; miRNA, microRNA.

*miRNAs abundant in both mammary glands and milk EVs.

has reported that meaningful amounts of miR-29b and miR-200c are absorbed when adults consumed 0.25, 0.5, and 1.0 L of milk in a randomized crossover design. However, Auerbach et al. (27) reported a failure to detect bovine miR-29b and miR-200c in human plasma after milk consumption. Title et al. (26) detected only trace amounts of miR-375 (magnitude below the threshold for target genes) in the plasma of miR-375–knockout mouse pups receiving wild-type milk. Subsequently, Zemleni's team (29) suggested that the integrity of the samples used in the study by Auerbach et al. (27) was compromised and the RNA was degraded. They also suggested that, unlike many other miRNAs, miR-375 in milk is subjected to “first passage elimination” in intestinal mucosa and liver, and therefore its concentrations in the blood circulation and peripheral tissues are low (76). More direct evidence about milk EV ncRNA uptake has been provided by Zemleni's team. They transfected synthetic, fluorophore-labeled miRNAs into bovine milk exosomes and administered these to mice, and found that distinct species of miRNAs demonstrated unique distribution profiles and accumulated in intestinal mucosa, spleen, liver, heart, and brain (25). Further, miRNAs present in milk are able to enter normal and tumor cells (77). Milk miRNAs encapsulated in exosomes have been confirmed to be able to cross the intestinal barrier (65, 78). Our previous study suggested porcine milk exosomal miRNAs could be taken up by intestinal epithelial cells (79, 80). Our recent work demonstrated that the concentrations of 4 miRNAs (miR-2284, miR-2291, miR-7134, and miR-1343) were significantly different in piglet serum after feeding porcine or bovine milk, which is in accordance with their original concentrations in porcine and bovine whey (which contains milk EVs). Interestingly, these milk-derived miRNAs showed differences in piglet serum at different time points (days 0, 3, 6, and 12),

which could be relevant to the variation in absorbance of miRNAs after milk feeding (81). Moreover, data from studies in dual-chamber systems have suggested that some miRNAs of milk EVs cross the intestinal mucosa more efficiently than others, and reverse transport from the basolateral to the luminal side is minimal in human Caco-2 colon carcinoma cells (30).

Biological Roles of ncRNAs in Milk EVs

Intestinal health

Milk EVs and their RNA cargoes, after resisting digestion by gastric juices, reach the intestines. Recent studies suggested that milk EVs and their RNA cargoes are beneficial for intestinal health. Intestinal epithelial cells play a crucial role in the regulation of development and health, forming an essential barrier between the exterior and the interior of the body, and are responsible for the first physiological step of transporting nutrients to the body's cells. It has been shown that milk exosomes promote intestinal epithelial cell growth (82) and protect them against intestinal injury under oxidative stress (83, 84), intestinal inflammation (85), and necrotizing enterocolitis (23, 86). Recent research has shown that dietary depletion of milk exosomes and their miRNA cargoes exacerbates cecal inflammation in multiple drug resistance (*Mdr*)1a^{-/-} mice (*Mdr*1a^{-/-} mice spontaneously develop clinical signs of inflammatory bowel disease). Bovine milk exosomal miR-200a-3p plays an important role in alleviating cecal inflammation by downregulating the expression of the proinflammatory chemokine (C-X-C motif) ligand 9 (*CXCL9*) (87). Furthermore, our recent work demonstrated that porcine exosomal miR-4334 and miR-219 reduce LPS-induced intestinal epithelial cell (IEC) inflammation through the NF- κ B pathway, porcine milk exosomal miR-338 inhibits

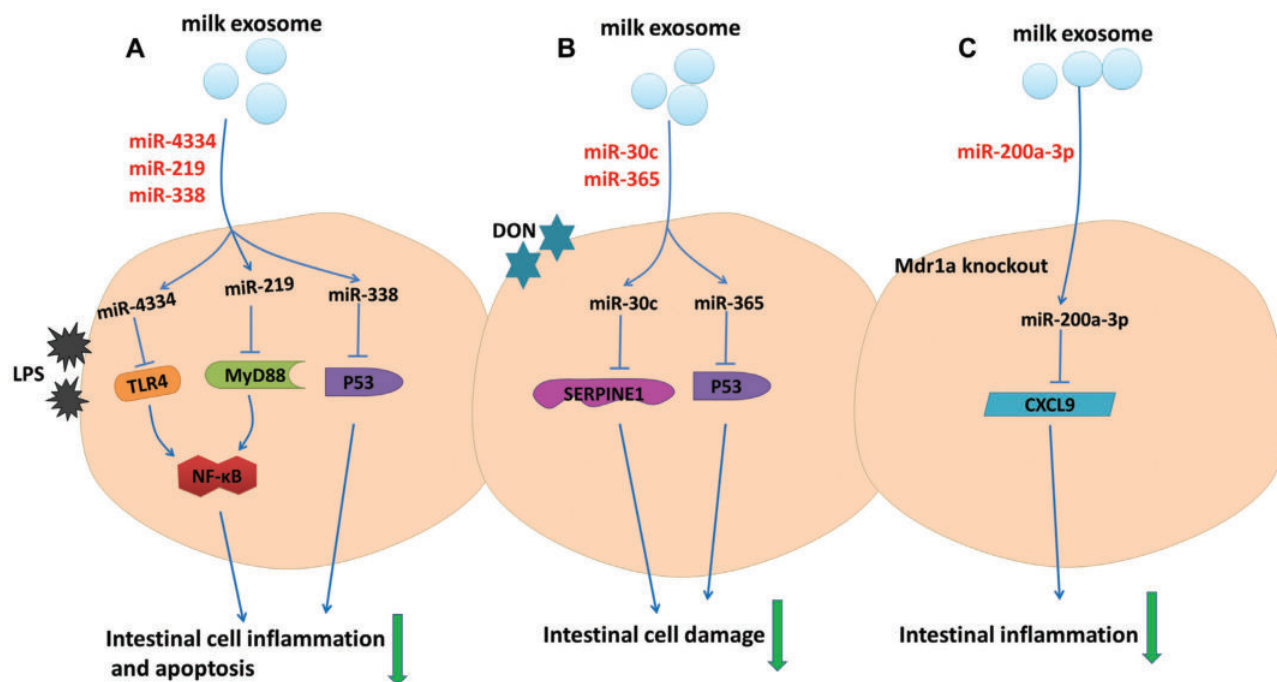


FIGURE 1 Milk exosomal miRNAs inhibit intestinal inflammation or damage caused by different factors. (A) Porcine milk exosomal miRNAs (miR-4334, miR-219, and miR-338) reduced LPS-induced intestinal cell inflammation and apoptosis. (B) Porcine milk exosomal miRNAs (miR-30c and miR-365-5p) attenuated deoxynivalenol (DON)-induced intestinal cell damage. (C) Bovine milk exosomal miR-200a-3p alleviated cecal inflammation in Mdr1a-knockout mice. CXCL9, chemokine (C-X-C motif) ligand 9; Mdr1a, multiple drug resistance 1a; miRNA, microRNA; MyD88, myeloid differentiation factor 88; p53, protein 53; SERPINE1, serine proteinase inhibitor, member 1; TLR4, toll-like receptor 4.

the LPS-induced IEC apoptosis via the p53 pathway (79), and porcine milk exosomal miR-30c and miR-365-5p attenuate deoxynivalenol-induced IEC damage by downregulating Serine proteinase inhibitor type-1 (*SERPINE1*) and protein 53 (*TP53*) expression (80). These findings show that several milk exosomal miRNAs are involved in the suppression of intestinal inflammation and damage by affecting target gene expression (Figure 1).

Many studies have indicated the potential of milk exosomal miRNAs to regulate intestinal health. Our previous study (88) and Gao et al. (22) suggested that both porcine and yak milk exosomes could promote intestinal proliferation by inhibiting protein 53 (*p53*) gene expression, and milk EV miR-2320, miR-181a, miR-1343, miR-128, and miR-769-3p concentrations were significantly increased in epithelial cells of porcine small intestine (IPEC-J2) after treatment with porcine milk-derived exosomes. Bioinformatics analysis suggested that TNF receptor superfamily member 6 (*FAS*) is targeted by miR-2320 and miR-181a and that *SERPINE* is targeted by miR-769-3p and miR-128 in the p53 signaling pathway. Breast milk exosomal miR-125b, miR-30d, and miR-25 can play an important role in attenuating cell death of intestinal epithelial cells (83). A recent study suggested that oral administration of moderate amounts of bovine milk-derived EVs enhances intestinal immunity in mice (89). Interestingly, highly abundant miRNAs in the milk EVs of

many species, including miR-148a and let-7 family and miR-30 family miRNAs (Table 1), have been reported to play a critical role in intestinal mucosal immunity regulation (90). For example, Paneth cell differentiation is important for producing defensins and antimicrobial peptides of the intestinal tract. The let-7 miRNA family facilitates Paneth cell differentiation by suppressing expression of their target genes [High mobility group AT-hook 2 (*Hmga2*) or insulin-like growth factor 2 binding protein 1 (*Igf2bp1*)] (91). Plasma cells are essential in IgA production in the intestinal tract. miR-30 family members have been reported to regulate the gene expression of *Blimp-1*, which is a transcription factor that is critical for the transition of germinal center B cells into plasma cells (92). miR-148a has been found to orchestrate the regulatory network to facilitate plasma cell differentiation by regulating Melanocyte inducing transcription factor (*Mitf*) and BTB domain and CNC homolog 2 (*Bach2*) expression (93). miR-375 is detected in the top 10 of human milk exosomes, and it is also thought to function in epithelial goblet cell differentiation (94). Together, these reports suggest the involvement and significance of highly expressed milk EV miRNAs in intestinal health, and provide sufficient hypotheses for future studies (Figure 2).

There is little literature about ncRNAs other than miRNAs in milk EVs in relation to intestinal health. Gene

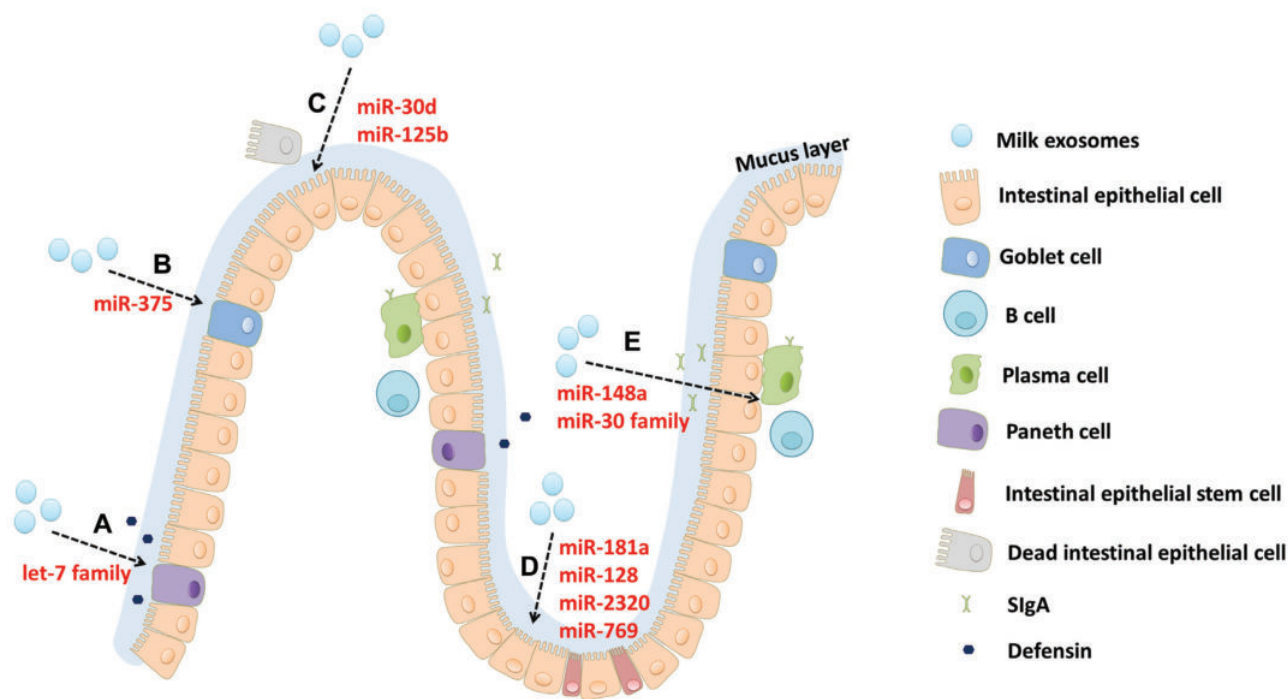


FIGURE 2 Potential regulation of milk exosomal miRNAs on intestinal health. (A) Paneth cell differentiation. (B) Goblet cell differentiation. (C) Attenuation of intestinal epithelial cell death. (D) Promotion of intestinal epithelial cell proliferation. (E) B-cell and plasma cell differentiation. miRNA, microRNA; SIgA, Secretory immunoglobulin A.

Ontology annotation indicated that the predicted target genes of bovine milk EV lncRNAs are enriched in the intestinal immune network for IgA production (21). In addition, gut microbiota and their metabolites play an important role in intestinal health. It has been reported that plant-derived exosome-like nanoparticles are taken up by the gut microbiota and contain miRNAs that alter microbiome composition and host physiology (95). Studies have reported that dietary milk EVs elicit changes in gut microbiota in mice (89, 96), but more research is necessary to determine whether milk EV ncRNAs influence the gut microbiota.

Immune regulation

Breast milk is important in the development of a child's immune system (97). Milk EVs have immune modulatory effects, and their ncRNA cargoes might play a role in this process, but research on the exact mechanism is still insufficient. A potential role for milk-derived EVs in immune modulation was first suggested by Admyre et al. (3), who found that human breast milk-derived EVs could facilitate regulatory T-cell induction. A recent publication showed that milk-derived EVs modulate cyclophosphamide-induced immunotoxicity in rats (98). Kosaka et al. (99) detected high abundances of immune-related miRNAs in the first 6 mo of lactation and proposed breast milk miRNA as a new immunoregulatory agent. Moreover, Sun et al. (51) found that bovine colostrum-derived EVs contain higher

concentrations of immune-related miRNAs and display immune modulatory effects. Bovine milk exosomes containing miRNAs have been found to be taken up by human macrophages (28) and peripheral blood mononuclear cells (72). Our previous work suggested 14 of the top 20 miRNAs in porcine milk EVs possibly participate in the regulation of the IgA immune network (16). Quan et al. (18) reported that 14 sheep milk EV miRNAs of the top 20, accounting for 98% of the total expression, are immune related. These reports suggest that miRNAs in milk EVs are potential immune protectors. As mentioned earlier, immune-related miRNAs are also found to be abundantly present in milk EVs of many species. miR-148a directly targets DNA methyltransferase 1 (*DNMT1*), which is associated with the forkhead box P3 (*FOXP3*) locus in CD4⁺ T cells. *DNMT1* deficiency results in highly efficient *FOXP3* induction following T-cell receptor stimulation (100). miR-148a functions as a critical regulator of B-cell tolerance and autoimmunity. Elevated miR-148a expression impairs B-cell tolerance by promoting the survival of immature B cells after engagement of the B-cell antigen receptor by suppressing the expression of the autoimmune suppressor growth arrest and DNA-damage-inducible 45 alpha (*Gadd45α*) (101). miR-30a directly targets myeloid differentiation factor 88 (*MyD88*) and suppresses Toll-like receptor (*TLR*)/*MyD88* activation and cytokine expression in Human acute monocytic leukemia (THP-1) cells during *Mycobacterium tuberculosis* H37Rv infection (102). Let-7f is involved in the promotion of memory cell generation

(103). Let-7a regulates the survival mechanisms mediated by the inflammatory cytokine IL-6 (104). In addition to miRNAs, the detection of specific lncRNAs in human breast milk EVs indicates that lncRNAs could also be important for programming the neonatal immune system (41). For instance, lnc-ZFAS1 appears to have an important role in cell cycle control (105), whereas lnc-GAS5 is essential in apoptosis and normal growth arrest in T cells (106). lnc-DANCR has been demonstrated to control the expression of IL-6 and TNF α in blood mononuclear cells (107). lnc-SRA1 could be important for the infant immune system because it regulates genes in the TNF α signaling pathway (108). In addition, functional enrichment analysis of the target genes of porcine milk EV lncRNAs indicated that these lncRNAs are involved in immune processes, including the regulation of the adaptive immune system, IL-8 production, and IL-6 secretion (59).

Epigenetic regulation

ncRNAs in milk EVs could be a class of key molecules in epigenetic regulation. miRNAs (109), lncRNAs (110), and circular RNAs (111) have been found to affect the epigenetic machinery. It is well known that the particular composition of breast milk gives it a role in epigenetics. Evidence is accumulating that epigenetic signaling of milk promotes the development of the infant's gastrointestinal tract and immune system, and also osteogenesis, myogenesis, adipogenesis, and neurogenesis (63). Milk nutritional epigenetics concerns the effects of nutrients on gene expression (112). In the past decade, ncRNAs have been found to be abundant in milk EVs, which has led to a new understanding of milk epigenetic regulation. Milk EVs provide high amounts of miR-148a, which targets DNMTs to potentially affect the whole genomic DNA methylation patterns (63). After incubation of normal and cancer cells with human milk-derived miRNAs, the expression of miR-148a was upregulated and the expression of its target, DNMT1, was downregulated (77). Milk EV miR-152, miR-29b, and miR-21 also target DNMTs (63). Moreover, milk EV miR-125b, miR-30d, and miR-25 might downregulate p53, which physically interacts with and stabilizes DNMT1 (113). Therefore, milk EV miRNAs can function as potential epigenetic modifiers of the milk recipient.

Metabolic disease

Milk EVs are rich in ncRNAs, some of which are associated with metabolic diseases. Many metabolic diseases, including obesity, type 2 diabetes mellitus (T2DM), osteoporosis, and Parkinson disease, have steadily increased in prevalence since the 1950s, the period of widespread distribution of refrigerated pasteurized cow milk (114). Much evidence has shown that ncRNAs in milk EVs can be absorbed by animals with potential benefits for intestinal health and immune function. But it raises concerns about metabolic diseases caused by ncRNAs in milk EVs. Young mice with long-term ad libitum access to commercial whole cow milk exhibit increased body weight and epididymal fat mass, compared

with controls with no access to dairy milk (115). However, whether obesity is promoted by milk EV ncRNAs is not clear. miR-148a, a highly abundant miRNA in milk EVs, suppresses its target gene Wnt family member 1 (*Wnt1*), an endogenous inhibitor of adipogenesis. Ectopic expression of miR-148a accelerates differentiation and partially rescues Wnt1-mediated inhibition of adipogenesis, whereas knockdown of miR-148a inhibits adipogenesis (116, 117). Remarkably, the miR-148a gene has been identified as an obesity risk gene in humans who are exhibiting single nucleotide polymorphisms (118, 119). miR-29b and miR-21, 2 other abundant mammalian milk EV-derived miRNAs (Table 1), are also involved in adipogenesis (120, 121). Notably, miR-29b also plays a role in T2DM. miR-29b mediates increases in branched-chain amino acid (BCAA) concentrations and BCAA-driven mammalian target of rapamycin complex 1 (*mTORC1*) activation in peripheral tissues, which explains why Ribosomal protein S6 kinase- (*S6K1*)-mediated inhibitory phosphorylation of insulin receptor substrate 1, a key checkpoint of insulin signaling, causes insulin resistance (122). Meanwhile, Kelch et al. (123) reported that miR-21 is significantly upregulated in serum and osteoclasts of patients with osteoporosis. miR-21 suppresses the expression of programmed cell death 4 (*PDCD4*) (124), which is important for the differentiation of preosteoclasts to osteoclasts (123). The above data indicate that milk EV ncRNAs can exert regulatory effects on metabolism of the recipient, but much more research is needed to determine the exact role of milk ncRNAs in this process.

Targeted Therapeutic Potential

Because of the therapeutic significance of exosomal miRNAs in an array of diseases, drug development focusing on the release of exosomal miRNA contents has begun (125). Due to their simplicity to obtain, stability in the gastrointestinal tract, and ability to efficiently shuttle small molecules to specific organs or the circulatory system, milk sEVs (exosomes) are an extremely promising therapeutic tool for numerous diseases. Munagala et al. (126) demonstrated that milk exosomes exhibit cross-species tolerance with no adverse immune and inflammatory response, and possess tremendous potential as drug carriers for hydrophilic and lipophilic agents. Shandilya et al. (78) encapsulated scrambled Alexa Fluor (AF)-488 short interfering RNA (siRNA) in milk exosomes using lipofection, and found that milk exosomal siRNAs are resistant to different digestive juices, and could be internalized by Caco-2 cells. The stable delivery of exosomal AF-488 siRNA and its transepithelial transport were confirmed by fluorescence microscopy and fluorescence intensity measurements. Of particular note, a recent study reported that siRNAs against specific genes, including vascular endothelial growth factor (*VEGF*), epidermal growth factor receptor (*EGFR*), protein kinase B (*AKT*), mitogen-activated protein kinase (*MAPK*), and v-Ki-ras2 Kirsten rat sarcoma viral oncogene homolog (*KRAS*), can be loaded in milk exosomes by electroporation or chemical transfection, and the expression levels of target genes after knockdown were 2- to

10-times lower in various cancers (127). Meanwhile, natural and unprocessed milk exosome ncRNAs also have potential for therapeutic applications. Metabolism-related miRNAs in breast milk are influenced by premature delivery (128), with miR-148a expression being higher and miR-320a expression being lower in preterm human milk compared with term human milk (129). Alterations in miRNA expression in milk EVs can affect biological function in infants and could serve as a nutritional therapeutic target (129). Our recent work suggested that miR-4334, miR-219, and miR-338 in porcine milk exosomes could have potential for application in therapies for necrotizing enterocolitis (79). However, there are bottlenecks in milk EV ncRNA-based target therapies. The transportation, uptake, and in vivo effector mechanisms of milk EV ncRNAs remain largely obscure. Moreover, milk EVs contain diverse contents and exert different functions. More methods must be developed to obtain milk EVs containing purified ncRNAs.

Questions and Perspectives of Milk EV ncRNAs

Because of its unique nutritional value and unique effects on humans and other mammals, the analysis of breast milk has never ceased. The field of milk EVs and their ncRNA cargoes has witnessed rapid expansion and progress in recent years. Collectively, milk EVs of humans and other mammals contain abundant ncRNAs, which have been proven: 1) to be stable under harsh conditions, and 2) to be able to enter the circulatory system through the intestinal barrier and influence target gene expression. Their roles as biological regulators in milk have been supported or predicted by many studies. All of these strongly indicate a potential function of milk EV ncRNAs in the recipient or offspring. However, a wide uncharted territory remains to be explored and verified, and the following issues should be considered in future research.

First, little is known about the expression profiles of the milk EV ncRNAs other than miRNAs. It is unknown whether highly expressed circRNAs and lncRNAs play a similar role in different mammalian milk EVs as miRNAs. From the perspective of milk nutrition evolution in different mammals, the ncRNAs in milk EVs could perform their characteristic nutritional regulatory functions just like lactose and proteins in milk. Therefore, exploration and analysis of ncRNAs in milk EVs is meaningful work. In addition, a quantitative survey of EV ncRNAs present in raw milk from different mammals and their products is equally important. This is an infrastructural project to replenish the milk ncRNA database. More research in this field will be helpful to elucidate the role of breast milk EV ncRNAs in infant or adult recipients.

Second, the exact origin, packaging mechanism, and uptake approach of milk EV ncRNAs remain unclear. For instance, the mammary gland is one of the possible sources of milk EV miRNAs (Table 3), but we still lack solid evidence supporting this hypothesis. Moreover, the following aspects remain unclear: 1) the mechanisms by which ncRNAs are selectively encapsulated into milk EVs; 2) the pathways

by which they enter intestinal epithelial cells and the circulatory system; and 3) the mechanisms by which they are distributed to target tissues and their final destination. These issues are important but challenging to elucidate. Moreover, although controversy about the absorption of milk EV ncRNAs into the circulatory system, tissues, or organs is decreasing, attention should be paid to the specific design of experimental protocols, such as animal models, applied dosage, and sampling time, to avoid controversial results.

Finally, the effects of milk containing EVs that are (partly) depleted of ncRNAs on offspring phenotypes and the underlying mechanisms need to be explored to determine the importance of maternal milk EV ncRNAs for babies. However, solid evidence that convincingly demonstrates the biological functions and exact mechanisms of milk EV ncRNAs under physiological or pathological conditions, especially in vivo, is still lacking, although many studies on this topic have been conducted. A progressive approach has been used to explore milk exosomes and RNA cargoes at Zemleni's laboratory. They fed mice with ultrasound-treated cow milk in which most of the exosomes and RNA cargoes were destroyed; this resulted in a series of phenotypic changes in mice (32, 87). Because milk or milk EVs are composed of multiple complex ingredients, ultrasound can also alter or degrade other components, not just EV RNAs. To this end, the construction of an animal model that lacks biogenesis of milk EV RNAs or certain ncRNA(s) in milk EVs is a potential key approach for further elucidating the physiological effects of milk EV ncRNAs. Importantly, it is necessary to distinguish milk EV ncRNA uptake from endogenous synthesis when a physiological feeding study is conducted in animals given milk EVs. Hopefully, a series of pioneering biotechnologies, including gene editing, nucleic acid tracing, isotopic tracing, and RNAscope, will rapidly advance this line of research in the near future.

Conclusions

ncRNAs in milk EVs represent a new research area in food science and milk nutrition. This field has expanded rapidly in recent years. Based on current studies, ncRNAs are abundant in milk EVs and have high stability. Some miRNAs are highly expressed in the milk EVs of different mammals and show a similar expression pattern. lncRNAs and circRNAs are present in milk EVs of humans, cows, and pigs. miRNAs in milk EVs are beneficial for intestinal health. These ncRNAs possibly also play biologically functional roles in immune regulation, epigenetic regulation, metabolic disease, and targeted therapy. Nevertheless, there are still many open questions that urgently require experimental analysis, such as the origin, uptake, and physiological effects of ncRNAs in milk EVs. Research in this field should be encouraged. As more detailed information in this field is being revealed, this will bring new insights into the importance of milk nutrition for human or animal health, and even into disease treatments.

Acknowledgments

The authors' responsibilities were as follows—BZ and TC: drafted the manuscript; J-YL, LZ, Q-YX, and Q-YJ: collected the data and organized the references; J-JS and Y-LZ: participated in the study design; and all authors: read and approved the final manuscript.

References

- Andreas NJ, Kampmann B, Le-Doare KM. Human breast milk: a review on its composition and bioactivity. *Early Hum Dev* 2015;91(11):629–35.
- Valadi H, Ekstrom K, Bossios A, Sjostrand M, Lee JJ, Lotvall JO. Exosome-mediated transfer of mRNAs and microRNAs is a novel mechanism of genetic exchange between cells. *Nat Cell Biol* 2007;9(6):654–9.
- Admyre C, Johansson SM, Qazi KR, Filen J-J, Laheesmaa R, Norman M, Neve EPA, Scheynius A, Gabrielsson S. Exosomes with immune modulatory features are present in human breast milk. *J Immunol* 2007;179(3):1969–78.
- Zhang L, Hou D, Chen X, Li D, Zhu L, Zhang Y, Li J, Bian Z, Liang X, Cai X, et al. Exogenous plant MIR168a specifically targets mammalian LDLRAP1: evidence of cross-kingdom regulation by microRNA. *Cell Res* 2012;22(1):107–26.
- Thery C, Witwer KW, Aikawa E, Jose Alcaraz M, Anderson JD, Andriantsitohaina R, Antoniou A, Arab T, Archer F, Atkin-Smith GK, et al. Minimal information for studies of extracellular vesicles 2018 (MISEV2018): a position statement of the International Society for Extracellular Vesicles and update of the MISEV2014 guidelines. *J Extracell Vesicles* [Internet] 2018;7(1). doi:10.1080/20013078.2018.1535750.
- Pegtel DM, Gould SJ. Exosomes. *Ann Rev Biochem* 2019;88:487–514.
- Xiao Y, Zheng L, Zou X, Wang J, Zhong J, Zhong T. Extracellular vesicles in type 2 diabetes mellitus: key roles in pathogenesis, complications, and therapy. *J Extracell Vesicles* [Internet] 2019;8(1). doi:10.1080/20013078.2019.1625677.
- Mathieu M, Martin-Jaular L, Lavieu G, Thery C. Specificities of secretion and uptake of exosomes and other extracellular vesicles for cell-to-cell communication. *Nat Cell Biol* 2019;21(1):9–17.
- Esteller M. Non-coding RNAs in human disease. *Nat Rev Genet* 2011;12(12):861–74.
- Mattick JS, Makunin IV. Non-coding RNA. *Hum Mol Genet* 2006;15:R17–29.
- Ying W, Riopel M, Bandyopadhyay G, Dong Y, Birmingham A, Seo JB, Ofrecio JM, Wollam J, Hernandez-Carretero A, Fu W, et al. Adipose tissue macrophage-derived exosomal miRNAs can modulate in vivo and in vitro insulin sensitivity. *Cell* 2017;171(2):372.
- Zheng R, Du M, Wang X, Xu W, Liang J, Wang W, Lv Q, Qin C, Chu H, Wang M, et al. Exosome-transmitted long non-coding RNA PTENP1 suppresses bladder cancer progression. *Mol Cancer* [Internet] 2018;17. doi:10.1186/s12943-018-0880-3.
- Zhang H, Deng T, Ge S, Liu Y, Bai M, Zhu K, Fan Q, Li J, Ning T, Tian F, et al. Exosome circRNA secreted from adipocytes promotes the growth of hepatocellular carcinoma by targeting deubiquitination-related USP7. *Oncogene* 2019;38(15):2844–59.
- Zhou Q, Li M, Wang X, Li Q, Wang T, Zhu Q, Zhou X, Wang X, Gao X, Li X. Immune-related microRNAs are abundant in breast milk exosomes. *Int J Biol Sci* 2012;8(1):118–23.
- Izumi H, Kosaka N, Shimizu T, Sekine K, Ochiya T, Takase M. Bovine milk contains microRNA and messenger RNA that are stable under degradative conditions. *J Dairy Sci* 2012;95(9):4831–41.
- Chen T, Xi Q-Y, Ye R-S, Cheng X, Qi Q-E, Wang S-B, Shu G, Wang L-N, Zhu X-T, Jiang Q-Y, et al. Exploration of microRNAs in porcine milk exosomes. *BMC Genomics* [Internet] 2014;15. doi:10.1186/1471-2164-15-100.100
- Ma J, Wang C, Long K, Zhang H, Zhang J, Jin L, Tang Q, Jiang A, Wang X, Tian S, et al. Exosomal microRNAs in giant panda (Ailuropoda melanoleuca) breast milk: potential maternal regulators for the development of newborn cubs. *Sci Rep* [Internet] 2017;7. doi:10.1038/s41598-017-03707-8.
- Quan S, Nan X, Wang K, Jiang L, Yao J, Xiong B. Characterization of sheep milk extracellular vesicle-miRNA by sequencing and comparison with cow milk. *Animals* [Internet] 2020;10(2). doi:10.3390/ani10020331.
- Pomar CA, Castro H, Pico C, Serra F, Palou A, Sanchez J. Cafeteria diet consumption during lactation in rats, rather than obesity per se, alters miR-222, miR-200a, and miR-26a levels in milk. *Mol Nutr Food Res* [Internet] 2019;63(8). doi:10.1002/mnfr.201800928.
- Modepalli V, Kumar A, Hinds LA, Sharp JA, Nicholas KR, Lefevre C. Differential temporal expression of milk miRNA during the lactation cycle of the marsupial tammar wallaby (*Macropus eugenii*). *BMC Genomics* [Internet] 2014;15. doi:10.1186/1471-2164-15-1012.
- Zeng B, Chen T, Xie M-Y, Luo J-Y, He J-J, Xi Q-Y, Sun J-J, Zhang Y-L. Exploration of long noncoding RNA in bovine milk exosomes and their stability during digestion in vitro. *J Dairy Sci* 2019;102(8):6726–37.
- Gao HN, Guo HY, Zhang H, Xie XL, Wen PC, Ren FZ. Yak-milk-derived exosomes promote proliferation of intestinal epithelial cells in an hypoxic environment. *J Dairy Sci* 2019;102(2):985–96.
- Pisano C, Galley J, Elbahrawy M, Wang Y, Farrell A, Brigstock D, Besner GE. Human breast milk-derived extracellular vesicles in the protection against experimental necrotizing enterocolitis. *J Pediatr Surg* 2020;55(1):54–8.
- Liao Y, Du X, Li J, Lonnerdal B. Human milk exosomes and their microRNAs survive digestion in vitro and are taken up by human intestinal cells. *Mol Nutr Food Res* [Internet] 2017;61(11). doi:10.1002/mnfr.201700082.
- Manca S, Upadhyaya B, Mutai E, Desaulniers AT, Cederberg RA, White BR, Zemleni J. Milk exosomes are bioavailable and distinct microRNA cargos have unique tissue distribution patterns. *Sci Rep* [Internet] 2018;8. doi:10.1038/s41598-018-29780-1.
- Title AC, Denzler R, Stoffel M. Uptake and function studies of maternal milk-derived microRNAs. *J Biol Chem* 2015;290(39):23680–91.
- Auerbach A, Vyas G, Li A, Halushka M, Witwer K. Uptake of dietary milk miRNAs by adult humans: a validation study. *FI000Res* [Internet] 2016;5:721. doi:10.12688/fi000research.8548.1.
- Izumi H, Tsuda M, Sato Y, Kosaka N, Ochiya T, Iwamoto H, Namba K, Takeda Y. Bovine milk exosomes contain microRNA and mRNA and are taken up by human macrophages. *J Dairy Sci* 2015;98(5):2920–33.
- Wang L, Sadri M, Giraud D, Zemleni J. RNase H2-dependent polymerase chain reaction and elimination of confounders in sample collection, storage, and analysis strengthen evidence that microRNAs in bovine milk are bioavailable in humans. *J Nutr* 2018;148(1):153–9.
- Wolf T, Baier SR, Zemleni J. The intestinal transport of bovine milk exosomes is mediated by endocytosis in human colon carcinoma Caco-2 cells and rat small intestinal IEC-6 cells. *J Nutr* 2015;145(10):2201–6.
- Kusuma RJ, Manca S, Friemel T, Sukreet S, Nguyen C, Zemleni J. Human vascular endothelial cells transport foreign exosomes from cow's milk by endocytosis. *Am J Physiol Cell Physiol* 2016;310(10):C800–C7.
- Zemleni J, Sukreet S, Zhou F, Wu D, Mutai E. Milk-derived exosomes and metabolic regulation. *Annu Rev Anim Biosci* 2019;7:245–62.
- Aguilar-Lozano A, Baier S, Grove R, Shu J, Giraud D, Leiferman A, Mercer KE, Cui J, Badger TM, Adamec J, et al. Concentrations of purine metabolites are elevated in fluids from adults and infants and in livers from mice fed diets depleted of bovine milk exosomes and their RNA cargos. *J Nutr* 2018;148(12):1886–94.
- Alsaweed M, Hepworth AR, Lefevre C, Hartmann PE, Geddes DT, Hassiotou F. Human milk microRNA and total RNA differ depending on milk fractionation. *J Cell Biochem* 2015;116(10):2397–407.
- Alsaweed M, Lai CT, Hartmann PE, Geddes DT, Kakulas F. Human milk cells contain numerous miRNAs that may change with milk

- removal and regulate multiple physiological processes. *Int J Mol Sci* [Internet] 2016;17(6). doi:10.3390/ijms17060956.
36. Li R, Dudemaine P-L, Zhao X, Lei C, Ibeagha-Awemu EM. Comparative analysis of the miRNome of bovine milk fat, whey and cells. *PLoS One* [Internet] 2016;11(4). doi:10.1371/journal.pone.0154129.
 37. Munch EM, Harris RA, Mohammad M, Benham AL, Pejerrey SM, Showalter L, Hu M, Shope CD, Maningat PD, Gunaratne PH, et al. Transcriptome profiling of microRNA by next-gen deep sequencing reveals known and novel miRNA species in the lipid fraction of human breast milk. *PLoS One* [Internet] 2013;8(2). doi:10.1371/journal.pone.0050564.
 38. Somiya M, Yoshioka Y, Ochiya T. Biocompatibility of highly purified bovine milk-derived extracellular vesicles. *J Extrac Vesicles* [Internet] 2018;7(1). doi:10.1080/20013078.2018.1440132.
 39. Reif S, Shiff YE, Golan-Gerstl R. Milk-derived exosomes (MDEs) have a different biological effect on normal fetal colon epithelial cells compared to colon tumor cells in a miRNA-dependent manner. *J Transl Med* [Internet] 2019;17(1). doi:10.1186/s12967-019-2072-3.
 40. Zonneveld MI, Brisson AR, van Herwijnen MJC, Tan S, van de Lest CHA, Redegeld FA, Garssen J, Wauben MHM, Nolte-^t Hoen ENM. Recovery of extracellular vesicles from human breast milk is influenced by sample collection and vesicle isolation procedures. *Journal of extracellular vesicles* 2014;3. doi:10.3402/jev.v3.24215.
 41. Karlsson O, Rodosthenous RS, Jara C, Brennan KJ, Wright RO, Baccarelli AA, Wright RJ. Detection of long non-coding RNAs in human breastmilk extracellular vesicles: implications for early child development. *Epigenetics* 2016;11(10):721–9.
 42. Ma Y, Feng S, Wang X, Qazi IH, Long K, Luo Y, Li G, Ning C, Wang Y, Hu S, et al. Exploration of exosomal microRNA expression profiles in pigeon "milk" during the lactation period. *BMC Genomics* [Internet] 2018;19. doi:10.1186/s12864-018-5201-0.
 43. Cui J, Zhou B, Ross SA, Zemleni J. Nutrition, microRNAs, and human health. *Adv Nutr* 2017;8(1):105–12.
 44. Chen X, Gao C, Li H, Huang L, Sun Q, Dong Y, Tian C, Gao S, Dong H, Guan D, et al. Identification and characterization of microRNAs in raw milk during different periods of lactation, commercial fluid, and powdered milk products. *Cell Res* 2010;20(10):1128–37.
 45. Hata T, Murakami K, Nakatani H, Yamamoto Y, Matsuda T, Aoki N. Isolation of bovine milk-derived microvesicles carrying mRNAs and microRNAs. *Biochem Biophys Res Commun* 2010;396(2):528–33.
 46. van Herwijnen MJC, Driedonks TAP, Snoek BL, Kroon AMT, Kleinjan M, Jorritsma R, Pieterse CMJ, Hoen E-t, Wauben MHM. Abundantly present miRNAs in milk-derived extracellular vesicles are conserved between mammals. *Front Nutr* [Internet] 2018;5. doi:10.3389/fnut.2018.00081.
 47. Simpson MR, Brede G, Johansen J, Johnsen R, Storro O, Saetrom P, Oien T. Human breast milk miRNA, maternal probiotic supplementation and atopic dermatitis in offspring. *PLoS One* [Internet] 2015;10(12). doi:10.1371/journal.pone.0143496.
 48. Cai M, He H, Jia X, Chen S, Wang J, Shi Y, Liu B, Xiao W, Lai S. Genome-wide microRNA profiling of bovine milk-derived exosomes infected with *Staphylococcus aureus*. *Cell Stress Chaperones* 2018;23(4):663–72.
 49. Sun J, Aswath K, Schroeder SG, Lippolis JD, Reinhardt TA, Sonstegard TS. MicroRNA expression profiles of bovine milk exosomes in response to *Staphylococcus aureus* infection. *BMC Genomics* [Internet] 2015;16. doi:10.1186/s12864-015-2044-9.
 50. Gu Y, Li M, Wang T, Liang Y, Zhong Z, Wang X, Zhou Q, Chen L, Lang Q, He Z, et al. Lactation-related microRNA expression profiles of porcine breast milk exosomes. *PLoS One* [Internet] 2012;7(8). doi:10.1371/journal.pone.0043691.
 51. Sun Q, Chen X, Yu J, Zen K, Zhang C-Y, Li L. Immune modulatory function of abundant immune-related microRNAs in microvesicles from bovine colostrum. *Protein Cell* 2013;4(3):197–210.
 52. Quan S-Y, Nan X-M, Wang K, Zhao Y-G, Jiang L-S, Yao J-H, Xiong B-H. Replacement of forage fiber with non-forage fiber sources in dairy cow diets changes milk extracellular vesicle-miRNA expression. *Food Funct* 2020;11(3):2154–62.
 53. Colitti M, Sgorlon S, Licastro D, Stefanon B. Differential expression of miRNAs in milk exosomes of cows subjected to group relocation. *Res Vet Sci* 2019;122:148–55.
 54. Kopp F, Mendell JT. Functional classification and experimental dissection of long noncoding RNAs. *Cell* 2018;172(3):393–407.
 55. Hansen TB, Jensen TI, Clausen BH, Bramsen JB, Finsen B, Damgaard CK, Kjems J. Natural RNA circles function as efficient microRNA sponges. *Nature* 2013;495(7441):384–8.
 56. Batista PJ, Chang HY. Long noncoding RNAs: cellular address codes in development and disease. *Cell* 2013;152(6):1298–307.
 57. Kulcheski FR, Christoff AP, Margis R. Circular RNAs are miRNA sponges and can be used as a new class of biomarker. *J Biotechnol* 2016;238:42–51.
 58. Wang Y, Li D, Wang Y, Li M, Fang X, Chen H, Zhang C. The landscape of circular RNAs and mRNAs in bovine milk exosomes. *J Food Compos Anal* 2019;76:33–8.
 59. Zeng B, Chen T, Luo J, Xie M, Wei L, Xi Q, Sun J, Zhang Y. Exploration of long non-coding RNAs and circular RNAs in porcine milk exosomes. *Front Genet* [Internet] 2020;11(652). doi:10.3389/fgene.2020.00652.
 60. Alsaweed M, Lai CT, Hartmann PE, Geddes DT, Kakulas F. Human milk miRNAs primarily originate from the mammary gland resulting in unique miRNA profiles of fractionated milk. *Sci Rep* [Internet] 2016;6. doi:10.1038/srep20680.
 61. Guillou SL, Leduc A, Laubier J, Barbey S, Rossignol MN, Lefebvre R, Marthey S, Laloe D, Provost FL. Characterization of Holstein and Normande whole milk miRNomes highlights breed specificities. *Sci Rep* [Internet] 2019;9(1):20345. doi.org/10.1038/s41598-019-56690-7.
 62. Hassiotou F, Geddes DT, Hartmann PE. Cells in human milk: state of the science. *J Hum Lact* 2013;29(2):171–82.
 63. Melnik BC, Kakulas F. Milk exosomes and microRNAs: potential epigenetic regulators. In: Patel V, Preedy V, editors. *Handbook of nutrition, diet, and epigenetics*. Springer Nature Switzerland AG; 2017. pp. 1–28. doi.org/10.1007/978-3-319-31143-2_86-1.
 64. Benmoussa A, Lee CHC, Laffont B, Savard P, Laugier J, Boilard E, Gilbert C, Fliss I, Provost P. Commercial dairy cow milk microRNAs resist digestion under simulated gastrointestinal tract conditions. *J Nutr* 2016;146(11):2206–15.
 65. Rani P, Vashisht M, Golla N, Shandilya S, Onteru SK, Singh D. Milk miRNAs encapsulated in exosomes are stable to human digestion and permeable to intestinal barrier in vitro. *J Funct Foods* 2017;34:431–9.
 66. Yu S, Zhao Z, Sun L, Li P. Fermentation results in quantitative changes in milk-derived exosomes and different effects on cell growth and survival. *J Agric Food Chem* 2017;65(6):1220–8.
 67. Howard KM, Kusuma RJ, Baier SR, Friemel T, Markham L, Vanamala J, Zemleni J. Loss of miRNAs during processing and storage of cow's (*Bos taurus*) milk. *J Agric Food Chem* 2015;63(2):588–92.
 68. Zhao Z, Yu S, Xu M, Li P. Effects of microwave on extracellular vesicles and microRNA in milk. *J Dairy Sci* 2018;101(4):2932–40.
 69. Leiferman A, Shu J, Grove R, Cui J, Adamec J, Zemleni J. A diet defined by its content of bovine milk exosomes and their RNA cargos has moderate effects on gene expression, amino acid profiles and grip strength in skeletal muscle in C57BL/6 mice. *J Nutr Biochem* 2018;59:123–8.
 70. Mulcahy LA, Pink RC, Carter DRF. Routes and mechanisms of extracellular vesicle uptake. *J Extracell Vesicles* [Internet] 2014;3. doi:10.3402/jev.v3.24641.
 71. Nishio M, Teranishi Y, Morioka K, Yanagida A, Shoji A. Real-time assay for exosome membrane fusion with an artificial lipid membrane based on enhancement of gramicidin A channel conductance. *Biosens Bioelectron* [Internet] 2019;150:111918. doi:10.1016/j.bios.2019.111918.
 72. Baier SR, Nguyen C, Xie F, Wood JR, Zemleni J. MicroRNAs are absorbed in biologically meaningful amounts from nutritionally relevant doses of cow milk and affect gene expression in peripheral

- blood mononuclear cells, HEK-293 kidney cell cultures, and mouse livers. *J Nutr* 2014;144(10):1495–500.
73. Li Z, Liu H, Jin X, Lo L, Liu J. Expression profiles of microRNAs from lactating and non-lactating bovine mammary glands and identification of miRNA related to lactation. *BMC Genomics* [Internet] 2012;13. doi:10.1186/1471-2164-13-731.
 74. Peng J, Zhao J-S, Shen Y-F, Mao H-G, Xu N-Y. MicroRNA expression profiling of lactating mammary gland in divergent phenotype swine breeds. *Int J Mol Sci* 2015;16(1):1448–65.
 75. Ji Z, Wang G, Xie Z, Zhang C, Wang J. Identification and characterization of microRNA in the dairy goat (*Capra hircus*) mammary gland by Solexa deep-sequencing technology. *Mol Biol Rep* 2012;39(10):9361–71.
 76. Zempeni J, Baier SR, Hirschi K. Diet-responsive microRNAs are likely exogenous. *J Biol Chem* [Internet] 2015;290(41):25197. doi:10.1074/jbc.L115.687830.
 77. Golan-Gerstl R, Shiff YE, Moshayoff V, Schechter D, Leshkowitz D, Reif S. Characterization and biological function of milk-derived miRNAs. *Mol Nutr Food Res* [Internet] 2017;61(10). doi:10.1002/mnfr.201700009.
 78. Shandilya S, Rani P, Onteru SK, Singh D. Small interfering RNA in milk exosomes is resistant to digestion and crosses the intestinal barrier in vitro. *J Agric Food Chem* 2017;65(43):9506–13.
 79. Xie M-Y, Hou L-J, Sun J-J, Zeng B, Xi Q-Y, Luo J-Y, Chen T, Zhang Y-L. Porcine milk exosome miRNAs attenuate LPS-induced apoptosis through inhibiting TLR4/NF-kappa B and p53 pathways in intestinal epithelial cells. *J Agric Food Chem* 2019;67(34):9477–91.
 80. Xie M-Y, Chen T, Xi Q-Y, Hou L-J, Luo J-Y, Zeng B, Li M, Sun J-J, Zhang Y-L. Porcine milk exosome miRNAs protect intestinal epithelial cells against deoxynivalenol-induced damage. *Biochem Pharmacol* [Internet] 2020;175:113898. doi:10.1016/j.bcp.2020.113898.
 81. Lin D, Chen T, Xie M, Li M, Zeng B, Sun R, Zhu Y, Ye D, Wu J, Sun J, et al. Oral administration of bovine and porcine milk exosome alter miRNAs profiles in piglet serum. *Sci Rep* [Internet] 2020;10(1):6983. doi:10.1038/s41598-020-63485-8.
 82. Hock A, Miyake H, Li B, Lee C, Ermini L, Koike Y, Chen Y, Maattanen P, Zani A, Pierro A. Breast milk-derived exosomes promote intestinal epithelial cell growth. *J Pediatr Surg* 2017;52(5):755–9.
 83. Martin C, Patel M, Williams S, Arora H, Sims B. Human breast milk-derived exosomes attenuate cell death in intestinal epithelial cells. *Innate Immun* 2018;24(5):278–84.
 84. Dong P, Zhang Y, Yan D-Y, Wang Y, Xu X, Zhao Y-C, Xiao T-T. Protective effects of human milk-derived exosomes on intestinal stem cells damaged by oxidative stress. *Cell Transplant* [Internet] 2020;29:096368972091269. doi:10.1177/0963689720912690.
 85. Gao R, Zhang R, Qian T, Peng X, He W, Zheng S, Cao Y, Pierro A, Shen C. A comparison of exosomes derived from different periods breast milk on protecting against intestinal organoid injury. *Pediatr Surg Int* 2019;35(12):1363–8.
 86. Li B, Hock A, Wu RY, Minich A, Botts SR, Lee C, Antounians L, Miyake H, Koike Y, Chen Y, et al. Bovine milk-derived exosomes enhance goblet cell activity and prevent the development of experimental necrotizing enterocolitis. *PLoS One* [Internet] 2019;14(1). doi:10.1371/journal.pone.0211431.
 87. Wu D, Kittana H, Shu J, Kachman SD, Cui J, Ramer-Tait AE, Zempeni J. Dietary depletion of milk exosomes and their microRNA cargos elicits a depletion of miR-200a-3p and elevated intestinal inflammation and chemokine (C-X-C motif) ligand 9 expression in Mdr1a-/- mice. *Curr Dev Nutr* [Internet] 2019;3(12):nzz122–nzz. doi:10.1093/cdn/nzz122.
 88. Chen T, Xie M-Y, Sun J-J, Ye R-S, Cheng X, Sun R-P, Wei L-M, Li M, Lin D-L, Jiang Q-Y, et al. Porcine milk-derived exosomes promote proliferation of intestinal epithelial cells. *Sci Rep* [Internet] 2016;6. doi:10.1038/srep33862.
 89. Tong L, Hao H, Zhang X, Zhang Z, Lv Y, Zhang L, Yi H. Oral administration of bovine milk-derived extracellular vesicles alters the gut microbiota and enhances intestinal immunity in mice. *Mol Nutr Food Res* [Internet] 2020. doi:10.1002/mnfr.201901251.
 90. Park EJ, Shimaoka M, Kiyono H. MicroRNA-mediated dynamic control of mucosal immunity. *Int Immunol* 2017;29(4):157–63.
 91. Madison BB, Liu Q, Zhong X, Hahn CM, Lin N, Emmett MJ, Stanger BZ, Lee J-S, Rustgi AK. LIN28B promotes growth and tumorigenesis of the intestinal epithelium via Let-7. *Genes Dev* 2013;27(20):2233–45.
 92. Zhang J, Jima DD, Jacobs C, Fischer R, Gottwein E, Huang G, Lugar PL, Lagoo AS, Rizzieri DA, Friedman DR, et al. Patterns of microRNA expression characterize stages of human B-cell differentiation. *Blood* 2009;113(19):4586–94.
 93. Porstner M, Winkelmann R, Daum P, Schmid J, Pracht K, Corte-Real J, Schreiber S, Haftmann C, Brandl A, Mashreghi M-F, et al. miR-148a promotes plasma cell differentiation and targets the germinal center transcription factors Mitf and Bach2. *Eur J Immunol* 2015;45(4):1206–15.
 94. Biton M, Levin A, Slyper M, Alkalay I, Horwitz E, Mor H, Kredor-Russo S, Avnit-Sagi T, Cojocaru G, Zreik F, et al. Epithelial microRNAs regulate gut mucosal immunity via epithelium-T cell crosstalk. *Nat Immunol* 2011;12(3):239–46.
 95. Teng Y, Ren Y, Sayed M, Hu X, Lei C, Kumar A, Hutchins E, Mu J, Deng Z, Luo C, et al. Plant-derived exosomal microRNAs shape the gut microbiota. *Cell Host Microbe* 2018;24(5):637–52.
 96. Zhou F, Paz HA, Sadri M, Cui J, Kachman SD, Fernando SC, Zempeni J. Dietary bovine milk exosomes elicit changes in bacterial communities in C57BL/6 mice. *Am J Physiol Gastrointest Liver Physiol* 2019;317(5):G618–G24.
 97. Mosconi E, Rekima A, Seitz-Polski B, Kanda A, Fleury S, Tissandie E, Monteiro R, Dombrowicz DD, Julia V, Glaichenhaus N, et al. Breast milk immune complexes are potent inducers of oral tolerance in neonates and prevent asthma development. *Mucosal Immunol* 2010;3(5):461–74.
 98. Ibrahim HM, Mohammed-Geba K, Tawfic AA, El-Magd MA. Camel milk exosomes modulate cyclophosphamide-induced oxidative stress and immuno-toxicity in rats. *Food Funct* 2019;10(11):7523–32.
 99. Kosaka N, Izumi H, Sekine K, Ochiya T. microRNA as a new immune-regulatory agent in breast milk. *Silence* [Internet] 2010;1(1):7. doi:10.1186/1758-907x-1-7.
 100. Josefowicz SZ, Wilson CB, Rudensky AY. Cutting edge: TCR stimulation is sufficient for induction of Foxp3 expression in the absence of DNA methyltransferase 1. *J Immunol* 2009;182(11):6648–52.
 101. Gonzalez-Martin A, Adams BD, Lai M, Shepherd J, Salvador-Bernaldez M, Salvador JM, Lu J, Nemazee D, Xiao C. The microRNA miR-148a functions as a critical regulator of B cell tolerance and autoimmunity. *Nat Immunol* [Internet] 2016;17(4):433. doi:10.1038/ni.3385.
 102. Wu Y, Sun Q, Dai L. Immune regulation of miR-30 on the Mycobacterium tuberculosis-induced TLR/MyD88 signaling pathway in THP-1 cells. *Exp Ther Med* 2017;14(4):3299–303.
 103. Wu H, Neilson JR, Kumar P, Manocha M, Shankar P, Sharp PA, Manjunath N. miRNA profiling of naive, effector and memory CD8 T cells. *PLoS One* [Internet] 2007;2(10). doi:10.1371/journal.pone.0001020.
 104. Meng F, Henson R, Wehbe-Janek H, Smith H, Ueno Y, Patel T. The microRNA let-7a modulates interleukin-6-dependent STAT-3 survival signaling in malignant human cholangiocytes. *J Biol Chem* 2007;282(11):8256–64.
 105. Askarian-Amiri ME, Crawford J, French JD, Smart CE, Smith MA, Clark MB, Ru K, Mercer TR, Thompson ER, Lakhani SR, et al. SNORD-host RNA Zfas1 is a regulator of mammary development and a potential marker for breast cancer. *RNA* 2011;17(5):878–91.
 106. Mourtada-Maarabouni M, Hedge VL, Kirkham L, Farzaneh F, Williams GT. Growth arrest in human T-cells is controlled by the non-coding RNA growth-arrest-specific transcript 5 (GAS5). *J Cell Sci* [Internet] 2010;123(7):1181. doi:10.1242/jcs.070631.
 107. Tong X, Gu P-c, Xu S-z, Lin X-j. Long non-coding RNA-DANCR in human circulating monocytes: a potential biomarker associated with postmenopausal osteoporosis. *Biosci Biotechnol Biochem* 2015;79(5):732–7.

108. Xu B, Gerin I, Miao H, Dang V-P, Johnson CN, Xu R, Chen X-W, Cawthorn WP, MacDougald OA, Koenig RJ. Multiple roles for the non-coding RNA SRA in regulation of adipogenesis and insulin sensitivity. *PLoS One* [Internet] 2010;5(12). doi:10.1371/journal.pone.0014199.
109. Saetrom P, Snove O, Jr, Rossi JJ. Epigenetics and microRNAs. *Pediatr Res* 2007;61(5):17R–23R.
110. Lee JT. Epigenetic regulation by long noncoding RNAs. *Science* 2012;338(6113):1435–9.
111. Cortes-Lopez M, Miura P. Emerging functions of circular RNAs. *Yale J Biol Med* 2016;89(4):527–37.
112. Verduci E, Banderali G, Barberi S, Radaelli G, Lops A, Betti F, Riva E, Giovannini M. Epigenetic effects of human breast milk. *Nutrients* 2014;6(4):1711–24.
113. Melnik BC, Schmitz G. DNA methyltransferase 1-targeting miRNA-148a of dairy milk: a potential bioactive modifier of the human epigenome. *Functional Foods in Health and Disease* 2017;7(9): 671–87.
114. Melnik BC. Milk exosomal miRNAs: potential drivers of AMPK-to-mTORC1 switching in beta-cell de-differentiation of type 2 diabetes mellitus. *Nutr Metab (Lond)* [Internet] 2019;16(1). doi:10.1186/s12986-019-0412-1.
115. Yamin HB, Barnea M, Genzer Y, Chapnik N, Froy O. Long-term commercial cow's milk consumption and its effects on metabolic parameters associated with obesity in young mice. *Mol Nutr Food Res* 2014;58(5):1061–8.
116. Shi C, Zhang M, Tong M, Yang L, Pang L, Chen L, Xu G, Chi X, Hong Q, Ni Y, et al. miR-148a is associated with obesity and modulates adipocyte differentiation of mesenchymal stem cells through Wnt signaling. *Sci Rep* [Internet] 2015;5. doi:10.1038/srep09930.
117. Shi C, Pang L, Ji C, Wang J, Lin N, Chen J, Chen L, Yang L, Huang F, Zhou Y, et al. Obesity-associated miR-148a is regulated by cytokines and adipokines via a transcriptional mechanism. *Mol Med Rep* 2016;14(6):5707–12.
118. Schwenk RW, Vogel H, Schuermann A. Genetic and epigenetic control of metabolic health. *Mol Metab* 2013;2(4):337–47.
119. Monda KL, Chen GK, Taylor KC, Palmer C, Edwards TL, Lange LA, Ng MCY, Adeyemo AA, Allison MA, Bielak LF, et al. A meta-analysis identifies new loci associated with body mass index in individuals of African ancestry. *Nat Genet* 2013;45(6):690.
120. Guglielmi V, D'Adamo M, Menghini R, Cardellini M, Gentileschi P, Federici M, Sbraccia P. MicroRNA 21 is up-regulated in adipose tissue of obese diabetic subjects. *Nutr Healthy Aging* 2017;4(2):141–5.
121. Bian Y, Lei Y, Wang C, Wang J, Wang L, Liu L, Liu L, Gao X, Li Q. Epigenetic regulation of miR-29s affects the lactation activity of dairy cow mammary epithelial cells. *J Cell Physiol* 2015;230(9):2152–63.
122. Melnik BC, Schmitz G. Exosomes of pasteurized milk: potential pathogens of Western diseases. *J Transl Med* [Internet] 2019;17. doi:10.1186/s12967-018-1760-8.
123. Kelch S, Balmayor ER, Seeliger C, Vester H, Kirschke JS, van Griensven M. miRNAs in bone tissue correlate to bone mineral density and circulating miRNAs are gender independent in osteoporotic patients. *Sci Rep* [Internet] 2017;7. doi:10.1038/s41598-017-16113-x.
124. Buscaglia LEB, Li Y. Apoptosis and the target genes of microRNA-21. *Chin J Cancer* 2011;30(6):371–80.
125. Hu G, Drescher KM, Chen X-M. Exosomal miRNAs: biological properties and therapeutic potential. *Front Gene* [Internet] 2012;3:56. doi:10.3389/fgene.2012.00056.
126. Munagala R, Aqil F, Jeyabalan J, Gupta RC. Bovine milk-derived exosomes for drug delivery. *Cancer Lett* 2016;371(1): 48–61.
127. Aqil F, Munagala R, Jeyabalan J, Agrawal AK, Kyakulaga A-H, Wilcher SA, Gupta RC. Milk exosomes – natural nanoparticles for siRNA delivery. *Cancer Lett* 2019;449:186–95.
128. Carney MC, Tarasiuk A, DiAngelo SL, Silveyra P, Podany A, Birch LL, Paul IM, Kelleher S, Hicks SD. Metabolism-related microRNAs in maternal breast milk are influenced by premature delivery. *Pediatr Res* 2017;82(2):226–36.
129. Shiff YE, Reif S, Marom R, Shiff K, Reifen R, Golan-Gerstl R. MiRNA-320a is less expressed and miRNA-148a more expressed in preterm human milk compared to term human milk. *J Funct Foods* 2019;57:68–74.

Article

Rno_circ_0001004 Acts as a miR-709 Molecular Sponge to Regulate the Growth Hormone Synthesis and Cell Proliferation

Jiali Xiong [†], Haojie Zhang ^{†‡}, Yuxuan Wang, Yunyun Cheng [§], Junyi Luo, Ting Chen, Qianyun Xi, Jiajie Sun ^{*} and Yongliang Zhang ^{*}

College of Animal Science, Guangdong Provincial Key Lab of Agro-Animal Genomics and Molecular Breeding, National Engineering Research Center for Breeding Swine Industry, South China Agricultural University, Guangzhou 510642, China; XJL00LJX@163.com (J.X.); zhanghj089@126.com (H.Z.); 13980686685@163.com (Y.W.); chengyy@jlu.edu.cn (Y.C.); luojunyi@scau.edu.cn (J.L.); allinchen@scau.edu.cn (T.C.); xqy0228@163.com (Q.X.)

^{*} Correspondence: jiajiesun@scau.edu.cn (J.S.); zhangyl@scau.edu.cn (Y.Z.); Tel: +86-139-2515-8841 (J.S.); +86-135-2780-3004 (Y.Z.)

[†] These authors contributed equally to this work.

[‡] Current address: College of Animal Science and Technology, Guangxi University, Nanning 530004, China.

[§] Current address: NHC Key Laboratory of Radiobiology, School of Public Health, Jilin University, Changchun 130062, China.

Abstract: (1) Background: As a novel type of non-coding RNA with a stable closed-loop structure, circular RNA (circRNA) can interact with microRNA (miRNA) and influence the expression of miRNA target genes. However, circRNA involved in pituitary growth hormone (GH) regulation is poorly understood. Our previous study revealed protein kinase C alpha (PRKCA) as the target gene of miR-709. Currently, the expression and function of rno_circRNA_0001004 in the rat pituitary gland is not clarified; (2) Methods: In this study, both bioinformatics analysis and dual-luciferase report assays showed a target relationship between rno_circRNA_0001004 and miR-709. Furthermore, the rno_circRNA_0001004 overexpression vector and si-circ_0001004 were constructed and transfected into GH₃ cells; (3) Results: We found that rno_circRNA_0001004 expression was positively correlated with the PRKCA gene and GH expression levels, while it was negatively correlated with miR-709. In addition, overexpression of rno-circ_0001004 also promoted proliferation and relieved the inhibition of miR-709 in GH₃ cells; (4) Conclusions: Our findings show that rno_circ_0001004 acts as a novel sponge for miR-709 to regulate GH synthesis and cell proliferation, and are the first case of discovery of the regulatory role of circRNA_0001004 in pituitary GH.

Keywords: pituitary; rno_circ_0001004; miR-709; GH; proliferation

Citation: Xiong, J.; Zhang, H.; Wang, Y.; Cheng, Y.; Luo, J.; Chen, T.; Xi, Q.; Sun, J.; Zhang, Y.

Rno_circ_0001004 Acts as a miR-709 Molecular Sponge to Regulate the Growth Hormone Synthesis and Cell Proliferation. *Int. J. Mol. Sci.* **2022**, *23*, 1413. <https://doi.org/10.3390/ijms23031413>

Academic Editor: Wolfgang Linert

Received: 28 December 2021

Accepted: 24 January 2022

Published: 26 January 2022

Publisher's Note: MDPI stays neutral with regard to jurisdictional claims in published maps and institutional affiliations.



Copyright: © 2022 by the authors. Licensee MDPI, Basel, Switzerland. This article is an open access article distributed under the terms and conditions of the Creative Commons Attribution (CC BY) license (<https://creativecommons.org/licenses/by/4.0/>).

1. Introduction

Growth hormone (GH) is a key hormone secreted from the anterior pituitary, and has received much attention as it regulates key physiological functions such as growth and development [1]. Studies have shown that microRNAs (miRNAs) can regulate the synthesis and secretion of GH [2–4]. MiRNAs are small single endogenous RNAs that regulate post-transcriptional silencing of target genes by binding to the 3'-untranslated region (UTR) or open reading frame (ORF) region of target mRNAs [5]. More and more evidence has demonstrated that miRNA functions broadly in development, physiology, and pathology by influencing cell proliferation, cell differentiation, cell migration, apoptosis, metabolism and signal transduction [6–11]. We have previously shown that the miR-709 is highly expressed in the pituitary and inhibits the GH synthesis and suppresses the viability of GH₃ cells [12] by targeting Protein Kinase C alpha (PKCA). Protein Kinase C (PKC) is a class of phospholipid-dependent kinases that participate in regulation of

protein secretion including GH and luteinizing hormone (LH) [13,14], as well as regulating cell proliferation [15].

Circular RNA (circRNA) is a special type of non-coding RNA (ncRNA) molecule that, unlike traditional linear RNA, forms covalently closed loop structures generated by pre-mRNA back splicing. CircRNAs are highly stable, abundant and conserved molecules with the characteristics of cell tissue specificity [16] and have received more attention due to their multiple regulation functions in animals and plants [17–19]. Similar to other regulatory ncRNAs, circRNAs play important roles in various biological processes, such as acting as a scaffold in the assembly of protein complexes [20–22], regulating alternative RNA splicing or transcription and RNA-protein interactions [23,24] and functioning as competing endogenous RNA (ceRNA) [25] or microRNA (miRNA) sponges [26–31]. However, reports of circRNAs involved in pituitary GH regulation have been very scarce up to the present [32,33].

The rno_circ_0001004 was firstly discovered in the rat anterior pituitary by using Illumina sequencing [34]. It is generated from exons 9 to 11 of the Wnk2 gene, with a length of 888 bp. However, the underlying regulatory role of rno_circ_0001004 in the pituitary remains unknown. Thus, in the present study, the role of rno_circ_0001004 in the regulation of GH and cell proliferation and the circRNA-miRNA-mRNA network were explored and identified.

2. Results

2.1. Characterization of Rno_circ_0001004 in GH₃ Cells

To characterize rno_circ_0001004 in GH₃ cells, we firstly detected the expression of rno_circ_0001004. Convergent and divergent primers were designed to amplify the linear or back-splicing products and total RNA from GH₃ cells with or without RNase R treatment was subjected to RT-PCR. As expected, endogenous circ_0001004, but not pre-mRNA, was resistant to RNase R digestion (Figure 1A). Sanger sequencing validated the back-spliced junction of rno_circ_0001004 (Figure 1B).

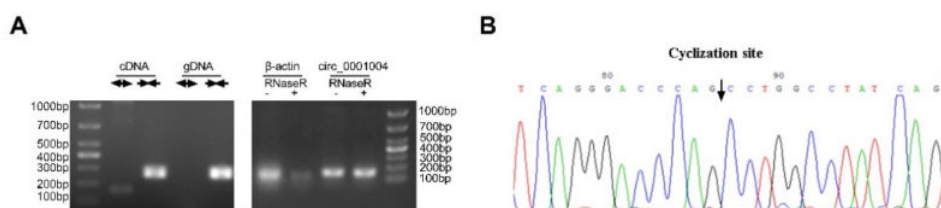


Figure 1. Characterization of rno_circ_0001004 in a GH₃ cell. (A) PCR analysis for rno_circ_0001004 in the cDNA and gDNA of a GH₃ cell. (left) Total RNA from GH₃ cells with or without RNase R treatment was subjected to RT-PCR. (right) (B) The back-splice junction of rno_circ_0001004 was identified by Sanger sequencing.

2.2. Rno_circ_0001004 Antagonizes miR-709-Mediated Repression of GH Synthesis and Secretion

Bioinformatics analysis with RNAhybird and miRanda was performed and indicated that rno_circ_0001004 has miR-709 binding sites (Figure 2A). Then, a dual-luciferase reporter assay showed that miR-709 overexpression was able to down-regulate the luciferase activity compared to miR-NC, and this inhibition was eliminated when the rno_circ_0001004 binding site was mutated (Figure 2B). To confirm their target relationship, the rno_circ_0001004 overexpression vector was constructed (Figure 2C), and after transfection into a GH₃ cell, rno_circ_0001004 was overexpressed and miR-709 was correspondingly down-regulated (Figure 2D). The results above suggest that rno_circ_0001004 is a molecular sponge for miR-709. Our previous studies demonstrated that miR-709 significantly inhibited the GH synthesis by targeting PKCA [12]. Thus, we further detected

the change in PKC α pathway and GH expression and release. Interestingly, our results show that rno_circ_0001004 obviously increases the mRNA and protein levels of PKC α , the phosphorylation of ERK1/2 (Figure 2E,F) and GH protein within cell as well as supernatant, compared to empty vectors (Figure 2F,G). These results confirm that rno_circ_0001004 antagonizes miR-709-mediated repression of the GH synthesis and secretion through the PKC α pathway.

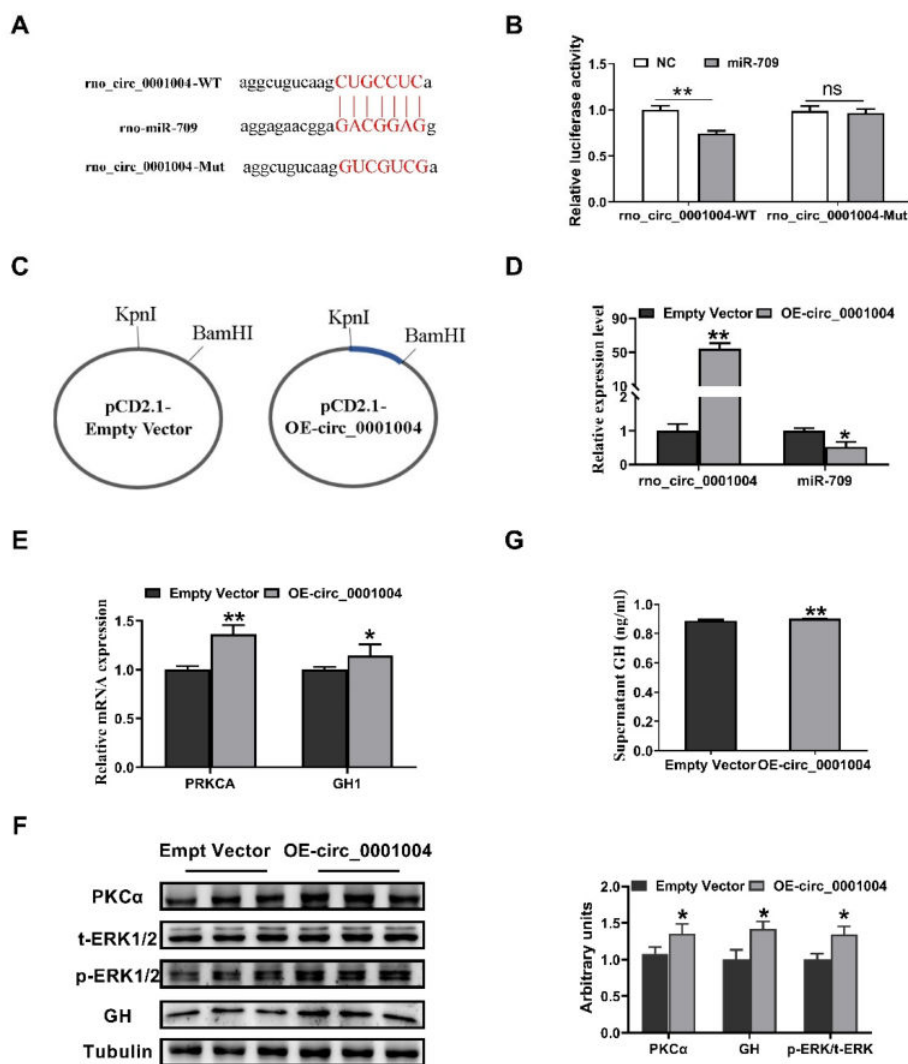


Figure 2. Rno_circ_0001004 antagonizes miR-709-mediated repression the synthesis and secretion of GH. (A) Bioinformatics target prediction. (B) Dual luciferase reporter gene assay verified. (C) Construction of rno_circ_0001004 overexpression vector. (D) Expression of rno_circ_0001004 along with miR-709 in empty vector and overexpression vector in GH₃ by qRT-PCR. (E) mRNA level of PKC α and GH1 after transfection of OE-circ_0001004. (F) Western blot evaluation results of PKC α , t-ERK1/2, p-ERK1/2 and GH protein expression following transfection with rno_circ_0001004 in GH₃ cells. (G) changes in supernatant GH level: average expression rose from 0.87 to 0.9 ng/mL. (* < 0.05; ** p < 0.01.)

2.3. Knockdown of *Rno_circ_0001004* Suppresses the GH Synthesis and Secretion in GH₃ Cell

In order to further verify the effect of *rno_circ_0001004* on GH, we transfected si-*circ_0001004* to GH₃ cells. As expected, si-*circ_0001004* significantly decreased the expression of *circ_0001004*, while it correspondingly increased the miR-709 expression level, followed by the inhibition of mRNA in *PRKCA* and *GH1* (Figure 3A). Furthermore, a Western blot revealed that the protein expression of PKC α , the phosphorylation of ERK1/2, and GH both in cell and supernatant all decreased with the inhibition of *circ_0001004* (Figure 3B,C). The above results further confirm that *rno_circ_0001004* regulates the synthesis and secretion of GH by acting as a molecular sponge for miR-709.

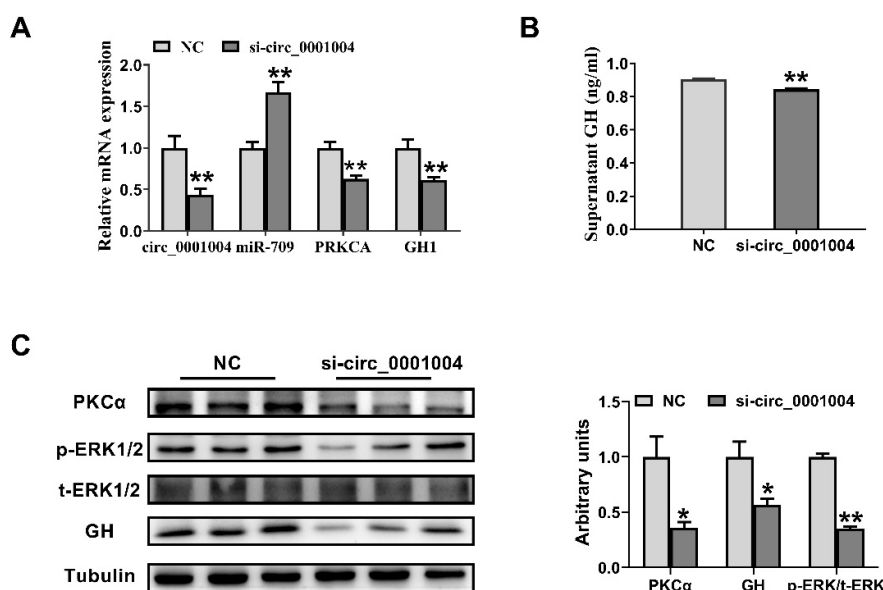


Figure 3. Knockdown of *rno_circ_0001004* promoted the GH synthesis and suppressed GH₃ cells. (A) The mRNA level of *PRKCA* and *GH1* along with *circ_0001004* and miR-709 expression after transfection si-*circ_0001004*. (B) The changes in supernatant GH level after transfection si-*circ_0001004*. (C) The PKC α , t-ERK1/2, p-ERK1/2 and GH protein expression levels in GH₃ cells after transfection si-*circ_0001004*. (* $p < 0.05$; ** $p < 0.01$.)

2.4. *Rno_circ_0001004* Promoted the Viability of GH₃ Cells

Our previous study showed that miR-709 suppressed the viability of GH₃ cells [12]. Thus, we performed CCK8 and EdU assays to determine the effect of *rno_circ_0001004* on GH₃ cell proliferation. Intriguingly, *circ_0001004* significantly promoted GH₃ cell proliferation (Figure 4A,B). Moreover, PCNA, the key marker of cell proliferation, was markedly up-regulated both in mRNA and protein levels (Figure 4C,D).

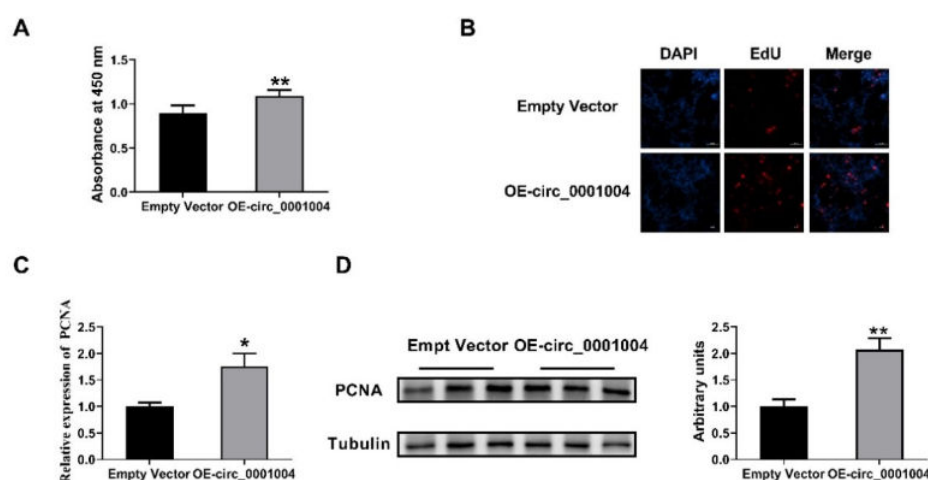


Figure 4. Rno_circ_0001004 promoted the viability of GH₃ cells (A) The GH₃ proliferation was evaluated with CCK-8 kits. (B) Cell proliferation tested by an EdU assay. (C) PCNA mRNA expression quantified by qRT-PCR. (D) Western blot assay for PCNA protein expression. (* $p < 0.05$; ** $p < 0.01$.)

2.5. Rno_circ_0001004 Reversed the Inhibition of Cell Proliferation by miR-709

In order to further confirm the idea that rno_circ_0001004 serves as a ceRNA for miR-709 to regulate the viability of GH₃ cells, we next co-transfected miR-709 mimics and circ_0001004 into GH₃ cells. The results demonstrates that overexpression of miR-709 obviously inhibits the cell proliferation of GH₃, and this inhibition is perfectly rescued by overexpression of rno_circ_0001004, as shown by CCK8 assay (Figure 5A), EdU assay (Figure 5B) and PCNA expression (Figure 5C,D). These results provide more profound evidence that rno_circ_0001004 is a sponge ceRNA for miR-709.

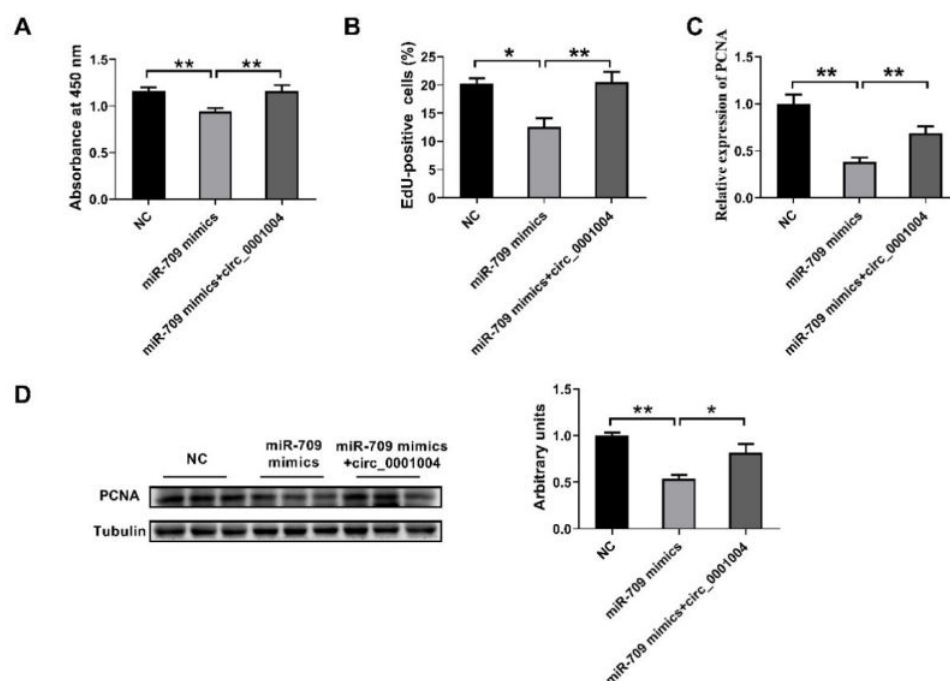


Figure 5. Effects of rno_circ_0001004 in reversing the inhibition of cell proliferation by miR-709. (A) The GH₃ proliferation was evaluated with CCK-8 kits. (B) EdU-positive cells. (C) PCNA mRNA

expression quantified by qRT-PCR. (D) Western blot assay for PCNA protein expression. (* $p < 0.05$; ** $p < 0.01$.)

3. Discussion

The pituitary gland, called the ‘master gland’ of the endocrine system, is the central regulator for growth, reproduction, metabolism and stress response [35]. The anterior pituitary accounts for 80% of the entire pituitary gland and secretes six major hormones, which are crucial to our physiological well-being [36,37]. As a major hormone in the pituitary gland, GH plays an important role in regulating the growth and metabolism of organisms [38,39].

MiRNAs are a class of small ncRNA with a length of about 22 nucleotides that post-transcriptionally regulate gene expression [40]. MiRNA generally functions primarily by binding to the 3′ untranslated region (UTR) of the target mRNA [41]. They play important roles in essential processes such as cell proliferation, cell apoptosis and cell differentiation [42,43]. miRNA was reported to participate in regulating GH. MiR-34b, miR-326, miR-432, miR-548c and miR-570 were found to regulate pituitary cell proliferation [44]. miR-126 played an important role in the development of GH-secreting pituitary adenomas [2]. Our previous study showed that miR-709 inhibited the GH synthesis and suppressed the viability of GH₃ cells by targeting PRKCA [12].

CircRNAs are derived from the exon or intron region of genes [45]. There are currently three hypothetical models for the mechanism of circRNA formation, including lariat-driven circularization, intron pairing-driven circularization, and RNA binding protein (RBP)-mediated circularization [46]. CircRNAs containing multiple competing miRNA binding sites are likely to act as ceRNA in reducing miRNA activity and up-regulating the expression of miRNA-related target genes [47]. Thousands of strongly and stably expressed circRNAs have been detected [26]. CircFGFR4 promotes the differentiation of myoblasts by binding miR-107 [48]. Circ0005276 can promote the proliferation and migration of prostate cancer cells [49]. Circ-ZNF609 regulates nasopharyngeal carcinoma cell growth via modulating miR-188 expression [50]. Some studies have identified circRNAs in the pituitary gland [51–54]. At present, there have been few reports of circRNA regulating GH.

In the present study, we firstly noted that rno_circ_0001004 has the potential to act as miR-709 binding sites. Then, characterization of rno_circ_0001004 was carried out and the target relationship with miR-709 was validated using a dual luciferase assay. To further probe the influence of rno_circ_0001004 on GH, the overexpression of a rno_circ_0001004 vector and si-circ_0001004 were constructed. Next, the genes and proteins in the pathway of miR-709 regulation of GH were all evaluated. The results show that the expression trend of rno_circ_0001004 is almost opposite to that of miR-709, but is consistent with the expression trend of PKC α , GH and the phosphorylation of ERK1/2. Thus, our findings firstly clarify the molecular mechanism by which rno_circ_0001004 can act as a sponge for miR-709 in regulating the synthesis and secretion of GH, providing novel insight into the regulatory mechanism of GH.

Our prior study also found that miR-709 repressed the viability of GH₃ cells [12]. Thus, we explored whether rno_circR_0001004 affected the proliferation of GH₃ cells. Compared with the empty vector, the rno_circ_0001004 overexpression group can significantly promote the proliferation of GH₃ cells, as determined by the CCK-8 assay, PCNA expression and the EdU incorporation assay. Moreover, rno_circ_0001004 was able to perfectly reverse the inhibitory effect of miR-709 on the proliferation of GH₃ cells. Therefore, our study reveals that rno_circ_0001004 is able to positively regulate GH₃ cell viability. These results indicate that rno_circ_0001004 plays an essential role in the regulation GH and pituitary cell proliferation. Furthermore, they lay a foundation for further study to explore the importance of circ_0001004 in regulation of animal and human growth and development.

4. Materials and Methods

4.1. Cell Culture and Transfection

GH₃ cell line (ATCC) was cultured in F12 (Gibco, New York, NY, USA) medium supplemented with 2.5% fetal bovine serum (FBS) (Gibco, New York, NY, USA), 15% horse serum (Hyclone, Logan, UT, USA) and 1% penicillin/streptomycin (Gibco, New York, NY, USA). Hela cells were cultured in PRMI 1640 (Gibco, New York, NY, USA) culture medium with 10% FBS and 1% penicillin/streptomycin. GH₃ cells were transfected with miR-709 mimic, rno_circ_0001004 or si-circ0001004 using Lipofectamine 2000 (Invitrogen, Carlsbad, CA, USA). The cells were incubated at 37 °C in a humidified atmosphere of 5% CO₂.

4.2. RAN Isolation, cDNA Synthesis, RT-PCR and Sanger Sequencing

Total RNA was isolated from GH₃ cells by Trizol reagent (Invitrogen, Carlsbad, CA, USA) according to the manufacturer's protocol. The cDNAs were obtained by Color Reverse Transcription Kit (with gDNA remover) (EZBioscience, Roseville, CA, USA). Genomic DNA (gDNA) was extracted using a Genomic DNA Isolation Kit (Sangon Biotech, Shanghai, China). Quantification of mRNA, miRNA, circRNA and gDNA was performed by using a SBRY Green PCR Kit (Takara, Tokyo, Japan), primers and Real-Time PCR System (Bio-Rad Laboratories, Inc., Hercules, CA, USA). The circRNA and mRNA levels were normalized to those of β -actin, while the miR-709 levels were normalized to the U6 and determined by 2- $\Delta\Delta$ Ct method. The primer sequences for the amplification of specific primers are listed in supplementary Table S1. Sanger sequencing (chain termination sequencing) is a method of DNA sequencing based upon the selective incorporation of chain-terminating dideoxynucleotides (ddNTPs) during in vitro DNA replication [55].

4.3. Vector Construction

The sequence for exons 9–11 of Wnk2 was PCR amplified using primers F (5'-GGGG-TACCTGAAATATGCTATCTTACAGCCTGGCCTATCAGTGGGC-3') and R (5'-CGG-GATCCTCAAGAAAAAATATATTCACCTGGGTCCCTGAGGCAGC-3'), then cloned into KpnI and BamHI restriction sites of a circular expression vector, the pcd2.1-ciR (GEN-ESEED, Guangzhou, China), by digestion to create rno_circ_0001004-overexpressing vector.

4.4. Dual-Luciferase Reporter Assay

Hela cells were seeded in 96-well cell culture plates. When their confluence reached about 80%, the miR-709 mimic and rno_circ_0001004-Wt or rno_circ_0001004-Mut were co-transfected into cells using Lipofectamine 2000. After incubation for 48 h, the cells were washed with PBS and the luciferase activity was measured by the Dual-GLO luciferase reporter assay system (Promega, Madison, WI, USA) according to the manufacturer's instructions.

4.5. Evaluation of GH₃ Proliferation

GH₃ proliferation was assessed by the cell counting kit-8 (CCK-8) method, 5-ethynyl-2'-deoxy uridine (EdU) incorporation assay and proliferating cell nuclear antigen (PCNA) expression. Firstly, the rate of GH₃ proliferation was determined with the CCK-8 kit (Bioss, Beijing, China) according to the manufacturer's instructions. The number of viable cells was assessed by measuring the absorbance at 450 nm using a Synergy 2 Multi-Mode Reader (Bio Tek Instruments, Inc., Winooski, VT, USA). Secondly, DNA synthesis was examined with EdU incorporation assay (YF® 555 Click-iT EdU Imaging Kit, Suzhou US EVERBRIGHT, Suzhou, China) to evaluate GH₃ proliferation. The EdU positive cells were counted and normalized by the total number of Hoechst 33,342 stained cells. Lastly, GH₃

proliferation was evaluated by PCNA expression, which is the auxiliary component of DNA polymerase δ and constitutes a useful proliferation marker.

4.6. Western Blot Analysis

GH₃ cells were lysed in a RIPA lysis buffer (Beyotime Institute of Biotechnology, Shanghai, China) containing 1mM phenyl methane sulfonyl fluoride (PMSF). The concentration of protein was measured using the BCA Protein Assay Kit (Thermo Fisher Scientific, Waltham, MA, USA) according to the manufacturer's instructions. Equal amounts of total protein were separated by SDS-PAGE and transferred to a PVDF membrane in a tris-glycine methanol buffer. The primary antibodies used in this study were as follows: GH monoclonal antibody (sc-374266, Santa Cruz, CA, USA), PKC α polyclonal antibody (BS1577, Bioworld, St. Louis Park, MN, USA), ERK1/2 monoclonal antibody (4695, CST, Danvers, MA, USA), Phospho-ERK1/2 monoclonal antibody (Tyr204) (4370, CST, Danvers, MA, USA), PCNA monoclonal antibody (200947-2E1, ZEN BIO, Chengdu, China) and Tubulin polyclonal antibody (AP0064, Bioworld, St. Louis Park, MN, USA), HRP conjugated goat anti-rabbit IgG (BS13278, Bioworld, St. Louis Park, MN, USA) and HRP conjugated goat anti-mouse IgG (BS12478, Bioworld, St. Louis Park, MN, USA) were used as secondary antibodies. The membranes were incubated with ImmobilonTM Western Chemiluminescent HRP Substrate (Millipore, Burlington, WA, USA) and scanned with a FluorChem M Fluorescent Western Imaging System (Protein Simple, Santa Clara, CA, USA). The protein band density was determined by the software Image J and normalized with a corresponding Tubulin intensity.

4.7. Quantification of Secretory GH by ELISA

The concentration of GH in a cell medium of GH₃ cells transfected with rno_circ_0001004 and si-circ_0001004 was determined using the reagents in the Rat Growth Hormone ELISA kit (Enzyme-linked Biotechnology, Shanghai, China) according to the manufacturer's protocols. Color alterations in the wells were read using the 96-well microplate reader (Bio Tek Instruments, Inc., Winooski, VT, USA).

4.8. Statistics Analysis

All experimental results are presented as the mean \pm S.E.M, with at least three independent replications. Statistical analysis was performed using SPSS 17.0 software. The statistically significant differences among groups were tested by one-way analysis of variance (ANOVA). $p < 0.05$ was considered as statistically significant. * $p < 0.05$; ** $p < 0.01$.

5. Conclusions

In summary, our study reveals that rno_circ_0001004 competitively binds miR-709 to regulate the GH synthesis and cell proliferation in rat pituitary cells (Figure 6). To the best of our knowledge, our findings are the first case to illustrate regulation of GH by circRNA_0001004 and provide novel evidence on the circRNA-miRNA-mRNA network in pituitary cells.

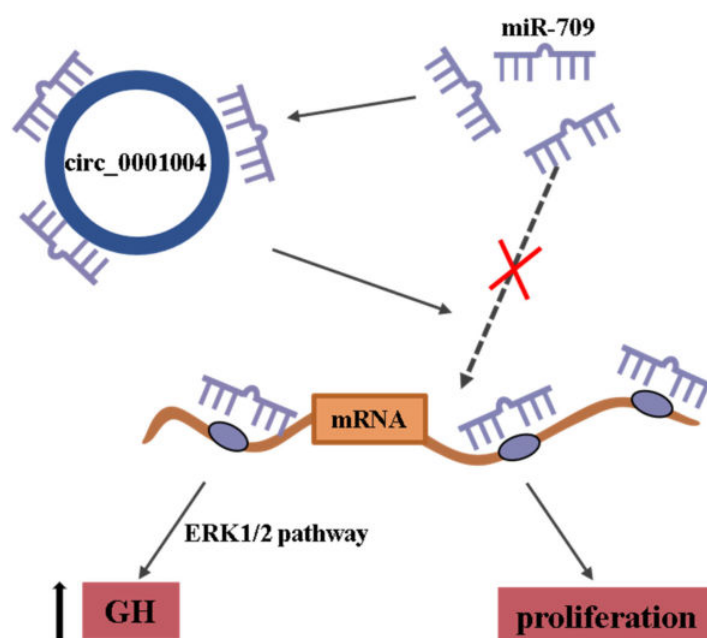


Figure 6. Rno_circ_0001004 has 3 miR-709 binding sites and can act as a miR-709 molecular sponge to regulate GH synthesis and cell proliferation.

Supplementary Materials: The following supporting information can be downloaded at: www.mdpi.com/article/10.3390/ijms23031413/s1.

Author Contributions: Methodology, Y.Z. and Q.X.; software, J.S.; validation, J.X., H.Z. and Y.W.; data curation, Y.C.; writing—original draft preparation, J.X.; writing—review and editing, Y.Z.; supervision, J.L. and T.C.; project administration, Y.Z. All authors have read and agreed to the published version of the manuscript.

Funding: This research was funded by the National Natural Science Foundation of China, grant numbers 31802156, 32072814 and 32072812; Natural Science Foundation of Guangzhou City, grant numbers 2021A1515011310 and 2020A1515010062.

Institutional Review Board Statement: Not applicable.

Informed Consent Statement: Not applicable.

Data Availability Statement: Not applicable.

Conflicts of Interest: The authors declare no conflict of interest.

References

1. Nyberg, F. Growth Hormone in the Brain: Characteristics of Specific Brain Targets for the Hormone and Their Functional Significance. *Front. Neuroendocrinol.* **2000**, *21*, 330–348.
2. Mao, Z.G.; He, D.S.; Zhou, J.; Yao, B.; Xiao, W.W.; Chen, C.H.; Zhu, Y.H.; Wang, H.J. Differential expression of microRNAs in GH-secreting pituitary adenomas. *Diagn. Pathol.* **2010**, *5*, 79.
3. Zhang, Z. Florez Sergio Gutierrez-Hartmann Arthur Martin James, F.; Amendt Brad, A. MicroRNAs Regulate Pituitary Development, and MicroRNA 26b Specifically Targets Lymphoid Enhancer Factor 1 (Lef-1), Which Modulates Pituitary Transcription Factor 1 (Pit-1) Expression. *J. Biol. Chem.* **2010**, *285*, 34718–34728.
4. Yu, Z.W.; Gao, W.; Feng, X.Y.; Zhang, J.Y.; Yuan, B. Roles of differential expression of miR-543-5p in GH regulation in rat anterior pituitary cells and GH3 cells. *PLoS ONE* **2019**, *14*, e0222340.
5. Liu, Y.W. MicroRNAs: Genomics, Biogenesis, Mechanism, and Function. *Cell* **2004**, *116*, 281–297.
6. Gee, H.E.; Camps, C.; Buffa, F.M.; Colella, S.; Sheldon, H.; Gleadow, J.M.; Ragoussis, J.; Harris, A.L. MicroRNA-10b and breast cancer metastasis. *Nature* **2008**, *455*, E8.
7. Kota, J.; Chivukula, R.R.; O'Donnell, K.A.; Wentzel, E.A.; Montgomery, C.L.; Hwang, H.W.; Chang, T.C.; Vivekanandan, P.; Torbenson, M.; Clark, K.R. Therapeutic delivery of miR-26a inhibits cancer cell proliferation and induces tumor-specific apoptosis. *Cell* **2009**, *137*, 1005.

8. Ma, L.; Teruya-Feldstein, J.; Weinberg, R.A. Tumour invasion and metastasis initiated by microRNA-10b in breast cancer. *Nature* **2007**, *449*, 682–688.
9. Png, K.J.; Halberg, N.; Yoshida, M.; Tavazoie, S.F. A microRNA regulon that mediates endothelial recruitment and metastasis by cancer cells. *Nature* **2012**, *481*, 190–194.
10. Tay, Y.; Zhang, J.; Thomson, A.M.; Bing, L.; Rigoutsos, I. MicroRNAs to Nanog, Oct4 and Sox2 coding regions modulate embryonic stem cell differentiation. *Nature* **2008**, *455*, 1124.
11. Felekis, K.; Touvana, E.; Stefanou, C.; Deltas, C. MicroRNAs: A newly described class of encoded molecules that play a role in health and disease. *Hippokratia* **2010**, *14*, 236–240.
12. Cheng, Y.; Chen, T.; Song, J.; Qi, Q.; Zhang, Y. miR-709 inhibits GHRP6 induced GH synthesis by targeting PRKCA in pituitary. *Mol. Cell. Endocrinol.* **2020**, *506*, 110763.
13. Grey, C.L.; Chang, J.P. Differential modulation of ghrelin-induced GH and LH release by PACAP and dopamine in goldfish pituitary cells. *Gen. Comp. Endocrinol.* **2013**, *191*, 215–224.
14. Pemberton, J.G.; Orr, M.E.; Stafford, J.L.; Chang, J.P. PI3K signalling in GnRH actions on dispersed goldfish pituitary cells: Relationship with PKC-mediated LH and GH release and regulation of long-term effects on secretion and total cellular hormone availability. *Gen. Comp. Endocrinol.* **2014**, *205*, 268–278.
15. Petiti, J.P.; Gutiérrez, S.; De Paul, A.L. Andreoli: GH3B6 Pituitary Tumor Cell Proliferation is Mediated by PKC α and PKC ϵ via ERK 1/2-dependent Pathway. *Cell Physiol. Biochem.* **2010**, *26*, 135–146.
16. Meng, S.; Zhou, H.; Feng, Z.; Xu, Z.; Ying, T.; Li, P.; Wu, M. CircRNA: Functions and properties of a novel potential biomarker for cancer. *Mol. Cancer* **2017**, *16*, 94.
17. Chen, L.L.; Yang, L. Regulation of circRNA biogenesis. *RNA Biol.* **2015**, *12*, 381–388.
18. Circular RNAs Are the Predominant Transcript Isoform from Hundreds of Human Genes in Diverse Cell Types. *PLoS ONE* **2012**, *7*, e30733.
19. Ye, C.Y.; Chen, L.; Liu, C.; Zhu, Q.H.; Fan, L. Widespread noncoding circular RNAs in plants. *New Phytol.* **2015**, *208*, 88–95.
20. Du, W.W.; Fang, L.; Yang, W.; Wu, N.; Awan, F.M.; Yang, Z.; Yang, B.B. Induction of tumor apoptosis through a circular RNA enhancing Foxo3 activity. *Cell Death Differ.* **2017**, *24*, 357–370.
21. Du, W.W.; Yang, W.; Liu, E.; Yang, Z.; Yang, B.B. Foxo3 circular RNA retards cell cycle progression via forming ternary complexes with p21 and CDK2. *Nucleic Acids Res.* **2016**, *44*, gkw027.
22. Zeng, Y.; Du, W.W.; Wu, Y.; Yang, Z.; Awan, F.M.; Li, X.; Yang, W.; Zhang, C.; Yang, Q.; Yee, A.; et al. A Circular RNA Binds To and Activates AKT Phosphorylation and Nuclear Localization Reducing Apoptosis and Enhancing Cardiac Repair. *Theranostics* **2017**, *7*, 3842–3855.
23. Ashwal-Fluss, R.; Meyer, M.; Pamudurti, N.R.; Ivanov, A.; Bartok, O.; Hanan, M.; Evtantal, N.; Memczak, S.; Rajewsky, N.; Kadener, S. circRNA Biogenesis Competes with Pre-mRNA Splicing—ScienceDirect. *Mol. Cell* **2014**, *56*, 55–66.
24. Salzman, J. Circular RNA Expression: Its Potential Regulation and Function. *Trends Genet.* **2016**, *32*, 309–316.
25. Huang, M.; Zhong, Z.; Lv, M.; Shu, J.; Tian, Q.; Chen, J. Comprehensive analysis of differentially expressed profiles of lncRNAs and circRNAs with associated co-expression and ceRNA networks in bladder carcinoma. *Oncotarget* **2016**, *7*, 47186.
26. Memczak, S.; Jens, M.; Elefsinioti, A.; Torti, F.; Krueger, J.; Rybak, A.; Maier, L.; Mackowiak, S.D.; Gregersen, L.H.; Munschauer, M.; et al. Circular RNAs are a large class of animal RNAs with regulatory potency. *Nature* **2013**, *495*, 333–338.
27. Hansen, T.B.; Jensen, T.I.; Clausen, B.H.; Bramsen, J.B.; Finsen, B.; Damgaard, C.K.; Kjems, J. Natural RNA circles function as efficient microRNA sponges. *Nature* **2013**, *495*, 384–388.
28. Lei, P.; Chen, G.; Zhu, Z.; Shen, Z.; Du, C.; Zang, R.; Yang, S.; Hua, X.; Li, H.; Xu, X. Circular RNA ZNF609 functions as a competitive endogenous RNA to regulate AKT3 expression by sponging miR-150-5p in Hirschsprung's disease. *Oncotarget* **2017**, *8*, 808.
29. Li, F.; Zhang, L.; Li, W.; Deng, J.; Zheng, J.; An, M.; Lu, J.; Zhou, Y. Circular RNA ITCH has inhibitory effect on ESCC by suppressing the Wnt/ β -catenin pathway. *Oncotarget* **2015**, *6*, 6001.
30. Wang, K.; Long, B.; Liu, F.; Wang, J.X.; Li, P.F. A circular RNA protects the heart from pathological hypertrophy and heart failure by targeting miR-223. *Eur. Heart J.* **2016**, *37*, ehv713.
31. Zheng, Q.; Bao, C.; Guo, W.; Li, S.; Chen, J.; Chen, B.; Luo, Y.; Lyu, D.; Li, Y.; Shi, G. Circular RNA profiling reveals an abundant circHIPK3 that regulates cell growth by sponging multiple miRNAs. *Nat. Commun.* **2016**, *7*, 11215.
32. Du, Q.; Zhang, W.; Feng, Q.; Hao, B.; Cheng, C.; Cheng, Y.; Li, Y.; Fan, X.; Chen, Z. Comprehensive circular RNA profiling reveals that hsa_circ_0001368 is involved in growth hormone-secreting pituitary adenoma development. *Brain Res. Bull.* **2020**, *161*, 65–77. <https://doi.org/10.1016/j.brainresbull.2020.04.018>.
33. Yu, Z.W.; Ren, W.Z.; Wang, T.; Zhang, W.D.; Yuan, B. CircAgtpbp1 Acts as a Molecular Sponge of miR-543-5p to Regulate the Secretion of GH in Rat Pituitary Cells. *Animals* **2021**, *11*, 558.
34. Han, D.X.; Sun, X.L.; Fu, Y.; Wang, C.J.; Liu, J.B.; Jiang, H.; Gao, Y.; Chen, C.Z.; Yuan, B.; Zhang, J.B. Identification of long non-coding RNAs in the immature and mature rat anterior pituitary. *Sci. Rep.* **2017**, *7*, 17780.
35. Scully, K.M.; Rosenfeld, M.G. Pituitary Development: Regulatory Codes in Mammalian Organogenesis. *Science* **2002**, *295*, 2231–2235.
36. Hagerjohnson, G. An Introduction to Behavioral Endocrinology. *Q. Rev. Biol.* **2011**, *2*, 273–282.
37. Tissier, P.; Hodson, D.J.; Lafont, C.; Fontanaud, P.; Mollard, P. Anterior pituitary cell networks. *Front. Neuroendocrinol.* **2012**, *33*, 252–266.

38. Isaksson, O.; Lindahl, A.; Nilsson, A.; Isgaard, J. Mechanism of the stimulatory effect of growth hormone on longitudinal bone growth. *Endocr. Rev.* **1987**, *8*, 426–438.
39. Salomon, F.; Cuneo, R.C. The effects of treatment with recombinant human growth hormone on body composition and metabolism. *N. Engl. J. Med.* **1989**, *321*, 1797–1797.
40. Carthew, R.W.; Sontheimer, E.J. Origins and mechanisms of miRNAs and siRNAs. *Cell* **2009**, *136*, 642–655.
41. He, L.; Hannon, G.J. MicroRNAs: Small RNAs with a big role in gene regulation. *Nat. Rev. Genet.* **2004**, *5*, 522–531.
42. Miska, E.A. How microRNAs control cell division, differentiation and death. *Curr. Opin. Genet. Dev.* **2005**, *15*, 563–568.
43. Zamore, P.; Haley, B. Ribo-gnome: The Big World of Small RNAs. *Science* **2005**, *309*, 1519–1524.
44. Daniela, D.A.; Dario, P.; Paula, M.; Magali, R.; Anne, W.; Gerald, R.; Monica, F.; Maria, C.C.; Jacqueline, T.; Alfredo, F. Altered microRNA expression profile in human pituitary GH adenomas: Down-regulation of miRNA targeting HMGA1, HMGA2, and E2F1. *J. Clin. Endocrinol. Metab.* **2012**, *97*, E1128–E1138.
45. Xiang, L.; Li, Y.; Chen, L.L. The Biogenesis, Functions, and Challenges of Circular RNAs. *Mol. Cell* **2018**, *71*, 428–442.
46. Jeck, W.R.; Sorrentino, J.A.; Wang, K.; Slevin, M.K.; Burd, C.E.; Liu, J.; Marzluff, W.F.; Sharpless, N.E. Circular RNAs are abundant, conserved, and associated with ALU repeats. *Rna* **2013**, *19*, 141–157.
47. Qu, S.; Zhong, Y.; Shang, R.; Zhang, X.; Song, W.; Kjems, J.; Li, H. The emerging landscape of circular RNA in life processes. *RNA Biol.* **2017**, *14*, 992–999.
48. Li, H.; Wei, X.; Yang, J.; Dong, D.; Hao, D.; Huang, Y.; Lan, X.; Plath, M.; Lei, C.; Ma, Y. circFGFR4 Promotes Differentiation of Myoblasts via Binding miR-107 to Relieve Its Inhibition of Wnt3a. *Mol. Ther. Nucleic Acids* **2018**, *11*, 272–283.
49. Feng, Y.; Yang, Y.; Zhao, X.; Fan, Y.; Zhou, L.; Rong, J.; Yu, Y. Circular RNA circ0005276 promotes the proliferation and migration of prostate cancer cells by interacting with FUS to transcriptionally activate XIAP. *Cell Death Dis.* **2019**, *10*, 792.
50. Li, M.; Li, Y.; Yu, M. CircRNA ZNF609 Knockdown Suppresses Cell Growth via Modulating miR-188/ELF2 Axis in Nasopharyngeal Carcinoma. *OncoTargets Ther.* **2020**, *13*, 2399–2409.
51. Guo, H.X.; Yuan, B.; Su, M.T.; Zheng, Y.; Zhang, J.B. Identification of Circular RNAs in the Anterior Pituitary in Rats Treated with GnRH. *Animals* **2021**, *11*, 2557.
52. Han, D.X.; Wang, C.J.; Sun, X.L.; Liu, J.B.; Zhang, J.B. Identification of circular RNAs in the immature and mature rat anterior pituitary. *J. Endocrinol.* **2019**, *240*, 393–402.
53. Li, C.; Li, X.; Ma, Q.; Zhang, X.; Cao, Y.; Yao, Y.; You, S.; Wang, D.; Quan, R.; Hou, X. Genome-wide analysis of circular RNAs in prenatal and postnatal pituitary glands of sheep. *Sci. Rep.* **2017**, *7*, 16143.
54. Zhang, H.; Hu, B.; Xiong, J.; Chen, T.; Zhang, Y. Genomewide analysis of circular RNA in pituitaries of normal and heat-stressed sows. *BMC Genom.* **2019**, *20*, 1013.
55. Sanger, F.; Nicklen, S.; Coulson, A.R. DNA sequencing with chain-terminating inhibitors. *Proc. Natl. Acad. Sci. USA* **1977**, *74*, 5463–5467.



Article

Skeletal Muscle-Derived Exosomal miR-146a-5p Inhibits Adipogenesis by Mediating Muscle-Fat Axis and Targeting GDF5-PPAR γ Signaling

Mengran Qin ^{1,†}, Lipeng Xing ^{1,†}, Jiahao Wu ¹, Shulei Wen ¹, Junyi Luo ¹, Ting Chen ¹, Yaotian Fan ¹, Jiahao Zhu ¹, Lekai Yang ¹, Jie Liu ¹, Jiali Xiong ¹, Xingping Chen ², Canjun Zhu ¹, Songbo Wang ¹, Lina Wang ¹, Gang Shu ¹, Qingyan Jiang ¹, Yongliang Zhang ¹, Jiajie Sun ^{1,*} and Qianyun Xi ^{1,*}

¹ Guangdong Provincial Key Laboratory of Animal Nutrition Control, State Key Laboratory of Livestock and Poultry Breeding, National Engineering Research Center for Breeding Swine Industry, College of Animal Science, South China Agricultural University, No. 483 Wushan Road, Guangzhou 510642, China

² Jiangxi Province Key Laboratory of Animal Nutrition, College of Animal Science and Technology, Jiangxi Agricultural University, Nanchang 330045, China

* Correspondence: jiajiesun@scau.edu.cn (J.S.); xqy0228@scau.edu.cn (Q.X.)

† These authors contributed equally to this work.

Abstract: Skeletal muscle-fat interaction is essential for maintaining organismal energy homeostasis and managing obesity by secreting cytokines and exosomes, but the role of the latter as a new mediator in inter-tissue communication remains unclear. Recently, we discovered that miR-146a-5p was mainly enriched in skeletal muscle-derived exosomes (SKM-Exos), 50-fold higher than in fat exosomes. Here, we investigated the role of skeletal muscle-derived exosomes regulating lipid metabolism in adipose tissue by delivering miR-146a-5p. The results showed that skeletal muscle cell-derived exosomes significantly inhibited the differentiation of preadipocytes and their adipogenesis. When the skeletal muscle-derived exosomes co-treated adipocytes with miR-146a-5p inhibitor, this inhibition was reversed. Additionally, skeletal muscle-specific knockout miR-146a-5p (mKO) mice significantly increased body weight gain and decreased oxidative metabolism. On the other hand, the internalization of this miRNA into the mKO mice by injecting skeletal muscle-derived exosomes from the Flox mice (Flox-Exos) resulted in significant phenotypic reversion, including down-regulation of genes and proteins involved in adipogenesis. Mechanistically, miR-146a-5p has also been demonstrated to function as a negative regulator of peroxisome proliferator-activated receptor γ (PPAR γ) signaling by directly targeting growth and differentiation factor 5 (GDF5) gene to mediate adipogenesis and fatty acid absorption. Taken together, these data provide new insights into the role of miR-146a-5p as a novel myokine involved in the regulation of adipogenesis and obesity via mediating the skeletal muscle-fat signaling axis, which may serve as a target for the development of therapies against metabolic diseases, such as obesity.

Keywords: skeletal muscle; exosomes; miR-146a-5p; adipogenesis; GDF5; crosstalk; PPAR γ



Citation: Qin, M.; Xing, L.; Wu, J.; Wen, S.; Luo, J.; Chen, T.; Fan, Y.; Zhu, J.; Yang, L.; Liu, J.; et al. Skeletal Muscle-Derived Exosomal miR-146a-5p Inhibits Adipogenesis by Mediating Muscle-Fat Axis and Targeting GDF5-PPAR γ Signaling. *Int. J. Mol. Sci.* **2023**, *24*, 4561. <https://doi.org/10.3390/ijms24054561>

Academic Editor: Antonio Gomez-Muñoz

Received: 24 January 2023

Revised: 13 February 2023

Accepted: 22 February 2023

Published: 25 February 2023



Copyright: © 2023 by the authors. Licensee MDPI, Basel, Switzerland. This article is an open access article distributed under the terms and conditions of the Creative Commons Attribution (CC BY) license (<https://creativecommons.org/licenses/by/4.0/>).

1. Introduction

Adipose tissue and skeletal muscle are highly heterogeneous endocrine organs that secrete several hormones, with myokines and adipokines participating in local autocrine/paracrine interactions and crosstalk with other tissues [1]. Myokines and adipokines are essential for the maintenance of body muscle and fat levels and modulation of the body composition [2]. Irisin stimulates uncoupling protein 1 (UCP1) expression on white adipose cells in vitro and in vivo, which results in brown-fat-like development, while muscle-specific expression of PPAR γ coactivator-1 α (PGC1 α) drives browning of subcutaneous white adipose tissue [3]. As reported, the muscle interleukin-6 (IL-6) influences the main neuropeptides for energy homeostasis in a sex-specific manner [4]. The hormone myostatin inhibits myogenesis and

promotes adipogenic differentiation of mesenchymal cells [5]. Prolyl hydroxylase 3 (PHD3) losses during endurance exercise challenges improve exercise capacity [6]. In mice with GR mKOs in the skeletal muscle, muscle mass is increased, while fat tissue is smaller [7]. The present study demonstrated that exercise induces myokines to counteract the negative effects of pro-inflammatory adipokines [8]. In recent years, there has been increased interest in investigating the effects of exercise training on adipose tissue [9].

Exosomes are small extracellular vesicles with a diameter of 50–150 nm, which are formed when multivesicular endosomes fuse with the plasma membrane and contained biologically active substances, such as proteins, RNA, DNA, cholesterol, etc. [10,11]. Secreted exosomes are taken up by and deliver their content to the recipient cells, thus representing a novel intercellular communication pathway [12]. Muscle and adipose exosomes can act as a mediator of intercellular communication to exert their physiological regulatory functions. There is increasing evidence that exosomes released by myogenic cells can transport their proteins, mRNAs, and miRNAs to recipient cells and regulate myocyte function in an autocrine or paracrine manner [13]. They can also enter the circulatory system, such as the blood, and may act on distant tissues [14,15]. The incorporation of muscle exosomes into various tissues in vivo, including the pancreas and liver, suggests that skeletal muscle (SKM) could transfer specific signals via the exosomal route to key metabolic tissues [16]. Endocytosis, membrane fusions, and receptor-mediated internalization are the mechanisms by which exosomes are absorbed intracellularly [17]. These variable internalization mechanisms and the signaling molecules presenting in exosomes are the reason why exosomes are widely accepted as important players of intercellular communication in the microenvironment and worthy of investigation [18].

The miRNA gene family adds a new layer of regulation and fine-tuning to gene expression that may affect a wide range of cellular functions, including metabolism, and numerous studies indicate that miRNAs play important roles in diverse aspects of signaling and metabolism, despite their unknown functions [19]. miR-27a released from adipocytes of high-fat diet-fed C57BL/6J mice was associated with a triglyceride accumulation. Exosomal miR-27a derived from adipocytes induces insulin resistance in C2C12 muscle cells through miR-27a-mediated repression of PPAR γ and downstream genes involved in obesity [20]. miR-130b's circulation could act as a metabolic mediator in adipose-muscle crosstalk, as well as a potential contributor to obesity-associated metabolic diseases [21]. MiR-124 secreted by adipose-derived stem cells has been implicated in skin wound healing, possibly by targeting MALAT1 and activating Wnt/catenin signaling pathways [22]. Accumulating evidence indicates that miR-146a-5p is a multifunctional miRNA that can act as a multidirectional target to regulate body metabolism. Mechanistically, miR-146a-5p attenuates TGF- β signaling by directly targeting SMAD family member 4 (SMAD4), thereby inhibiting cell proliferation, and attenuates AKT/mTORC1 signaling by targeting TNF receptor-associated factor 6 (TRAF6) to inhibit the differentiation of intramuscular preadipocytes [23]. Further studies revealed that hepatic miR-146a-5p overexpression significantly improved glucose and insulin tolerance as well as lipid accumulation in the liver by targeting the mediator complex subunit 1 gene (MED1) to promote the oxidative metabolism of fatty acids [24]. In long-living Ame's dwarf (df/df) mice, miR-146a-5p mimetic treatment increased cellular senescence and inflammation and decreased pro-apoptotic factors in visceral adipose tissue [25]. Furthermore, the miR-146a gene might be a powerful target for preventing age-related bone dysfunctions such as the formation of bone marrow adiposity and osteoporosis [26]. However, whether skeletal muscle-derived exosomes by transferring miRNAs and then affects adipogenesis associated signaling pathways remains elusive.

Recently, we compared the expression profiles of miRNA between exosomes derived from skeletal muscle and adipose tissue [27]. The findings showed that the content of miR-146a-5p in skeletal muscle-derived exosomes was more than 50 times higher than that in fat-derived exosomes, indicating that the miR-146a-5p may play a crucial role in regulating the skeletal muscle-fat axis. In this study, we intend to explore the connection between skeletal muscle and adipose tissue via the mediation of exosomes, especially,

miR-146a-5p from skeletal muscle-derived exosomes mediating crosstalk between skeletal muscle and adipose tissue. Through transwell assay, gain-of-function and loss-of-function strategies in cell models, and skeletal muscle-specific miR-146a-5p knockout animal models, in vitro and in vivo studies have gradually revealed the exosomal miR-146a-5p released from skeletal muscle as a new myokine involved in the regulation of adipogenesis via mediating the skeletal muscle-fat signaling axis.

2. Results

2.1. Transwell Co-Culture of C2C12 Cells Inhibits the Adipogenesis of 3T3-L1 Cells

To further determine whether muscle cells can regulate adipocyte differentiation and lipid deposition via secreted exosomes, we used the transwell co-culture experiments with C2C12 cells and 3T3-L1 cells to test this possibility (Figure 1a). C2C12 myoblasts during proliferation (Pro) were cultured in vitro and induced to differentiate into mature myofibroblasts (Diff) (Figure 1b). The result showed that the differentiated C2C12 cells promoted the deposition of lipid droplets (Figure 1c), and significantly increased the content of TG in 3T3-L1 cells (Figure 1d). Next, we extracted the exosomes from the proliferation stage (Pro-Exos) and differentiation stage (Diff-Exos), respectively, and determined the morphology of Pro-Exos and Diff-Exos by electron microscopy (Figure 1e); nanoparticle tracking analysis (NTA) showed that the exosomes were mainly concentrated at 130–150 nm (Figure 1f), and the exosome marker proteins such as apoptosis-linked gene 2-interacting protein X (Alix), tumor susceptibility gene 101 (TSG101), CD9, and CD63 were mainly enriched in Pro-Exos and Diff-Exos, while the endoplasmic reticulum marker protein Calnexin was mainly enriched in cells (Figure 1g), indicating that the exosomes were successfully extracted. Interestingly, we found that the expression of miR-146a-5p in the C2C12 cells' proliferation stage was significantly higher than that in the differentiation stage of C2C12 cells, and the same expression level of miR-146a-5p also existed in the secreted exosomes (Pro-Exos and Diff-Exos) (Figure 1h). Then, 3T3-L1 cells were treated with Pro-Exos and Diff-Exos and induced to differentiate. RT-qPCR showed that Pro-Exos inhibited the mRNA levels of adipogenesis-related transcriptional factors PPAR γ and C/EBP α (Figure 1i–j), and fatty acid synthesis-related genes CD36 and FABP4 (Figure 1k–l), on the contrary, the results of Diff-Exos treatment are reversed. These results suggest that the co-culture of C2C12 cells can inhibit adipogenesis of 3T3-L1 cells, and the reason may be related to exosomal miR-146a-5p secreted by C2C12 cells.

2.2. C2C12 Cells-Derived Exosomes Affect Glucose and Fatty Acid Uptake in 3T3-L1 Cells via Transferring of miR-146a-5p

To further explore whether skeletal muscle-derived exosomes are involved in regulating adipogenesis and metabolism, especially via miR-146a-5p, we cultured 3T3-L1 adipose precursor cells in vitro to induce their maturation. The results showed that the deposition of lipid droplets and the content of TG in the Pro-Exos treated group was significantly smaller than that of the Diff-Exos group. However, Pro-Exos + i group the miR-146a-5p inhibitor co-treated with Pro-Exos 3T3-L1 cells obtained a similar phenotype to Diff-Exos, indicating that the downregulation of muscle exosomal miR-146a-5p can improve adipogenesis. Similarly, after co-treatment of Diff-Exos with miR-146a-5p mimics (Diff-Exos + m), lipid droplet phenotype and TG content are similar to that of Pro-Exos (Figure 2a,b). Subsequently, the expressions of adipogenesis-related proteins GDF5, PPAR γ , C/EBP α , and fatty acid synthesis-related proteins FABP4 and FASN were detected in 3T3-L1 cells of each group. The expression of these proteins was found to be significantly lower in the Pro-Exos and Diff-Exos + m treated groups than in the Diff-Exos and Pro-Exos + i treated groups (Figure 2c,d). To further explore whether skeletal muscle-derived exosomes can affect adipogenesis by affecting glucose and fatty acid uptake in adipocytes, we used fluorescently labeled glucose (2-NBDG) and fatty acids (Bodipy-FA) to observe glycolipid absorption. The amount of glucose absorbed by 3T3-L1 cells in the Pro-Exos treatment group was significantly smaller than that in the Diff-Exos treatment group for the same

period. In the Pro-Exos + i group, the glucose uptake of 3T3-L1 cells was significantly greater than that in the Pro-Exos group, and in the Diff-Exos + m group, the absorption of glucose by 3T3-L1 cells was significantly lower than that in the Diff-Exos group (Figure 2e,f). Pro-Exos and Diff-Exos + m treated 3T3-L1 cells had significantly less uptake of free fatty acids than Diff-Exos and Pro-Exos + i treated groups (Figure 2g,h). Experiments showed that C2C12 cells-derived Pro-Exos can inhibit glucose and fatty acid uptake in 3T3-L1 cells, while Diff-Exos can promote glucose and fatty acid uptake in 3T3-L1 cells. Adding the inhibitor and mimics of miR-146a-5p to pro-Exos and diff-Exos, respectively, could reverse the effects of exosomal treatment alone on adipogenesis and glycolipid transport metabolism in 3T3-L1 cells. In summary, the above results highlight the important roles of exosomal miR-146a-5p in mediating the interactions between skeletal muscle cells and the adipocytes' microenvironment.

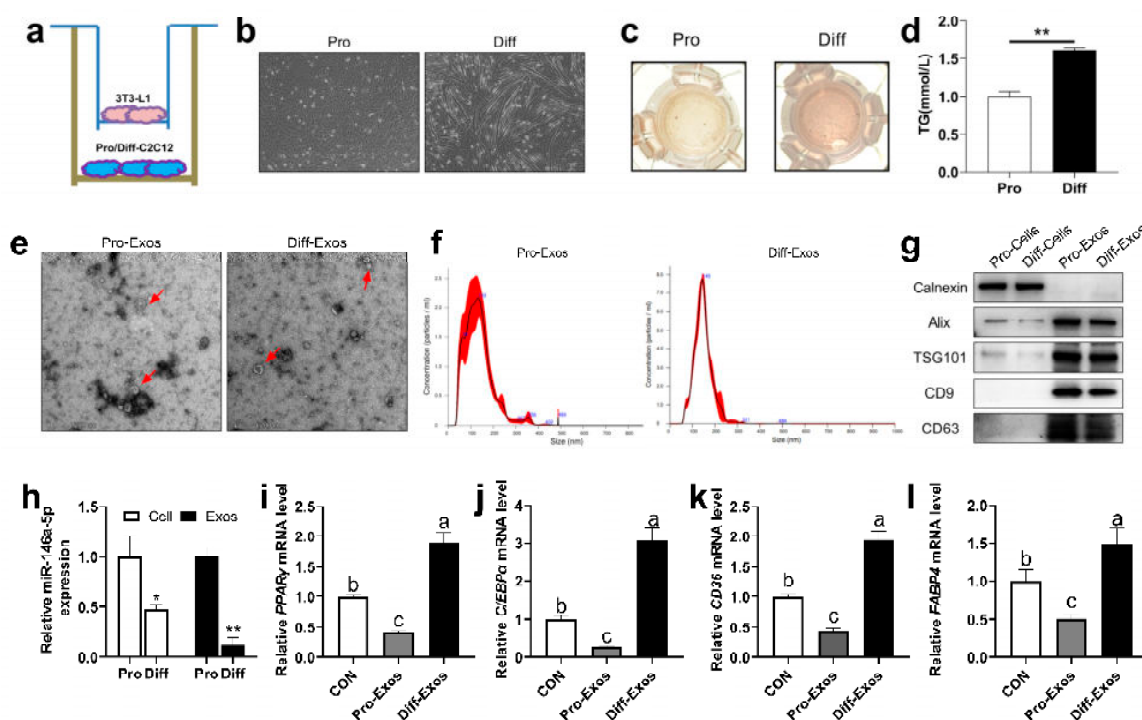


Figure 1. Effects of skeletal muscle-derived exosomes on adipogenesis in 3T3-L1 cells. (a) C2C12 cells were co-cultured with 3T3-L1 cells, and the cells were grown in a transwell. (b) The morphology of C2C12 cells before and after differentiation was observed under a microscope (scale bar = 100 μ m). (c) During co-culture, differentiated 3T3-L1 adipogenic precursor cells were induced to mature, and oil red O staining was performed. (d) During co-culture, the differentiation of 3T3-L1 adipocyte precursor cells was induced to mature to examine TG content ($n = 6$). (e) Electron microscopy photographs of C2C12 cells-derived exosomes proliferation (Pro-Exos) and differentiation (Diff-Exos) (scale bar = 200 nm). (f) Nanoparticle tracking analysis (NTA) was used to determine the size distribution and concentration of exosomes. (g) Marker proteins Alix, TSG101, CD9, and CD63 in exosomes extracted from C2C12 cells, and the Western Blot detection bands of endoplasmic reticulum marker protein Calnexin. (h) The expression of miR-146a-5p in C2C12 cells proliferation and differentiation ($n = 6$), and the expression of miR-146a-5p in C2C12 cells-derived exosomes of the proliferation and differentiation ($n = 4$). (i–l) After treatment with skeletal muscle-derived exosomes (Pro-Exos, Diff-Exos), adipogenesis-related genes PPAR γ and C/EBP α , and fatty acid synthesis-related genes CD36 and FABP4, were detected by real-time quantitative PCR after induced differentiation in 3T3-L1 preadipocytes ($n = 6$). Values are presented as means \pm SEM, * $p < 0.05$, and ** $p < 0.01$, according to the non-paired Student's t -test or one-way ANOVA between individual groups. Different letters mean significant difference ($p < 0.05$), and the same letters mean no significant difference ($p > 0.05$).

2.3. miR-146a-5p Significantly Inhibits Adipogenesis, Glucose Uptake and Fatty Acid Absorption in 3T3-L1 Cells

To further determine the role of skeletal muscle-derived exosomes in affecting adipogenesis mediated through miR-146a-5p, 3T3-L1 cells were transfected with miR-146a-5p mimics (Mimics) and miR-146a-5p inhibitor (Inhibitor) and induced to mature. The transfection efficiency of miR-146a-5p was quantitatively analyzed first. The expression of miR-146a-5p in 3T3-L1 cells transfected with miR-146a-5p mimics increased 166 times. However, the expression of miR-146a-5p in the miR-146a-5p inhibitor transfected group was also reduced by 33%, and both reached a statistically significant level (Figure 3a). For TG content in each group, it was significantly decreased for miR-146a-5p mimics and significantly increased for miR-146a-5p inhibitor (Figure 3b). At the same time, the results of Oil Red O staining showed that miR-146a-5p mimics could significantly reduce lipid droplet synthesis, while there is a significant increase in miR-146a-5p inhibitor (Figure 3c). To confirm the effect of skeletal muscle-derived exosomes on adipocyte glucose uptake and fatty acid absorption is mediated by miR-146a-5p, we used 2-NBDG and Bodipy-FA to examine the efficiency of glycolipid uptake in 3T3-L1 cells. The 3T3-L1 cells with miR-146a-5p inhibitor treatment significantly increased the uptake of glucose and the absorption of free fatty acids, while miR-146a-5p mimics treatment significantly reduced glucose uptake and free fatty acid uptake (Figure 3d–g). It was found by qPCR that miR-146a-5p mimics could significantly reduce the expression of adipogenesis-related genes PPAR γ , C/EBP α , and fatty acid synthesis-related genes CD36, FABP4, and FASN, while miR-146a-5p inhibitor significantly increased the expression levels of these genes (Figure 3h). Western blot results were consistent with the quantitative results that miR-146a-5p mimics significantly decreased the expression of adipogenesis-related proteins PPAR γ , C/EBP α , and fatty acid synthesis-related proteins CD36, FABP4, and FASN, while miR-146a-5p inhibitor significantly increased the expression of these proteins (Figure 3i–j). The results showed that miR-146a-5p significantly inhibited the differentiation, glucose uptake, and fatty acid absorption of 3T3-L1 preadipocytes.

2.4. miR-146a-5p as a Negative Regulator of PPAR γ Signaling by Directly Targeting GDF5 to Inhibit Adipogenesis

To determine the targeting mechanism of miR-146a-5p inhibiting adipogenesis, the bioinformatics database miRDB was used to identify putative target genes for miR-146a-5p given the above adipogenesis-related genes and found that miR-146a-5p has a target interaction with the 3'UTR of GDF5 (Figure 4a). Subsequently, the relationship between miR-146a-5p and GDF5 was verified by dual luciferase and miR-146a-5p targeted the 3'UTR of GDF5 and reduced dual-luciferase expression (Figure 4b). In addition, we examined the protein and gene expression changes of GDF5 after miR-146a-5p overexpression and knockdown. As expected, miR-146a-5p overexpression decreased GDF5 protein expression, whereas miR-146a-5p knockdown increased GDF5 protein expression (Figure 4c,d). At the same time, overexpression of miR-146a-5p reduced GDF5 gene expression, and knockdown of miR-146a-5p increased GDF5 gene expression (Figure 4e), which is in line with the trend of miRNA regulation of target genes, and also indicated that miR-146a-5p targeted GDF5. To verify that miR-146a-5p regulates the PPAR γ signaling pathway by targeting GDF5, three siRNAs against GDF5 were designed. First, the protein knockdown efficiency of GDF5 siRNA were verified, and GDF5 siRNA-3 significantly reduced GDF5 protein expression (Figure 4f,g). 3T3-L1 cells were transfected with different miR-146a-5p nucleic acid analogs and siRNA (NC, GDF5 siRNA, miR-146a-5p inhibitor + GDF5 siRNA), and the cells were cultured until mature. In 3T3-L1 cells treated with GDF5 siRNA, the expression levels of adipogenesis-related genes GDF5, PPAR γ , C/EBP α and fatty acid synthesis-related genes CD36, FABP4 and FASN were significantly decreased, while in those co-treated with GDF5 siRNA and miR-146a-5p inhibitor, the gene expressions of adipogenesis-related genes GDF5, PPAR γ , C/EBP α and fatty acid synthesis-related genes CD36, FABP4 and FASN were significantly increased compared with just GDF5 siRNA treatment (Figure 4h). Western

blotting results further verified that 3T3-L1 cells transfected GDF5 siRNA significantly reduced the expressions of adipogenesis-related proteins GDF5, PPAR γ , C/EBP α , and fatty acid synthesis-related proteins CD36, FABP4, and FASN, while in those co-transfected with miR-146a-5p inhibitor and GDF5 siRNA, the expressions of adipogenesis-related proteins GDF5, PPAR γ , C/EBP α and fatty acid synthesis-related proteins CD36, FABP4, and FASN were significantly increased (Figure 4i–j). We found that the content of TG and lipid droplets in the GDF5 siRNA treatment group were significantly lower than NC group, while the co-treatment of GDF5 siRNA and miR-146a-5p inhibitor significantly increased TG and lipid droplet content (Figure 4k–l). Co-immunoprecipitation (co-IP) test further showed that GDF5 has a protein-protein interaction relationship with PPAR γ , C/EBP α , CD36, and FASN (Figure 4m). These results suggested that GDF5 participated in adipogenesis by regulating the PPAR γ signaling pathway, indicating that miR-146a-5p regulated the PPAR γ signaling pathway by targeting GDF5.

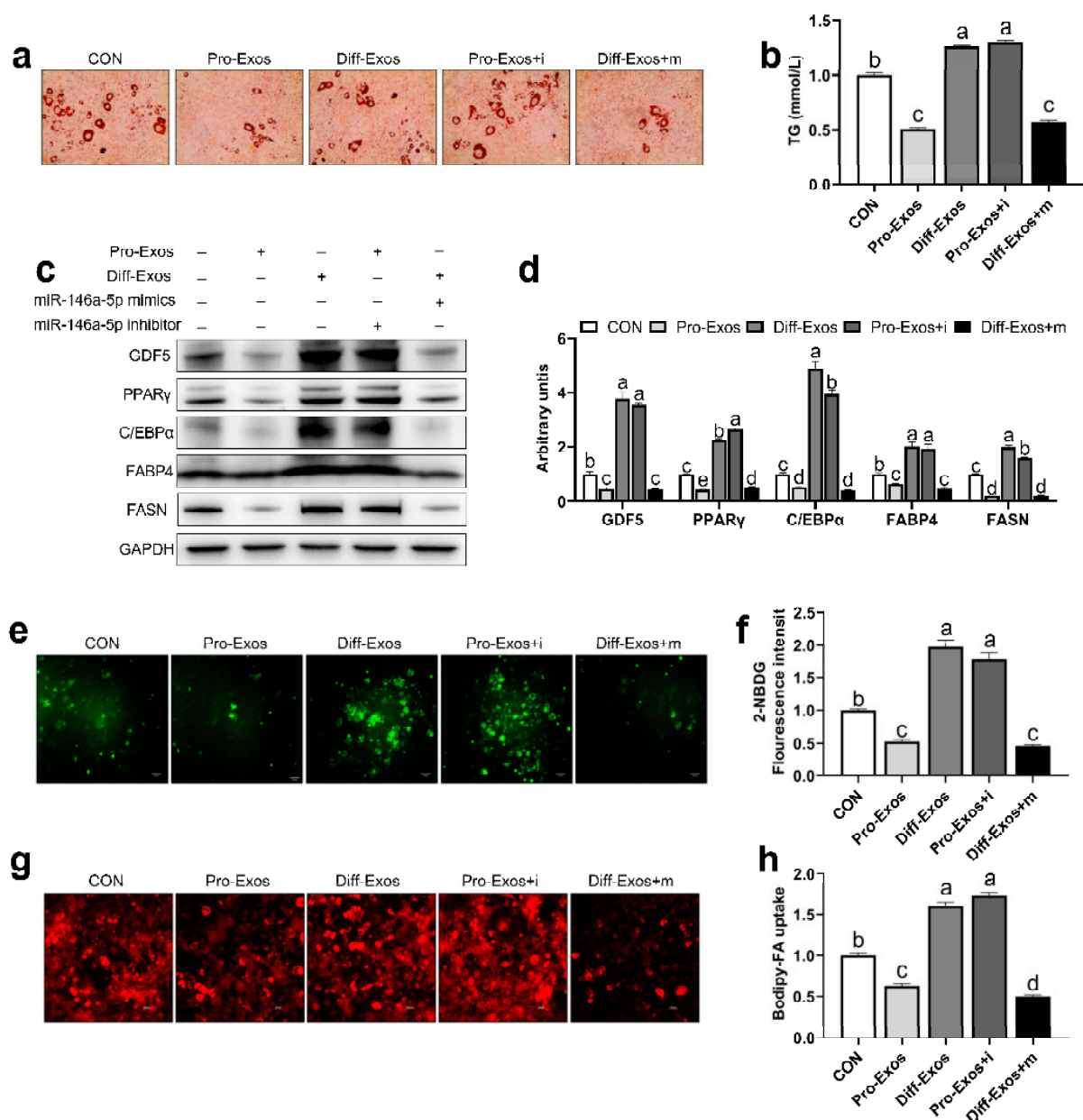


Figure 2. miR-146a-5p reversed the effect of skeletal muscle-derived exosomes on adipogenesis,

glucose uptake, and fatty acid absorption in 3T3-L1 cells. (a) After treatment of exosomes (Pro-Exos, Diff-Exos) and transfections of miR-146a-5p mimics and miR-146a-5p inhibitor, 3T3-L1 adipogenic precursor cells were induced to mature, and oil red O staining was performed (scale bar = 50 μ m). (b) After treatment with exosomes (Pro-Exos, Diff-Exos) and transfecting miR-146a-5p mimics (mimics) and miR-146a-5p inhibitor (inhibitor), 3T3-L1 adipocytes were induced to mature, and TG content was assayed (n = 6). (c,d) After treatment of exosomes (Pro-Exos, Diff-Exos) and transfections of mimics and inhibitor, adipogenesis-related proteins and fatty acid synthesis-related protein bands were detected by Western Blot in mature 3T3-L1 cells (n = 4). (e) 2-NBDG fluorescence profile of 3T3-L1 cells after treatment of exosomes (Pro-Exos, Diff-Exos) and transfections of mimics and inhibitor for 24 h (scale bar = 50 μ m). (f) 2-NBDG fluorescence values of 3T3-L1 cell after treatment of exosomes (Pro-Exos, Diff-Exos) and transfections of mimics and inhibitor for 24h (n = 6). (g) Bodipy-FA fluorescence image of 3T3-L1 cells after treatment with exosomes (Pro-Exos, Diff-Exos) and transfections of mimics and inhibitor for 24 h (scale bar = 50 μ m). (h) Bodipy-FA for 4 h, 3T3-L1 cell fluorescence values after treatment of exosomes (Pro-Exos, Diff-Exos) and transfections of mimics and inhibitor for 24 h (n = 6). Values are presented as means \pm SEM, according to the non-paired Student's *t*-test or one-way ANOVA between individual groups. Different letters mean significant difference ($p < 0.05$), and the same letters mean no significant difference ($p > 0.05$).

2.5. Skeletal Muscle-Specific Knockout miR-146a-5p Significantly Increased Body Weight Gain and Decreased Oxidative Metabolism in Mice

To further explore the function of miR-146a-5p, we constructed a skeletal muscle-specific knockout mouse model of miR-146a-5p. Through Sanger sequencing and genotyping results, we confirmed that the mKO mice were successfully constructed (Figure 5a,b). By qPCR, the expression of miR-146a-5p was significantly knocked down in the gastrocnemius (GAS) and tibialis anterior (TA) of mKO mice compared with Flox mice (Figure 5c). Flox and mKO mice were induced with a high-fat diet (HFD) to observe the effect on the growth and metabolism of the mice. During the experiment, it was found that the HFD induction significantly increased the body weight gain of the mKO mice (Figure 5d). We found a significant decrease in muscle mass in both GAS and TA in mKO mice (Figure 5e). However, there was no difference in feed intake (Figure 5f). The skeletal muscle had no significant effect on insulin resistance in miR-146a-5p knockout mice (Figure 5g), but significantly improved glucose tolerance (Figure 5h). In terms of respiratory metabolism, O₂ inhalation and CO₂ exhalation in the skeletal muscle of miR-146a-5p knockout mice (mKO) were significantly lower than those in the Flox mice (control group) (Figure 5i–l). To a certain extent, O₂ inhalation and CO₂ exhalation reflect the energy metabolism level of the body. Therefore, the experiment showed that the skeletal muscle-specific miR-146a-5p knockout could increase body weight gain and reduce oxidative metabolism in mice.

2.6. Skeletal Muscle-Specific Knockout miR-146a-5p Significantly Increased Adipogenesis in Mice by Up-Regulating GDF5 and PPAR γ

To further explore how miR-146a-5p knockdown in the skeletal muscle regulates adipogenesis in vivo, the body composition and body imaging of the mice were observed, and the lean mass content of mKO mice was significantly reduced; interestingly, the fat mass content and fat enrichment increased instead, which successfully confirmed the crosstalk in the skeletal muscle and fat axis (Figure 6a,b). For further verification, the tissue weights of inguinal white adipose tissue (IngWAT) and epididymal white adipose tissue (EpiWAT) in mKO mice were found to be significantly higher than those in Flox mice (Figure 6c). At the same time, the HE-stained sections of IngWAT and EpiWAT tissues intuitively revealed that the adipocytes in mKO mice were larger and plumper (Figure 6d). qPCR analysis of adipogenesis-related gene expression showed that the expressions of GDF5, PPAR γ , C/EBP α , and fatty acid synthesis-related genes CD36, FABP4, FASN in IngWAT of mKO mice were significantly increased compared with that of Flox mice (Figure 6e). Consistent with the quantitative results, the proteins of these genes were also more highly expressed in the IngWAT tissues of mKO mice (Figure 6f,g). Similarly, in the EpiWAT tissue

of mKO mice, the expression of GDF5, PPAR γ , C/EBP α , and fatty acid synthesis-related genes CD36, FABP4, FASN was significantly higher than that of Flox mice (Figure 6h), and the protein expressions of these genes were also significantly higher than those of Flox mice (Figure 6i–j). These results suggested that skeletal muscle miR-146a-5p knockout significantly increased adipogenesis in mice.

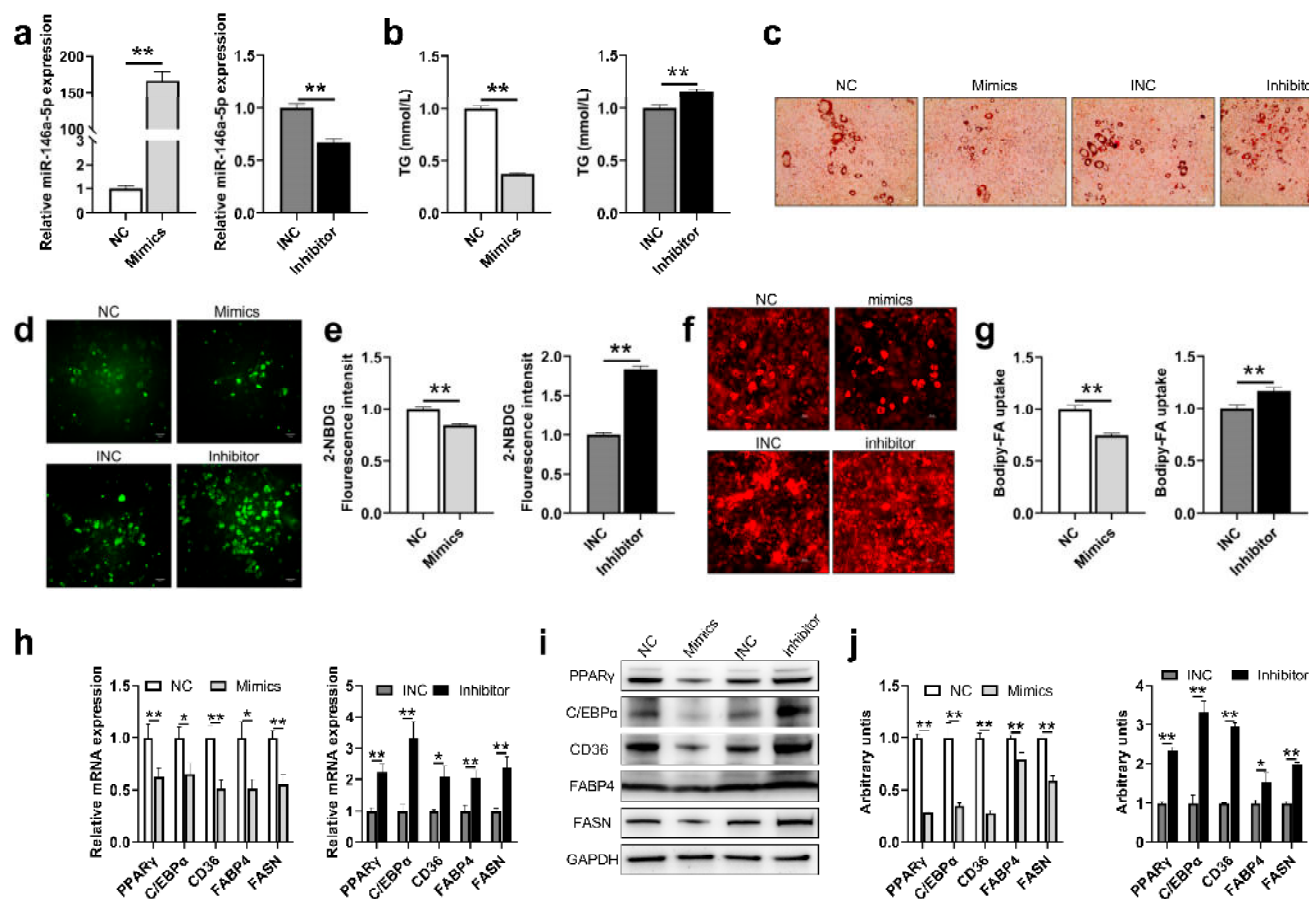


Figure 3. miR-146a-5p was associated with adipogenesis and glucose uptake and fatty acid absorption. (a) miR-146a-5p gene expressions in 3T3-L1 adipose mature cells after transfections of miR-146a-5p mimics (Mimics) and miR-146a-5p inhibitor (Inhibitor) (n = 6). (b) TG content in 3T3-L1 adipose mature cells after transfections of mimics and inhibitor (n = 6). (c) Oil red O staining photographs in 3T3-L1 adipose mature cells after transfections of mimics and inhibitor (scale bar = 50 μ m). (d) Fluorescence image of 3T3-L1 cells treated with glucose analog 2-NBDG for 1 h after transfections of mimics and inhibitor for 24 h (bar = 50 μ m). (e) Statistical graph of fluorescence value of 3T3-L1 cells treated with glucose analog 2-NBDG (n = 4). (f) Fluorescence image of 3T3-L1 cells treated with free fatty acid analog Bodipy-FA for 4 h after transfections of mimics and inhibitor for 24 h (bar = 50 μ m). (g) Statistical graph of fluorescence value of 3T3-L1 cells treated with free fatty acid analog Bodipy-FA (n = 4). (h) After transfection of mimics and inhibitor adipogenesis-related genes PPAR γ , C/EBP α , and fatty acid synthesis-related genes CD36, FABP4, and FASN were detected by real-time quantitative PCR in mature 3T3-L1 (n = 6). (i,j) After transfection of mimics and inhibitor, adipogenesis-related proteins PPAR γ , C/EBP α , and fatty acid synthesis-related proteins CD36, FABP4, and FASN were detected by Western Blot (n = 6). Values are presented as means \pm SEM, * p < 0.05, and ** p < 0.01, according to the non-paired Student's t-test or one-way ANOVA between individual groups.

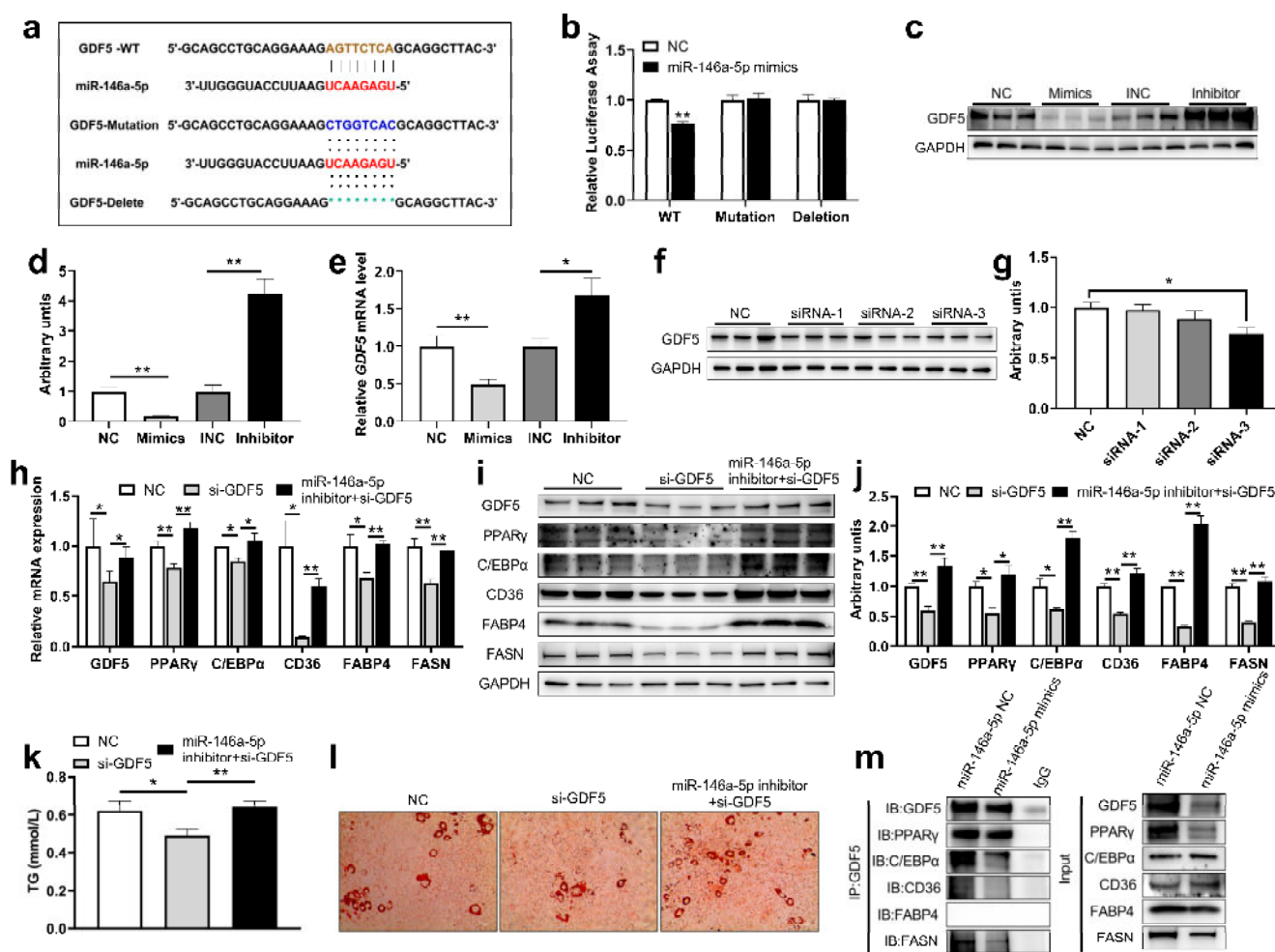


Figure 4. miR-146a-5p regulated PPAR γ signaling pathway by targeting GDF5. (a) miR-146a-5p has a target interaction with the 3'UTR of GDF5. (b) Statistical chart of miR-146a-5p and GDF5 dual luciferase validation fluorescence values ($n = 8$). (c,d) After transfections of miR-146a-5p mimics (Mimics) and miR-146a-5p inhibitor (Inhibitor), GDF5 was detected by Western Blot in mature 3T3-L1 cells ($n = 6$). (e) After transfections of mimics and inhibitor, GDF5 gene expression was detected by real-time quantitative PCR ($n = 6$). (f,g) 3T3-L1 cells were transfected with GDF5 siRNA for 48 h, and GDF5 was detected by Western Blot ($n = 6$). (h) After transfection (NC, GDF5 siRNA, miR-146a-5p inhibitor + GDF5 siRNA), GDF5, PPAR γ C/EBP α , CD36, FABP4 and FASN expressions were detected by real-time quantitative PCR ($n = 6$). (i,j) After transfection (NC, GDF5 siRNA, miR-146a-5p inhibitor + GDF5 siRNA), proteins GDF5, PPAR γ C/EBP α , CD36, FABP4 and FASN were detected by Western Blot ($n = 6$). (k) After transfection (NC, GDF5 siRNA, miR-146a-5p inhibitor + GDF5 siRNA), TG content was assayed ($n = 6$). (l) After transfection (NC, GDF5 siRNA, miR-146a-5p inhibitor + GDF5 siRNA), oil red O staining was performed (scale bar = 50 μ m). (m) Oil Red O readings ($n = 6$). (n) Immunoprecipitation assay revealed enrichment of PPAR γ C/EBP α , CD36, FABP4, and FASN when introduced with GDF5. Values are presented as means \pm SEM, * $p < 0.05$, and ** $p < 0.01$, according to the non-paired Student's t -test or one-way ANOVA between individual groups.

2.7. The Internalization of miR-146a-5p into the mKO Mice by Injecting Flox-Exos Inhibits Adipogenesis

To further explore the function of skeletal muscle-derived exosomes, two different skeletal muscle-derived exosomes (Flox-Exos, mKO-Exos) were extracted and identified (Supplementary Figure S1a–c), and the expression level of miR-146a-5p was detected (Figure 7a). The skeletal muscle-derived exosomes were labeled with PKH67 and injected into mice via the tail vein, which was distributed in different organs after 24 h. Interest-

ingly, imaging showed that PKH67-labeled exosomes were mainly distributed in IngWAT, EpiWAT, visceral adipose tissue (VAT), brown adipose tissue (BAT), GAS, TA, liver, lung, kidney (with a small enrichment in extensor digitorum longus (EDL)), soleus (SOL), heart, and spleen (Figure 7b). This indicated that skeletal muscle-derived exosomal miR-146a-5p could be specifically taken up into the fat tissues through humoral circulation (Figure 7c). When mice were continuously injected with skeletal muscle-derived exosomes for 3 weeks (Figure 7d), the body weight gain of Flox-Exos injected mice was significantly reduced at 2 weeks (Figure 7e), and the body weight was also different at 3 weeks (Figure 7f), but there was no difference in feed intake (Figure 7g). After aKO mice were injected with Flox-Exos, IngWAT and EpiWAT tissue weight in mice was significantly reduced (Figure 7h), and the fat mass in body composition decreased significantly, while the lean content showed an increasing trend (Figure 7i), and in vivo imaging also showed fat enrichment was decreased compared to injected with mKO-Exos (Figure 7j). In tissue sections, we found decreased accumulation of lipid droplets in the adipose tissue of mice injected with Flox-Exos (Figure 7k,o). Further studies found that IngWAT adipogenesis and fatty acid synthesis-related mRNA levels were significantly reduced in Flox-Exos-injected mice (Figure 7l), and protein levels were also significantly reduced (Figure 7m,n). Similar results were seen for EpiWAT adipogenesis and fatty acid synthesis-related mRNA and protein levels (Figure 7p–r). These results suggested that miR-146a-5p in skeletal muscle-derived exosomes can be specifically enriched in the adipose tissue, further affecting adipogenesis. Taken together, SKM-Exos-mediated intercellular miR-146a-5p has great potential for the prevention and treatment of obesity.

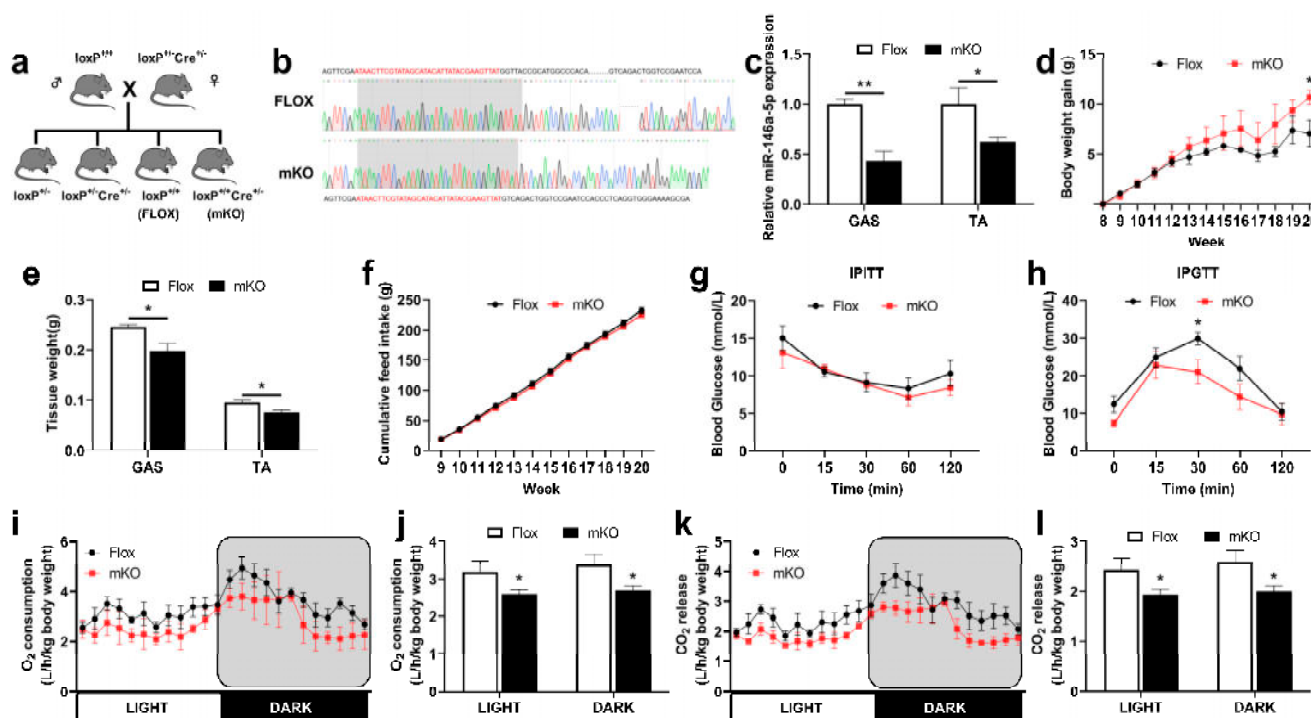


Figure 5. Regulations of growth and metabolism in transgenic mice. (a) Mice breeding atlas. (b) Sequence alignment of skeletal muscle-specific miR-146a-5p knockout (mKO) and Flox. (c) The expression of miR-146a-5p in GAS and TA of mKO mice was detected by quantitative PCR ($n = 4$). (d) Body weight change curve of Flox and mKO mice fed a high-fat diet ($n = 4$). (e) The muscle weight for GAS and TA of Flox and mKO mice fed a high-fat diet ($n = 4$). (f) Accumulate feed intake of Flox and mKO fed HFD ($n = 4$). (g) IPITT blood glucose changes in Flox and mKO mice ($n = 4$). (h) IPGTT blood glucose changes in Flox and mKO mice ($n = 4$). (i,j) Oxygen consumption ($n = 4$). (k,l) CO₂ release ($n = 4$). Values are presented as means \pm SEM, * $p < 0.05$, and ** $p < 0.01$, according to the non-paired Student's t-test or one-way ANOVA between individual groups.

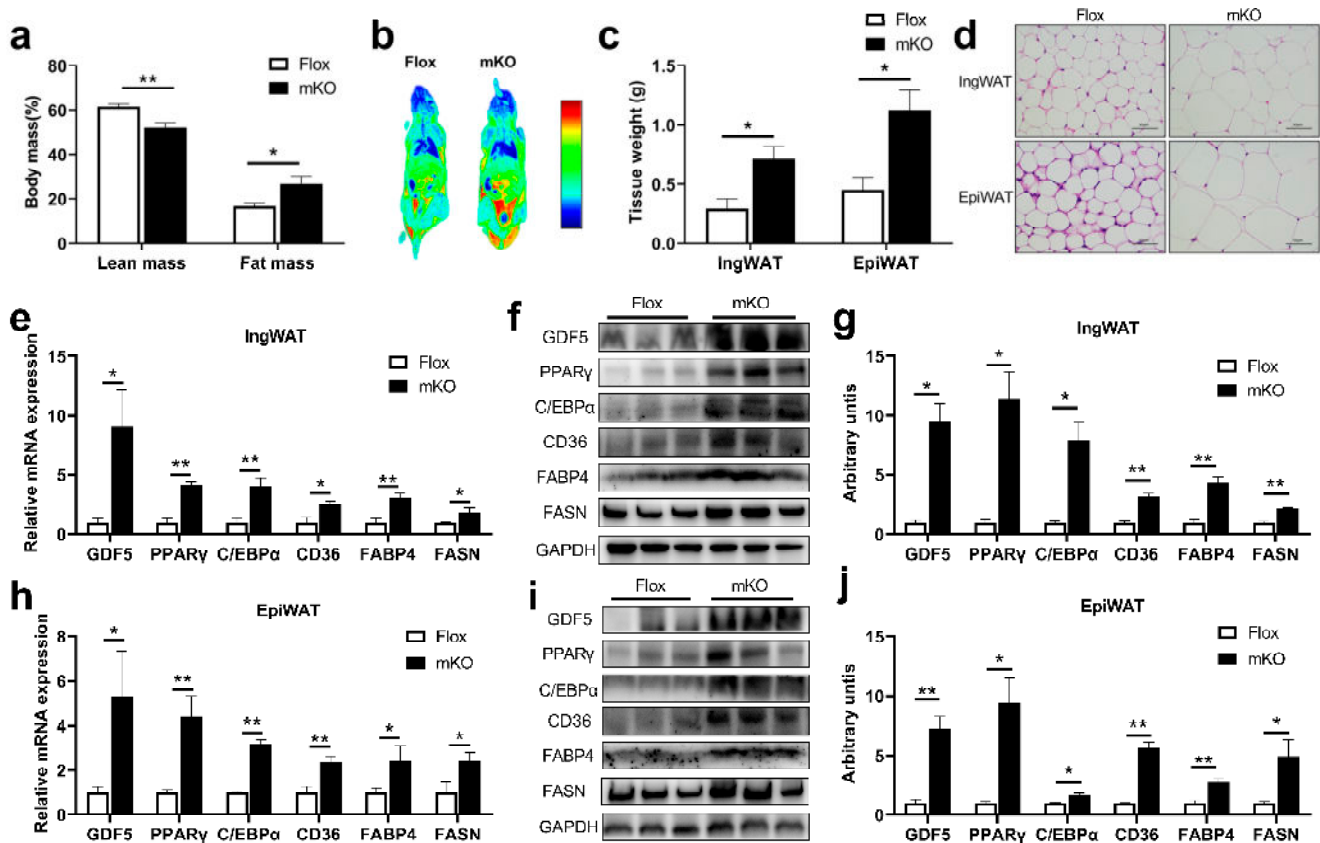


Figure 6. Effects of skeletal muscle-specific miR-146a-5p knockout on adipogenesis in mice. **(a)** Body composition of Flox and mKO mice. **(b)** Body imaging of Flox and mKO mice. **(c)** Tissue weight (IngWAT and EpiWAT) of Flox and mKO mice after feeding with a high-fat diet (HFD) ($n = 4$). **(d)** HE staining image of IngWAT and EpiWAT in Flox and mKO mice fed with HFD (scale bar = 50 μ m). **(e)** Fluorescence quantitative PCR detection of adipogenesis-related genes GDF5, PPAR γ , C/EBP α , and fatty acid synthesis-related genes CD36, FABP4, FASN in IngWAT of Flox and mKO mice ($n = 4$). **(f,g)** Western Blot detection of adipogenesis-related proteins GDF5, PPAR γ , C/EBP α , and fatty acid synthesis-related proteins CD36, FABP4, and FASN in IngWAT of Flox and mKO mice ($n = 4$). **(h)** Fluorescence quantitative PCR detection of adipogenesis-related genes GDF5, PPAR γ , C/EBP α , and fatty acid synthesis-related genes CD36, FABP4, FASN in EpiWAT of Flox and mKO mice ($n = 4$). **(i,j)** Western Blot detection of adipogenesis-related proteins GDF5, PPAR γ , C/EBP α , and fatty acid synthesis-related proteins CD36, FABP4, FASN in EpiWAT of Flox and mKO mice ($n = 4$). Values are presented as means \pm SEM, * $p < 0.05$, and ** $p < 0.01$, according to the non-paired Student's t -test or one-way ANOVA between individual groups.

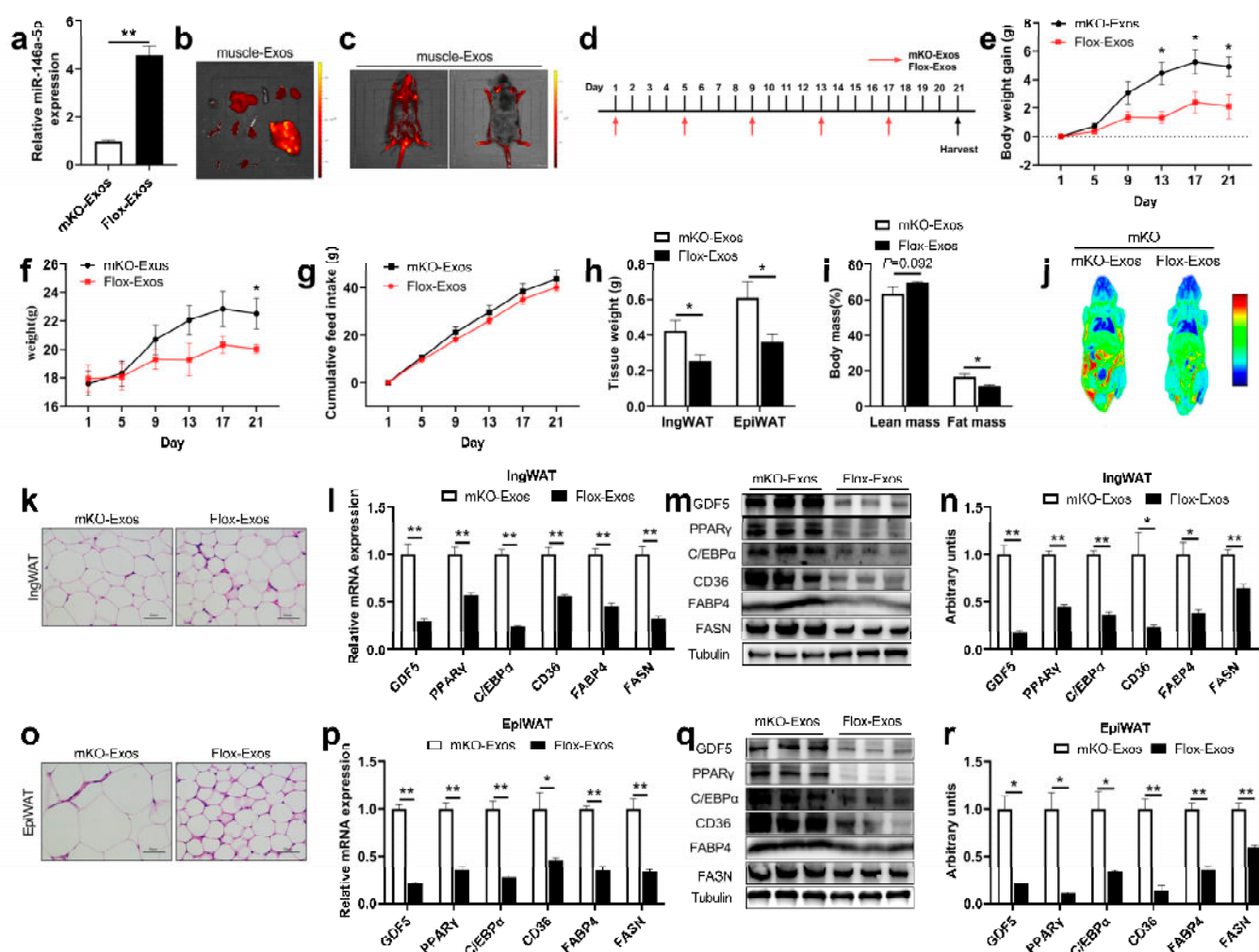


Figure 7. The intravenous injection of Flox-Exos into mKO mice reversed the inhibition of adipogenesis. **(a)** Expressions of miR-146a-5p were determined in skeletal muscle-derived exosomes from mKO and Flox mice ($n = 6$). **(b)** The fluorescence signal of skeletal muscle-derived exosomes in isolated mKO mice organs 24 h after tail vein injection. The isolated organs from left to right are as follows: heart, liver, spleen, lung, kidney, BAT, IngWAT, EpiWAT, whole intestine, TA, EDL, GAS, SOL. **(c)** In vivo imaging of mKO mice 24 h after tail vein injection of PKH67-labeled skeletal muscle-derived exosomes. **(d)** Schematic diagram of tail-vein injections of Flox-Exos and mKO-Exos administered to HFD-fed mKO mice at the age of 6 weeks. **(e)** Body weight gain in mKO mice ($n = 3$). **(f)** Body weight of mKO mice ($n = 3$). **(g)** Accumulate feed intake of mKO mice fed HFD ($n = 3$). **(h)** Tissue weight (IngWAT and EpiWAT) of mKO mice ($n = 3$). **(i)** Body Composition of mKO mice ($n = 3$). **(j)** Body imaging of mKO mice. **(k)** IngWAT HE staining image of mKO mice. **(l)** Expression of adipogenesis and fatty acid synthesis-related genes 21 days after exosome injection in IngWAT ($n = 3$). **(m,n)** Expression of adipogenesis and fatty acid synthesis-related proteins in IngWAT ($n = 3$). **(o)** EpiWAT HE staining image of mKO mice. **(p)** Expression of adipogenesis and fatty acid synthesis-related genes 21 days after exosome injection in EpiWAT ($n = 3$). **(q,r)** Expression of adipogenesis and fatty acid synthesis-related proteins in EpiWAT ($n = 3$). Values are presented as means \pm SEM, * $p < 0.05$, and ** $p < 0.01$, according to the non-paired Student's t -test or one-way ANOVA between individual groups.

3. Discussion

By binding the 3'UTR of mRNA, miRNAs regulate metabolic homeostasis by repressing or degrading the translation of target mRNA [28]. miR-146a is lowered in obese and type 2 diabetic patients, and mice fed a high-fat diet (HFD) show exaggerated weight gain,

increased adiposity, hepatosteatosis, and dysregulated blood glucose levels compared to wild-type controls [29]. miR-146a may be involved in the regulation of inflammation in orbital fibroblasts, contributing to GO pathogenesis [30]. Exosomes derived from miR-146a-modified ADSCs reduced acute myocardial infarction (AMI)-induced myocardial damage by downregulating early growth response factor 1 (EGR1) [31]. Both in vitro and in vivo, miR-146a negatively regulates osteogenesis and bone regeneration in ADSCs [32]. In WAT, miR-146a may contribute to the regulation of inflammatory processes and prevent an overreaction to inflammation [33]. However, some studies suggest that miR-146a deficiency increases inflammation in the liver tissue without affecting lipid deposition in the liver [34]. Our findings indicate that low-abundance miR-146a-5p skeletal muscle-derived exosomes could be circulated to adipose tissue and increase adipogenesis. This indicates that miR-146a-5p plays different roles in different organs.

The interaction between skeletal muscle and fat is dynamic, in which excessive accumulation of fat can cause skeletal muscle atrophy that in turn increases fat differentiation [35]. Adipose tissue is an important fuel reservoir for animal bodies, providing energy for energy-consuming tissues such as the skeletal muscle and ensuring the normal energy operation of the body. The exosome is a natural vehicle for intercellular communication that can penetrate tissues, and diffuse into the blood [36]. These exosomes carry proteins, mRNA, and miRNA for mediating intercellular communication and regulating the function of the recipient cells [37,38]. Previous studies have shown that miR-146a-5p mimics inhibit the proliferation and differentiation of porcine intramuscular adipocyte precursor cells, whereas miR-146a-5p inhibitors promote cell proliferation and adipogenic differentiation of adipogenic precursor cells [23]. After miR-146a-/- systemic knockout, mice were fed a high-fat diet, and their body weight gain was significantly higher; additionally, the sliced cells in the adipose tissue of the mice were significantly larger than those of the control group [39], which is consistent with the phenotype of muscle-specific miR-146a knockout mice in this study. Our study demonstrated that after knocking out miR-146a-5p in mouse skeletal muscle tissue, the adipose tissue showed a promotion effect the same as a miR-146a-5p inhibitor on adipogenic formation, revealing that the skeletal muscle tissue has a potential regulatory effect on adipose development, and the skeletal muscle-derived exosome is the bridge between the two tissues. Thus, the miR-146a-5p is critical for regulating the balance between normal skeletal muscle development and adipogenesis.

In this study, the target gene of miR-146a-5p, GDF5, is a member of the TGF- β superfamily. GDF5 is mainly expressed in developing joints and lateral edges of joints and is a key regulator of cartilage and bone formation [40–42]. In addition, GDF5 also plays a key role in embryogenesis, limb development, and connective tissue repair [43]. Overexpression of GDF5 promotes brown adipocyte development in a transgenic mouse model [44]. PPAR γ is the main regulatory gene of adipocyte proliferation and differentiation, which promotes adipocyte differentiation and increases the expression of lipid metabolism-related genes. As an important marker gene of adipose differentiation, PPAR γ is of great significance to study the regulation of miRNAs. Up to now, a large number of studies have reported that miRNAs can directly or indirectly target the PPAR γ signaling pathway to regulate lipid metabolism [45,46]. Subsequent studies found that there is a positive correlation between the gene and protein expressions of GDF5 and PPAR γ during the differentiation of 3T3-L1 cells [47]. As research continues, the types of miRNAs found that regulate the expression of PPAR γ have increased, and their regulatory mechanisms are gradually explored, providing more selectivity for future applications such as obesity treatment. The present study thus shows that miR-146a-5p internalization plays a critical role in SKM-Exos-mediated adipogenesis, although other signaling pathways being regulated by GDF5/PPAR γ -related cannot be completely excluded.

4. Materials and Methods

4.1. Animals

The mice were housed under a 12 h light/12 h dark cycle at a constant temperature (23 ± 2 °C) with free access to food and water. The animals were fed ad libitum with standard mouse chow (18% protein, 4.5% fat, and 58% carbohydrate, purchased from Guangdong Medical Science Experiment Center, Guangzhou, Guangdong, China) for the first 8 weeks and high-fat chow (60 kcal% Fat from Research Diets, Cat No. D12492) from 8 to 20 weeks. All animal experiments used female mice aged 20 weeks at the time when they were sacrificed. The miR-146a-5p flox/flox (miR-146a^{flox+/+}) and Myf5-Cre mice using CRISPR/Cas9/Cre method were generated (Cyagen, Suzhou, China) and maintained on a C57BL/6 background. They were used to study the metabolic effects of long-term HFD supplementation. To generate skeletal muscle-specific miR-146a-5p knockout (mKO) mice, miR-146a^{flox+/+} mice were first crossed with Myf5-Cre mice to obtain F1(miR-146a^{flox+/-}, Cre^{+/-}). Then the F1 mice mated with miR-146a^{flox+/+} mice to produce the mKO mice (miR-146a^{flox+/+, Cre+/-}). The primer sequence of mouse genotype identification is shown in Table S1. The care of all animals and procedures at South China Agricultural University complies with “The Instructive Notions with Respect to Caring for Laboratory Animals” issued by the Ministry of Science and Technology of the People’s Republic of China and approved by the Animal Subjects Committee of South China Agricultural University.

4.2. NMR Analysis of the Whole-Body Composition

Body composition of mice was determined using quantitative magnetic resonance (QMR, Niumag Corporation, Shanghai, China).

4.3. IPITT and IPGTT

Before the intraperitoneal glucose tolerance test (IPGTT), mice fasted for 12 h. By using a blood glucose meter, blood glucose levels were measured at 0, 15, 30, 60, and 120 min after glucose ($1 \text{ g} \cdot \text{kg}^{-1}$) was injected intraperitoneally. In the intraperitoneal insulin tolerance test (IPITT), mice fasted for 6 h prior to the experiment. Insulin ($0.7 \text{ U} \cdot \text{kg}^{-1}$) was injected, and blood glucose levels were measured at 0, 15, 30, 60, and 120 min after injection.

4.4. In Vivo Oxygen Consumption Assay

Utilizing the promotion metabolism measurement system (Sable Systems International, North Las Vegas, NV, USA), we analyzed O₂ consumption (VO₂) and CO₂ production (VCO₂) in HFD.

4.5. Imaging Experiments

The tissue distribution of PKH67 (Sigma-Aldrich) labeled exosomes were visualized using fluorescence parameters as detected by the IVIS Lumina LT SeriesIII[®] imaging system after injection of PKH67-labeled exosomes into the tail vein. We isolated all tissue samples within a 1-h post-mortem, rinsed them in cold PBS to remove blood, and observed them. Exosomes labeled with PKH67 (Sigma-Aldrich, St. Louis, MI, USA) were measured at 490 nm and 520 nm.

4.6. HE Staining

Briefly, an aliquot of IngWAT (inguinal white adipose tissue) and EpiWAT (epididymal white adipose tissue) was fixed with 10% formalin and embedded with paraffin. Then, fixed IngWAT and EpiWAT were sectioned and stained with hematoxylin-eosin (HE).

4.7. Cell Lines, Culture Conditions, Transfection

The 3T3-L1 cells were grown in high-glucose Dulbecco’s Modified Eagle Medium (DMEM, Gibco) with 10% fetal bovine serum (FBS, Gibco) and 1% penicillin-streptomycin (P/S, Gibco) in a 5% CO₂ atmosphere at 37 °C. The differentiation was induced by incu-

bating confluent cells (in 12-well plates) for 2 days in differentiation media, which was comprised of DMEM supplemented with 10% FBS, 0.5 mM 3-isobutyl-1-methylxanthine (IBMX), 1 μ M dexamethasone, and 10 μ g/mL of insulin. Then the cells were cultured with 10 μ g/mL insulin in 10% FBS medium by changing the medium every 2 days until a mature lipid droplet appeared. For miR-146a-5p mimics or miR-146a-5p inhibitor (40 nM) (GenePharma, Shanghai, China) or si-GDF5 (50 nM) (Tsingke, Beijing, China) or exosome (10 μ g/mL) transfection, 3T3-L1 cells were plated in 12-well dishes at a density of 1.0×10^5 per well and lipofectamine 2000 (Thermo Fisher, Waltham, MA, USA) transfection started at the cell density reached 60 to 70%. The sequence of siRNA transfected by 3T3L-1 cells is shown in Table S2.

4.8. Cell Co-Culture

Transwell chambers (BIOFIL, TCS016012) were used to construct the co-culture systems. At the beginning of the test, the upper layer of the cell chamber was inoculated with 3T3-L1 cells (2.0×10^4 cells per well), and the lower layer with C2C12 cells (8.0×10^4 cells per well). They were cultured separately, co-cultured, and contacted for 48 h to detect indicators.

4.9. Collection of C2C12 Cell Culture Medium Supernatant

The C2C12 cells were seeded in 75 cm² cell culture flasks (1.0×10^6 cells/flasks) (Corning, Corning, NY, USA) exosome-free 10% FBS DMEM and grown for 48 h. Then, the cellular supernatant was collected. The C2C12 cells were plated in 12-well plates (Corning, 3513), seeded with 8.0×10^4 cells per well in DMEM supplemented with 10% FBS and 1% P/S. By adding 2% horse serum (HS, Gibco) after reaching 80% confluency, C2C12 cells became myotubes for 4 days. The supernatant was collected by contacting the cells with 2% exosome-free HS DMEM for 48 h.

4.10. Collection of Skeletal Muscle Tissue Culture Medium Supernatant

In order to obtain the mice skeletal muscle tissue-derived exosomes, the mice's were first identified by genotype. After identification, Flox mice and mKO mice were sacrificed by cervical dislocation and immersed in a beaker of 75% alcohol and isolated in a sterile environment. The skeletal muscle tissue of mice was removed, washed with PBS (containing 1% P/S), and placed in a medium containing exosome-free 10% FBS DMEM. Then, the skeletal muscle tissue was carefully cut into 1 mm³ pieces with fine scissors for 10 min and washed with PBS 3 times. Then, they were placed in a petri dish and kept in an incubator of a 5% CO₂ atmosphere at 37 °C for 24 h to collect the medium supernatant. The exosomes were named Flox-Exos and mKO-Exos, respectively.

4.11. Exosome Isolation

Isolation of exosomes in culture supernatant by ultracentrifugation. The specific steps were as follows. After centrifuging the culture supernatant at $2000 \times g$ for 10 min and $12,000 \times g$ for 30 min, large debris and dead cells were removed. An ultracentrifuge of $100,000 \times g$ for 70 min was performed on the supernatant. Finally, the cells were rinsed in 38 mL PBS and ultracentrifuged for 70 min at $100,000 \times g$. We resuspended the pellets in 100 μ L of PBS and stored them at -80 °C.

4.12. Transmission Electron Microscopy Analysis

Exosomes of 10 μ L were placed on copper grids coated with formvar, incubated for 5 min, and excess liquid was discarded. Uranyl acetate was added to the grid for negative stain for 1 min, and excess liquid was discarded. At 100 kV, samples were examined using transmission electron microscopy.

4.13. Dual-Luciferase Reporter Experiments

We seeded HEK293T cells in 96-well plates (Corning) at 2.5×10^4 cells per well and grew them overnight to 70–80% confluence. The dual-luciferase reporter plasmids were co-transfected with miRNA into HEK293T cells and the dosage of miR-146a-5p NC/mimic and wild-type/mutation/deletion dual-luciferase gene reporter vector per well was 3 pmol and 100 ng, respectively. The Dual-Luciferase Reporter Assay System (Promega) was used to detect luciferase activity after 48 h.

4.14. Nanoparticle Tracking Analysis

The exosomes were diluted to appropriate concentrations with PBS. The size of exosomes derived from cells or skeletal muscle tissue was measured by nanoparticle tracking analysis (NTA). Refer to the manual for the specific use of the instrument, including sample loading, photo-taking, and result statistics in brief.

4.15. Co-IP Experiment

The specific steps are shown in the instructions. In short, Pierce™ Protein A/G Magnetic Beads (88803, Thermo Scientific, Waltham, MA, USA) were used to bind GDF5 antibody and added to the lysed samples. The magnetic beads were pulled down with a magnet, and the resulting precipitate was detected using a western blot to confirm whether the target protein exists, and the sample lysate was directly used as the Input group control to detect the target protein.

4.16. Oil Red O Staining

After being treated and induced to mature, 3T3-L1 cells (24-well plates, Corning) were washed 3 times with PBS buffer, fixed in 4% formaldehyde for 30 min at room temperature, washed 3 times with PBS for 5 min each, and then stained with oil red O (Sigma-Aldrich, Shanghai, China) for 1 h. To create a working solution, oil red O was first diluted with water (3:2) and filtered through filter paper. After staining the cells, the plates were washed 3 times in PBS for 5 min each and then photographed under a microscope (TE2000-E; Nikon, Japan).

4.17. Triglyceride Accumulation

Triglyceride (TG) content was determined using a colorimetric/fluorometric assay kit (Biovision, Milpitas, CA, USA). 3T3-L1 cells were seeded into a 96-well plate and differentiated with CTE (500–1000 $\mu\text{g/mL}$) until they became mature adipocytes. A lipid droplet was then extracted by extraction buffer and converted by lipase to glycerol and fatty acid. A wavelength of 570 nm was used to measure the released glycerol.

4.18. Fatty Acid and Glucose Uptake Assay

Fatty acid and glucose uptake assays were carried out using Bodipy-FA (Invitrogen Cat No. D3835) and 2-NBDG (Sigma Cat No. 186689-07-6), which are fluorescent tracers.

4.19. Quantitative Real-Time PCR

We extracted the total RNA using TRIzol (Thermo Fisher). 1 μg of RNA was converted into complementary deoxyribonucleic acid (cDNA) using Color Reverse Transcription Kit (EZBioscience, Roseville, MN, USA, Cat No. A0010CGQ). We performed quantitative real-time PCR (qPCR) using a QuantStudio Real-Time PCR System (Bio-Rad C1000 Touch) using $2 \times$ RealStar Fast SYBR qPCR Mix (GenStar, Cat No. A301). The mRNA and miRNA internal references were GAPDH and U6. Quantitative real-time PCR primer sequence is shown in Table S3, and reverse transcription primer sequences are shown in Table S4.

4.20. Protein Extraction and Western Blot Analysis

Radioimmunoprecipitation assay (RIPA) buffer containing protease and phosphatase inhibitors (BestBio Cat No. BB-3101) was used to extract proteins. The protein concentration

was assessed using the Rapid Gold BCA Protein Assay Kit (Thermo Fisher). Western blotting analysis was performed by loading 15 µg of lysate onto sodium dodecyl sulfate-polyacrylamide gel electrophoresis (SDS-PAGE) gels, transferring the gels to polyvinylidene difluoride (PVDF) membranes (Millipore), and incubated with rabbit anti-GDF5 (1:1000, #A13167; ABclonal), rabbit anti-PPAR γ (1:1000, #2443; CST), rabbit anti-FASN (1:1000, #D262701; Sangon Biotech), rabbit anti-C/EBP α (1:1000, #2295; CST), rabbit anti-FABP4 (1:1000, #2120; CST), rabbit anti-CD36 (1:1000, #ab1336-25; Abcam), rabbit anti-GAPDH (1:5000, #BS65529; Bioworld), rabbit anti-CD9 (1:1000, #AP68-965-100; Abcepta), rabbit anti-CD63 (1:2000, #D160973; Sangon Biotech), rabbit anti-TSG101 (1:2000, #381538; ZEN BIO), rabbit anti-Alix (1:1000, #D262028; Sangon Biotech) or rabbit anti-Calnexin (1:1000, #D262986; Sangon Biotech). Afterward, goat anti-rabbit secondary antibody (1:50000, #BS13278, Bioworld) conjugated with HRP was used. GAPDH levels served as the loading control. The amount of protein was measured using ImageJ software.

4.21. Statistical Analysis

SPSS 25 and Graphpad prism 9.0 were used for one-way ANOVA and stand-alone sample t-test analysis and plotting. The results were presented as mean \pm standard error of the mean (SEM). The significance of the difference was judged by a level of * $p < 0.05$ or ** $p < 0.01$. The letters a, b, and c represent the level of statistical significance of the difference between the groups. Different letters mean a significant difference, and the same letters mean the difference is not significant.

5. Conclusions

In conclusion, our results suggest that high levels of miR-146a-5p in mice are inversely correlated with adipogenesis. Skeletal muscle secreted large quantities of exosomes containing abundant proteins, mRNA, and miRNAs. Additionally, there were notably high levels of miR-146a-5p. Under the uptake of adipocytes to skeletal muscle-derived exosomes, the skeletal muscle exosomal miR-146a-5p inhibits the synthesis of lipid droplets and adipocyte differentiation by down-regulating the expression of GDF5 in adipocytes and repressing the PPAR γ signaling pathway. In addition, miR-146a-5p blocked fatty acid uptake by decreasing CD36 expression. miR-146a-5p-specific knockout in skeletal muscle can improve the body weight, fat ratio, and glucose tolerance, and reduce the body's oxidative respiratory metabolism in mice. Our study provides new insights into the role of miR-146a-5p as a novel myokine in the cross-talk between skeletal muscle and fat tissue and contributes to the prevention and improvement of obesity by maintaining an appropriate ratio of skeletal muscle to fat.

Supplementary Materials: The following supporting information can be downloaded at: <https://www.mdpi.com/article/10.3390/ijms24054561/s1>.

Author Contributions: Data curation, M.Q.; formal analysis, M.Q.; funding acquisition, T.C., Y.Z., J.S. and Q.X.; investigation, M.Q., L.X., J.W., S.W. (Shulei Wen), J.L. (Junyi Luo), T.C., Y.F., J.Z., L.Y., J.L. (Jie Liu), J.X., X.C., C.Z., S.W. (Songbo Wang), L.W., G.S., Q.J., Y.Z., J.S. and Q.X.; methodology, M.Q.; project administration Q.J., Y.Z., J.S. and Q.X.; software, M.Q.; supervision, Q.X.; validation, L.X.; visualization, M.Q.; writing—original draft, M.Q.; writing—review & editing, M.Q., L.X., J.L. (Junyi Luo), J.S. and Q.X. All authors have read and agreed to the published version of the manuscript.

Funding: This research was funded by the Natural Science Foundation of China (32072814, 32072812, and 32072714) and the Project of Guangdong Provincial Nature Science Foundation (2023A1515012511, 2019A15150117734 and 2021A1515011310).

Institutional Review Board Statement: All of the experimental protocols and methods were approved by the College of Animal Science, South China Agricultural University (Ethical code number: SCAU-AEC-2015–0527). All of the experiments were conducted following the “The Instructive Notions with Respect to Caring for Laboratory Animals” issued by the Ministry of Science and Technology of the People’s Republic of China.

Informed Consent Statement: Not applicable.

Data Availability Statement: Not applicable.

Conflicts of Interest: The authors declare no conflict of interest.

Abbreviations

CD36: Cluster of differentiation 36 receptor; C/EBP α : CCAAT/enhancer binding protein alpha; EpiWAT: Epididymal white adipose tissue; Exos: Exosomes; FABP4: Fatty acid binding proteins4; Flox-Exos: Skeletal muscle-derived exosomes from the Flox mice; GDF5: Growth and differentiation factor 5; HE: Hematoxylin-eosin; IngWAT: Inguinal white adipose tissue; IPGTT: Intraperitoneal glucose tolerance test; IPITT: Intraperitoneal insulin tolerance test; miRNAs: microRNAs; mKO: skeletal muscle-specific knockout miR-146a-5p; NTA: Nanoparticle tracking analysis; PPAR γ : Peroxisome proliferator-activated receptor γ ; SKM: Skeletal muscle; SKM-Exos: Skeletal muscle-derived exosomes; TG: triglyceride.

References

1. Graf, C.; Ferrari, N. Metabolic Health—The Role of Adipo-Myokines. *Int. J. Mol. Sci.* **2019**, *20*, 6159. [\[CrossRef\]](#) [\[PubMed\]](#)
2. Manole, E.; Ceafalan, L.C.; Popescu, B.O.; Dumitru, C.; Bastian, A.E. Myokines as Possible Therapeutic Targets in Cancer Cachexia. *J. Immunol. Res.* **2018**, *2018*, 8260742. [\[CrossRef\]](#) [\[PubMed\]](#)
3. Boström, P.; Wu, J.; Jedrychowski, M.P.; Korde, A.; Ye, L.; Lo, J.C.; Rasbach, K.A.; Boström, E.A.; Choi, J.H.; Long, J.Z.; et al. A PGC1- α -dependent myokine that drives brown-fat-like development of white fat and thermogenesis. *Nature* **2012**, *481*, 463–468. [\[CrossRef\]](#)
4. Ferrer, B.; Navia, B.; Giralt, M.; Comes, G.; Carrasco, J.; Molinero, A.; Quintana, A.; Señarís, R.M.; Hidalgo, J. Muscle-specific interleukin-6 deletion influences body weight and body fat in a sex-dependent manner. *Brain Behav. Immun.* **2014**, *40*, 121–130. [\[CrossRef\]](#) [\[PubMed\]](#)
5. Artaza, J.N.; Bhasin, S.; Magee, T.R.; Reisz-Porszasz, S.; Shen, R.; Groome, N.P.; Meerasahib, M.F.; Gonzalez-Cadavid, N.F. Myostatin inhibits myogenesis and promotes adipogenesis in C3H 10T(1/2) mesenchymal multipotent cells. *Endocrinology* **2005**, *146*, 3547–3557. [\[CrossRef\]](#)
6. Yoon, H.; Spinelli, J.B.; Zaganjor, E.; Wong, S.J.; German, N.J.; Randall, E.C.; Dean, A.; Clermont, A.; Paulo, J.A.; Garcia, D.; et al. PHD3 Loss Promotes Exercise Capacity and Fat Oxidation in Skeletal Muscle. *Cell Metab.* **2020**, *32*, 215–228. [\[CrossRef\]](#)
7. Shimizu, N.; Maruyama, T.; Yoshikawa, N.; Matsumiya, R.; Ma, Y.; Ito, N.; Tasaka, Y.; Kuribara-Souta, A.; Miyata, K.; Oike, Y.; et al. A muscle-liver-fat signalling axis is essential for central control of adaptive adipose remodelling. *Nat. Commun.* **2015**, *6*, 6693. [\[CrossRef\]](#)
8. Pedersen, B.K.; Febbraio, M.A. Muscles, exercise and obesity: Skeletal muscle as a secretory organ. *Nat. Rev. Endocrinol.* **2012**, *8*, 457–465. [\[CrossRef\]](#)
9. Stanford, K.I.; Goodyear, L.J. Exercise regulation of adipose tissue. *Adipocyte* **2016**, *5*, 153–162. [\[CrossRef\]](#)
10. Kowal, J.; Arras, G.; Colombo, M.; Jouve, M.; Morath, J.P.; Primdal-Bengtson, B.; Dingli, F.; Loew, D.; Tkach, M.; Théry, C. Proteomic comparison defines novel markers to characterize heterogeneous populations of extracellular vesicle subtypes. *Proc. Natl. Acad. Sci. USA* **2016**, *113*, E968–E977. [\[CrossRef\]](#)
11. Yang, D.; Zhang, W.; Zhang, H.; Zhang, F.; Chen, L.; Ma, L.; Larcher, L.M.; Chen, S.; Liu, N.; Zhao, Q.; et al. Progress, opportunity, and perspective on exosome isolation—Efforts for efficient exosome-based theranostics. *Theranostics* **2020**, *10*, 3684–3707. [\[CrossRef\]](#)
12. Wang, Y.; Balaji, V.; Kaniyappan, S.; Krüger, L.; Irsen, S.; Tepper, K.; Chandupatla, R.; Maetzler, W.; Schneider, A.; Mandelkow, E.; et al. The release and trans-synaptic transmission of Tau via exosomes. *Mol. Neurodegener.* **2017**, *12*, 5. [\[CrossRef\]](#) [\[PubMed\]](#)
13. Severinsen, M.C.K.; Pedersen, B.K. Muscle-Organ Crosstalk: The Emerging Roles of Myokines. *Endocr. Rev.* **2020**, *41*, 594–609. [\[CrossRef\]](#) [\[PubMed\]](#)
14. Guescini, M.; Canonico, B.; Lucertini, F.; Maggio, S.; Annibalini, G.; Barbieri, E.; Luchetti, F.; Papa, S.; Stocchi, V. Muscle Releases Alpha-Sarcoglycan Positive Extracellular Vesicles Carrying miRNAs in the Bloodstream. *PLoS ONE* **2015**, *10*, e0125094. [\[CrossRef\]](#)
15. Fulzele, S.; Mendhe, B.; Khayrullin, A.; Johnson, M.; Kaiser, H.; Liu, Y.; Isales, C.M.; Hamrick, M.W. Muscle-derived miR-34a increases with age in circulating extracellular vesicles and induces senescence of bone marrow stem cells. *Aging* **2019**, *1*, 1791–1803. [\[CrossRef\]](#) [\[PubMed\]](#)
16. Aswad, H.; Forterre, A.; Wiklander, O.P.; Vial, G.; Danty-Berger, E.; Jalabert, A.; Lamazière, A.; Meugnier, E.; Pesenti, S.; Ott, C.; et al. Exosomes participate in the alteration of muscle homeostasis during lipid-induced insulin resistance in mice. *Diabetologia* **2014**, *57*, 2155–2164. [\[CrossRef\]](#)
17. Kourembanas, S. Exosomes: Vehicles of intercellular signaling, biomarkers, and vectors of cell therapy. *Annu. Rev. Physiol.* **2015**, *77*, 13–27. [\[CrossRef\]](#)

18. Donzelli, J.; Proestler, E.; Riedel, A.; Nevermann, S.; Hertel, B.; Guenther, A.; Gattenlöhner, S.; Savai, R.; Larsson, K.; Saul, M.J. Small extracellular vesicle-derived miR-574-5p regulates PGE2-biosynthesis via TLR7/8 in lung cancer. *J. Extracell. Vesicles* **2021**, *10*, e12143. [\[CrossRef\]](#)
19. Krützfeldt, J.; Stoffel, M. MicroRNAs: A new class of regulatory genes affecting metabolism. *Cell Metab.* **2006**, *4*, 9–12. [\[CrossRef\]](#)
20. Yu, Y.; Du, H.; Wei, S.; Feng, L.; Li, J.; Yao, F.; Zhang, M.; Hatch, G.M.; Chen, L. Adipocyte-Derived Exosomal MiR-27a Induces Insulin Resistance in Skeletal Muscle through Repression of PPAR γ . *Theranostics* **2018**, *8*, 2171–2188. [\[CrossRef\]](#)
21. Wang, Y.C.; Li, Y.; Wang, X.Y.; Zhang, D.; Zhang, H.; Wu, Q.; He, Y.Q.; Wang, J.Y.; Zhang, L.; Xia, H.; et al. Circulating miR-130b mediates metabolic crosstalk between fat and muscle in overweight/obesity. *Diabetologia* **2013**, *56*, 2275–2285. [\[CrossRef\]](#)
22. He, L.; Zhu, C.; Jia, J.; Hao, X.Y.; Yu, X.Y.; Liu, X.Y.; Shu, M.G. ADSC-Exos containing MALAT1 promotes wound healing by targeting miR-124 through activating Wnt/ β -catenin pathway. *Biosci. Rep.* **2020**, *40*, BSR20192549. [\[CrossRef\]](#) [\[PubMed\]](#)
23. Zhang, Q.; Cai, R.; Tang, G.; Zhang, W.; Pang, W. MiR-146a-5p targeting SMAD4 and TRAF6 inhibits adipogenesis through TGF- β and AKT/mTORC1 signal pathways in porcine intramuscular preadipocytes. *J. Anim. Sci. Biotechnol.* **2021**, *12*, 12. [\[CrossRef\]](#)
24. Li, K.; Zhao, B.; Wei, D.; Wang, W.; Cui, Y.; Qian, L.; Liu, G. miR-146a improves hepatic lipid and glucose metabolism by targeting MED1. *Int. J. Mol. Med.* **2020**, *45*, 543–555. [\[CrossRef\]](#)
25. Nunes, A.D.C.; Weigl, M.; Schneider, A.; Noureddine, S.; Yu, L.; Lahde, C.; Saccon, T.D.; Mitra, K.; Beltran, E.; Grillari, J.; et al. miR-146a-5p modulates cellular senescence and apoptosis in visceral adipose tissue of long-lived Ames dwarf mice and in cultured pre-adipocytes. *Geroscience* **2022**, *44*, 503–518. [\[CrossRef\]](#) [\[PubMed\]](#)
26. Saferding, V.; Hofmann, M.; Brunner, J.S.; Niederreiter, B.; Timmen, M.; Magilnick, N.; Hayer, S.; Heller, G.; Steiner, G.; Stange, R.; et al. microRNA-146a controls age-related bone loss. *Aging Cell* **2020**, *19*, e13244. [\[CrossRef\]](#) [\[PubMed\]](#)
27. Li, W.; Wen, S.; Wu, J.; Zeng, B.; Chen, T.; Luo, J.; Shu, G.; Wang, S.B.; Zhang, Y.; Xi, Q. Comparative Analysis of MicroRNA Expression Profiles between Skeletal Muscle- and Adipose-Derived Exosomes in Pig. *Front. Genet.* **2021**, *12*, 631230. [\[CrossRef\]](#) [\[PubMed\]](#)
28. Bose, M.; Bhattacharyya, S.N. Target-dependent biogenesis of cognate microRNAs in human cells. *Nat. Commun.* **2016**, *7*, 12200. [\[CrossRef\]](#)
29. Runtsch, M.C.; Nelson, M.C.; Lee, S.H.; Voth, W.; Alexander, M.; Hu, R.; Wallace, J.; Petersen, C.; Panic, V.; Villanueva, C.J.; et al. Anti-inflammatory microRNA-146a protects mice from diet-induced metabolic disease. *PLoS Genet.* **2019**, *15*, e1007970. [\[CrossRef\]](#)
30. Jang, S.Y.; Chae, M.K.; Lee, J.H.; Lee, E.J.; Yoon, J.S. Role of miR-146a in the Regulation of Inflammation in an In Vitro Model of Graves' Orbitopathy. *Investig. Ophthalmol. Vis. Sci.* **2016**, *57*, 4027–4034. [\[CrossRef\]](#)
31. Pan, J.; Alimujiang, M.; Chen, Q.; Shi, H.; Luo, X. Exosomes derived from miR-146a-modified adipose-derived stem cells attenuate acute myocardial infarction-induced myocardial damage via downregulation of early growth response factor 1. *J. Cell. Biochem.* **2019**, *120*, 4433–4443. [\[CrossRef\]](#)
32. Xie, Q.; Wei, W.; Ruan, J.; Ding, Y.; Zhuang, A.; Bi, X.; Sun, H.; Gu, P.; Wang, Z.; Fan, X. Effects of miR-146a on the osteogenesis of adipose-derived mesenchymal stem cells and bone regeneration. *Sci. Rep.* **2017**, *7*, 42840. [\[CrossRef\]](#) [\[PubMed\]](#)
33. Roos, J.; Enlund, E.; Funcke, J.B.; Tews, D.; Holzmann, K.; Debatin, K.M.; Wabitsch, M.; Fischer-Posovszky, P. miR-146a-mediated suppression of the inflammatory response in human adipocytes. *Sci. Rep.* **2016**, *6*, 38339. [\[CrossRef\]](#) [\[PubMed\]](#)
34. Javidan, A.; Jiang, W.; Okuyama, M.; Thiagarajan, D.; Yang, L.; Moorleghen, J.J.; Muniappan, L.; Subramanian, V. miR-146a Deficiency Accelerates Hepatic Inflammation without Influencing Diet-Induced Obesity in Mice. *Sci. Rep.* **2019**, *9*, 12626. [\[CrossRef\]](#) [\[PubMed\]](#)
35. Shan, T.; Liu, W.; Kuang, S. Fatty acid binding protein 4 expression marks a population of adipocyte progenitors in white and brown adipose tissues. *FASEB J.* **2013**, *27*, 277–287. [\[CrossRef\]](#) [\[PubMed\]](#)
36. Abbas, T.O.; Ali, T.A.; Uddin, S. Urine as a Main Effector in Urological Tissue Engineering-A Double-Edged Sword. *Cells* **2020**, *9*, 538. [\[CrossRef\]](#) [\[PubMed\]](#)
37. Hu, H.; Dong, L.; Bu, Z.; Shen, Y.; Luo, J.; Zhang, H.; Zhao, S.; Lv, F.; Liu, Z. miR-23a-3p-abundant small extracellular vesicles released from Gelma/nanoclay hydrogel for cartilage regeneration. *J. Extracell. Vesicles* **2020**, *9*, 1778883. [\[CrossRef\]](#)
38. Sato, K.; Kennedy, L.; Liangpunsakul, S.; Kusumanchi, P.; Yang, Z.; Meng, F.; Glaser, S.; Francis, H.; Alpini, G. Intercellular Communication between Hepatic Cells in Liver Diseases. *Int. J. Mol. Sci.* **2019**, *20*, 2180. [\[CrossRef\]](#) [\[PubMed\]](#)
39. Roos, J.; Dahlhaus, M.; Funcke, J.B.; Kustermann, M.; Strauss, G.; Halbgebauer, D.; Boldrin, E.; Holzmann, K.; Möller, P.; Trojanowski, B.M.; et al. miR-146a regulates insulin sensitivity via NPR3. *Cell. Mol. Life Sci.* **2021**, *78*, 2987–3003. [\[CrossRef\]](#)
40. Francis-West, P.H.; Abdelfattah, A.; Chen, P.; Allen, C.; Parish, J.; Ladher, R.; Allen, S.; MacPherson, S.; Luyten, F.P.; Archer, C.W. Mechanisms of GDF-5 action during skeletal development. *Development* **1999**, *126*, 1305–1315. [\[CrossRef\]](#)
41. Takahara, M.; Harada, M.; Guan, D.; Otsuji, M.; Naruse, T.; Takagi, M.; Ogino, T. Developmental failure of phalanges in the absence of growth/differentiation factor 5. *Bone* **2004**, *35*, 1069–1076. [\[CrossRef\]](#) [\[PubMed\]](#)
42. Oshin, A.O.; Caporali, E.; Byron, C.R.; Stewart, A.A.; Stewart, M.C. Phenotypic maintenance of articular chondrocytes in vitro requires BMP activity. *Vet. Comp. Orthop. Traumatol.* **2007**, *20*, 185–191. [\[CrossRef\]](#)
43. Hatakeyama, Y.; Tuan, R.S.; Shum, L. Distinct functions of BMP4 and GDF5 in the regulation of chondrogenesis. *J. Cell. Biochem.* **2004**, *91*, 1204–1217. [\[CrossRef\]](#) [\[PubMed\]](#)
44. Hinoi, E.; Nakamura, Y.; Takada, S.; Fujita, H.; Iezaki, T.; Hashizume, S.; Takahashi, S.; Odaka, Y.; Watanabe, T.; Yoneda, Y. Growth differentiation factor-5 promotes brown adipogenesis in systemic energy expenditure. *Diabetes* **2014**, *63*, 162–175. [\[CrossRef\]](#)

45. Karbiener, M.; Fischer, C.; Nowitsch, S.; Opriessnig, P.; Papak, C.; Ailhaud, G.; Dani, C.; Amri, E.Z.; Scheideler, M. microRNA miR-27b impairs human adipocyte differentiation and targets PPAR γ . *Biochem. Biophys. Res. Commun.* **2009**, *390*, 247–251. [[CrossRef](#)] [[PubMed](#)]
46. Lee, E.K.; Lee, M.J.; Abdelmohsen, K.; Kim, W.; Kim, M.M.; Srikantan, S.; Martindale, J.L.; Hutchison, E.R.; Kim, H.H.; Marasa, B.S.; et al. miR-130 suppresses adipogenesis by inhibiting peroxisome proliferator-activated receptor gamma expression. *Mol. Cell. Biol.* **2011**, *31*, 626–638. [[CrossRef](#)] [[PubMed](#)]
47. Pei, Z.; Yang, Y.; Kiess, W.; Sun, C.; Luo, F. Dynamic profile and adipogenic role of growth differentiation factor 5 (GDF5) in the differentiation of 3T3-L1 preadipocytes. *Arch. Biochem. Biophys.* **2014**, *560*, 27–35. [[CrossRef](#)]

Disclaimer/Publisher’s Note: The statements, opinions and data contained in all publications are solely those of the individual author(s) and contributor(s) and not of MDPI and/or the editor(s). MDPI and/or the editor(s) disclaim responsibility for any injury to people or property resulting from any ideas, methods, instructions or products referred to in the content.

Article

Plant MIR167e-5p Inhibits Enterocyte Proliferation by Targeting β -Catenin

Meng Li [†], Ting Chen [†], Jia-Jian He, Jia-Han Wu, Jun-Yi Luo, Rui-Song Ye, Mei-Ying Xie, Hao-Jie Zhang, Bin Zeng, Jie Liu, Qian-Yun Xi, Qing-Yan Jiang, Jia-Jie Sun ^{*} and Yong-Liang Zhang ^{*,†}

Guangdong Provincial Key Laboratory of Animal Nutritional Control, National Engineering Research Center for Breeding Swine Industry, College of Animal Science, South China Agricultural University, Guangzhou 510642, China; limengscau@163.com (M.L.); allinchen@scau.edu.cn (T.C.); scauhejiajian@163.com (J.-J.H.); jiahan94@foxmail.com (J.-H.W.); luojunyi@scau.edu.cn (J.-Y.L.); yiguangnian2004@163.com (R.-S.Y.); xxiemy@163.com (M.-Y.X.); zhanghj089@126.com (H.-J.Z.); zhanghj089@126.com (B.Z.); 15800202206@163.com (J.L.); xqy0228@163.com (Q.-Y.X.); qyjiang@scau.edu.cn (Q.-Y.J.)

^{*} Correspondence: jiajiekong@126.com (J.-J.S.); zhangyl@scau.edu.cn (Y.-L.Z.); Tel.: +86-20-85281269 (Y.-L.Z.); Fax: +86-20-85280740 (Y.-L.Z.)

[†] These authors contributed equally to this work.

[‡] Present Address: Yong-Liang Zhang, College of Animal Science, South China Agricultural University, 483 Wushan Road, Guangzhou 510642, China.

Received: 5 June 2019; Accepted: 31 October 2019; Published: 4 November 2019



Abstract: MicroRNAs (miRNAs) are important negative regulators of genes involved in physiological and pathological processes in plants and animals. It is worth exploring whether plant miRNAs play a cross-kingdom regulatory role in animals. Herein, we found that plant MIR167e-5p regulates the proliferation of enterocytes in vitro. A porcine jejunum epithelial cell line (IPEC-J2) and a human colon carcinoma cell line (Caco-2) were treated with 0, 10, 20, and 40 pmol of synthetic 2'-O-methylated plant MIR167e-5p, followed by a treatment with 20 pmol of MIR167e-5p for 0, 24, 48, and 72 h. The cells were counted, and IPEC-J2 cell viability was determined by the MTT and EdU assays at different time points. The results showed that MIR167e-5p significantly inhibited the proliferation of enterocytes in a dose- and time-dependent manner. Bioinformatics prediction and a luciferase reporter assay indicated that MIR167e-5p targets β -catenin. In IPEC-J2 and Caco-2 cells, MIR167e-5p suppressed proliferation by downregulating β -catenin mRNA and protein levels. MIR167e-5p relieved this inhibition. Similar results were achieved for the β -catenin downstream target gene c-Myc and the proliferation-associated gene PCNA. This research demonstrates that plant MIR167e-5p can inhibit enterocyte proliferation by targeting the β -catenin pathway. More importantly, plant miRNAs may be a new class of bioactive molecules for epigenetic regulation in humans and animals.

Keywords: MIR167e-5p; β -catenin; enterocyte; proliferation

1. Introduction

MicroRNAs (miRNAs) are critical biological molecules and have attracted much attention for more than a decade. The functions of miRNA are well established in plants and animals. These single-stranded molecules impact on fundamental biological processes, including proliferation, differentiation, immune responses, and metabolism in different species. The recent detection of plant miRNAs in body fluids, including serum [1], urine [2], saliva [3], and milk [4], suggests that these endogenous circulating miRNAs may be broadly implicated in miRNA-mediated control of gene expression. Subsequent studies

have suggested that plant miRNAs might regulate gene expression in mammalian cells. In mouse liver, plant MIR168a targets low-density lipoprotein receptor adapter protein 1 (LDLRAP1), which results in the elevation of LDL-cholesterol level in the plasma [5]. Plant MIR2911 has been reported to target the *PB2* and *NS1* genes encoded by influenza A viruses (IAVs) H1N1, inhibiting H1N1 viral replication [6]. MIR159 is capable of inhibiting cancer proliferation by targeting T cell factor (TCF) 7 [7]. MIR156a can directly target junction adhesion molecule-A (JAM-A), reducing inflammatory cytokine-induced monocytes adhesion [8]. Plant MIR162a in bee bread can even regulate honeybee caste development [9]. Surprisingly, a recent study shows that *Cuscuta campestris* miRNAs were induced through the haustorium to target and reduce the accumulation of mRNAs, such as those for F-box/RNI-like superfamily protein (TIR1) and sieve element occlusion amino-terminus protein 1 (SEOR1), in host plants [10]. These findings provide new evidence that food-derived miRNAs may elicit the regulation of gene expression and be used in nutritional therapies for animal and human beings.

Some researchers have identified all intestinal miRNAs and shown that miRNAs play a vital role in the differentiation and function of the intestine by using gene ablation of Dicer1 [11]. A study demonstrated that grape exosome-like nanoparticles (GELNs) could penetrate the intestinal mucus barrier and were taken up by mouse intestinal stem cells, causing a significant induction of Lgr5 intestinal stem cells through the Wnt/ β -catenin pathway and protecting the mice from dextran sulphate sodium (DSS)-induced colitis [12]. Subsequently, it was found that edible plant-derived exosome-like nanoparticles (EPDELNs) could instigate EPDELN-mediated interspecies communication by inducing the expression of genes for anti-inflammatory cytokines, antioxidation, and activation of Wnt signaling, which are crucial for maintaining intestinal homeostasis [13]. Many EPDELNs have anti-inflammatory properties. MiRNAs have been detected in 11 EPDELNs and found to have the potential to regulate human mRNA [14]. Exosome-like nanoparticles (ELNs) mediate miR7267-3p-mediated targeting of *Lactobacillus rhamnosus* (LGG) monooxygenase *ycnE* yielded increased indole-3-carboxaldehyde, inducing the production of interleukin (IL)-22 and ameliorating mouse colitis via IL-22-dependent mechanisms [15]. MiRNAs can be selectively encapsulated in extracellular vesicles and perform anti-inflammatory functions. These findings suggest that plant miRNAs have important effects on the regulation of intestinal functions.

The intestinal tract not only is the first line of defense against harmful pathogens, but also is the main place for the digestion and absorption of nutrients. Ontogenetic development of the mammalian intestine is a topologically and temporally highly organized process. Intestinal stem cells (ISCs) constantly produce enterocytes and endocrine cells to maintain homeostasis in the intestinal epithelium [16]. One of the crucial results of this process is the formation of a specialized intestinal epithelium that exerts digestive and absorptive functions, as well as certain endocrine and immunological roles [16]. The survival of newborns and the maintenance of homeostasis require the regulation of the intestinal epithelium operating as a crucial unit [17]. Therefore, it is particularly important to maintain normal intestinal morphology and structure. The morphogenetic process and the acquisition of particular cell fates are coordinated by a relatively small number of highly evolutionarily conserved signaling pathways, including the canonical Wnt signaling pathway [18]. The standard model of Wnt/ β -catenin signaling states that, upon stimulation by the Wnt ligand, β -catenin accumulates and subsequently translocates to the nucleus to activate the TCF-dependent transcription of a variety of target genes, including cellular myelocytomatosis oncogene (c-Myc) [19]. This pathway has been shown to play a central role in cell proliferation, differentiation, and stem cell maintenance [18]. Sun et al. found that miR-320a can target the β -catenin gene and inhibit the proliferation of colorectal cancer cells [20]. While plant miRNAs have been involved in canonical Wnt activity regulatory processes, their effects on the proliferation of intestinal cells remain to be explored.

We hypothesized that plant miRNA might be an exogenous regulator influencing animal enterocytes' functions. We found that plant MIR167e-5p could inhibit enterocyte proliferation and further identified β -catenin as a target of MIR167e-5p. This study demonstrates that plant miRNAs can influence the growth of enterocytes and thus serve as important bioactive molecules.

2. Materials and Methods

2.1. Cell Culture and Transfection of Cells with MIR167e-5p

IPEC-J2, STC-1, and Caco-2 cells were seeded at a density of 1×10^5 , 4×10^5 , and 2×10^5 cells, respectively, in 12-well plates overnight (70–80% confluency) and transfected for 6 hours (h) the following day using Lipofectamine 2000 (Invitrogen, Carlsbad, CA, USA), according to the manufacturer's instructions. The treatment groups were as follow: MIR167e-5p group (MIR167e-5p mimics, 20 pmol), NC group (normal control, 20 pmol), MIR167e-5p inhibitor group (MIR167e-5p inhibitor, 20 pmol), i-NC group (inhibitor normal control, 20 pmol), MIR167e-5p+inhibitor group (20 pmol MIR167e-5p mimics +40 pmol MIR167e-5p inhibitor). The cells were harvested at 0, 24, 48, or 72h after transfection for cell counting, real-time quantitative PCR (qPCR), and western blot analysis.

2.2. RNA Isolation

Total RNA was extracted from the cells using TRIzol Reagent (Invitrogen) according to the manufactures' instruction. RNA concentration was determined by an ND-2000 Nanodrop spectrophotometer (NanoDrop Technology, Wilmington, DE, USA). RNA integrity was examined by gel electrophoresis using a 0.8% agarose gel. The RNA was used for further PCR and qPCR analyses.

2.3. PCR and qPCR Analyses

Total RNA (2 µg) was reverse-transcribed to cDNA using M-MLV-R transcriptase (Promega, Madison, WI, USA) with OligodT18 (for mRNA) or a specific stem-loop RT primer (for miRNA). The samples were amplified by PCR using complementary primers. To quantify miRNAs and mRNAs, cDNA was diluted 5-fold with ddH₂O, and qPCR (20 µL) was performed on a Bio-Rad CFX Manager 3.1 instrument (Applied Biosystems, Waltham, MA, USA) with U6 (miRNA control) or β-actin (mRNA control) as internal controls. The reactions contained 2 µL cDNA, 10 µL 2× GoTaq Qpcr Master Mix (Promega), and 0.4 µL of each primer (10 µM). The thermal profile of real-time PCR involved an initial denaturation step at 95 °C for 5 min (min), followed by 40 cycles at 94 °C for 15 s, 15 s at the corresponding annealing temperature (T_m), extension at 72 °C for 30 s, followed by a quick denaturation at 95 °C for 10 s, plus a slow ramp from T_m to 95 °C to generate a melting curve to confirm the specificity of the amplified product. A no template (NT) negative control was included for each miRNA and mRNA, and all reactions were performed in triplicate. The 2^{−ΔC_t} method was employed to quantify and normalize the expression data. The miRNAs, mRNAs primers, and specific stem-loop RT primers were designed with Premier Primer 5.0 (Premier Software, San Jose, CA, USA) (Table 1).

Table 1. qPCR and PCR primers.

Gen	Sequences	Product Length (bp)	T _M	Gene Accession
Stem-loop-RT-MIR167e-5p primer	GTCGTATCCAGTGCCTGTCGTG GAGTCGGCAATTGCACT GGATACGAC CAGATC	74		
MIR167e-5p-F Stem-loop Universal	TGAAGCTGCCAGCATGAT ATCCAGTGCCTGTCGTGGA	68	56	
Ssc-PCNA-F Ssc-PCNA-R	TTCTTCCACCTGTAGCCG TTGGACATGCTGGTGAGG	269	60	NM_001291925.1
Ssc-c-Myc-F Ssc-c-Myc-R	GTCCAAGCAGAGGAGCAAA ATGGGCAAGAGTTCCGTAG	103	58	HF549032.1
Ssc-β-catenin-F Ssc-β-catenin-R	TGAACCTGCCATCTGTGC TCCGTAGTGAAGGCGAAC	88	58	AB046171.1
Homo-PCNA-F Homo-PCNA-R	AGGCACTCAAGGACCTCATC GCCAAGGTATCCGCGTTATC	250	58	CR541799.1

Table 1. Cont.

Gen	Sequences	Product Length (bp)	TM	Gene Accession
Homo- β -catenin-F	CTGGCAGCAACAGTCTTACC	224	58	X87838.1
Homo- β -catenin-R	ACATAGCAGCTCGTACCCTC			
Homo-c-Myc-F	CACATCAGCACAACTACGCA	119	58	NM_002467.6
Homo-c-Myc-R	GGTGCATTTTCGGTTGTTGC			
β -actin-F	CCAGCACCATGAAGATCAAGATC	55	60	AY550069.1
β -actin-R	ACATCTGCTGGAAGGTGGACA			
U6-F	CTCGCTTCGGCAGCACACA	71	60	NR_004394
U6-R	AACGCTTCACGAATTTGCGT			

2.4. Western Blot Analysis

Total proteins were isolated from the cells using RIPA buffer with 1 nM phenylmethylsulphonyl fluoride (PMSF) and quantified with a BCA Total Protein Assay Kit (Thermo Fisher, Waltham, MA, USA). The protein suspension (30 μ g) was supplemented with β -mercaptoethanol, boiled for 10 min, resolved by 5% and 10% sodium dodecyl sulphate-polyacrylamide gel electrophoresis (SDS-PAGE), and transferred to a polyvinylidene difluoride membrane. β -catenin and c-Myc were detected by incubation with primary anti-human β -catenin (1:500, Sangon Biotech, Shanghai, China) and anti-human c-Myc (1:1000, Sangon Biotech) antibodies, followed by incubation with rabbit HRP-linked IgG1 secondary antibodies (1:50,000, Bioworld Technology, St Louis Park, MN, USA). β -actin (1:5000, Bioworld Technology) served as a control. Band intensities were measured using Image J and were normalized against β -actin band intensity.

2.5. Dual-Luciferase Reporter Assay

On the basis of the predicted miRNA–mRNAs binding sequences, normal sequences bearing an MIR167e-5p target site or with MIR167e-5p target site-deleted β -catenin 3'-UTR were generated by two complementary chemically synthesized primers (Sangon Biotech) as follows: wt- β -catenin-3'UTR-sense (tcgagttgtatctaaagtcggtgttgccagcttcagttggttctgt), wt- β -catenin-3'UTR-antisense (ctagaggaaccaactga agctggcaacaccggacttagatacaac), del- β -catenin-3'UTR-sense (tcgagttgtatctaaagtcggtgttgccagttggttctgt), and del- β -catenin-3'UTR-antisense (ctagacaggaaccaactgaacaccggacttagatacaac). The complementary oligonucleotides were re-suspended at a 1:1 ratio (1 μ g/ μ L each) in annealing buffer (10 mM TRIS, pH 7.5–8.0, 50 mM NaCl, 1 mM EDTA) and heated at 95 °C for 10 min to denature the secondary structures. The temperature was then gradually lowered to room temperature. Annealed products were cloned into the pmir-GLO vector (Promega) downstream from the firefly luciferase coding region (between *XhoI* and *XbaI* sites). HeLa cells were seeded in 96-well cell culture plates (3.5 \times 10⁴ cells per well) and cultured in RPMI 1640 (Life Technologies, Grand Island, NY, USA) with 10% fetal bovine serum (FBS). The next day, the cells were transfected with recombinant pmirGLO-3'UTR vector (100 ng/well) mixed with their corresponding MIR167e-5p mimics or NC (3 pmol/well, RiboBio, Guangzhou, Guangdong, China) for 6 h using Lipofectamine 2000 (Invitrogen). The cells were harvested 24 h after transfection, and luciferase activity was detected by a dual luciferase reporter assay system (Promega) according to the manufacturer's recommendations. The normalized firefly luciferase activity (firefly luciferase activity/Renilla luciferase activity) of each construct was compared with that of the pmirGLO vector.

2.6. 3-(4,5-Dimethyl-2-thiazolyl)-2,5-diphenyl-2H-tetrazolium bromide (MTT) Assay

The MTT kit was purchased from Beyotime Biotechnology (Shanghai, China) and used according to the manufacturer's protocol. Briefly, IPEC-J2 cells were seeded in 96-well plates at a density of 4000 cells per well with 200 μ L of complete culture medium. After being allowed to adhere and spread for 12 h, the cells were treated with 3 pmol of MIR167e-5p, NC, inhibitor, and i-NC for 0, 24, 48, and 72 h. MTT assays were performed by incubating the treated IPEC-J2 cells with 20 μ L (5 mg/mL) of

MTT labelling solution. After 4 h of incubation, IPEC-J2 were lysed with 150 μ L of DMSO, and the purple formazan crystals were solubilized for detection at 570 nm.

2.7. 5-Ethynyl-2'-deoxyuridine (EdU) Incorporation Assay

Cell proliferation was assessed by a Cell-Light EdU Apollo 488 In Vitro Imaging Kit (Ribobio), according to the manufacturer's instructions. IPEC-J2 cells were incubated with 1:1000 EdU diluted in culture solution for 2 h at 37 °C before harvesting. After several washes, the cells were fixed with 4% paraformaldehyde (pH 7.4) for 30 min and incubated with glycine (2 mg/mL) for 5 min. The fixed cells were washed with 0.5% Triton-100 (diluted in phosphate-buffered saline (PBS)) for 10 min, followed by staining with Apollo buffer (RiboBio) for 30 min at room temperature in the dark. The cells were incubated with Hoechst 33342 dye at room temperature for 30 min in the dark. Finally, images were captured using fluorescent microscopy and IR-DIC imaging on an Eclipse FN-1 upright microscope (Nikon, Tokyo, Japan) at a magnification of 100 \times .

2.8. Statistical Analyses

Least significant difference (LSD) tests were used for multiple comparisons, and *t*-tests were employed for pairwise comparisons ($p < 0.05$ was considered statistically significant). Data are presented as the mean \pm standard error (S.E.), and all analyses were performed using GraphPad Prism software 6.0 (GraphPad Software, San Diego, Canada).

3. Results

3.1. Synthetic MIR167e-5p Suppresses the Proliferation of Enterocytes

Recent studies indicated that exosomes from plants can protect mice from colitis [12], and miRNAs can be packaged into ELNs to regulate the intestinal microbiota [13,15]. Therefore, we hypothesized that plant miRNAs might also regulate mammalian enterocytes. To explore this idea, three species of intestinal cells were selected for experiments. Porcine jejunum epithelial cells IPEC-J2, mouse endocrine cells STC-1, and human colon carcinoma cells Caco-2 were transfected with either synthetic 2'-O-methylated plant MIR167e-5p or 2'-O-methylated control nucleic acids (NC). The cell number in each sample was calculated 24 h after treatment with 0, 10, 20, and 40 pmol MIR167e-5p. We observed that 10 pmol MIR167e-5p determined a remarkable decrease of IPEC-J2 ($p < 0.01$, Figure 1A), STC-1 ($p < 0.01$, Figure 1B), and Caco-2 ($p < 0.01$, Figure 1C) cells. Furthermore, to test the time-dependence of MIR167e-5p effect, the cells were treated with 20 pmol MIR167e-5p, and the cell number was determined after 0, 24, 48, and 72 h of treatment. The results showed an obvious decrease of IPEC-J2 cell number after 24 h (8.1%), 48 h (24.8%), and 72 h (24.6%) of treatment, compared to NC cells (Figure 1D). STC-1 cell number also decreased after 24 h (8.2%) and 48 h (10.9%) of treatment, but no significant difference at 72 h was found, compared to NC cells (Figure 1E). Similarly, Caco-2 cell number also decreased after 24 h (18.7%), 48 h (11.2%), and 72 h (17.0%) of treatment, compared to NC cells (Figure 1F). These results indicate that MIR167e-5p significantly inhibited the proliferation of intestinal cells. The MTT assay and the EdU incorporation assay were performed to further confirm the inhibition of MIR167e-5p. The MTT assay showed that the proliferation of IPEC-J2 cells was significantly suppressed after 72 h by MIR167e-5p, while MIR167e-5p inhibitor did not show any effect (Figure 1G). The EdU incorporation assay showed that the fluorescence intensity of IPEC-J2 cells was significantly reduced after both 24 and 48 h of MIR167e-5p treatment but not after treatment with MIR167e-5p inhibitor (Figure 1H,I), indicating significantly reduced DNA replication activity. Taken together, these results indicate that MIR167e-5p is capable of inhibiting enterocyte proliferation.

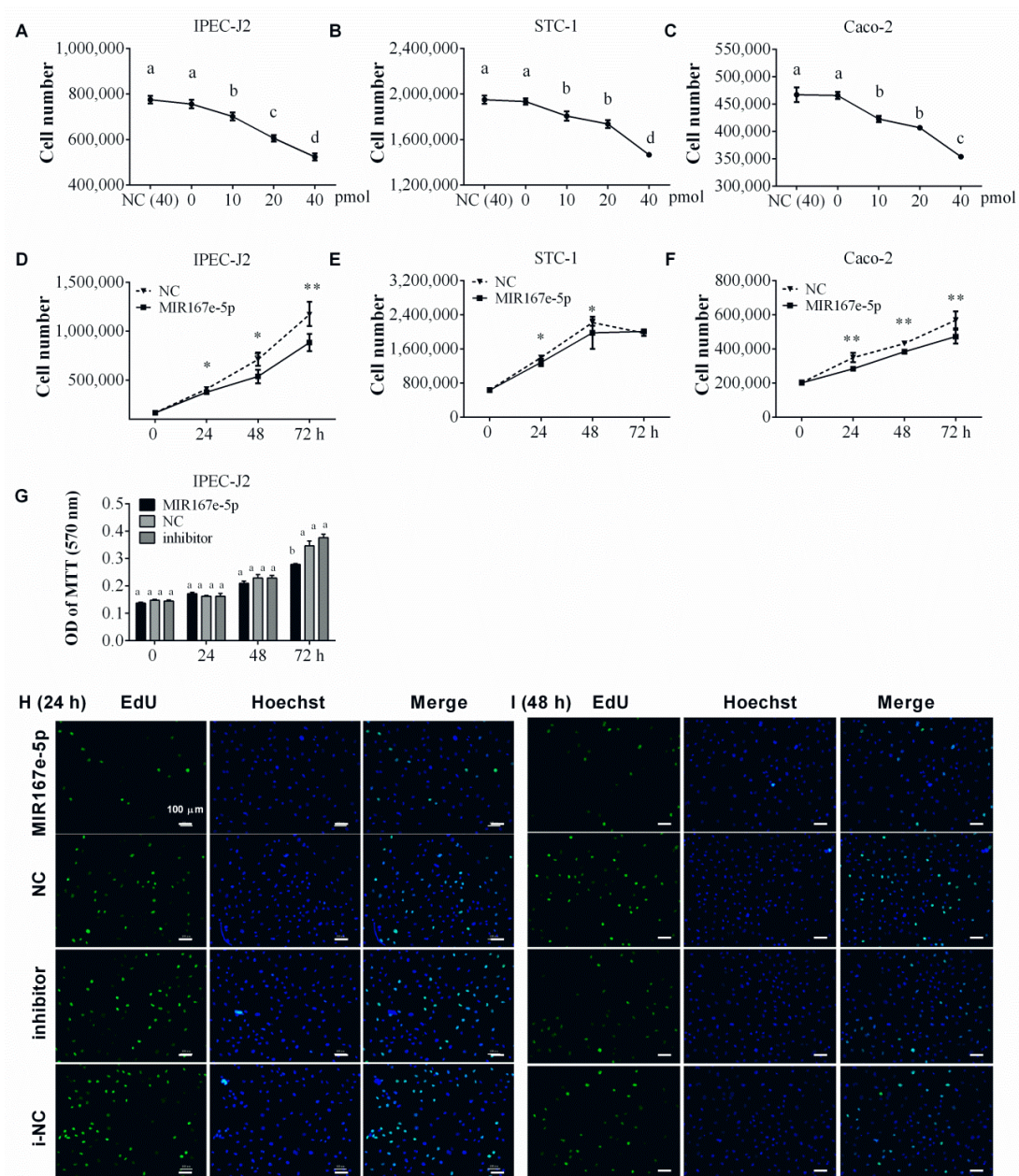


Figure 1. Synthetic MIR167e-5p suppresses the proliferation of IPEC-J2, STC-1, and Caco-2 cells. (A–C) Number of IPEC-J2 (A), STC-1 (B), and Caco-2 (C) cells transfected with different doses of MIR167e-5p ($n = 6$, LSD tests). (D–F) IPEC-J2 (D), STC-1 (E), and Caco-2 (F) cells proliferation after transfection with NC or MIR167e-5p mimics at 0, 24, 48, and 72 h. Cell counting was performed to evaluate cell proliferation ($n = 6$, t -tests). (G) Cell metabolic activity was examined by the MTT assay 0, 24, 48, and 72 h after transfection with MIR167e-5p, NC, inhibitor, or i-NC ($n = 7$, LSD tests). (H,I) Immunofluorescence staining for EdU incorporation in IPEC-J2 cells 24 and 48 h after treatment with MIR167e-5p, NC, inhibitor, or i-NC (Scale bars, 100 μ m, $n = 6$); * $p < 0.05$; ** $p < 0.01$; the same superscripts denote a non-significant difference ($p > 0.05$), and different superscripts denote a significant difference ($p < 0.05$).

3.2. MIR167e-5p Targets the Transcript of β -Catenin

MIR167e-5p regulates various aspects of development in plants by targeting the auxin response factors ARF6 and ARF8 [21]. To identify targets of MIR167e-5p in mammals, miRanda was employed, and the results showed that MIR167e-5p might target β -catenin, a key molecule in the Wnt/ β -catenin

pathway. A putative binding site conserved among various species was located in β -catenin (Figure 2A). To confirm this relationship, a β -catenin partially normal 3'-UTR sequence and a sequence in which the MIR167e-5p binding site was deleted were cloned into a luciferase reporter plasmid (Figure 2A). HeLa cells were transfected with the reporter plasmids along with synthetic MIR167e-5p mimics or NC. The results showed that MIR167e-5p significantly reduced luciferase activity, and deletion of the MIR167e-5p binding site diminished this reduction (Figure 2B), which was preliminary evidence of their binding.

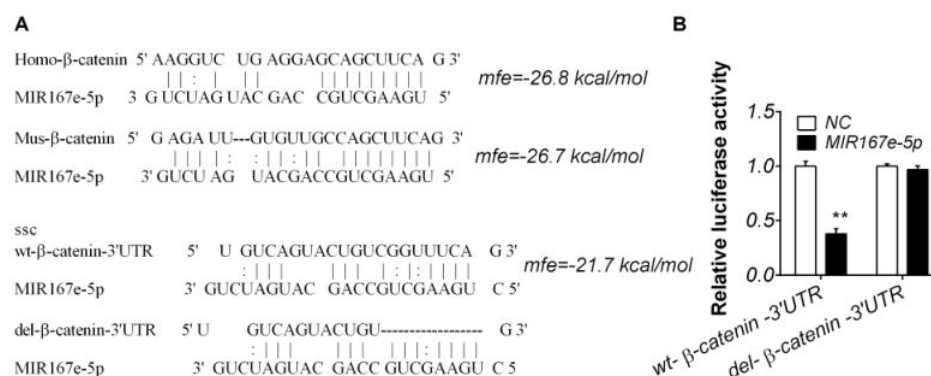


Figure 2. MIR167e-5p targets β -catenin. (A) The predicted target β -catenin 3'-UTR (untranslated region) and MIR167e-5p. Black lines and two-dotted labels represent the paired and G:U paired sequences for normal and 3'-UTR-deleted β -catenin, respectively. Note that the potential binding site of MIR167e-5p in the β -catenin 3'-UTR is highly conserved across species. (B) HeLa cells were transfected with each of the constructed plasmids, together with MIR167e-5p or NC. MIR167e-5p significantly decreased luciferase activity in cells transfected with wild-type (wt) β -catenin but not in cells transfected with 3'-UTR-deleted β -catenin (firefly luciferase activity/Renilla luciferase activity, ** $p < 0.01$, $n = 8$).

3.3. MIR167e-5p Inhibits the β -Catenin Pathway

To determine whether MIR167e-5p inhibits the β -catenin pathway, two enterocyte cell lines, IPEC-J2 and Caco-2 cells, were transfected with synthetic MIR167e-5p. Interestingly, the transfection led to a remarkable increase of MIR167e-5p in the cells, and MIR167e-5p inhibitor restored MIR167e-5p levels to the levels in NC cells (Figure 3A,E). More importantly, as the potential target of MIR167e-5p, β -catenin mRNA level was decreased after MIR167e-5p transfection compared to NC transfection (Figure 3B) in IPEC-J2 cells, indicating that MIR167e-5p probably enhanced the degradation of β -catenin mRNA. As a proliferative marker gene for intestine cell, PCNA mRNA examined by qPCR was significantly reduced by MIR167e-5p compared to NC and restored to a normal level by MIR167e-5p inhibitor (Figure 3C). We also examined c-Myc, a downstream molecule of β -catenin. Analysis by qPCR revealed that MIR167e-5p significantly reduced c-Myc mRNA level compared to NC, and this reduction was prevented by MIR167e-5p inhibitor (Figure 3D). Similarly, these three mRNAs were significantly reduced by MIR167e-5p in Caco-2 cells (Figure 3E–H), and β -catenin mRNA level was recovered to that in NC cells by MIR167e-5p inhibitor. These results indicate that MIR167e-5p may regulate the β -catenin pathway.

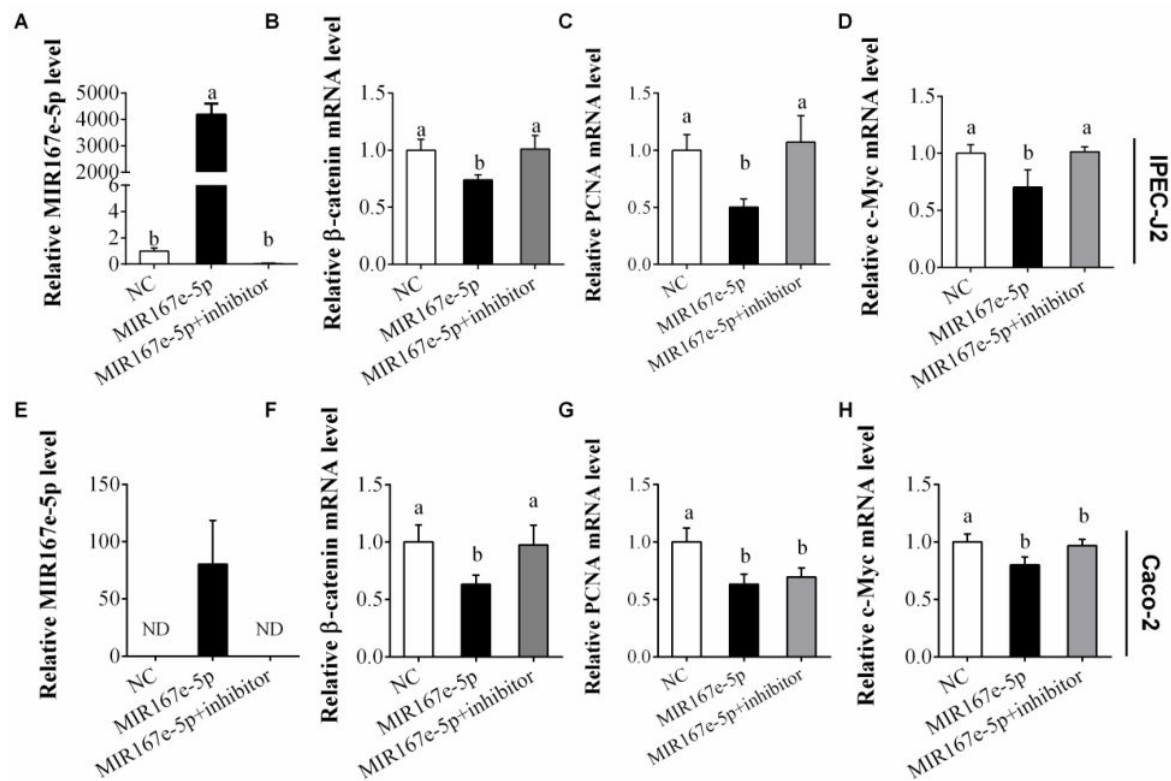


Figure 3. MIR167e-5p suppresses β -catenin, PCNA, and c-Myc mRNA expression. (A,E) qPCR analysis of relative MIR167e-5p levels in IPEC-J2 and Caco-2 cells after transfection with NC, MIR167e-5p, or MIR167e-5p+inhibitor (normalized against U6; $n = 6$). (B–D) qPCR analysis of relative β -catenin (B), PCNA (C), and c-Myc (D) mRNA levels in IPEC-J2 cells after transfection with NC, MIR167e-5p, or MIR167e-5p+inhibitor (normalized against β -actin; $n = 6$). (F–H) qPCR analysis of relative β -catenin (F), PCNA (G), and c-Myc (H) mRNA levels in Caco-2 cells after transfection with NC, MIR167e-5p, or MIR167e-5p+inhibitor (normalized against β -actin; $n = 6$). Statistical significance was determined by LSD tests. The same superscripts denote non-significant differences ($p > 0.05$), different superscripts denote significant differences ($p < 0.05$).

To further confirm the inhibition of MIR167e-5p, β -catenin and c-Myc proteins were examined by western blot. As shown in the results, MIR167e-5p seemed to downregulate β -catenin. β -catenin protein levels in IPEC-J2 cells were reduced, and this reduction could be restored by the inhibitor (Figure 4A,B). C-Myc was downregulated too, as shown in Figure 4A,C and recovered in the presence of the inhibitor. A similar inhibitory effect of MIR167e-5p was observed in Caco-2 cells (Figure 4D–F). These results provided further evidence that MIR167e-5p may inhibit the β -catenin pathway.

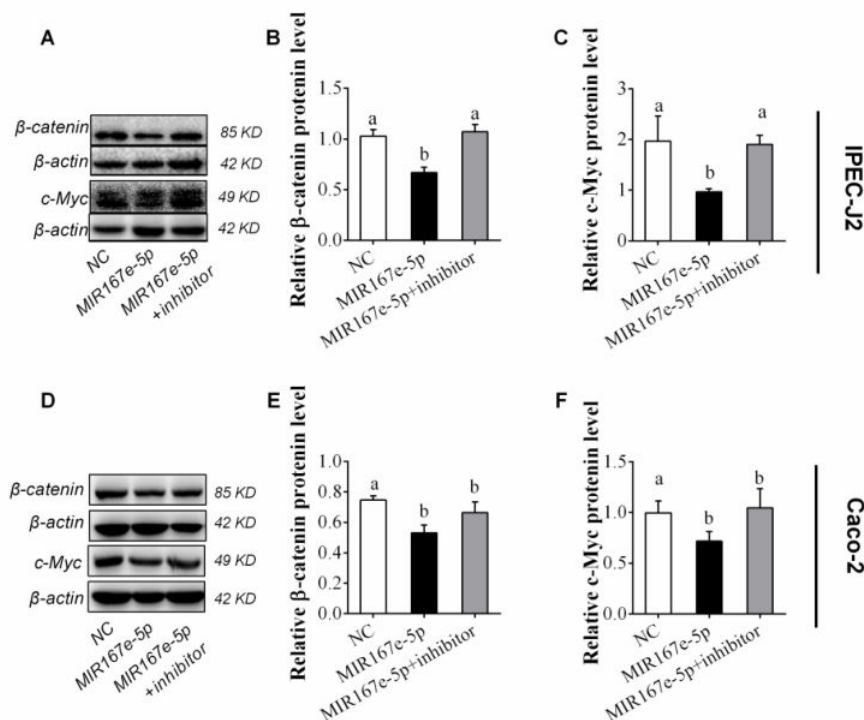


Figure 4. MIR167e-5p suppresses β -catenin and c-Myc protein expression. (A–C) Western blot was used to evaluate β -catenin (A,B) and c-Myc (A,C) protein levels in IPEC-J2 cells after transfection with NC, MIR167e-5p, or MIR167e-5p+inhibitor ($n = 6$; LSD tests). (D–F) β -catenin (D,E) and c-Myc (D,F) protein levels in Caco-2 cells after transfection with NC, MIR167e-5p, or MIR167e-5p+inhibitor ($n = 6$; LSD tests). The same superscripts denote non-significant differences ($p > 0.05$), different superscripts denote significant differences ($p < 0.05$).

4. Discussion

MiRNAs are important negative regulators of genes involved in physiological and pathological processes in plants and animals. Whether plant miRNAs play a cross-kingdom regulatory role in animals is still disputed. Animal and plant miRNAs are processed and spliced differently, and present differences also in their sequences, precursor structures, evolutionary origins, and biogenesis mechanisms [22–24]. Plant miRNAs are methylated on the ribose of the 3'-end nucleotide, and methylation makes plant naked miRNAs highly stable relative to animal miRNAs [25], since most animal miRNAs are not methylated. It is believed the methylation at the 3' ends by Hua Enhancer 1 (HEN1) distinguishes plant miRNAs from animal miRNAs [26]. The recent detection of plant miRNAs in body fluids suggests that these circulating miRNAs may have broad implications for miRNA-mediated gene expression control. These miRNAs could be associated with Ago2 [5], packaged into secreted ELNs [13] or exosomes [3], and thus be resistant to harsh internal environments, such as the acidic gastric environment, different temperature conditions, and nuclease enzymes [27]. This can provide favorable conditions for plant miRNA regulation in mammals.

MIR167e-5p is a conserved and highly expressed miRNA throughout the plant kingdom. In miRBase (<http://www.mirbase.org/>), there are 63 miRNAs sharing identical sequences (UGAAGCUGCCAGCAUGAUCUG). These miRNAs have been found in 27 plants, including soybean [28], wheat [29], and maize [30], which together account for a significant proportion of the diets of humans and other animals. Furthermore, MIR167e-5p has been found in *Moringa oleifera*, a widespread plant with substantial nutritional and medicinal value, and has a potential for cross-species control of human gene expression [31]. It was also found in human serum [32], human breast milk [33], porcine breast milk [34], and honey [9]. Maize MIR167e-5p was present in porcine nonsolid (blood) and solid tissues [35]. A study found that the basal level of MIR167a in human plasma was negligible but

significantly increased after drinking watermelon juice, reaching 797.47 fM at the end point [36]. Ginger MIR167a downregulates the expression of SpaC in *Lactobacillus rhamnosus* in the mouse intestine [15]. These studies have proved that MIR167e-5p may be absorbed by mammals, may mediate cross-kingdom communication, and therefore may be a bioactive ingredient for epigenetic regulation in humans and animals.

Plant miRNAs are of potential biological function in mammalian cells. Plant MIR2911 has been reported to target the *PB2* and *NS1* genes and inhibit H1N1 viral replication [6]. MIR159 was capable of inhibiting cancer proliferation by targeting TCF7 [7]. MIR156a can directly target JAM-A and reduce inflammatory cytokine-induced monocyte adhesion [8]. Plant MiR162a in beebread can even regulate honeybee caste development [9]. In our research, we proved that MIR167e-5p could inhibit the proliferation of IPEC-J2 and Caco-2 cells in vitro, as indicated by cell counting, MTT assay, and EdU incorporation assay. PCNA, which is a nuclear polypeptide expressed only in proliferating cells, has been taken as a good indicator of cell proliferation [37]. In the present study, PCNA mRNA level was significantly decreased by MIR167e-5p. These results provide sufficient evidence that MIR167e-5p can inhibit the proliferation of enterocytes.

β -catenin is a crucial component of the Wnt signaling pathway, which is crucial in many developmental processes [38], including the development of the intestinal epithelium [39–41]. In our research, plant MIR167e-5p could target β -catenin, as supported by bioinformatics analysis and luciferase report system experiments. qPCR and western blot further proved that β -catenin mRNA and protein levels were significantly decreased by MIR167e-5p mimics, while MIR167e-5p inhibitor relieved this inhibition. In previous studies, blockade of β -catenin or overexpression of the Wnt inhibitor Dkk-1 resulted in a severe loss of proliferative epithelial cells in the intestine [42]. Mutations in the negative regulator of Wnt signaling, the adenomatous polyposis coli (APC) protein, or overexpression of oncogenic forms of β -catenin resulted in hyperproliferation of the epithelium [43]. In our research, β -catenin mRNA levels recovered to the levels observed in NC control cells after treatment with MIR167e-5p inhibitor, but the protein levels were only mildly recovered in Caco-2 cells, similar to PCNA and c-Myc levels. The Wnt/ β -catenin signaling pathway is abnormally activated in colon cancer [44]. Caco-2 cells differ from normal enterocytes, bearing mutations in the APC and β -catenin genes, which are involved in the transcriptional control of the myc gene during enterocyte differentiation. The ability of APC to regulate β -catenin levels in the cytosol and nucleus has been well demonstrated and involves binding of APC to β -catenin and stimulation of its phosphorylation and degradation [45]. Mutations or regulatory changes that disrupt APC or inhibit the APC-mediated β -catenin turnover may lead to altered levels of cytosolic and nuclear β -catenin. Some evidence has indicated that cell fate determination and lineage commitment of enterocytes are not governed by a simple rule, but by a complex and multilayered interaction between several pathways [46]. This means that β -catenin is regulated in many ways, for example, NOTCH1 plays a key role in the Wnt pathway, and activation of NOTCH1 is associated with the translocation of β -catenin to the nucleus in colon cancer [47]. Axin expression is positively regulated by β -catenin, and this generates a negative feedback loop that would be expected to decrease cytosolic β -catenin levels [48]. Besides, altering the level and distribution of β -catenin may affect the paralogous protein plakoglobin (γ -catenin) which, like β -catenin, can bind cadherins, APC, and TCFs, mimicking the effects of Wnt signaling [49]. The c-Myc transcription factor is a potent inducer of proliferation and is required for Wnt/ β -catenin signaling in the intestinal epithelium. C-Myc appears essential to provide crypt progenitor cells with the necessary biosynthetic capacity to successfully progress through the cell cycle. C-Myc-deficient crypts are lost within weeks and replaced by c-Myc-proficient crypts through a fission process of crypts that have escaped gene deletion [50]. Considering with these observations, we can confirm that MIR167e-5p may inhibit enterocyte proliferation by targeting the β -catenin pathway.

As an essential organ for digestion and absorption, the intestine is the largest immune organ and plays a key role in maintaining animal health and growth. Recent studies have indicated that miRNAs can regulate gene expression in different species, and plant miRNAs regulate the intestinal flora

and, thus, intestinal development. MiRNAs in EPDELNs have been detected and found to have the potential to regulate human mRNAs [14]. GELNs cause significant induction of Lgr5 intestinal stem cells through the Wnt/ β -catenin pathway, protecting mice from DSS-induced colitis [12]. EPDELNs could induce the expression of genes encoding anti-inflammatory cytokines, anti-oxidation proteins, and proteins activating Wnt signaling [13]. GELNs mdo-miR7267-3p-mediated targeting of the LGG monooxygenase ycnE leads to increased indole-3-carboxaldehyde, inducing the production of IL-22 and thus ameliorating mouse colitis via IL-22-dependent mechanisms [15]. Our study suggests that plant MIR167e-5p might execute its inhibitory function in porcine and human enterocytes. These results demonstrate that plant miRNAs can regulate intestinal growth in vitro. Previous studies have been suggested that food-derived plant miRNAs may be important factors regulating intestinal health and development.

In conclusion, this study provides new evidence supporting the idea that plant miRNAs can exert cross-kingdom regulatory functions in mammals. We provide the first evidence that plant MIR167e-5p suppresses intestinal cell proliferation by targeting β -catenin. We suggest that the large variety of plant miRNAs should be considered as a new class of nutrients, which has been neglected for centuries.

Author Contributions: M.L. and T.C. were the main contributors to the study conduction, data collection and analysis, data interpretation, and manuscript writing. J.J.-H., R.-S.Y., B.Z., H.-J.Z., J.-Y.L., J.-H.W., and M.-Y.X. contributed to the conduction of the study. Q.-Y.X., J.L., and Q.-Y.J. contributed to manuscript writing and data interpretation. Y.-L.Z. and J.-J.S. contributed to study design, data interpretation, and manuscript writing.

Funding: This study was supported by grants from the National Key Research and Development Program of China (2016YFD0500503), the Natural Science Foundation of China Program (No. 31802156, 31872435, 31802037), the Natural Science Foundation of Guangdong Provincial Key Program (2018B030311015) and the Natural Science Foundation of Guangdong Provincial Program (2019A1515011734).

Conflicts of Interest: The authors declare that there is no conflict of interest that could be perceived as prejudicing the impartiality of the research reported.

Abbreviations

c-Myc	Cellular myelocytomatosis oncogene
Caco-2	Colon carcinoma cell line 2
DAPI	4',6-Diamidino-2-Phenylindole, Dihydrochloride
EdU	5-ethynyl-2'-deoxyuridine
EPDELNs	exosome-like nanoparticles
FBS	fetal bovine serum
GSK-3 β	glycogen synthase kinase-3 β
i-NC	inhibitor normal control
IPEC-J2	porcine jejunum epithelial cell line
LEF	lymphoid enhancing factor
MTT	3-(4,5-Dimethyl-2-thiazolyl)-2,5-diphenyl-2H-tetrazolium bromide
NC	normal control
PCNA	proliferating cell nuclear antigen
PMSF	phenylmethylsulphonyl fluoride
STC-1	Invasive small intestinal neuroendocrine carcinoma 1
TCF	T cell factor
UTR	untranslated region
Wnt	Wingless Int1

References

1. Arroyo, J.D.; Chevillet, J.R.; Kroh, E.M.; Ruf, I.K.; Pritchard, C.C.; Gibson, D.F.; Mitchell, P.S.; Bennett, C.F.; Pogossovaagadjanyan, E.L.; Stirewalt, D.L. Argonaute2 complexes carry a population of circulating microRNAs independent of vesicles in human plasma. *Proc. Natl. Acad. Sci. USA* **2011**, *108*, 5003–5008. [[CrossRef](#)]
2. Andrey, T.; Ludmila, W.; Anne, L.; Barbara, B. Characterization of extracellular circulating microRNA. *Nucleic Acids Res.* **2011**, *39*, 7223–7233.

3. Gallo, A.; Tandon, M.; Alevizos, I.; Illei, G.G. The majority of microRNAs detectable in serum and saliva is concentrated in exosomes. *PLoS ONE* **2012**, *7*, e30679. [[CrossRef](#)] [[PubMed](#)]
4. Mohammed, A.; Hepworth, A.R.; Christophe, L.; Hartmann, P.E.; Geddes, D.T.; Foteini, H. Human Milk MicroRNA and Total RNA Differ Depending on Milk Fractionation. *J. Cell. Biochem.* **2015**, *116*, 2397–2407.
5. Zhang, L.; Hou, D.; Chen, X.; Li, D.; Zhu, L.; Zhang, Y.; Li, J.; Bian, Z.; Liang, X.; Cai, X. Exogenous plant MIR168a specifically targets mammalian LDLRAP1: Evidence of cross-kingdom regulation by microRNA. *Cell Res.* **2012**, *22*, 107–126. [[CrossRef](#)] [[PubMed](#)]
6. Zhou, Z.; Li, X.; Liu, J.; Dong, L.; Chen, Q.; Liu, J.; Kong, H.; Zhang, Q.; Qi, X.; Hou, D. Honeysuckle-encoded atypical microRNA2911 directly targets influenza A viruses. *Cell Res.* **2014**, *25*, 39–49. [[CrossRef](#)] [[PubMed](#)]
7. Chin, A.R.; Fong, M.Y.; Somlo, G.; Wu, J.; Swiderski, P.; Wu, X.; Wang, S.E. Cross-kingdom inhibition of breast cancer growth by plant miR159. *Cell Res.* **2016**, *26*, 217–228. [[CrossRef](#)]
8. Hou, D.; He, F.; Ma, L.; Cao, M.; Zhou, Z.; Wei, Z.; Xue, Y.; Sang, X.; Chong, H.; Tian, C.; et al. The potential atheroprotective role of plant MIR156a as a repressor of monocyte recruitment on inflamed human endothelial cells. *J. Nutr. Biochem.* **2018**, *57*, 197–205. [[CrossRef](#)]
9. Zhu, K.; Liu, M.; Fu, Z.; Zhou, Z.; Kong, Y.; Liang, H.; Lin, Z.; Luo, J.; Zheng, H.; Wan, P. Plant microRNAs in larval food regulate honeybee caste development. *PLoS Genet.* **2017**, *13*, e1006946. [[CrossRef](#)]
10. Shahid, S.; Kim, G.; Johnson, N.R.; Wafula, E.; Wang, F.; Coruh, C.; Bernal-Galeano, V.; Phifer, T.; dePamphilis, C.W.; Westwood, J.H.; et al. MicroRNAs from the parasitic plant *Cuscuta campestris* target host messenger RNAs. *Nature* **2018**, *553*, 82–85. [[CrossRef](#)]
11. Mckenna, L.B.; Schug, J.; Vourekas, A.; Mckenna, J.B.; Bramswig, N.C.; Friedman, J.R.; Kaestner, K.H. MicroRNAs Control Intestinal Epithelial Differentiation, Architecture, and Barrier Function. *Gastroenterology* **2010**, *139*, 1654–1664. [[CrossRef](#)] [[PubMed](#)]
12. Ju, S.; Mu, J.; Dokland, T.; Zhuang, X.; Wang, Q.; Jiang, H.; Xiang, X.; Deng, Z.B.; Wang, B.; Zhang, L. Grape exosome-like nanoparticles induce intestinal stem cells and protect mice from DSS-induced colitis. *Mol. Ther.* **2013**, *21*, 1345–1357. [[CrossRef](#)] [[PubMed](#)]
13. Mu, J.; Zhuang, X.; Wang, Q.; Jiang, H.; Deng, Z.B.; Wang, B.; Zhang, L.; Kakar, S.; Jun, Y.; Miller, D. Interspecies communication between plant and mouse gut host cells through edible plant derived exosome-like nanoparticles. *Mol. Nutr. Food Res.* **2014**, *58*, 1561–1573. [[CrossRef](#)] [[PubMed](#)]
14. Xiao, J.; Feng, S.; Xun, W.; Long, K.; Yi, L.; Wang, Y.; Ma, J.; Tang, Q.; Long, J.; Li, X. Identification of exosome-like nanoparticle-derived microRNAs from 11 edible fruits and vegetables. *PeerJ* **2018**, *6*, e5186. [[CrossRef](#)]
15. Teng, Y.; Ren, Y.; Sayed, M.; Hu, X.; Lei, C.; Kumar, A.; Hutchins, E.; Mu, J.; Deng, Z.; Luo, C.; et al. Plant-Derived Exosomal MicroRNAs Shape the Gut Microbiota. *Cell Host Microbe* **2018**, *24*, 637–652. [[CrossRef](#)]
16. Gonzalez, L.M. Intestinal Epithelial Stem Cells. In *The Equine Acute Abdomen*, 3rd ed.; John Wiley & Sons, Inc.: Hoboken, NJ, USA, 2017; pp. 19–23.
17. Moeser, A.J.; Borst, L.B.; Overman, B.L.; Pittman, J.S. Defects in small intestinal epithelial barrier function and morphology associated with peri-weaning failure to thrive syndrome (PFTS) in swine. *Res. Vet. Sci.* **2012**, *93*, 975–982. [[CrossRef](#)]
18. Guonan, L.; Na, X.; Rongwen, X. Paracrine Wingless signalling controls self-renewal of *Drosophila* intestinal stem cells. *Nature* **2008**, *455*, 1119–1123.
19. Kikuchi, A.; Yamamoto, H.; Sato, A.; Matsumoto, S. New Insights into the Mechanism of Wnt Signaling Pathway Activation. *Int. Rev. Cell Mol. Biol.* **2011**, *291*, 21–71.
20. Sun, J.Y.; Huang, Y.; Li, J.P.; Zhang, X.; Wang, L.; Meng, Y.L.; Yan, B.; Bian, Y.Q.; Zhao, J.; Wang, W.Z. MicroRNA-320a suppresses human colon cancer cell proliferation by directly targeting β -catenin. *Biochem. Biophys. Res. Commun.* **2012**, *420*, 787–792. [[CrossRef](#)]
21. Ying, H.S.; Yu, B.L.; Chao, Z.; Xiao, M.L.; Xian, S.Z. The microRNA167 controls somatic embryogenesis in *Arabidopsis* through regulating its target genes ARF6 and ARF8. *Plant. Cell Tissue Organ. Cult.* **2016**, *124*, 405–417.
22. Narry, K.V. MicroRNA biogenesis: Coordinated cropping and dicing. *Nat. Rev. Mol. Cell Biol.* **2005**, *6*, 376–385.

23. Millar, A.A.; Waterhouse, P.M. Plant and animal microRNAs: Similarities and differences. *Funct. Integr. Genomics* **2005**, *5*, 129–135. [[CrossRef](#)] [[PubMed](#)]
24. Xuemei, C. MicroRNA biogenesis and function in plants. *FEBS Lett.* **2005**, *579*, 5923–5931.
25. Bin, Y.; Zhiyong, Y.; Junjie, L.; Svetlana, M.; Maocheng, Y.; Padgett, R.W.; Ruth, S.; Xuemei, C. Methylation as a crucial step in plant microRNA biogenesis. *Science* **2005**, *307*, 932–935.
26. Baohong, Z.; Xiaoping, P.; Cobb, G.P.; Anderson, T.A. Plant microRNA: A small regulatory molecule with big impact. *Dev. Biol.* **2006**, *289*, 3–16.
27. Chen, X.; Ba, Y.; Ma, L.; Cai, X.; Yin, Y.; Wang, K.; Guo, J.; Zhang, Y.; Chen, J.; Guo, X. Characterization of microRNAs in serum: A novel class of biomarkers for diagnosis of cancer and other diseases. *Cell Res.* **2008**, *18*, 997–1006. [[CrossRef](#)]
28. Chen, S.Y.; Ma, B.; Zhang, W.K.; Hu, X.Y.; Liu, Y.F.; Song, Q.X.; Zhang, J.S. Identification of miRNAs and their target genes in developing soybean seeds by deep sequencing. *BMC Plant Biol.* **2011**, *11*, 5.
29. Sun, F.; Guo, G.; Du, J.; Guo, W.; Peng, H.; Ni, Z.; Sun, Q.; Yao, Y. Whole-genome discovery of miRNAs and their targets in wheat (*Triticum aestivum* L.). *BMC Plant Biol.* **2014**, *14*, 142. [[CrossRef](#)]
30. Ding, D.; Wang, Y.; Han, M.; Fu, Z.; Li, W.; Liu, Z.; Hu, Y.; Tang, J. MicroRNA transcriptomic analysis of heterosis during maize seed germination. *PLoS ONE* **2012**, *7*, e39578. [[CrossRef](#)]
31. Pirrò, S.; Zanella, L.; Kenzo, M.; Montesano, C.; Minutolo, A.; Potestà, M.; Sobze, M.S.; Canini, A.; Cirilli, M.; Muleo, R. MicroRNA from *Moringa oleifera*: Identification by High Throughput Sequencing and Their Potential Contribution to Plant Medicinal Value. *PLoS ONE* **2016**, *11*, e0149495. [[CrossRef](#)]
32. Witwer, K.W. XenomiRs and miRNA homeostasis in health and disease. *RNA Biol.* **2012**, *9*, 1147–1154. [[CrossRef](#)] [[PubMed](#)]
33. Lukasik, A.; Brzozowska, I.; Zielenkiewicz, U.; Zielenkiewicz, P. Detection of Plant miRNAs Abundance in Human Breast Milk. *Int. J. Mol. Sci.* **2018**, *19*, 37. [[CrossRef](#)] [[PubMed](#)]
34. Lukasik, A.; Zielenkiewicz, P. In Silico Identification of Plant miRNAs in Mammalian Breast Milk Exosomes—A Small Step Forward? *PLoS ONE* **2014**, *9*, e99963. [[CrossRef](#)] [[PubMed](#)]
35. Luo, Y.; Wang, P.; Wang, X.; Wang, Y.; Mu, Z.; Li, Q.; Fu, Y.; Xiao, J.; Li, G.; Ma, Y. Detection of dietetically absorbed maize-derived microRNAs in pigs. *Sci. Rep.* **2017**, *7*, 645. [[CrossRef](#)] [[PubMed](#)]
36. Hongwei, L.; Suyang, Z.; Zheng, F.; Yanbo, W.; Nan, W.; Yanqing, L.; Chihao, Z.; Jinhui, W.; Yiqiao, H.; Junfeng, Z. Effective detection and quantification of dietetically absorbed plant microRNAs in human plasma. *J. Nutr. Biochem.* **2015**, *116*, 505–512.
37. Kelman, Z. PCNA: Structure, functions and interactions. *Oncogene* **1997**, *14*, 629–640. [[CrossRef](#)]
38. MacDonald, B.T.; Tamai, K.; Xi, H. Wnt/ β -Catenin Signaling: Components, Mechanisms, and Diseases. *Dev. Cell* **2009**, *17*, 9–26. [[CrossRef](#)]
39. Daniel, P.; Alex, G.; Harry, B.; Hans, C. Canonical Wnt signals are essential for homeostasis of the intestinal epithelium. *Genes Dev.* **2003**, *17*, 1709–1713.
40. Wong, M.H.; Rubinfeld, B.; Gordon, J.I. Effects of forced expression of an NH₂-terminal truncated beta-Catenin on mouse intestinal epithelial homeostasis. *J. Cell Biol.* **1998**, *141*, 765–777. [[CrossRef](#)]
41. Hardiman G1, K.R.; Bazan, J.F. Isolation, characterization and chromosomal localization of human WNT10B. *Cytogenet. Cell Genet.* **1997**, *77*, 278–282. [[CrossRef](#)]
42. Fauser, J.K.; Donato, R.P.; Woenig, J.A.; Proctor, S.J.; Trotta, A.P.; Grover, P.K.; Howarth, G.S.; Penttila, I.A.; Cummins, A.G. Wnt blockade with dickkopf reduces intestinal crypt fission and intestinal growth in infant rats. *J. Pediatr. Gastroenterol. Nutr.* **2012**, *55*, 26–31. [[CrossRef](#)] [[PubMed](#)]
43. Pauline, A.; Sabine, C.; Cécile, G.; Sophie, G.; Philippe, C.; Michiko, N.K.; Pierre, L.P.; Axel, K.; Sylvie, R.; Christine, P. Crypt-restricted proliferation and commitment to the Paneth cell lineage following Apc loss in the mouse intestine. *Development* **2005**, *132*, 1443–1451. [[CrossRef](#)]
44. Sparks, A.B.; Morin, P.J.; Vogelstein, B.; Kinzler, K.W. Mutational analysis of the APC/beta-catenin/Tcf pathway in colorectal cancer. *Cancer Res.* **1998**, *58*, 1130–1134. [[PubMed](#)]
45. Näthke, I.S. The Adenomatous Polyposis Coli Protein: The Achilles Heel of the Gut Epithelium. *Annu. Rev. Cell Dev. Biol.* **2004**, *20*, 337–366. [[CrossRef](#)] [[PubMed](#)]
46. Nakamura, T.; Tsuchiya, K.; Watanabe, M. Crosstalk between Wnt and Notch signaling in intestinal epithelial cell fate decision. *J. Gastroenterol.* **2007**, *42*, 705–710. [[CrossRef](#)] [[PubMed](#)]

47. Ishiguro, H.; Okubo, T.; Kuwabara, Y.; Kimura, M.; Mitsui, A.; Sugito, N.; Ogawa, R.; Katada, T.; Tanaka, T.; Shiozaki, M. NOTCH1 activates the Wnt/ β -catenin signaling pathway in colon cancer. *Oncotarget* **2017**, *8*, 60378. [[CrossRef](#)] [[PubMed](#)]
48. Jho, E.H.; Zhang, T.; Domon, C.; Joo, C.K.; Freund, J.N.; Costantini, F. Wnt/beta-catenin/Tcf signaling induces the transcription of Axin2, a negative regulator of the signaling pathway. *Mol. Cell. Biol.* **2002**, *22*, 1172–1183. [[CrossRef](#)]
49. Ozawa, M.; Baribault, H.; Kemler, R. The cytoplasmic domain of the cell adhesion molecule uvomorulin associates with three independent proteins structurally related in different species. *EMBO J.* **1989**, *8*, 1711–1717. [[CrossRef](#)]
50. Muncan, V.; Sansom, O.J.; Tertoolen, L.; Plesse, T.J.; Begthel, H.; Sancho, E.; Cole, A.M.; Gregorieff, A.; de Alboran, I.M.; Clevers, H.; et al. Rapid loss of intestinal crypts upon conditional deletion of the Wnt/Tcf-4 target gene c-Myc. *Mol. Cell. Biol.* **2006**, *26*, 8418–8426. [[CrossRef](#)]



© 2019 by the authors. Licensee MDPI, Basel, Switzerland. This article is an open access article distributed under the terms and conditions of the Creative Commons Attribution (CC BY) license (<http://creativecommons.org/licenses/by/4.0/>).



Exploration of Long Non-coding RNAs and Circular RNAs in Porcine Milk Exosomes

Bin Zeng[†], Ting Chen[†], Junyi Luo, Meiying Xie, Limin Wei, Qianyun Xi, Jiajie Sun* and Yongliang Zhang*

Guangdong Provincial Key Laboratory of Animal Nutrition Control, National Engineering Research Center for Breeding Swine Industry, College of Animal Science, South China Agricultural University, Guangzhou, China

OPEN ACCESS

Edited by:

Yadong Zheng,
Lanzhou Institute of Veterinary
Research (CAAS), China

Reviewed by:

Chi-Ming Wong,
The Hong Kong Polytechnic
University, Hong Kong
Si-Yang Huang,
Yangzhou University, China

*Correspondence:

Jiajie Sun
jjiesun@scau.edu.cn
Yongliang Zhang
zhangyl@scau.edu.cn

[†] These authors have contributed
equally to this work

Specialty section:

This article was submitted to
RNA,
a section of the journal
Frontiers in Genetics

Received: 23 February 2020

Accepted: 28 May 2020

Published: 02 July 2020

Citation:

Zeng B, Chen T, Luo J, Xie M,
Wei L, Xi Q, Sun J and Zhang Y (2020)
Exploration of Long Non-coding
RNAs and Circular RNAs in Porcine
Milk Exosomes. *Front. Genet.* 11:652.
doi: 10.3389/fgene.2020.00652

RNA in milk exosomes can be absorbed in the mammalian intestinal tract and function in gene expression regulations. Our previous work demonstrated that porcine milk exosomes (PME) contain large amounts of miRNAs and mRNAs. Increasing evidence suggests that long non-coding RNAs (lncRNAs) and circular RNAs (circRNAs) are of particular interest, given their key role in diverse biological processes of animals. However, the expression profiles and the potential functions of lncRNAs and circRNAs in PME are still unknown. In the present study, we isolated PME by ultracentrifugation and performed a comprehensive analysis of lncRNA and circRNA in PME by using RNA sequencing. As a result, 2,466 novel lncRNAs, 809 annotated lncRNAs, and 61 circRNAs were identified in PME. The lncRNAs shared similar characteristics with other mammals in terms of length, exon number, and open reading frames. However, lncRNAs showed a higher level compared with mRNAs. Eight lncRNAs and five circRNAs in PME were selected for PCR identification. A functional enrichment analysis on the target genes of lncRNAs indicated that these genes were involved in cellular macromolecule metabolic, RNA metabolic, and immune processes. The circRNAs host genes were enriched in nucleic acid binding and adherence junction. We also evaluated the potential interaction targets between miRNAs and PME lncRNAs or circRNAs, and the results showed that the PME lncRNAs and the circRNAs have a high density of miRNA target sites. The top 20 highly expressed lncRNAs were found to interact with the proliferation-related miRNAs, and the circRNAs potentially targeted many miRNAs that are associated with the intestinal barrier. This study is the first to provide a resource for lncRNA and circRNA research of porcine milk. Moreover, the potential interaction between lncRNA/circRNA and miRNA is revealed. The present study expands our knowledge of non-coding RNAs in milk, and additional research is necessary to confirm their exactly physiological functions.

Keywords: long non-coding RNAs, circular RNAs, milk exosomes, porcine, milk

INTRODUCTION

Exosomes (30–200 nm in diameter) are natural nanoparticles, defined as a subtype of extracellular vesicles (Pegtel and Gould, 2019). It plays a significant role as a mediator in intercellular communication that is achieved by the transfer of cargos, such as lipids, proteins, and RNAs, from donor to recipient cells (Mathieu et al., 2019). Among exosome cargos, non-coding RNAs (ncRNAs) are of particular interest because they participate in cellular homeostasis and diseases (Esteller, 2011) and regulate a majority of genes in mammals (Mattick and Makunin, 2006). In recent years, the exosome-mediated transfer of ncRNAs, including miRNAs (Ying et al., 2017), long non-coding RNAs (lncRNAs) (Zheng et al., 2018), and circular RNAs (circRNAs) (Zhang et al., 2019), can result in a genetic exchange between cells or tissues and regulate the gene expression of receptors. The exosomes are released from most cell cultures *in vitro* and can be found in tissues and biological fluids including blood, saliva, urine, milk, and cerebrospinal fluid (Aqil et al., 2019). The total RNA concentration in breast milk was higher than in other body fluids (Weber et al., 2010). Remarkably, unlike other exosomes, milk exosomes can transmit information to the progeny and even to other species. Milk exosome-derived RNA, which serves as a biomolecular software, is significant for epigenetic gene regulations that are required for the developmental processes of the newborn infant (Melnik et al., 2016).

Breast milk exosomes from many species including human (Zhou et al., 2012), cow (Izumi et al., 2012), pig (Chen et al., 2014), and panda (Ma J. et al., 2017) have been shown to contain RNAs. Evidence has demonstrated that the exosome lipid membrane helps to protect the milk-derived RNAs against degradation by RNases (Izumi et al., 2012), low pH (Liao et al., 2017), and digestive enzymes (Rani et al., 2017) *in vitro*, suggesting a significant function of milk exosome-encapsulated RNAs in the communication from mother to child. The milk exosome-derived RNA can be absorbed by intestinal and immune cells *in vitro* (Izumi et al., 2015; Liao et al., 2017). The milk exosomes and their RNA cargo could enter the circulatory system of the milk consumer and distribute into many tissues of mice after the oral administration of labeled bovine milk exosomes (Manca et al., 2018; Wang et al., 2018). Exosomes derived from human (Martin et al., 2018), yak (Gao et al., 2019), rat (Hock et al., 2017), and pig (Chen T. et al., 2016) milk are found to facilitate the proliferation of intestinal epithelial cells and those from bovine milk could enhance intestinal goblet cell activity (Li et al., 2019). Interestingly, recent papers have reinforced the evidence that mice fed with bovine milk exosome and RNA-depleted diet exhibit elevated purine metabolites and lower fecundity and elicit moderate changes in intestinal immunity compared with milk exosome and RNA-sufficient diet control (Aguilar-Lozano et al., 2018; Zemleni et al., 2019). In addition, loading milk exosomes with siRNA can knockdown target gene expression in A549 cells (Aqil et al., 2019). Based on these researches, it is extremely likely that milk exosome RNAs can be absorbed by the mammalian intestinal tract and cause significant regulatory effects.

lncRNAs are defined as transcripts of more than 200 nucleotides in length that are not translated into proteins. An increased number of studies highlight their important biological roles in processes such as post-transcriptional regulation, cell cycle regulation and cell apoptosis, and protein localization (Bryzghalov et al., 2020). circRNAs are a recently identified genetic element that are covalently closed and evolutionarily conserved. Some circRNAs are abundant in eukaryotes with cell-specific and tissue-specific expression profiles. Many circRNAs exert significant biological functions by acting as microRNA inhibitors (sponges) (Kristensen et al., 2019). Recent studies have indicated that lncRNAs and circRNAs are stable in exosomes and can play their biological roles after the exosomes are taken up by recipient cells (Li et al., 2015; Zhou et al., 2018). Current research suggests that lncRNAs in human breast milk are implicational for the early development of a child (Karlsson et al., 2016). circRNAs (Wang Y. et al., 2019) and lncRNAs (Zeng et al., 2019) have been detected in bovine milk exosomes. However, the expression profile of lncRNAs and circRNAs in porcine milk exosomes (PME) is currently unknown. Pig, as a kind of important livestock and medical model for human beings [its milk yield by body weight (BW) being 11 kg milk/180 kg BW, 0.06] (Strathe et al., 2016), is more efficient than cow (35 kg milk/700 kg BW, 0.05) (Vallimont et al., 2010). The total RNA content in an equal volume of pig's milk is 50–100 times more than that in cow's milk (our unpublished data). Our previous work has demonstrated that PME contains abundant miRNAs (Chen et al., 2014) and mRNAs (Chen et al., 2017). Therefore, at present, we performed RNA sequencing and analysis of lncRNAs and circRNAs in PME, which may help to establish a further understanding of porcine milk in molecular events and physiological functions.

MATERIALS AND METHODS

Milk Sample Preparation and Milk Exosomes Isolation

Fresh milk was collected from six Landrace female pigs within 3 days postpartum at the farm of the Wens (Guangdong, China) with the permission of the farm owner. Equal volumes of milk from the six pigs were mixed as a pool. The milk exosomes were separated by ultracentrifugation, a commonly reported method of extraction. Briefly, about 40 ml of fresh milk samples was centrifuged at $2,000 \times g$, 4°C , for 30 min to remove fat, cells, and large debris. The defatted supernatant was then centrifuged at $15,000 \times g$, 4°C , for 30 min to remove residual fat, cell debris, and partial casein. This supernatant, now devoid of fat, cells, and debris, was stored at -20°C immediately and then transferred to the laboratory and kept at -80°C until ready for use. After the milk was thawed, it went through a $0.45 \mu\text{m}$ filter to obtain a clear whey fraction. Subsequently, the clear whey fraction was prepared for ultracentrifugation ($160,000 \times g$, 4°C , 90 min) by an SW70Ti rotor (OPTIMA XPN-100, Beckman Coulter Instruments, Fullerton, CA, United States), and the pellets were re-suspended in 3 ml phosphate-buffered saline

and then passed through a 0.22 μm filter to obtain the exosome solutions.

Transmission Electron Microscopy and Particle Size Analysis

Ten microliters of purified exosomal fractions was analyzed by transmission electron microscopy (TEM). The sample was placed on formvar-coated copper grids for 2 min, washed briefly with ultrapure water, negatively stained with 1% uranyl acetate, and then observed by TEM (JEOLJEM2000EX, Tokyo, Japan). The size distribution was measured by the use of Zetasizer Nano ZS 90 (Malvern, United Kingdom) at 25°C.

Western Blot Analyses

To confirm the presence of porcine milk exosome, two positive markers (CD9 and CD63) of exosomes were used for Western blot. The PME protein content was assayed by Pierce BCA Protein Assay Kit. The proteins (20 μg) were first separated by sodium dodecyl sulfate-polyacrylamide gel electrophoresis (10%) and then transferred to a polyvinylidene difluoride membrane. After blocking with 5% skimmed milk for 2 h, the membranes were incubated overnight at 4°C with CD9 and CD63 antibodies (1:1,000, Sangon Biotech, China), respectively. Horseradish peroxidase-conjugated goat antirabbit IgG (H + L) (1:50,000, Jackson ImmunoResearch, United States) was applied as a secondary antibody for 1 h at 25°C. The proteins were measured using the FluorChem M Fluorescent Imaging System.

RNA Extraction and RNA Sequencing

Total RNA from PME samples was extracted using Trizol reagent (Invitrogen, Carlsbad, CA, United States). PME RNA was verified by agarose gel, and the quality was assessed using the RNA Nano 6000 Assay Kit of the Bioanalyzer 2100 system. Two micrograms of total RNA was used as input material for constructing a cDNA library. The library was constructed using a NEBNext Ultra Directional RNA Library Prep Kit for Illumina (NEB, United States) after the removal of ribosomal RNAs. Library sequencing was performed on an Illumina HiSeq 4000 platform and 150 bp paired-end reads were generated.

Data Analysis for Quality Control and Transcriptome Assembly

Firstly, the raw reads were processed through in-house perl scripts. The clean reads were obtained by wiping off the adapter reads, reads with over 10% N sequence, and unqualified reads in which the number of bases with a quality value $Q \leq 10$ was greater than 50%. At the same time, the Q20, Q30, and GC contents were calculated. The index of the reference genome was built using bowtie2 v2.2.8, and paired-end clean reads were aligned to the reference genome (*Sscrofa11.1*)¹ using HISAT2 v2.0.4 (Langmead and Salzberg, 2012). The mapped reads were assembled by StringTie (v1.3.1) software in a reference-based approach (Pertea et al., 2016).

¹ ftp://ftp.ensembl.org/pub/release-94/fasta/sus_scrofa/dna/

Identification of lncRNAs and Quantification of Expression Level

To identify lncRNAs, these steps were followed: (1) the transcripts with exon number < 2 were deleted, (2) the transcripts (length < 200 bp) were removed, (3) the transcripts that overlapped with the exon region of the database-annotated RNAs were removed through the Cuffcompare software (meanwhile, the transcripts overlapped with the known lncRNA exon regions in the database as the annotated lncRNAs), (4) the transcripts [fragments per kilobase million (FPKMs) < 0.5] were removed, (5) the transcripts that did not pass the protein-coding-score test were removed using four coding potential analysis software, including CPC (Kong et al., 2007), PhyloCSF (Lin et al., 2011), CNCI (Sun et al., 2013), and Pfam-scan (Finn et al., 2014). The intersecting results of all software were defined, as well those that were appointed as candidate lncRNAs (novel lncRNAs). The phyloFit program in the Phast package (Siepel et al., 2005) was used for the phylogenetic reconstruction of conserved and non-conserved regions among different species. Cufflink software was used to calculate FPKMs (representing the expression levels of the transcripts) of both lncRNAs and mRNAs (Trapnell et al., 2010).

Identification of circRNAs and Quantification of Expression Level

To identify circRNA, three different software including find-circ (Memczak et al., 2013), CIRCexplorer2 (Zhang et al., 2016) and CIRI2 (Gao et al., 2018) were performed on RNAseq library. Only circRNA candidates identified by all the three algorithms were considered for next evaluation. The raw counts were normalized using TPM (Zhou et al., 2010). Normalized expression level = (read count*1,000,000)/libsize (libsize is the sum of circRNA read count). Circos software was used to construct the circos figure.

Validation of lncRNAs/circRNAs by PCR and Sanger Sequencing

PME total RNAs were extracted by Trizol reagent. cDNA was synthesized by a reverse transcription kit (PrimeScript™ RT reagent Kit) with 500 ng of total RNA. PCR was performed on a Bio-Rad system (BIO-RAD, United States) in a 20 μl volume reaction containing 2 μl cDNA, 7 μl Nuclease-Free water, 1 mM of each primer, and 10 μl of 2 \times Tap Master Mix (Vazyme, Nanjing, China). The PCR program was as follows: 5 min at 95°C, 39 cycles of 30 s at 95°C, 30 s at the corresponding annealing temperature and 72°C for 30 s, and followed by 10 min at 72°C. The primers were designed using Primer 5.0 (detailed information shown in **Supplementary Tables 1, 2**). The PCR products of randomly selected eight lncRNAs and five circRNAs were confirmed by agarose gel. The PCR products of five circRNA divergent primers were confirmed by Sanger sequencing.

Target Gene Prediction of lncRNAs

The lncRNA target genes located in cis were predicted based on the assumption of lncRNAs that regulate their neighboring

regions. The coding genes 100 kb downstream and upstream of lncRNAs were searched and analyzed for their functional roles.

Function Enrichment Analysis of lncRNA Target Genes and circRNA Host Genes

Gene Ontology (GO) enrichment analyses for lncRNAs target genes or host genes of circRNAs were performed with the GOSecR package (Young et al., 2010). The corrected *P*-values less than 0.05 were considered as significantly enriched. Statistical enrichment of lncRNA target genes or circRNA host genes was identified using the Kyoto Encyclopedia of Genes and Genomes (KEGG) pathways, conducted by using the KOBAS software (Mao et al., 2005).

Interacted-Network Analysis of lncRNA and circRNA With miRNA

Putative interaction targets between the miRNAs and PME ncRNAs (lncRNAs or circRNAs) were predicted using RNAhybrid (Krueger and Rehmsmeier, 2006) and miRanda (Betel et al., 2010). The selected candidate miRNAs were shared by the abovementioned two tools. Cytoscape software was used to build and visualize the interacted network between miRNA and ncRNA (lncRNAs and circRNAs) or mRNA. In these networks, the interaction targets between the miRNAs and the mRNAs have been confirmed in previous studies.

RESULTS

Isolation and Characterization of Porcine Milk Exosomes and Their RNA Cargo

Porcine milk exosome was prepared by ultracentrifugation. The intact spherical morphology of PME was confirmed by TEM, and small spherical vesicles were observed (Figure 1A). The main particle size of PME ranged from 100 to 200 nm, and the average particle size was 155.7 nm (Figure 1B). The exosomes' positive common surface markers, CD9 and CD63, were detected by western blotting (Figure 1C). These results indicate that we have successfully isolated exosomes from porcine milk. Agarose gel and Agilent 2100 analyses showed that PME contained abundant RNAs, including few quantities of 28s and 18s rRNAs (Figures 1D,E).

Identification of lncRNAs and circRNAs in Porcine Milk Exosomes by RNA-Seq

For RNA-Seq data, we totally gained 100,528,942 raw reads and 93,361,890 clean reads, which were obtained after wiping off low-quality sequences, adaptor sequences, and sequences with over 10% N. The data output quality is shown in Supplementary Table 3. We aligned all clean reads onto the porcine *Sscrofa11.1* reference genome and found that 74,178,283 reads (79.45%) could be mapped successfully to the genome (detailed information shown in Supplementary Table 4). Based on lncRNAs' structural and non-coding functional characteristics, 2,466 novel lncRNAs were identified after filtering out the annotation transcripts (Figures 2A,B; detailed

information shown in Supplementary Files 2, 3), including 68% lincRNA, 31.6% antisense lncRNA, and 0.4% intronic lncRNAs (Figure 2C). Meanwhile, 809 annotated lncRNAs (detailed information shown in Supplementary Files 4, 5) were detected in PME². In order to explore the circular RNA expression profiles of PME, we identified 61 circRNAs with at least two unique back-spliced reads through RNA-seq analyses (detailed information shown in Supplementary Files 6, 7). A vast majority of the circRNAs were located in the exons and were distributed in different chromosomes (Figures 3A–C).

Genomic Features of lncRNAs in Porcine Milk Exosomes

To systematically identify differences between the lncRNAs and the mRNAs, gene structure and expression analyses were performed. In agreement with previous studies (Trapnell et al., 2010), the lncRNAs (novel and annotated lncRNAs) were shorter in length than the mRNAs (Figure 2D), and their genes tend to contain fewer exons (Figure 2E) and open reading frames (Figure 2F). However, our result showed that the lncRNAs were of a higher expression level compared with mRNAs in PME (Figure 2G).

Identification of lncRNAs and circRNAs by PCR Analysis

To verify the deep sequencing results, eight lncRNAs and five circRNAs in PME were randomly selected respectively from their top 20 in expression levels for PCR amplification. Agarose gel electrophoresis revealed that the product size of all selected lncRNAs and circRNAs (amplified with convergent primers and divergent primers) was fully matched (Figures 2H, 3D). In addition, five circRNA-amplified products with specific divergent primers were verified by Sanger sequencing, and the results were in accordance with high-throughput sequencing (Figure 3E).

Functional Enrichment Analysis of lncRNAs and circRNAs in Porcine Milk Exosomes

Recent studies have indicated that lncRNAs may act in cis and affect the gene expression at 100 kb upstream and downstream of their chromosomal neighborhood (Orom et al., 2010). To investigate the relationship between lncRNAs and their neighboring coding genes, we identified lncRNAs in PME corresponding to 8,075 protein-coding genes (detailed information shown in Supplementary File 8). GO annotation indicated that the predicted target genes were significantly enriched in cellular macromolecule metabolic process, RNA metabolic process, hematopoietic progenitor cell differentiation, regulation of adaptive immune response, interleukin-8 production, interleukin-6 secretion, intracellular membrane-bounded organelle, and early endosome and nucleic acid binding (Figure 4A). The KEGG pathway analysis showed that the lncRNA target genes were significantly enriched in olfactory transduction. Meanwhile, the T cell receptor signaling

²<http://asia.ensembl.org/index.html>

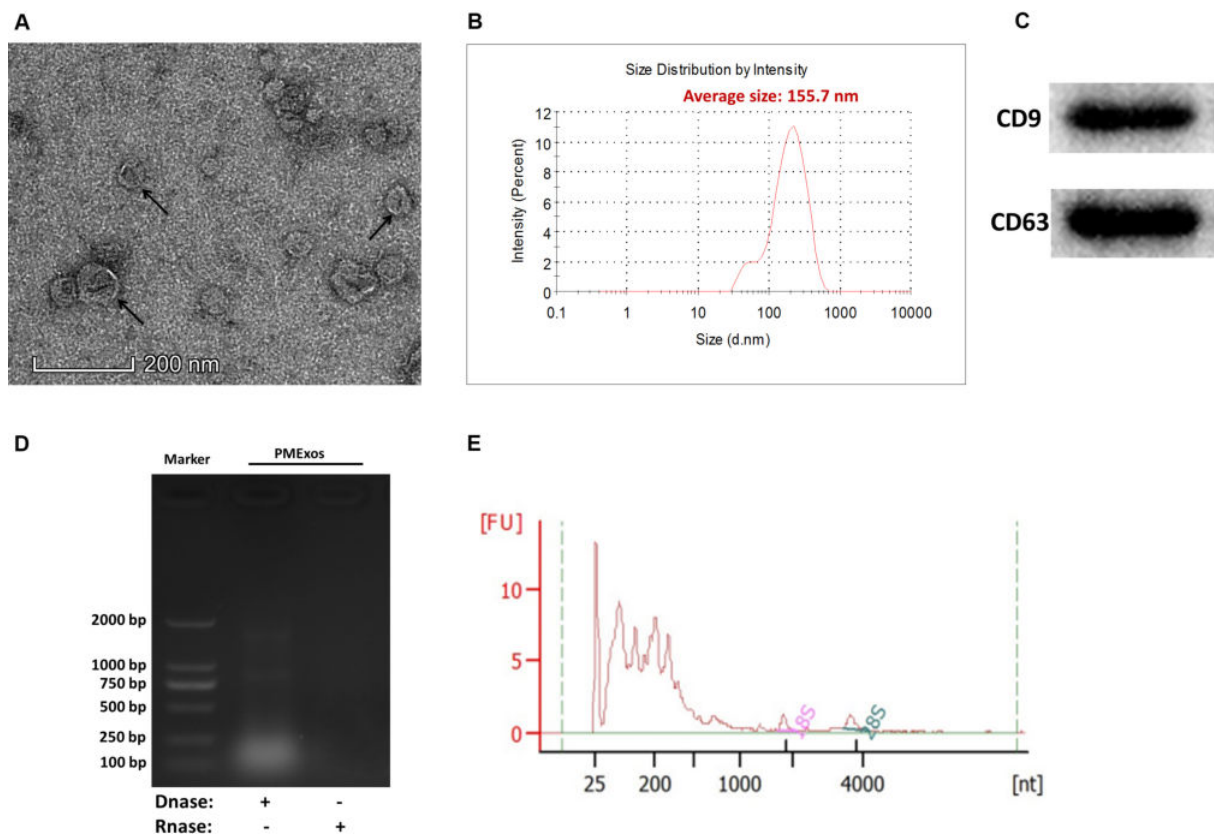


FIGURE 1 | Characterization of porcine milk exosomes. **(A)** Transmission electron microscopy analysis of porcine milk exosomes. The arrows indicate “milk exosomes.” **(B)** Size distribution analysis of porcine milk exosomes. **(C)** Porcine milk exosome proteins resolved by sodium dodecyl sulfate-polyacrylamide gel electrophoresis and analyzed by Western blot (two positive markers, CD9 and CD63). **(D)** Agarose gel analysis of RNA extracted from porcine milk exosomes. **(E)** RNA sample of porcine milk exosomes analyzed by Agilent Bioanalyzer 2100.

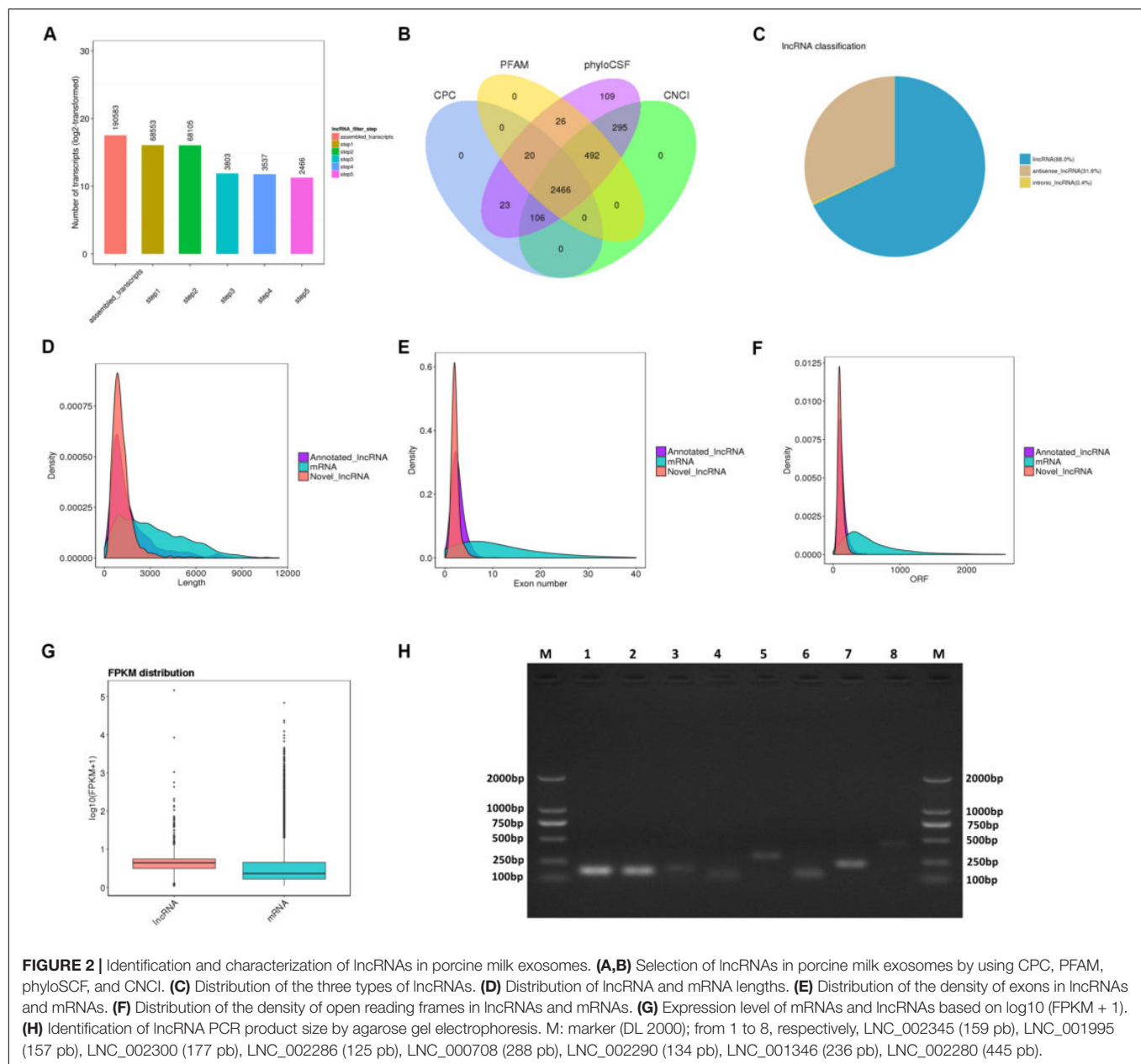
pathway, RIG-I-like receptor signaling pathway, mTOR signaling pathway, and MAPK signaling pathway were also enriched (**Figure 4B**). These findings suggested that lncRNAs may act in cis on mRNAs to regulate the immune reaction and the growth metabolism in PME.

The GO analysis of circRNA host genes showed that PME circRNAs were involved in nucleic acid binding, intracellular organelle, heterocycle metabolic processes, organic cyclic compound metabolic processes, and RNA metabolic processes (**Figure 5A**). The KEGG pathway analysis revealed that circRNA host genes were enriched in tight junction, adherence junction, inflammatory bowel disease, leukocyte transendothelial migration, spliceosome, and RNA degradation (**Figure 5B**). These findings hinted the potential roles of PME circRNAs in the functional areas, which are related to the intestinal barrier and nucleic acid metabolism.

lncRNA and circRNA Target Prediction in miRNAs

We aimed to compute the possible interactions of the top 100 expressed lncRNAs and all circRNAs with miRNAs. The PME lncRNAs and circRNAs had a high density of miRNA target

sites. The predicted target miRNAs of the top 100 lncRNAs are shown in **Supplementary File 9**. We selected the top 20 expressed lncRNAs, their potential miRNAs, and mRNAs that were reported to target these potential miRNAs to construct the lncRNA-miRNA-mRNA interaction network (**Figure 4C**). In this network, many proliferation-related miRNAs have been observed. For instance, miR-149, miR-125a, miR-383, miR-769, miR-1343, and miR-615 have been demonstrated to inhibit proliferation or induce apoptosis by suppressing the target gene expression. It was also shown that some miRNAs might each interact with multiple lncRNAs, such as miR-383 interacting with LNC_002286, LNC_000994, LNC_000708, and LNC_002276. So, those lncRNAs in PME could be considered as candidates for cell proliferation regulation. Meanwhile, 61 circRNAs in PME were predicted to target 154 miRNAs (detailed information shown in **Supplementary File 10**). As the KEGG pathway showed, the circRNA host genes were related to the intestinal barrier. More interestingly, the miRNA-circRNA interaction analysis showed that many target miRNAs of circRNA have been reported to be associated with the intestinal barrier and mucosal immunity. Superimposing these miRNAs, the target mRNAs and the predicted target circRNAs enabled the construction of a circRNA-miRNA-mRNA interaction network, which is



associated with regulating the intestinal barrier. In total, the network contains 42 connections between 19 circRNAs, 11 miRNAs, and 12 mRNAs (Figure 5C).

DISCUSSION

It has been well evidenced that exosomes are presented in porcine milk, and miRNAs (Chen et al., 2014; Ma et al., 2018) and mRNAs (Chen et al., 2017) were identified from these extracellular vesicles. In the present study, we identified a total of 3,275 lncRNAs and 61 circRNAs in PME. Comparisons of the genomic features between lncRNAs and mRNAs showed that the observed characteristics are coincident with those of previous

studies (Ren et al., 2016; Ma Q. et al., 2017). The PCR product sequencing of five circRNAs in PME was completely matched. To the best of our knowledge, this is the first work to report two novel types of RNAs (lncRNA and circRNA) presented in porcine milk, although the presence of lncRNA in human milk exosomes (Karlsson et al., 2016) and the presence of lncRNA (Zeng et al., 2019) and circRNA (Wang Y. et al., 2019) in bovine milk exosomes have been reported. As such, our study provides a comprehensive foundation for the expression profiles of lncRNA and circRNA in porcine milk and, thus, will greatly enrich the transcript genomic database of pig.

For newborn animals, breast milk plays an irreplaceable role in the growth, development, intestinal health, and improvement of the immune system from birth to adulthood. Traditionally,

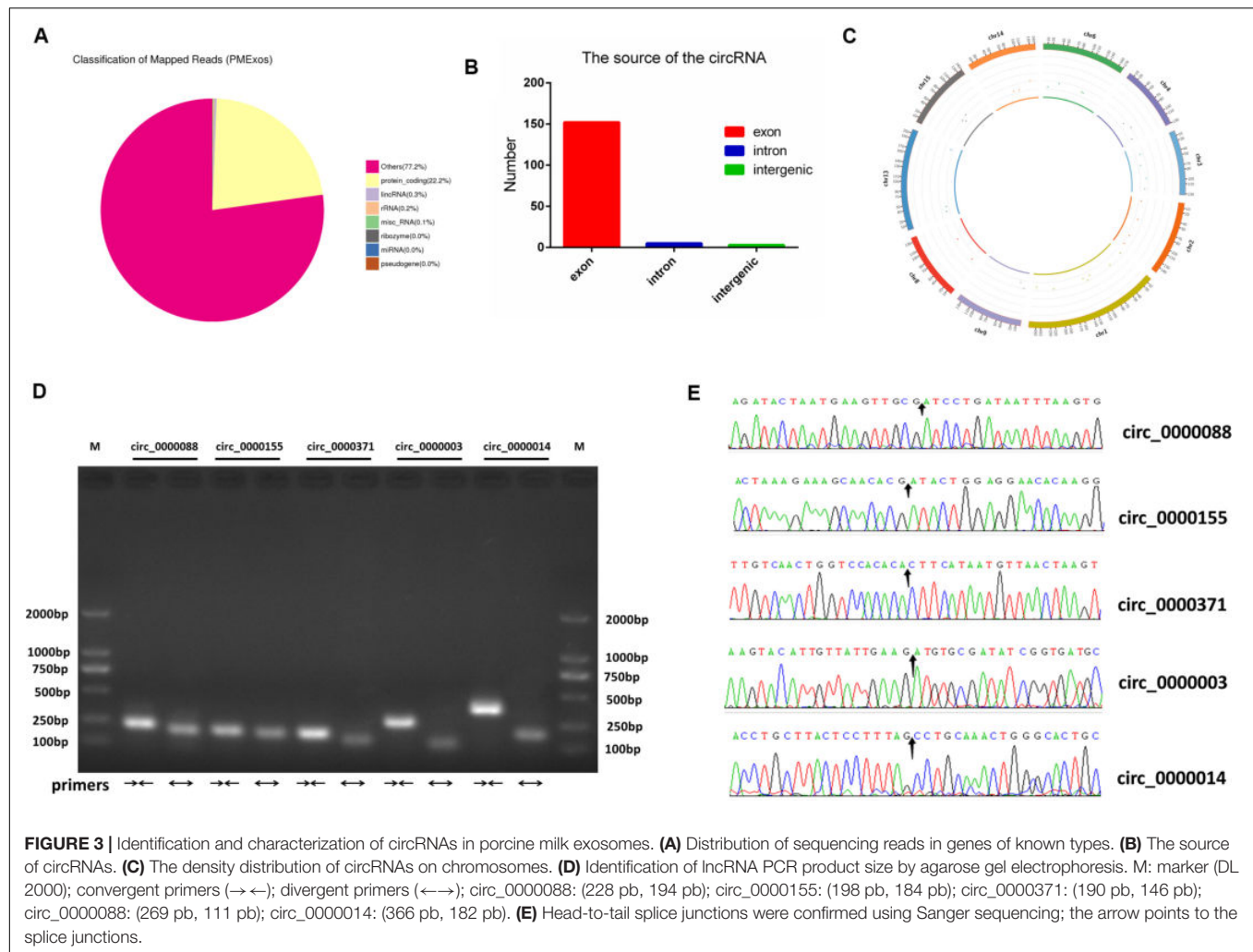
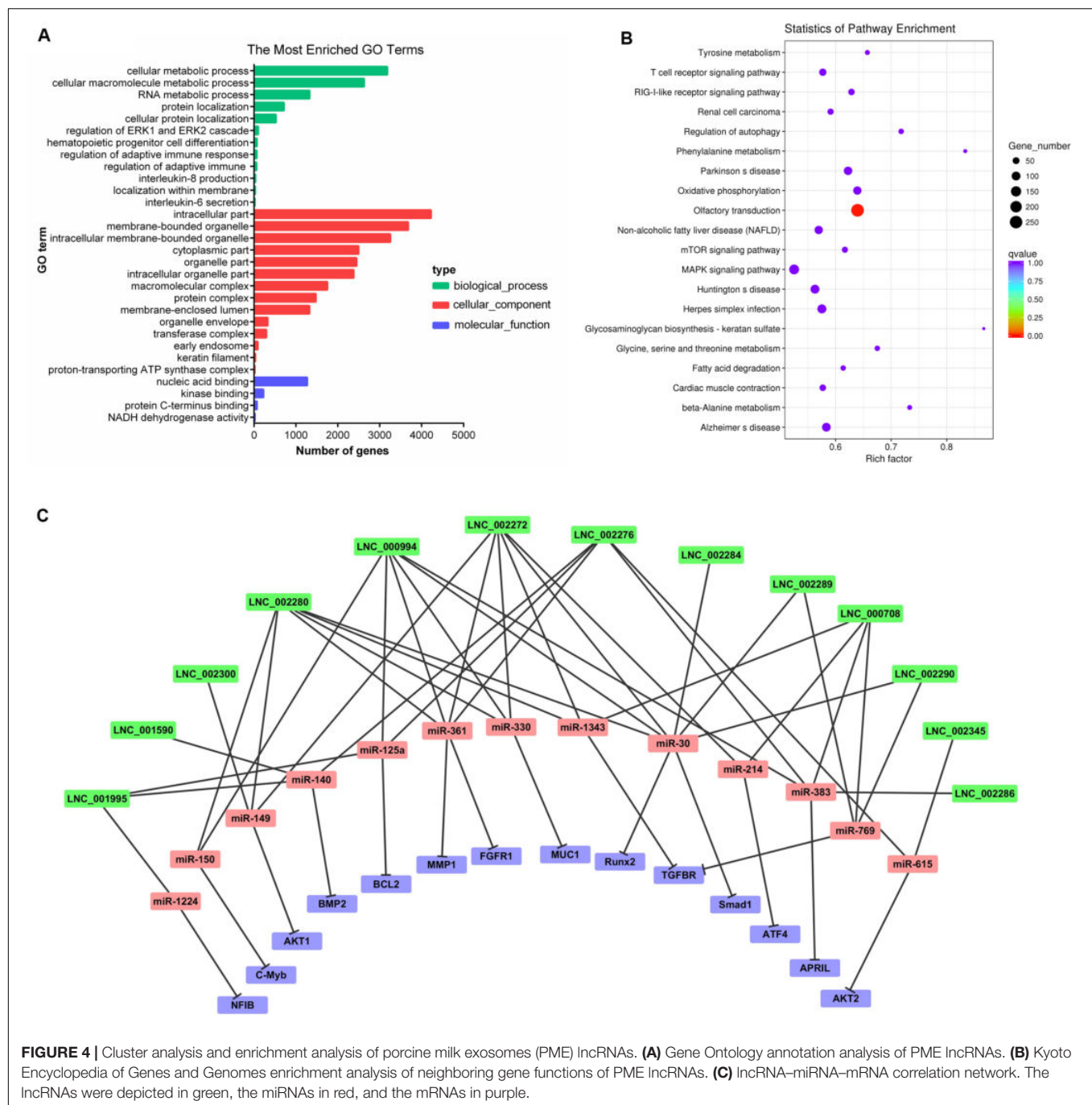


FIGURE 3 | Identification and characterization of circRNAs in porcine milk exosomes. **(A)** Distribution of sequencing reads in genes of known types. **(B)** The source of circRNAs. **(C)** The density distribution of circRNAs on chromosomes. **(D)** Identification of lncRNA PCR product size by agarose gel electrophoresis. M: marker (DL 2000); convergent primers (→←); divergent primers (←→); circ_0000088: (228 pb, 194 pb); circ_0000155: (198 pb, 184 pb); circ_0000371: (190 pb, 146 pb); circ_0000088: (269 pb, 111 pb); circ_0000014: (366 pb, 182 pb). **(E)** Head-to-tail splice junctions were confirmed using Sanger sequencing; the arrow points to the splice junctions.

immunoglobulins and non-nutritional bioactive factors in milk have been considered as the main functional substances in organismic regulations. More recently, the scientific enthusiasm to study the modulating function of milk exosomal RNAs has soared because milk RNAs were found to be stable to acidic conditions and resistant to RNase (Izumi et al., 2012) and digestive enzymes degradation (Rani et al., 2017) and could be taken up by intestinal cells (Liao et al., 2017) and macrophages (Izumi et al., 2015). Moreover, cargo selection into exosomes is a regulated, non-random process. A previous study has indicated that the RNAs are selectively encapsulated into exosomes (Skog et al., 2008). In our research, we found that the lncRNAs, encapsulated in PME, were in higher levels compared with mRNAs (Figure 2G). The high abundance of these lncRNAs in PME may indicate that they would play a relatively important role in physiological function. A functional analysis showed that the PME lncRNA target genes were enriched in many biological processes which were essential for infants' growth and development. BME lncRNAs have been predicted to be involved in hematopoietic progenitor cell differentiation, regulation of adaptive immune response,

interleukin-8 production, interleukin-6 secretion, T cell receptor signaling pathway, and RIG-I-like receptor signaling pathway, which are related to immune responses (Quicke et al., 2017). Zemleni et al. (2019) suggest that cargos in milk exosomes, RNAs in particular, are important information communicative and regulatory substances. The abundant lncRNAs in PME may be absorbed and play a significant role in infants. The circular structure of circRNAs makes them more stable than the other types of RNAs. Many circRNAs are conserved in mammals, which might have potential biological functions (Rybak-Wolf et al., 2015). Previous studies have found that exosomes derived from human (Martin et al., 2018), yak (Gao et al., 2019), rat (Hock et al., 2017), and pig (Chen T. et al., 2016) milk promote the proliferation or attenuate the death of intestinal epithelial cells. In our study, a functional analysis showed that the circRNA host genes were associated with intestinal barrier, including in tight junction, adherence junction, inflammatory bowel disease, and leukocyte transendothelial migration.

Increasing studies suggest that lncRNA or circRNA play a role in piglet immunity, development, and oxidative stress. Shuangbao Gun's team provides a novel understanding of



lncRNAs on regulating piglet ileum immune response against *Clostridium perfringens* infectious diseases (CPID) (Huang et al., 2019). Interestingly, the differentially expressed lncRNA (ALDBSSCG0000001631) involved in ileum immune response in CPID was found in porcine milk exosome. They also reported the potential lncRNA (Yan et al., 2018a) and circRNA (Yan et al., 2018b) functions in the spleen of diarrheic piglets caused by CPID. Liu et al. (2018) and Chen et al. (2019) revealed the potential role of lncRNA or circRNA in muscle and fat development in piglets. lncRNA was also found to be associated

with oxidative stress in piglet (Wang J. et al., 2019). Currently, the dominant perception is that milk-derived RNAs could be transferred from mother to infant and regulate gene expression in target tissues and cells (Baier et al., 2014; Aqil et al., 2019). The delivery of lncRNAs and circRNAs through breast milk exosomes could therefore allow effects in gene expression in recipient cells and play an important role in infant/piglet development (Figure 6). Our finding raises the exciting possibility that PME-encapsulated ncRNAs might provide biological signals that regulate gene expression in piglets.

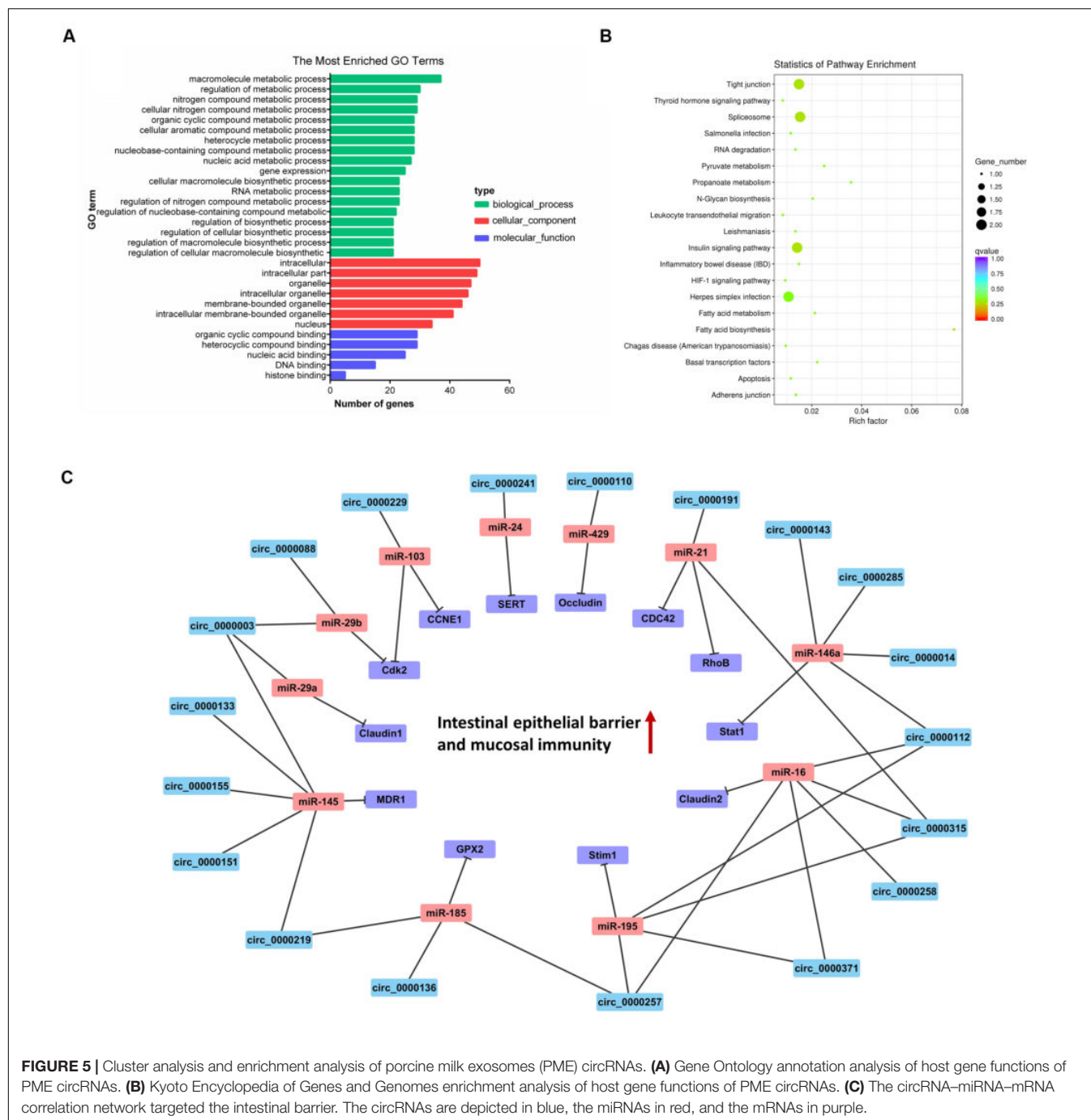
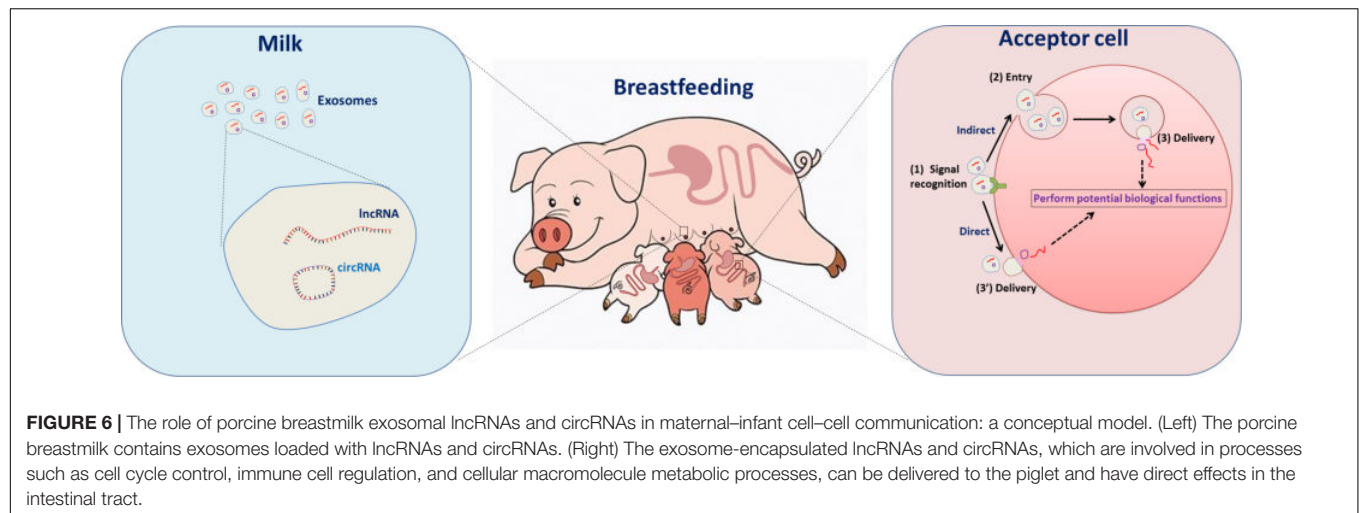


FIGURE 5 | Cluster analysis and enrichment analysis of porcine milk exosomes (PME) circRNAs. **(A)** Gene Ontology annotation analysis of host gene functions of PME circRNAs. **(B)** Kyoto Encyclopedia of Genes and Genomes enrichment analysis of host gene functions of PME circRNAs. **(C)** The circRNA-miRNA-mRNA correlation network targeted the intestinal barrier. The circRNAs are depicted in blue, the miRNAs in red, and the mRNAs in purple.

Examples of classic RNA-RNA interactions associated with the post-transcriptional regulation of miRNAs have been described in many species (Tay et al., 2014). Recently, evidence indicates that exosomal ncRNAs communicated and co-regulated with each other by competing to bind with shared miRNAs, acting as competitive endogenous RNAs (ceRNAs) (Zheng et al., 2018; Zhang et al., 2019). Therefore, exosomal lncRNAs and circRNAs may inhibit or relieve the repression of miRNA in translation. In this study, the top 20 high-expression lncRNAs had high-density binding sites for the proliferation-related

miRNAs, such as miR-149 (Pan et al., 2012), miR-615 (Bai et al., 2015), and miR-383 (Chen L. et al., 2016), which inhibit cell proliferation by targeting AKT1, AKT2, and APRIL, respectively. Other targeted miRNAs such as miR-769 (Yang et al., 2017) and miR-1343 (Stolzenburg et al., 2016) could suppress cell proliferation by targeting TGFBR. We found that the PME circRNAs could interact with miRNAs that were associated with the intestinal barrier. For instance, circ_0000003 and circ_0000088 in PME were predicted to target miR-29a/b, which were involved in increased intestinal permeability and suppressed



proliferation and mucosal growth (Xiao et al., 2013; Zhou et al., 2015). Previous studies showed that miR-146a was expressed in a variety of gut tissues to reduce luminal IgA levels (Runtsch et al., 2015) and mediated Treg cell immune homeostasis by direct targeting to signal transducer and activator transcription 1 (Stat1) (Lu et al., 2010). Interestingly, circ_0000143, circ_0000285, circ_0000014, and circ_0000112 in PME have binding sites to miR-146a. Our previous and recent work showed that porcine milk exosomal RNAs play an important role in promoting proliferation and attenuating the lipopolysaccharide-induced apoptosis of intestinal epithelial cells (Chen T. et al., 2016; Xie et al., 2019). Based on our findings, we suggest that these predicted binding sites implicate lncRNAs and circRNAs as a miRNA sponge and may be an attractive regulatory substance in cell proliferation and intestinal barrier process. These findings also provide new perspectives on lncRNA/circRNA-associated ceRNA networks in porcine milk and piglets for future research.

CONCLUSION

The present study firstly explored PME lncRNA and circRNA profiles by high-throughput sequencing. We demonstrated here that porcine milk exosome contained abundant lncRNAs and circRNAs, and most of them were predicted to participate in cell proliferation and intestinal barrier functions. These findings provide significant information and contribute to an increased understanding of the role of lncRNAs and circRNAs in milk and build a basis for future researches on their physiological functions and regulatory mechanisms. Further experimental studies are warranted to elucidate their roles in piglets' development and long-term health.

DATA AVAILABILITY STATEMENT

The datasets generated for this study can be found in the all sequencing raw data sets were deposited into the National Center for Biotechnology Information (NCBI) Sequence

Read Archive (SRA) database under BioProject accession number PRJNA556770 (<https://dataview.ncbi.nlm.nih.gov/object/PRJNA556770?reviewer=nshbepi58ifirg7nerp7j2o35q&archive=sra>). Sequencing files can be found under accession numbers SRR9843080.

ETHICS STATEMENT

The animal study was reviewed and approved by the laboratory animal management and welfare regulations approved by Standing Committee of Guangdong People's Congress.

AUTHOR CONTRIBUTIONS

BZ and YZ conceived and designed the experimental plan. BZ, TC, MX, and LW collected the samples and measurement data. QX and JS participated in the bioinformatics analyses. BZ, TC, JL, and YZ drafted and revised this manuscript. All authors contributed to the article and approved the submitted version.

FUNDING

This work was supported by grants from the National Key Research and Development Program of China (2016YFD0500503), the Natural Science Foundation of China program (31802156), and the Key Project of Guangdong Provincial Nature Science Foundation (2018B030311015). The funders had no role in the study design, sample collection and analysis, decision to publish, or preparation of the manuscript.

SUPPLEMENTARY MATERIAL

The Supplementary Material for this article can be found online at: <https://www.frontiersin.org/articles/10.3389/fgene.2020.00652/full#supplementary-material>

REFERENCES

- Aguilar-Lozano, A., Baier, S., Grove, R., Shu, J., Giraud, D., Leiferman, A., et al. (2018). Concentrations of purine metabolites are elevated in fluids from adults and infants and in livers from mice fed diets depleted of bovine milk exosomes and their RNA cargos. *J. Nutr.* 148, 1886–1894. doi: 10.1093/jn/nxy223
- Aqil, F., Munagala, R., Jayabalan, J., Agrawal, A. K., Kyakulaga, A.-H., Wilcher, S. A., et al. (2019). Milk exosomes - natural nanoparticles for siRNA delivery. *Cancer Lett.* 449, 186–195. doi: 10.1016/j.canlet.2019.02.011
- Bai, Y., Li, J., Li, J., Liu, Y., and Zhang, B. (2015). MiR-615 inhibited cell proliferation and cell cycle of human breast cancer cells by suppressing of AKT2 expression. *Int. J. Clin. Exp. Med.* 8, 3801–3808.
- Baier, S. R., Nguyen, C., Xie, F., Wood, J. R., and Zemleni, J. (2014). MicroRNAs are absorbed in biologically meaningful amounts from nutritionally relevant doses of cow milk and affect gene expression in peripheral blood mononuclear cells, HEK-293 kidney cell cultures, and mouse livers. *J. Nutr.* 144, 1495–1500. doi: 10.3945/jn.114.196436
- Betel, D., Koppal, A., Agius, P., Sander, C., and Leslie, C. (2010). Comprehensive modeling of microRNA targets predicts functional non-conserved and non-canonical sites. *Genome Biol.* 11:R90. doi: 10.1186/gb-2010-11-8-r90
- Bryzghalov, O., Szcześniak, M. W., and Makołowska, I. (2020). SyntDB: defining orthologues of human long noncoding RNAs across primates. *Nucleic Acids Res.* 48, D238–D245.
- Chen, L., Guan, H., Gu, C., Cao, Y., Shao, J., and Wang, F. (2016). miR-383 inhibits hepatocellular carcinoma cell proliferation via targeting APRIL. *Tumor Biol.* 37, 2497–2507. doi: 10.1007/s13277-015-4071-1
- Chen, L., Shi, G., Chen, G., Li, J., Li, M., Zou, C., et al. (2019). Transcriptome analysis suggests the roles of long intergenic non-coding RNAs in the growth performance of weaned piglets. *Front. Genet.* 10:196. doi: 10.3389/fgene.2019.00196
- Chen, T., Xi, Q.-Y., Sun, J.-J., Ye, R.-S., Cheng, X., Sun, R.-P., et al. (2017). Revelation of mRNAs and proteins in porcine milk exosomes by transcriptomic and proteomic analysis. *BMC Vet. Res.* 13:101. doi: 10.1186/s12917-017-1021-8
- Chen, T., Xi, Q.-Y., Ye, R.-S., Cheng, X., Qi, Q.-E., Wang, S.-B., et al. (2014). Exploration of microRNAs in porcine milk exosomes. *BMC Genomics* 15:100. doi: 10.1186/1471-2164-15-100
- Chen, T., Xie, M.-Y., Sun, J.-J., Ye, R.-S., Cheng, X., Sun, R.-P., et al. (2016). Porcine milk-derived exosomes promote proliferation of intestinal epithelial cells. *Sci. Rep.* 6:33862. doi: 10.1038/srep33862
- Esteller, M. (2011). Non-coding RNAs in human disease. *Nat. Rev. Genet.* 12, 861–874. doi: 10.1038/nrg3074
- Finn, R. D., Bateman, A., Clements, J., Coghill, P., Eberhardt, R. Y., Eddy, S. R., et al. (2014). Pfam: the protein families database. *Nucleic Acids Res.* 42, D222–D230. doi: 10.1093/nar/gkt1223
- Gao, H. N., Guo, H. Y., Zhang, H., Xie, X. L., Wen, P. C., and Ren, F. Z. (2019). Yak-milk-derived exosomes promote proliferation of intestinal epithelial cells in an hypoxic environment. *J. Dairy Sci.* 102, 985–996. doi: 10.3168/jds.2018-14946
- Gao, Y., Zhang, J., and Zhao, F. (2018). Circular RNA identification based on multiple seed matching. *Brief. Bioinform.* 19, 803–810. doi: 10.1093/bib/bbx014
- Hock, A., Miyake, H., Li, B., Lee, C., Ermini, L., Koike, Y., et al. (2017). Breast milk-derived exosomes promote intestinal epithelial cell growth. *J. Pediatr. Surg.* 52, 755–759. doi: 10.1016/j.jpedsurg.2017.01.032
- Huang, X., Sun, W., Yan, Z., Shi, H., Yang, Q., Wang, P., et al. (2019). Integrative analyses of long non-coding RNA and mRNA involved in piglet ileum immune response to *Clostridium perfringens* type C infection. *Front. Cell. Infect. Microbiol.* 9:130. doi: 10.3389/fcimb.2019.00130
- Izumi, H., Kosaka, N., Shimizu, T., Sekine, K., Ochiya, T., and Takase, M. (2012). Bovine milk contains microRNA and messenger RNA that are stable under degradative conditions. *J. Dairy Sci.* 95, 4831–4841. doi: 10.3168/jds.2012-5489
- Izumi, H., Tsuda, M., Sato, Y., Kosaka, N., Ochiya, T., Iwamoto, H., et al. (2015). Bovine milk exosomes contain microRNA and mRNA and are taken up by human macrophages. *J. Dairy Sci.* 98, 2920–2933. doi: 10.3168/jds.2014-9076
- Karlsson, O., Rodosthenous, R. S., Jara, C., Brennan, K. J., Wright, R. O., Baccarelli, A. A., et al. (2016). Detection of long non-coding RNAs in human breastmilk extracellular vesicles: implications for early child development. *Epigenetics* 11, 721–729. doi: 10.1080/15592294.2016.1216285
- Kong, L., Zhang, Y., Ye, Z.-Q., Liu, X.-Q., Zhao, S.-Q., Wei, L., et al. (2007). CPC: assess the protein-coding potential of transcripts using sequence features and support vector machine. *Nucleic Acids Res.* 35, W345–W349. doi: 10.1093/nar/gkm391
- Kristensen, L. S., Andersen, M. S., Stagsted, L. V., Ebbesen, K. K., Hansen, T. B., and Kjems, J. (2019). The biogenesis, biology and characterization of circular RNAs. *Nat. Rev. Genet.* 20, 675–691.
- Krueger, J., and Rehmsmeier, M. (2006). RNAhybrid: microRNA target prediction easy, fast and flexible. *Nucleic Acids Res.* 34, W451–W454. doi: 10.1093/nar/gkl243
- Langmead, B., and Salzberg, S. L. (2012). Fast gapped-read alignment with Bowtie 2. *Nat. Methods* 9, 357–359. doi: 10.1038/nmeth.1923
- Li, B., Hock, A., Wu, R. Y., Minich, A., Botts, S. R., Lee, C., et al. (2019). Bovine milk-derived exosomes enhance goblet cell activity and prevent the development of experimental necrotizing enterocolitis. *PLoS One* 14:e0211431. doi: 10.1371/journal.pone.0211431
- Li, Y., Zheng, Q., Bao, C., Li, S., Guo, W., Zhao, J., et al. (2015). Circular RNA is enriched and stable in exosomes: a promising biomarker for cancer diagnosis. *Cell Res.* 25, 981–984. doi: 10.1038/cr.2015.82
- Liao, Y., Du, X., Li, J., and Lonnerdal, B. (2017). Human milk exosomes and their microRNAs survive digestion in vitro and are taken up by human intestinal cells. *Mol. Nutr. Food Res.* 61:1700082. doi: 10.1002/mnfr.201700082
- Lin, M. F., Jungreis, I., and Kellis, M. (2011). PhyloCSF: a comparative genomics method to distinguish protein coding and non-coding regions. *Bioinformatics* 27, 1275–1282. doi: 10.1093/bioinformatics/btr209
- Liu, X., Liu, K., Shan, B., Wei, S., Li, D., Han, H., et al. (2018). A genome-wide landscape of mRNAs, lncRNAs, and circRNAs during subcutaneous adipogenesis in pigs. *J. Anim. Sci. Biotechnol.* 9:76.
- Lu, L.-F., Boldin, M. P., Chaudhry, A., Lin, L.-L., Taganov, K. D., Hanada, T., et al. (2010). Function of miR-146a in controlling treg cell-mediated regulation of Th1 responses. *Cell* 142, 914–929. doi: 10.1016/j.cell.2010.08.012
- Ma, J., Wang, C., Long, K., Zhang, H., Zhang, J., Jin, L., et al. (2017). Exosomal microRNAs in giant panda (*Ailuropoda melanoleuca*) breast milk: potential maternal regulators for the development of newborn cubs. *Sci. Rep.* 7:3507.
- Ma, Q., Li, L., Tang, Y., Fu, Q., Liu, S., Hu, S., et al. (2017). Analyses of long non-coding RNAs and mRNA profiling through RNA sequencing of MDBK cells at different stages of bovine viral diarrhea virus infection. *Res. Vet. Sci.* 115, 508–516. doi: 10.1016/j.rvsc.2017.09.020
- Ma, Y., Feng, S., Wang, X., Qazi, I. H., Long, K., Luo, Y., et al. (2018). Exploration of exosomal microRNA expression profiles in pigeon 'Milk' during the lactation period. *BMC Genomics* 19:828. doi: 10.1186/s12864-018-5201-0
- Manca, S., Upadhyaya, B., Mutai, E., Desaulniers, A. T., Cederberg, R. A., White, B. R., et al. (2018). Milk exosomes are bioavailable and distinct microRNA cargos have unique tissue distribution patterns. *Sci. Rep.* 8:11321.
- Mao, X. Z., Cai, T., Olyarchuk, J. G., and Wei, L. P. (2005). Automated genome annotation and pathway identification using the KEGG Orthology (KO) as a controlled vocabulary. *Bioinformatics* 21, 3787–3793. doi: 10.1093/bioinformatics/bti430
- Martin, C., Patel, M., Williams, S., Arora, H., and Sims, B. (2018). Human breast milk-derived exosomes attenuate cell death in intestinal epithelial cells. *Innate Immun.* 24, 278–284. doi: 10.1177/1753425918785715
- Mathieu, M., Martin-Jaulat, L., Lavieu, G., and Thery, C. (2019). Specificities of secretion and uptake of exosomes and other extracellular vesicles for cell-to-cell communication. *Nat. Cell Biol.* 21, 9–17. doi: 10.1038/s41556-018-0250-9
- Mattick, J. S., and Makunin, I. V. (2006). Non-coding RNA. *Hum. Mol. Genet.* 15, R17–R29. doi: 10.1093/hmg/ddl046
- Melnik, B. C., Kakulas, F., Geddes, D. T., Hartmann, P. E., John, S. M., Carrera-Bastos, P., et al. (2016). Milk miRNAs: simple nutrients or systemic functional regulators? *Nutr. Metab.* 13:42.
- Memczak, S., Jens, M., Elefsinioti, A., Torti, F., Krueger, J., Rybak, A., et al. (2013). Circular RNAs are a large class of animal RNAs with regulatory potency. *Nature* 495, 333–338. doi: 10.1038/nature11928
- Orom, U. A., Derrien, T., Beringer, M., Gumireddy, K., Gardini, A., Bussotti, G., et al. (2010). Long noncoding RNAs with enhancer-like function in human cells. *Cell* 143, 46–58. doi: 10.1016/j.cell.2010.09.001
- Pan, S. J., Zhan, S. K., Pei, B. G., Sun, Q. F., Bian, L. G., and Sun, B. M. (2012). microRNA-149 inhibits proliferation and invasion of glioma cells via blockade of AKT1 signaling. *Int. J. Immunopathol. Pharmacol.* 25, 871–881. doi: 10.1177/039463201202500405
- Pegtel, D. M., and Gould, S. J. (2019). Exosomes. *Annu. Rev. Biochem.* 88, 487–514.

- Pertea, M., Kim, D., Pertea, G. M., Leek, J. T., and Salzberg, S. L. (2016). Transcript-level expression analysis of RNA-seq experiments with HISAT, StringTie and Ballgown. *Nat. Protoc.* 11, 1650–1667. doi: 10.1038/nprot.2016.095
- Quicke, K. M., Diamond, M. S., and Suthar, M. S. (2017). Negative regulators of the RIG-I-like receptor signaling pathway. *Eur. J. Immunol.* 47, 615–628. doi: 10.1002/eji.201646484
- Rani, P., Vashisht, M., Golla, N., Shandilya, S., Onteru, S. K., and Singh, D. (2017). Milk miRNAs encapsulated in exosomes are stable to human digestion and permeable to intestinal barrier in vitro. *J. Funct. Foods* 34, 431–439. doi: 10.1016/j.jff.2017.05.009
- Ren, H., Wang, G., Chen, L., Jiang, J., Liu, L., Li, N., et al. (2016). Genome-wide analysis of long non-coding RNAs at early stage of skin pigmentation in goats (*Capra hircus*). *BMC Genomics* 17:67. doi: 10.1186/s12864-016-2365-3
- Runtsch, M. C., Hu, R., Alexander, M., Wallace, J., Kagele, D., Petersen, C., et al. (2015). MicroRNA-146a constrains multiple parameters of intestinal immunity and increases susceptibility to DSS colitis. *Oncotarget* 6, 28556–28572. doi: 10.18632/oncotarget.5597
- Rybák-Wolf, A., Stottmeister, C., Glazar, P., Jens, M., Pino, N., Giusti, S., et al. (2015). Circular RNAs in the mammalian brain are highly abundant, conserved, and dynamically expressed. *Mol. Cell* 58, 870–885. doi: 10.1016/j.molcel.2015.03.027
- Siepel, A., Bejerano, G., Pedersen, J. S., Hinrichs, A. S., Hou, M. M., Rosenbloom, K., et al. (2005). Evolutionarily conserved elements in vertebrate, insect, worm, and yeast genomes. *Genome Res.* 15, 1034–1050. doi: 10.1101/gr.3715005
- Skog, J., Wuerdinger, T., van Rijn, S., Meijer, D. H., Gainche, L., Sena-Esteves, M., et al. (2008). Glioblastoma microvesicles transport RNA and proteins that promote tumour growth and provide diagnostic biomarkers. *Nat. Cell Biol.* 10, 1470–1476. doi: 10.1038/ncb1800
- Stolzenburg, L. R., Wachtel, S., Dang, H., and Harris, A. (2016). miR-1343 attenuates pathways of fibrosis by targeting the TGF-beta receptors. *Biochem. J.* 473, 245–256. doi: 10.1042/bj20150821
- Strathe, A. V., Bruun, T. S., Zerrahn, J. E., Tauson, A. H., and Hansen, C. F. (2016). The effect of increasing the dietary valine-to-lysine ratio on sow metabolism, milk production, and litter growth. *J. Anim. Sci.* 94, 155–164. doi: 10.2527/jas2015-9267
- Sun, L., Luo, H., Bu, D., Zhao, G., Yu, K., Zhang, C., et al. (2013). Utilizing sequence intrinsic composition to classify protein-coding and long non-coding transcripts. *Nucleic Acids Res.* 41:e166. doi: 10.1093/nar/gkt646
- Tay, Y., Rinn, J., and Pandolfi, P. P. (2014). The multilayered complexity of ceRNA crosstalk and competition. *Nature* 505, 344–352. doi: 10.1038/nature12986
- Trapnell, C., Williams, B. A., Pertea, G., Mortazavi, A., Kwan, G., van Baren, M. J., et al. (2010). Transcript assembly and quantification by RNA-Seq reveals unannotated transcripts and isoform switching during cell differentiation. *Nat. Biotechnol.* 28, 511–515. doi: 10.1038/nbt.1621
- Vallimont, J. E., Dechow, C. D., Daubert, J. M., Dekleva, M. W., Blum, J. W., Barlieb, C. M., et al. (2010). Genetic parameters of feed intake, production, body weight, body condition score, and selected type traits of Holstein cows in commercial tie-stall barns. *J. Dairy Sci.* 93, 4892–4901. doi: 10.3168/jds.2010-3189
- Wang, J., Li, Z.-X., Yang, D.-D., Liu, P.-Q., Wang, Z.-Q., Zeng, Y.-Q., et al. (2019). Diquat determines a deregulation of lncRNA and mRNA expression in the liver of postweaned piglets. *Oxid. Med. Cell. Longev.* 2019:9148535. doi: 10.1155/2019/9148535
- Wang, L., Sadri, M., Giraud, D., and Zemleni, J. (2018). RNase H2-dependent polymerase chain reaction and elimination of confounders in sample collection, storage, and analysis strengthen evidence that microRNAs in bovine milk are bioavailable in humans. *J. Nutr.* 148, 153–159. doi: 10.1093/jn/nxx024
- Wang, Y., Li, D., Wang, Y., Li, M., Fang, X., Chen, H., et al. (2019). The landscape of circular RNAs and mRNAs in bovine milk exosomes. *J. Food Compos. Anal.* 76, 33–38. doi: 10.1016/j.jfca.2018.12.004
- Weber, J. A., Baxter, D. H., Zhang, S., Huang, D. Y., Huang, K. H., Lee, M. J., et al. (2010). The MicroRNA spectrum in 12 body fluids. *Clin. Chem.* 56, 1733–1741. doi: 10.1373/clinchem.2010.147405
- Xiao, L., Rao, J. N., Zou, T., Liu, L., Cao, S., Martindale, J. L., et al. (2013). miR-29b represses intestinal mucosal growth by inhibiting translation of cyclin-dependent kinase 2. *Mol. Biol. Cell* 24, 3038–3046. doi: 10.1091/mbc.e13-05-0287
- Xie, M.-Y., Hou, L.-J., Sun, J.-J., Zeng, B., Xi, Q.-Y., Luo, J.-Y., et al. (2019). Porcine milk exosome miRNAs attenuate LPS-induced apoptosis through inhibiting TLR4/NF-κB and p53 pathways in intestinal epithelial cells. *J. Agric. Food Chem.* 67, 9477–9491. doi: 10.1021/acs.jafc.9b02925
- Yan, Z., Huang, X., Sun, W., Yang, Q., Shi, H., Jiang, T., et al. (2018a). Analyses of long non-coding RNA and mRNA profiling in the spleen of diarrheic piglets caused by *Clostridium perfringens* type C. *PeerJ* 6:e5997. doi: 10.7717/peerj.5997
- Yan, Z., Jiang, T., Wang, P., Huang, X., Yang, Q., Sun, W., et al. (2018b). Circular RNA expression profile of spleen in a *Clostridium perfringens* type C-induced piglet model of necrotizing enteritis. *FEBS Open Bio* 8, 1722–1732. doi: 10.1002/2211-5463.12512
- Yang, Z., He, J., Gao, P., Niu, Y., Zhang, J., Wang, L., et al. (2017). miR-769-5p suppressed cell proliferation, migration and invasion by targeting TGFBR1 in non-small cell lung carcinoma. *Oncotarget* 8, 113558–113570. doi: 10.18632/oncotarget.23060
- Ying, W., Riopel, M., Bandyopadhyay, G., Dong, Y., Birmingham, A., Seo, J. B., et al. (2017). Adipose tissue macrophage-derived exosomal miRNAs can modulate in vivo and in vitro insulin sensitivity. *Cell* 171, 372–384.e12. doi: 10.1016/j.cell.2017.08.035
- Young, M. D., Wakefield, M. J., Smyth, G. K., and Oshlack, A. (2010). Gene ontology analysis for RNA-seq: accounting for selection bias. *Genome Biol.* 11:R14. doi: 10.1186/gb-2010-11-2-r14
- Zemleni, J., Sukreet, S., Zhou, F., Wu, D., and Mutai, E. (2019). Milk-derived exosomes and metabolic regulation. *Annu. Rev. Anim. Biosci.* 7, 245–262. doi: 10.1146/annurev-animal-020518-115300
- Zeng, B., Chen, T., Xie, M.-Y., Luo, J.-Y., He, J.-J., Xi, Q.-Y., et al. (2019). Exploration of long noncoding RNA in bovine milk exosomes and their stability during digestion in vitro. *J. Dairy Sci.* 102, 6726–6737. doi: 10.3168/jds.2019-16257
- Zhang, H. Y., Deng, T., Ge, S. H., Liu, Y., Bai, M., Zhu, K. G., et al. (2019). Exosome circRNA secreted from adipocytes promotes the growth of hepatocellular carcinoma by targeting deubiquitination-related USP7. *Oncogene* 38, 2844–2859. doi: 10.1038/s41388-018-0619-z
- Zhang, X.-O., Dong, R., Zhang, Y., Zhang, J.-L., Luo, Z., Zhang, J., et al. (2016). Diverse alternative back-splicing and alternative splicing landscape of circular RNAs. *Genome Res.* 26, 1277–1287. doi: 10.1101/gr.202895.115
- Zheng, R., Du, M., Wang, X., Xu, W., Liang, J., Wang, W., et al. (2018). Exosome-transmitted long non-coding RNA PTENP1 suppresses bladder cancer progression. *Mol. Cancer* 17:143.
- Zhou, L., Chen, J., Li, Z., Li, X., Hu, X., Huang, Y., et al. (2010). Integrated profiling of MicroRNAs and mRNAs: microRNAs located on Xq27.3 associate with clear cell renal cell carcinoma. *PLoS One* 5:e15224. doi: 10.1371/journal.pone.0015224
- Zhou, Q., Costinean, S., Croce, C. M., Brasier, A. R., Merwat, S., Larson, S. A., et al. (2015). MicroRNA 29 targets nuclear factor-kappa B-repressing factor and claudin 1 to increase intestinal permeability. *Gastroenterology* 148, 158–169.e8. doi: 10.1053/j.gastro.2014.09.037
- Zhou, Q., Li, M., Wang, X., Li, Q., Wang, T., Zhu, Q., et al. (2012). Immune-related MicroRNAs are abundant in breast milk exosomes. *Int. J. Biol. Sci.* 8, 118–123. doi: 10.7150/ijbs.8.118
- Zhou, R., Chen, K. K., Zhang, J., Xiao, B., Huang, Z., Ju, C., et al. (2018). The decade of exosomal long RNA species: an emerging cancer antagonist. *Mol. Cancer* 17:75. doi: 10.1186/s12943-018-0823-z

Conflict of Interest: The authors declare that the research was conducted in the absence of any commercial or financial relationships that could be construed as a potential conflict of interest.

Copyright © 2020 Zeng, Chen, Luo, Xie, Wei, Xi, Sun and Zhang. This is an open-access article distributed under the terms of the Creative Commons Attribution License (CC BY). The use, distribution or reproduction in other forums is permitted, provided the original author(s) and the copyright owner(s) are credited and that the original publication in this journal is cited, in accordance with accepted academic practice. No use, distribution or reproduction is permitted which does not comply with these terms.

畜禽环境生物学

张宏福 等 著



内 容 简 介

本书重点阐述温热、有害气体、光照、饲养密度、环境颗粒物及微生物气溶胶等主要环境因子影响畜禽生长、免疫、繁殖、泌乳健康的生理机制,并对环境生物学的新技术、新方法做了较详细的介绍。全书共十章,第一、二章介绍畜禽环境生物学概论和畜禽环境应激的生理响应机制;第三至五章讨论温热环境对畜禽健康的影响机制,包括温热环境对畜禽生长健康、繁殖健康和泌乳健康的影响机制;第六、七章讨论有害气体对畜禽生产健康的影响机制、光照对畜禽繁殖健康的影响机制;第八、九章讨论畜禽群体与环境互动机制、畜禽舍环境颗粒物和微生物气溶胶形成与危害健康机制;第十章重点论述畜禽环境生物学研究的新技术和新方法。

本书可作为畜牧、兽医、养殖、生物学、动物营养、环境工程等专业教师、研究生和科研人员的教材和参考书,对其他从事生物科学技术工作的教学和科研人员也有重要的参考价值。

图书在版编目(CIP)数据

畜禽环境生物学/张宏福等著. —北京:科学出版社, 2021.8
ISBN 978-7-03-069585-7

I. ①畜… II. ①张… III. ①畜禽-环境生物学 IV. ①S81

中国版本图书馆 CIP 数据核字 (2021) 第 162982 号

责任编辑: 武仙山 / 责任校对: 王万红
责任印制: 吕春珉 / 封面设计: 金舵手世纪

科学出版社 出版

北京东黄城根北街 16 号
邮政编码: 100717
<http://www.sciencep.com>

北京中科印刷有限公司 印刷

科学出版社发行 各地新华书店经销

*

2021 年 8 月第 一 版 开本: 787×1092 1/16
2021 年 8 月第一次印刷 印张: 25 插页: 1
字数: 596 000

定价: 288.00 元

(如有印装质量问题, 我社负责调换〈中科〉)
销售部电话 010-62136230 编辑部电话 010-62135235

版权所有, 侵权必究

《畜禽环境生物学》著者名单

主 著：张宏福

副主著：赵茹茜 张永亮 吴 信 伊 宝 陈 亮 解竞静

其他著者（按姓氏笔画排序）：

王 丽	王 敏	王月影	王军军	王松波	王修启
毛晨羽	方 微	方正锋	石志芳	龙定彪	史彬林
白世平	冯 丹	冯京海	伊 宝	刘 杰	刘 真
刘红云	刘作华	刘建新	刘静波	齐智利	汤善龙
孙 鹏	孙加节	孙研研	李延森	李春梅	杨晓静
吴 芬	吴 信	吴中红	吴维达	张永亮	张宏福
张金枝	张恩平	张敏红	张腾飞	陈 亮	陈昭辉
陈继兰	林 海	赵 辛	赵占中	赵茹茜	郝 月
南雪梅	施振旦	姚 文	贺 斌	袁建敏	夏 东
夏 冰	高 峰	郭振东	黄飞若	崔茂盛	程建波
解竞静	臧建军	魏凤仙			

目 录

第一章 畜禽环境生物学概论	1
1.1 畜禽（健康）养殖与环境	1
1.1.1 养殖环境与畜禽健康	1
1.1.2 国外畜禽养殖环境研究进展	1
1.1.3 我国畜禽养殖环境研究进展	2
1.1.4 畜禽环境生物学研究	2
1.2 畜禽舍内环境因子概述	3
1.2.1 畜禽舍内主要环境因子	3
1.2.2 温湿度	3
1.2.3 有害气体	5
1.2.4 光照	7
1.2.5 饲养密度	8
1.2.6 空气颗粒物和微生物气溶胶	10
参考文献	11
第二章 畜禽环境应激的生理响应机制	16
2.1 应激的生理响应机制	16
2.1.1 应激研究的历史	16
2.1.2 应激的自主性神经和神经内分泌系统响应	16
2.1.3 应激反应中枢机制	17
2.1.4 应激中枢系统的结构	17
2.1.5 HPA 轴的负反馈调节作用	21
2.1.6 应激反应的适应过程	23
2.2 畜禽自主神经系统	23
2.2.1 自主神经系统的结构	23
2.2.2 自主神经系统的功能	26
2.3 畜禽神经内分泌系统	29
2.3.1 温热环境对畜禽神经内分泌系统的影响	29
2.3.2 运输应激对畜禽神经内分泌系统的影响	34
2.3.3 有害气体和颗粒物对畜禽神经内分泌系统的影响	36
2.3.4 饲养管理对畜禽神经内分泌系统的影响	38
2.4 环境诱发的氧化应激及对线粒体的损伤	42

2.4.1	环境诱发的氧化应激及其机制	42
2.4.2	ROS 产生及线粒体损伤	45
2.5	热休克蛋白家族对环境应激的响应机制	49
2.5.1	热休克蛋白的发现及命名	49
2.5.2	热休克蛋白的分类	50
2.5.3	热休克蛋白的生物学特点	50
2.5.4	应激条件下热休克蛋白的变化	51
2.5.5	热休克蛋白的调控	52
2.5.6	热休克蛋白对环境应激的响应机制	53
	参考文献	56
第三章	温热环境对畜禽生长健康的影响及其机制	61
3.1	温热环境对家禽体温调节的影响及评估模型	61
3.1.1	家禽的产热和散热	61
3.1.2	环境温度对家禽体温调节的影响	62
3.1.3	环境湿度对家禽体温调节的影响	64
3.1.4	环境风速对家禽体温调节的影响	64
3.1.5	环境温湿度等因素对家禽的综合影响及评估模型	64
3.2	温热环境对肉鸡采食量及养分代谢的影响及其调控机制	65
3.2.1	环境温湿度对肉鸡采食量的影响及其调控机制	66
3.2.2	环境温湿度对肉鸡养分代谢的影响及其调控机制	71
3.3	温热环境对畜禽肠道健康的影响及其机制	74
3.3.1	温热环境对单胃动物肠道健康的影响及其机制	74
3.3.2	温热环境对反刍动物肠道健康的影响及其机制	78
3.4	热应激对畜禽肠道黏膜屏障功能的影响及其机制	82
3.4.1	热应激对畜禽肠道黏膜屏障功能的影响	83
3.4.2	热应激损伤肠道干细胞	85
3.4.3	热应激影响肠道信号传导	86
3.4.4	热应激损伤肠道黏膜屏障的营养调控	87
	参考文献	90
第四章	温热环境对畜禽繁殖健康的影响及其机制	102
4.1	热应激对母猪卵泡发育和卵母细胞成熟的影响	102
4.1.1	卵泡发育和卵母细胞成熟概述	102
4.1.2	热应激对卵母细胞成熟的影响	105
4.1.3	热应激对颗粒细胞的影响	106
4.1.4	热应激对卵丘—卵母细胞通讯结构的影响	108
4.2	热应激对妊娠母猪肠道菌群及胚胎发育的影响	110

4.2.1	热应激对母猪繁殖性能和仔猪发育的影响	110
4.2.2	热应激对动物病理生理和肠道菌群的影响	111
4.3	妊娠期和哺乳期母猪热应激对子代生长发育的影响	113
4.3.1	妊娠期和哺乳期热应激对母猪的影响	113
4.3.2	妊娠期和哺乳期母猪热应激对子代的影响	115
4.3.3	母猪热应激对子代表观遗传的影响	117
4.4	热应激对动物精子发生和精子活力的影响	117
4.4.1	热应激对动物精子发生的影响	118
4.4.2	热应激对动物精子活力的影响	120
4.5	热应激条件下畜禽转录组应答	121
4.5.1	热应激条件下猪转录组应答	121
4.5.2	热应激条件下家禽转录组应答	122
4.5.3	热应激条件下反刍动物转录组应答	126
	参考文献	130
第五章 温热环境对家畜泌乳健康的影响及其机制		146
5.1	热应激对母猪内分泌系统的影响	146
5.1.1	家畜内分泌系统概述	146
5.1.2	热应激对母猪内分泌系统的影响	146
5.2	热应激对母猪乳腺发育和乳品质的影响	149
5.2.1	母猪乳腺发育及其影响因素	150
5.2.2	热应激对母猪乳腺发育的影响	150
5.2.3	热应激条件下母猪乳腺发育不良的改善措施	151
5.2.4	热应激对母猪乳品质的影响	151
5.3	热应激对泌乳母猪采食量及泌乳性能的影响	155
5.3.1	热应激对泌乳母猪采食量的影响	156
5.3.2	热应激对泌乳母猪泌乳量的影响	157
5.3.3	热应激对泌乳母猪乳成分的影响	158
5.3.4	热应激对泌乳母猪泌乳行为的影响	158
5.4	热应激对奶牛代谢的影响	159
5.4.1	奶牛适宜温度范围	159
5.4.2	热应激对奶牛能量代谢的影响	160
5.4.3	热应激对奶牛蛋白代谢的影响	161
5.4.4	热应激对奶牛脂代谢的影响	162
5.4.5	热应激对奶牛碳水化合物代谢的影响	164
5.5	热应激对奶牛生产及乳腺炎症的影响	165
5.5.1	热应激对奶牛生产性能的影响	165
5.5.2	热应激对奶牛瘤胃发酵及微生物的影响	166

5.5.3	热应激对奶牛内分泌代谢的影响	167
5.5.4	热应激对奶牛乳成分的影响	167
5.5.5	热应激对奶牛乳腺炎症的影响	167
	参考文献	171
第六章	有害气体对畜禽生产健康的影响及其机制	179
6.1	畜禽舍有害气体及其生成机制	179
6.1.1	NH_3 前体物生成机制	179
6.1.2	H_2S 前体物生成机制	180
6.2	有害气体对家禽生产健康的影响及其调控	182
6.2.1	NH_3 对家禽的影响	182
6.2.2	H_2S 对家禽的影响	184
6.2.3	家禽舍内有害气体的调控	184
6.3	有害气体对奶牛生产健康的影响及其调控	188
6.3.1	奶牛场空气污染物种类及产生途径	188
6.3.2	奶牛场空气污染物的危害	192
6.3.3	奶牛场空气污染物的调控	194
6.4	NH_3 排放规律及对畜禽健康的危害	197
6.4.1	畜禽舍 NH_3 产生及排放影响因素	197
6.4.2	NH_3 对畜禽健康的影响	201
6.5	NH_3 对畜禽肌肉品质的影响及其机制	204
6.5.1	畜禽舍内 NH_3 的产生及代谢途径	205
6.5.2	NH_3 对畜禽生长及肉品质的影响	205
6.5.3	NH_3 影响肉品质可能的分子机制	207
6.6	H_2S 对炎症反应和细胞凋亡的影响	211
6.6.1	畜禽舍内 H_2S 的生成	211
6.6.2	舍内 H_2S 对畜禽健康的影响	212
6.6.3	内源性 H_2S 的生成及调节	212
6.6.4	H_2S 在炎症反应中的双重作用	213
6.6.5	H_2S 在细胞凋亡中的作用	214
	参考文献	215
第七章	光照对畜禽繁殖健康的影响及其机制	230
7.1	光照对母猪卵泡发育的影响及其机制	230
7.1.1	光照影响母猪繁殖性能的基本原理	230
7.1.2	光照对母猪促性腺激素和性腺激素的影响	232
7.1.3	光照对母猪卵巢、卵泡和卵子发育的影响	232

7.2	光照对母猪繁殖性能的影响及其机制	234
7.2.1	光照周期对母猪繁殖性能的影响	234
7.2.2	光照强度对母猪繁殖性能的影响	236
7.2.3	光线波长对母猪繁殖性能的影响	237
7.2.4	光照影响母猪繁殖性能的机制	237
7.3	光照对公猪繁殖性能的影响	241
7.3.1	野公猪短日照繁殖特性	241
7.3.2	现代公猪繁殖性能的季节性变化	241
7.3.3	光照周期对公猪繁殖性能的影响	242
7.4	光照对蛋鸡和种鸡繁殖性能的影响	244
7.4.1	鸡对光照环境的感受	244
7.4.2	光照强度对鸡繁殖性能的影响	245
7.4.3	光照周期对鸡繁殖性能的影响	246
7.4.4	光照波长对鸡繁殖性能的影响	250
7.5	生物钟对蛋鸡排卵产蛋过程的调控	251
7.5.1	生物钟通过 HPG 轴调控排卵	252
7.5.2	生物钟整合能量/物质代谢调控产蛋	253
7.6	光照对反刍动物生产和繁殖的影响及其机制	256
7.6.1	光照对奶牛、绒山羊增重的影响	257
7.6.2	光照对绒山羊产绒的影响	257
7.6.3	光照对奶牛、奶山羊产奶的影响	258
7.6.4	光照周期影响反刍动物生产的机制	258
7.6.5	光照对反刍动物繁殖的影响	259
7.7	畜禽季节性生理活动及其光照调控	261
7.7.1	畜禽季节性生理活动	261
7.7.2	畜禽季节性生理活动的光照调控	263
	参考文献	268
第八章	畜禽饲养密度和群体规模与环境的互作	281
8.1	饲养密度对猪生产健康的影响	281
8.1.1	饲养密度对猪生产的影响	281
8.1.2	饲养密度对猪舍环境和猪健康的影响	284
8.1.3	饲养密度对猪营养代谢的影响	285
8.1.4	饲养密度与动物福利	285
8.2	饲养密度对肉牛生产健康的影响	286
8.2.1	饲养密度对肉牛生产的影响	286
8.2.2	饲养密度对肉牛舍内环境的影响	289
8.2.3	饲养密度对肉牛行为及动物福利的影响	290

8.3 饲养密度和群体规模对肉鸡生产健康的影响	291
8.3.1 肉鸡饲养密度和群体规模	291
8.3.2 饲养密度和群体规模对肉鸡生产性能和效益的影响	292
8.3.3 饲养密度和群体规模对肉鸡健康的影响	294
参考文献	297
第九章 畜禽舍环境颗粒物和微生物气溶胶的形成及危害动物健康的机制	304
9.1 畜禽舍环境颗粒物和微生物气溶胶组分及形成	304
9.1.1 颗粒物分类及组成	304
9.1.2 畜禽舍内颗粒物来源	306
9.1.3 畜禽舍内的微生物气溶胶	307
9.1.4 畜禽舍颗粒物的危害	308
9.1.5 颗粒物的传播	310
9.1.6 影响微生物气溶胶的因素	310
9.2 畜禽舍环境颗粒物和微生物气溶胶时空分布特点	311
9.2.1 畜禽舍环境颗粒物和微生物气溶胶的时间变化动态特征	312
9.2.2 畜禽舍环境颗粒物和微生物气溶胶的空间分布规律	315
9.2.3 畜禽舍环境颗粒物和微生物气溶胶时空分布特点形成的因素分析	316
9.3 畜禽舍环境颗粒物和微生物气溶胶对动物生产健康的影响及其机制	318
9.3.1 畜禽舍环境颗粒物和微生物气溶胶对动物生产健康的影响	318
9.3.2 畜禽舍环境颗粒物和微生物气溶胶对动物健康损伤的机制	320
9.3.3 机体缓解畜禽舍环境颗粒物诱导的呼吸道损伤的路径	328
9.4 封闭式畜禽舍环境颗粒物和微生物气溶胶检测技术及减排措施	329
9.4.1 封闭式畜禽舍环境颗粒物和微生物气溶胶检测技术	330
9.4.2 源头控制	331
9.4.3 过程控制	332
参考文献	336
第十章 畜禽环境生物学的新技术和新方法	345
10.1 宏基因组学技术在畜禽环境生物学研究中的应用	345
10.1.1 宏基因组概述	345
10.1.2 宏基因组分析的流程	346
10.1.3 宏基因组学技术在畜禽环境生物学研究中的应用	349
10.2 蛋白质组学技术在畜禽环境生物学研究中的应用	351
10.2.1 蛋白质组学概述	351
10.2.2 蛋白质组学的分类	352
10.2.3 质谱技术的发展	353
10.2.4 蛋白质组学主要研究方法	353

10.2.5 蛋白质组学技术在畜禽环境生物学研究中的应用	353
10.3 代谢组学在畜禽环境生物学研究中的应用	354
10.3.1 代谢组学研究方法	355
10.3.2 代谢组学技术在畜禽环境生物学研究中的应用	358
10.4 Meta 方法在畜禽环境生物学研究中的应用	361
10.4.1 Meta 分析的概念及作用	361
10.4.2 Meta 分析的步骤	362
10.4.3 Meta 分析的常用软件	364
10.4.4 Meta 方法在畜禽环境生物学研究中的应用	365
10.4.5 Meta 方法的局限性及注意的问题	367
10.5 表观遗传学及其在畜禽环境生物学研究中的应用进展	368
10.5.1 表观遗传学概述	368
10.5.2 环境与表观遗传学的关系	369
10.5.3 表观遗传学的调节机制及研究方法	369
参考文献	376
附图	385



中国黄牛遗传学

陈 宏 主编



科学出版社

内 容 简 介

本书较为全面、系统地阐述了中国黄牛遗传学研究领域的最新进展,内容包括中国黄牛选育的遗传学基础、体型外貌的遗传学、免疫遗传学、生化遗传与蛋白质组学、行为遗传学、细胞遗传学、分子数量遗传学、mtDNA 遗传多样性与母系起源、Y 染色体 DNA 多态性与父系起源、微卫星标记、功能基因的分子遗传变异、全基因组学、转录组学、表观遗传学、分子群体遗传学以及分子遗传技术与育种应用等研究。

本书可作为动物科学、动物医学、智慧牧业、生物科学、生物技术等专业的学生、教师及科研人员的参考资料,同时也是肉牛、奶牛遗传育种与繁殖领域的教学人员、科研人员、生产人员的有益参考书。

审图号: GS 京(2023) 2403 号

图书在版编目(CIP)数据

中国黄牛遗传学/陈宏主编. —北京:科学出版社, 2024.6

ISBN 978-7-03-077509-2

I. ①中… II. ①陈… III. ①黄牛—遗传育种—研究—中国 IV. ①S823.8

中国国家版本馆 CIP 数据核字(2024)第 013691 号

责任编辑:李 迪 田明霞 / 责任校对:杨 赛

责任印制:肖 兴 / 封面设计:无极书装

科 学 出 版 社 出 版

北京东黄城根北街 16 号

邮政编码: 100717

<http://www.sciencep.com>

北京建宏印刷有限公司印刷

科学出版社发行 各地新华书店经销

*

2024 年 6 月第 一 版 开本: 787×1092 1/16

2024 年 6 月第一次印刷 印张: 41 3/4

字数: 987 000

定价: 598.00 元

(如有印装质量问题, 我社负责调换)

《中国黄牛遗传学》编写人员

主 编：陈 宏

副 主 编：雷初朝 蓝贤勇 黄永震 黄锡霞 宋恩亮

编写人员：陈 宏 雷初朝 蓝贤勇 黄永震 王 昕 蔡 欣

潘传英 陈宁博 党瑞华 张春雷 张建勤 黄锡霞

宋恩亮 曹修凯 田全召 房兴堂 周 扬 汪聪勇

高 雪 张良志 王二耀 刘 梅 刘 贤 魏雪锋

赵杨杨 李明勋 徐美芳 栗福星 乐祥鹏 宋成创

孙加节 陈秋明 李 辉 杨东英 蔡含芳 孙雨佳

张 丽 成海建 马志杰 张梦华 韩浩园 曾璐岚

黄洁萍 程 杰 王 珂 夏小婷 张晓燕 张思欢

主 审：张英汉

目 录

第一章 中国黄牛选育的遗传学基础.....	1
第一节 中国地方黄牛的种质特性.....	1
一、中国地方黄牛数量的分布情况.....	1
二、中国地方黄牛优良的种质特性.....	1
三、中国地方黄牛种质特性的缺点.....	3
第二节 中国黄牛重要经济性状的测定.....	3
一、生长发育性状的测定.....	4
二、产肉性能的测定.....	7
三、产乳性状的测定.....	10
四、繁殖性状的测定.....	11
第三节 中国黄牛选育的遗传学三大要素.....	12
一、种质资源.....	12
二、遗传学理论.....	12
三、品种内遗传多态性.....	12
本章小结	13
参考文献	13
第二章 中国黄牛体型外貌的遗传学研究.....	14
第一节 黄牛体型大小的遗传.....	14
一、黄牛的体型.....	14
二、黄牛体型大小的多基因控制.....	14
第二节 黄牛毛色的遗传.....	16
一、家牛毛色的形成机理.....	16
二、国外家牛被毛表型与基本毛色.....	18
三、中国黄牛被毛表型与基本毛色.....	29
第三节 黄牛角的遗传.....	30
一、牛无角的遗传.....	30
二、牛畸形角的遗传.....	31
三、无角牛的培育.....	32

第四节 黄牛头型的形态特征与遗传.....	34
一、牛头骨的形态差异.....	34
二、牛头型特征.....	34
三、牛头型的遗传.....	35
第五节 黄牛乳房形态的遗传.....	35
一、牛乳房的内部结构.....	36
二、牛乳房的外部形态.....	36
三、牛乳房相关性状的遗传.....	38
第六节 黄牛特殊体型外貌的遗传.....	39
一、瘤牛肩峰的遗传.....	39
二、瘤牛腹垂的遗传.....	39
三、牛双肌的遗传.....	40
四、牛耳型的遗传.....	41
第七节 黄牛的畸形遗传.....	43
一、牛蜘蛛腿综合征.....	43
二、牛脊椎畸形综合征.....	43
三、牛并趾症.....	44
四、牛短脊椎综合征.....	44
五、牛侏儒症.....	44
六、牛肺发育不全和水肿综合征.....	45
七、中国牛畸形遗传病的研究现状.....	45
本章小结	45
参考文献	46
第三章 中国黄牛免疫遗传学研究.....	50
第一节 中国黄牛红细胞抗原遗传与生产性状.....	50
一、中国黄牛红细胞抗原遗传系统.....	50
二、中国黄牛红细胞抗原多态性与生产性状.....	52
第二节 中国黄牛 BoLA 遗传与生产性状.....	53
一、中国黄牛 BoLA 及其基因的分布、组成和染色体定位.....	53
二、中国黄牛 BoLA 基因及其编码产物.....	53
三、中国黄牛 BoLA 基因的遗传特征.....	55
四、中国黄牛 BoLA 及其基因的遗传分型.....	56

五、黄牛 <i>BoLA</i> 基因多态性与生产性状	57
六、中国黄牛 <i>BoLA</i> 及其基因与疾病	58
七、中国黄牛 <i>BoLA</i> 基因与抗病育种	59
第三节 中国黄牛免疫球蛋白及其多样性	60
一、免疫球蛋白的基本结构和功能	60
二、黄牛免疫球蛋白重链基因	62
三、黄牛免疫球蛋白轻链基因	66
四、黄牛免疫球蛋白多样性	67
第四节 中国黄牛 Toll 样受体与抗病性状	69
一、Toll 样受体结构及其功能	69
二、中国黄牛 <i>TLR</i> 基因多态性与抗病性	74
第五节 中国黄牛细胞因子与抗病性	76
一、细胞因子概述	76
二、中国黄牛白细胞介素及其抗病性	77
三、中国黄牛干扰素及其抗病性	80
本章小结	83
参考文献	84
第四章 中国黄牛生化遗传与蛋白质组学研究	91
第一节 血液蛋白多态性研究	91
一、血液蛋白多态性的概念	91
二、血液蛋白多态性的测定方法	91
三、中国黄牛血液蛋白多态性的类型与频率	92
第二节 血液同工酶及其多态性研究	97
一、同工酶的概念与分类	97
二、血液同工酶多态性测定方法	98
三、中国黄牛血液同工酶多态性的研究	99
第三节 乳蛋白多态性研究	101
一、乳蛋白多态性的概念	101
二、乳蛋白多态性的测定方法	101
三、黄牛乳蛋白多态性研究	101
第四节 生化遗传学在黄牛育种中的应用	103
一、血液蛋白多态性的应用研究	103

二、同工酶多态性的应用研究.....	105
三、乳蛋白多态性的应用研究.....	107
第五节 可变剪接与蛋白质多态性.....	108
一、可变剪接的定义及分类.....	108
二、黄牛基因的可变剪接及其特征.....	109
三、可变剪接对基因表达蛋白质的影响.....	111
第六节 蛋白质组学研究.....	112
一、蛋白质组学的定义及研究方法.....	112
二、黄牛蛋白质组学研究进展.....	114
本章小结	116
参考文献	117
第五章 中国黄牛行为遗传学研究.....	120
第一节 黄牛的性情遗传学研究.....	120
一、黄牛性情的定义和检测方法.....	120
二、黄牛性情的遗传变异.....	123
三、黄牛性情选育的壁垒和前景.....	124
第二节 黄牛耐热的遗传学研究.....	125
一、热应激原理.....	125
二、黄牛耐热性的遗传.....	127
第三节 黄牛的采食行为研究.....	129
一、黄牛的采食行为概述.....	129
二、影响牛采食行为的因素.....	131
第四节 黄牛高海拔适应性的遗传学研究.....	134
一、牛高海拔适应基因研究.....	134
二、牛高海拔适应基因的渗入.....	135
三、人类与畜禽高海拔适应性的候选基因.....	136
本章小结	137
参考文献	137
第六章 中国黄牛细胞遗传学研究.....	140
第一节 黄牛染色体数目和形态特征.....	141
一、黄牛染色体的数目.....	141
二、黄牛染色体的大小.....	142

三、黄牛染色体的形态特征.....	143
四、黄牛染色体的核型及其分析.....	144
第二节 黄牛性染色体及其多态性.....	148
一、黄牛的性染色体.....	148
二、性染色体的多态性.....	148
第三节 黄牛染色体显带研究.....	152
一、Q 带的研究.....	152
二、G 带的研究.....	153
三、C 带的研究.....	157
四、Ag-NOR 的研究.....	159
五、R 带的研究.....	164
六、T 带的研究.....	164
七、姐妹染色单体交换的研究.....	165
八、高分辨显带.....	166
九、染色体显带的命名与识别.....	166
第四节 黄牛染色体变异类型与频率.....	167
一、黄牛染色体的多型性.....	167
二、黄牛染色体的变异类型.....	170
第五节 染色体标记与牛起源、进化.....	177
一、染色体进化与牛的起源.....	177
二、染色体进化与品种的形成.....	177
三、染色体标记与牛品种的分类.....	177
第六节 黄牛染色体研究与育种及生产.....	179
一、染色体与家畜育种.....	179
二、染色体与黄牛的亲缘关系.....	179
三、染色体与环境检测及黄牛的饲养管理.....	180
四、染色体与性别的早期诊断与控制.....	180
本章小结.....	181
参考文献.....	181
第七章 中国黄牛分子数量遗传学研究.....	186
第一节 分子数量遗传学的研究内容和方法.....	186
一、分子标记辅助选择与 QTL 定位技术.....	186

二、分子标记的高通量分型技术与基因组选择.....	192
三、分子设计育种与基因编辑技术.....	195
第二节 体尺性状的分子数量遗传学研究.....	198
一、黄牛体尺性状测量的基本知识.....	199
二、体型外貌的线性评定.....	199
三、体尺性状的遗传参数研究.....	200
四、体尺性状的关联分析研究进展.....	201
第三节 生长发育性状的数量遗传学研究.....	202
一、衡量生长发育性状的主要指标.....	202
二、生长发育性状的遗传参数估计.....	203
第四节 屠宰性状的分子数量遗传学研究.....	203
一、屠宰性状的遗传参数估计.....	203
二、屠宰性状的主效基因及 SNP 研究.....	204
第五节 泌乳性状的分子数量遗传学研究.....	204
一、泌乳性状的遗传评定与遗传参数估计.....	205
二、泌乳性状的 QTL 研究.....	205
三、泌乳性状与相关基因的关联分析.....	206
四、泌乳性状与体尺性状的关联分析.....	206
第六节 其他性状的分子数量遗传学研究.....	206
一、繁殖性状的分子数量遗传学研究.....	207
二、牛角性状的分子数量遗传学研究.....	207
三、奶牛乳头长度的分子数量遗传学研究.....	207
第七节 重要经济性状的因果突变的鉴定.....	207
一、表达数量性状位点的鉴定.....	208
二、三维基因组学鉴定.....	208
本章小结.....	216
参考文献.....	216
第八章 中国黄牛 mtDNA 遗传多样性与母系起源研究.....	220
第一节 mtDNA 的遗传.....	220
一、mtDNA 的基本结构.....	220
二、mtDNA 的遗传特征.....	220
三、mtDNA 的应用.....	221

第二节 mtDNA RFLP 研究	222
第三节 mtDNA D-loop 序列多态性研究	222
第四节 mtDNA 基因多态性研究	226
一、mtDNA <i>Cytb</i> 基因多态性研究	226
二、mtDNA 12S rRNA 和 16S rRNA 基因多态性研究	228
第五节 mtDNA 全基因组研究	228
第六节 中国古代黄牛的 mtDNA 研究	232
第七节 mtDNA 多态性与黄牛的起源进化	233
本章小结	234
参考文献	234
第九章 中国黄牛 Y 染色体 DNA 多态性与父系起源研究	237
第一节 Y 染色体 DNA 大小、组成与基因数目	237
一、牛 Y 染色体的 DNA 大小	237
二、牛 MSY 组成和基因数目	238
第二节 Y-STR 研究	240
一、Y-STR 标记分型技术的原理和方法	240
二、中国黄牛 Y-STR 标记研究	240
三、普通牛 Y-STR 分布特征	242
第三节 Y-SNP 研究	247
第四节 Y 染色体 DNA 类型与起源进化	248
一、中国黄牛 Y 染色体类型	248
二、中国黄牛 Y 染色体单倍型与起源进化	249
本章小结	250
参考文献	250
第十章 中国黄牛微卫星标记研究	252
第一节 微卫星 DNA 的概念与特点	252
一、微卫星 DNA 的概念	252
二、微卫星 DNA 的特点	253
第二节 微卫星多位点 DNA 指纹的研究与应用	254
一、DNA 指纹的概念	254
二、DNA 指纹的制备方法	255
三、DNA 指纹的遗传特点	255

四、DNA 指纹的分析方法	256
五、牛 DNA 指纹的研究与应用	257
第三节 微卫星 DNA 多态性分型研究与应用	260
一、微卫星 DNA 多态性分型的一般检测步骤	260
二、微卫星引物与 PCR 扩增	260
三、微卫星 DNA 的电泳分型	260
四、微卫星 DNA 多态性的研究与应用	264
第四节 微卫星多态性与重要性状的关联性研究	266
一、中国地方黄牛微卫星多态性与重要性状的关联研究	266
二、中国培育牛品种微卫星多态性与重要性状的关联研究	267
第五节 利用微卫星 DNA 标记进行黄牛的亲子鉴定	269
一、微卫星 DNA 亲子鉴定统计分析方法	269
二、亲子鉴定在黄牛生产中的应用	272
三、展望	273
本章小结	273
参考文献	274
第十一章 中国黄牛功能基因的分子遗传特征研究	277
第一节 肉质与脂肪相关基因的分子遗传特征	277
一、IGF1R 基因的分子遗传特征	277
二、TCAP 基因的分子遗传特征	278
三、DECRI 基因的分子遗传特征	278
四、PRKAG3 基因的分子遗传特征	279
五、PPAR γ 基因的分子遗传特征	279
六、CIDEA 基因的分子遗传特征	279
七、CAST 基因的分子遗传特征	280
八、LEP 基因的分子遗传特征	280
九、TG 基因的分子遗传特征	281
十、FABP3 基因的分子遗传特征	281
十一、CACNA2D1 基因的分子遗传特征	281
十二、LPL 基因的分子遗传特征	282
十三、MRF 家族基因的分子遗传特征	282
十四、CDIPT 基因的分子遗传特征	283

十五、 <i>DNMT</i> 家族基因的分子遗传特征.....	283
十六、 <i>SSTR2</i> 基因的分子遗传特征.....	284
十七、 <i>HSP70-1</i> 基因的分子遗传特征.....	284
十八、 <i>SCD1</i> 基因的分子遗传特征.....	285
十九、 <i>DGAT1</i> 基因的分子遗传特征.....	285
二十、 <i>AdPLA</i> 基因的分子遗传特征.....	286
二十一、 <i>PRDM16</i> 基因的分子遗传特征.....	286
二十二、 <i>SIRT</i> 家族基因的分子遗传特征.....	286
二十三、 <i>PNPLA3</i> 基因的分子遗传特征.....	287
二十四、 <i>FLII</i> 基因的分子遗传特征.....	287
二十五、 <i>PPAR</i> 家族基因的分子遗传特征.....	288
二十六、 <i>HSD17B8</i> 基因的分子遗传特征.....	288
二十七、 <i>STAT3</i> 基因的分子遗传特征.....	289
二十八、 <i>Foxa2</i> 基因的分子遗传特征.....	289
二十九、 <i>SREBP1c</i> 基因的分子遗传特征.....	290
三十、总结与展望.....	290
第二节 繁殖相关基因的分子遗传特征.....	291
一、 <i>GPR54</i> 基因的分子遗传特征.....	291
二、 <i>TMEM95</i> 基因的分子遗传特征.....	292
三、 <i>GRB10</i> 基因的分子遗传特征.....	292
四、 <i>HIF-3α</i> 基因的分子遗传特征.....	292
五、 <i>FSHR</i> 基因的分子遗传特征.....	293
六、 <i>PGR</i> 基因的分子遗传特征.....	293
七、 <i>ESRα</i> 基因的分子遗传特征.....	293
八、 <i>RXRG</i> 基因的分子遗传特征.....	293
九、 <i>ADCY5</i> 基因的分子遗传特征.....	294
十、 <i>HSD17B3</i> 基因的分子遗传特征.....	294
十一、 <i>SEPT7</i> 基因的分子遗传特征.....	295
十二、 <i>ITGβ5</i> 基因的分子遗传特征.....	295
十三、 <i>DENND1A</i> 基因的分子遗传特征.....	296
十四、 <i>PROPI</i> 基因的分子遗传特征.....	297
十五、总结与展望.....	297
第三节 生长相关基因的分子遗传特征.....	297

一、NPC 家族基因的分子遗传特征.....	298
二、GLI3 基因的分子遗传特征.....	298
三、STAM2 基因的分子遗传特征.....	299
四、Pax7 基因的分子遗传特征.....	299
五、TMEM18 基因的分子遗传特征.....	300
六、GHRHR 基因的分子遗传特征.....	300
七、AZGP1 基因的分子遗传特征.....	301
八、Angptl4 基因的分子遗传特征.....	301
九、GHRL 基因的分子遗传特征.....	301
十、IGFBP-5 基因的分子遗传特征.....	301
十一、PCSK1 基因的分子遗传特征.....	302
十二、Ghrelin 基因的分子遗传特征.....	303
十三、GDF10 基因的分子遗传特征.....	303
十四、RARRES2 基因的分子遗传特征.....	303
十五、SH2B1 基因的分子遗传特征.....	304
十六、VEGF-B 基因的分子遗传特征.....	304
十七、KCNJ12 基因的分子遗传特征.....	305
十八、PLA2G2D 基因的分子遗传特征.....	305
十九、FHL1 基因的分子遗传特征.....	306
二十、SHH 基因的分子遗传特征.....	306
二十一、GBP6 基因的分子遗传特征.....	306
二十二、NCSTN 基因的分子遗传特征.....	307
二十三、MLLT10 基因的分子遗传特征.....	308
二十四、PLIN2 基因的分子遗传特征.....	308
二十五、ACTL8 基因的分子遗传特征.....	309
二十六、MXD3 基因的分子遗传特征.....	309
二十七、SPARC 基因的分子遗传特征.....	310
二十八、ACVRI 基因的分子遗传特征.....	310
二十九、RET 基因的分子遗传特征.....	311
三十、TRP 基因的分子遗传特征.....	311
三十一、SERPINA3 基因的分子遗传特征.....	312
三十二、PLAG1 基因的分子遗传特征.....	312
三十三、ADD1 基因的分子遗传特征.....	312

三十四、 <i>MYLK4</i> 基因的分子遗传特征	313
三十五、 <i>TNF</i> 基因的分子遗传特征	313
三十六、 <i>GBP2</i> 基因的分子遗传特征	313
三十七、 <i>IGF1</i> 基因的分子遗传特征	314
三十八、 <i>MC4R</i> 基因的分子遗传特征	314
三十九、 <i>LEPR</i> 基因的分子遗传特征	315
四十、 <i>MT-ND5</i> 基因的分子遗传特征	315
四十一、 <i>SMAD3</i> 基因的分子遗传特征	316
四十二、 <i>Nanog</i> 基因的分子遗传特征	316
四十三、 <i>I-mfa</i> 基因的分子遗传特征	317
四十四、 <i>CaSR</i> 基因的分子遗传特征	317
四十五、 <i>NOTCH1</i> 基因的分子遗传特征	318
四十六、 <i>ATBF1</i> 基因的分子遗传特征	318
四十七、 <i>Wnt8A</i> 基因的分子遗传特征	319
四十八、 <i>AR</i> 基因的分子遗传特征	319
四十九、 <i>SDC3</i> 基因的分子遗传特征	319
五十、 <i>BMPER</i> 基因的分子遗传特征	320
五十一、 <i>SMO</i> 基因的分子遗传特征	320
五十二、 <i>ANGPTL3</i> 基因的分子遗传特征	321
五十三、 <i>CIDEA</i> 基因的分子遗传特征	321
五十四、 <i>CFL2</i> 基因的分子遗传特征	322
五十五、 <i>LHX3</i> 基因的分子遗传特征	323
五十六、 <i>MC3R</i> 基因的分子遗传特征	323
五十七、 <i>NCAPG</i> 基因的分子遗传特征	324
五十八、 <i>HNF-4α</i> 基因的分子遗传特征	324
五十九、 <i>Pax3</i> 基因的分子遗传特征	324
六十、 <i>IGFALS</i> 基因的分子遗传特征	325
六十一、 <i>LXRα</i> 基因的分子遗传特征	325
六十二、 <i>IGF2</i> 基因的分子遗传特征	326
六十三、 <i>ZBED6</i> 基因的分子遗传特征	327
六十四、 <i>SIRT2</i> 基因的分子遗传特征	327
六十五、 <i>BMP7</i> 基因的分子遗传特征	328
六十六、 <i>PROPI</i> 基因的分子遗传特征	328

六十七、 <i>PAX6</i> 基因的分子遗传特征	329
六十八、 <i>SH2B2</i> 基因的分子遗传特征	329
六十九、 <i>SIRT1</i> 基因的分子遗传特征	329
七十、 <i>HGF</i> 基因的分子遗传特征	330
七十一、 <i>Wnt7a</i> 基因的分子遗传特征	331
七十二、 <i>RXRα</i> 基因的分子遗传特征	331
七十三、 <i>FBXO32</i> 基因的分子遗传特征	331
七十四、 <i>VEGF</i> 基因的分子遗传特征	332
七十五、 <i>MyoG</i> 基因的分子遗传特征	332
七十六、 <i>NPY</i> 基因的分子遗传特征	333
七十七、 <i>SST</i> 基因的分子遗传特征	333
七十八、 <i>KLF7</i> 基因的分子遗传特征	333
七十九、 <i>PRLR</i> 基因的分子遗传特征	334
八十、 <i>GDF5</i> 基因的分子遗传特征	334
八十一、 <i>RBP4</i> 基因的分子遗传特征	334
八十二、 <i>MEF2A</i> 基因的分子遗传特征	335
八十三、 <i>GAD1</i> 基因的分子遗传特征	335
八十四、 <i>NUCB2</i> 基因的分子遗传特征	335
八十五、 <i>POMC</i> 基因的分子遗传特征	336
八十六、 <i>GHSR</i> 基因的分子遗传特征	336
八十七、 <i>ADIPOQ</i> 基因的分子遗传特征	336
八十八、 <i>NPM1</i> 基因的分子遗传特征	336
八十九、 <i>MICAL-L2</i> 基因的分子遗传特征	337
九十、 <i>MYH3</i> 基因的分子遗传特征	337
九十一、 <i>SDC1</i> 基因的分子遗传特征	337
九十二、 <i>ANGPTL8</i> 基因的分子遗传特征	338
九十三、 <i>LHX4</i> 基因的分子遗传特征	338
九十四、 <i>POU1F1</i> 基因的分子遗传特征	338
九十五、 <i>PROPI</i> 基因的分子遗传特征	339
九十六、总结与展望	339
第四节 能量代谢相关基因的分子遗传特征	340
一、 <i>SOD1</i> 基因的分子遗传特征	340
二、 <i>HSPB7</i> 基因的分子遗传特征	340

三、 <i>EIF2AK4</i> 基因的分子遗传特征	341
四、 <i>HSF1</i> 基因的分子遗传特征	341
五、 <i>NR1P1</i> 基因的分子遗传特征	341
六、 <i>MGAT2</i> 基因的分子遗传特征	342
七、 <i>BMP8b</i> 基因的分子遗传特征	342
八、 <i>Orexin</i> 基因的分子遗传特征	343
九、 <i>CRTC3</i> 基因的分子遗传特征	343
十、 <i>OLR1</i> 基因的分子遗传特征	344
十一、 <i>CART</i> 基因的分子遗传特征	344
十二、总结与展望	344
第五节 泌乳相关基因的分子遗传特征	345
一、 β - <i>Lg</i> 基因的分子遗传特征	345
二、 κ - <i>Cn</i> 基因的分子遗传特征	345
三、 <i>CSN1S2</i> 基因的分子遗传特征	346
四、 <i>IGFBP-3</i> 基因的分子遗传特征	346
五、 <i>MBL1</i> 基因的分子遗传特征	346
六、 <i>LAP3</i> 基因的分子遗传特征	347
七、 <i>GABRG2</i> 基因的分子遗传特征	347
八、 <i>PLSCR5</i> 基因的分子遗传特征	347
九、 <i>CLASP1</i> 基因的分子遗传特征	348
十、 <i>SMARCA2</i> 基因的分子遗传特征	348
十一、 <i>FHIT</i> 基因的分子遗传特征	348
十二、 <i>ADIPOQ</i> 基因的分子遗传特征	349
本章小结	350
参考文献	351
第十二章 中国黄牛全基因组学研究	357
第一节 全基因组遗传变异特征	357
一、全基因组基本特征	357
二、全基因组 SNP 和 InDel 分布特征	358
三、全基因组 SNP 与性状的关联研究	362
第二节 全基因组拷贝数变异 (CNV) 的特征	363
一、拷贝数变异 (CNV) 的概念	363

二、中国黄牛全基因组 CNV 数目与分布特征	366
三、中国黄牛全基因组 CNV 与起源进化	368
四、中国黄牛全基因组 CNV 与性状的关系研究	378
五、结论与展望	382
第三节 全基因组 DNA 甲基化遗传特征	383
一、不同发育阶段黄牛全基因组 DNA 甲基化遗传特征	383
二、牛肌肉组织中功能基因 DNA 甲基化与基因表达的关系	385
三、启动子 DNA 甲基化与基因表达的关系	388
四、基因本体 DNA 甲基化与基因表达的关系	390
本章小结	391
参考文献	392
第十三章 中国黄牛转录组学研究	397
第一节 肌肉组织转录组及其特征	397
一、转录组学概述	397
二、骨骼肌的生长发育规律	397
三、黄牛不同发育阶段肌肉组织转录组及其特征	399
第二节 脂肪组织转录组及其特征	400
一、脂肪组织的分类及特征	400
二、牛脂肪组织转录组研究	401
三、不同发育阶段牛脂肪组织转录组特征	402
第三节 睾丸组织及精子转录组及其特征	405
一、精子发生机制	405
二、睾丸组织转录组研究	408
三、精子转录组研究	409
四、犏牛雄性不育症的转录组测序	412
第四节 卵巢组织转录组及其特征	413
一、卵巢概述	413
二、不同发育阶段卵巢组织的转录组研究进展	415
第五节 胚胎发育的转录组及其特征	418
一、黄牛的胚胎发育	418
二、牛胚胎发育的转录组研究	420
第六节 乳腺组织转录组及其特征	421

一、乳腺的结构及发育阶段.....	421
二、影响奶牛乳腺发育及泌乳的信号通路.....	422
三、乳腺组织转录组研究.....	423
第七节 肝脏转录组及其特征.....	425
一、肝脏与能量代谢.....	425
二、肝脏的转录组学研究.....	425
第八节 其他组织转录组及其特征.....	428
一、肺脏转录组学研究.....	428
二、皮肤转录组学研究.....	429
本章小结	429
参考文献	429
第十四章 中国黄牛表观遗传学研究.....	435
第一节 miRNA 组学研究.....	435
一、miRNA 概述	435
二、黄牛肌肉组织 miRNA 组学研究	443
三、黄牛脂肪组织 miRNA 组学研究	449
四、奶牛乳腺组织 miRNA 组学研究	456
五、其他组织 miRNA 组学研究	462
六、中国黄牛 miRNA 的功能研究	462
第二节 lncRNA 组学研究	470
一、lncRNA 概述	470
二、肌肉组织不同发育阶段 lncRNA 组学研究	474
三、脂肪组织不同发育阶段 lncRNA 组学研究	477
四、乳腺 lncRNA 组学研究	480
五、其他组织 lncRNA 组学研究	481
六、中国黄牛 lncRNA 的功能研究	482
第三节 circRNA 组学研究	501
一、circRNA 概述	501
二、黄牛肌肉组织 circRNA 组学研究	510
三、不同发育阶段脂肪组织 circRNA 组学研究	513
四、其他组织 circRNA 组学研究	515
五、中国黄牛 circRNA 的功能研究	516

第四节 DNA 甲基化研究.....	535
一、DNA 甲基化概述.....	536
二、DNA 甲基化影响黄牛肌肉发育研究.....	541
三、DNA 甲基化影响黄牛脂肪沉积研究.....	546
四、DNA 甲基化影响黄牛胚胎发育研究.....	550
第五节 RNA 修饰研究.....	552
一、 N^6 甲基化修饰 (m^6A).....	553
二、 N^1 甲基化修饰 (m^1A).....	554
三、 $N^6,2'-O$ -二甲基腺嘌呤 (m^6Am).....	554
四、5-甲基胞嘧啶 (m^5C) 和 5-羟甲基胞嘧啶 (5hmC).....	554
五、尿苷异构化.....	555
六、核糖修饰.....	555
第六节 蛋白质修饰研究.....	556
一、磷酸化.....	556
二、甲基化.....	556
三、泛素化.....	557
四、乙酰化.....	557
五、脂基化.....	558
六、糖基化.....	558
本章小结.....	558
参考文献.....	559
第十五章 中国黄牛分子群体遗传学研究.....	567
第一节 分子群体遗传学的概念和研究内容.....	567
一、分子群体遗传学的概念及发展简史.....	567
二、分子群体遗传学的研究内容及进展.....	568
第二节 编码序列的分子群体遗传学分析.....	569
一、基因组 DNA 多态性.....	569
二、连锁不平衡.....	569
三、基因组重组对 DNA 多态性的影响.....	569
四、基因进化方式.....	570
五、外显子的分子群体遗传学分析.....	570
第三节 非编码序列的分子群体遗传学分析.....	589

一、内含子的分子群体遗传学分析.....	590
二、启动子的分子群体遗传学分析.....	599
三、基因间隔序列的分子群体遗传学分析.....	602
四、UTR 的分子群体遗传学分析.....	603
第四节 中国黄牛与国外品种的分子群体遗传学分析.....	606
第五节 中国黄牛各基因位点分子群体遗传学结构分析.....	607
本章小结	608
参考文献	609
第十六章 中国黄牛分子遗传技术与育种应用研究.....	611
第一节 分子标记辅助选择.....	611
一、分子标记的概念.....	611
二、分子标记辅助选择概述.....	612
三、分子标记辅助选择在中国黄牛育种中的应用	613
第二节 全基因组选择.....	616
一、全基因组选择的原理方法.....	616
二、全基因组选择的优势及影响因素	617
三、全基因组选择在牛遗传育种上的应用	617
四、全基因组选择的发展展望.....	620
第三节 胚胎克隆和体细胞克隆.....	620
一、卵母细胞的来源和质量.....	621
二、细胞周期组合.....	622
三、供体细胞的类型和体外培养.....	622
四、融合和激活的时间.....	623
五、组蛋白脱乙酰酶抑制剂 (HDI) 处理.....	623
第四节 基因编辑与育种.....	624
一、DNA 同源重组 (HR) 在牛基因组修饰中的应用.....	625
二、牛基因多位点修饰.....	626
三、牛动物繁殖辅助顺次基因组工程.....	626
四、设计核酸酶用于牛基因组工程.....	627
第五节 转基因与生物反应器.....	628
一、转基因生物反应器的概念.....	628
二、生物反应器的分类.....	629

三、转基因动物生物反应器.....	630
四、转基因牛生物反应器.....	632
五、转基因牛生物反应器的功能.....	633
第六节 性别控制.....	633
一、牛性别控制在生产实践中的意义.....	633
二、性别形成的遗传学基础.....	634
三、牛性别控制的方法研究及其应用.....	634
本章小结	637
参考文献	638

证书号第 4093621 号



发明专利证书

发明名称：与猪胴体肉品质相关的 circRNA 标志物及其应用

发明人：孙加节;张永亮;江青艳;习欠云;陈婷;罗君谊;谢月琴
王伶

专利号：ZL 2018 1 0496311.X

专利申请日：2018 年 05 月 22 日

专利权人：华南农业大学

地址：510642 广东省广州市天河区五山路 483 号

授权公告日：2020 年 11 月 13 日

授权公告号：CN 108676894 B

国家知识产权局依照中华人民共和国专利法进行审查，决定授予专利权，颁发发明专利证书并在专利登记簿上予以登记。专利权自授权公告之日起生效。专利权期限为二十年，自申请日起算。

专利证书记载专利权登记时的法律状况。专利权的转移、质押、无效、终止、恢复和专利权人的姓名或名称、国籍、地址变更等事项记载在专利登记簿上。



局长
申长雨

申长雨



第 1 页 (共 2 页)

其他事项参见续页

642

证书号第 4259381 号



发明专利证书

发明名称：一种区分水牛和奶牛奶的 miRNA 标记物及其应用

发明人：孙加节;张永亮;江青艳;刘德武;李耀坤;习欠云;陈婷
罗君谊

专利号：ZL 2018 1 0269310.1

专利申请日：2018 年 03 月 29 日

专利权人：华南农业大学

地址：510642 广东省广州市天河区五山路 483 号

授权公告日：2021 年 02 月 19 日

授权公告号：CN 108315440 B

国家知识产权局依照中华人民共和国专利法进行审查，决定授予专利权，颁发发明专利证书并在专利登记簿上予以登记。专利权自授权公告之日起生效。专利权期限为二十年，自申请日起算。

专利证书记载专利权登记时的法律状况。专利权的转移、质押、无效、终止、恢复和专利权人的姓名或名称、国籍、地址变更等事项记载在专利登记簿上。



局长
申长雨

申长雨



第 1 页 (共 2 页)

其他事项参见续页

证书号第 4448413 号



发明专利证书

发明名称：与猪胴体瘦肉率相关的 miRNA 标志物及其应用

发明人：孙加节;张永亮;江青艳;习欠云;陈婷;罗君谊

专利号：ZL 2018 1 0269264.5

专利申请日：2018 年 03 月 29 日

专利权人：华南农业大学

地址：510642 广东省广州市天河区五山路 483 号

授权公告日：2021 年 05 月 28 日

授权公告号：CN 108300792 B

国家知识产权局依照中华人民共和国专利法进行审查，决定授予专利权，颁发发明专利证书并在专利登记簿上予以登记。专利权自授权公告之日起生效。专利权期限为二十年，自申请日起算。

专利证书记载专利权登记时的法律状况。专利权的转移、质押、无效、终止、恢复和专利权人的姓名或名称、国籍、地址变更等事项记载在专利登记簿上。



局长
申长雨

申长雨



第 1 页 (共 2 页)

其他事项参见续页

644

证书号第 5284485 号



发明专利证书

发明名称：一种与猪肌纤维类型相关的 lncRNA 标志物及其应用

发明人：孙加节;张永亮;江青艳;习欠云;陈婷;罗君谊

专利号：ZL 2020 1 0496135.7

专利申请日：2020 年 06 月 03 日

专利权人：华南农业大学

地址：510642 广东省广州市天河区五山路 483 号

授权公告日：2022 年 07 月 05 日

授权公告号：CN 111662988 B

国家知识产权局依照中华人民共和国专利法进行审查，决定授予专利权，颁发发明专利证书并在专利登记簿上予以登记。专利权自授权公告之日起生效。专利权期限为二十年，自申请日起算。

专利证书记载专利权登记时的法律状况。专利权的转移、质押、无效、终止、恢复和专利权人的姓名或名称、国籍、地址变更等事项记载在专利登记簿上。



局长
申长雨

申长雨



第 1 页 (共 2 页)

其他事项参见续页

645

证书号第5969432号



发明专利证书

发 明 名 称：与猪肌间脂肪相关的分子标记及其应用

发 明 人：孙加节;林泽堃;谢芳;张永亮;江青艳;习欠云;陈婷
罗君谊

专 利 号：ZL 2021 1 1436662.X

专利申请日：2021年11月29日

专 利 权 人：华南农业大学

地 址：510642 广东省广州市天河区五山路483号

授权公告日：2023年05月16日

授权公告号：CN 113897445 B

国家知识产权局依照中华人民共和国专利法进行审查，决定授予专利权，颁发发明专利证书并在专利登记簿上予以登记。专利权自授权公告之日起生效。专利权期限为二十年，自申请日起算。

专利证书记载专利权登记时的法律状况。专利权的转移、质押、无效、终止、恢复和专利权人的姓名或名称、国籍、地址变更等事项记载在专利登记簿上。



局长
申长雨

申长雨



证书号第6641173号



发明专利证书

发明名称：与猪肌纤维类型发育相关的circKANSL1L及其应用

发明人：孙加节;庄晓娜;张永亮;江青艳;习欠云;陈婷;罗君谊
林泽堃;谢芳

专利号：ZL 2021 1 1435261.2

专利申请日：2021年11月29日

专利权人：华南农业大学

地址：510642 广东省广州市天河区五山路483号

授权公告日：2024年01月23日

授权公告号：CN 113999851 B

国家知识产权局依照中华人民共和国专利法进行审查，决定授予专利权，颁发发明专利证书并在专利登记簿上予以登记。专利权自授权公告之日起生效。专利权期限为二十年，自申请日起算。

专利证书记载专利权登记时的法律状况。专利权的转移、质押、无效、终止、恢复和专利权人的姓名或名称、国籍、地址变更等事项记载在专利登记簿上。



局长
申长雨

申长雨



荣誉证书

孙加节 同志：

被评为华南农业大学动物科学学院 2019 年度
“青年教师成长奖”。

特发此证，以资鼓励。

华南农业大学动物科学学院

2020 年 1 月 7 日

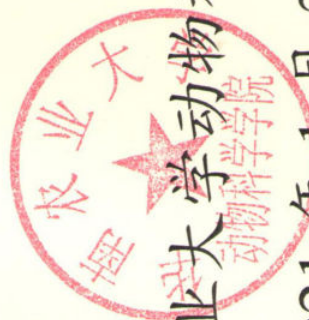


荣誉证书

孙如节 同志：

被评为华南农业大学动物科学学院 2020 年度
“服务管理工作先进个人”。

特发此证，以资鼓励！



华南农业大学动物科学学院

2021 年 1 月 27 日

荣誉证书

孙加节 同志：

被评为华南农业大学动物科学学院 2020 年度
“青年教师优秀奖”。

特发此证，以资鼓励！



华南农业大学动物科学学院

2021 年 1 月 27 日

荣誉证书

孙如节同志：

被评为华南农业大学动物科学学院 2021 年度

“服务育人先进个人”。

特发此证，以资鼓励。

中国共产党华南农业大学动物科学学院委员会 华南农业大学动物科学学院

2022 年 1 月 10 日



广东省高等教育学会
第二届高等教育研究优秀成果奖
(学术论文类)

获奖证书

获奖成果：饲料生物技术课程改革与教
果评价

获奖者：孙加节、罗君谊、陈婷、
习欠云、张永亮

获奖等级：三等奖

广东省高等教育学会

2022年10月24日